NUMERICAL SIMULATION OF COMPOSITE SLABS WITH STEEL DECK UNDER FIRE CONDITIONS

Fernando Freire Ribeiro

Final report of the thesis presented to the

School of Technology and Management (ESTiG)

Polytechnic Institute of Bragança – IPB

For the fulfilment of the requirements for a Master's Degree in

Construction Engineering

July, 2019

NUMERICAL SIMULATION OF COMPOSITE SLABS WITH STEEL DECK UNDER FIRE CONDITIONS

Fernando Freire Ribeiro

Final report of the thesis presented to the

School of Technology and Management

Polytechnic Institute of Bragança – IPB

For the fulfilment of the requirements for a Master's Degree in

Construction Engineering

In the scope of the double degree program with the

Federal University of Technology – Paraná (UTFPR)

Supervised by:

Prof. Dr. Paulo Alexandre Gonçalves Piloto (IPB)

Prof. Dr. Carlos Jorge da Rocha Balsa (IPB)

Prof. Dr. Ronaldo Rigobello (UTFPR-CM)

July, 2019

This thesis is dedicated to my family, for the confidence and support.

ACKNOWLEDGEMENTS

First and foremost, I would like to thank God for taking me through the most challenging and incredible episode of my life. Furthermore, I should express my very profound gratitude to my parents, grandparents and my little brother, for their constant support and belief in me. Without their encouragement this work could not have been successfully conducted.

Special thanks to my supervisors at IPB, Professor Paulo Alexandre Gonçalves Piloto and Professor Carlos Jorge da Rocha Balsa, for their friendship, invaluable support, patience and guidance throughout the development of this work. Thank you for sharing expertise and providing important advices that made this project possible.

Professor Ronaldo Rigobello, my supervisor at UTFPR, is cordially thanked for his friendship, help and dedication. In addition, I would like to thank Professor Leandro Waidemam of the UTFPR for encouraging me on this journey. I would also like to thank all the professors of IPB and UTFPR, for helping me to construct knowledge along my graduation.

Completing this investigation would have been way more difficult without the company, advices, suggestions and support provided by my friends of IPB and UTFPR. I must express my sincere gratitude to all who have contributed to the research reported in this thesis.

ABSTRACT

A composite steel-concrete slab consists of a concrete topping cast on the top of a profiled steel deck. Normally, the concrete is reinforced with an anti-crack mesh positioned on the upper part and individual reinforcing bars placed within the ribs. The steel deck acts as a permanent formwork and the composite action between the steel and concrete is generally achieved by indentations or embossments in this component.

Composite slabs play an important role in the overall stability of buildings during fire exposure, and should be designed in accordance with regulations and standards. The fire rating of this structural element is defined with respect to fire exposure from below and is normally determined through standard fire tests. Three different criteria should be taken into consideration: load bearing (R), integrity (E) and thermal insulation (I).

The Annex D of the EN 1994 – 1-2 and the Annex C of the NBR 14323 provide guidelines for the calculation of the fire resistance (I), as well as the temperature of the rebars and the parts of the steel deck of unprotected fire exposed composite slabs. However, no revisions were made to these methods during the last two decades.

The underlying work presents the development of numerical models for 3-D thermal analysis in the software ANSYS Mechanical APDL 18.2, and MATLAB R2018a through the PDE Toolbox. A total of 208 numerical simulations should be performed considering perfect thermal contact between all the materials, with the aim to investigate the influence of different parameters on the fire resistance (I) and the temperature of the steel components.

During experimental fire tests, the steel deck separates from concrete, which increases the thermal resistance in this interface. In order to simulate debonding effects, another thermal model is established for more 40 numerical simulations, including an air gap with a constant thickness between the steel deck and concrete topping.

The thermal models shall be validated against the results of different experimental fire tests. It is concluded that the calculation rules given in the European and Brazilian standard are generally on the unsafe side and do not consider important parameters. This work proposes improved equations for the estimation of the fire resistance (I) and the temperature of the parts of the steel deck and the rebars as well.

Keywords: Composite slabs; Fire resistance; Thermal insulation; Numerical simulation; Finite Element Method.

RESUMO

Uma laje mista aço-concreto consiste em uma cobertura de concreto no topo de uma chapa de aço. Geralmente, o concreto é reforçado com uma malha anti-fissuração posicionada na parte superior e barras de reforço individuais colocadas dentro das nervuras. A chapa de aço atua como fôrma permanente e a ação composta entre o aço e o concreto é normalmente obtida por entalhes ou mossas neste componente.

As lajes mistas desempenham um papel importante na estabilidade dos edifícios durante a exposição ao fogo, e devem ser projetadas de acordo com regulamentos e normas. A classificação de incêndio deste elemento estrutural é definida com relação à exposição ao fogo em sua parte inferior e é normalmente determinada por meio de testes de incêndio padrão. Três diferentes critérios devem ser levados em consideração: capacidade de carga (R), integridade (E) e isolamento térmico (I).

O Anexo D do Eurocódigo EN 1994 - 1-2 e o Anexo C da NBR 14323 fornecem instruções para o cálculo da resistência ao fogo (I), bem como a temperatura das barras de reforço e das partes da chapa de aço de lajes mistas em situação de incêndio, sem material de revestimento contra fogo. Entretanto, nenhuma revisão foi feita a estes métodos durante as duas últimas décadas.

Este trabalho apresenta a descrição de modelos numéricos para análise térmica 3-D nos programas ANSYS Mechanical APDL 18.2, e MATLAB R2018a através da PDE Toolbox. Assim, 208 simulações serão realizadas considerando contato térmico perfeito entre os materiais, com o objetivo de investigar a influência de diferentes parâmetros na resistência ao fogo (I) e na temperatura dos componentes do aço.

Durante testes experimentais, a chapa de aço separa-se do concreto, o que aumenta a resistência térmica nessa interface. Para simular os efeitos da descolagem, outro modelo térmico é empregado para mais 40 simulações numéricas, incluindo uma camada de ar com espessura constante entre a chapa de aço e a cobertura de concreto.

Os modelos térmicos devem ser validados com base nos resultados de diferentes testes experimentais. Conclui-se que as regras de cálculo dadas na norma Europeia e Brasileira são geralmente inseguras e não levam em consideração parâmetros importantes. Este trabalho propõe novas equações para a estimativa da resistência ao fogo (I) e da temperatura das partes da chapa de aço e das barras de reforço.

Palavras-chave: Lajes mistas; Resistência ao fogo; Isolamento térmico; Simulação numérica; Método dos Elementos Finitos.

LIST OF FIGURES

Figure 1.1: Typical layout of composite slabs: trapezoidal and re-entrant profiles. 1
Figure 1.2: Schematization of the profile of composite slabs with trapezoidal steel deck (adapted from EN 1994-1-2 [13]). 4
Figure 1.3: Schematization of the profile of composite slabs with re-entrant steel deck (adapted from EN 1994-1-2 [13]). 4
Figure 1.4: Theoretical temperature distribution at the unexposed surface of a fire exposed composite slab (adapted from Both [1]). 19
Figure 2.1: Schematic for the calculation of the view factor (adapted from Jiang et al. [9]). 30
Figure 2.2: View of the composite floor slab above the fire at Broadgate, UK [30]. 32
Figure 2.3: The Cardington fire test building structure [58]. 33
Figure 2.4: Cracked slab in region of non-overlapped steel mesh and external view of the fire test [30]. 34
Figure 2.5: Fire curve for the complete process of fire development (adapted from Abu [60]). 35
Figure 2.6: Nominal time-temperature fire curves. 37
Figure 2.7: Examples of temperature-time parametric curves. 40
Figure 2.8: TRRF for structural elements of buildings in Brazil (adapted from IT No. 08/2018 [72]). 47
Figure 2.9: Examples of fire protection measures: active (a) and passive (b) systems. . 48
Figure 2.10: Suspended ceiling after a fire test in Australia [30]. 49
Figure 2.11: Specific heat of concrete as function of temperature. 51
Figure 2.12: Thermal conductivity of concrete: lower and upper limits. 52
Figure 2.13: Density of concrete as function of temperature. 53
Figure 2.14: Variation of the specific heat of carbon steel with temperature. 54
Figure 2.15: Thermal conductivity of carbon steel as function of temperature. 54
Figure 2.16: Thermal properties of air as function of temperature at 1 atm pressure. ... 56
Figure 2.17: Parameters for the position of the rebars (adapted from EN 1994 – 1-2 [13]). 60
Figure 3.1: Heat fluxes acting on a volumetric infinitesimal element. 62
Figure 3.2: Perfect thermal contact model and air gap model. 66
Figure 3.3: Representation of the boundary conditions. 67

Figure 3.4: Modelling of composite slabs in ANSYS: areas and volumes [76]..... 68
Figure 3.5 The SHELL131 finite element [76]. 69
Figure 3.6: The SOLID70 finite element [76]. 69
Figure 3.7: The LINK33 finite element [76]. 70
Figure 3.8: Finite element meshes created in ANSYS [76]. 70
Figure 3.9: Full solution method (Newton-Raphson iteration scheme) [76]..... 71
Figure 3.10: Incremental solution technique for nonlinear problems, combined with the Newton-Raphson iteration scheme [1]. 72
Figure 3.11: Modelling of composite slabs in MATLAB [77]. 73
Figure 3.12: The tetrahedral finite element: linear and quadratic order [77]. 74
Figure 3.13: Finite element meshes created in MATLAB [77]..... 75
Figure 3.14: Mesh convergence study [77]. 75
Figure 4.1: Steel deck geometries for the first parametric study (dimensions in millimetres)..... 79
Figure 4.2: Temperature distribution in slabs 1 and 2 after 60 minutes of fire exposure (ANSYS, first parametric study). 81
Figure 4.3: Influence of diameter of rebar on fire resistance (I) of all the slabs (ANSYS, first parametric study)..... 82
Figure 4.4: Influence of the parameters of the anti-crack mesh on fire resistance (I) (ANSYS, first parametric study). 83
Figure 4.5: Influence of concrete cover for rebar on fire resistance (I) of all the slabs (ANSYS, first parametric study). 84
Figure 4.6: Influence of concrete thickness on fire resistance (I) of all the slabs (ANSYS, first parametric study). 84
Figure 4.7: Average and maximum temperature development on the unexposed side of the slabs (ANSYS, first parametric study) – dimensions in millimetres..... 85
Figure 4.8: Influence of concrete thickness on fire resistance (I) of slab 1 (ANSYS, second parametric study) – dimensions in millimetres. 86
Figure 4.9: Average and maximum temperature development on the unexposed side of slab 1 for the perfect contact model (ANSYS, second parametric study) – dimensions in millimetres. 87
Figure 4.10: Temperature distribution in slab 1 after 90 minutes of fire exposure for different concrete thicknesses (MATLAB, second parametric study). 87

Figure 4.11: Influence of the air gap thickness on fire resistance (I) of slab 1 (ANSYS, second parametric study) – dimensions in millimetres. 88
Figure 4.12: Average and maximum temperature development on the unexposed side of slab 1 for different air gaps (ANSYS, second parametric study) – dimensions in millimetres. 89
Figure 4.13: Temperature distribution in slab 1 after 120 minutes of fire exposure for different air gap thicknesses (ANSYS, second parametric study)..... 89
Figure 4.14: Critical temperatures of the steel components for all the slabs (ANSYS, first parametric study)..... 90
Figure 4.15: Temperatures of the lower flange for different classes of fire resistance (R) for all the slabs (ANSYS, first parametric study)..... 92
Figure 4.16: Temperatures of the web for different classes of fire resistance (R) for all the slabs (ANSYS, first parametric study). 93
Figure 4.17: Temperatures of the upper flange for different classes of fire resistance (R) for all the slabs (ANSYS, first parametric study)..... 93
Figure 4.18: Relationship between the temperature of the rebars for R60 and its diameter, for different concrete thicknesses (ANSYS, first parametric study). 94
Figure 4.19: Relationship between the temperature of the rebars for R90 and its diameter (ANSYS, first parametric study). 95
Figure 4.20: Relationship between the temperature of the rebars for R120 and its diameter (ANSYS, first parametric study). 95
Figure 5.1: Numerical and experimental results for slab 1 – Points 1, 2 and 3 at distance 50, 85 and 70 mm from the top. 96
Figure 5.2: Numerical and experimental results for slab 2 – Points 1, 2 and 3 at distance 20, 74 and 123 mm from the top. 97
Figure 5.3: Numerical and experimental results for slab 3 – Points 1, 2 and 3 at distance 20, 70 and 130 mm from the top. 97
Figure 5.4: Numerical and experimental results for slab 4 – Points 1, 2 and 3 at distance 20, 15 and 15 mm from the top. 97
Figure 5.5: Comparison between the numerical results: ANSYS and MATLAB. 101
Figure 5.6: Comparison between the numerical results from ANSYS and Eurocode 4 – Part 1-2 for the fire resistance (I)..... 102

Figure 5.7: Comparison between the numerical results (ANSYS) and EN 1994 – 1-2 provisions for the temperatures of the lower flange for different classes of fire resistance (R). 102
Figure 5.8: Comparison between the numerical results (ANSYS) and EN 1994 – 1-2 provisions for the temperatures of the web for different classes of fire resistance (R). 103
Figure 5.9: Comparison between the numerical results (ANSYS) and EN 1994 – 1-2 provisions for the temperatures of the upper flange for different classes of fire resistance (R). 103
Figure 5.10: Comparison between the numerical results (ANSYS) and EN 1994 – 1-2 provisions for the temperatures of the rebars for R60. 104
Figure 5.11: Comparison between the numerical results (ANSYS) and EN 1994 – 1-2 provisions for the temperatures of the rebars for R90. 104
Figure 5.12: Comparison between the numerical results (ANSYS) and EN 1994 – 1-2 provisions for the temperatures of the rebars for R120. 105
Figure 5.13: Comparison between the numerical results from ANSYS and NBR 14323 for the fire resistance (I). 105
Figure 5.14: Comparison between numerical, experimental and analytical results for fire resistance (I): second parametric study. 106
Figure 5.15: Results of the proposed new equation for the fire resistance (I) of composite slabs. 107

LIST OF TABLES

Table 1.1: Field of application of the Annex D of EN 1994-1-2 [13]. 21
Table 2.1: Classification of buildings according to DL No. 224/2015 [71]. 45
Table 2.2: Categories of fire risk for office buildings [71]. 45
Table 2.3: Minimum standard fire resistance for structural elements of buildings in Portugal (adapted from Ordinance No. 1532/2008 [69]). 46
Table 2.4: Thermal properties of air at 1 atm pressure (adapted from Çengel and Ghajar [53]). 55
Table 2.5: Coefficients for the determination of the fire resistance of composite slabs with NWC and LWC (adapted from EN 1994 – 1-2 [13]). 57
Table 2.6: Minimum effective thickness according to the standard fire resistance: Eurocode 4 – Part 1-2 (adapted from EN 1994-1-2 [13]). 58
Table 2.7: Coefficients for the determination of the temperatures of the parts of the steel deck for slabs with NWC (adapted from EN 1994 – 1-2 [13]). 58
Table 2.8: Coefficients for the determination of the temperatures of the rebars in the rib for slabs with NWC (adapted from EN 1994 – 1-2 [13]). 59
Table 2.9: Minimum effective thickness according to the required fire resistance: NBR 14323 (adapted from NBR 14323 [14]). 60
Table 4.1: Investigated parameters of the first parametric study. 78
Table 4.2: Calculated view factors. 80
Table 4.3: Investigated parameters of the second parametric study. 80
Table 5.1: Parameters considered for the validation models. 96
Table 5.2: Fire resistance (I) of slab 1: numerical, experimental and analytical results. 99
Table 5.3: Fire resistance (I) of slab 2: numerical, experimental and analytical results. 99
Table 5.4: Fire resistance (I) of slab 3: numerical, experimental and analytical results. 100
Table 5.5: Fire resistance (I) of slab 4: numerical, experimental and analytical results. 100
Table 5.6: Validation models: numerical, experimental and analytical results. 108
Table 5.7: Proposed new coefficients for the temperature of the parts of the steel deck for slabs with NWC. 108
Table 5.8: Proposed new coefficients for the determination of the temperatures of the rebars in the rib for slabs with NWC (Part 1). 109

Table 5.9: Proposed new coefficients for the determination of the temperatures of the rebars in the rib for slabs with NWC (Part 2)..... 109

SYMBOLS

Latin letters

A/L_r	The rib geometry factor
A_t	Total area of enclosure (walls, ceiling and floor, including openings)
A_v	Total are of vertical openings on all walls
b	Thermal absorptivity for the total enclosure
c	Specific heat
c_a	Specific heat of carbon steel
c_{air}	Specific heat of air
c_p	Specific heat of dry concrete
$c_{p,peak}$	Peak of specific heat of concrete according to a certain moisture content
D	Maximum deflection
d	Distance from the extreme fibre of the cold design compression zone to the extreme fibre of the cold design tensile zone
d'_{reb}	Concrete cover for rebar
E	Integrity criterion
E_b	Maximum amount of thermal radiation which can be emitted from a surface
h_1	Height of the concrete part of a composite slab above the steel deck
h_2	Height of the concrete part of a composite slab within the steel deck
h_3	Thickness of the screed situated on top of the concrete
h_{eff}	Effective thickness of a composite slab
h_{eq}	Weighted average of window heights on all walls
$\dot{h}_{net}$	Design value of the net heat flux per unit area
$\dot{h}_{cd}$	Conduction heat flux
$\dot{h}_{net,cv}$	Design value of the net heat flux per unit area by convection
$\dot{h}_{net,r}$	Design value of the net heat flux per unit area by radiation
I	Thermal insulation criterion
L	Clear span of the structural element
l_1, l_2, l_3	Specific dimensions of the trapezoidal or re-entrant steel deck profile
$\vec{n}$	Normal vector
O	Opening factor of the fire compartment
Q	External heat flux
$q_{t,d}$	Design fire load density related to the total surface area A_t
R	Load bearing criterion

s_{mesh}	Anti-crack mesh spacing
T	The temperature
T_∞	Bulk temperature
$\dot{T}$	Time derivative
T_0	Initial temperature
T_{crit}	Critical temperature of the composite slab
T_g	Gas temperature
t	Time
t_a	Air gap thickness
t_d	Thickness of the steel deck profile
t_{fi}	The fire resistance with respect to thermal insulation criterion
$t_{fi,d}$	Design value of standard fire resistance of a member in fire situation
$t_{fi,r}$	Required standard fire resistance in the fire situation
t_{lim}	Time for maximum gas temperature in case of fuel controlled fire
t_{max}	Time for maximum gas temperature
U	Internal energy
u	Moisture content
u_1; u_2	Shortest distance of the centre of the rebar to any point of the webs of the steel deck
u_3	Distance of the centre of the rebar to the lower flange

Greek letters

α	Angle of the web
α_{cv}	Convective heat transfer coefficient
Δ	Variation
ε	Emissivity
ε_f	Emissivity coefficient of the fire
ε_m	Emissivity coefficient related to the surface material of the member
ε_{res}	Resulting emissivity
Φ	View factor
Φ_{low}	View factor of the lower flange
Φ_{up}	View factor of the upper flange
Φ_{web}	View factor of the web
ϕ	Conduction heat flux
ϕ_{reb}	Diameter of the rebar

Θ_g	Gas temperature in the vicinity of the fire exposed element
Θ_m	Surface temperature of the element
Θ_r	Effective radiation temperature of the fire environment
θ	Temperature
θ_a	Temperature of the parts of the steel deck
θ_s	Temperature of the rebars in the rib
Γ	Time factor function of the opening factor O and the thermal absorptivity b
λ	Thermal conductivity
λ_a	Thermal conductivity of carbon steel
λ_{air}	Thermal conductivity of air
λ_c	Thermal conductivity of concrete
ρ	Density
ρ_a	Density of carbon steel
ρ_{air}	Density of air
ρ_c	Density of concrete
σ	Stefan-Boltzmann constant

INDEX

1. INTRODUCTION 1
1.1 General 1
1.2 Objectives 5
1.3 Motivation 5
1.4 Methodology 6
1.5 Background 7
1.6 Fire resistance of composite slabs 18
1.6.1 Eurocode 4 – Part 1-2 20
1.6.2 Brazilian standard NBR 14323 21
1.7 Outline 22
2. FIRE BEHAVIOUR OF COMPOSITE STRUCTURES 24
2.1 Introduction 24
2.2 Heat transfer and thermal actions 25
2.2.1 Conduction 26
2.2.2 Convection 27
2.2.3 Radiation 28
2.2.3.1 View factor 30
2.3 Fires in multi-storey buildings 31
2.3.1 Broadgate 31
2.3.2 Churchill Plaza 32
2.3.3 Cardington fire tests 33
2.4 Fire curves 34
2.4.1 Natural fire curve 35
2.4.2 Nominal standard fire curves 36
2.4.2.1 Standard fire curve ISO 834 37

2.4.3 Parametric temperature-time curves 38
2.5 Fire resistance criteria 40
2.5.1 Insulation 41
2.5.2 Integrity 41
2.5.3 Load bearing capacity 42
2.6 Fire safety on buildings 42
2.6.1 Fire resistance requirements 43
2.6.2 Portuguese regulations 43
2.6.3 Brazilian regulations 46
2.6.4 Fire protection measures 48
2.7 Thermal properties of materials 49
2.7.1 Concrete 50
2.7.2 Carbon steel 53
2.7.3 Air 55
2.8 Simplified calculation methods 56
2.8.1 Eurocode 4 – Part 1-2 56
2.8.2 Brazilian standard NBR 14323 60
3. ADVANCED CALCULATION METHOD 61
3.1 Introduction 61
3.2 Finite element method (FEM) 61
3.3 Description of the thermal models 64
3.3.1 Initial and boundary conditions 66
3.4 ANSYS 67
3.4.1 General 67
3.4.2 Finite element models for thermal analysis 68
3.4.2.1 Finite elements 68
3.4.3 Initial and boundary conditions 70

3.4.4 Solution method 71
3.5 MATLAB 72
3.5.1 General 72
3.5.2 Finite element models for thermal analysis 73
3.5.2.1 Finite elements 74
3.5.3 Initial and boundary conditions 75
3.5.4 Solution method 76
4. PARAMETRIC STUDIES 78
4.1 Description 78
4.2 Numerical results 80
4.2.1 Influence of different parameters on fire resistance (I) 81
4.2.1.1 Steel deck geometry 81
4.2.1.2 Rebar diameter 82
4.2.1.3 Anti-crack mesh diameter and spacing 83
4.2.1.4 Concrete cover for rebar 83
4.2.1.5 Concrete thickness 84
4.2.1.6 Air gap thickness 88
4.2.2 Critical temperatures 90
4.2.3 Temperatures of the steel components 91
4.2.3.1 Parts of the steel deck 91
4.2.3.2 Reinforcement bars 94
5. COMPARISONS OF RESULTS 96
5.1 Validation of the thermal models 96
5.2 ANSYS and MATLAB results 100
5.3 Numerical results and Eurocode 4 – Part 1-2 101
5.4 Numerical results and NBR 14323 105
5.5 General comparison 106

5.5.1 Proposed new formulae 107

6. CONCLUSIONS AND RECOMMENDATIONS 111

6.1 Recommendations for future research 112

7. REFERENCES 114

APPENDIX A 120

APPENDIX B 127

APPENDIX C 336

APPENDIX D 347

APPENDIX E 351

APPENDIX F 392

APPENDIX G 397

1. INTRODUCTION

1.1 General

A composite steel-concrete slab consists of cold-formed profiled steel deck which acts as a permanent formwork to the concrete topping. Usually, the concrete is reinforced with individual longitudinal reinforcement bars placed within the ribs and an anti-crack mesh, as illustrated in Figure 1.1. The composite action between the steel and concrete is generally achieved by indentations or embossments in the steel deck [1].

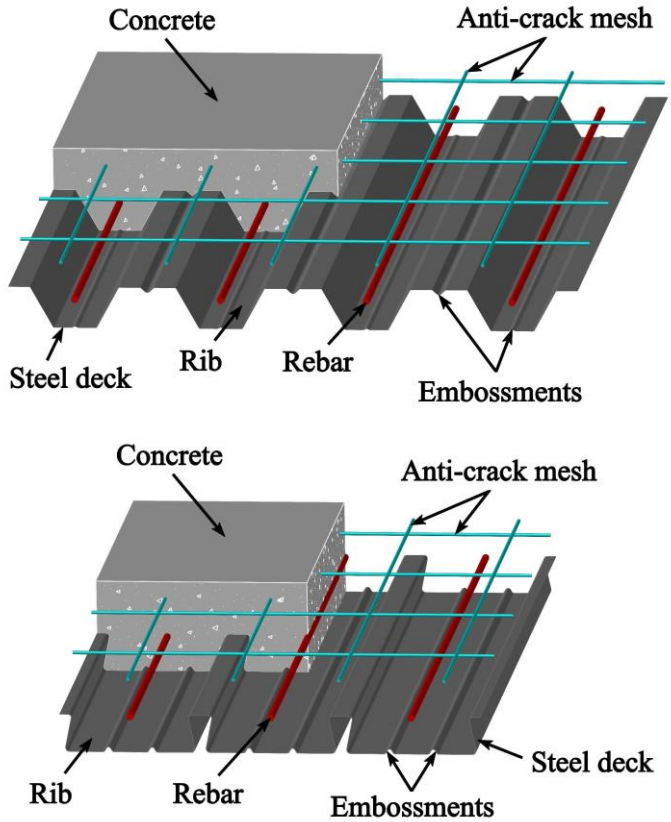

Figure 1.1: Typical layout of composite slabs: trapezoidal and re-entrant profiles.

The additional steel reinforcing elements incorporated within the concrete layer on composite slabs have several functions such as reinforcing the structure hence permitting openings, distributing the effects of concentrated and linear loads, improving the fire resistance and controlling concrete cracking [2].

The steel deck has three different functions: before concrete pouring, it acts as a work platform and safety screen; during casting, the deck serves as permanent shuttering; and after hardening of the concrete, the deck serves as reinforcement [1].

Owing to the relative ease of casting concrete, trapezoidal deck slabs are more popular than re-entrant ones [3].

Fire resistance of an assembly or material can be defined as the property to endure fire or protect from it. On structural engineering elements, it is measured by the time and can be associated to the capacity of confining a fire or to maintain performing the structural function during fire exposure, or both. On composite slabs, the fire resistance is principally affected by the thickness of the steel deck, type of aggregate in concrete and the thickness of the concrete layer [4]. Several other aspects may influence on the fire endurance of composite slabs such as the diameter and concrete cover for the reinforcement bars, for example.

The concept of fire safety engineering consists in the prevention of the catastrophic failure of structures during fires. Consequently, the objective is to guarantee that every person in a building can escape safely from a fire [5]. Therefore, the application of protective actions and appropriate fire design is essential to reduce the damage to the whole building and assure life safety in case of fire.

The employment of composite slabs in construction has been usual in North America for several years and since the 80s, a significant increase has taken place in Europe [6]. Thus, different types of profiled steel deck started to be developed likewise researches concerning the structural and thermal behaviour of composite slabs has significantly increased.

Composite slabs have an important paper in preventing the spread of fire in buildings. The fire resistance of this type of building element should be determined according to three different criteria, namely, load bearing (R), integrity (E) and insulation (I).

Presently, several types of profiled steel deck are marketed in Europe with thicknesses usually ranging from 0.7 mm to 1.2 mm. Generally, with the aim of providing protection against corrosion, the steel deck is made from galvanized cold-formed steel with a thin zinc layer applied on both faces [7]. This measure increases considerably the durability of the structure as a whole and hence decreases the number of pathologies.

The overall depth of composite slabs, that is, the height of the steel deck added to the height of the concrete layer typically varies between 100 and 170 mm. The span length usually varies between 2.5 and 4.0 m when the slab is not propped during the construction phase [8].

This type of structural engineering element is mainly used in multi-storey office buildings however, it is common to encounter this structural element in various types of buildings such as airports, industrial constructions, parking spaces and hospitals, among others [2].

After completing the construction stage, the steel deck acts as an external reinforcement. Therefore, this solution requires less additional reinforcement and provide reduced construction time in comparison with conventional flat slabs due to the application of the steel deck as a permanent formwork [9]. In addition, the structural efficiency and the reduction/elimination of propping are other advantages of the use of composite slabs.

Another advantage of the use of composite slabs is the reduction of the dead load of the structure. Owing to the hollow shape of the deck, a significant area of concrete can be saved providing a decrease on the self-weight and therefore resulting in a more economical and efficient building. The flexibility, simplicity of installation/transportation and elevated quality control on the production of the steel deck are other positive points of this solution [10].

Structural elements have to meet fire-safety requirements and additional measures have to be taken if necessary. For composite slabs with profiled steel deck, the direct exposure of the steel deck to fire leads to fast loss of stiffness and strength degradation. Therefore, additional reinforcement is commonly used to increase the fire resistance and comply with the requirements of design codes [11].

An appropriate prediction of the behaviour of structural engineering elements in use is essential for a safe and economic design. Large scale fire tests on elements of construction are expensive and time-consuming. As a workaround, numerical methods can provide a rapid and cost effective approach to problems of heat transfer and even afford accurate predictions of the fire performance of structures [12].

Simplified calculation methods for determining the fire resistance of composite slabs are presented by the European Standard EN 1994 Part 1-2 [13] and Brazilian standard NBR 14323: 2013 [14]. The calculation rules are suitable for a specific range of unprotected composite slabs with trapezoidal and re-entrant steel deck exposed to fire according to standard temperature-time curves.

The calculation of fire resistance according to insulation criterion incorporated in the actual version of Eurocode 4 – Part 1-2 is based on approximate closed-form expressions [7], which depends on the geometric parameters of the slab. The simplified

procedures for determining the fire resistance presented in the NBR 14323 are similar to those specified in the European Standard. Figures 1.2 and 1.3 illustrate the geometric parameters of composite slabs with trapezoidal and re-entrant profiles, respectively. The parameter h_3 represents the thickness of the screed layer if any on top of the slab.

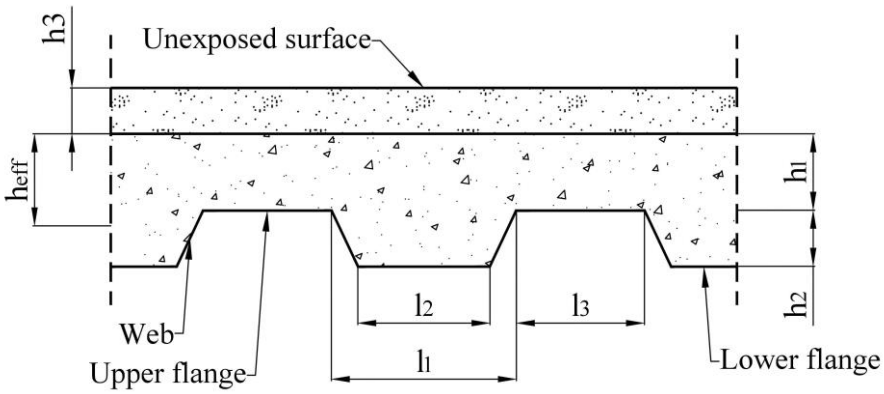

Figure 1.2: Schematization of the profile of composite slabs with trapezoidal steel deck (adapted from EN 1994-1-2 [13]).

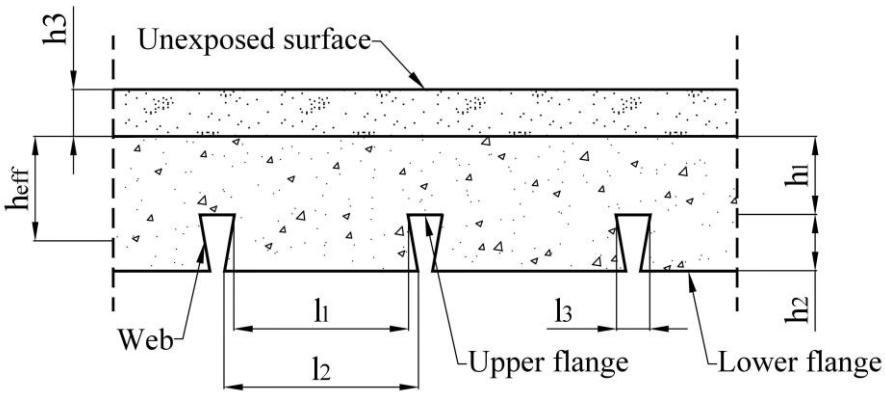

Figure 1.3: Schematization of the profile of composite slabs with re-entrant steel deck (adapted from EN 1994-1-2 [13]).

During fire exposure, the steel deck heats up rapidly, expands and can separate from the concrete topping. The loss of thermal contact between these components may also be attributed to the evaporation of concrete moisture, which occurs at a temperature of 100 °C. Effectively, previous studies mention the separation of the steel deck from the concrete in fire exposed composite slabs, which increases the thermal resistance in this interface (see, for instance Both, Fellinger and Twilt [15]).

The underlying work deals with numerical simulations of the fire behaviour of composite slabs using different steel deck geometries, concrete thicknesses, and rebar diameters, among other parameters.

1.2 Objectives

The main objective of this study is to develop three-dimensional thermal models in order to investigate the fire behaviour of composite steel-concrete slabs with profiled steel deck. Toward this end, a new tool must be developed on the software MATLAB R2018a for three-dimensional thermal analyses, which shall be validated against the commercial finite element software ANSYS Mechanical APDL 18.2. Moreover, the developed finite element models should be validated against experimental data provided by different authors.

The final goal of this work is to investigate the influence of different parameters on the fire resistance (I), as well as on the temperature of the rebars and the parts of the steel deck of composite slabs. The numerical results shall be compared to the simplified calculation methods of the EN 1994-1-2 and the Brazilian standard NBR 14323:2013.

If necessary, a new formula must be proposed for determining the fire resistance of composite slabs from the thermal insulation standpoint. Additionally, new proposals may be presented for the calculation of the temperature of the rebars and the parts of the steel deck, which are important for the load bearing fire resistance.

1.3 Motivation

The increasing use of composite structures in buildings has highlighted the necessity for accurate and refined analysis concerning the thermal and structural behaviour of these elements in case of a fire. In this way, it is possible to adopt economical solutions but at the same time enable safe and efficient buildings.

The analytical solution of problems involving complicated geometries and material properties is usually difficult and oftentimes impossible. An alternative for these cases is the application of numerical methods, such as the finite element method (FEM) [16].

Owing to the exponential growth of computing in last decades, several computer programs based on FEM were developed. Along with the increase of processing power of computers, complex problems of engineering have been solved by means of numerical simulations using these programs. As a result, several studies have evidenced that numerical analyses constitute an efficient approach for determining responses of structures, hence providing reasonable results.

A great number of numerical investigations provided valuable insight and improved the knowledge about the behaviour of composite slabs with steel deck during fire exposure. Nevertheless, the majority of these studies have focused on the structural response, using the thermal analysis to furnish input for the structural model. Thus, a small number of researches have consistently investigated the temperature gradient in composite slabs under fire and its sensitivity to different parameters [7].

The Annex D of EN 1994-1-2 [13] presents a simplified calculation method for the calculation of the fire resistance of unprotected composite slabs subjected to the standard fire curve ISO 834 from below. During the last years, no revisions were made to this method and the range of geometric parameters of the profiles that are commercialized nowadays has increased considerably in comparison to the range used in the decade of 1990. For these reasons, it is felt that thermal analyses shall be made in order to evaluate the precision of these calculation rules.

In the present investigation, it is expected that the development of the new tool for the assessment of the fire resistance, along with the results of the numerical simulations, provide consistent data for the development of future studies. In addition, this work intends to contribute to the community by increasing the knowledge about the fire performance of composite slabs and fomenting the scientific development, thus providing buildings increasingly safer.

1.4 Methodology

In order to determine the fire resistance of composite slabs regarding the thermal insulation criterion, and calculate the temperature of the steel components, two different solution methods are used: the simplified calculation method of standards and the advanced calculation method. The latter is based on a three-dimensional finite element models which include the effect of additional steel reinforcement.

Two different parametric studies should be performed in order to analyse possible relevant parameters for fire resistance. Commonly used values of concrete thicknesses and rebar diameters are selected for the range of studied parameters. A total of 264 numerical simulations shall be performed, including the analyses for validation.

The first parametric study (208 simulations) comprises slabs with four different commercial steel deck profiles, being two trapezoidal and two re-entrant. In addition, the effect of three different rebar diameters with two different values of concrete cover

for rebar, four different concrete thicknesses and two different anti-crack mesh configurations should be analysed separately. A perfect thermal contact model shall be utilized in these analyses.

The second parametric study (40 simulations) involves a single trapezoidal steel deck profile and eight different concrete thicknesses. An air gap thermal model should be used in these numerical simulations in order to simulate the effects of debonding of the steel deck from the concrete. The insulating layer (air gap) has constant thickness and is introduced between the steel deck and the concrete topping. In this regard, three different air gap thicknesses are analysed.

A representative portion of one square meter of each composite slab is selected to perform the numerical analyses. The composite slabs are exposed to fire on the bottom surface according to standard fire curve ISO 834.

1.5 Background

In this section, a literature review of several studies about composite steel-concrete slabs under fire conditions is presented. Therefore, the background and the current knowledge about the thematic will be presented, according to numerical and experimental investigations developed throughout history.

The first reference of the application of steel deck as a structure to support a concrete floor occurs at the 1920 decade. In 1926, based on the demand for new construction solutions, Loucks and Gillet developed and patented the steel deck system [17]. At that time, only the steel deck provided the structural resistance and the concrete layer was responsible to level the surface and assure the fire resistance. This solution demonstrated to be more efficient than conventional reinforced concrete floors, due to the fact that the steel deck worked as a permanent formwork and construction platform [2].

In the decade of 1950, the first composite slab with profiled steel deck called *Cofar* was produced and marketed by Granco Steel Products Company, Missouri [18]. The developed composite solution consisted of a trapezoidal deck section with a mesh of cold drawn wires welded transversely across the deck troughs, associated with a concrete topping.

In 1954, Friberg [19] published the primordial expressive article about design criteria of composite slabs after numerical and experimental evaluations of the system

Cofar. This research provided a cost comparison between the composite system and traditional reinforced concrete slabs. The results of the tests demonstrated good equivalence with what was expected and it was observed that this solution had similar structural resistance with analogue reinforced concrete slabs.

With the objective to avert the use of welded mesh and assure horizontal shear transfer between the steel and concrete to achieve composite action, a new steel deck profile with embossments and re-entrant parts was developed by Inland-Ryerson Company in 1961 [17]. Named as *HiBond*, the new trapezoidal profile was the forerunner of modern profiled steel decks for composite slabs that use indentations as mechanism of shear transference [2].

The first concept of "fire engineering" applied to steel structures was introduced by Petterson et al. [20] in 1976. The publication exposes principles which govern rational fire engineering design, comparisons between suspended ceilings carrying floor slabs of lightweight concrete under fire exposure conditions and a description of prevailing materials and methods used for structural fire insulation.

In Europe, the use of composite steel-concrete structural components increased significantly in the decade of 1980. Until this time, the structural fire resistance was calculated mostly by experimental tests, which are substantially expensive and time-consuming [6]. In 1983, recognizing the need for a calculation method, the ECCS (European Convention for Constructional Steelwork) [21] published the first instructions for the practical design of composite slabs under fire conditions. This technical note introduced simple calculation methods based on criteria for fire resistance of the standard ISO 834 [22], hence inspiring the diffusion of the use of composite slabs.

Between 1983 and 1985, a test programme sponsored by the dominant steel deck manufacturers in the United Kingdom was performed by the Construction Industry Research & Information Association (CIRIA). The fire tests were conducted on one large-scale and five smaller-scale loaded composite slabs with reinforcement meshes. The investigation indicated that design recommendations were generally conservative and slabs with dovetail profiles normally provided better fire resistance in comparison to slabs with trapezoidal profiles, among other conclusions [8].

In parallel, between the years of 1984 and 1986, with the support of the Fire Research Station (FRS), the British Steel Corporation (BSC) executed a test programme on three different large-scale specimens. The research consisted of loaded fire tests

carried out on continuous composite slabs with welded bars as reinforcement. From the results of the tests, it was concluded that some requirements for minimum slab depth were too conservative and several cautions must be taken concerning the use of high tensile drawn reinforcement due to the breaking of some bars over the supports during the tests [8].

In the Netherlands, a research project was started in 1989 with the association between the TNO Institute for Building Materials and Structures, and both Delft and Eindhoven Universities of Technology. This project consisted of extensive numerical and experimental studies comprising the behaviour of composite slabs under fire conditions and was divided into two phases: the first involved principally simply supported slabs and in the second, main focus was given to continuous slabs. This research was part of an international project co-sponsored by the European Coal and Steel Community (ECSC) with the final goal of introducing practical calculation rules for fire resistance assessment, which should be proposed as revisions of the existing European recommendations [23]. In particular, this investigation was focused on the positive effect of thermal shielding and partial protection of composite slabs near internal supports.

In 1990, a research related to the first phase of the ECSC project was carried out at TNO with the purpose of studying the influence of fire exposure on the behaviour of reinforced composite slabs. For that matter, Hamerlinck et al. [24] developed a thermal and a mechanical numerical models which were experimentally verified with loaded and unloaded tests. For galvanized steel decks, owing to the melting of the zinc layer and surface blackening, the resulting emissivity of the steel deck was obtained in the calculations as function of the temperature. Based on the comparisons between calculated and measured results, it was concluded that the models satisfactorily predicted the behaviour of the simply supported tested slabs.

In 1991, a mathematical model was developed by Hamerlinck [6] in order to analyse the mechanical and thermal behaviour of reinforced composite slabs under fire conditions. The research took into account the most important parameters in the testing programme and a new computer program based on the model was implemented, enabling an extensive number of simulations at low computational cost (low time processing). As a conclusion, it was observed that the developed two-dimensional model provided satisfactory results on the thermal behaviour of fire-exposed composite slabs although not including three-dimensional thermal effects.

In the same year, Newman [25] from the Steel Construction Institute (SCI) of the United Kingdom published instructions about the most used methods at this time for verifying the fire resistance of composite slabs: the fire engineering method and the simplified method. Moreover, dimensions requirements, design examples and a comparison between the methods were also presented. This investigation presented a number of conclusions and recommendations, such as the fire protection of beams supporting composite floors and the required thickness of concrete, in both trapezoidal and re-entrant composite slabs, for a specified fire rating.

In 1993, in the scope of the second phase of the ECSC project, an investigation about the effect of thermal shielding and partial protection near internal supports of continuous composite slabs was carried out by Both et al. [23]. This study highlighted the benefits of applying partial protection and showed a comparison between the results of partial protected and unprotected models. All things considered, it was noticed that the use of partial protection as an insulated steel section near internal supports was a simple and economical alternative that could increase the fire resistance of composite slabs up to 20%. Beyond that, it was also concluded that existing rules for the calculation of the fire resistance were conservative.

In the United Kingdom, a numerical research was conducted in 1994 by Davies and Wang [12] based on previous experimental studies. With the main purpose of determining the temperature distribution in the cross-section of composite slabs subjected to standard fire conditions, a two-dimensional Finite Element Method was applied. Furthermore, a simple engineering approach was developed with the objective of better accounting the influence of the moisture content of the concrete on the heat transfer through the slab. The results of the analysis demonstrated excellent agreement with the experimental results obtained in 1990 by P.W. van de Haar et al., and evidenced that an accurate prediction of the temperature development in composite slabs under fire conditions was available.

In 1995, Hamerlinck and Twilt [26] published a paper with the main objective of describing the calculation method of the first draft of Eurocode 4 – “Design of composite steel and concrete structures - Part 1-2: Structural fire design”. Moreover, this publication presented a general discussion around the fire resistance of composite slabs, summarized research developments at that time and highlighted some modifications incorporated in the final draft of Eurocode 4 in 1993. The authors concluded that although providing a simple and quick calculation method, the Eurocode

4 required special attention at some points as the contribution of the steel deck for the sagging moment capacity and the influence of the reinforcement in regions of hogging moment to avoid premature failure.

In the next year, a study was published by Both [27] which summarized research conclusions of that time as well as proposed new calculation rules to Eurocode 4 for the prediction of the hogging moment capacity. In this publication, a quantitative description of the behaviour of fire exposed composite slabs and the validation of the numerical models were presented. Moreover, a parametric study was performed comprising most of available steel deck in Europe and conclusions obtained from the new proposed calculation rules were compared to numerical results. In summary, it was concluded that a good accordance was given between the results of the numerical models, described by two and three-dimensional heat flow, and experimental evidence.

In the late nineties, calculations rules of Eurocode 4 for the assessment of the fire resistance were based on a limited number of experimental tests and thus required a fundamental basis since often led to conservative solutions [1].

In 1997, a numerical investigation was performed by Fellinger and Twilt [28] after the conclusion of a full-scale standard fire test conducted on a composite flooring system. The tested specimen consisted of a continuous composite slab adopting deep steel deck profiles, supported by integrated steel beams which were almost completely encased. The DIANA Finite Element Method program was used to perform the numerical simulations. In addition, the radiative heat exchange between the web and the upper flange, the reduced contact between the steel deck and concrete, and the effect of thermal shielding of the slab were taken into account. The responses of the thermal and structural models showed satisfactory agreement with the test results.

During the same year, a similar research was carried out by Both et al. [15] encompassing the fire behaviour of shallow floor systems. In this paper, full-scale fire tests were summarised and the numerical modelling comprising these tests was performed using DIANA program. The debonding of the steel deck owing to the evaporation of moisture was taken into consideration (assumed to occur over temperatures of 100 ºC). Ultimately, a parametric study was performed with the main objective of developing simplified calculation rules for easy assessment of fire resistance. The thermal and mechanical behaviour of shallow floor systems was satisfactorily predicted using the program and the simple calculation rules were successfully established.

Within the scope of the second phase of the ECSC project, Both [1] performed a numerical and experimental study in 1998 with the main objective of introducing easy to handle calculation rules as well as providing more insight on the fire behaviour and failure mechanisms mainly of continuous composite slabs. In this doctoral thesis, the experimental work was clearly described and the numerical model was developed and validated with the tests results in conjunction with results of previous researches. The package DIANA with some modifications and extensions in particular modules was used to perform the numerical simulations. It is noteworthy that the three-dimensional heat flow near internal supports, concrete cracking behaviour and the melting of the zinc layer of the steel deck were taken into account. Finally, a parameter study was performed and simple calculation rules were derived from the results using standard regression techniques. It was concluded that the thermal model was able to describe the two and three-dimensional heat flow in composite slabs during fire exposure and the assessment rules for the fire resistance given in the Eurocode 4 at that time could be considerably improved, among other conclusions.

In 1999, Bailey et al. [29] published a paper with the main aim of discussing in detail two of six fire tests performed between 1995 and 1996 on a full-scale eight-storey building at the Building Research Establishment (BRE) Cardington Laboratory, in the UK. The structural system of the tested building comprised 130 mm deep composite slabs with trapezoidal deck, shrinkage mesh and lightweight concrete. In consonance with previous small-scale fire tests, the composite floor achieved good fire resistance, providing dominant contribution to the frame endurance. In general, accordingly to observations of the tests, no collapse occurred and the fire behaviour was better than presented in standard fire tests.

In the same year, Abdel-Halim et al. [4] published a paper with the main goal of providing relevant data about the behaviour of fire exposed composite slabs adopting a model fire test facility. For this purpose, one sample with and another without additional longitudinal reinforcement bars were subjected to the ISO standard fire in the University of Salford, UK. Thereupon, the research focused on the investigation of the effect of additional bars on the fire resistance as well as on the comparison of the fire resistance of the specimens with respect to integrity and insulation. Conclusively, it was observed that the sample without additional bars presented a lower rate of rise of temperatures at the unexposed surface than the reinforced sample and thus, a higher fire resistance in both insulation and integrity criteria.

The first design instructions for composite steel framed buildings based on Cardington fire tests were introduced in 2000 by Newman et al. [30]. This publication highlighted details of the fire test programme as well as proposed design rules adopting design tables based on a simple structural model developed by the BRE Cardington. The suggested recommendations required a division of each floor into floor design zones which had some limitations and should be applied only to composite steel-framed buildings of the general form tested at Cardington. The calculations were simple to apply but were based on some assumptions, hence leading to conservative solutions. As also observed by Bailey et al. [29], the performance of entire buildings in fire was very different from the behaviour of isolated members in standard fire tests.

In 2001, Lamont et al. [31] published an article in which numerical simulations of Cardington fire tests were performed using the adaptive heat transfer program HADAPT. In addition, this publication also presented a description of four fire tests at Cardington and described the two models that were used to predict the temperature development in composite slabs. The first model excluded the steel deck and was used to execute a sensitivity analysis around important parameters in a relatively decreased processing time. On the other hand, the second model included the steel deck and consisted in a rigorous approach to the problem. In general, the developed models successfully predicted the temperatures in the slabs. However, the second model overpredicted the steel temperatures due to inadequacies considering the moisture evaporation.

In the year of 2002, Lim and Wade [32] published a report which describes the fire tests performed on six large-scale slabs carried out at Building Research Association of New Zealand (BRANZ) furnace. The main objective of the tests was to analyse the behaviour of unrestrained simply supported slabs in a controlled furnace, providing consistent data for the verification of numerical models. Three reinforced concrete flat slabs and three composite slabs were loaded as well as exposed to a standard fire for three hours. All the tested slabs performed well despite suffering loss of moisture and extensive surface cracking on the unexposed side. In brief, the fire resistance in the tests was higher than calculated from normative recommendations and the results evidenced the important effect of membrane action on preserving the structural stability of the slabs under fire conditions.

Still in 2002, a research was performed by Both and Stark [33] with the main goal of establishing fundamental basis to the calculation rules of fire exposed composite

slabs and thereafter, introducing more precise rules. Part of this research was executed within the scope of the ECSC research project. The investigation comprised a briefly description of the performed experimental work as well as the validation of the sophisticated finite element models. Besides that, a parametric study was carried out in order to develop new improved calculation rules for the assessment of the fire resistance of composite slabs. In this regard, an innovative aspect was the computing of the contribution of the steel deck to the load bearing capacity. Finally, a comparison between the results of the parameter study and the calculation rules available at that time was presented with the view to show the betterment.

In 2003, Lim [34] published his doctoral thesis which comprised an analysis of the influence of both compressive membrane action on the behaviour of restrained one-way flat slabs and tensile membrane action on unrestrained two-way composite and flat slabs. In the first case, different boundary conditions were analysed to study and compare the various types of support conditions in structures. In the second case, fire tests on axially unrestrained slabs and numerical modelling of the tested slabs were performed. The main objectives of this research were to ascertain if tensile membrane forces could avoid failure of simply supported two-way slabs during fire exposure and whether axial restraint could enhance the fire resistance of one-way slabs. The numerical simulations were performed using shell and beam elements in the non-linear finite element program SAFIR and the validation of the developed numerical model was accomplished based on experimental fire tests. In general, it was observed that the behaviour of one-way slabs in fire conditions had great dependence on the support conditions and owing to tensile membrane action, two-way slabs had better fire resistance than one-way slabs. Moreover, the results of modelling of the fire tests showed good accordance with the experimental results, among other conclusions.

A new fire design method incorporating the membrane action of slab/beam composite floor systems was introduced in 2004 by Bailey [35]. The new method was an extension of a previous simplified design approach developed by the author and included the membrane action of the slab and beam acting compositely as well as the effects of oscillations in the deflected shape of the slab. In this paper, focus was placed on a brief explanation of the concepts of membrane action and a comparison between the new and previous approach. In essence, the new design approach enabled the membrane capacity of the system to be satisfactorily computed and evidenced that simplifications of the previous method were conservative.

In 2008, an orthotropic slab finite element was implemented by X. Yu et al. [3] to perform numerical simulations on composite slabs under fire conditions. The continuous part of the slab was represented by solid slab elements and the ribbed part by special beam elements with uniaxial attributes. The thermal analyses were carried out on software VULCAN and took into consideration the moisture evaporation in the concrete and the temperature-dependent thermal properties of both steel and concrete. The model was validated against three fire tests and a parametric study was conducted to evaluate the influence of the rib shapes on the thermal and structural performance of fire exposed composite slabs. The results of the parametric study showed that the orthotropic model sensitively considered the influence of the deck shape and a simple calculation method to estimate the fire resistance level was proposed.

In 2011, Guo and Bailey [36] executed an experimental research with the aim of providing more insight on the performance of composite slabs during heating and cooling phases of fire. Nine equal composite slab specimens were tested: two of them at room temperature and the other ones at three different fire scenarios which were controlled by burners and fans within the furnace. In addition, the specimens were loaded with representative values found in practice to investigate the structural behaviour. In short, the tests results showed that the maximum temperature and both heating and cooling rates strongly influenced the fire behaviour of composite slabs. For all the tests, the maximum temperatures at the unexposed surface and on the anti-crack mesh were both higher during the cooling stages, due to the thermal inertial effect, which highlighted that insulation failure is likely to occur not only during heating but also during cooling phase. The obtained results provided consistent data for the validation of future numerical models.

In 2012, Banerjee [37] from the National Institute of Standards and Technology (NIST) published a report which summarized the description and the results of two full-scale standard fire tests of the same composite floor system employed in the towers of the World Trade Centre. The principal goals of these tests were to comprehend the effects of thickness of fire protection, scale of test and restraint conditions on the fire performance of composite floor systems. In order to simulate the transient heat transfer, a finite element model was developed in the software ANSYS and the numerical results for a representative section were confronted to experimental measurements. The study provided an outlined statistical analysis of the thermal data as well as a quantitative comparison between the numerical and experimental results. In general, the numerical

model required improvements such as considering more realistic evidence for heat transfer parameters, thermophysical properties and geometric changes in fire.

In 2014, Kolšek et al. [38] published an article in which a generalized model for numerical simulations of composite structures was presented and validated against experimental tests performed by other authors. The developed model took into account material hardening/softening and creep as well as geometrical and material nonlinearities to consider interlayer slips and uplifts. In addition, a finite element formulation was presented for the mechanical study and an investigation of the contribution of the steel deck and the flexibility of the interlayer connection of a trapezoidal composite slab to the overall fire resistance was carried out. The results evidenced that when the proportion between the tensile stiffness of the reinforcing bars and the tensile stiffness of the deck is small, a reasonable contribution of the steel deck to the fire endurance can be mobilized. On the whole, the research resulted in a model which was suitable for the development of parametric studies to analyse the influence of physical phenomena, for example.

In the next year, a numerical study was conducted by Tan and Nguyen [39] which described the experimental behaviour of three composite floor systems exposed to fire conditions that were part of a test programme carried out at Nanyang Technological University in 2012. The finite element model was developed using Abaqus/Explicit software and validated against the experimental data from the tests. The main aim of the research was to comprehend the effect of bending stiffness of the protected secondary beam on the system performance. A good correspondence between the simulations and tests results was observed, that is, the numerical model satisfactorily predicted the thermal and structural behaviour of the systems although not considering the degradation of composite action between the concrete and steel. After all, it was observed that as the stiffness of the secondary edge beams increased, the central deflection of the slab decreased at the beginning and failure happened later.

In 2017, Guo-Qiang Li et al. [40] performed experimental investigations on the thermal and mechanical performance of four full-scale composite floors with the main objective of studying the influence of the boundary conditions, reinforcement location, slab layout and the effect of unprotected secondary beams on tensile membrane action. During the tests, debonding between the steel deck and concrete was observed and the highest temperature in the reinforcement and steel deck occurred on the cooling phase. The results were compared to Eurocode 4 provisions and it was concluded that the

temperature on the reinforcement was considerably affected by its location and Eurocode 4 predictions were conservative in terms of fire resistance and temperature of the steel deck.

Still in 2017, a numerical study based on detailed and reduced-order models of heat transfer in composite slabs was carried out by Jian Jiang et al. [9], from the NIST. The main objective of this research was to develop a reduced-order modelling approach applicable for both thermal and structural analysis, in order to simplify the analysis of the structural behaviour under fire conditions. Solid elements were used for the concrete slab and shell elements for the steel deck. Both detailed and reduced-order models were validated against experimental evidence and a parametric study using the detailed model was conducted to evaluate the effect of some components on temperature development such as thermal boundary conditions, thermal properties of materials and slab geometry. In addition, the specific heat of the concrete was modified to better estimate the heat input in the web, and thereafter an equation for the modification was suggested. In order to consider the effects of the change in emissivity of the galvanized steel deck due to the melting of the zinc layer, a novel method to calculate the temperature-dependent emissivity was proposed. Generally speaking, it was observed that satisfactory results did not require a great refinement of the finite element mesh and temperatures at the unexposed side were mainly affected by the thickness of the concrete topping. The results of the proposed model for emissivity showed better conformity with experimental results than those calculated from Eurocode 4.

In 2018, an investigation of the thermal performance of composite slabs under standard fire conditions was conducted by Prates [41]. The key objective of this study was to develop two-dimensional numerical models using the software MATLAB and ANSYS in order to evaluate the fire resistance of different slab configurations according to the insulation criterion. Several numerical simulations were performed with the aim of analysing the effect of both concrete and steel deck thicknesses on the temperatures at the unexposed side. Considering that the thermal behaviour is not influenced by the mechanical behaviour, experimental fire tests were conducted on two unloaded samples. Moreover, the results of the numerical simulations were compared against results obtained with the experimental tests as well as the simplified method given in Eurocode 4 and NBR 14323. On the whole, the fire resistance ratings obtained from the numerical models were considerably smaller than those measured on the experimental tests. A comparison between the numerical results and the simplified calculation method of

Eurocode 4 evidenced that the current design rules are unsafe. According to the numerical results, a new and better approach considering a quadratic dependence between the fire resistance and the effective thickness of the composite slab was proposed.

In 2019, Jian Jiang et al. [42] conducted a numerical investigation around different parameters that may influence on the fire resistance of composite slabs with respect to the thermal insulation criterion (I). An improved algebraic expression for the calculation of the fire resistance that explicitly accounts for moisture content of concrete was proposed. The formulation is applicable to an extended range of geometries in comparison to the limitations of the calculation method presented in the current version of Eurocode 4. A set of 54 composite slabs was selected for numerical analyses using a high-fidelity finite element approach. It was concluded that the concrete thickness and the moisture content were the parameters that most influenced the fire resistance. The proposed expression for fire resistance was validated against additional analyses and experimental data, resulting in maximum deviations of 15 and 18 minutes, respectively.

In 2019, Piloto et al. [43] [44] [45] [46] carried out a numerical research concerning the fire behaviour of composite slabs under standard fire conditions. The main objective of this investigation was to evaluate the fire resistance of this structural element from the thermal insulation standpoint. Three-dimensional thermal models were implemented using ANSYS and MATLAB PDE toolbox, considering slabs with perfect thermal contact between all materials, and an insulating layer with constant thickness (air gap) between the steel deck and the concrete topping in order to simulate debonding effects. It was concluded that the perfect contact model underestimates the fire resistance (I) and the results of the air gap model present good agreement with experimental results. Further research was conducted by the authors [47] with the aim to propose an improved method for the estimation of the temperature of the parts of the steel deck and the rebars of composite slabs subjected to standard fire exposure. It was observed that the assessment rules given in the EN 1994 – 1-2 for the temperature of the steel components of composite slabs were generally on the unsafe side and do not considered important parameters.

1.6 Fire resistance of composite slabs

Normally, experimental fire tests are expensive and time-consuming. As an alternative solution, the fire resistance of composite slabs can be determined by means of numerical simulations and simple calculation methods. The fire resistance of composite slabs is defined considering only standard fire exposure from below, which in practical situations is always decisive.

During fire exposure, determining the temperature field in the cross section of composite slabs is complex due to existence of ribs, which result in orthotropic profiles with large temperature gradients. Thus, calculating the temperatures at the unexposed surface and predicting the fire resistance of composite slabs represent difficult challenges in fire design. Figure 1.4 illustrates the theoretical temperature distribution and the resulting average temperature in the cross section of an arbitrary composite slab with trapezoidal steel deck.

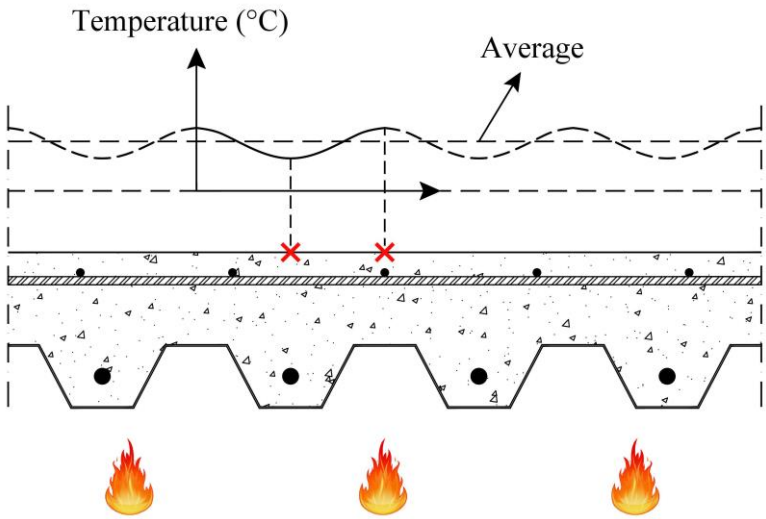

Figure 1.4: Theoretical temperature distribution at the unexposed surface of a fire exposed composite slab (adapted from Both [1]).

The Eurocode 4 and the standard NBR 14323 present simple calculation rules for determining the fire resistance of composite slabs compound by either normal weight or lightweight concrete. In addition, the fire resistance concerning the integrity criterion is assumed to be verified for this structural element. The current calculation methods of these standards are suitable for the determination the fire endurance of simply supported and continuous composite slabs exposed to standard fire conditions.

The following topics present specific aspects of each standard concerning the fire resistance of composite slabs as well as a short review of the development of the codes.

1.6.1 Eurocode 4 – Part 1-2

The first recommendations for the assessment of the fire resistance of composite slabs in Eurocode 4 were based on the model introduced by the ECCS [21] in 1983. This model, however, was based on limited experimental data available at the time it was developed hence leading to the adoption of conservative assumptions and uneconomical designs.

In 1990, the first draft of Eurocode 4 "Design of composite steel and concrete structures – Part 1-2: Structural fire design" was presented at a symposium in Luxembourg. Members of the European Community were invited to contribute by sending comments and suggestions. A redrafting started in 1991, but the final version for voting was approved in 1993 [26].

With the aim of enhancing these design rules, substantial research effort was initiated in Europe with the ECSC research project. Several experimental fire tests provided consistent data for the development of improved simple calculation rules. The actual version of Eurocode 4 – Part 1-2 was released in 2005 and incorporated the proposal new rules for the calculation of the fire resistance of composite slabs introduced by Both [1] in 1998.

The simplified calculation method provides guidelines for determining the fire resistance of composite slabs subjected to standard fire conditions according to the thermal insulation criterion (I). The proposed model is based on the slab geometry, partial factors and other parameters, being proper to composite slabs with trapezoidal and re-entrant steel deck. Moreover, these rules are exclusively applicable to composite slabs without any protection against fire, that is, slabs with fire containment measures are not covered.

The simplified calculation method for the fire resistance (I) has a field of application limited to a range of commonly used composite slab geometries from the decade of 1990. Table 1.1 presents the range of applicability of the method of Eurocode 4 for unprotected composite slabs with trapezoidal and re-entrant profiles, valid for slabs with either normal weight concrete or lightweight concrete. The geometric parameters of the slab are illustrated in Figures 1.2 and 1.3.

Table 1.1: Field of application of the Annex D of EN 1994-1-2 [13].

For trapezoidal steel deck profiles	For re-entrant steel deck profiles
$80.0 \leq l_1 \leq 155.0$ mm	$77.0 \leq l_1 \leq 135.0$ mm
$32.0 \leq l_2 \leq 132.0$ mm	$110.0 \leq l_2 \leq 150.0$ mm
$40.0 \leq l_3 \leq 115.0$ mm	$38.5 \leq l_3 \leq 97.5$ mm
$50.0 \leq h_1 \leq 125.0$ mm	$50.0 \leq h_1 \leq 130.0$ mm
$50.0 \leq h_2 \leq 100.0$ mm	$30.0 \leq h_2 \leq 60.0$ mm

Still with regard to the thermal insulation criterion, the Eurocode 4 considers orthotropic slabs as equivalent solid slabs with an effective thickness (h_{eff}) which depends on the geometry of the steel deck as well as the concrete depth. The standard presents two different formulae for the calculation of h_{eff} and specifies the minimum effective thickness according to standard fire resistance classes. These normative recommendations are discussed in section 2.8.

With respect to the load bearing criterion (R), the Eurocode 4 – Part 1-2 determines that if a composite slab with profiled steel deck, with or without additional reinforcement, is properly designed according to EN 1994-1-1 [48], the fire resistance (R) is at least 30 minutes.

This standard also states that the integrity criterion (E) is assumed to be satisfied for composite slabs with profiled steel deck.

1.6.2 Brazilian standard NBR 14323

In the nineties, with the objective of providing more insight on the fire safety of buildings, a group involving members of fire brigade of São Paulo, manufacturers of steel structures and fire-retardant materials as well as representatives of the steel industry and Technological Research Institute (IPT) started the elaboration of normative recommendations. Based on these instructions, the first version of the Brazilian code for fire design NBR 14323 “Fire design of steel and composite structures for buildings” was approved and published in 1999 [49].

In the late 2000s, a revision process of this standard was carried out and changed its name to “Structural fire design of steel and composite steel and concrete structures for buildings”. The current version was published in 2013 and included several modifications regarding the previous publication. In addition to the practical fire design of different structural members, the NBR 14323 also presents other important aspects

such as the requirements for the design of hot rolled and welded steel profiles; bolted and welded joints; and composite steel-concrete elements. Some parts of this standard, namely the simplified calculation methods and the thermal properties of steel and concrete are based on the Eurocode.

The Annex C describes a simplified method for the calculation of the fire resistance of composite slabs with re-entrant and trapezoidal profiled steel deck. The model for determining the fire resistance according to insulation criterion is based on the effective thickness of the composite slab.

Minimum effective thickness requirements are specified as a function of the fire resistance rating. For protected composite slabs, these minimum requirements can be reduced using an equivalent concrete thickness of the fire-retardant material, provided that a verification is conducted via thermal analysis or experimental tests [14].

The fire resistance of composite slabs with profiled steel deck, with or without additional steel reinforcement is considered to be of at least 30 minutes when the thermal insulation criterion is verified.

The NBR 14323 also states that the integrity criterion (E) is considered to be satisfied for composite slabs due to the presence of the profiled steel deck.

1.7 Outline

In the present work, Chapter 1 gives an introduction to the research theme and presents the working methodology; a summary of relevant investigations in the field of study; and a brief description of concepts concerning the fire resistance of composite slabs.

Chapter 2 deals with the description of different fire curves, heat transfer mechanisms, thermal properties of materials and other aspects with respect to the fire behaviour of composite structures.

Chapter 3 presents a description of FEM principles as well as the development of finite element models for the development of numerical simulations using the software MATLAB and ANSYS.

In Chapter 4, the description and the results of the parametric studies are outlined. A discussion around the influence of each studied parameter is given in this chapter as well.

The validation of the thermal models and comparisons between the outcome of the numerical simulations and existing calculation rules are presented in Chapter 5. Based on the general evaluation of the results, new proposal formulae regarding the calculation of the fire resistance (I) and the temperatures of the steel components should also be given.

The conclusions of the investigation and recommendations for further research can be found in Chapter 6.

The appendices comprise the following information:

- Appendix A: Technical files for the validation models.
- Appendix B: Technical files for the first parametric study.
- Appendix C: Critical temperatures of the steel components for the first parametric study (tabulated data).
- Appendix D: Numerical and Eurocode 4 results for the temperatures of the parts of the steel deck and the rebars for the first parametric study (tabulated data).
- Appendix E: Technical files for the second parametric study.
- Appendix F: Description of the parameters of the simulations and fire resistance of the composite slabs (I) for the second parametric study (tabulated data).
- Appendix G: Comparison between the results of the proposed new equations, ANSYS and Eurocode 4 for the temperature of the parts of the steel deck, and the temperature of the rebars in the rib (tabulated data).

2. FIRE BEHAVIOUR OF COMPOSITE STRUCTURES

2.1 Introduction

Before analysing the fire behaviour of composite structural elements, it is important to understand the different mechanisms of heat transfer as well as the distinct ways of transmission. The present chapter deals with the most relevant concepts of fire safety engineering, heat transfer, thermal properties of the materials, fire resistance criteria and other relevant aspects for the fire behaviour of structures during fire exposure.

The physical parameters which determine the conditions for fire development have influence on the duration and severity of fire, as well as on the thermal effects on structural components. The fire load density, combustion characteristics of materials, compartment shape and dimensions, ventilation conditions and the thermal properties of the boundary of enclosure are the most important factors [50].

According to EN 1991-1-2 [51], the actions on structures from fire exposure are classified as accidental actions. The fire effect increases the temperature on structural elements of a building, affecting its performance and resulting on additional loads and displacements. These consequences may result in the collapse or even ruin of the framework, which highlights the necessity to evaluate the fire behaviour of building components under fire conditions [52].

Basically, the concept of design for fire of building elements can be defined through a transient analysis, satisfying the following condition:

$$t_{fi,d} \geq t_{fi,r} \tag{2.1}$$

In the equation above, $t_{fi,d}$ represents the design value of fire resistance and $t_{fi,r}$ is the nominal required fire resistance, both components in compatible units of time. Other parameters must be verified such as the critical temperature and the structural resistance, for example.

Due to the orthotropic ribbed lower portion, composite slabs present a complex temperature distribution across the cross section during fire exposure. In view of that, the thermal gradient on the unexposed side of the slab is strongly affected by the

geometry of the steel deck and the position of the ribs. The thicker portion is subjected to lower temperatures than the thinner portion, see Figure 1.4. The last one plays a substantial role in the thermal insulation criterion of composite slabs.

The critical temperature of the steel components of composite slabs is defined as the average temperature of each steel component (steel deck, rebars and anti-crack mesh) at the time of failure concerning the thermal insulation criterion.

2.2 Heat transfer and thermal actions

In order to better comprehend the mechanisms of heat transfer, it is necessary to make clear some basic concepts. “Temperature” can be defined as the measure of the amount of kinetic energy present in the molecules of a given substance. In other words, it is a measure of the coldness or warmth of a substance. Çengel and Ghajar [53] define “heat” as the form of energy which can be transferred from one system to another as a consequence of temperature difference.

A thermodynamic analysis deals with the amount of heat transfer as an energy system undergoes a process from one equilibrium state to another. The heat transfer is the science which concerns the determination of the rates of these energy transfers. The heat transfer between two substances requires the existence of temperature differences and occurs from the high-temperature medium to the lower-temperature medium [53].

There are three different modes of heat transfer: conduction, convection and radiation. As a matter of fact, the temperature distribution in a system is dependent on the combined effects of these three modes of heat transfer [49].

In order to calculate the rate of temperature increase in structural components, it is fundamental to determine the amount of heat which affects these components. The Eurocode 1 – Part 1-2 [51] presents thermal actions for temperature analysis, which are given by the net heat flux $\dot{h}_{net}$ (W/m^2) to the boundary surface of the element. On the fire exposed surfaces, the net heat flux is divided into two components: the first considers heat transfer by convection ($\dot{h}_{net,cv}$) and the second by radiation ($\dot{h}_{net,r}$), as presented below.

$$\dot{h}_{net} = \dot{h}_{net,cv} + \dot{h}_{net,r} \tag{2.2}$$

The following subsections present the formulation used to determine each component of the equation above and give a brief description of the three modes of heat transfer.

2.2.1 Conduction

Conduction can be defined as the transfer of energy in a body from the more energetic particles of a substance (higher temperature) to the less energetic ones (lower temperature), due to interactions between the particles [53]. The heat transfer through conduction can occur in solids, gases or liquids. This phenomenon is governed by the Fourier's law of heat conduction, introduced in 1822. According to this law, the conduction heat flux $\dot{h}_{cd}$ (W/m^2) is directly proportional to the temperature gradient in the direction of the flow of heat $\frac{dT}{dx}$ (K/m), as presented in Eq. 2.3.

$$\dot{h}_{cd} = -\lambda \cdot \frac{dT}{dx} \tag{2.3}$$

In the last equation, λ represents the thermal conductivity (W/mK), which is a measure of the capacity of the material to conduct heat. As stated before, the heat is transferred from the higher temperature particles to the lower temperature particles, resulting in a negative temperature variation. In this regard, the negative sign is necessary because the heat transfer in the positive x direction is a positive value

According to Regobello [49], the conduction heat flux is a vector quantity ($\vec{\dot{h}}_{cd}$). Therefore, in the three-dimensional space, this component can be written as:

$$\vec{\dot{h}}_{cd} = -\lambda \cdot \left(\partial x, \partial y, \partial z\right)^T T \tag{2.4}$$

In the equation above, the vector derivative is the gradient operator (∇) applied to the temperature T.

A good heat conductor presents a high thermal conductivity and a poor heat conductor (insulator) presents a low thermal conductivity. This thermal property varies from material to material and depends on the physical state, chemical constitution and temperature of the material. Consequently, in a transient analysis, it is necessary to determine this property in each time step of the solution.

2.2.2 Convection

Convection heat transfer is defined as the mode of energy transfer between a solid surface and a fluid (liquid or gas) in movement on its boundaries, involving combined effects of conduction and fluid motion. The greater the velocity of the fluid is, the greater the convection heat transfer. Whether there is no bulk fluid motion, the heat transfer between the solid and adjacent fluid is governed by conduction [53].

The convection heat transfer occurs through two different manners, namely the natural (or free) convection and the forced convection. The first takes place if the fluid motion is caused by resulting forces that are induced by temperature differences between its layers. In contrast, the second occurs whether the fluid is forced to flow over a solid by using hydraulic machines such as pumps, for example [49].

The overall effect of convection is well defined through the Newton's law of cooling, which states that the rate of convection heat transfer is proportional to the temperature difference between the surface and fluid temperatures.

The Eurocode 1 – Part 1-2 [51] determines that the net convective heat flux component $\dot{h}_{net,cv}$ (W/m^2) for temperature analysis shall be calculated according to the following equation:

$$\dot{h}_{net,cv} = \alpha_{cv} \cdot \left(\Theta_g - \Theta_m\right) \tag{2.5}$$

Where, α_{cv} is the coefficient of heat transfer by convection (W/m^{2}K), relevant for nominal temperature-time curves; Θ_g represents the gas temperature in the vicinity of the fire exposed element (°C); and Θ_m is the surface temperature of the element (°C).

The EN 1991 – 1-2 also states that the net convective heat flux on the unexposed surface of separating elements should be calculated with α_{cv} = 4 (W/m^{2}K). Otherwise, this value should be taken as α_{cv} = 9 (W/m^{2}K) when assuming it contains the effects of radiation heat transfer. Regarding the fire exposed surface, the coefficient of heat transfer by convection should be adopted as α_{cv} = 25 (W/m^{2}K) if the element is exposed to the standard fire curve ISO 834 or the external fire curve. In case of surfaces exposed to the hydrocarbon curve, a value of α_{cv} = 50 (W/m^{2}K) should be taken.

It is noteworthy that a mean value is assumed for this coefficient by means of simplification, since the convection heat transfer is complex and depends on several factors such as the velocity field of the fluid.

2.2.3 Radiation

Radiation consists of the energy emitted by matter in the form of electromagnetic waves (photons) due to changes in the electronic configurations of atoms or molecules. In opposition to conduction and convection, this mean of heat transfer does not require a material medium, that is, the heat can also be transferred through regions of vacuum [53].

For heat transfer analyses, the radiation is restricted to the thermal radiation, which is propagated as a result of temperature differences in a system. This means that other forms of electromagnetic radiation (e.g. x-rays and microwaves) do not influence on the temperature distribution. In the heating process of a fire, the radiation is the main mechanism of heat transfer, especially when high temperatures are reached. The radiation heat transfer is a complex phenomenon due to its dependence on the relative positions of the flames [52].

The maximum amount of thermal radiation E_b (W/m^2) which can be emitted from a surface is determined by the Stefan-Boltzmann law. This law states that an idealized surface called blackbody (ideal thermal radiator) emits thermal radiation proportionally to the fourth power of the absolute temperature T (K), as given below.

$$E_b = \sigma \cdot T^4 \tag{2.6}$$

In Eq. 2.6, σ is a proportionality constant called Stefan-Boltzmann constant, which is equal to 5.67E-8 (W/m^2K^4). This equation is suitable only for radiation emitted by a blackbody, which is of fundamental importance to radiant heat transfer [54].

A blackbody is a perfect radiation emitter and thus, no other body can emit more thermal radiation than a blackbody at the same temperature. Given these points, the radiation emitted by real surfaces must take into consideration an additional factor. This factor is called emissivity (ε), which is a value between 0 and 1 defined as the ratio of the energy emitted by the real surface to the energy emitted by a blackbody, both at the same temperature [55]. For a general surface, the total radiant energy E (W/m^2) can be expressed as:

$$E = \varepsilon \cdot \sigma \cdot T^4 \tag{2.7}$$

Commonly, the emissivity of a surface is associated to the wavelength of radiant energy, the surface temperature and the angle of radiation. For simplification purposes, whether the emissivity is independent of these factors, the surface is called a greybody surface. The greybody radiation is applied in fire engineering approaches and calculations.

According to Eurocode 1 – Part 1-2 [51] and considering the concepts presented above, the net radiative heat flux component $\dot{h}_{net,r}$ (W/m^2) for temperature analysis of structural members should be determined according to the following equation.

$$\dot{h}_{net,r} = \Phi \cdot \varepsilon_m \cdot \varepsilon_f \cdot \sigma \cdot \left[\left(\Theta_r + 273\right)^4 - \left(\Theta_m + 273\right)^4 \right] \tag{2.8}$$

In the last equation, Φ (dimensionless) is the view factor, which takes into consideration position and shadow effects; ε_m (dimensionless) represents the surface emissivity of the element; ε_f (dimensionless) represents the emissivity of the fire; σ is the Stefan-Boltzmann constant (W/m^{2}K^4); Θ_r is the effective radiation temperature of the fire environment (°C); and Θ_m is the surface temperature of the element (°C).

The EN 1992-1-2 [56] states that the emissivity related to the concrete surface should be equal to 0.7. The EN 1993-1-2 [57] determines that the emissivity concerning the steel surface should be taken as 0.7 for carbon steel and taken as 0.4 for stainless steel. Regarding the fire emissivity, the EN 1991-1-2 [51] states that this parameter should be taken as 1. The methods of calculation of the view factor are given in subsection 2.2.3.1.

In the numerical modelling performed in this investigation, the gas temperature is assumed to be the effective radiation temperature of the fire environment, approximated by the Stefan-Boltzmann law. Therefore, considering convection and radiation heat transfer, the net heat flux which affects a structural member under fire conditions can be written as:

$$\dot{h}_{net} = \alpha_{cv} \cdot \left(\Theta_g - \Theta_m\right) + \Phi \cdot \varepsilon_{res} \cdot 5.67E-8 \cdot \left[\left(\Theta_g + 273\right)^4 - \left(\Theta_m + 273\right)^4 \right] \tag{2.9}$$

In the equation above, ε_{res} (dimensionless) represents the resulting emissivity, which is the product between the surface emissivity of the member and the emissivity of the fire. This equation represents the boundary conditions applied on the fire exposed surface of the composite slabs numerically tested in this work.

2.2.3.1 View factor

The view factor (Φ), see Eq. 2.9, quantifies the geometric relation between the surface emitting radiation and the surface receiving radiation. In other words, the view factor is a measure of how much the emitter is "seen" by the surface receiving radiation. This factor depends on the area and orientation of the surface emitting radiation in relation to the surface receiving radiation, as well as the distance between them [42].

The view factor of the lower flange of composite slabs is given as $\Phi_{low} = 1$. Owing to the obstruction to direct exposure caused by the ribs of the steel deck, the view factor of the web and upper flange are smaller than one. These view factors can be calculated following the simple crossed-strings method (see Figure 2.1), developed by H. C. Hottel in the 1950s [53]. This approach is also adopted by the standards EN 1994-1-2 and NBR 14323; however, only the expression for the upper flange view factor is given.

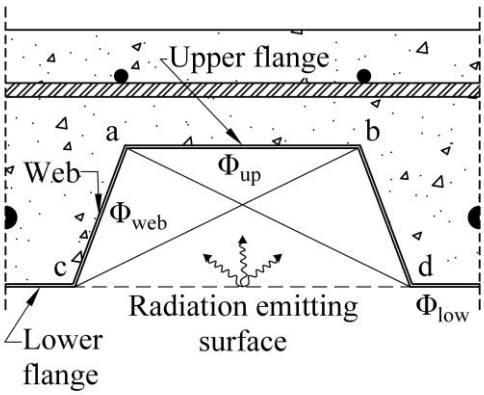

Figure 2.1: Schematic for the calculation of the view factor (adapted from Jiang et al. [9]).

The view factors of the upper flange (Φ_{up}) and web (Φ_{web}) can be calculated as function of the distances between the parts of the steel deck or using the geometric parameters of the composite slab, see Figures 1.2 and 1.3. The expressions for the calculation of these view factors of composite slabs with either trapezoidal or re-entrant profiles are presented in Eqs. 2.10a and 2.10b.

$$\Phi_{up} = \frac{ad + cb - ab - cd}{2 \cdot ab} = \frac{\sqrt{h_2^2 + \left(l_3 + \frac{l_1 - l_2}{2}\right)^2} - \sqrt{h_2^2 + \left(\frac{l_1 - l_2}{2}\right)^2}}{l_3} \tag{2.10a}$$

$$\Phi_{web} = \frac{ac + cd - ad}{2 \cdot ac} = \frac{\sqrt{h_2^2 + \left(\frac{l_1 - l_2}{2}\right)^2} + \left(l_3 + l_1 - l_2\right) - \sqrt{h_2^2 + \left(l_3 + \frac{l_1 - l_2}{2}\right)^2}}{2 \cdot \sqrt{h_2^2 + \left(\frac{l_1 - l_2}{2}\right)^2}} \quad (2.10b)$$

2.3 Fires in multi-storey buildings

Besides consisting in big tragedies and usually resulting in several losses, accidental fires provide an opportunity for humanity to understand the performance of entire buildings when subjected to fire. Thus, the design of buildings is improved as long as the experience from these fires and large-scale fire tests is obtained.

In the first part of the decade of 1990, two fires occurred in multi-storey buildings in England, namely Broadgate and Churchill Plaza. In 1996, a programme of fire tests conducted on an eight-storey composite steel-framed building was finished at the Building Research Establishment's Cardington Laboratory. These fires and fire tests considerably increased the insight about how buildings shall be designed to resist fire.

2.3.1 Broadgate

In 1990, a fire accident occurred in a partly completed 14-storey office building on the Broadgate development, London. The fire began on the first level of the building and lasted for four hours and a half. The floor system consisted of a composite slab (designed to achieve 90 minutes fire resistance) supported by composite long-span lattice trusses and composite beams [30].

At the time of the fire, both active and passive fire protection features to the steelwork were incomplete. According to estimates, the fire temperatures reached over 1000 °C. Besides being exposed to the severe fire, the steel structure survived without collapsing and the integrity of the composite floor slab was preserved. Large deformations in the composite slab were observed after the fire, with a maximum vertical displacement of about 600 mm. In some places, debonding of the steel deck from the concrete and failure of the reinforcement were also observed. Figure 2.2 presents a view of the deformed floor above the fire, after the fire accident.

Figure 2.2: View of the composite floor slab above the fire at Broadgate, UK [30].

The structural repairs were concluded in 30 days and the direct fire loss amounted to £25M, of which approximately £2M was attributed to the restoration of the structural frame and floor damage. The other costs were related to smoke damages [30]. The accident provided more insight into the performance of complete composite steel-concrete structures in fire and fortunately, no lives were lost.

2.3.2 Churchill Plaza

In 1991, a fire occurred in a 12-storey building (Churchill Plaza) in Basingstoke, UK. The structure of the building was designed to achieve 90 minutes of fire resistance and the underside of the composite slabs did not present fire protection. The fire started on the eighth floor and spread rapidly to the others floors.

In some areas, the re-entrant steel deck presented signs of debonding from the concrete, as also observed in the Broadgate fire. After the accident, load tests were carried out on the most affected areas applying a load of 1.5 times the total design load of the element. The results evidenced that the composite slab had sufficient load bearing capacity to be used without being repaired [30].

The structural steelwork which was fire protected suffered no damages and the total cost of repair of the building was approximately of £15M, of which most part was attributed to smoke contamination.

2.3.3 Cardington fire tests

Between 1995 and 1996, a programme of large scale fire tests was carried out in a complete building at the Cardington Laboratory in Bedfordshire, UK. The 8-storey steel framed composite building was designed according to the British standard BS 5950 – Part 1 to recreate a typical multi-storey office building [55]. Figure 2.3 illustrates the Cardington multi-storey test frame during the installation of the profiled steel deck of the composite slabs.

Figure 2.3: The Cardington fire test building structure [58].

The objective of the six major fire tests was to investigate the behaviour of a real structure when subjected to real fire conditions and provide data for the validation of numerical simulations of structures under fire conditions [30].

The test building was composed by composite floor slabs with profiled steel deck in composite action with the supporting beams and using cast *in situ* concrete. Sandbags distributed over each floor were used to impose the loads with load levels that were typically found in office buildings in the UK, see Figure 2.4. Due to mistakes in the placement of the reinforcement, such as the non-overlapping of the mesh in some regions, large cracks occurred in the slabs. Figure 2.4 presents a cracked region in a floor slab around one column as well as an external view of the fire during the test.

Figure 2.4: Cracked slab in region of non-overlapped steel mesh and external view of the fire test [30].

Although suffering extensive cracking, the composite floors preserved its integrity and separating function during all the fire tests, presenting an important contribution to the survival of the test frame.

In general, the structural elements presented a good performance and the overall structural stability was retained. It was observed that the fire behaviour of all the elements acting together was different from the performance of single members in standard fire tests. Therefore, the Cardington fire tests evidenced that steel frames with composite floor slabs provided a greater fire resistance than that normally assumed at that time.

2.4 Fire curves

Fires occur with the existence of the three factors in simultaneous: heat source (responsible for the initial ignition); fuel (e.g. paper, oil and wood); and oxygen. Whether one of these factors is missing, the fire does not ignite or reach a significant level.

Although consisting of complex and stochastic events, a fire can be represented by temperature-time curves. In a structure subjected to elevated temperatures, these curves allow the determination of the maximum temperature reached on the elements and its correspondent fire resistance as well [49]. A short discussion about some fire curves is presented in the following subsections.

2.4.1 Natural fire curve

In real natural fire models, the complete process of fire development can be described as being composed by four different stages, see Figure 2.5. Not necessarily all fires follow this curve, because in some situations it may disappear naturally or do not reach flashover, mainly if the fuel materials are isolated or if there is not enough air to maintain the combustion [59].

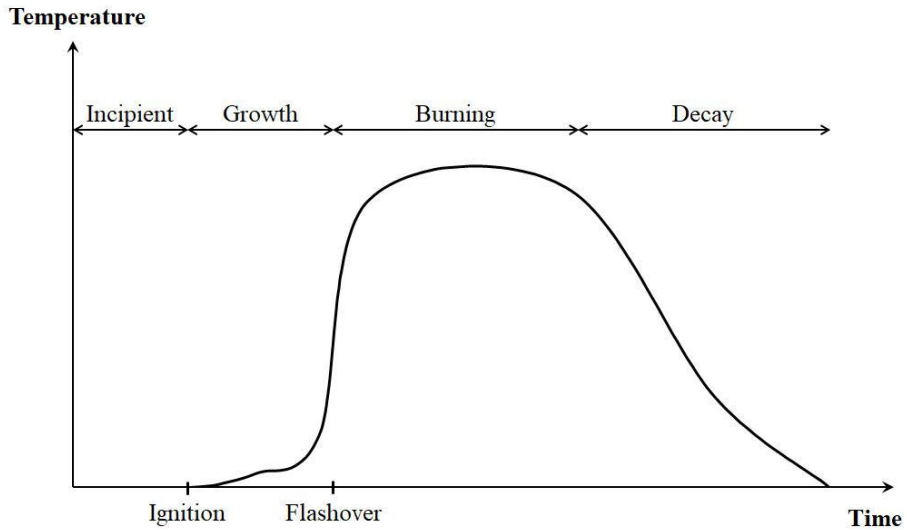

Figure 2.5: Fire curve for the complete process of fire development (adapted from Abu [60]).

The incipient stage is characterized by the heating of potential combustible materials. The transition from the incipient stage to the growth stage is called ignition, representing the start of combustion. In the growth stage, most fires spread slowly on the available combustible surfaces, and then more rapidly as long as the fire grows and there is radiant feedback from flames to other fuel materials. The flashover represents the transition from the growth stage to the burning period, characterized by a rapid increase in the burning rate. In the burning period, the temperatures and radiant heat flux within the compartment are of such level that all exposed surfaces are burning. Finally, after all the fuel materials in the environment have burned out, the temperatures drop and the fire dies in the decay period [59].

These curves are determined from experimental fire tests in compartments using real fire conditions and present an ascending segment (heating phase), and a descending segment (cooling phase). Results of tests evidenced that the parameters that most influence on the shape of the natural fire curves are the level of fire and ventilation, as well as the thermal properties of the materials of the compartment wall [49].

2.4.2 Nominal standard fire curves

In view of the conditioning factors regarding the natural fire curves, standard fire curves were created with the aim of determining a convention for the development of numerical simulations and experimental fire tests. These fire curves present only a heating phase and do not depend on the characteristics of the compartment.

The Eurocode 1 – Part 1-2 [51] specifies three different nominal fire curves for the fire design of structures, namely the standard temperature-time curve, the external fire curve and the hydrocarbon curve. These fire curves allow the calculation of the temperature in a fire compartment as function of time. The equations which describe these curves are presented below, where T_g represents the gas temperature (°C), and t is the time (min).

- Standard fire curve (ISO 834):

$$T_g = 20 + 345 \cdot \log_{10}(8t + 1) \tag{2.11}$$

- External fire curve:

$$T_g = 660 \cdot \left(1 - 0.687 \cdot e^{-0.32t} - 0.313 \cdot e^{-3.8t}\right) + 20 \tag{2.12}$$

- Hydrocarbon curve:

$$T_g = 1080 \cdot \left(1 - 0.325 \cdot e^{-0.167t} - 0.675 \cdot e^{-2.5t}\right) + 20 \tag{2.13}$$

The American Society for Testing and Materials (ASTM) presents a fire curve through the ASTM E119 [61] which is defined by a number of discrete points. There are several equations that approximate this curve; one of the most used is given by Lie [62], as presented in Eq. 2.14.

$$T_g = T_0 + 750 \cdot \left(1 - e^{-3.79553\sqrt{t}}\right) + 170.41\sqrt{t} \tag{2.14}$$

In the equation above, T_g is the gas temperature within the fire compartment (°C); T_0 is the initial room temperature (°C), usually adopted as 20 °C; and t is the time (h).

A comparison between the temperature developments of the nominal standard fire curves cited in this subsection is illustrated in Figure 2.6.

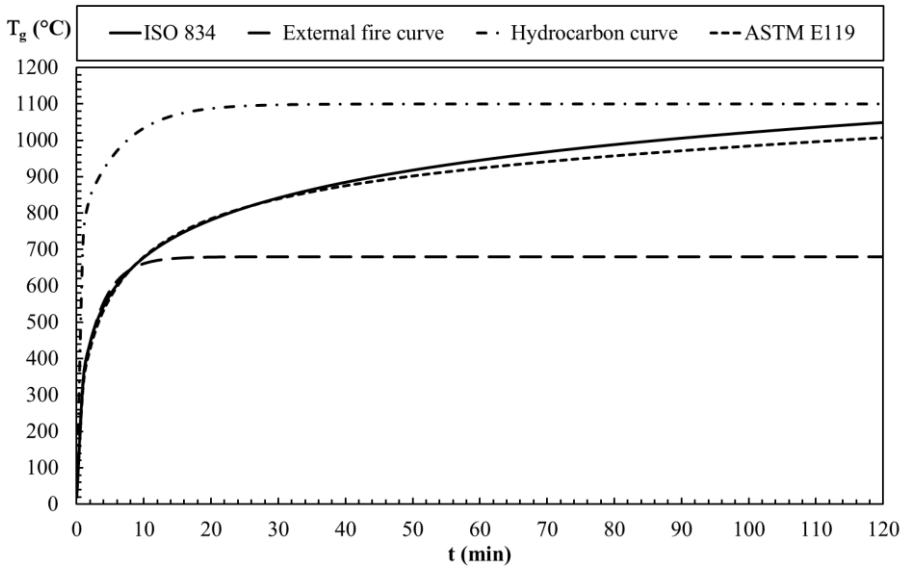

Figure 2.6: Nominal time-temperature fire curves.

The numerical model which is developed in this investigation concerns only the standard fire curve ISO 834. The following subsection presents a short discussion about this time-temperature fire curve.

2.4.2.1 Standard fire curve ISO 834

In 1975, the International Organization for Standardization (ISO) introduced the standard fire curve through the international standard ISO 834:1975 – "Fire resistance tests – Elements of building construction". In 1999, this version of the standard was replaced by the first edition of ISO 834-1 [22], changing the tolerances applied to the deviation of the curve of the average furnace temperature in comparison to the standard heating curve.

This fire curve presents a logarithmic relationship between temperature and time and is one of the most widely used nominal fire curves for the determination of the fire resistance of structural elements (see Eq. 2.11 and Figure 2.6). In addition to Eurocode 1, other standards adopt the standard fire curve, such as the Brazilian standard NBR 14432:2000 – "Fire resistance requirements for building construction elements" [63]; and the British standard BS 476-20:1987 – "Fire tests on building materials and structures – Part 20: Method for determination of the fire resistance of elements of construction (general principles)" [64].

2.4.3 Parametric temperature-time curves

In the Annex A of Eurocode 1 – Part 1-2, a model for the determination of parametric temperature-time curves is defined. These curves are valid for fire compartments up to 500 m^2 of floor area, without openings in the roof and for a maximum compartment height of 4 m.

Unlike the nominal fire curves, the parametric curves present both heating and cooling phases, and depend on several factors such as the thermal properties of the boundary of enclosure, fire load density, and area of enclosure, among others. The temperature-time curves in the heating phase shall be calculated according to Eq. 2.15.

$$T_g = 20 + 1325 \cdot \left(1 - 0.324 \cdot e^{-0.2t^*} - 0.204 \cdot e^{-1.7t^*} - 0.472 \cdot e^{-19t^*}\right) \tag{2.15}$$

In the formula above, T_g is the gas temperature in the fire compartment (°C); and t* represents a fictitious time (h), which should be calculated according to Eq. 2.16, where t is the time (h).

$$t^* = t \cdot \Gamma \tag{2.16}$$

The factor Γ is dimensionless and must be determined as follows.

$$\Gamma = \left[O/b\right]^2 \Big/ \left(0.04/1160\right)^2 \tag{2.17}$$

Where:

$$O = A_v \cdot \sqrt{h_{eq}} \Big/ A_t \tag{2.18a}$$

$$b = \sqrt{\left(\rho \cdot c \cdot \lambda\right)} \tag{2.18b}$$

In the equations above, O is the opening factor of the fire compartment ($m^{1/2}$), respecting the limits $0.02 \leq O \leq 0.20$; A_v is the total area of vertical openings on all walls (m^2); h_{eq} is the weighted average of window heights on all walls (m); and A_t is the total area of enclosure including openings (m^2). The factor b is given in $J/m^2s^{1/2}K$, respecting the limits $100 \leq b \leq 2200$; ρ is the density of boundary of enclosure (kg/m^3); c is the specific heat of boundary of enclosure (J/kgK); and λ is the thermal conductivity of boundary of enclosure (W/mK).

The heating phase of fire occurs until the maximum temperature T_{max}, defined by $t^* = t^*_{max}$. This temperature should be determined using Eqs. 2.19 and 2.15.

$$t^*_{max} = t_{max} \cdot \Gamma \tag{2.19a}$$

$$t_{max} = \max\left[\left(0.2 \cdot 10^{-3} \cdot q_{t,d} / O\right); t_{lim}\right] \tag{2.19b}$$

In the equations above, t^*_{max}, t_{max} and t_{lim} are given in hours; $q_{t,d}$ is the design value of the fire load density related to the total surface area of the enclosure (MJ/m^2), within the limits $50 \leq q_{t,d} \leq 1000$; and t_{lim} is the time limit, which separates the heating phase from the cooling phase as function of the fire growth rate.

The segment of the parametric curves related to the cooling phase of fire presents a decreasing linear relationship between temperature and time. The temperature-time curves in this phase should be calculated using the following equations.

$$T_g = T_{max} - 625 \cdot \left(t^* - t^*_{max} \cdot x\right) \qquad \text{for } t^*_{max} \leq 0.5 \tag{2.20a}$$

$$T_g = T_{max} - 250 \cdot \left(3 - t^*_{max}\right) \cdot \left(t^* - t^*_{max} \cdot x\right) \qquad \text{for } 0.5 < t^*_{max} < 2 \tag{2.20b}$$

$$T_g = T_{max} - 250 \cdot \left(t^* - t^*_{max} \cdot x\right) \qquad \text{for } t^*_{max} \geq 2 \tag{2.20c}$$

Where:

$$t^*_{max} = \left(0.2 \cdot 10^{-3} \cdot q_{t,d} / O\right) \cdot \Gamma \tag{2.21}$$

In the equations above, t^* shall be determined according to Eq. 2.16. The factor x is dimensionless and is given as x= 1.0 if $t_{max} > t_{lim}$; or x= $(t_{lim} \cdot \Gamma)/t^*_{max}$ if $t_{max} = t_{lim}$.

Figures 2.7a and 2.7b illustrate a comparison between different examples of parametric curves applying the method of Eurocode 1 – Part 1-2 and the standard fire curve ISO 834. The parameters utilized in both analyses are b= 2144.76 J/m^{2}s$^{1/2}$K and t_{lim} = 20 min or 0.333 h (medium fire growth rate). For the first analysis, see Figure 2.7a, a fixed value of 200 MJ/m^2 is used for $q_{t,d}$. In the second analysis, see Figure 2.7b, a fixed value of 0.1 m$^{1/2}$ is used for O.

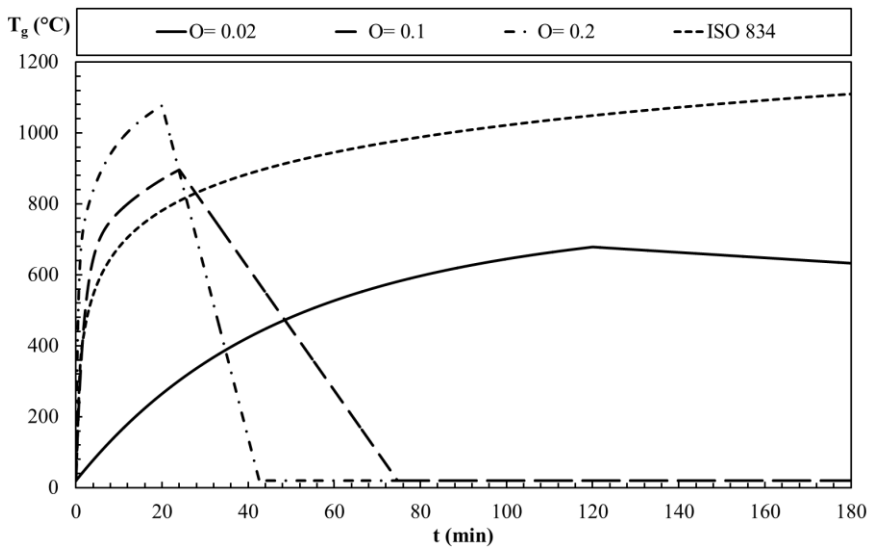

a) Parameter O in $m^{1/2}$.

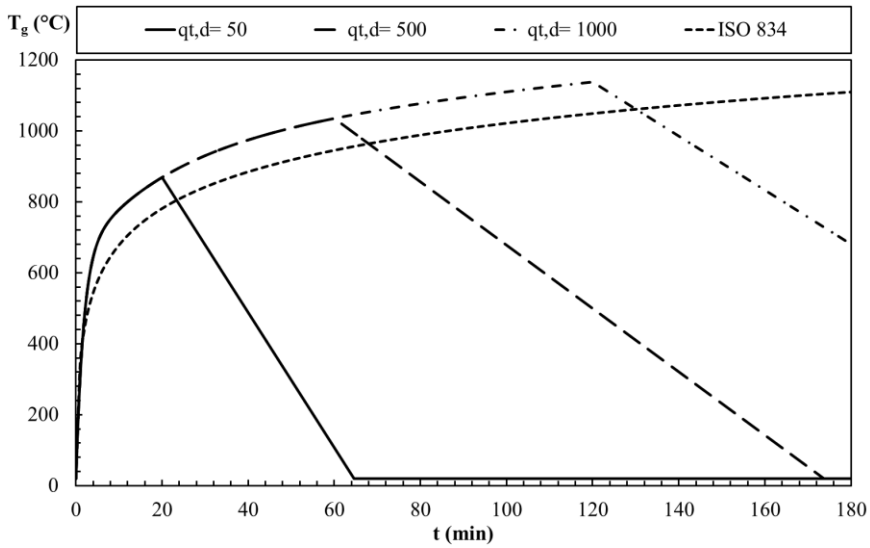

b) Parameter $q_{t,d}$ in MJ/m^2.

Figure 2.7: Examples of temperature-time parametric curves.

Concerning the first analysis, it can be observed that as long as the opening factor of the compartment increases, the duration of the heating phase decreases and the maximum temperature increases, leading to more severe fires. With respect to the second analysis, it is noteworthy that as the fire load density related to the total surface area of the enclosure increases, the maximum temperature increases along with t_{max}, resulting in longer and more severe fires.

2.5 Fire resistance criteria

Structural elements need to meet fire-safety requirements according to building codes. The fire rating of composite slabs is usually made using standard fire tests and

should take into account the criteria of insulation (I), integrity (E) and load bearing (R). Usually, the fire resistance is expressed in classes, ranging from 30 to 180 minutes (and beyond) with intervals of 30 minutes [1].

The steel deck of composite slabs acts as a diaphragm and as a shield, preventing the passage of flames and hot gases as well as reducing the heat flow through the slab. These characteristics play an important part on improving the fire resistance according to the insulation and integrity aspects [6].

In this work, focus is given to the fire resistance according to the thermal insulation criterion (I). The following subsections present a description about the three different criteria of fire resistance for composite slabs.

2.5.1 Insulation

The thermal insulation criterion (I) can be defined as the ability to withstand fire in one side and prevent excessive transmission of heat, with the purpose of preventing the fire propagation caused by the ignition of any material at the unexposed surface. In this regard, the temperature development at the unexposed surface is the primary concern of this criterion.

The assessment of the thermal insulation criterion shall be made on the basis of the average temperature rise on the unexposed surface limited to 140 °C above the initial average temperature; or on the basis of the maximum temperature rise at any point on the unexposed surface limited to 180 °C above the initial average temperature. Therefore, the fire resistance (I) is the time, expressed in minutes, necessary to reach any of these criteria, whichever governs [7].

2.5.2 Integrity

The integrity criterion (E) is the capacity to withstand fire in one side and resist penetration of hot gases and flames through cracks and openings. The assessment should be made on the basis of the measurement of cracks or openings in excess of given dimensions; or of the ignition of a cotton pad; or of sustained flaming on the unexposed side. For cast *in situ* composite slabs, the integrity criterion is normally satisfied provided that the joints are adequately sealed.

2.5.3 Load bearing capacity

The load bearing resistance (R) is the ability to support the structural loading without collapsing or suffering excessive deformations. When ignoring the membrane action, three different failure modes are relevant: flexural failure, longitudinal shear failure and vertical shear [1].

The international standard ISO 834 [22] specifies performance criteria for flexural elements for the maximum deflection D (mm) and the maximum deflection rate dD/dt (mm/min), as presented below.

$$D = \frac{L^2}{400 \cdot d} \tag{2.22a}$$

$$\frac{dD}{dt} = \frac{L^2}{9000 \cdot d} \tag{2.22b}$$

In the last equations, L is the clear span of the structural element (mm), and d is the distance from the extreme fibre of the cold design compression zone to the extreme fibre of the cold design tensile zone of the structural section (mm).

2.6 Fire safety on buildings

Elements of construction shall be properly designed to resist fire, which is one of the most severe hazards that buildings are subjected. The major goal of fire protection is to limit the risks of death, property loss and environmental damage to acceptable levels in a fire [59]. The design for fire safety should allow the fire brigade access and ensure safety for the occupants in case of fire by providing proper means of escape (with adequate fire exits), inhibiting the spread of smoke and hot gases in the rooms, and preserving the structural stability during a period of time, among others.

Regulations were created to prevent the spread of fire to neighbouring buildings and ensure that the framework does not collapse with the occurrence of disastrous fires. These regulations consist of provisions of minimum thicknesses of concrete and areas of reinforcement/insulation of steelwork. The regulatory control depends on several circumstances and should be determined through legislations as well as national and international standards. The legislative control is usually based on local building regulations and specific legal requirements [65].

2.6.1 Fire resistance requirements

The assessment rules of most standards are based on the premises that buildings are divided by separating members into fire compartments and the fire is confined to only one compartment, which should be designed to contain it for a specified failure time, or fire resistance time [66].

The British standard BS 13501-2 [67] determines that the assessment of the fire resistance of structural members should take into account the criteria of insulation (I), integrity (E) and load bearing capacity (R). Further optional criteria are also specified, namely smoke leakage (S), self-closing ability (C), radiation (W) and mechanical action (M). The necessity of classification based on these optional criteria is dependent on national regulations.

Normally, the fire resistance is expressed in classes and is determined using nominal standard fire curves. For example, supposing that the standard fire resistance class of an element is I 60, the failure time according to the insulation criterion should not be less than 60 minutes. For the different criteria of fire resistance, classification periods of 10, 15, 20, 30, 45, 60, 90, 120, 180, 240 or 360 minutes are specified in BS 13501-2 [67].

Concerning the thermal insulation criterion (I), the Brazilian standard NBR 14323 [14] specifies classes of 30, 60, 90, 120 and 180 minutes; and the EN 1994-1-2 [13] establishes classes of 30, 60, 90, 120, 180 and 240 minutes.

Regarding the performance of the entire building, requirements are established for the minimum periods of fire resistance for the structural elements and compartments. These requirements are prescribed by national building codes and generally depend on the purpose and total height of the building, as well as on the presence of active/passive control systems. Subsections 2.6.2 and 2.6.3 present a brief description of regulations concerning the fire safety engineering in Brazil and Portugal, respectively.

2.6.2 Portuguese regulations

In Portugal, the fire protection regulation was significantly modified through the Decree-Law No. 220/2008 [68] and the Ordinance No. 1532/2008 [69], which came into force on 1st January, 2009. However, these regulations presented some

inadequacies such as not covering prisons and ammunition/explosives storages, among others [70]. With the aim of correcting these problems and allowing the implementation of technological innovations for new buildings, the Decree-Law No. 224/2015 [71] introduces the first modifications with respect to the DL 220/2008.

The documents cited above consist of the most important regulations which establish the general conditions and specifications of the legal regime of Fire Safety in Buildings (SCIE) in Portugal. The publication of these regulatory documents corrects inconsistences in the legislation and facilitates the application of measures concerning the SCIE.

The technical provisions for the SCIE, published through the Ordinance No. 1532/2008, consist of specifications regarding exterior conditions, fire performance, insulation and protection, evacuation, technical installations, equipment and safety systems, as well as auto protection. These conditions involve not only buildings with exclusive purposes but also mixed use constructions [69].

The article 8th of DL 224/2015 classifies buildings into 12 different types according to its purpose, as presented in Table 2.1. In addition, this document defines 14 different classes of fire resistance for construction elements, as follows:

a) R – Load bearing capacity;
b) E – Integrity;
c) I – Thermal insulation;
d) W – Radiation;
e) M – Mechanical action;
f) C – Self-closing ability;
g) S – Smoke leakage;
h) P or PH – Power and/or signal supply continuity;
i) G – Soot fire resistance;
j) K – Fire protection;
k) D – Stability when subjected to constant temperatures;
l) DH – Stability when subjected to temperature-time fire curves;
m) F – Functionality for electric ventilation;
n) B – Functionality for natural ventilation of smoke and heat.

Table 2.1: Classification of buildings according to DL No. 224/2015 [71].

Class of the building	Purpose
Type I	Residential
Type II	Parking lot
Type III	Office
Type IV	Educational
Type V	Health services and nursing home
Type VI	Shows and public place
Type VII	Hotel and restoration
Type VIII	Commercial and transportation
Type IX	Sports and leisure
Type X	Museum and art gallery
Type XI	Library and file room
Type XII	Industry, repair workshop and storage

Regarding the above classification, each type of building is divided into 4 categories of fire risk depending on several factors such as the total height, modified fire load and occupant capacity of the construction. Table 2.2 presents these categories referred to office buildings (Type III).

Table 2.2: Categories of fire risk for office buildings [71].

Category	Total height of the building (m)	Occupant capacity
1st	≤ 9	≤ 100
2nd	≤ 28	≤ 1000
3rd	≤ 50	≤ 5000
4th	> 50	> 5000

The requirements concerning the fire resistance of structural elements with supporting and compartmentation functions are established by the Ordinance No. 1532/2008. Table 2.3 gives the minimum requirements for the fire resistance of structural components (classes R, E and I) defined by this regulation.

In Portugal, the structural fire design of elements of construction shall be made complying with the normative recommendations from the Eurocode. The EN 1994-1-2 provides guidelines for the design of composite steel-concrete structures under standard fire conditions, including composite slabs with profiled steel deck. The methodology for the assessment of the fire resistance of unprotected composite slabs is discussed in the subsection 2.8.1 of this work.

Table 2.3: Minimum standard fire resistance for structural elements of buildings in Portugal (adapted from Ordinance No. 1532/2008 [69]).

Class of the building	**Category of fire risk**				**Function of the structural element**
	1st	**2nd**	**3rd**	**4th**	
I, III, IV, V, VI, VII, VIII, IX and X	R 30	R 60	R 90	R 120	Only supporting
	REI 30	REI 60	REI 90	REI 120	Supporting and compartmentation
II, XI and XII	R 60	R 90	R 120	R 180	Only supporting
	REI 60	REI 90	REI 120	REI 180	Supporting and compartmentation

2.6.3 Brazilian regulations

Since the decade of 1970, due to large fires occurred in stores and multi-storey buildings, a significant increase in the publication of standards and regional regulations concerning the fire safety engineering has taken place in Brazil [70]. In view of the limited knowledge about fire safety engineering in the country, some normative recommendations are based on regulations from other countries.

After the publication of the Brazilian standard NBR 14323 [14] in 1999, the necessity arose to specifications for the required conditions that should be fulfilled concerning the fire performance of structural elements. In this regard, the standard NBR 14432 “Fire resistance requirements for building construction elements – Procedure” [63] was published in 2000. This standard defines the Fire Resistance Required Time (TRRF) as the minimum (fictitious) period of time in which a structural member, when subjected to standard fire exposure, shall maintain its fire resistance criterion, not presenting failure. The Annex A of this regulation presents a table describing the TRRF for different classes of buildings, in minutes. For slabs, the NBR 14432 states that the TRRF does not need to be more than 90 minutes, except for buildings with total height superior to 45 m.

In 2018, the Technical Instruction IT No. 08/2018 “Structural fire safety” [72] was developed by the fire brigade of the state of São Paulo. This manual has the main goal to establish instructions and required conditions for structural elements and compartments under fire conditions. In Brazil, this is one of the most up-to-date documents regarding the requirements for fire resistance [41]. Since these recommendations are updated in comparison to the Brazilian standard, this subsection highlights the requirements of the technical instruction.

The IT No. 08/2018 classifies the buildings into 12 principal groups which are divided into subgroups according to its specific purpose and usage. The detailed classification (group and subgroup) shall be made using the Table 1 of the Decree No. 56819/2011 [73]. For instance, a building of group B (hotel services) can be classified as B-1 (hotel and similar) or B-2 (residential hotel). In this document, buildings are also divided into 8 classes according to the height of the top floor above ground and 2 classes according to the basement depth. Similarly to NBR 14432, this technical instruction presents a table in the Annex A comprising the TRRF for elements of structure, which is illustrated in Figure 2.8.

FIRE RESISTANCE REQUIRED TIME (MIN)												
Group	Purpose/ usage	Subgroup	Basement depth h_s		Total height of the building h							
			Class S_2 h_s > 10 m	Class S_1 $h_s \leq 10$ m	Class P_1 $h \leq 6$ m	Class P_2 6 m < h ≤ 12 m	Class P_3 12 m < h ≤ 23 m	Class P_4 23 m < h ≤ 30 m	Class P_5 30 m < h ≤ 80 m	Class P_6 80 m < h ≤ 120 m	Class P_7 120 m < h ≤ 150 m	Class P_8 150 m < h ≤ 250 m
A	Residential	A-1 to A-3	90	60	30	30	60	90	120	120	150	180
B	Hotel services	B-1 and B-2	90	60	30	60	60	90	120	150	180	180
C	Commercial	C-1	90	60	60	60	60	90	120	150	150	180
		C-2 and C-3	90	60	60	60	60	90	120	150	150	180
D	Professional services	D-1 to D-4	90	60	30	60	60	90	120	120	150	180
E	Educational and physical culture	E-1 to E-6	90	60	30	30	60	90	120	120	150	180
F	Public places	F-1, F-2, F-5, F-6, F-8 and F-10	90	60	60	60	60	90	120	150	180	-
		F-3, F-4 and F-7	90	60	See item A.2.3.3		30	60	60	90	120	-
		F-9	90	60	30	60	60	90	120	-	-	-
G	Automotive services and similar	G-1 and G-2 without lateral opening and G-3 to G-5	90	60	30	60	60	90	120	120	150	180
		G-1 and G-2 with lateral opening	90	60	30	30	30	30	60	120	120	150
H	Institutional health services	H-1 and H-4	90	60	30	60	60	90	120	150	180	180
		H-2, H-3, H-5 and H6	90	60	30	60	60	90	120	150	180	180
I	Industrial	I-1	90	60	30	30	30	60	120	-	-	-
		I-2	120	90	30	30	60	90	120	-	-	-
		I-3	120	90	60	60	90	120	120	-	-	-
J	Storages	J-1	60	30	See item A.2.3.4		30	30	60	-	-	-
		J-2	90	60	60	60	60	60	60	-	-	-
		J-3	90	60	60	60	60	120	120	-	-	-
		J-4	120	90	60	60	90	120	120	-	-	-
L	Explosives	L-1, L-2 and L-3	120	120	120	-				-	-	-
M	Special	M-1	150	150	150	-				-	-	-
		M-2	-		120	120	-	-	-	-	-	-
		M-5	120	90	60	60	90	120	-	-	-	-
		M-3	120	90	90	90	120	120	120	150	-	-

Figure 2.8: TRRF for structural elements of buildings in Brazil (adapted from IT No. 08/2018 [72]).

In Brazil, the NBR 14323 presents instructions for the design of composite structures under fire conditions, including composite slabs. The method for the

calculation of the fire resistance of unprotected composite slabs is given in the subsection 2.8.2 of this work.

The Annex F of NBR 14323 introduces the method of equivalent time whereby the TRRF is calculated taking into consideration the building features that reduce the spread of fire, among other aspects. For buildings with favourable fire safety characteristics, the fire resistance requirements depicted in Figure 2.8 can be reduced by up to 30 minutes using this method [14].

2.6.4 Fire protection measures

In fire safety engineering, fire protection measures are defined as solutions used to mitigate/control fire hazards. These measures have great importance in the behaviour of structural components, flame and smoke management, and consequently, in the occupants safety during a fire.

Nowadays, fire protection strategies are divided into active and passive systems. The active measures refer to control of the fire by an action executed by a person or an automatic fire protection device. Automatic sprinkler systems, foam systems, smoke control systems and fire alarm systems are examples of active measures. The passive measures are static systems that are built into the structure or fabric of the building and do not require human or automatic operation. The passive systems include the application of suitable materials on the structural members (intumescent paint and vermiculite mortar, for example), adequate compartmentation, and provision of escape routes, among others. Figure 2.9 illustrates examples of active and passive fire protection measures.

a) Fire sprinkler system [74].

b) Application of intumescent paint [75].

Figure 2.9: Examples of fire protection measures: active (a) and passive (b) systems.

Fire safety objectives are normally achieved with a combination of active and passive fire protection systems [59]. Further measures such as the inclusion of fire hydrants, extinguishers and hose stations increase the level of fire safety of the buildings.

For composite slabs, the ECCS Technical Note [21] specifies three different means of additional fire protection: additional reinforcement, insulating coatings and suspended ceilings. This document states that the additional reinforcement, placed within the ribs, may significantly contribute to the fire resistance with respect to the load bearing capacity (R). Insulating coatings such as sprayed coatings containing mineral fibres or vermiculite, for example, are usually applied when extremely high fire resistance ratings are required, resulting in a considerable extra cost. Suspended ceilings act as a heat shield for the structural elements above, increasing the fire resistance of the floor assembly. In addition, this mean of fire protection can be combined with decorative elements, thermal and acoustic insulation systems, and also serve to conceal wires and installations within the gap between the ceiling and the slab. Figure 2.10 shows a non-fire-rated suspended ceiling system after a fire test carried out in Collins Street, Melbourne.

Figure 2.10: Suspended ceiling after a fire test in Australia [30].

2.7 Thermal properties of materials

The thermal properties of materials have significant influence on the results of numerical simulations of structural members under fire conditions. In this regard, better results are achieved whether the thermal model considers thermal properties that are closer to the reality.

Nonlinear transient heat transfer analyses require the calculation of the specific heat, thermal conductivity and density of the materials at each time step. The specific heat can be defined as "the energy required to raise the temperature of a unit mass of a substance by one degree in a specified way". The thermal conductivity is "a measure of the ability of a material to conduct heat" [53]. The density of a material is defined as the quantity of mass per unit volume.

These thermal properties vary according to the standards used for composite slabs [13], steel structures [57] and concrete structures [56]. In the following subsections, a brief discussion around the thermal properties of each material of interest is given.

2.7.1 Concrete

The Eurocode 2 – Part 1-2 [56] determines that the specific heat of dry concrete (u = 0%), using either siliceous or calcareous aggregates, is temperature dependent and shall be determined according to the following equations.

$$c_p(\theta) = 900 \qquad \text{for } 20\ °C \leq \theta \leq 100\ °C \qquad (2.23a)$$

$$c_p(\theta) = 900 + (\theta - 100) \qquad \text{for } 100\ °C < \theta \leq 200\ °C \qquad (2.23b)$$

$$c_p(\theta) = 1000 + (\theta - 200)/2 \qquad \text{for } 200\ °C < \theta \leq 400\ °C \qquad (2.23c)$$

$$c_p(\theta) = 1100 \qquad \text{for } 400\ °C < \theta \leq 1200\ °C \qquad (2.23d)$$

In the equations above, c_p is the specific heat of dry concrete (J/kgK), and θ is the concrete temperature (°C).

Still with regard to EN 1992 – 1-2, whether the moisture content of the concrete is not considered explicitly in the calculation method, the function for the specific heat of concrete should be modelled using a constant value ($c_{p,peak}$), situated between 100 °C and 115 °C, presenting a linear decrease between 115 °C and 200 °C. The following equations present the values specified by this standard for $c_{p,peak}$ as function of different moisture contents of concrete (u).

$$c_{p,peak} = 900\ \text{J/kgK} \qquad \text{for } u = 0\% \qquad (2.24a)$$

$$c_{p,peak} = 1470\ \text{J/kgK} \qquad \text{for } u = 1.5\% \qquad (2.24b)$$

$$c_{p,peak} = 2020\ \text{J/kgK} \qquad \text{for } u = 3.0\% \qquad (2.24c)$$

For other values of moisture contents, linear interpolation is acceptable. Figure 2.11 presents the specific heat of concrete as function of temperature at 5 different moisture contents by weight.

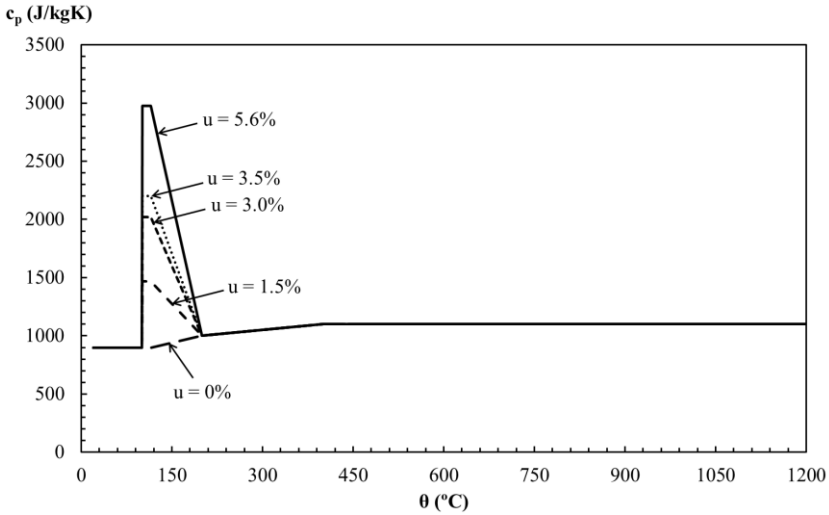

Figure 2.11: Specific heat of concrete as function of temperature.

It can be observed that the specific heat of concrete is increased for temperatures between 100 °C and 200 °C. This is due to the influence of moisture evaporation in the early stage of heating [9]. This investigation applies the models for the specific heat of concrete considering moisture contents of 3.0% for the parametric studies, and of 3.0%, 3.5% and 5.6% for the validation models.

The EN 1992 – 1-2 also states that the thermal conductivity of concrete λ_c depends on the temperature of the concrete and should be determined between lower and upper limit values.

The lower limit of thermal conductivity λ_c [W/mK] of normal weight concrete should be calculated according to Eq. 2.25.

$$\lambda_c = 1.36 - 0.136 \cdot (\theta/100) + 0.0057 \cdot (\theta/100)^2 \quad \text{for } 20\ °C \le \theta \le 1200\ °C \qquad (2.25)$$

In the equation above, θ is the concrete temperature (°C).

On the other hand, the upper limit of thermal conductivity λ_c (W/mK) of normal weight concrete shall be calculated according to Eq. 2.26.

$$\lambda_c = 2 - 0.2451 \cdot (\theta/100) + 0.0107 \cdot (\theta/100)^2 \quad \text{for } 20\ °C \le \theta \le 1200\ °C \qquad (2.26)$$

In the equation above, θ is the concrete temperature (°C). Figure 2.12 illustrates the variation of the thermal conductivity of concrete with temperature for both lower and upper limits.

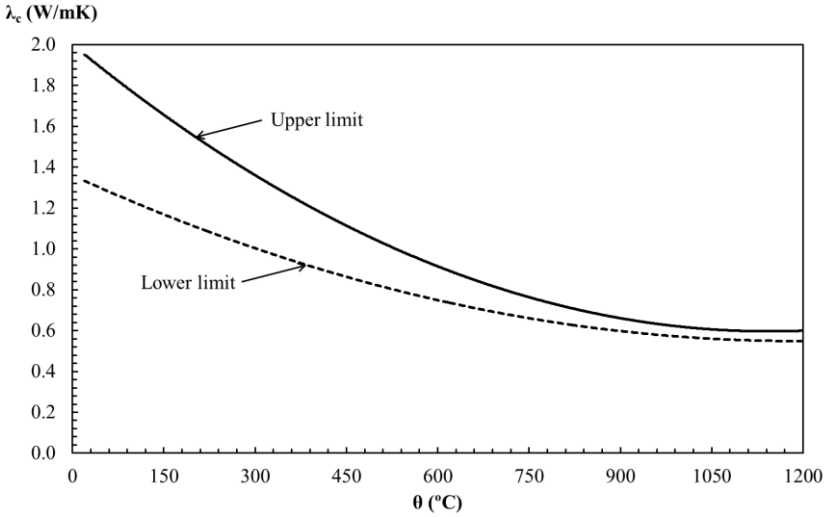

Figure 2.12: Thermal conductivity of concrete: lower and upper limits.

The upper limit model for the thermal conductivity of concrete is used in this study, which is indicated for numerical analyses. Jian Jiang et al. [9] concluded that the thermal conductivity of concrete has larger influence on the temperature at the unexposed surface than the exposed surface.

According to the EN 1992 – 1-2, the density of concrete varies with temperature and is influenced by water loss. This variation with temperature is defined in Eqs. 2.27. The density of normal weight concrete at room temperature ρ_c (20 °C) is equal to 2300 kg/m^3.

- For 20 °C ≤ θ ≤ 115 °C:

$$\rho_c(\theta) = \rho_c(20°C) \tag{2.27a}$$

- For 115 °C < θ ≤ 200 °C:

$$\rho_c(\theta) = \rho_c(20°C)\cdot\left(1 - 0.02\cdot(\theta - 115)/85\right) \tag{2.27b}$$

- For 200 °C < θ ≤ 400 °C:

$$\rho_c(\theta) = \rho_c(20°C)\cdot\left(0.98 - 0.03\cdot(\theta - 200)/200\right) \tag{2.27c}$$

- For 400 °C < θ ≤ 1200 °C:

$$\rho_c(\theta) = \rho_c(20°C)\cdot\left(0.95 - 0.07\cdot(\theta - 400)/800\right) \tag{2.27d}$$

In the equations above, ρ_c (θ) is the density of concrete (kg/m^3) and θ is the concrete temperature (°C). The relationship between the temperature and the density of concrete is graphically represented in Figure 2.13.

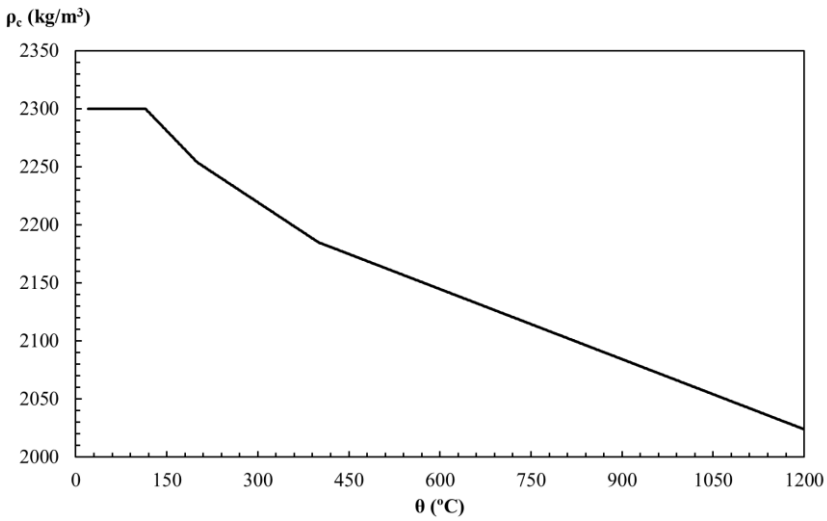

Figure 2.13: Density of concrete as function of temperature.

2.7.2 Carbon steel

According to the Eurocode 3 – Part 1-2 [57], the specific heat of carbon steel c_a (J/kgK) is temperature dependent and shall be determined from the following equations.

- For 20 °C $\leq \theta_a <$ 600 °C:

$$c_a = 425 + 7.73\times10^{-1}\cdot\theta_a - 1.69\times10^{-3}\cdot\theta_a^2 + 2.22\times10^{-6}\cdot\theta_a^3 \tag{2.28a}$$

- For 600 °C $\leq \theta_a <$ 735 °C:

$$c_a = 666 + 13002/(738 - \theta_a) \tag{2.28b}$$

- For 735 °C $\leq \theta_a <$ 900 °C:

$$c_a = 545 + 17820/(\theta_a - 731) \tag{2.28c}$$

- For 900 °C $\leq \theta_a \leq$ 1200 °C:

$$c_a = 650 \tag{2.28d}$$

In the equations above, θ_a is the steel temperature (°C). The variation of the specific heat of carbon steel with temperature is presented in Figure 2.14.

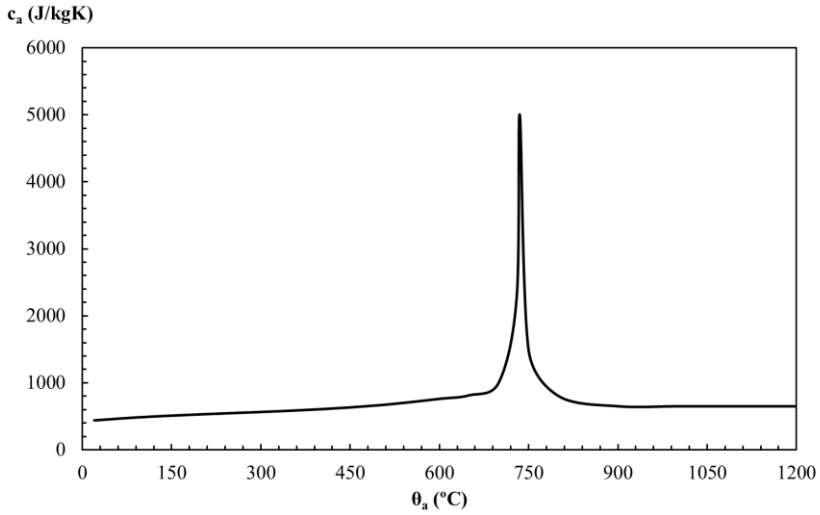

Figure 2.14: Variation of the specific heat of carbon steel with temperature.

It can be noticed that the specific heat of steel has an abrupt variation for temperatures between 700 °C and 800 °C. This is due to the allotropic phase transformation, which can affect the temperature development on steel components.

The EN 1993 – 1-2 states that the thermal conductivity of carbon steel λ_a (W/mK) varies with temperature and should be calculated according to the following equations.

$$\lambda_a = 54 - 3.33 \times 10^{-2} \cdot \theta_a \qquad \text{for } 20\ °C \leq \theta_a < 800\ °C \qquad (2.29a)$$

$$\lambda_a = 27.3 \qquad \text{for } 800\ °C \leq \theta_a \leq 1200\ °C \qquad (2.29b)$$

In the equations above, θ_a is the steel temperature (°C). Figure 2.15 represents the variation of this thermal property with temperature.

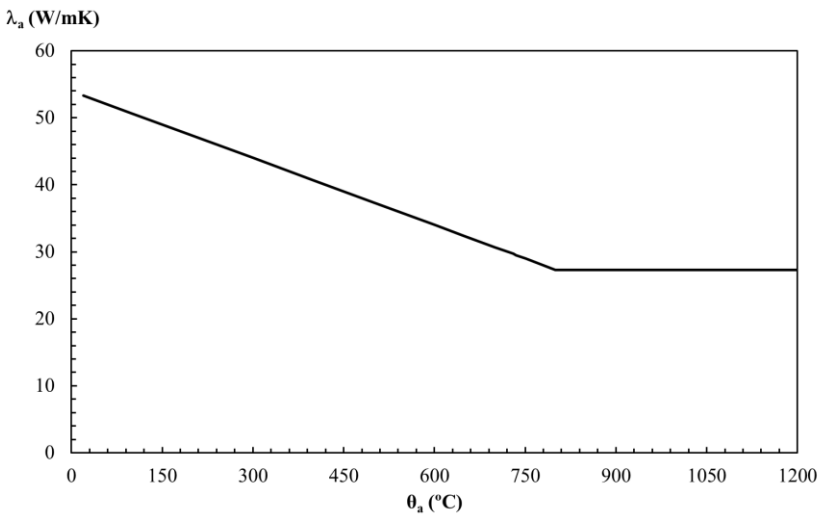

Figure 2.15: Thermal conductivity of carbon steel as function of temperature.

Analysing the graph above, it can be observed that this thermal property has a linear decrease until 800 °C, and after that, assumes a constant value. The development of the thermal conductivity of steel is reversible after the cooling stage of fire [52].

According to the EN 1993 – 1-2, the unit mass of carbon steel ρ_a (kg/m^3) may be considered to be independent of the steel temperature. In this regard, a constant value of ρ_a = 7850 kg/m^3 should be taken.

2.7.3 Air

The thermal properties of air are temperature dependent and should be used to simulate the interface between the steel deck and the bottom surface of the concrete topping. In addition, these thermal properties vary with the air pressure. This work considers the thermal properties of air at 1 atm pressure [53].

Presently, there is no standard which specifies the thermal properties of air. However, computer programs and experimental tests provide reliable data for numerical analyses. Table 2.4 presents the variation of the main thermal properties of air with temperature θ_{air} (°C), namely the specific heat c_{air} (J/kgK), the thermal conductivity λ_{air} (W/mK) and the density ρ_{air} (kg/m^3). These thermal properties are graphically represented in Figure 2.16.

Table 2.4: Thermal properties of air at 1 atm pressure (adapted from Çengel and Ghajar [53]).

θ_{air} (°C)	c_{air} (J/kgK)	λ_{air} (W/mK)	ρ_{air} (kg/m^3)
20	1007	0.02514	1.2040
30	1007	0.02588	1.1640
60	1007	0.02808	1.0590
100	1009	0.03095	0.9458
200	1023	0.03779	0.7459
300	1044	0.04418	0.6158
400	1069	0.05015	0.5243
500	1093	0.05572	0.4565
600	1115	0.06093	0.4042
700	1135	0.06581	0.3627
800	1153	0.07037	0.3289
900	1169	0.07465	0.3008
1000	1184	0.07868	0.2772
1500	1234	0.09599	0.1990

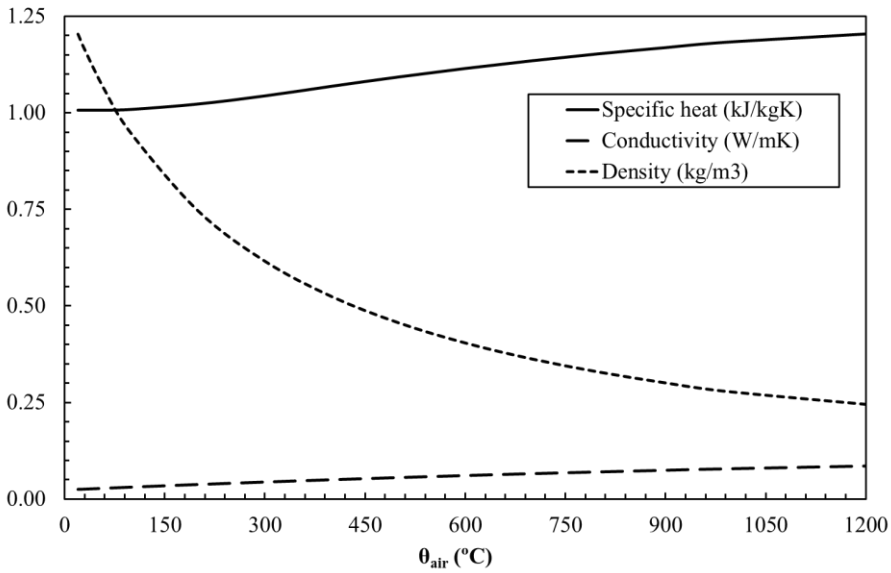

Figure 2.16: Thermal properties of air as function of temperature at 1 atm pressure.

2.8 Simplified calculation methods

Simplified calculation models from standards are generally derived from experimental fire tests and numerical analyses. These models allow the calculation of important parameters regarding the fire behaviour of composite slabs (e.g. fire resistance and temperature of the steel components) through simple analytical expressions.

The simplified calculation methods for composite slabs with profiled steel deck presented in the Annex D of the Eurocode 4 – Part 1-2 [13] and Annex C of the NBR 14323 [14] are discussed in the subsections below.

2.8.1 Eurocode 4 – Part 1-2

The analytical expressions for composite slabs given in the current version of the EN 1994 – 1-2 are based on the study conducted by Both [1], in 1998. As stated before, no revisions were made to these methods during the last years.

The fire resistance of composite slabs with respect to the thermal insulation criterion t_{fi} (min) depends linearly on different parameters and should be determined according to Eq. 2.30.

$$t_{fi} = a_0 + a_1 \cdot h_1 + a_2 \cdot \Phi_{up} + a_3 \cdot \frac{A}{L_r} + a_4 \cdot \frac{1}{l_3} + a_5 \cdot \frac{A}{L_r} \cdot \frac{1}{l_3} \tag{2.30}$$

In the equation above, h_1 is the concrete thickness (mm); Φ_{up} is the view factor of the upper flange (dimensionless); A/L_r is the rib geometry factor (mm); and l_3 is the width of the upper flange (mm). The partial factors a_i are tabulated coefficients which are different for normal weight concrete (NWC) and lightweight concrete (LWC). These coefficients are given in the following table.

Table 2.5: Coefficients for the determination of the fire resistance of composite slabs with NWC and LWC (adapted from EN 1994 – 1-2 [13]).

	a_0 (min)	**a_1 (min/mm)**	**a_2 (min)**	**a_3 (min/mm)**	**a_4 (mm min)**	**a_5 (min)**
NWC	-28.8	1.55	-12.6	0.33	-735.0	48.0
LWC	-79.2	2.18	-2.44	0.56	-542.0	52.3

The scope of this investigation comprises only composite slabs with normal weight concrete.

The rib geometry factor is defined as the ratio between the concrete volume of the rib per metre of rib length A (mm^3/m) and the exposed area of the rib per metre of rib length L_r (mm^2/m). This factor can be calculated using the geometric parameters of the slab as follows.

$$A/L_r = h_2 \cdot \left(\left(l_1 + l_2\right)/2\right) \Big/ \left(l_2 + 2\sqrt{h_2^2 + \left(\left(l_1 - l_2\right)/2\right)^2}\right) \tag{2.31}$$

The EN 1994 – 1-2 states that the effective thickness of a composite slab h_{eff} (mm) should be calculated according to Eqs. 2.32.

$$h_{eff} = h_1 + 0.5 \cdot h_2 \cdot \left(\frac{l_1 + l_2}{l_1 + l_3}\right) \qquad \text{for } h_2/h_1 \leq 1.5 \text{ and } h_1 > 40 \text{ mm} \tag{2.32a}$$

$$h_{eff} = h_1 \cdot \left[1 + 0.75 \cdot \left(\frac{l_1 + l_2}{l_1 + l_3}\right)\right] \qquad \text{for } h_2/h_1 > 1.5 \text{ and } h_1 > 40 \text{ mm} \tag{2.32b}$$

The geometric parameters of the slab h_1, h_2, l_1, l_2 and l_3 are illustrated in Figures 1.2 and 1.3. The effective thickness may be adopted as h_1 if $l_3 > 2\ l_1$.

Table 2.6 presents the relation between the minimum effective slab thickness and the standard fire resistance (I). The parameter "h_3" represents the thickness of the screed layer, if any on top of the composite slab, see Figures 1.2 and 1.3.

Table 2.6: Minimum effective thickness according to the standard fire resistance: Eurocode 4 – Part 1-2 (adapted from EN 1994-1-2 [13]).

Standard fire resistance	**Minimum effective thickness h_{eff} (mm)**
I 30	60 - h_3
I 60	80 - h_3
I 90	100 - h_3
I 120	120 - h_3
I 180	150 - h_3
I 240	175 - h_3

Concerning the load bearing capacity (R), the EN 1994 – 1-2 provides guidelines for the calculation of the sagging moment resistance. In this regard, a method is introduced for the calculation of the temperatures of the lower flange, web or upper flange θ_a (°C) for different levels of fire resistance. The temperatures of the parts of the steel deck should be calculated according to Eq. 2.33.

$$\theta_a = b_0 + b_1 \cdot \frac{1}{l_3} + b_2 \cdot \frac{A}{L_r} + b_3 \cdot \Phi_{up} + b_4 \cdot \Phi_{up}^2 \tag{2.33}$$

The partial factors b_i are coefficients that differ for slabs with normal weight concrete and lightweight concrete. Table 2.7 presents these coefficients for each part of the steel deck for slabs with normal weight concrete. For intermediate values, linear interpolation is allowed.

Table 2.7: Coefficients for the determination of the temperatures of the parts of the steel deck for slabs with NWC (adapted from EN 1994 – 1-2 [13]).

Standard fire resistance	**Part of the steel deck**	**b_0 (°C)**	**b_1 (°C mm)**	**b_2 (°C mm)**	**b_3 (°C)**	**b_4 (°C)**
R60	Lower flange	951	-1197	-2.32	86.4	-150.7
	Web	661	-833	-2.96	537.7	-351.9
	Upper flange	340	-3269	-2.62	1148.4	-679.8
R90	Lower flange	1018	-839	-1.55	65.1	-108.1
	Web	816	-959	-2.21	464.9	-340.2
	Upper flange	618	-2786	-1.79	767.9	-472.0
R120	Lower flange	1063	-679	-1.13	46.7	-82.8
	Web	925	-949	-1.82	344.2	-267.4
	Upper flange	770	-2460	-1.67	592.6	-379.0

Still regarding the load bearing capacity (R), the temperature of the rebars in the rib θ_s (°C) shall be determined as follows.

$$\theta_s = c_0 + \left(c_1 \cdot \frac{u_3}{h_2}\right) + \left(c_2 \cdot z\right) + \left(c_3 \cdot \frac{A}{L_r}\right) + \left(c_4 \cdot \alpha\right) + \left(c_5 \cdot \frac{1}{l_3}\right) \tag{2.34}$$

In the equation above, u_3 is the distance of the rebar to the lower flange (mm); z is an indication of the position in the rib ($mm^{-0.5}$); and α is the angle of the web (degrees). The partial factors c_i depend on the fire resistance R and differ for slabs with normal weight concrete and lightweight concrete. Table 2.8 gives these coefficients for slabs with normal weight concrete. For intermediate values, linear interpolation is allowed.

Table 2.8: Coefficients for the determination of the temperatures of the rebars in the rib for slabs with NWC (adapted from EN 1994 – 1-2 [13]).

Standard fire resistance	**c_0 (°C)**	**c_1 (°C)**	**c_2 (°C $mm^{0.5}$)**	**c_3 (°C mm)**	**c_4 (°C/°)**	**c_5 (°C mm)**
R60	1191	-250	-240	-5.01	1.04	-925
R90	1342	-256	-235	-5.30	1.39	-1267
R120	1387	-238	-227	-4.79	1.68	-1326

The z-factor should be calculated according to the following equation.

$$\frac{1}{z} = \frac{1}{\sqrt{u_1}} + \frac{1}{\sqrt{u_2}} + \frac{1}{\sqrt{u_3}} \tag{2.35}$$

In Eq. 2.35, u_1 and u_2 are defined as the shortest distances of the centre of the rebar to any point of the webs of the steel deck (mm); and u_3 is the distance of the centre of the rebar to the lower flange of the steel deck (mm). These parameters are illustrated in Figure 2.17 for composite slabs with trapezoidal and re-entrant profiles.

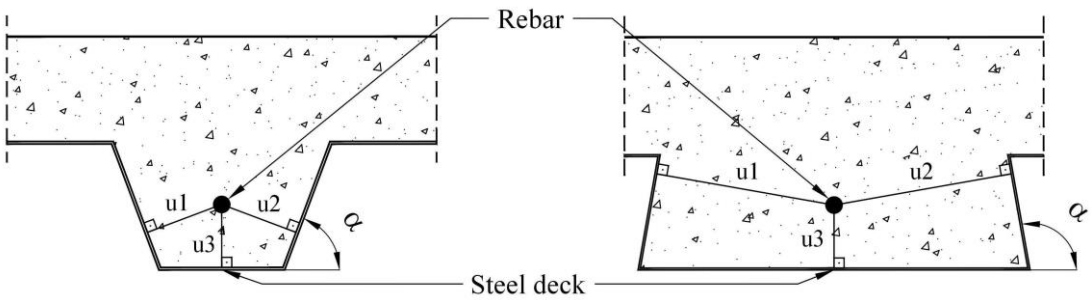

Figure 2.17: Parameters for the position of the rebars (adapted from EN 1994 – 1-2 [13]).

2.8.2 Brazilian standard NBR 14323

According to the Brazilian standard NBR 14323 [14], for the fulfilment of the thermal insulation criterion of fire resistance, the effective thickness of the slab should not be less than a minimum value, which depends on the fire resistance required time (TRRF). Table 2.9 presents the minimum effective slab thickness as function of the required fire resistance.

Table 2.9: Minimum effective thickness according to the required fire resistance: NBR 14323 (adapted from NBR 14323 [14]).

TRRF (min)	**Minimum effective thickness h_{eff} (mm)**
30	60
60	80
90	100
120	120
180	150

The equations for the calculation of the effective thickness presented in this standard are the same as those given in the EN 1994 – 1-2, see Eqs. 2.32.

This standard states that whether lightweight concrete is used, the values for the effective thickness of the Table 2.9 can be multiplied by a correction factor of 0.9.

Regarding the calculation of the sagging moment resistance, the methodology for the determination of the temperature of the parts of the steel deck θ_a and the rebars θ_s is the same of that introduced by the EN 1994 – 1-2, see subsection 2.8.1.

3. ADVANCED CALCULATION METHOD

3.1 Introduction

Advanced calculation models are based on numerical methods (e.g. finite element method and finite difference method) and shall provide realistic analysis of structures under fire exposure. However, these methods require the use of computer programs due to its high complexity.

In comparison with simple calculation models, the advanced calculation models give an improved approximation of the real structural performance under fire conditions. These models should be used in association with time-temperature curves and the thermal material properties must be known for a relevant temperature range.

According to the EN 1994 – 1-2 [13], the advanced calculation models shall include different models for the determination of the temperature distribution within structural components (thermal model), as well as the mechanical behaviour of the structure (mechanical model).

Normally, the fire behaviour of building structures is studied assuming that the influence of the mechanical response on the thermal response, on both material and structural level, can be neglected [1].

This investigation is concerned with the development and application of three-dimensional thermal models for the analysis of the fire behaviour of composite slabs. These models should be implemented using the software ANSYS Mechanical APDL 18.2 and the software MATLAB R2018a, through the Partial Differential Equation (PDE) Toolbox™.

3.2 Finite element method (FEM)

The analytical mathematical solution of complex engineering problems is generally not possible because it normally requires the solution of ordinary or partial differential equations which are not usually obtainable. Numerical methods represent an efficient alternative to these problems and can provide satisfactory results.

The finite element method is a powerful numerical method which is widely used by computer programs to solve problems of heat transfer and fluid flow, for example. In this method, the process of modelling a body (discretization) consist of dividing it into smaller bodies (finite elements) interconnected at common points (nodes) with a specific number of degrees of freedom (DOF). Therefore, instead of solving the problem for the entire body in one operation, the FEM formulates the equations for each finite element and combine them to obtain the solution for the whole body [16].

Consider an arbitrary solid body on which heat fluxes act. For an infinitesimal volume element dV = (dx · dy · dz), the conduction heat flux ϕ can be described on all surface edges, see Figure 3.1.

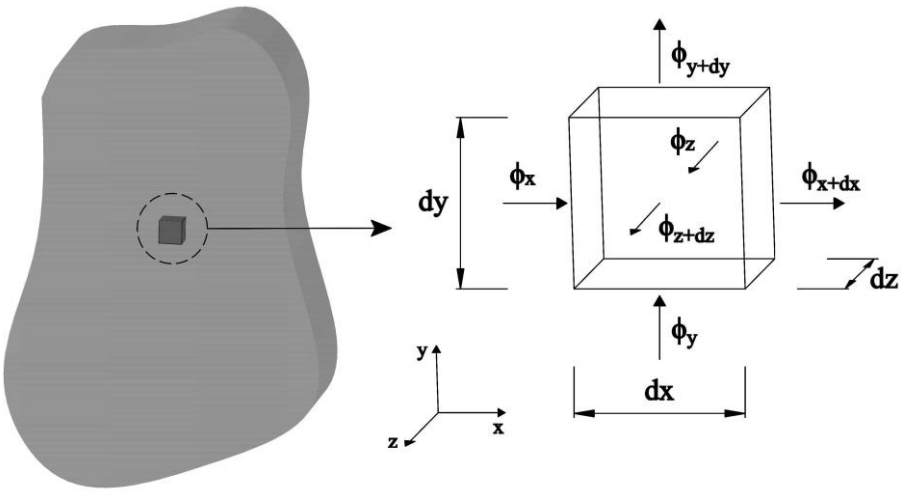

Figure 3.1: Heat fluxes acting on a volumetric infinitesimal element.

According to the Fourier's law for conduction of heat, see Eq. 2.3, the heat flux for the x-direction into the element at the surface edge ϕ_x and the heat flux out of the element at the surface edge ϕ_{x+xd} can be defined as:

$$\phi_x = -\left(\lambda \frac{\partial T}{\partial x}\right)_x \tag{3.1a}$$

$$\phi_{x+dx} = -\left(\lambda \cdot \frac{\partial T}{\partial x}\right)_{x+dx} \tag{3.1b}$$

Using a two-term Taylor series to approximate the heat flux equation at x+dx, results:

$$\left(\lambda \cdot \frac{\partial T}{\partial x}\right)_{x+dx} = \left(\lambda \cdot \frac{\partial T}{\partial x}\right)_{x} + \frac{\partial}{\partial x}\left(\lambda \cdot \frac{\partial T}{\partial x}\right)_{x} \cdot dx \tag{3.2}$$

The internal energy variation for the infinitesimal element ΔU (thermal balance) is expressed through the following general equation.

$$\Delta U = \sum \phi_{in} - \sum \phi_{out} \tag{3.3}$$

In transient-state analyses, the temperature changes with time. In this case, the change in the internal energy can be written as:

$$\Delta U = \rho \cdot c \cdot dV \cdot \frac{\partial T}{\partial t} \tag{3.4}$$

Where ρ is the specific mass; c is the specific heat; dV is the infinitesimal volume; T is the temperature; and t is the time.

Substituting Eqs. 3.1, 3.2 and 3.4 into Eq. 3.3, and writing the in/out heat fluxes for the x-direction with respect to the infinitesimal area, results:

$$\rho \cdot c \cdot dV \cdot \frac{\partial T}{\partial t} = -\left(\lambda \cdot \frac{\partial T}{\partial x}\right)_{x} \cdot (dy \cdot dz) - \left[-\left(\lambda \cdot \frac{\partial T}{\partial x}\right)_{x} - \frac{\partial}{\partial x}\left(\lambda \cdot \frac{\partial T}{\partial x}\right)_{x} \cdot dx\right] \cdot (dy \cdot dz) \tag{3.5}$$

Performing mathematical operations in Eq. 3.5 and simplifying, the one-dimensional heat conduction equation can be written as:

$$\rho \cdot c \cdot \frac{\partial T}{\partial t} = \frac{\partial}{\partial x}\left(\lambda \cdot \frac{\partial T}{\partial x}\right)_{x} \tag{3.6}$$

Analogously, this process can be performed for y and z directions. Therefore, the conduction heat transfer considering all the directions for the heat flow can be expressed by:

$$\rho \cdot c \cdot \frac{\partial T}{\partial t} = \frac{\partial}{\partial x}\left(\lambda \cdot \frac{\partial T}{\partial x}\right)_{x} + \frac{\partial}{\partial y}\left(\lambda \cdot \frac{\partial T}{\partial y}\right)_{y} + \frac{\partial}{\partial z}\left(\lambda \cdot \frac{\partial T}{\partial z}\right)_{z} \tag{3.7}$$

Writing the Eq, 3.7 in a compact form, the following expression is obtained:

$$\nabla(\lambda \cdot \nabla T) = \rho \cdot c \cdot \frac{\partial T}{\partial t} \rightarrow (\Omega) \tag{3.8}$$

In the underlying investigation, the composite slab is discretized to numerically solve a nonlinear transient thermal problem. The FEM requires the solution of the heat equation in the domain (Ω), see Eq. 3.8. In addition, it is necessary to define the boundary conditions on both exposed and unexposed surfaces of the composite slab ($\partial\Omega$), according to Eq. 3.9.

$$\lambda \cdot \nabla T \cdot \vec{n} = \alpha_{cv} \cdot \left(T_g - T\right) + \Phi \cdot \varepsilon_m \cdot \varepsilon_f \cdot \sigma \cdot \left(T_g^4 - T^4\right) \rightarrow \left(\partial\Omega\right) \tag{3.9}$$

In the equation above, T is the temperature of each material; $\vec{n}$ represents the normal vector; α_{cv} is the convection coefficient. T_g represents the gas temperature of the fire compartment, following the standard fire ISO 834 applied on the bottom part of the slab; Φ is the view factor; ε_m is the emissivity of each material; ε_f represents the emissivity of fire and σ represents the Stefan-Boltzmann constant.

The Method of Weighted Residuals (MWR) along with the Galerkin Formulation are employed to solve the thermal differential equation through the FEM. Based on the weak integral formulation, several mathematical theorems are applied in order to reduce the requirements for temperature differentiability, hence increasing the weighting function differentiability.

For more specific details, reference is made to Logan [16].

3.3 Description of the thermal models

Considering the finite element analysis of an arbitrary structure, after its division into a finite number of elements, the unknown temperatures at the nodes (DOF's) can be calculated. The degrees of freedom are assumed to vary along the element according to shape functions. Using these shape functions, combined with the Fourier's law for conduction of heat, the system conductivity matrix can be constructed, which establishes the relationship between all nodal temperatures and external fluxes. With the aim to obtain a solution, time integration needs to be performed. Therefore, the time derivative $\dot{T}$ is given as:

$$\dot{T} \approx \frac{T_{t+\Delta t} - T_t}{\Delta t} \tag{3.10}$$

By means of illustration, the fully implicit method is presented in Eq. 3.11. Using this method, the solution is unconditionally stable, which means that the time step

in the integration process is not restricted, at least for almost linear material behaviour [1].

$$[L]\cdot\{T\}+[C]\cdot\{\dot{T}\}=\{Q\} \tag{3.11a}$$

$$[L]\cdot\{T_{t+\Delta t}\}+[C]\cdot\frac{\{T_{t+\Delta t}-T_t\}}{\Delta t}=\{Q_{t+\Delta t}\} \tag{3.11b}$$

$$\left[L+\frac{C}{\Delta t}\right]\cdot\{T_{t+\Delta t}\}=\left\{Q_{t+\Delta t}+C\cdot\frac{T_t}{\Delta t}\right\} \tag{3.11c}$$

$$[L_{eff}]\cdot\{T_{t+\Delta t}\}=\{Q_{eff}\} \tag{3.11d}$$

In the equations above, [L] is the system conductivity matrix; {T} is the vector with nodal temperatures; [C] is the capacitance matrix; $\{\dot{T}\}$ represents the vector of time derivative; and {Q} is the vector with external fluxes.

Whether the thermal material properties are temperature dependent, an iterative method is required for the solution of the Eq. 3.11. This is called a nonlinear problem. The external fluxes can be applied in increments ΔQ using the iterative procedure [1]. The solution method used by ANSYS and MATLAB are discussed in subsections 3.4.4 and 3.5.4, respectively.

In this investigation, two different three-dimensional thermal models are developed: the first considers perfect thermal contact between all the materials, and the second presents an air gap with a constant thickness t_a between the steel deck and the concrete topping in order to simulate debonding effects. Due to the very small thickness of the air gap, only heat flow by conduction is considered through this layer. Figure 3.2 illustrates the material components of each thermal model for an arbitrary composite slab with trapezoidal profile.

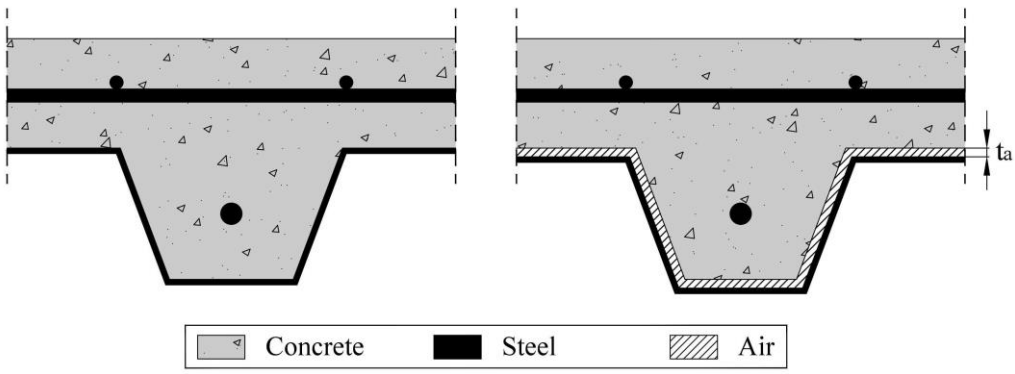

Figure 3.2: Perfect thermal contact model and air gap model.

It is noteworthy that there is a limitation concerning the air gap model. The air layer has constant thickness during the whole simulation time. In experimental fire tests, the air gap thickness may not be constant: the test starts with perfect thermal contact between all the materials (t_a = 0 mm) and as long as the specimen is heated, the steel deck may be (slowly) separated from the concrete topping, hence increasing the air gap thickness.

Regarding the thermal material properties, see section 2.7, the relationship between the temperature and the thermal properties of the concrete and steel are adopted from the European standards. The effect of evaporation of free moisture in concrete is implicitly included in the specific heat of concrete c_p by changing the peaks. The thermal properties of air are adopted from Çengel and Ghajar [53].

3.3.1 Initial and boundary conditions

The boundary conditions employed in the thermal analyses of this investigation follow the recommendations of the EN 1991 – 1-2 [51]. Concerning the parametric studies, all the nodes are set with an initial condition for temperature of 20 °C. For the validation models, a temperature equal to the measured initial average temperature for each fire test is considered as the initial condition for temperature.

The exposed surface of the composite slab is submitted to a heat flux by convection and radiation, using different values for view factors for each part of the steel deck, and a bulk temperature following the standard fire ISO 834. In addition, it is assumed a convection coefficient of 25 W/m^{2}K and an emissivity of fire equal to 1.

The unexposed surface of the composite slab is subjected to a convective heat flux considering a constant bulk temperature according to the initial temperature. A

convective coefficient of 9 W/m^{2}K is applied on this boundary surface in order to include the effects of heat transfer by radiation.

Figure 3.3 illustrates the boundary conditions which should be considered in the numerical simulations for composite slabs with either trapezoidal or re-entrant steel deck profile.

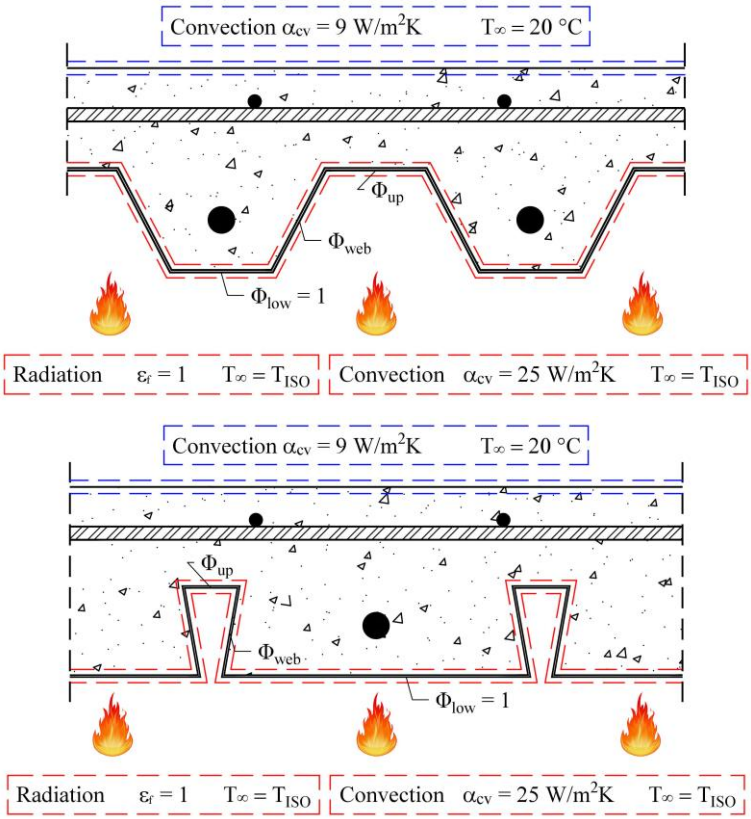

Figure 3.3: Representation of the boundary conditions.

3.4 ANSYS

3.4.1 General

ANSYS is a general commercial finite element analysis package which was released in the decade of 1970. Nowadays, this tool is widely used in engineering simulation for the solution of problems involving thermal, structural and fluid analysis.

The ANSYS Mechanical APDL 18.2 [76] is a powerful software which utilizes the FEM to solve linear and nonlinear problems in either steady-state or transient regime, comprising 2-D or 3-D geometries. This computer program utilizes various

types of finite elements and allows the introduction of commands through graphical user interface and command prompt as well.

3.4.2 Finite element models for thermal analysis

In ANSYS, the three-dimensional geometric models of the composite slab are manually created using the graphical user interface to define *keypoints*, *lines*, *areas* and *volumes* (through the extrusion of *areas*). Figure 3.4 presents the geometric model of a composite slab introduced in the software.

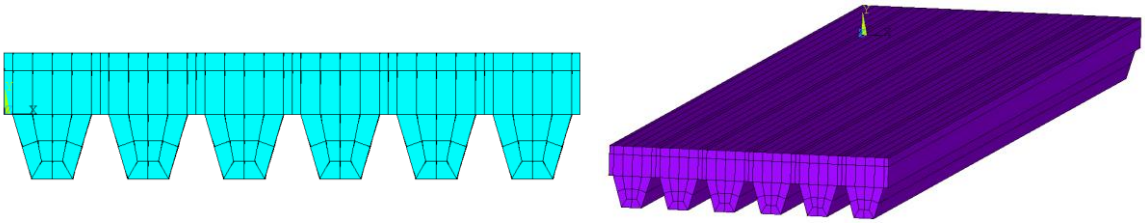

Figure 3.4: Modelling of composite slabs in ANSYS: areas and volumes [76].

The thermal properties, see section 2.7, are introduced on the software by creating material models for each material; that is, manually inserting the values of each property for different instants of time. These material models can be written to a *MP* file to be read in posterior simulations.

A specific number of divisions are given for each line in order to generate the meshes. The finite element model is created by meshing areas and volumes using different 3-D elements, appropriate for thermal analysis, for each subdomain (steel components, concrete topping and air gap).

3.4.2.1 Finite elements

Three different types of finite elements from the ANSYS library are used, namely SHELL131, SOLID70 and LINK33.

The SHELL131 element has four nodes with up to 32 degrees of freedom (temperature) per node, depending on the number of layers (one layer). This element presents linear interpolation functions in the plane of the element, using full Gauss integration method 2x2 and linear interpolation functions through the layer thickness (three Gauss points). The bottom temperature of the shell element nodes is assumed to be equal to the temperature of solid element nodes using the function “Paint (TBOT →

TEMP)", when both nodes are coincident. The shell element is used to model the steel deck of the composite slab. Figure 3.5 presents the geometry, node locations and the global and local coordinates systems of the SHELL131 element.

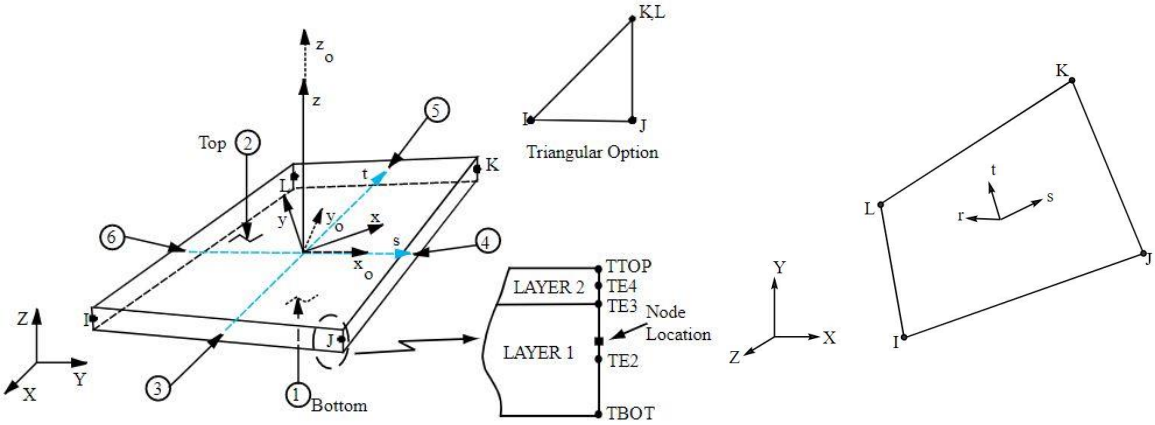

Figure 3.5 The SHELL131 finite element [76].

The SOLID70 element presents eight nodes with a single degree of freedom (temperature) at each node. Linear interpolation functions are used for this element and the full Gauss integration method 2x2x2 is also applied. This finite element is used to model the concrete topping and the air gap volume of the composite slab. Figure 3.6 illustrates the SOLID70 geometry in global and local coordinate systems as well as the node locations.

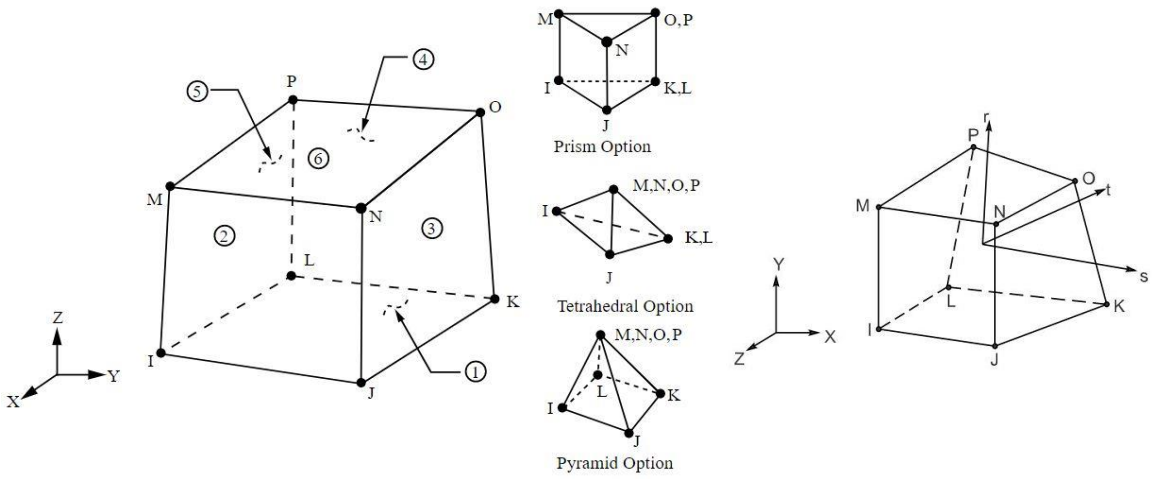

Figure 3.6: The SOLID70 finite element [76].

The LINK33 element has two nodes with a single degree of freedom (temperature) per node. This uniaxial element presents linear interpolation functions as well as exact integration. The LINK33 element is defined by a cross-sectional area (*real constant*) and is used to model the anti-crack mesh and the rebars as well. It is

noteworthy that, by means of simplification, the cross-section of these steel components is assumed to be a square with the same area of that of the bars. Figure 3.7 presents the geometry, node locations and coordinate systems of the LINK33 element.

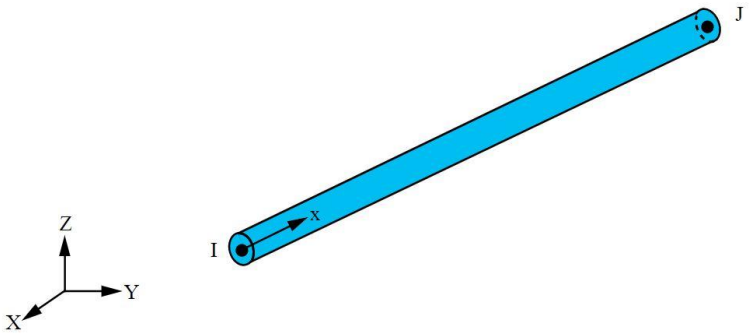

Figure 3.7: The LINK33 finite element [76].

Regarding the 3-D finite element models, in the regions of the rebars and anti-crack mesh, there is a coincidence of two different materials (concrete and steel) on the same node. Figure 3.8 presents two different examples of 3-D finite element meshes created in ANSYS.

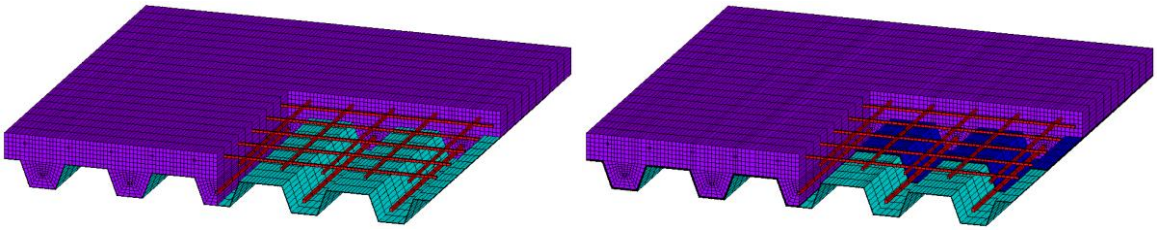

a) Perfect contact model. b) Air gap model.

Figure 3.8: Finite element meshes created in ANSYS [76].

3.4.3 Initial and boundary conditions

The initial and boundary conditions specified in subsection 3.3.1 are applied in the ANSYS finite element model.

The initial conditions for temperature are set for all nodes and all degrees of freedom. A table containing the temperature development based on the standard fire curve ISO 834 is introduced in the software through the command prompt. After that, a node is created to represent the compartment temperature following the standard fire curve.

The convective boundary conditions are applied on the boundary areas of the elements which comprise the exposed and unexposed surfaces of the composite slab.

With respect to the radiation options, a value of 5.67E-8 is defined for the Stefan-Boltzmann constant, and a value of 273.15 is set for the temperature difference between absolute zero and zero of the active temperature scale (*temperature offset*). Thereafter, the space node following the standard fire curve is assigned to the enclosure.

Finally, the radiative boundary conditions are applied on the elements of the fire exposed surface (steel deck elements), following the temperature of the enclosure previously defined. Different view factors should be adopted for each part of the steel deck, namely the lower flange, web and upper flange.

3.4.4 Solution method

The ANSYS Mechanical APDL 18.2 has two different solution methods for transient analysis (TRNOPT), namely the full method (FULL – default) and the mode-superposition method (MSUP).

In the underlying investigation, the full method has been selected for the solution of the nonlinear transient thermal analysis. In this case, the Newton-Raphson method is used along with the Newmark assumptions. This method is the most frequently used iteration scheme for nonlinear finite element analysis in which the effective conductivity matrix is updated in each iteration [1]. The following figure illustrates how the solution is obtained using the Newton-Raphson method.

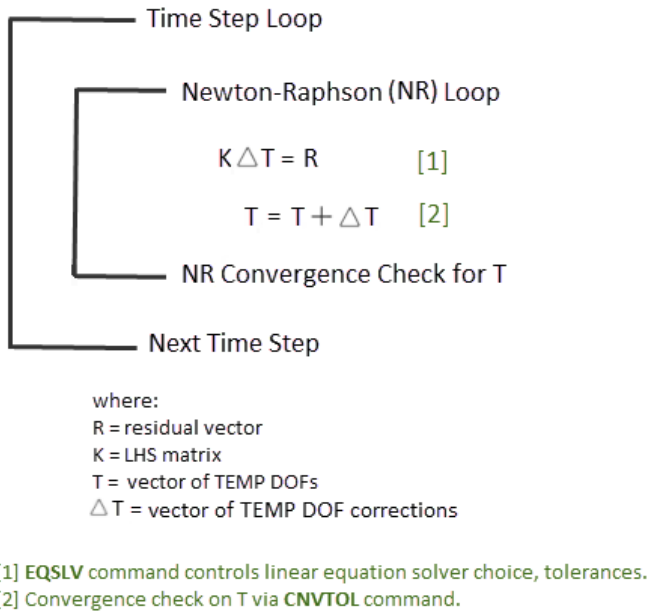

Figure 3.9: Full solution method (Newton-Raphson iteration scheme) [76].

The Newton-Raphson method proved to be efficient because normally results in faster convergence. However, this method causes higher CPU consumption in comparison to other procedures [1]. Figure 3.10 illustrates the Newton-Raphson iteration scheme for a one-dimensional case with two external flux increments. In the second increment, three iteration steps are given.

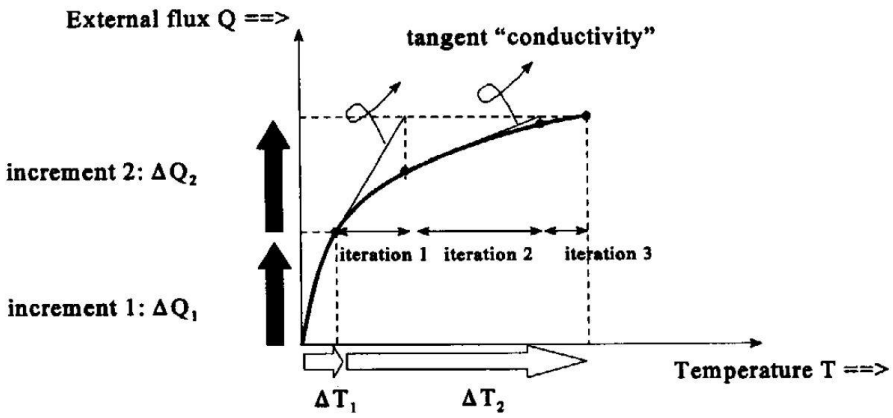

Figure 3.10: Incremental solution technique for nonlinear problems, combined with the Newton-Raphson iteration scheme [1].

For each external flux increment, the iterative process continues until converge is achieved. In ANSYS, the convergence is obtained when "size of the residual (disequilibrium) is less than a tolerance times a reference value and/or when the size of the DOF increment is less than a tolerance times a reference value" [76]. In this regard, the heat flow criterion is chosen for the convergence criterion, using a tolerance value of 1E-3 and a minimum reference value of 1E-6.

The method of automatic time stepping is adopted in the numerical simulations. In this method, the time step size is automatically calculated depending on the current state of the analysis [76]. Therefore, the time control is based on time increments, with a time step size of 60 s, a minimum time step of 1 s and a maximum time step of 60 s.

3.5 MATLAB

3.5.1 General

The MATLAB (MAtrix LABoratory) software is a multi-paradigm programming environment developed by MathWorks. This software has been selected

for the development of the new tool for nonlinear transient thermal analysis due to its flexibility and large number of functions for finite element analysis.

The MATLAB PDE Toolbox^{TM} [77] is a widely used tool for solving partial differential equations (PDEs) involving problems of heat transfer, structural mechanics, and electrostatics, among others. Its algorithm uses FEM principles for problems defined on bounded domains in 2-D or 3-D space, and allows the performance of steady-state and transient heat transfer analysis.

3.5.2 Finite element models for thermal analysis

Modelling complex 3-D multidomain geometries in MATLAB PDE Toolbox is a challenge because, at the present time, there is no specific function for creating such geometries. In this work, complementary programs for the creation of the composite slab geometry are utilized, namely AutoCAD Mechanical and Gmsh. In addition, the QuickerSim CFD Toolbox is also used for this task.

Thermal analyses in MATLAB PDE Toolbox require the definition of a thermal model object which contains information about the heat transfer problem, such as the geometry, material properties, and boundary conditions, among others.

By means of simplification, the rebars and the anti-crack mesh are not included in the MATLAB numerical models. The geometry is created through the function *geometryFromMesh* considering an imported mesh data in [p,e,t] form (for more details, see MathWorks [77]). Figure 3.11 presents the geometric model of a composite slab created in MATLAB.

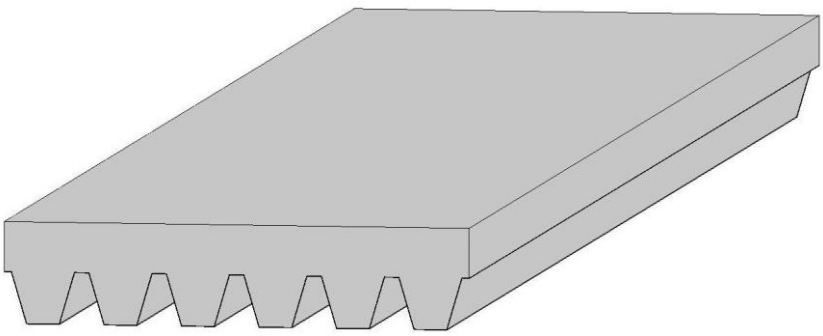

Figure 3.11: Modelling of composite slabs in MATLAB [77].

For the thermal material properties, see section 2.7, individual auxiliary functions have been created for each thermal property of all materials of interest. As the thermal properties are temperature dependent, the auxiliary functions recalculate these

values at each time step of the solution. These properties are assigned to each subdomain (*cell*) of the geometry using the function *thermalProperties*.

The mesh of the composite (multidomain) geometry is generated through the function *generateMesh* and stored in the thermal model object. This function allows the use of either linear or quadratic elements, and provides few options for mesh-size control, namely the mesh growth rate (*Hgrad*), and the maximum and minimum mesh edge length (*Hmax*, *Hmin*). Generally, quadratic elements result in more accurate solutions; however, require higher computational power in comparison to linear elements.

3.5.2.1 Finite elements

For 3-D geometries, the PDE Toolbox uses uniform meshes with tetrahedral elements and adopts quadratic elements by default, not supporting meshes with elements of different types (mixed meshes) [77].

The tetrahedral elements are defined by four nodes (at the corners) for linear elements, or ten nodes (at its corners and edge centres) for quadratic elements. Figure 3.12 illustrates the tetrahedral finite element for both linear and quadratic geometric order, as well as the ordering of the nodes.

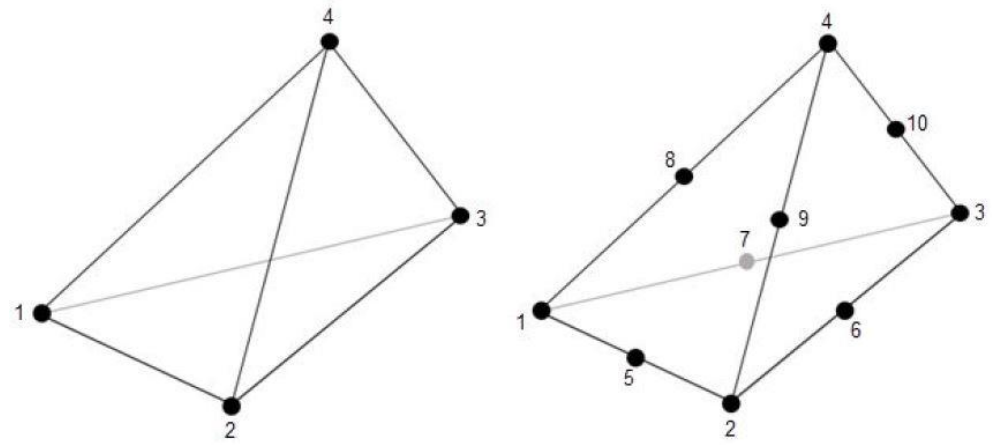

Figure 3.12: The tetrahedral finite element: linear and quadratic order [77].

In the underlying investigation, the linear tetrahedral element has been chosen for the numerical simulations in order to reduce the processing time. This element presents linear interpolation functions and a single degree of freedom (temperature) at each node. The following figure illustrates examples of 3-D meshes generated in MATLAB, regarding the perfect contact model and air gap model.

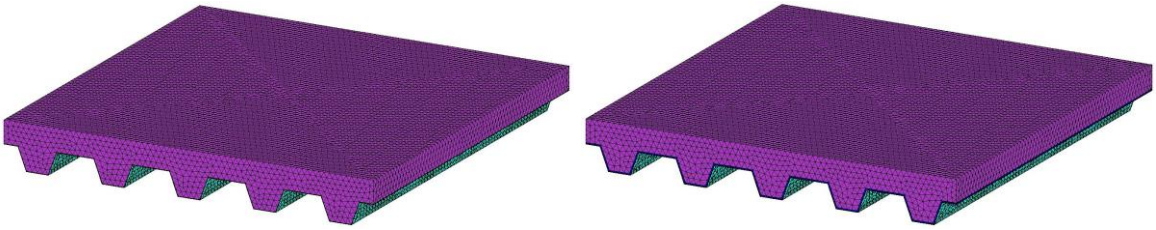

a) Perfect contact model. b) Air gap model.

Figure 3.13: Finite element meshes created in MATLAB [77].

In the numerical simulations, the maximum mesh edge length *Hmax* varies from analysis to analysis, usually standing between 0.015 and 0.02. These values have been selected according to convergence tests using different mesh sizes. Figure 3.14 presents the convergence of results with the mesh refinement, for the temperature at one point on the unexposed surface of a composite slab, after 60 minutes of fire exposure.

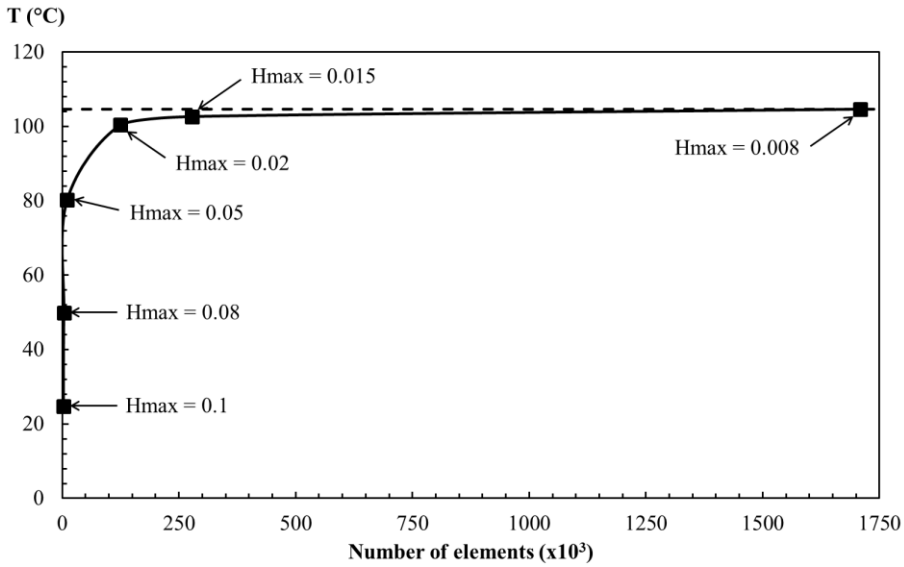

Figure 3.14: Mesh convergence study [77].

From the results above, it can be observed that the use of coarse finite element meshes leads to unpleasant results (Hmax = 0.1, 0.08 and 0.05). The results are significantly improved as long as the mesh is refined. However, finite element problems involving very dense meshes require large computational effort and result in considerable memory consumption, hence increasing the elapsed time of the analysis.

3.5.3 Initial and boundary conditions

The initial and boundary conditions specified in subsection 3.3.1 are applied in the MATLAB finite element model.

The initial conditions for temperature are set to the entire geometry of the thermal model (all the subdomains) through the function *thermalIC*.

Similarly to the approach adopted for the thermal material properties, auxiliary functions have been created for the thermal boundary conditions. These functions are set to the slab geometry boundaries using the PDE Toolbox function *thermalBC*.

The convective boundary conditions are applied on the exposed and unexposed boundary faces of the geometry using appropriate convection coefficients and bulk temperatures.

The view factors of each component of the steel deck are automatically calculated based on the geometric parameters of the slab. The radiation boundary conditions are applied on the fire exposed faces of the geometry through the heat flux boundary condition. The heat fluxes (including radiation and convection) are calculated at each time step by calling the auxiliary functions and adopting different values for view factors.

3.5.4 Solution method

The Gauss-Newton iteration method, which is a modification of Newton's method, is local and can be used for the solution of nonlinear equations. For the so-called "small-residual problems", the Gauss-Newton method ultimately converges at the same rate as Newton's method, despite the fact that only first derivatives are required [78]. In this case, the convergence of the problem is assured only when the guess is close enough to the solution.

The solution method of the PDE Toolbox consists of using the weak formulation $r(u) = 0$, integrating in the domain of the structure, and using the Green's formula based on guesses to find the solution. Whether the guess is close enough to the exact solution, the Gauss-Newton iteration tends to be the minimizer of the residual by providing an improved approximation with the solution of a linearized system [77].

For further details, reference is made to Gill and Murray [78], and MathWorks [77].

With respect to the PDE solver options, the absolute tolerance determines the accuracy when the solution approaches zero and is adopted as 1E-2. The relative tolerance is defined as a measure of the error relative to the size of each solution component and is assumed as 1E-1. The nonlinear solver continues the iterative process

until the residual size is less than the residual tolerance, which is adopted as 1E-2. The maximal number of Gauss-Newton iterations allowed for the nonlinear solver is set as 15.

Finally, the temperature development at specific points can be obtained through the function *interpolateTemperature* by specifying its x, y and z coordinates.

4. PARAMETRIC STUDIES

4.1 Description

Two different parametric studies comprising composite slabs with commercial steel deck profiles have been performed in this investigation. A representative portion of 1 m by 1 m of each slab is selected to perform the thermal analyses considering standard fire conditions. In addition, a moisture content of 3% of concrete weight is considered.

All the composite slabs are fire exposed for 7200 seconds (2 hours). In cases where none or only one of the two fire resistance criteria (AVE_T crit. and MAX_T crit.) is achieved, the numerical simulation should be performed again, considering fire exposure for 14400 seconds (4 hours).

In the first parametric study, focus is given to the influence of the steel components of the slab on the fire resistance (I). In addition, this parametric study is concerned with the influence of different parameters on the temperatures of the parts of the steel deck and the rebars. A total of 208 numerical simulations have been conducted in ANSYS using the perfect contact model and all the parameters are compared separately. The following table resumes the ranges of the investigated parameters.

Table 4.1: Investigated parameters of the first parametric study.

Steel deck profile	**h_1 (mm)**	**ϕ_{reb} (mm)**	**d'_{reb} (mm)**	**Steel mesh (mm//mm)**
O Feliz H60 (Trapezoidal) t_d = 1.2 mm	50, 60, 70, 80	8, 10, 12	30, 60	ϕ6//100, ϕ6//150
ArcelorMittal Polydeck 59S (Trapezoidal) t_d = 1.25 mm	51, 61, 71, 81	8, 10, 12	30, 60	ϕ5//100, ϕ6//100
Vulcraft 3.5D Dovetail Formlok (Re-entrant) t_d = 0.9 mm	51, 61, 71, 81	8, 10, 12	30, 60	ϕ6//100, ϕ6//150
Lysaght Bondek (Re-entrant) t_d = 0.9 mm	56, 66, 76, 86	8, 10, 12	30, 60	ϕ6.75//200, ϕ7.6//200

The ranges of selected parameters comprise commonly used values. The diameters and spacing of the anti-crack meshes have been determined from technical catalogues.

For the determination of the fire resistance (I) of each composite slab, the average temperature on the unexposed side (AVE_T) is calculated from a weighted mean between 9 points located on the central section. The maximum temperature on the unexposed side (MAX_T) is obtained from these points as well. Figure 4.1 illustrates the geometry of the steel deck profiles and the position of the points on the unexposed surface.

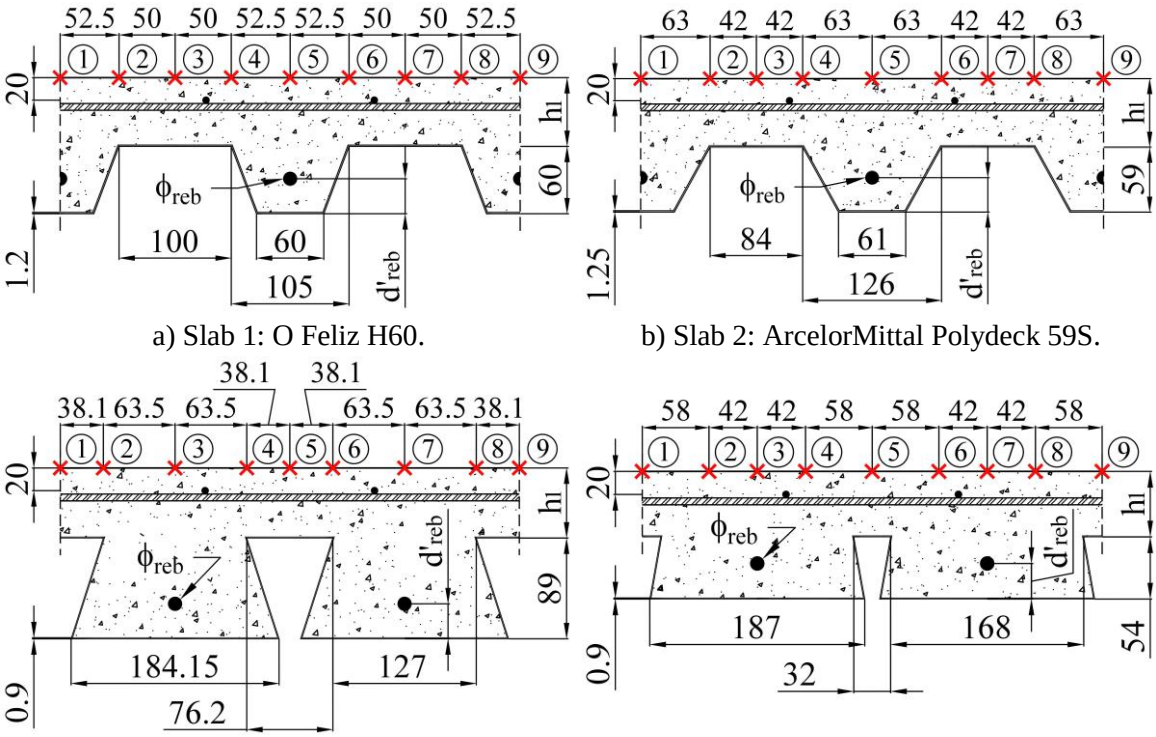

a) Slab 1: O Feliz H60.

b) Slab 2: ArcelorMittal Polydeck 59S.

c) Slab 3: Vulcraft 3.5D Dovetail Formlok.

d) Slab 4: Lysaght Bondek.

Figure 4.1: Steel deck geometries for the first parametric study (dimensions in millimetres).

The maximum temperature should occur on points 3 and 7 for trapezoidal profiles, and on points 1, 5 and 9 for re-entrant profiles. This is because these points are positioned on the centre of the thinner part of concrete layer (over the upper flange), which means that they are less protected by concrete from fire exposure.

Table 4.2 presents the view factor of the upper flange and web, calculated according to Eqs. 2.10a and 2.10b, for each steel deck profile. As discussed before, the view factor of the lower flange is always assumed as 1.

Table 4.2: Calculated view factors.

Steel deck profile	Φ_{up}	Φ_{web}
O Feliz H60	0.72325	0.56707
ArcelorMittal PD 59S	0.75273	0.63667
Vulcraft 3.5D	0.09799	0.06196
Lysaght Bondek	0.11471	0.08508

It can be observed that there is a significant difference between the view factors of trapezoidal and re-entrant profiles. The lower values for re-entrant profiles are due to the large obstruction from the ribs.

The second parametric study is concerned with the influence of the thickness of concrete (h_1) and air gap (t_a) on the fire resistance according to the insulation criterion. A total of 40 numerical simulations have been carried out, of which 32 performed in ANSYS, using the perfect contact model and the air gap model; and 8 performed in MATLAB, using the air gap model. In ANSYS, the air layer is divided into elements with 0.5 mm through the thickness.

The O Feliz H60 steel deck profile (slab 1) has been selected to perform the numerical analyses. Furthermore, some parameters have been fixed, namely the rebar diameter ϕ_{reb} = 8 mm, the concrete cover for rebar d'_{reb} = 30 mm, and the anti-crack mesh configuration ϕ6//100 mm. Table 4.3 presents the ranges of investigated parameters of the second parametric study.

Table 4.3: Investigated parameters of the second parametric study.

	h_1 (mm)	t_a (mm)
ANSYS	50, 60, 70, 80, 90, 100, 110, 120	0 (perfect thermal contact), 1, 2, 3
MATLAB	50, 60, 70, 80, 90, 100, 110, 120	3

The view factors and the points for the calculation of the AVE_T and MAX_T are the same as those of the first parametric study, see Table 4.2 and Figure 4.1a).

4.2 Numerical results

With respect to the first parametric study, the fire resistance (I) of the composite slabs is predominantly governed by the average temperature rise criterion, which is decisive for 71.6% of the numerical analyses. For the temperatures of the parts of the

steel deck, see Appendix E, the results are given only for slabs with d'_{reb} = 30 mm and one type of anti-crack mesh. With respect to the temperatures of the rebars, see Appendix E, the results are given for slabs with the same parameters, however only for the thinnest concrete thickness for each steel deck family, which is the critical case (highest temperature). The results for the Vulcraft steel deck were ignored because they consisted of inconsistent values according to the geometry, which has geometric parameters outside the range of common values.

Concerning the second parametric study, the fire resistance (I) of the composite slabs is governed by the average temperature rise criterion for most of the analyses (92.5%).

The following subsection discusses the influence of each investigated parameter on the fire resistance of composite slabs according to thermal insulation criterion.

4.2.1 Influence of different parameters on fire resistance (I)

4.2.1.1 Steel deck geometry

The trapezoidal steel deck profiles present similar geometric parameters between each other, namely the height of the steel deck h_2 and the width of the lower flange l_2, see Figure 4.1. For similar concrete thicknesses, it is observed that slab 2 presents slightly higher fire resistance in comparison to slab 1, with differences ranging from 1 °C to 4 °C. This is because the higher inclination of the web results in the presence of a greater volume of concrete over the ribs of the composite slab. The following figure presents the temperature distribution through slab 1 and slab 2 with similar concrete thicknesses after 60 minutes of fire exposure.

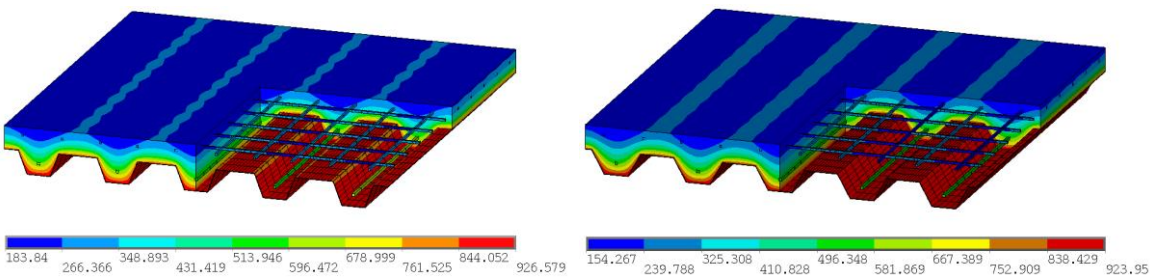

a) Slab 1 – h_1 = 60 mm. b) Slab 2 – h_1 = 61 mm.

Figure 4.2: Temperature distribution in slabs 1 and 2 after 60 minutes of fire exposure (ANSYS, first parametric study).

From the temperature contours above, it can be observed that the temperatures on the unexposed surface of slab 1 are higher than those of slab 2. In addition, the temperature distribution along the upper flange on the unexposed side is more homogeneous in slab 2. The sinuosity in the temperature distribution on the unexposed side is caused by the presence of the anti-crack mesh. This effect is more evident in slab 1 due to the more accentuated temperature gradient through the cross-section.

According to Jian Jiang et al. [9], increasing the width at the top of the rib l_1 should lead to a reduction of temperatures in the thick portion of the slab, however shall not present a considerable effect on the temperatures in the thin portion. In addition, decreasing the width of the upper flange l_3, the temperatures in the thin portion also decrease, but this effect is very small.

The slabs with re-entrant steel deck profiles (slabs 3 and 4) cannot be directly compared to each other because they present very different geometric parameters which may influence on the fire resistance, such as the height of the steel deck profile and the width of the upper flange.

4.2.1.2 Rebar diameter

Figure 4.3 presents the relationship between the fire resistance of the composite slabs t_{fi} and the diameter of rebars ϕ_{reb}, considering the concrete cover for rebar d'_{reb} of 30 mm and the smallest concrete thickness h_1 for each group of slabs. In addition, the values for the fire resistance of composite slabs without rebars (ϕ_{reb} = 0 mm) are given.

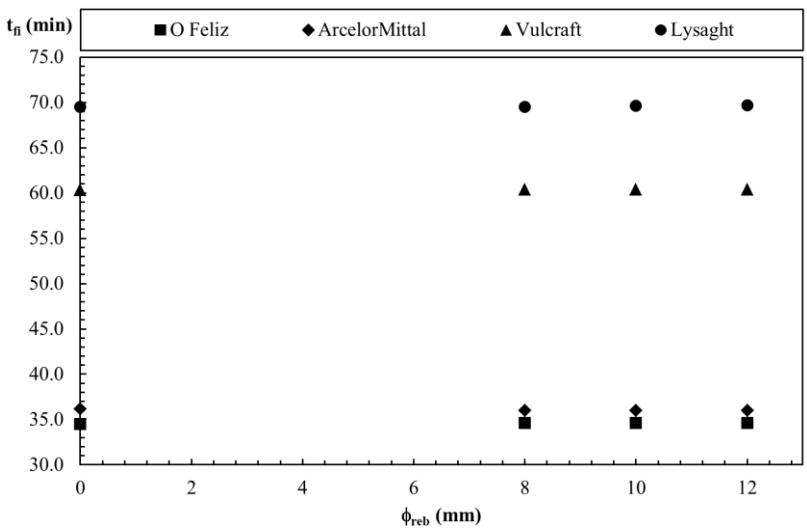

Figure 4.3: Influence of diameter of rebar on fire resistance (I) of all the slabs (ANSYS, first parametric study).

According to the graph above, it can be concluded that the effect of the diameter of rebars as well as the existence of rebars have no influence on the fire resistance (I) of composite slabs.

4.2.1.3 Anti-crack mesh diameter and spacing

For slabs 2 and 4, two anti-crack meshes with different diameters have been employed in the numerical simulations and for slabs 1 and 3, two anti-crack meshes with different spacing have been selected.

Figure 4.4 gives the relationship between the fire resistance of the slabs t_{fi} and the anti-crack mesh diameter ϕ_{reb} and spacing s_{mesh}, considering slabs with the smallest concrete thickness h_1 for each group of slabs.

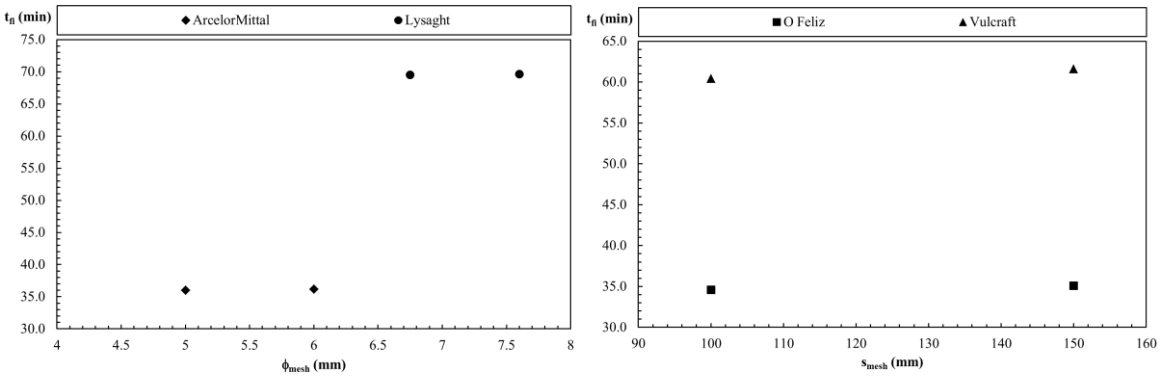

a) Diameter. b) Spacing.

Figure 4.4: Influence of the parameters of the anti-crack mesh on fire resistance (I) (ANSYS, first parametric study).

From the results above, it can be concluded that the diameter of the anti-crack mesh has no effect on the fire resistance (I) of both trapezoidal and re-entrant steel deck profile. In addition, it can also be concluded that the anti-crack mesh spacing has fairly small effect on the fire resistance of composite slabs. The fire resistance is slightly higher when the mesh spacing is increased, resulting in maximum differences of 0.6 °C for slab 1, and 1.2 °C for slab 3.

4.2.1.4 Concrete cover for rebar

Two different values for the concrete cover for rebar d'_{reb} have been selected to be evaluated: 30 mm and 60 mm. Figure 4.5 presents the relationship between the fire

resistance t_{fi} and the concrete cover for rebar, considering slabs with the thinnest concrete thickness h_1 for each group of slabs.

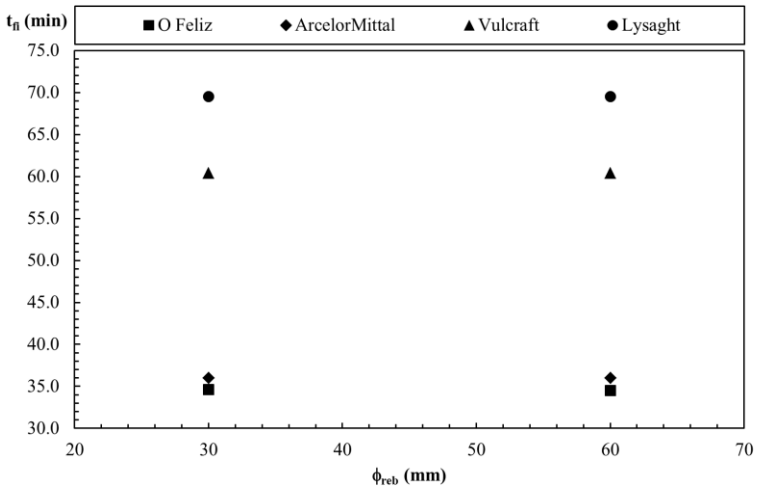

Figure 4.5: Influence of concrete cover for rebar on fire resistance (I) of all the slabs (ANSYS, first parametric study).

From the results above, it can be concluded that the distance between the centre of the rebars and the lowest portion of the steel deck (lower flange) does not affect the fire resistance (I) for all the groups of slabs.

4.2.1.5 Concrete thickness

For the first parametric study, four different concrete thicknesses have been selected for each group of composite slabs, see Table 4.1. The following figure presents the relationship between the fire resistance t_{fi} and the concrete thickness for all the groups of slabs, considering a rebar diameter of 8 mm.

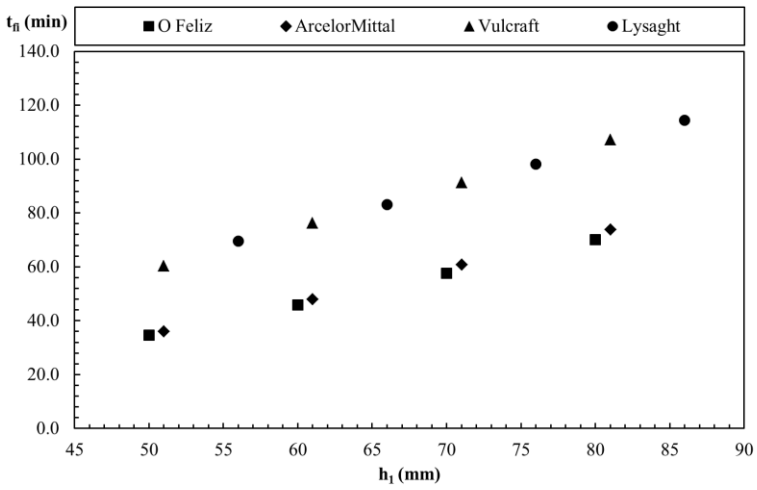

Figure 4.6: Influence of concrete thickness on fire resistance (I) of all the slabs (ANSYS, first parametric study).

According to the results above, it is observed that the fire resistance (I) considerably increases with the concrete thickness for all the groups of slabs. In addition, the results for the slabs with re-entrant steel deck profiles present an almost linear increase pattern. The same is observed for the slabs with trapezoidal steel deck profiles.

Comparing the results for simulations with the same concrete thickness, the slabs with re-entrant profiles present higher fire resistance in comparison to the slabs with trapezoidal profiles. These differences are situated between 24 min and 34 min, approximately. This is explained by the fact that the re-entrant profiles allow the employment of more uniform volume of concrete along the cross section, resulting in more homogeneous temperature distributions.

Figure 4.7 illustrates the influence of the concrete thickness h_1 in the average and maximum temperature development on the unexposed surface of each slab of the first parametric study.

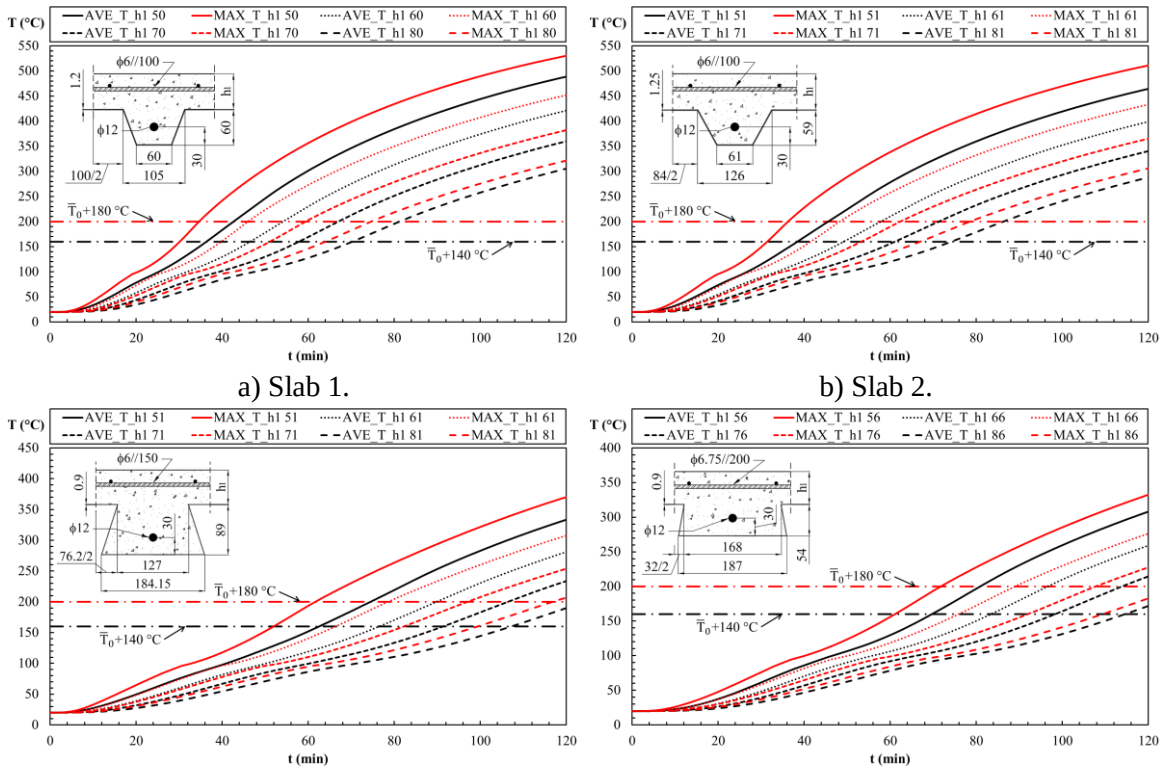

a) Slab 1. b) Slab 2.

c) Slab 3. d) Slab 4.

Figure 4.7: Average and maximum temperature development on the unexposed side of the slabs (ANSYS, first parametric study) – dimensions in millimetres.

According to the results above, it is observed that whereas the concrete thickness is increased, both average and maximum temperature curves are horizontally translated,

hence increasing the fire resistance time. In addition, a slight plateau at about 100 °C is evident for all the curves due to moisture evaporation. It is noticeable that the slabs with re-entrant profile present less accentuated temperature development in comparison to the slabs with trapezoidal profile. For slab 4, the curves of the average and maximum temperature are closer to each other in comparison to the other slabs.

With respect to the second parametric study, eight different concrete thicknesses have been selected for the numerical analyses, see Table 4.3. The following figure presents a comparison between the fire resistance t_{fi} and the concrete thickness h_1 for different air gap thicknesses t_a.

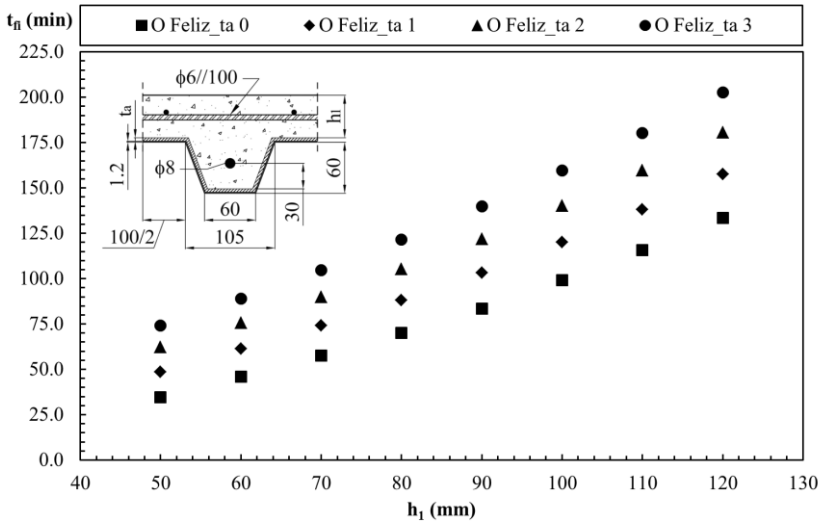

Figure 4.8: Influence of concrete thickness on fire resistance (I) of slab 1 (ANSYS, second parametric study) – dimensions in millimetres.

Analysing the graph above, it can be observed that the fire resistance presents similar rate of increase with concrete thickness in comparison to the slabs of the first parametric study, see Figure 4.6. In addition, a significant increase in the fire resistance is obtained by increasing the air gap thickness. The differences between the results for the perfect contact model (O Feliz_ta 0) and the air gap models (O Feliz_ta 1, O Feliz_ta 2 and O Feliz_ta 3) are greater for the highest concrete thicknesses.

Figure 4.9 presents the variation of the average and maximum temperature development on the unexposed surface of slab 1 with concrete thickness, for the second parametric study.

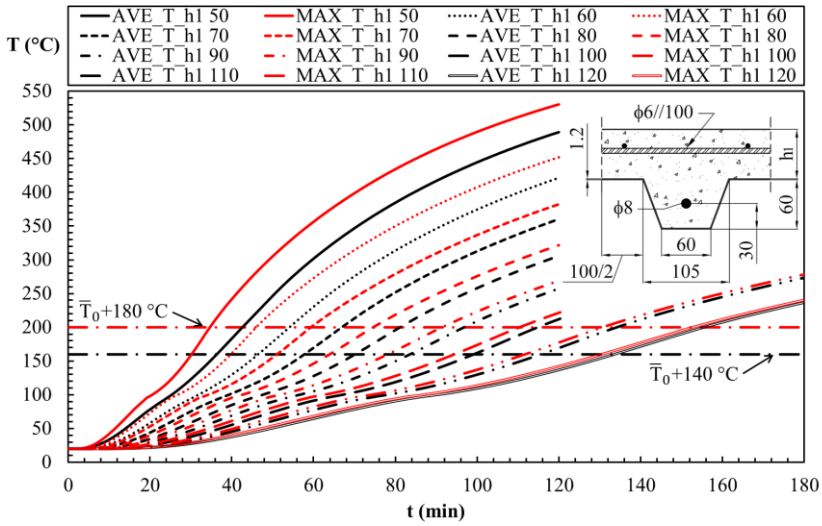

Figure 4.9: Average and maximum temperature development on the unexposed side of slab 1 for the perfect contact model (ANSYS, second parametric study) – dimensions in millimetres.

From the results above, it is observed that the higher the concrete thickness, the smaller the difference between the average and maximum temperature curves. This means that the temperature gradient on the unexposed side is more homogeneous for slabs with higher concrete thicknesses. Furthermore, the extension of the plateaus at about 100 °C increases with h_1 due to the increased moisture content, caused by the greater volume of concrete.

Figure 4.10 presents the temperature distribution through slab 1 after 90 minutes of fire exposure for four different concrete thicknesses.

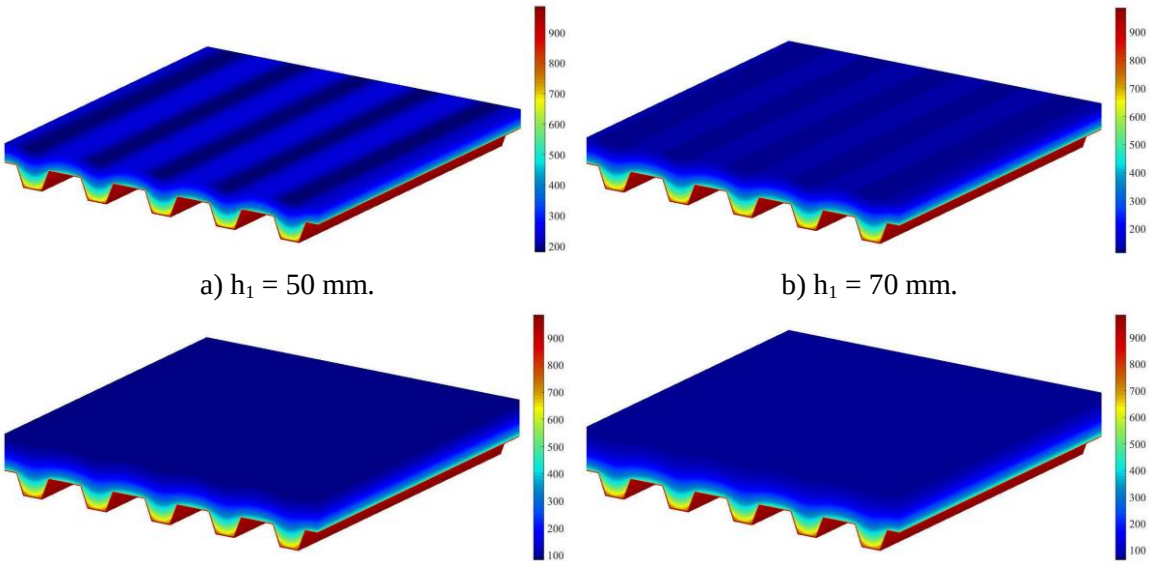

a) h_1 = 50 mm. b) h_1 = 70 mm.

c) h_1 = 100 mm. d) h_1 = 120 mm.

Figure 4.10: Temperature distribution in slab 1 after 90 minutes of fire exposure for different concrete thicknesses (MATLAB, second parametric study).

According to the temperature contours above, it is observed that the temperatures on the unexposed side of the slab with the smallest h_1 are considerably higher in comparison to the slab with the highest h_1. For the slabs with h_1 = 50 mm and h_1 = 70 mm, the segment with higher temperatures on the unexposed side (over the upper flange) should be highlighted. These segments are not noticed in the slabs with higher concrete thickness because the concrete layer allows a more uniform distribution of temperatures through the cross-section.

Therefore, for considerably high concrete thicknesses, the temperature distribution on the unexposed side of composite slabs is quite similar to the temperature distribution of flat concrete slabs.

4.2.1.6 Air gap thickness

Three different air gap thicknesses have been selected for the numerical analyses, see Table 4.3. Figure 4.11 presents the relationship between the fire resistance t_{fi} and the air gap thickness t_a for different concrete thicknesses h_1.

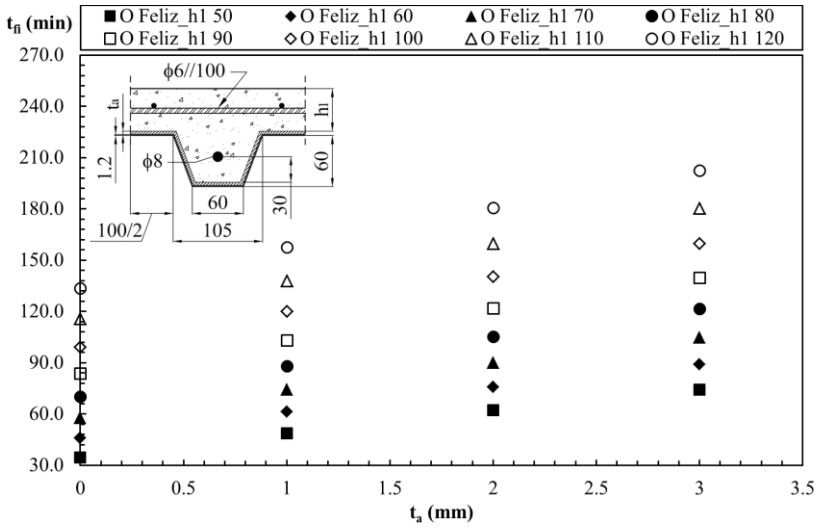

Figure 4.11: Influence of the air gap thickness on fire resistance (I) of slab 1 (ANSYS, second parametric study) – dimensions in millimetres.

Analysing the results above, it can be concluded that the air gap thickness has great influence on the fire resistance of composite slabs. The effect of increasing the air gap thickness by 1 mm is almost the same as increasing the concrete thickness by 10 mm. The variation of the fire resistance with the air layer thickness is practically linear.

Figure 4.12 illustrates the influence of the air gap thickness on the average and maximum temperature development on the unexposed surface of slab 1.

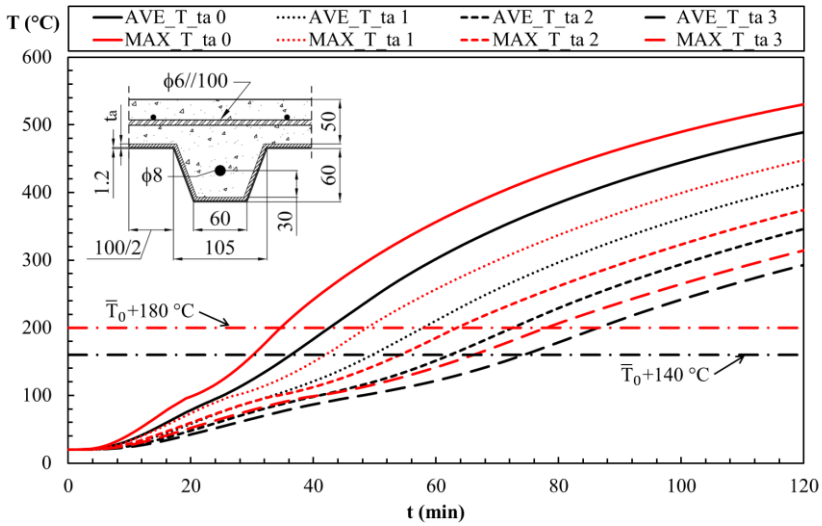

Figure 4.12: Average and maximum temperature development on the unexposed side of slab 1 for different air gaps (ANSYS, second parametric study) – dimensions in millimetres.

From the results above, it can be observed that the effect of increasing the air gap thickness on the average and maximum temperature is similar to the effect of increasing the concrete thickness, see Figure 4.9.

Figure 4.13 presents the temperature gradient in slab 1 after 120 minutes of fire exposure for different air gap thicknesses.

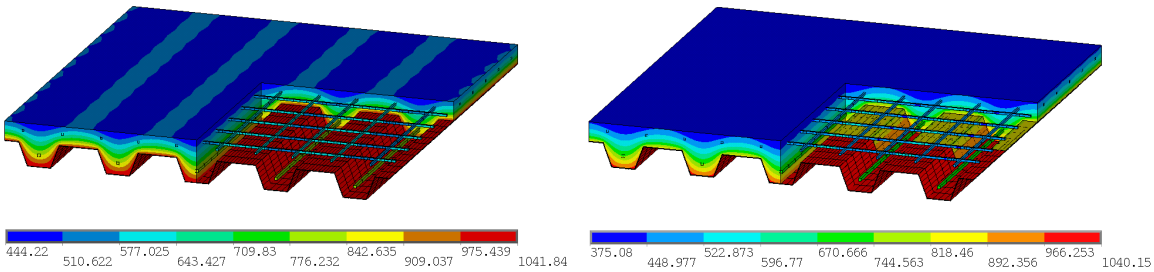

a) Perfect contact (t_a = 0 mm). b) t_a = 1 mm.

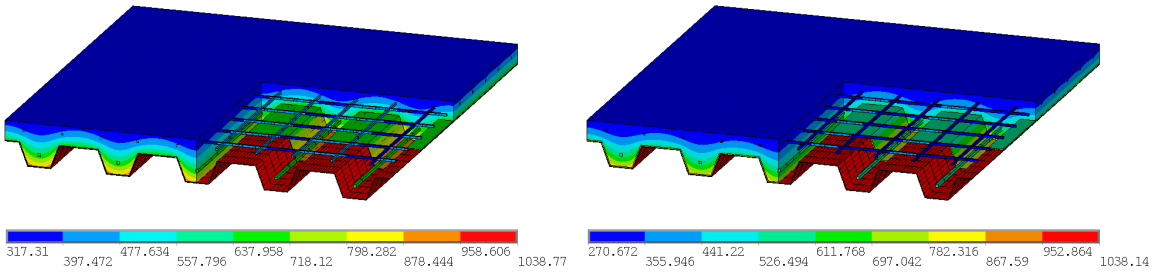

c) t_a = 2 mm. d) t_a = 3 mm.

Figure 4.13: Temperature distribution in slab 1 after 120 minutes of fire exposure for different air gap thicknesses (ANSYS, second parametric study).

According to the results above, it can be observed that the temperatures on the unexposed side of the slab are strongly affected by the air gap thickness. This means that this parameter plays a fundamental role on the fire resistance of composite slabs. In

addition, the temperature distribution within the ribs is also influenced by the thickness of the air layer however the temperature oscillation through the upper continuous part of the slab is not significantly affected.

4.2.2 Critical temperatures

The critical temperatures for each steel component have been determined from the first parametric study, considering perfect thermal contact between the materials.

Figure 4.14 presents the relationship between the critical temperature of each steel component T_{crit} and the effective thickness h_{eff} for all slabs. The critical temperatures of the rebars are given only for slabs with a rebar diameter of 8 mm, which is the critical situation because result in higher temperatures in comparison to the slabs with larger diameters. Furthermore, these critical temperatures are given for the concrete covers of rebar d'_{reb} of 30 mm and 60 mm.

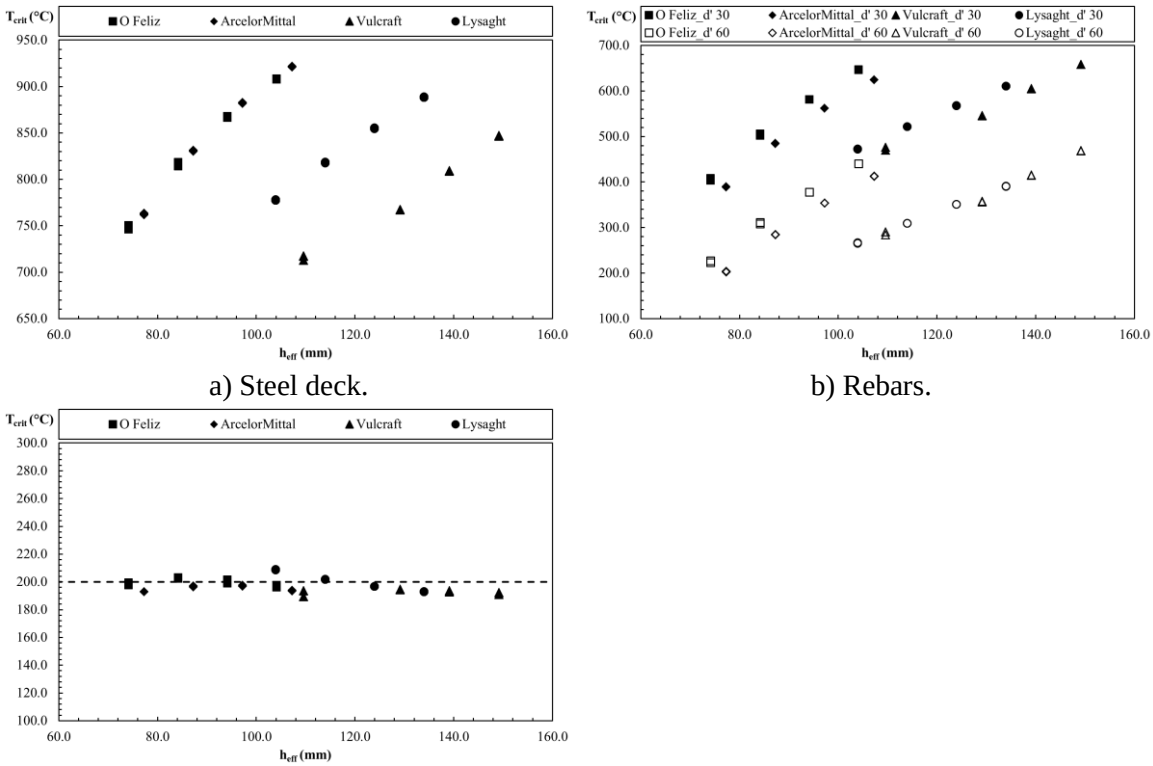

a) Steel deck. b) Rebars.

c) Anti-crack mesh.

Figure 4.14: Critical temperatures of the steel components for all the slabs (ANSYS, first parametric study).

For the critical temperatures of the steel deck, it is observed that the slabs with trapezoidal profiles present results close to each other and follow a similar pattern of

increase with the effective thickness. On the other hand, the slabs with re-entrant profile present different results between each other and have an almost linear increase pattern.

With respect to the critical temperatures of the rebars, a similar pattern of increase is noticed between slabs with both trapezoidal and re-entrant steel deck profile. The critical temperatures are considerably higher for slabs with d'_{reb} = 30 mm in comparison to slabs with d'_{reb} = 60 mm. These remarkable differences are due to the fact that higher concrete covers for rebar provide higher fire protection to these elements, reflecting on reduced temperatures in these components.

For the critical temperatures of the anti-crack mesh, all the results obtained for the slabs with trapezoidal and re-entrant steel deck are around a constant temperature of 200 °C. This is due to the fact that the fire resistance time increases with the effective thickness, and the position of the anti-crack mesh does not change from simulation to simulation.

4.2.3 Temperatures of the steel components

The temperatures of the steel components of the composite slabs have been determined from the first parametric study, considering perfect thermal contact between all the materials.

4.2.3.1 Parts of the steel deck

The results presented in this subsection are related to slabs with rebar diameter of 8 mm and concrete cover for rebar of 30 mm.

Figure 4.15 presents the relationship between the effective thickness h_{eff} and the temperature of the lower flange of the steel deck θ_a for different classes of fire resistance, namely R60, R90 and R120.

According to the results below, it is observed that all the temperatures present a slight decrease with the effective thickness. The temperatures of the slabs with trapezoidal steel deck are considerably close to each other. Otherwise, for the temperatures of the slabs with re-entrant profile, greater differences are obtained. The discrepancy observed in the temperature for the Lysaght profile for the fire resistance class R90 is probably due to numerical errors.

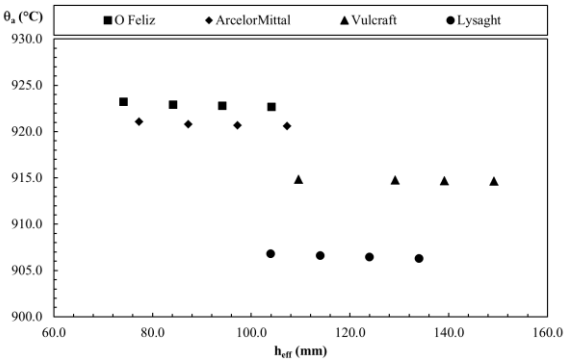

a) R60.

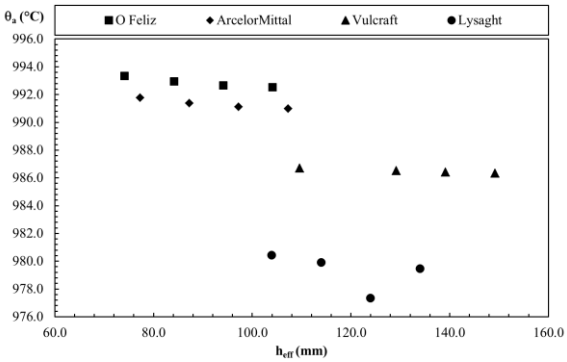

b) R90.

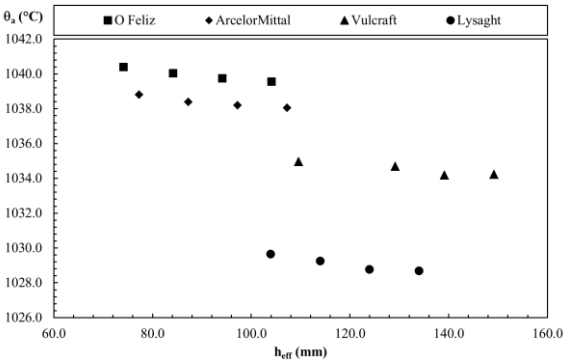

c) R120.

Figure 4.15: Temperatures of the lower flange for different classes of fire resistance (R) for all the slabs (ANSYS, first parametric study).

Figure 4.16 illustrates the relationship between the effective thickness h_{eff} and the temperature of the web θ_a for different classes of fire resistance for all the slabs.

From the results below, it can be concluded that, as observed for the temperatures of the lower flange, the temperatures of the slabs with trapezoidal steel deck are closer to each other when compared to the slabs with re-entrant steel deck. In addition, the slabs with trapezoidal profiles result in considerably higher temperatures in comparison to the slabs with re-entrant profiles. These differences can be explained by the great difference between the view factors of these slabs.

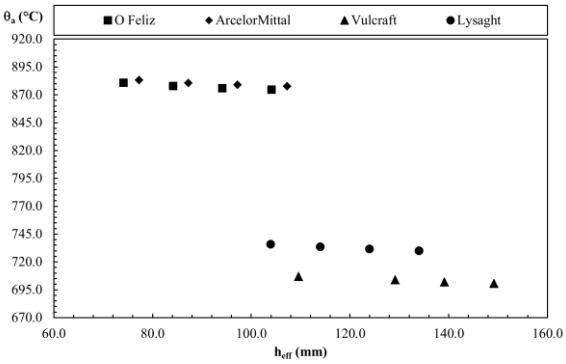

a) R60.

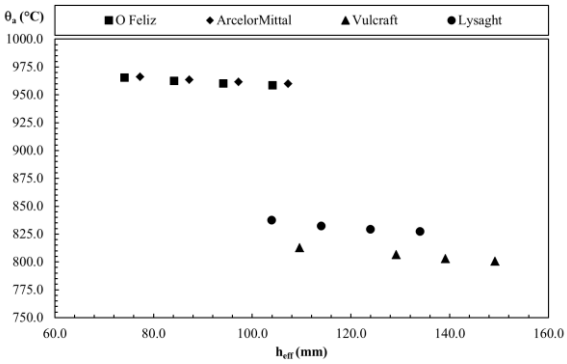

b) R90.

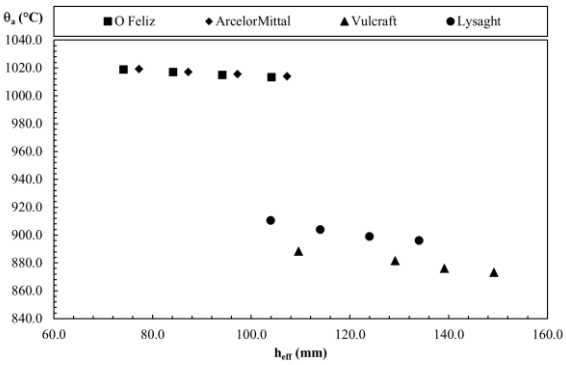

c) R120.

Figure 4.16: Temperatures of the web for different classes of fire resistance (R) for all the slabs (ANSYS, first parametric study).

The following figure illustrates the relationship between the effective thickness h_{eff} and the temperatures of the upper flange θ_a for the classes of fire resistance (R) for all the slabs.

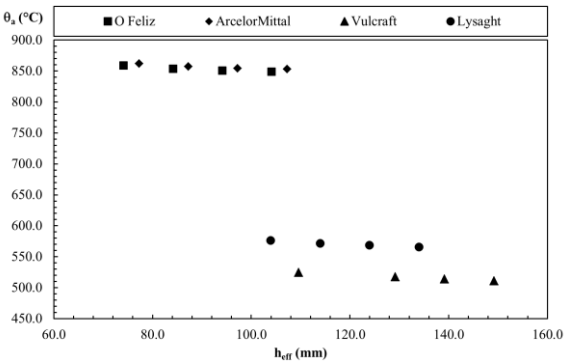

a) R60.

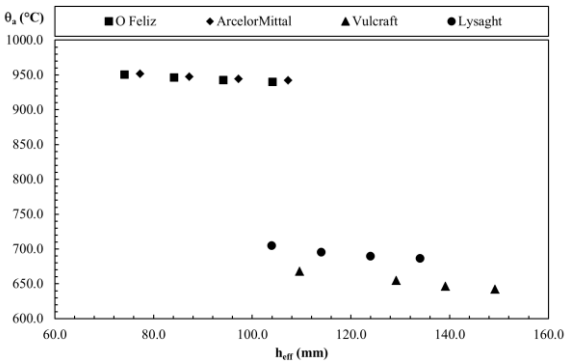

b) R90.

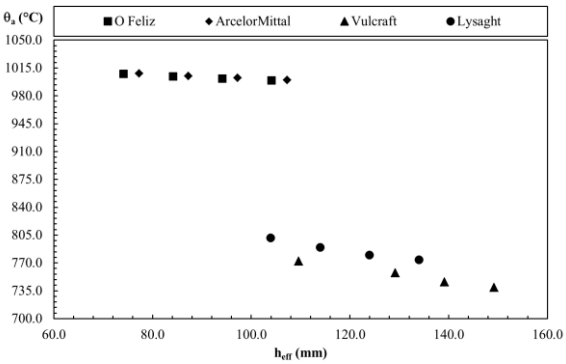

c) R120.

Figure 4.17: Temperatures of the upper flange for different classes of fire resistance (R) for all the slabs (ANSYS, first parametric study).

According to the results above, it is observed that the differences between the temperatures of the upper flange of slabs with trapezoidal and re-entrant profiles are even greater than those of the web. The temperatures of the slabs with trapezoidal steel deck are also quite similar.

4.2.3.2 Reinforcement bars

The temperatures of the rebars have been determined for slabs with concrete cover for rebar d'_{reb} of 30 mm. The results for slab 3 are not included in this subsection due to some discrepancies which were detected.

Figure 4.18 presents the relationship between the temperature of the rebars θ_a for the fire resistance class R60 and the diameter of the rebars ϕ_{reb}, for slabs with trapezoidal and re-entrant steel deck profiles.

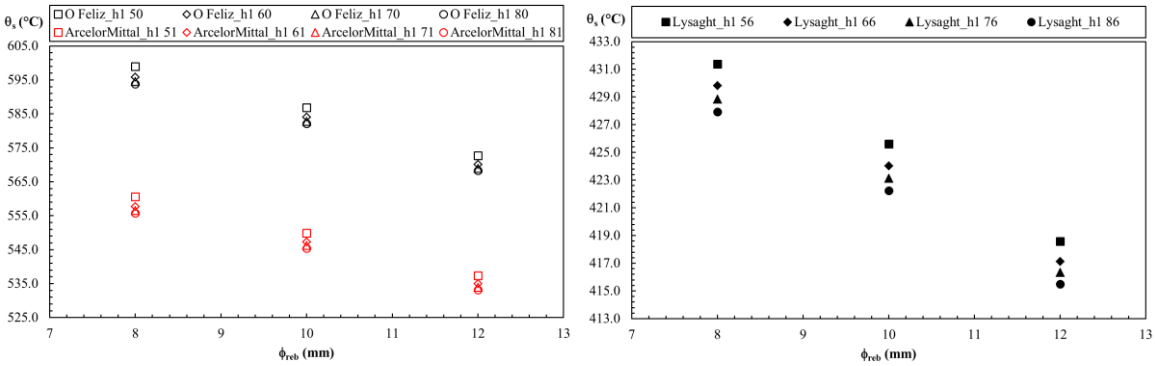

a) Trapezoidal profiles. b) Re-entrant profile.

Figure 4.18: Relationship between the temperature of the rebars for R60 and its diameter, for different concrete thicknesses (ANSYS, first parametric study).

From the results above, it can be observed that the concrete thickness has fairly small effect on the fire resistance and the smaller the thickness of this layer, the higher the temperature of the rebars. On the other hand, the diameter of these components has considerable influence on its temperature. The temperature θ_a significantly decreases with the diameter of the rebars, resulting in maximum temperature differences of 26.2 °C for slab 1, 23.2 °C for slab 2, and 12.8 °C for slab 4. Furthermore, a noticeable difference is observed between the temperatures of the slabs with trapezoidal and re-entrant profiles.

Figures 4.19 and 4.20 present the variation of the temperature of the rebars θ_a with its diameter ϕ_{reb} for the fire resistance classes R90 and R120, respectively. The results are given only for slabs with the smallest concrete thickness for each group of slabs, which is the critical case because result in higher temperatures.

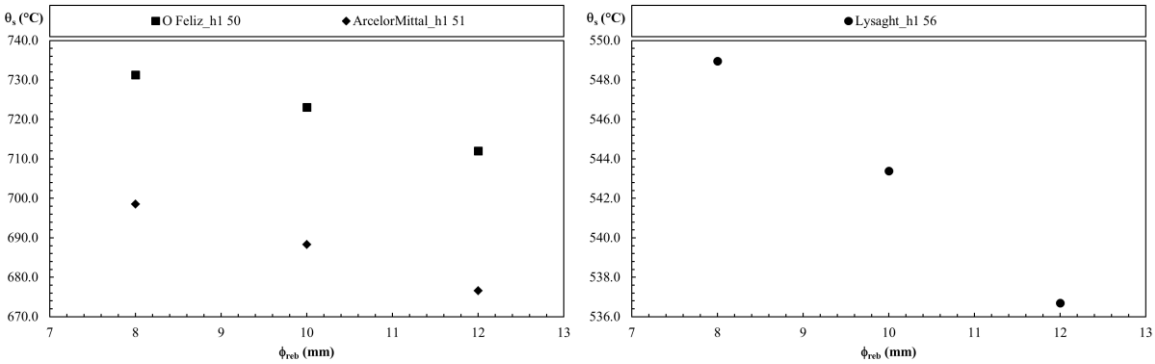

a) Trapezoidal profiles. b) Re-entrant profile.

Figure 4.19: Relationship between the temperature of the rebars for R90 and its diameter (ANSYS, first parametric study).

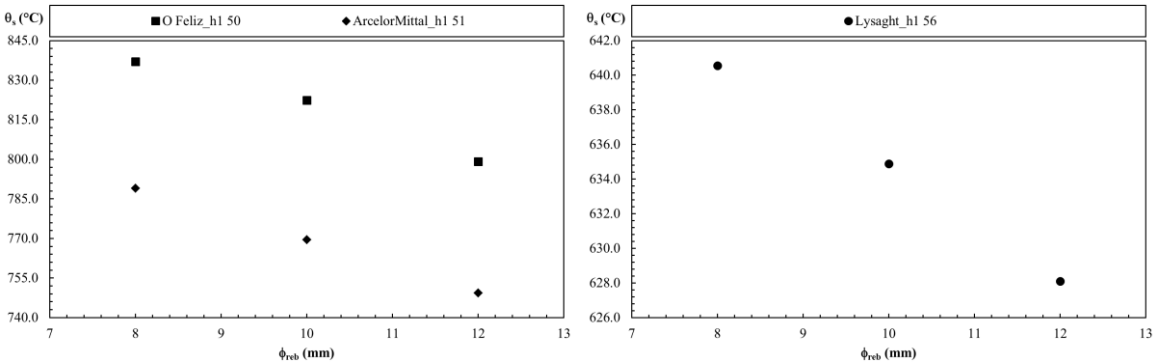

a) Trapezoidal profiles. b) Re-entrant profile.

Figure 4.20: Relationship between the temperature of the rebars for R120 and its diameter (ANSYS, first parametric study).

With respect to the temperatures for the fire resistance class R90, a reasonable decrease is observed in the temperature θ_a with the increase of the diameter of the rebars, resulting in maximum temperature differences of 19.3 °C for slab 1, 22.0 °C for slab 2, and 12.3 °C for slab 4. For the fire resistance class R120, these differences are of 37.8 °C for slab 1, 39.7 °C for slab 2, and 12.5 °C for slab 4.

5. COMPARISONS OF RESULTS

5.1 Validation of the thermal models

For the validation of the numerical thermal models, four different experimental fire tests have been selected: Abdel-Halim, Hakmi and O'Leary [4] (test no. 2); Hamerlinck [6] (test no. 2); Lim [34] (test no. 4); and Prates [41] (test no. 1). A description of the test setup and the results of each fire test are given in the Appendix A.

Table 5.1 presents some characteristics of the slabs and parameters which have been considered in the numerical analyses for the validation of the thermal models, according to information of each fire test.

Table 5.1: Parameters considered for the validation models.

Slab no.	Experimental fire test	Steel deck profile	Φ_{up}	Φ_{web}	u (%)	T_0 (°C)
1	Abdel-Halim, Hakmi and O'Leary	-	0.78032	0.62147	3.0	20
2	Hamerlinck	Prins PSV 73	0.39357	0.36221	3.5	20
3	Lim	Dimond Hibond	0.80007	0.63442	5.6	13
4	Prates	O Feliz H60	0.72325	0.56707	3.0	20

The specific heat of concrete c_p as function of temperature at these values of moisture content u is given in Figure 2.11.

Figures 5.1, 5.2, 5.3 and 5.4 illustrate the temperature development (numerical and experimental) at different selected points as well as the average and maximum temperatures at the unexposed surface of the slab for the four validation models.

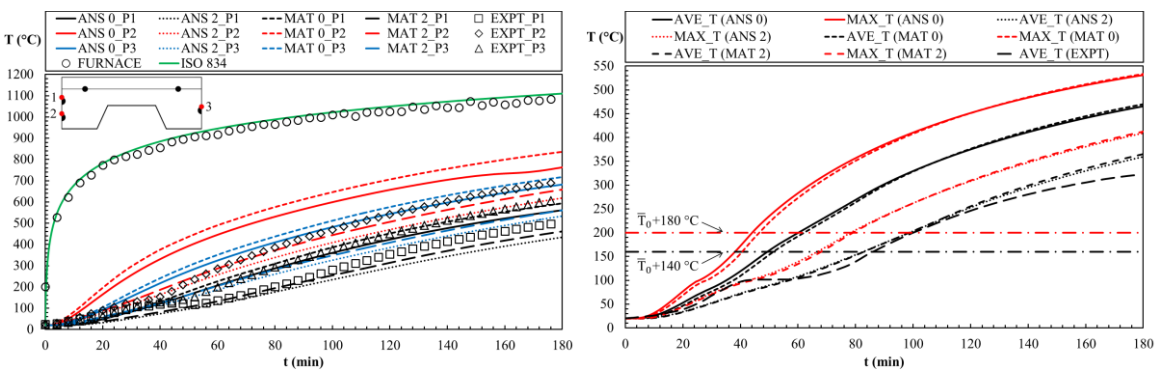

a) Selected points. b) Unexposed side.

Figure 5.1: Numerical and experimental results for slab 1 – Points 1, 2 and 3 at distance 50, 85 and 70 mm from the top.

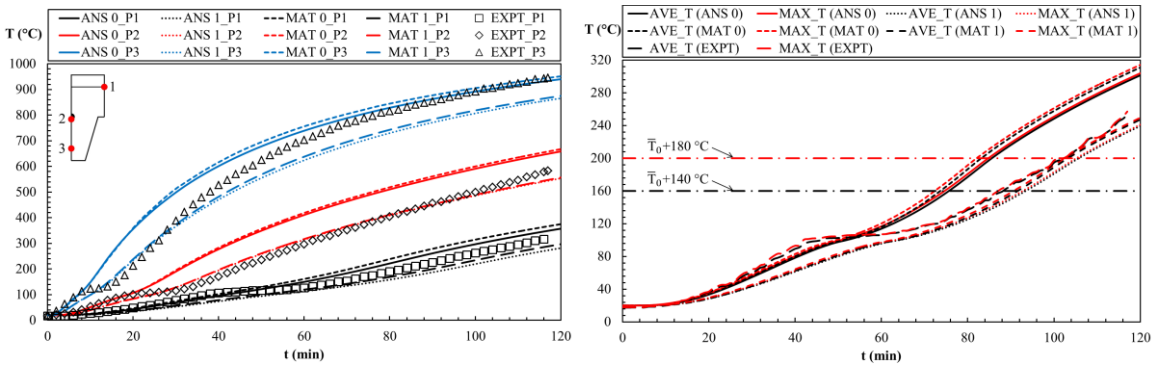

a) Selected points. b) Unexposed side.

Figure 5.2: Numerical and experimental results for slab 2 – Points 1, 2 and 3 at distance 20, 74 and 123 mm from the top.

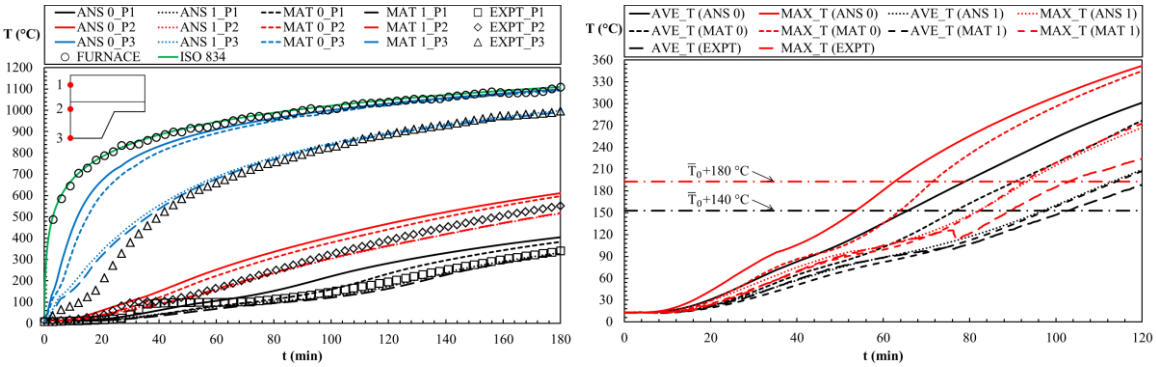

a) Selected points. b) Unexposed side.

Figure 5.3: Numerical and experimental results for slab 3 – Points 1, 2 and 3 at distance 20, 70 and 130 mm from the top.

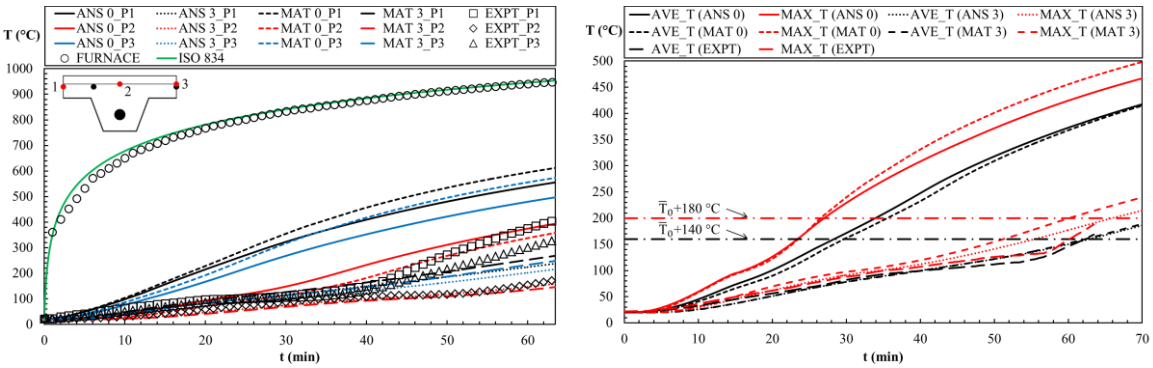

a) Selected points. b) Unexposed side.

Figure 5.4: Numerical and experimental results for slab 4 – Points 1, 2 and 3 at distance 20, 15 and 15 mm from the top.

With respect to the results for slab 1, it is noteworthy that the furnace temperature is under the standard fire curve ISO 834, which was used for the numerical simulations. Consequently, the numerical results should be higher than experimental results. For the perfect contact models ANS 0 and MAT 0, a good agreement with experimental results (EXPT) is observed for point 1 until the first 44 minutes of fire.

After that, better results are obtained using the air gap models ANS 2 and MAT 2 (air gap thickness of 2 mm). This is because during a fire, the debonding of the steel deck from concrete occurs after a period of time. A delay in the rate of temperature increase is observed in the last minutes of fire on curve ANS 0_P2. It can be justified by the coincidence of two different materials (steel and concrete) on the same node and the abrupt change in the specific heat of steel for temperatures between 700 °C and 800 °C, see Figure 2.14. In general, the results for the air gap models present better agreement with measured temperatures in comparison to the results for the perfect contact models. For the selected points, the models ANS 0 and MAT 2 present better agreement with experimental results when compared to the models MAT 0 and ANS 2, respectively. Considerable differences between ANSYS and MATLAB models are evident, mainly for the curves ANS 0_P2 and MAT 0_P2. On the other hand, the results for these models are very close to each other for the unexposed surface.

From the results for slab 2, it can be observed that the temperature development on the selected points is quite similar between the experimental results EXPT and the perfect contact models ANS 0 and MAT 0 at the first minutes of heating. After that, better results are obtained using the air gap models ANS 1 and MAT 1 (air gap thickness of 1 mm), with exception to point 3. Regarding the temperature development on point 2, the air gap models present good agreement with experimental results for temperatures over 100 °C. For point 3, at the last minutes of heating, the perfect contact model presents better agreement with measured temperatures in comparison to the air gap model. Concerning the temperature development on the unexposed surface, the maximum and average temperature curves are very close to each other for all the models. In this case, better agreement with the experimental results is observed using the air gap models.

Regarding the results for slab 3, a reasonable agreement is observed between the furnace temperature and the standard fire curve ISO 834. For both perfect contact models ANS 0 and MAT 0, a considerable difference to experimental results (EXPT) can be observed in the first stages of heating. The numerical results from MATLAB are slightly closer to experimental results than results from ANSYS. The air gap models ANS 1 and MAT 1 (air gap thickness of 1 mm) provide a good agreement to measured temperatures for all selected points. With respect to the unexposed surface, a big difference between the results for the perfect contact models and the air gap models is verified. For the models ANS 1 and MAT 1, the agreement between the computed and

measured temperatures is very good for both average and maximum temperatures until 76 minutes. After that, some differences are noticed, probably due to experimental deviations such as the furnace temperature, for example. In general, small differences between the results of ANSYS and MATLAB models are observed.

Concerning the results for slab 4, the furnace temperature is very close to the standard fire curve ISO 834, although presenting a small deviation in the first minutes of fire. For the perfect contact models ANS 0 and MAT 0, the temperatures are higher than the experimental results (EXPT) throughout the entire duration of the test. The temperatures for the air gap models ANS 3 and MAT 3 (air gap thickness of 3 mm) are considerably smaller than those for the perfect contact models, and present satisfactory agreement with measured temperatures, mainly for points 2 and the average temperature on the unexposed side. For points 1 and 3, the results for the air gap models present good agreement with measured temperatures until the first 42 minutes of fire. Some differences are observed between the results of ANSYS and MATLAB models, being greater for the perfect contact models.

The following tables present the numerical, experimental and analytical results obtained for the fire resistance according to the insulation criterion, with respect to the average temperature rise (t_{fi} Ave) and the maximum temperature rise (t_{fi} Max) on the unexposed surface of each slab.

Table 5.2: Fire resistance (I) of slab 1: numerical, experimental and analytical results.

Fire resistance	**Model ANS 0**	**Model MAT 0**	**Model ANS 2**	**Model MAT 2**	**EXPT result**	**EN 1994-1-2**
t_{fi} Ave (min)	49.4	51.4	82.6	82.9	*80.0*	*73.9*
t_{fi} Max (min)	*44.1*	*46.5*	*78.3*	*79.1*	-	

Table 5.3: Fire resistance (I) of slab 2: numerical, experimental and analytical results.

Fire resistance	**Model ANS 0**	**Model MAT 0**	**Model ANS 1**	**Model MAT 1**	**EXPT result**	**EN 1994-1-2**
t_{fi} Ave (min)	*75.6*	*73.6*	*93.5*	*91.6*	*88.2*	*106.5*
t_{fi} Max (min)	84.8	82.0	105.1	102.5	102.1	

Table 5.4: Fire resistance (I) of slab 3: numerical, experimental and analytical results.

Fire resistance	Model ANS 0	Model MAT 0	Model ANS 1	Model MAT 1	EXPT result	EN 1994-1-2
t_{fi} Ave (min)	65.6	76.7	97.0	97.7	*102.7*	*95.8*
t_{fi} Max (min)	*62.6*	*71.4*	*93.3*	*92.5*	103.0	

Table 5.5: Fire resistance (I) of slab 4: numerical, experimental and analytical results.

Fire resistance	Model ANS 0	Model MAT 0	Model ANS 3	Model MAT 3	EXPT result	EN 1994-1-2
t_{fi} Ave (min)	28.3	29.7	*62.8*	62.3	*62.2*	*38.0*
t_{fi} Max (min)	*27.0*	*26.5*	65.9	*60.1*	-	

Regarding the slab 1, the results evidence that the fire resistance obtained using the air gap models is slightly underestimated, with a relative error of 2.1% for ANSYS and 1.1% for MATLAB. In addition, a good agreement between EN 1994-1-2 calculations and experimental data is observed, resulting in a relative error of 7.6%.

According to the results for slab 2, it can be concluded that the air gap models slightly overestimated the fire resistance, with a relative error of 6.0% for ANSYS and 3.9% for MATLAB. A bigger discrepancy is obtained using the perfect contact models, with a relative error of 14.3% for ANSYS and 16.6% for MATLAB. The EN 1994-1-2 provisions overestimated the fire resistance, providing an unsafe result with a relative error of 20.7%.

The results obtained with the air gap models underestimate the fire resistance for slab 3, with a relative error of 9.2% for ANSYS and 9.9% for MATLAB. Better approximation to experimental results is observed for the EN 1994-1-2 provisions, with a relative error of 6.7%.

With respect to slab 4, a good agreement between the fire resistance obtained with the air gap models and experimental results is achieved, resulting in a relative error of 1.0% for ANSYS and 3.4% for MATLAB. An underestimated value is obtained using the EN 1994-1-2 provisions, with a relative error of 38.9%.

The thicknesses of the air layer t_a used in the air gap models were determined from parametric analyses, selecting the values that best fit with the experimental results.

5.2 ANSYS and MATLAB results

In general, the numerical results from ANSYS and MATLAB are very similar to each other, see Tables 5.2 to 5.5. Figure 5.5 presents the relationship between the effective thickness h_{eff} and the ratio between the fire resistance t_{fi} obtained in ANSYS and MATLAB. The results are given for the slabs of the second parametric study (air gap models) and the validation models (perfect contact models and air gap models).

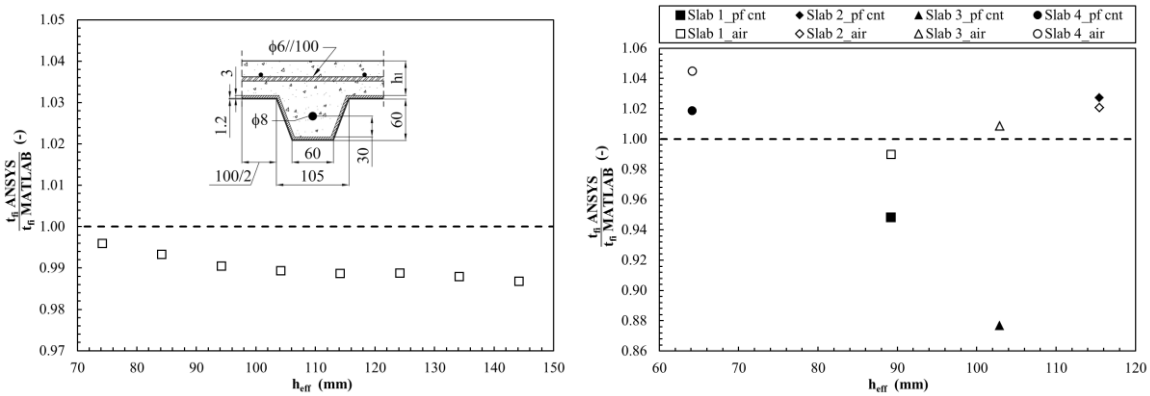

a) Second parametric study. b) Validation models.

Figure 5.5: Comparison between the numerical results: ANSYS and MATLAB.

According to the results for the second parametric study, it is observed that all the results for fire resistance from MATLAB are higher than those from ANSYS, presenting a maximum difference of 2.7 min. These differences increase with the effective thickness of the slab.

For the results of the validation models, it can be observed that the results from ANSYS and MATLAB for the perfect contact models are quite similar, with exception to slab 3, which presents a difference of 8.8 min. For most of the cases the values for the fire resistance from MATLAB were smaller than those of ANSYS.

5.3 Numerical results and Eurocode 4 – Part 1-2

As the results from ANSYS and MATLAB are quite similar, this subsection deals only with the results from ANSYS.

Figure 5.6 presents a comparison between the results obtained numerically (ANSYS) and through the simplified calculation method of Eurocode 4 – Part 1-2 (EC4) for the fire resistance (I), according to the effective thickness h_{eff} of the composite slabs. The results are given for the slabs of the first parametric study (perfect contact model) and second parametric study (perfect contact and air gap model).

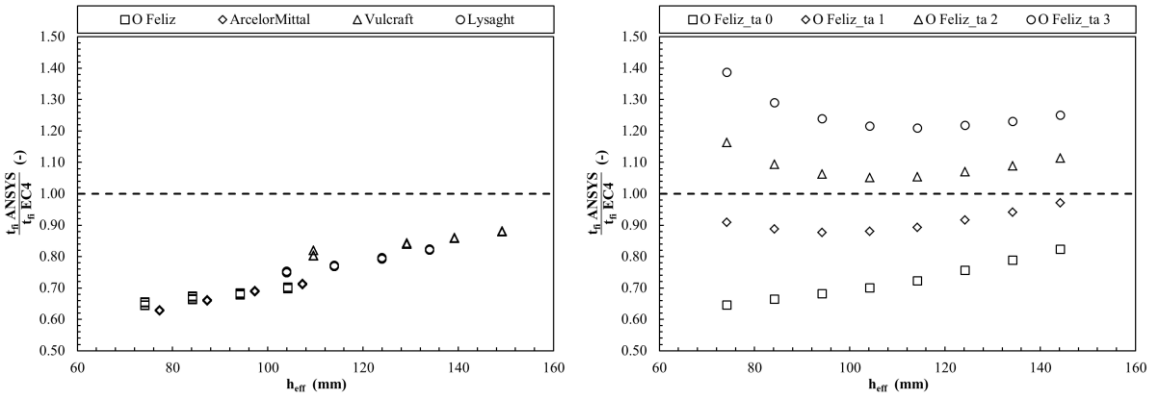

a) First parametric study. b) Second parametric study.

Figure 5.6: Comparison between the numerical results from ANSYS and Eurocode 4 – Part 1-2 for the fire resistance (I).

For the first parametric study, it is observed that all the results obtained in ANSYS are smaller than the Eurocode 4 provisions, presenting a maximum difference of 30.2 min. Concerning the second parametric study, it can be observed that the numerical results from ANSYS for the air gap model O Feliz_ta 2 (air gap thickness of 2 mm) present good agreement with the Eurocode 4 provisions.

Figures 5.7, 5.8 and 5.9 present the numerical results obtained in ANSYS and the Eurocode 4 provisions (EC4) for the temperatures of the lower flange, web and upper flange, according to different classes of fire resistance (R).

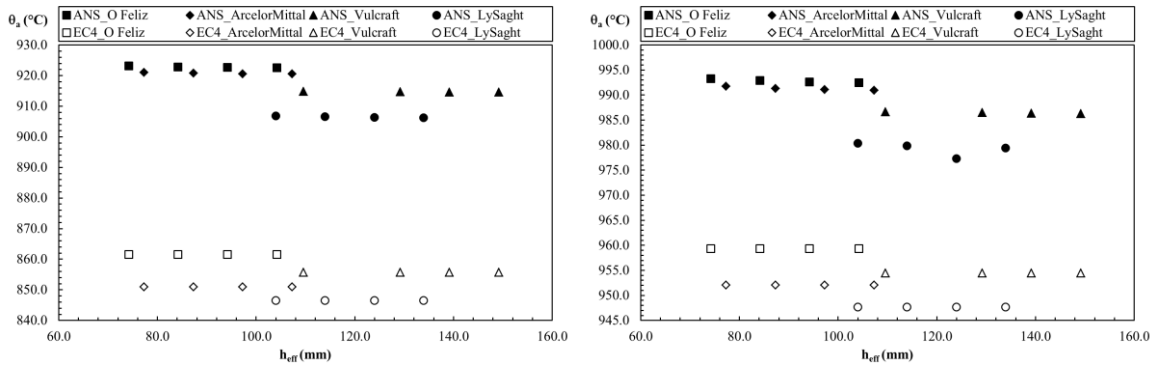

a) R60. b) R90.

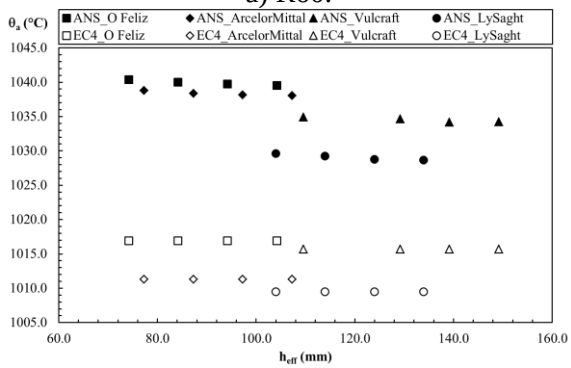

c) R120.

Figure 5.7: Comparison between the numerical results (ANSYS) and EN 1994 – 1-2 provisions for the temperatures of the lower flange for different classes of fire resistance (R).

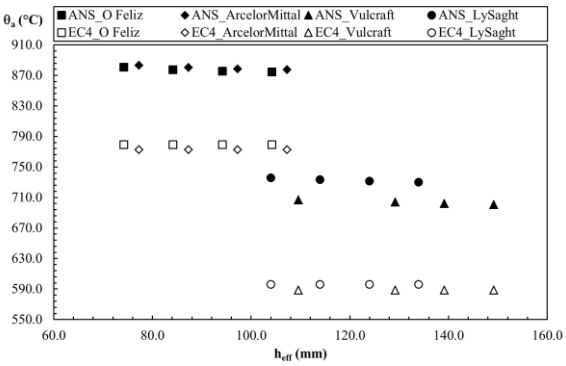

a) R60.

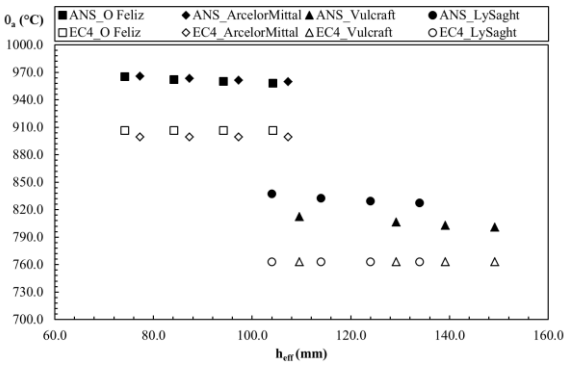

b) R90.

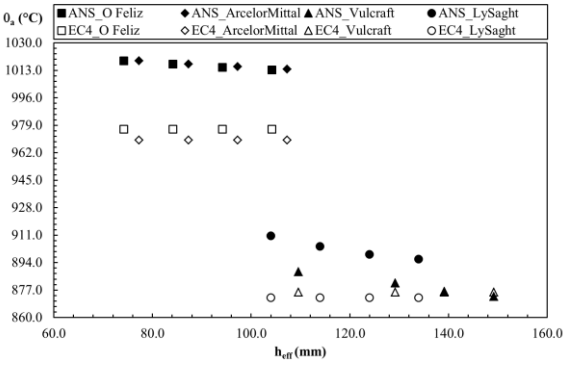

c) R120.

Figure 5.8: Comparison between the numerical results (ANSYS) and EN 1994 – 1-2 provisions for the temperatures of the web for different classes of fire resistance (R).

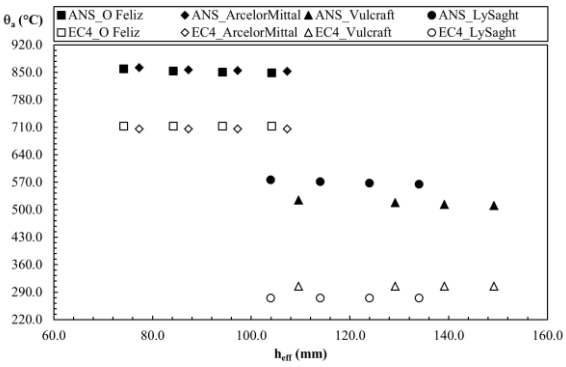

a) R60.

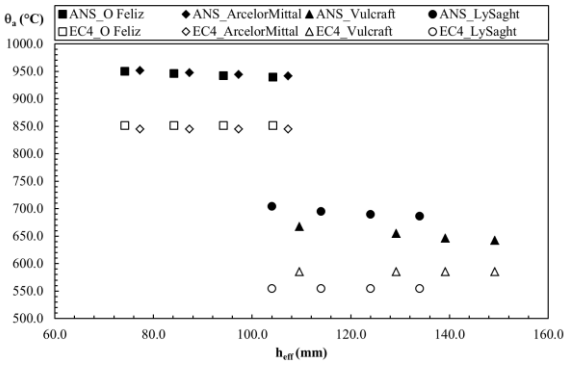

b) R90.

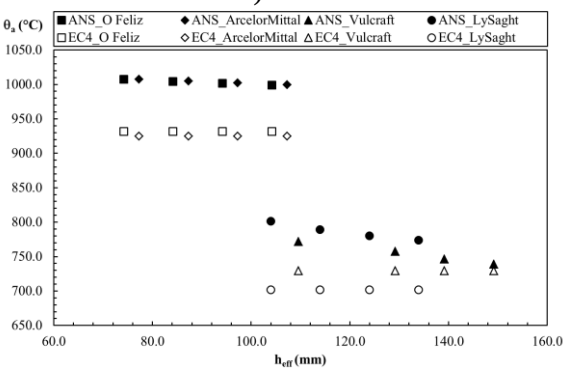

c) R120.

Figure 5.9: Comparison between the numerical results (ANSYS) and EN 1994 – 1-2 provisions for the temperatures of the upper flange for different classes of fire resistance (R).

In general, it is observed that the results from the Eurocode 4 – Part 1-2 for the temperature of the parts of the steel deck θ_a are considerably inferior to the numerical results.

Figures 5.10, 5.11 and 5.12 give the relationship between the diameter of the rebars ϕ_{reb} and the results for its temperature θ_s, obtained numerically (ANSYS) and through the Eurocode 4 calculation rules (EC4), for different classes of fire resistance (R).

Analysing the results below, it can be concluded that the temperatures obtained numerically are higher than the Eurocode 4 results for most of the analyses (81.5%). In addition, it is noteworthy that the simplified calculation method of the standard does not include the effect of the diameter of the rebars on its temperature.

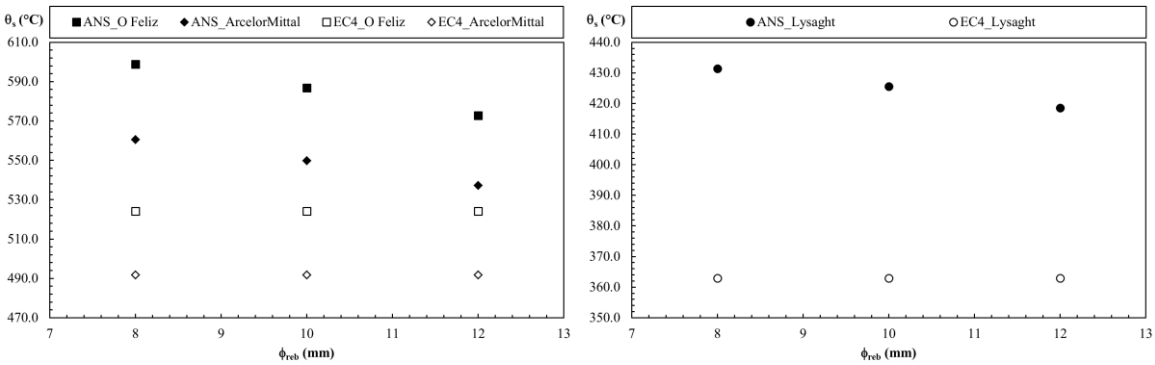

a) Trapezoidal profiles. b) Re-entrant profile.

Figure 5.10: Comparison between the numerical results (ANSYS) and EN 1994 – 1-2 provisions for the temperatures of the rebars for R60.

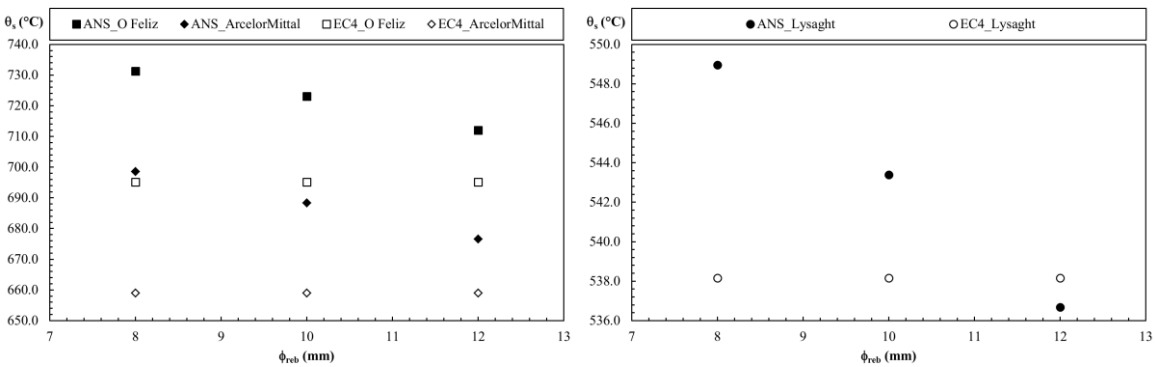

a) Trapezoidal profiles. b) Re-entrant profile.

Figure 5.11: Comparison between the numerical results (ANSYS) and EN 1994 – 1-2 provisions for the temperatures of the rebars for R90.

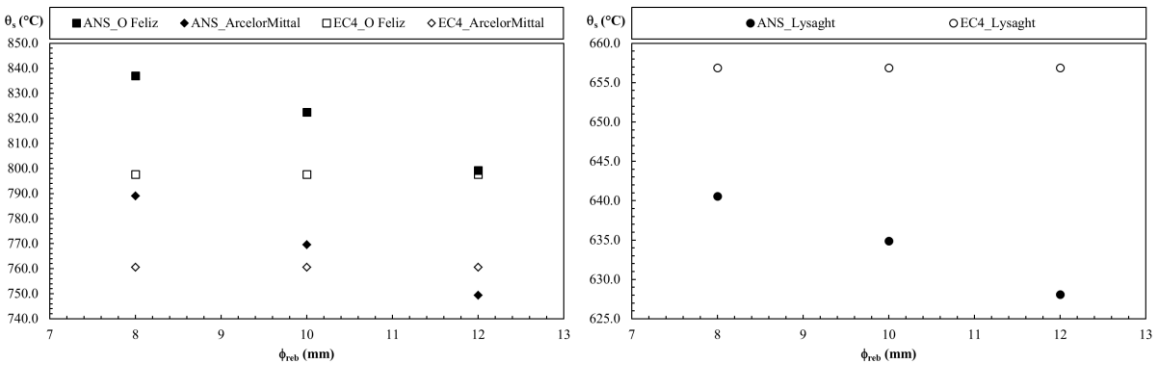

a) Trapezoidal profiles. b) Re-entrant profile.

Figure 5.12: Comparison between the numerical results (ANSYS) and EN 1994 – 1-2 provisions for the temperatures of the rebars for R120.

5.4 Numerical results and NBR 14323

As the results from ANSYS and MATLAB are quite similar, this subsection deals only with the results from ANSYS.

Figure 5.13 presents the relationship between the ratios of the numerical results (ANSYS) to the calculation rules of NBR 14323 (NBR) for the fire resistance (I), and the effective thickness h_{eff} of the composite slabs. The results are given for the slabs of the first parametric study (perfect contact model) and second parametric study (perfect contact and air gap model).

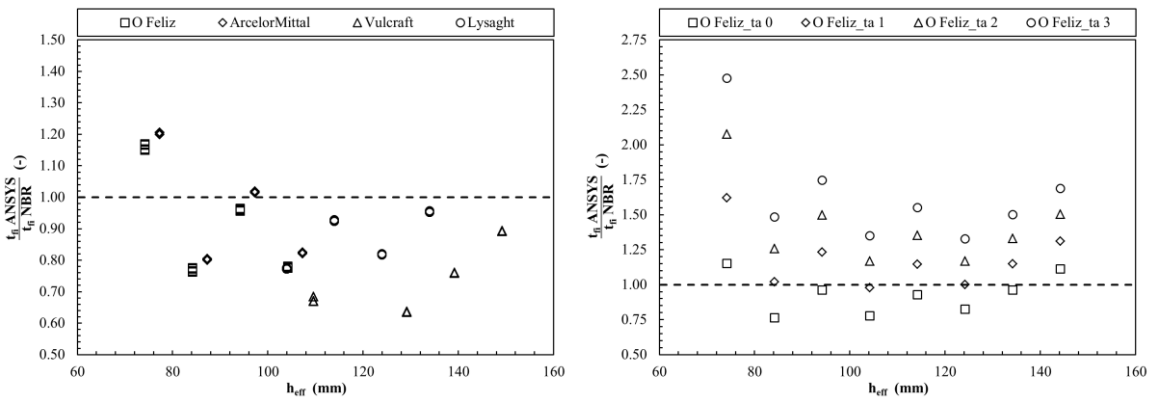

a) First parametric study. b) Second parametric study.

Figure 5.13: Comparison between the numerical results from ANSYS and NBR 14323 for the fire resistance (I).

With respect to the first parametric study, it can be observed that most of the numerical results for the fire resistance are smaller than the results from the NBR 14323 (81.3%). For the second parametric study, it can be concluded that the results from the

perfect contact model (O Feliz_ta 0) presented better agreement with the results from the Brazilian Standard in comparison to the air gap models.

The calculation rules for the temperatures of the steel components of the NBR 14323, for the calculation of the sagging moment resistance, are the same as those from the Eurocode 4 – Part 1-2. Therefore, for the comparison between these results and numerical results refer to the previous subsection.

5.5 General comparison

Figure 5.14 presents the results for the fire resistance (I) obtained through the numerical models (ANSYS and MATLAB); experimental fire tests (EXPT); and simplified calculation methods (EN 1994 – 1-2 and NBR 14323:2013). These results are given as function of the effective thickness h_{eff} for the slabs of the second parametric study.

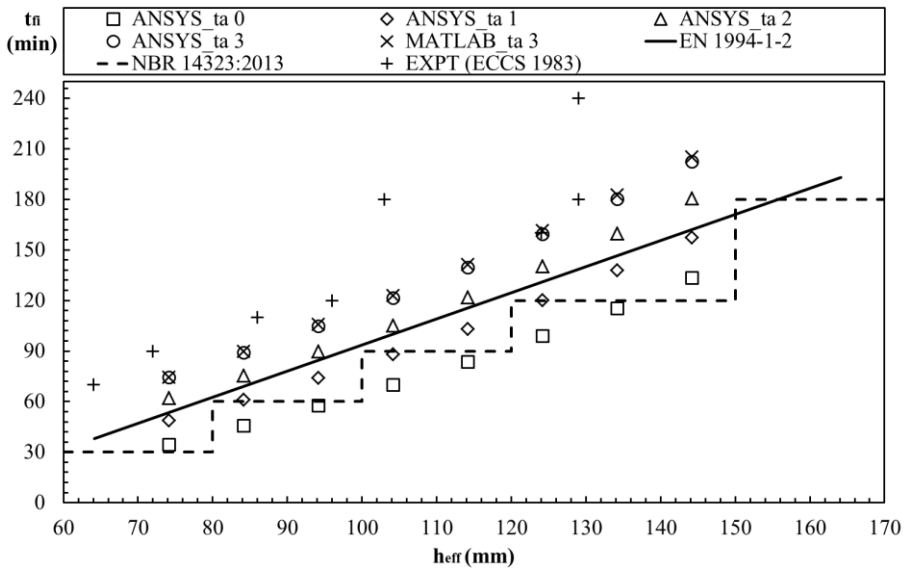

Figure 5.14: Comparison between numerical, experimental and analytical results for fire resistance (I): second parametric study.

From the results above, it can be observed that the numerical results of the air gap models ANSYS_ta 3 and MATLAB_ta 3 (air gap thickness of 3 mm) present better agreement with experimental results in comparison to the other numerical models. Furthermore, the model which presents results that best approximate to those of the European standard is the air gap model ANSYS_ta 2 (air gap thickness of 2 mm). The numerical model ANSYS_ta 0 (perfect contact model) presents good agreement with the results of the Brazilian standard.

According to the numerical results, there is a non-linear dependence between the fire resistance t_{fi} and the effective thickness h_{eff} which is not considered in the simplified calculation methods of both European and Brazilian standard. In addition, the thickness of the air layer t_a is an important parameter which can significantly affect the fire resistance and may be considered in calculation methods.

5.5.1 Proposed new formulae

A model with quadratic dependence between the fire resistance t_{fi} and the effective thickness h_{eff} is chosen to fit the results of the numerical simulations. A linear relationship between the effective thickness and the thickness of the air gap t_a is considered in order to take into account the increase of fire resistance. The proposed new equation for the fire resistance of composite slabs is given in Eq. 5.1.

$$t_{fi} = 0.0059 \cdot h_{eff}{}^2 + 0.1127 \cdot h_{eff} - 5.8065 + \left(0.1424 \cdot h_{eff} + 2.4672\right) \cdot t_a \qquad (5.1)$$

Where t_{fi} is given in minutes, and h_{eff} and t_a are given in millimetres; with the following limits: $70 \leq h_{eff} \leq 150$ mm and $0 \leq t_a \leq 3$ mm.

Figure 5.15 illustrates the results obtained with the application of Eq. 5.1 (New Eq) for different air gap thicknesses.

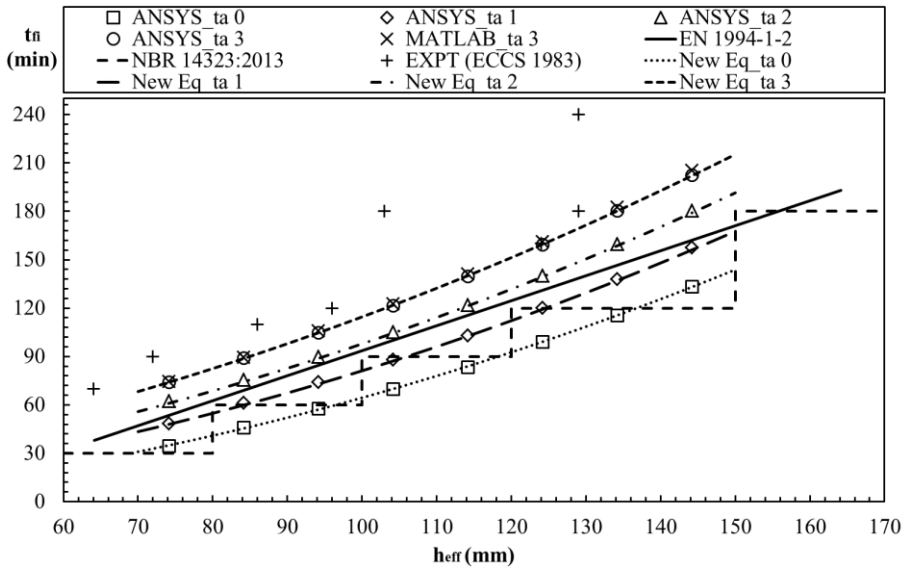

Figure 5.15: Results of the proposed new equation for the fire resistance (I) of composite slabs.

Analysing the graph above, a good agreement is observed between the results of the proposed new equation and the numerical results.

Table 5.6 presents a comparison between the results of the proposed new equation for t_{fi}, and numerical and experimental results for the validation models. The results for "Eq. 5.1 air gap" for each slab were obtained using the same air gap thickness of the corresponding numerical model.

Table 5.6: Validation models: numerical, experimental and analytical results.

t_{fi} (min)	Abdel-Halim, Hakmi and O'Leary	Hamerlinck	Lim	Prates
ANSYS pf. contact	44.1	75.6	62.6	27.0
ANSYS air gap	78.3	93.5	93.3	62.8
Eq. 5.1 pf. contact	51.2	85.9	68.2	25.7
Eq. 5.1 air gap	81.5	104.8	85.3	60.5
EN 1994 – 1-2	73.9	106.5	95.8	38.0
Experimental	80.0	88.2	102.7	62.2

Based on the differences between the numerical results and the Eurocode 4 calculation rules for the temperature of the parts of the steel deck, new coefficients are proposed for composite slabs with normal weight concrete. The following table presents these coefficients for different classes of fire resistance (R).

Table 5.7: Proposed new coefficients for the temperature of the parts of the steel deck for slabs with NWC.

Standard fire resistance	Part of the steel deck	b_0 (°C)	b_1 (°C mm)	b_2 (°C mm)	b_3 (°C)	b_4 (°C)
R60	Lower flange	*1015*	-1197	-2.32	86.4	*-147.5*
	Web	*725*	*600*	*-2.00*	537.7	*-356.0*
	Upper flange	*474*	*1300*	*-1.95*	1148.4	*-777.0*
R90	Lower flange	*939.5*	*95.0*	*1.00*	*93.0*	*-78.3*
	Web	*848.0*	*345.0*	-2.21	464.9	*-308.6*
	Upper flange	*641.5*	*854.0*	*-1.55*	*700.0*	*-315.0*
R120	Lower flange	*1106.0*	*-995.0*	*-1.55*	46.7	-82.8
	Web	*920.0*	*300.0*	-1.82	344.2	*-199.0*
	Upper flange	*764.0*	*660.0*	-1.67	592.6	*-271.0*

In the table above, the numbers which are not highlighted were not modified in relation to the current calculation rules of the European standard. A comparison between the results of the proposed new formulation, ANSYS and Eurocode 4 is given in the Appendix G of the underlying work.

With respect to the temperature of the rebars in the rib, a new equation is also proposed, presenting a quadratic dependence between the diameter ϕ_{reb} (mm) and the temperature θ_s (°C) of the rebars. As the concrete thickness has fairly small effect on the results, this component is not included in the new proposal. The proposed new equation is given in Eq. 5.2.

$$\theta_s = c_0 + \left(c_1 \cdot \frac{u_3}{h_2}\right) + \left(c_2 \cdot z\right) + \left(c_3 \cdot \frac{A}{L_r}\right) + \left(c_4 \cdot \alpha\right) + \left(c_5 \cdot \frac{1}{l_3}\right) + \left(c_6 \cdot \phi_{reb}{}^2\right) + \left(c_7 \cdot \phi_{reb}\right) \quad (5.2)$$

The last equation is based on the current calculation rules of the EN 1994 – 1-2. The partial coefficients c_i are given in the following tables for slabs with normal weight concrete, and with either trapezoidal or re-entrant steel deck profile.

Table 5.8: Proposed new coefficients for the determination of the temperatures of the rebars in the rib for slabs with NWC (Part 1).

Steel deck profile	**Standard fire resistance**	**c_0 (°C)**	**c_1 (°C)**	**c_2 (°C mm$^{0.5}$)**	**c_3 (°C mm)**	**c_4 (°C/°)**	**c_5 (°C mm)**
Trapezoidal	R60	*1294.90*	-250	-240	-5.01	1.04	-925
	R90	*1406.81*	-256	-235	-5.30	1.39	-1267
	R120	*1407.65*	-238	-227	*-6.80*	*2.85*	-1326
Re-entrant	R60	*1269.67*	-250	-240	-5.01	1.04	-925
	R90	*1363.63*	-256	-235	-5.30	1.39	-1267
	R120	*1382.02*	-238	-227	-4.79	1.68	-1326

Table 5.9: Proposed new coefficients for the determination of the temperatures of the rebars in the rib for slabs with NWC (Part 2).

Steel deck profile	**Standard fire resistance**	**c_6 (°C/mm^2)**	**c7 (°C/mm)**
Trapezoidal	R60	*-0.2425*	*-1.70*
	R90	*-0.1938*	*-1.6075*
	R120	*-0.7544*	*5.1688*
Re-entrant	R60	*-0.160*	*-0.005*
	R90	*-0.1425*	*-0.215*
	R120	*-0.1413*	*-0.2875*

In the tables above, the numbers which are not highlighted were not modified in relation to the current calculation rules of the European standard. Appendix G gives the

results of the application of the proposed new equation for the temperature of the rebars, compared to numerical and Eurocode 4 results.

With respect to the critical temperatures of the steel components T_{crit} (°C), the following equations are proposed for the steel deck, according to the effective thickness of the slab h_{eff} (mm).

- For trapezoidal steel deck profiles:

$$T_{crit} = -0.0588 \cdot h_{eff}^{2} + 15.784 \cdot h_{eff} - 95.706 \tag{5.3a}$$

- For Vulcraft steel deck profile (re-entrant):

$$T_{crit} = 0.0306 \cdot h_{eff}^{2} - 4.6049 \cdot h_{eff} + 853.94 \tag{5.3b}$$

- For Lysaght steel deck profile (re-entrant):

$$T_{crit} = -0.017 \cdot h_{eff}^{2} + 7.7274 \cdot h_{eff} + 159.12 \tag{5.3c}$$

The following equations are proposed for the critical temperatures of the rebars in the rib, according to the effective thickness of the slab h_{eff} (mm) and the concrete cover for rebar d'_{reb} (mm), within the limits $30 \leq d'_{reb} \leq 60$ mm.

- For trapezoidal steel deck profiles:

$$\begin{aligned} T_{crit} &= -0.0813 \cdot h_{eff}^{2} + 22.397 \cdot h_{eff} - 804.85 + \\ &- \left[\left(-0.0009 \cdot h_{eff}^{2} + 0.1846 \cdot h_{eff} - 2.8367 \right) \cdot \left(d'_{reb} - 30 \right) \right] \end{aligned} \tag{5.4a}$$

- For re-entrant steel deck profiles:

$$\begin{aligned} T_{crit} &= -0.0284 \cdot h_{eff}^{2} + 11.305 \cdot h_{eff} - 395.84 + \\ &- \left[\left(-0.0012 \cdot h_{eff}^{2} + 0.298 \cdot h_{eff} - 10.944 \right) \cdot \left(d'_{reb} - 30 \right) \right] \end{aligned} \tag{5.4b}$$

As the critical temperatures of the anti-crack mesh are around 200 °C for all the numerical simulations, see Figure 4.14 c), no equation is proposed for this case.

6. CONCLUSIONS AND RECOMMENDATIONS

The underlying work deals with 3-D numerical simulations of the fire behaviour of composite slabs with profiled steel deck using the software ANSYS Mechanical APDL and MATLAB, through the PDE Toolbox. In this regard, numerical models have been established considering either perfect thermal contact between all the materials, or an insulating layer (air gap) with constant thickness between the concrete topping and the steel deck to simulate debonding effects. Two parametric studies have been performed with 208 and 40 different composite slabs, in order to evaluate the influence of different parameters on the temperature of the steel components, and on the fire resistance according to thermal insulation criterion (I).

The thermal models have been validated on the basis of four standard fire tests conducted by different authors. Furthermore, the numerical results have been compared to the results of simplified calculation methods of the EN 1994 – 1-2 and the NBR 14323:2013.

Generally speaking, the developed numerical models satisfactorily predicted the fire behaviour of composite slabs by describing the three-dimensional heat flow through this structural element in good agreement with experimental results. In particular, the air gap model resulted in better results in comparison to the perfect thermal contact model for most of the cases. For the second parametric study, good agreement between experimental and numerical results was obtained considering an air gap thickness t_a of 3 mm. The fire resistance (I) obtained through the perfect contact model was considerably smaller than the measured fire resistance for all the numerical simulations.

For the experimental results of validation models, a plateau at about 100 °C (due to moisture evaporation) should be highlighted, consisting of a decrease in the rate of temperature increase. The results of the numerical simulations do not present this pronounced plateau, probably because localized moisture concentrations in the tests were higher than the uniform moisture content introduced in the thermal models for each slab.

The fire resistance t_{fi} was governed by the average temperature rise criterion for most of the numerical analyses of the parametric studies. The results of the new tool developed for thermal analysis in MATLAB programming language presented good

agreement with the results of the commercial finite element software ANSYS, although not including the steel reinforcing components within the concrete layer (rebars and anti-crack mesh). In some cases, the results of ANSYS and MATLAB models presented noticeable differences for the same situation, that is, for a same point and type of model (perfect contact or air gap model). These differences can be justified by the presence of the steel components within the concrete layer in the ANSYS model, which are not included in the MATLAB model. Despite not significantly affecting the fire resistance (I), these components can affect the temperature development at specific points.

With respect to the normative recommendations, the fire resistance t_{fi} and the temperature of the steel components obtained through the calculation rules from EN 1994 – 1-2 were on the unsafe side for most of the cases, regarding the results of the perfect thermal contact model. Better agreement between the results for fire resistance (I) of the European standard and the numerical simulations was obtained using an air gap thickness of 2 mm. For the Brazilian standard NBR 14323:2013, better agreement between the results for fire resistance (I) of the calculation rules and the numerical simulations was observed for the perfect thermal contact model.

The parameters that most affected the fire resistance of composite slabs according to thermal insulation criterion were the thickness of the air gap and the thickness of the concrete topping above the steel deck. For considerably high concrete thicknesses, the composite slab presents a temperature distribution on the unexposed side similar to a flat concrete slab.

Based on the numerical results, a new equation has been proposed for the calculation of the fire resistance t_{fi}, depending on the effective thickness of the composite slab and the air gap thickness. In addition, new calculation methods have been proposed for the determination of the temperature of the steel components of the slab (steel deck and rebars), and the critical temperature of each component as well. These equations present good agreement with numerical results and consider parameters which are not included in the current calculation rules of standards.

6.1 Recommendations for future research

The research related to the fire behaviour of structures is of great importance and complexity in the field of civil and construction engineering. Additional research shall be carried out in the future in order to complement the results of this work:

a) Perform a numerical investigation considering different fire curves, such as natural fire curve models.
b) Conduct experimental fire tests with composite slabs with trapezoidal and re-entrant steel deck profile.
c) Experimentally verify the thermal material properties.
d) Carry out parametric studies comprising a series of different steel deck profiles, air gap thicknesses and both normal weight and lightweight concrete.

7. REFERENCES

[1] C. Both, “The fire resistance of composite steel-concrete slabs,” Delft University of Technology, 1998.

[2] L. Calado and J. Santos, *Steel-concrete composite structures [in portuguese]*. Lisbon: IST press, 2010.

[3] X. Yu, Z. Huang, I. Burgess, and R. Plank, “Nonlinear analysis of orthotropic composite slabs in fire,” *Eng. Struct.*, vol. 30, pp. 67–80, 2008.

[4] M. A. H. Abdel-Halim, M. R. Hakmi, and D. C. O’Leary, “Fire resistance of composite floor slabs using a model fire test facility,” *Eng. Struct.*, vol. 21, no. 2, pp. 176–182, 1999.

[5] M. Gillie, A. Usmani, M. Rotter, and M. O’Connor, “Modelling of heated composite floor slabs with reference to the Cardington experiments,” *Fire Saf. J.*, vol. 36, no. 8, pp. 745–767, 2001.

[6] R. Hamerlinck, “The behaviour of fire-exposed composite steel/concrete slabs,” Eindhoven University of Technology, 1991.

[7] J. Jiang, J. A. Main, J. M. Weigand, and F. H. Sadek, “Thermal performance of composite slabs with profiled steel decking exposed to fire effects,” *Fire Saf. J.*, vol. 95, no. May 2017, pp. 25–41, 2018.

[8] G. M. E. Cooke, R. M. Lawson, and G. M. Newman, “Fire resistance of composite deck slabs,” *Struct. Eng.*, vol. 66, no. 16, pp. 253–267, 1988.

[9] J. Jiang, J. A. Main, F. Sadek, and J. M. Weigand, “Numerical modeling and analysis of heat transfer in composite slabs with profiled steel decking,” 2017.

[10] M. Crisinel and D. O’Leary, “Composite floor slab design and construction,” *Struct. Eng. Int.*, vol. 6, no. Special Issue 1, pp. 41–46, 1996.

[11] D. Pantousa and E. Mistakidis, “Advanced modeling of composite slabs with thin-walled steel sheeting submitted to fire,” *Fire Technol.*, vol. 49, no. 2, pp. 293–327, 2013.

[12] J. M. Davies and H. B. Wang, “Numerical temperature calculation for composite deck slabs exposed to fire,” *Trans. Eng. Sci.*, vol. 5, pp. 331–338, 1994.

[13] CEN - European Committee for Standardization, *EN 1994-1-2: Design of composite steel and concrete structures - Part 1-2: General rules - Structural fire design*. Brussels, 2005.

[14] *ABNT NBR 14323: Structural fire design of steel and composite steel and concrete structures for buildings [in portuguese]*. Brazil: ABNT/CB-002, 2013, p. 66.

[15] C. Both, J. H. H. Fellinger, and L. Twilt, "Shallow floor construction with deep composite deck: from fire tests to simple calculation rules," *Heron*, vol. 42, no. 3, pp. 145–158, 1997.

[16] D. L. Logan, *A first course in the Finite Element Method*, 4th ed. Platteville: Thomson, 2007.

[17] D. A. . Nethercot, *Composite Construction*. London: Spon Press, 2004.

[18] A. Penza, "Composite Slabs with Lightweight Concrete: Experimental evaluation of steel decking and lightweight concrete," Politecnico di Milano, 2009.

[19] B. F. Friberg, "Combined Form and Reinforcement to Concrete Slabs," *J. Am. Concr. Inst.*, vol. 50, no. 5, pp. 697–716, 1954.

[20] O. Pettersson, S. E. Magnusson, and J. Thor, "Fire engineering design of steel structures," Lund, 1976.

[21] European Convention for Constructional Steelwork - Committee T3 - Fire Safety of Steel Structures, "Calculation of the fire resistance of composite concrete slabs with profiled steel sheet exposed to the standard fire," Brussels, 1983.

[22] International Standard ISO 834, "Fire-resistance tests - Elements of building construction." 1975.

[23] C. Both, J. W. B. Stark, and L. Twilt, "Partial fire protection of composite slabs," *J. Constr. Steel Res.*, vol. 27, no. 1–3, pp. 143–158, 1993.

[24] R. Hamerlinck, L. Twilt, and J. W. B. Stark, "A numerical model for fire-exposed composite steel/concrete slabs," *10th Int. Spec. Conf. Cold-Formed Steel Struct. - Int. Spec. Conf. Cold-Formed Steel Struct. 5*, pp. 115–130, 1990.

[25] G. M. Newman, "The Fire Resistance of Composite Floors with Steel Decking," *Steel Constr. Inst.*, no. 056, p. 35, 1991.

[26] R. Hamerlinck and L. Twilt, "Fire resistance of composite slabs," *J. Constr. Steel Res.*, vol. 33, no. 94, pp. 71–85, 1995.

[27] K. Both, "Fire-exposed continuous span composite steel-concrete slabs," *Heron*, vol. 41, no. 3, pp. 187–199, 1996.

[28] J. H. H. Fellinger and L. Twilt, "Fire behaviour of long span composite floor centre for fire research," in *Fire safety science - proceedings of the fifth International Symposium*, 1997, pp. 1093–1104.

[29] C. G. Bailey, T. Lennon, and D. B. Moore, “The behaviour of full-scale steel-framed buildings subjected to compartment fires,” *Struct. Eng.*, vol. 77, no. 8, pp. 15–21, 1999.

[30] G. M. Newman, J. T. Robinson, and C. G. Bailey, “Fire safe design: A new approach to multi-storey steel framed buildings,” Ascot, 2000.

[31] S. Lamont, A. S. Usmani, and D. D. Drysdale, “Heat transfer analysis of the composite slab in the Cardington frame fire tests,” *Fire Saf. J.*, vol. 36, no. 8, pp. 815–839, 2001.

[32] L. Lim and C. Wade, “Experimental fire tests of two-way concrete slabs,” Christchurch, 2002.

[33] C. Both and J. W. B. Stark, “Fire exposed composite steel-concrete slabs,” in *Composite Construction in Steel and Concrete IV*, 2002, pp. 756–767.

[34] L. Lim, “Membrane action in fire exposed concrete floor systems,” University of Canterbury, 2003.

[35] C. G. Bailey, “Membrane action of slab/beam composite floor systems in fire,” *Eng. Struct.*, vol. 26, pp. 1691–1703, 2004.

[36] S. Guo and C. G. Bailey, “Experimental behaviour of composite slabs during the heating and cooling fire stages,” *Eng. Struct.*, vol. 33, pp. 563–571, 2011.

[37] D. Banerjee, “A study of thermal behavior of a composite floor system in standard fire resistance tests,” 2012.

[38] J. Kolšek, M. Saje, I. Planinc, and T. Hozjan, “A fully generalised approach to modelling fire response of steel-RC composite structures,” *Int. J. Non. Linear. Mech.*, vol. 67, pp. 382–393, 2014.

[39] K. H. Tan and T. T. Nguyen, “Experimental and numerical evaluation of composite floor systems under fire conditions,” *J. Constr. Steel Res.*, vol. 105, pp. 86–96, 2015.

[40] G.-Q. Li, N. Zhang, and J. Jiang, “Experimental investigation on thermal and mechanical behaviour of composite floors exposed to standard fire,” *Fire Saf. J.*, vol. 89, pp. 63–76, 2017.

[41] L. M. S. Prates, “Numerical simulation of the fire behaviour of composite structures (slabs) [in portuguese],” Polytechnic Institute of Bragança, 2018.

[42] J. Jiang, A. Pintar, J. M. Weigand, J. A. Main, and F. Sadek, “Improved calculation method for insulation-based fire resistance of composite slabs,” *Fire Saf. J.*, 2019.

[43] P. A. G. Piloto, C. Balsa, F. Ribeiro, L. Santos, R. Rigobello, and E. Kimura, "Critical temperature for the components of composite slabs with steel deck under fire for load-bearing rating," in *4th International Conference on Numerical and Symbolic Computation Developments and Applications - SYMCOMP 2019*, 2019, no. ISBN 978-989-99410-5-2, pp. 119–135.

[44] P. A. G. Piloto, C. Balsa, F. Ribeiro, L. Santos, R. Rigobello, and E. Kimura, "Fire resistance of composite slabs with steel deck: experimental and numerical investigation," *MATTER Int. J. Sci. Technol.*, no. ISSN 2454-5880, 2019.

[45] P. Piloto, C. Balsa, F. Ribeiro, R. Rigobello, L. Santos, and E. Kimura, "Validation models on the fire resistance of composite slab with steel deck," in *Congress on Numerical Methods in Engineering – CMN 2019*, 2019, no. ISBN: 978-989-54496-0-6, pp. 625–642.

[46] C. Balsa, F. F. Ribeiro, P. A. G. Piloto, and R. Rigobello, "Numerical simulation of composite slabs with steel deck under fire conditions," in *5th Iberian-Latin-American Congress on Fire Safety - V CILASCI*, 2019.

[47] P. A. G. Piloto, C. Balsa, F. F. Ribeiro, and R. Rigobello, "Improved calculation methods for the temperature of the steel components of composite slabs under fire conditions," in *Conference on Steel and Composite Construction - XII CMM*, 2019.

[48] CEN- European Committee for Standardization, *EN 1994-1-1: Design of composite steel and concrete structures - Part 1-1: General rules and rules for buildings*. Brussels: CEN - European Committee for Standardization, 2004.

[49] R. Regobello, "Numerical analysis of steel and composite steel-concrete cross sections and structural elements in fire situation [in portuguese]," University of São Paulo, 2007.

[50] J.-M. Franssen, "Analysis of the fire behaviour of composite steel-concrete structures [in french]," University of Liège, 1987.

[51] CEN - European Committee for Standardization, *EN 1991-1-2: Actions on structures - Part 1-2: General actions - Actions on structures exposed to fire*. Brussels, 2002.

[52] P. A. G. Piloto, "Experimental and numerical analisys of metalic structures behaviour under fire conditions [in portuguese]," University of Porto, 2000.

[53] Y. A. Çengel and A. J. Ghajar, *Heat and mass transfer: fundamentals & applications*, Fifth edit. New York: McGraw-Hill Education, 2015.

[54] J. P. Holman, *Heat transfer*, Tenth edit. New York: McGraw-Hill Education, 2010.

[55] Y. Wang, *Steel and composite structures: behaviour and design for fire safety*, vol. 1. London: Spon Press, 2002.

[56] CEN - European Committee for Standardization, *EN 1992-1-2: Design of concrete structures - Part 1-2: General rules - Structural fire design*. Brussels, 2004.

[57] CEN - European Committee for Standardization, *EN 1993-1-2: Design of steel structures - Part 1-2: General rules - Structural fire design*. Brussels, 2005.

[58] C. Engineering, "BRE's multi storey test frame - Cardington," *Caunton Engineering Ltd.* [Online]. Available: http://www.caunton.co.uk/media/10/1091/1091.pdf. [Accessed: 02-May-2019].

[59] A. H. Buchanan and A. K. Abu, *Structural design for fire safety*, Second Ed. Chichester, UK: John Wiley & Sons Ltd., 2017.

[60] A. K. Abu, "Behaviour of Composite Floor Systems in Fire," The University of Sheffield, 2008.

[61] ASTM International, *American Society for Testing and Materials ASTM E119 - 00a: Standard test methods for fire tests of building construction and materials*. United States, 2000.

[62] T. T. Lie, "Fire temperature-time relations," in *Society of Fire Protection Engineers - SFPE: Handbook of fire protection engineering*, Third edit., O. Typography, Ed. Quincy, Massachusetts: National Fire Protection Association, 2002, pp. 4–201.

[63] *ABNT NBR 14432: Fire resistance requirements for building construction elements - Procedure [in portuguese]*. Brazil: ABNT/CB-24, 2001, p. 15.

[64] *BS 476-20: Fire tests on building materials and structures - Part 20: Method for determination of the fire resistance of elements of construction (general principles)*. United Kingdom, 1987, p. 41.

[65] J. A. Purkiss and L. Li, *Fire safety engineering design of structures*, Third edit. New York: CRC Press, 2013.

[66] R. P. Johnson, *Composite structures of steel and concrete: Beams, slabs, columns, and frames for buildings*, Third edit., vol. 19, no. 4. Oxford: Blackwell Scientific Publications, 2004.

[67] *BS 13501-2: Fire classification of construction products and building elements -*

Part 2: Classification using data from fire resistance tests, excluding ventilation services. United Kingdom, 2009, p. 80.

[68] *Decree-Law No. 220/2008 [in portuguese]*. Portugal: Ministry of Internal Administration, 2008, pp. 7903–7922.

[69] *Ordinance No. 1532/2008 [in portuguese]*. Portugal: Ministry of Internal Administration, 2008, pp. 9050–9127.

[70] E. E. C. Rodrigues, "Management system of fire safety in buildings: fundamentation for a national regulation [in portuguese]," Federal University of Rio Grande do Sul, 2015.

[71] *Decree-Law No. 224/2015 [in portuguese]*. Portugal: Ministry of Internal Administration, 2015, pp. 8740–8774.

[72] *Technical Instruction No. 08/2018: Structural fire safety [in portuguese]*. State of São Paulo, Brazil: Fire brigade of the state of São Paulo, 2018, p. 11.

[73] *Decree No. 56819: Fire safety regulation [in portuguese]*. State of São Paulo, Brazil: Fire brigade of the state of São Paulo, 2011, p. 50.

[74] "Fire sprinkler service," *Fireserv*, 2019. [Online]. Available: https://www.fireserv.info/services/fire-sprinkler-service. [Accessed: 19-May-2019].

[75] "Intumescent paint," *TBL Fire Protection*. [Online]. Available: http://tblfireprotection.com/intumescent-paint.html. [Accessed: 19-May-2019].

[76] ANSYS, "Mechanical APDL 18.2 - Academic version." 2018.

[77] MathWorks, "Partial Differential Equation Toolbox ™ User's Guide R2019a," Natick, MA, 2019.

[78] P. E. Gill and W. Murray, "Algorithms for the solution of the nonlinear least-squares problem," *SIAM J. Numer. Anal.*, vol. 15, no. 5, pp. 977–992, 1978.

APPENDIX A

TECHNICAL FILES FOR THE VALIDATION MODELS

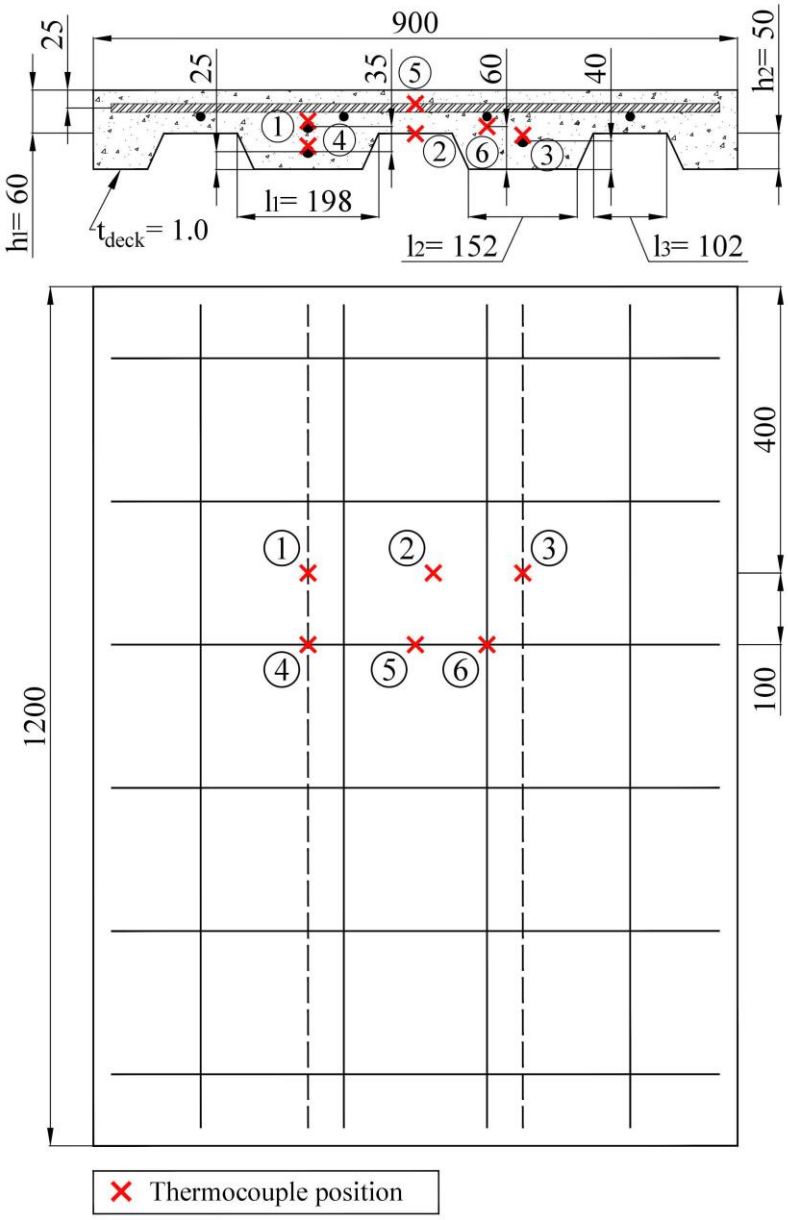

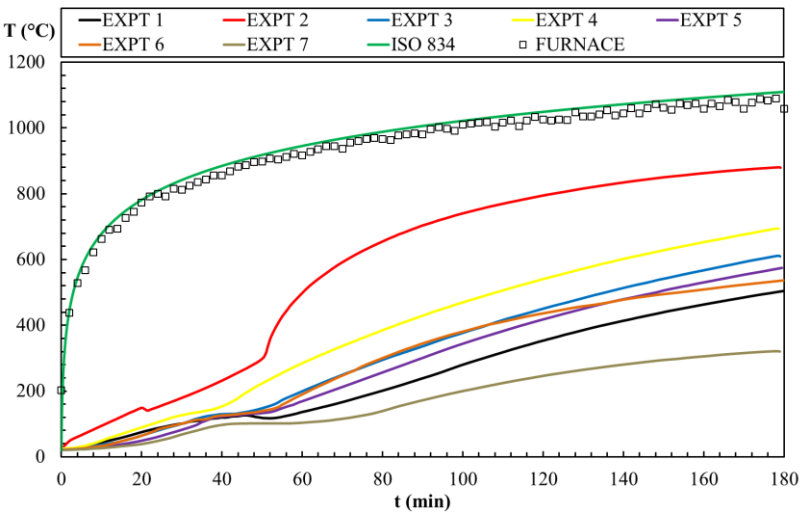

Description

Authors: Abdel-Halim, Hakmi and O'Leary [4]		Test no.: 2
Local: University of Salford, UK		Year: 1997
Load: 0 kPa	Rebar: ϕ16	Mesh: ϕ12//200
Concrete compressive strength: 25 MPa		
Yield strength of rebar/mesh: -		
Yield strength of steel deck: -		

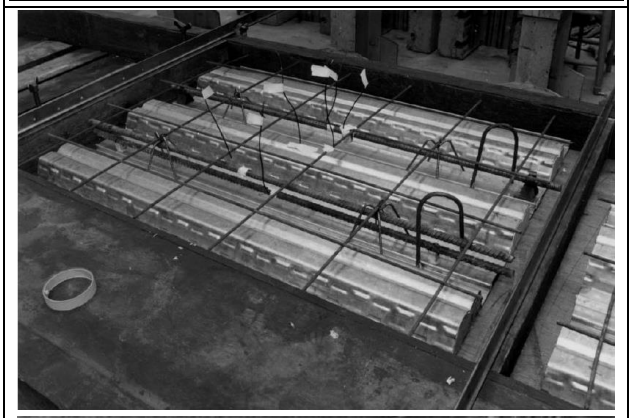

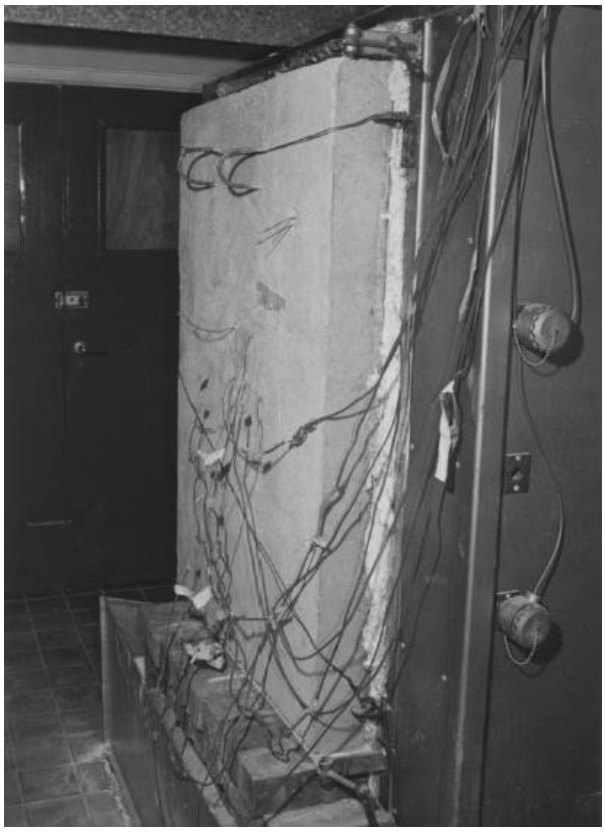

Observations:

- Dimensions in millimetres;
- The specimen was tested vertically in the furnace;
- The curve "EXPT 7" represents the average temperature at the unexposed surface.

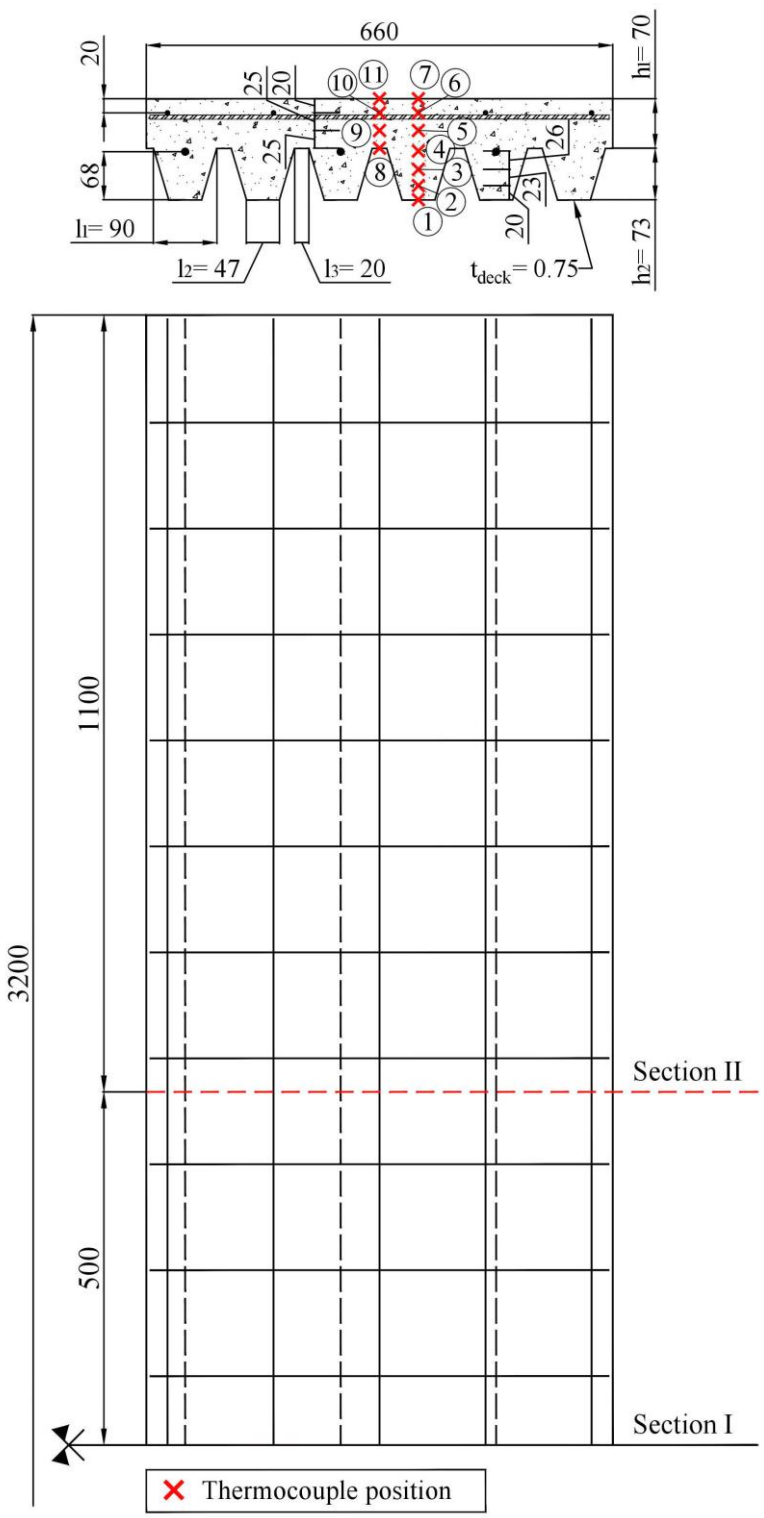

Description

Author: Alphonse Florentinus Hamerlinck [6]		Test no.: 2
Local: Eindhoven University of Technology, NL		Year: 1991
Load: 3.0 kPa	Rebar: ϕ10	Mesh: ϕ6//150
Concrete compressive strength: 25 MPa		
Yield strength of rebar/mesh: 500 MPa		
Yield strength of steel deck: 280 MPa		

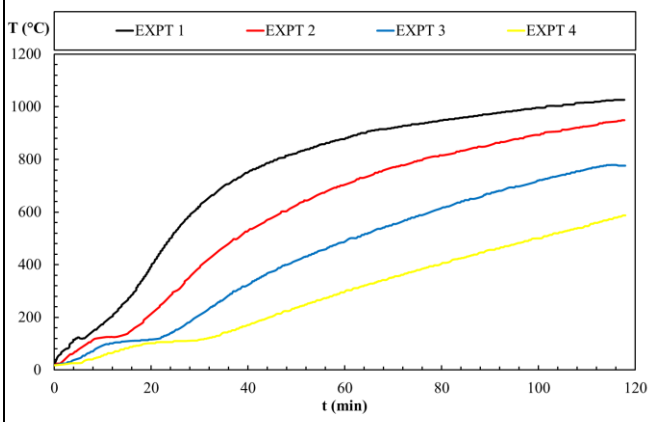

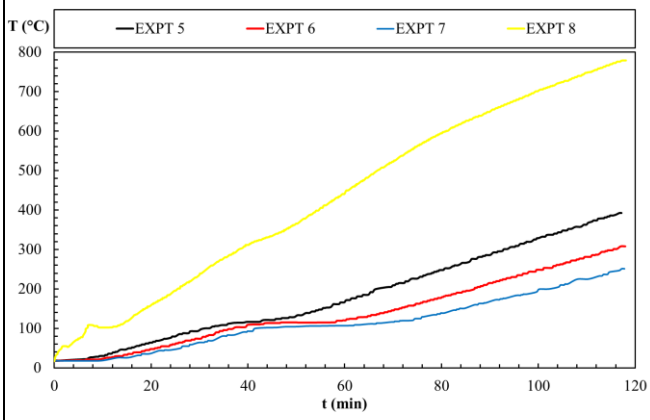

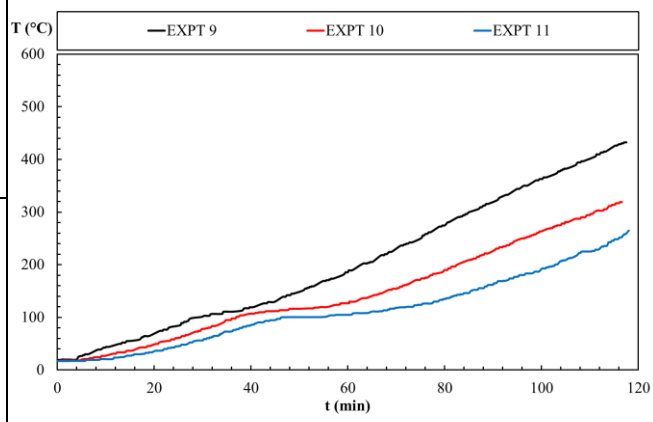

Observations:

- Dimensions in millimetres;
- Temperatures correspond to the average temperatures between sections I and II.

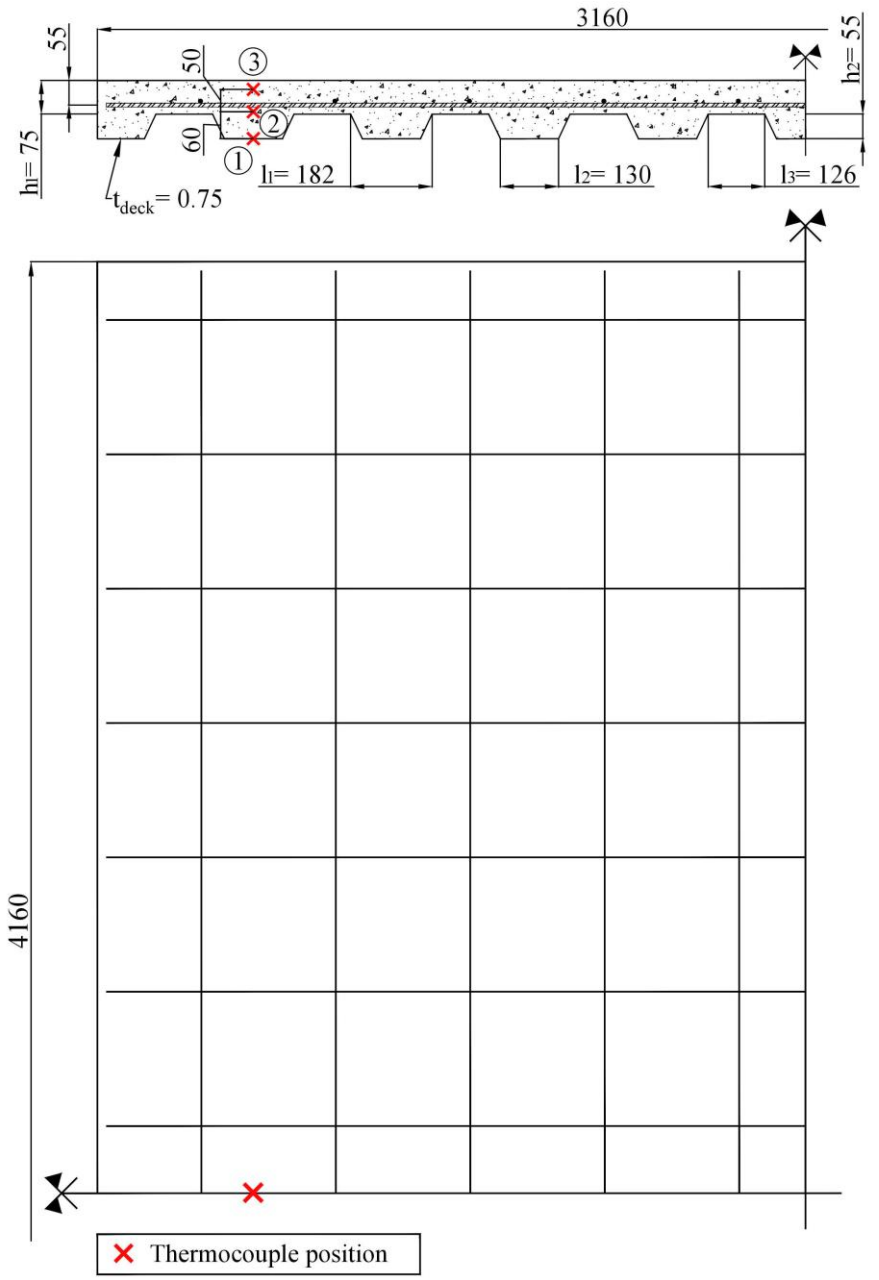

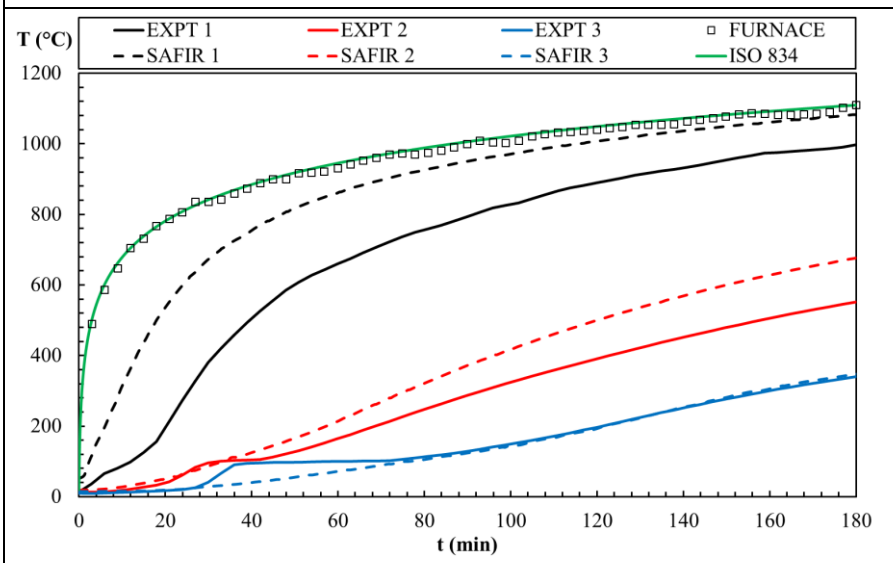

Description

Author: Linus Lim [34]		Test no.: 4
Local: University of Canterbury, NZ		Year: 2002
Load: 5.43 kPa	Rebar: -	Mesh: ϕ8.7//300
Concrete compressive strength: 32 MPa		
Yield strength of rebar/mesh: 565 MPa		
Yield strength of steel deck: 550 MPa		

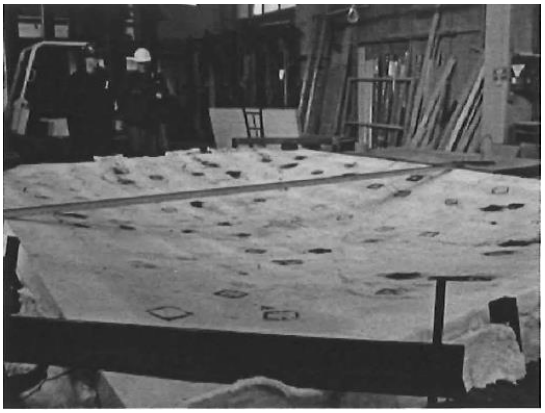

Numerical model

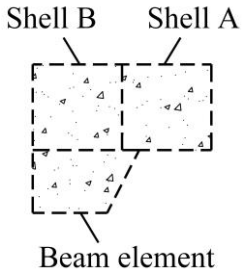

Observations:

- Dimensions in millimetres;
- Normal weight concrete with siliceous aggregates was used;
- SAFIR represents the numerical results obtained by the author.

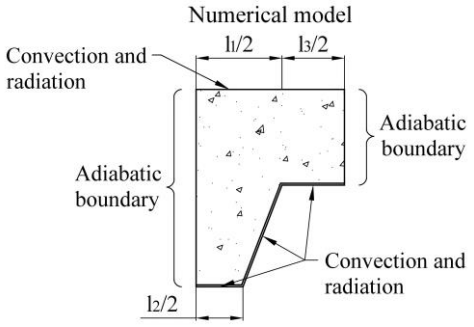

Description

Authors: Jian Jiang et al. [7]	Test no.: 2
Local: National Institute of Standards and Technology, USA	Year: 2018
Load: 5.43 kPa	Concrete compressive strength: 32 MPa
Rebar: -	Yield strength of rebar/mesh: 565 MPa
Mesh: ϕ8.7//300	Yield strength of steel deck: 550 MPa

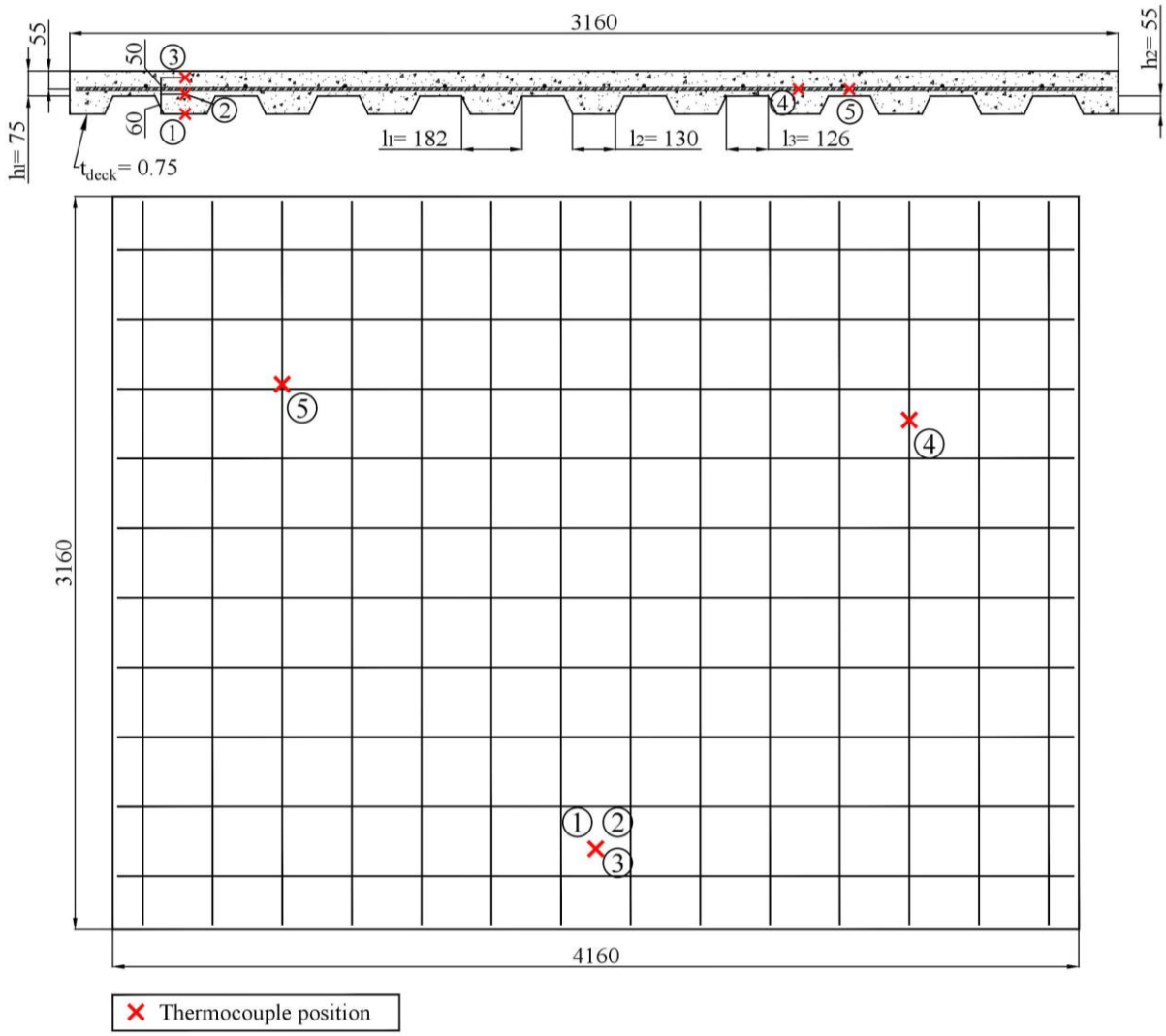

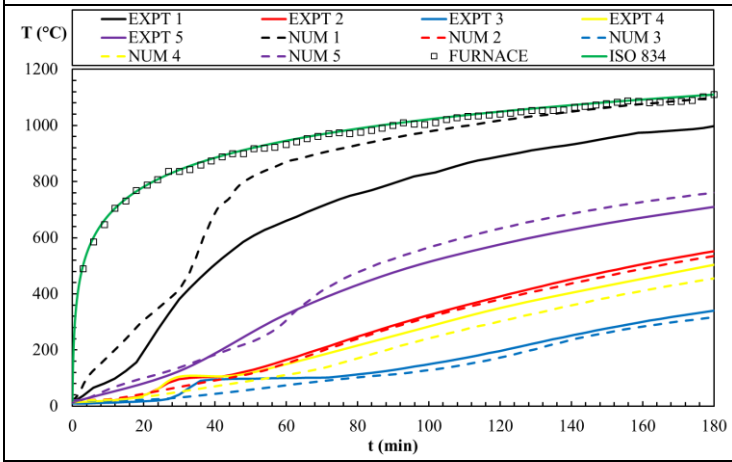

Observations:

- Dimensions in millimetres;
- Normal weight concrete with siliceous aggregates was used;
- NUM represents the numerical results obtained by the authors;
- Experimental results from Lim [32].

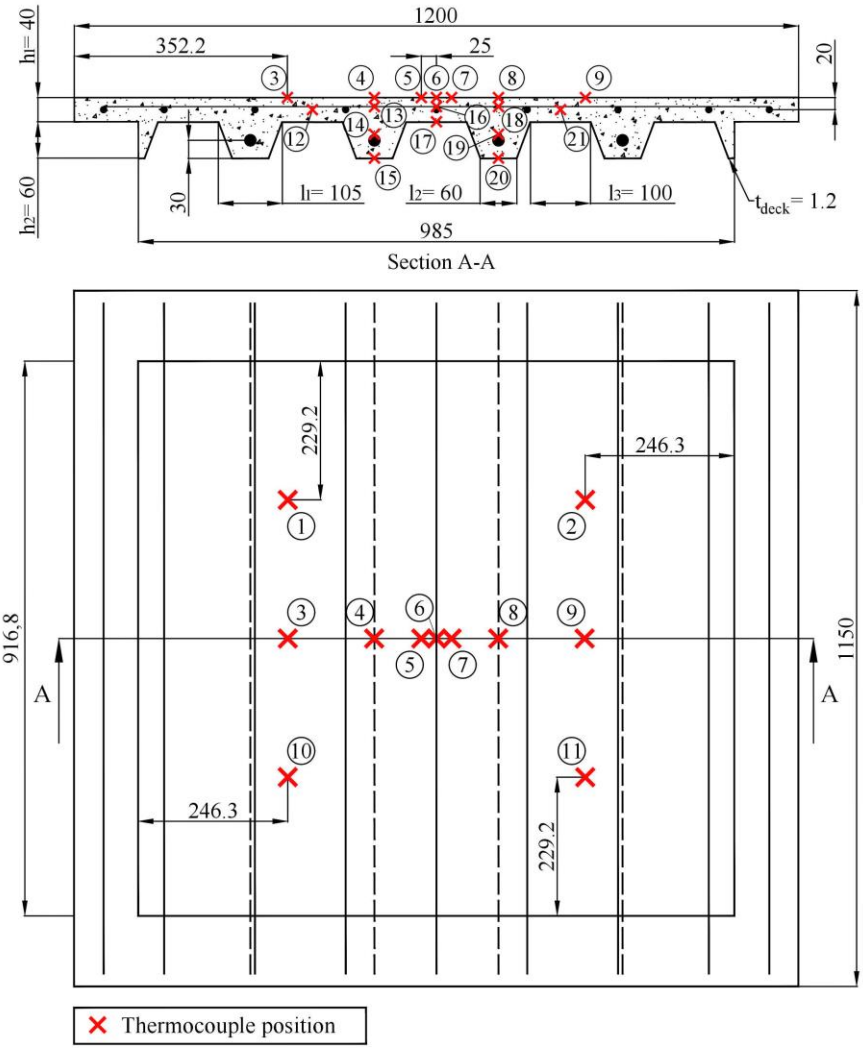

Description

Author: Lucas M. S. Prates [41]		Test no.: 1
Local: Polytechnic Institute of Bragança, PT		Year: 2018
Load: 0 kPa	Rebar: ϕ20	Mesh: ϕ10//150
Concrete compressive strength: 20 MPa		
Yield strength of rebar/mesh: 500 MPa		
Yield strength of steel deck: 320 MPa		

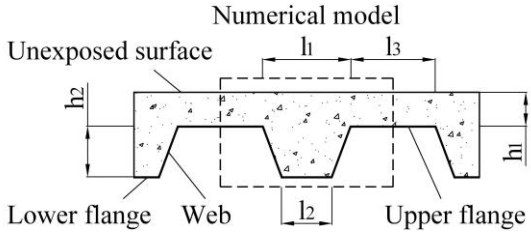

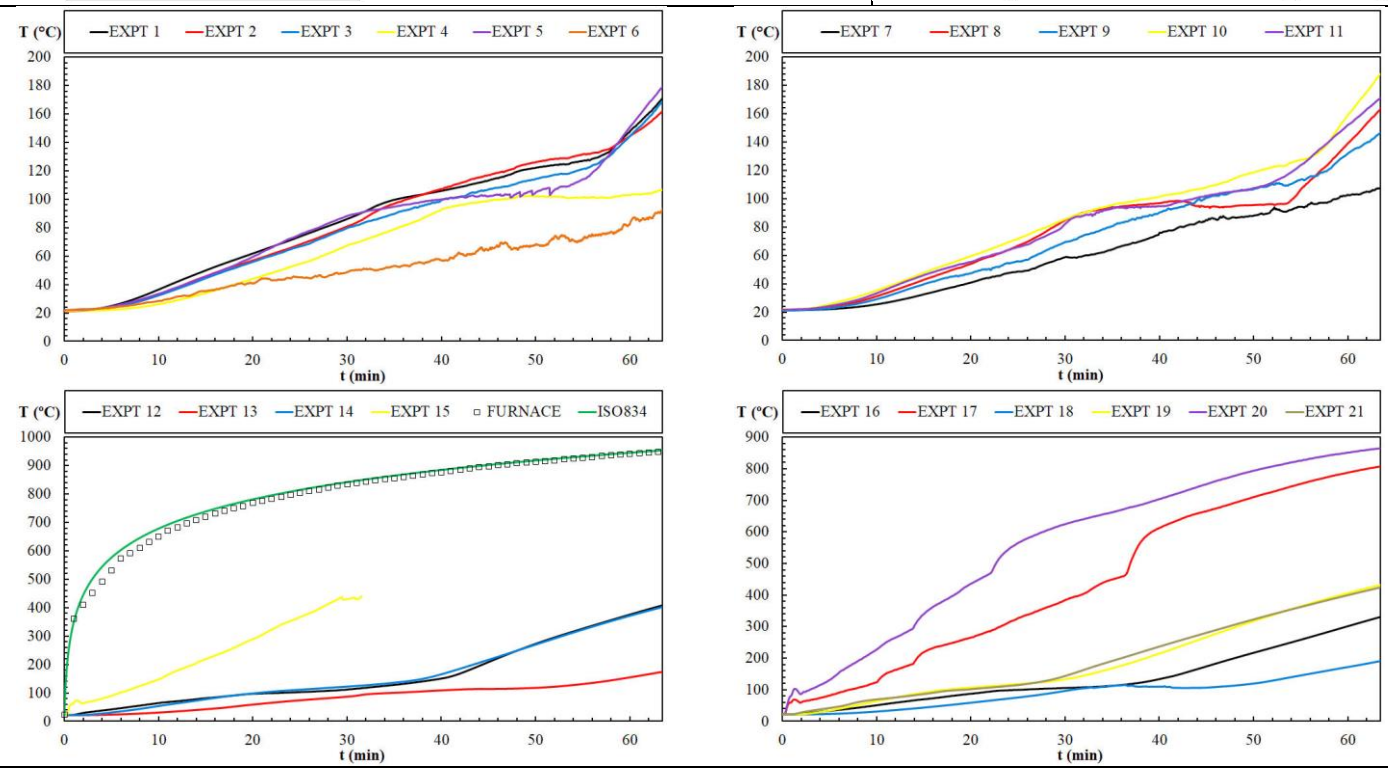

Observations: dimensions in millimetres.

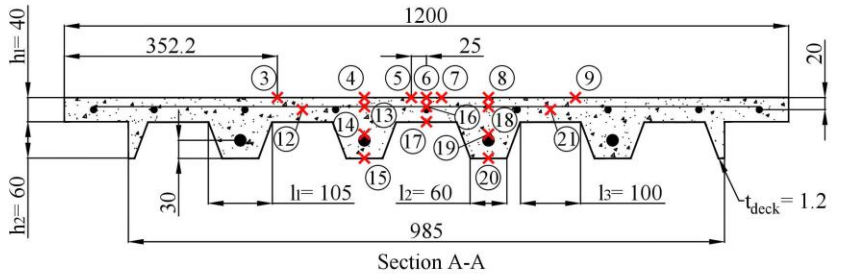

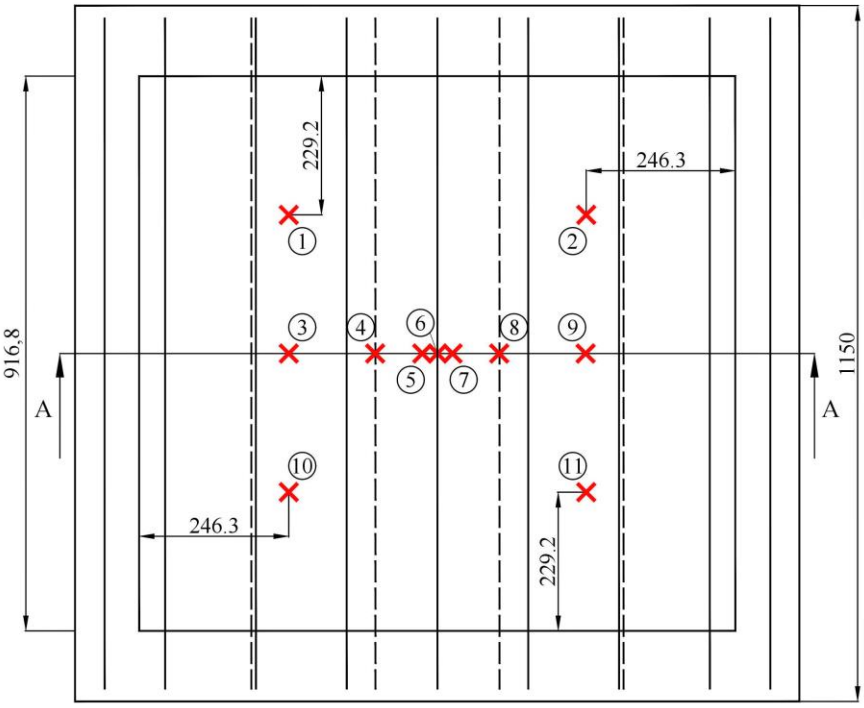

Description

Author: Lucas M. S. Prates [41]		Test no.: 2
Local: Polytechnic Institute of Bragança, PT		Year: 2018
Load: 0 kPa	Rebar: ϕ20	Mesh: ϕ10//150
Concrete compressive strength: 20 MPa		
Yield strength of rebar/mesh: 500 MPa		
Yield strength of steel deck: 320 MPa		

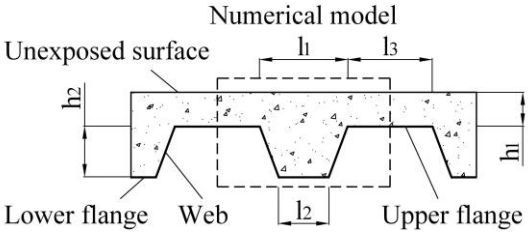

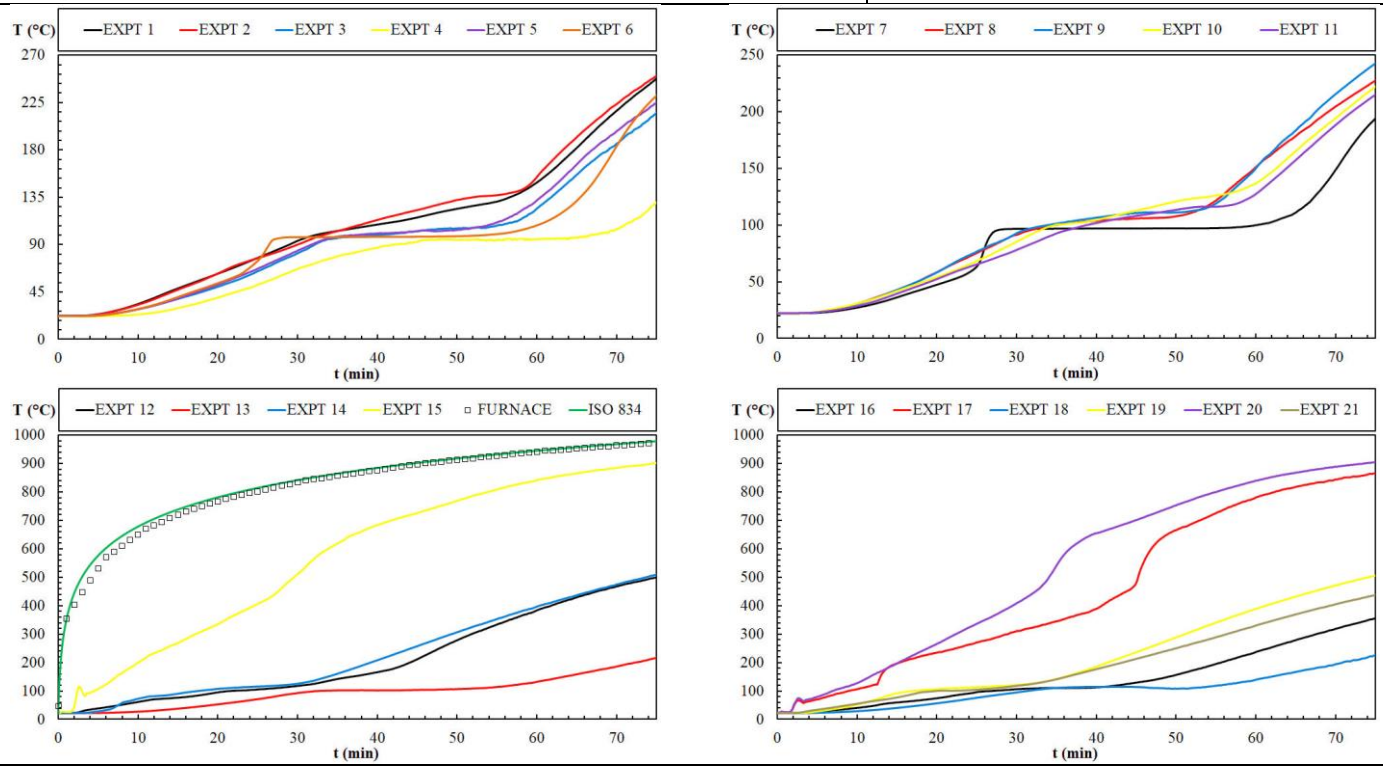

Observations: dimensions in millimetres.

APPENDIX B

TECHNICAL FILES FOR THE FIRST PARAMETRIC STUDY

SIM. 1	**Steel deck:** Trapezoidal – O Feliz H60	**Rebar (mm):** ϕ8	**Fire resistance (min)**	
	Mesh (mm//mm): ϕ6//100 (FNQ 60)	**h_1 (mm):** 50	Ave: 36.3	Max: *34.6*

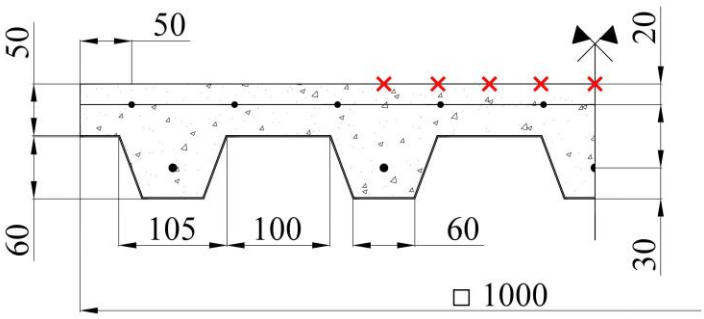

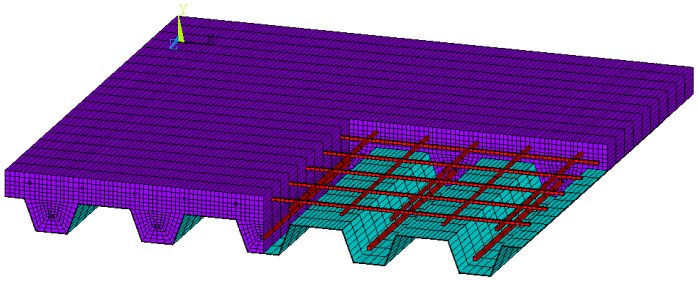

Finite element mesh

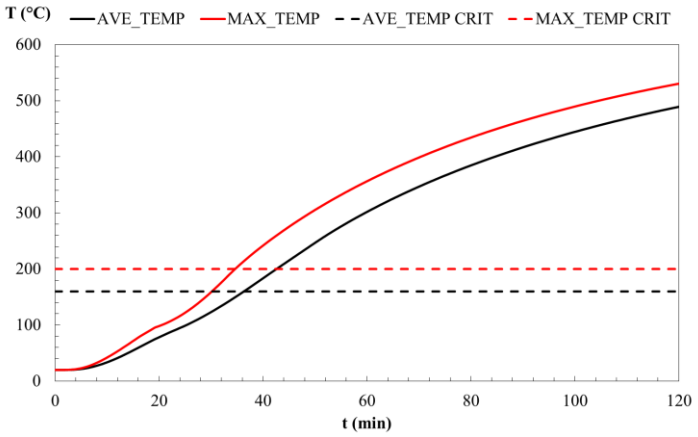

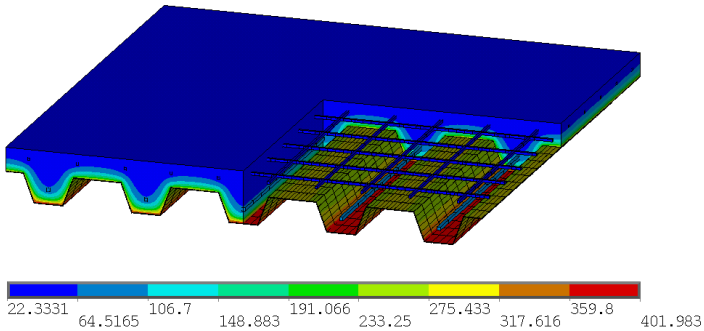

t= 8.7 min

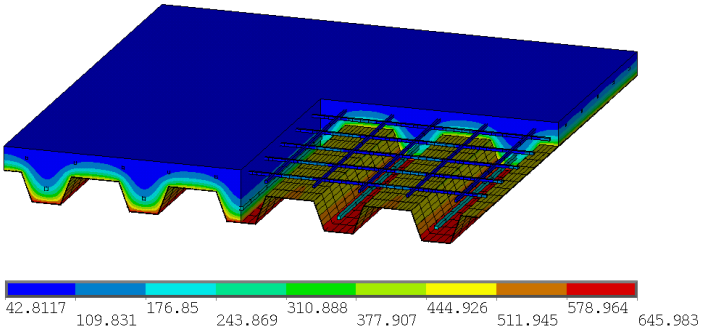

t= 17.3 min

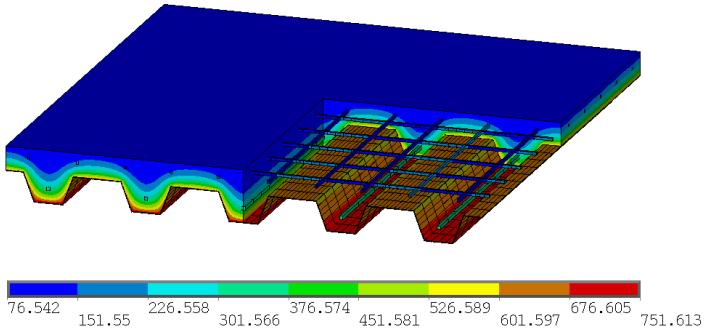

t= 26.0 min

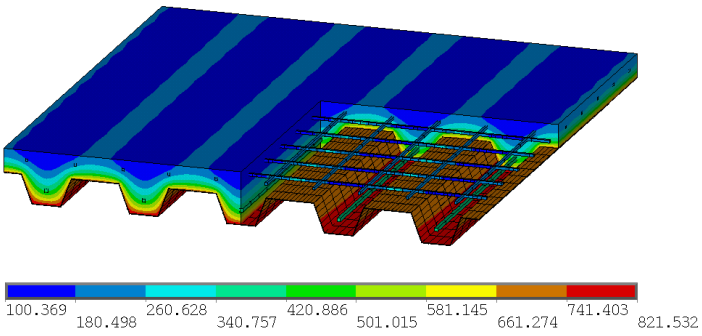

t= 34.6 min

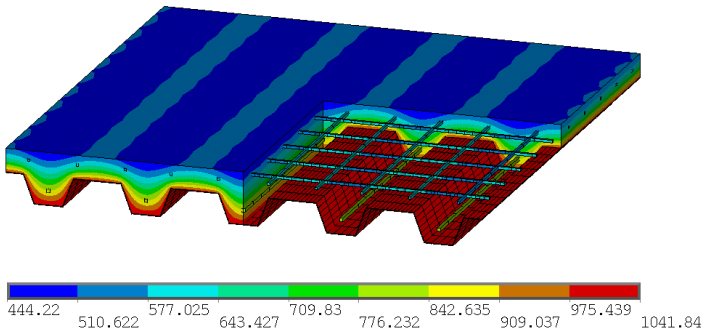

t= 120.0 min

SIM. 2	**Steel deck:** Trapezoidal – O Feliz H60	**Rebar (mm):** ϕ8	**Fire resistance (min)**	
	Mesh (mm//mm): ϕ6//100 (FNQ 60)	**h_1 (mm):** 60	Ave: 46.4	Max: *45.9*

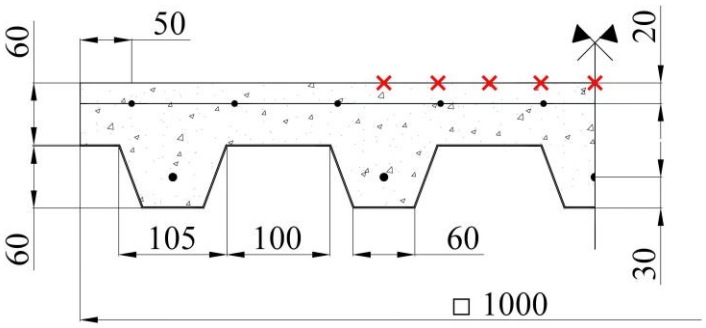

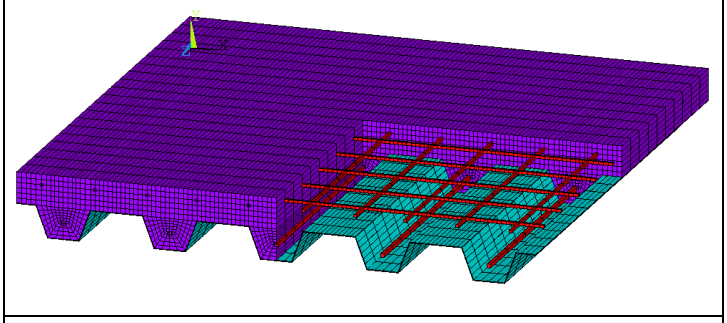

Finite element mesh

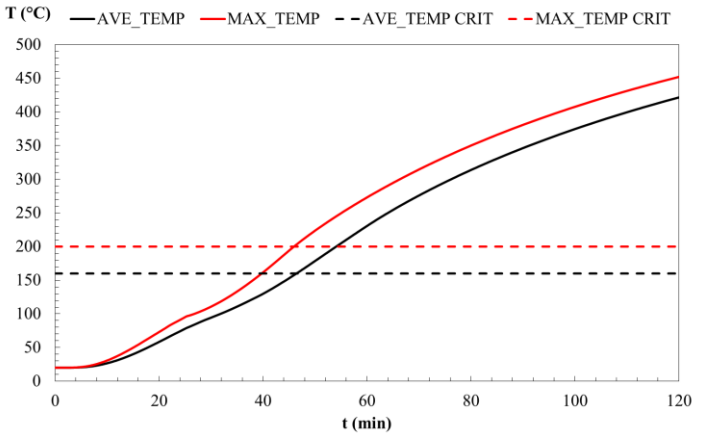

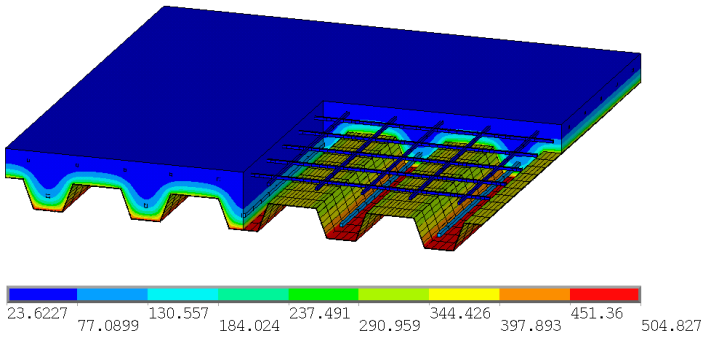

t= 11.5 min

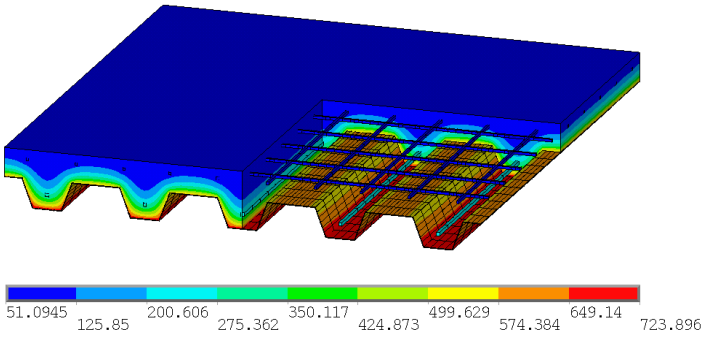

t= 23.0 min

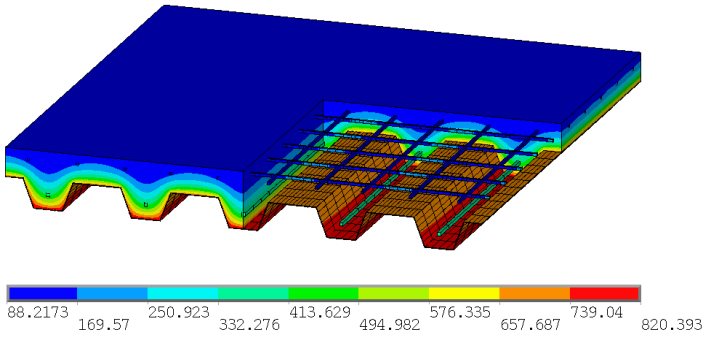

t= 34.4 min

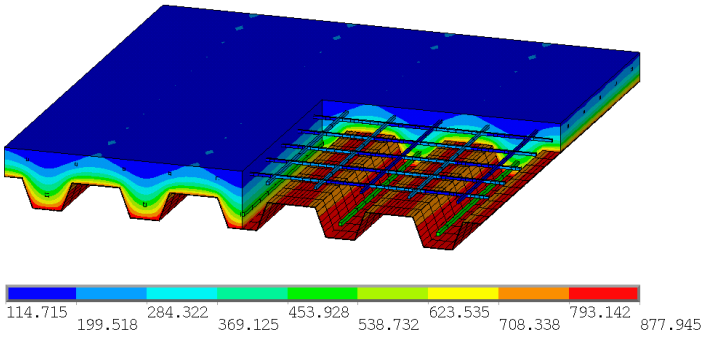

t= 45.9 min

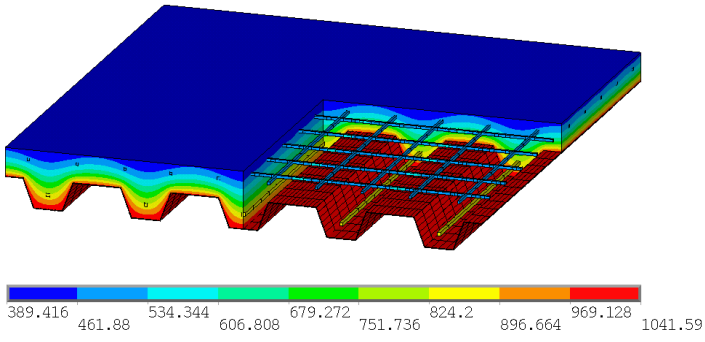

t= 120.0 min

SIM. 3	**Steel deck:** Trapezoidal – O Feliz H60	**Rebar (mm):** ϕ8	**Fire resistance (min)**	
	Mesh (mm//mm): ϕ6//100 (FNQ 60)	**h_1 (mm):** 70	Ave: *57.7*	Max: 59.3

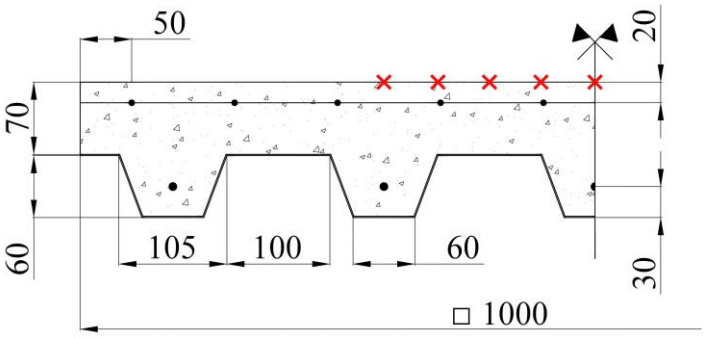

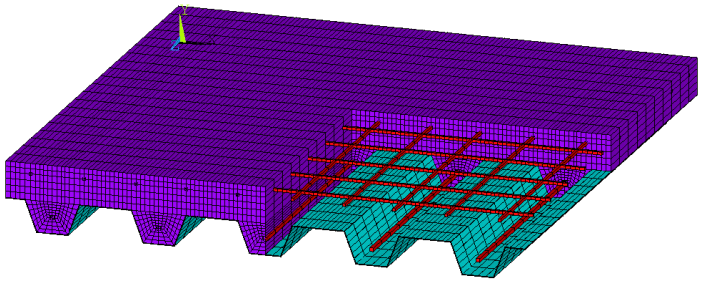

Finite element mesh

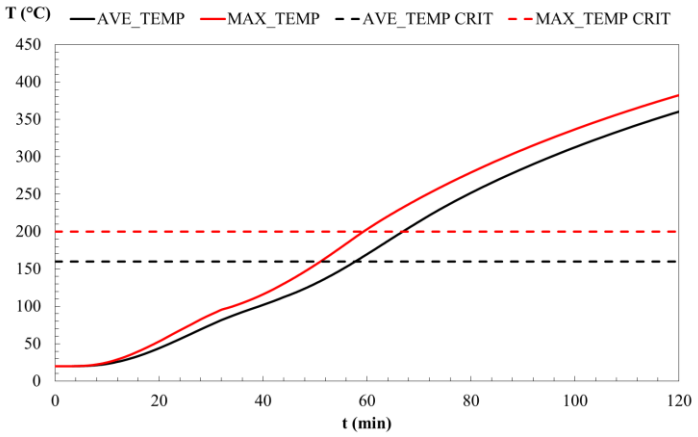

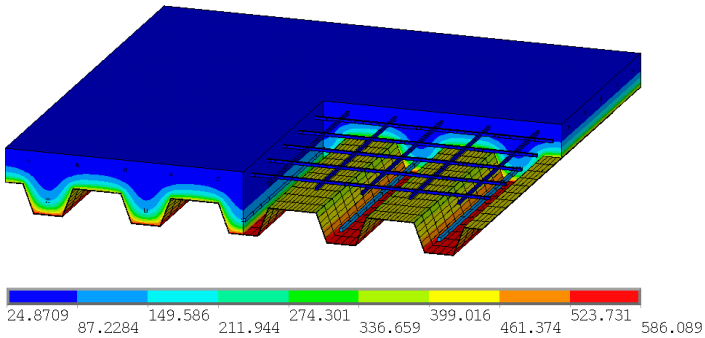

t= 14.4 min

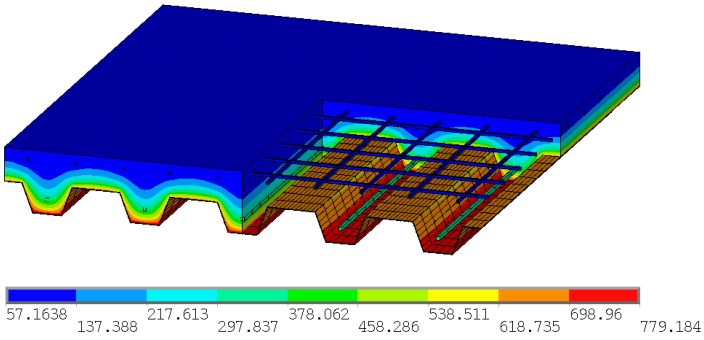

t= 28.9 min

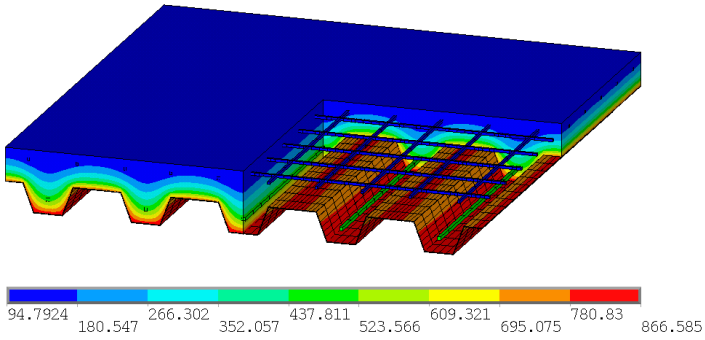

t= 43.3 min

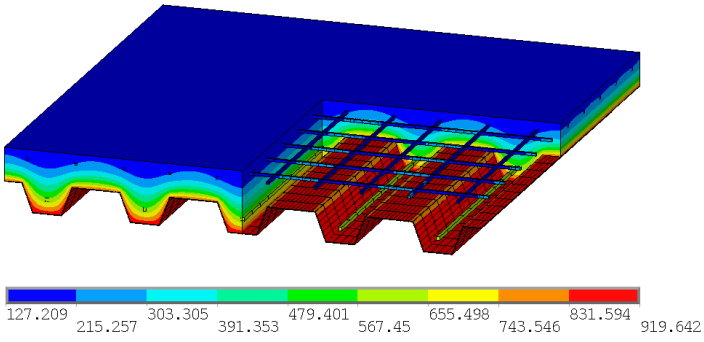

t= 57.7 min

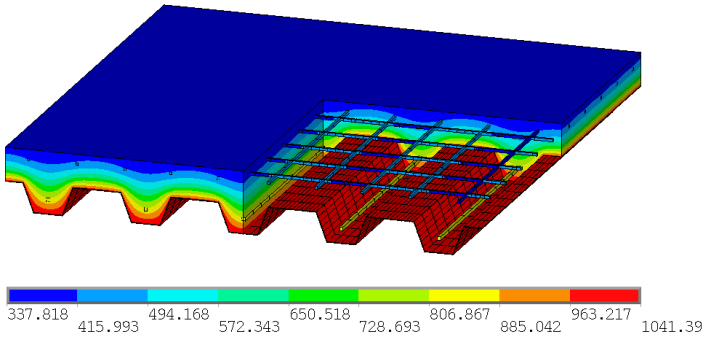

t= 120.0 min

SIM. 4	**Steel deck:** Trapezoidal – O Feliz H60	**Rebar (mm):** ϕ8	**Fire resistance (min)**	
	Mesh (mm//mm): ϕ6//100 (FNQ 60)	**h_1 (mm):** 80	Ave: *70.1*	Max: 74.5

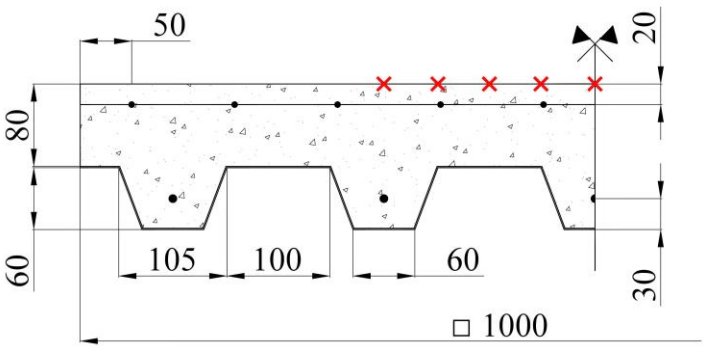

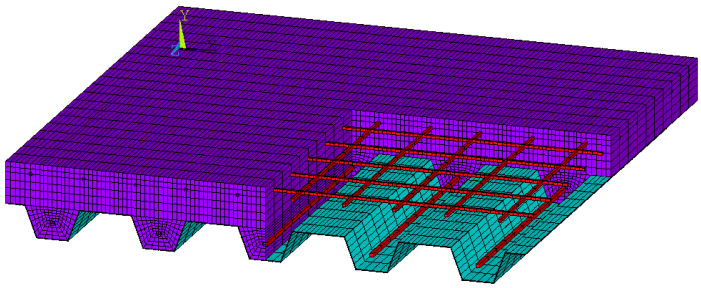

Finite element mesh

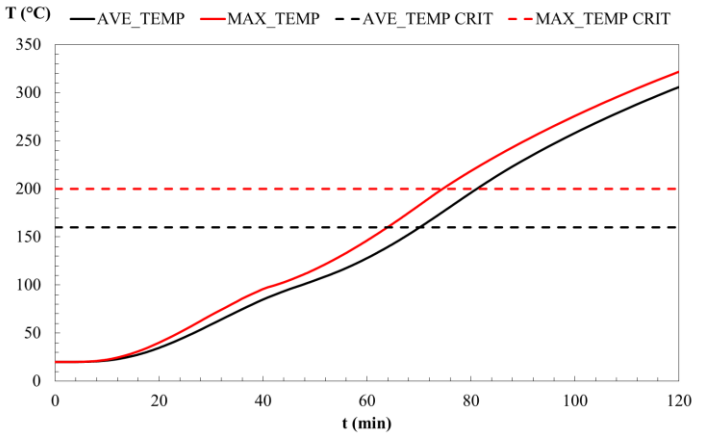

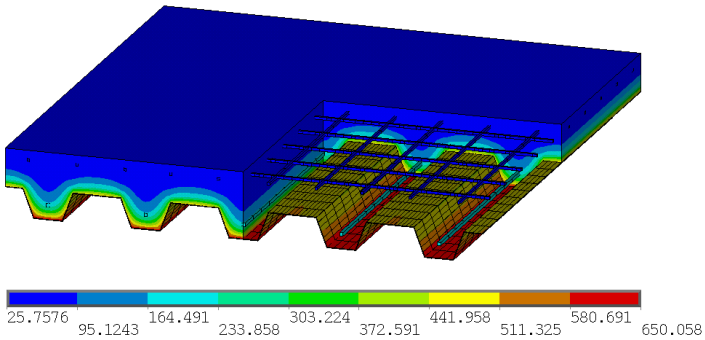

t= 17.5 min

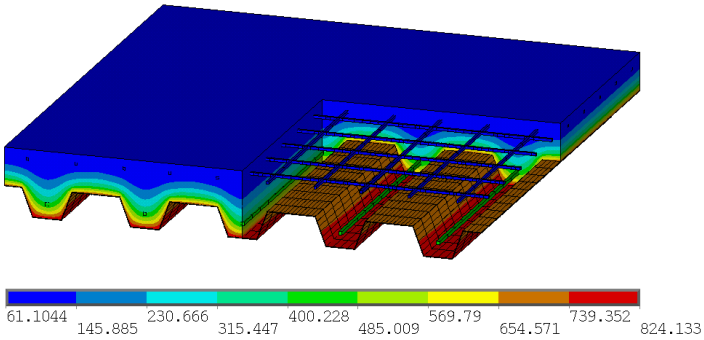

t= 35.1 min

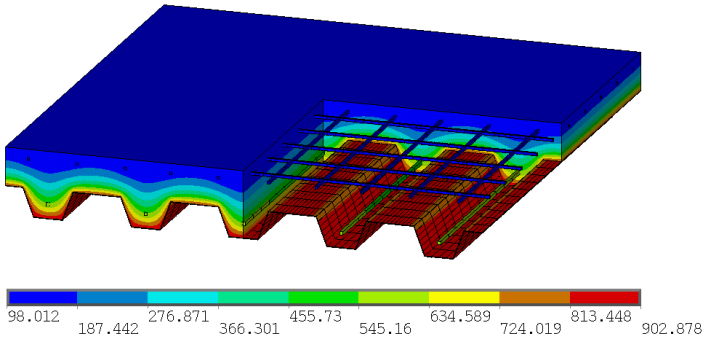

t= 52.6 min

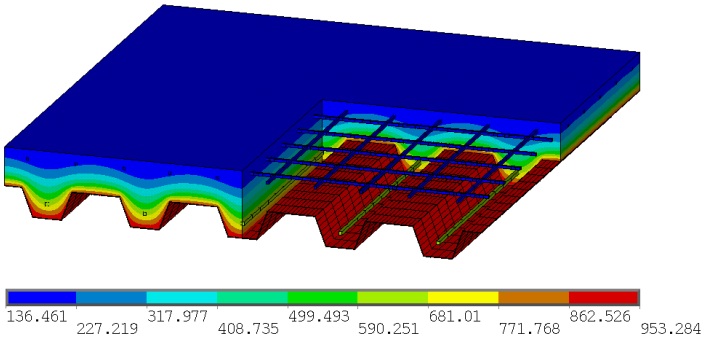

t= 70.1 min

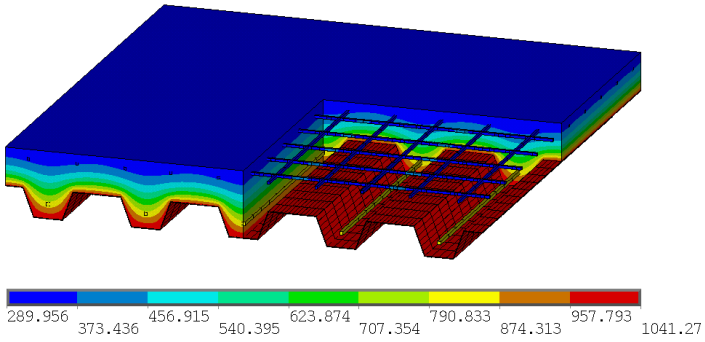

t= 120.0 min

SIM. 5	**Steel deck:** Trapezoidal – O Feliz H60	**Rebar (mm):** ϕ8	**Fire resistance (min)**	
	Mesh (mm//mm): ϕ6//100 (FNQ 60)	**h_1 (mm):** 50	Ave: 36.2	Max: *34.5*

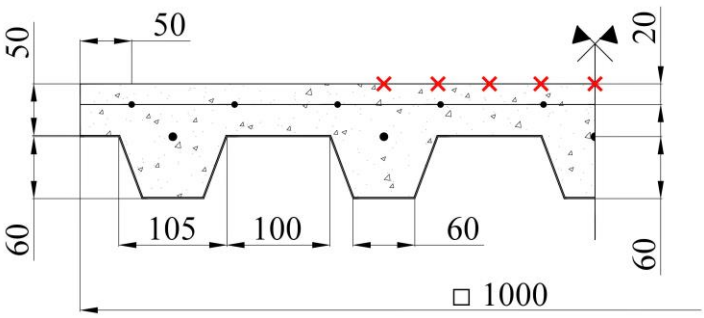

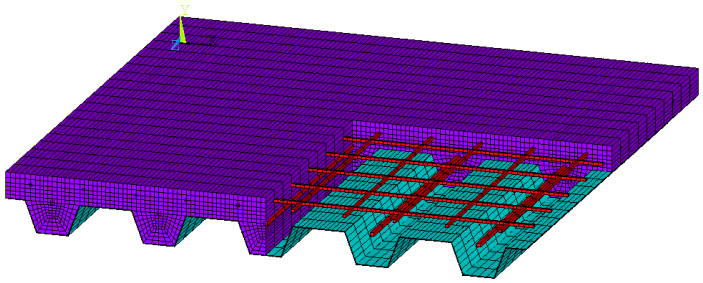

Finite element mesh

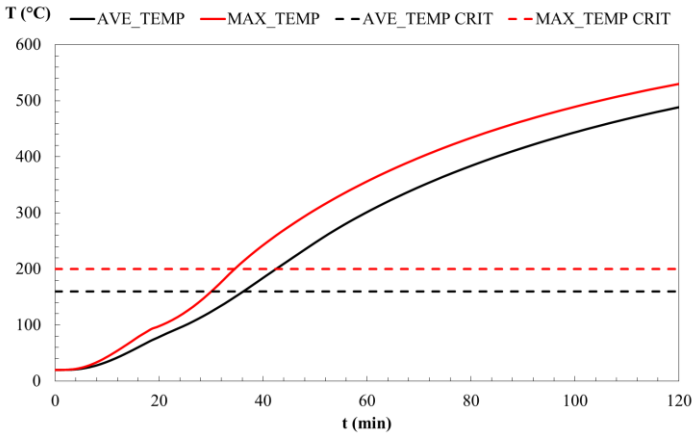

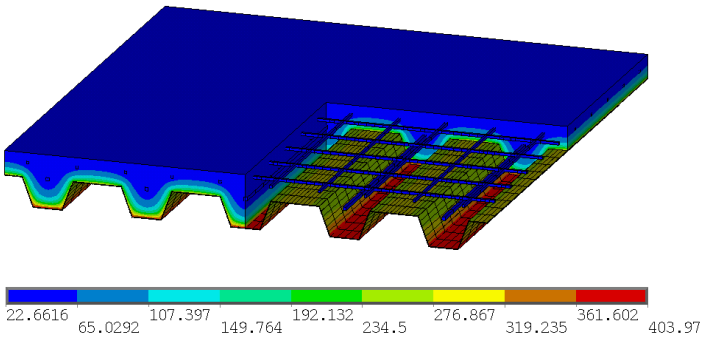

t= 8.6 min

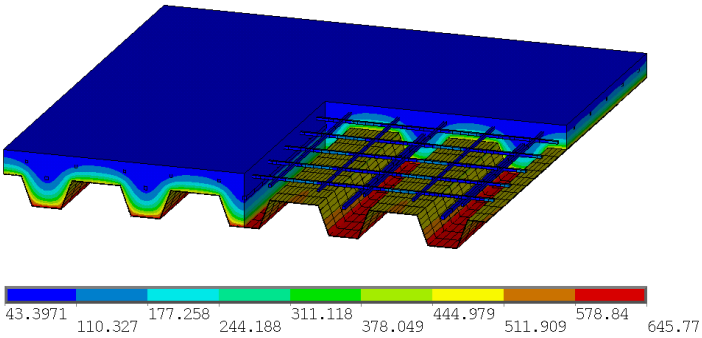

t= 17.3 min

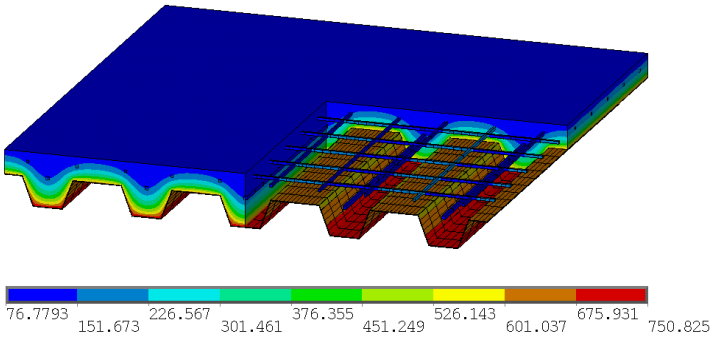

t= 25.9 min

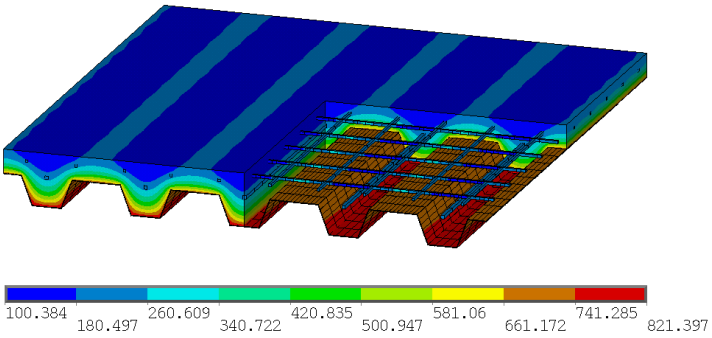

t= 34.5 min

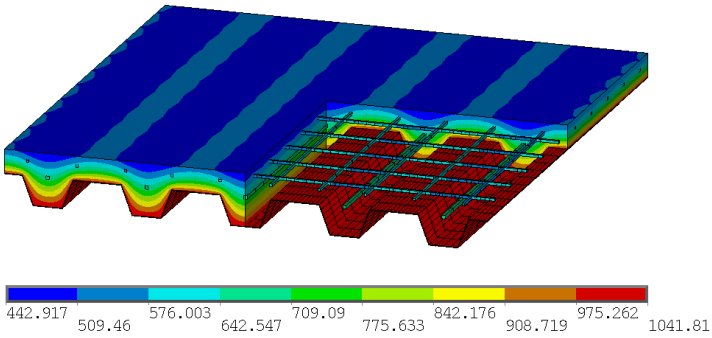

t= 120.0 min

SIM. 6	**Steel deck:** Trapezoidal – O Feliz H60	**Rebar (mm):** ϕ8	**Fire resistance (min)**	
	Mesh (mm//mm): ϕ6//100 (FNQ 60)	**h_1 (mm):** 60	Ave: 46.3	Max: *45.9*

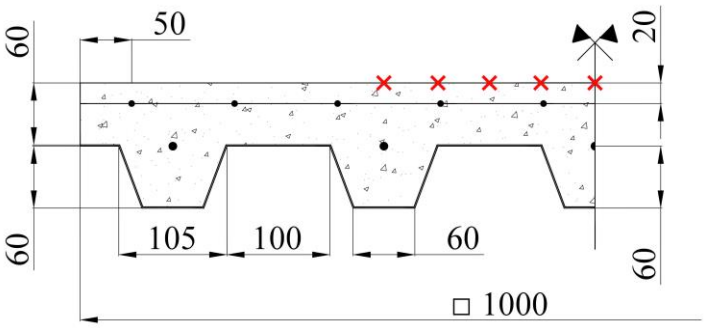

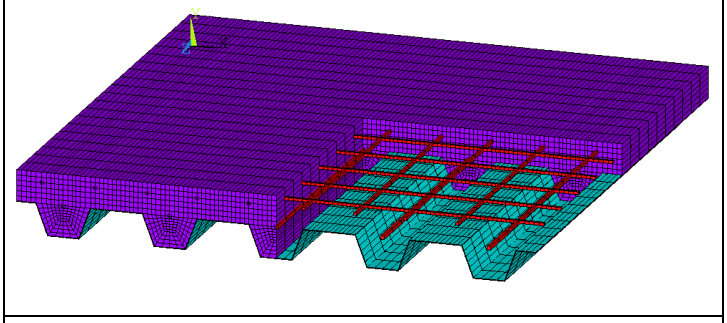

Finite element mesh

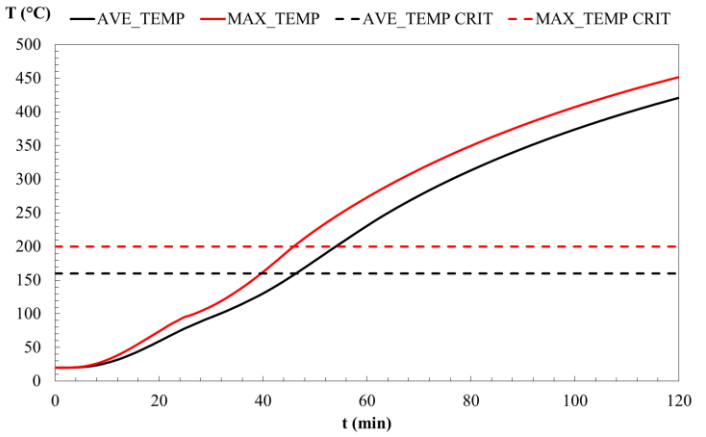

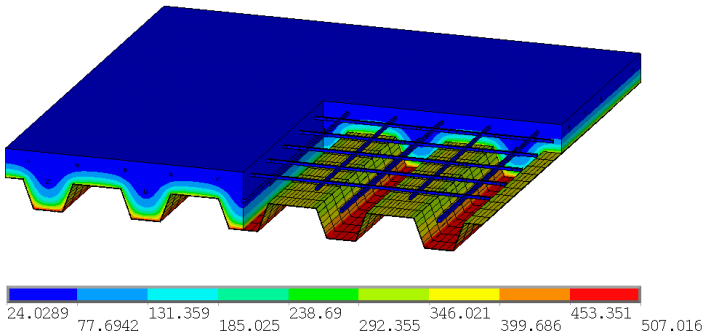

t= 11.5 min

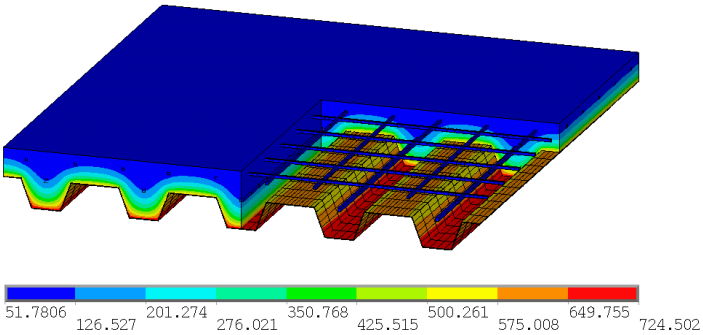

t= 23.0 min

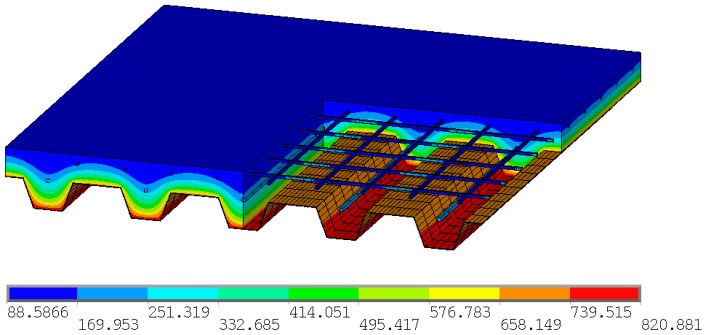

t= 34.4 min

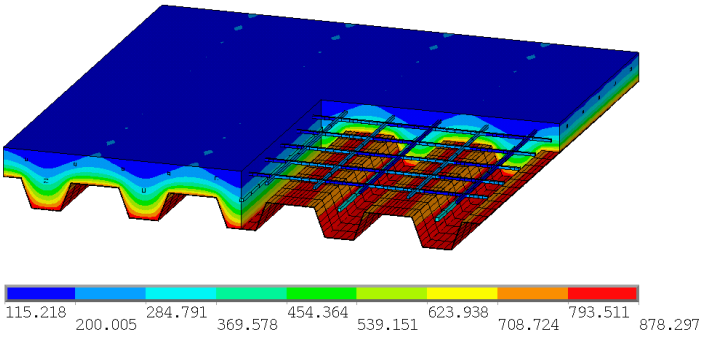

t= 45.9 min

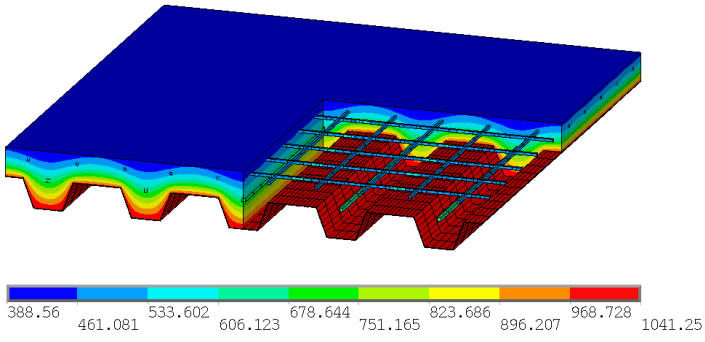

t= 120.0 min

SIM. 7	**Steel deck:** Trapezoidal – O Feliz H60	**Rebar (mm):** ϕ8	**Fire resistance (min)**	
	Mesh (mm//mm): ϕ6//100 (FNQ 60)	**h_1 (mm):** 70	Ave: *57.5*	Max: 59.2

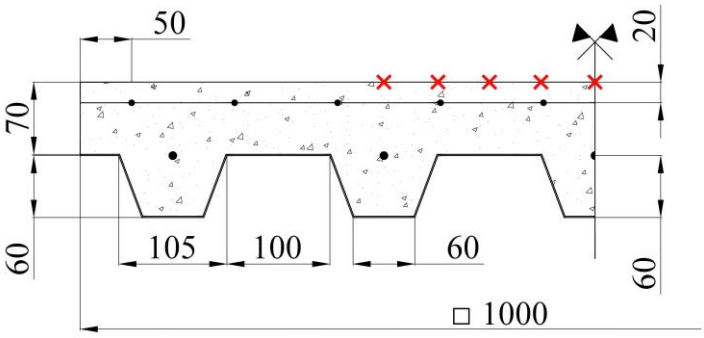

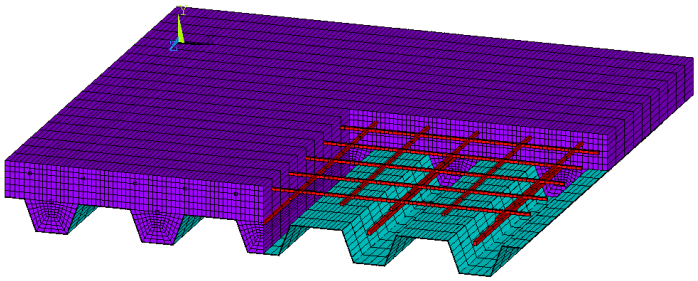

Finite element mesh

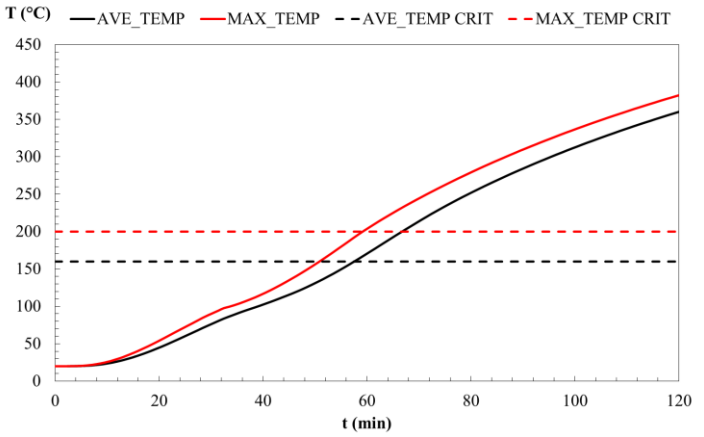

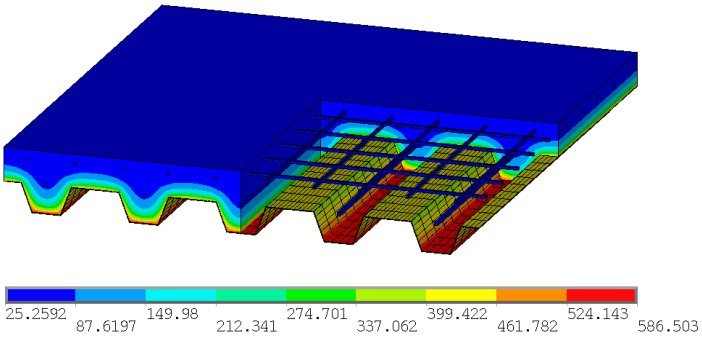

t= 14.4 min

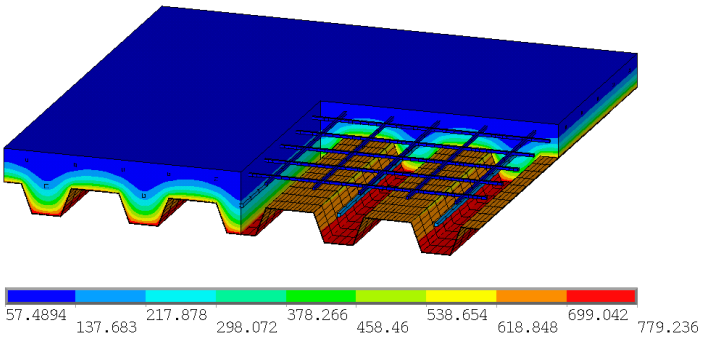

t= 28.8 min

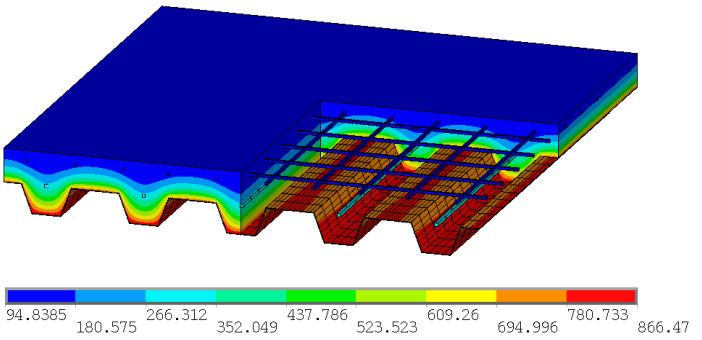

t= 43.1 min

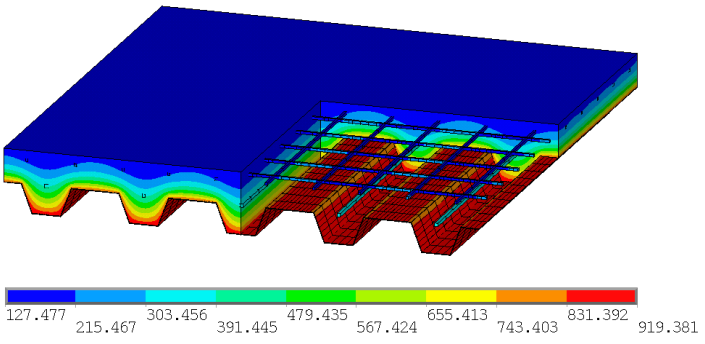

t= 57.5 min

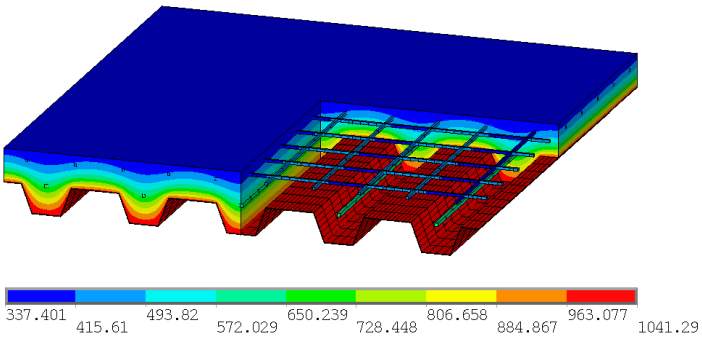

t= 120.0 min

SIM. 8	**Steel deck:** Trapezoidal – O Feliz H60	**Rebar (mm):** ϕ8	**Fire resistance (min)**	
	Mesh (mm//mm): ϕ6//100 (FNQ 60)	**h_1 (mm):** 80	Ave: *70.0*	Max: 74.4

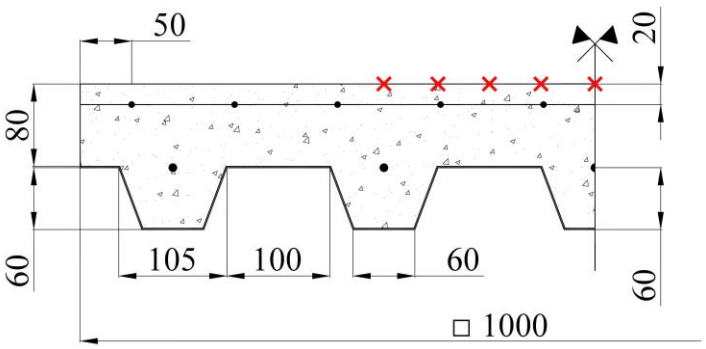

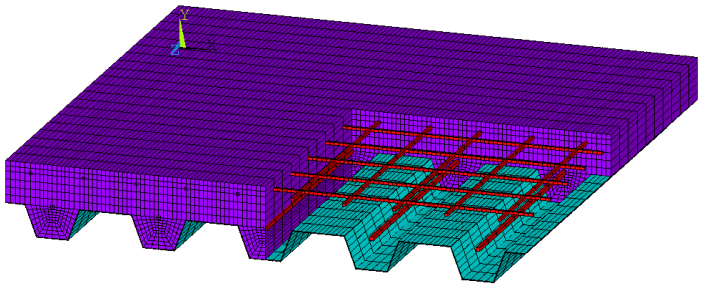

Finite element mesh

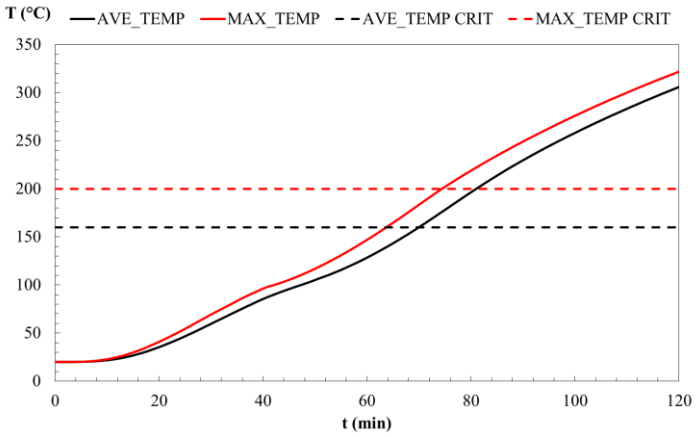

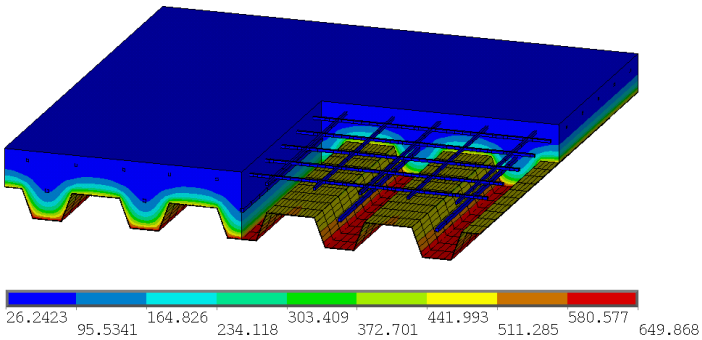

t= 17.5 min

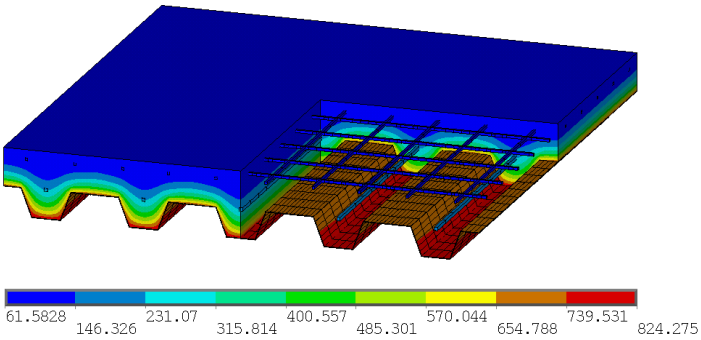

t= 35.0 min

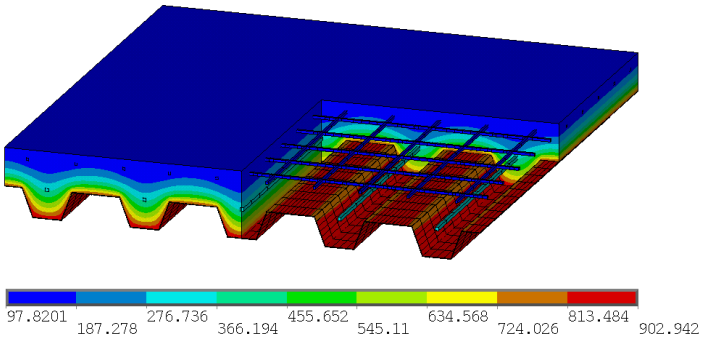

t= 52.5 min

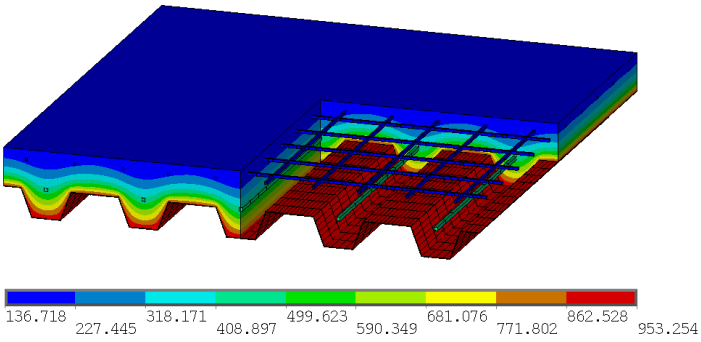

t= 70.0 min

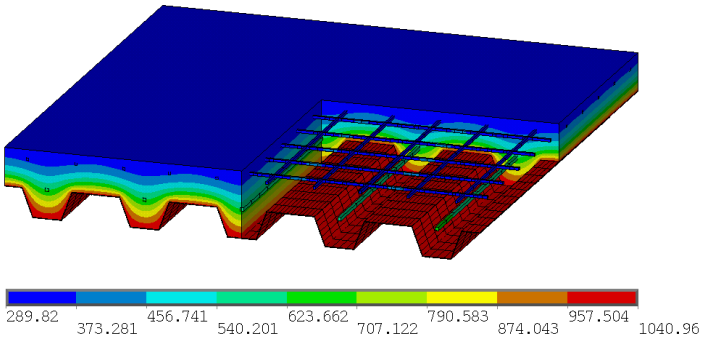

t= 120.0 min

SIM. 9	**Steel deck:** Trapezoidal – O Feliz H60	**Rebar (mm):** ϕ8	**Fire resistance (min)**	
	Mesh (mm//mm): ϕ6//150 (FND 60)	**h_1 (mm):** 50	Ave: 36.4	Max: *35.1*

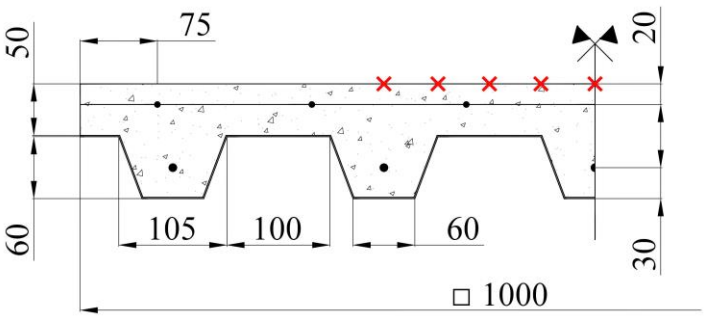

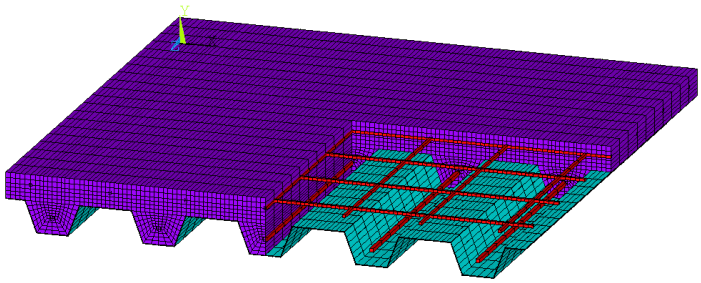

Finite element mesh

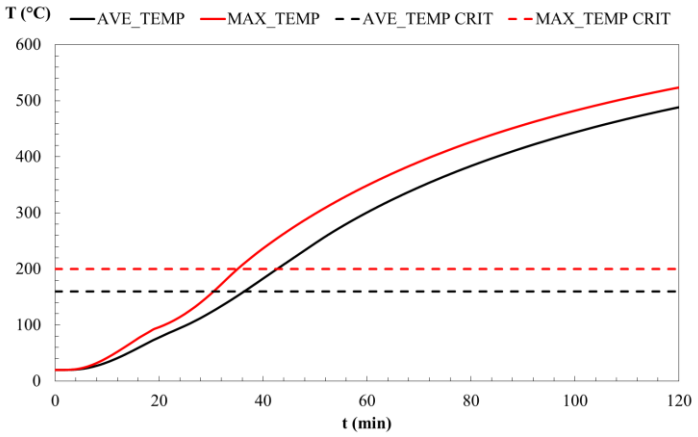

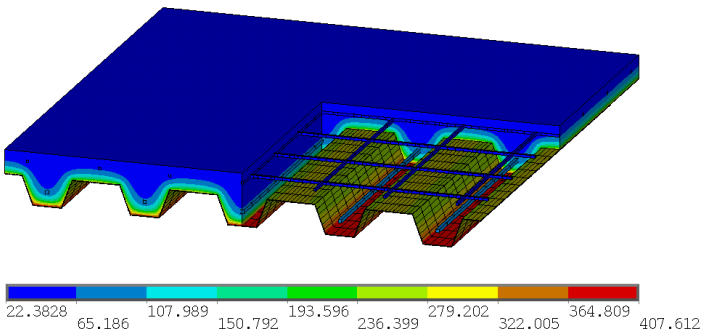

t= 8.8 min

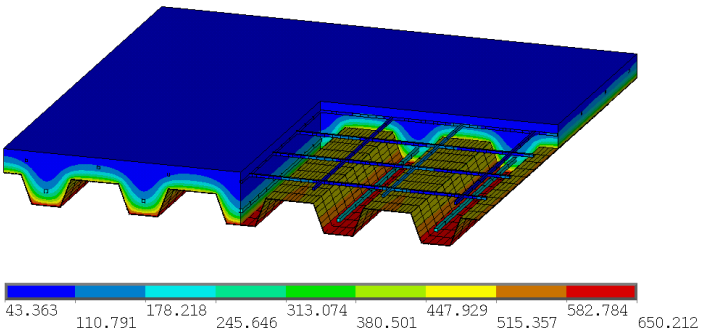

t= 17.6 min

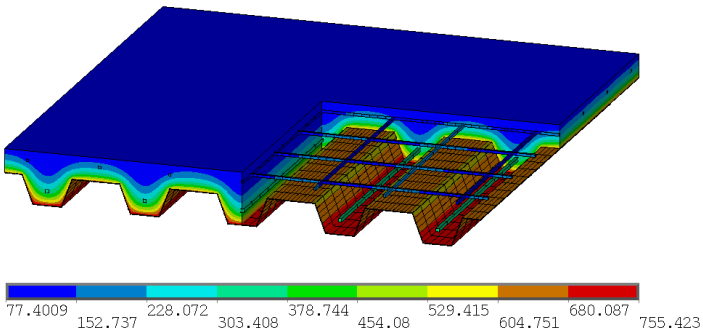

t= 26.3 min

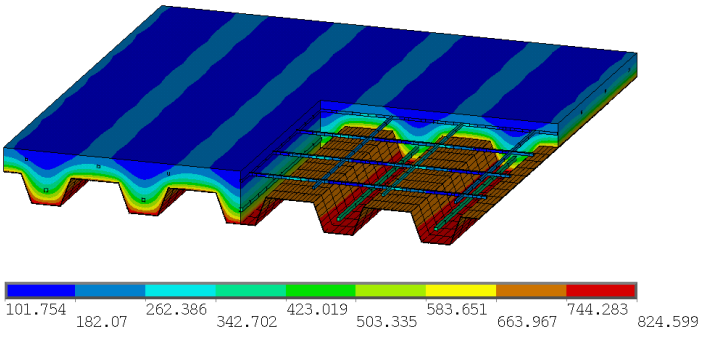

t= 35.1 min

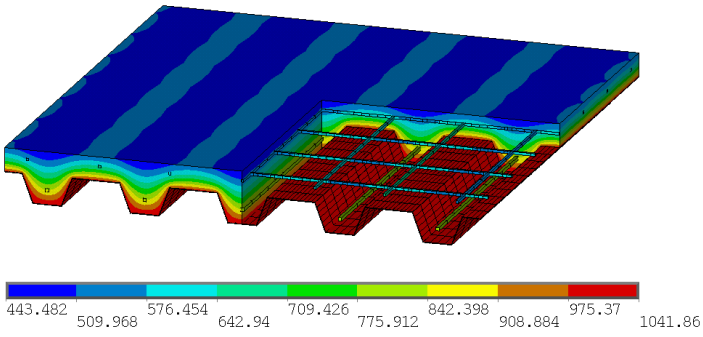

t= 120.0 min

SIM. 10	**Steel deck:** Trapezoidal – O Feliz H60	**Rebar (mm):** ϕ8	**Fire resistance (min)**	
	Mesh (mm//mm): ϕ6//150 (FND 60)	**h_1 (mm):** 60	Ave: *46.5*	Max: 46.5

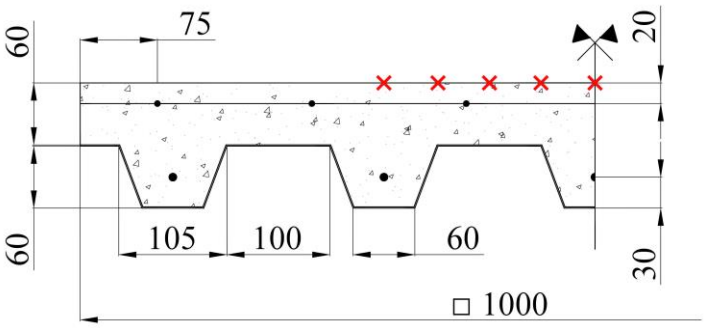

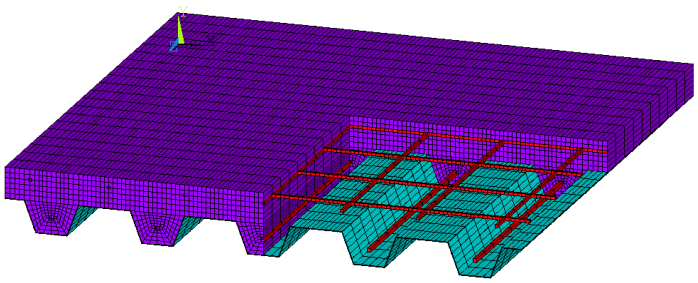

Finite element mesh

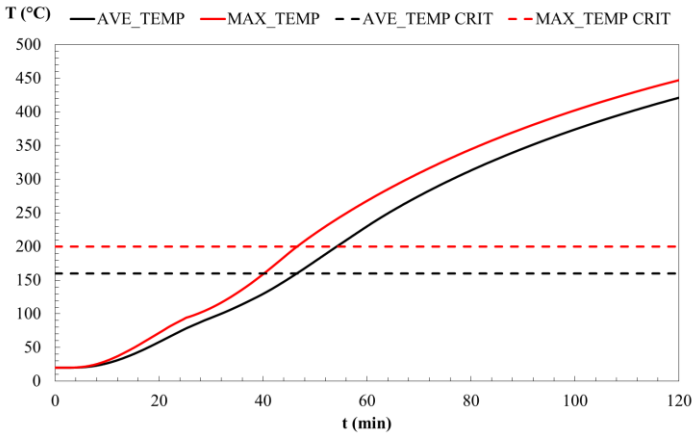

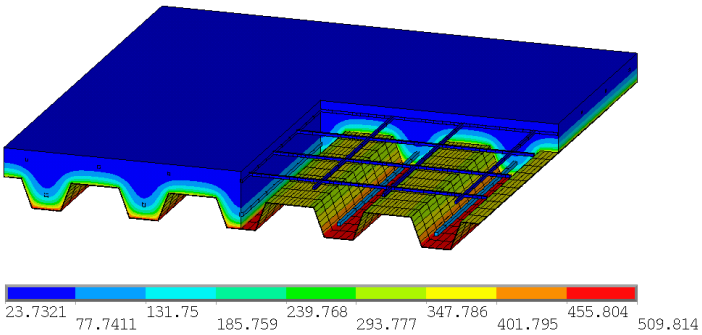

t= 11.6 min

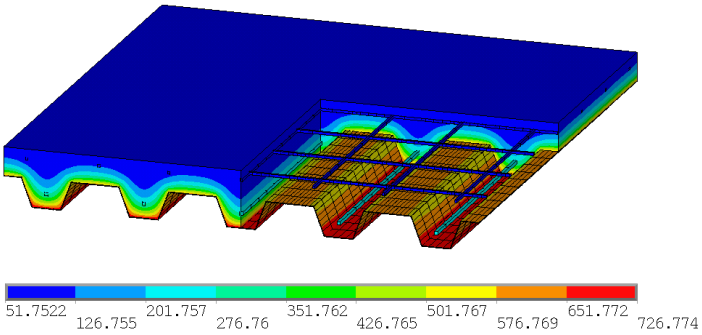

t= 23.3 min

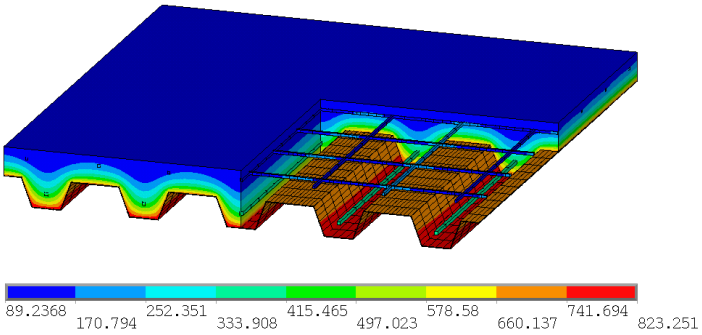

t= 34.9 min

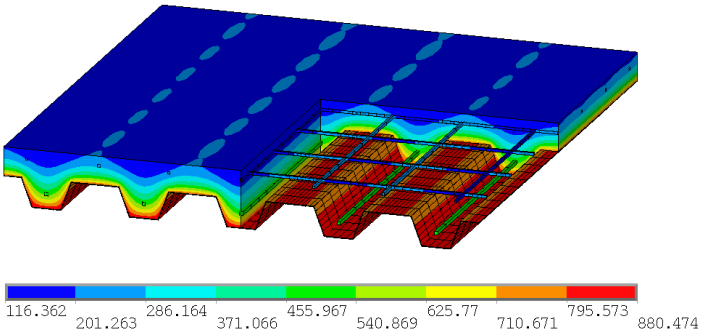

t= 46.5 min

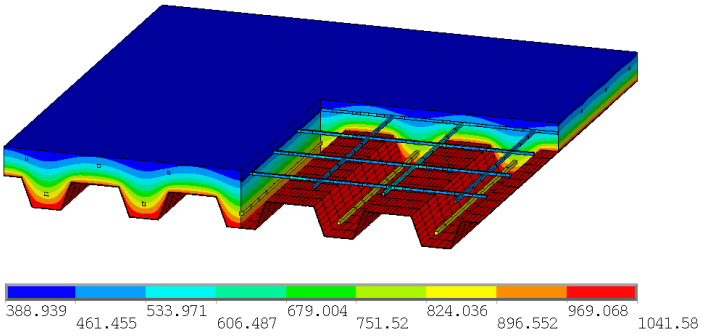

t= 120.0 min

SIM. 11	**Steel deck:** Trapezoidal – O Feliz H60	**Rebar (mm):** ϕ8	**Fire resistance (min)**	
	Mesh (mm//mm): ϕ6//150 (FND 60)	**h_1 (mm):** 70	Ave: *57.8*	Max: 60.0

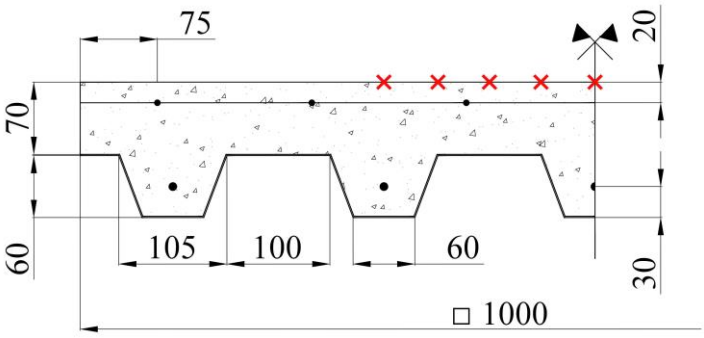

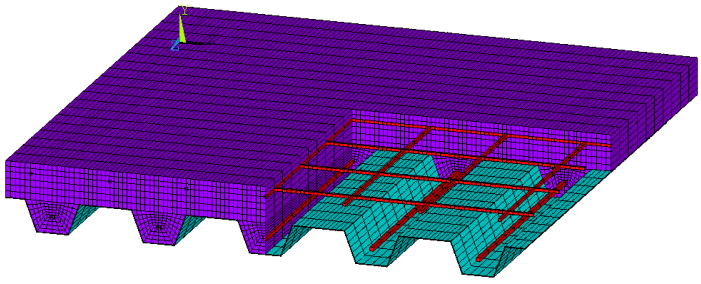

Finite element mesh

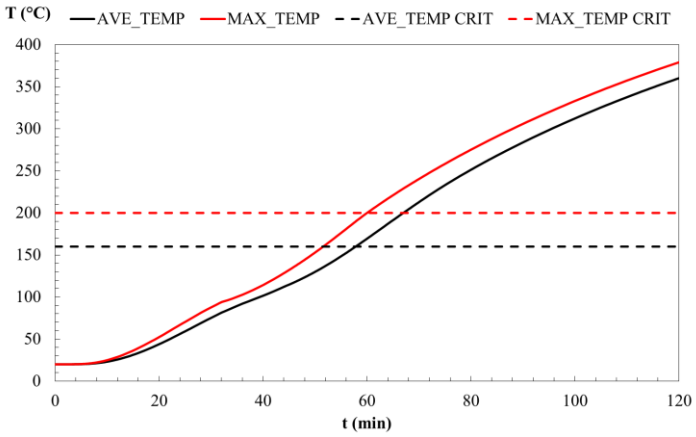

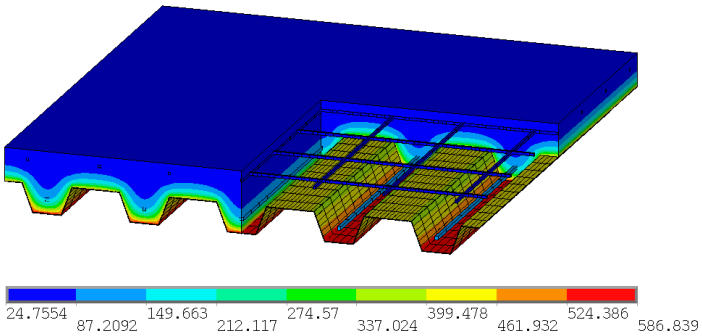

t= 14.5 min

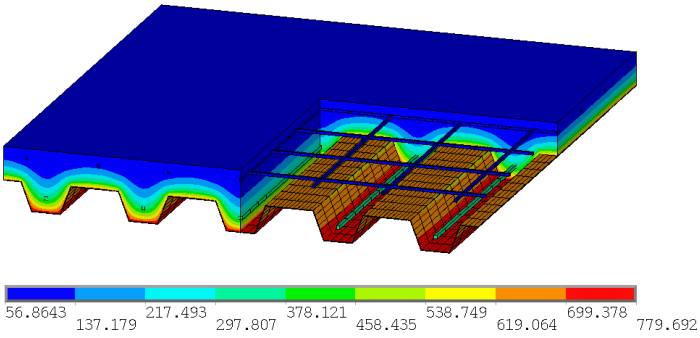

t= 28.9 min

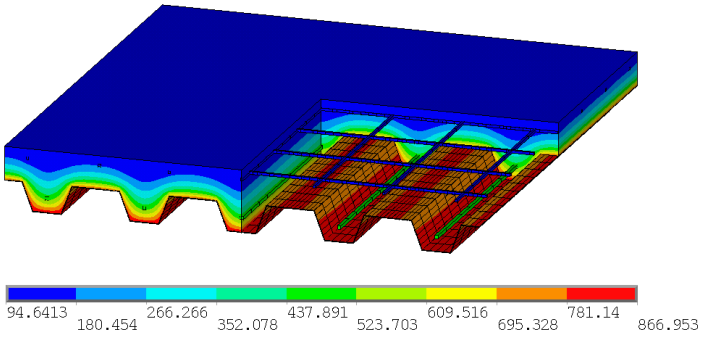

t= 43.4 min

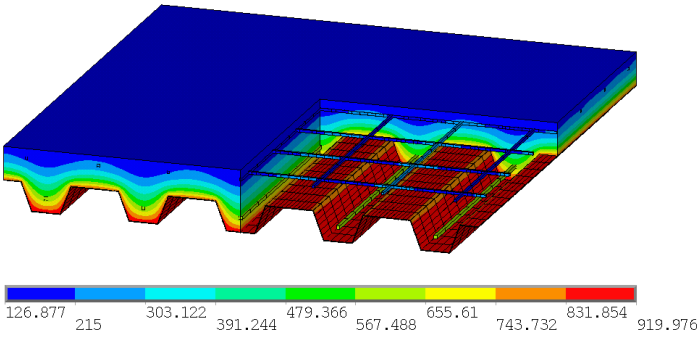

t= 57.8 min

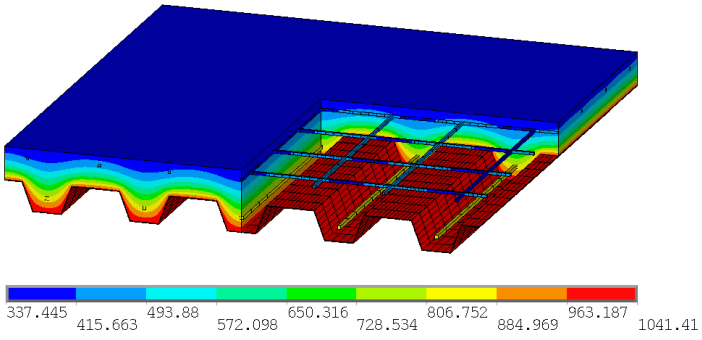

t= 120.0 min

SIM. 12	**Steel deck:** Trapezoidal – O Feliz H60	**Rebar (mm):** ϕ8	**Fire resistance (min)**	
	Mesh (mm//mm): ϕ6//150 (FND 60)	**h_1 (mm):** 80	Ave: *70.2*	Max: 75.2

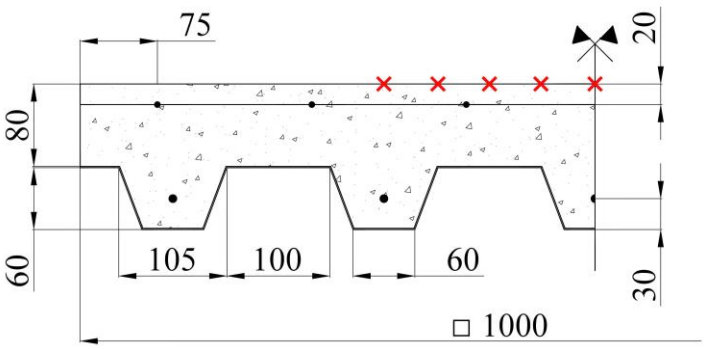

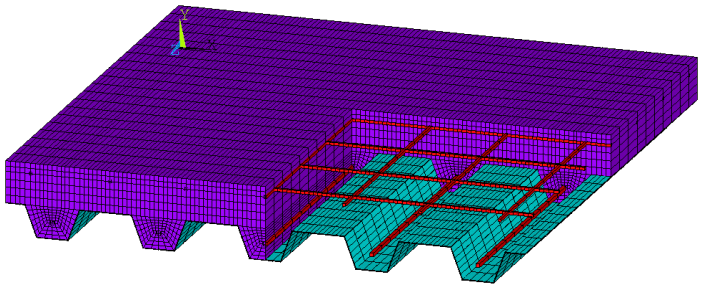

Finite element mesh

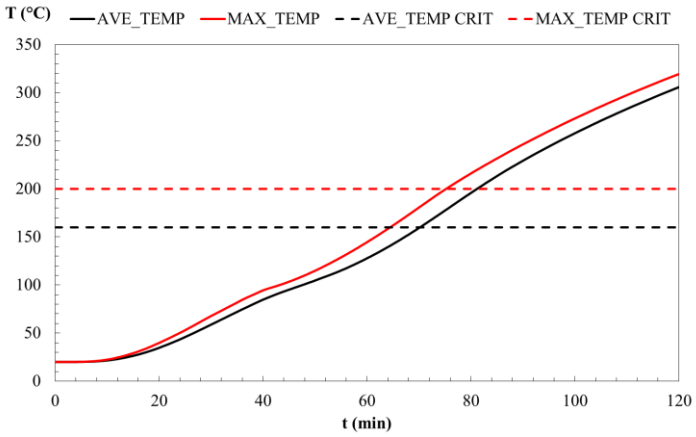

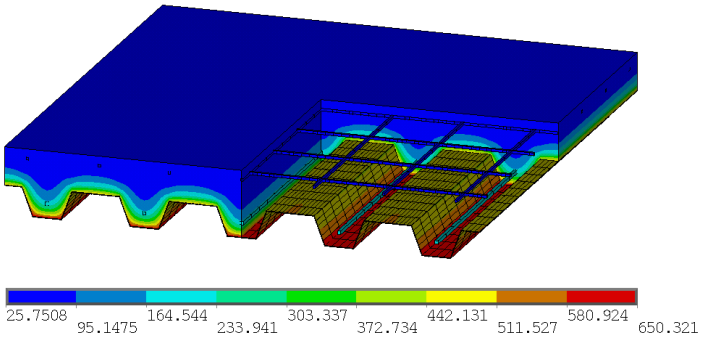

t= 17.6 min

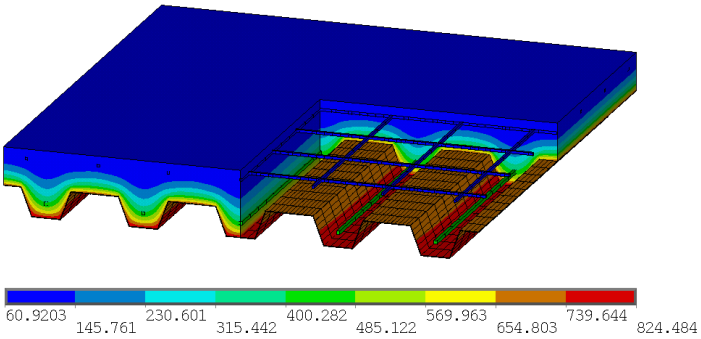

t= 35.1 min

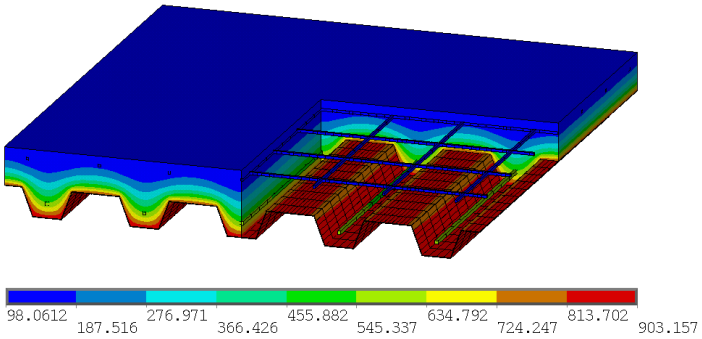

t= 52.7 min

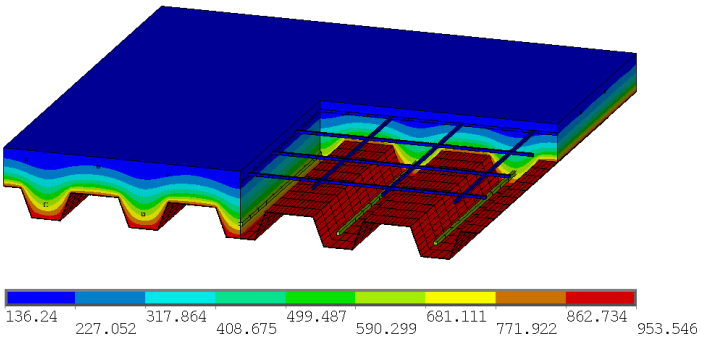

t= 70.2 min

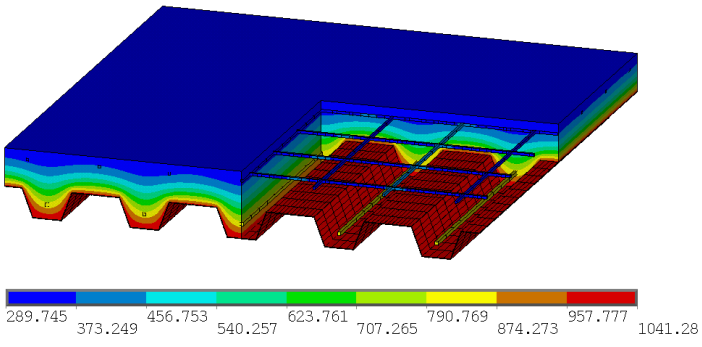

t= 120.0 min

SIM. 13	**Steel deck:** Trapezoidal – O Feliz H60	**Rebar (mm):** ϕ8	**Fire resistance (min)**	
	Mesh (mm//mm): ϕ6//150 (FND 60)	**h_1 (mm):** 50	Ave: 36.3	Max: *35.0*

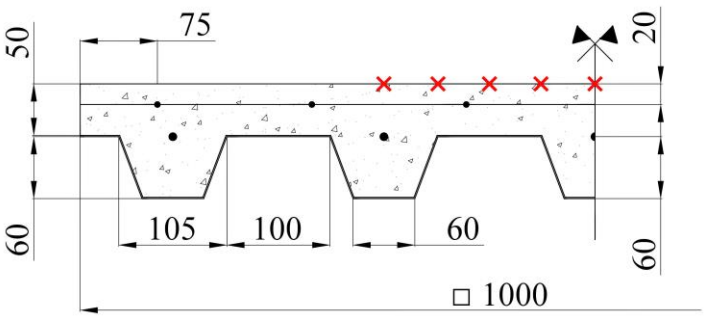

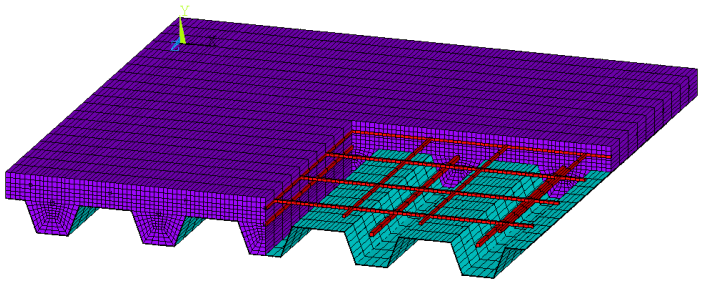

Finite element mesh

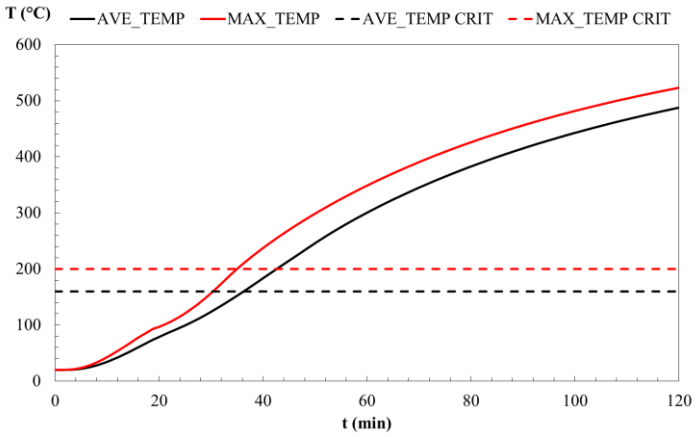

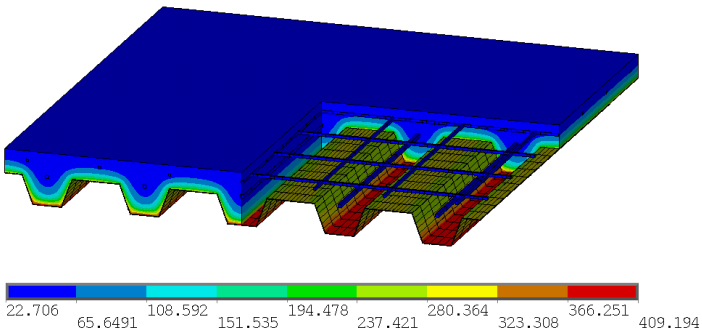

t= 8.8 min

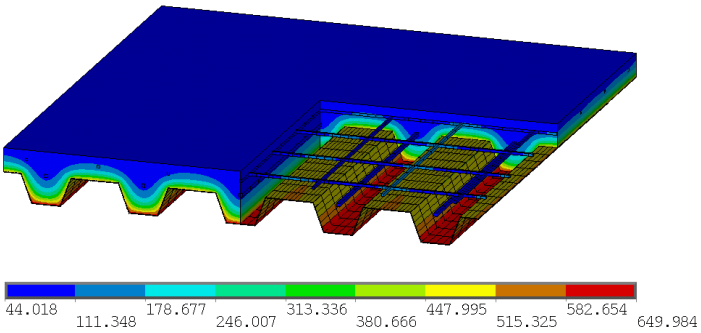

t= 17.5 min

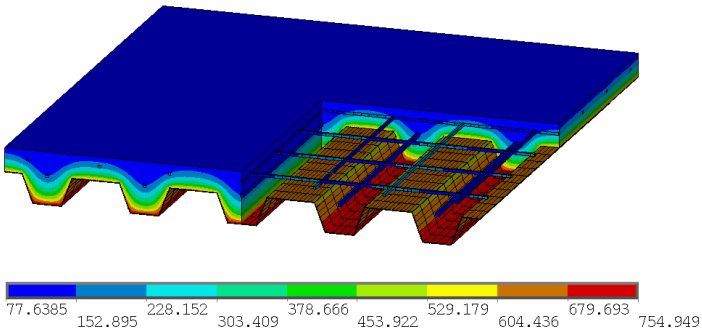

t= 26.3 min

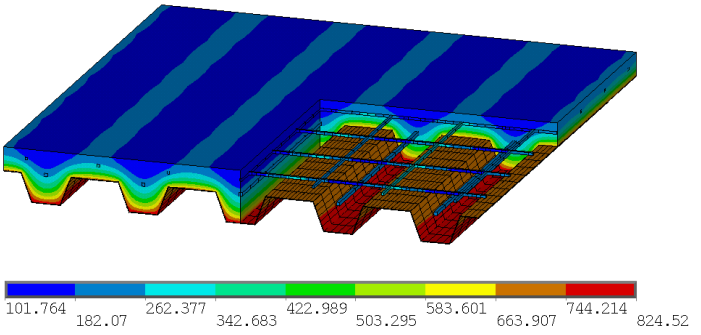

t= 35.0 min

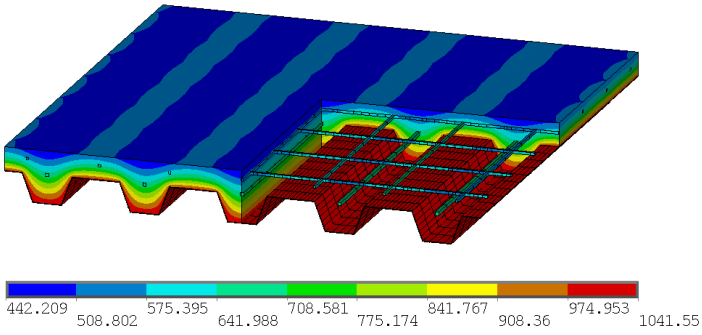

t= 120.0 min

SIM. 14	**Steel deck:** Trapezoidal – O Feliz H60	**Rebar (mm):** ϕ8	**Fire resistance (min)**	
	Mesh (mm//mm): ϕ6//150 (FND 60)	**h_1 (mm):** 60	Ave: *46.4*	Max: 46.5

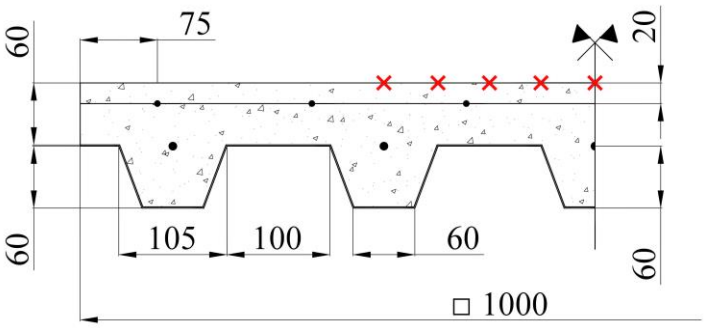

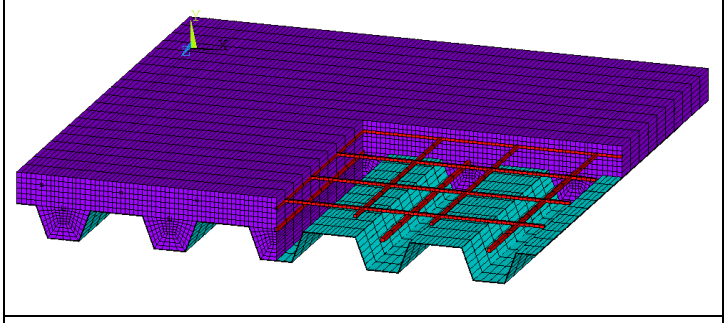

Finite element mesh

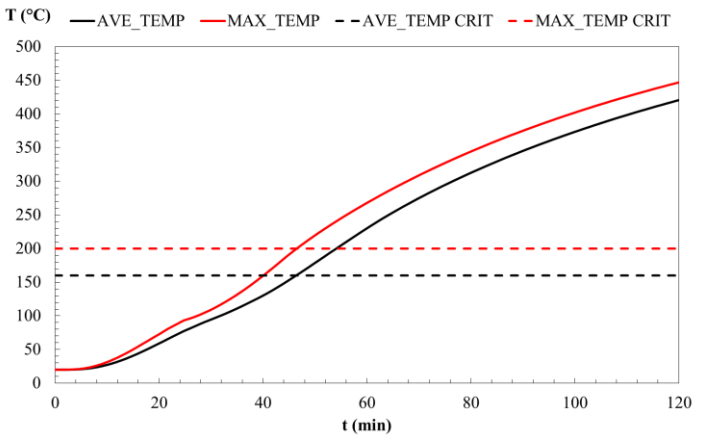

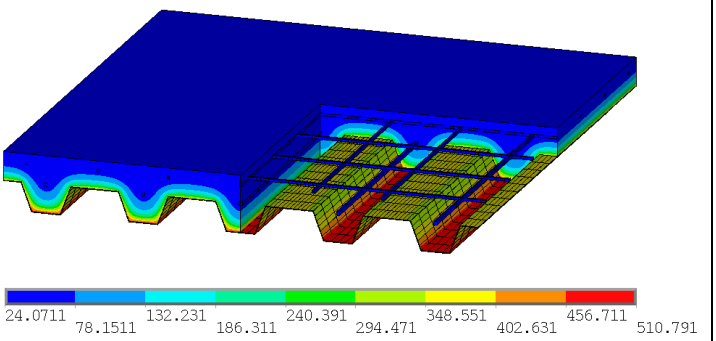

t= 11.6 min

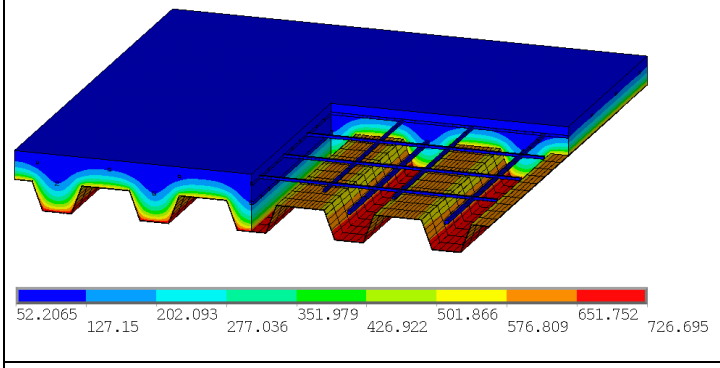

t= 23.2 min

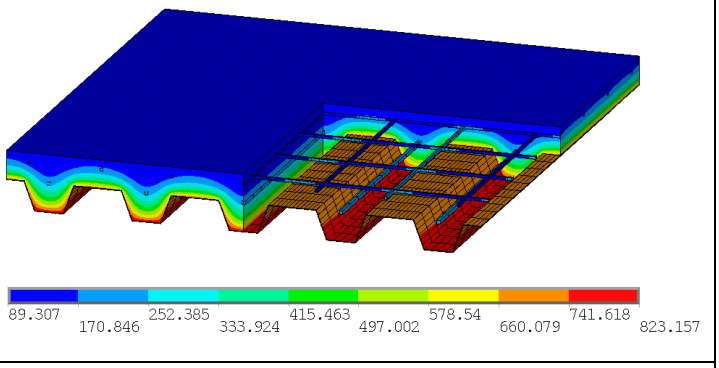

t= 34.8 min

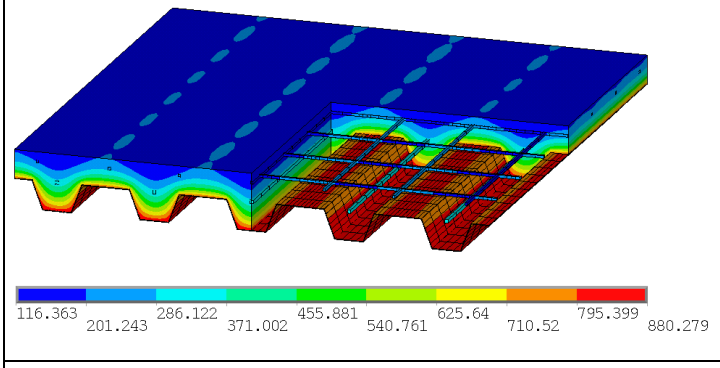

t= 46.4 min

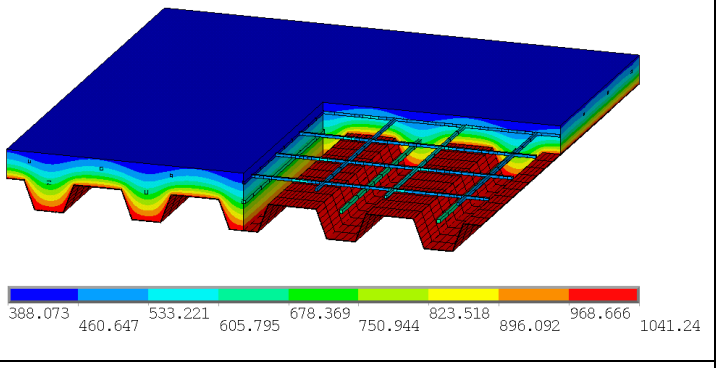

t= 120.0 min

SIM. 15	**Steel deck:** Trapezoidal – O Feliz H60	**Rebar (mm):** ϕ8	**Fire resistance (min)**	
	Mesh (mm//mm): ϕ6//150 (FND 60)	**h_1 (mm):** 70	Ave: *57.6*	Max: 59.9

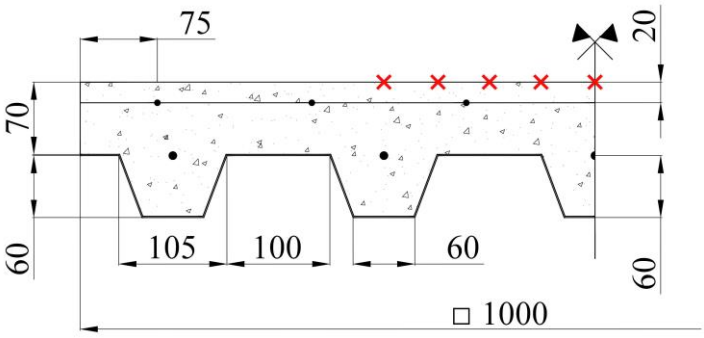

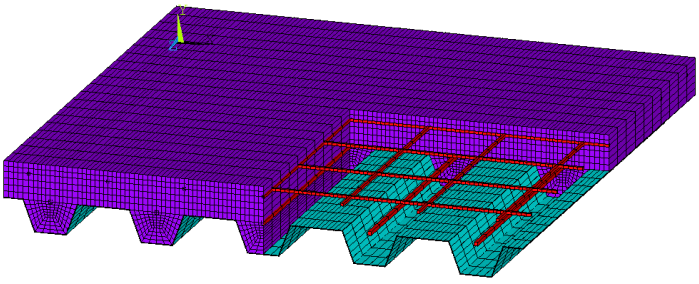

Finite element mesh

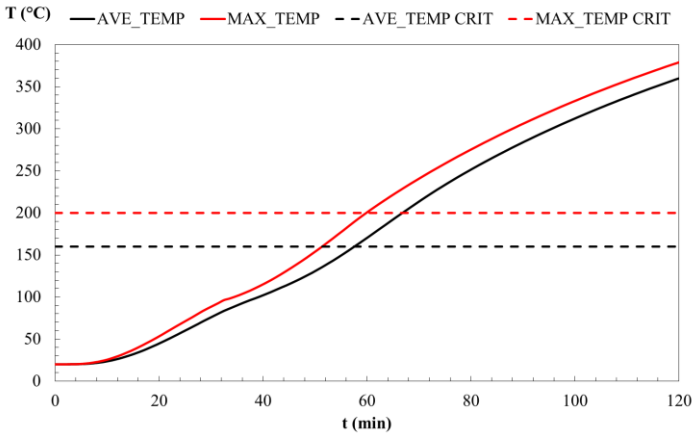

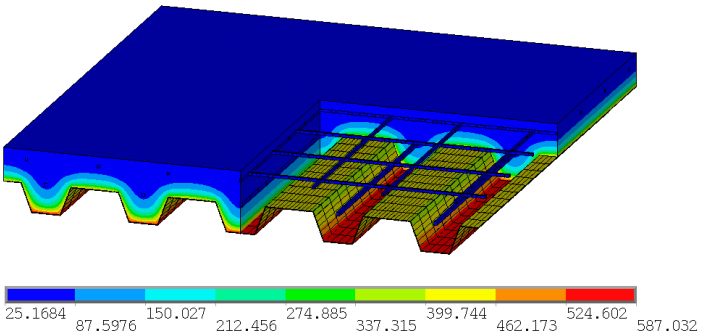

t= 14.4 min

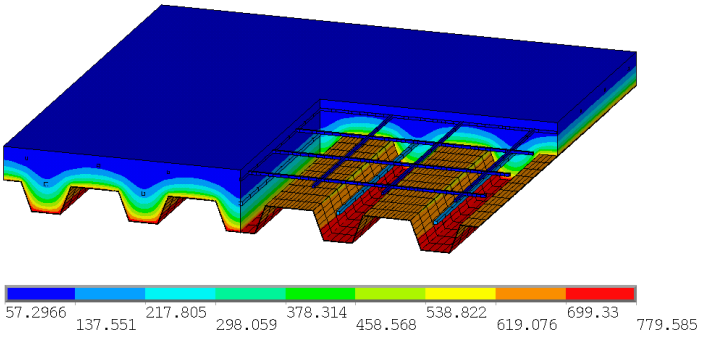

t= 28.8 min

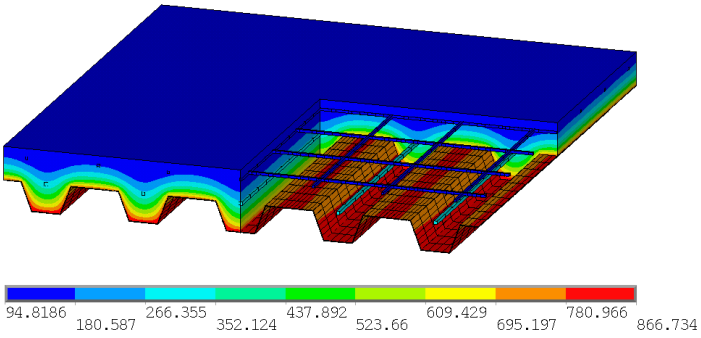

t= 43.2 min

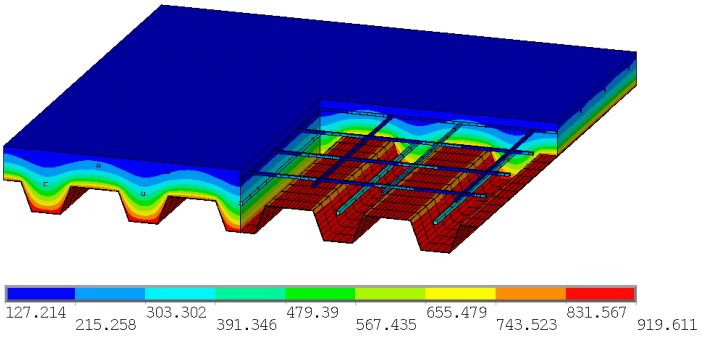

t= 57.6 min

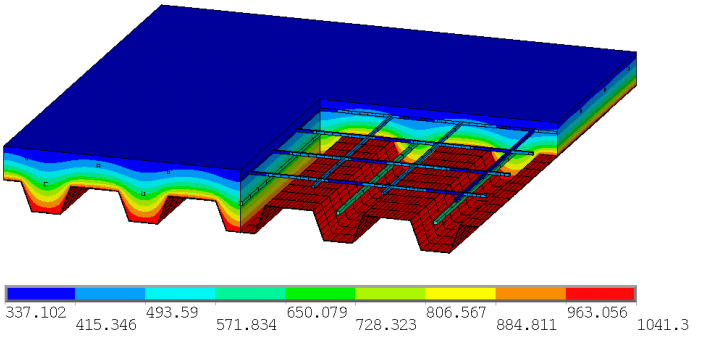

t= 120.0 min

SIM. 16	**Steel deck:** Trapezoidal – O Feliz H60	**Rebar (mm):** ϕ8	**Fire resistance (min)**	
	Mesh (mm//mm): ϕ6//150 (FND 60)	**h_1 (mm):** 80	Ave: *70.0*	Max: 75.1

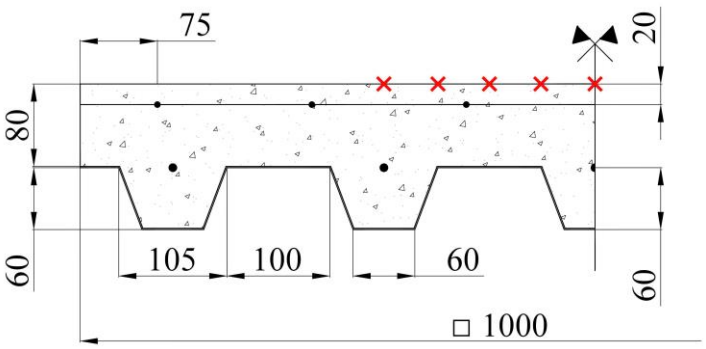

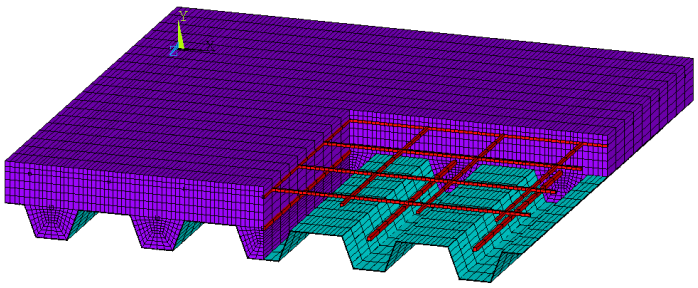

Finite element mesh

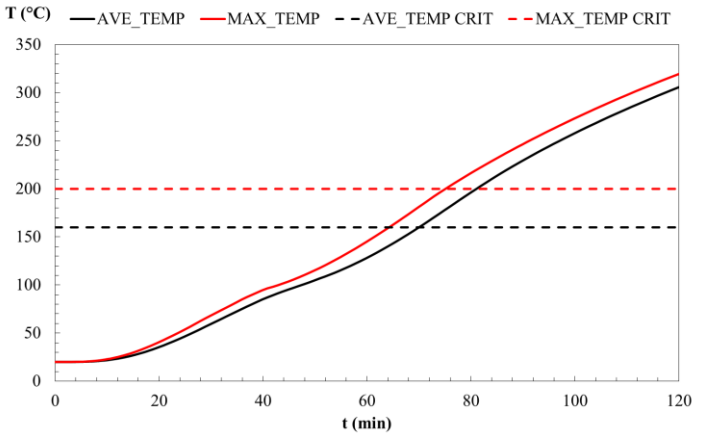

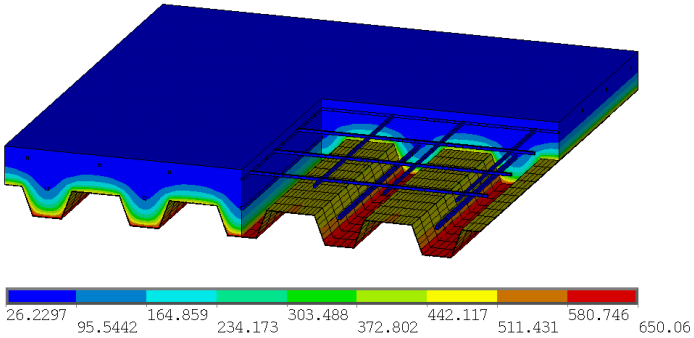

t= 17.5 min

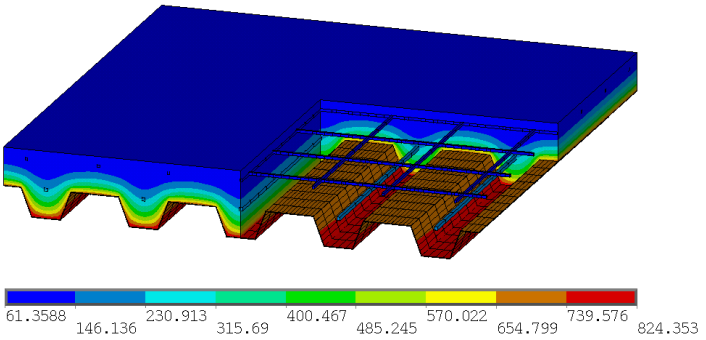

t= 35.0 min

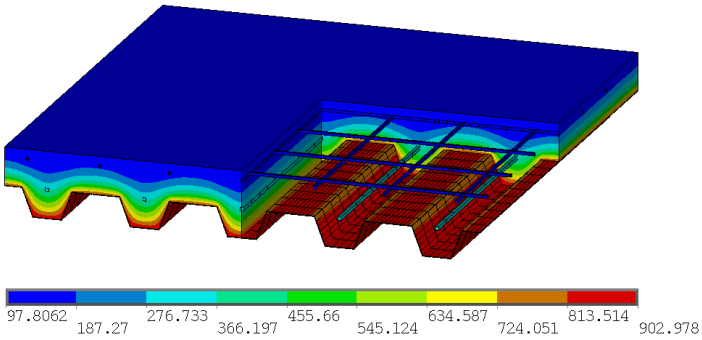

t= 52.5 min

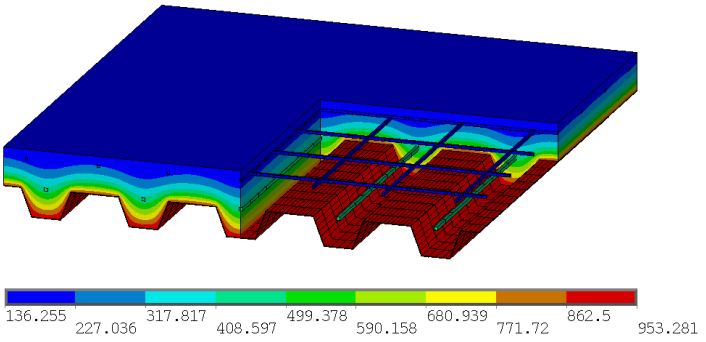

t= 70.0 min

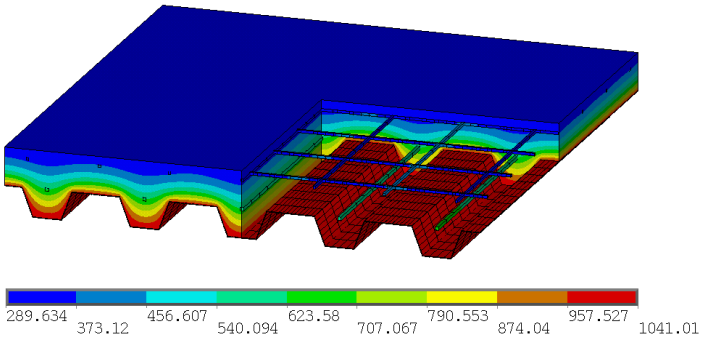

t= 120.0 min

SIM. 17	**Steel deck:** Trapezoidal – O Feliz H60	**Rebar (mm):** ϕ10	**Fire resistance (min)**	
	Mesh (mm//mm): ϕ6//100 (FNQ 60)	**h_1 (mm):** 50	Ave: 36.3	Max: *34.6*

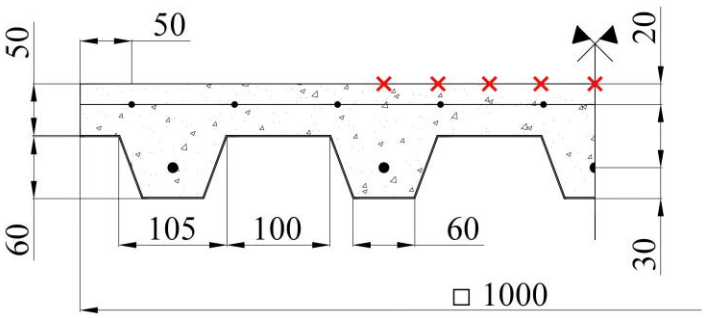

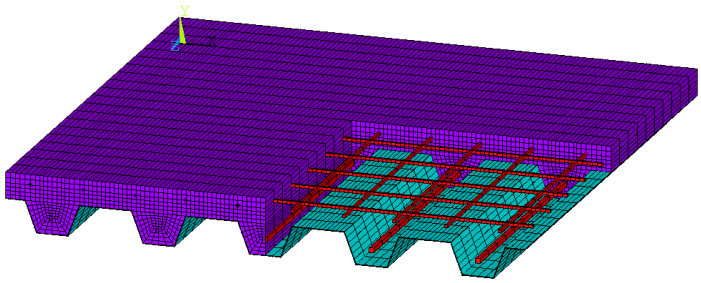

Finite element mesh

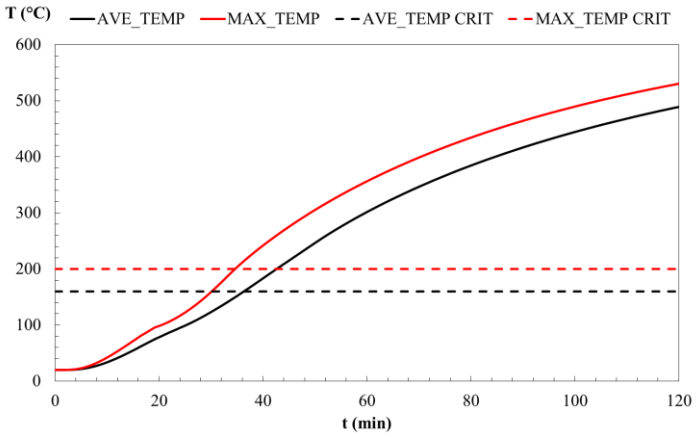

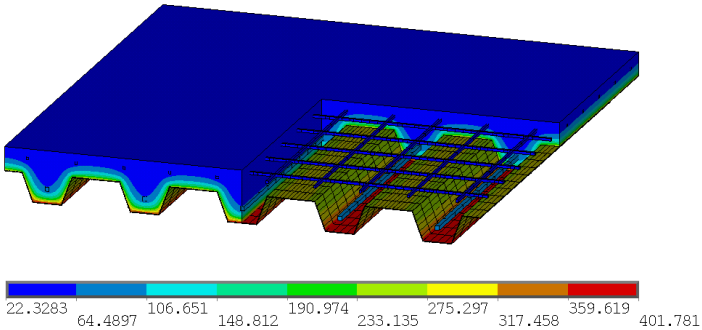

t= 8.7 min

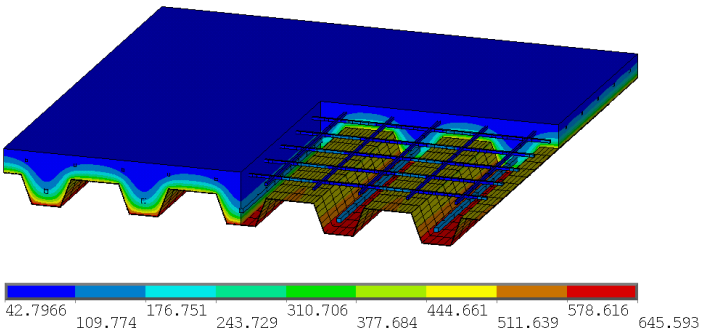

t= 17.3 min

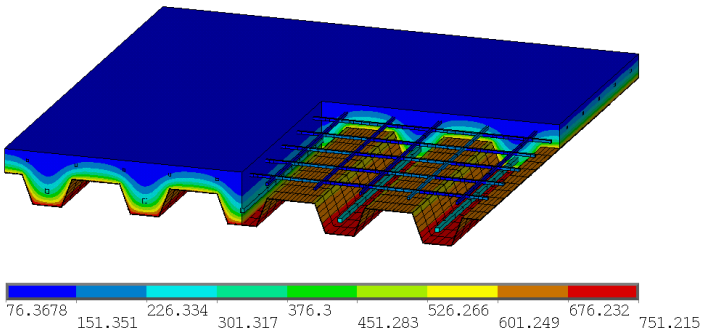

t= 26.0 min

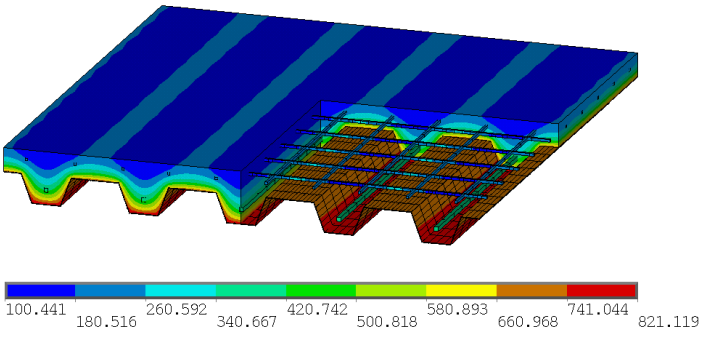

t= 34.6 min

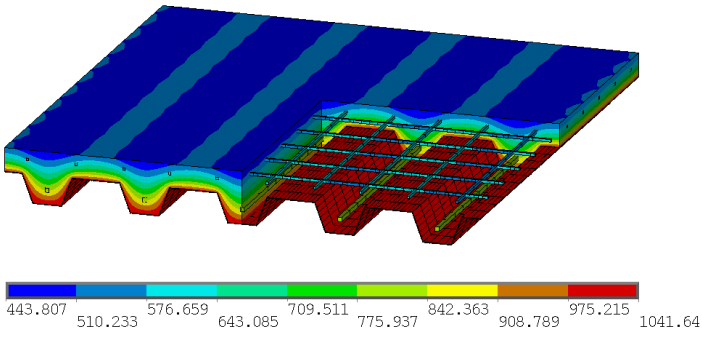

t= 120.0 min

SIM. 18	**Steel deck:** Trapezoidal – O Feliz H60	**Rebar (mm):** ϕ10	**Fire resistance (min)**	
	Mesh (mm//mm): ϕ6//100 (FNQ 60)	**h_1 (mm):** 60	Ave: 46.4	Max: *45.9*

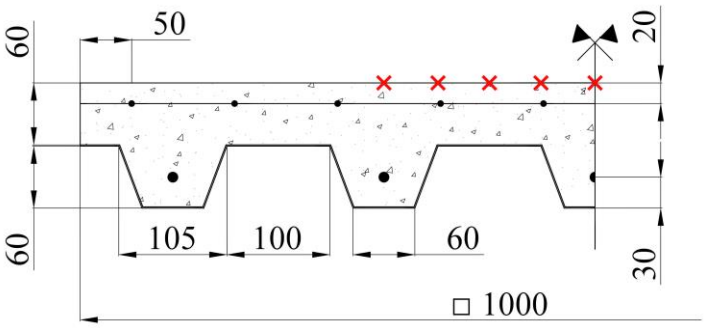

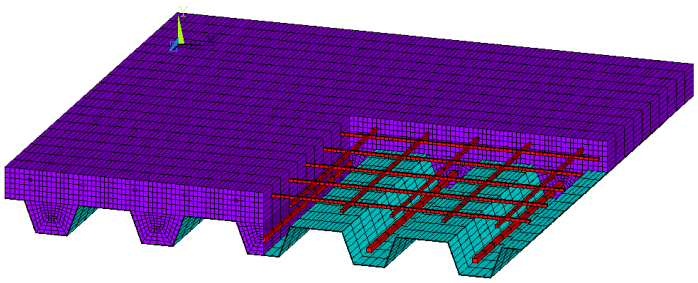

Finite element mesh

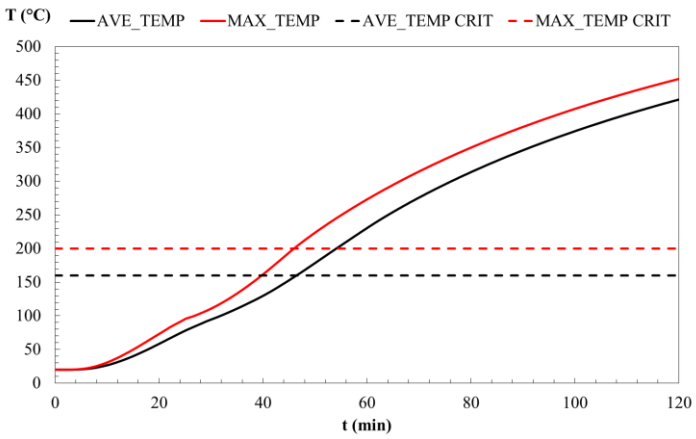

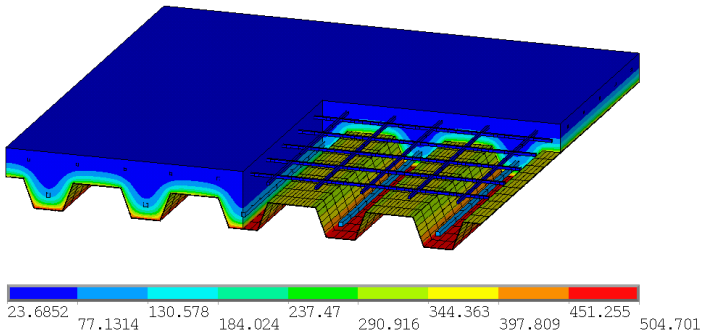

t= 11.5 min

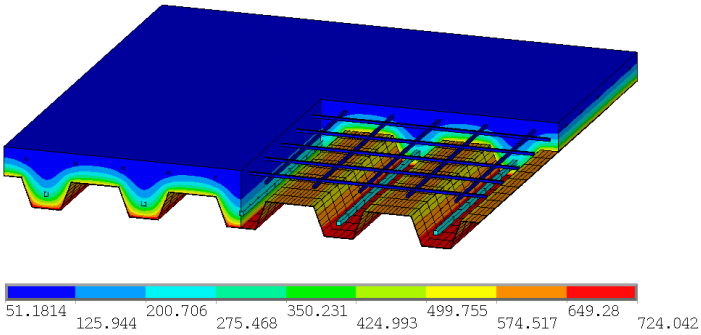

t= 23.0 min

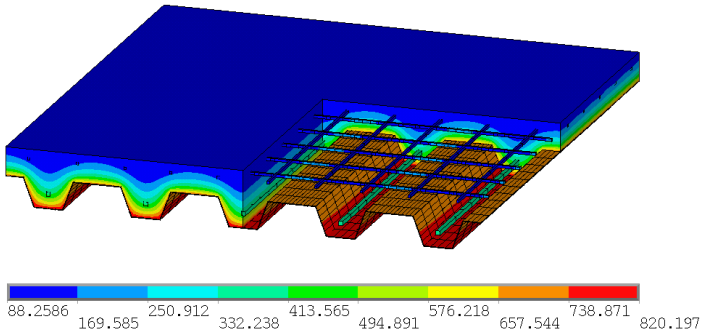

t= 34.4 min

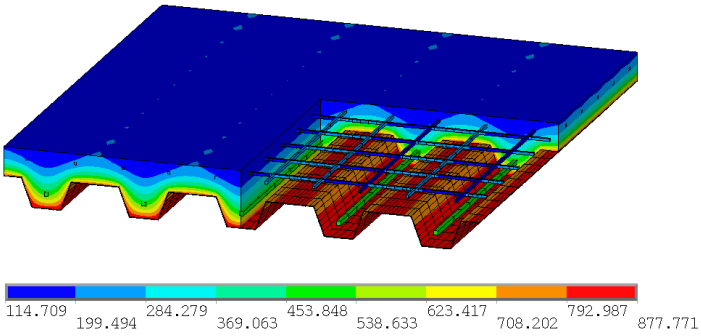

t= 45.9 min

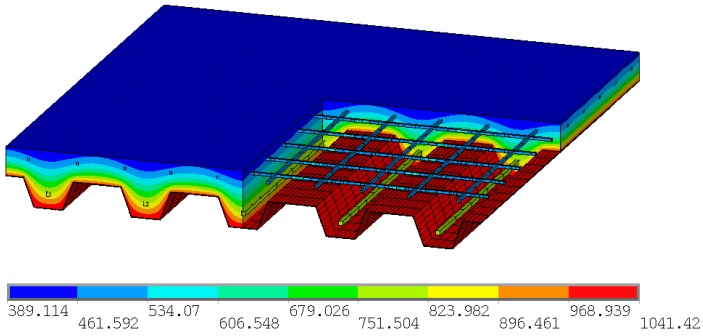

t= 120.0 min

SIM. 19	**Steel deck:** Trapezoidal – O Feliz H60	**Rebar (mm):** ϕ10	**Fire resistance (min)**	
	Mesh (mm//mm): ϕ6//100 (FNQ 60)	**h_1 (mm):** 70	Ave: *57.8*	Max: 59.3

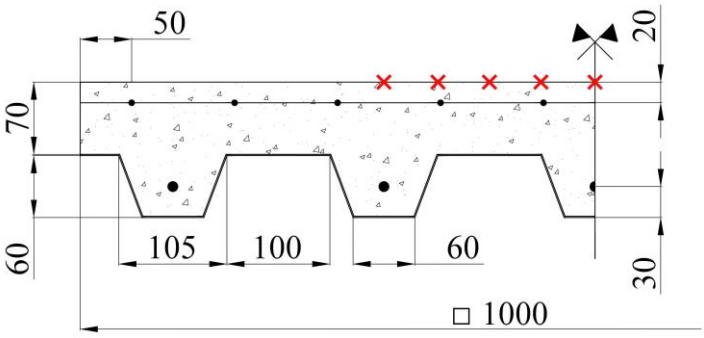

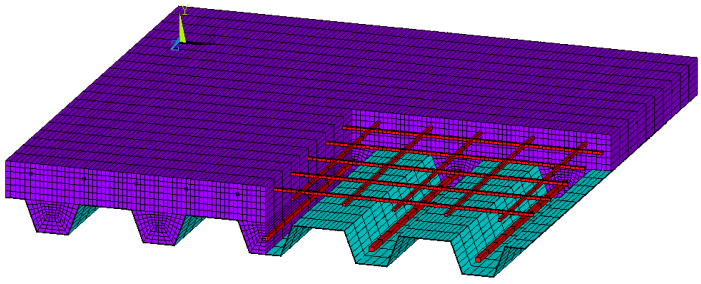

Finite element mesh

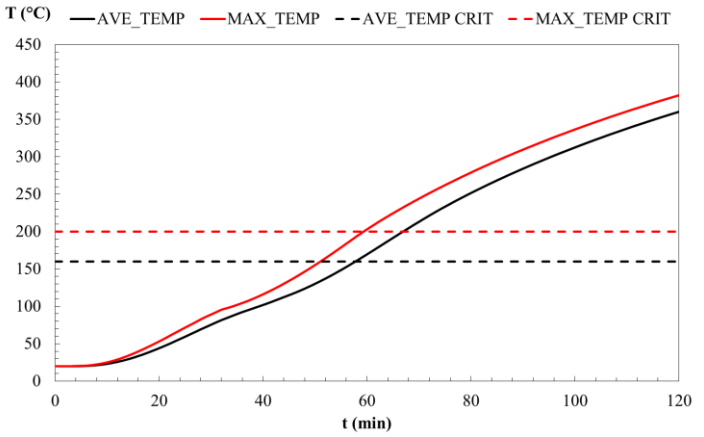

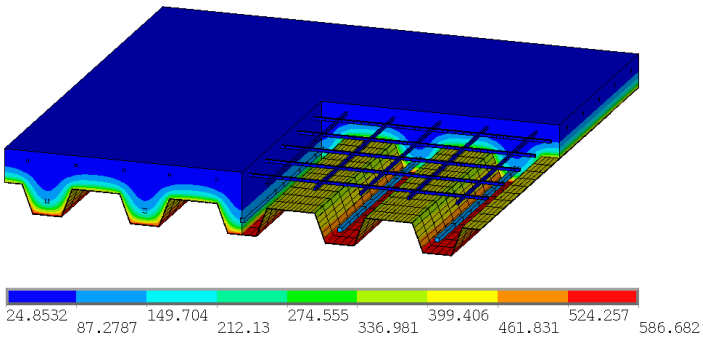

t= 14.5 min

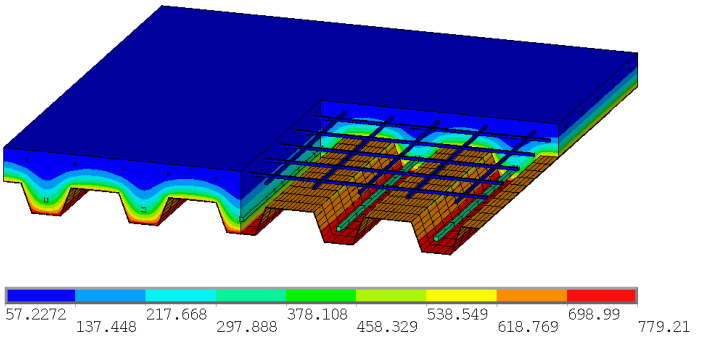

t= 28.9 min

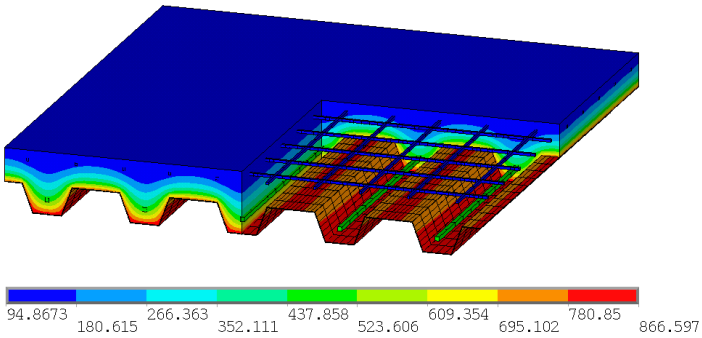

t= 43.4 min

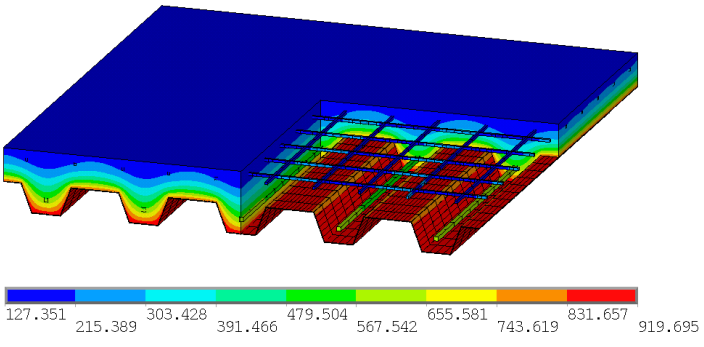

t= 57.8 min

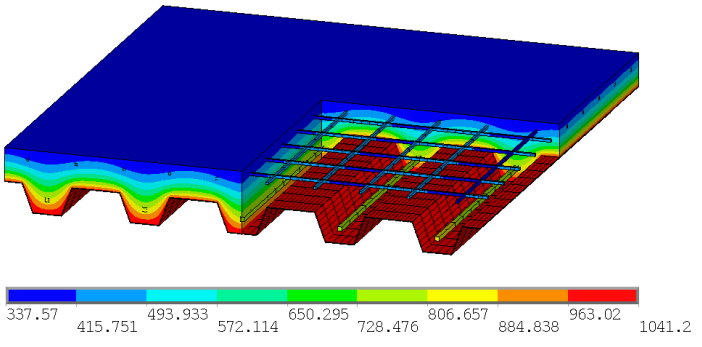

t= 120.0 min

SIM. 20	**Steel deck:** Trapezoidal – O Feliz H60	**Rebar (mm):** ϕ10	**Fire resistance (min)**	
	Mesh (mm//mm): ϕ6//100 (FNQ 60)	**h_1 (mm):** 80	Ave: *70.2*	Max: 74.6

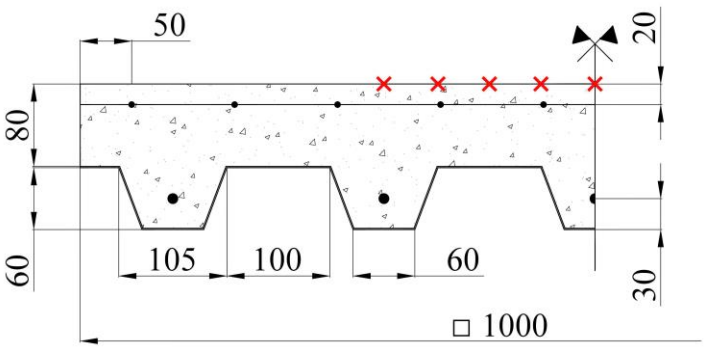

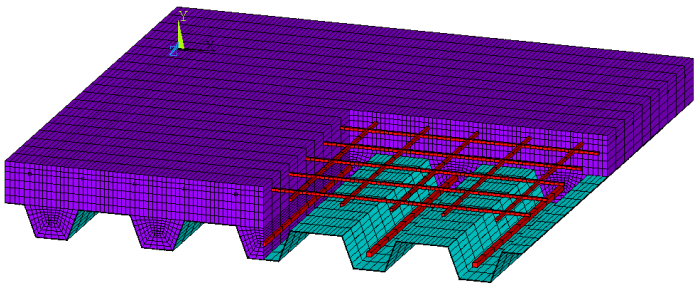

Finite element mesh

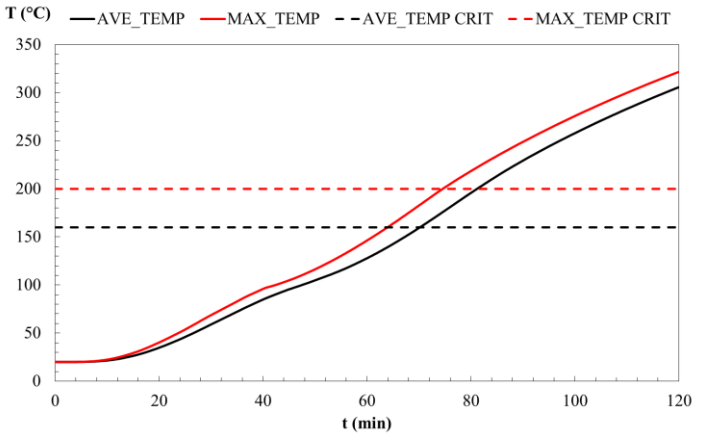

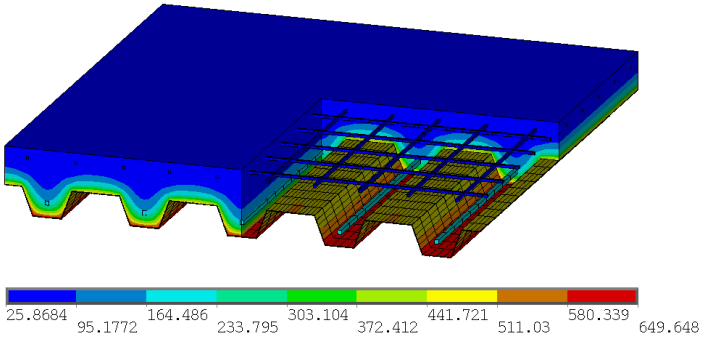

t= 17.6 min

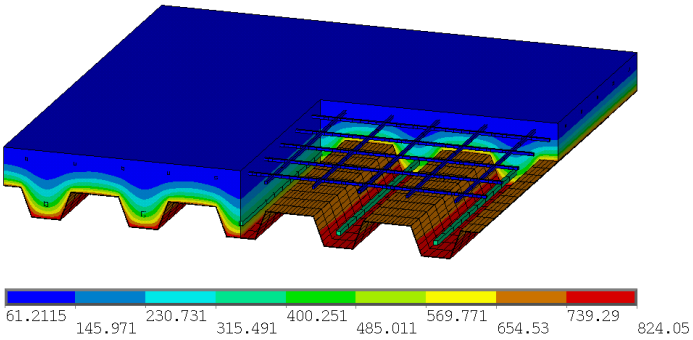

t= 35.1 min

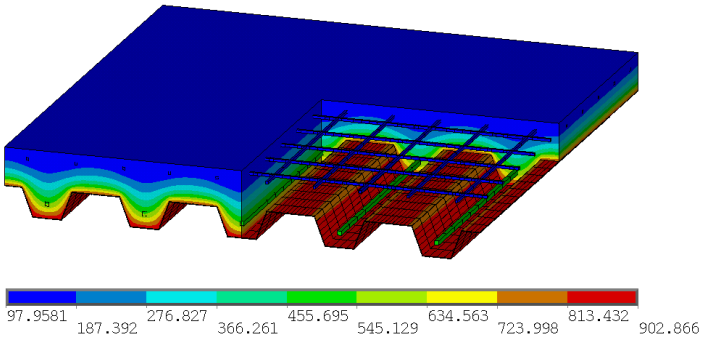

t= 52.7 min

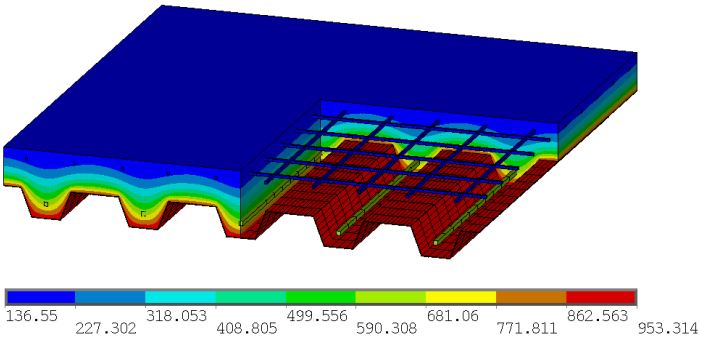

t= 70.2 min

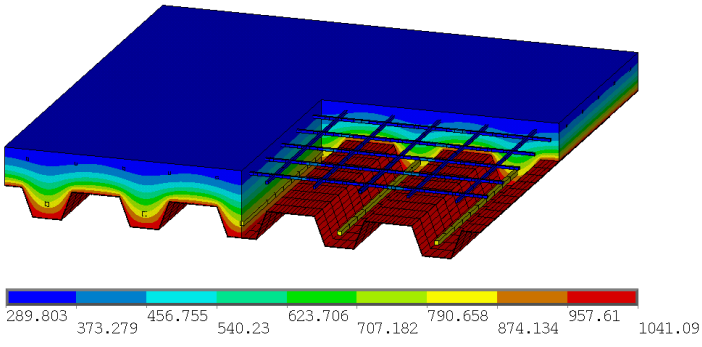

t= 120.0 min

SIM. 21	**Steel deck:** Trapezoidal – O Feliz H60	**Rebar (mm):** ϕ10	**Fire resistance (min)**	
	Mesh (mm//mm): ϕ6//100 (FNQ 60)	**h_1 (mm):** 50	Ave: 36.2	Max: *34.5*

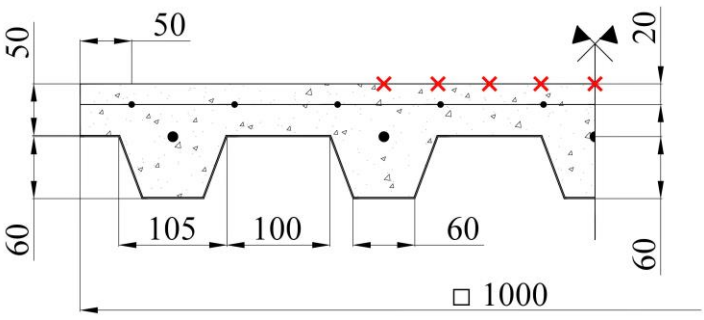

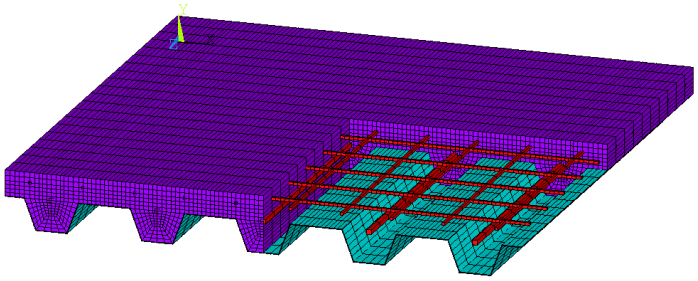

Finite element mesh

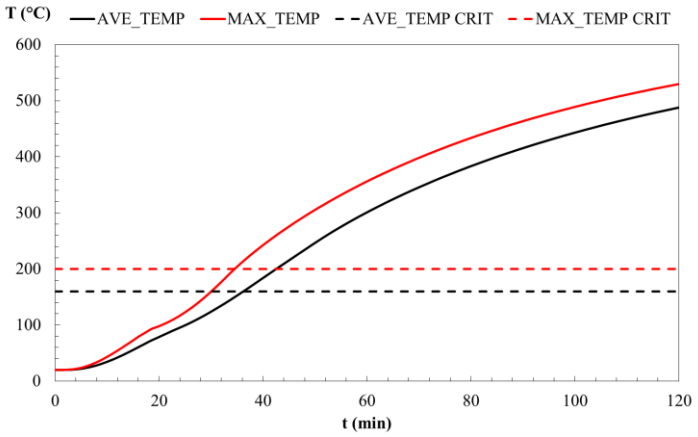

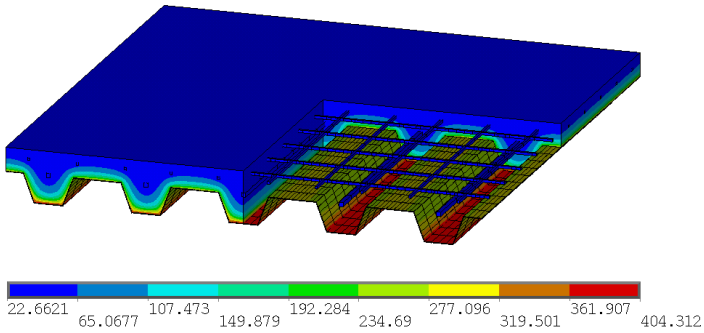

t= 8.6 min

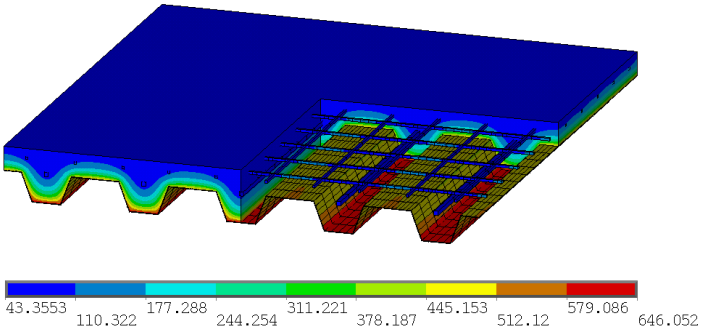

t= 17.3 min

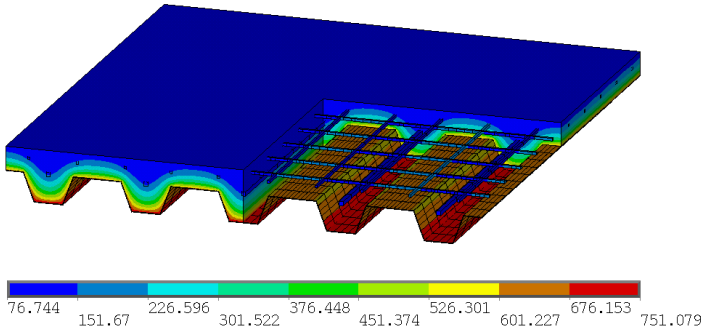

t= 25.9 min

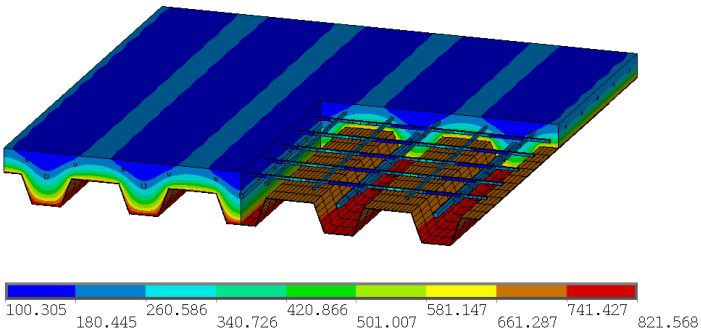

t= 34.5 min

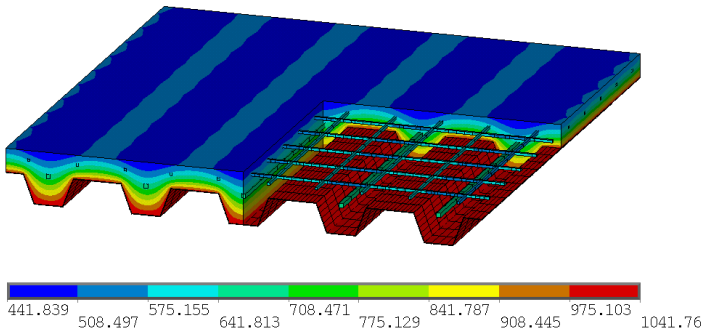

t= 120.0 min

SIM. 22	**Steel deck:** Trapezoidal – O Feliz H60	**Rebar (mm):** ϕ10	**Fire resistance (min)**	
	Mesh (mm//mm): ϕ6//100 (FNQ 60)	**h_1 (mm):** 60	Ave: 46.4	Max: *45.9*

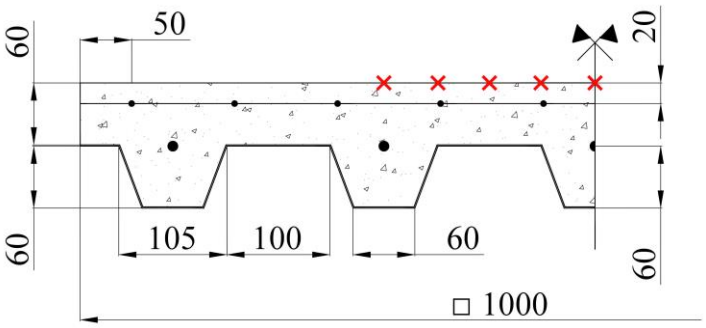

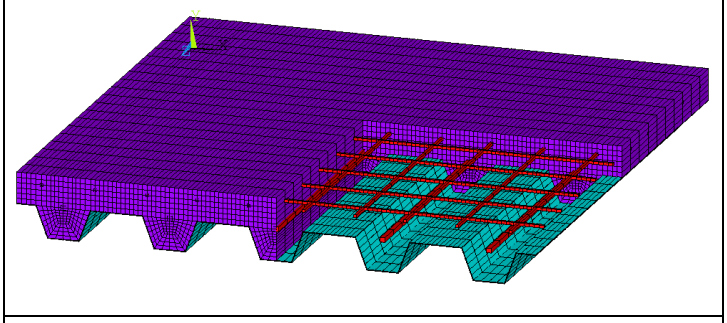

Finite element mesh

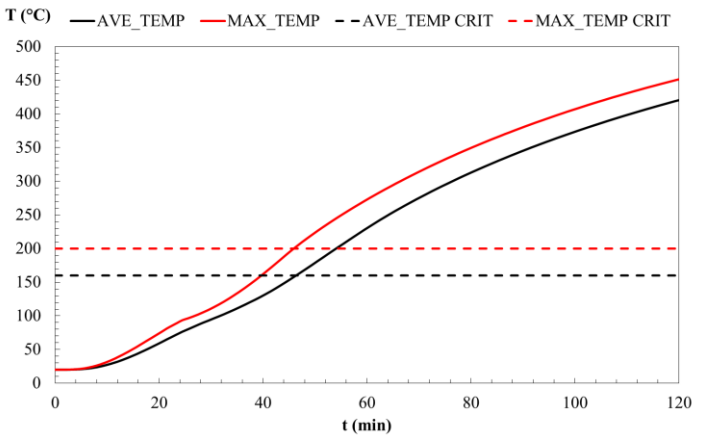

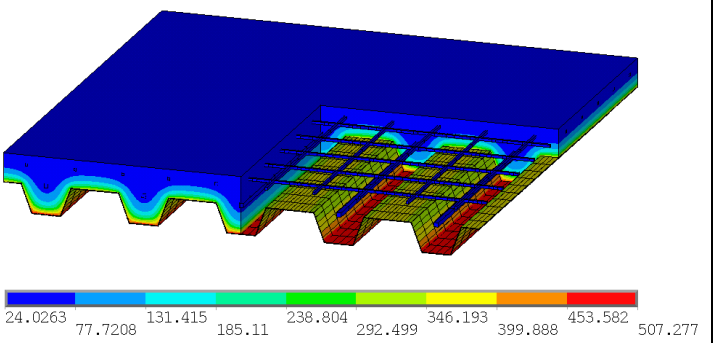

t= 11.5 min

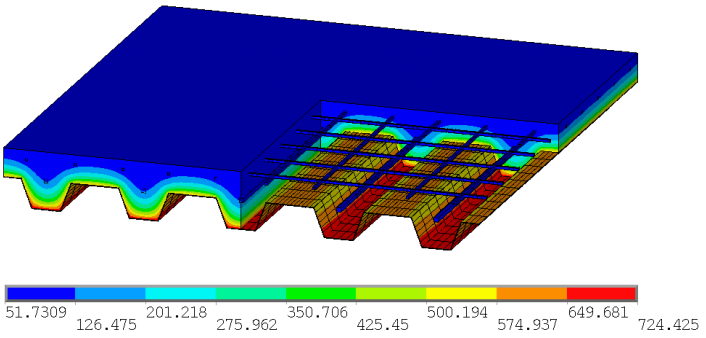

t= 23.0 min

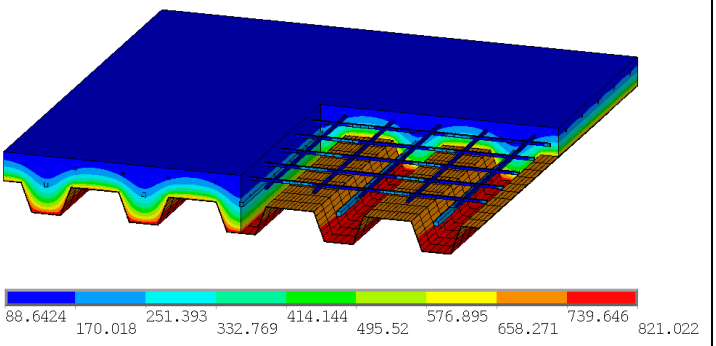

t= 34.4 min

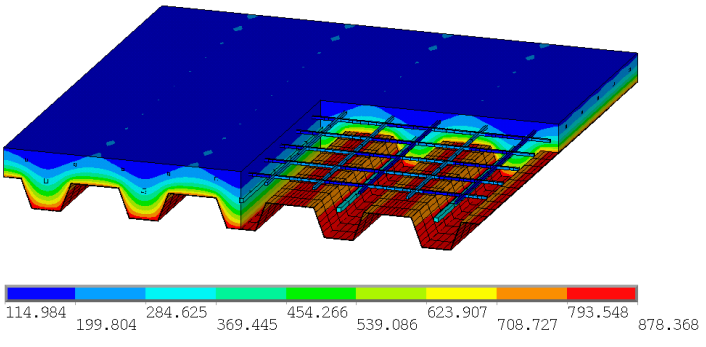

t= 45.9 min

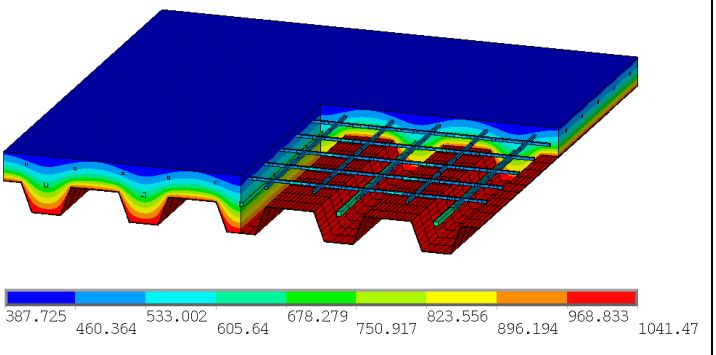

t= 120.0 min

SIM. 23	**Steel deck:** Trapezoidal – O Feliz H60	**Rebar (mm):** ϕ10	**Fire resistance (min)**	
	Mesh (mm//mm): ϕ6//100 (FNQ 60)	**h_1 (mm):** 70	Ave: *57.6*	Max: 59.2

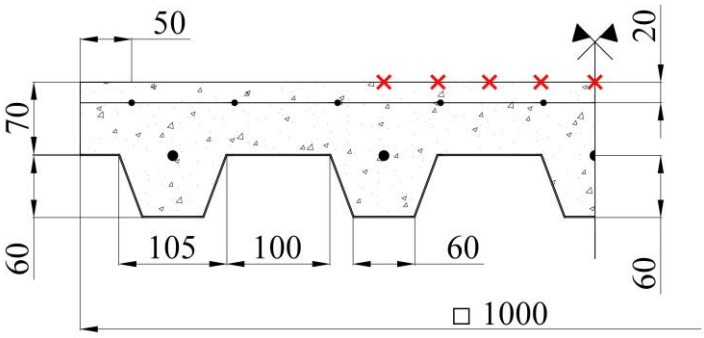

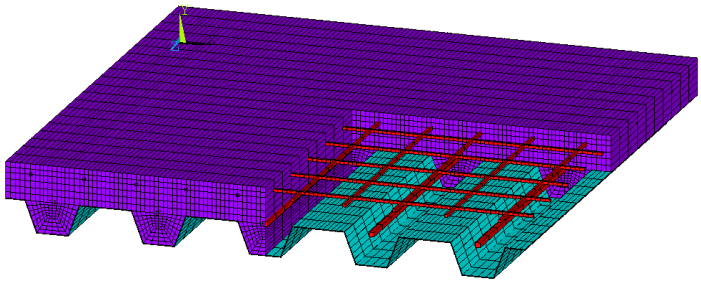

Finite element mesh

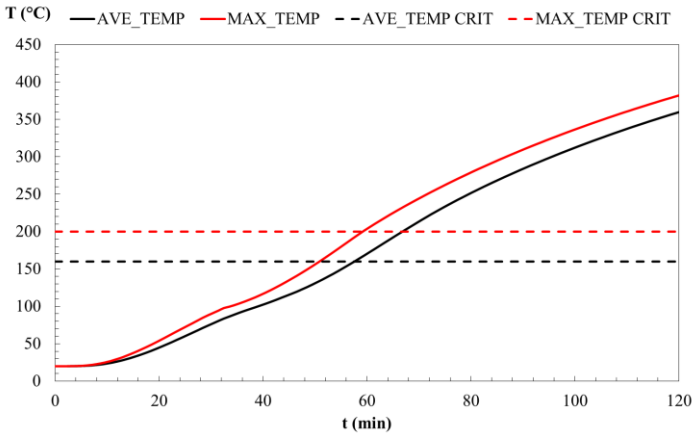

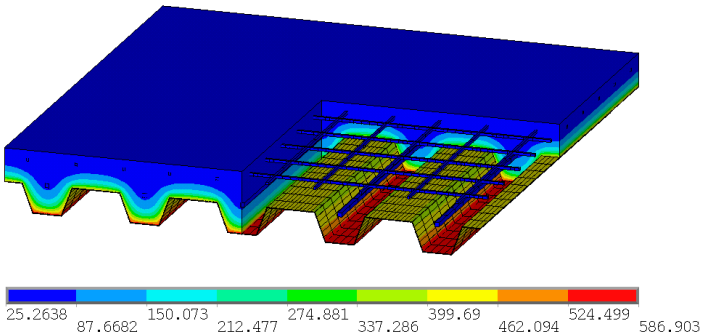

t= 14.4 min

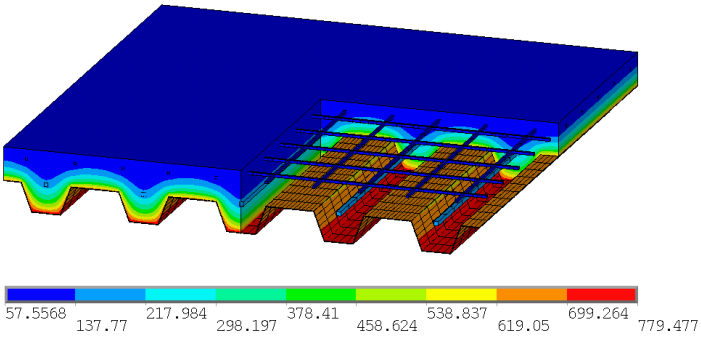

t= 28.8 min

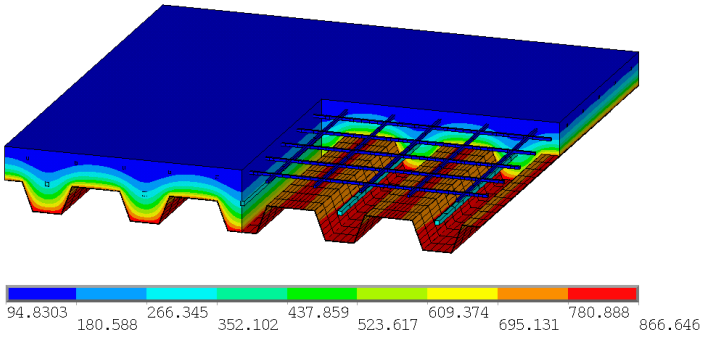

t= 43.2 min

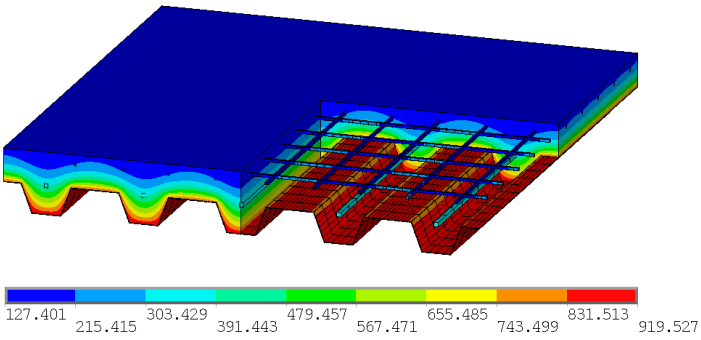

t= 57.6 min

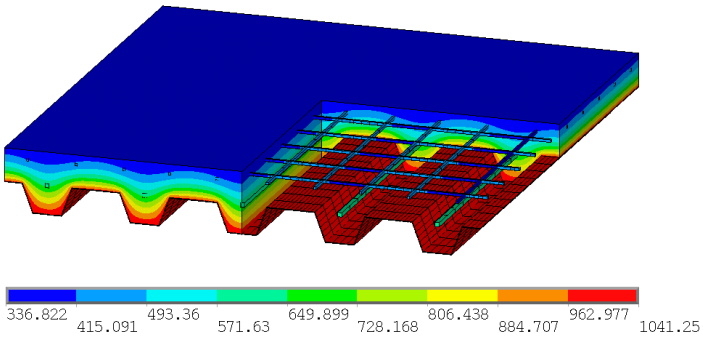

t= 120.0 min

SIM. 24	**Steel deck:** Trapezoidal – O Feliz H60	**Rebar (mm):** ϕ10	**Fire resistance (min)**	
	Mesh (mm//mm): ϕ6//100 (FNQ 60)	**h_1 (mm):** 80	Ave: *70.0*	Max: 74.4

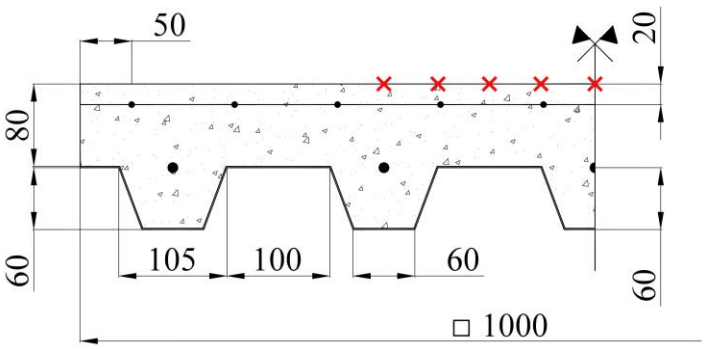

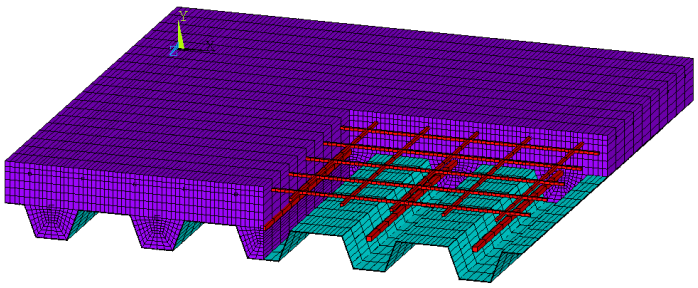

Finite element mesh

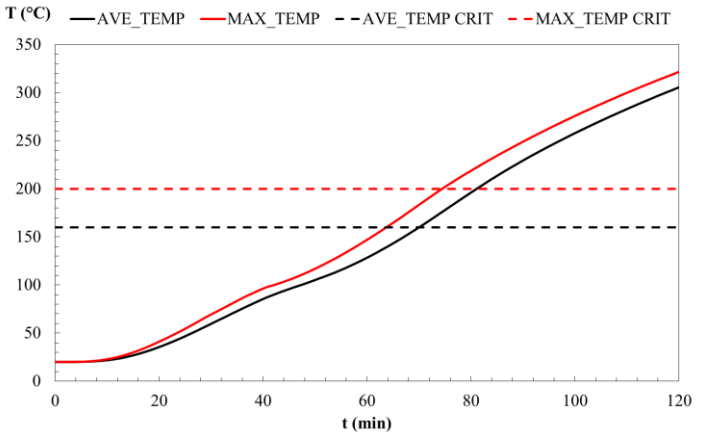

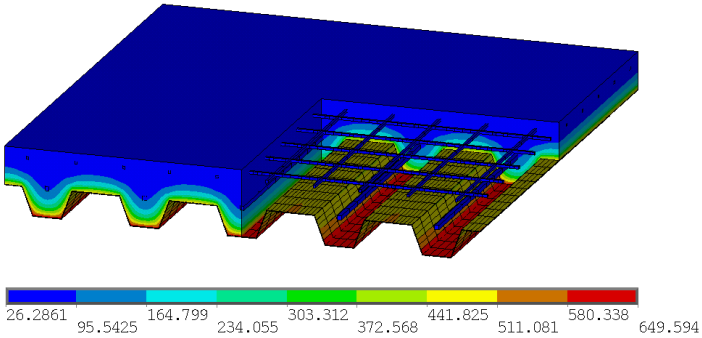

t= 17.5 min

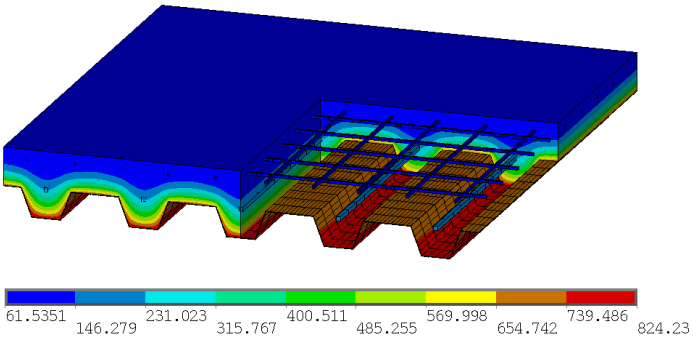

t= 35.0 min

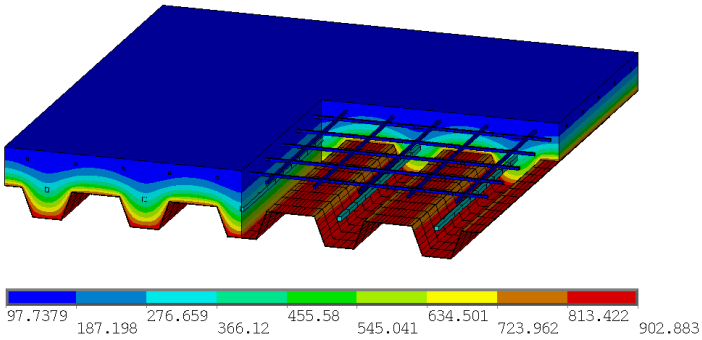

t= 52.5 min

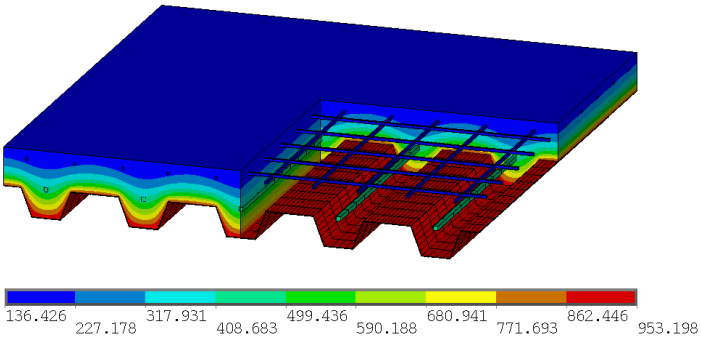

t= 70.0 min

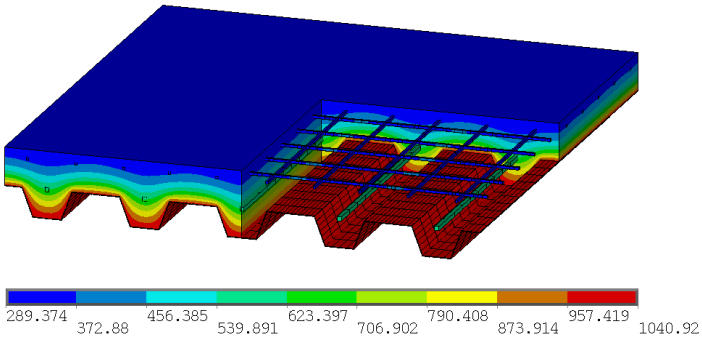

t= 120.0 min

SIM. 25	**Steel deck:** Trapezoidal – O Feliz H60	**Rebar (mm):** ϕ10	**Fire resistance (min)**	
	Mesh (mm//mm): ϕ6//150 (FND 60)	**h_1 (mm):** 50	Ave: 36.4	Max: *35.1*

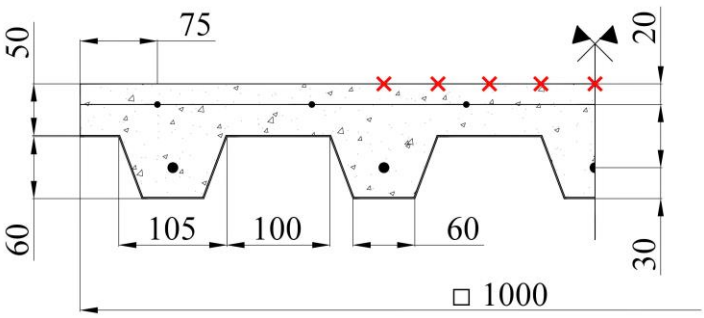

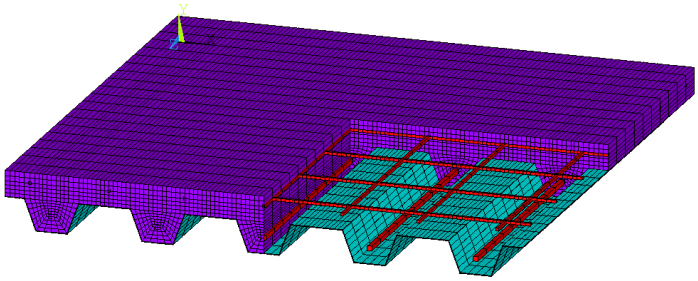

Finite element mesh

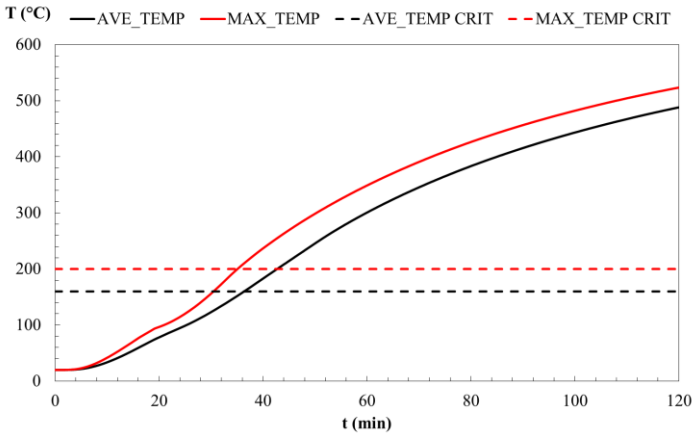

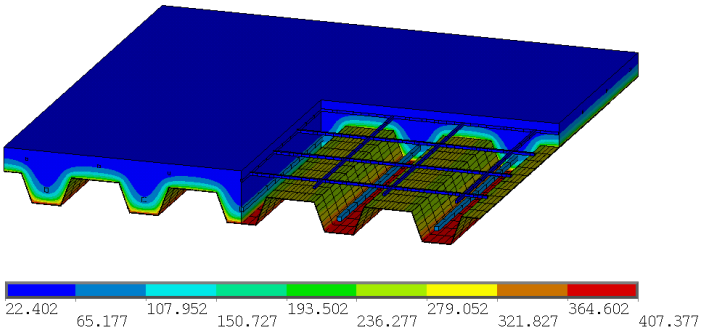

t= 8.8 min

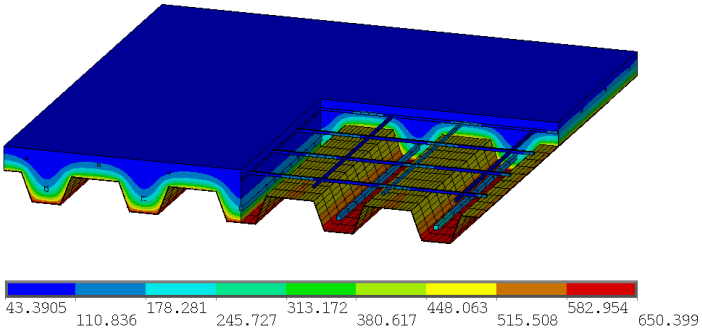

t= 17.6 min

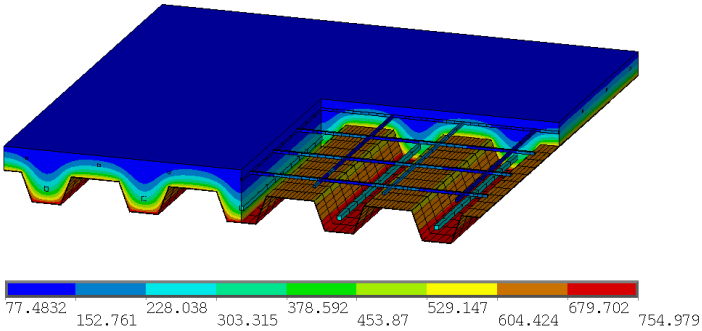

t= 26.3 min

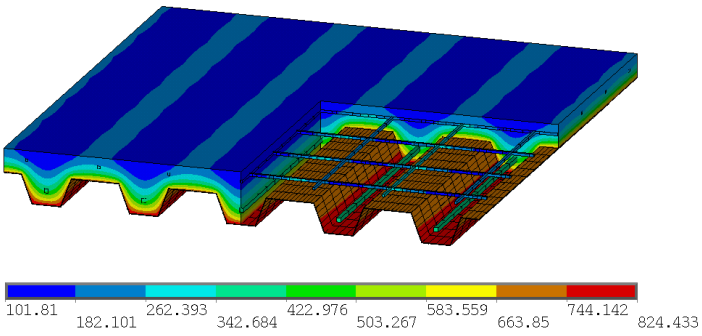

t= 35.1 min

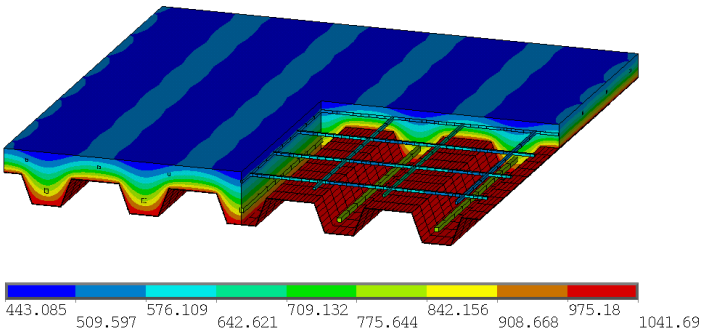

t= 120.0 min

SIM. 26	**Steel deck:** Trapezoidal – O Feliz H60	**Rebar (mm):** ϕ10	**Fire resistance (min)**	
	Mesh (mm//mm): ϕ6//150 (FND 60)	**h_1 (mm):** 60	Ave: *46.6*	Max: 46.6

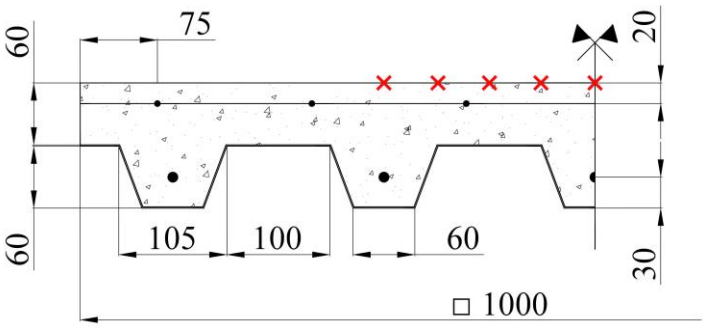

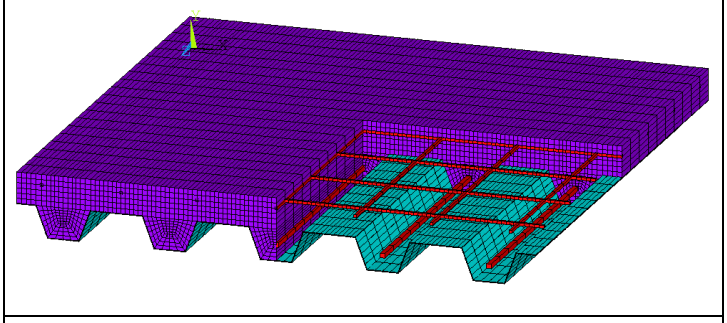

Finite element mesh

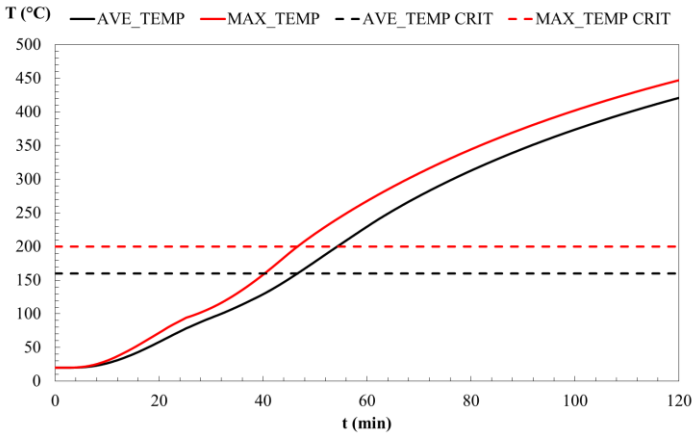

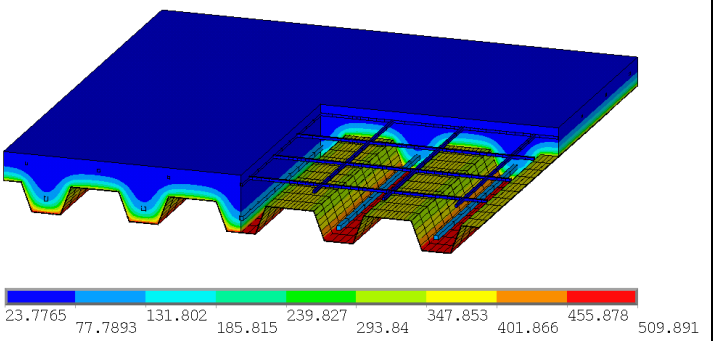

t= 11.7 min

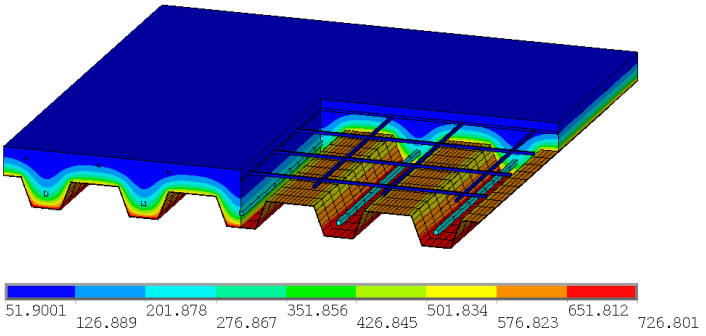

t= 23.3 min

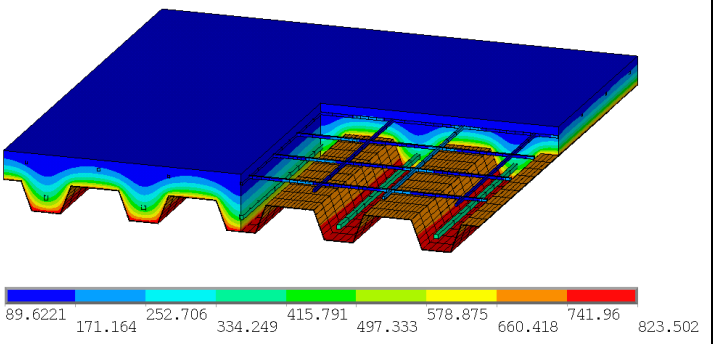

t= 35.0 min

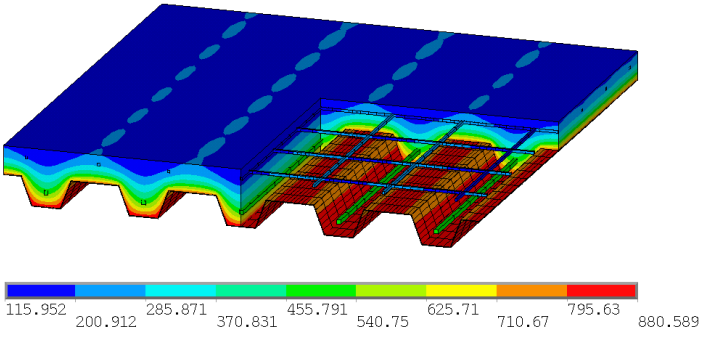

t= 46.6 min

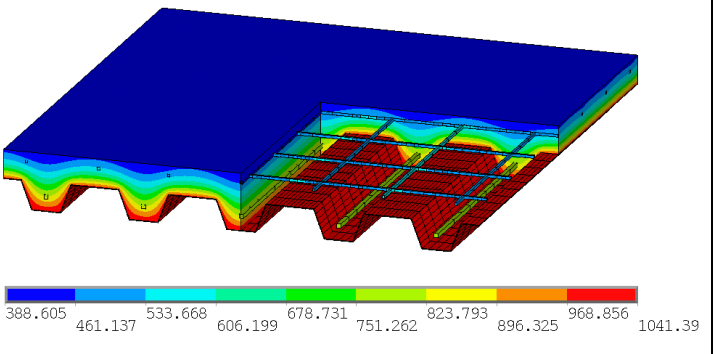

t= 120.0 min

SIM. 27	**Steel deck:** Trapezoidal – O Feliz H60	**Rebar (mm):** ϕ10	**Fire resistance (min)**	
	Mesh (mm//mm): ϕ6//150 (FND 60)	**h_1 (mm):** 70	Ave: *57.8*	Max: 60.0

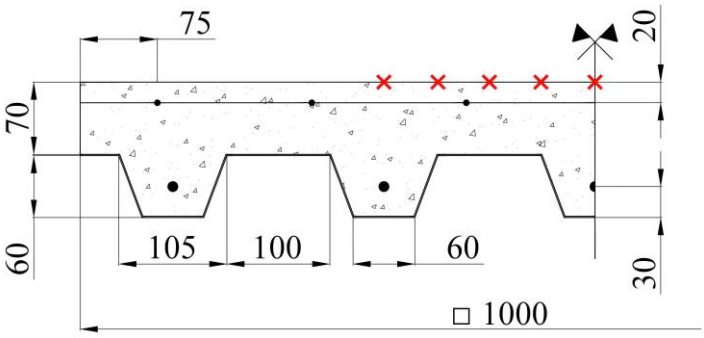

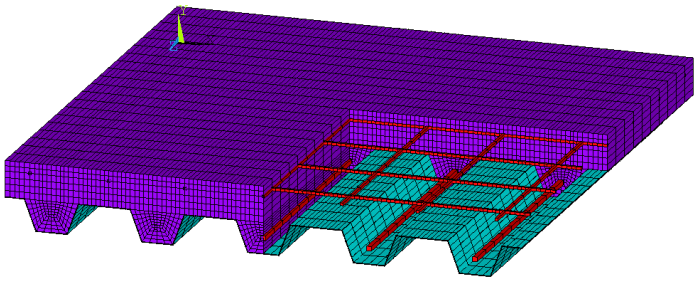

Finite element mesh

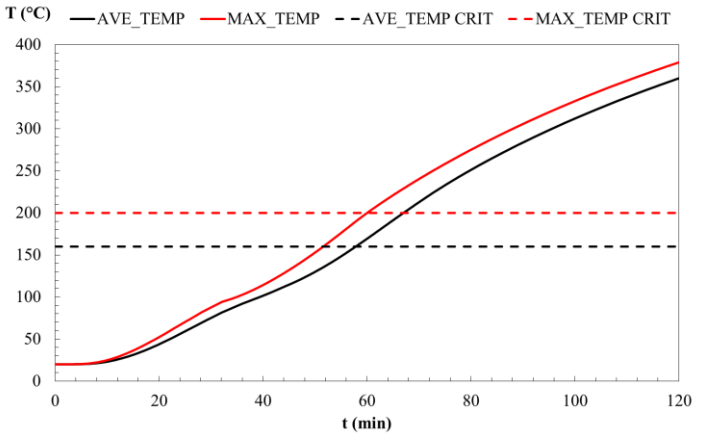

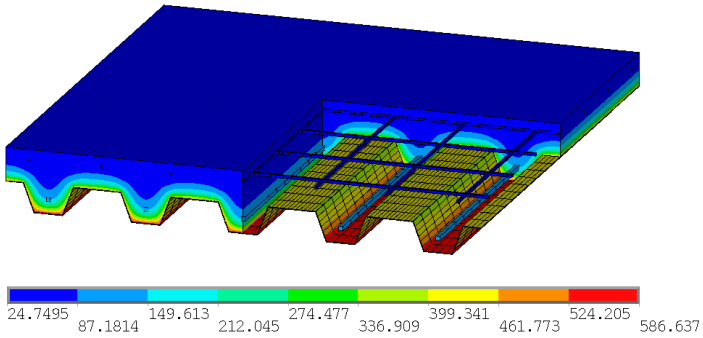

t= 14.5 min

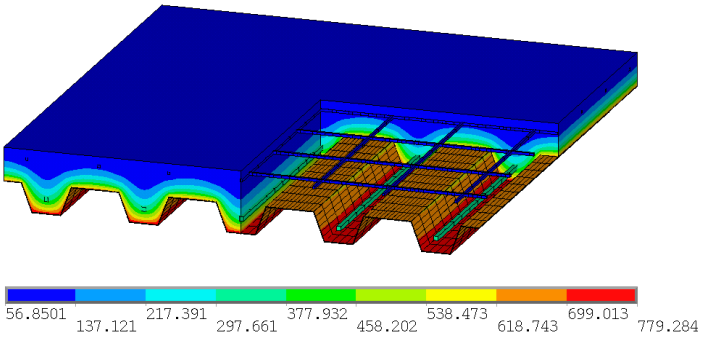

t= 28.9 min

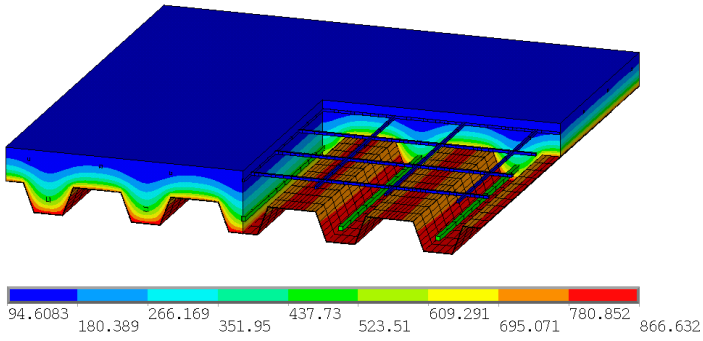

t= 43.4 min

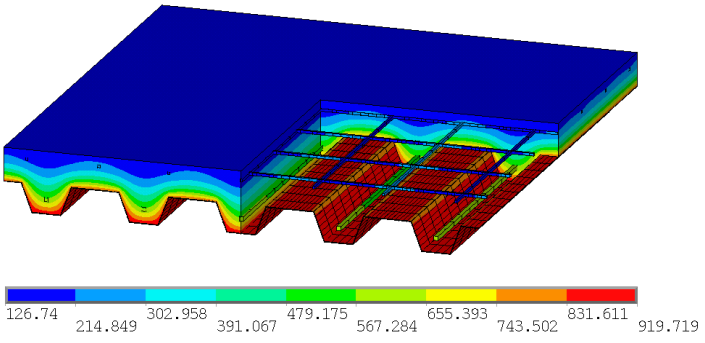

t= 57.8 min

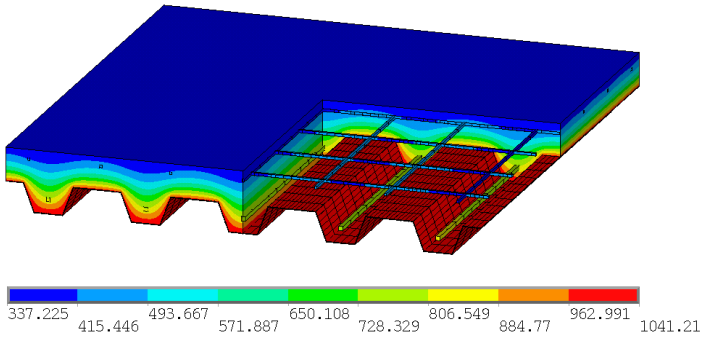

t= 120.0 min

SIM. 28	**Steel deck:** Trapezoidal – O Feliz H60	**Rebar (mm):** ϕ10	**Fire resistance (min)**	
	Mesh (mm//mm): ϕ6//150 (FND 60)	**h_1 (mm):** 80	Ave: *70.2*	Max: 75.2

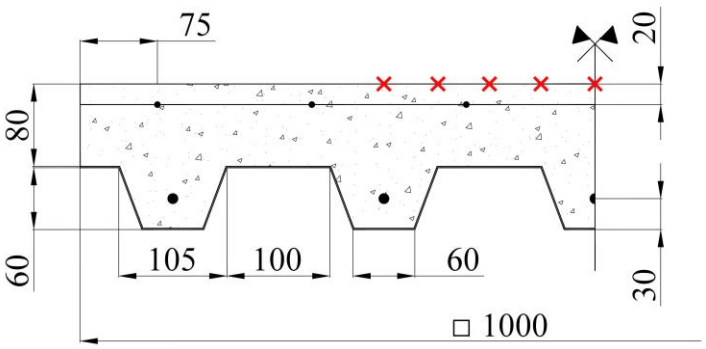

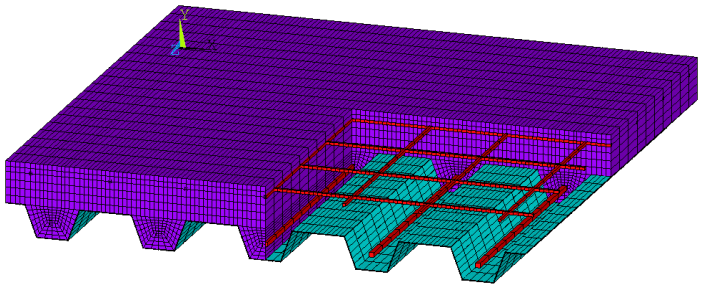

Finite element mesh

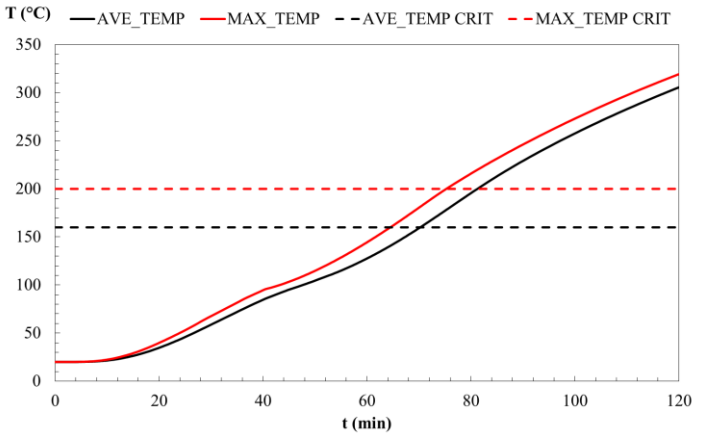

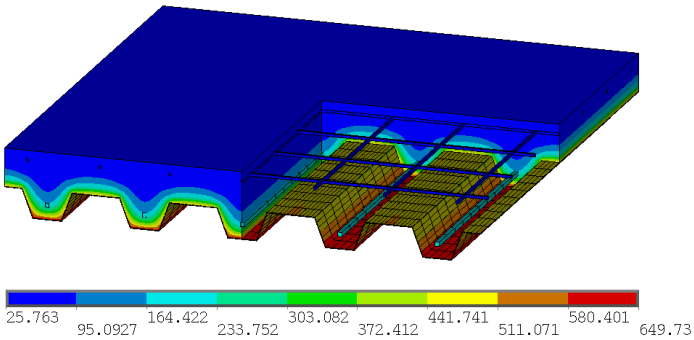

t= 17.6 min

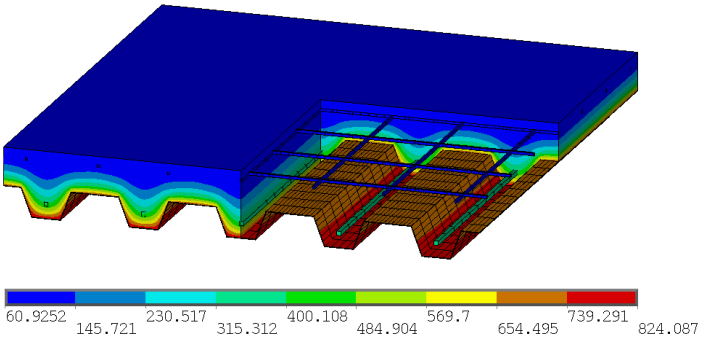

t= 35.1 min

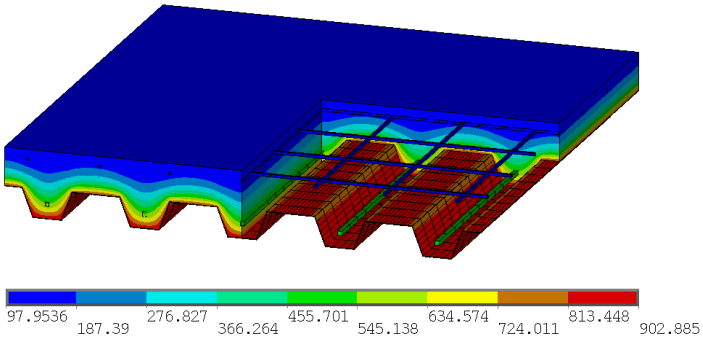

t= 52.7 min

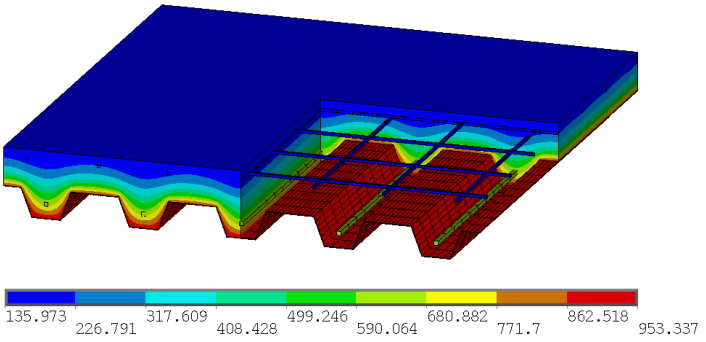

t= 70.2 min

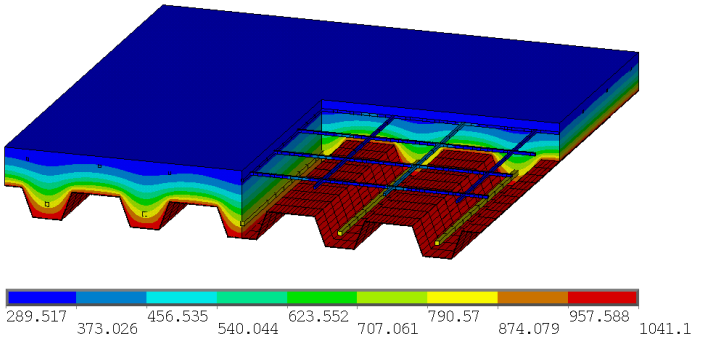

t= 120.0 min

SIM. 29	**Steel deck:** Trapezoidal – O Feliz H60	**Rebar (mm):** ϕ10	**Fire resistance (min)**	
	Mesh (mm//mm): ϕ6//150 (FND 60)	**h_1 (mm):** 50	Ave: 36.3	Max: *35.0*

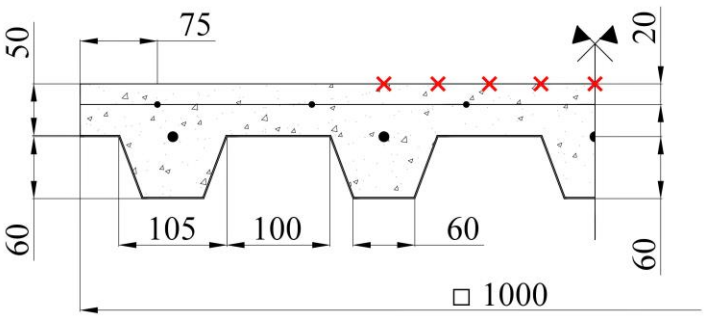

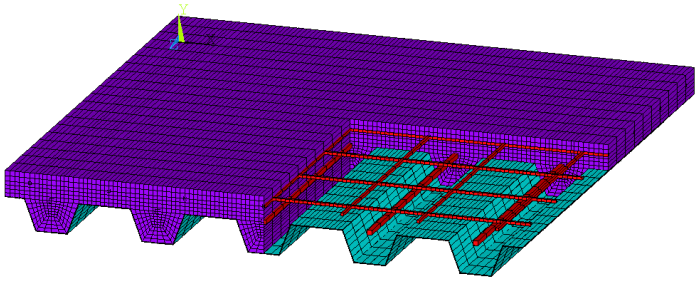

Finite element mesh

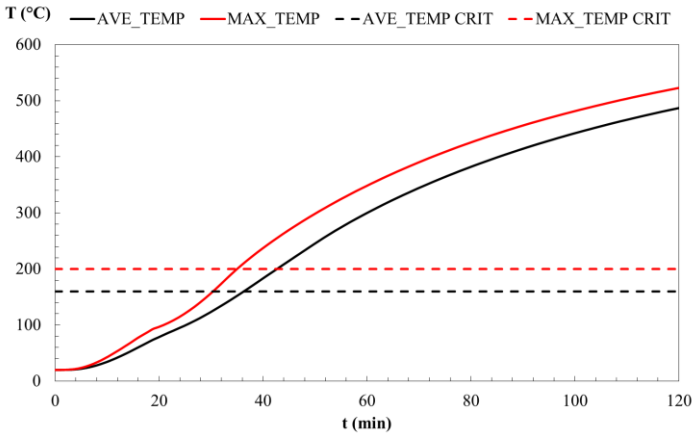

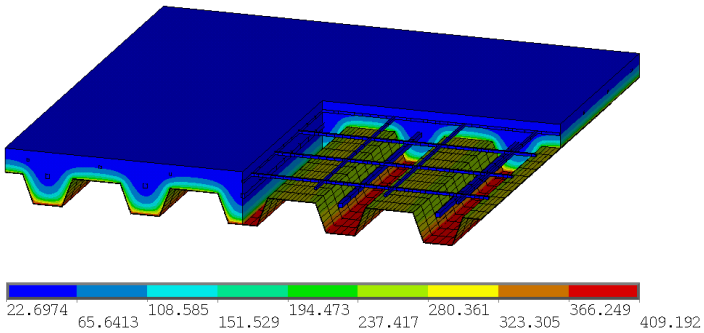

t= 8.8 min

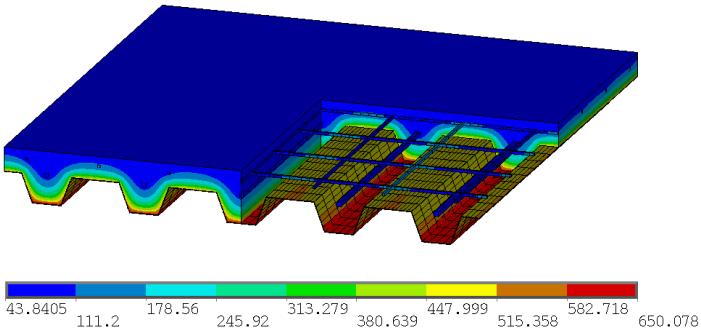

t= 17.5 min

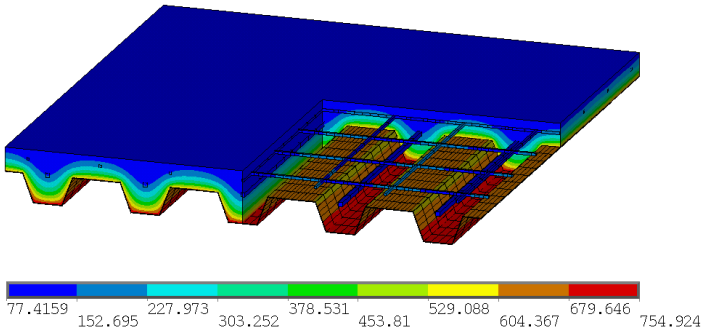

t= 26.3 min

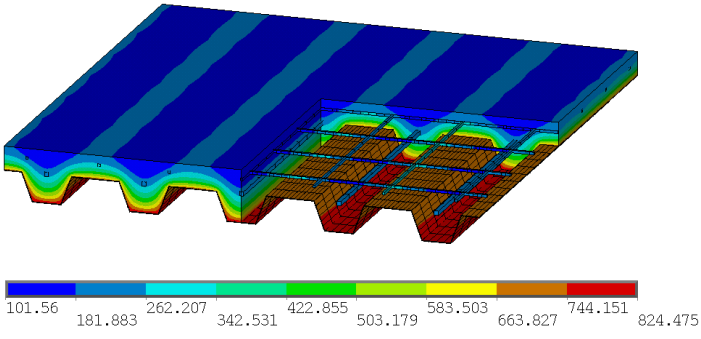

t= 35.0 min

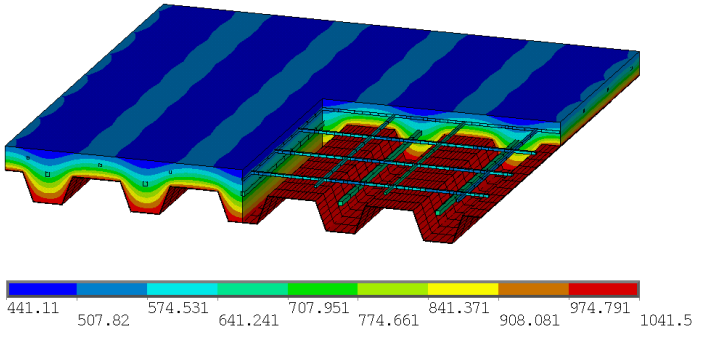

t= 120.0 min

SIM. 30	**Steel deck:** Trapezoidal – O Feliz H60	**Rebar (mm):** ϕ10	**Fire resistance (min)**	
	Mesh (mm//mm): ϕ6//150 (FND 60)	**h_1 (mm):** 60	Ave: *46.4*	Max: 46.5

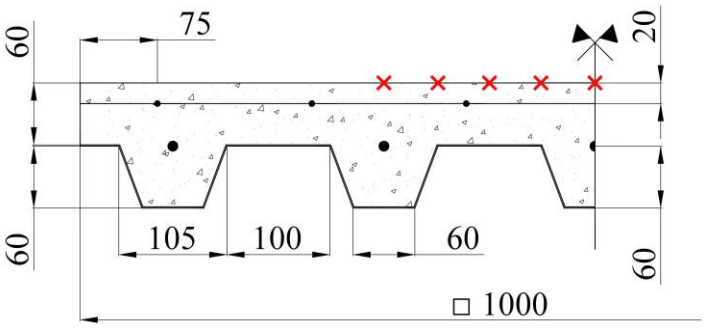

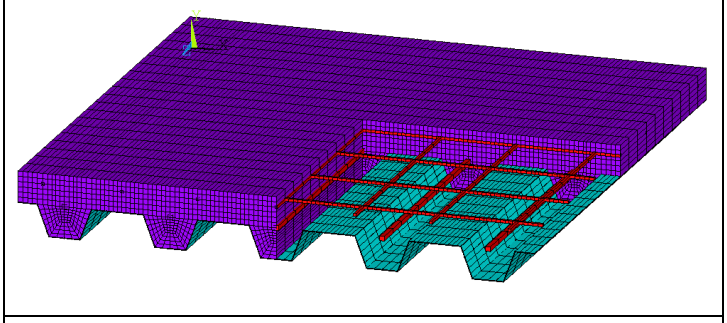

Finite element mesh

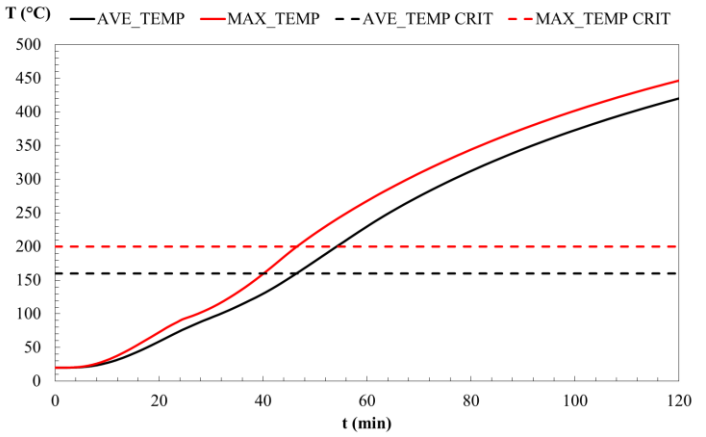

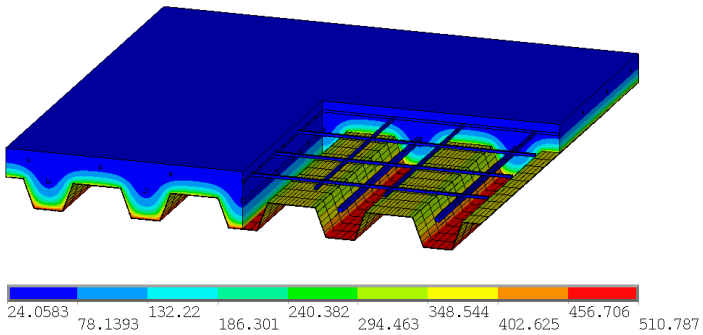

t= 11.6 min

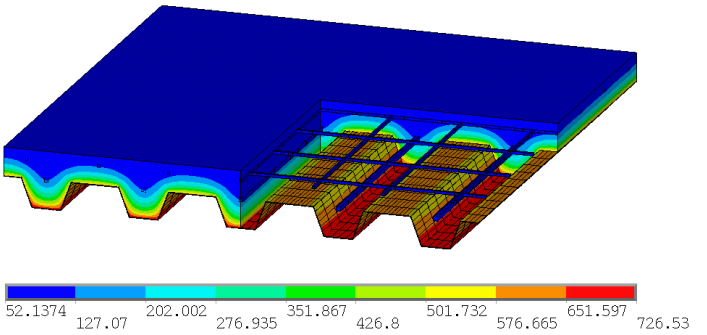

t= 23.2 min

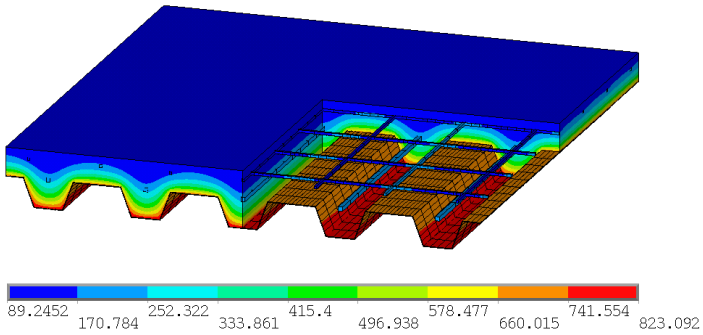

t= 34.8 min

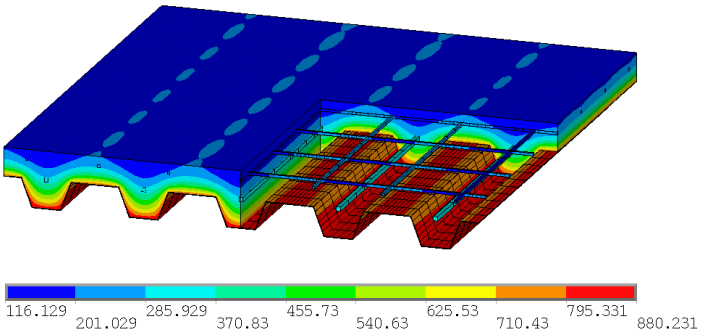

t= 46.4 min

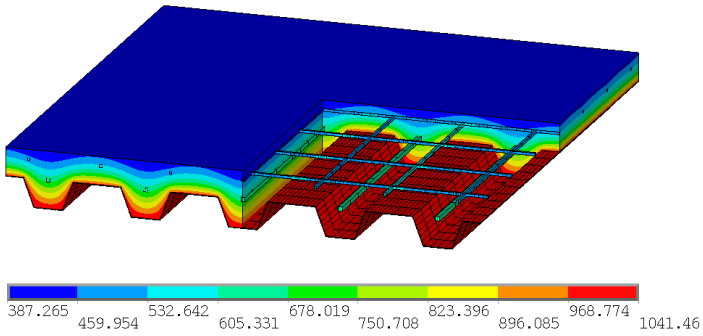

t= 120.0 min

SIM. 31	**Steel deck:** Trapezoidal – O Feliz H60	**Rebar (mm):** ϕ10	**Fire resistance (min)**	
	Mesh (mm//mm): ϕ6//150 (FND 60)	**h_1 (mm):** 70	Ave: *57.6*	Max: 59.9

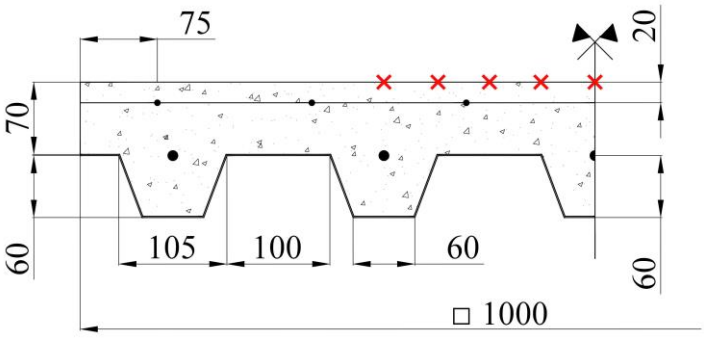

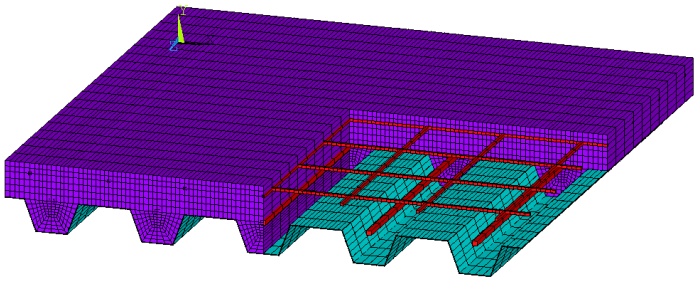

Finite element mesh

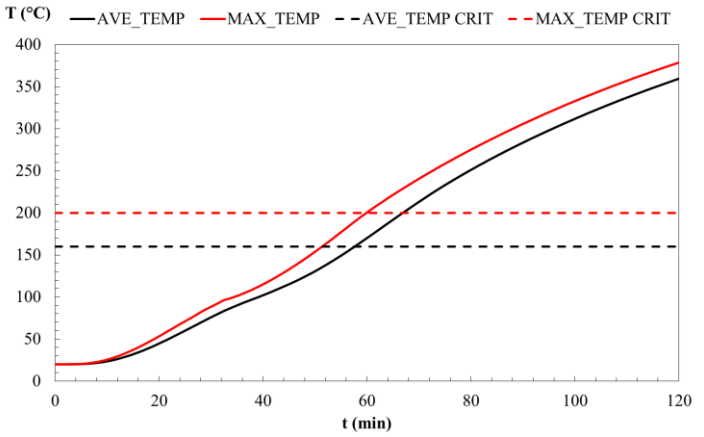

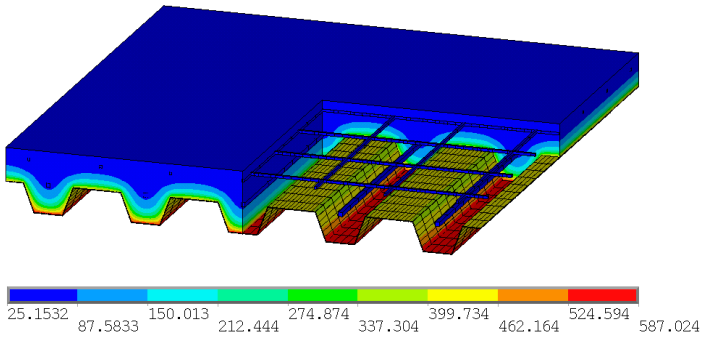

t= 14.4 min

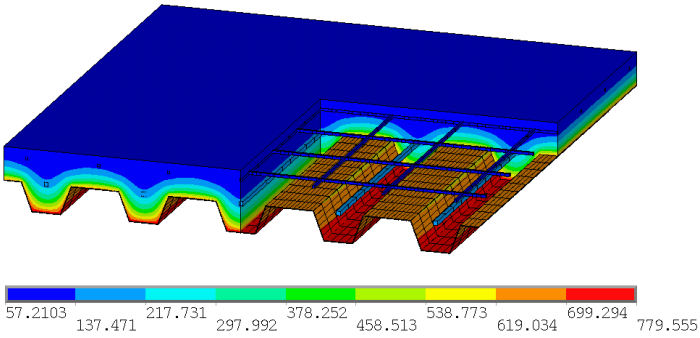

t= 28.8 min

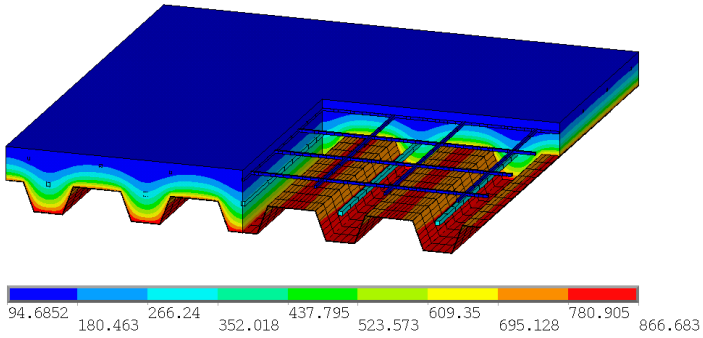

t= 43.2 min

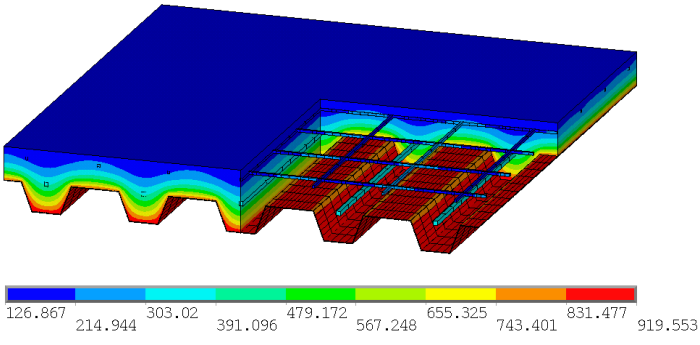

t= 57.6 min

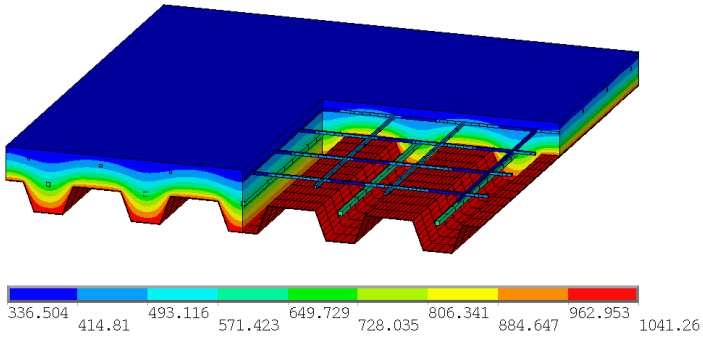

t= 120.0 min

SIM. 32	**Steel deck:** Trapezoidal – O Feliz H60	**Rebar (mm):** ϕ10	**Fire resistance (min)**	
	Mesh (mm//mm): ϕ6//150 (FND 60)	**h_1 (mm):** 80	Ave: *70.1*	Max: 75.1

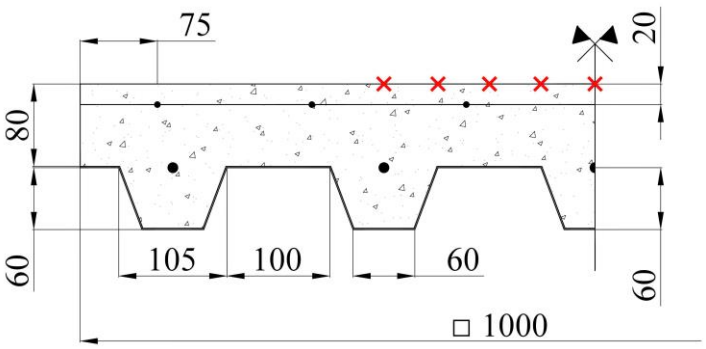

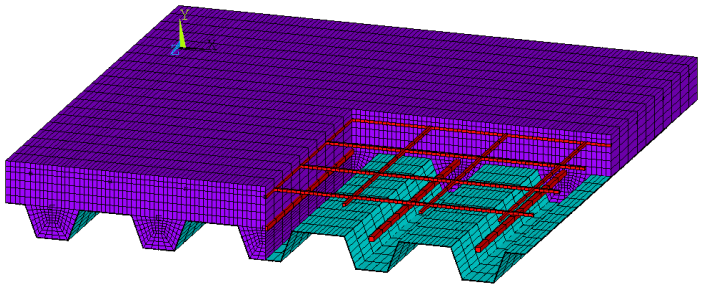

Finite element mesh

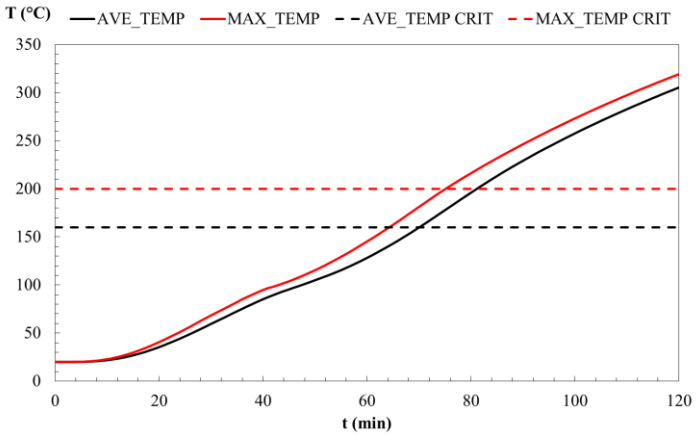

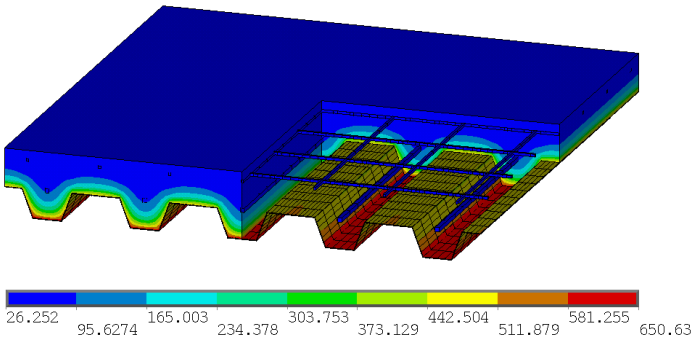

t= 17.5 min

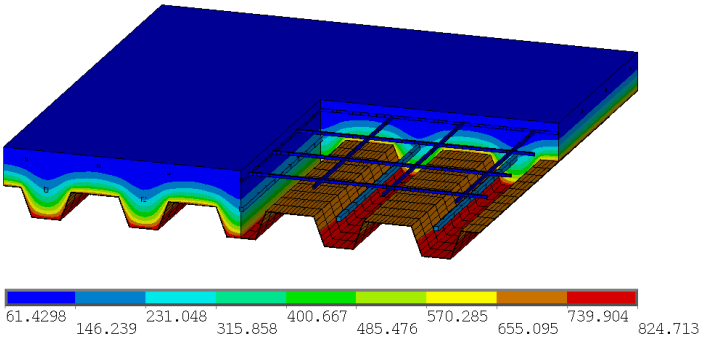

t= 35.1 min

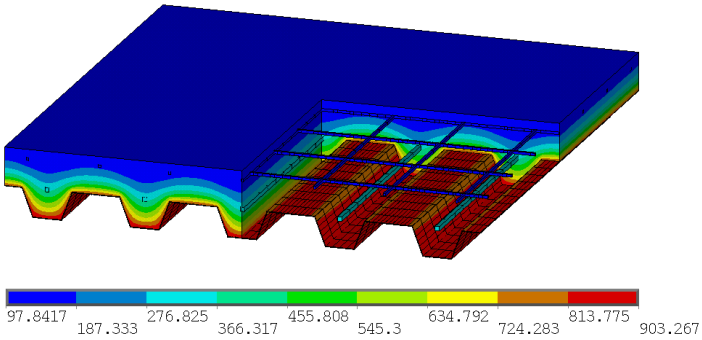

t= 52.6 min

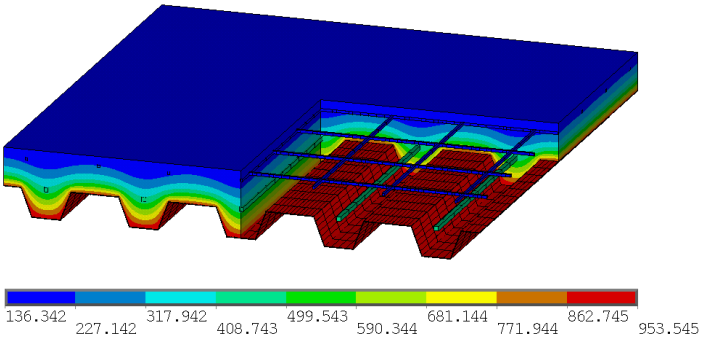

t= 70.1 min

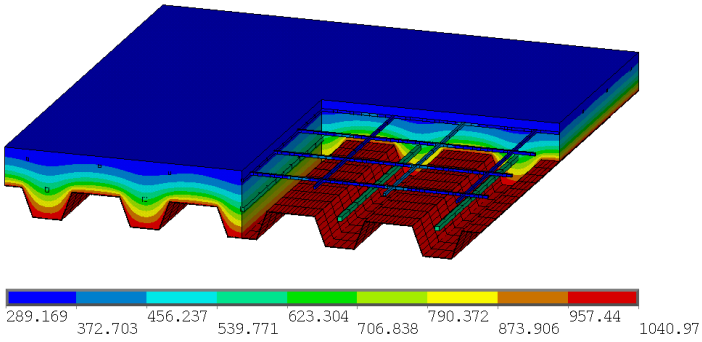

t= 120.0 min

SIM. 33	**Steel deck:** Trapezoidal – O Feliz H60	**Rebar (mm):** ϕ12	**Fire resistance (min)**	
	Mesh (mm//mm): ϕ6//100 (FNQ 60)	**h_1 (mm):** 50	Ave: 36.3	Max: *34.6*

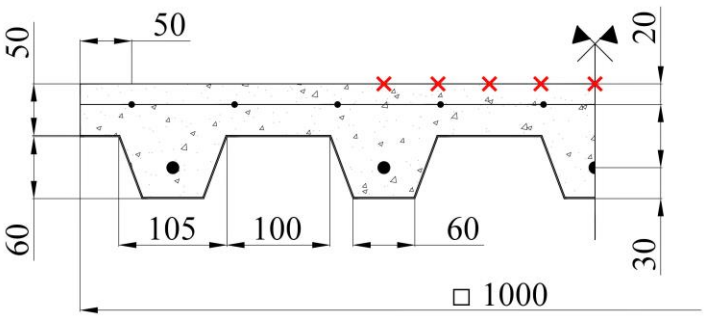

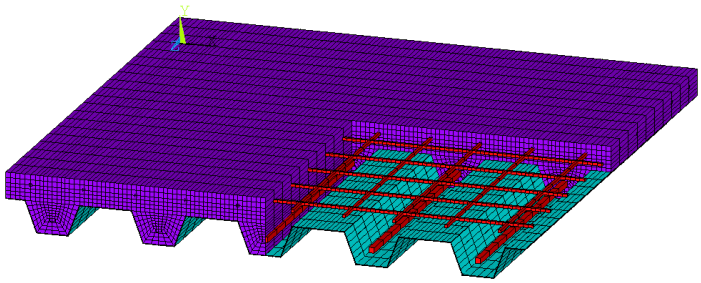

Finite element mesh

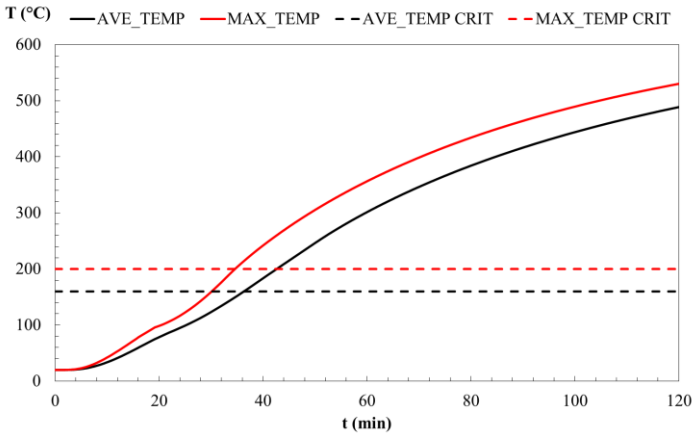

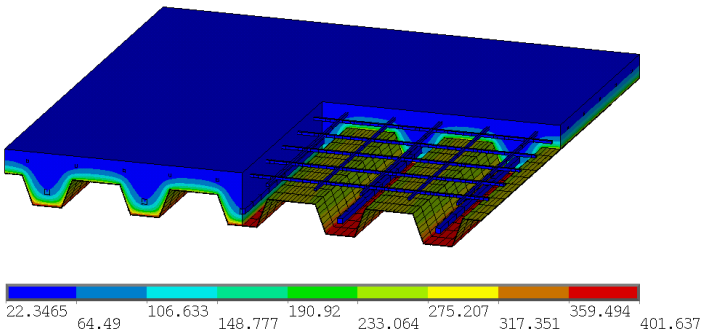

t= 8.7 min

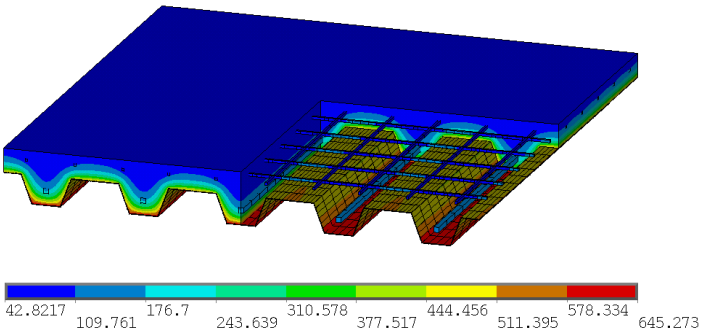

t= 17.3 min

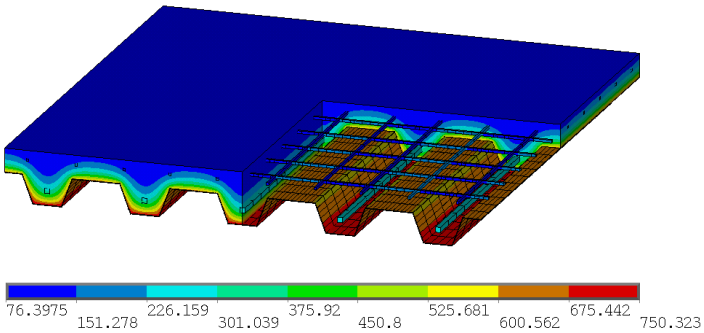

t= 26.0 min

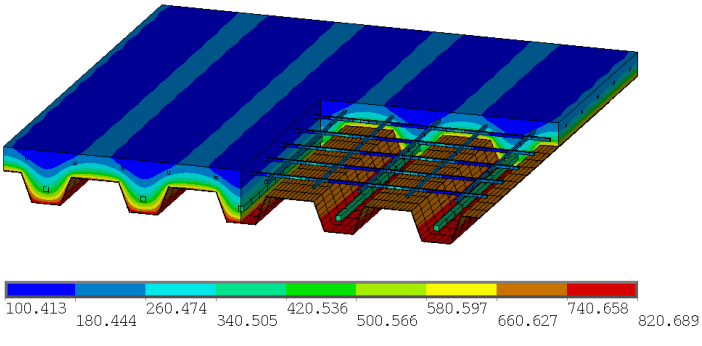

t= 34.6 min

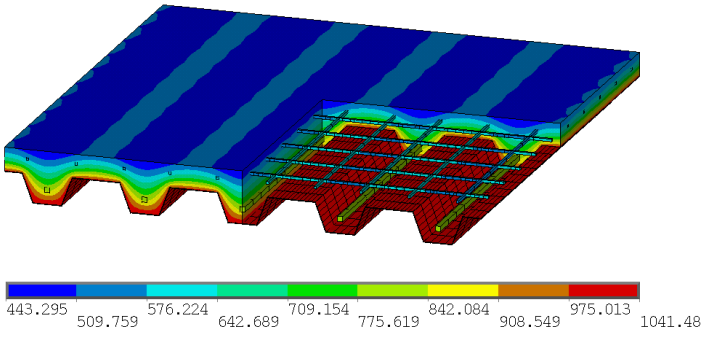

t= 120.0 min

SIM. 34	**Steel deck:** Trapezoidal – O Feliz H60	**Rebar (mm):** ϕ12	**Fire resistance (min)**	
	Mesh (mm//mm): ϕ6//100 (FNQ 60)	**h_1 (mm):** 60	Ave: 46.5	Max: *46.0*

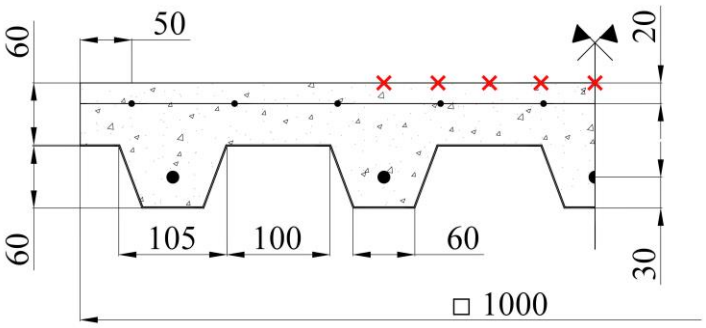

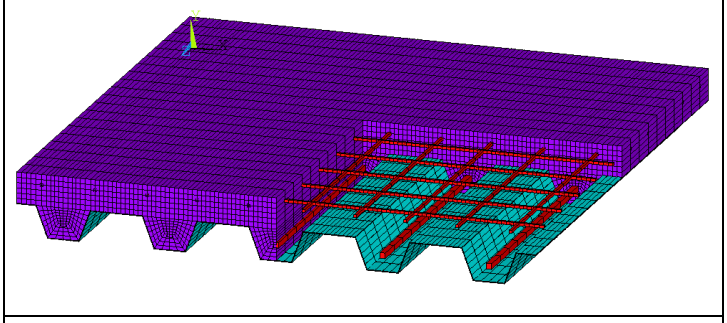

Finite element mesh

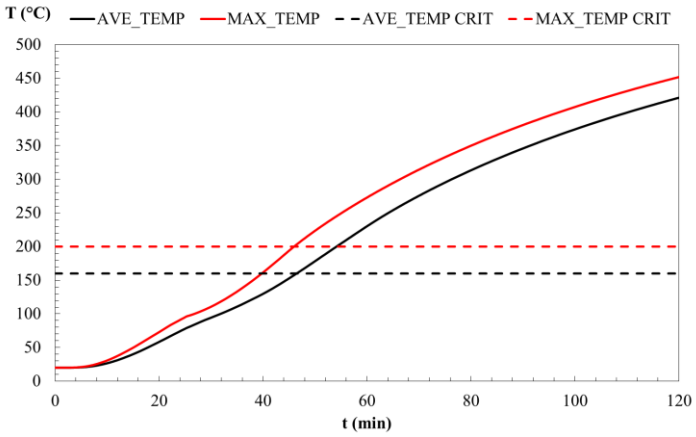

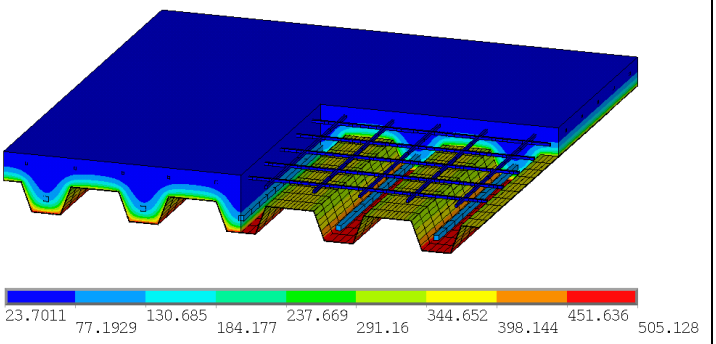

t= 11.5 min

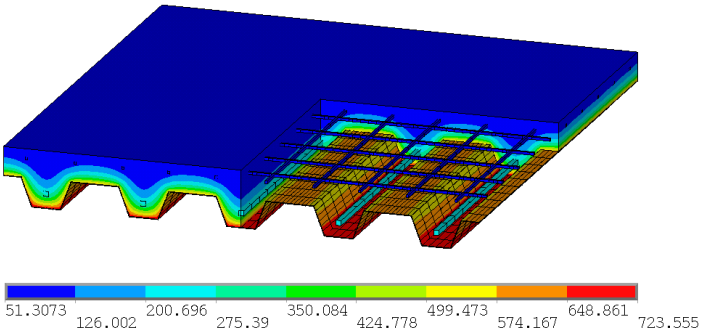

t= 23.0 min

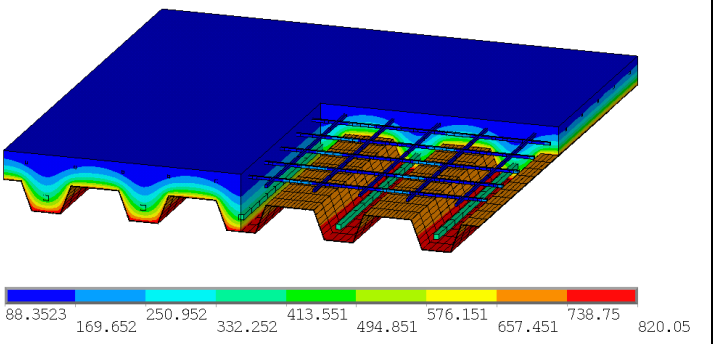

t= 34.5 min

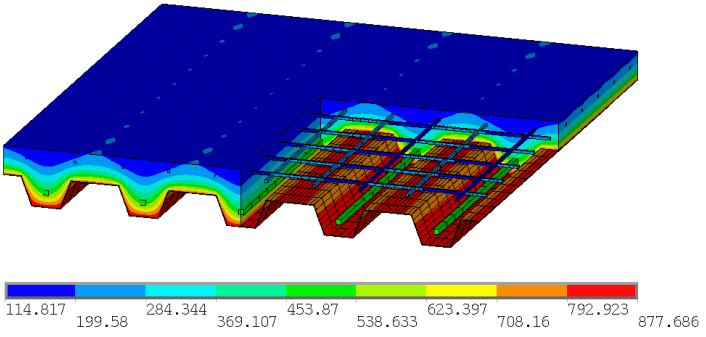

t= 46.0 min

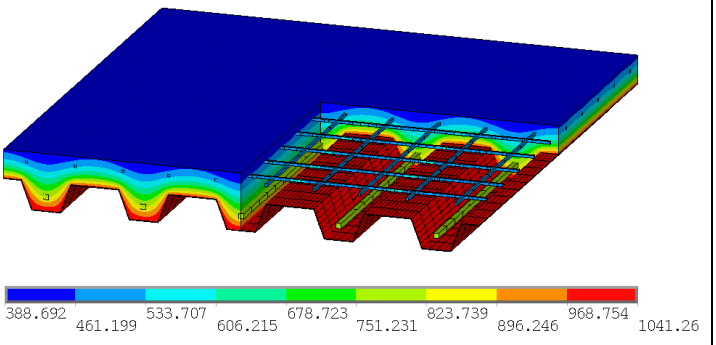

t= 120.0 min

SIM. 35	**Steel deck:** Trapezoidal – O Feliz H60	**Rebar (mm):** ϕ12	**Fire resistance (min)**	
	Mesh (mm//mm): ϕ6//100 (FNQ 60)	**h_1 (mm):** 70	Ave: *57.8*	Max: 59.3

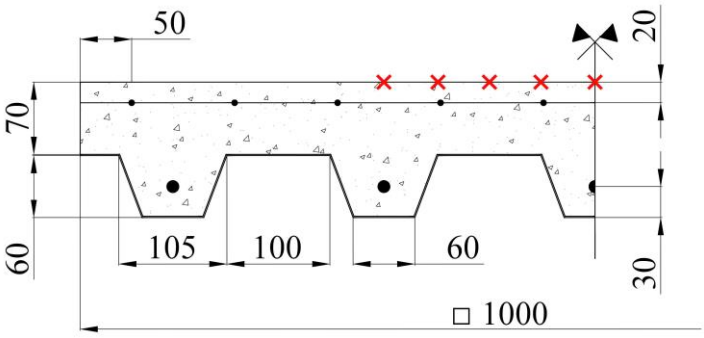

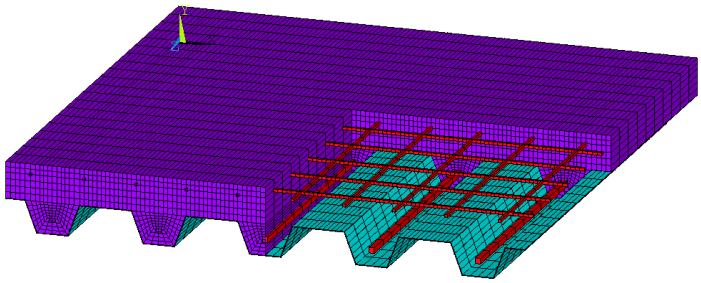

Finite element mesh

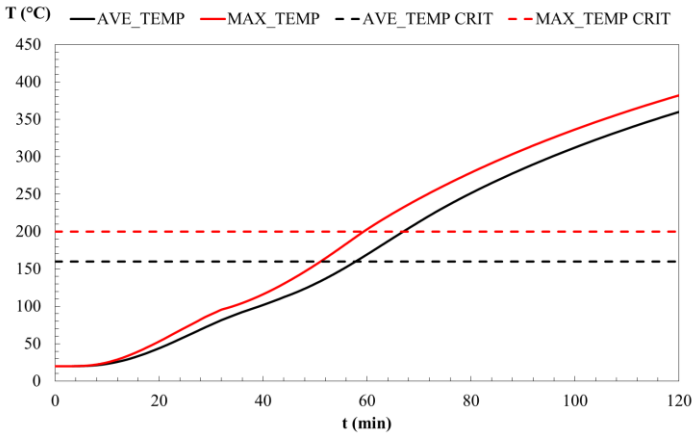

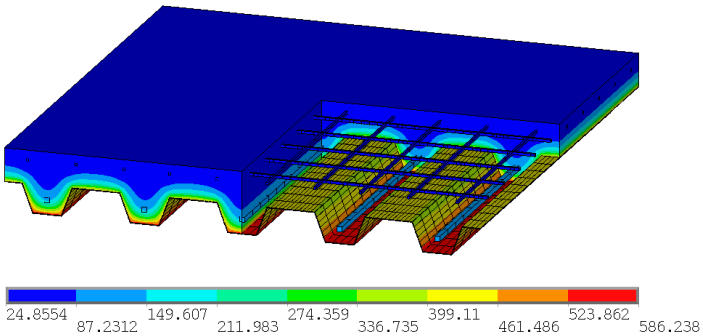

t= 14.5 min

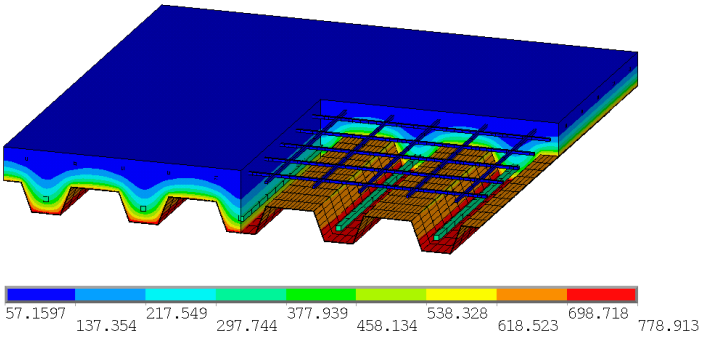

t= 28.9 min

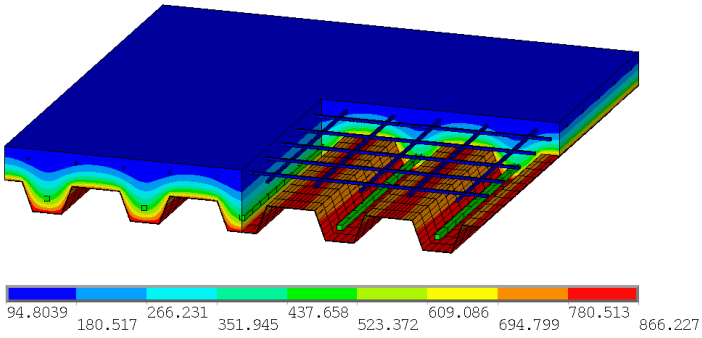

t= 43.4 min

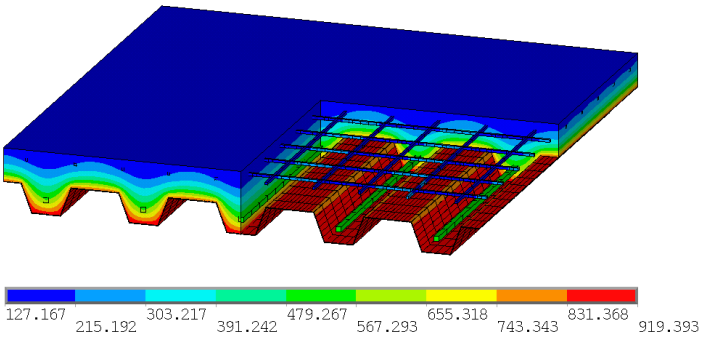

t= 57.8 min

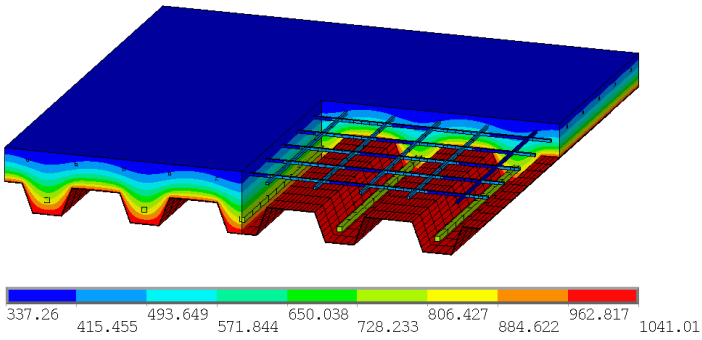

t= 120.0 min

SIM. 36	**Steel deck:** Trapezoidal – O Feliz H60	**Rebar (mm):** ϕ12	**Fire resistance (min)**	
	Mesh (mm//mm): ϕ6//100 (FNQ 60)	**h_1 (mm):** 80	Ave: *70.2*	Max: 74.6

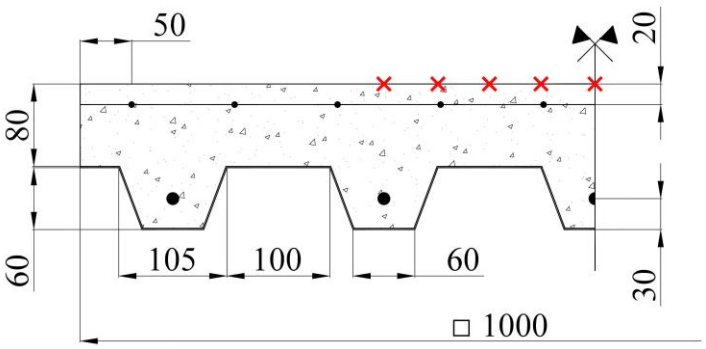

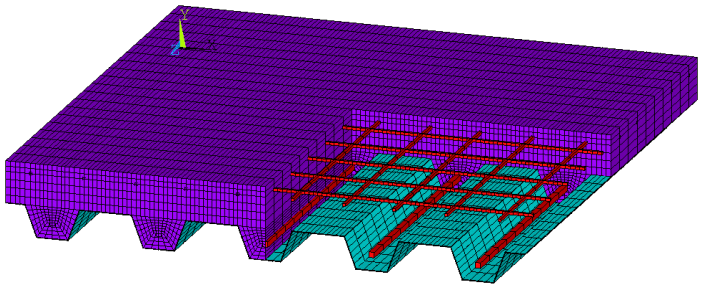

Finite element mesh

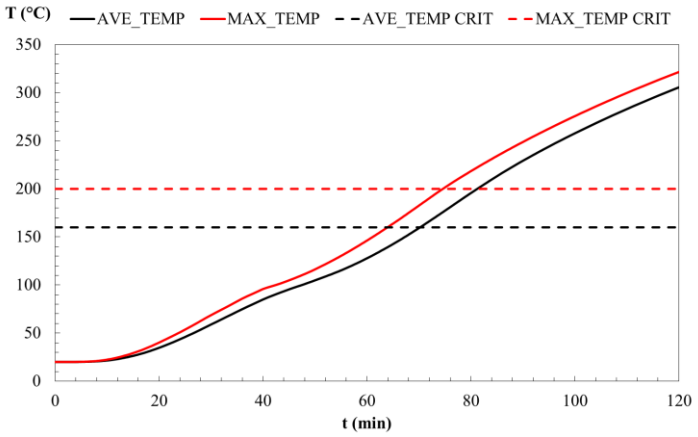

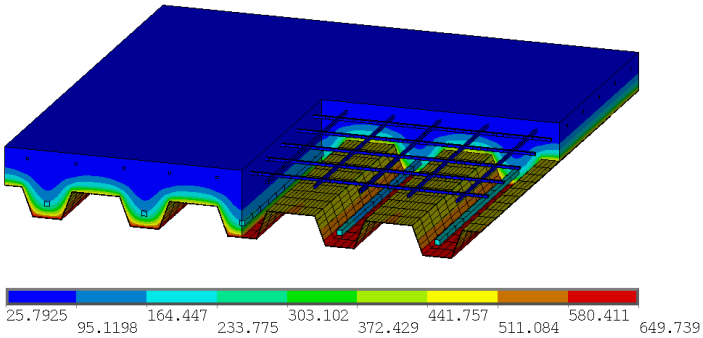

t= 17.6 min

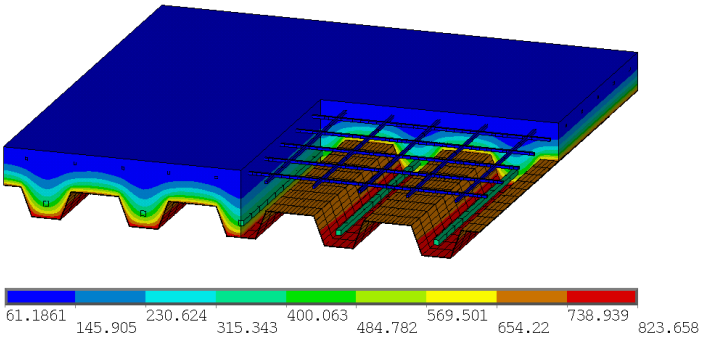

t= 35.1 min

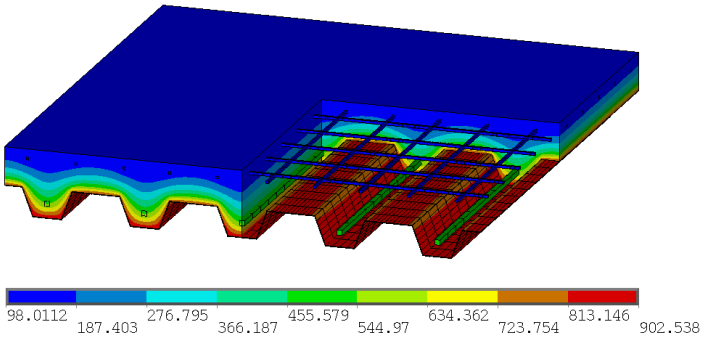

t= 52.7 min

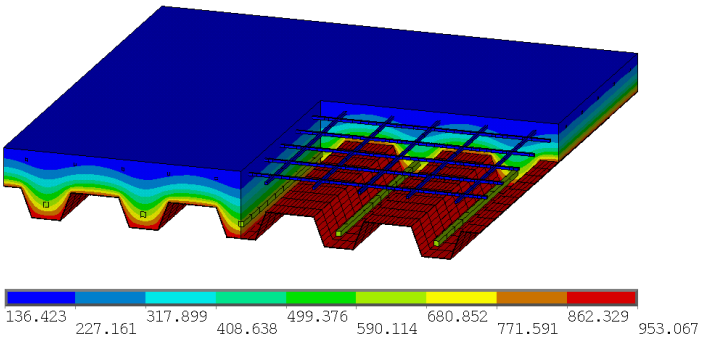

t= 70.2 min

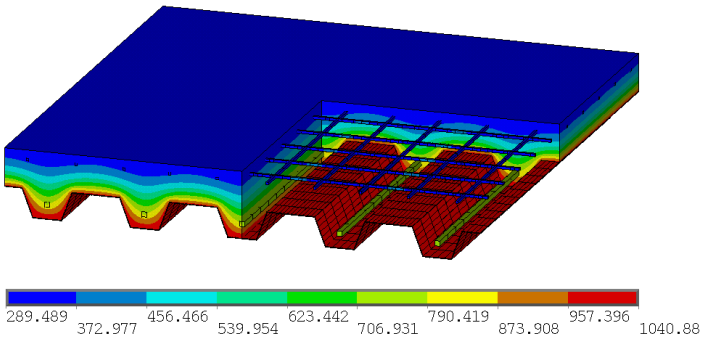

t= 120.0 min

SIM. 37	**Steel deck:** Trapezoidal – O Feliz H60	**Rebar (mm):** ϕ12	**Fire resistance (min)**	
	Mesh (mm//mm): ϕ6//100 (FNQ 60)	**h_1 (mm):** 50	Ave: 36.2	Max: *34.5*

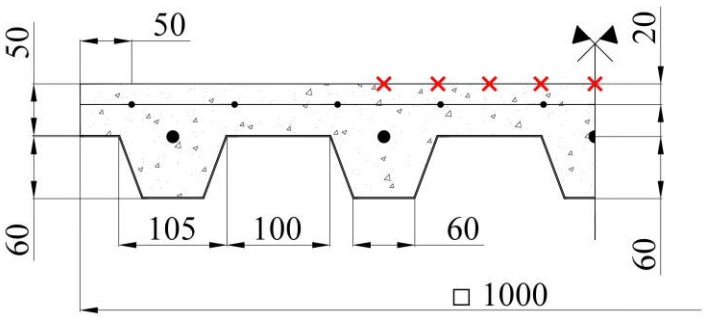

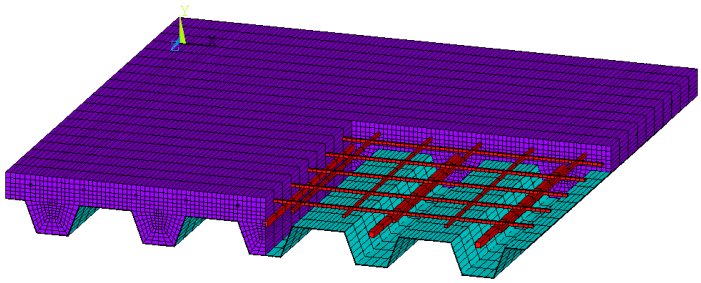

Finite element mesh

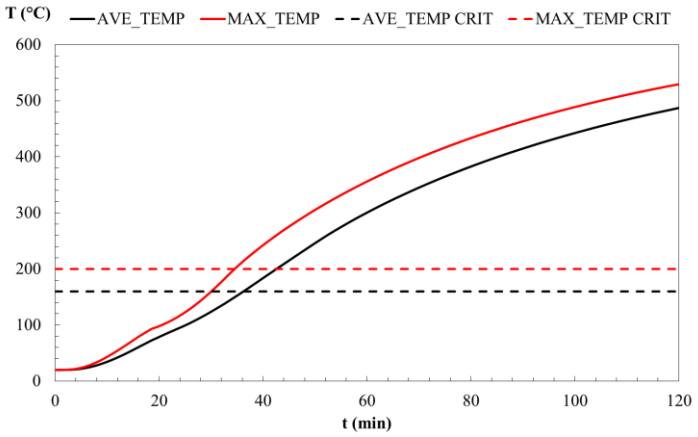

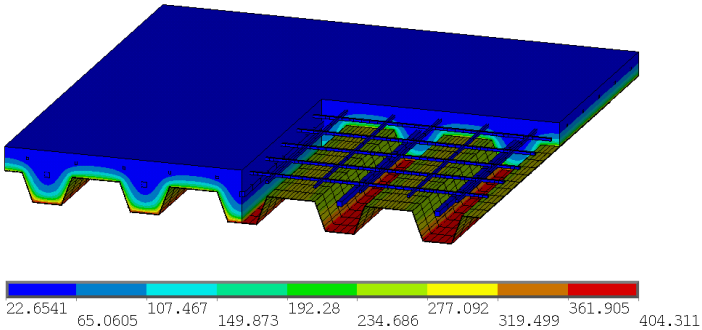

t= 8.6 min

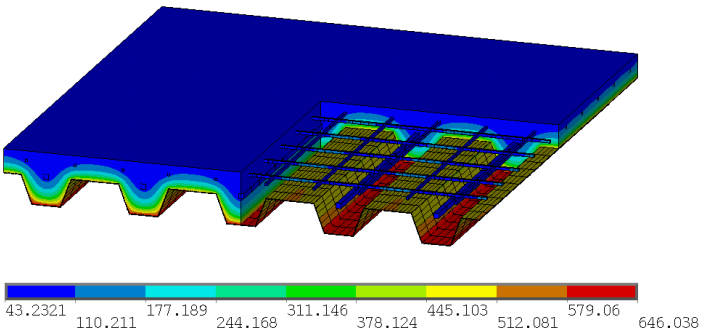

t= 17.3 min

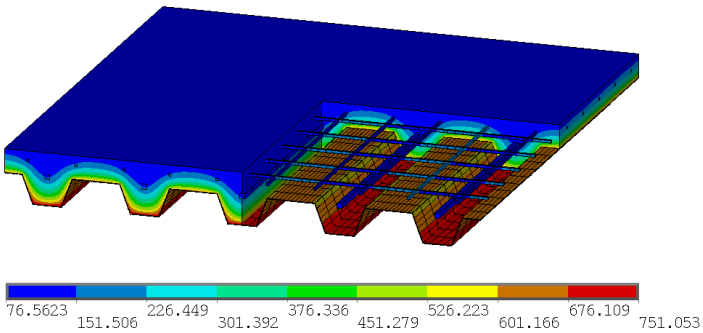

t= 25.9 min

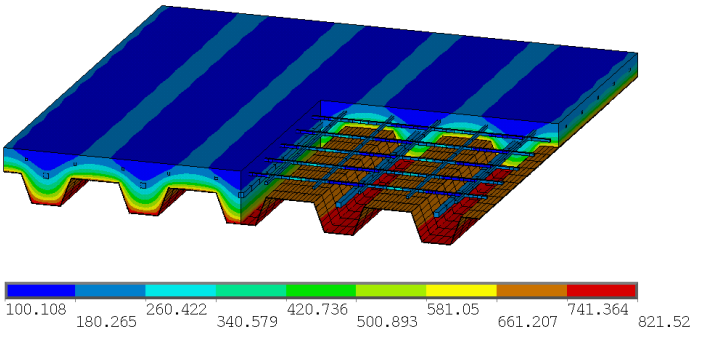

t= 34.5 min

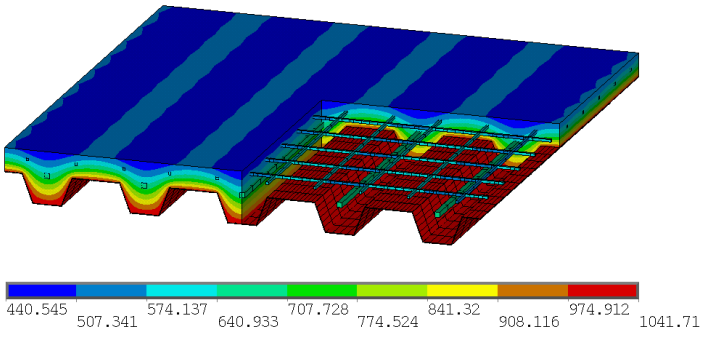

t= 120.0 min

SIM. 38	**Steel deck:** Trapezoidal – O Feliz H60	**Rebar (mm):** ϕ12	**Fire resistance (min)**	
	Mesh (mm//mm): ϕ6//100 (FNQ 60)	**h_1 (mm):** 60	Ave: 46.4	Max: *45.9*

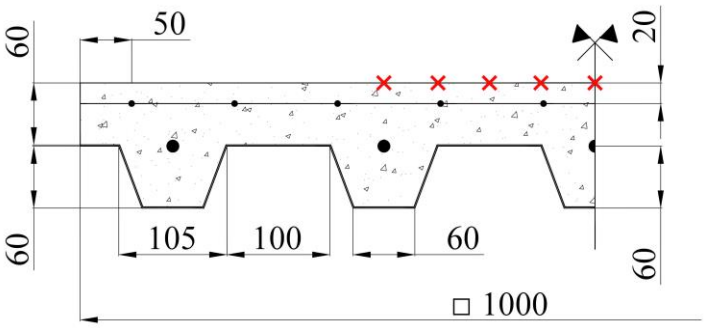

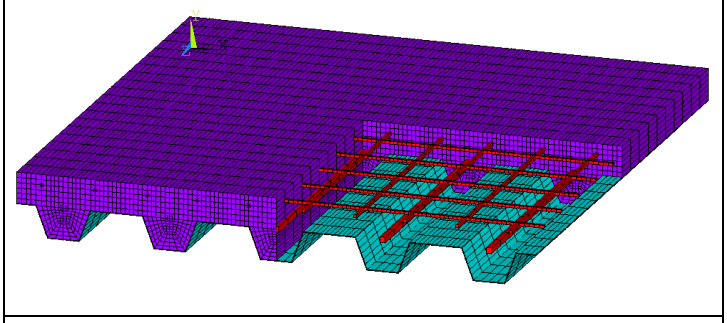

Finite element mesh

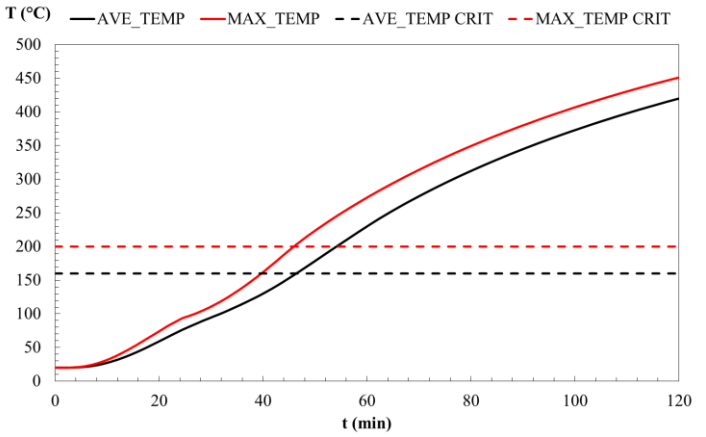

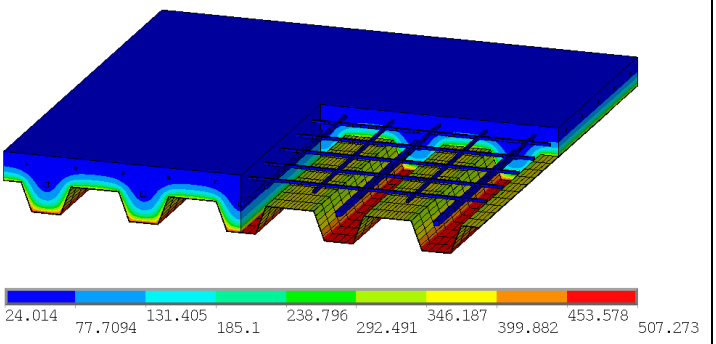

t= 11.5 min

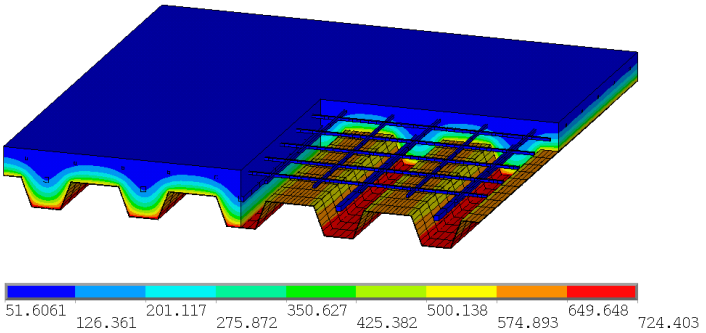

t= 23.0 min

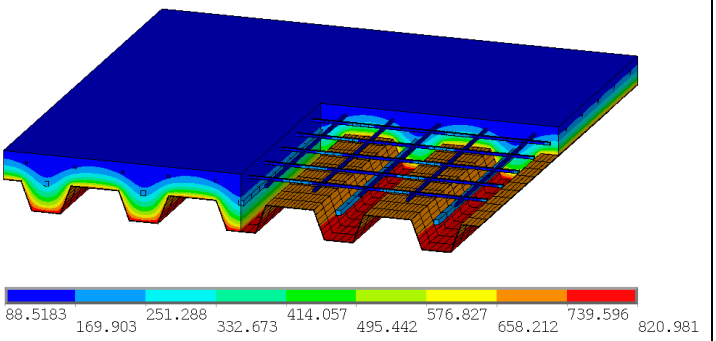

t= 34.4 min

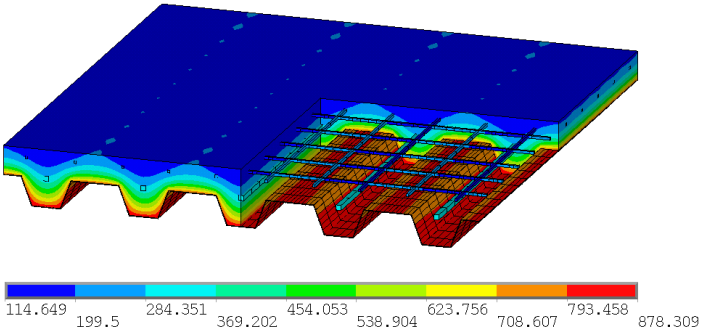

t= 45.9 min

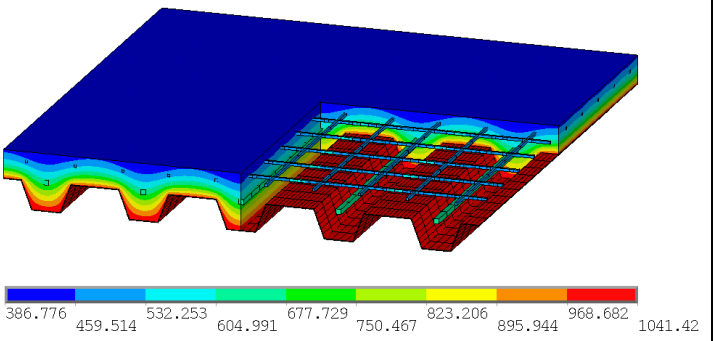

t= 120.0 min

SIM. 39	**Steel deck:** Trapezoidal – O Feliz H60	**Rebar (mm):** ϕ12	**Fire resistance (min)**	
	Mesh (mm//mm): ϕ6//100 (FNQ 60)	**h_1 (mm):** 70	Ave: *57.6*	Max: 59.2

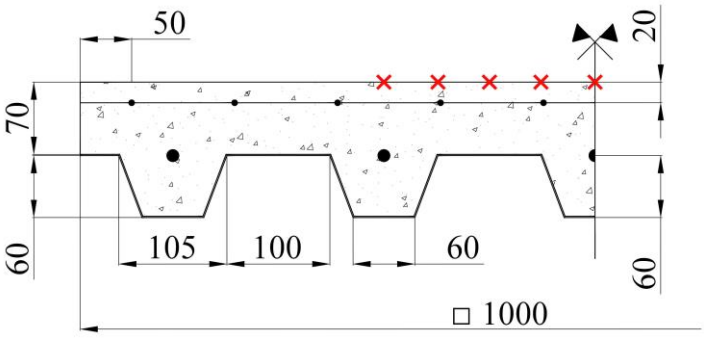

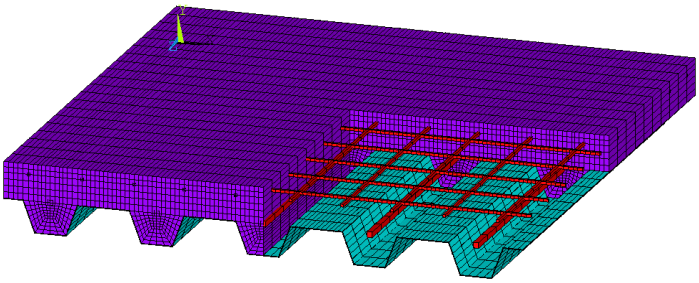

Finite element mesh

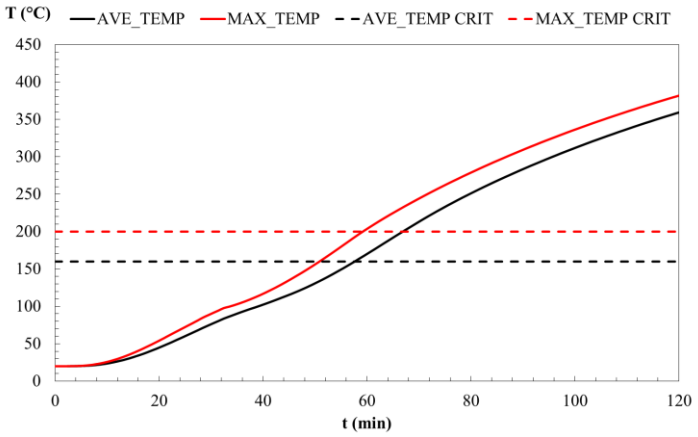

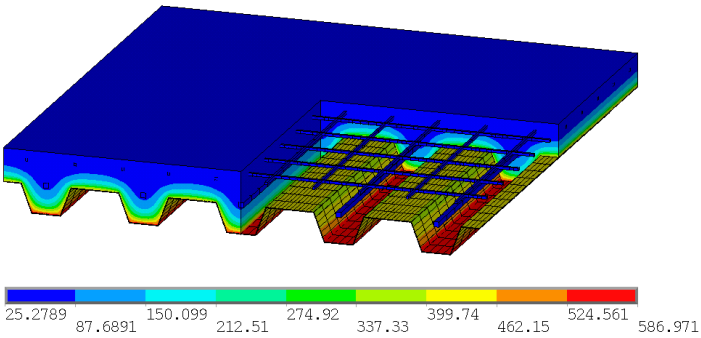

t= 14.4 min

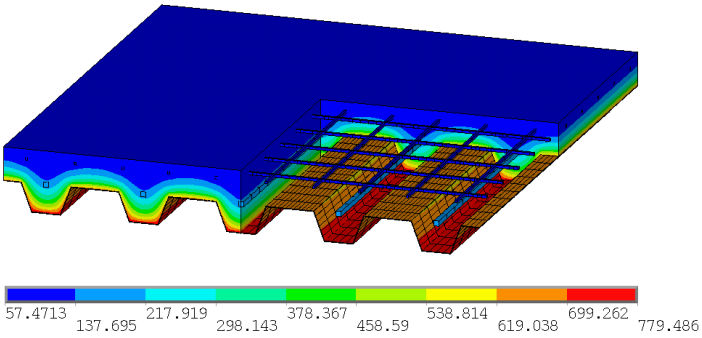

t= 28.8 min

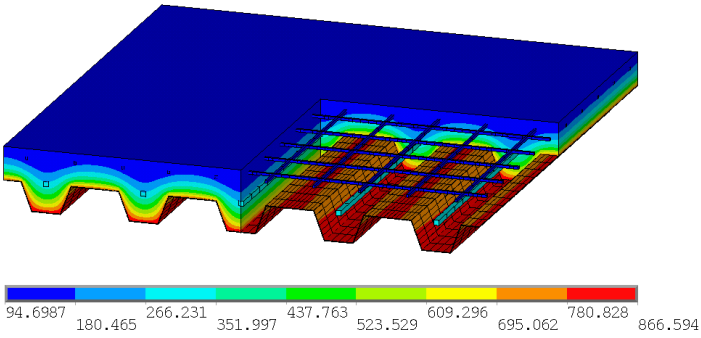

t= 43.2 min

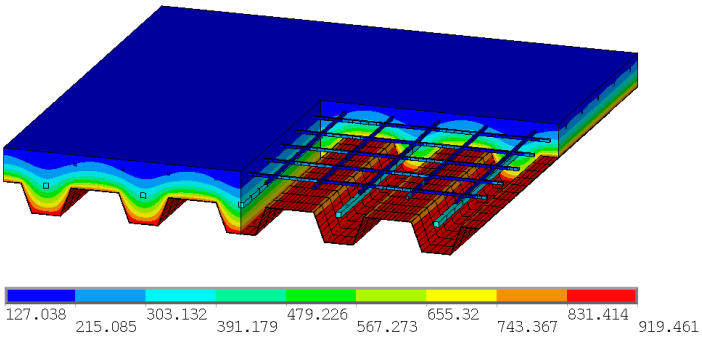

t= 57.6 min

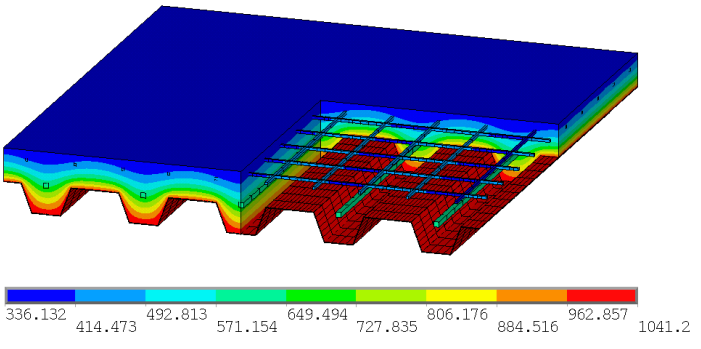

t= 120.0 min

SIM. 40	**Steel deck:** Trapezoidal – O Feliz H60	**Rebar (mm):** ϕ12	**Fire resistance (min)**	
	Mesh (mm//mm): ϕ6//100 (FNQ 60)	**h_1 (mm):** 80	Ave: *70.1*	Max: 74.5

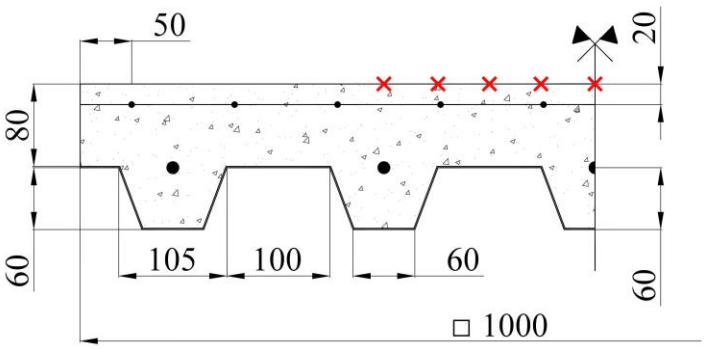

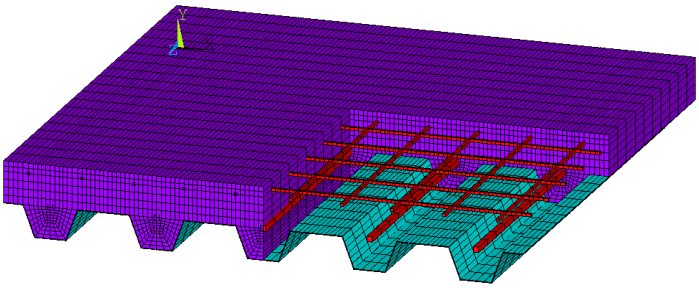

Finite element mesh

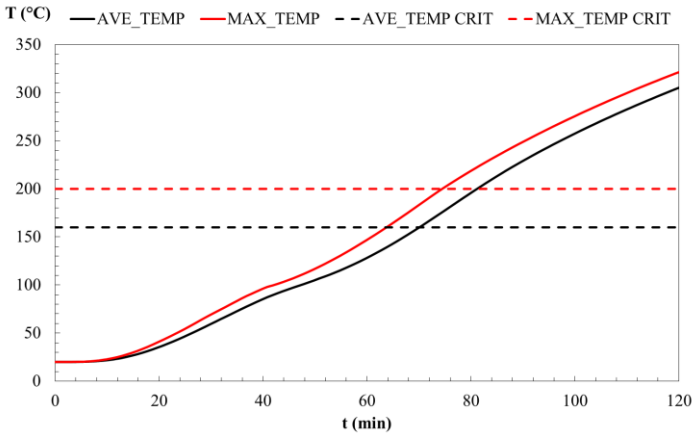

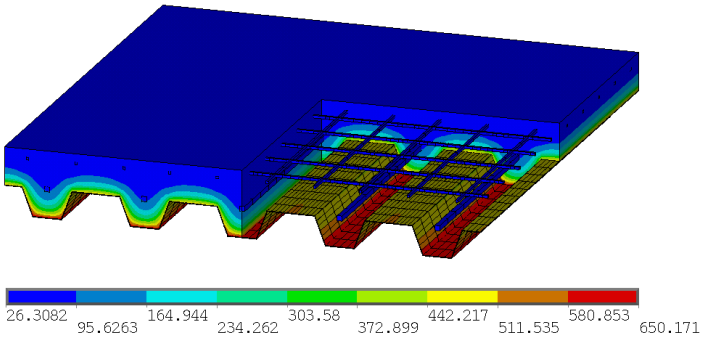

t= 17.5 min

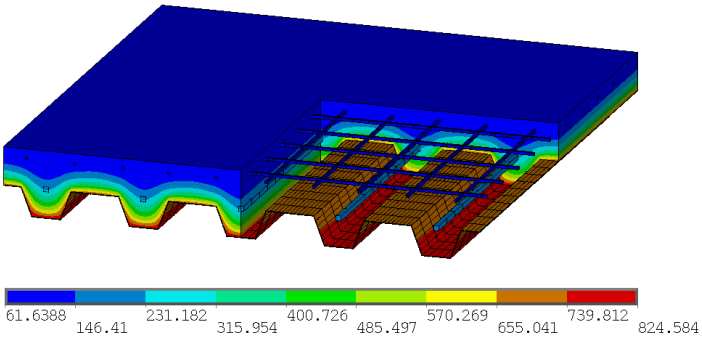

t= 35.1 min

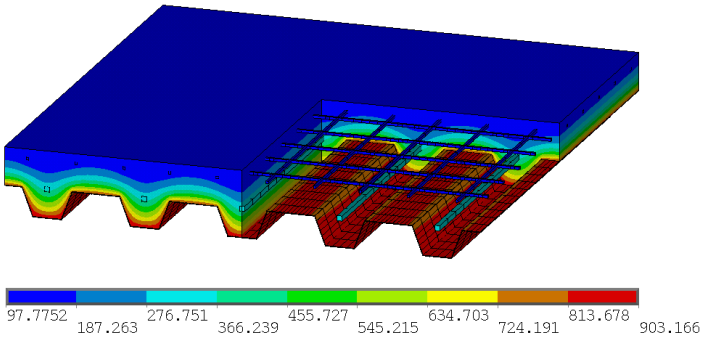

t= 52.6 min

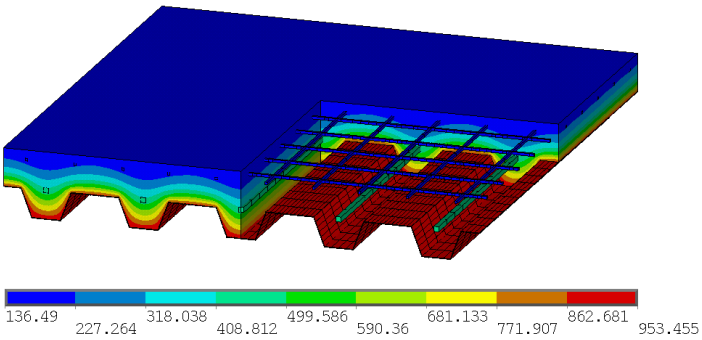

t= 70.1 min

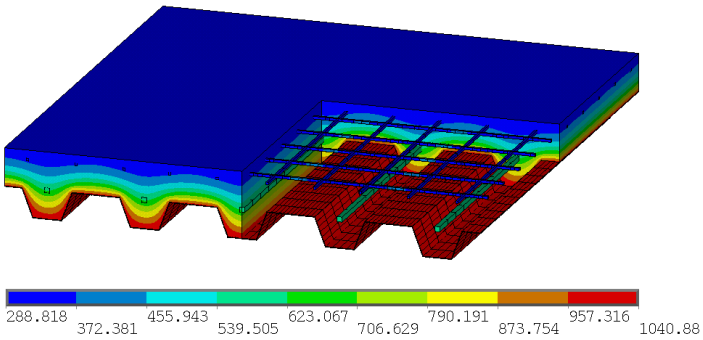

t= 120.0 min

SIM. 41	**Steel deck:** Trapezoidal – O Feliz H60	**Rebar (mm):** ϕ12	**Fire resistance (min)**	
	Mesh (mm//mm): ϕ6//150 (FND 60)	**h_1 (mm):** 50	Ave: 36.4	Max: *35.1*

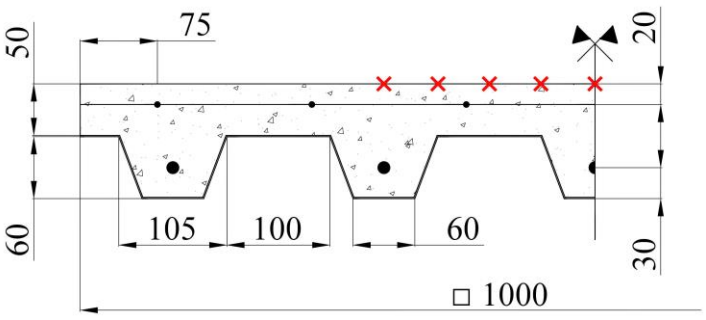

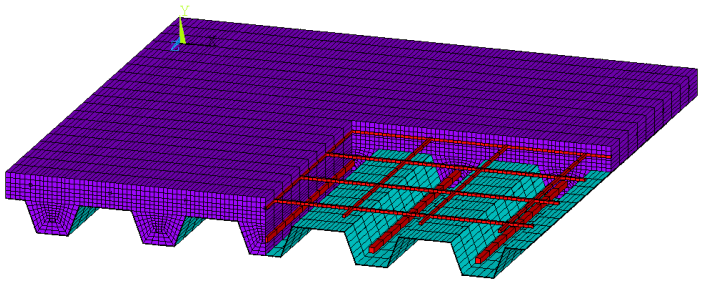

Finite element mesh

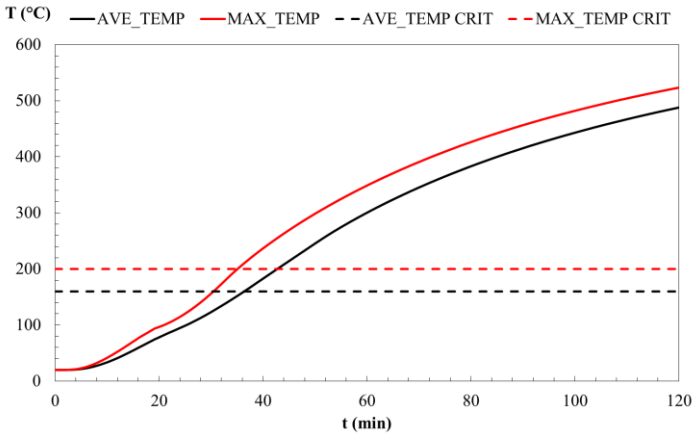

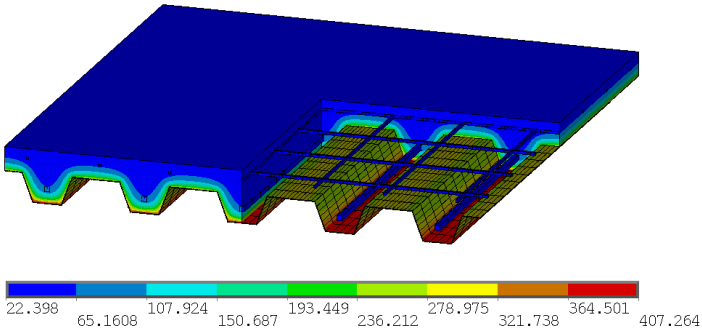

t= 8.8 min

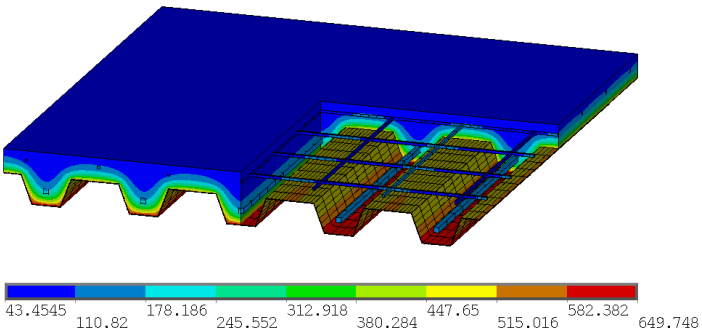

t= 17.6 min

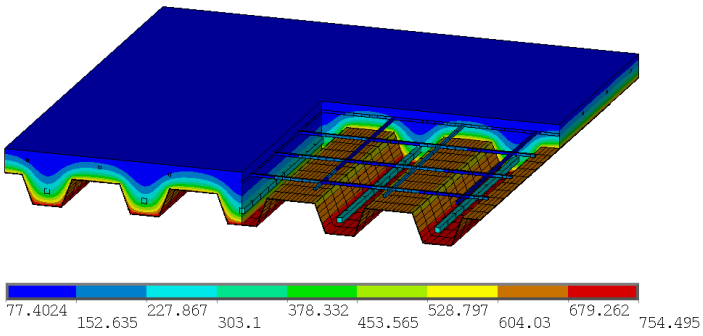

t= 26.3 min

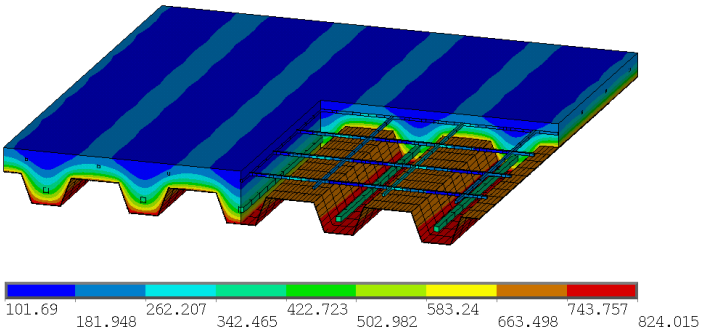

t= 35.1 min

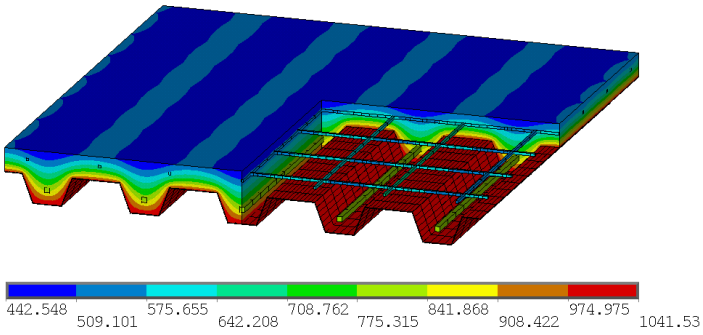

t= 120.0 min

SIM. 42	**Steel deck:** Trapezoidal – O Feliz H60	**Rebar (mm):** ϕ12	**Fire resistance (min)**	
	Mesh (mm//mm): ϕ6//150 (FND 60)	**h_1 (mm):** 60	Ave: *46.5*	Max: 46.5

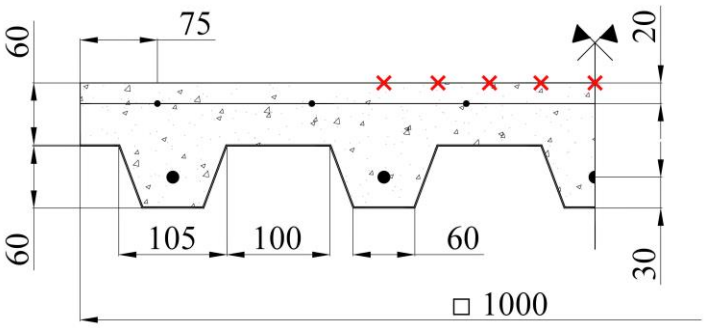

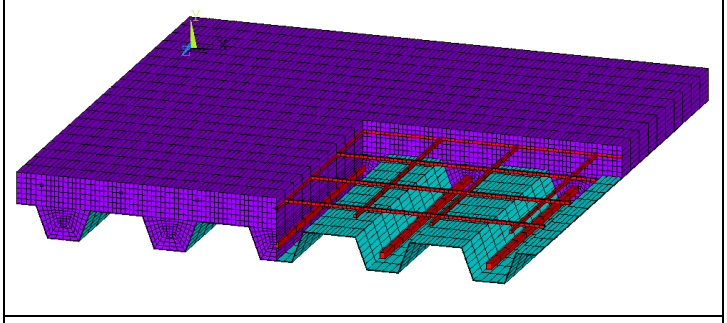

Finite element mesh

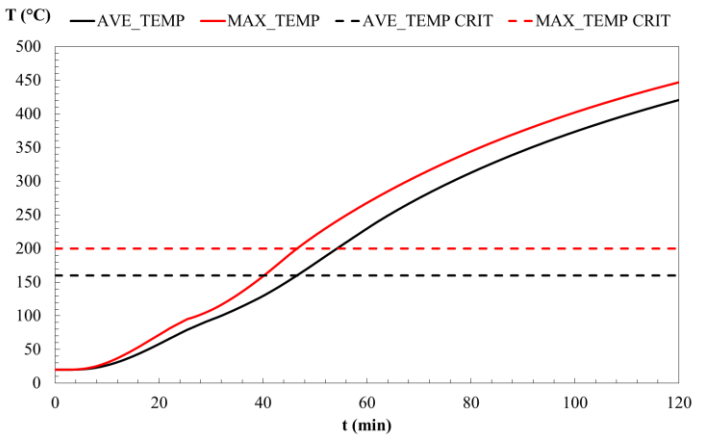

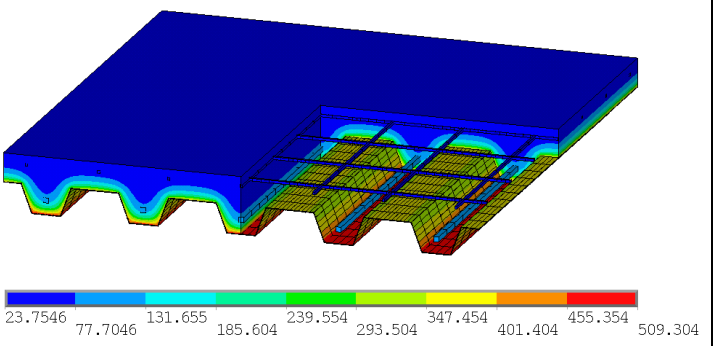

t= 11.6 min

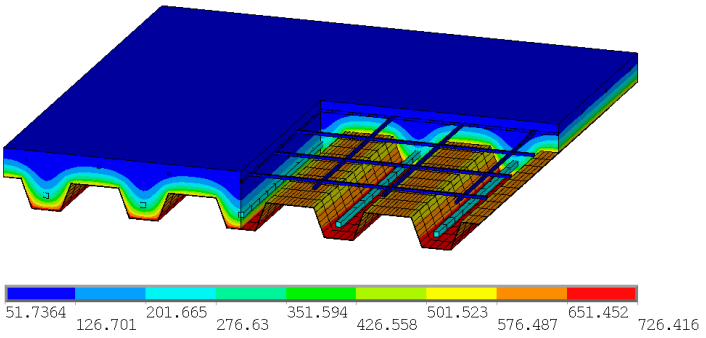

t= 23.3 min

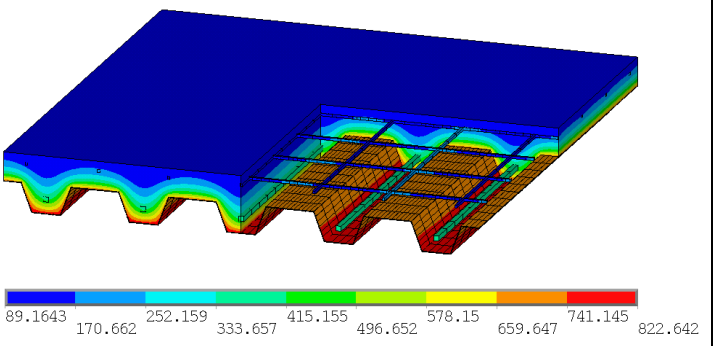

t= 34.9 min

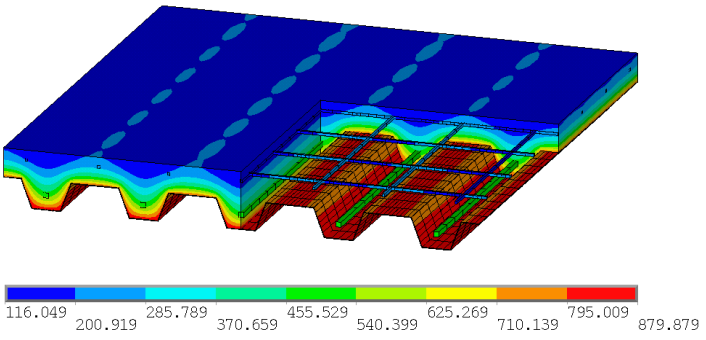

t= 46.5 min

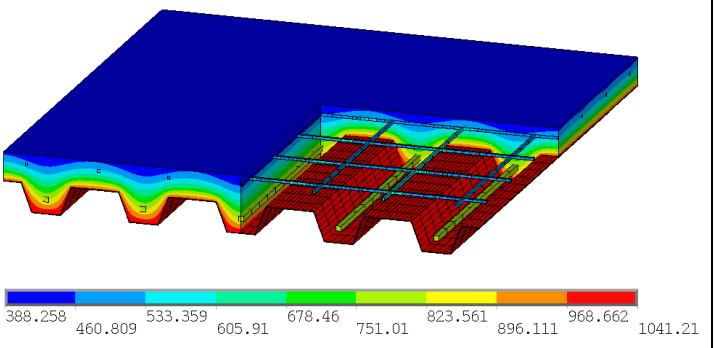

t= 120.0 min

SIM. 43	**Steel deck:** Trapezoidal – O Feliz H60	**Rebar (mm):** ϕ12	**Fire resistance (min)**	
	Mesh (mm//mm): ϕ6//150 (FND 60)	**h_1 (mm):** 70	Ave: *57.9*	Max: 60.1

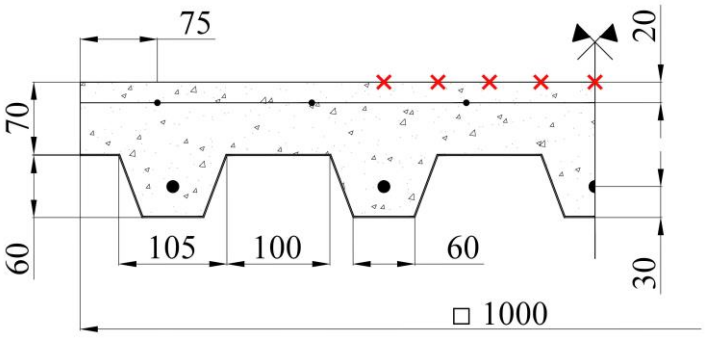

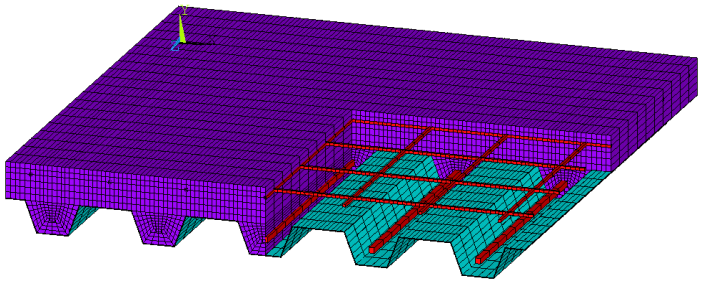

Finite element mesh

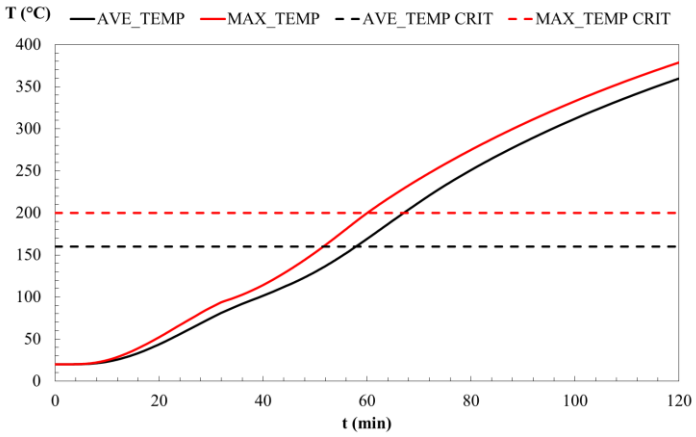

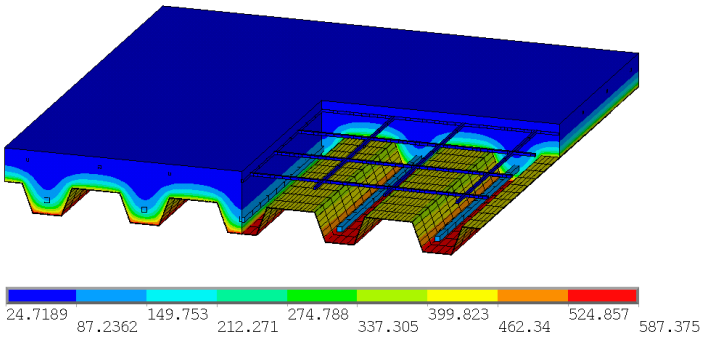

t= 14.5 min

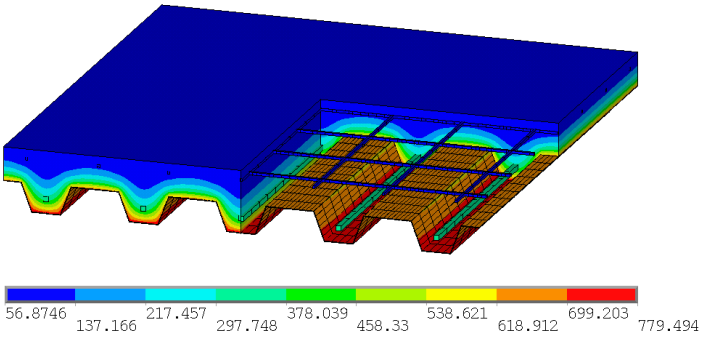

t= 29.0 min

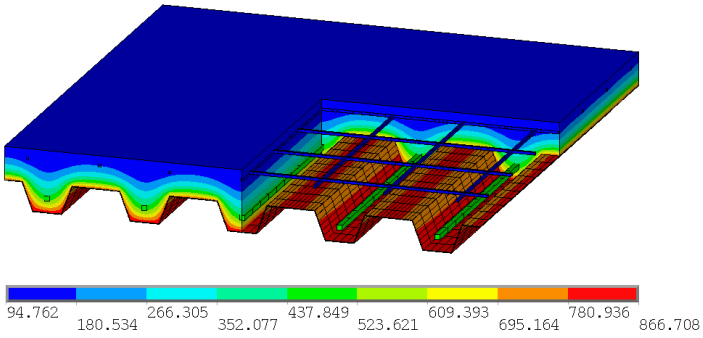

t= 43.4 min

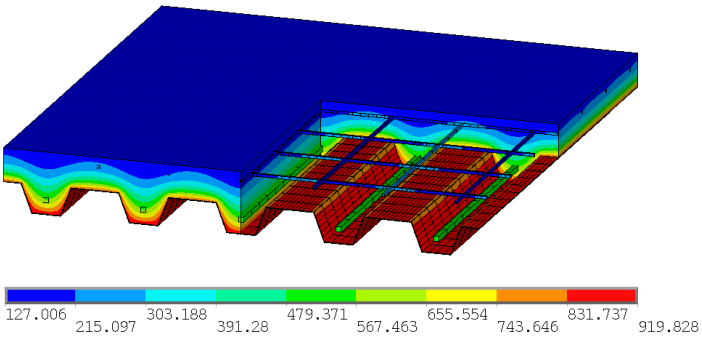

t= 57.9 min

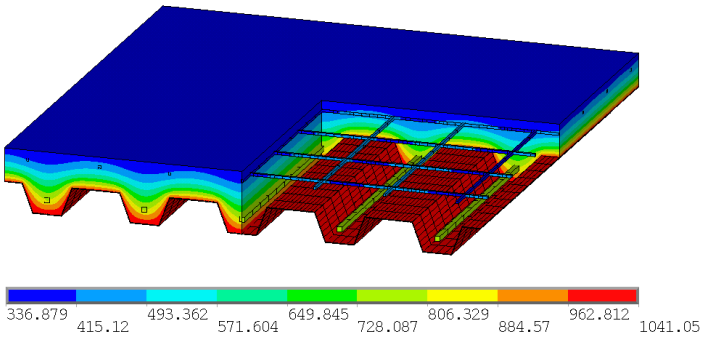

t= 120.0 min

SIM. 44	**Steel deck:** Trapezoidal – O Feliz H60	**Rebar (mm):** ϕ12	**Fire resistance (min)**	
	Mesh (mm//mm): ϕ6//150 (FND 60)	**h_1 (mm):** 80	Ave: *70.3*	Max: 75.3

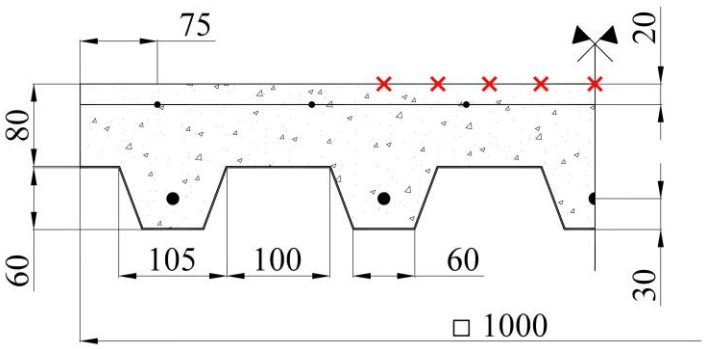

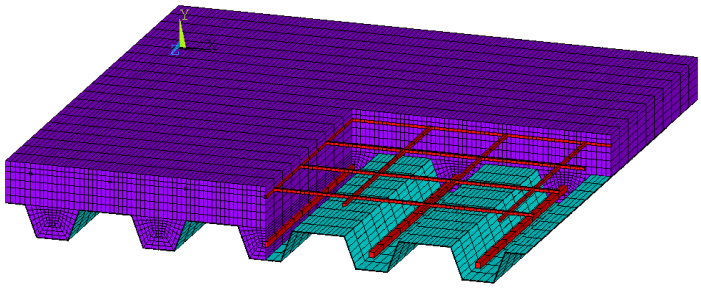

Finite element mesh

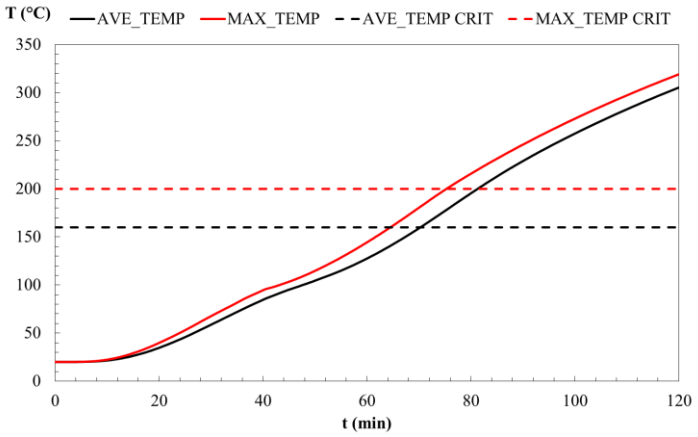

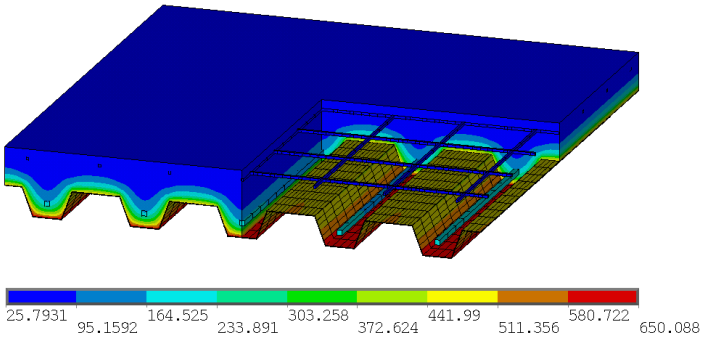

t= 17.6 min

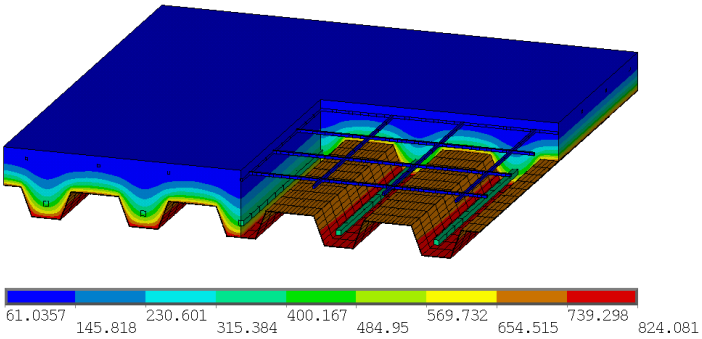

t= 35.2 min

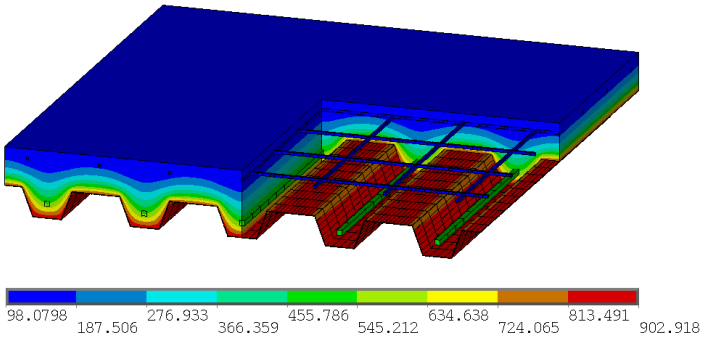

t= 52.7 min

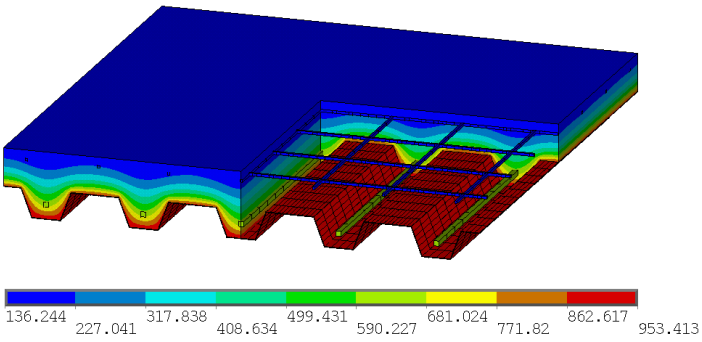

t= 70.3 min

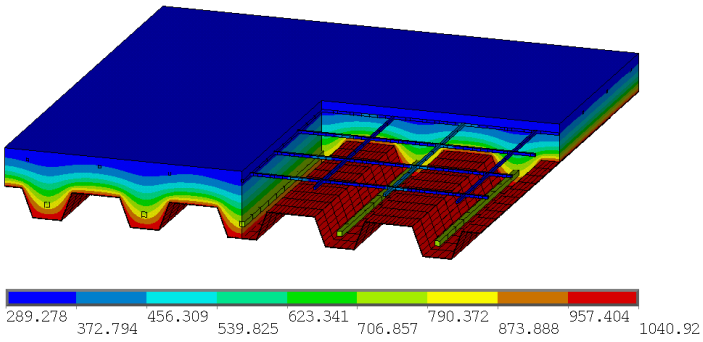

t= 120.0 min

SIM. 45	**Steel deck:** Trapezoidal – O Feliz H60	**Rebar (mm):** ϕ12	**Fire resistance (min)**	
	Mesh (mm//mm): ϕ6//150 (FND 60)	**h_1 (mm):** 50	Ave: 36.3	Max: *35.0*

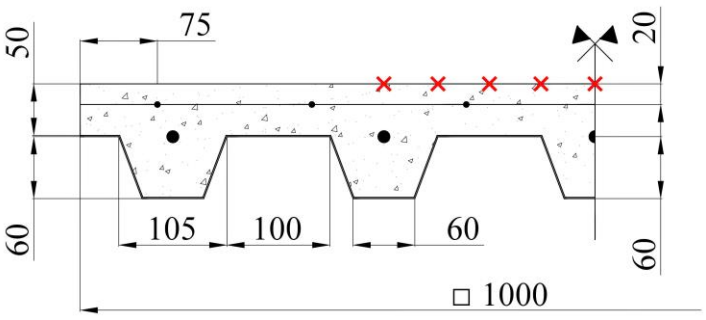

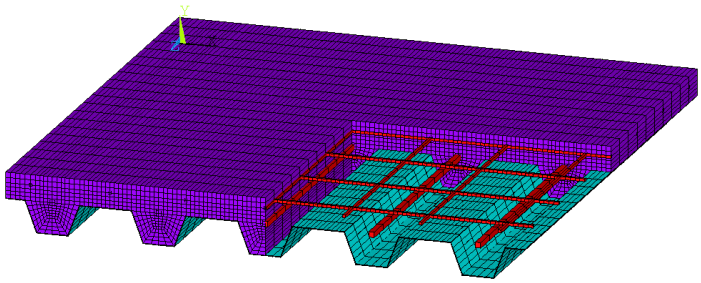

Finite element mesh

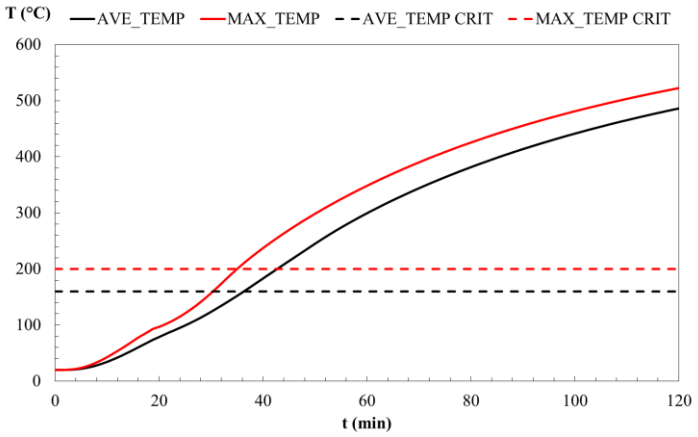

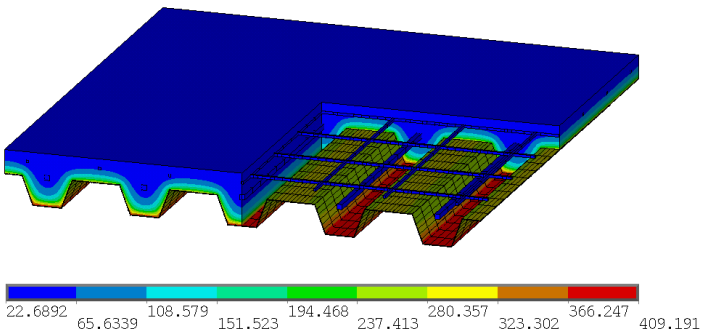

t= 8.8 min

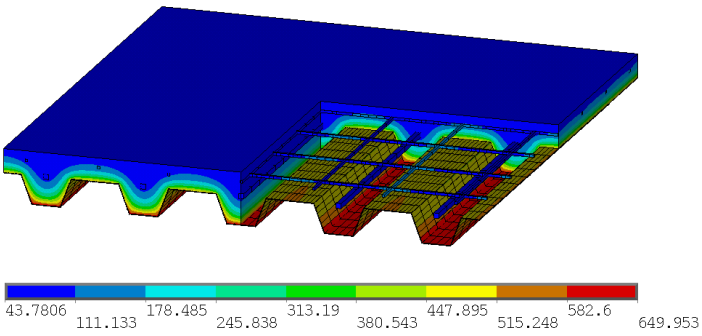

t= 17.5 min

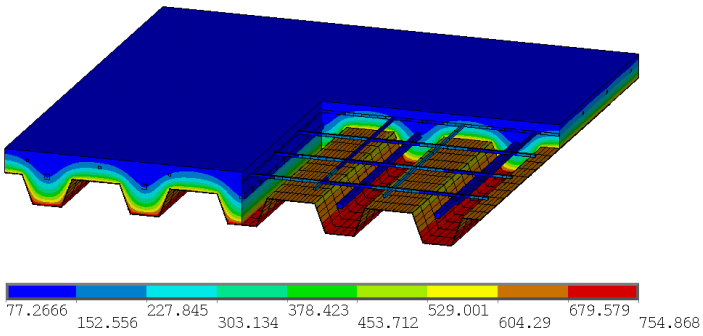

t= 26.3 min

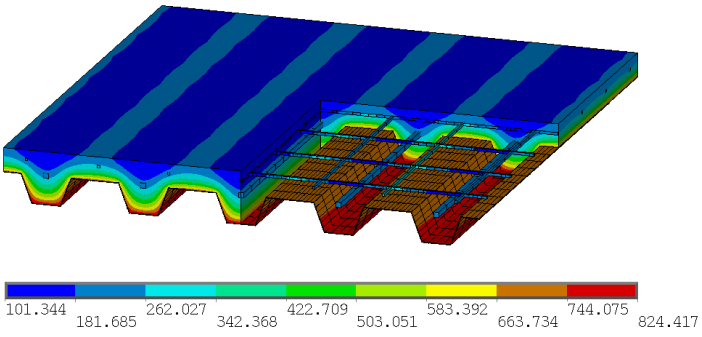

t= 35.0 min

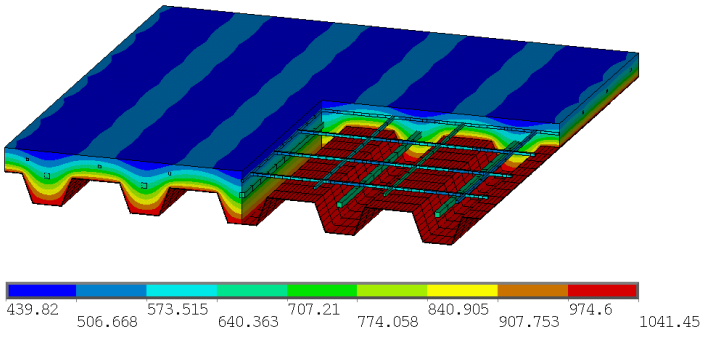

t= 120.0 min

SIM. 46	**Steel deck:** Trapezoidal – O Feliz H60	**Rebar (mm):** ϕ12	**Fire resistance (min)**	
	Mesh (mm//mm): ϕ6//150 (FND 60)	**h_1 (mm):** 60	Ave: *46.5*	Max: 46.5

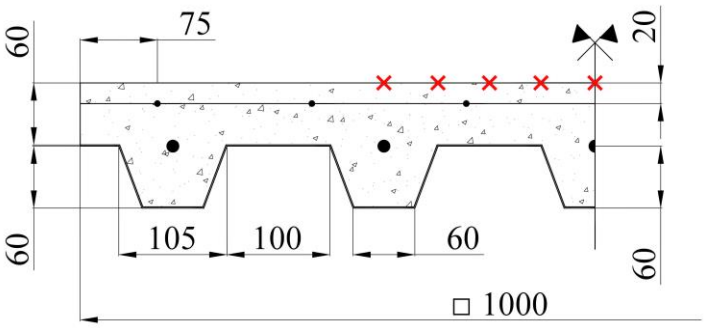

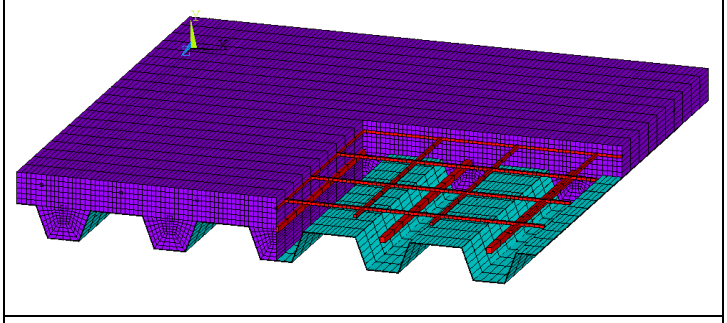

Finite element mesh

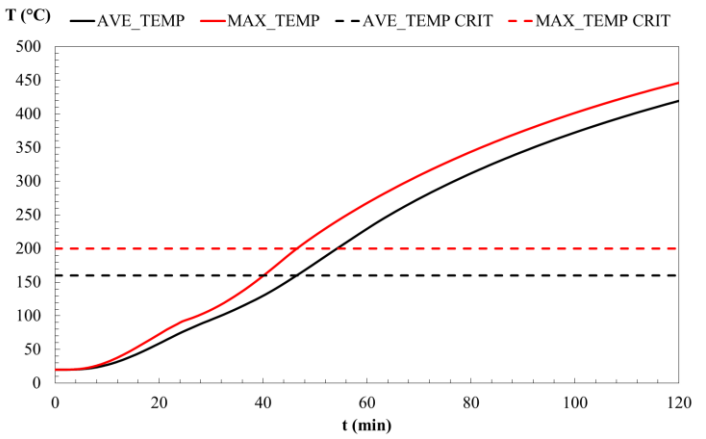

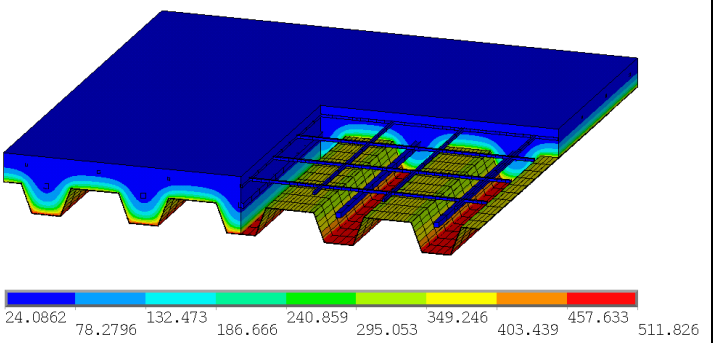

t= 11.6 min

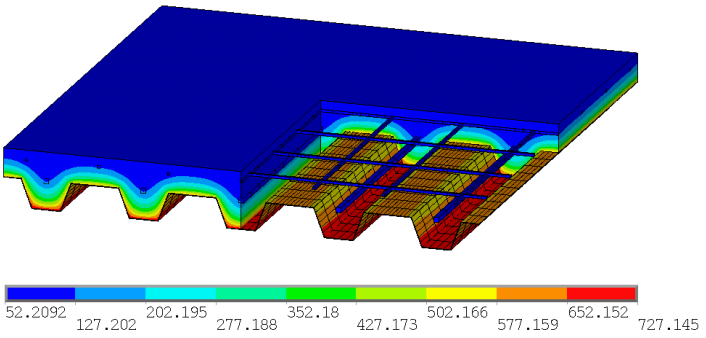

t= 23.3 min

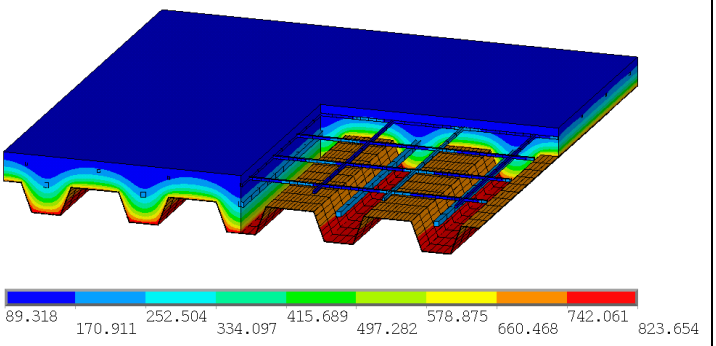

t= 34.9 min

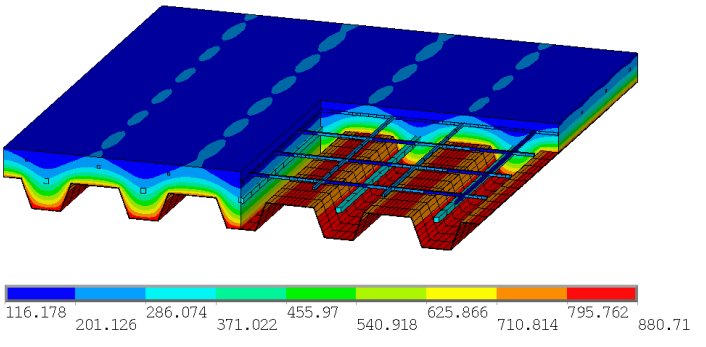

t= 46.5 min

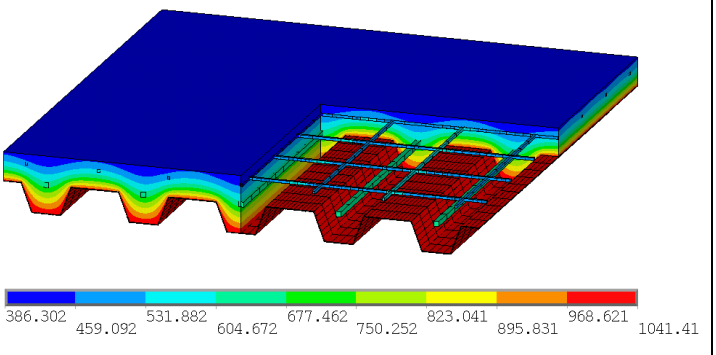

t= 120.0 min

SIM. 47	**Steel deck:** Trapezoidal – O Feliz H60	**Rebar (mm):** ϕ12	**Fire resistance (min)**	
	Mesh (mm//mm): ϕ6//150 (FND 60)	**h_1 (mm):** 70	Ave: *57.7*	Max: 59.9

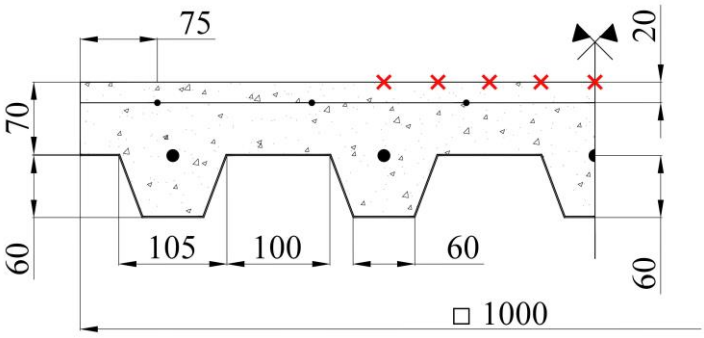

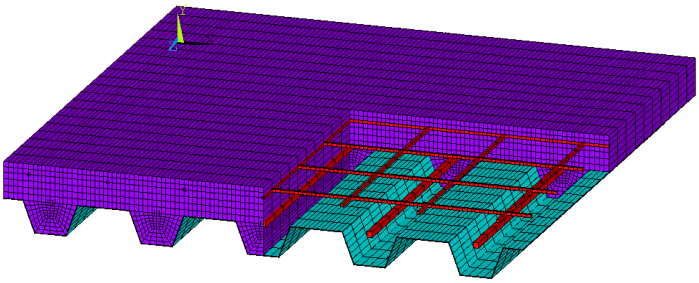

Finite element mesh

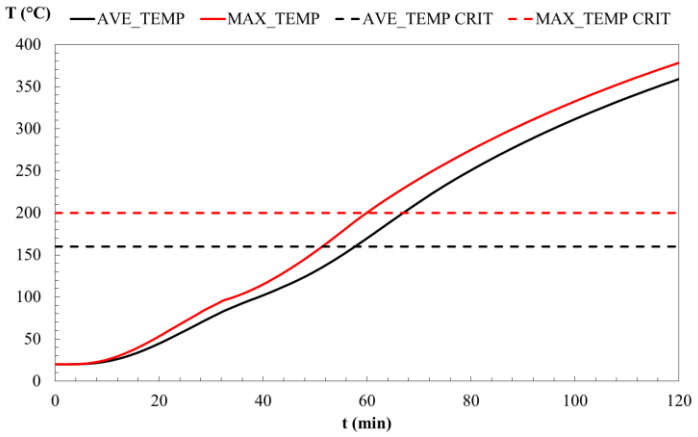

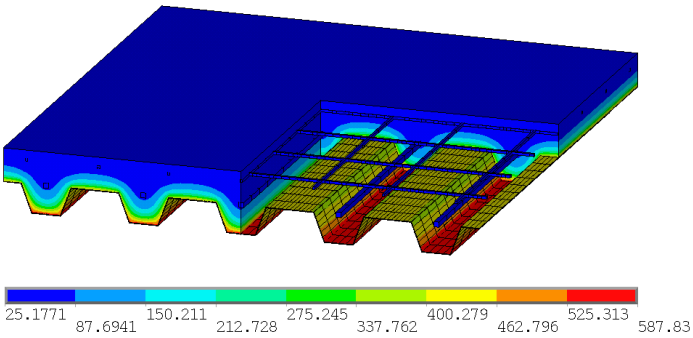

t= 14.4 min

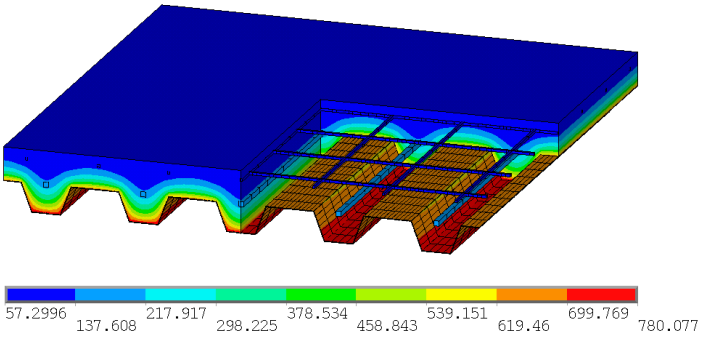

t= 28.9 min

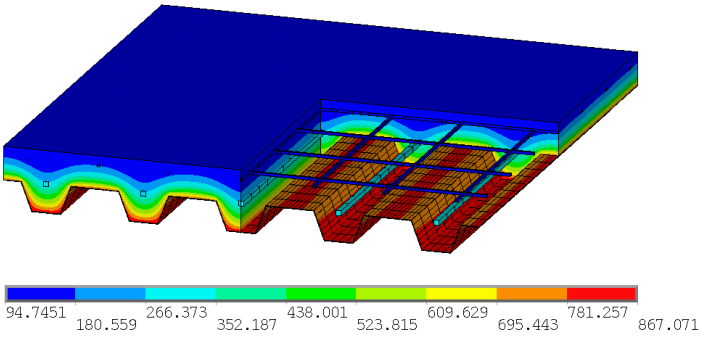

t= 43.3 min

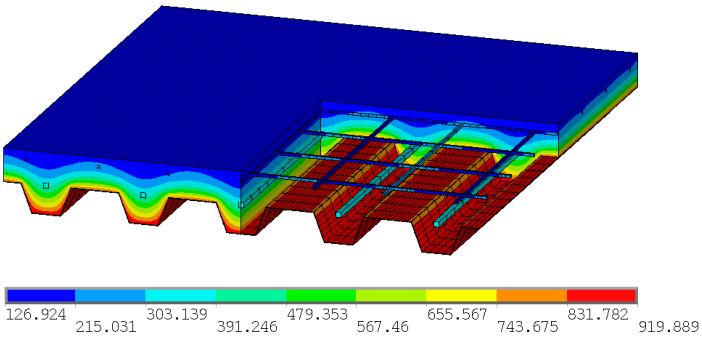

t= 57.7 min

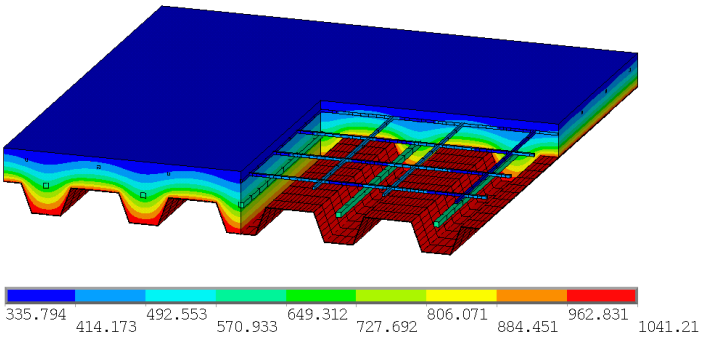

t= 120.0 min

SIM. 48	**Steel deck:** Trapezoidal – O Feliz H60	**Rebar (mm):** ϕ12	**Fire resistance (min)**	
	Mesh (mm//mm): ϕ6//150 (FND 60)	**h_1 (mm):** 80	Ave: *70.1*	Max: 75.1

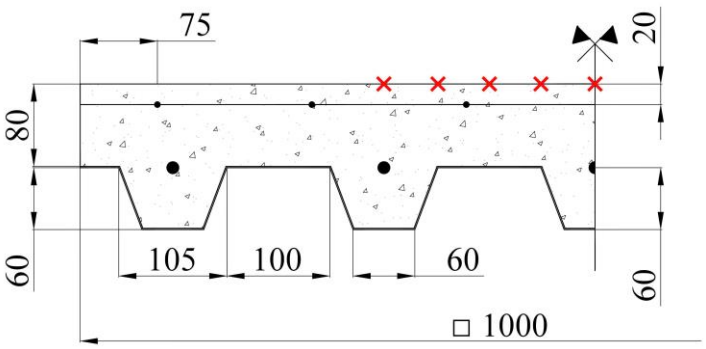

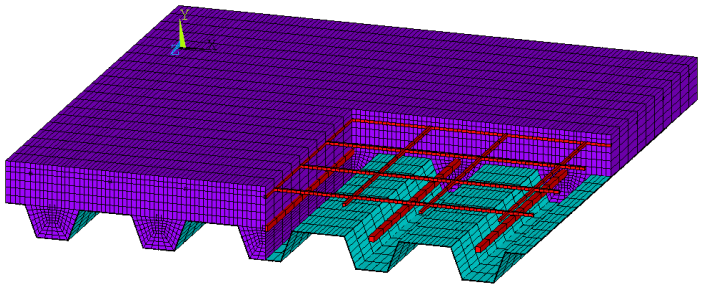

Finite element mesh

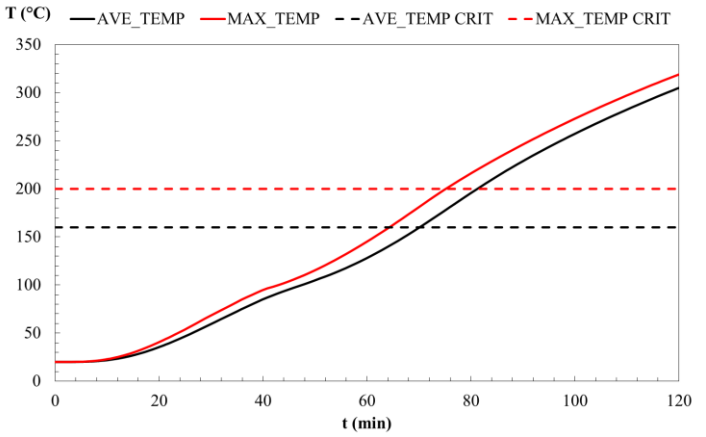

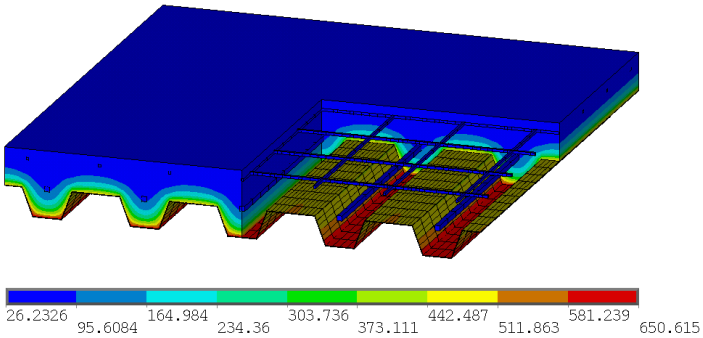

t= 17.5 min

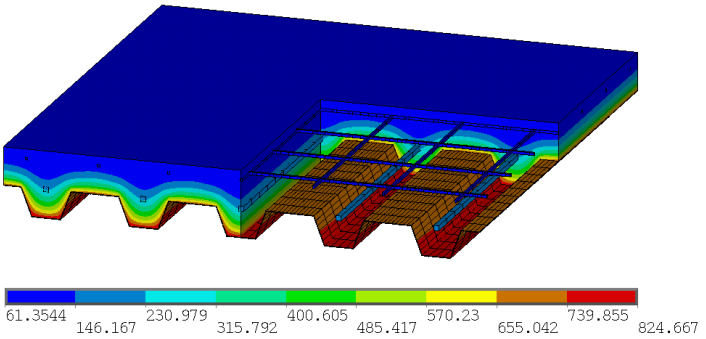

t= 35.1 min

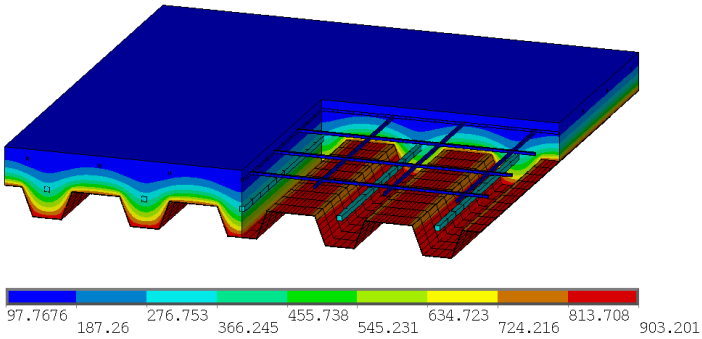

t= 52.6 min

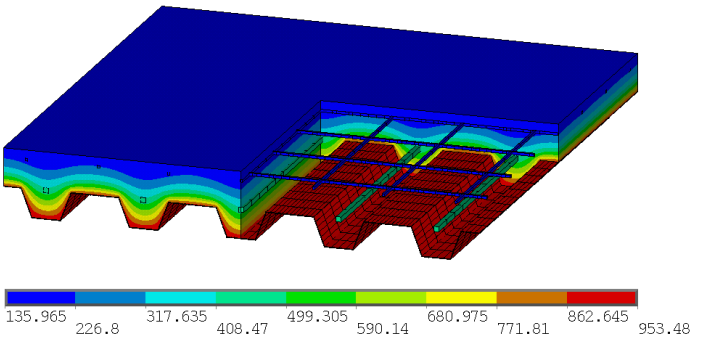

t= 70.1 min

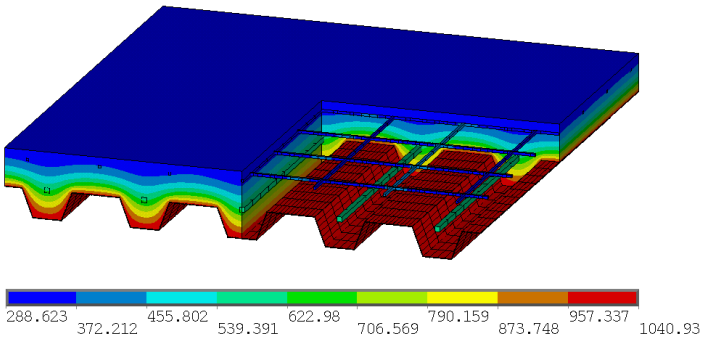

t= 120.0 min

SIM. 49	**St. deck:** Trapezoidal – ArcelorMittal Polydeck 59S	**Rebar (mm):** ϕ8	**Fire resistance (min)**	
	Mesh (mm//mm): ϕ5//100 (Q 196)	**h_1 (mm):** 51	Ave: 38.2	Max: *36.0*

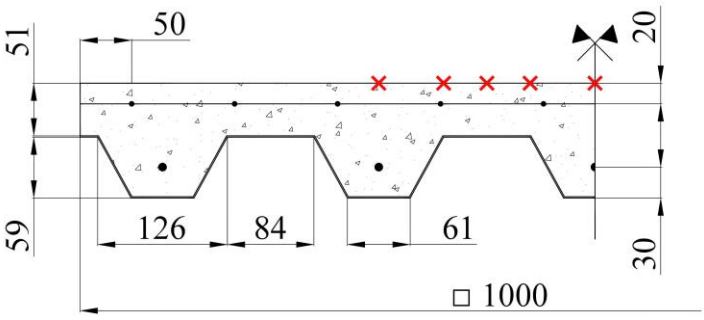

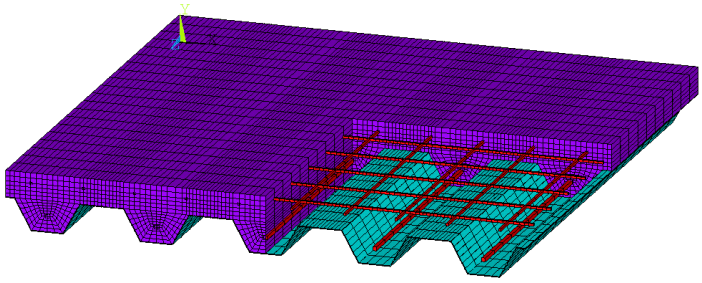

Finite element mesh

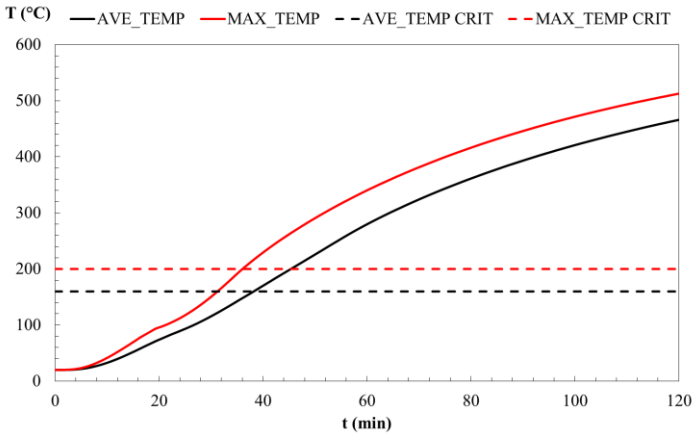

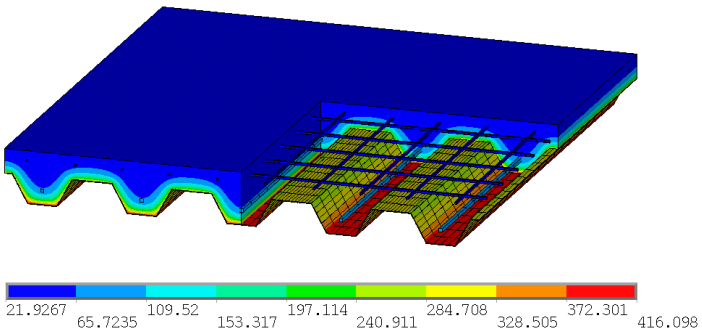

t= 9.0 min

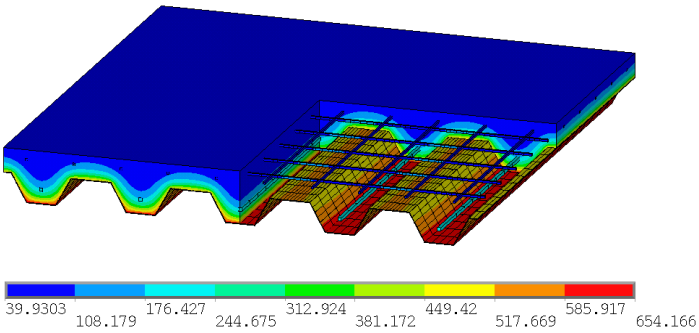

t= 18.0 min

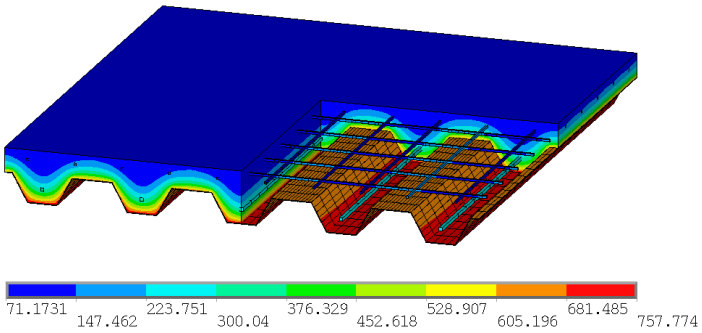

t= 27.0 min

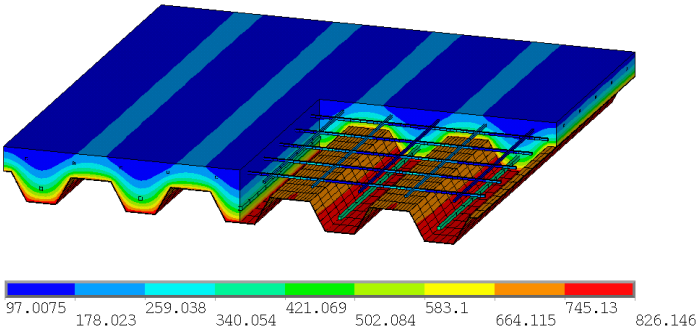

t= 36.0 min

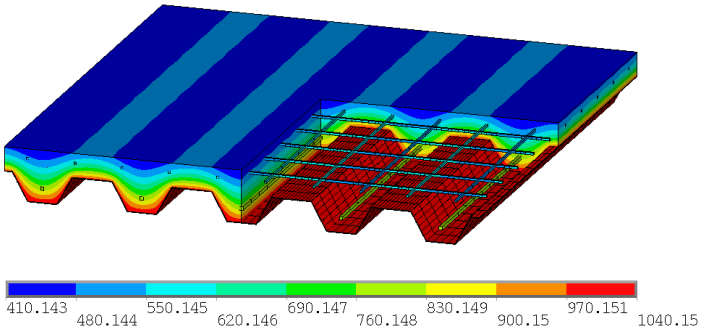

t= 120.0 min

SIM. 50	**St. deck:** Trapezoidal – ArcelorMittal Polydeck 59S	**Rebar (mm):** ϕ8	**Fire resistance (min)**	
	Mesh (mm//mm): ϕ5//100 (Q 196)	**h_1 (mm):** 61	Ave: 49.0	Max: *48.1*

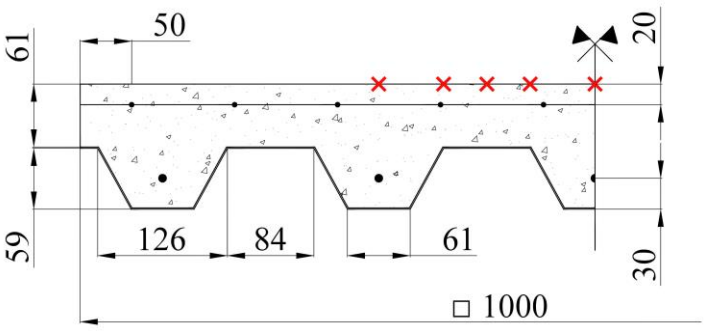

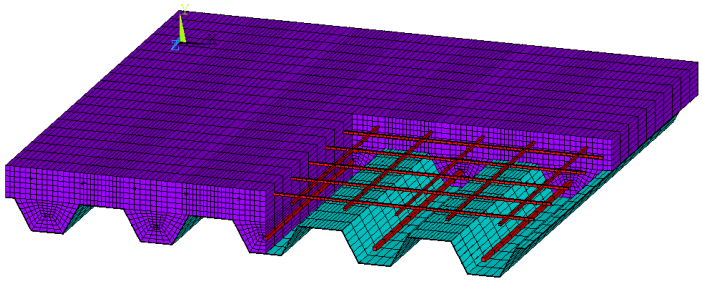

Finite element mesh

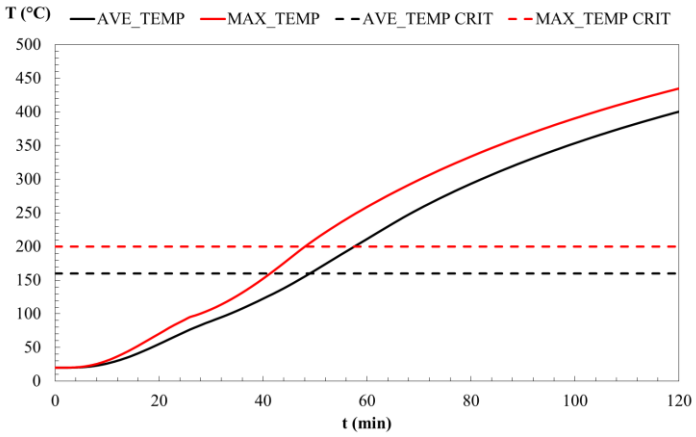

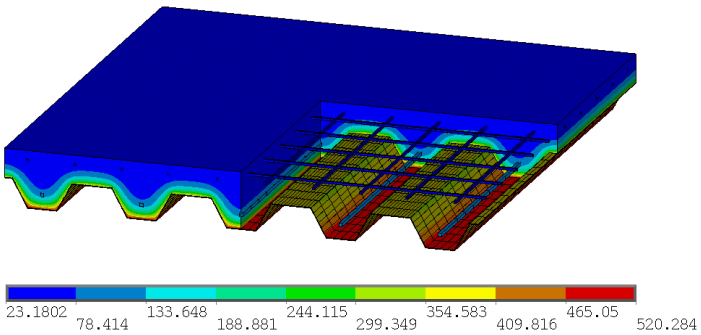

t= 12.0 min

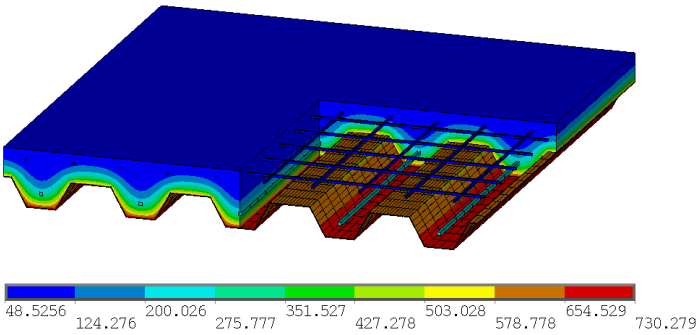

t= 24.1 min

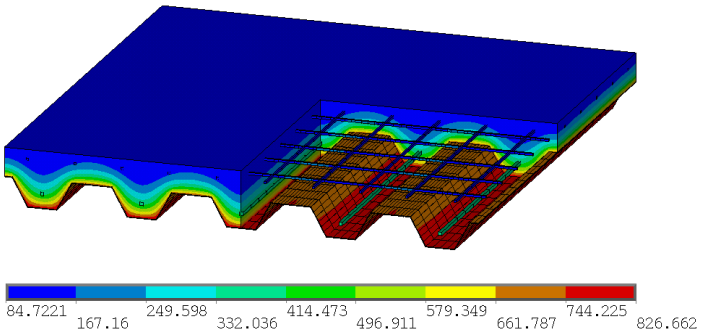

t= 36.1 min

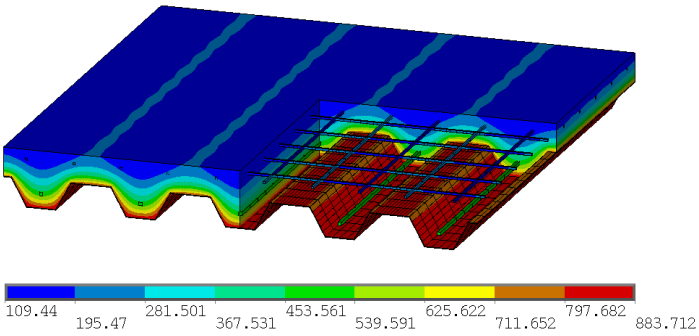

t= 48.1 min

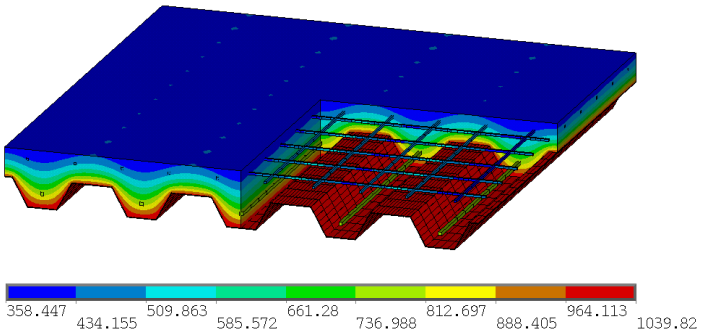

t= 120.0 min

SIM. 51	**St. deck:** Trapezoidal – ArcelorMittal Polydeck 59S	**Rebar (mm):** ϕ8	**Fire resistance (min)**	
	Mesh (mm//mm): ϕ5//100 (Q 196)	**h_1 (mm):** 71	Ave: *60.9*	Max: 62.1

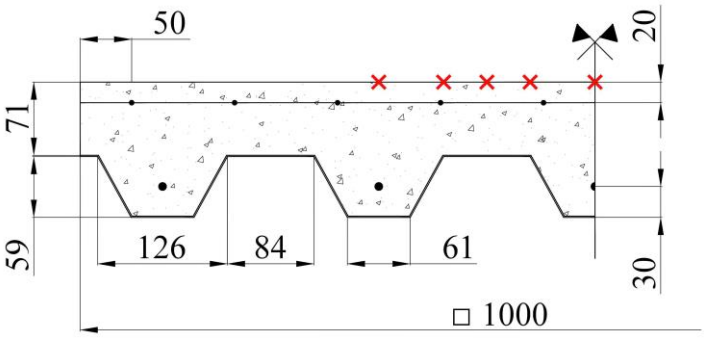

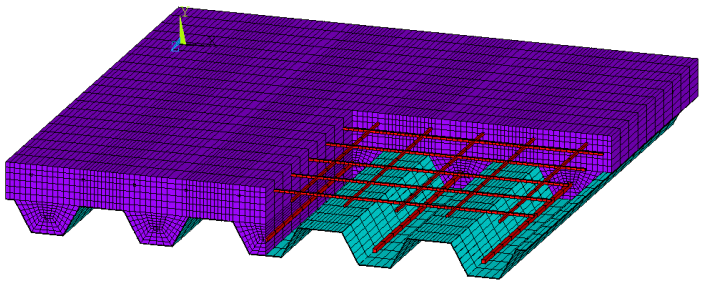

Finite element mesh

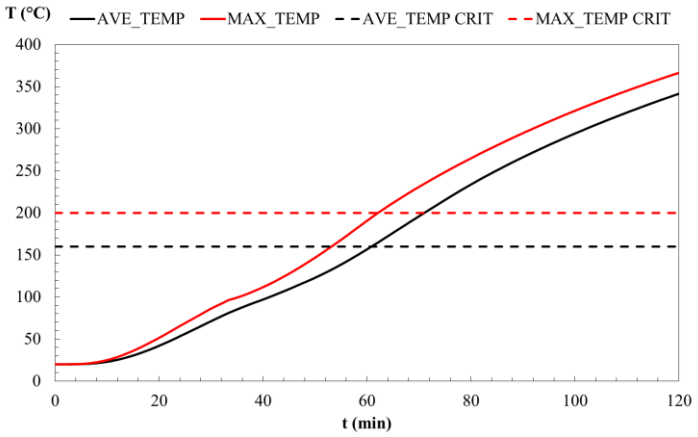

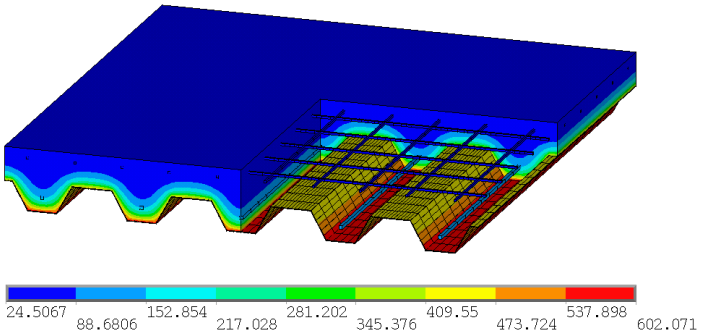

t= 15.2 min

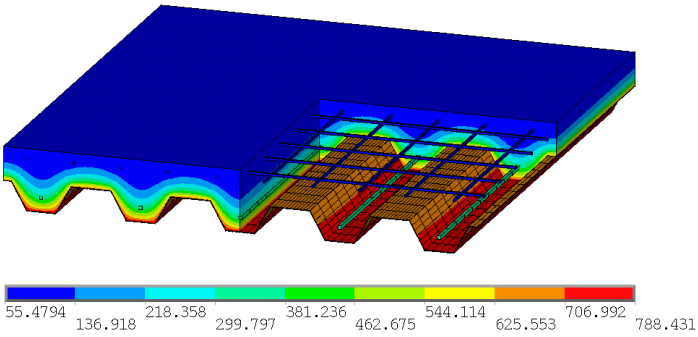

t= 30.5 min

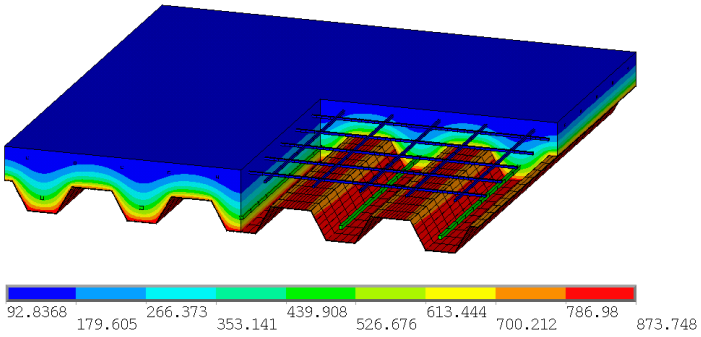

t= 45.7 min

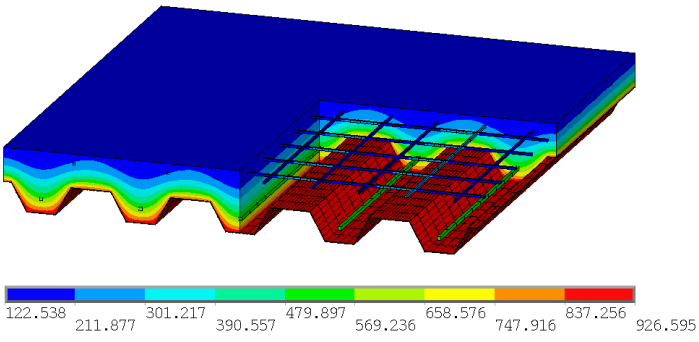

t= 60.9 min

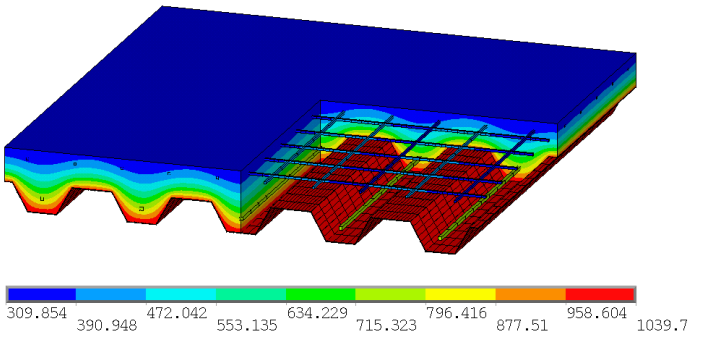

t= 120.0 min

SIM. 52	**St. deck:** Trapezoidal – ArcelorMittal Polydeck 59S	**Rebar (mm):** ϕ8	**Fire resistance (min)**	
	Mesh (mm//mm): ϕ5//100 (Q 196)	**h_1 (mm):** 81	Ave: *73.9*	Max: 78.1

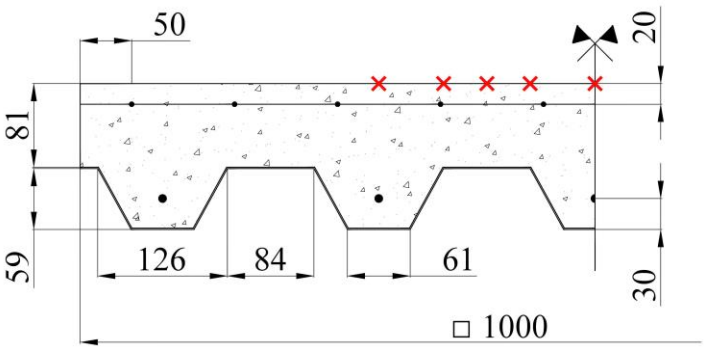

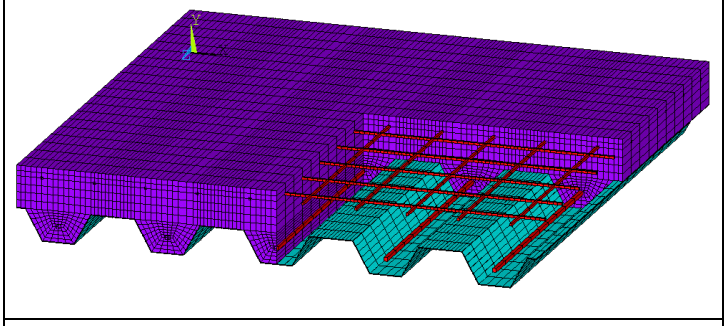

Finite element mesh

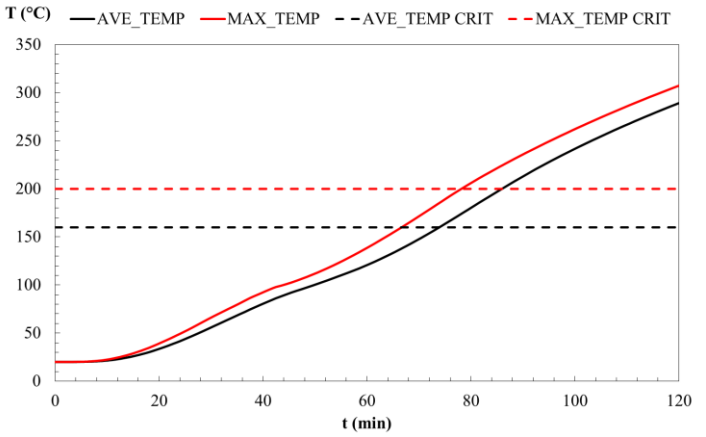

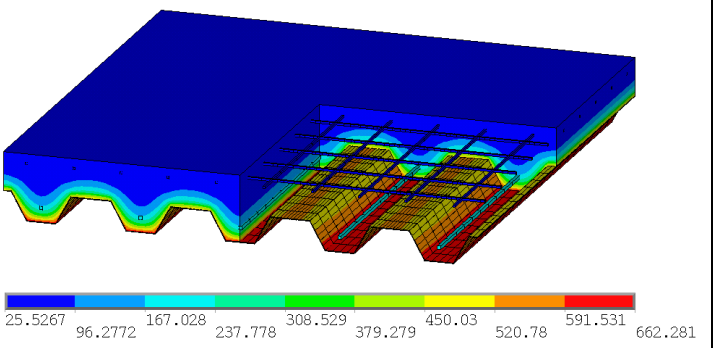

t= 18.5 min

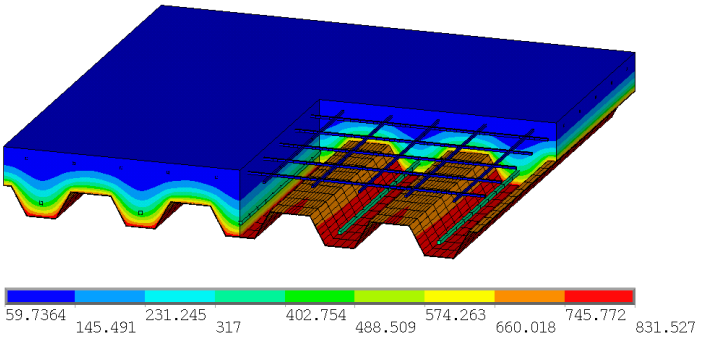

t= 37.0 min

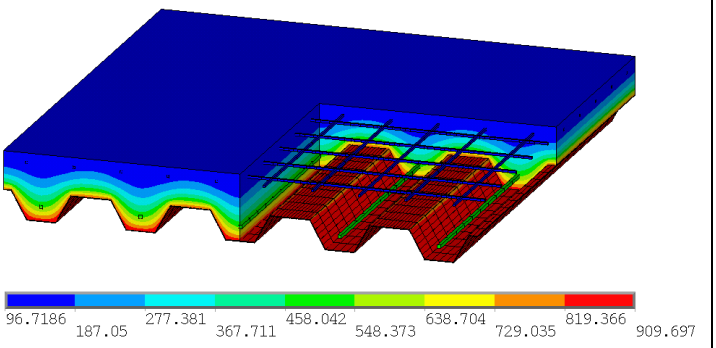

t= 55.4 min

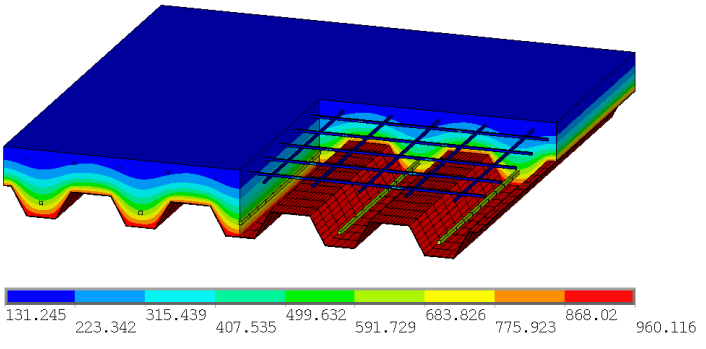

t= 73.9 min

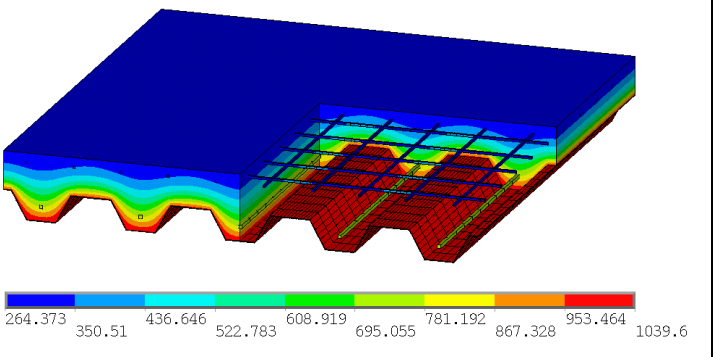

t= 120.0 min

SIM. 53	**St. deck:** Trapezoidal – ArcelorMittal Polydeck 59S	**Rebar (mm):** ϕ8	**Fire resistance (min)**	
	Mesh (mm//mm): ϕ5//100 (Q 196)	**h_1 (mm):** 51	Ave: 38.2	Max: *36.0*

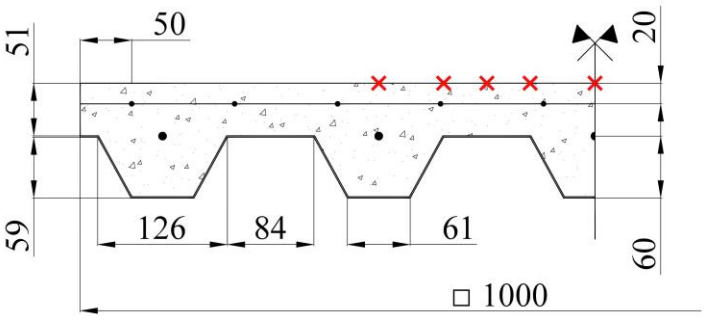

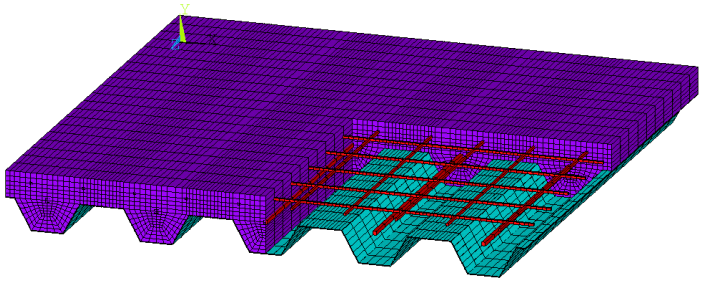

Finite element mesh

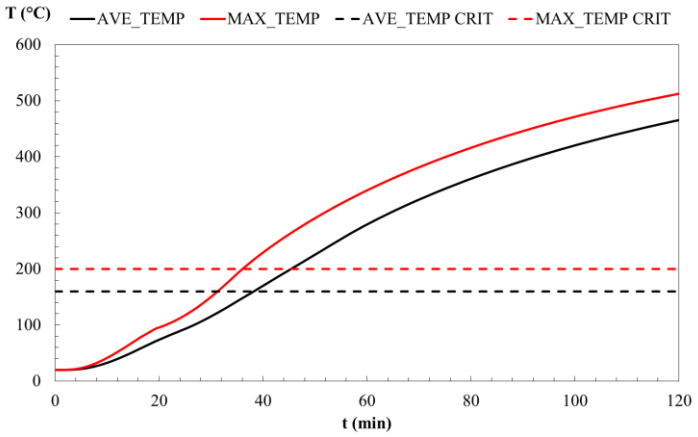

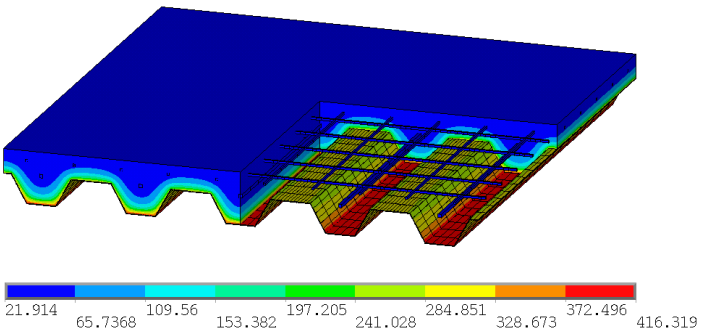

t= 9.0 min

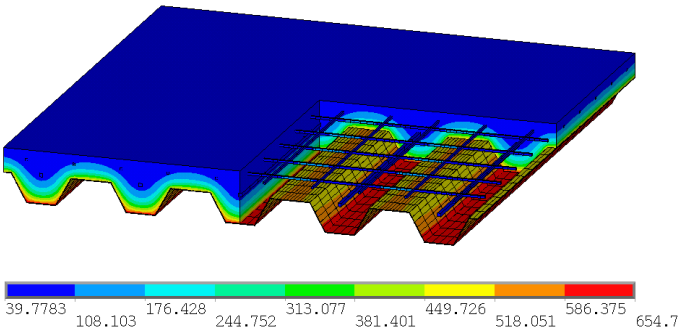

t= 18.0 min

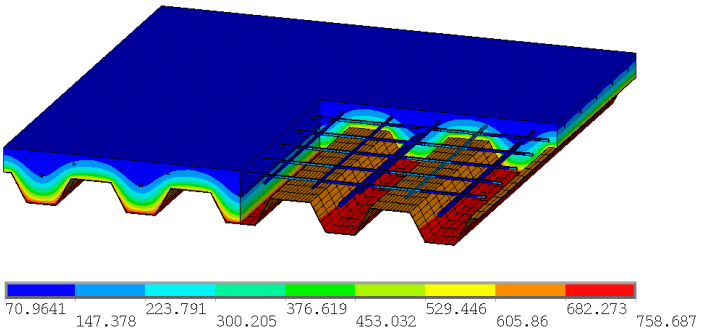

t= 27.0 min

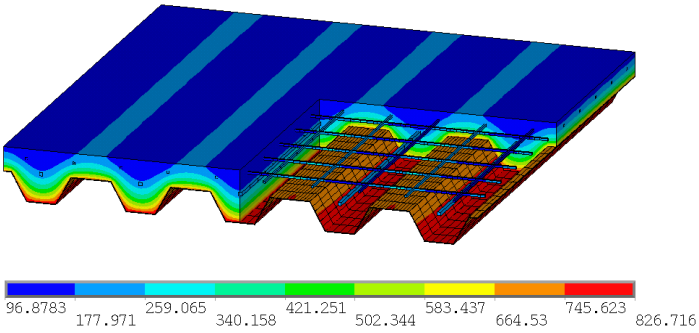

t= 36.0 min

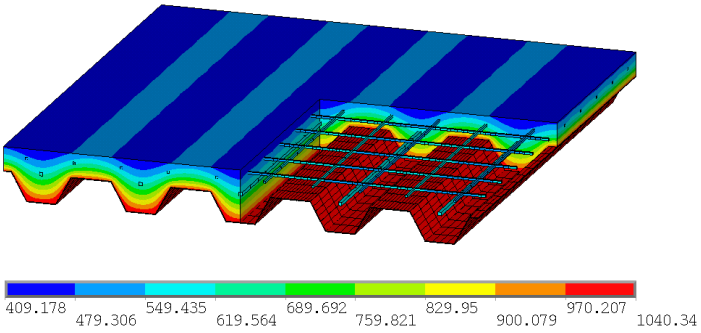

t= 120.0 min

SIM. 54	**St. deck:** Trapezoidal – ArcelorMittal Polydeck 59S	**Rebar (mm):** ϕ8	**Fire resistance (min)**	
	Mesh (mm//mm): ϕ5//100 (Q 196)	**h_1 (mm):** 61	Ave: 49.0	Max: *48.1*

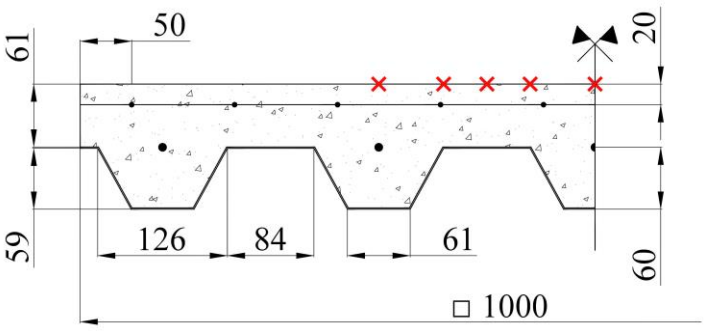

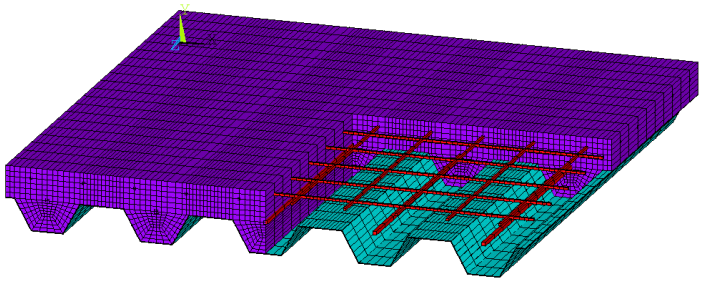

Finite element mesh

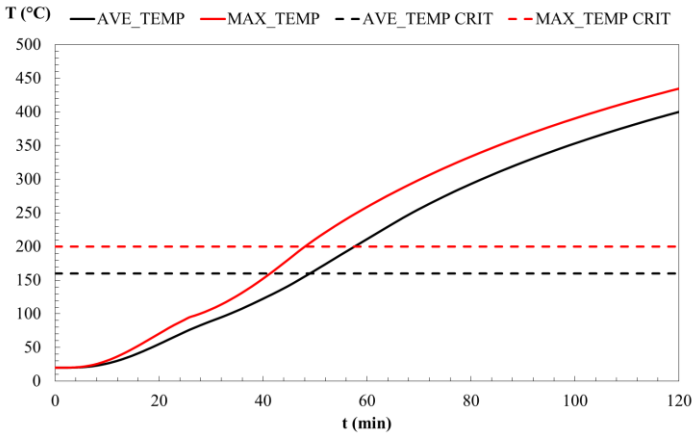

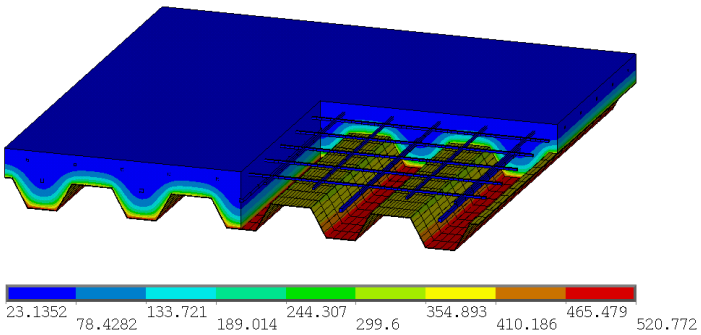

t= 12.0 min

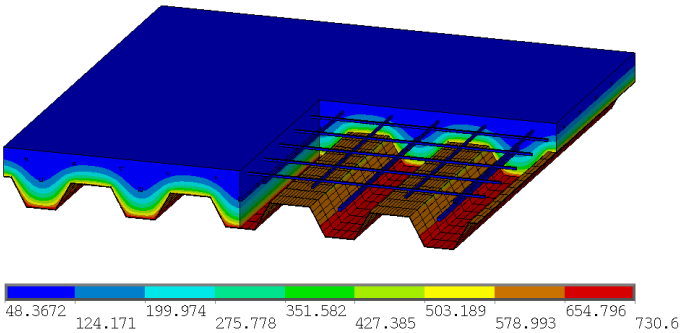

t= 24.1 min

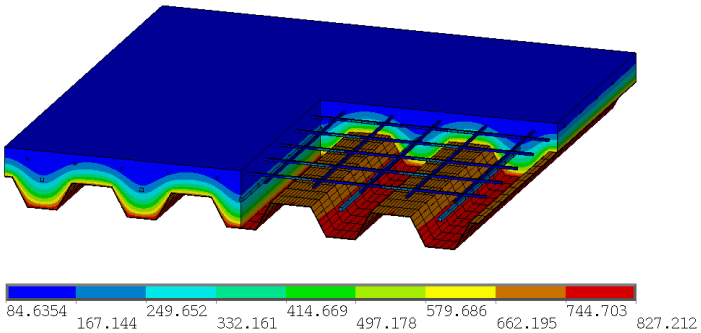

t= 36.1 min

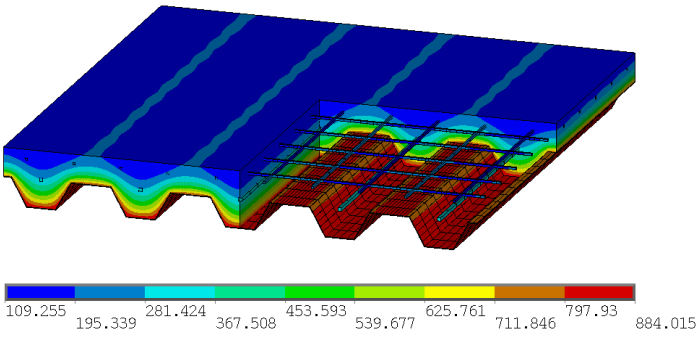

t= 48.1 min

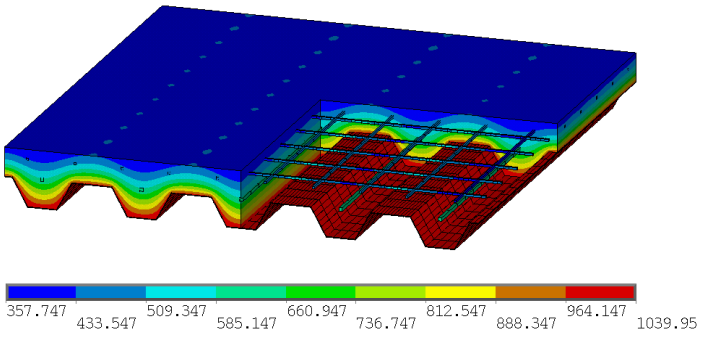

t= 120.0 min

SIM. 55	**St. deck:** Trapezoidal – ArcelorMittal Polydeck 59S	**Rebar (mm):** ϕ8	**Fire resistance (min)**	
	Mesh (mm//mm): ϕ5//100 (Q 196)	**h_1 (mm):** 71	Ave: *60.9*	Max: 62.1

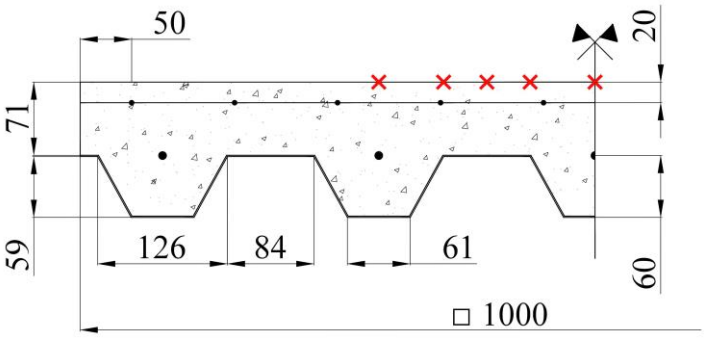

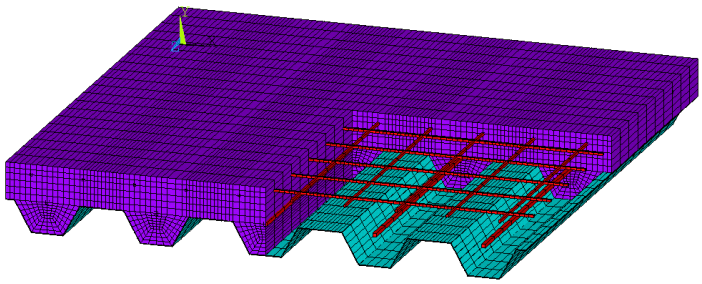

Finite element mesh

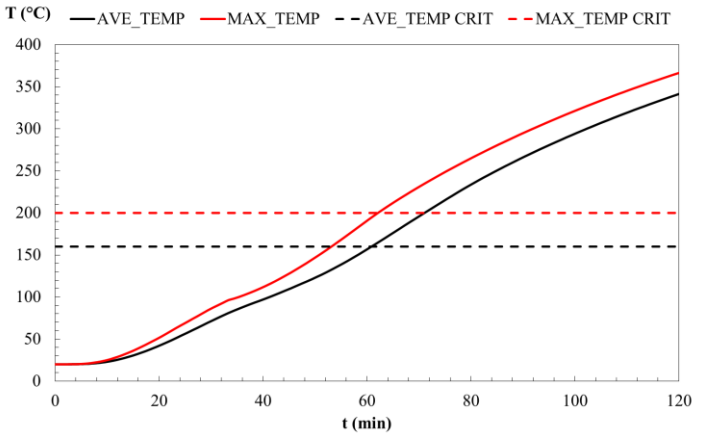

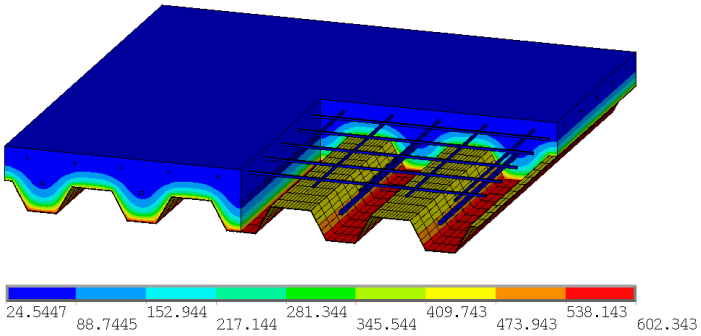

t= 15.2 min

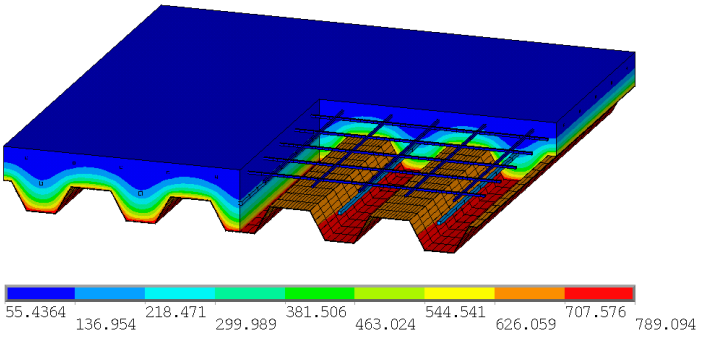

t= 30.5 min

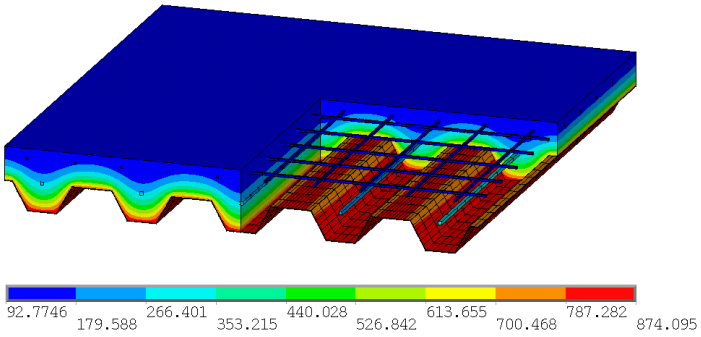

t= 45.7 min

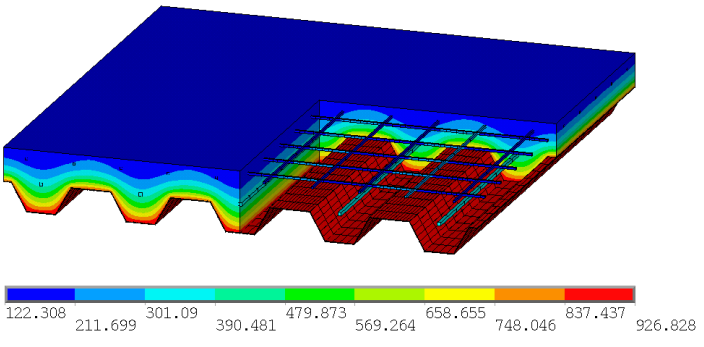

t= 60.9 min

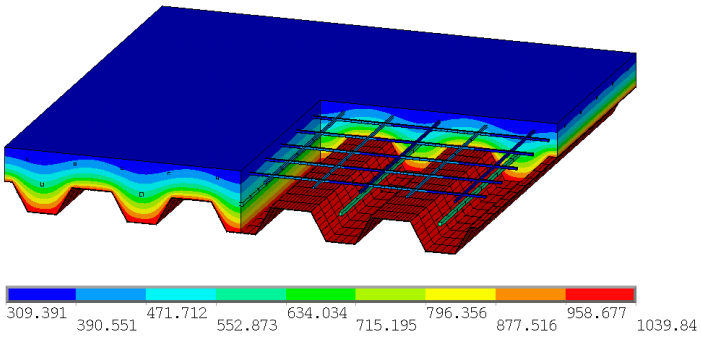

t= 120.0 min

SIM. 56	**St. deck:** Trapezoidal – ArcelorMittal Polydeck 59S	**Rebar (mm):** ϕ8	**Fire resistance (min)**	
	Mesh (mm//mm): ϕ5//100 (Q 196)	**h_1 (mm):** 81	Ave: *73.9*	Max: 78.2

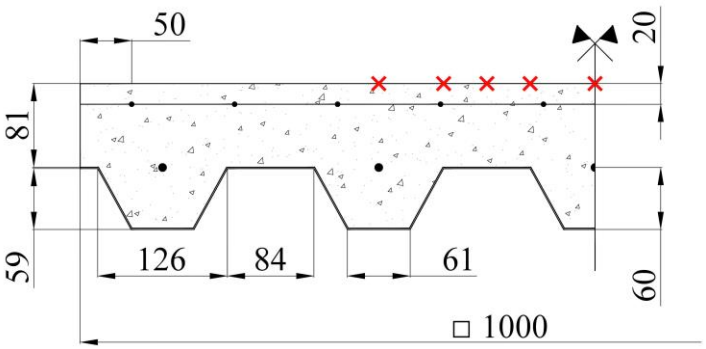

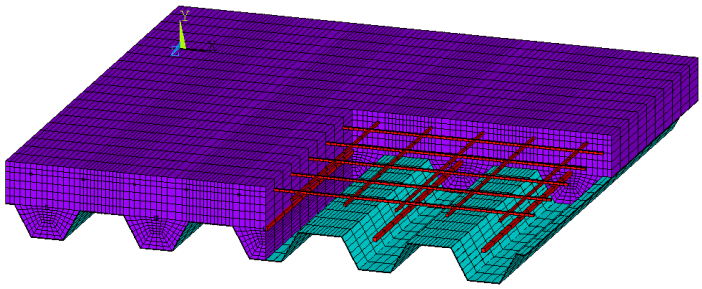

Finite element mesh

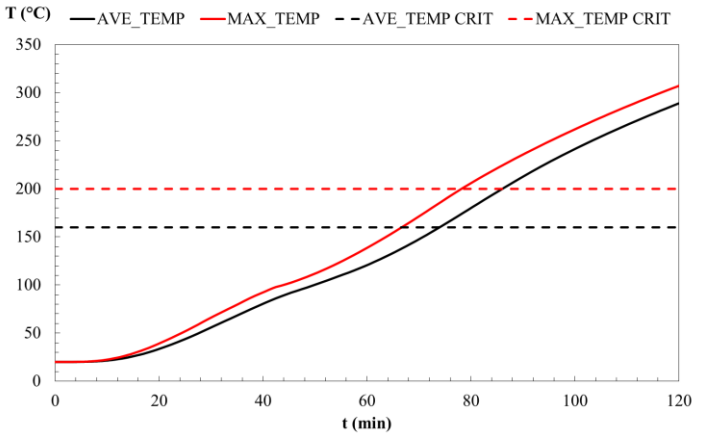

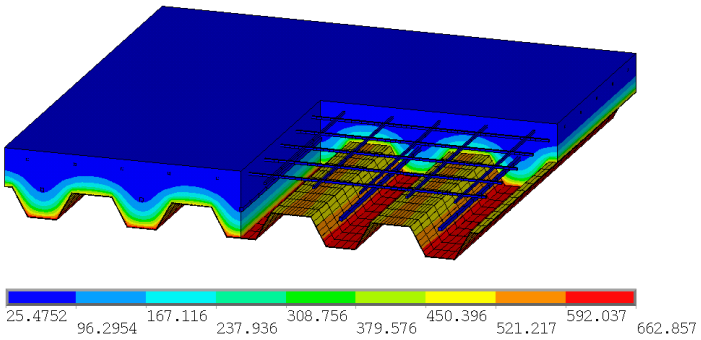

t= 18.5 min

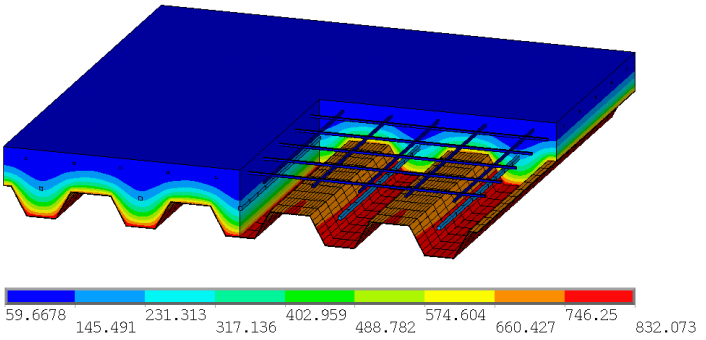

t= 37.0 min

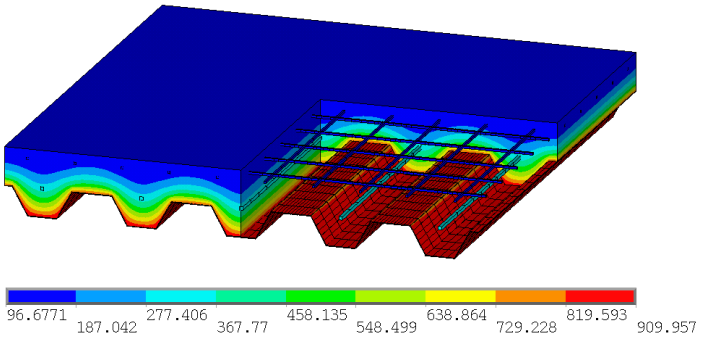

t= 55.4 min

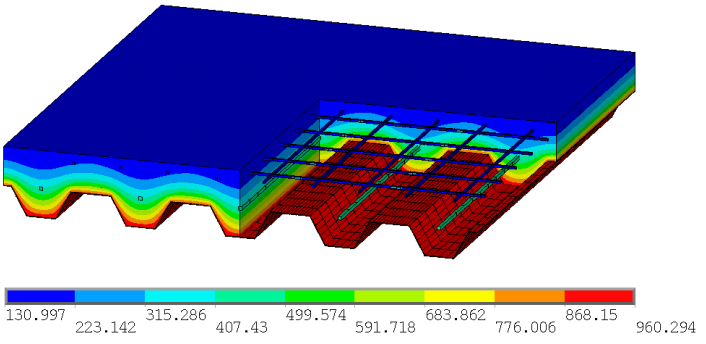

t= 73.9 min

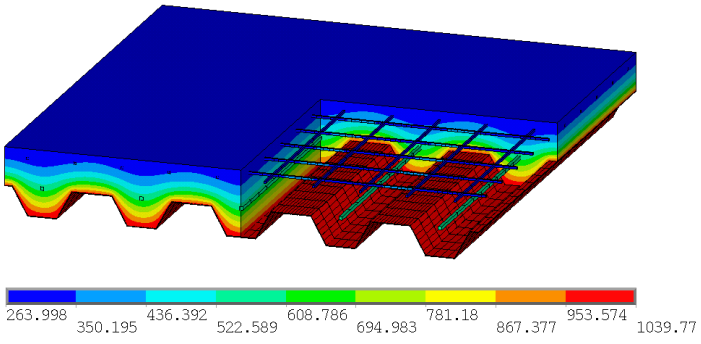

t= 120.0 min

SIM. 57	**St. deck:** Trapezoidal – ArcelorMittal Polydeck 59S	**Rebar (mm):** ϕ8	**Fire resistance (min)**	
	Mesh (mm//mm): ϕ6//100 (Q 283)	**h_1 (mm):** 51	Ave: 38.3	Max: *36.2*

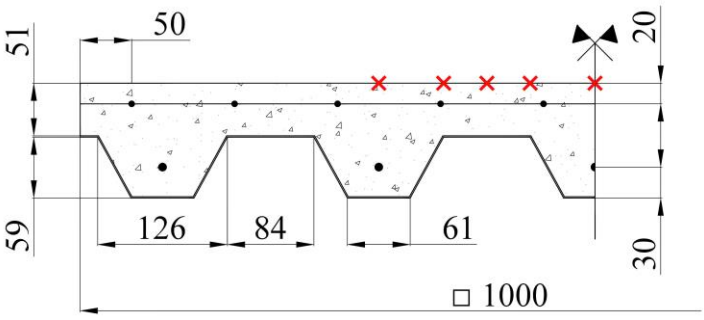

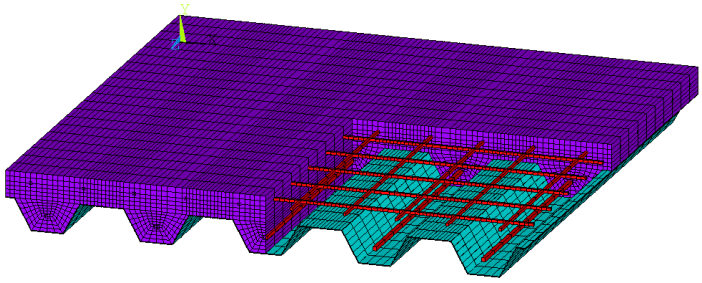

Finite element mesh

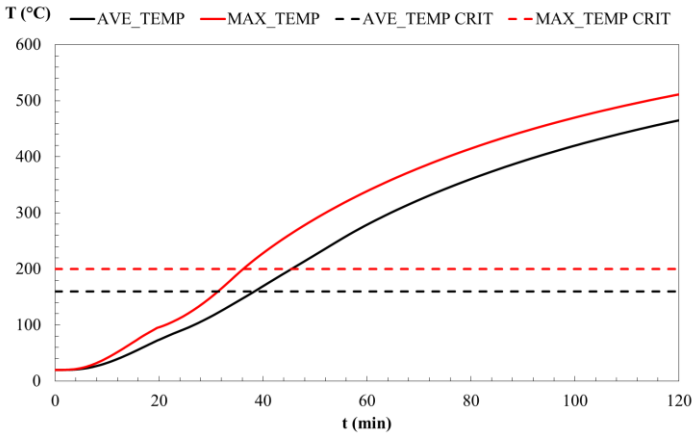

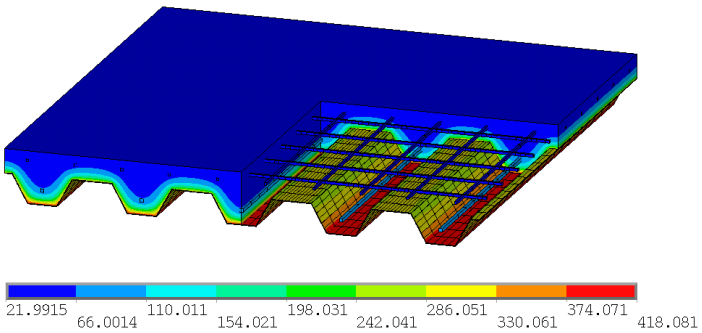

t= 9.1 min

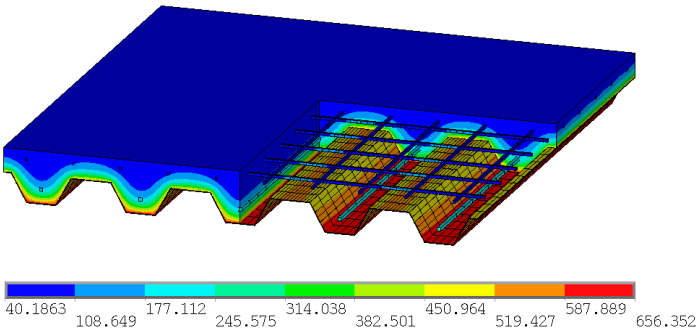

t= 18.1 min

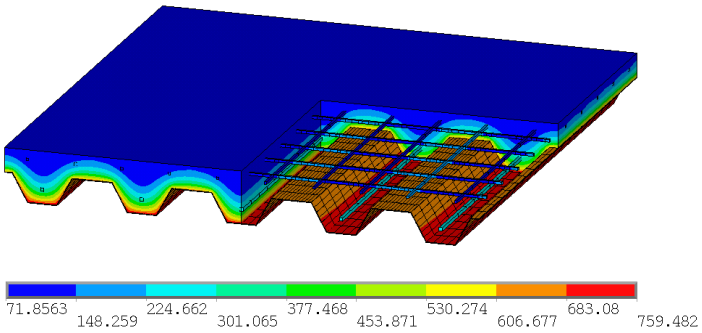

t= 27.2 min

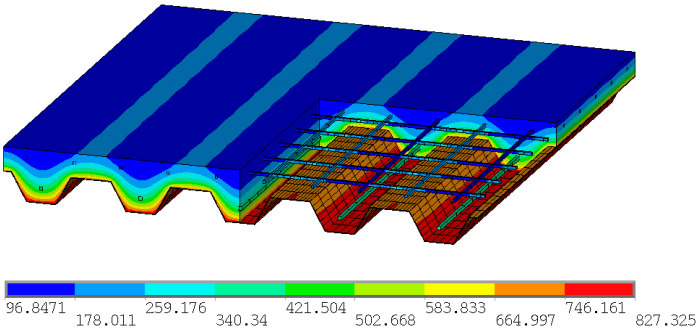

t= 36.2 min

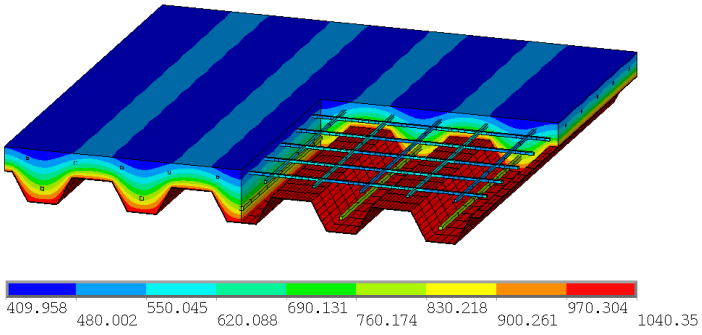

t= 120.0 min

SIM. 58	**St. deck:** Trapezoidal – ArcelorMittal Polydeck 59S	**Rebar (mm):** ϕ8	**Fire resistance (min)**	
	Mesh (mm//mm): ϕ6//100 (Q 283)	**h_1 (mm):** 61	Ave: 49.2	Max: *48.3*

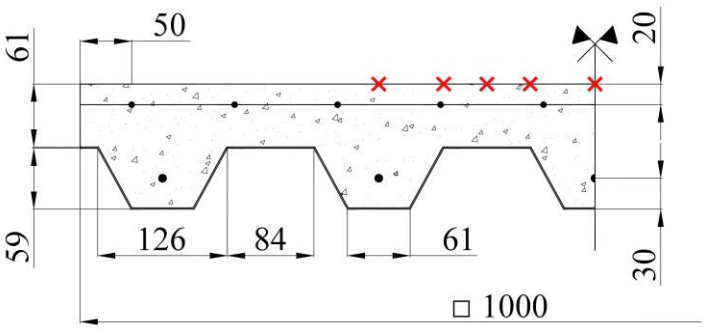

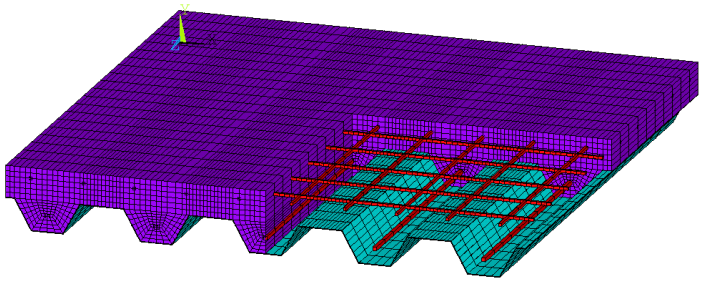

Finite element mesh

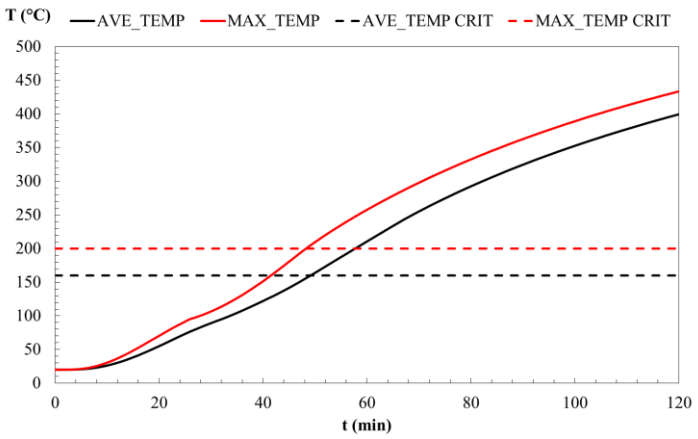

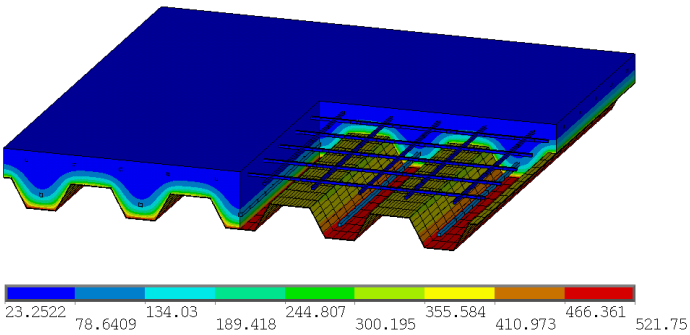

t= 12.1 min

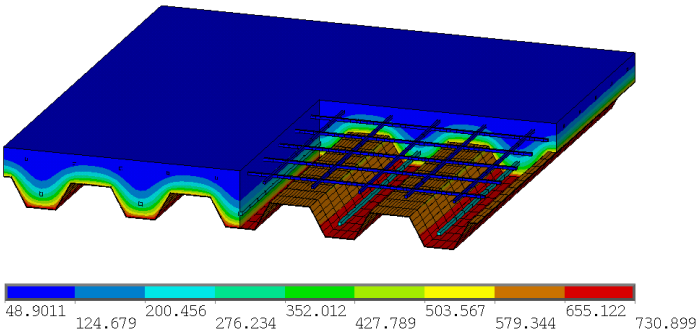

t= 24.2 min

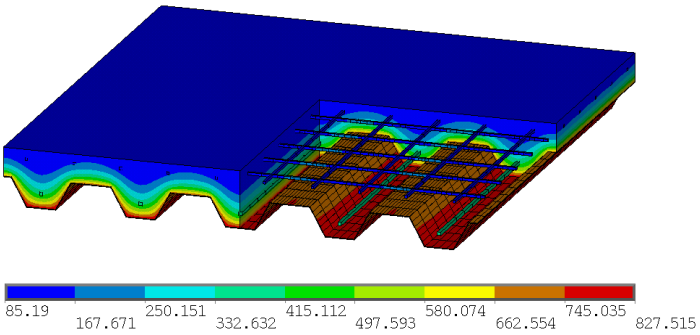

t= 36.2 min

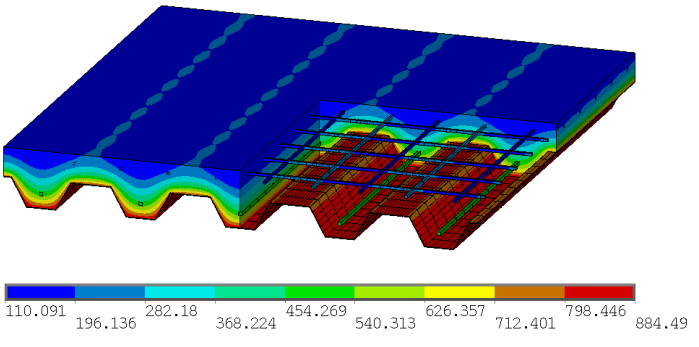

t= 48.3 min

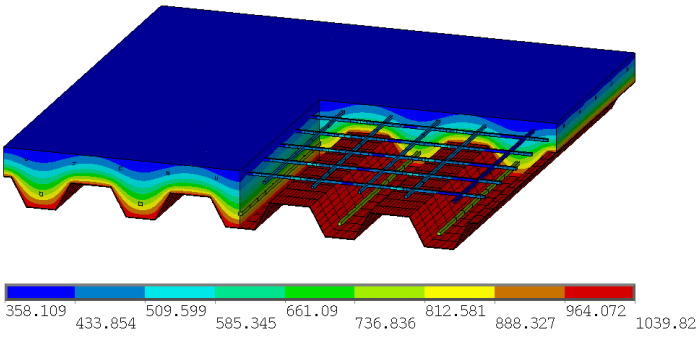

t= 120.0 min

SIM. 59	**St. deck:** Trapezoidal – ArcelorMittal Polydeck 59S	**Rebar (mm):** ϕ8	**Fire resistance (min)**	
	Mesh (mm//mm): ϕ6//100 (Q 283)	**h_1 (mm):** 71	Ave: *61.0*	Max: 62.4

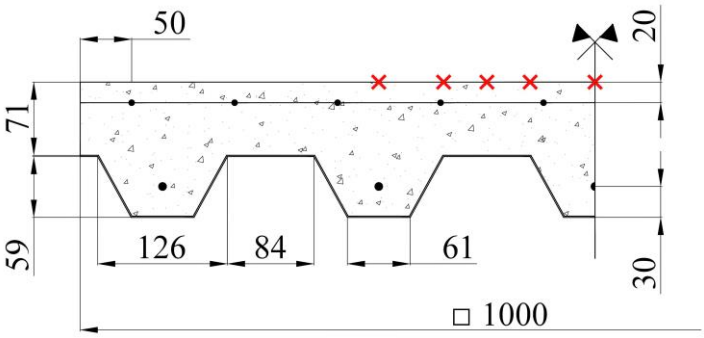

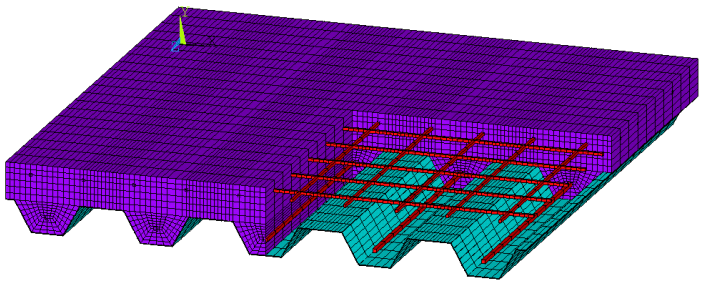

Finite element mesh

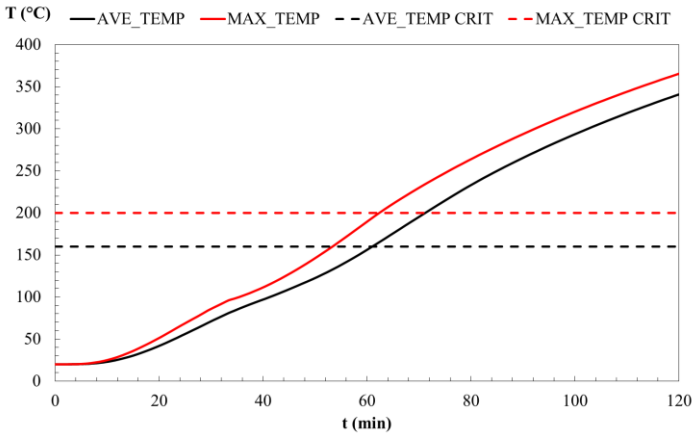

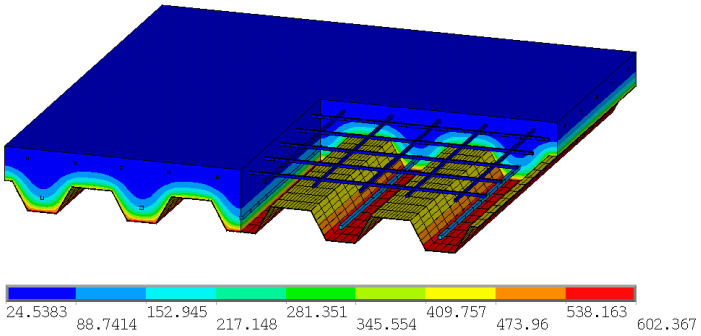

t= 15.3 min

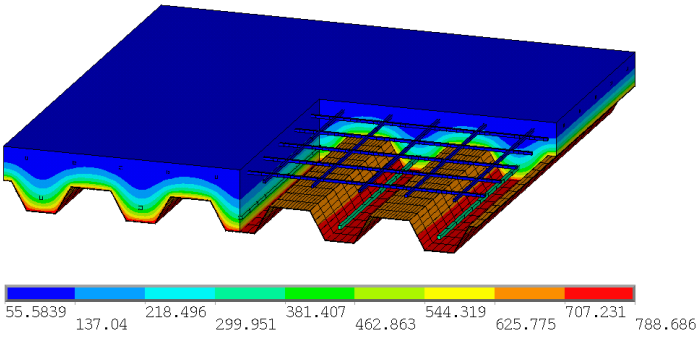

t= 30.5 min

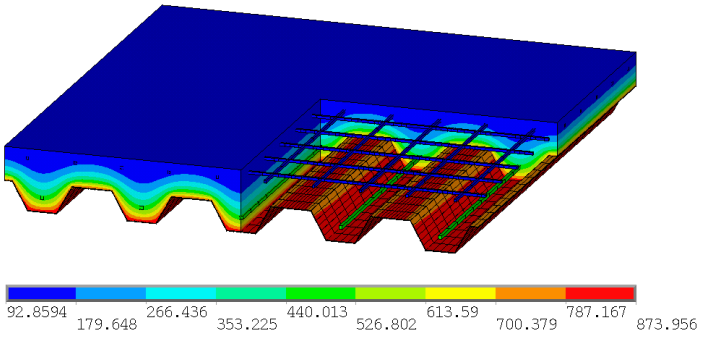

t= 45.8 min

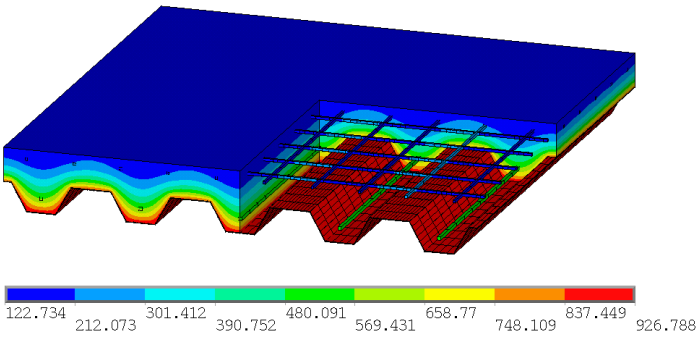

t= 61.0 min

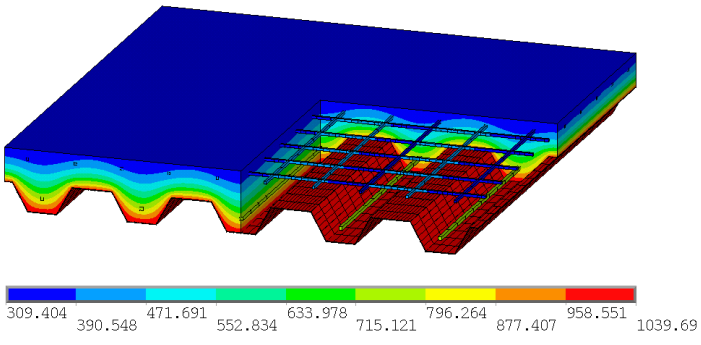

t= 120.0 min

SIM. 60	**St. deck:** Trapezoidal – ArcelorMittal Polydeck 59S	**Rebar (mm):** ϕ8	**Fire resistance (min)**	
	Mesh (mm//mm): ϕ6//100 (Q 283)	**h_1 (mm):** 81	Ave: *74.1*	Max: 78.4

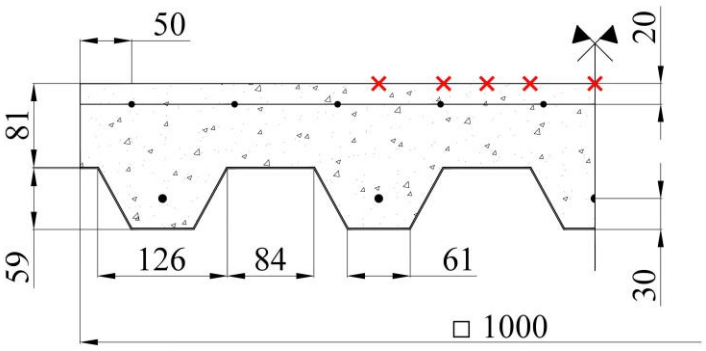

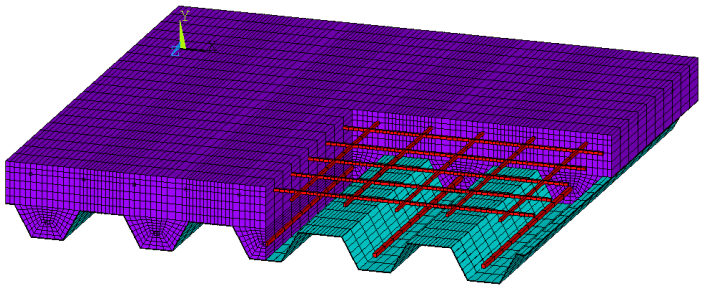

Finite element mesh

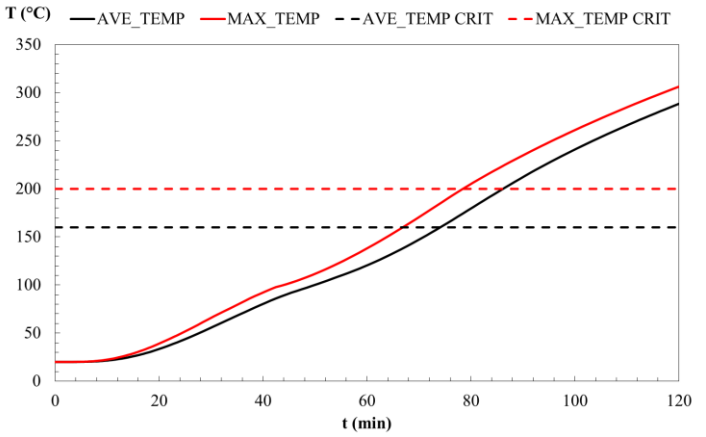

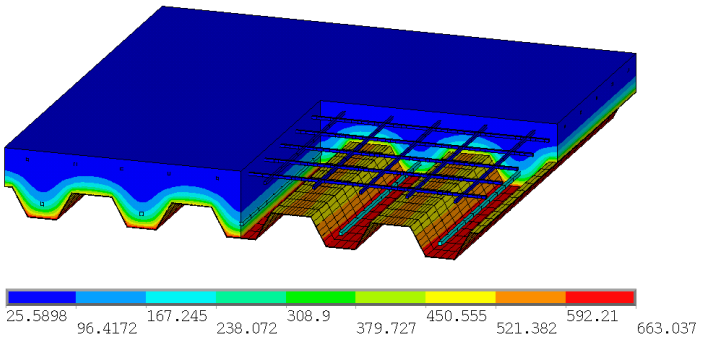

t= 18.5 min

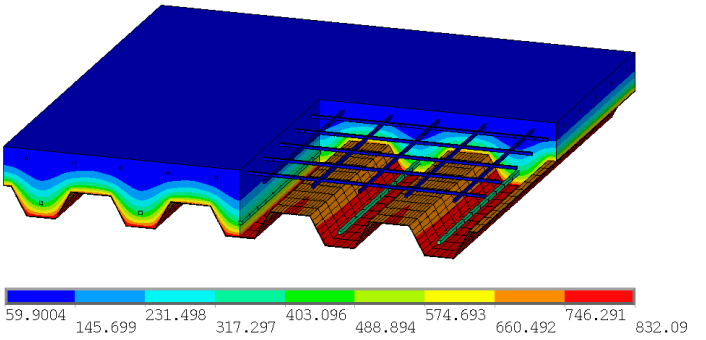

t= 37.1 min

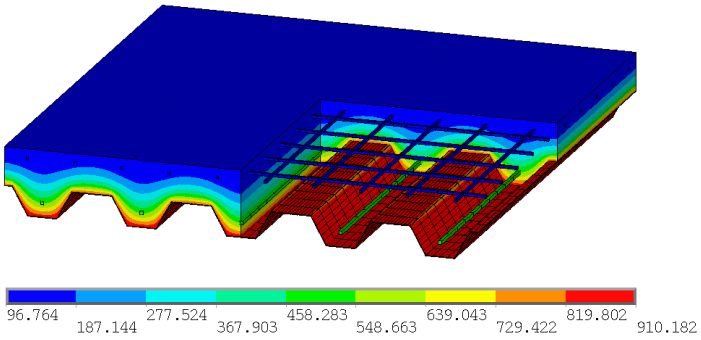

t= 55.6 min

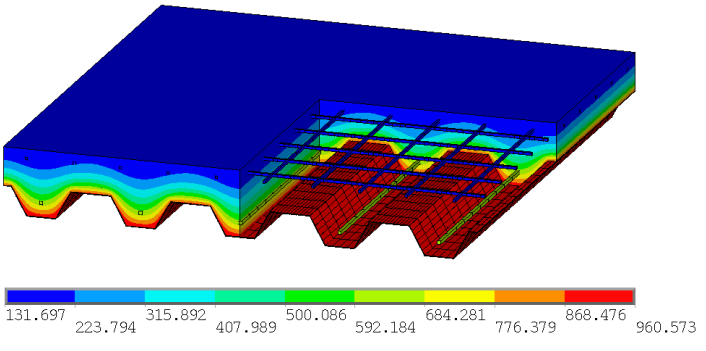

t= 74.1 min

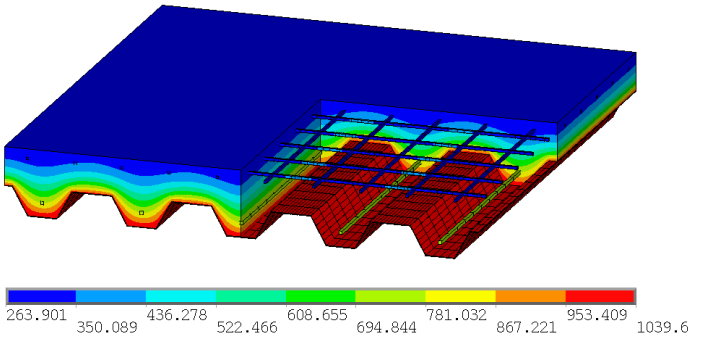

t= 120.0 min

SIM. 61	**St. deck:** Trapezoidal – ArcelorMittal Polydeck 59S	**Rebar (mm):** ϕ8	**Fire resistance (min)**	
	Mesh (mm//mm): ϕ6//100 (Q 283)	**h_1 (mm):** 51	Ave: 38.3	Max: *36.2*

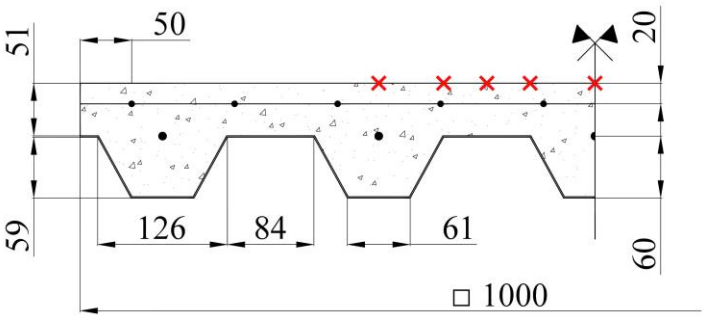

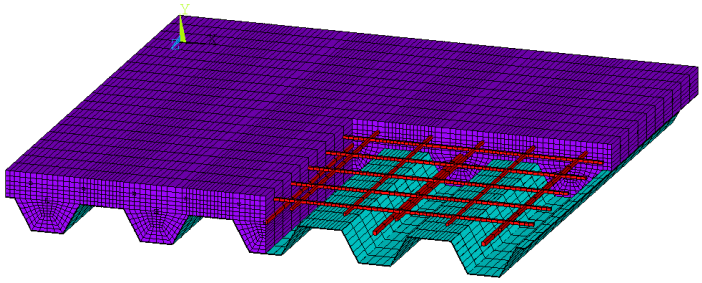

Finite element mesh

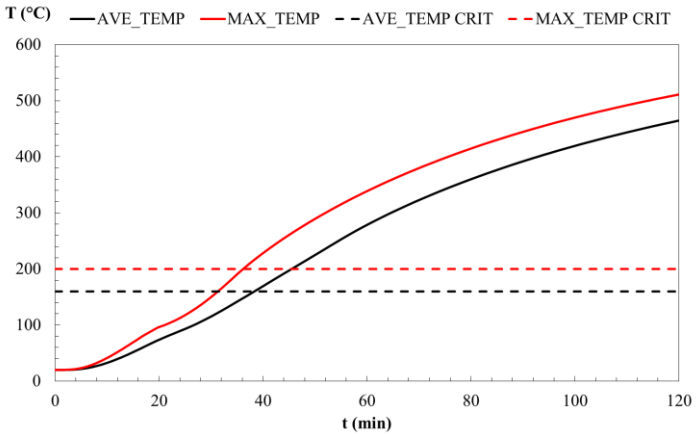

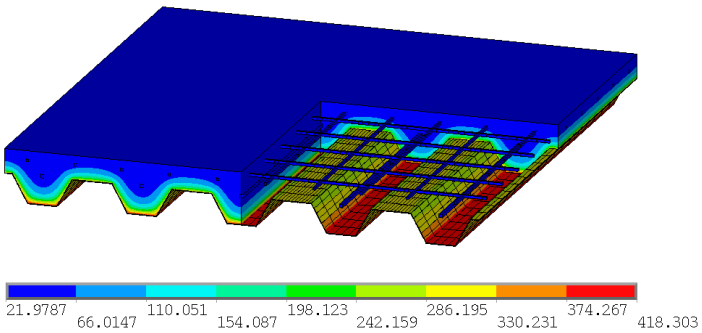

t= 9.1 min

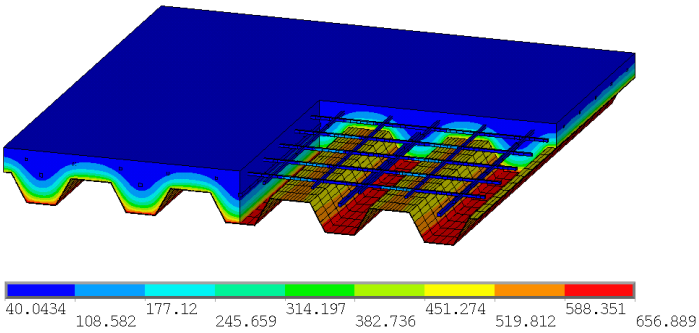

t= 18.1 min

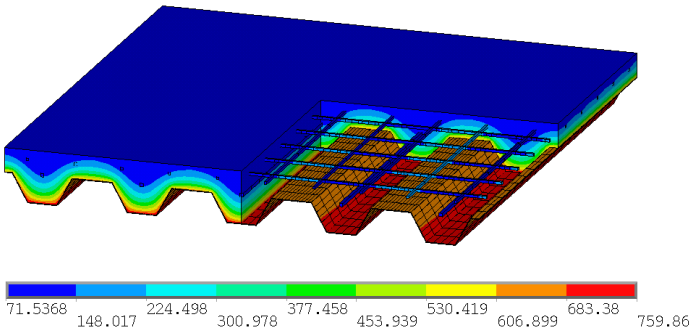

t= 27.2 min

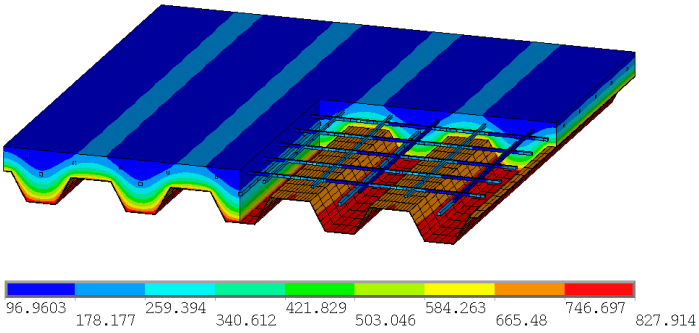

t= 36.2 min

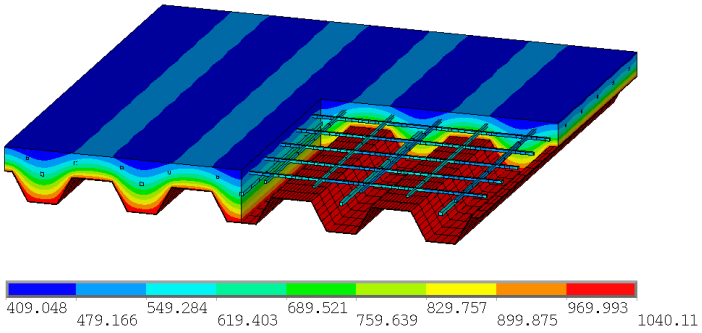

t= 120.0 min

SIM. 62	**St. deck:** Trapezoidal – ArcelorMittal Polydeck 59S	**Rebar (mm):** ϕ8	**Fire resistance (min)**	
	Mesh (mm//mm): ϕ6//100 (Q 283)	**h_1 (mm):** 61	Ave: 49.2	Max: *48.2*

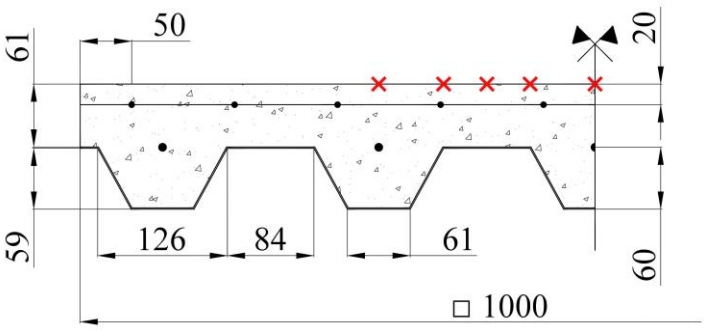

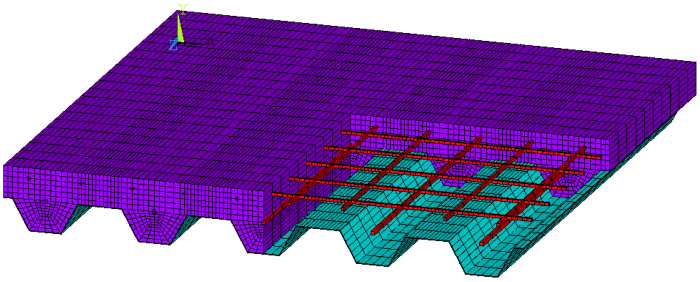

Finite element mesh

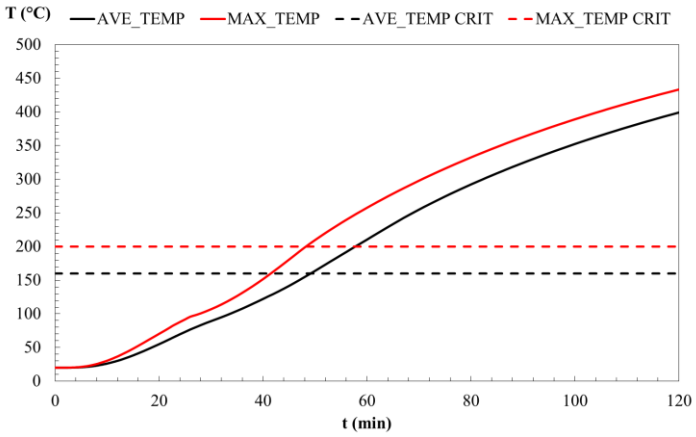

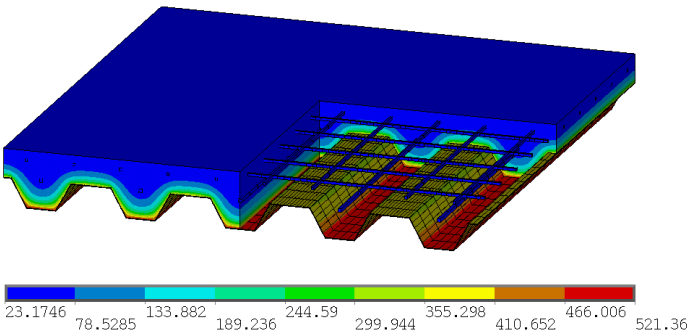

t= 12.1 min

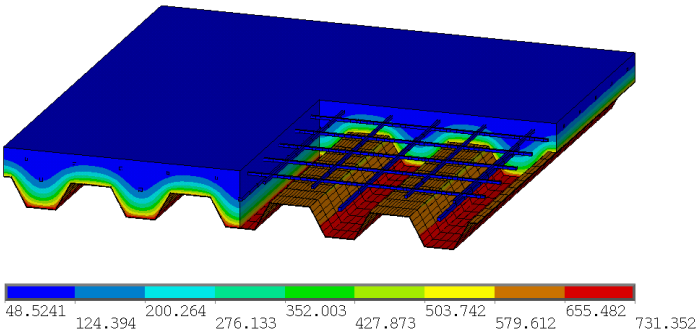

t= 24.1 min

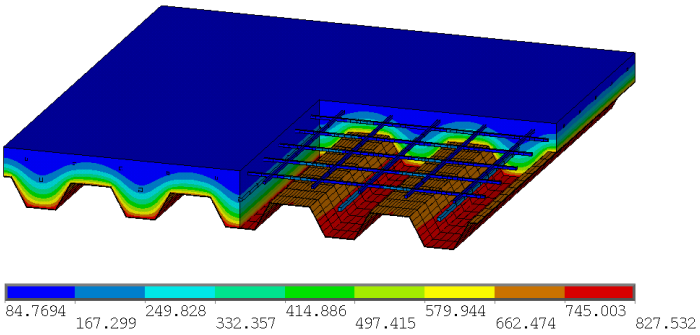

t= 36.2 min

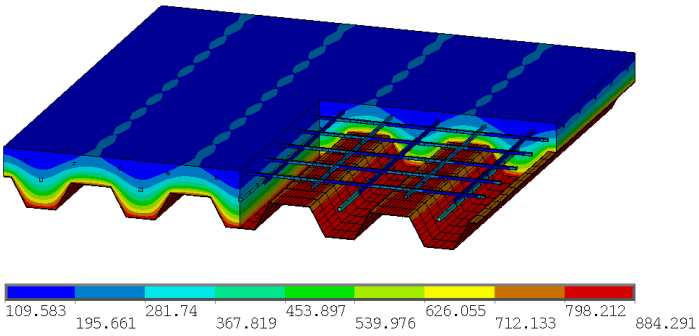

t= 48.2 min

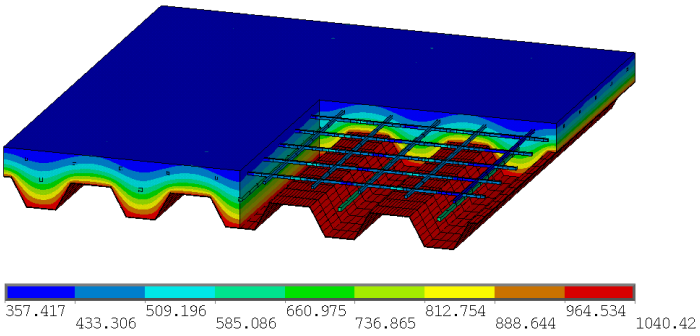

t= 120.0 min

SIM. 63	**St. deck:** Trapezoidal – ArcelorMittal Polydeck 59S	**Rebar (mm):** ϕ8	**Fire resistance (min)**	
	Mesh (mm//mm): ϕ6//100 (Q 283)	**h_1 (mm):** 71	Ave: *61.0*	Max: 62.3

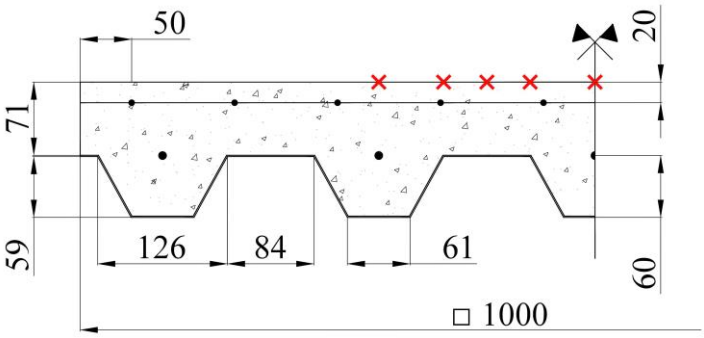

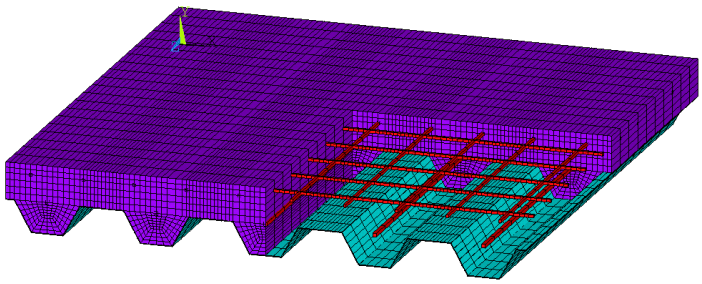

Finite element mesh

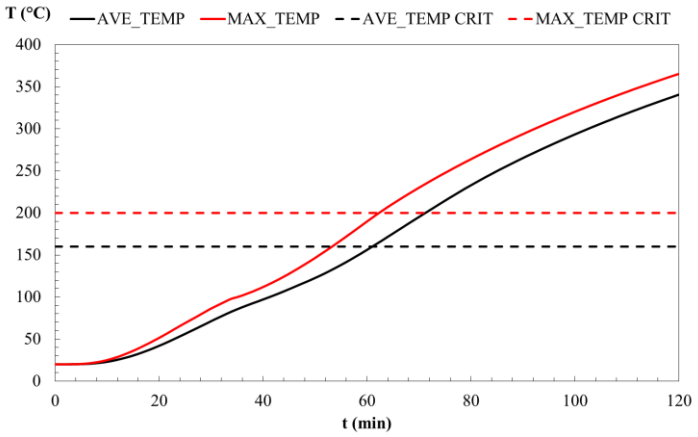

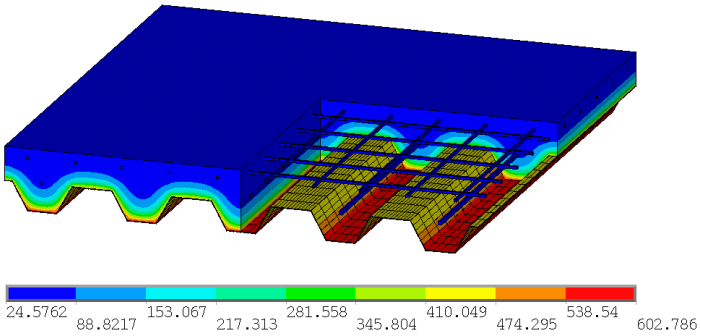

t= 15.3 min

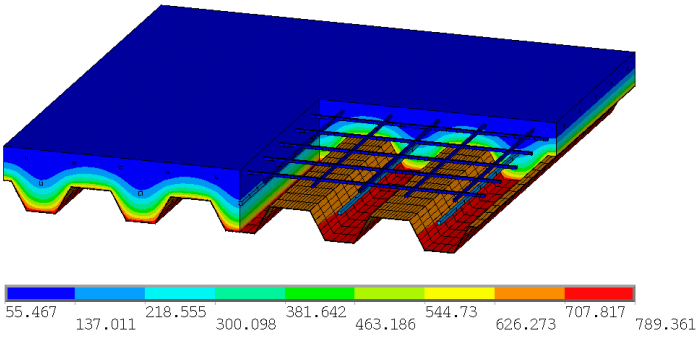

t= 30.5 min

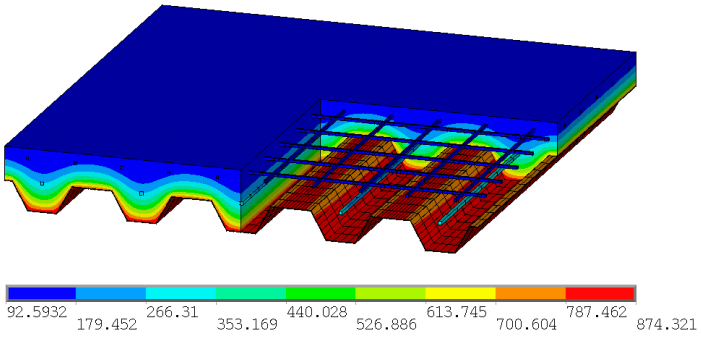

t= 45.8 min

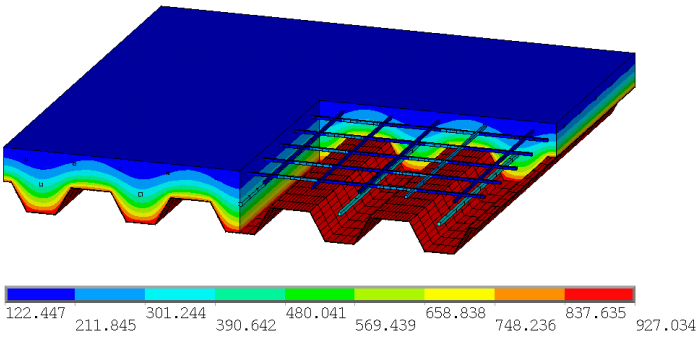

t= 61.0 min

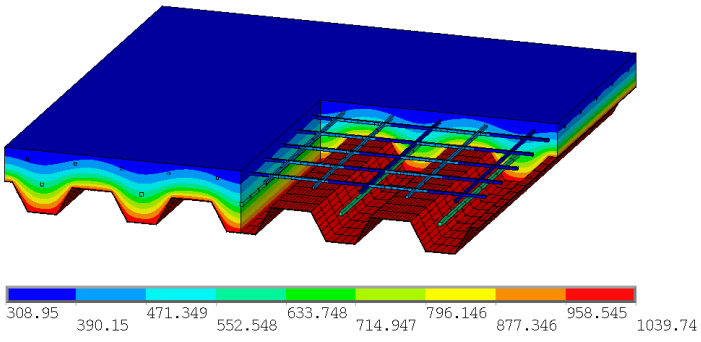

t= 120.0 min

SIM. 64	**St. deck:** Trapezoidal – ArcelorMittal Polydeck 59S	**Rebar (mm):** ϕ8	**Fire resistance (min)**	
	Mesh (mm//mm): ϕ6//100 (Q 283)	**h_1 (mm):** 81	Ave: *74.1*	Max: 78.4

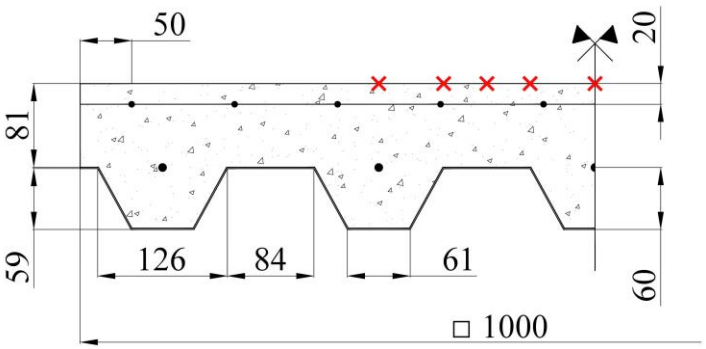

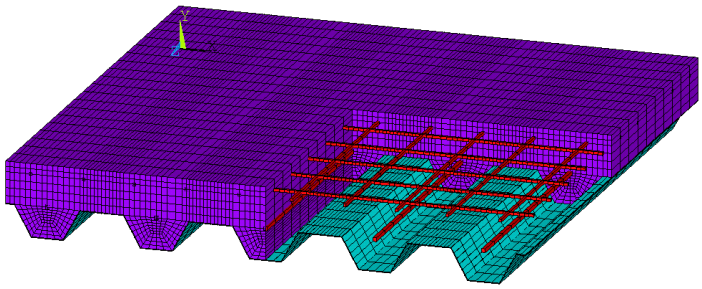

Finite element mesh

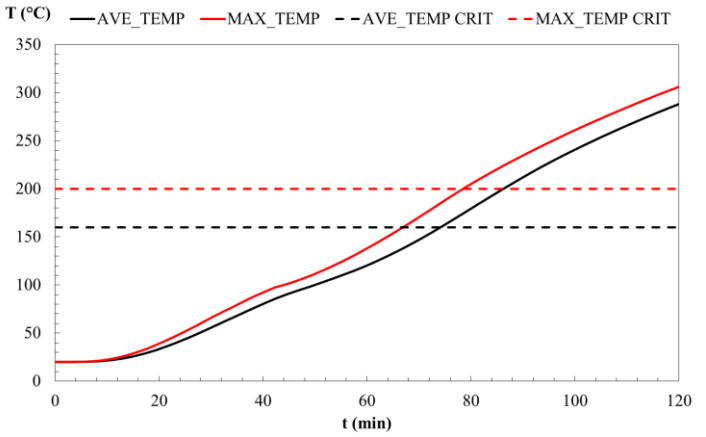

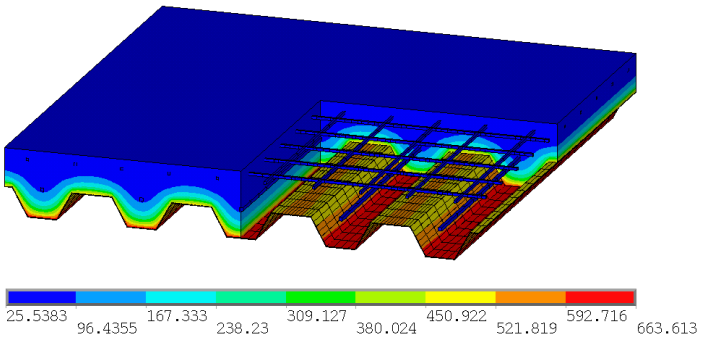

t= 18.5 min

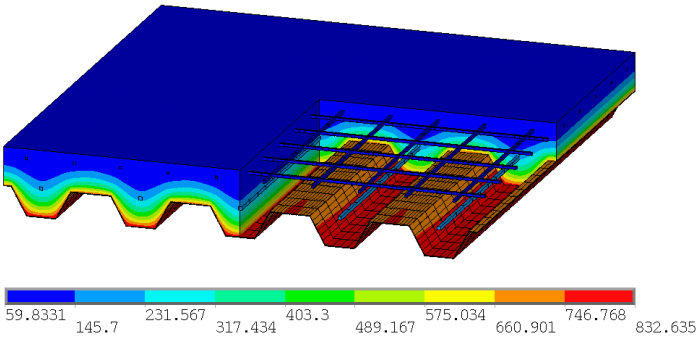

t= 37.1 min

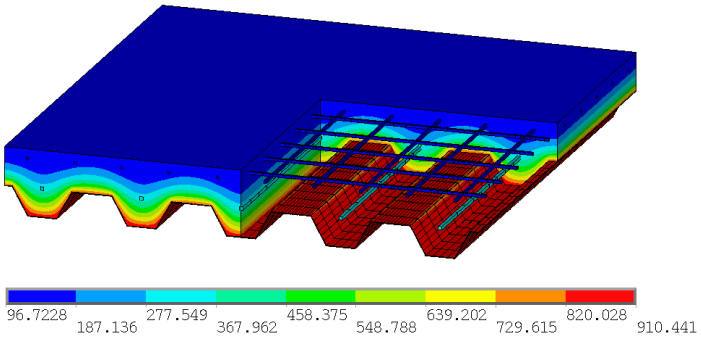

t= 55.6 min

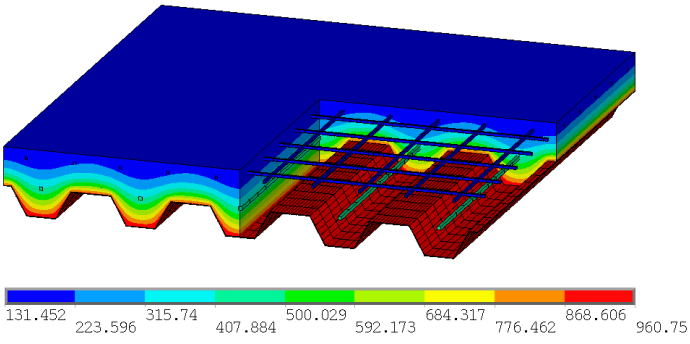

t= 74.1 min

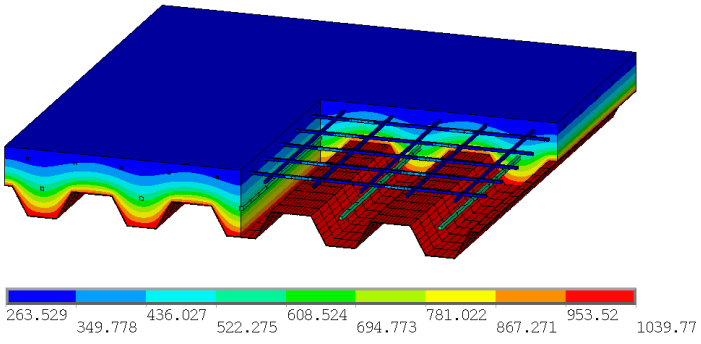

t= 120.0 min

SIM. 65	**St. deck:** Trapezoidal – ArcelorMittal Polydeck 59S	**Rebar (mm):** ϕ10	**Fire resistance (min)**	
	Mesh (mm//mm): ϕ5//100 (Q 196)	**h_1 (mm):** 51	Ave: 38.2	Max: *36.0*

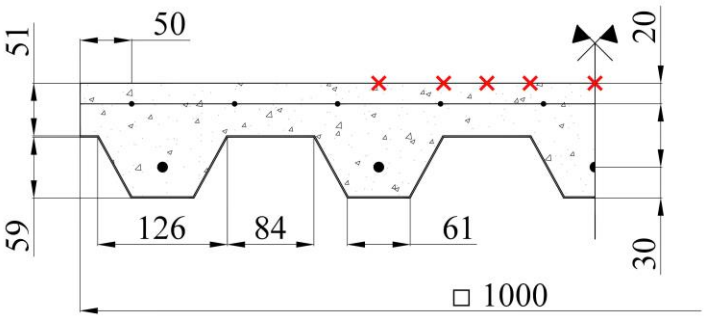

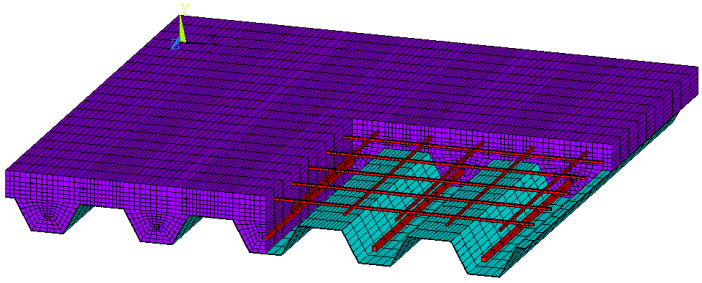

Finite element mesh

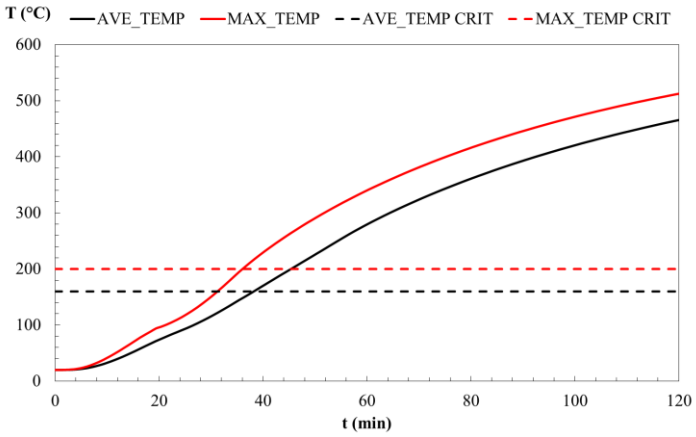

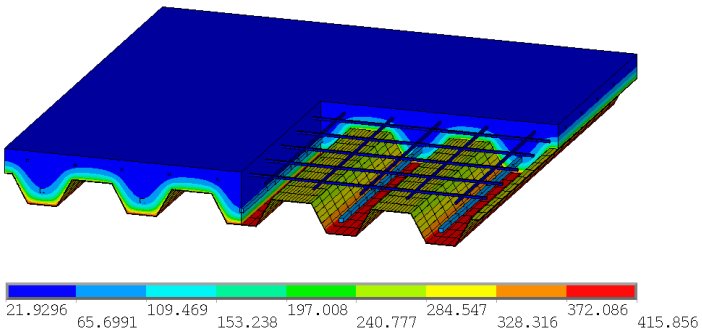

t= 9.0 min

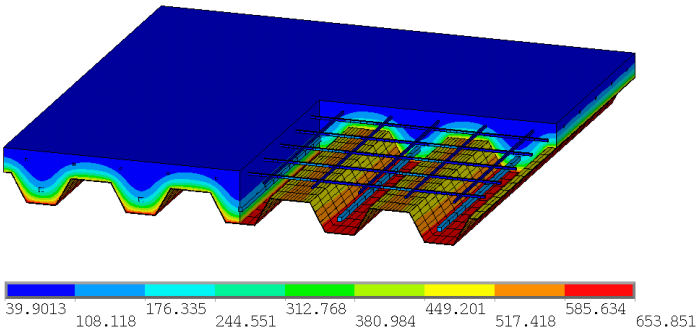

t= 18.0 min

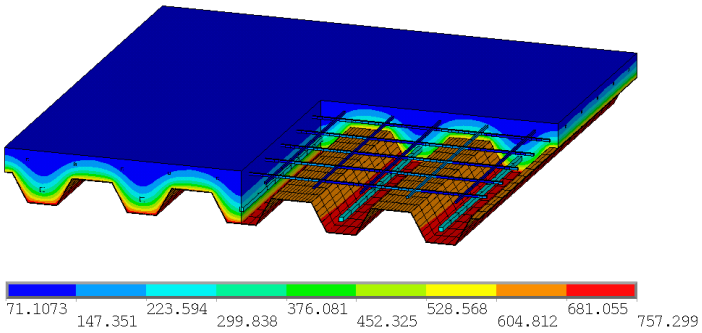

t= 27.0 min

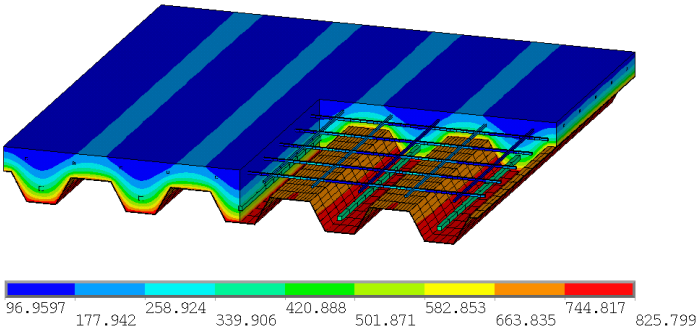

t= 36.0 min

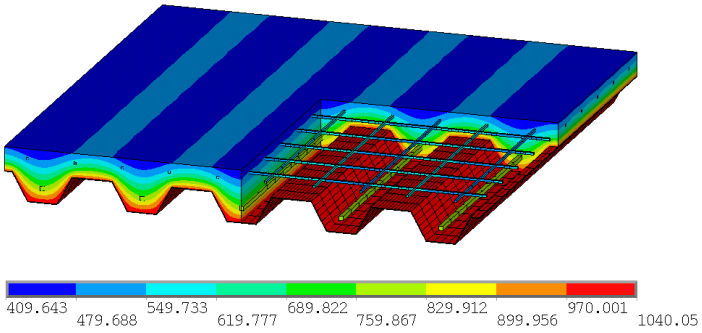

t= 120.0 min

SIM. 66	**St. deck:** Trapezoidal – ArcelorMittal Polydeck 59S	**Rebar (mm):** ϕ10	**Fire resistance (min)**	
	Mesh (mm//mm): ϕ5//100 (Q 196)	**h_1 (mm):** 61	Ave: 49.0	Max: *48.1*

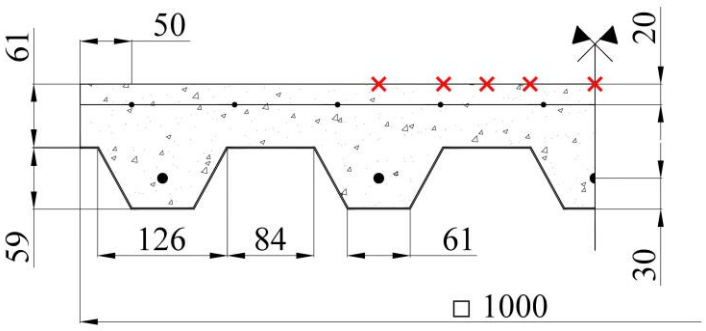

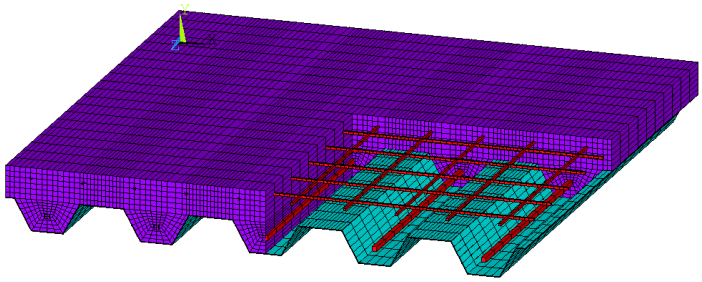

Finite element mesh

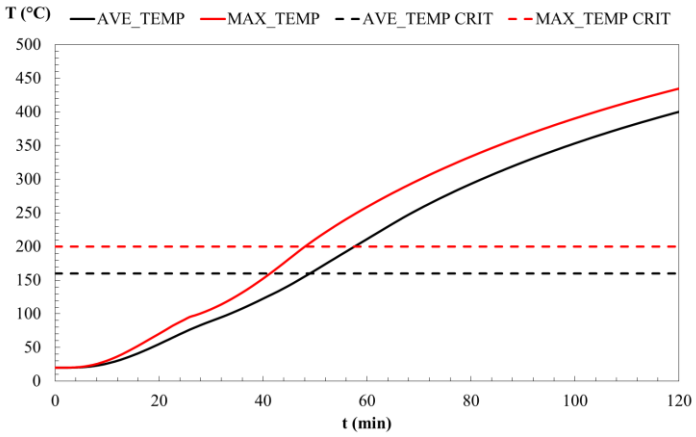

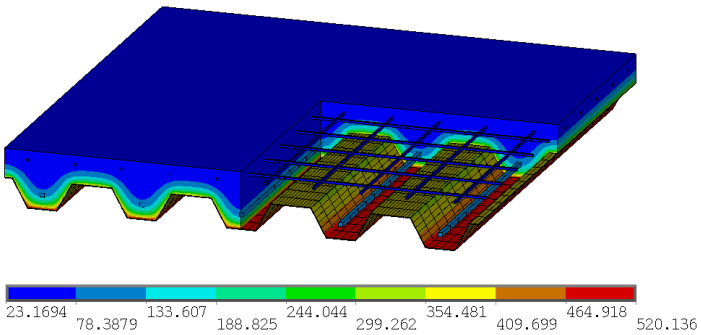

t= 12.0 min

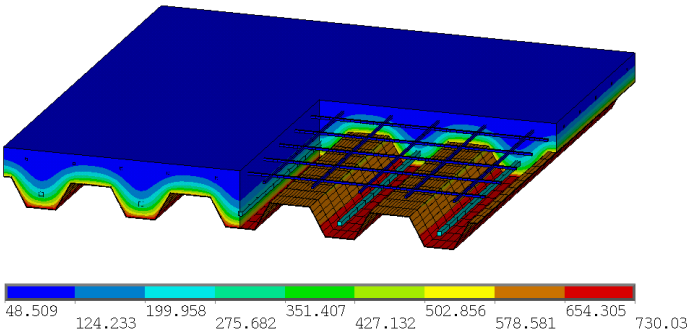

t= 24.1 min

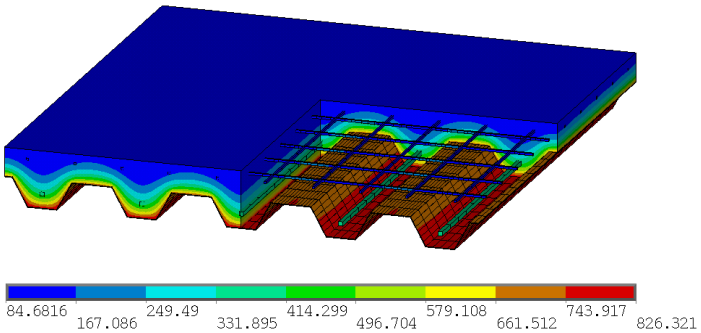

t= 36.1 min

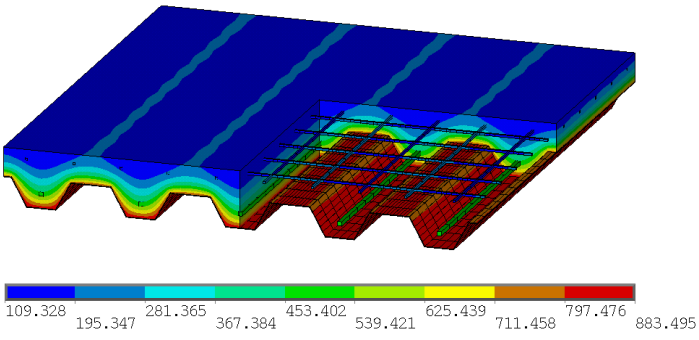

t= 48.1 min

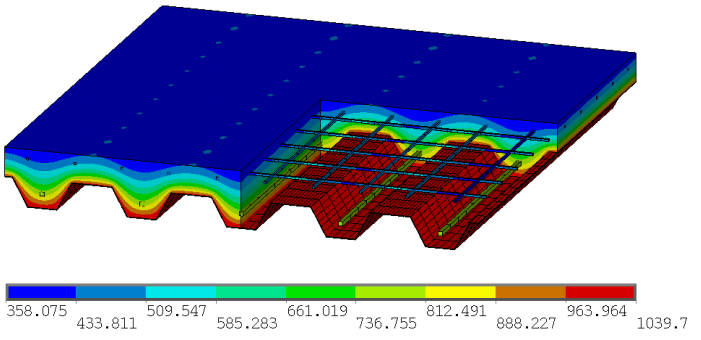

t= 120.0 min

SIM. 67	**St. deck:** Trapezoidal – ArcelorMittal Polydeck 59S	**Rebar (mm):** ϕ10	**Fire resistance (min)**	
	Mesh (mm//mm): ϕ5//100 (Q 196)	**h_1 (mm):** 71	Ave: *60.9*	Max: 62.1

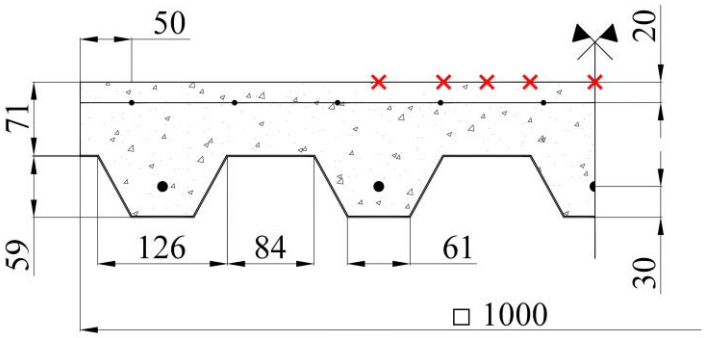

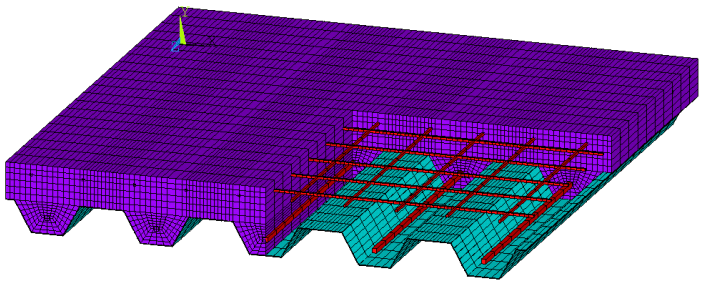

Finite element mesh

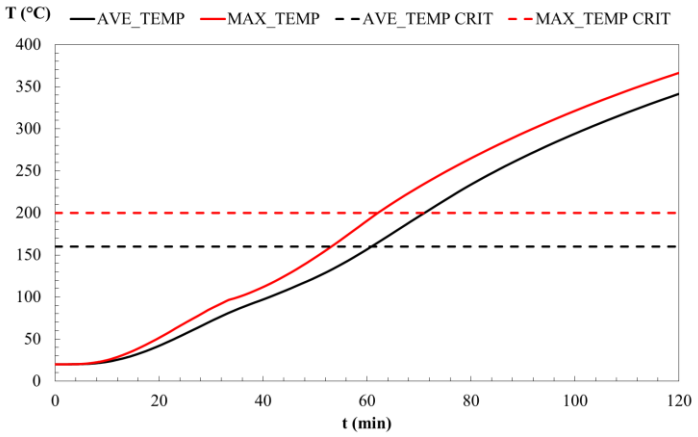

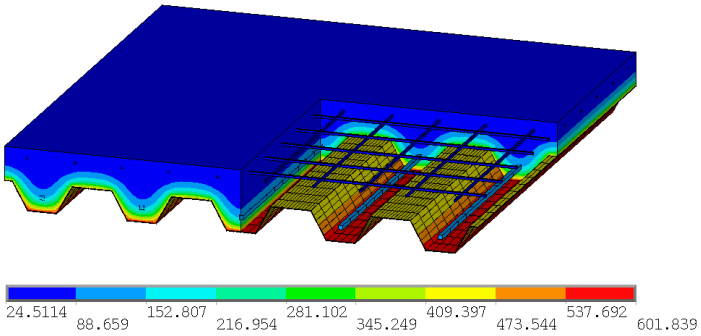

t= 15.2 min

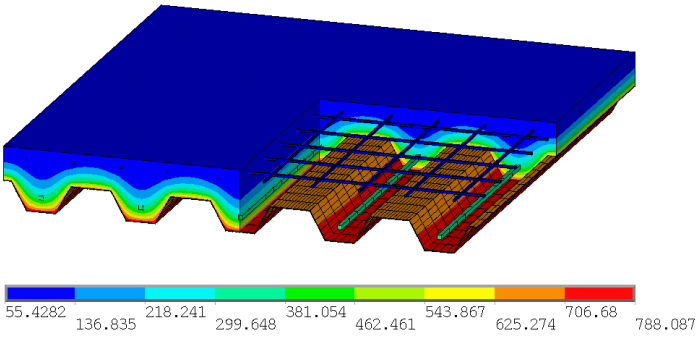

t= 30.5 min

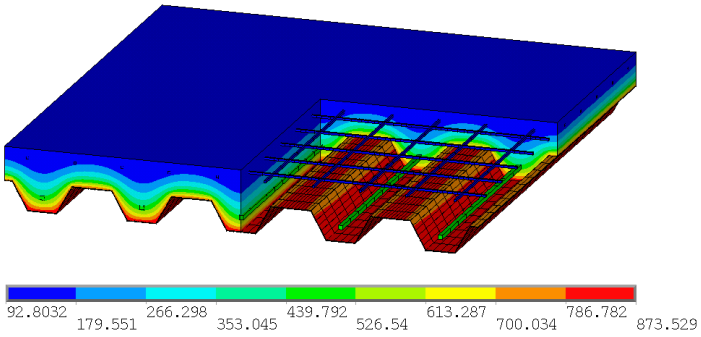

t= 45.7 min

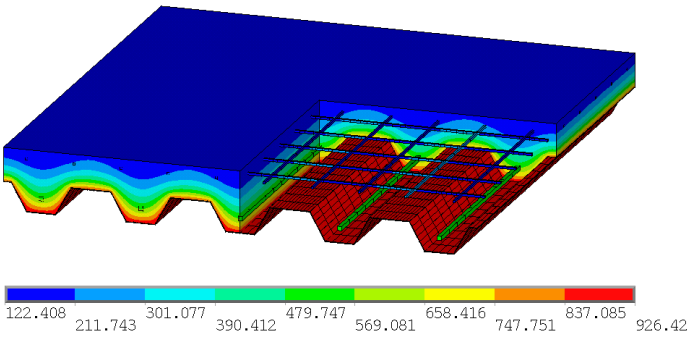

t= 60.9 min

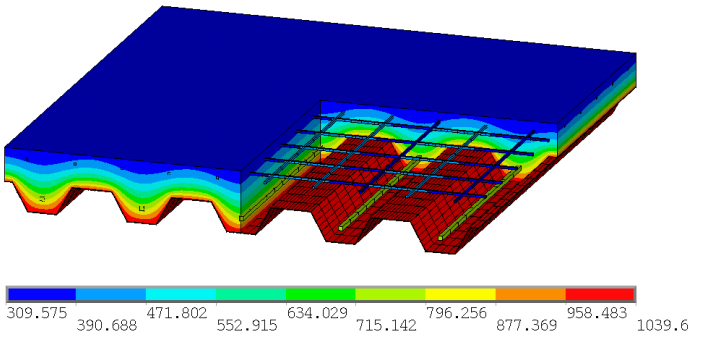

t= 120.0 min

SIM. 68	**St. deck:** Trapezoidal – ArcelorMittal Polydeck 59S	**Rebar (mm):** ϕ10	**Fire resistance (min)**	
	Mesh (mm//mm): ϕ5//100 (Q 196)	**h_1 (mm):** 81	Ave: *74.0*	Max: 78.1

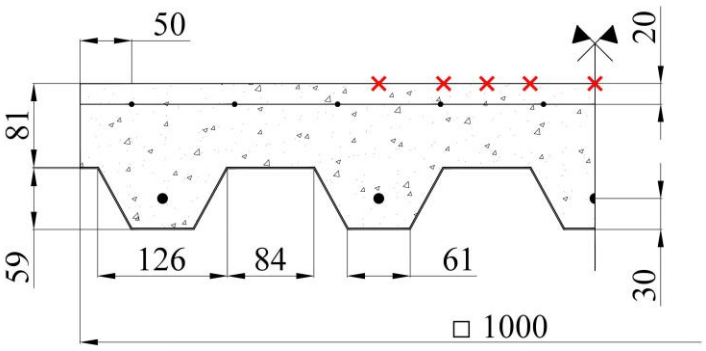

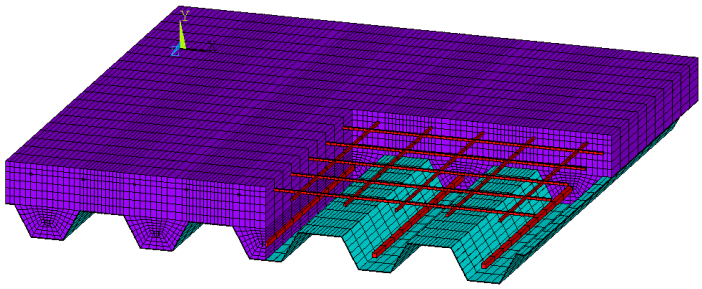

Finite element mesh

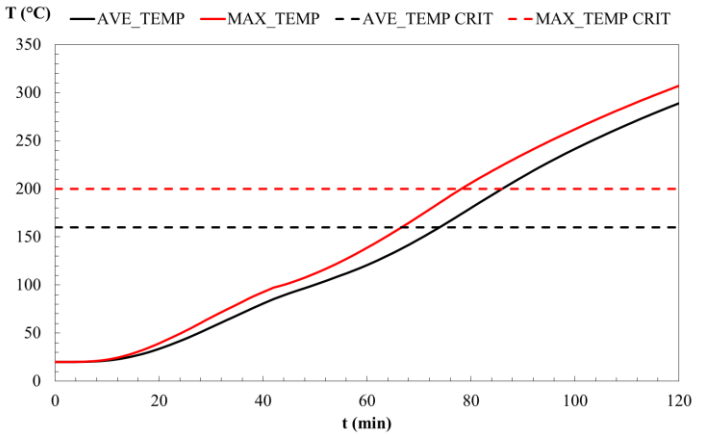

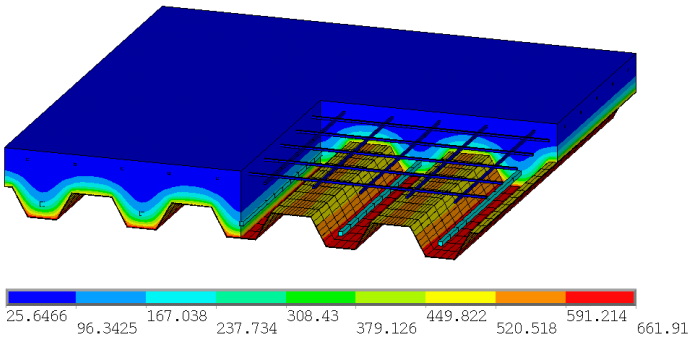

t= 18.5 min

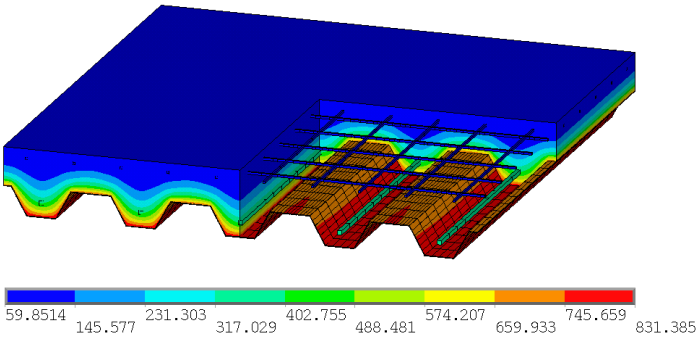

t= 37.0 min

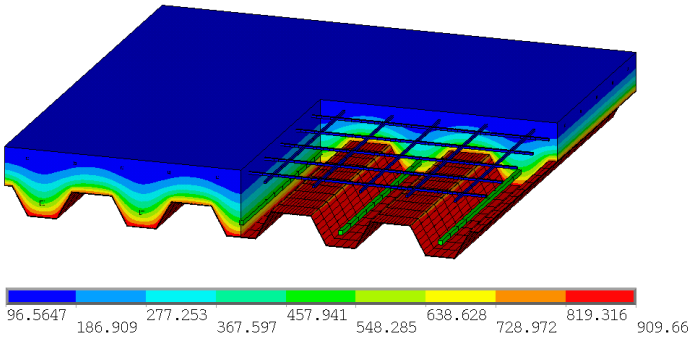

t= 55.5 min

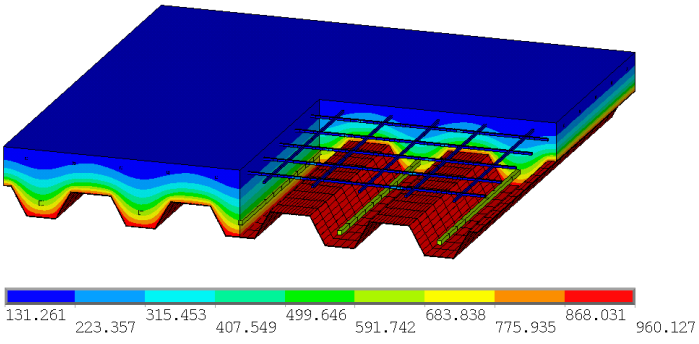

t= 74.0 min

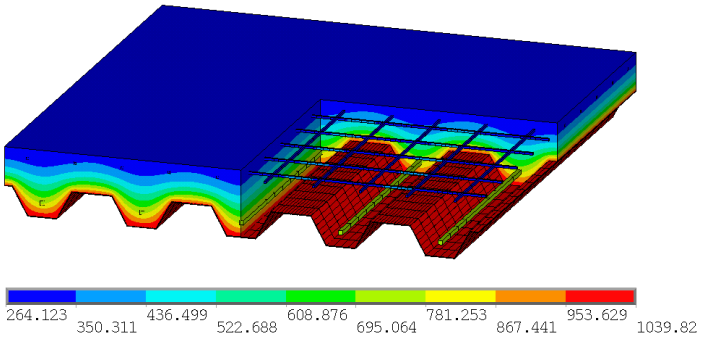

t= 120.0 min

SIM. 69	**St. deck:** Trapezoidal – ArcelorMittal Polydeck 59S	**Rebar (mm):** ϕ10	**Fire resistance (min)**	
	Mesh (mm//mm): ϕ5//100 (Q 196)	**h_1 (mm):** 51	Ave: 38.2	Max: *36.0*

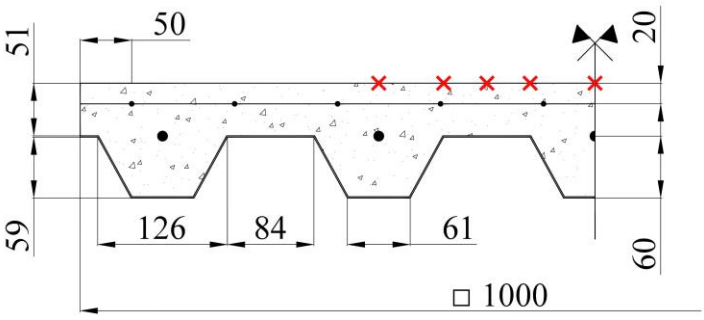

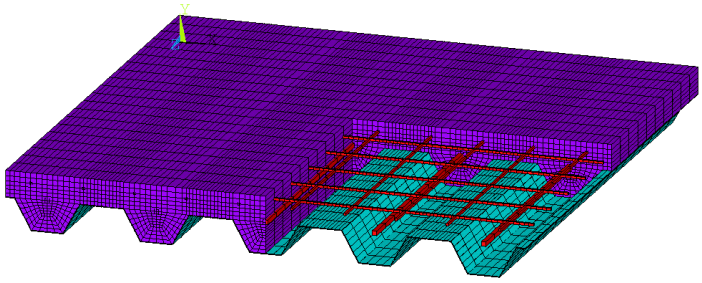

Finite element mesh

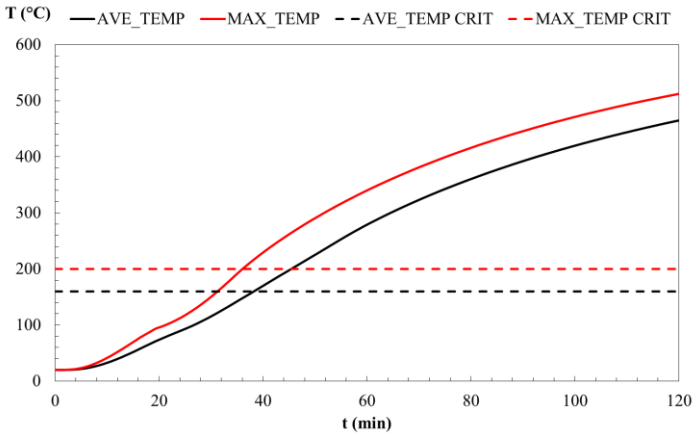

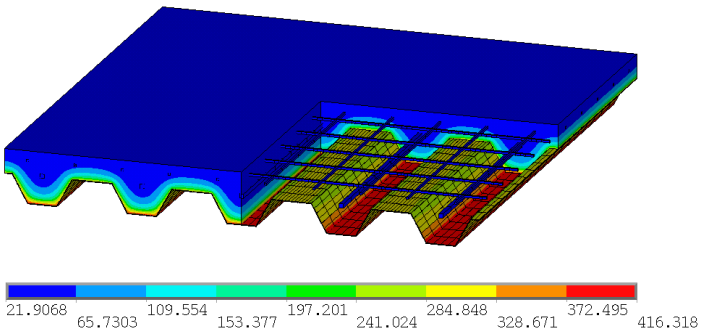

t= 9.0 min

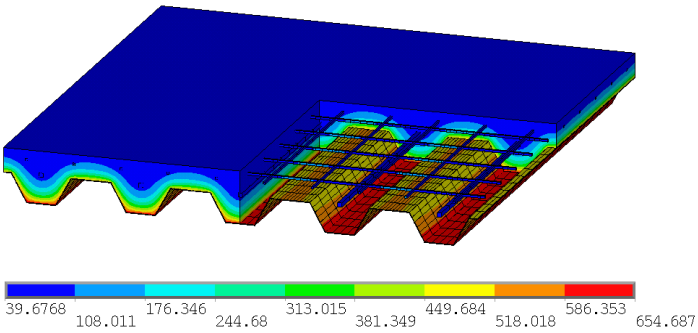

t= 18.0 min

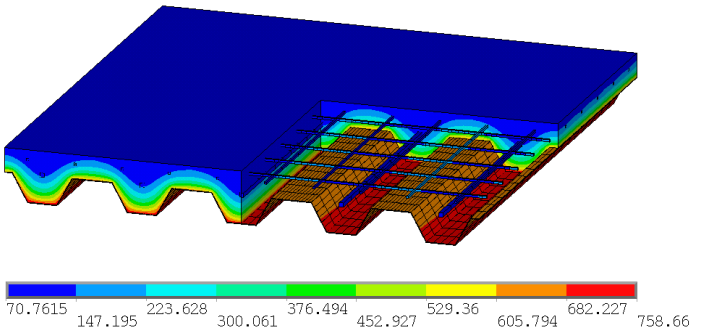

t= 27.0 min

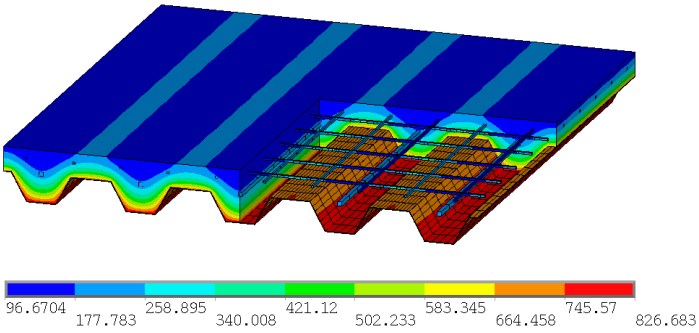

t= 36.0 min

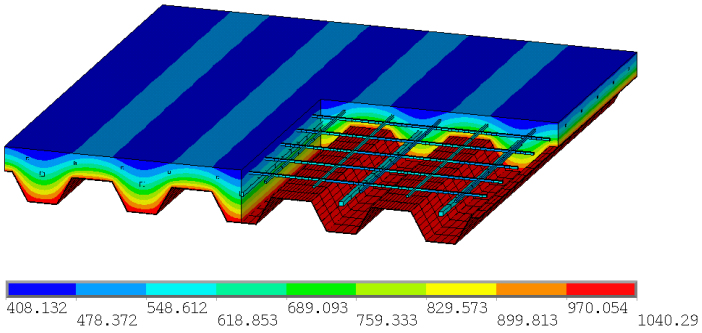

t= 120.0 min

SIM. 70	**St. deck:** Trapezoidal – ArcelorMittal Polydeck 59S	**Rebar (mm):** ϕ10	**Fire resistance (min)**	
	Mesh (mm//mm): ϕ5//100 (Q 196)	**h_1 (mm):** 61	Ave: 49.0	Max: *48.1*

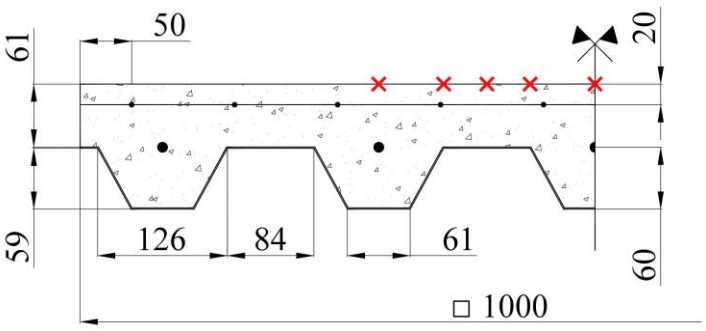

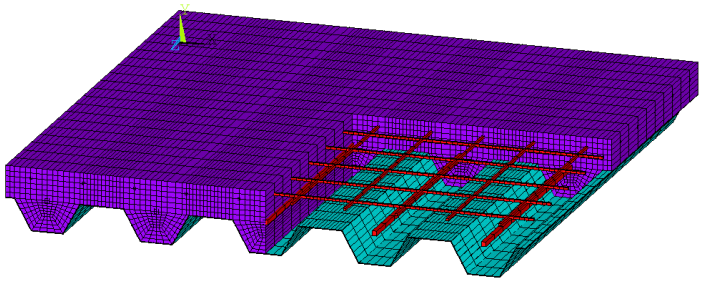

Finite element mesh

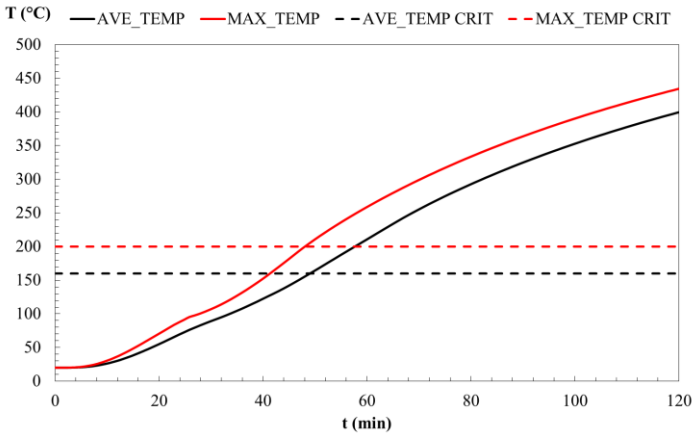

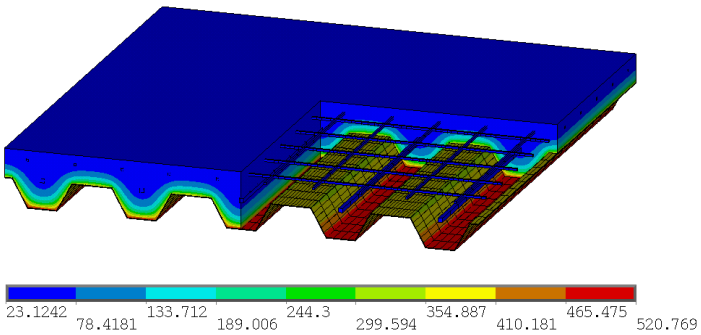

t= 12.0 min

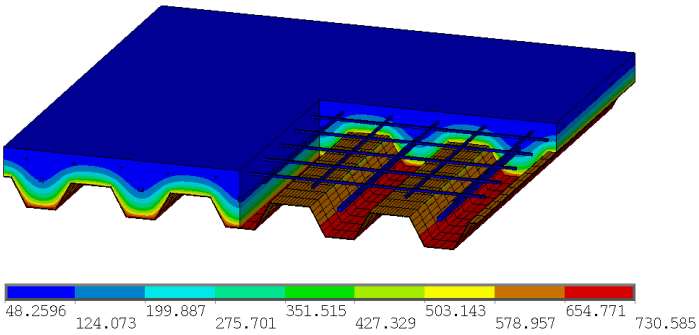

t= 24.1 min

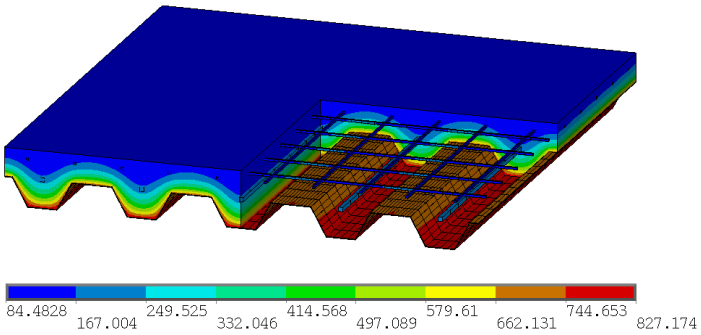

t= 36.1 min

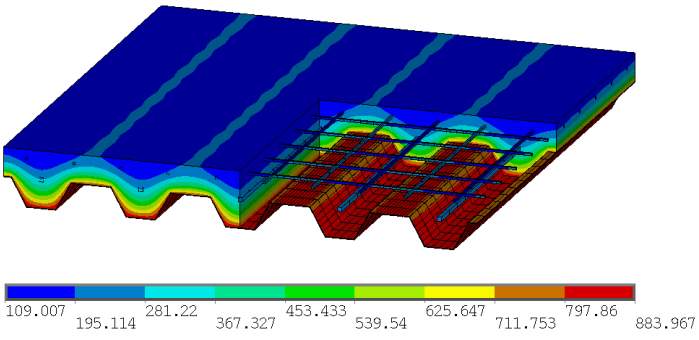

t= 48.1 min

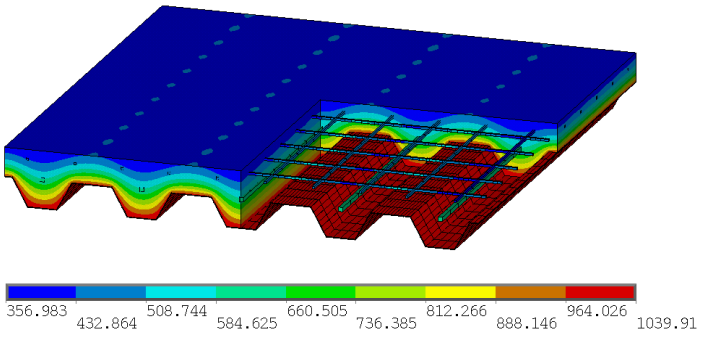

t= 120.0 min

SIM. 71	**St. deck:** Trapezoidal – ArcelorMittal Polydeck 59S	**Rebar (mm):** ϕ10	**Fire resistance (min)**	
	Mesh (mm//mm): ϕ5//100 (Q 196)	**h_1 (mm):** 71	Ave: *60.9*	Max: 62.1

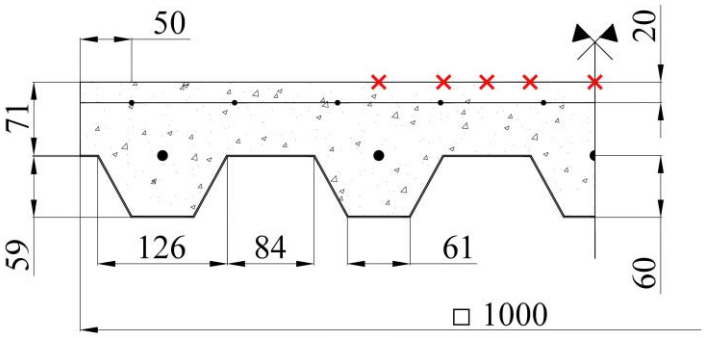

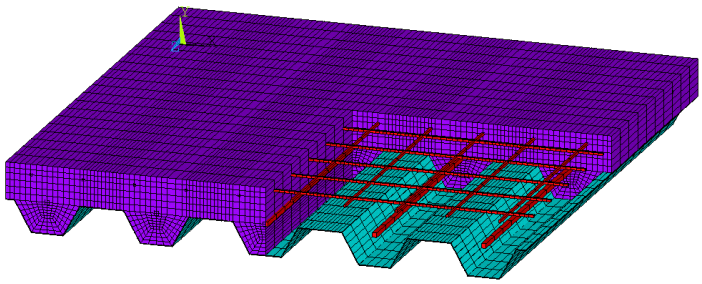

Finite element mesh

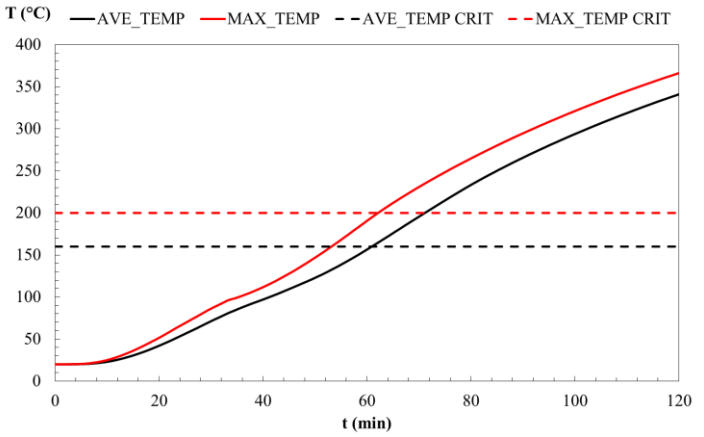

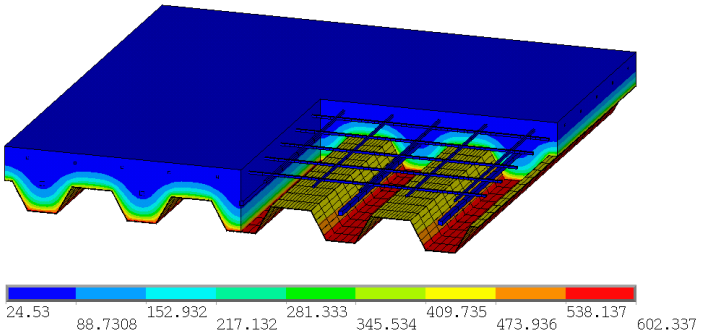

t= 15.2 min

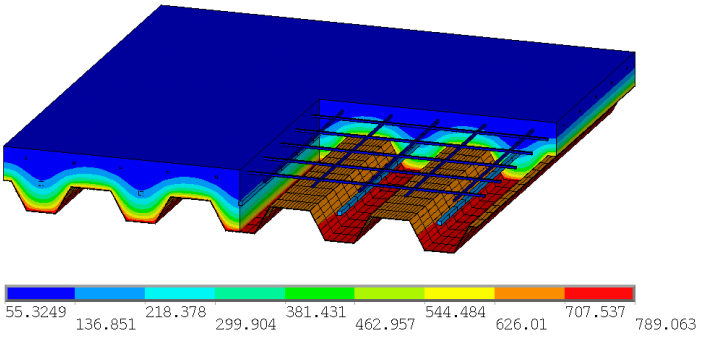

t= 30.5 min

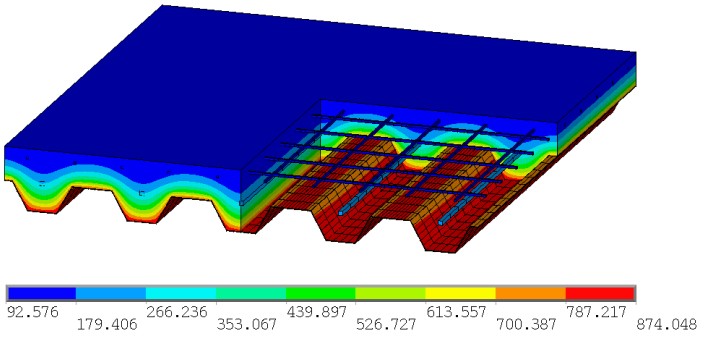

t= 45.7 min

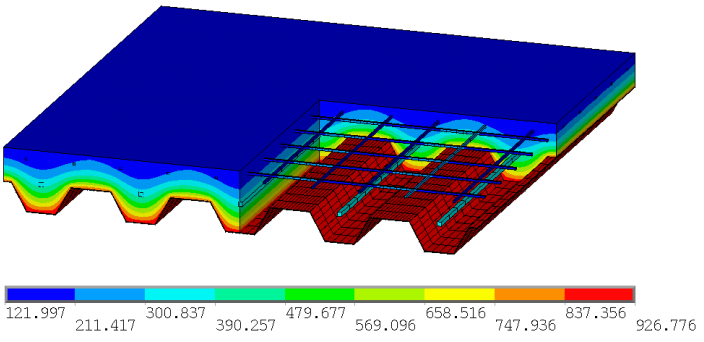

t= 60.9 min

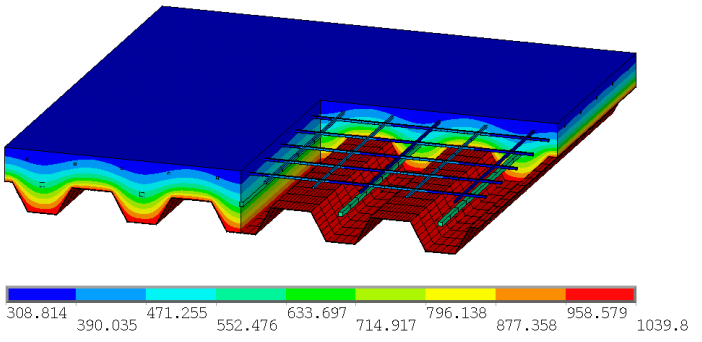

t= 120.0 min

SIM. 72	**St. deck:** Trapezoidal – ArcelorMittal Polydeck 59S	**Rebar (mm):** ϕ10	**Fire resistance (min)**	
	Mesh (mm//mm): ϕ5//100 (Q 196)	**h_1 (mm):** 81	Ave: *74.0*	Max: 78.2

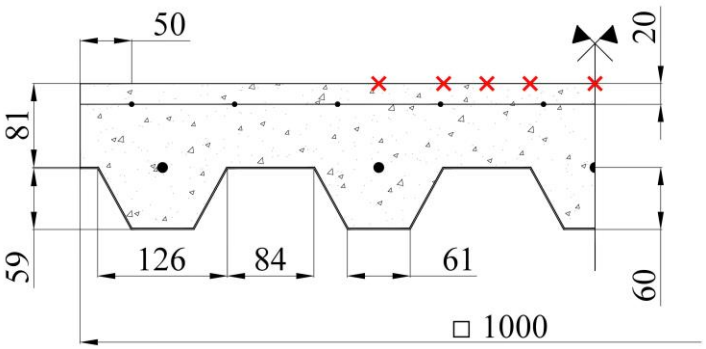

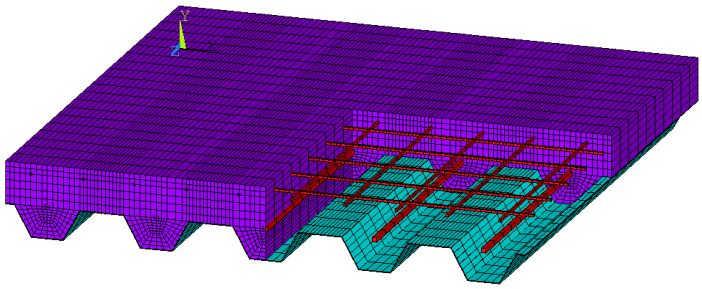

Finite element mesh

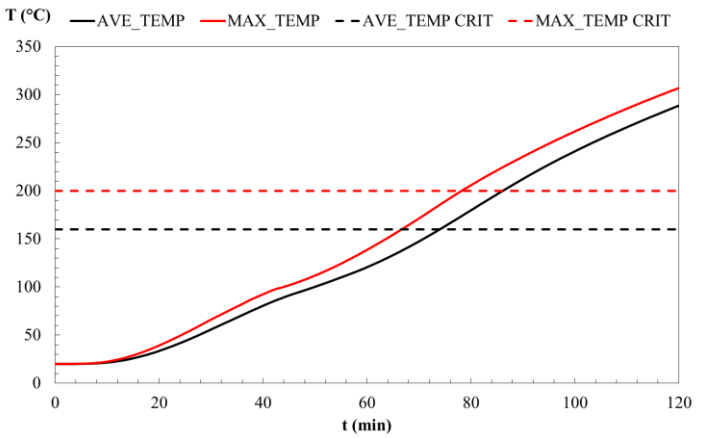

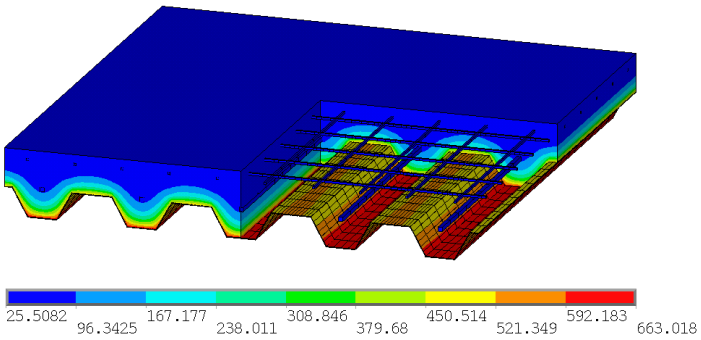

t= 18.5 min

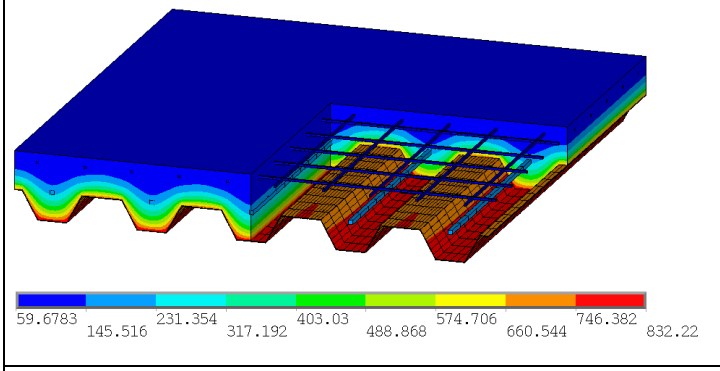

t= 37.0 min

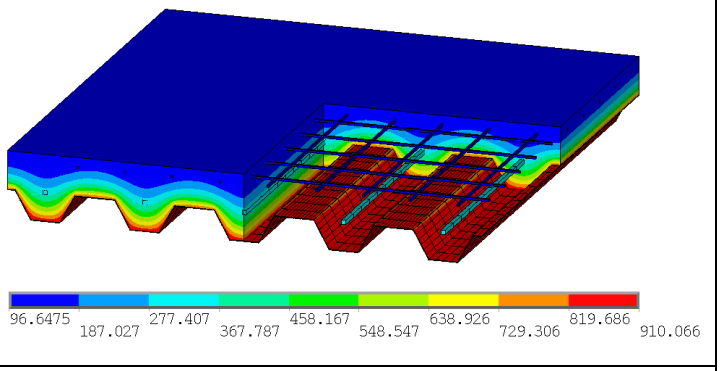

t= 55.5 min

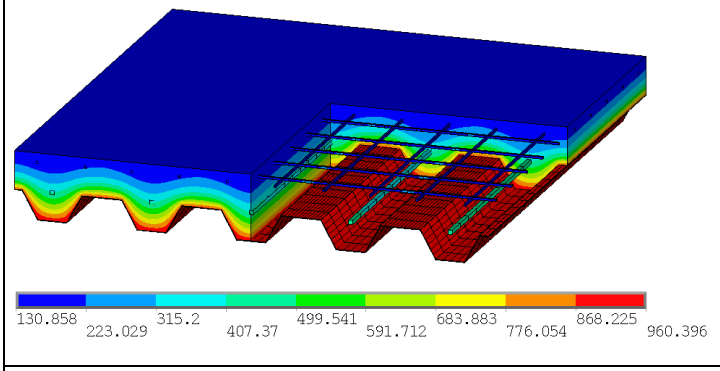

t= 74.0 min

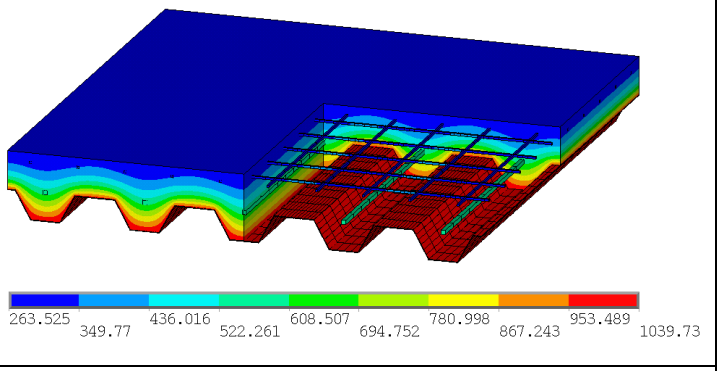

t= 120.0 min

SIM. 73	**St. deck:** Trapezoidal – ArcelorMittal Polydeck 59S	**Rebar (mm):** ϕ10	**Fire resistance (min)**	
	Mesh (mm//mm): ϕ6//100 (Q 283)	**h_1 (mm):** 51	Ave: 38.4	Max: *36.2*

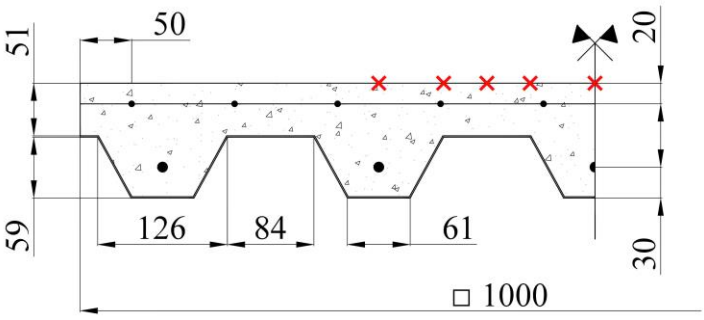

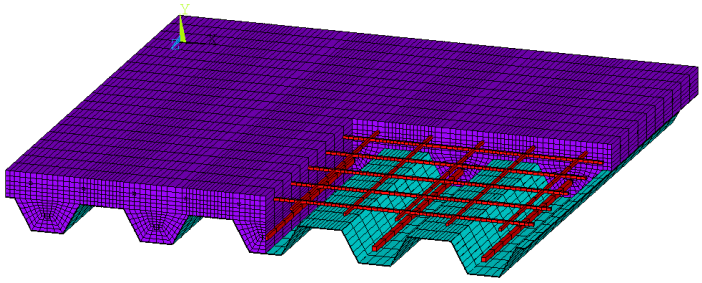

Finite element mesh

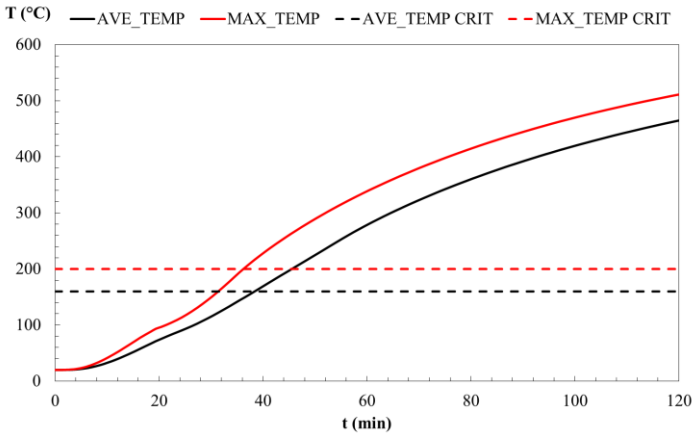

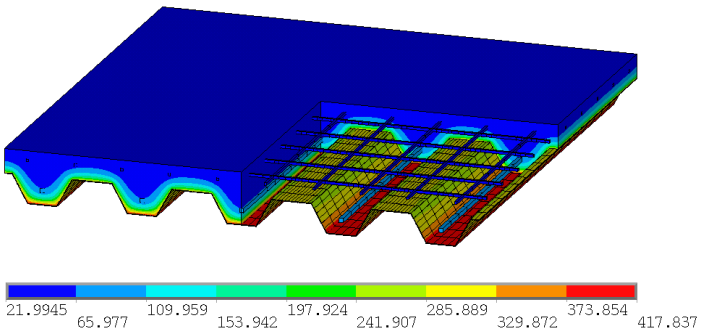

t= 9.1 min

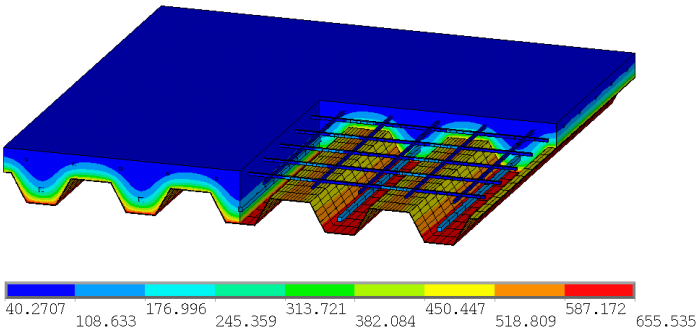

t= 18.1 min

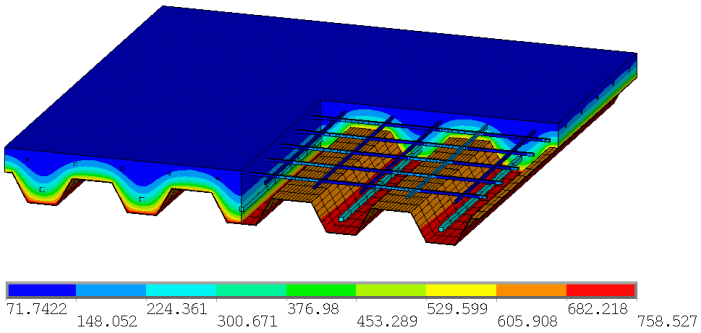

t= 27.2 min

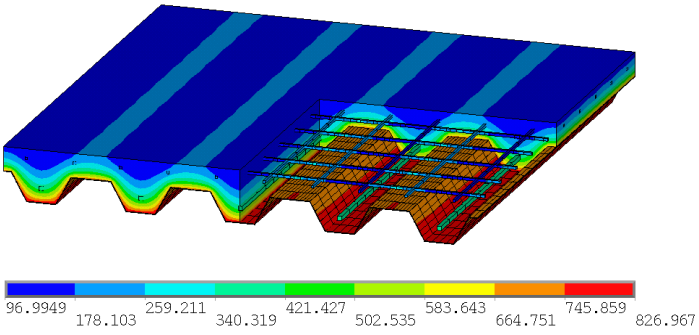

t= 36.2 min

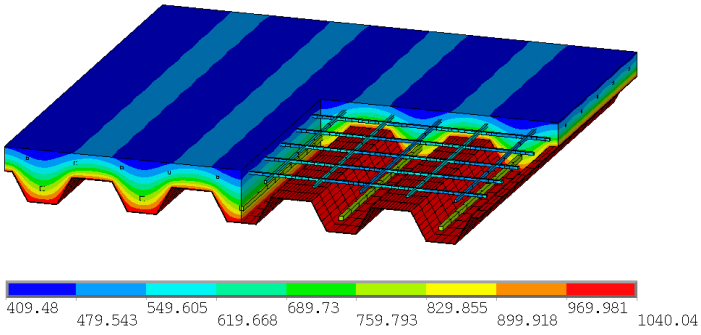

t= 120.0 min

SIM. 74	**St. deck:** Trapezoidal – ArcelorMittal Polydeck 59S	**Rebar (mm):** ϕ10	**Fire resistance (min)**	
	Mesh (mm//mm): ϕ6//100 (Q 283)	**h_1 (mm):** 61	Ave: 49.2	Max: *48.3*

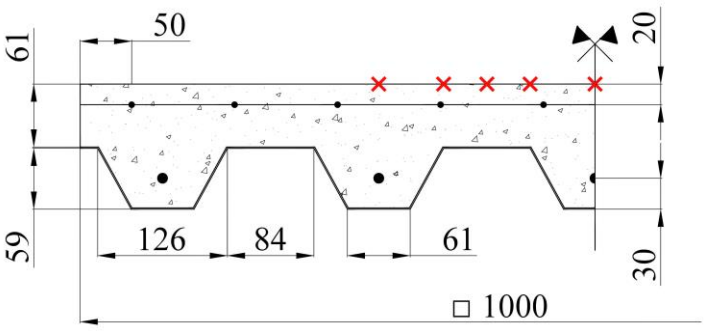

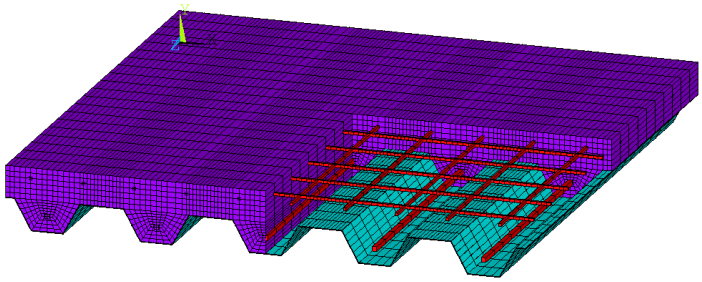

Finite element mesh

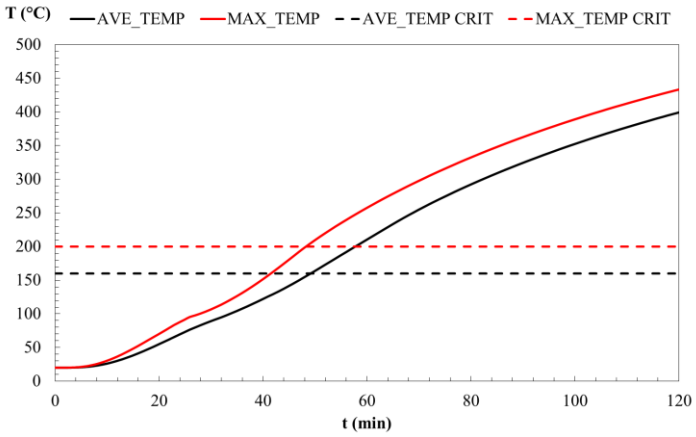

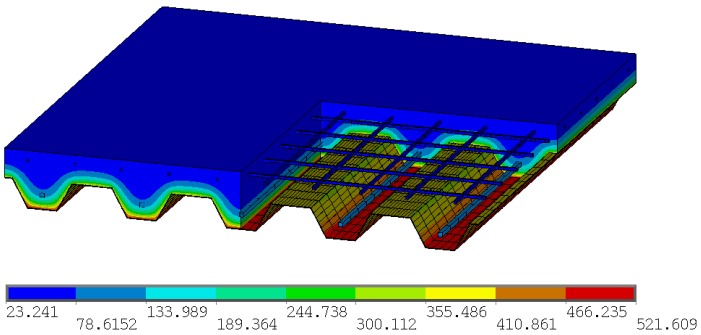

t= 12.1 min

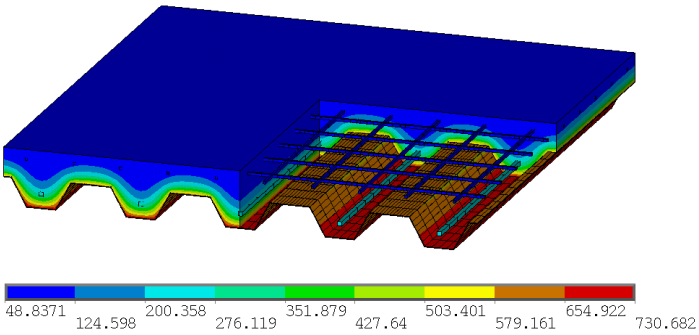

t= 24.2 min

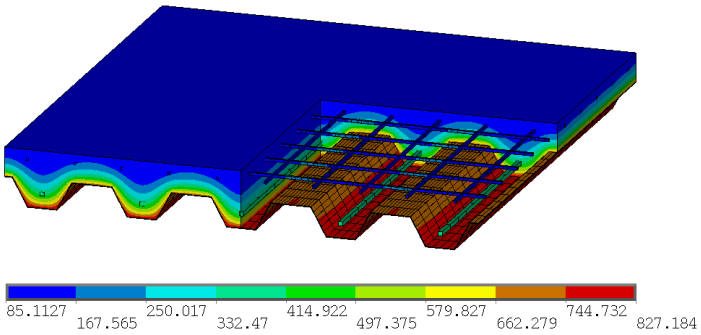

t= 36.2 min

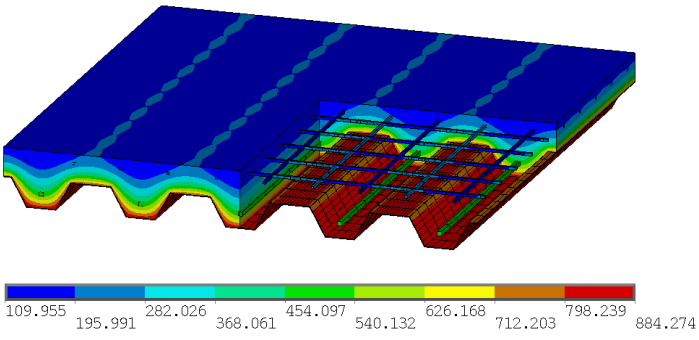

t= 48.3 min

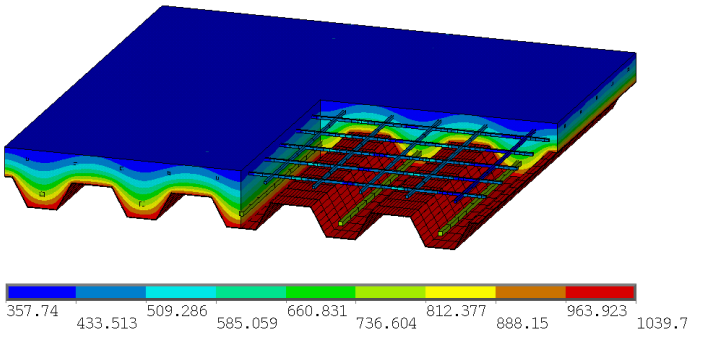

t= 120.0 min

SIM. 75	**St. deck:** Trapezoidal – ArcelorMittal Polydeck 59S	**Rebar (mm):** ϕ10	**Fire resistance (min)**	
	Mesh (mm//mm): ϕ6//100 (Q 283)	**h_1 (mm):** 71	Ave: *61.0*	Max: 62.4

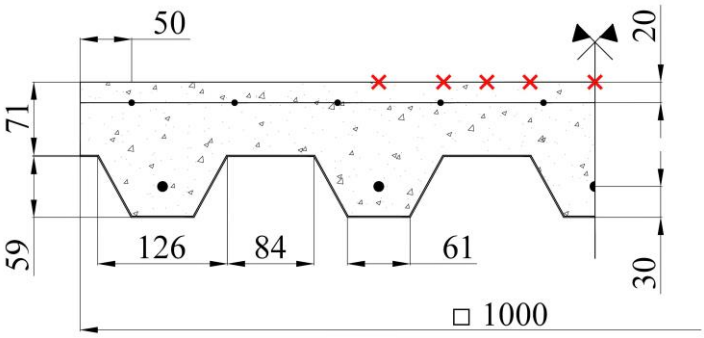

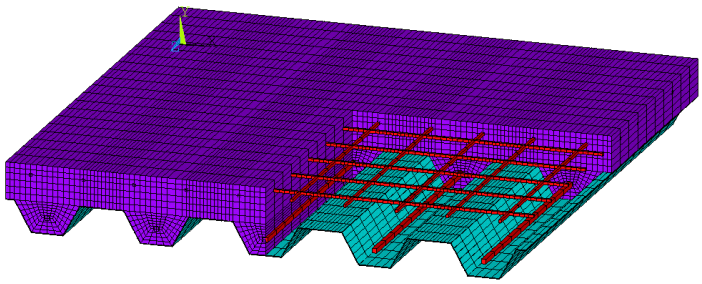

Finite element mesh

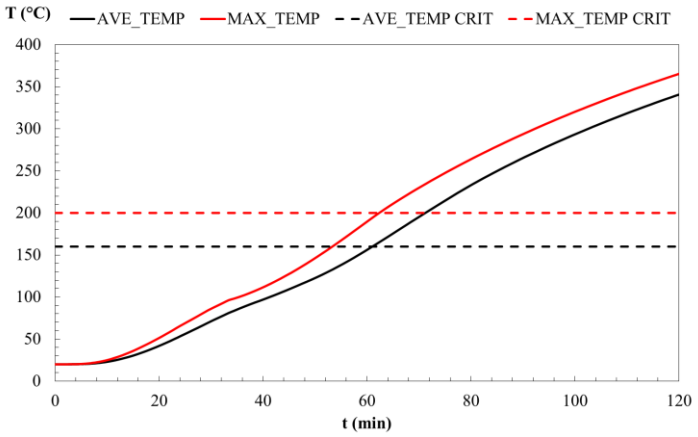

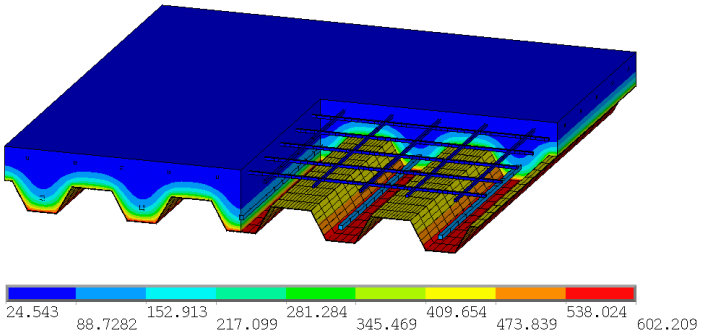

t= 15.3 min

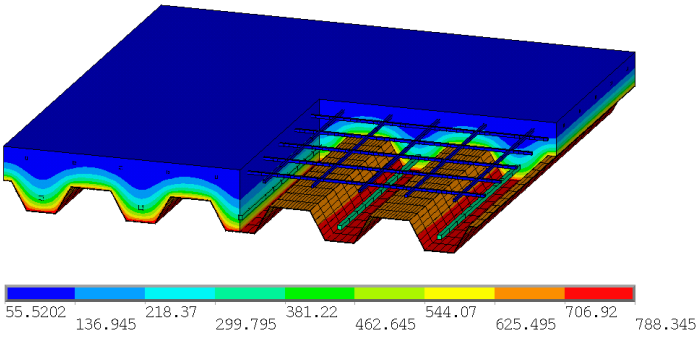

t= 30.5 min

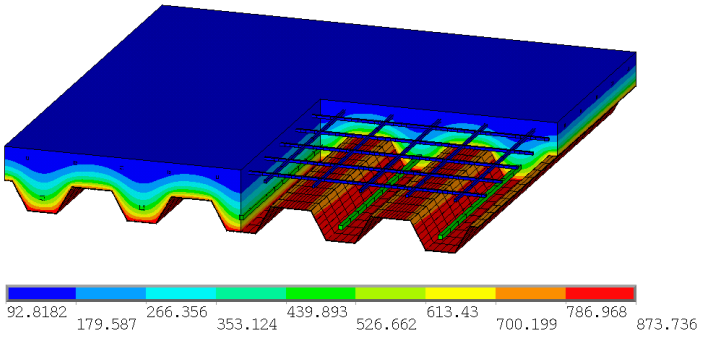

t= 45.8 min

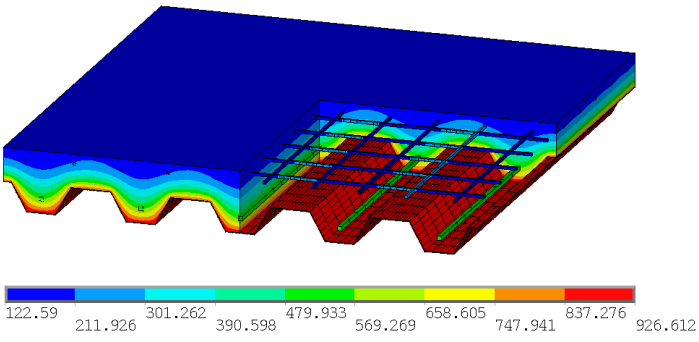

t= 61.0 min

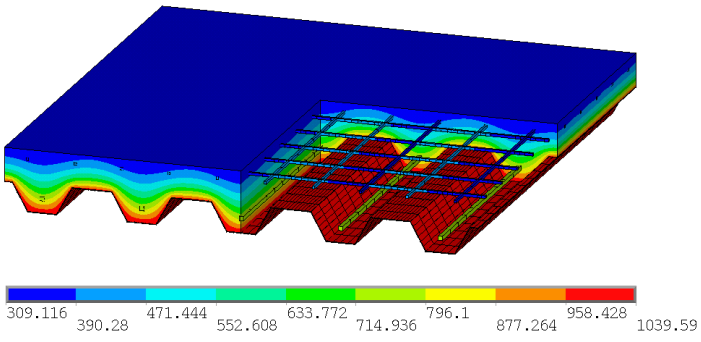

t= 120.0 min

SIM. 76	**St. deck:** Trapezoidal – ArcelorMittal Polydeck 59S	**Rebar (mm):** ϕ10	**Fire resistance (min)**	
	Mesh (mm//mm): ϕ6//100 (Q 283)	**h_1 (mm):** 81	Ave: *74.1*	Max: 78.4

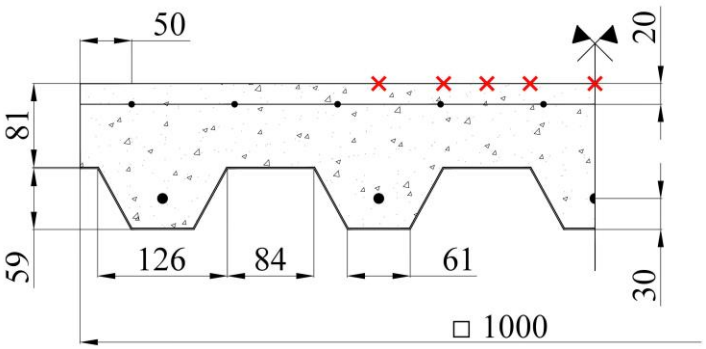

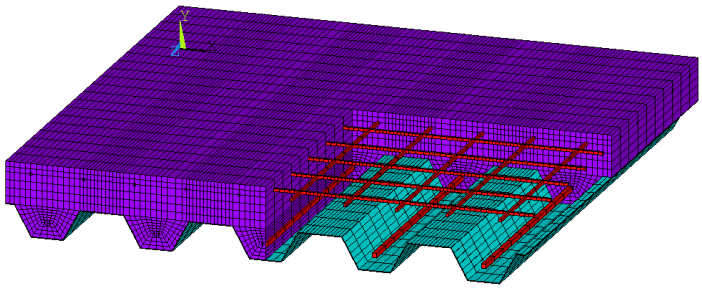

Finite element mesh

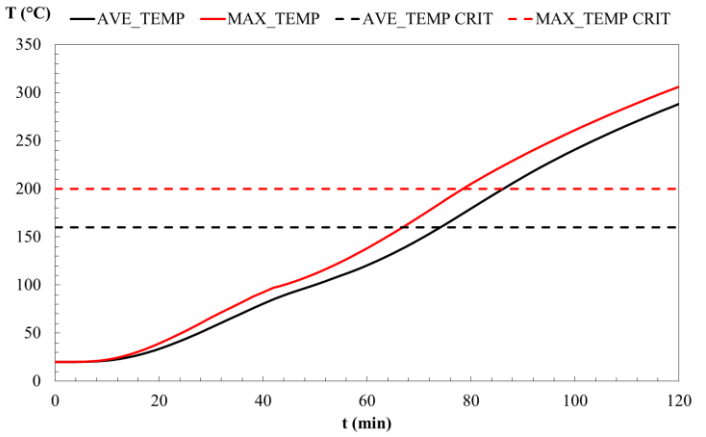

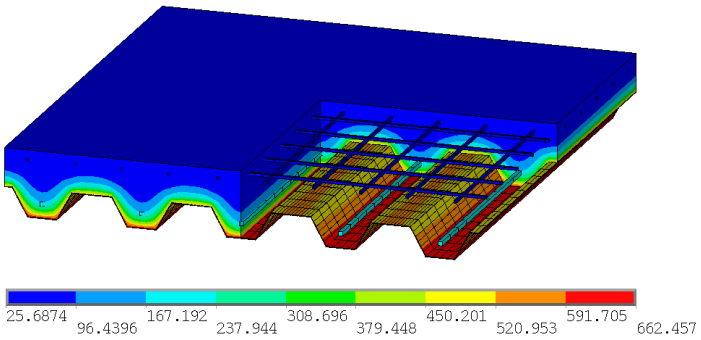

t= 18.5 min

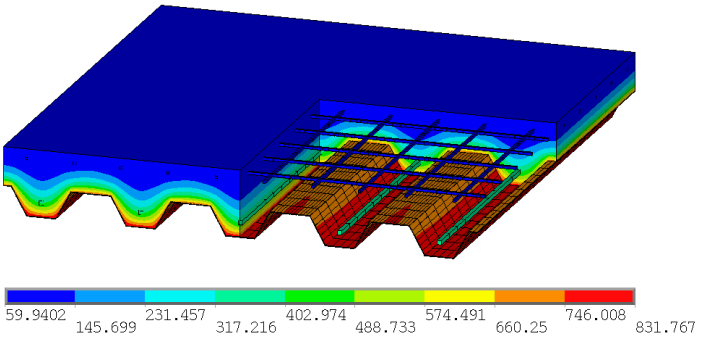

t= 37.1 min

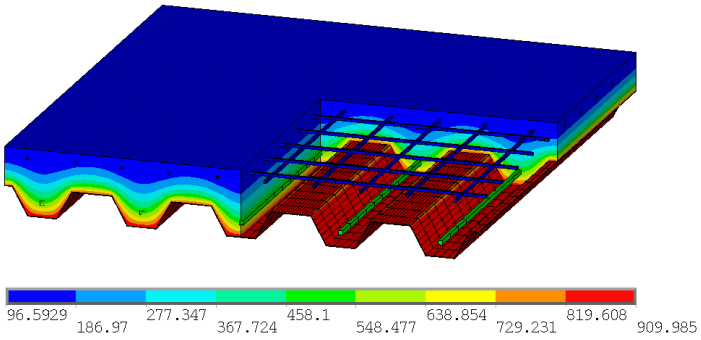

t= 55.6 min

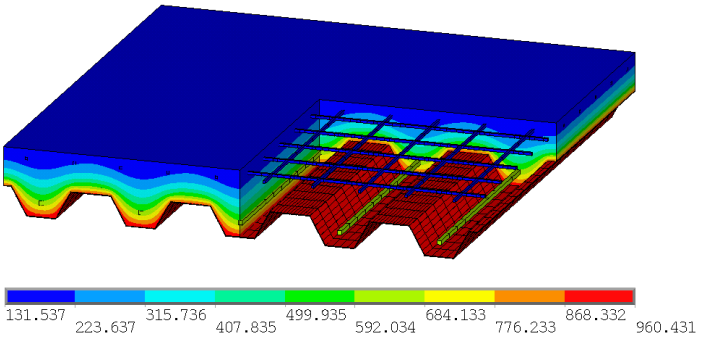

t= 74.1 min

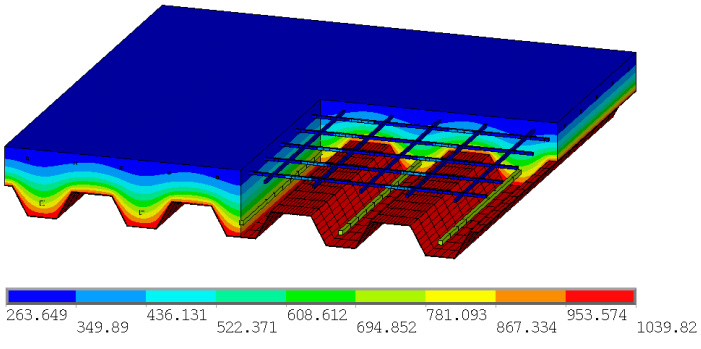

t= 120.0 min

SIM. 77	**St. deck:** Trapezoidal – ArcelorMittal Polydeck 59S	**Rebar (mm):** ϕ10	**Fire resistance (min)**	
	Mesh (mm//mm): ϕ6//100 (Q 283)	**h_1 (mm):** 51	Ave: 38.4	Max: *36.2*

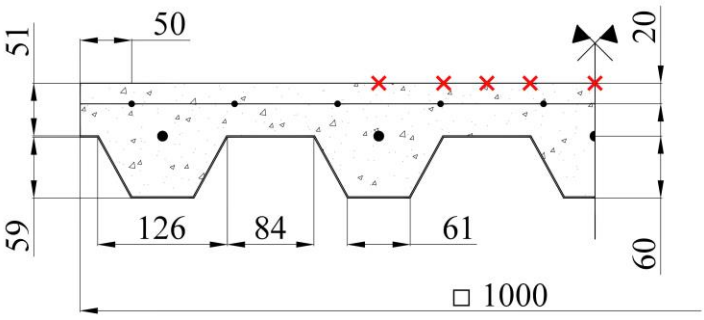

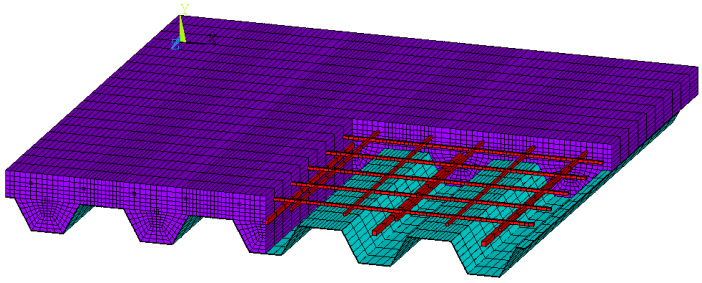

Finite element mesh

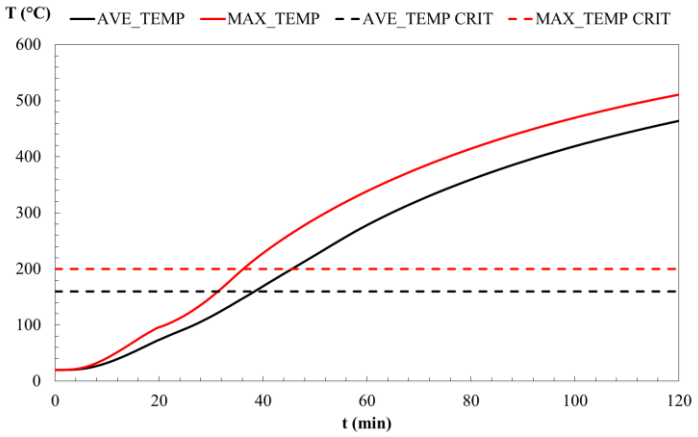

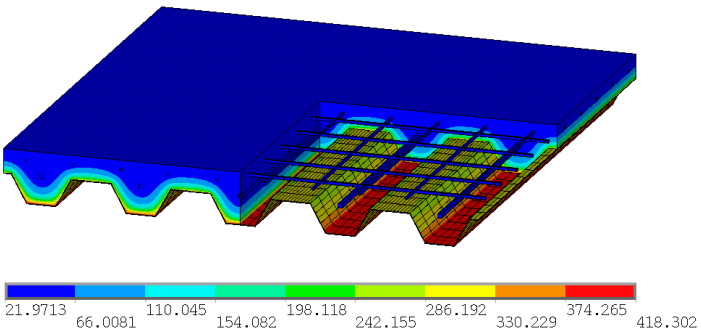

t= 9.1 min

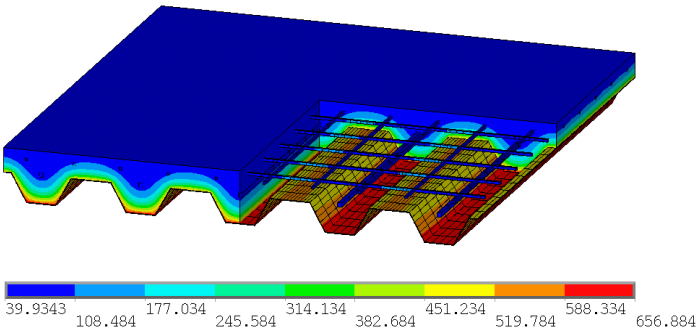

t= 18.1 min

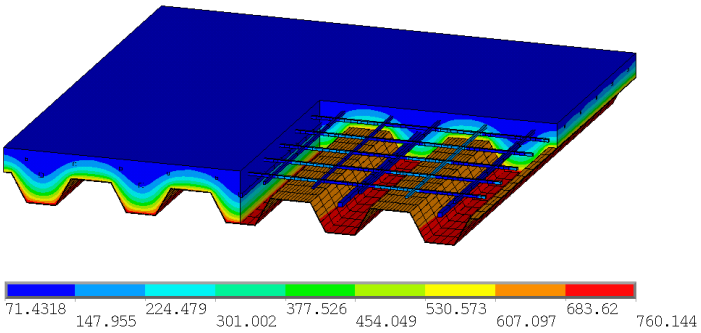

t= 27.2 min

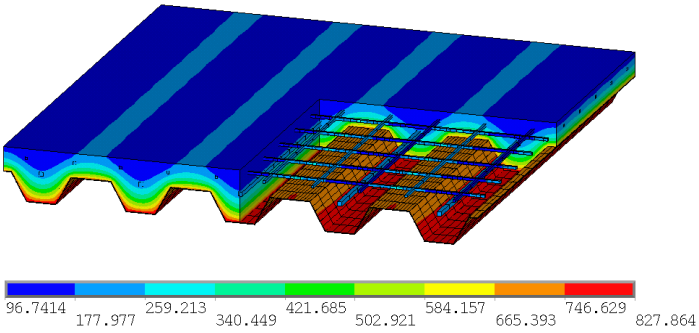

t= 36.2 min

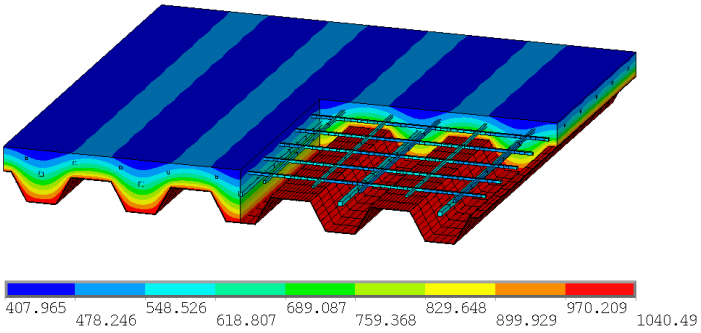

t= 120.0 min

SIM. 78	**St. deck:** Trapezoidal – ArcelorMittal Polydeck 59S	**Rebar (mm):** ϕ10	**Fire resistance (min)**	
	Mesh (mm//mm): ϕ6//100 (Q 283)	**h_1 (mm):** 61	Ave: 49.2	Max: *48.3*

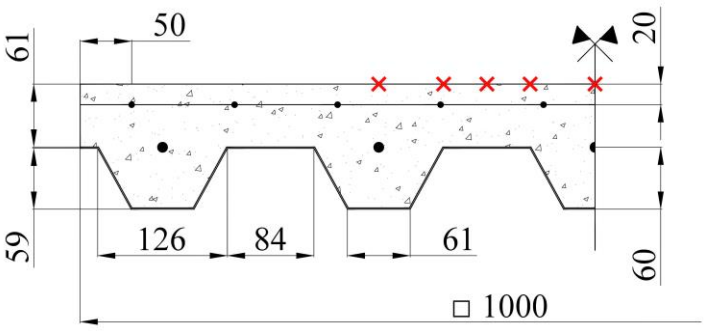

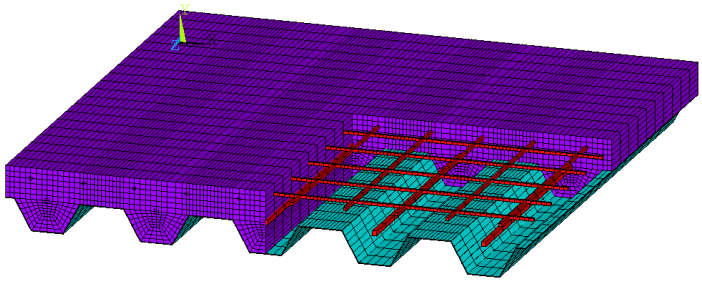

Finite element mesh

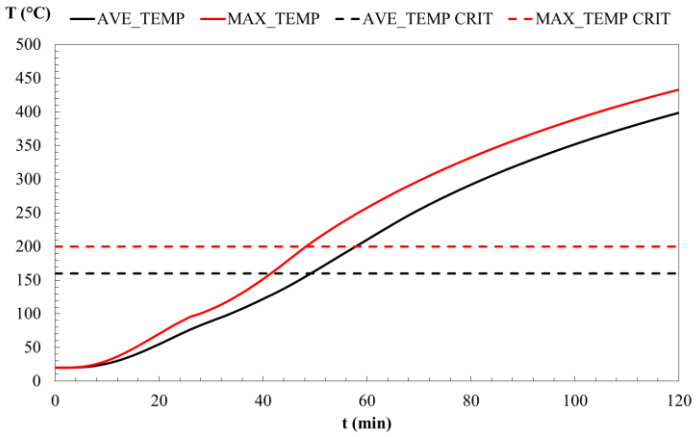

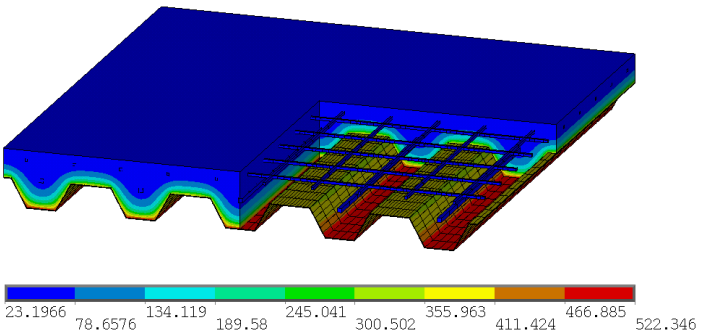

t= 12.1 min

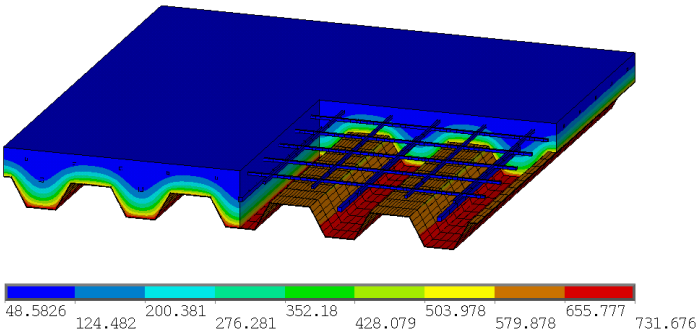

t= 24.2 min

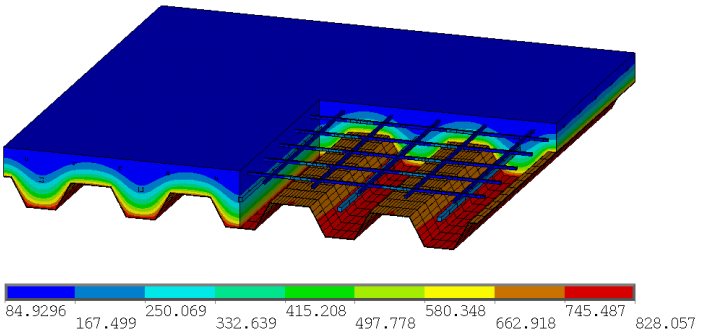

t= 36.2 min

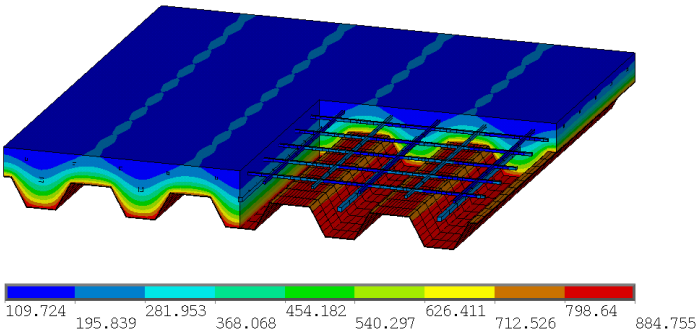

t= 48.3 min

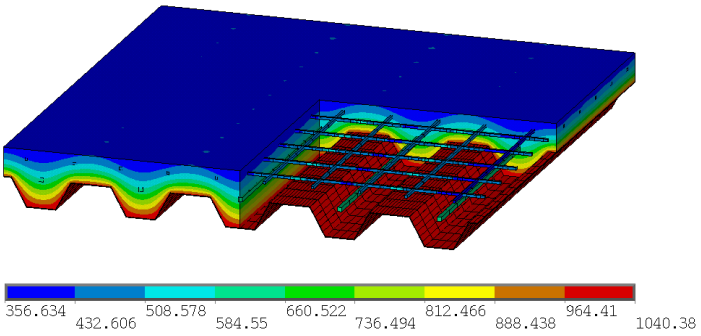

t= 120.0 min

SIM. 79	**St. deck:** Trapezoidal – ArcelorMittal Polydeck 59S	**Rebar (mm):** ϕ10	**Fire resistance (min)**	
	Mesh (mm//mm): ϕ6//100 (Q 283)	**h_1 (mm):** 71	Ave: *61.1*	Max: 62.3

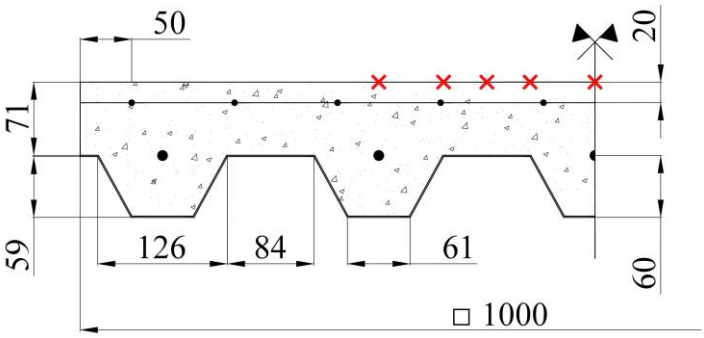

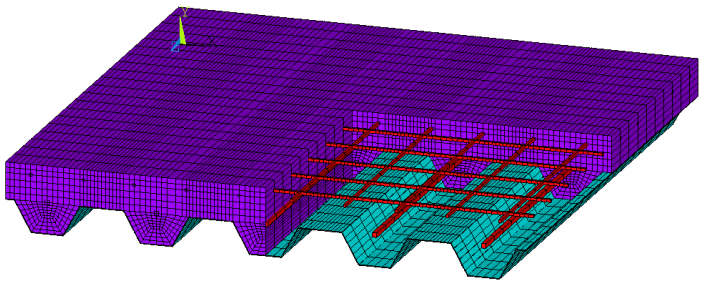

Finite element mesh

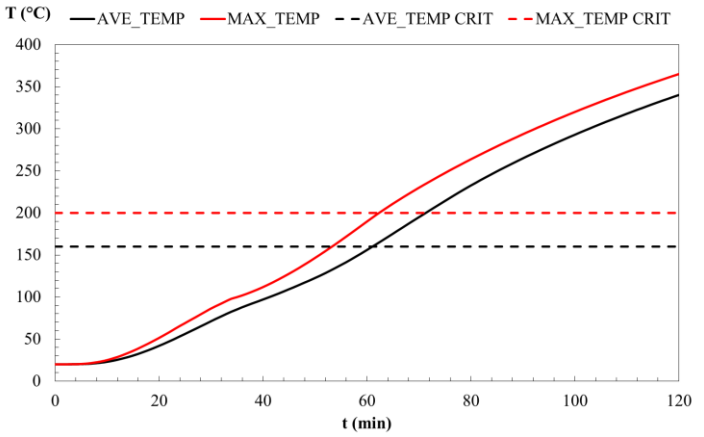

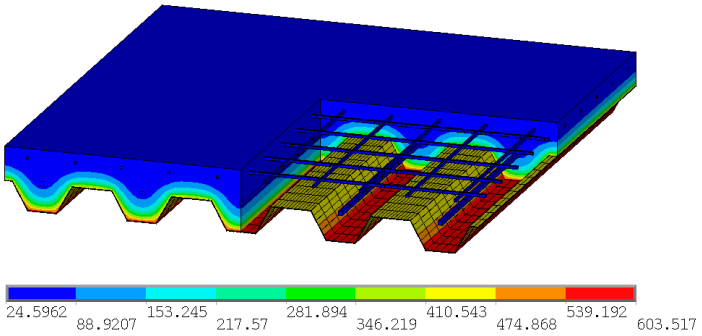

t= 15.3 min

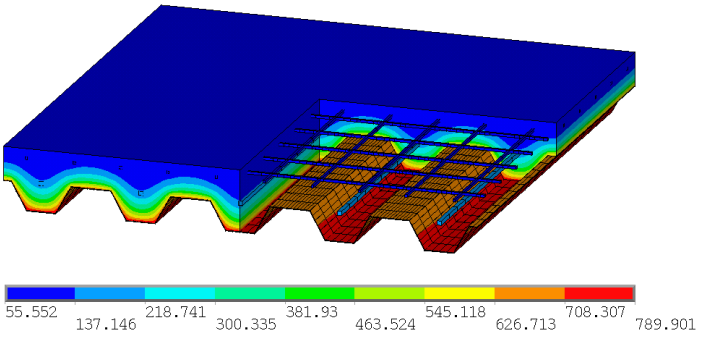

t= 30.6 min

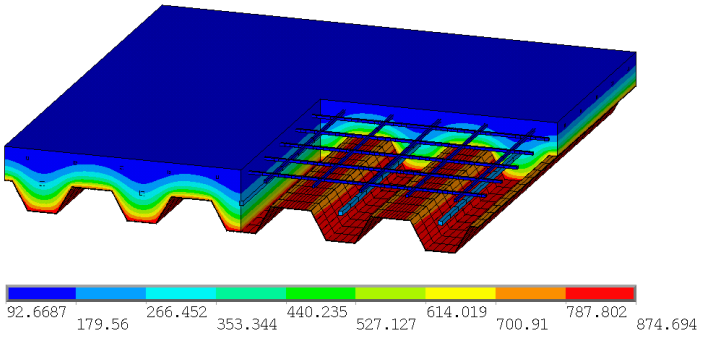

t= 45.8 min

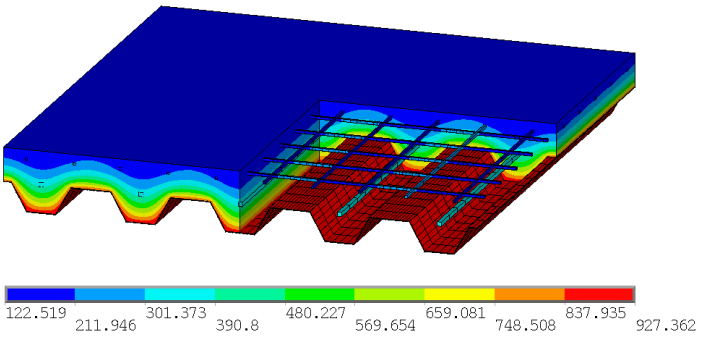

t= 61.1 min

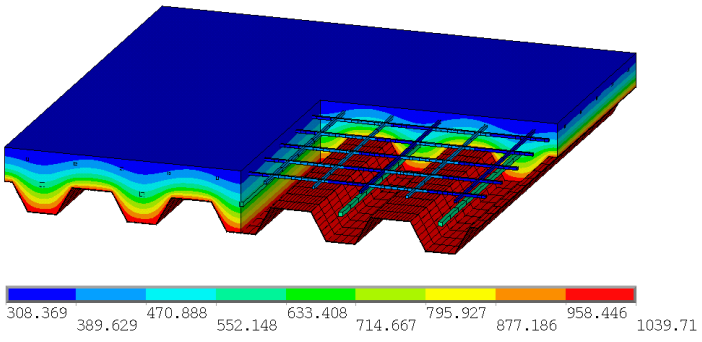

t= 120.0 min

SIM. 80	**St. deck:** Trapezoidal – ArcelorMittal Polydeck 59S	**Rebar (mm):** ϕ10	**Fire resistance (min)**	
	Mesh (mm//mm): ϕ6//100 (Q 283)	**h_1 (mm):** 81	Ave: *74.2*	Max: 78.4

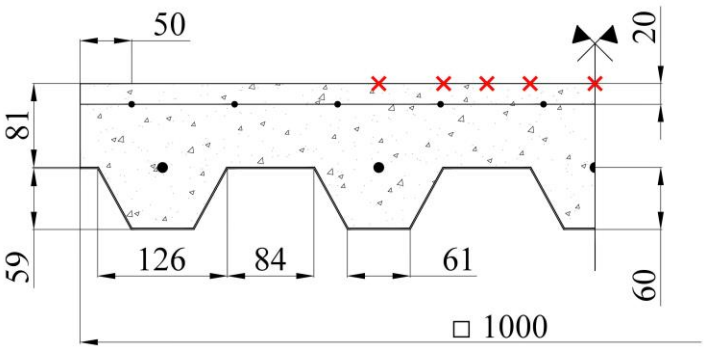

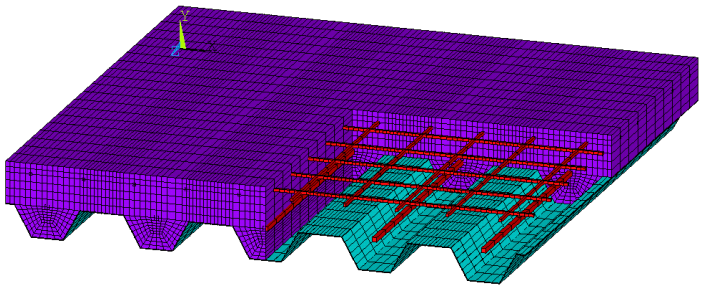

Finite element mesh

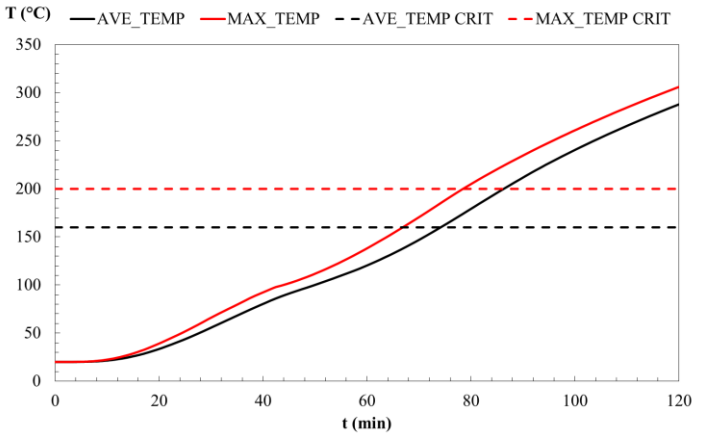

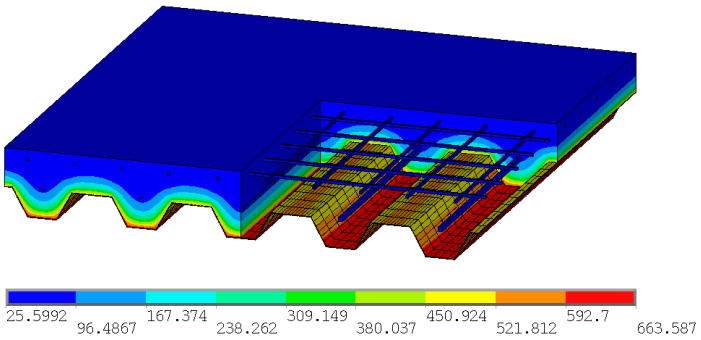

t= 18.6 min

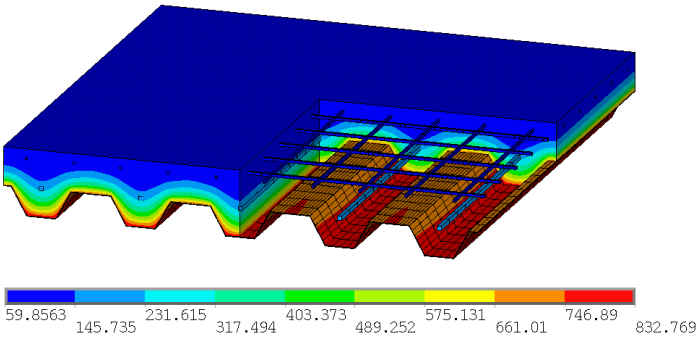

t= 37.1 min

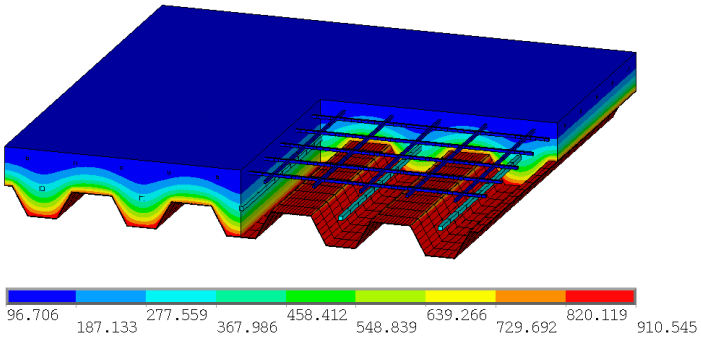

t= 55.7 min

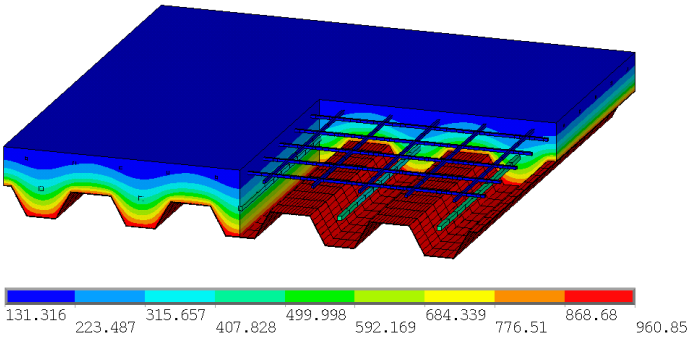

t= 74.2 min

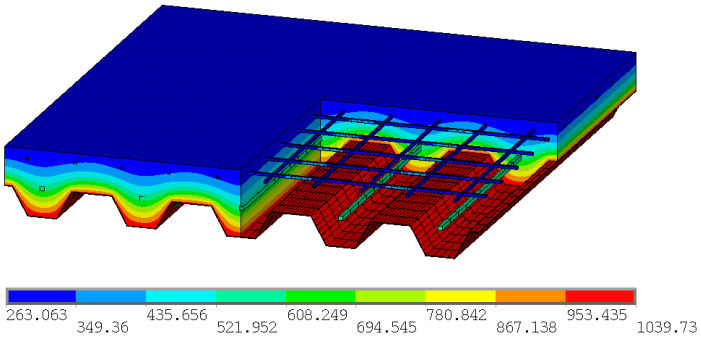

t= 120.0 min

SIM. 81	**St. deck:** Trapezoidal – ArcelorMittal Polydeck 59S	**Rebar (mm):** ϕ12	**Fire resistance (min)**	
	Mesh (mm//mm): ϕ5//100 (Q 196)	**h_1 (mm):** 51	Ave: 38.2	Max: *36.0*

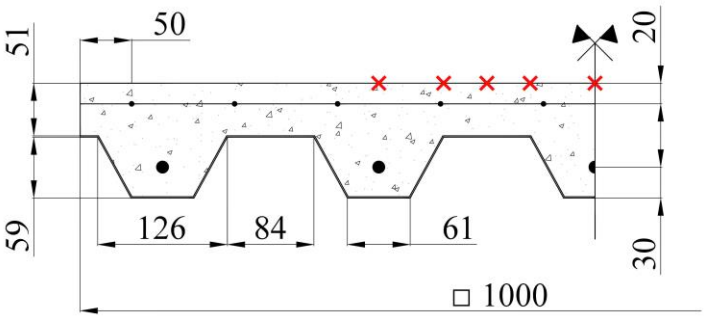

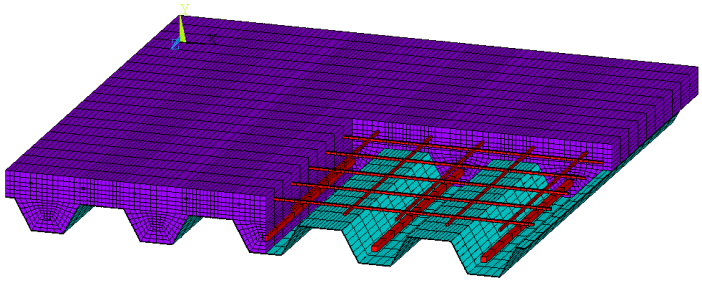

Finite element mesh

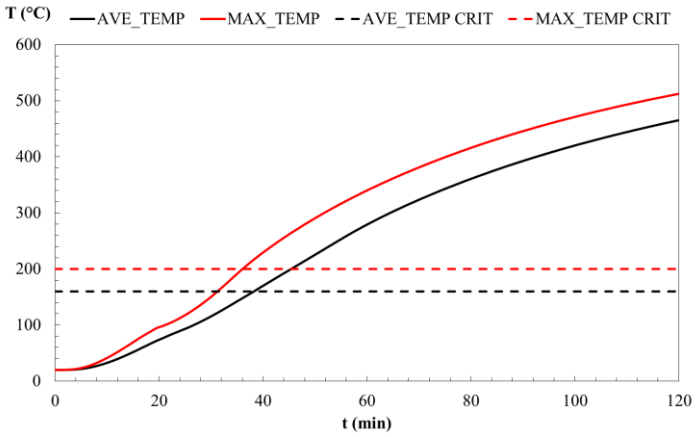

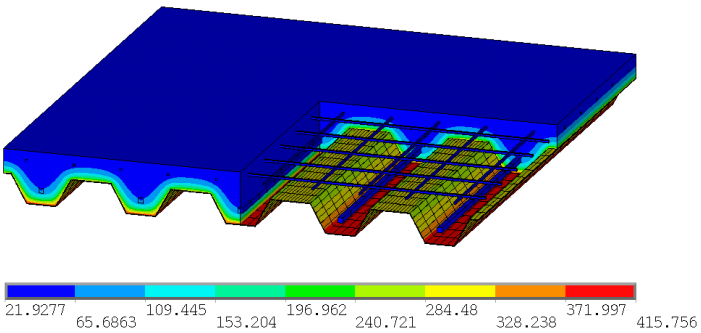

t= 9.0 min

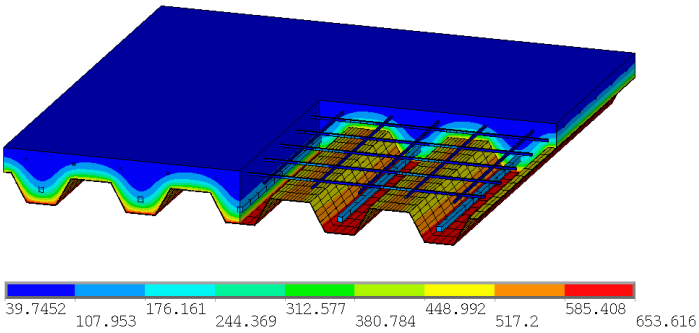

t= 18.0 min

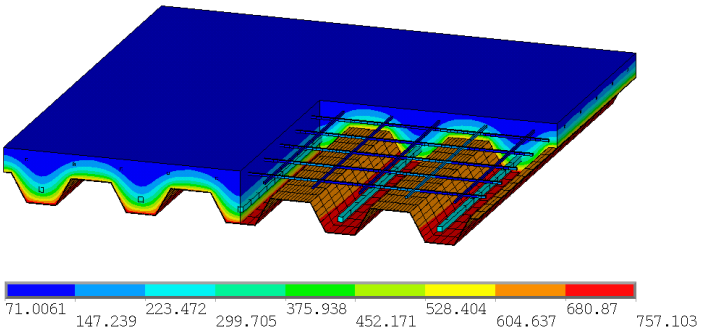

t= 27.0 min

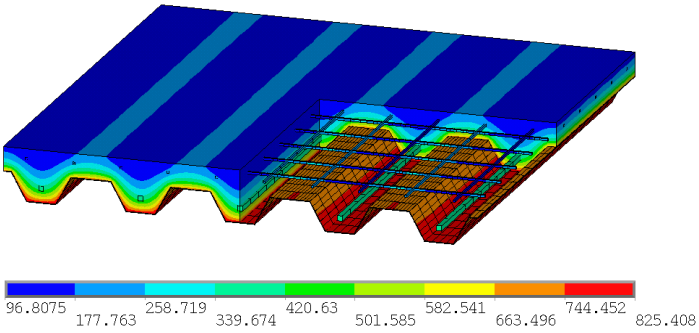

t= 36.0 min

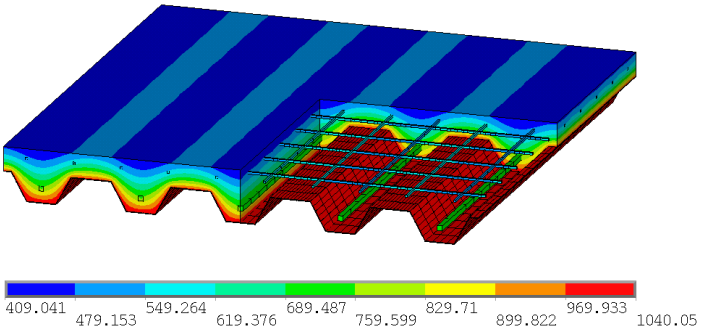

t= 120.0 min

SIM. 82	**St. deck:** Trapezoidal – ArcelorMittal Polydeck 59S	**Rebar (mm):** ϕ12	**Fire resistance (min)**	
	Mesh (mm//mm): ϕ5//100 (Q 196)	**h_1 (mm):** 61	Ave: 49.0	Max: *48.1*

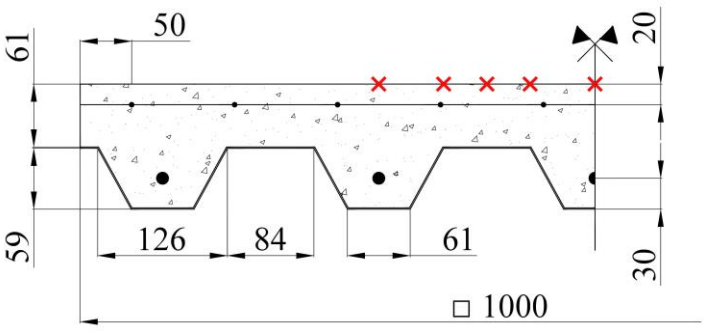

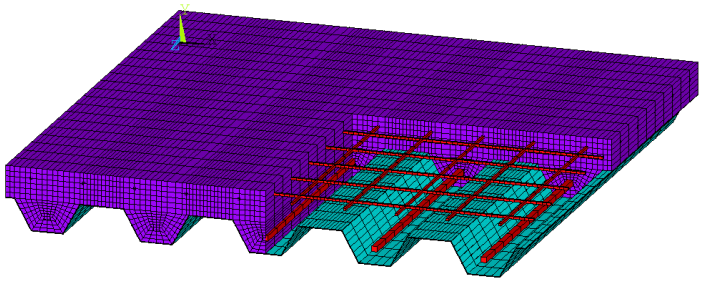

Finite element mesh

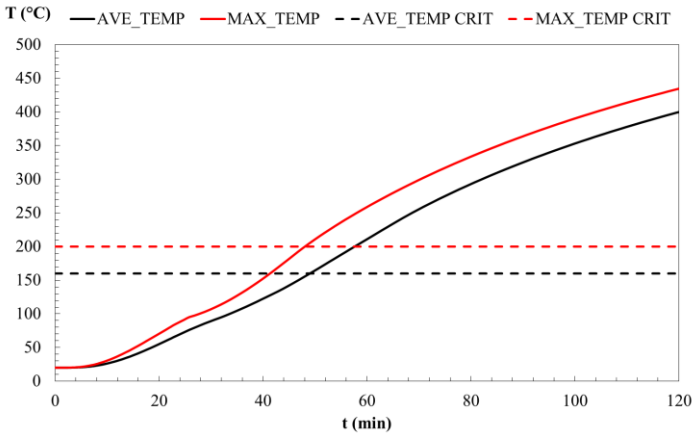

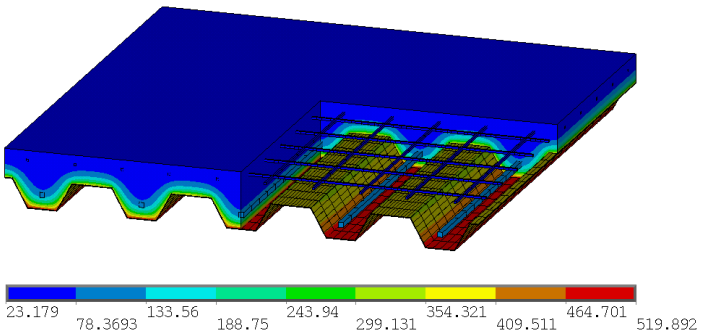

t= 12.0 min

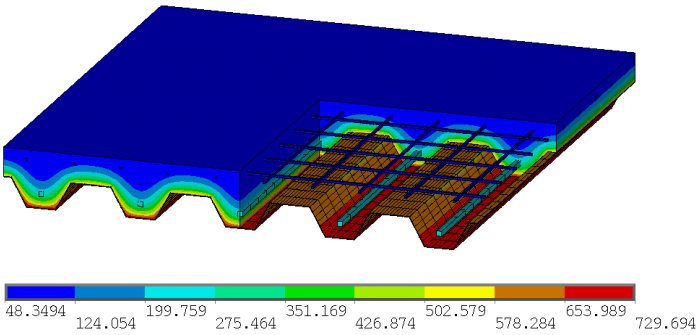

t= 24.1 min

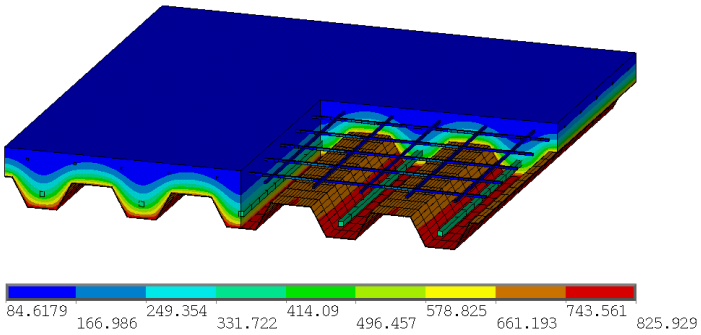

t= 36.1 min

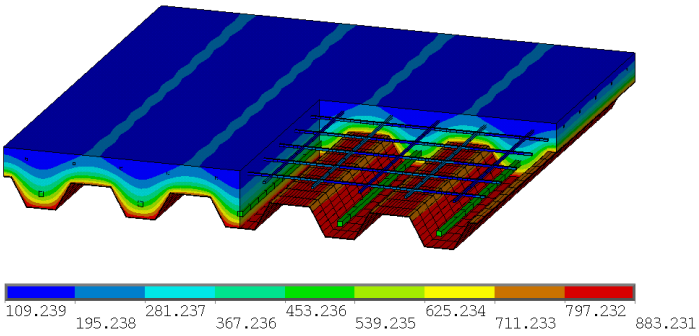

t= 48.1 min

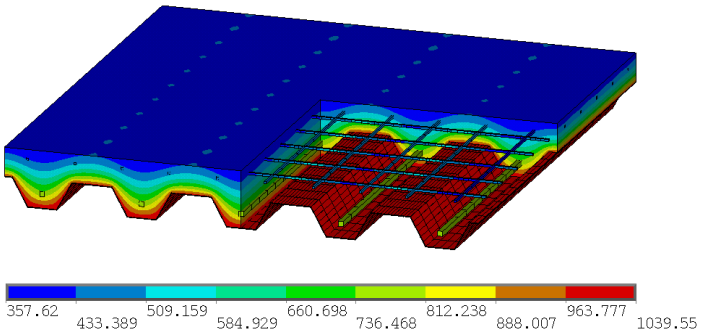

t= 120.0 min

SIM. 83	**St. deck:** Trapezoidal – ArcelorMittal Polydeck 59S	**Rebar (mm):** ϕ12	**Fire resistance (min)**	
	Mesh (mm//mm): ϕ5//100 (Q 196)	**h_1 (mm):** 71	Ave: *60.9*	Max: 62.1

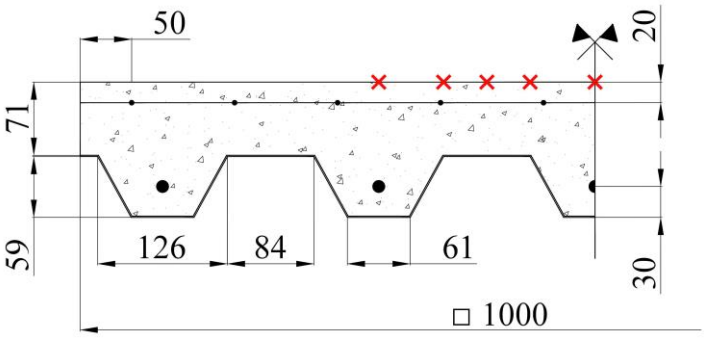

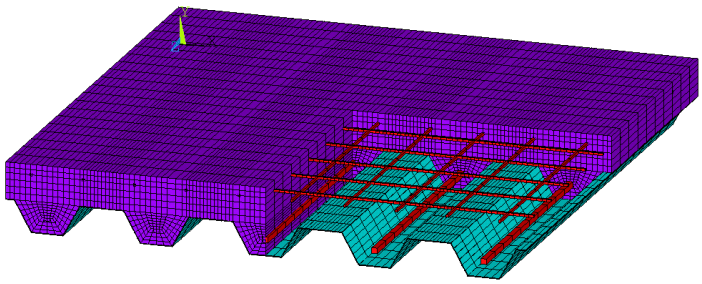

Finite element mesh

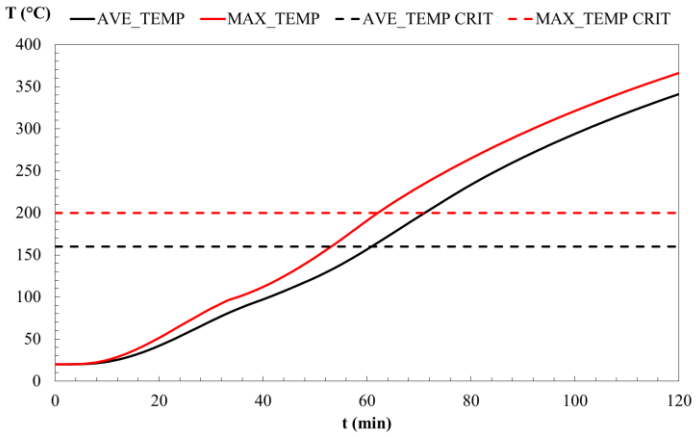

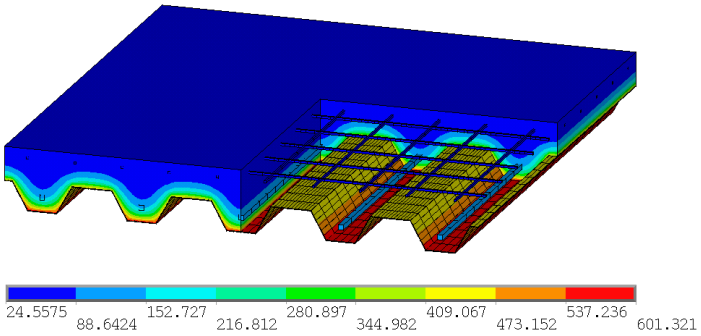

t= 15.2 min

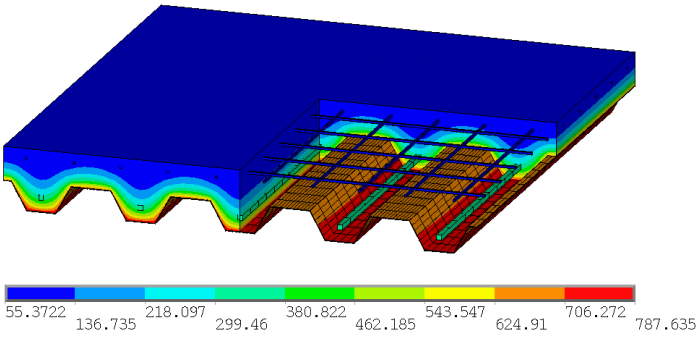

t= 30.5 min

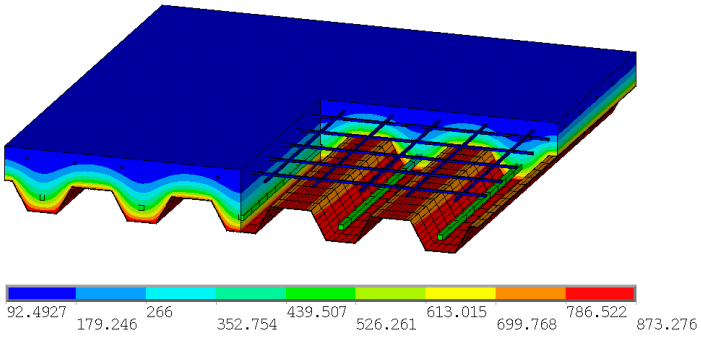

t= 45.7 min

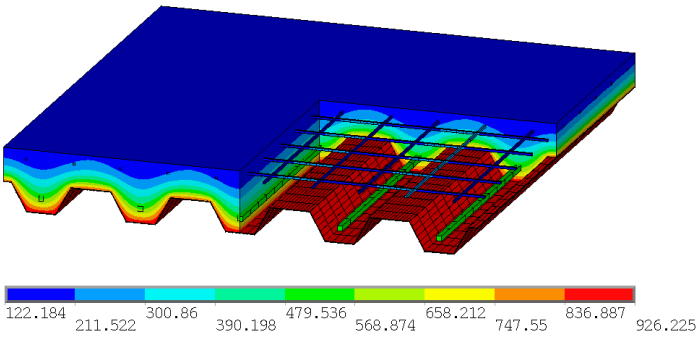

t= 60.9 min

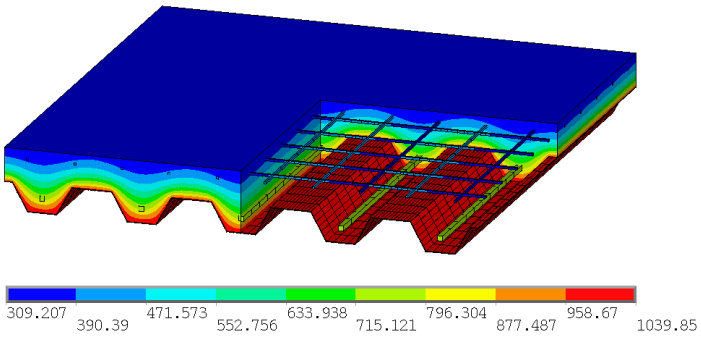

t= 120.0 min

SIM. 84	**St. deck:** Trapezoidal – ArcelorMittal Polydeck 59S	**Rebar (mm):** ϕ12	**Fire resistance (min)**	
	Mesh (mm//mm): ϕ5//100 (Q 196)	**h_1 (mm):** 81	Ave: *74.0*	Max: 78.2

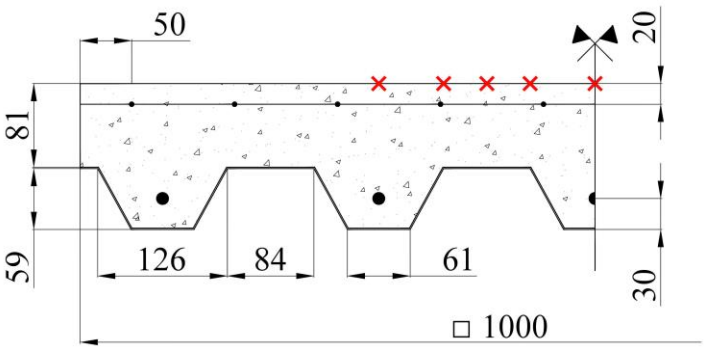

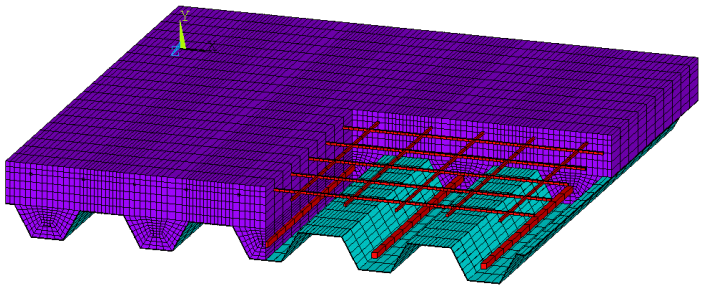

Finite element mesh

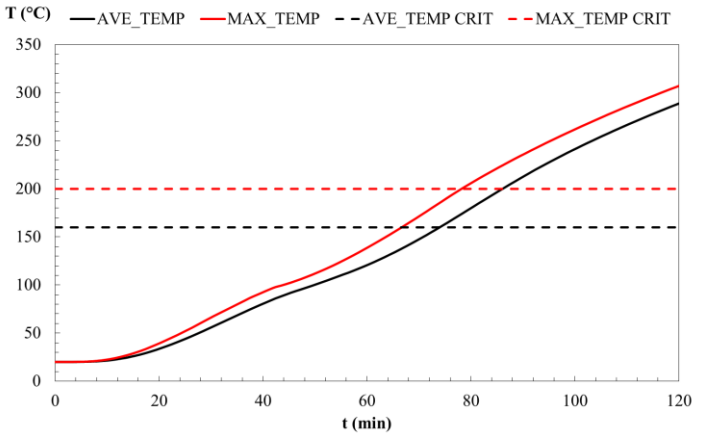

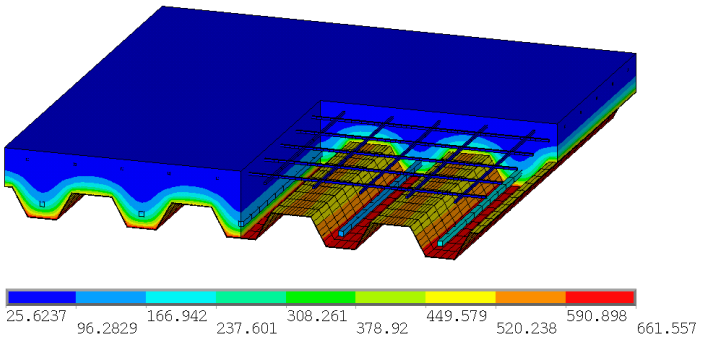

t= 18.5 min

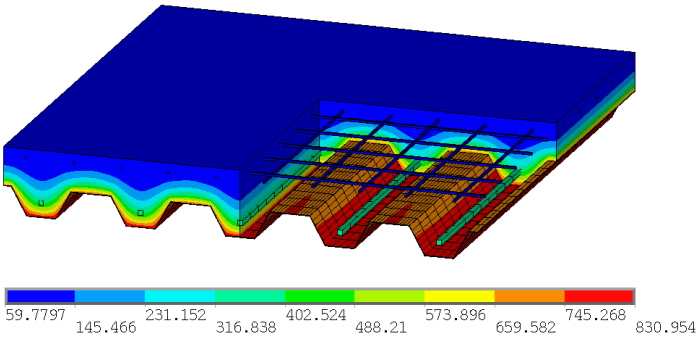

t= 37.0 min

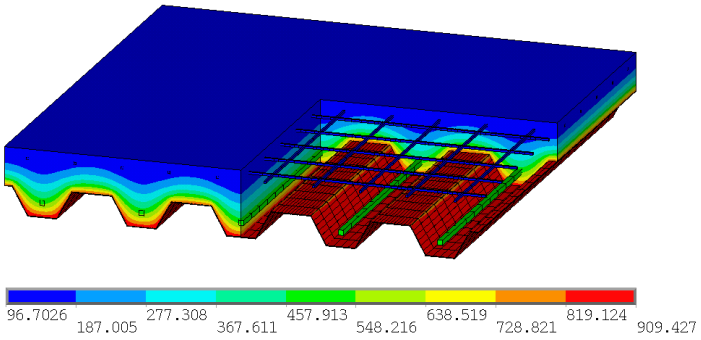

t= 55.5 min

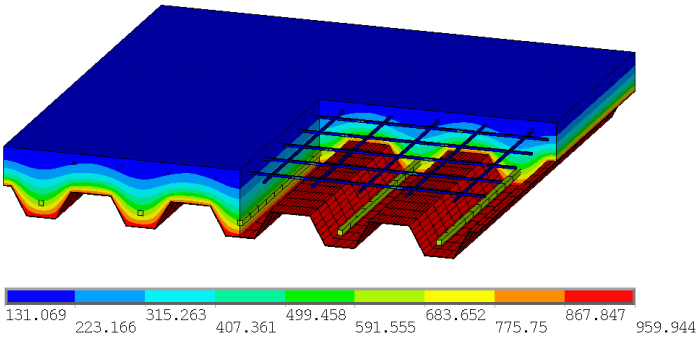

t= 74.0 min

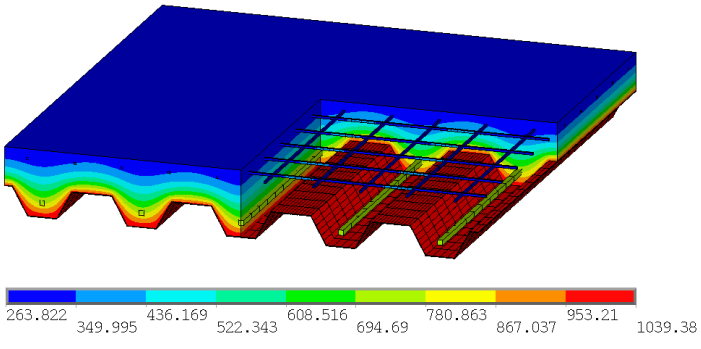

t= 120.0 min

SIM. 85	**St. deck:** Trapezoidal – ArcelorMittal Polydeck 59S	**Rebar (mm):** ϕ12	**Fire resistance (min)**	
	Mesh (mm//mm): ϕ5//100 (Q 196)	**h_1 (mm):** 51	Ave: 38.2	Max: *36.0*

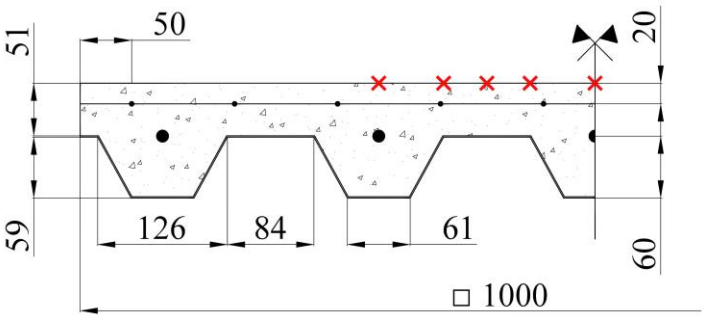

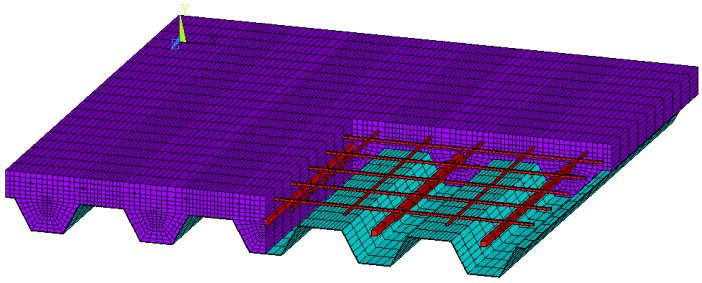

Finite element mesh

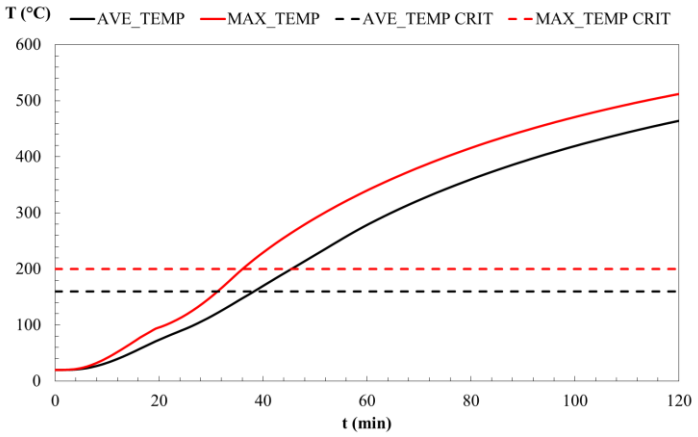

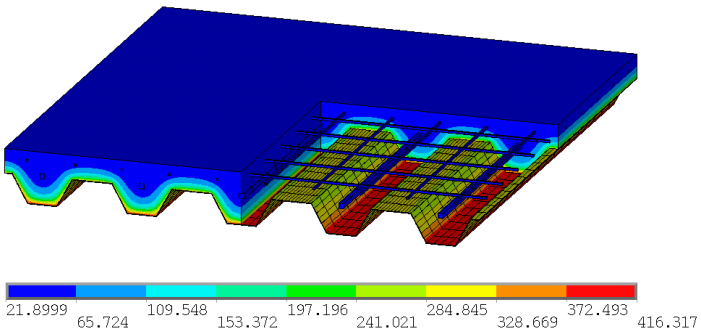

t= 9.0 min

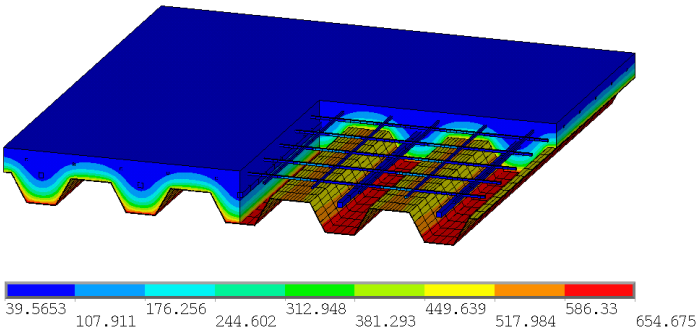

t= 18.0 min

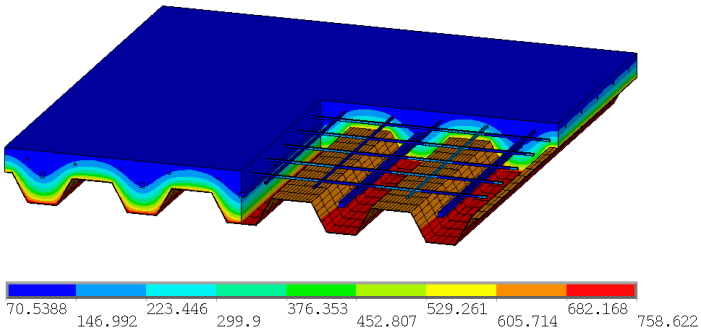

t= 27.0 min

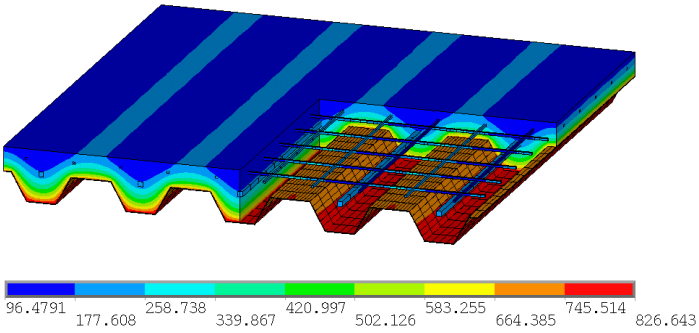

t= 36.0 min

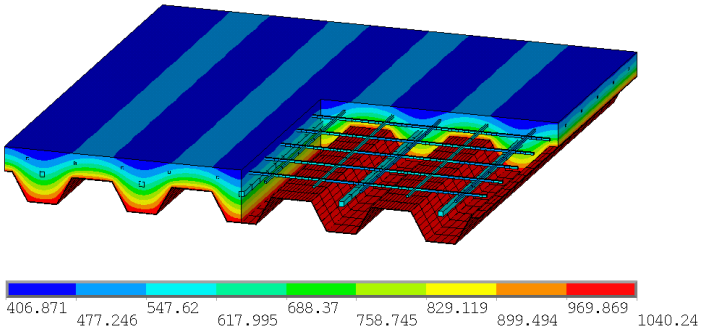

t= 120.0 min

SIM. 86	**St. deck:** Trapezoidal – ArcelorMittal Polydeck 59S	**Rebar (mm):** ϕ12	**Fire resistance (min)**	
	Mesh (mm//mm): ϕ5//100 (Q 196)	**h_1 (mm):** 61	Ave: 49.0	Max: *48.0*

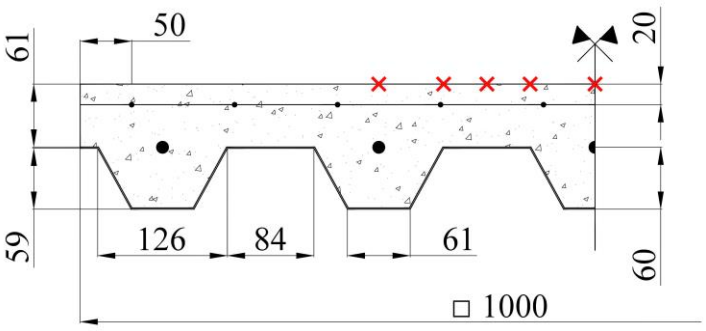

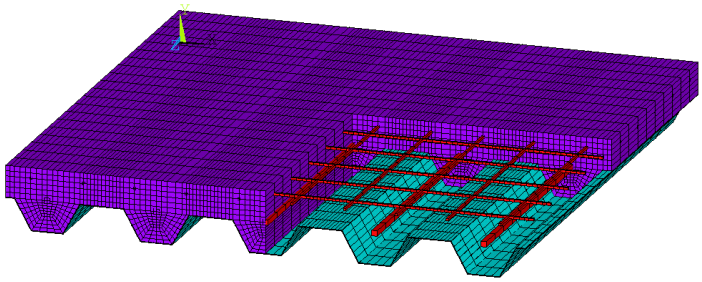

Finite element mesh

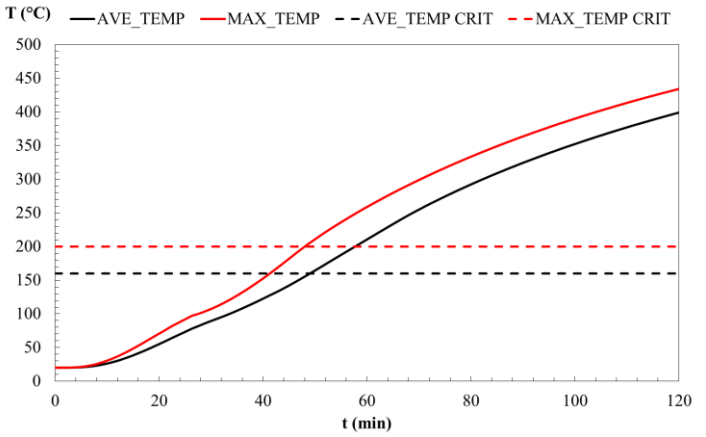

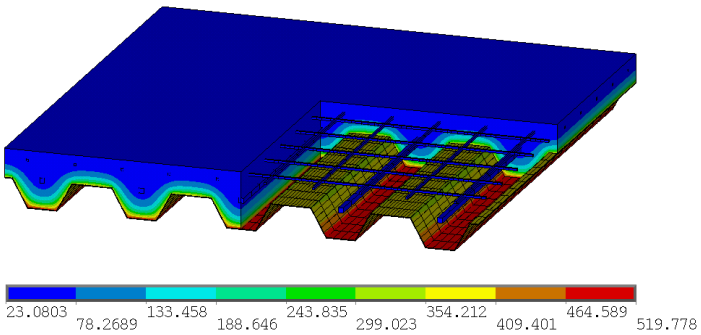

t= 12.0 min

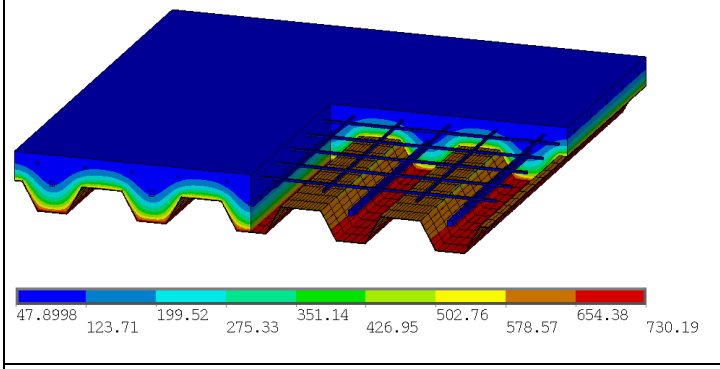

t= 24.0 min

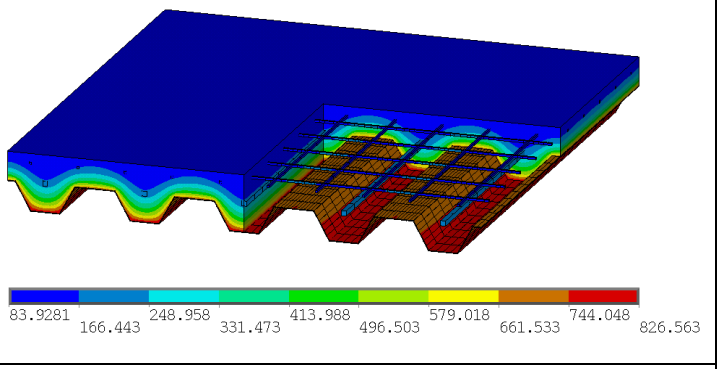

t= 36.0 min

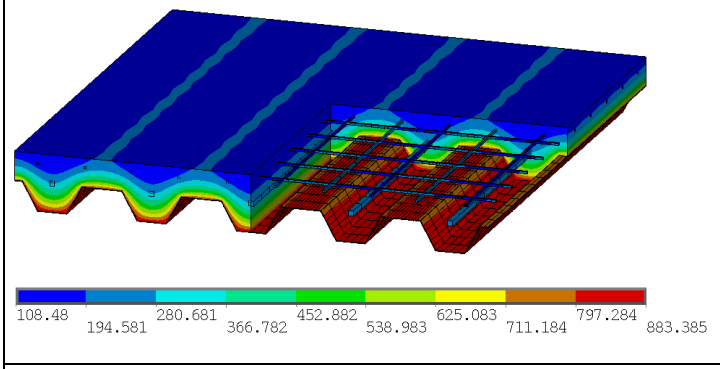

t= 48.0 min

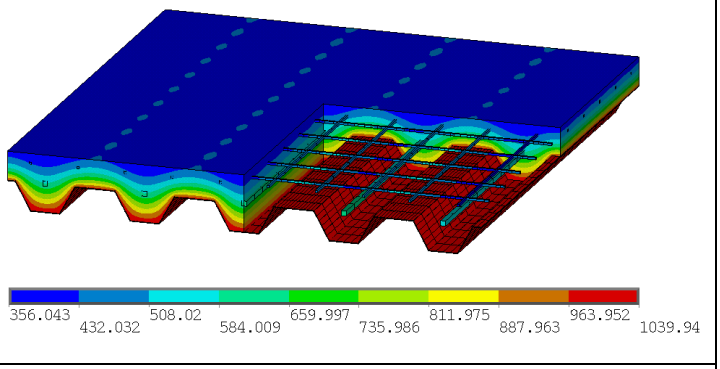

t= 120.0 min

SIM. 87	**St. deck:** Trapezoidal – ArcelorMittal Polydeck 59S	**Rebar (mm):** ϕ12	**Fire resistance (min)**	
	Mesh (mm//mm): ϕ5//100 (Q 196)	**h_1 (mm):** 71	Ave: *61.0*	Max: 62.2

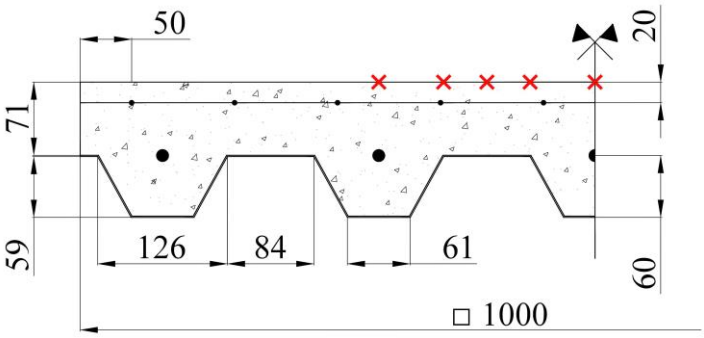

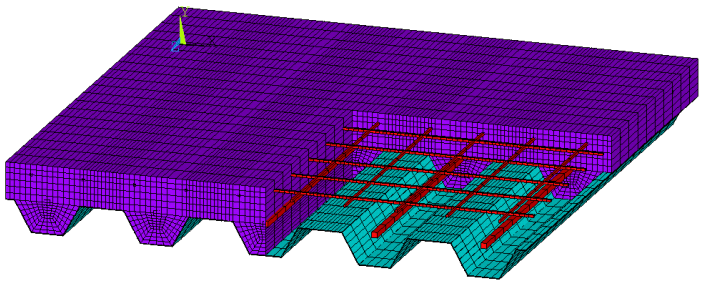

Finite element mesh

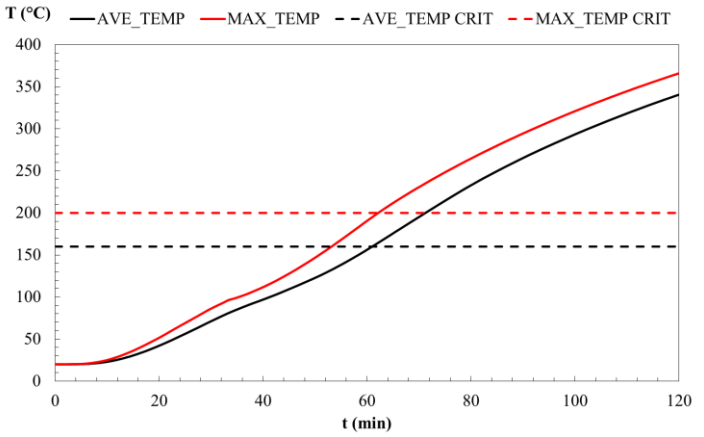

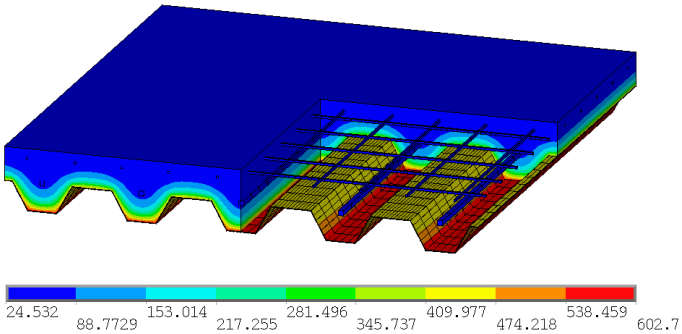

t= 15.3 min

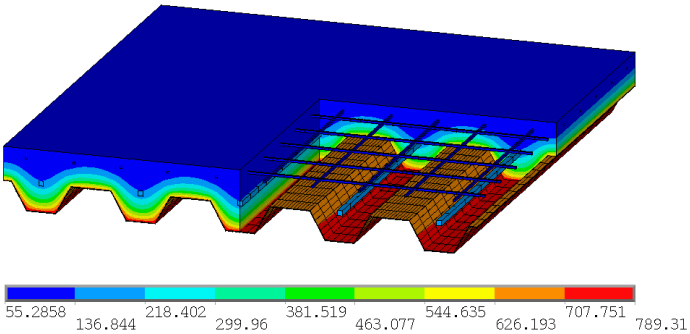

t= 30.5 min

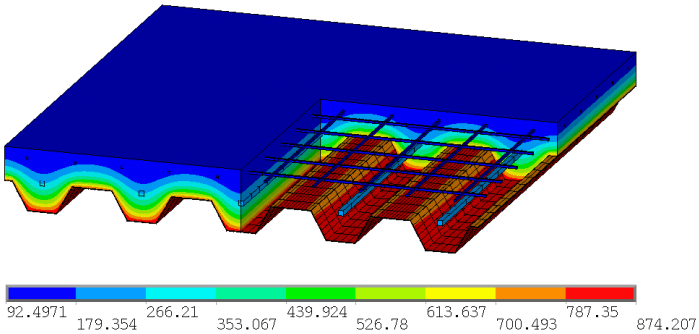

t= 45.8 min

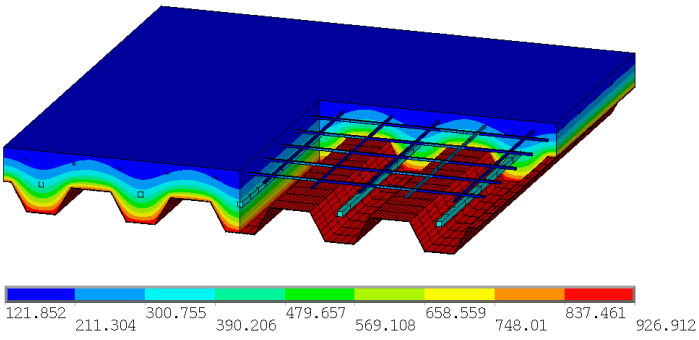

t= 61.0 min

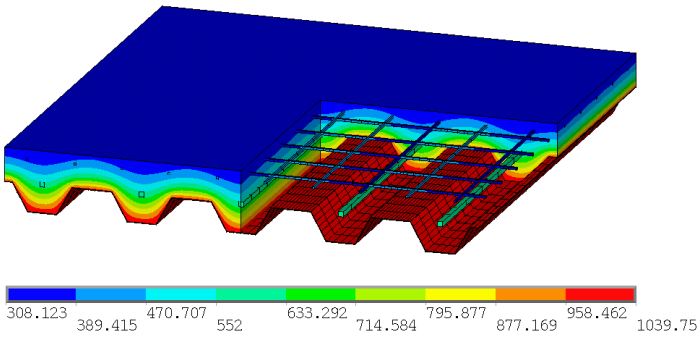

t= 120.0 min

SIM. 88	**St. deck:** Trapezoidal – ArcelorMittal Polydeck 59S	**Rebar (mm):** ϕ12	**Fire resistance (min)**	
	Mesh (mm//mm): ϕ5//100 (Q 196)	**h_1 (mm):** 81	Ave: *74.1*	Max: 78.2

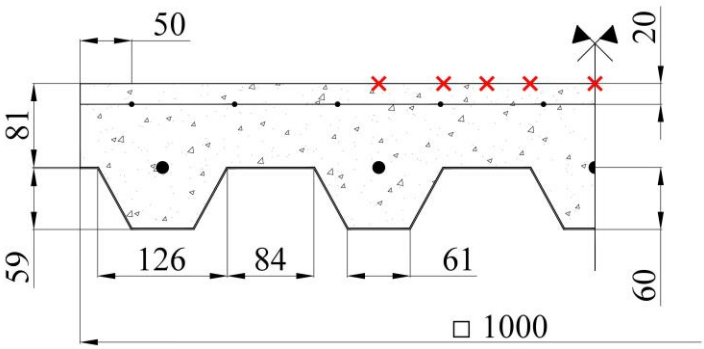

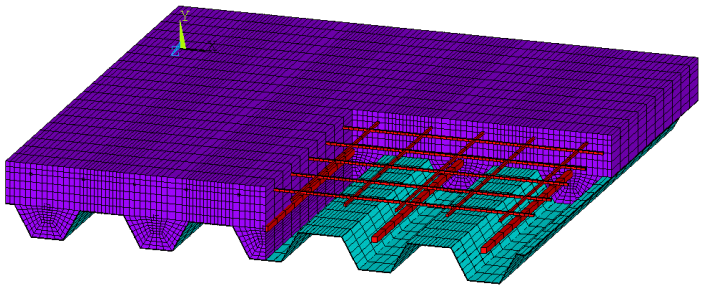

Finite element mesh

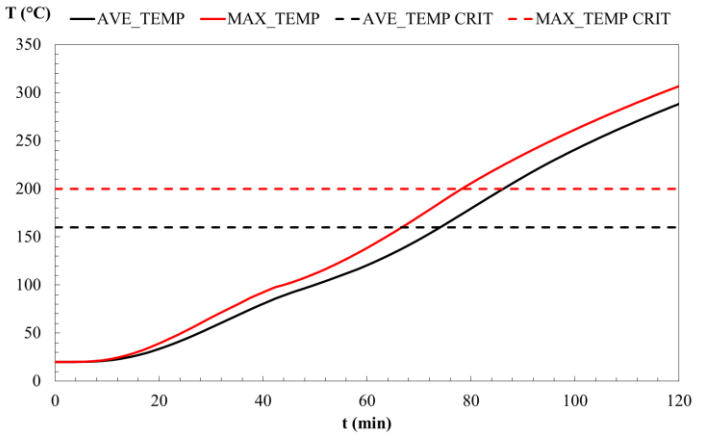

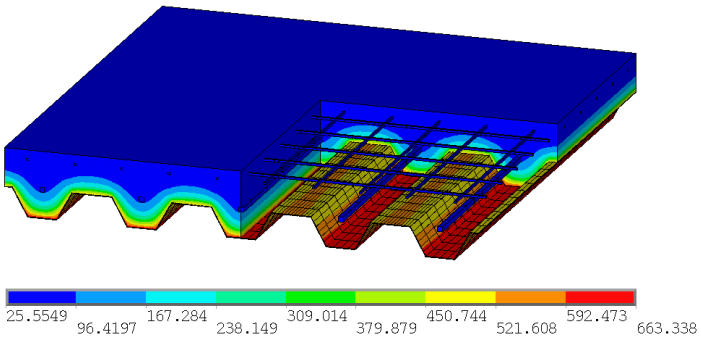

t= 18.5 min

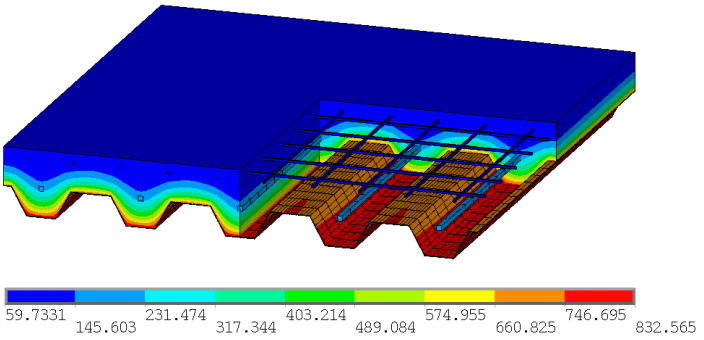

t= 37.1 min

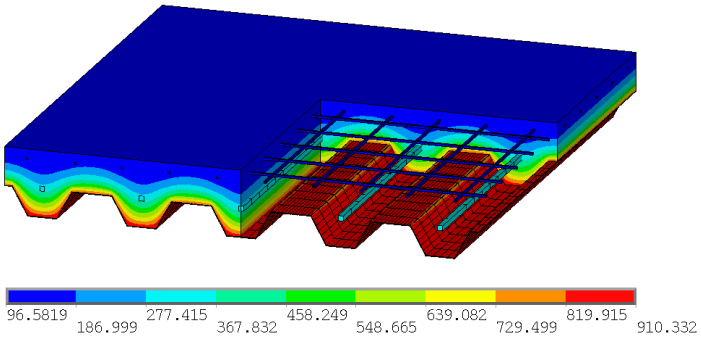

t= 55.6 min

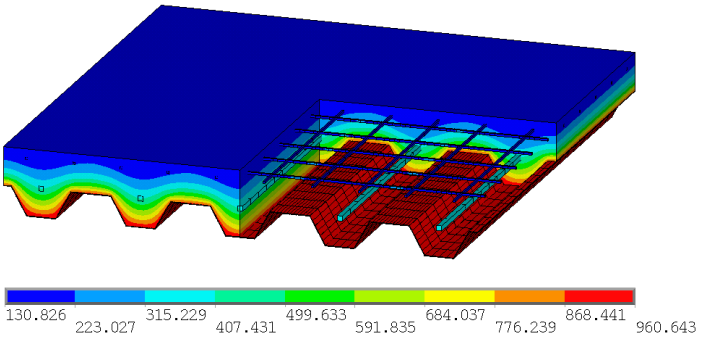

t= 74.1 min

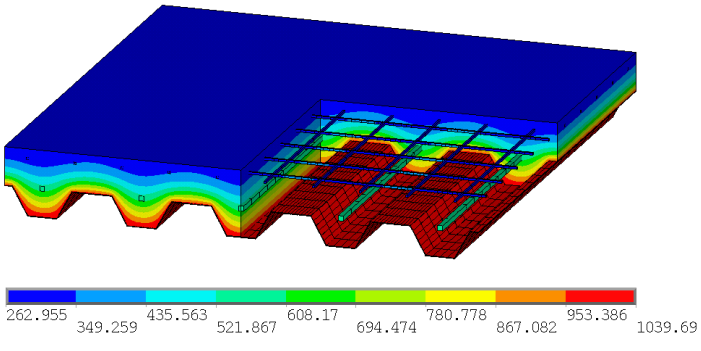

t= 120.0 min

SIM. 89	**St. deck:** Trapezoidal – ArcelorMittal Polydeck 59S	**Rebar (mm):** ϕ12	**Fire resistance (min)**	
	Mesh (mm//mm): ϕ6//100 (Q 283)	**h_1 (mm):** 51	Ave: 38.4	Max: *36.2*

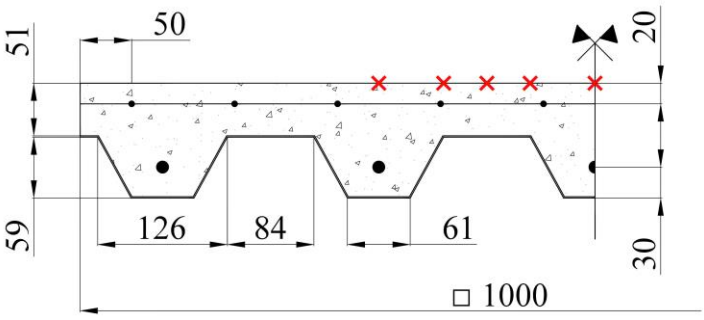

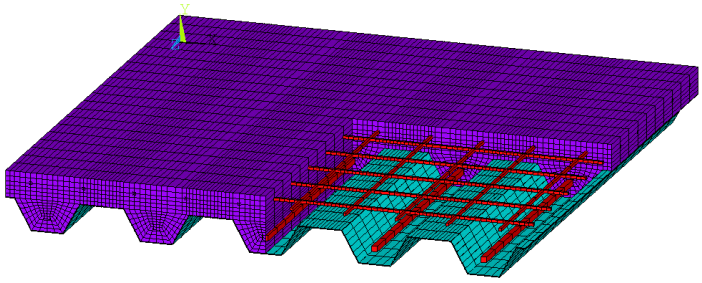

Finite element mesh

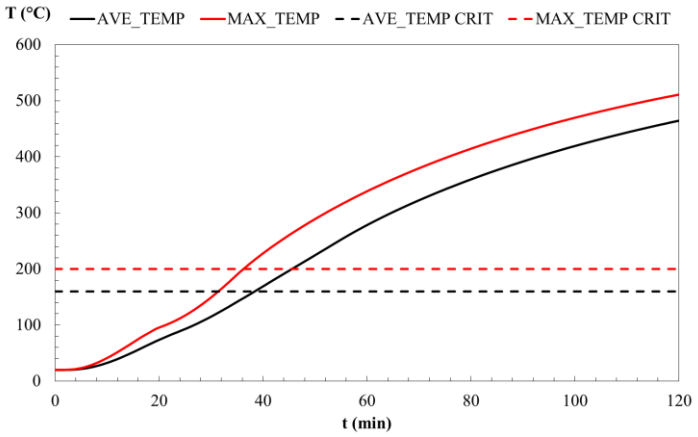

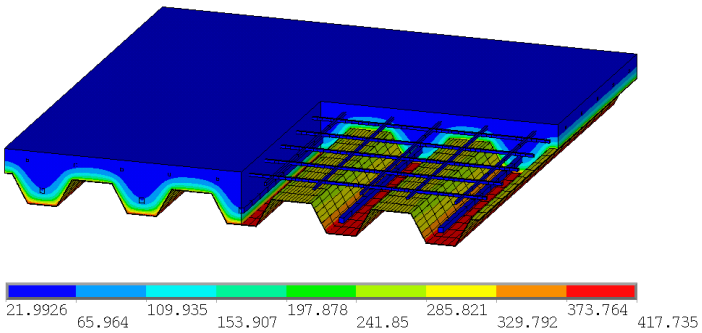

t= 9.1 min

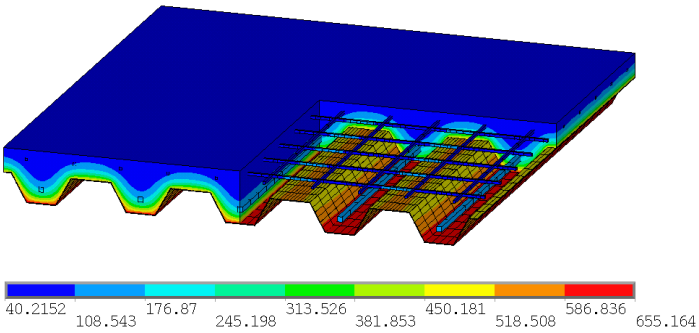

t= 18.1 min

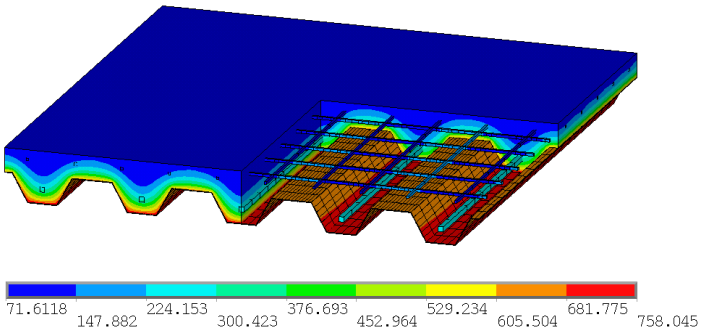

t= 27.2 min

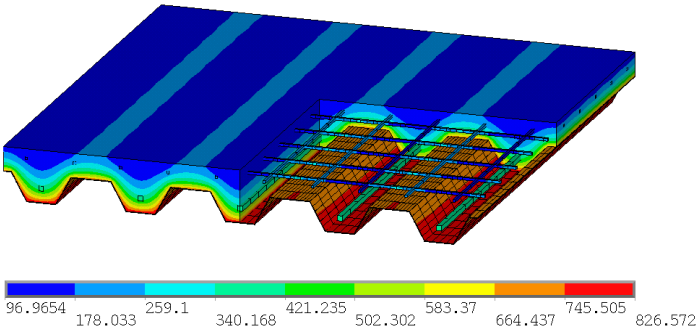

t= 36.2 min

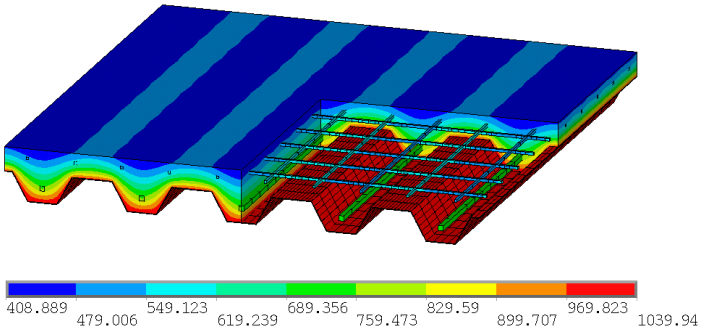

t= 120.0 min

SIM. 90	**St. deck:** Trapezoidal – ArcelorMittal Polydeck 59S	**Rebar (mm):** ϕ12	**Fire resistance (min)**	
	Mesh (mm//mm): ϕ6//100 (Q 283)	**h_1 (mm):** 61	Ave: 49.2	Max: *48.2*

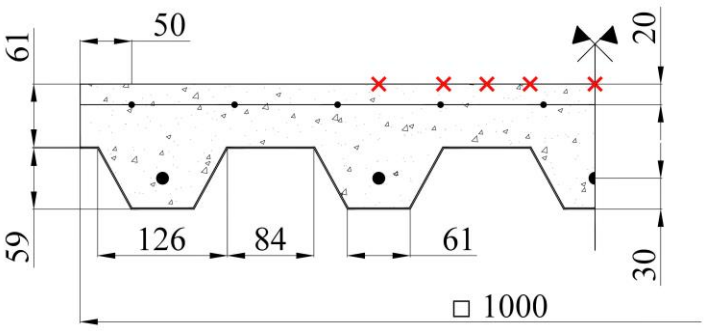

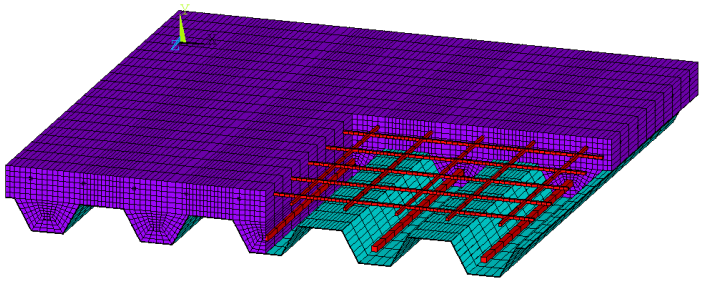

Finite element mesh

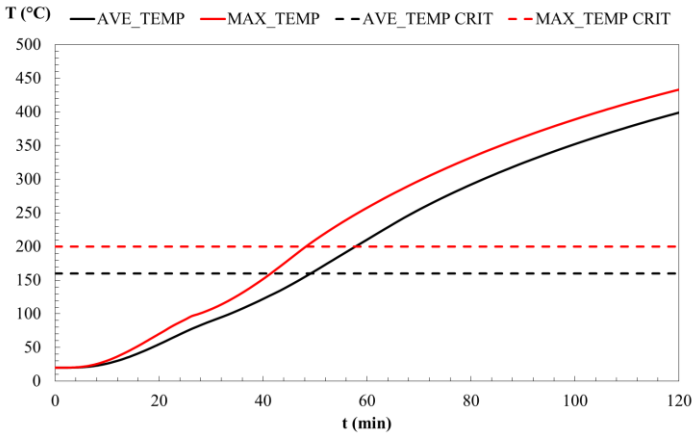

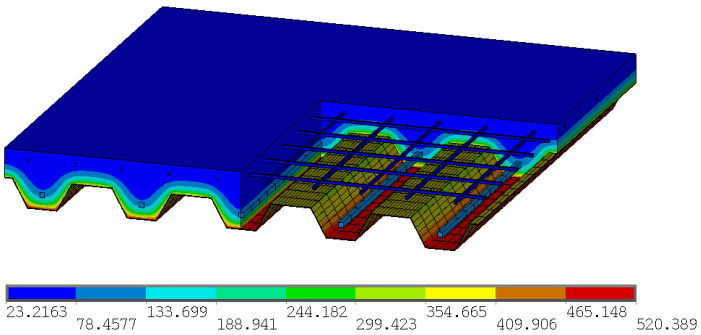

t= 12.1 min

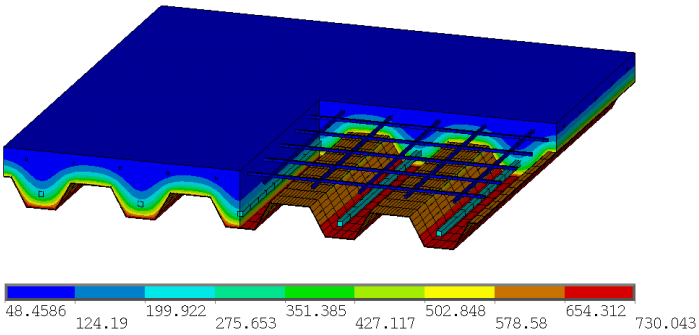

t= 24.1 min

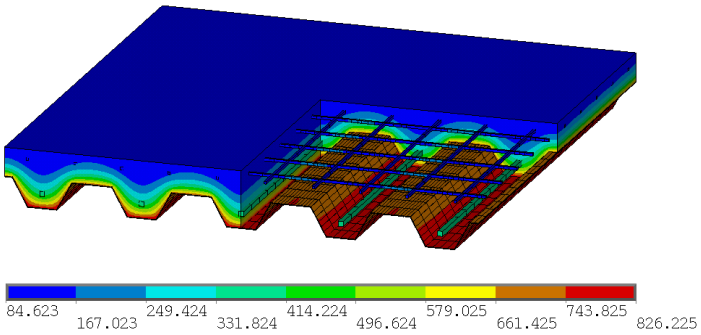

t= 36.2 min

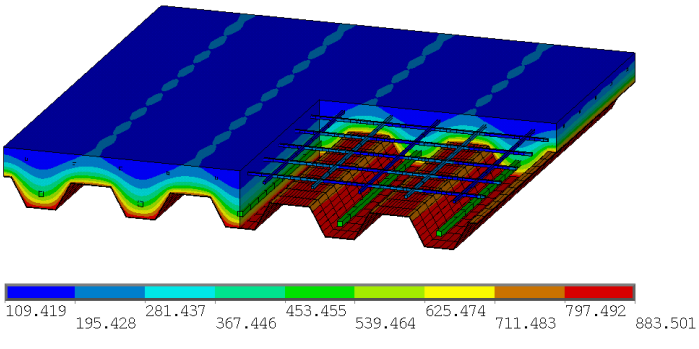

t= 48.2 min

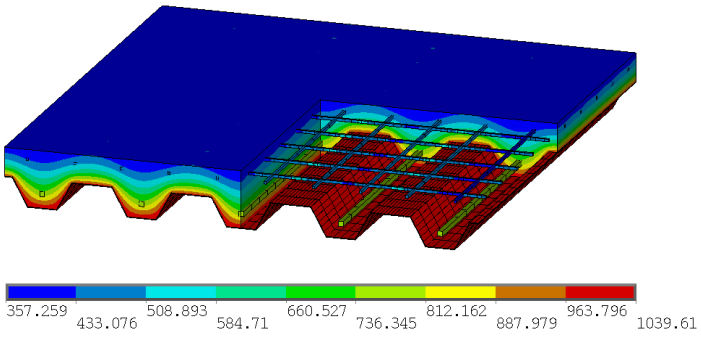

t= 120.0 min

SIM. 91	**St. deck:** Trapezoidal – ArcelorMittal Polydeck 59S	**Rebar (mm):** ϕ12	**Fire resistance (min)**	
	Mesh (mm//mm): ϕ6//100 (Q 283)	**h_1 (mm):** 71	Ave: *61.0*	Max: 62.3

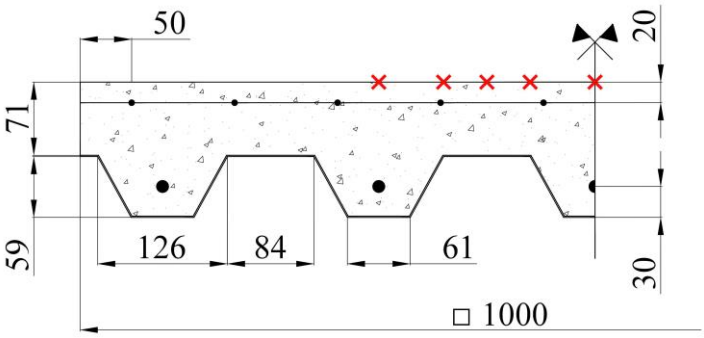

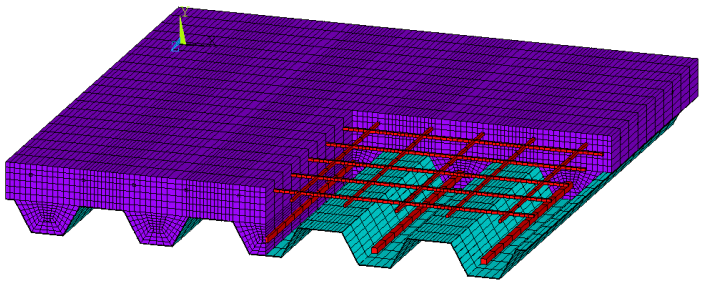

Finite element mesh

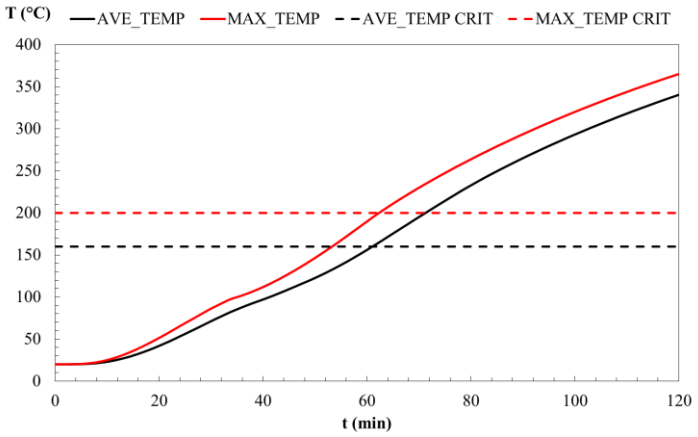

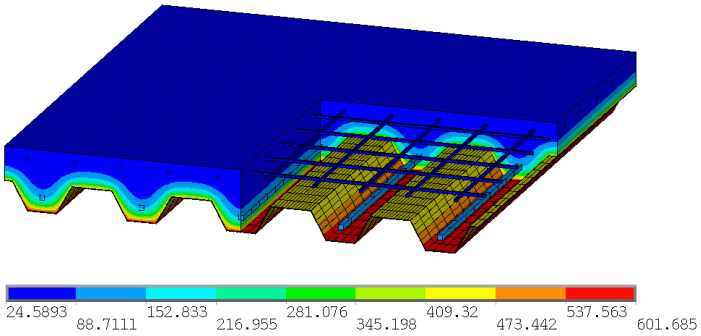

t= 15.3 min

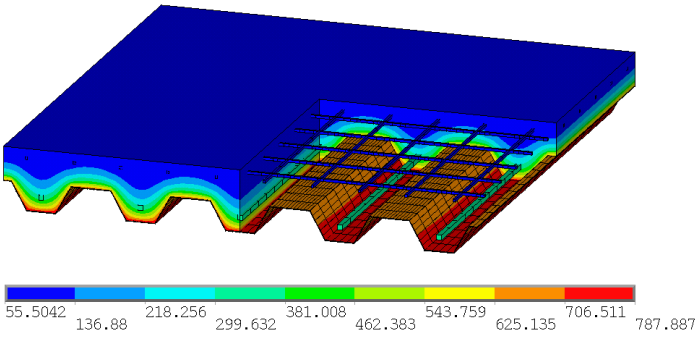

t= 30.5 min

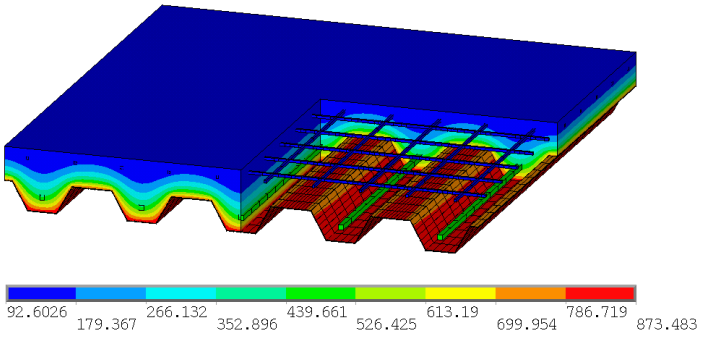

t= 45.8 min

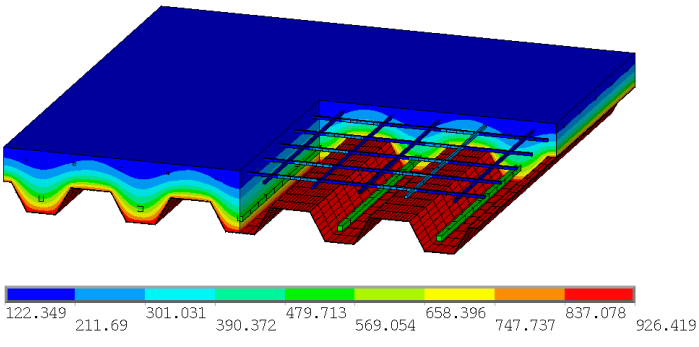

t= 61.0 min

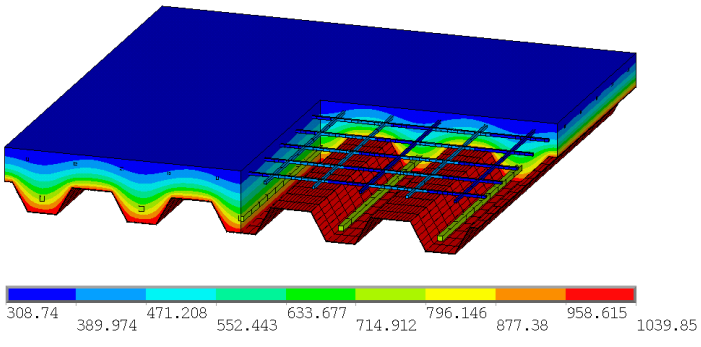

t= 120.0 min

SIM. 92	**St. deck:** Trapezoidal – ArcelorMittal Polydeck 59S	**Rebar (mm):** ϕ12	**Fire resistance (min)**	
	Mesh (mm//mm): ϕ6//100 (Q 283)	**h_1 (mm):** 81	Ave: *74.2*	Max: 78.5

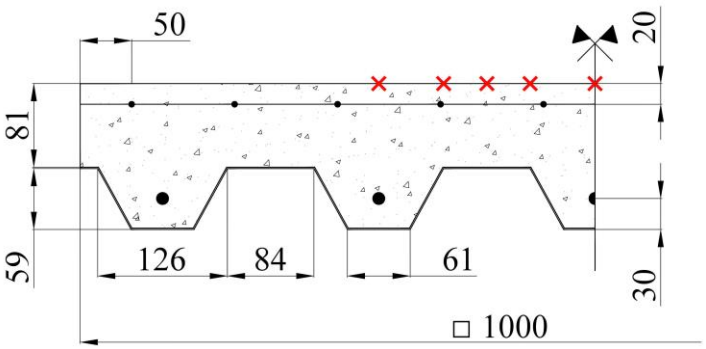

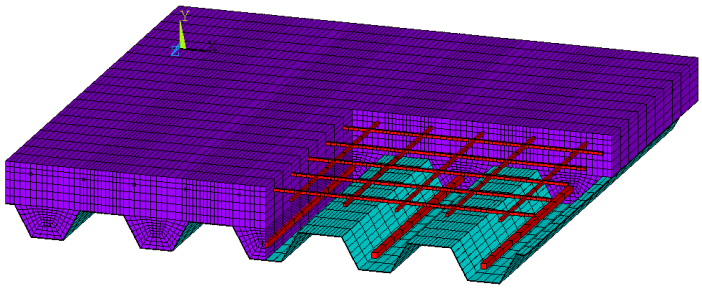

Finite element mesh

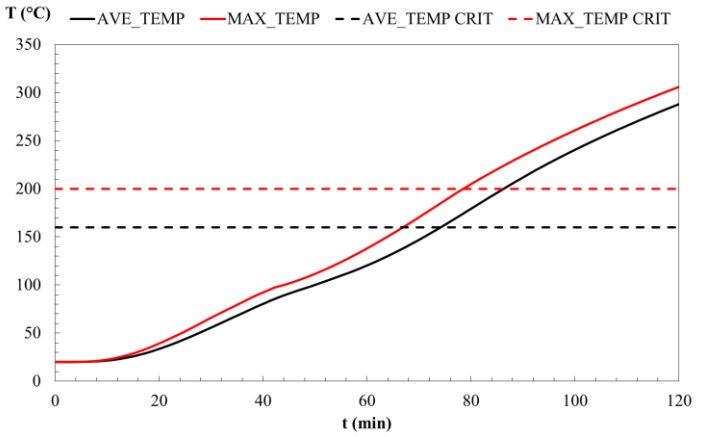

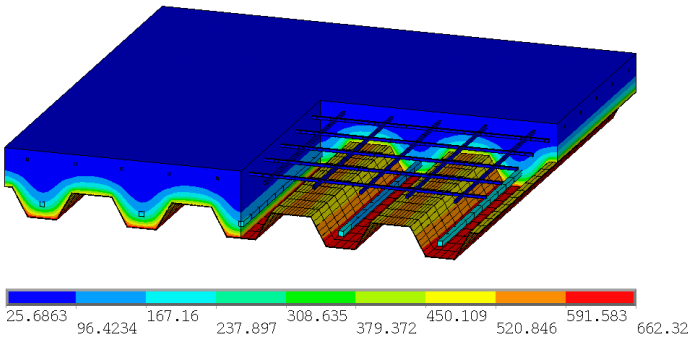

t= 18.6 min

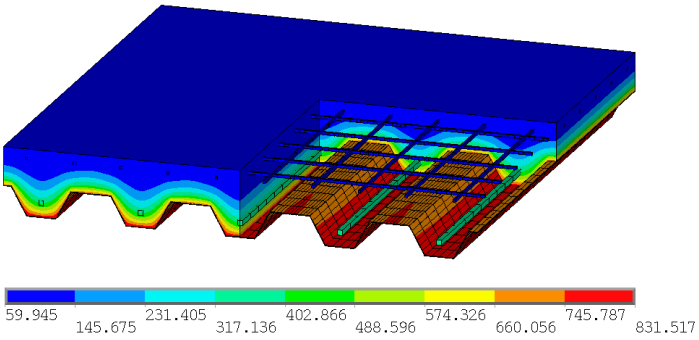

t= 37.1 min

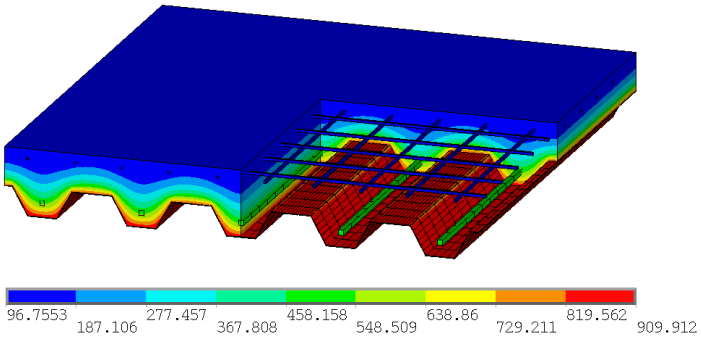

t= 55.7 min

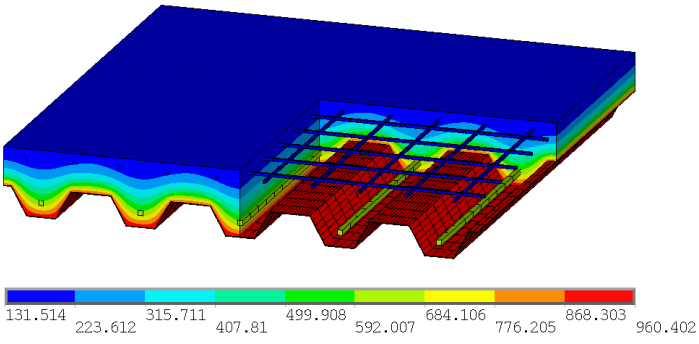

t= 74.2 min

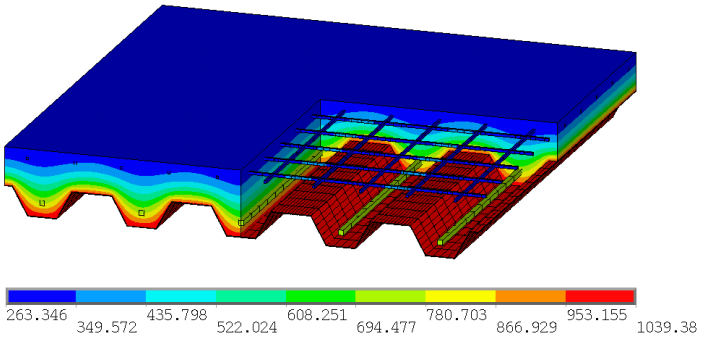

t= 120.0 min

SIM. 93	**St. deck:** Trapezoidal – ArcelorMittal Polydeck 59S	**Rebar (mm):** ϕ12	**Fire resistance (min)**	
	Mesh (mm//mm): ϕ6//100 (Q 283)	**h_1 (mm):** 51	Ave: 38.4	Max: *36.2*

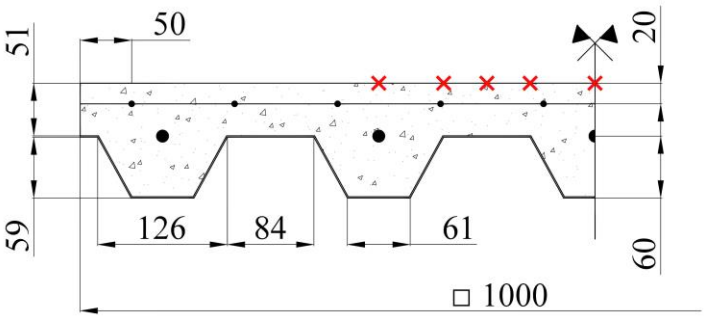

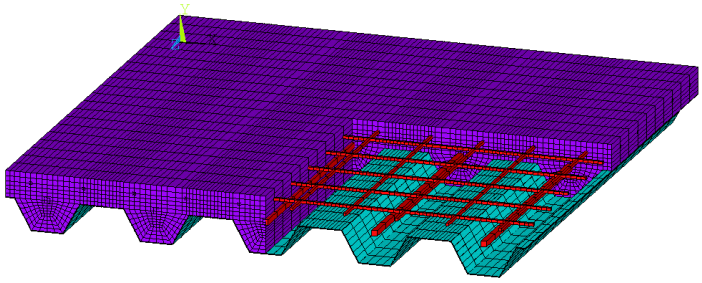

Finite element mesh

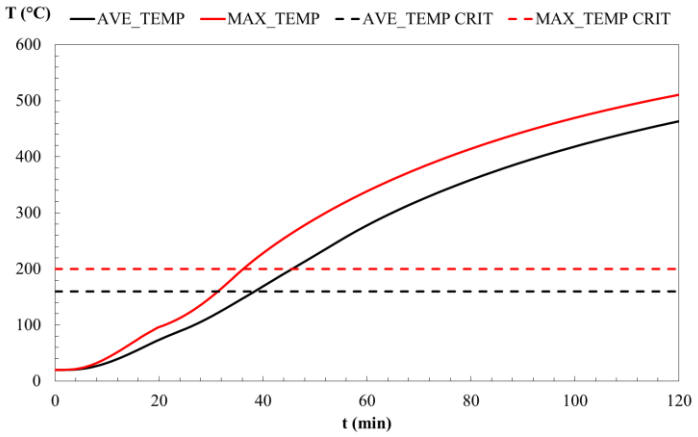

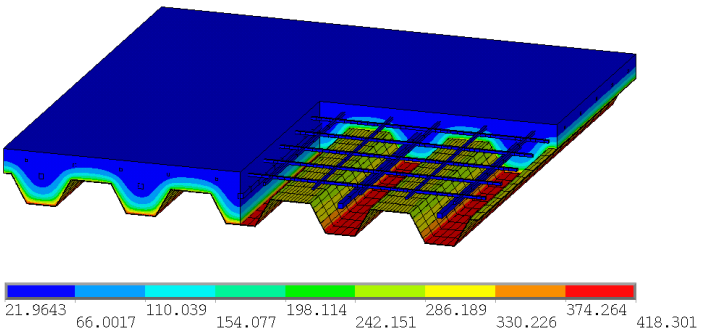

t= 9.1 min

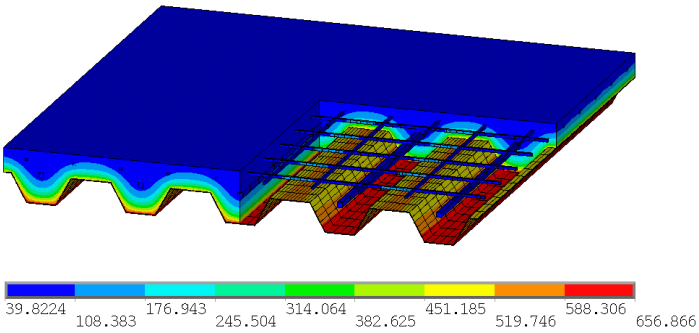

t= 18.1 min

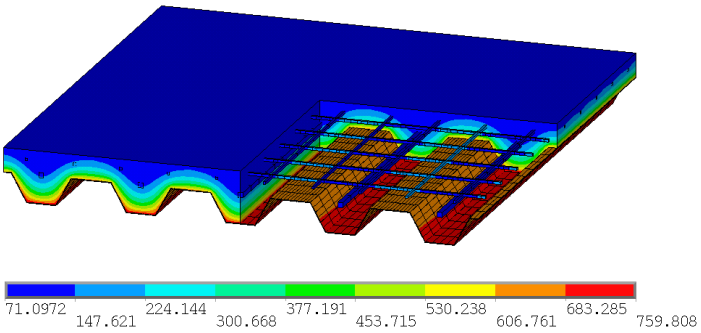

t= 27.2 min

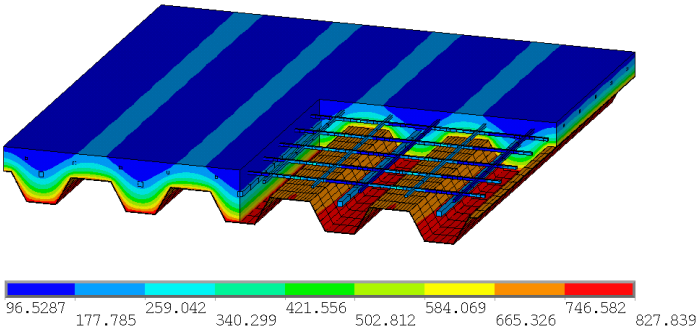

t= 36.2 min

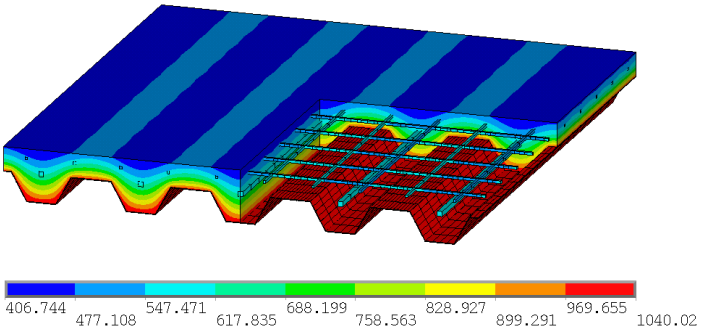

t= 120.0 min

SIM. 94	**St. deck:** Trapezoidal – ArcelorMittal Polydeck 59S	**Rebar (mm):** ϕ12	**Fire resistance (min)**	
	Mesh (mm//mm): ϕ6//100 (Q 283)	**h_1 (mm):** 61	Ave: 49.2	Max: *48.3*

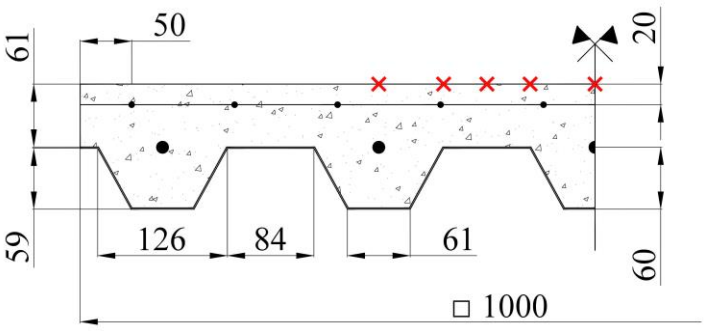

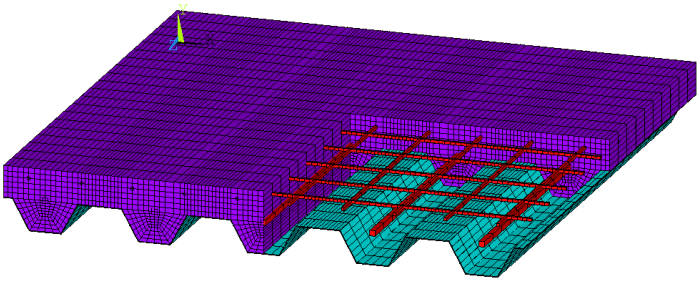

Finite element mesh

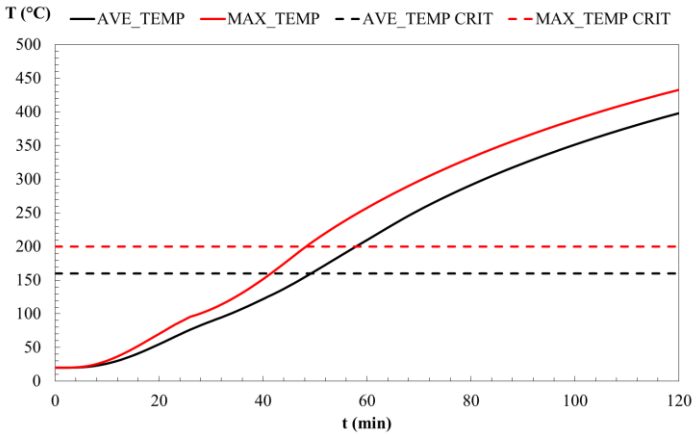

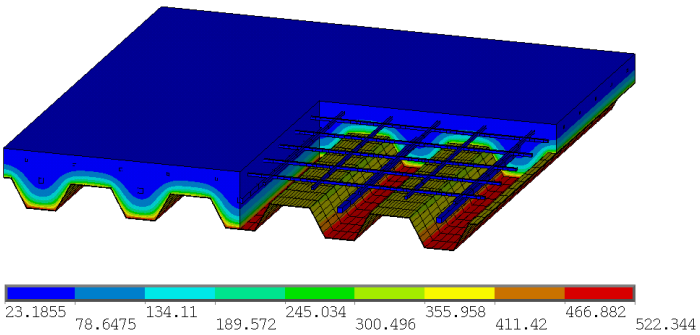

t= 12.1 min

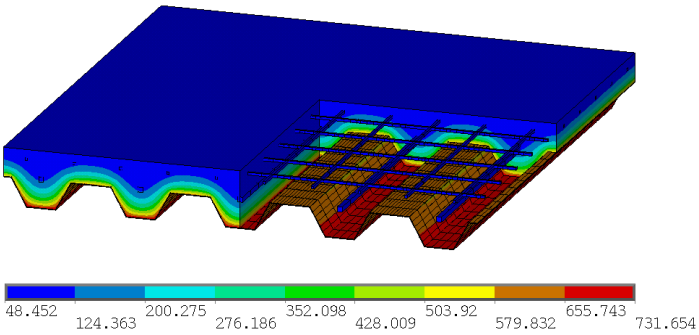

t= 24.2 min

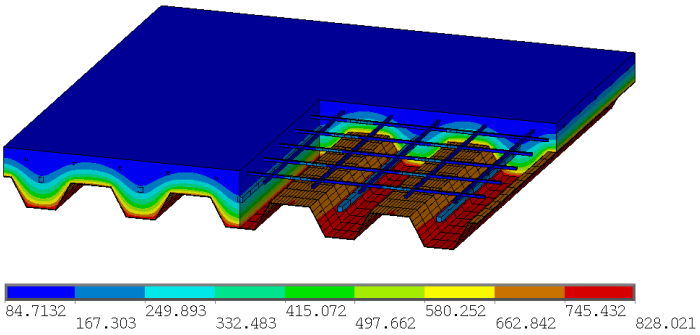

t= 36.2 min

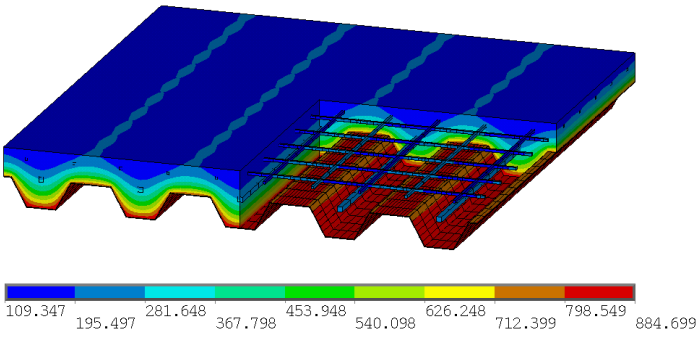

t= 48.3 min

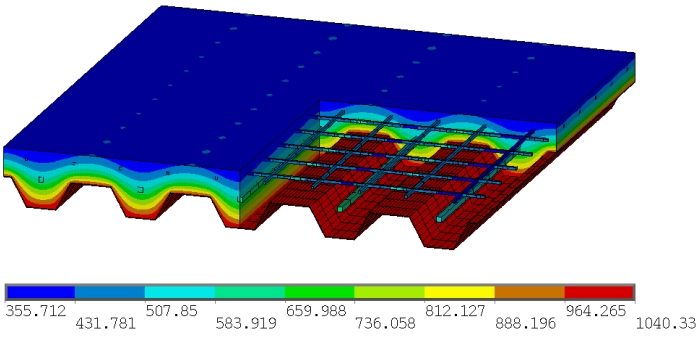

t= 120.0 min

SIM. 95	**St. deck:** Trapezoidal – ArcelorMittal Polydeck 59S	**Rebar (mm):** ϕ12	**Fire resistance (min)**	
	Mesh (mm//mm): ϕ6//100 (Q 283)	**h_1 (mm):** 71	Ave: *61.2*	Max: 62.4

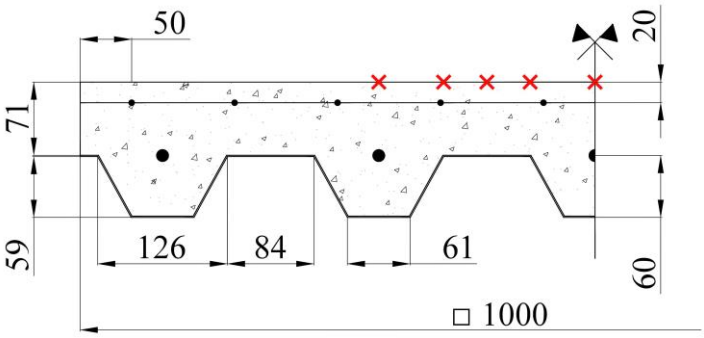

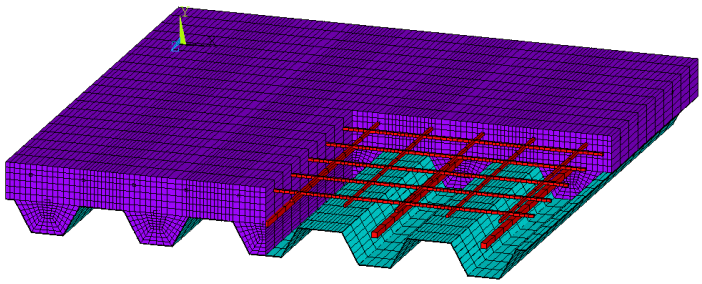

Finite element mesh

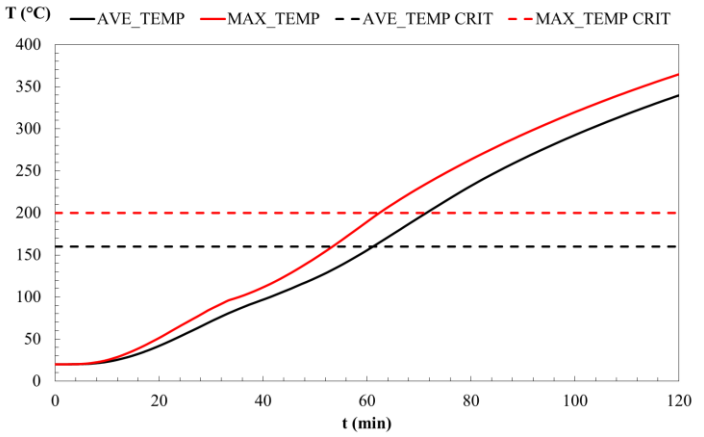

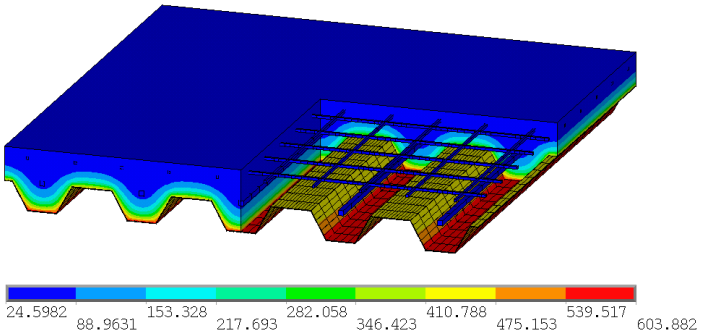

t= 15.3 min

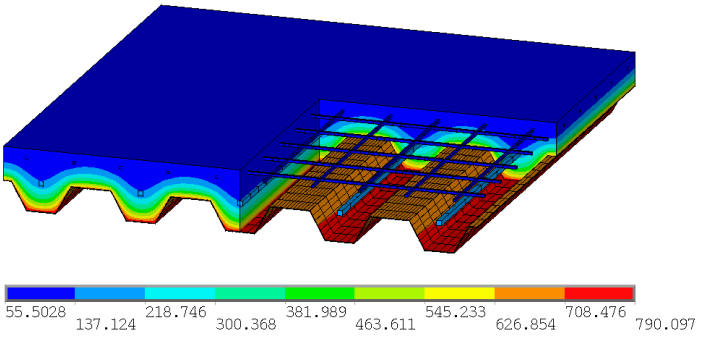

t= 30.6 min

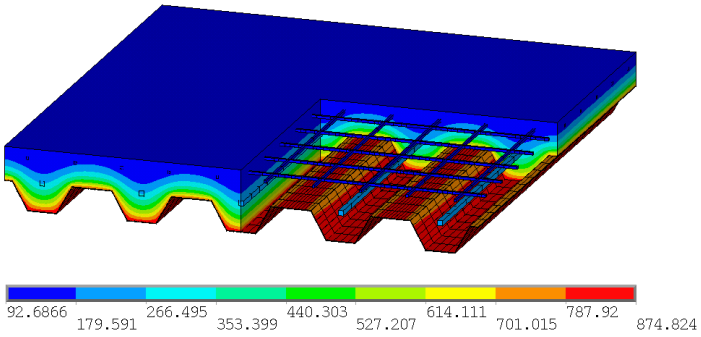

t= 45.9 min

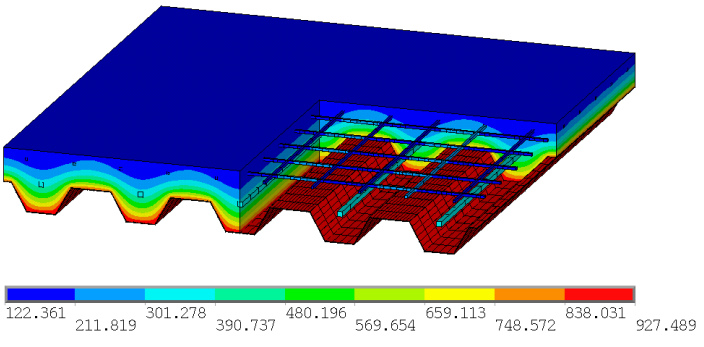

t= 61.2 min

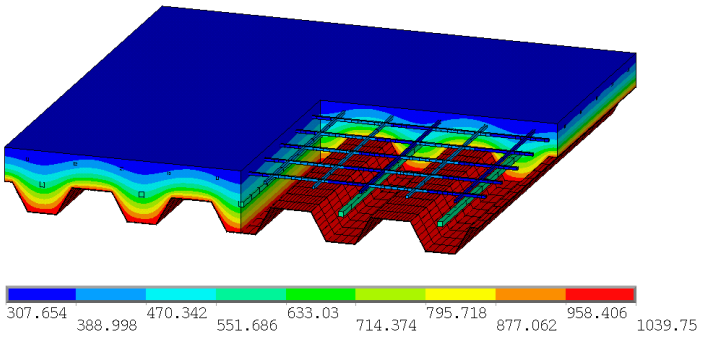

t= 120.0 min

SIM. 96	**St. deck:** Trapezoidal – ArcelorMittal Polydeck 59S	**Rebar (mm):** ϕ12	**Fire resistance (min)**	
	Mesh (mm//mm): ϕ6//100 (Q 283)	**h_1 (mm):** 81	Ave: *74.3*	Max: 78.5

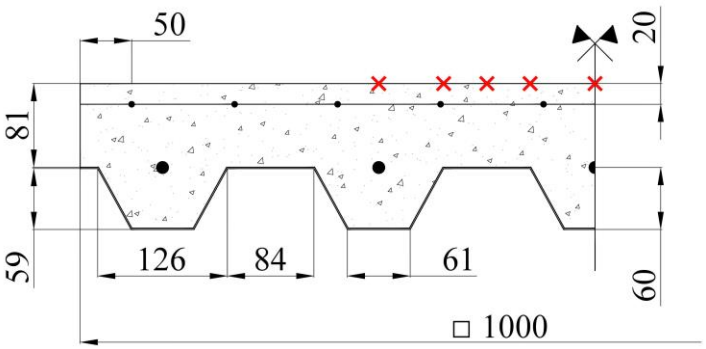

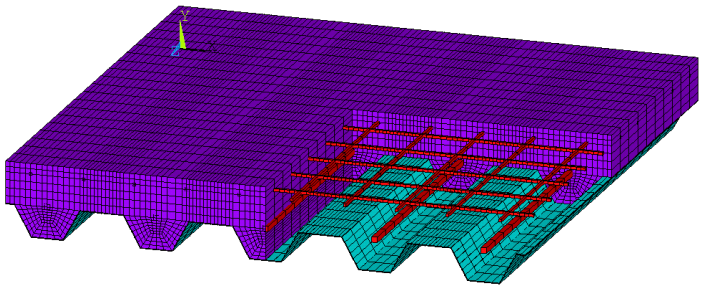

Finite element mesh

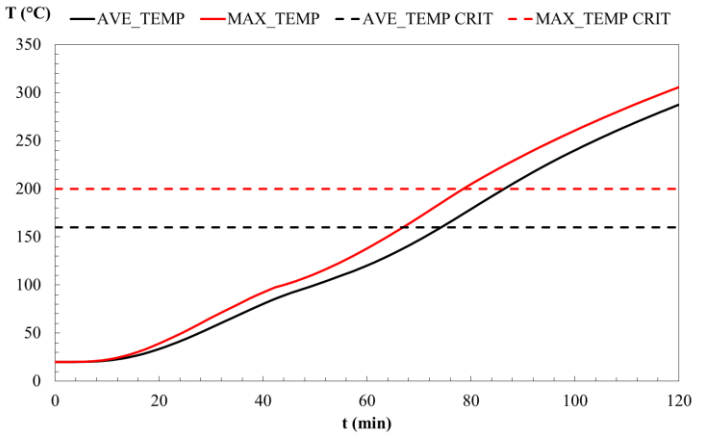

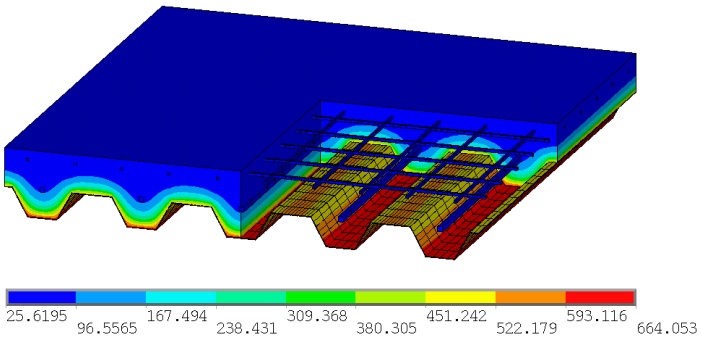

t= 18.6 min

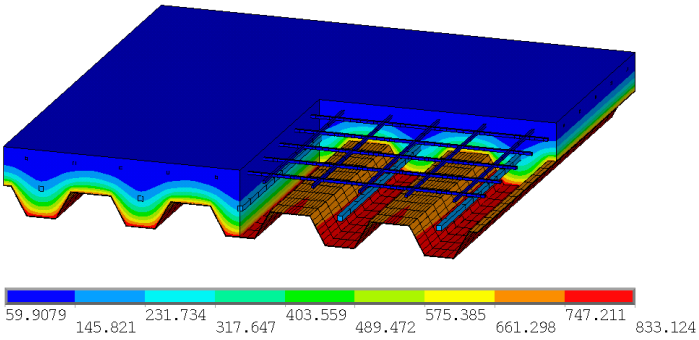

t= 37.2 min

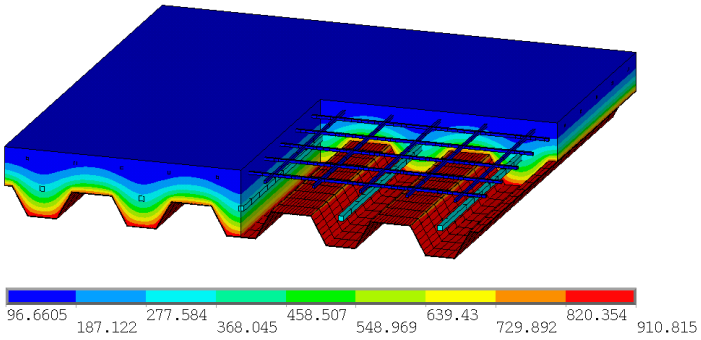

t= 55.7 min

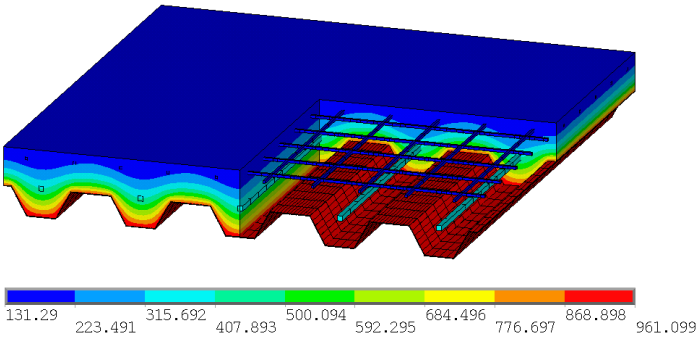

t= 74.3 min

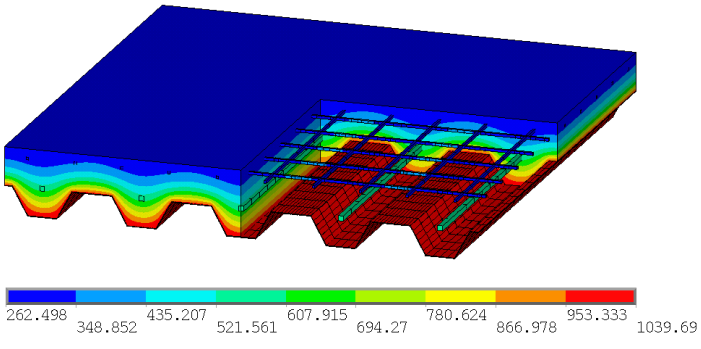

t= 120.0 min

SIM. 97	**Steel deck:** Re-entrant – Vulcraft 3.5D Formlok	**Rebar (mm):** ϕ8	**Fire resistance (min)**	
	Mesh (mm//mm): ϕ6//100 (W4.5)	**h_1 (mm):** 51	Ave: 62.2	Max: *60.4*

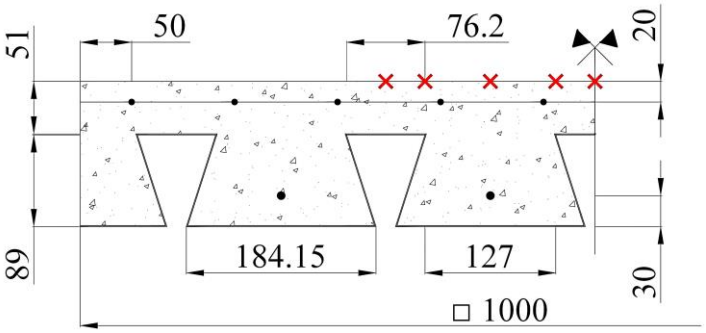

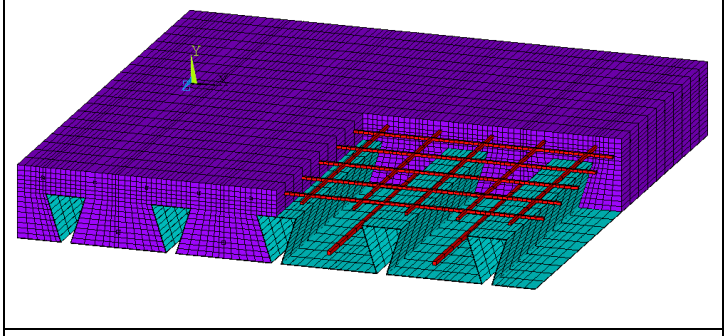

Finite element mesh

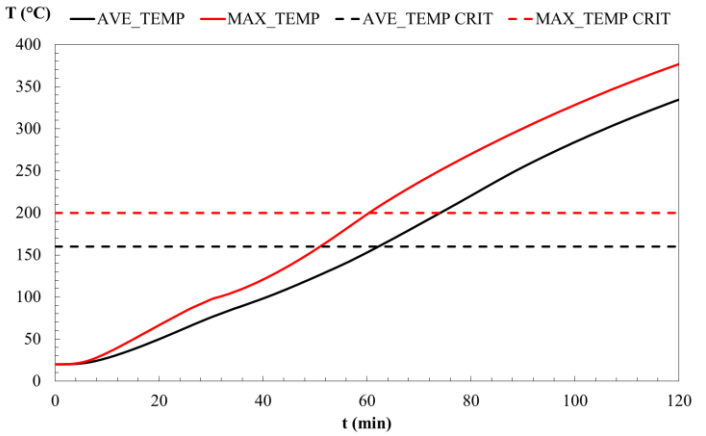

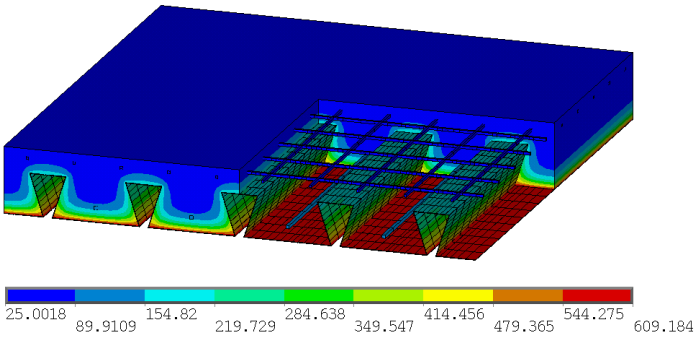

t= 15.1 min

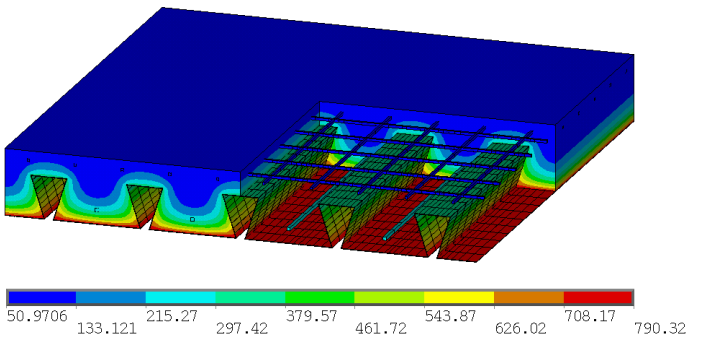

t= 30.2 min

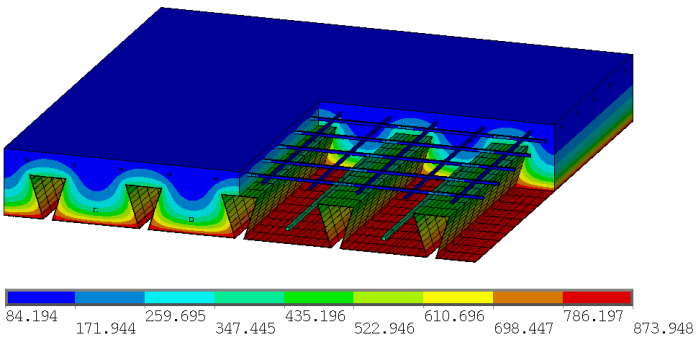

t= 45.3 min

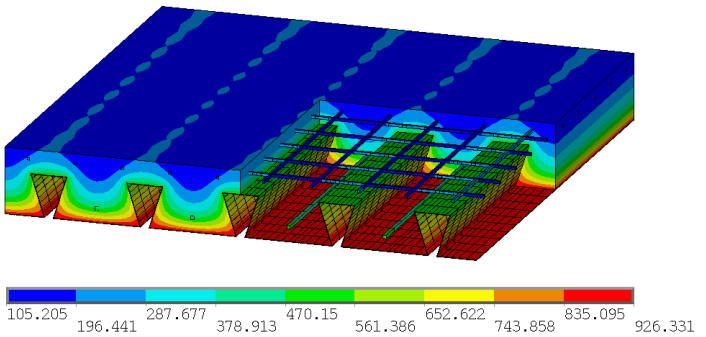

t= 60.4 min

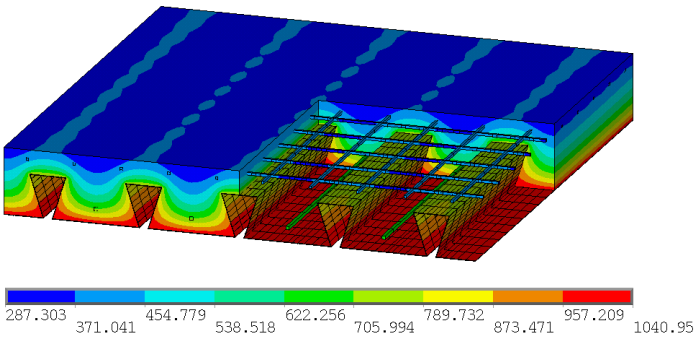

t= 120.0 min

SIM. 98	**Steel deck:** Re-entrant – Vulcraft 3.5D Formlok	**Rebar (mm):** ϕ8	**Fire resistance (min)**	
	Mesh (mm//mm): ϕ6//100 (W4.5)	**h_1 (mm):** 61	Ave: *76.2*	Max: 77.3

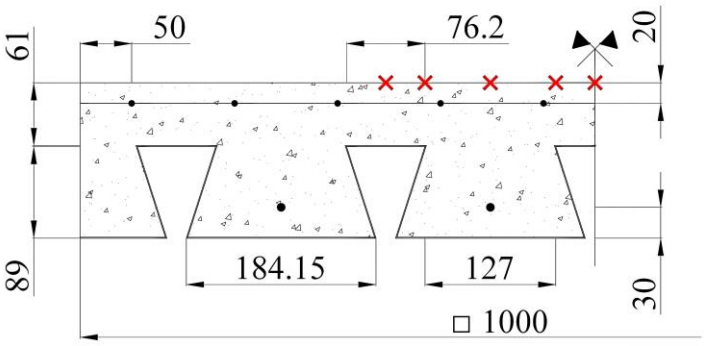

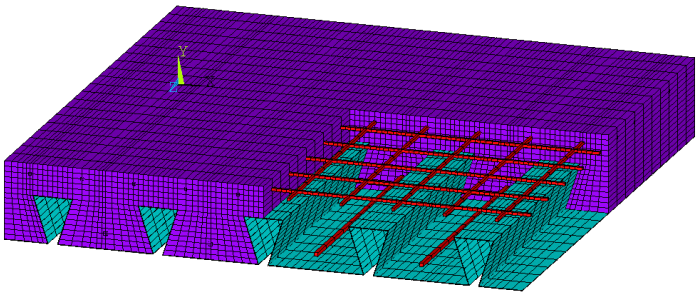

Finite element mesh

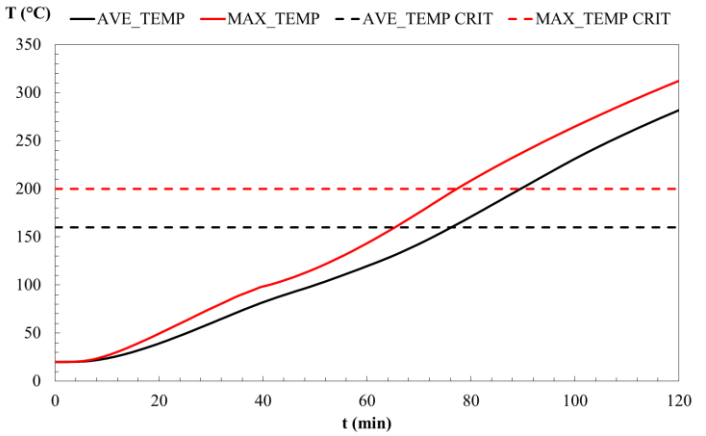

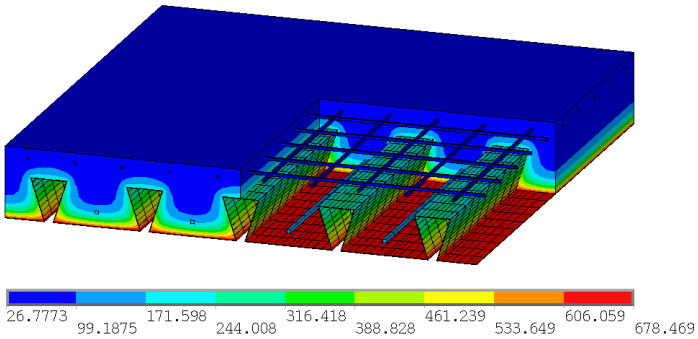

t= 19.1 min

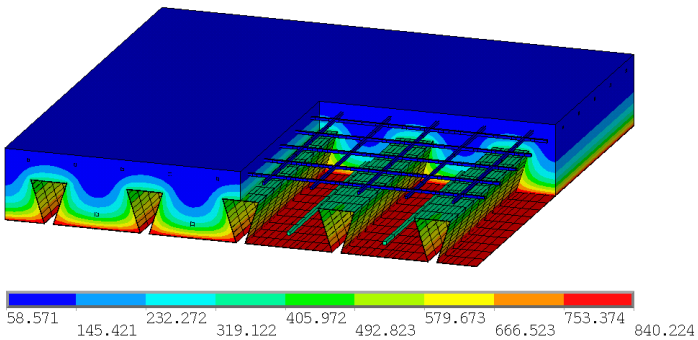

t= 38.1 min

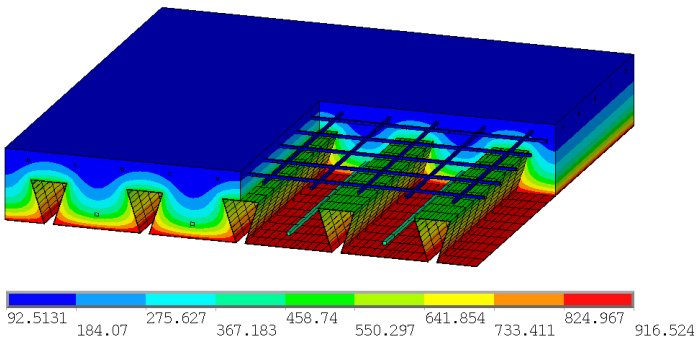

t= 57.2 min

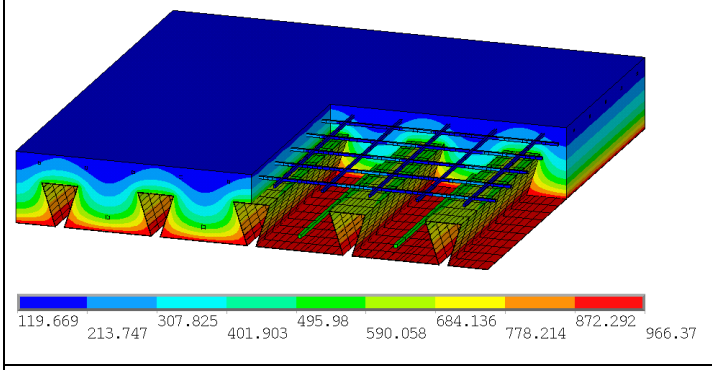

t= 76.2 min

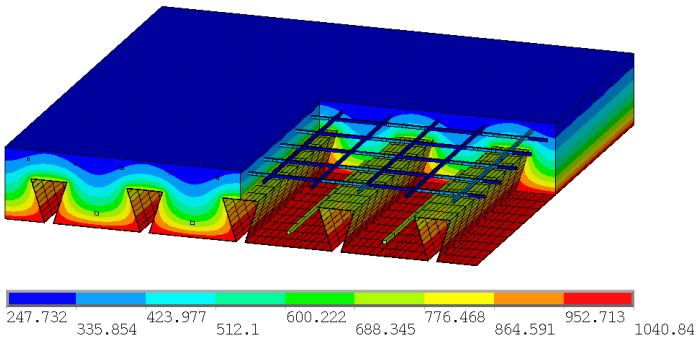

t= 120.0 min

SIM. 99	**Steel deck:** Re-entrant – Vulcraft 3.5D Formlok	**Rebar (mm):** ϕ8	**Fire resistance (min)**	
	Mesh (mm//mm): ϕ6//100 (W4.5)	**h_1 (mm):** 71	Ave: *91.2*	Max: 95.8

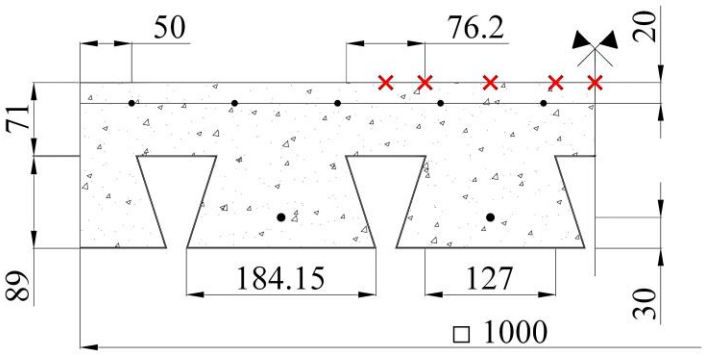

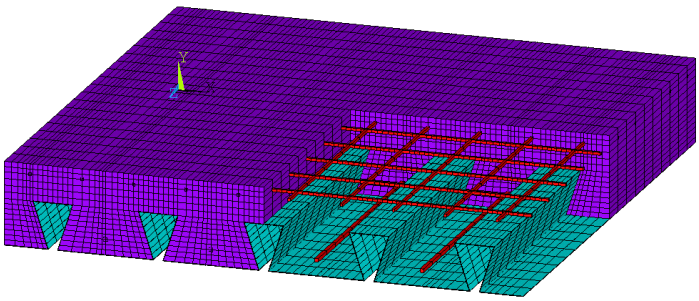

Finite element mesh

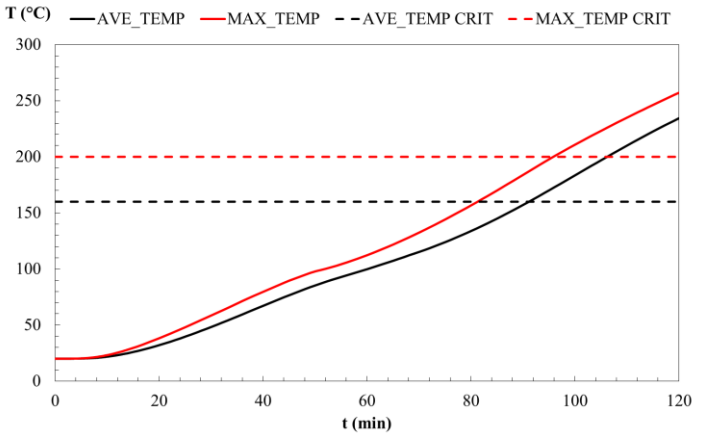

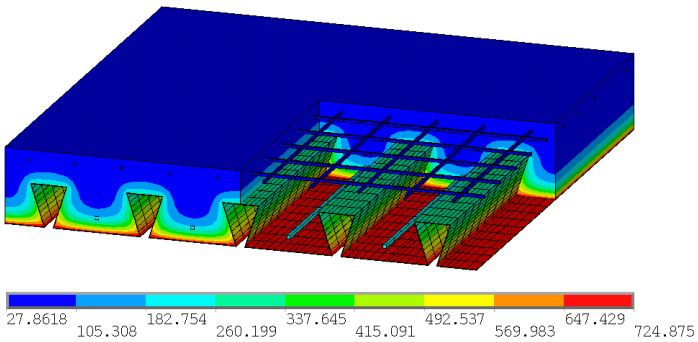

t= 22.8 min

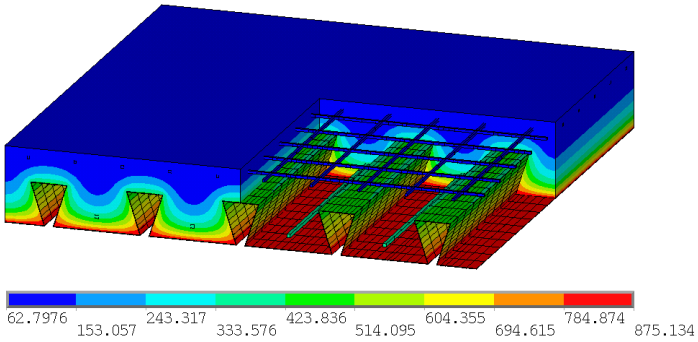

t= 45.6 min

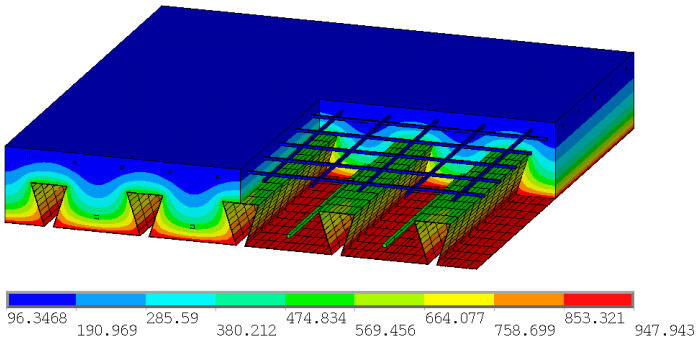

t= 68.4 min

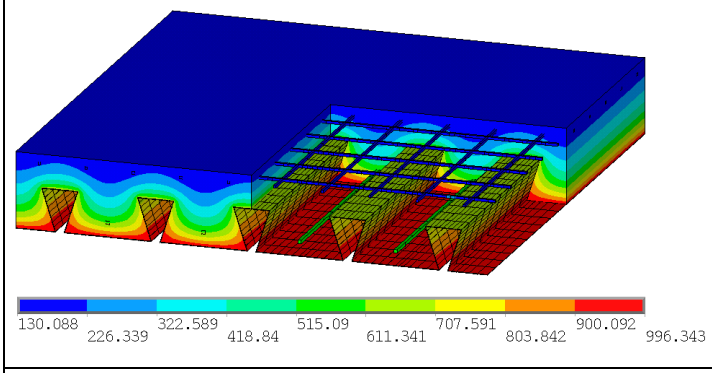

t= 91.2 min

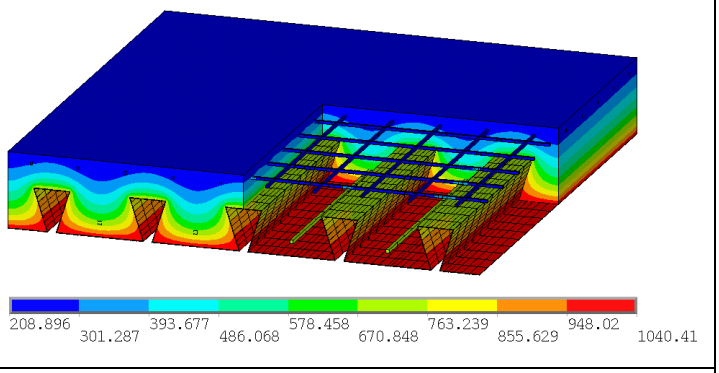

t= 120.0 min

SIM. 100	**Steel deck:** Re-entrant – Vulcraft 3.5D Formlok	**Rebar (mm):** ϕ8	**Fire resistance (min)**	
	Mesh (mm//mm): ϕ6//100 (W4.5)	**h_1 (mm):** 81	Ave: *107.1*	Max: 115.8

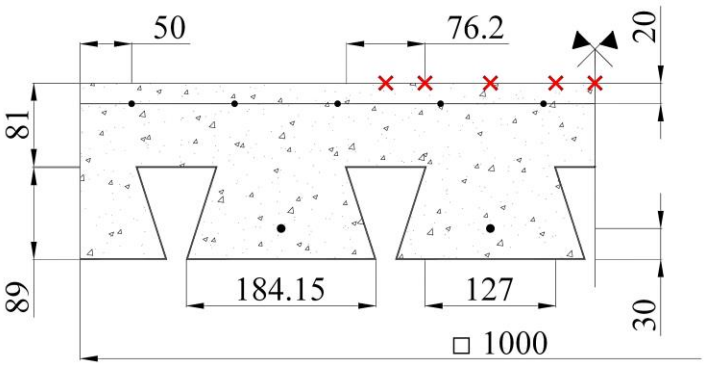

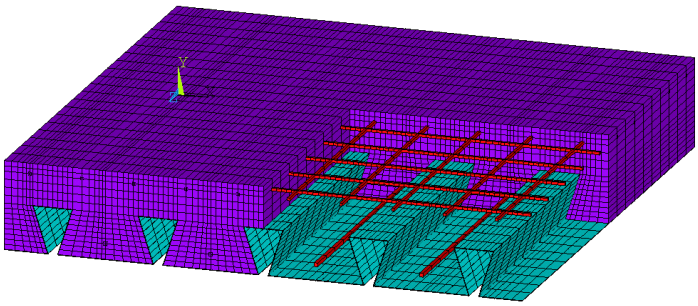

Finite element mesh

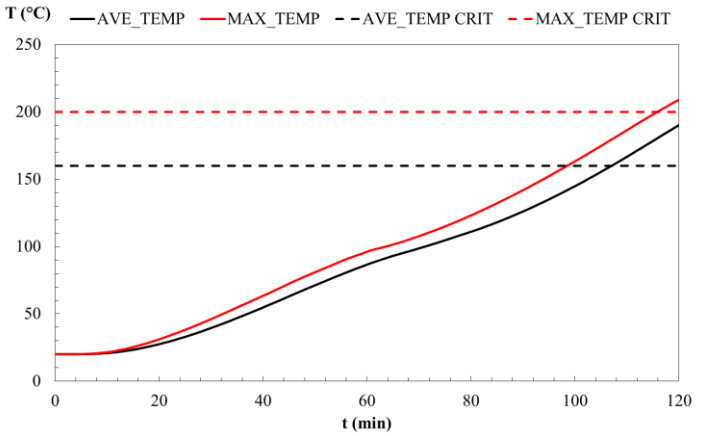

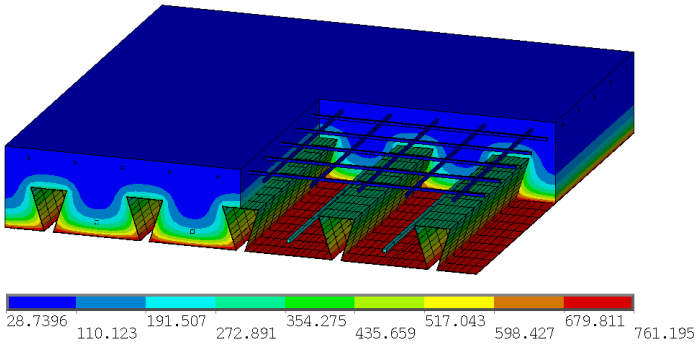

t= 26.8 min

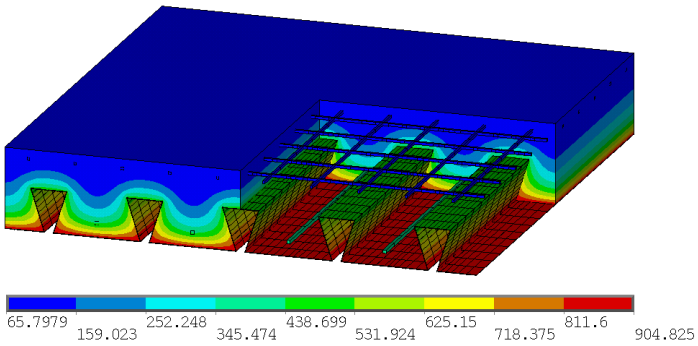

t= 53.6 min

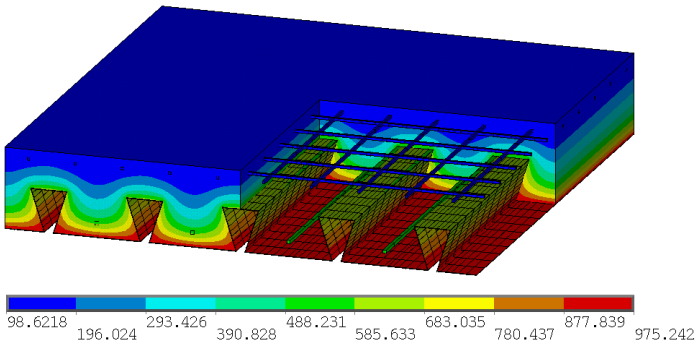

t= 80.3 min

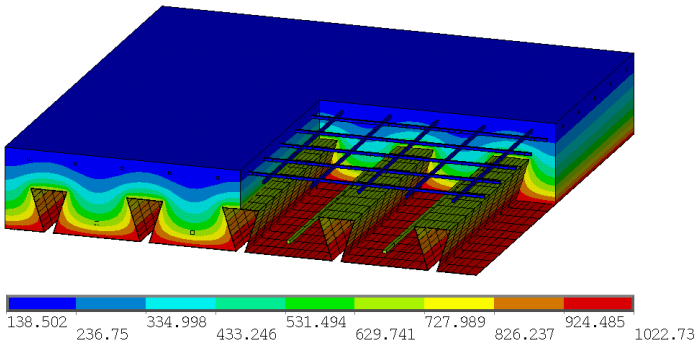

t= 107.1 min

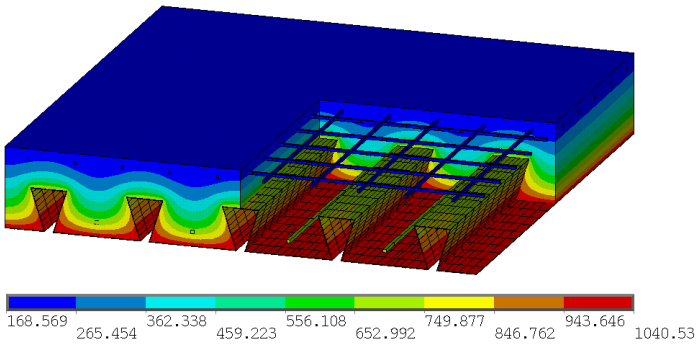

t= 120.0 min

SIM. 101	**Steel deck:** Re-entrant – Vulcraft 3.5D Formlok	**Rebar (mm):** ϕ8	**Fire resistance (min)**	
	Mesh (mm//mm): ϕ6//100 (W4.5)	**h_1 (mm):** 51	Ave: 62.2	Max: *60.4*

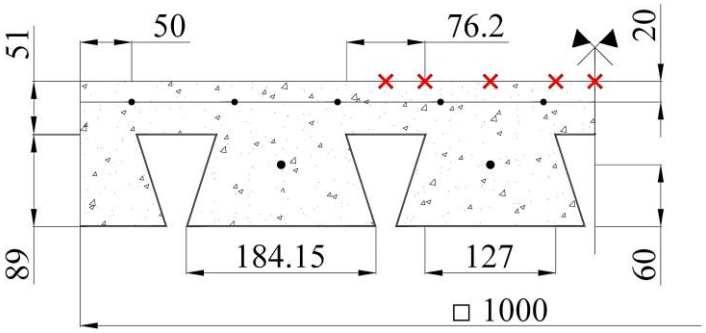

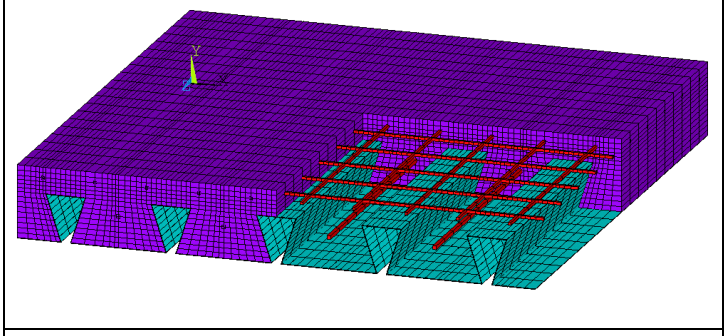

Finite element mesh

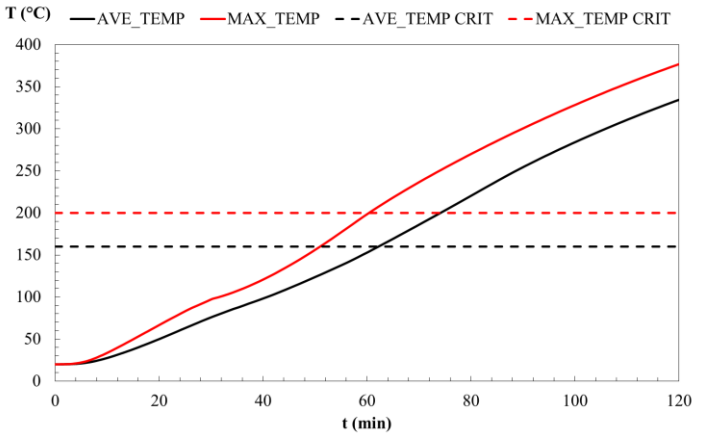

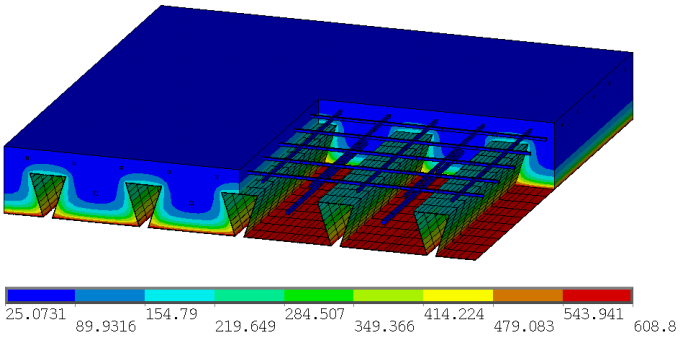

t= 15.1 min

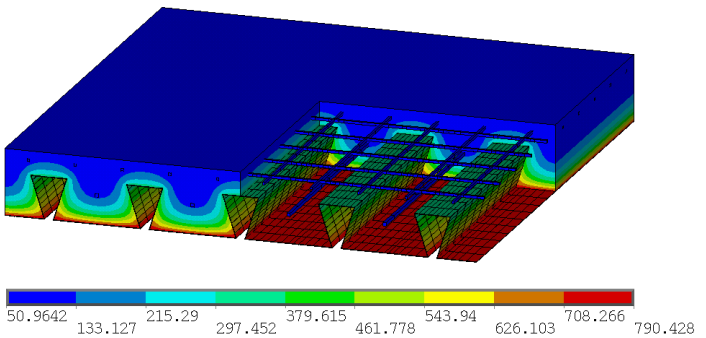

t= 30.2 min

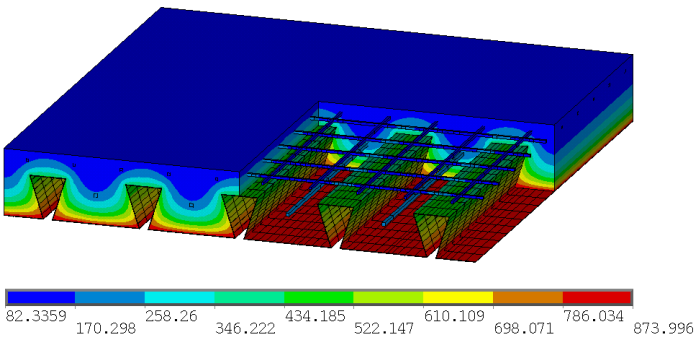

t= 45.3 min

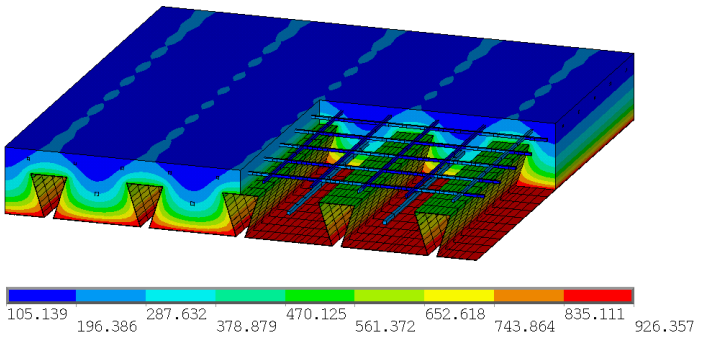

t= 60.4 min

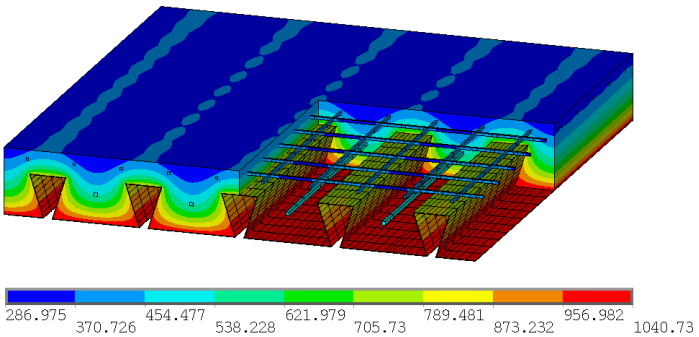

t= 120.0 min

SIM. 102	**Steel deck:** Re-entrant – Vulcraft 3.5D Formlok	**Rebar (mm):** ϕ8	**Fire resistance (min)**	
	Mesh (mm//mm): ϕ6//100 (W4.5)	**h_1 (mm):** 61	Ave: *76.2*	Max: 77.3

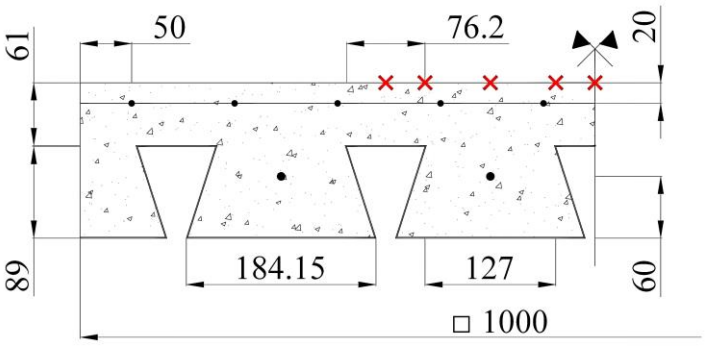

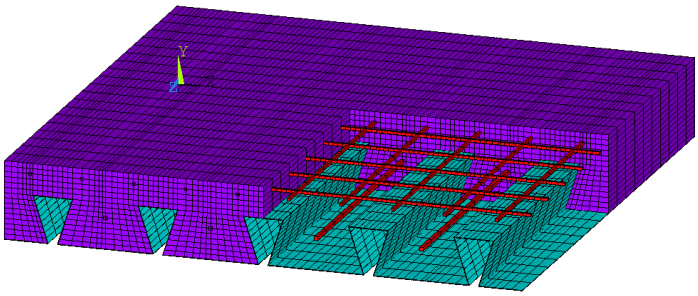

Finite element mesh

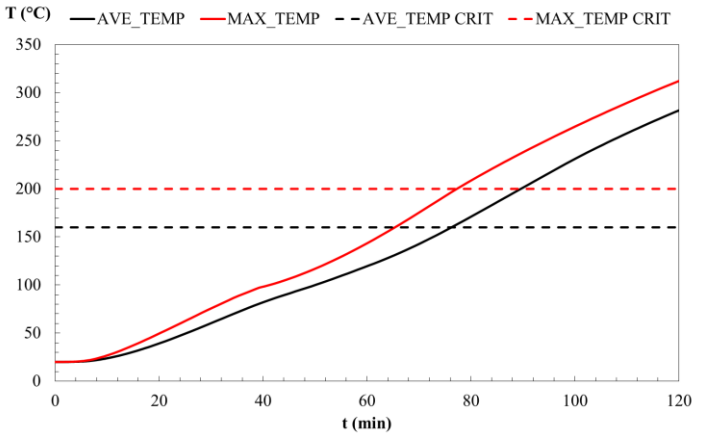

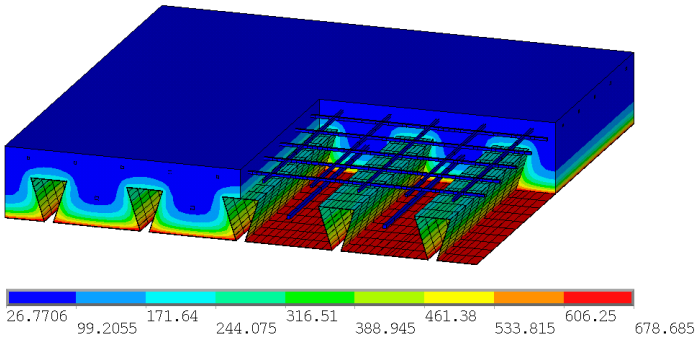

t= 19.1 min

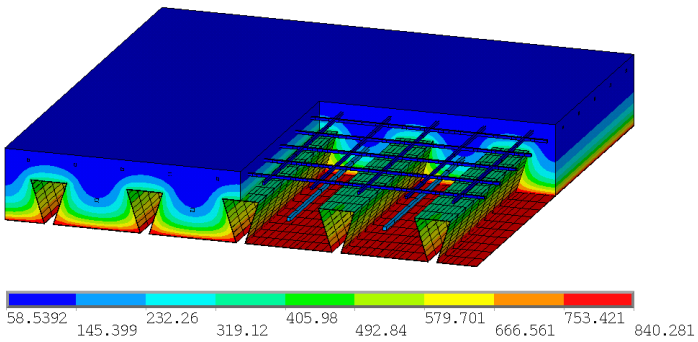

t= 38.1 min

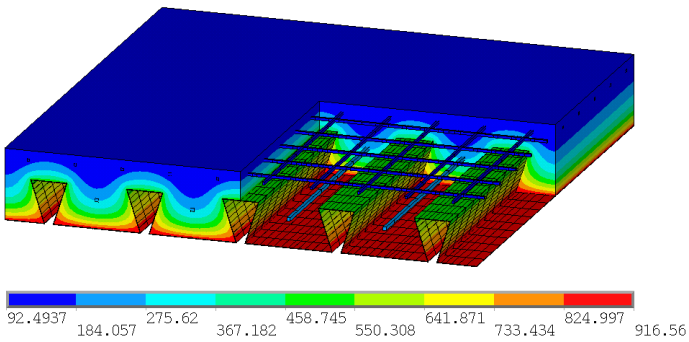

t= 57.2 min

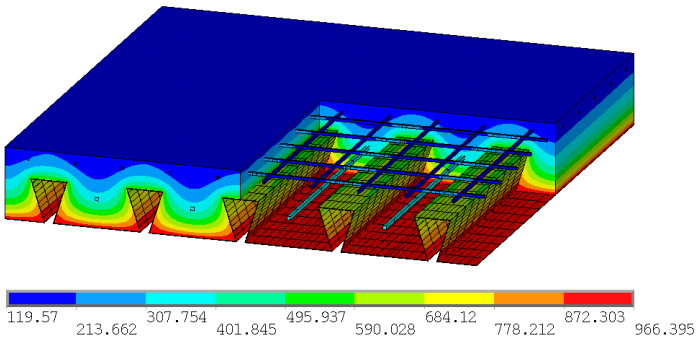

t= 76.2 min

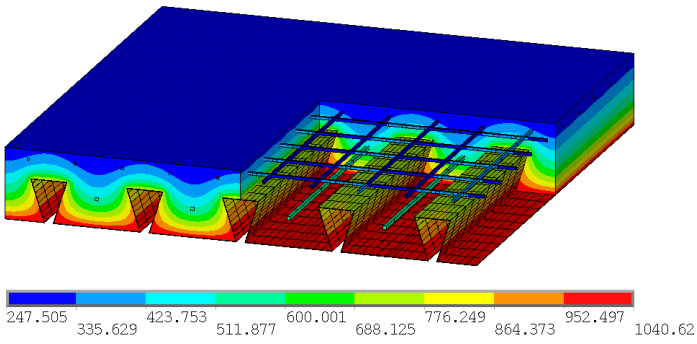

t= 120.0 min

SIM. 103	**Steel deck:** Re-entrant – Vulcraft 3.5D Formlok	**Rebar (mm):** ϕ8	**Fire resistance (min)**	
	Mesh (mm//mm): ϕ6//100 (W4.5)	**h_1 (mm):** 71	Ave: *91.2*	Max: 95.9

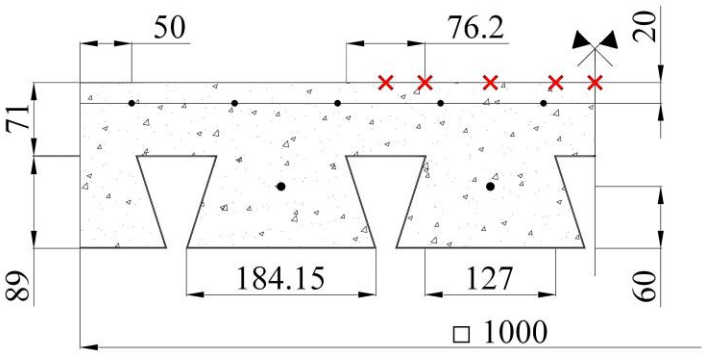

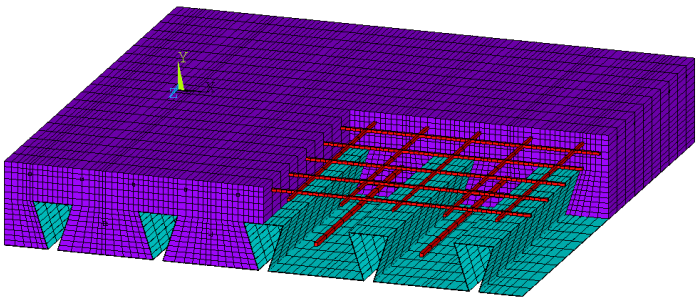

Finite element mesh

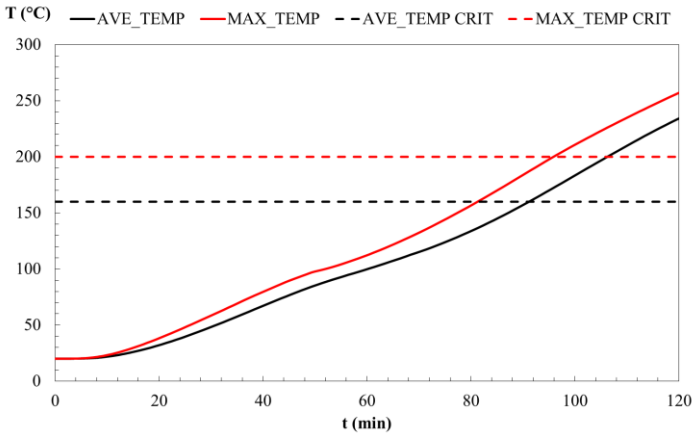

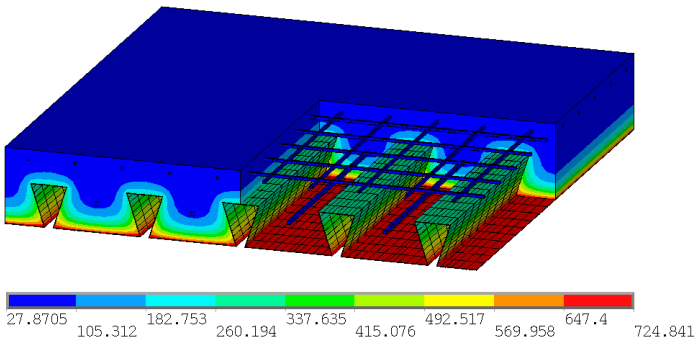

t= 22.8 min

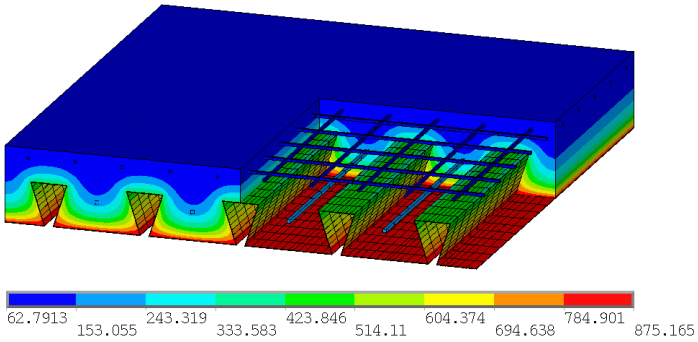

t= 45.6 min

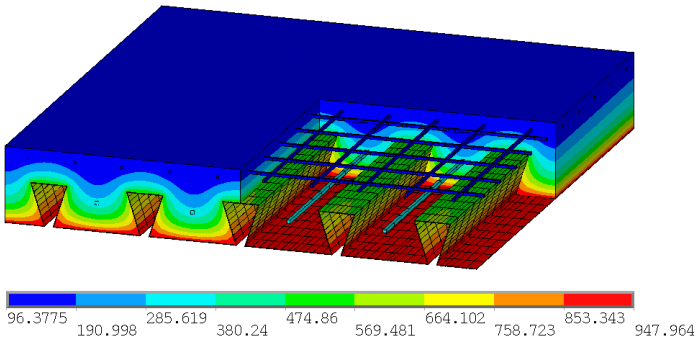

t= 68.4 min

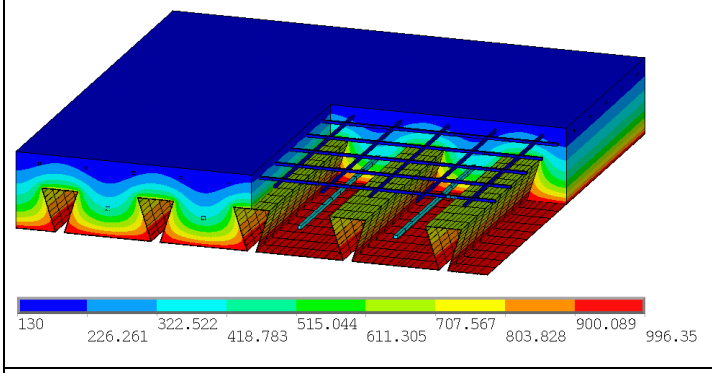

t= 91.2 min

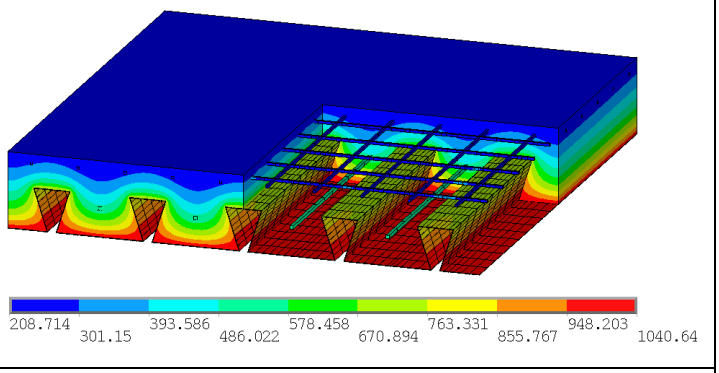

t= 120.0 min

SIM. 104	**Steel deck:** Re-entrant – Vulcraft 3.5D Formlok	**Rebar (mm):** ϕ8	**Fire resistance (min)**	
	Mesh (mm//mm): ϕ6//100 (W4.5)	**h_1 (mm):** 81	Ave: *107.1*	Max: 115.9

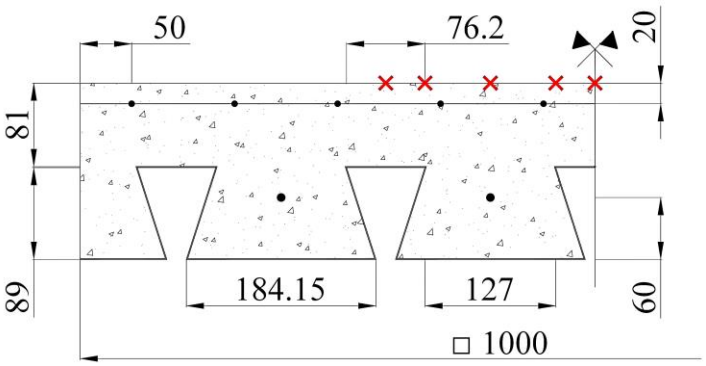

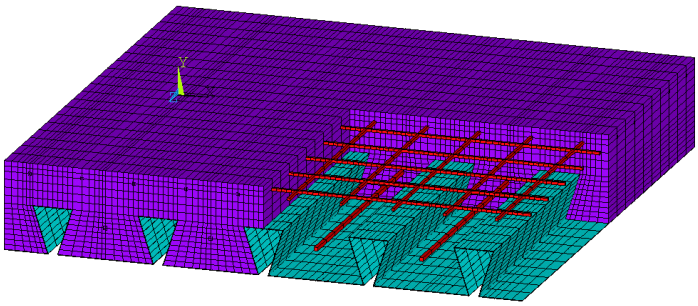

Finite element mesh

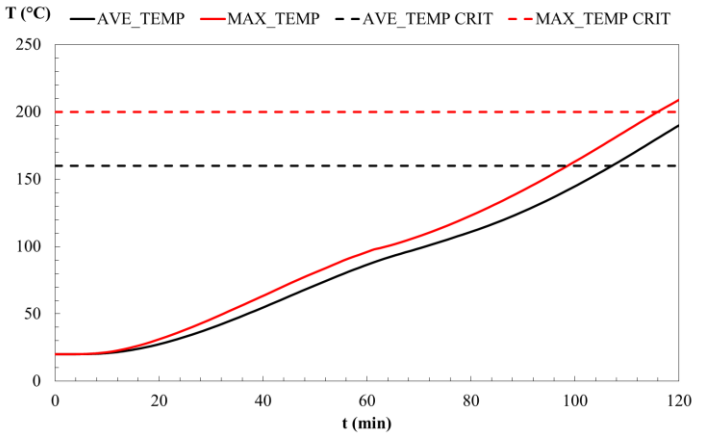

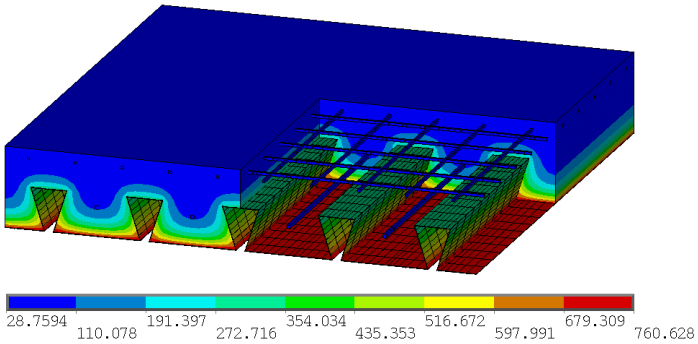

t= 26.8 min

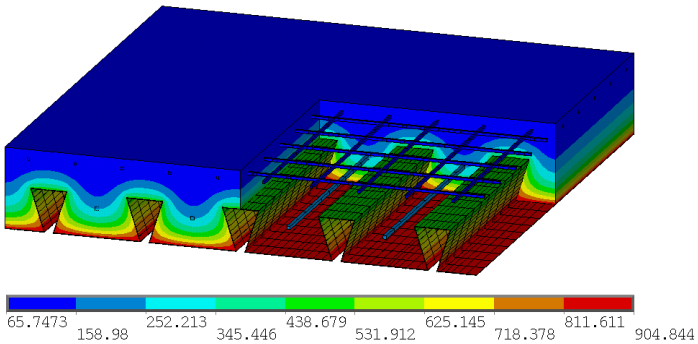

t= 53.6 min

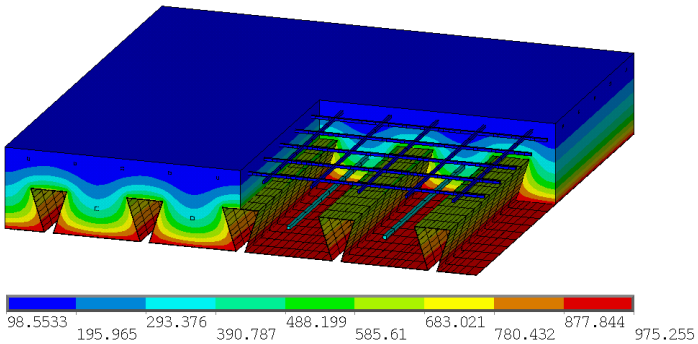

t= 80.3 min

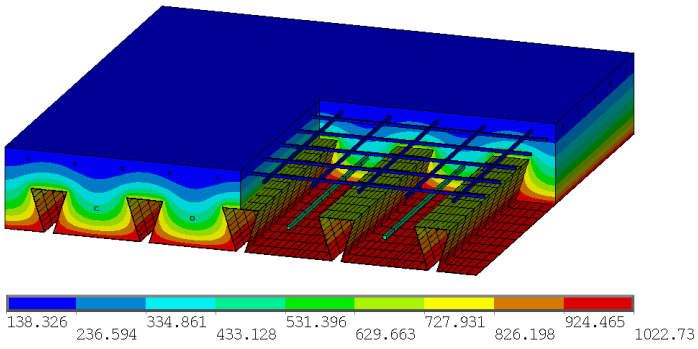

t= 107.1 min

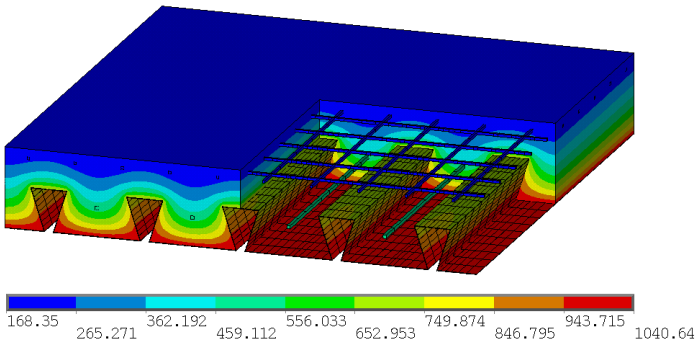

t= 120.0 min

SIM. 105	**Steel deck:** Re-entrant – Vulcraft 3.5D Formlok	**Rebar (mm):** ϕ8	**Fire resistance (min)**	
	Mesh (mm//mm): ϕ6//150 (W4.5)	**h_1 (mm):** 51	Ave: 62.5	Max: *61.6*

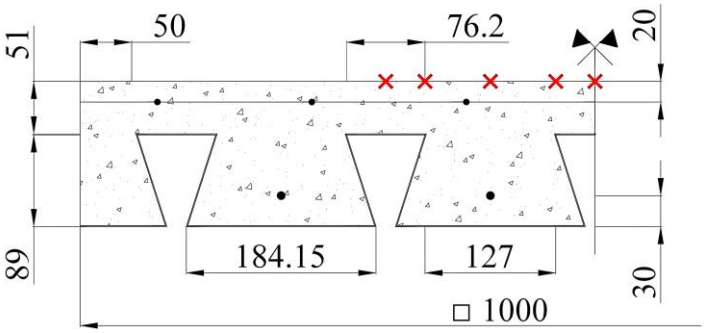

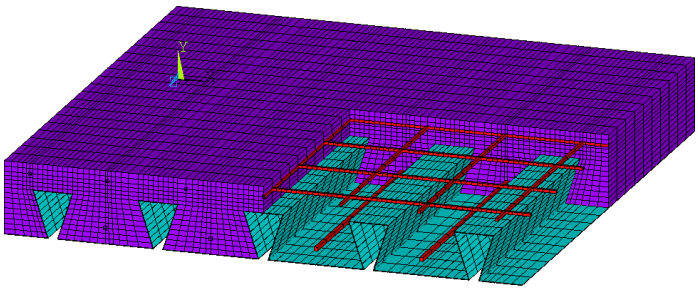

Finite element mesh

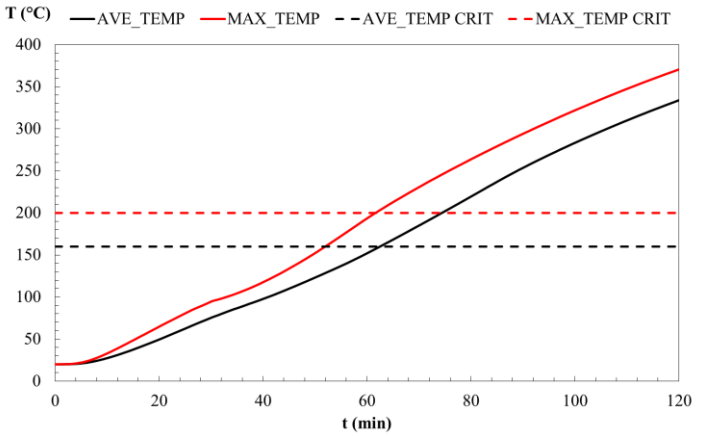

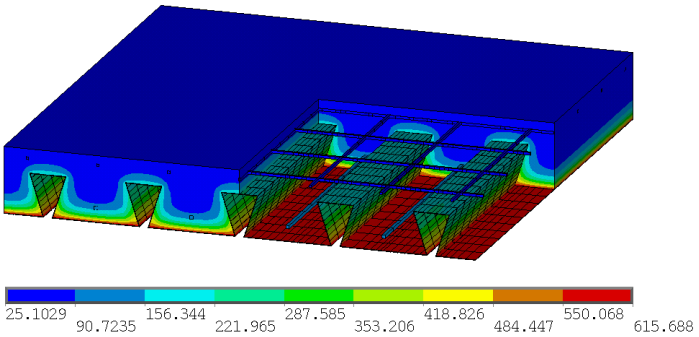

t= 15.4 min

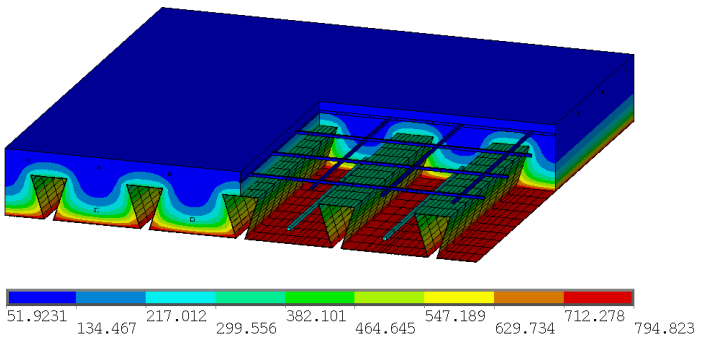

t= 30.8 min

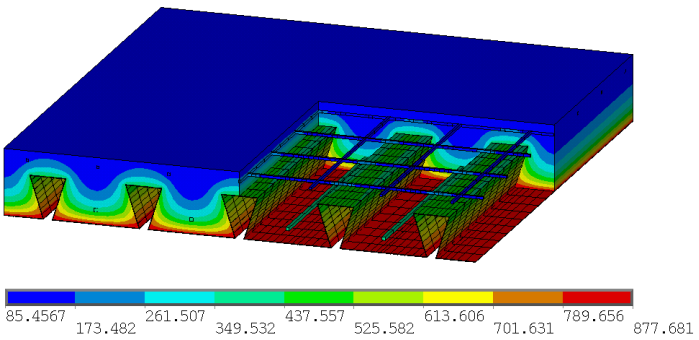

t= 46.2 min

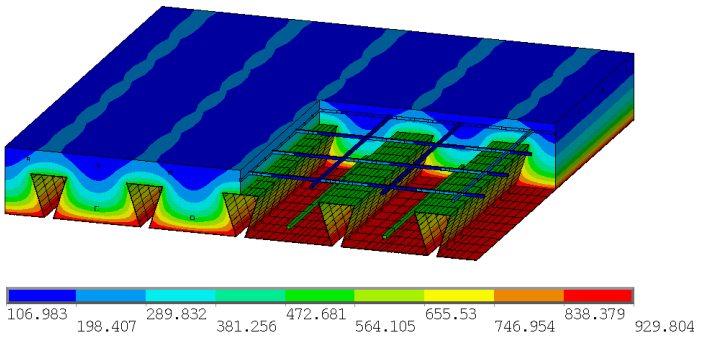

t= 61.6 min

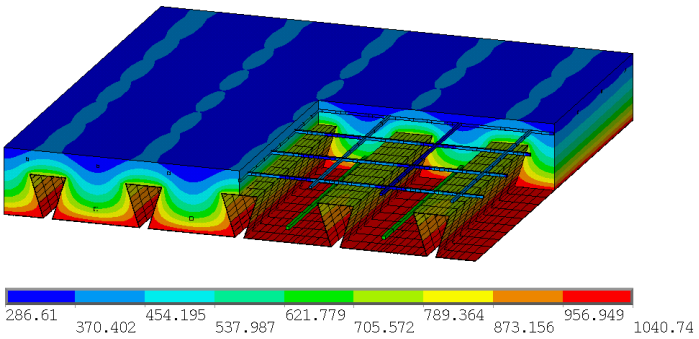

t= 120.0 min

SIM. 106	**Steel deck:** Re-entrant – Vulcraft 3.5D Formlok	**Rebar (mm):** ϕ8	**Fire resistance (min)**	
	Mesh (mm//mm): ϕ6//150 (W4.5)	**h_1 (mm):** 61	Ave: *76.4*	Max: 78.5

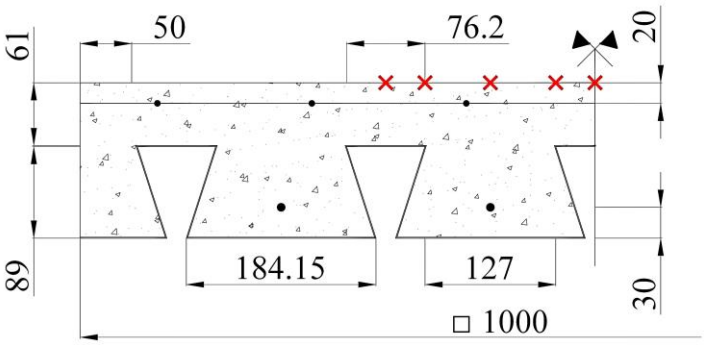

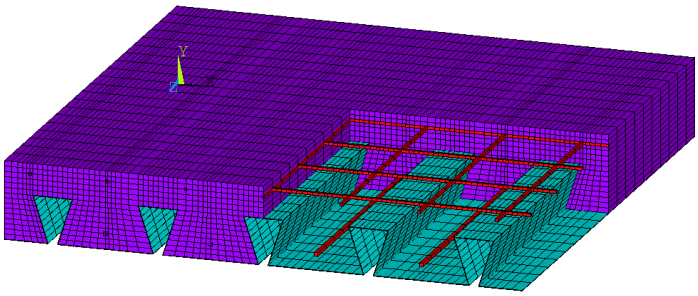

Finite element mesh

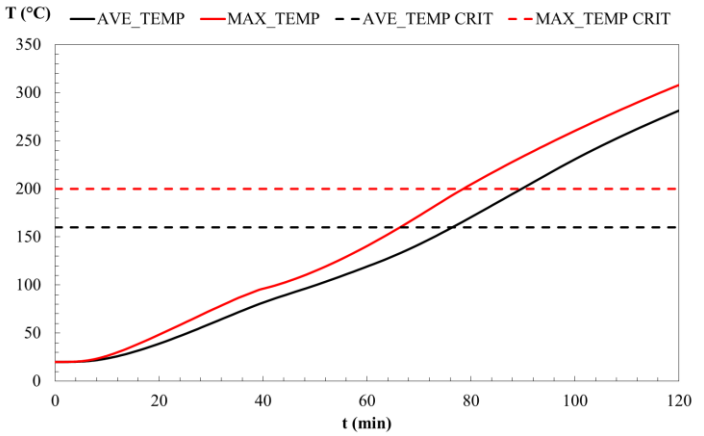

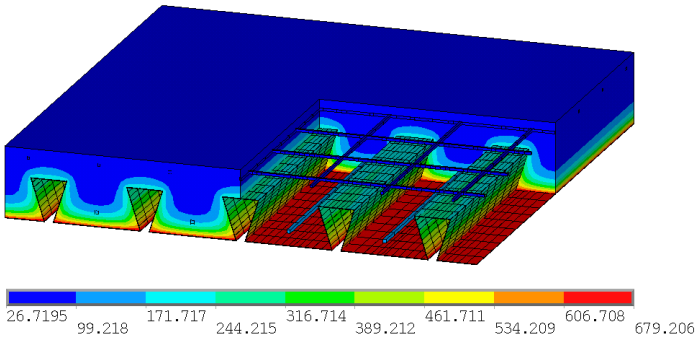

t= 19.1 min

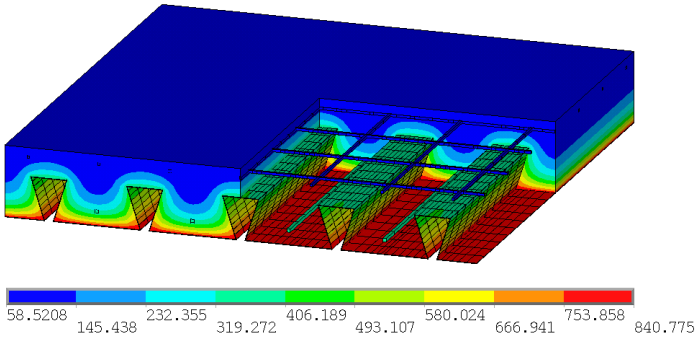

t= 38.2 min

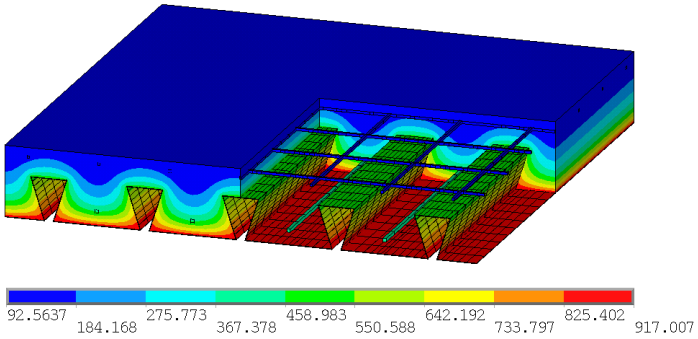

t= 57.3 min

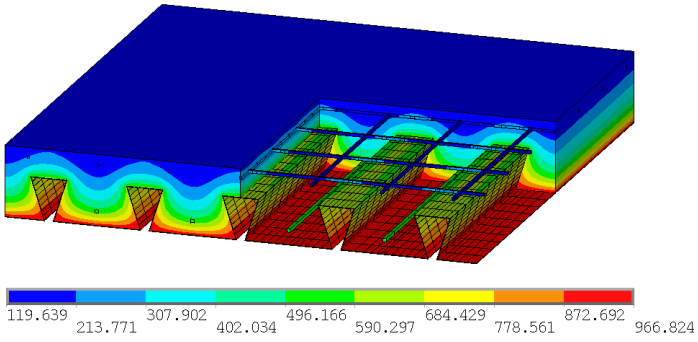

t= 76.4 min

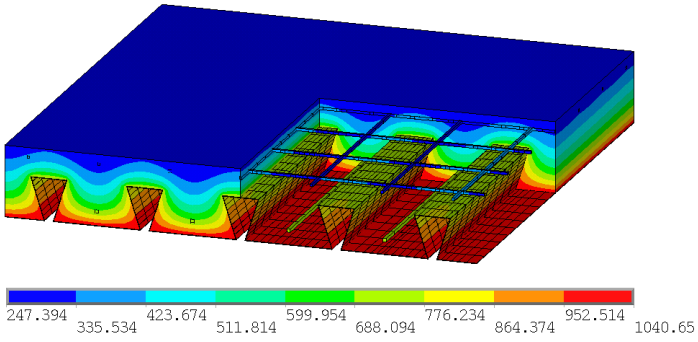

t= 120.0 min

SIM. 107	**Steel deck:** Re-entrant – Vulcraft 3.5D Formlok	**Rebar (mm):** ϕ8	**Fire resistance (min)**	
	Mesh (mm//mm): ϕ6//150 (W4.5)	**h_1 (mm):** 71	Ave: *91.3*	Max: 96.9

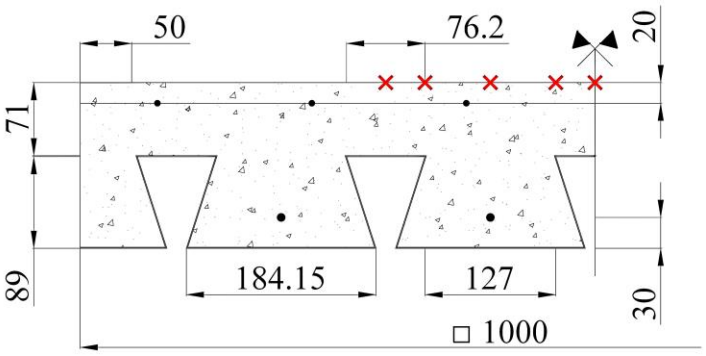

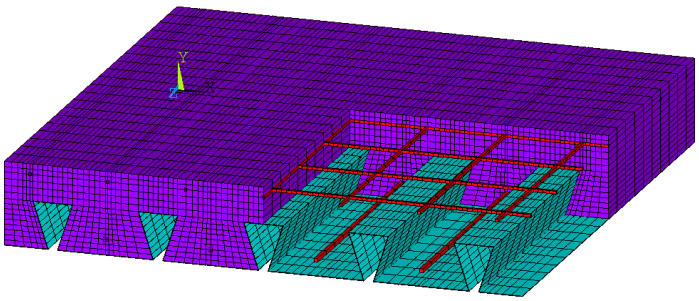

Finite element mesh

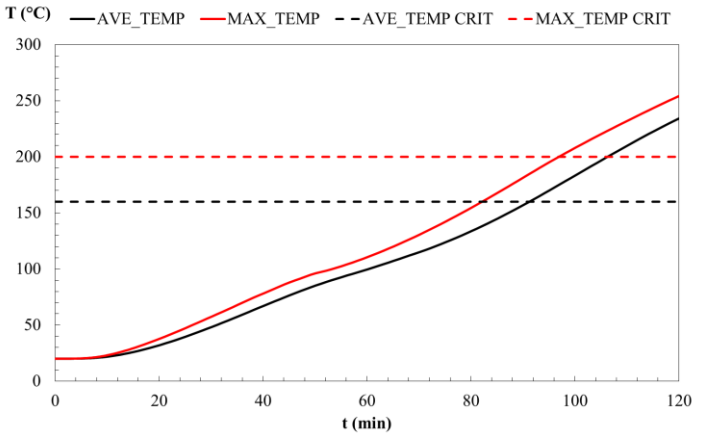

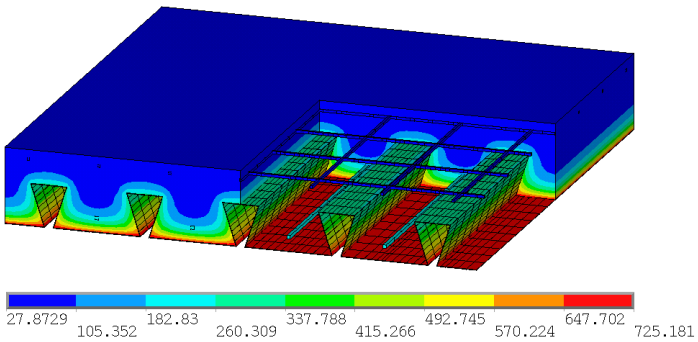

t= 22.8 min

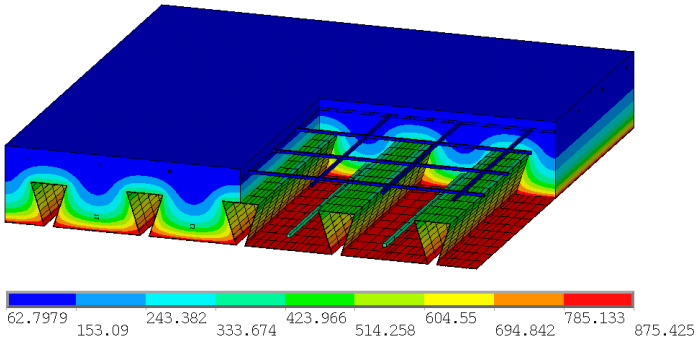

t= 45.7 min

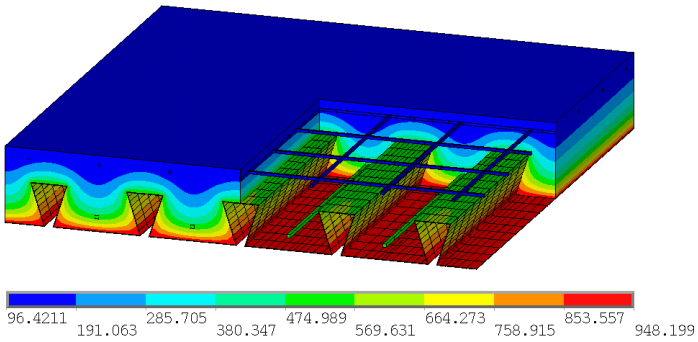

t= 68.5 min

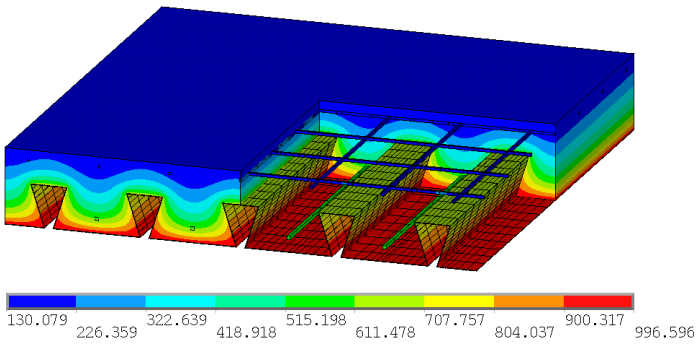

t= 91.3 min

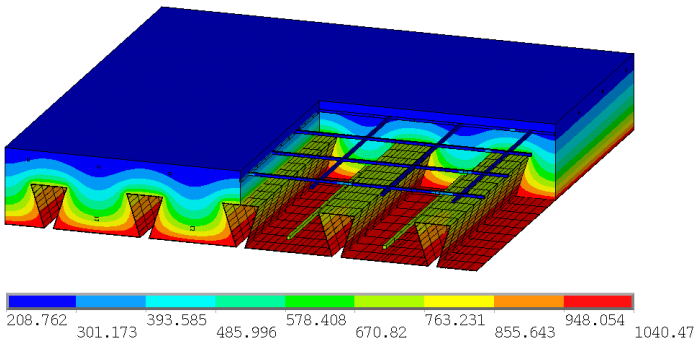

t= 120.0 min

SIM. 108	**Steel deck:** Re-entrant – Vulcraft 3.5D Formlok	**Rebar (mm):** ϕ8	**Fire resistance (min)**	
	Mesh (mm//mm): ϕ6//150 (W4.5)	**h_1 (mm):** 81	Ave: *107.1*	Max: 116.7

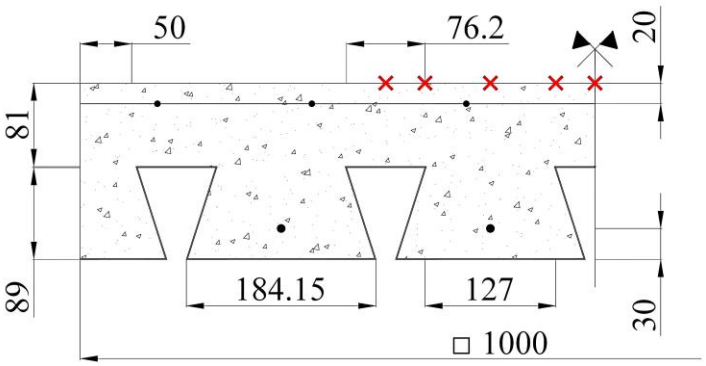

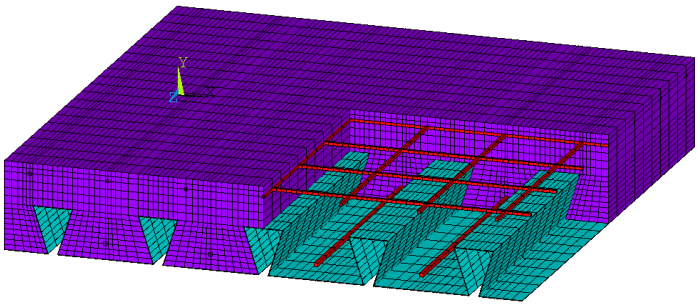

Finite element mesh

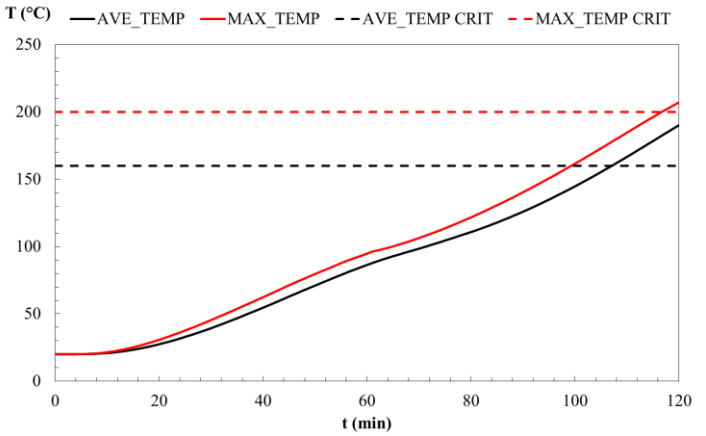

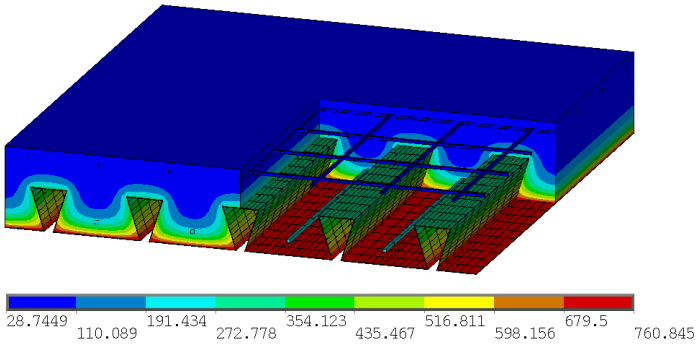

t= 26.8 min

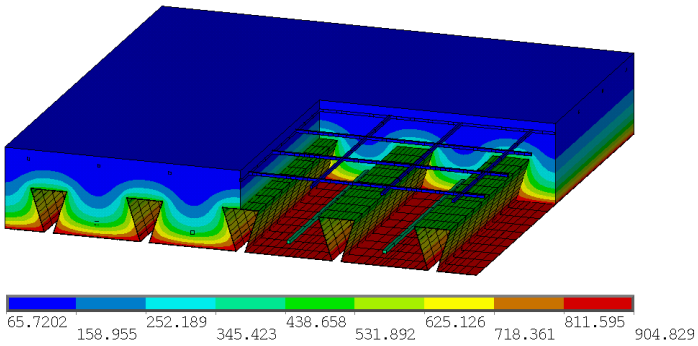

t= 53.6 min

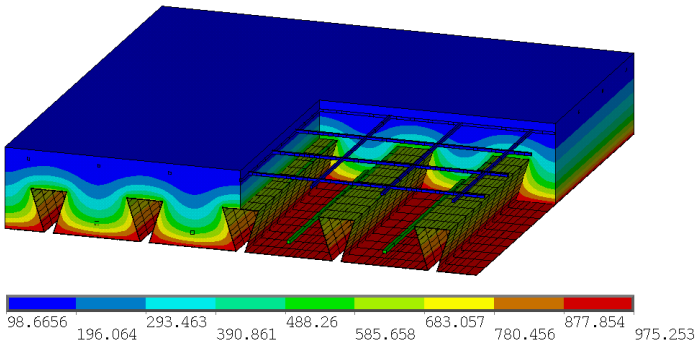

t= 80.3 min

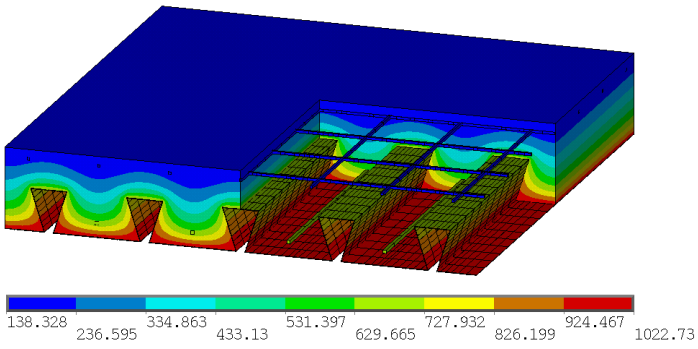

t= 107.1 min

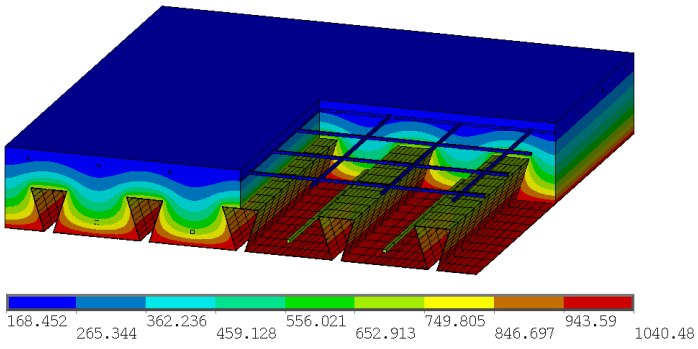

t= 120.0 min

SIM. 109	**Steel deck:** Re-entrant – Vulcraft 3.5D Formlok	**Rebar (mm):** ϕ8	**Fire resistance (min)**	
	Mesh (mm//mm): ϕ6//150 (W4.5)	**h_1 (mm):** 51	Ave: 62.5	Max: *61.6*

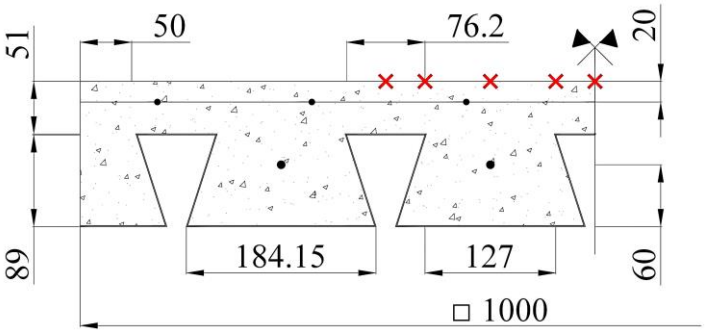

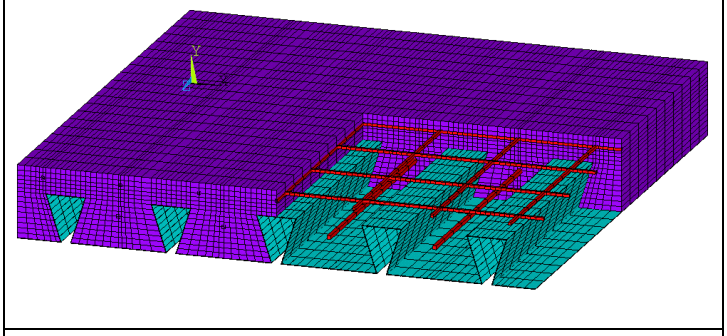

Finite element mesh

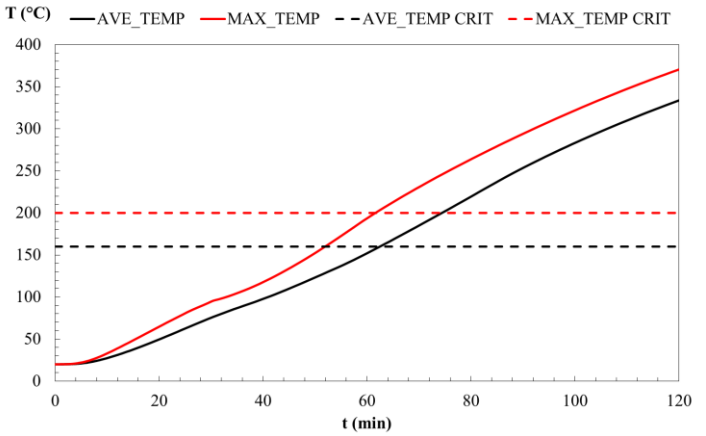

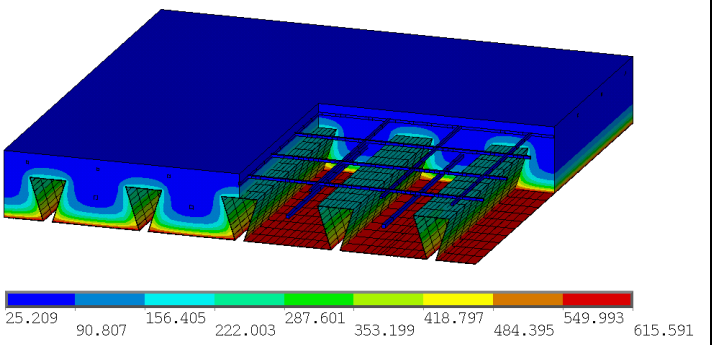

t= 15.4 min

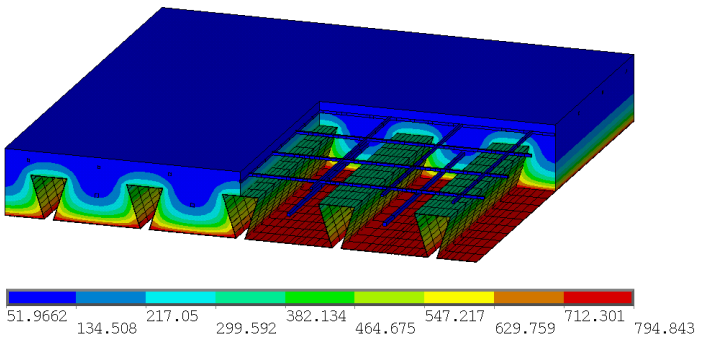

t= 30.8 min

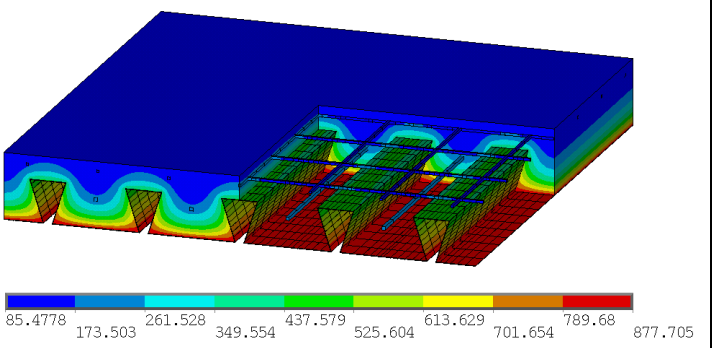

t= 46.2 min

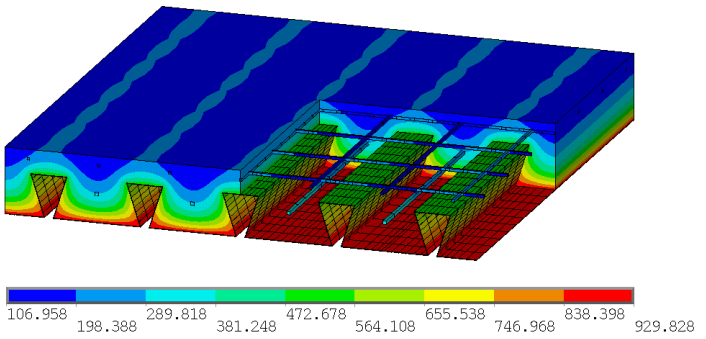

t= 61.6 min

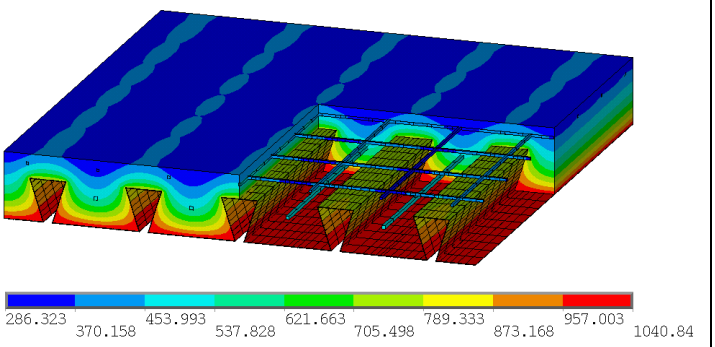

t= 120.0 min

SIM. 110	**Steel deck:** Re-entrant – Vulcraft 3.5D Formlok	**Rebar (mm):** ϕ8	**Fire resistance (min)**	
	Mesh (mm//mm): ϕ6//150 (W4.5)	**h_1 (mm):** 61	Ave: *76.4*	Max: 78.5

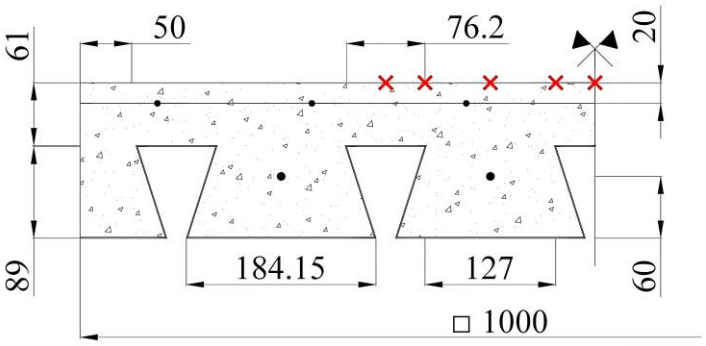

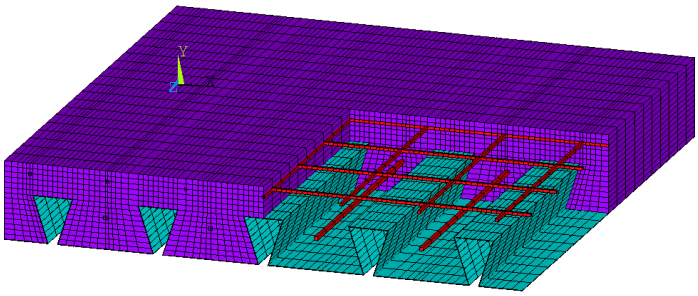

Finite element mesh

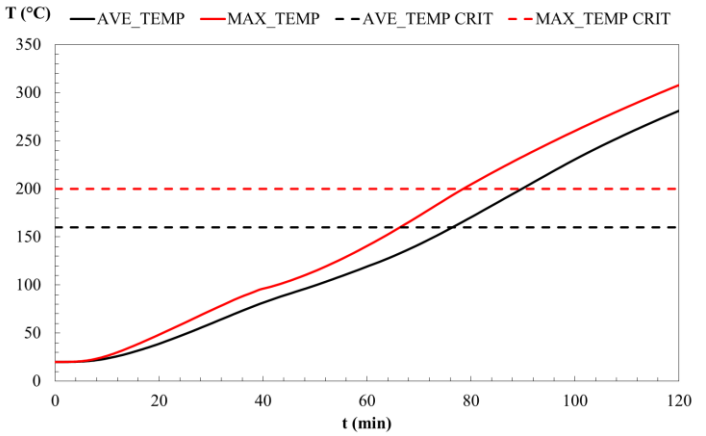

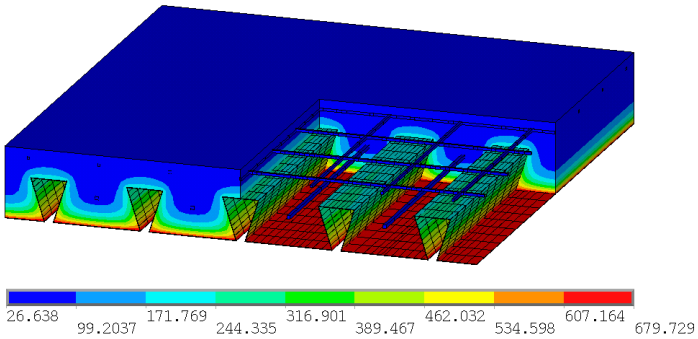

t= 19.1 min

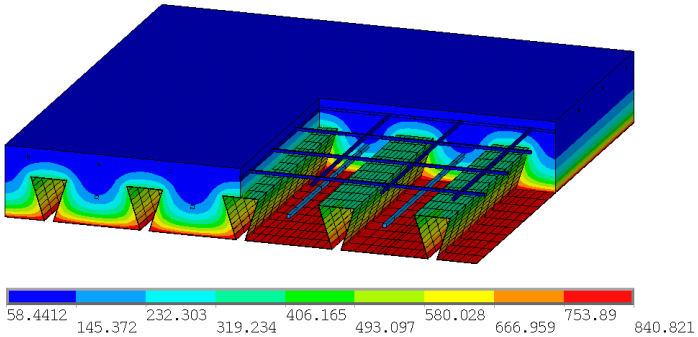

t= 38.2 min

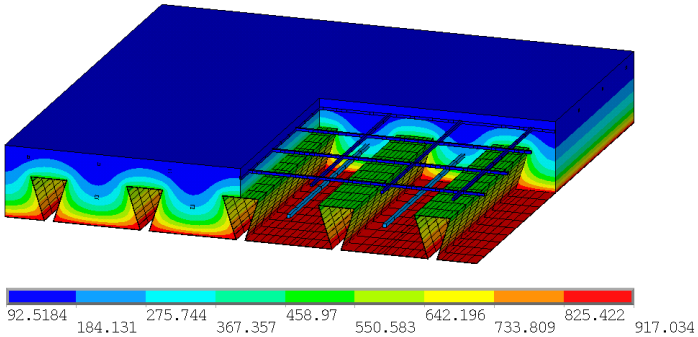

t= 57.3 min

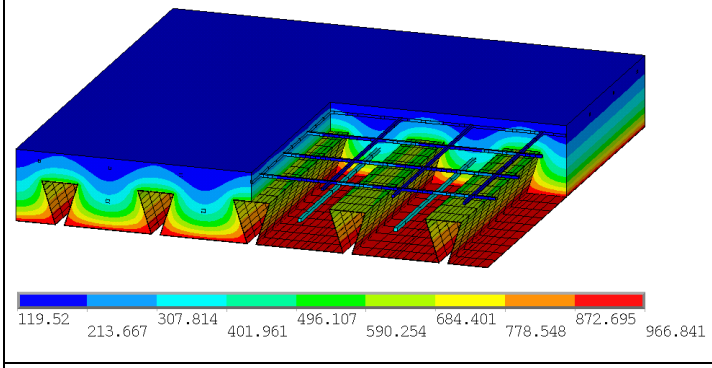

t= 76.4 min

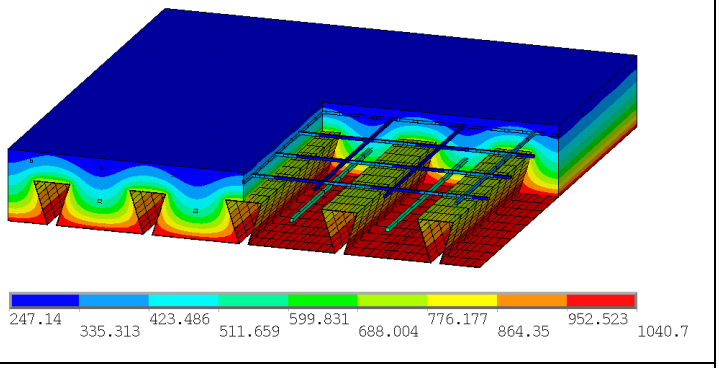

t= 120.0 min

SIM. 111	**Steel deck:** Re-entrant – Vulcraft 3.5D Formlok	**Rebar (mm):** ϕ8	**Fire resistance (min)**	
	Mesh (mm//mm): ϕ6//150 (W4.5)	**h_1 (mm):** 71	Ave: *91.3*	Max: 96.9

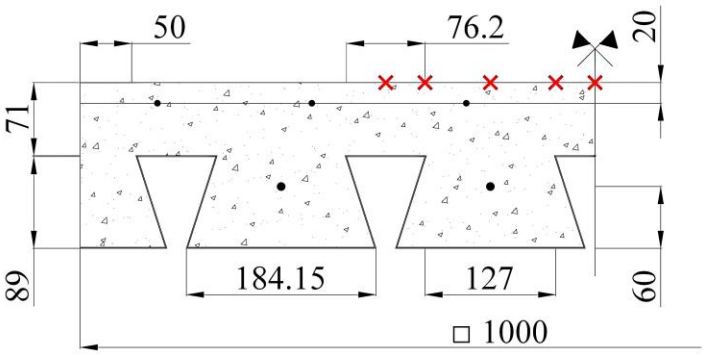

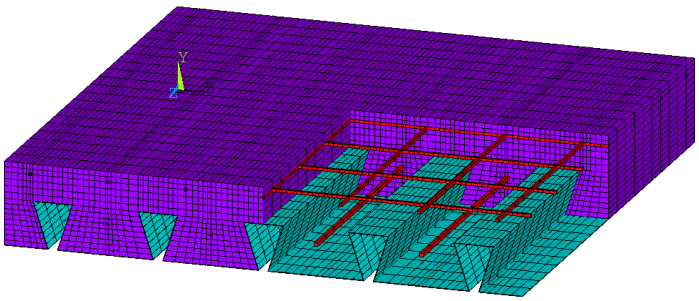

Finite element mesh

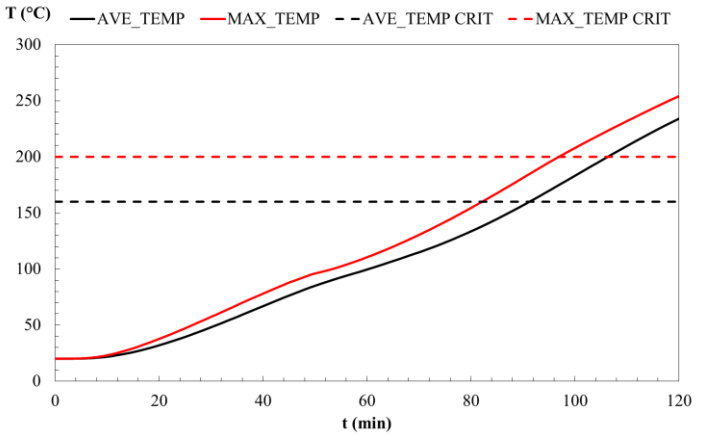

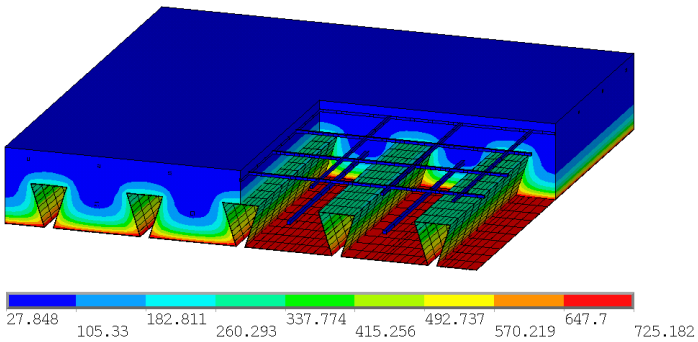

t= 22.8 min

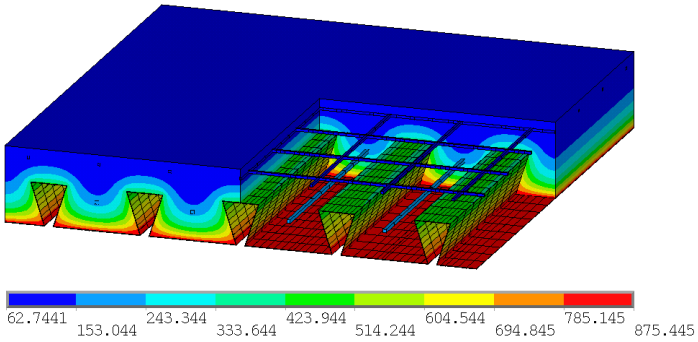

t= 45.7 min

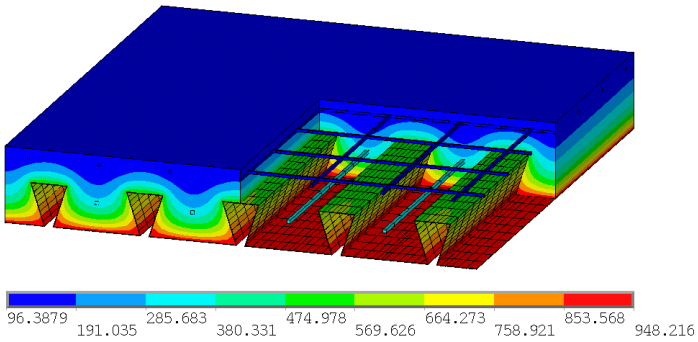

t= 68.5 min

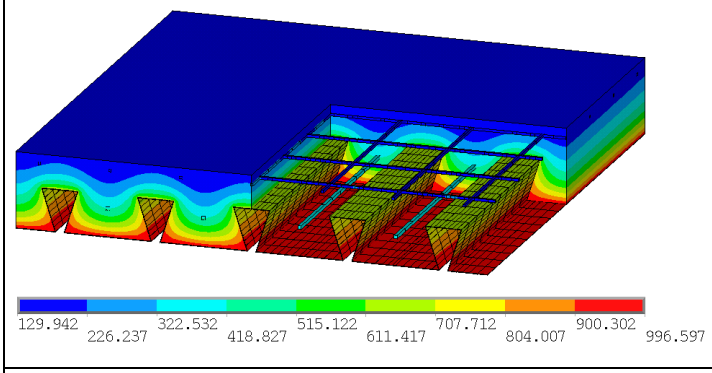

t= 91.3 min

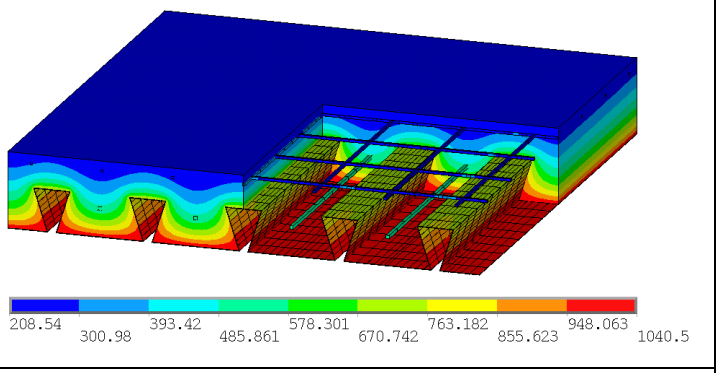

t= 120.0 min

SIM. 112	**Steel deck:** Re-entrant – Vulcraft 3.5D Formlok	**Rebar (mm):** ϕ8	**Fire resistance (min)**	
	Mesh (mm//mm): ϕ6//150 (W4.5)	**h_1 (mm):** 81	Ave: *107.2*	Max: 116.8

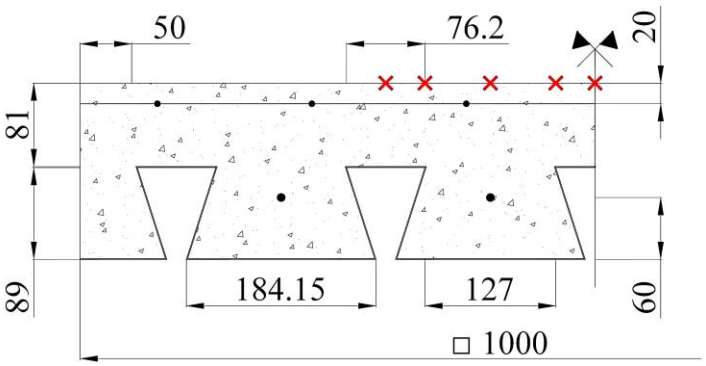

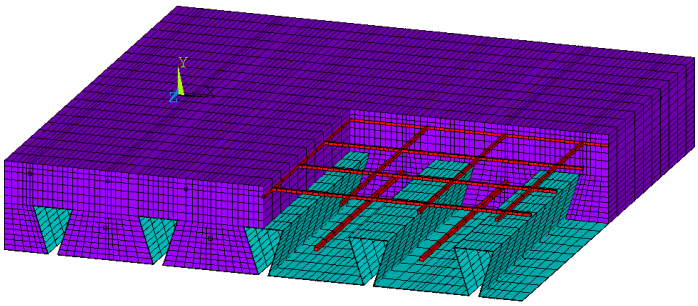

Finite element mesh

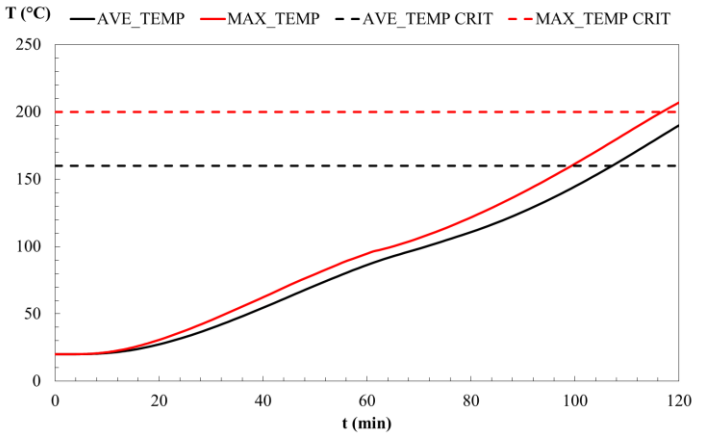

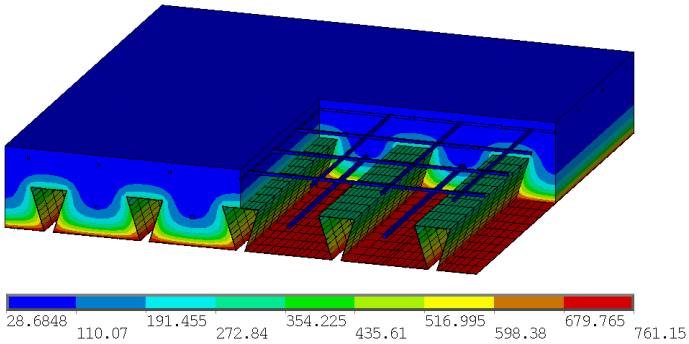

t= 26.8 min

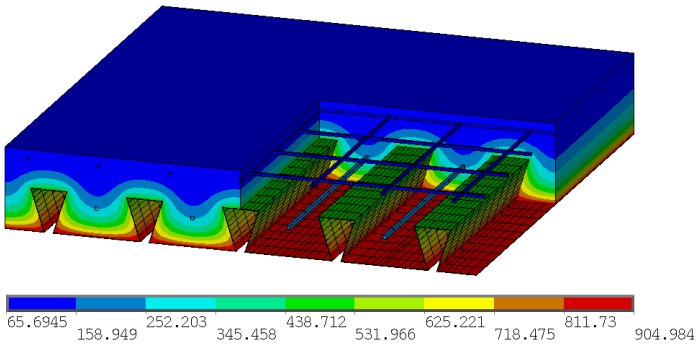

t= 53.6 min

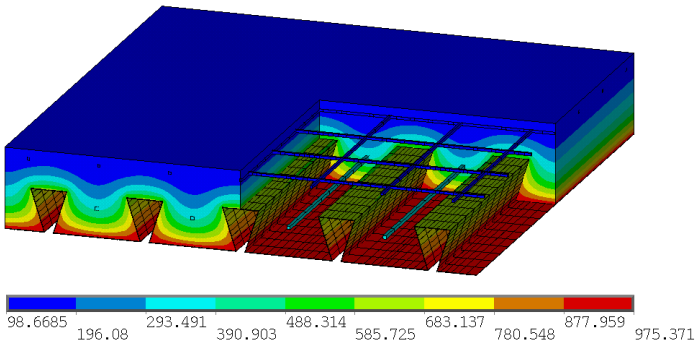

t= 80.4 min

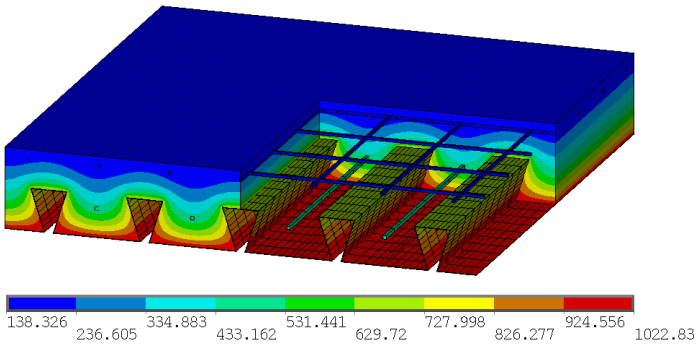

t= 107.2 min

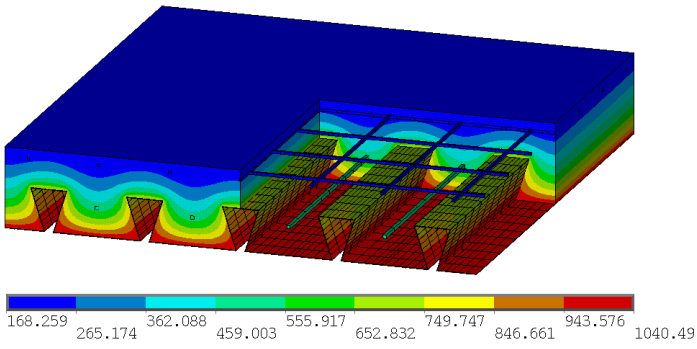

t= 120.0 min

SIM. 113	**Steel deck:** Re-entrant – Vulcraft 3.5D Formlok	**Rebar (mm):** ϕ10	**Fire resistance (min)**	
	Mesh (mm//mm): ϕ6//100 (W4.5)	**h_1 (mm):** 51	Ave: 62.2	Max: *60.4*

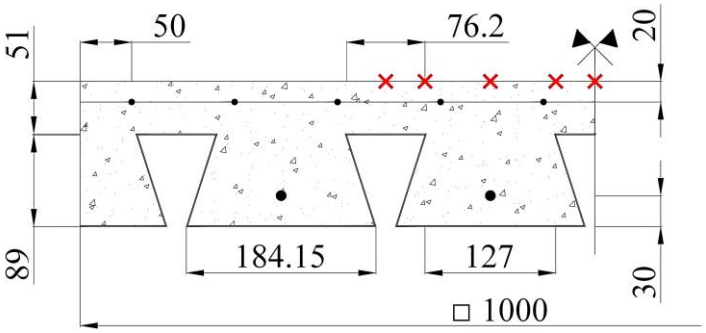

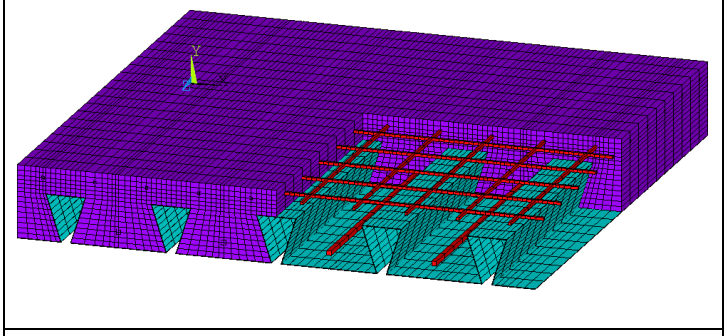

Finite element mesh

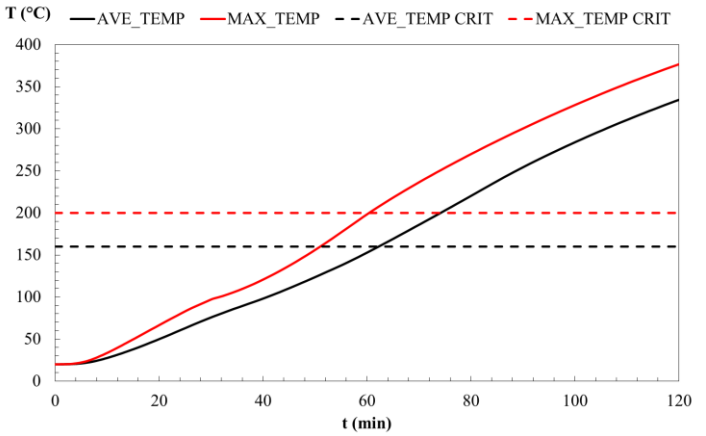

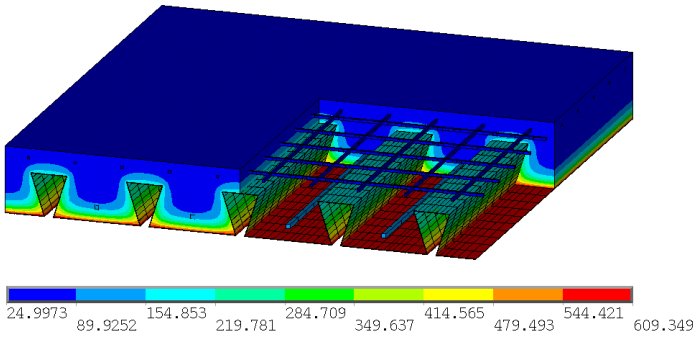

t= 15.1 min

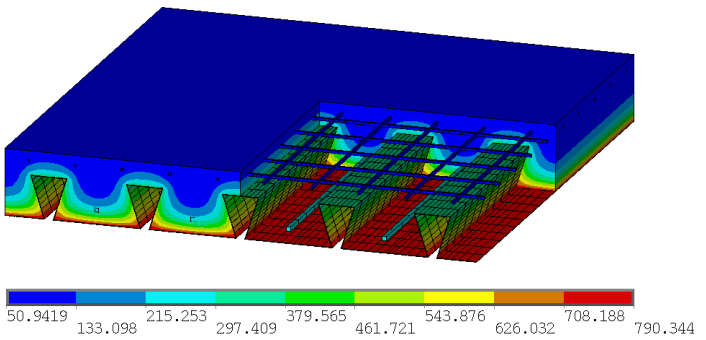

t= 30.2 min

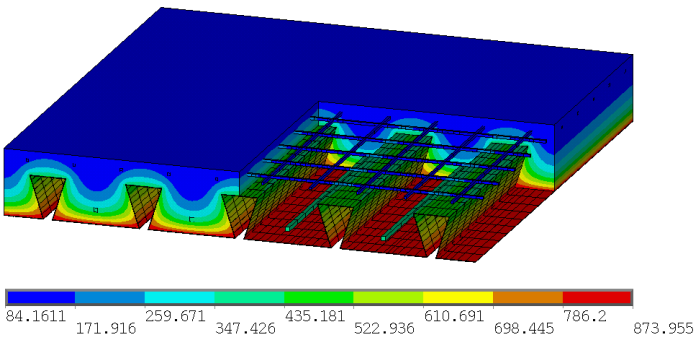

t= 45.3 min

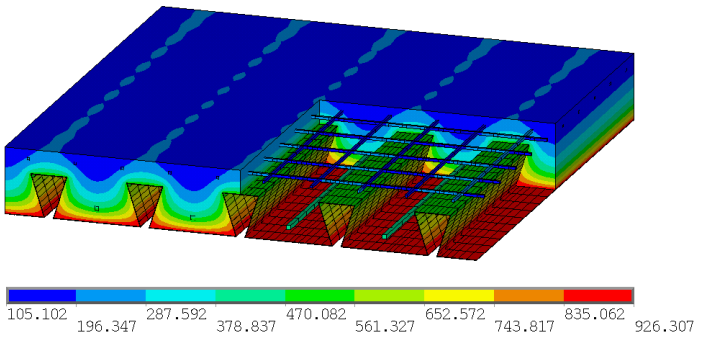

t= 60.4 min

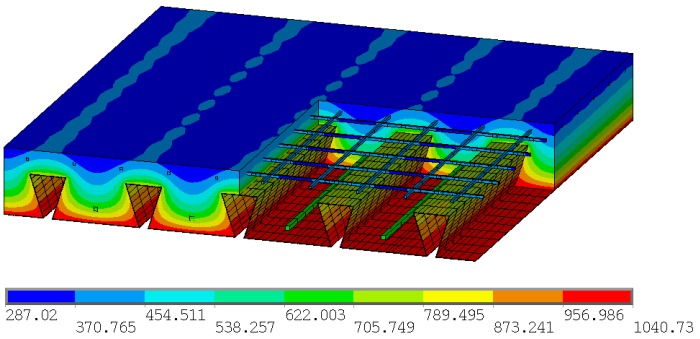

t= 120.0 min

SIM. 114	**Steel deck:** Re-entrant – Vulcraft 3.5D Formlok	**Rebar (mm):** ϕ10	**Fire resistance (min)**	
	Mesh (mm//mm): ϕ6//100 (W4.5)	**h_1 (mm):** 61	Ave: *76.2*	Max: 77.3

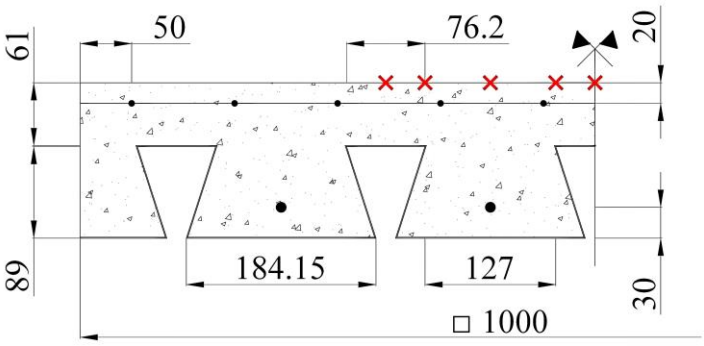

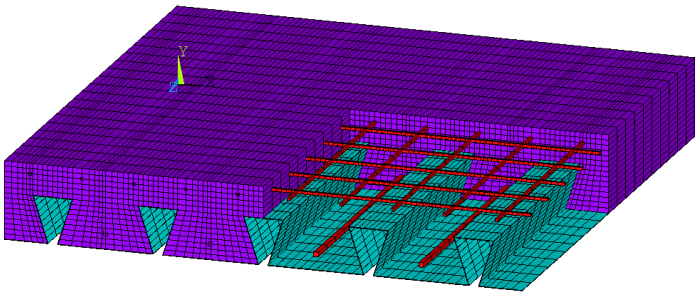

Finite element mesh

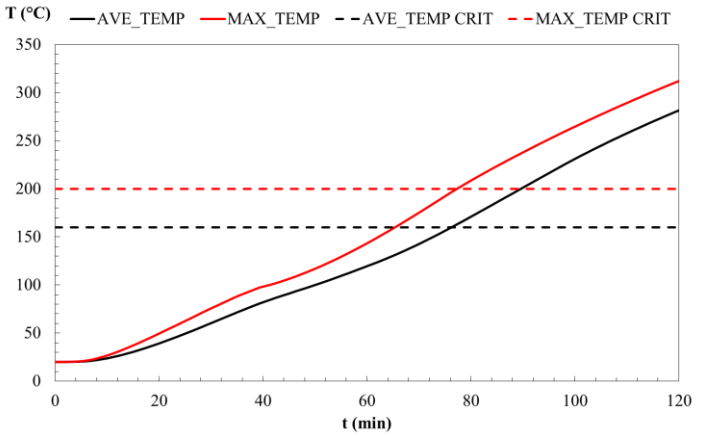

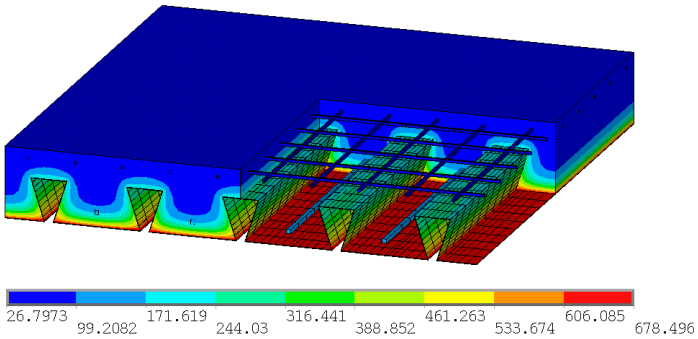

t= 19.1 min

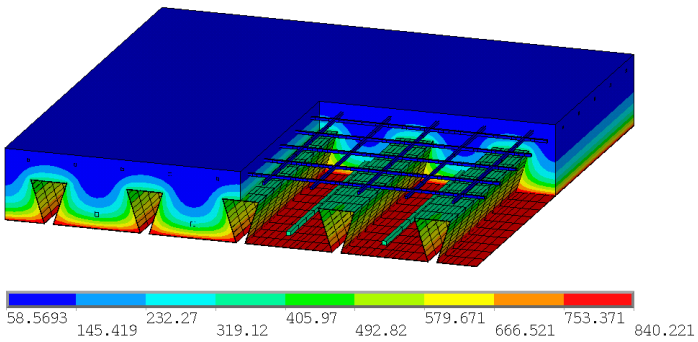

t= 38.1 min

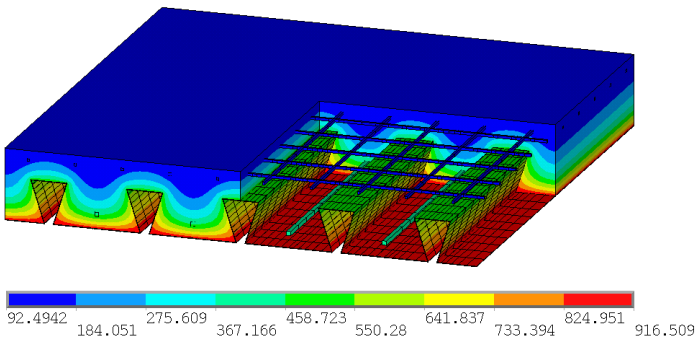

t= 57.2 min

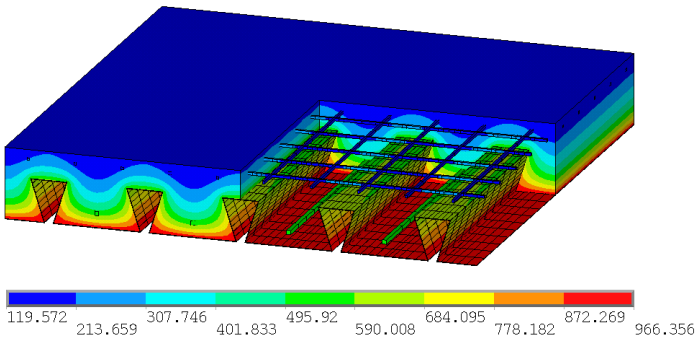

t= 76.2 min

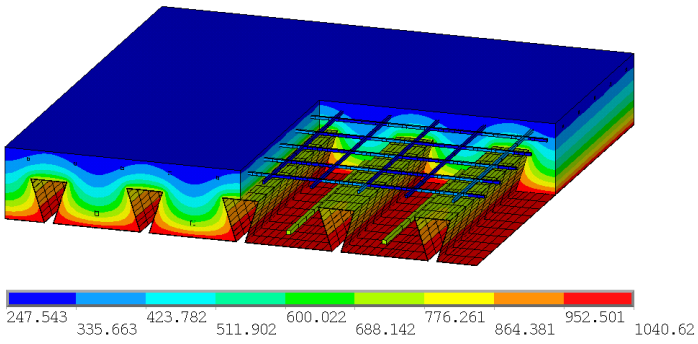

t= 120.0 min

SIM. 115	**Steel deck:** Re-entrant – Vulcraft 3.5D Formlok	**Rebar (mm):** ϕ10	**Fire resistance (min)**	
	Mesh (mm//mm): ϕ6//100 (W4.5)	**h_1 (mm):** 71	Ave: *91.2*	Max: 95.9

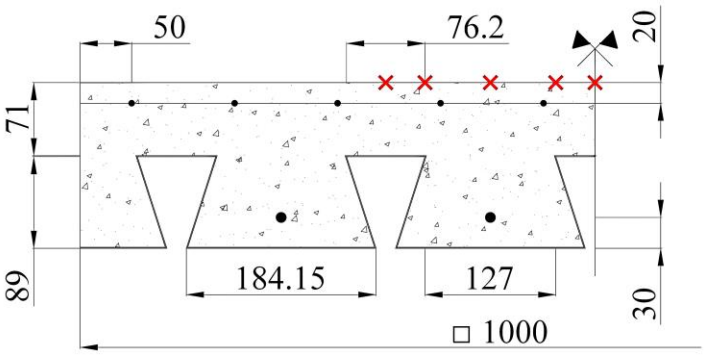

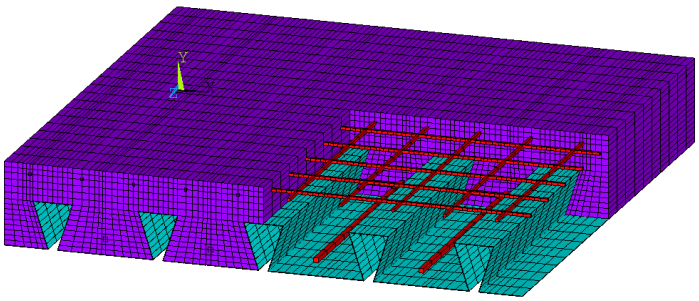

Finite element mesh

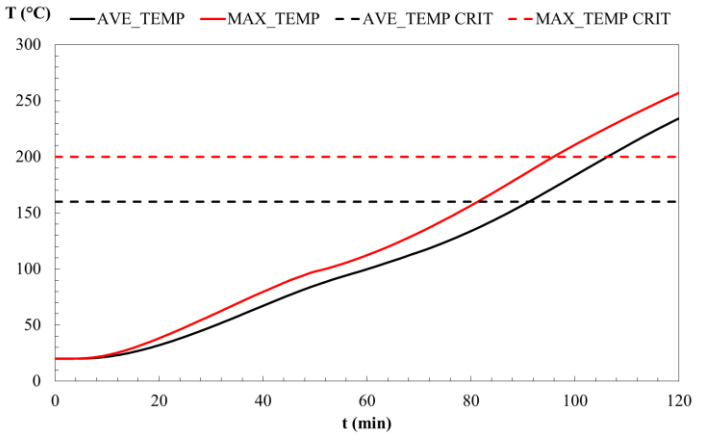

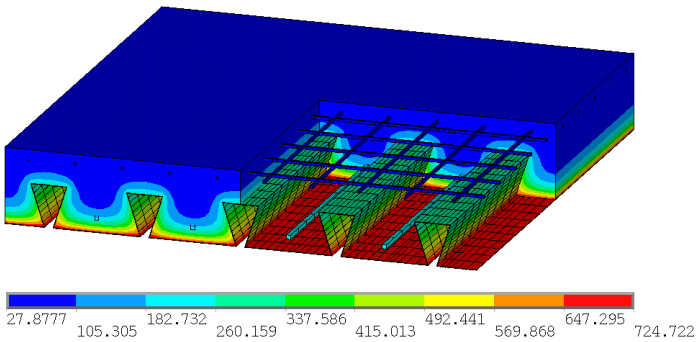

t= 22.8 min

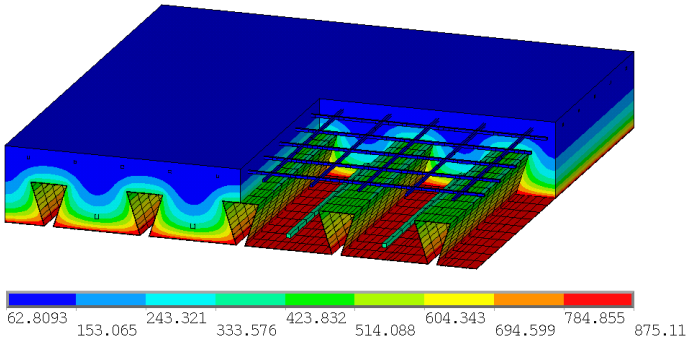

t= 45.6 min

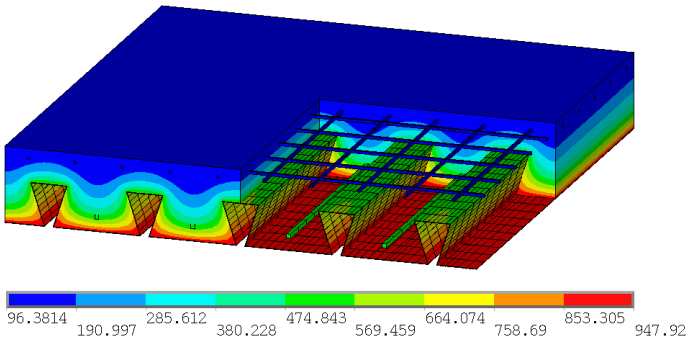

t= 68.4 min

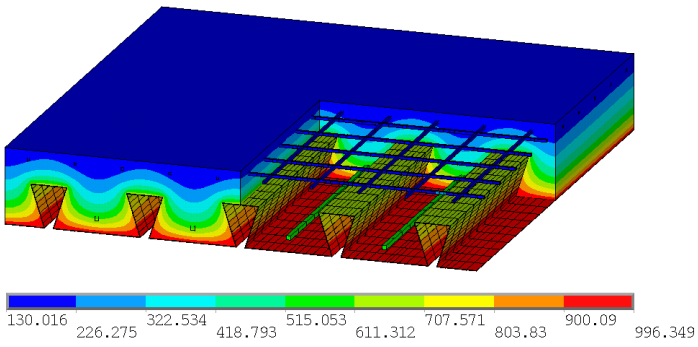

t= 91.2 min

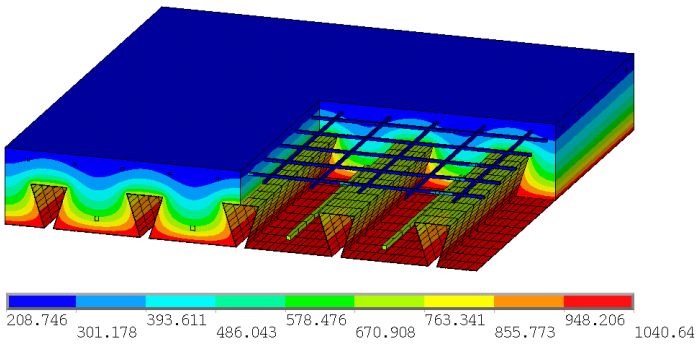

t= 120.0 min

SIM. 116	**Steel deck:** Re-entrant – Vulcraft 3.5D Formlok	**Rebar (mm):** ϕ10	**Fire resistance (min)**	
	Mesh (mm//mm): ϕ6//100 (W4.5)	**h_1 (mm):** 81	Ave: *107.1*	Max: 115.9

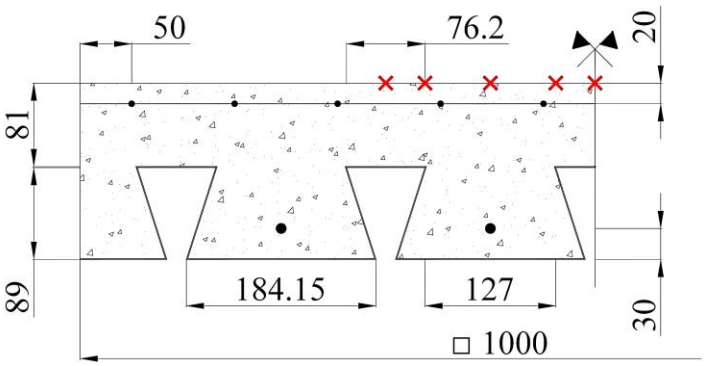

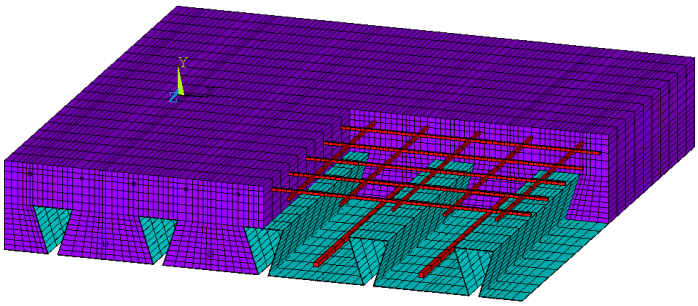

Finite element mesh

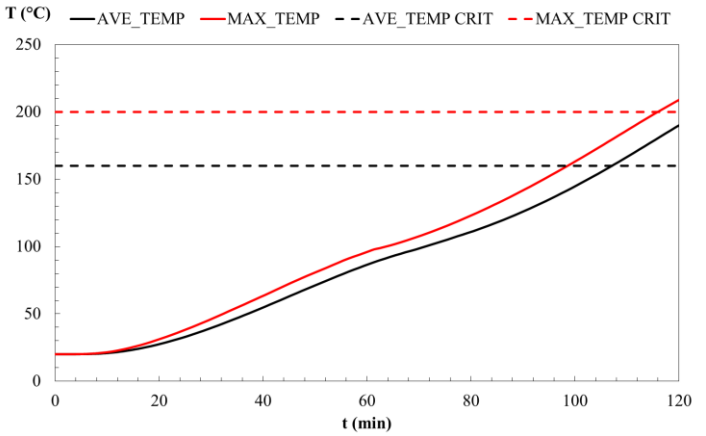

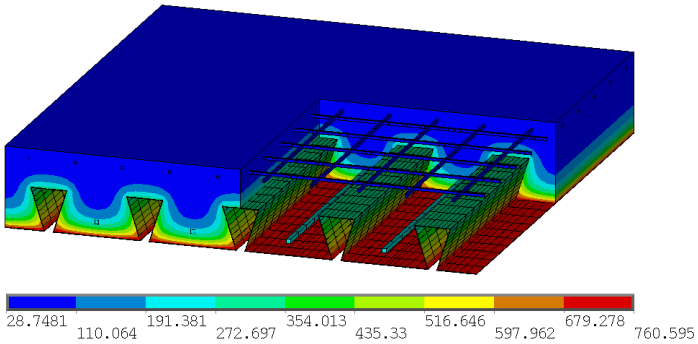

t= 26.8 min

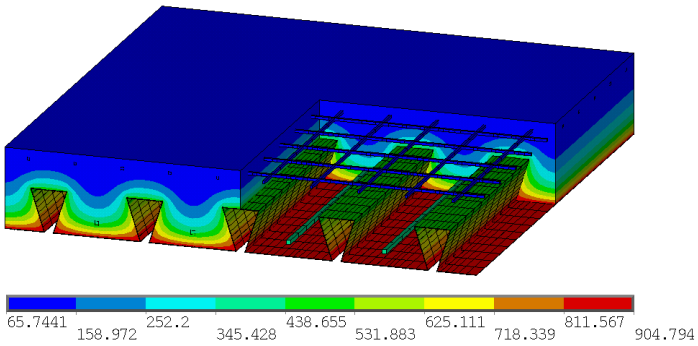

t= 53.6 min

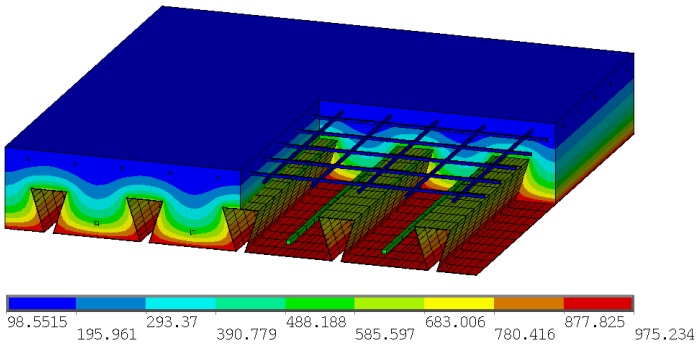

t= 80.3 min

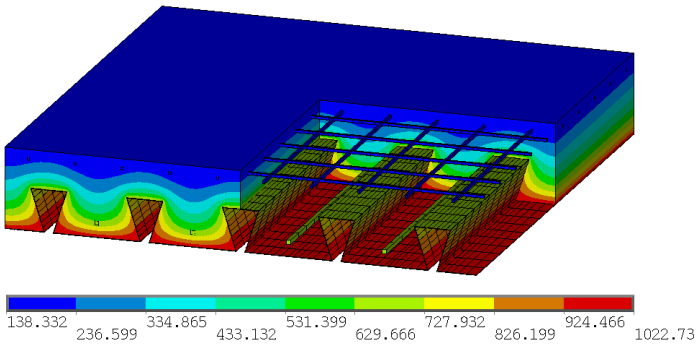

t= 107.1 min

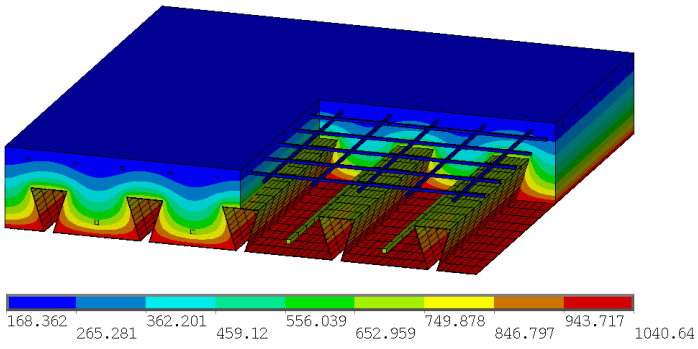

t= 120.0 min

SIM. 117	**Steel deck:** Re-entrant – Vulcraft 3.5D Formlok	**Rebar (mm):** ϕ10	**Fire resistance (min)**	
	Mesh (mm//mm): ϕ6//100 (W4.5)	**h_1 (mm):** 51	Ave: 62.2	Max: *60.4*

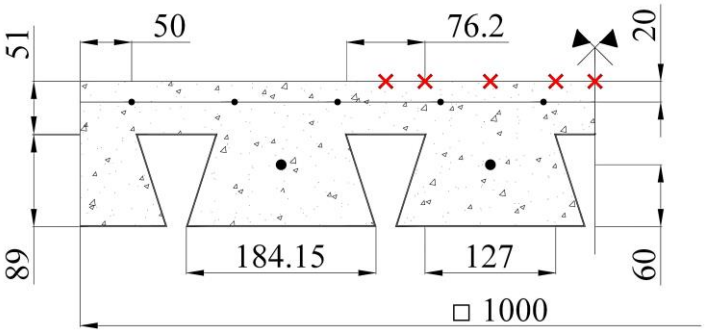

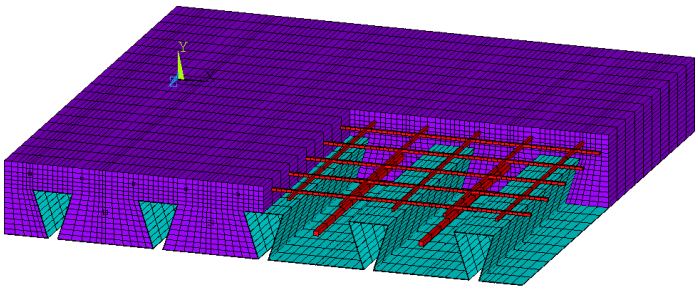

Finite element mesh

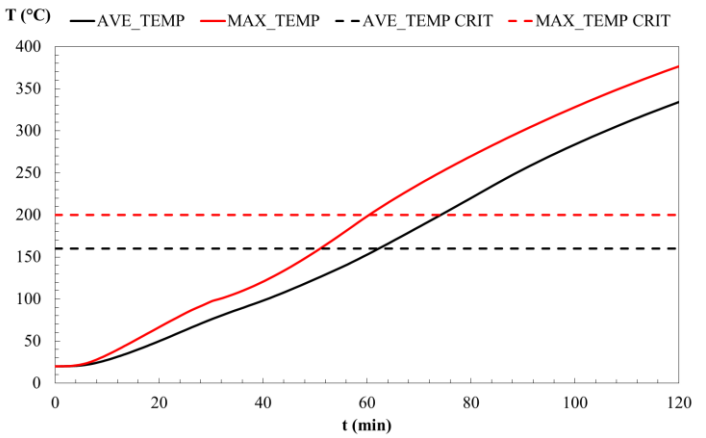

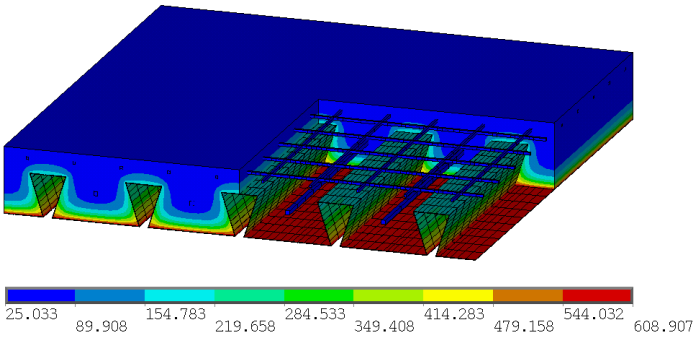

t= 15.1 min

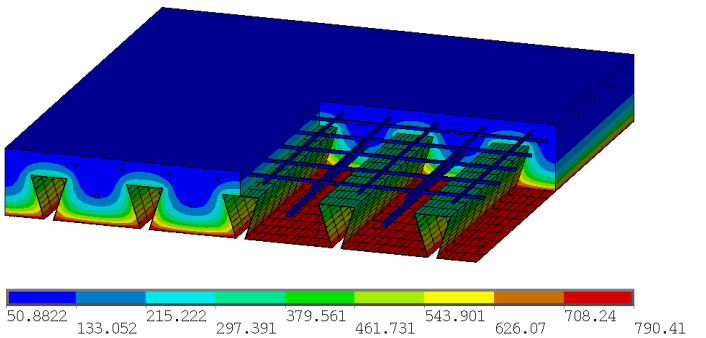

t= 30.2 min

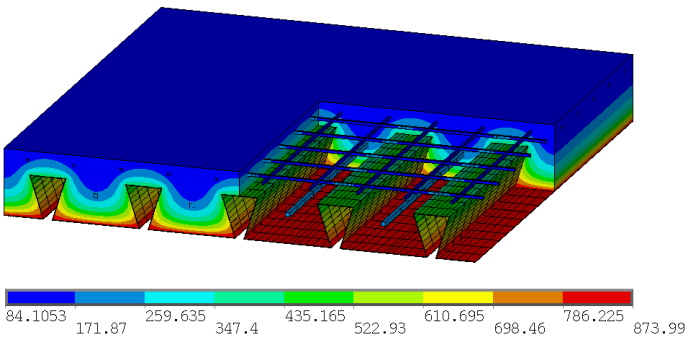

t= 45.3 min

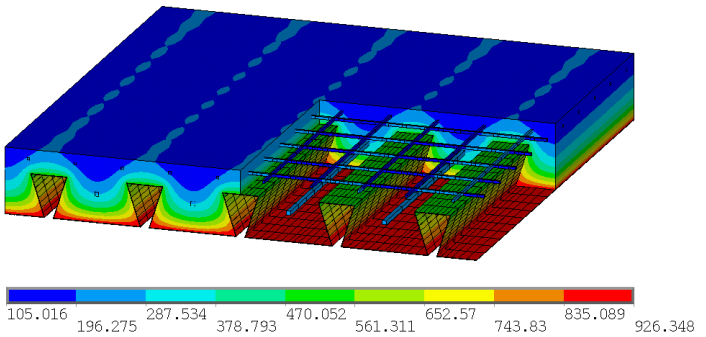

t= 60.4 min

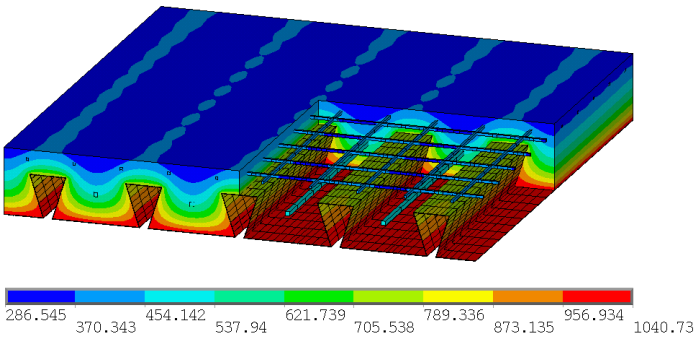

t= 120.0 min

SIM. 118	**Steel deck:** Re-entrant – Vulcraft 3.5D Formlok	**Rebar (mm):** ϕ10	**Fire resistance (min)**	
	Mesh (mm//mm): ϕ6//100 (W4.5)	**h_1 (mm):** 61	Ave: *76.3*	Max: 77.3

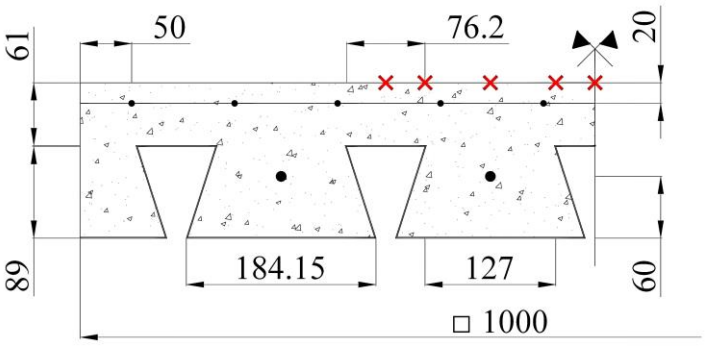

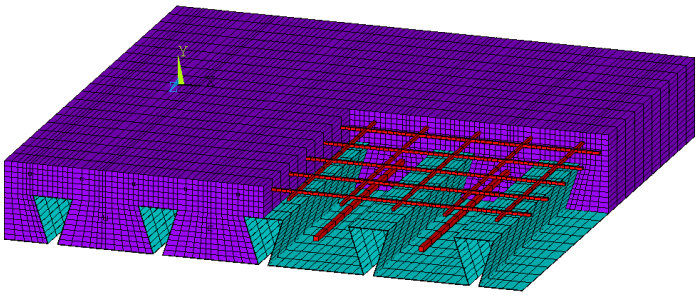

Finite element mesh

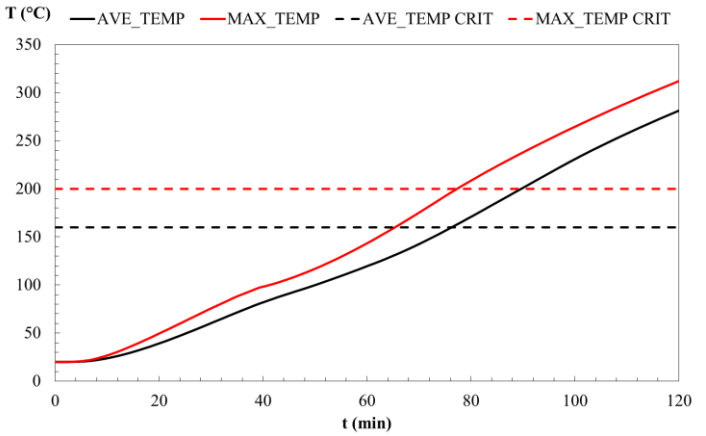

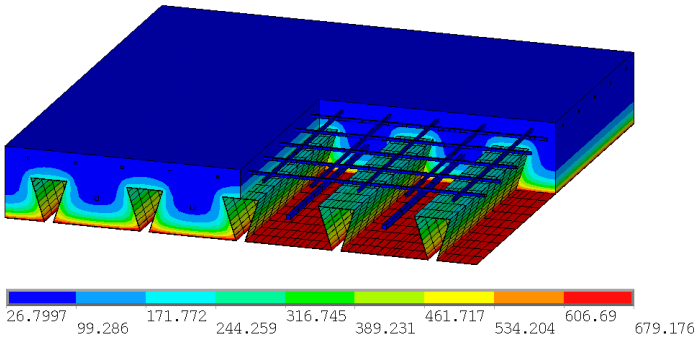

t= 19.1 min

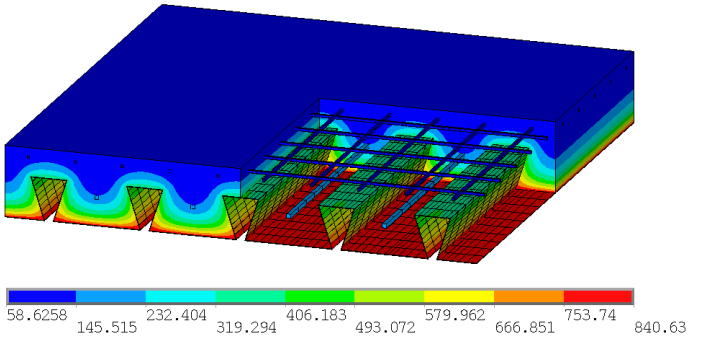

t= 38.2 min

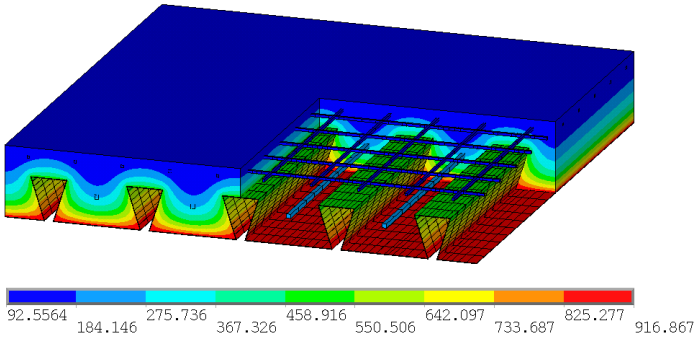

t= 57.2 min

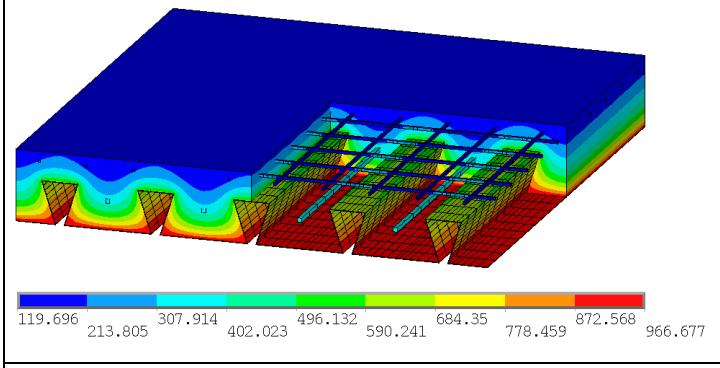

t= 76.3 min

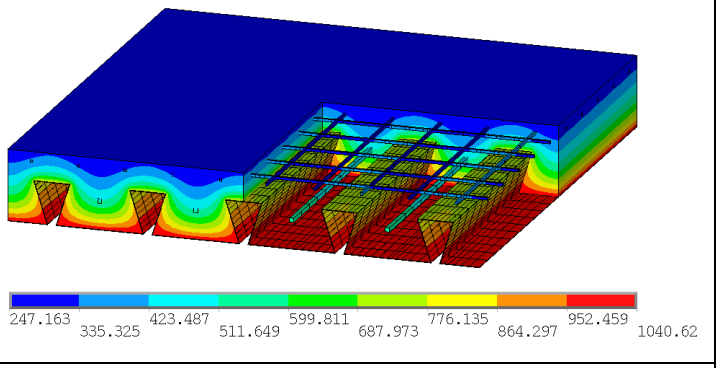

t= 120.0 min

SIM. 119	**Steel deck:** Re-entrant – Vulcraft 3.5D Formlok	**Rebar (mm):** ϕ10	**Fire resistance (min)**	
	Mesh (mm//mm): ϕ6//100 (W4.5)	**h_1 (mm):** 71	Ave: *91.2*	Max: 95.9

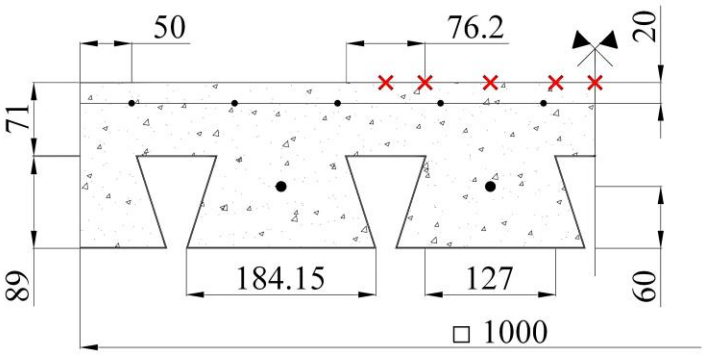

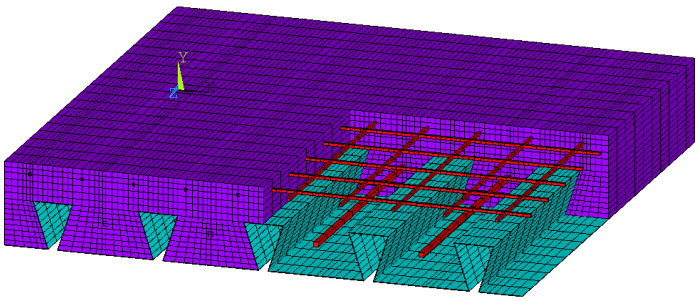

Finite element mesh

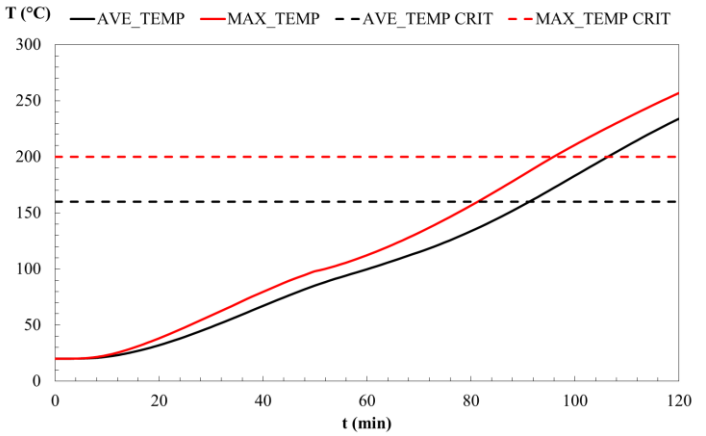

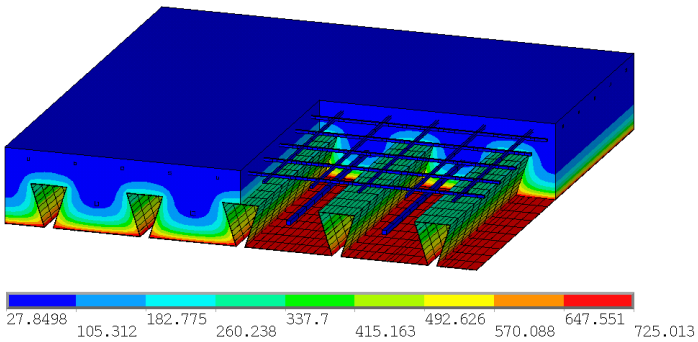

t= 22.8 min

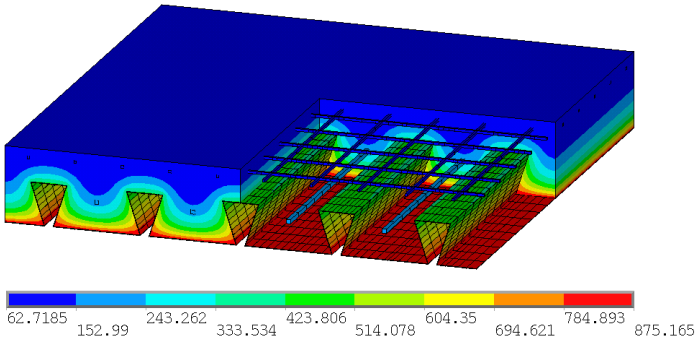

t= 45.6 min

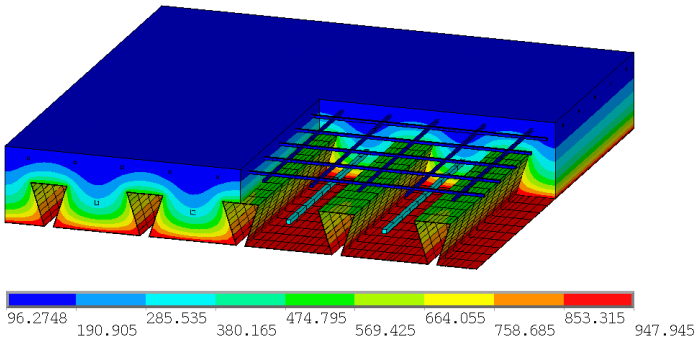

t= 68.4 min

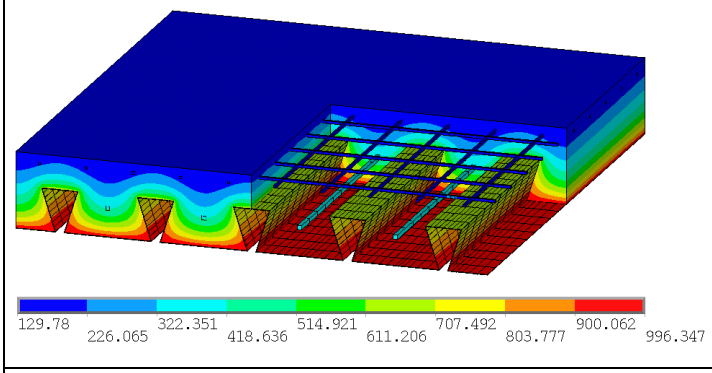

t= 91.2 min

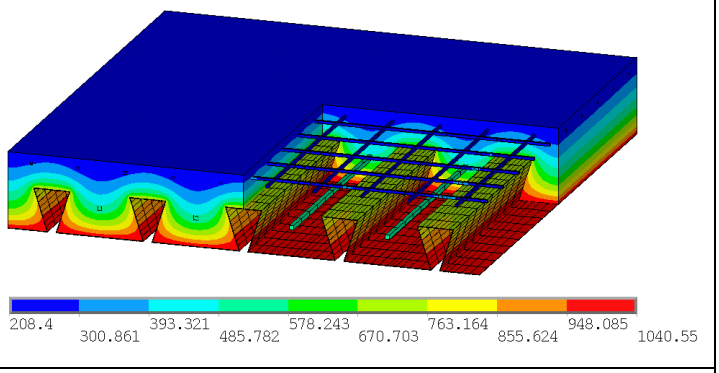

t= 120.0 min

SIM. 120	**Steel deck:** Re-entrant – Vulcraft 3.5D Formlok	**Rebar (mm):** ϕ10	**Fire resistance (min)**	
	Mesh (mm//mm): ϕ6//100 (W4.5)	**h_1 (mm):** 81	Ave: *107.2*	Max: 116.0

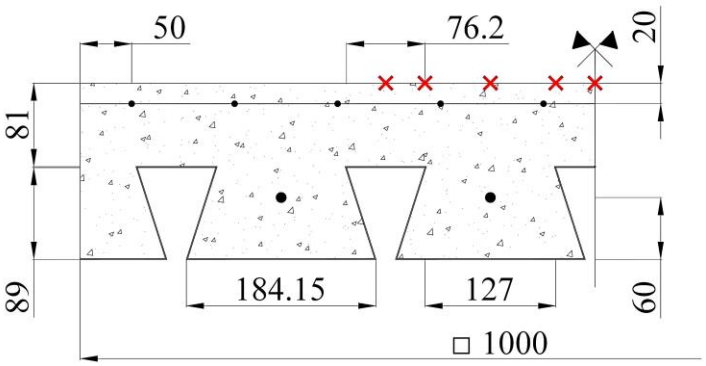

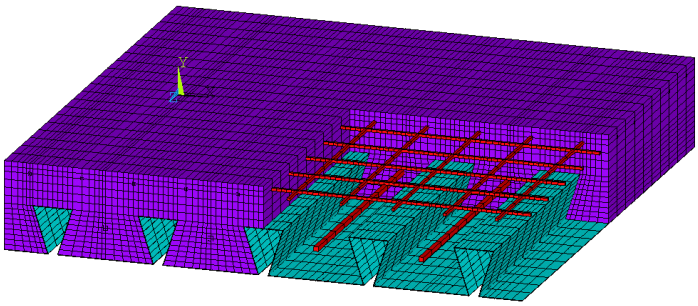

Finite element mesh

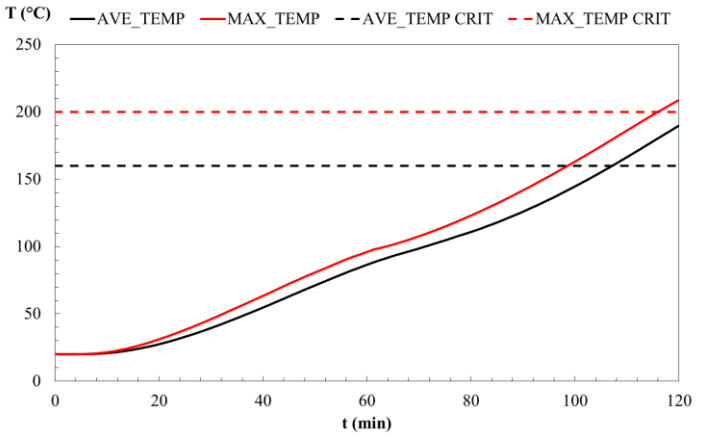

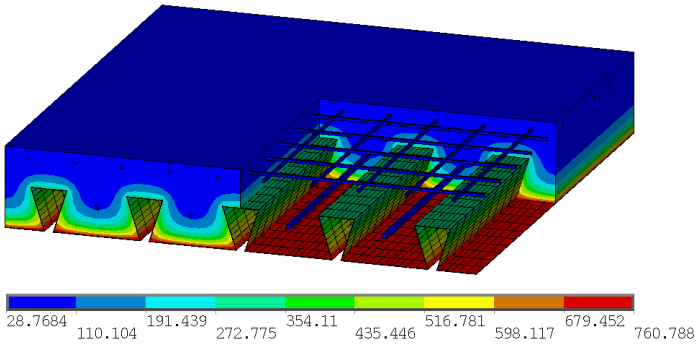

t= 26.8 min

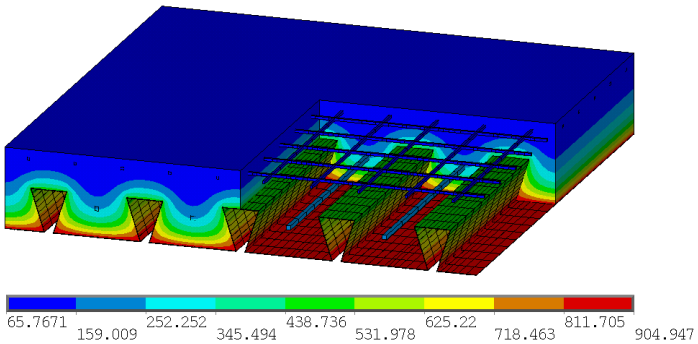

t= 53.6 min

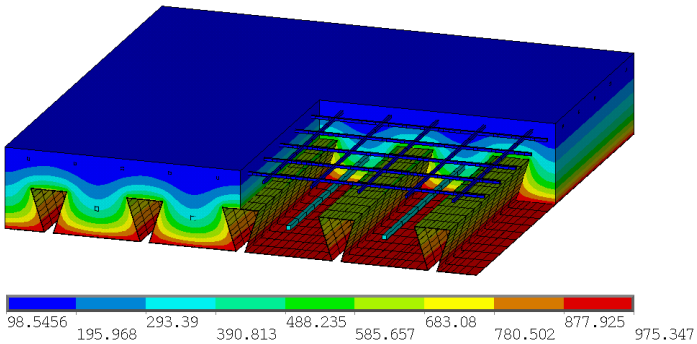

t= 80.4 min

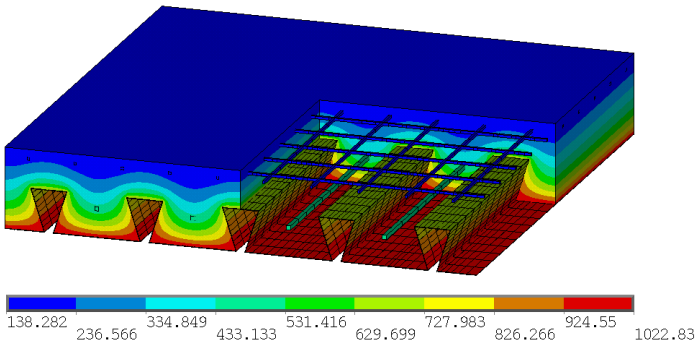

t= 107.2 min

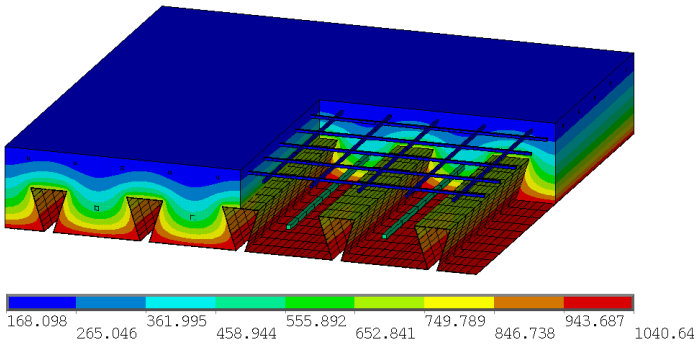

t= 120.0 min

SIM. 121	**Steel deck:** Re-entrant – Vulcraft 3.5D Formlok	**Rebar (mm):** ϕ10	**Fire resistance (min)**	
	Mesh (mm//mm): ϕ6//150 (W4.5)	**h_1 (mm):** 51	Ave: 62.5	Max: *61.6*

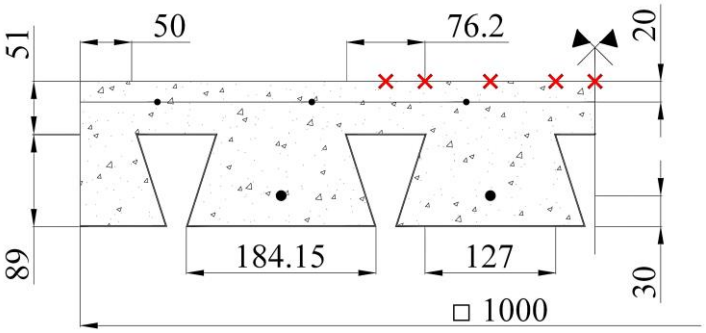

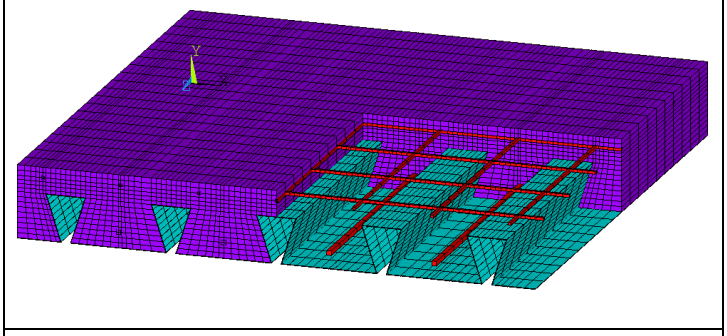

Finite element mesh

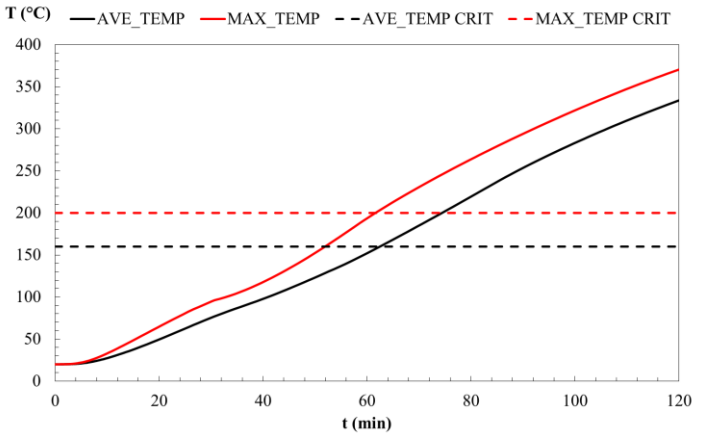

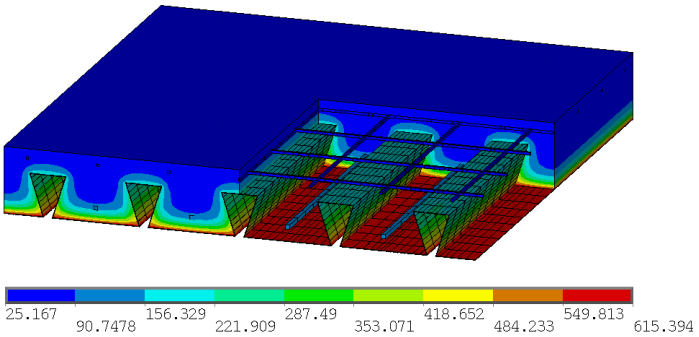

t= 15.4 min

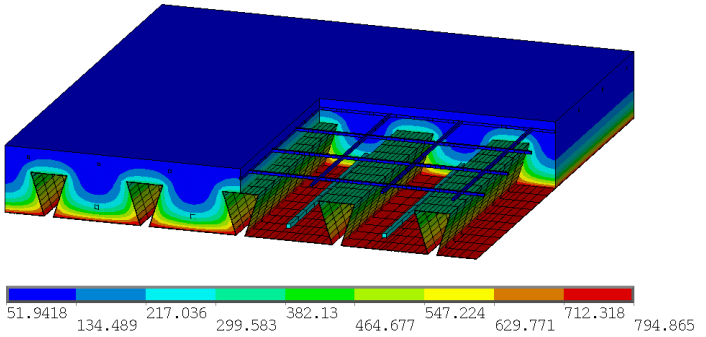

t= 30.8 min

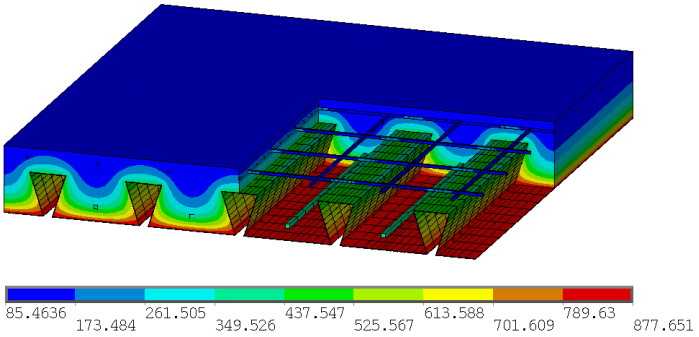

t= 46.2 min

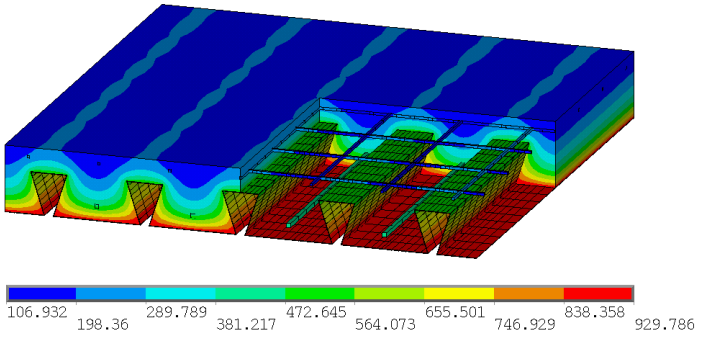

t= 61.6 min

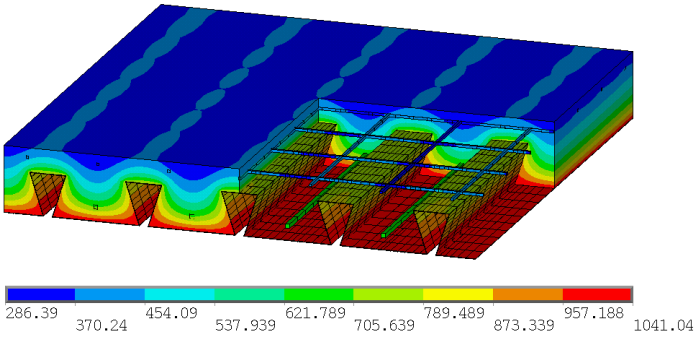

t= 120.0 min

SIM. 122	**Steel deck:** Re-entrant – Vulcraft 3.5D Formlok	**Rebar (mm):** ϕ10	**Fire resistance (min)**	
	Mesh (mm//mm): ϕ6//150 (W4.5)	**h_1 (mm):** 61	Ave: *76.5*	Max: 78.5

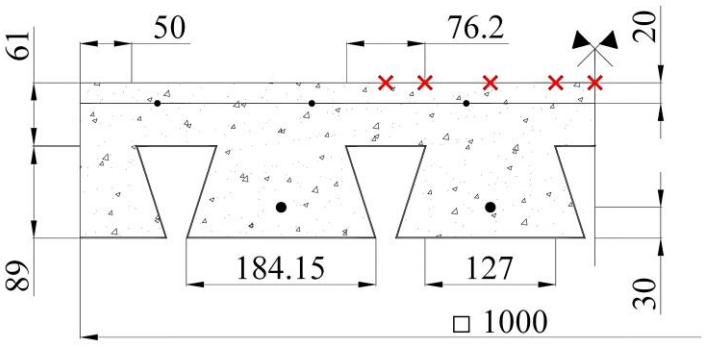

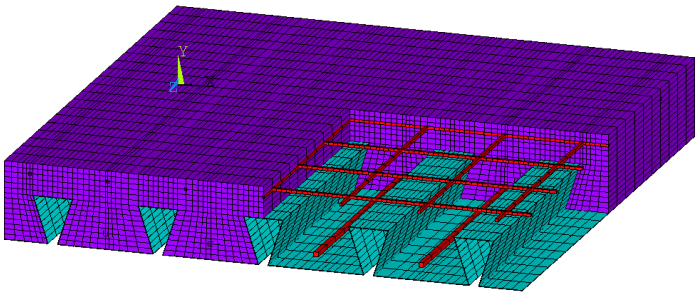

Finite element mesh

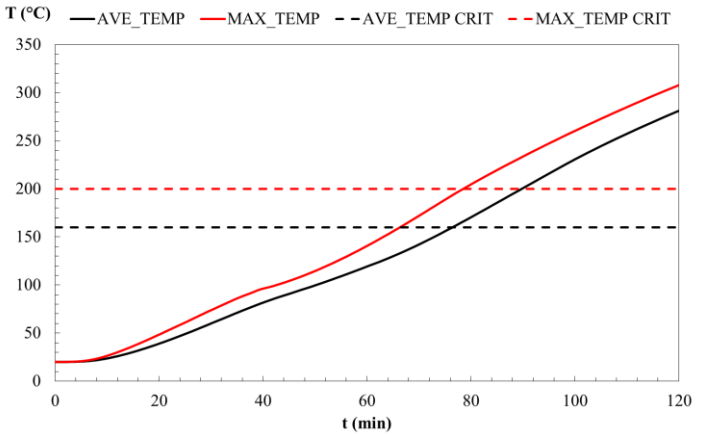

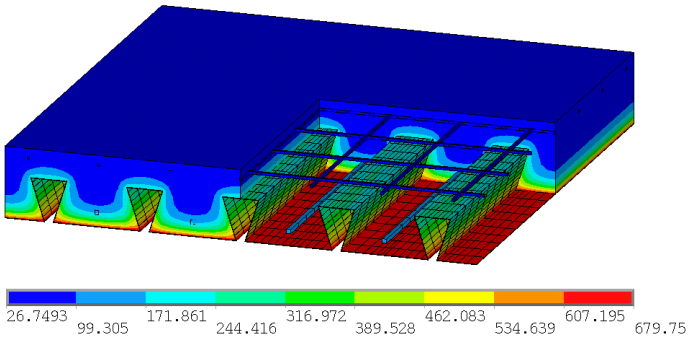

t= 19.1 min

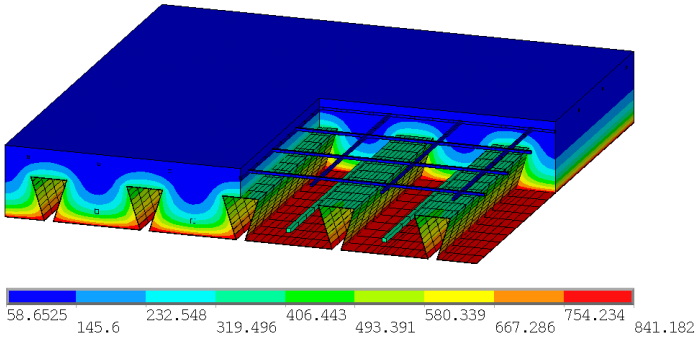

t= 38.3 min

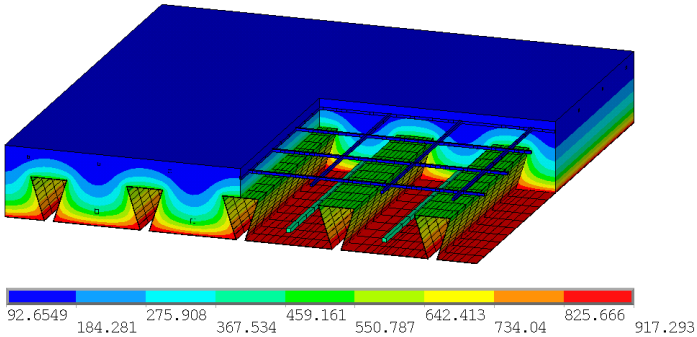

t= 57.4 min

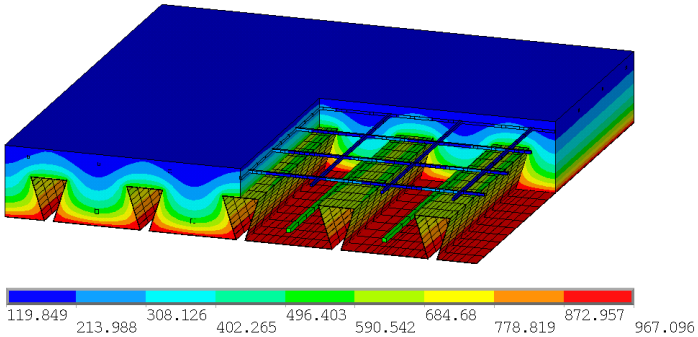

t= 76.5 min

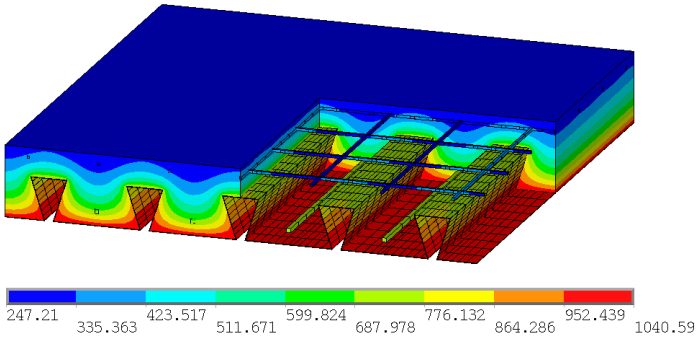

t= 120.0 min

SIM. 123	**Steel deck:** Re-entrant – Vulcraft 3.5D Formlok	**Rebar (mm):** ϕ10	**Fire resistance (min)**	
	Mesh (mm//mm): ϕ6//150 (W4.5)	**h_1 (mm):** 71	Ave: *91.3*	Max: 97.0

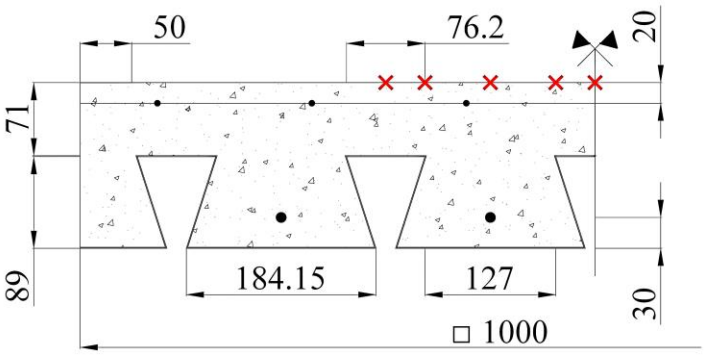

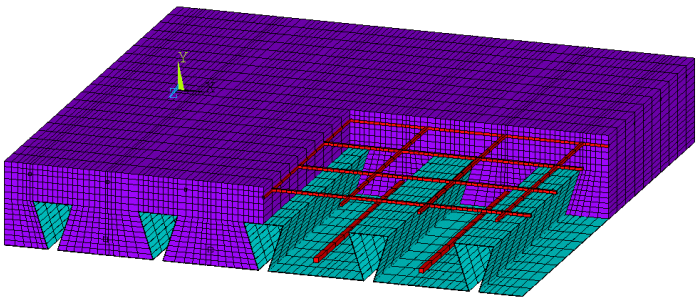

Finite element mesh

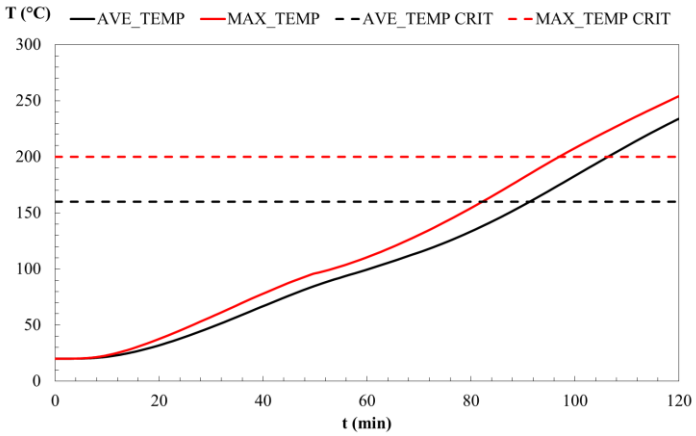

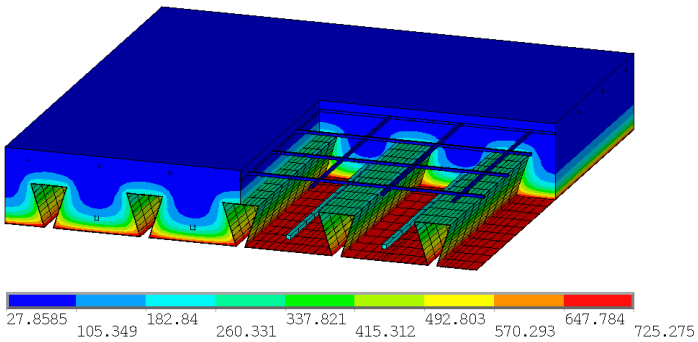

t= 22.8 min

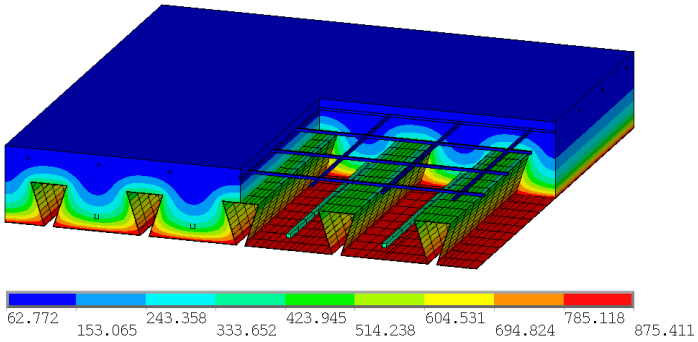

t= 45.7 min

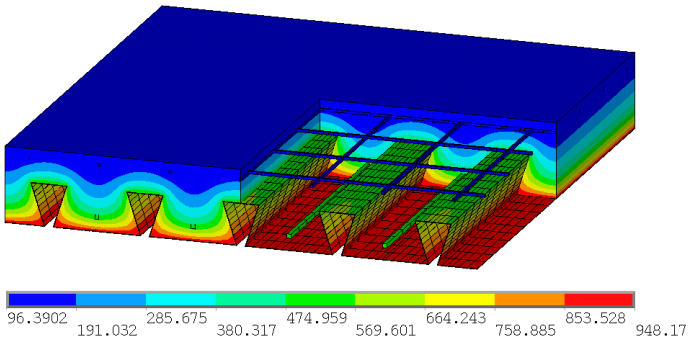

t= 68.5 min

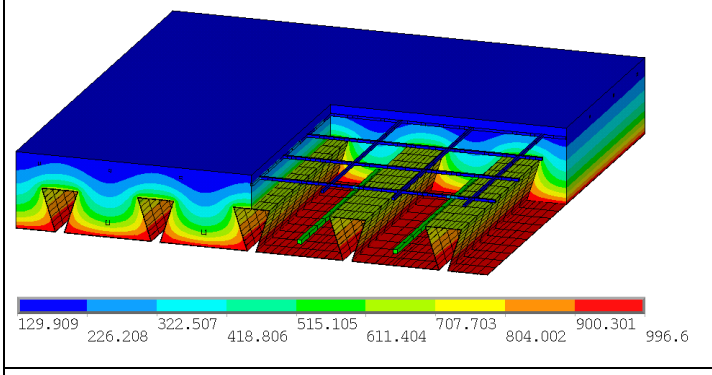

t= 91.3 min

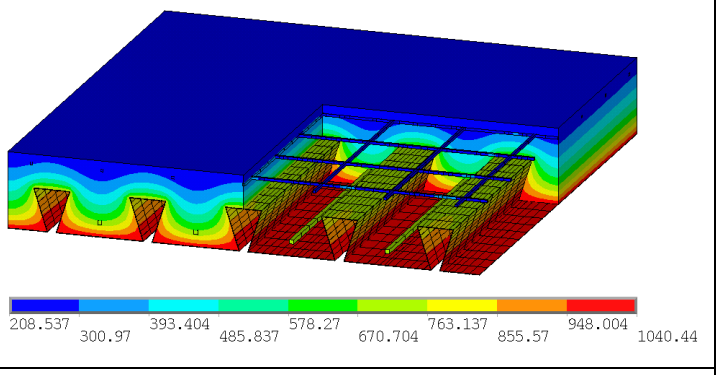

t= 120.0 min

SIM. 124	**Steel deck:** Re-entrant – Vulcraft 3.5D Formlok	**Rebar (mm):** ϕ10	**Fire resistance (min)**	
	Mesh (mm//mm): ϕ6//150 (W4.5)	**h_1 (mm):** 81	Ave: *107.2*	Max: 116.7

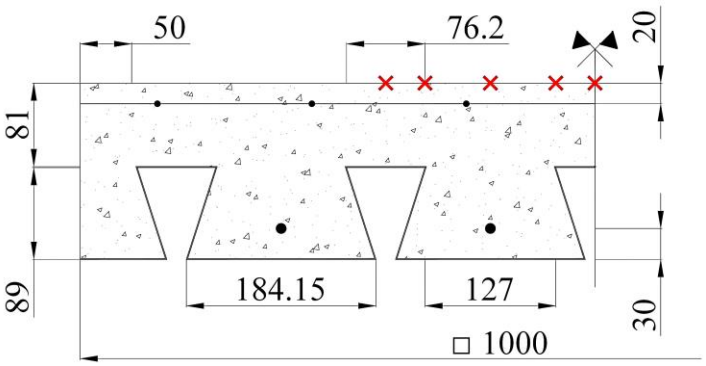

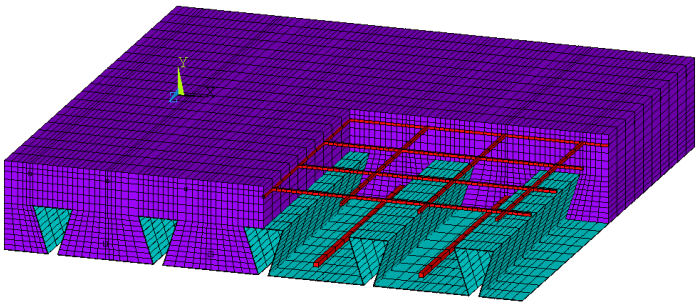

Finite element mesh

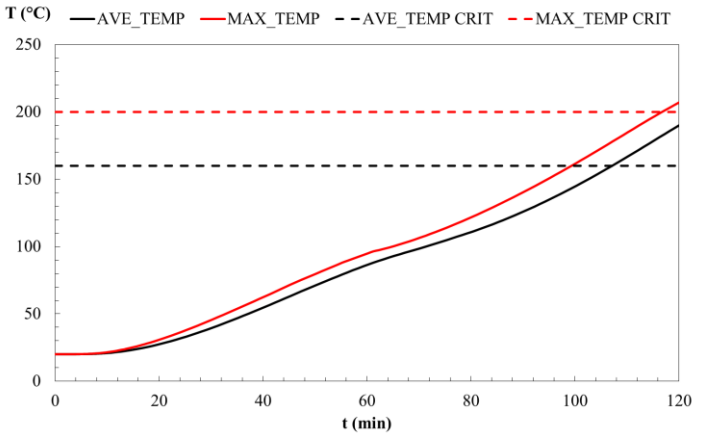

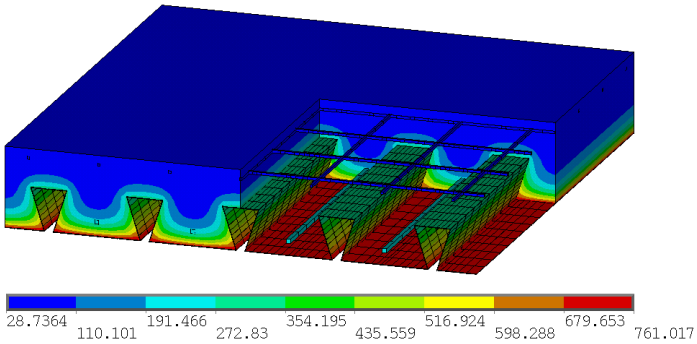

t= 26.8 min

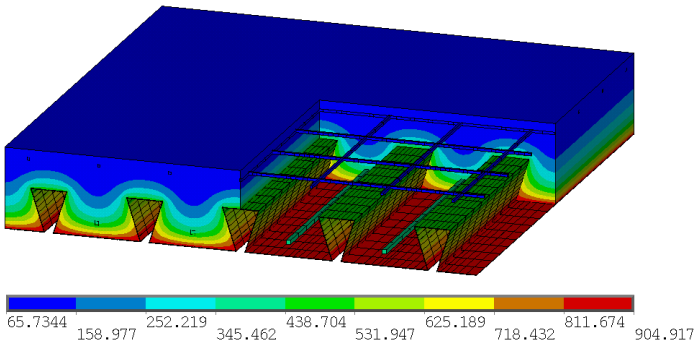

t= 53.6 min

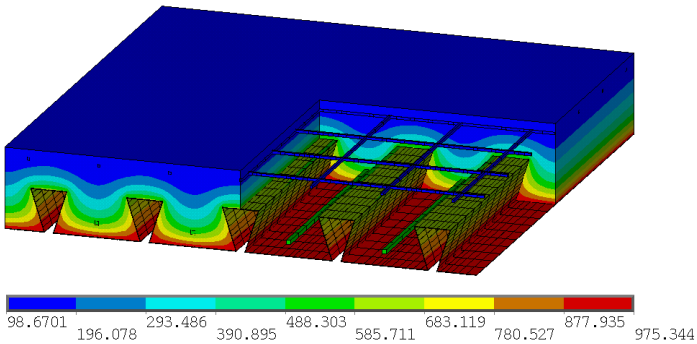

t= 80.4 min

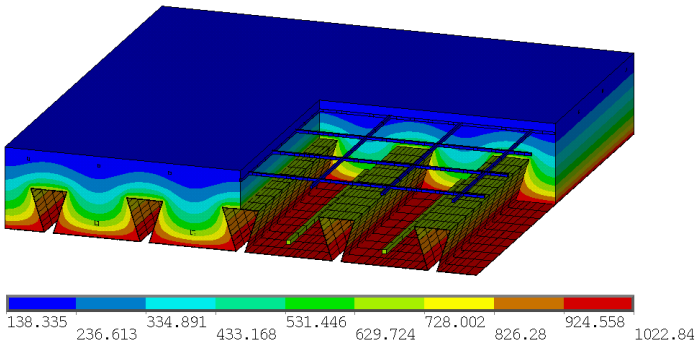

t= 107.2 min

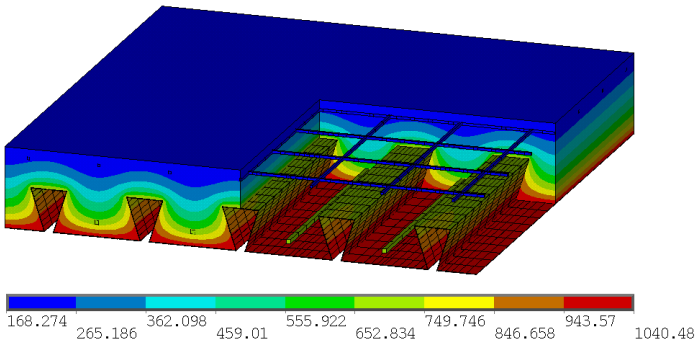

t= 120.0 min

SIM. 125	**Steel deck:** Re-entrant – Vulcraft 3.5D Formlok	**Rebar (mm):** ϕ10	**Fire resistance (min)**	
	Mesh (mm//mm): ϕ6//150 (W4.5)	**h_1 (mm):** 51	Ave: 62.5	Max: *61.6*

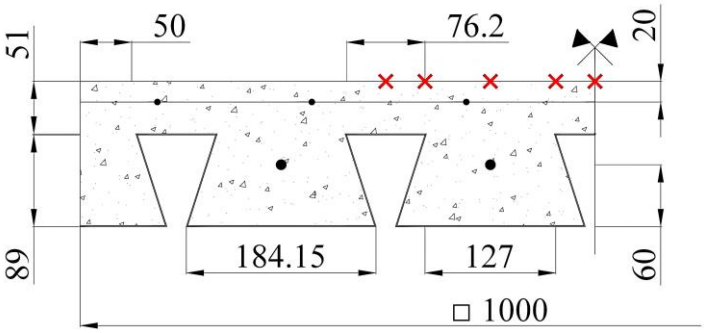

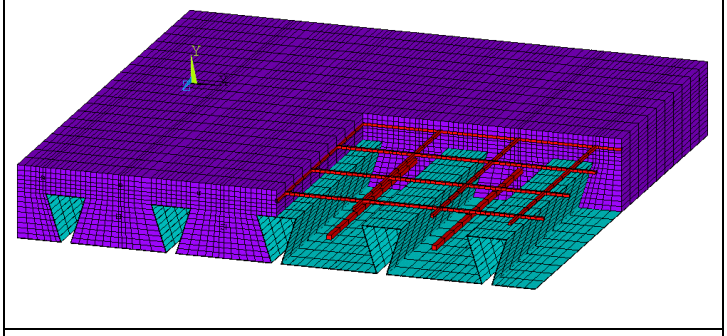

Finite element mesh

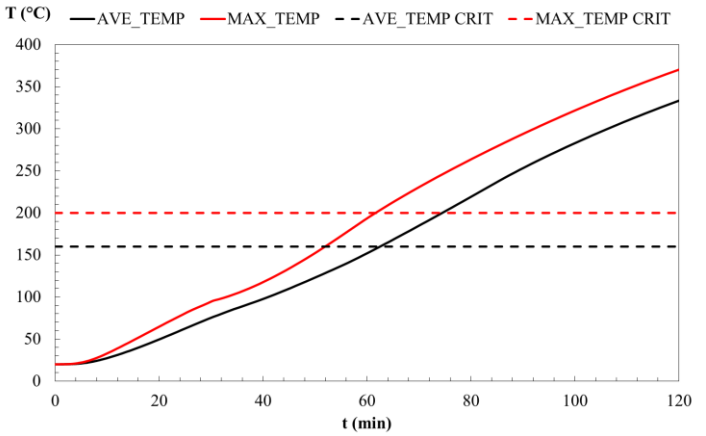

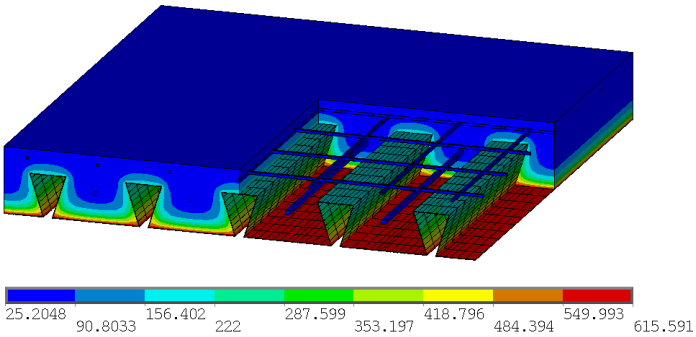

t= 15.4 min

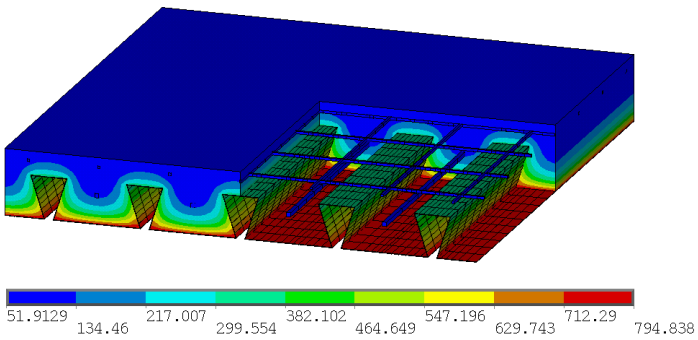

t= 30.8 min

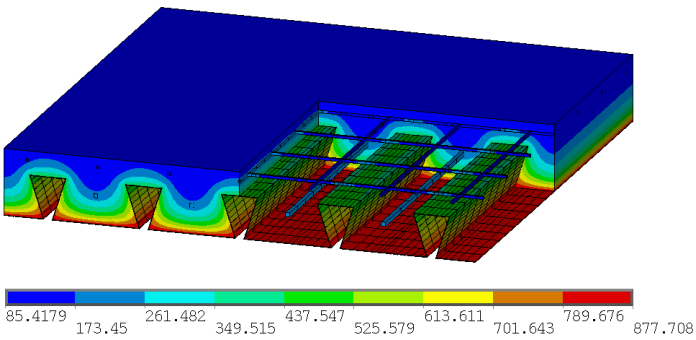

t= 46.2 min

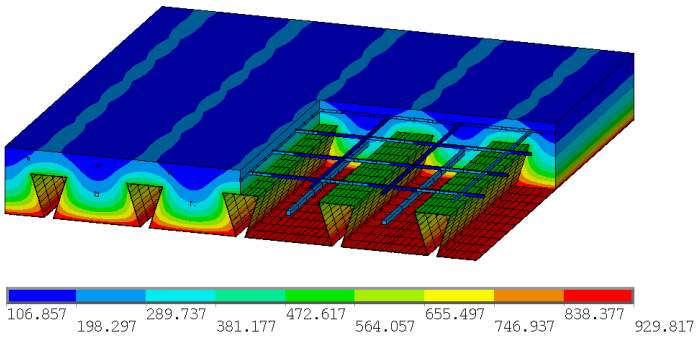

t= 61.6 min

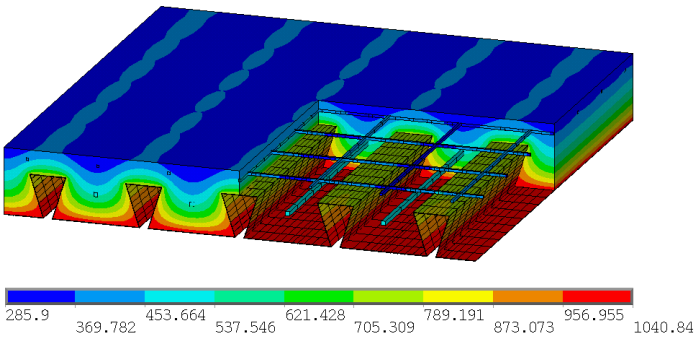

t= 120.0 min

SIM. 126	**Steel deck:** Re-entrant – Vulcraft 3.5D Formlok	**Rebar (mm):** ϕ10	**Fire resistance (min)**	
	Mesh (mm//mm): ϕ6//150 (W4.5)	**h_1 (mm):** 61	Ave: *76.5*	Max: 78.5

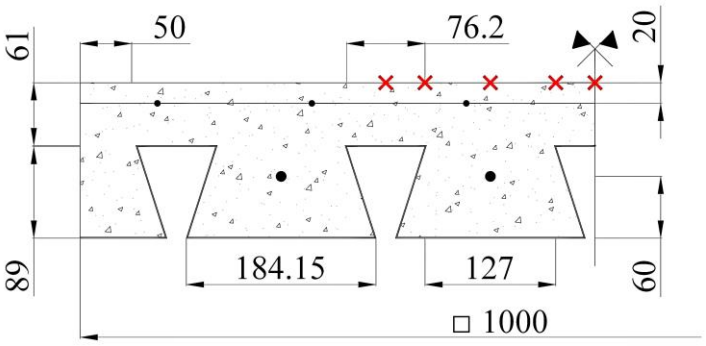

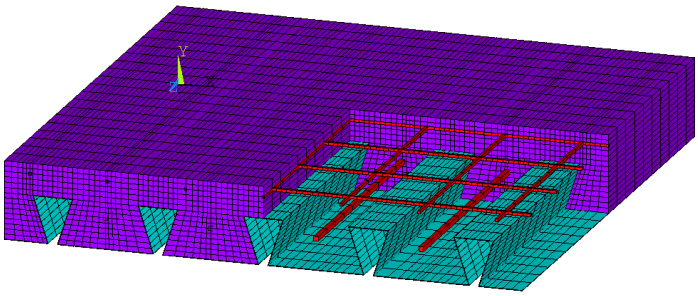

Finite element mesh

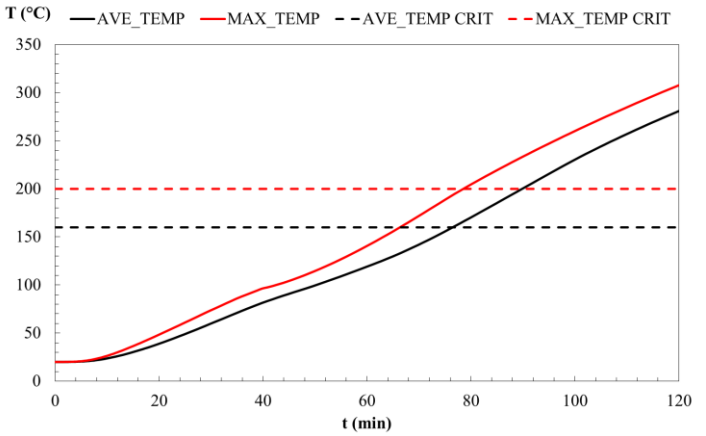

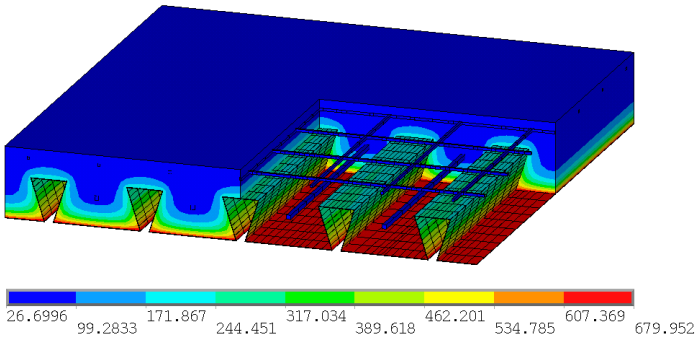

t= 19.1 min

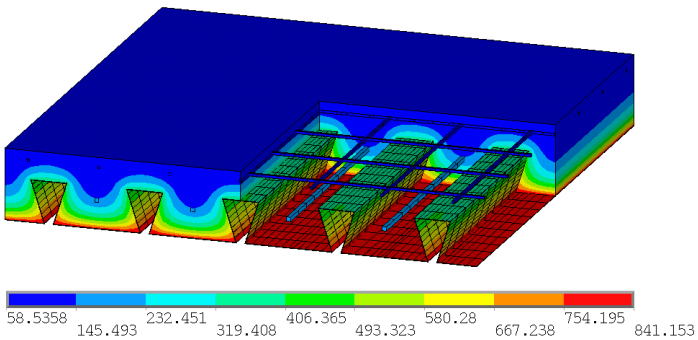

t= 38.3 min

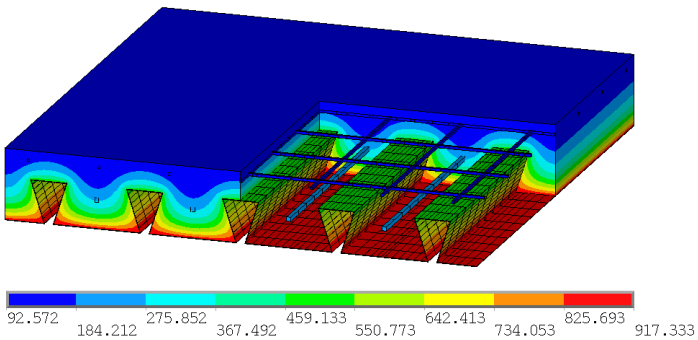

t= 57.4 min

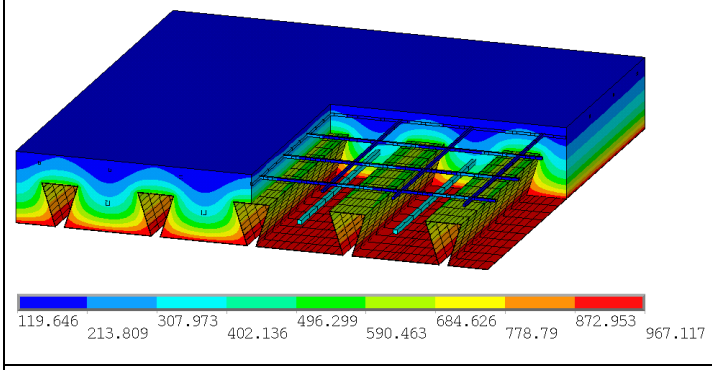

t= 76.5 min

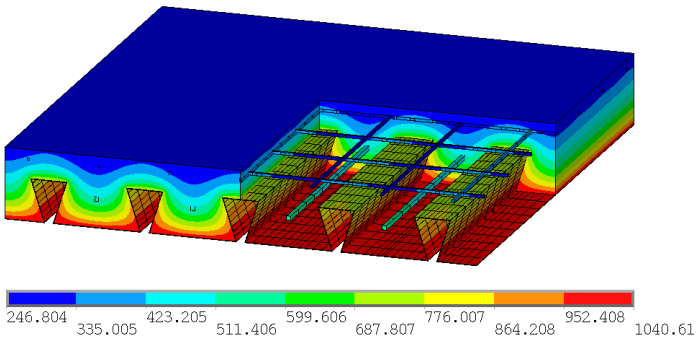

t= 120.0 min

SIM. 127	**Steel deck:** Re-entrant – Vulcraft 3.5D Formlok	**Rebar (mm):** ϕ10	**Fire resistance (min)**	
	Mesh (mm//mm): ϕ6//150 (W4.5)	**h_1 (mm):** 71	Ave: *91.3*	Max: 97.0

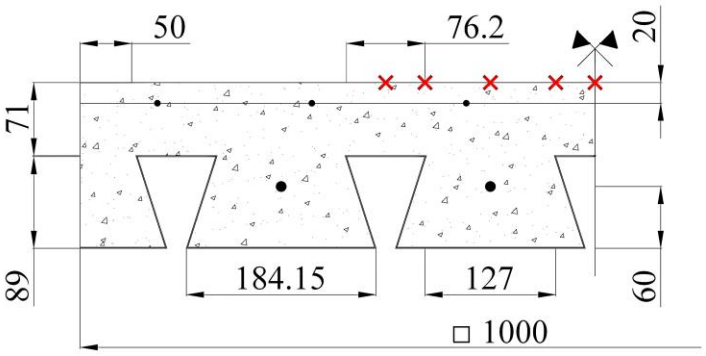

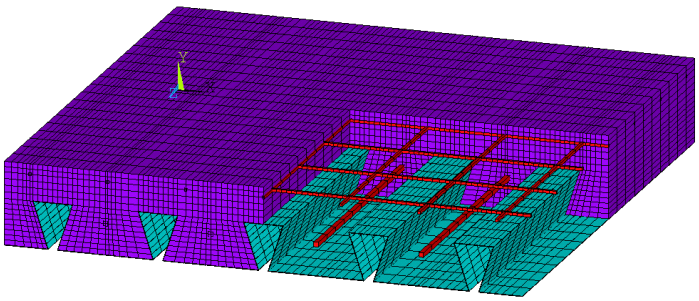

Finite element mesh

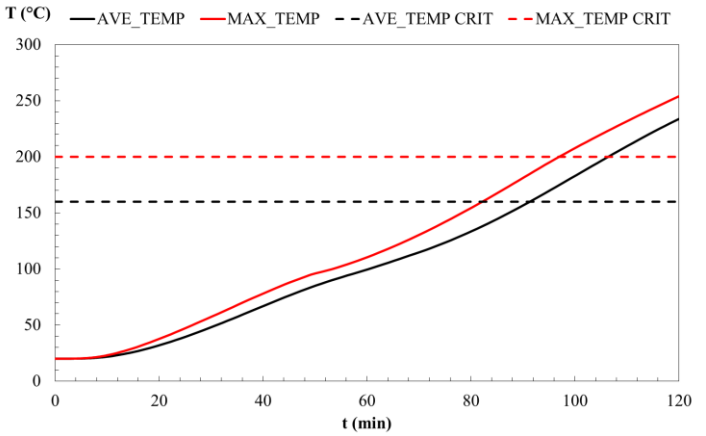

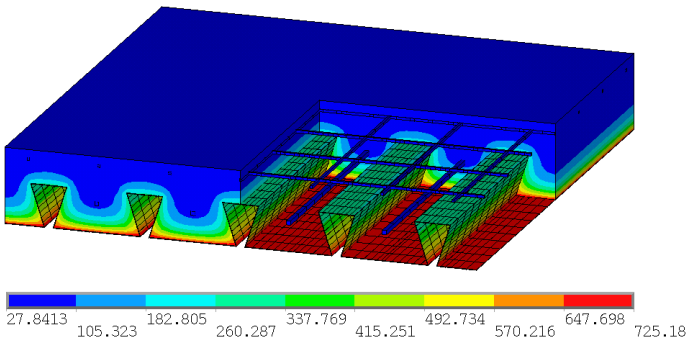

t= 22.8 min

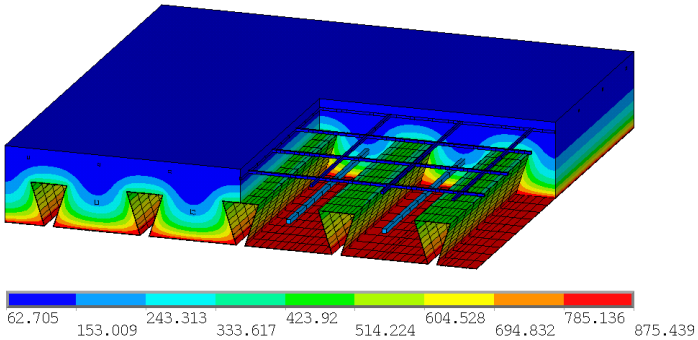

t= 45.7 min

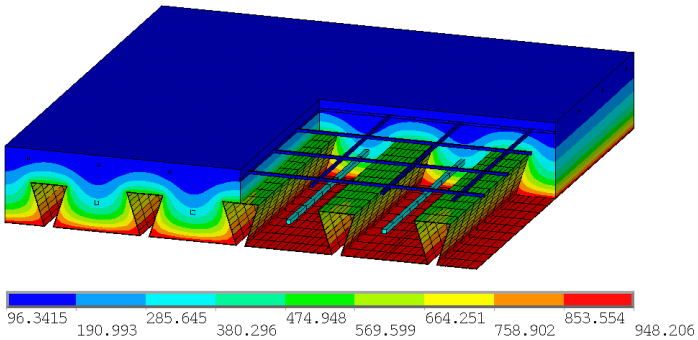

t= 68.5 min

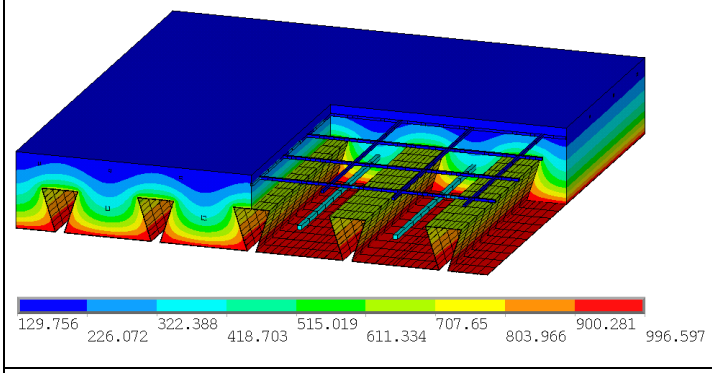

t= 91.3 min

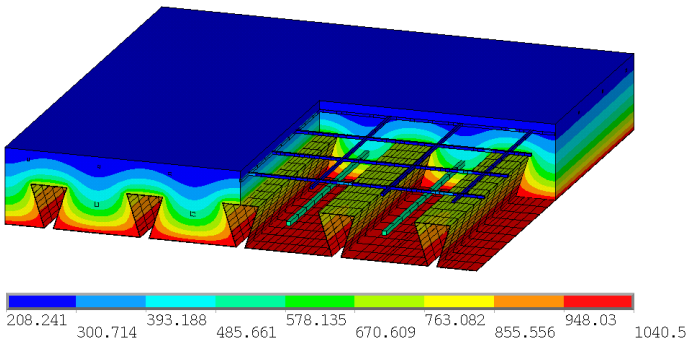

t= 120.0 min

SIM. 128	**Steel deck:** Re-entrant – Vulcraft 3.5D Formlok	**Rebar (mm):** ϕ10	**Fire resistance (min)**	
	Mesh (mm//mm): ϕ6//150 (W4.5)	**h_1 (mm):** 81	Ave: *107.2*	Max: 116.8

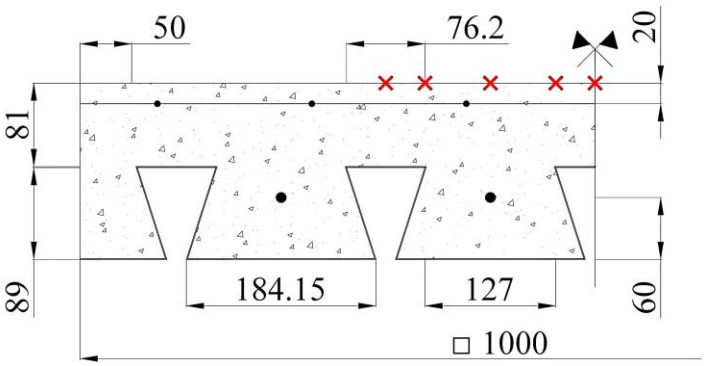

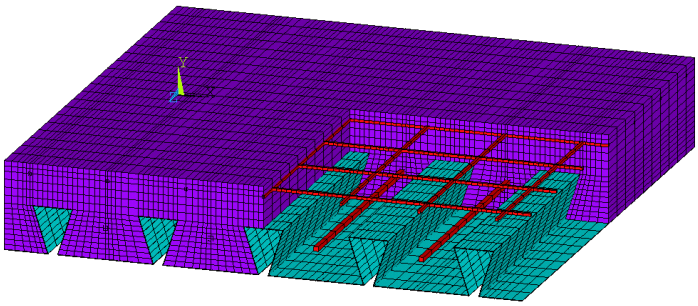

Finite element mesh

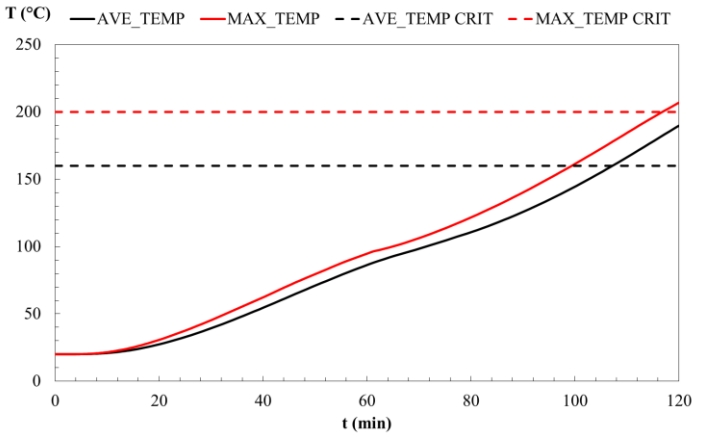

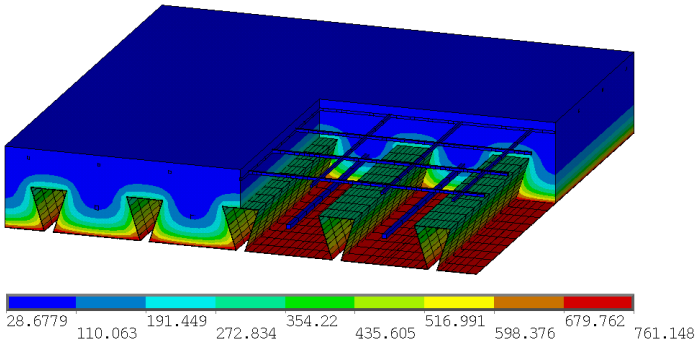

t= 26.8 min

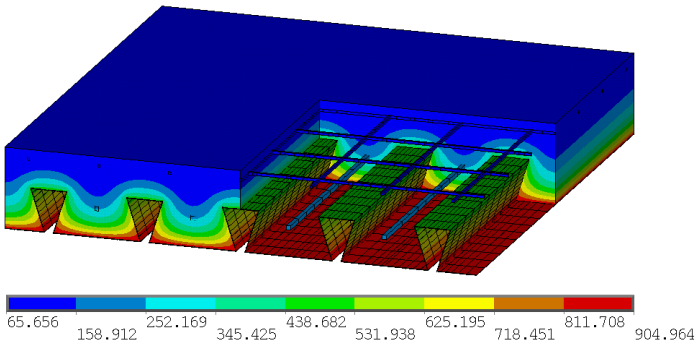

t= 53.6 min

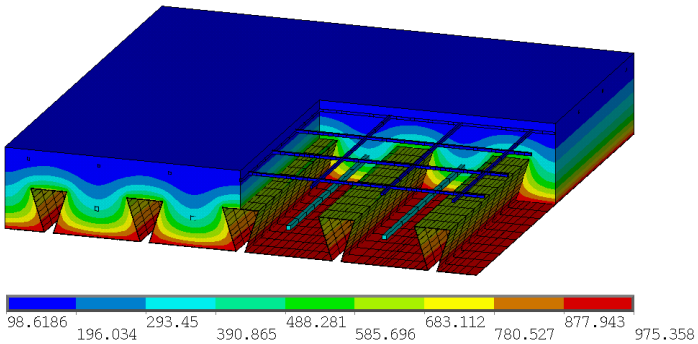

t= 80.4 min

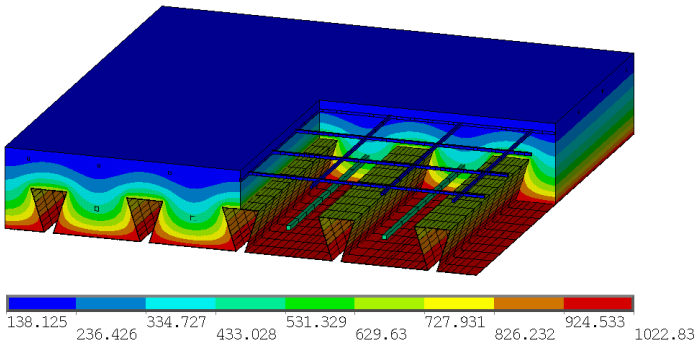

t= 107.2 min

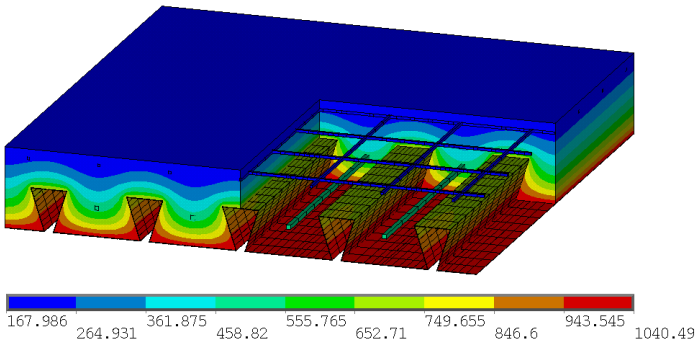

t= 120.0 min

SIM. 129	**Steel deck:** Re-entrant – Vulcraft 3.5D Formlok	**Rebar (mm):** ϕ12	**Fire resistance (min)**	
	Mesh (mm//mm): ϕ6//100 (W4.5)	**h_1 (mm):** 51	Ave: 62.2	Max: *60.4*

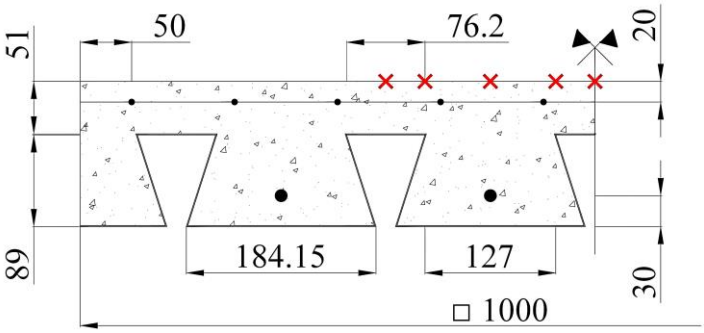

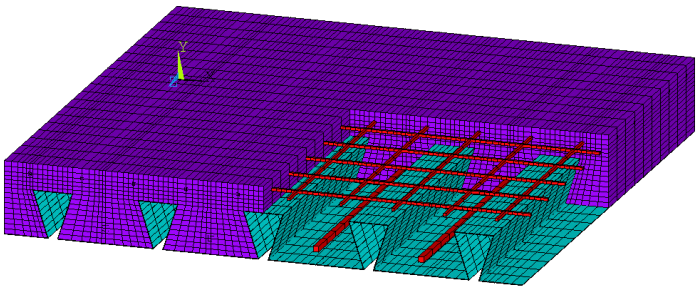

Finite element mesh

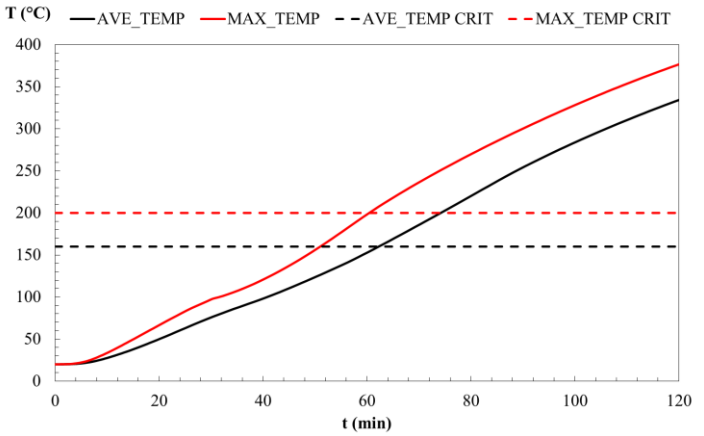

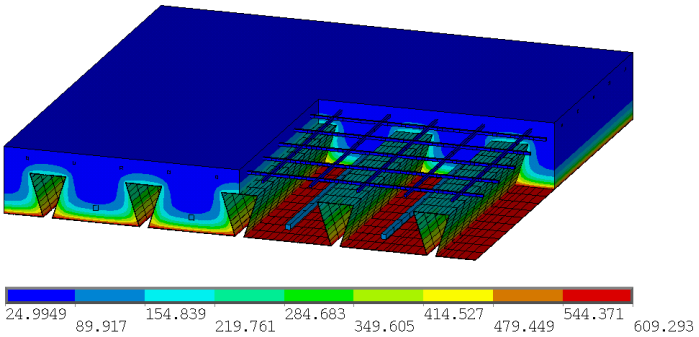

t= 15.1 min

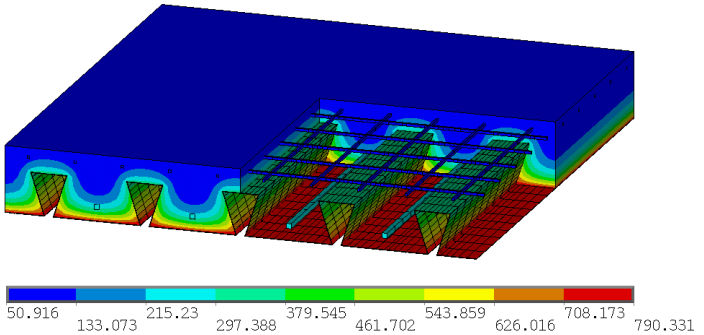

t= 30.2 min

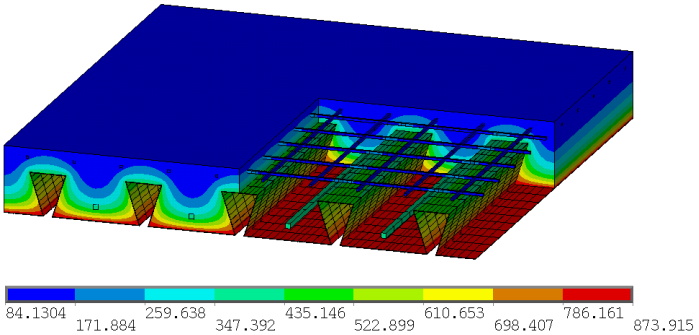

t= 45.3 min

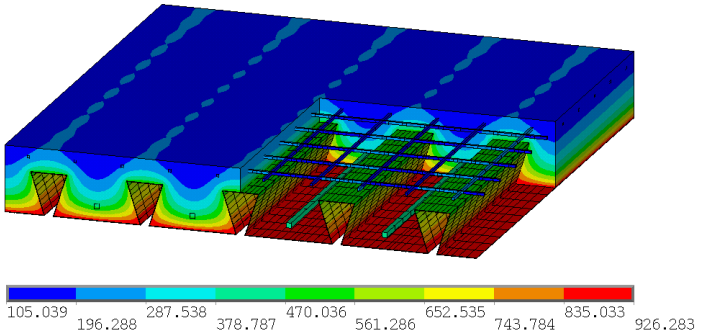

t= 60.4 min

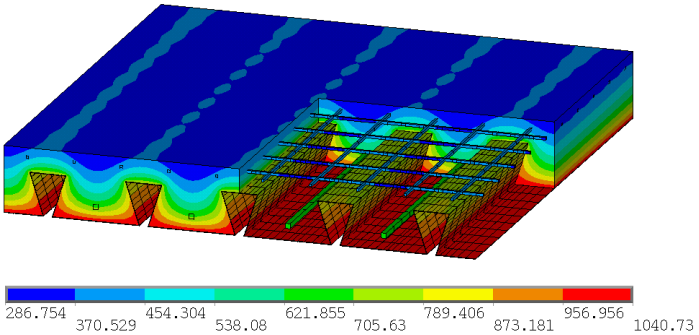

t= 120.0 min

SIM. 130	**Steel deck:** Re-entrant – Vulcraft 3.5D Formlok	**Rebar (mm):** ϕ12	**Fire resistance (min)**	
	Mesh (mm//mm): ϕ6//100 (W4.5)	**h_1 (mm):** 61	Ave: *76.3*	Max: 77.3

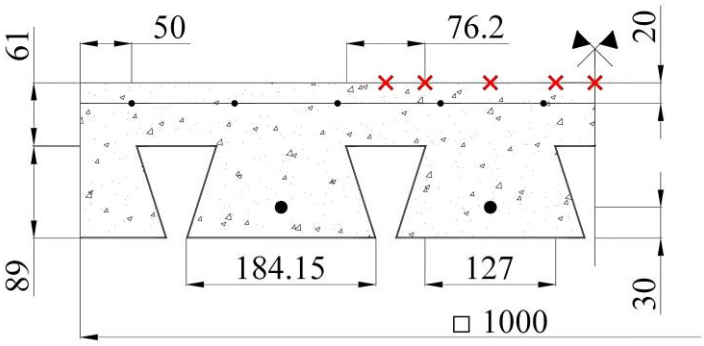

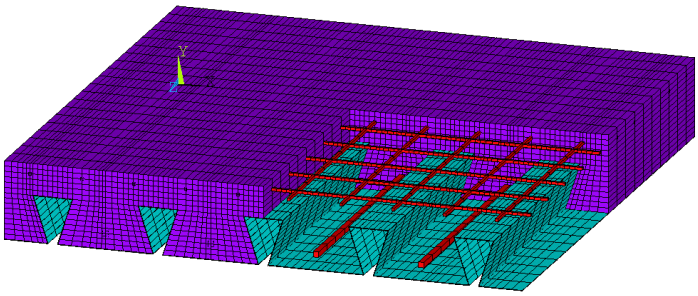

Finite element mesh

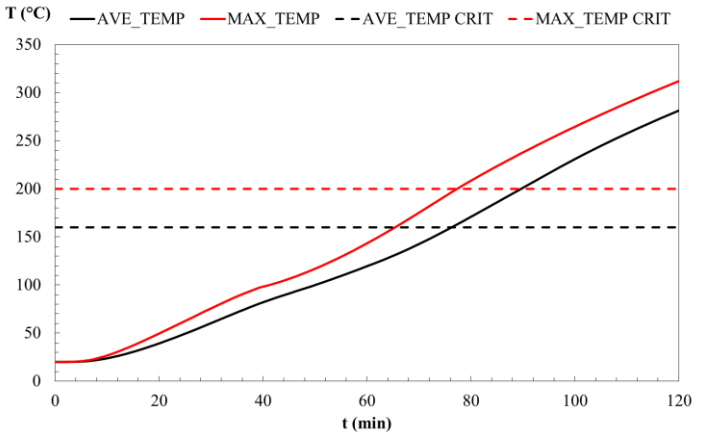

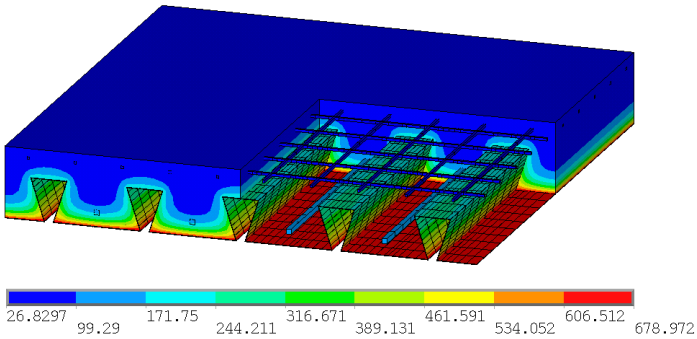

t= 19.1 min

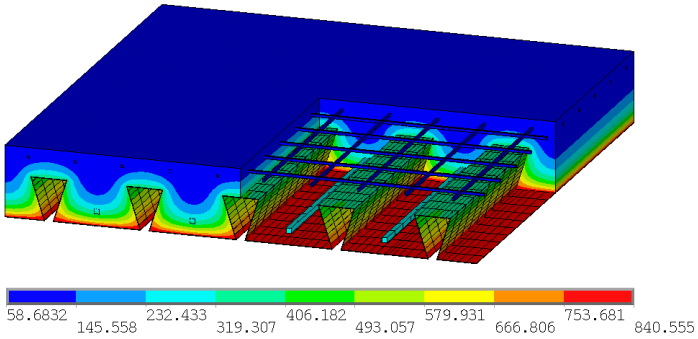

t= 38.2 min

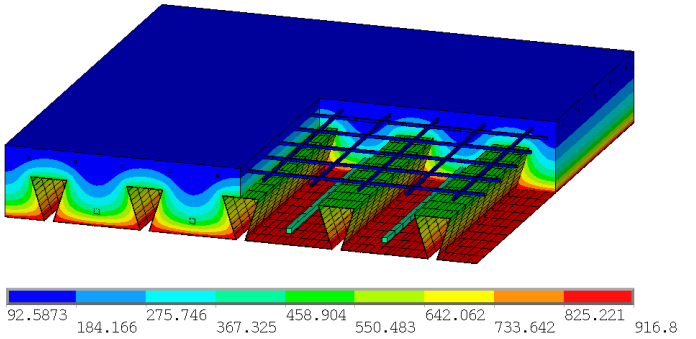

t= 57.2 min

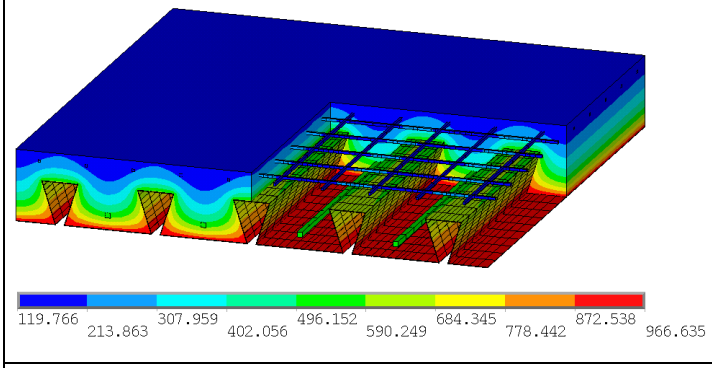

t= 76.3 min

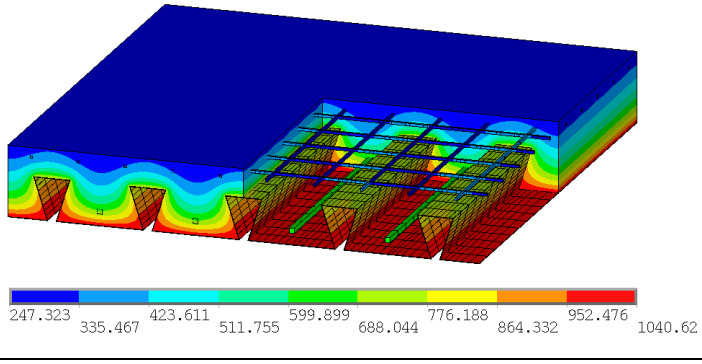

t= 120.0 min

SIM. 131	**Steel deck:** Re-entrant – Vulcraft 3.5D Formlok	**Rebar (mm):** ϕ12	**Fire resistance (min)**	
	Mesh (mm//mm): ϕ6//100 (W4.5)	**h_1 (mm):** 71	Ave: *91.2*	Max: 95.9

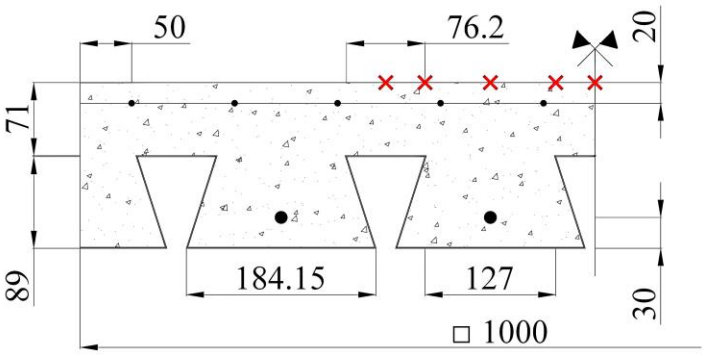

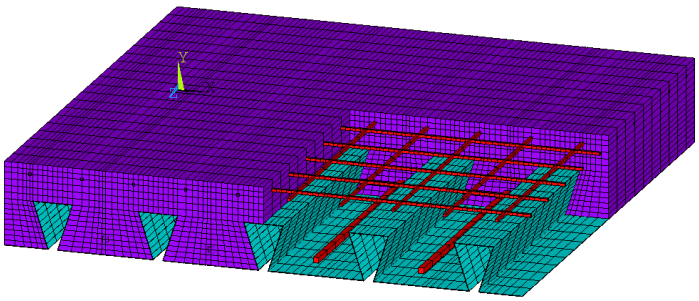

Finite element mesh

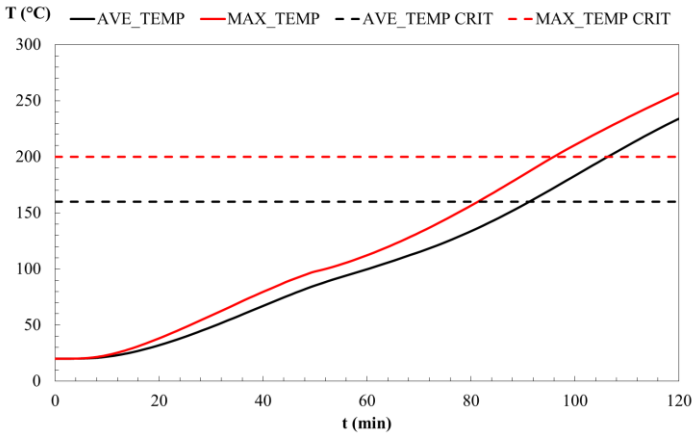

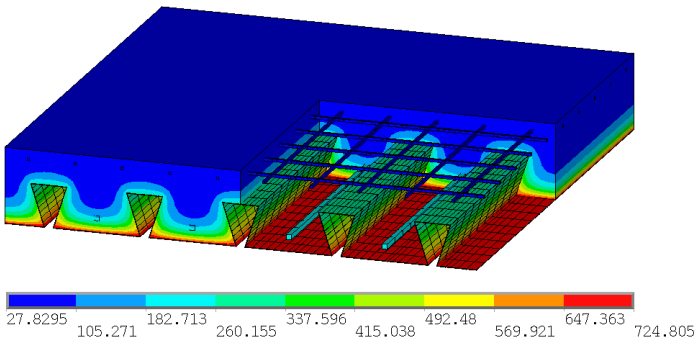

t= 22.8 min

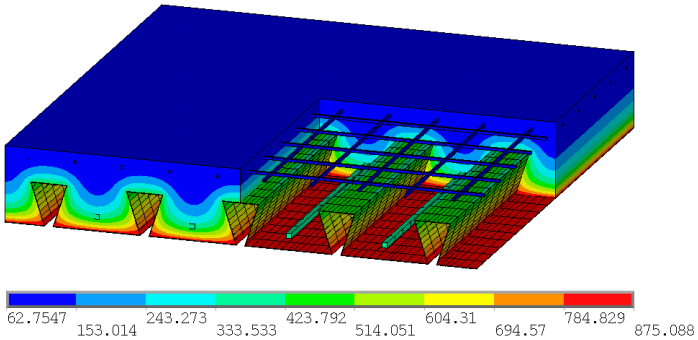

t= 45.6 min

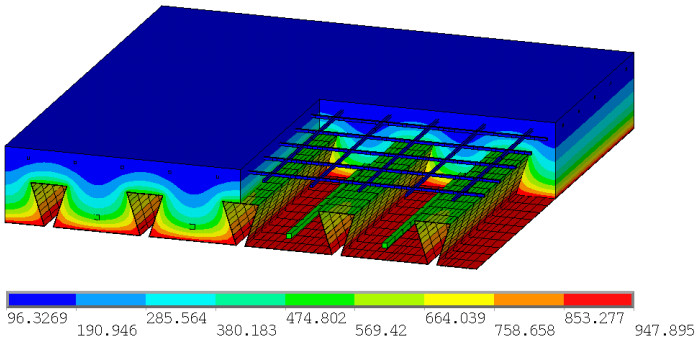

t= 68.4 min

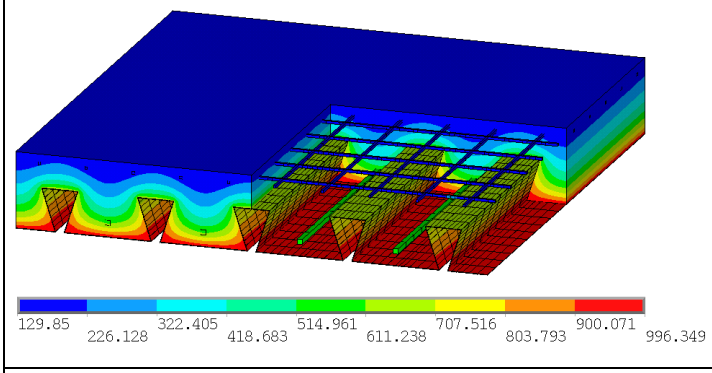

t= 91.2 min

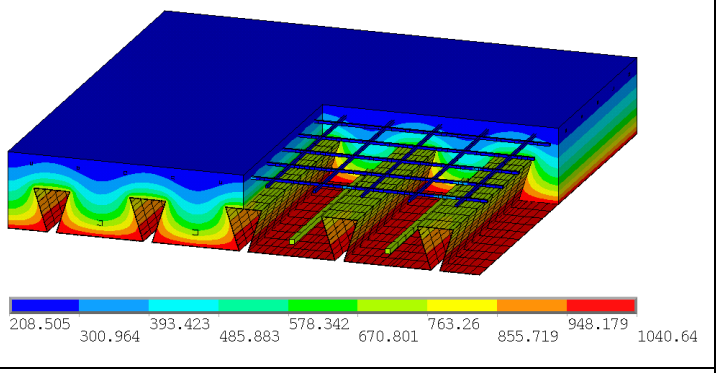

t= 120.0 min

SIM. 132	**Steel deck:** Re-entrant – Vulcraft 3.5D Formlok	**Rebar (mm):** ϕ12	**Fire resistance (min)**	
	Mesh (mm//mm): ϕ6//100 (W4.5)	**h_1 (mm):** 81	Ave: *107.2*	Max: 115.9

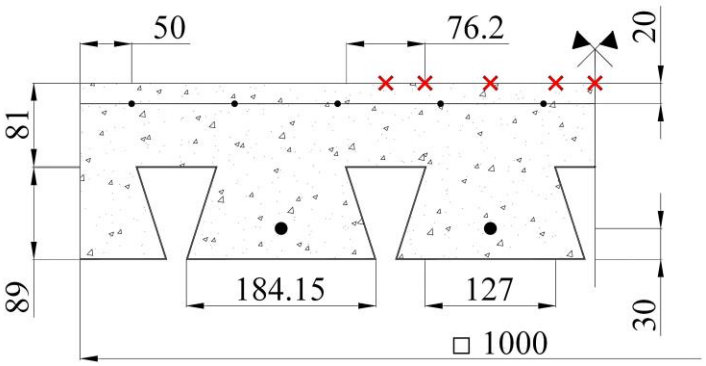

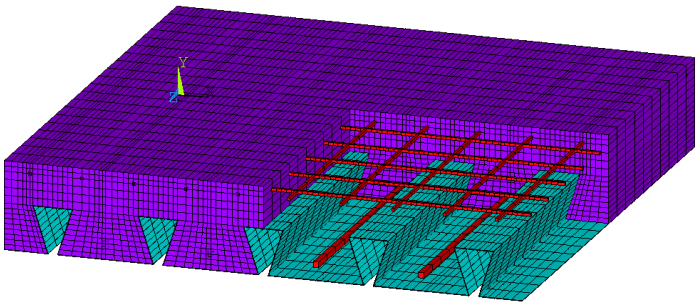

Finite element mesh

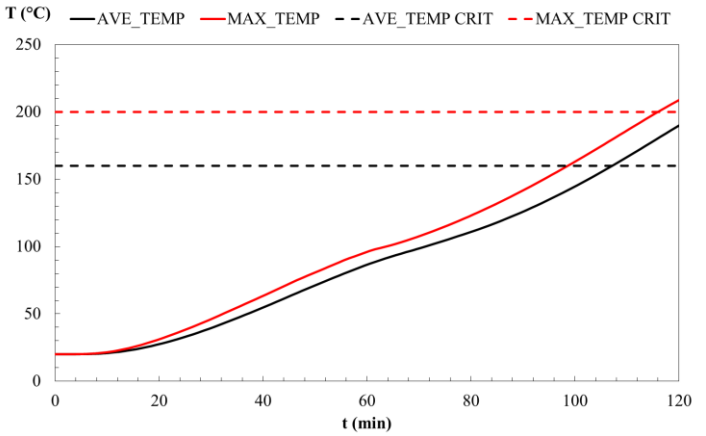

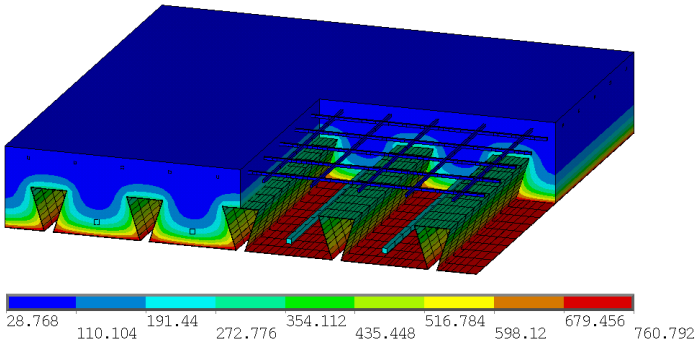

t= 26.8 min

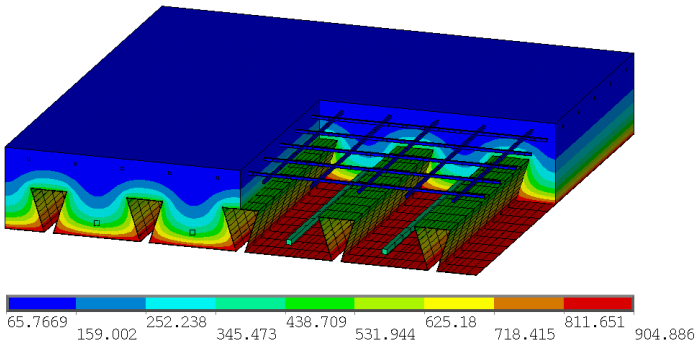

t= 53.6 min

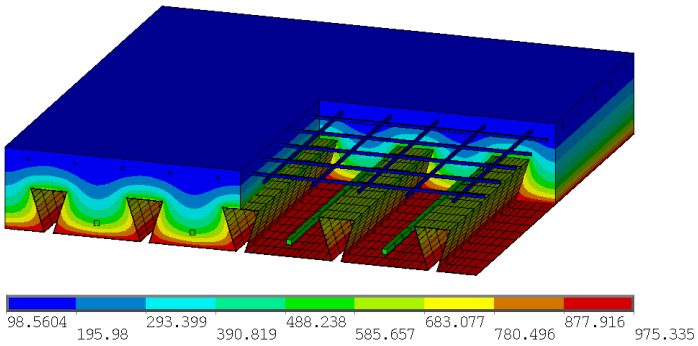

t= 80.4 min

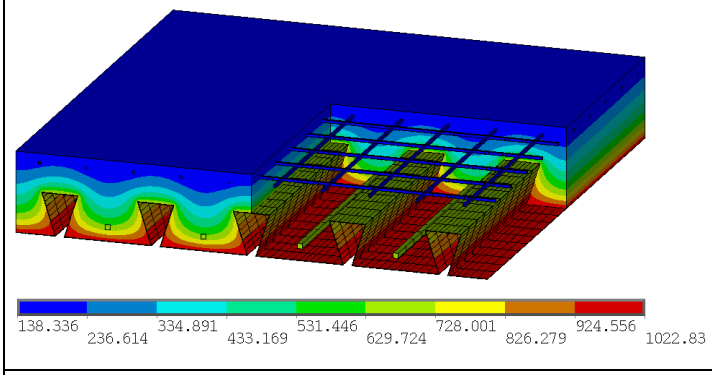

t= 107.2 min

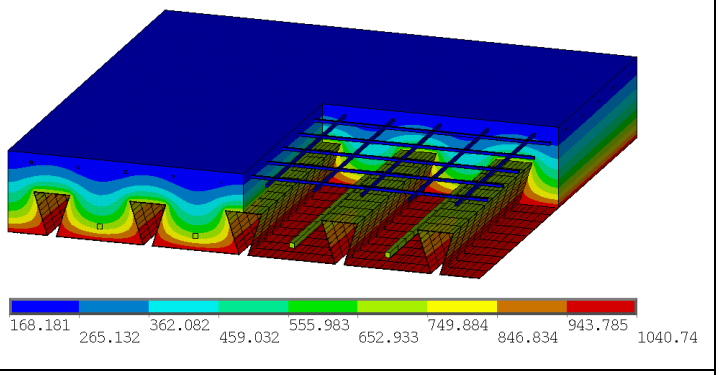

t= 120.0 min

SIM. 133	**Steel deck:** Re-entrant – Vulcraft 3.5D Formlok	**Rebar (mm):** ϕ12	**Fire resistance (min)**	
	Mesh (mm//mm): ϕ6//100 (W4.5)	**h_1 (mm):** 51	Ave: 62.3	Max: *60.4*

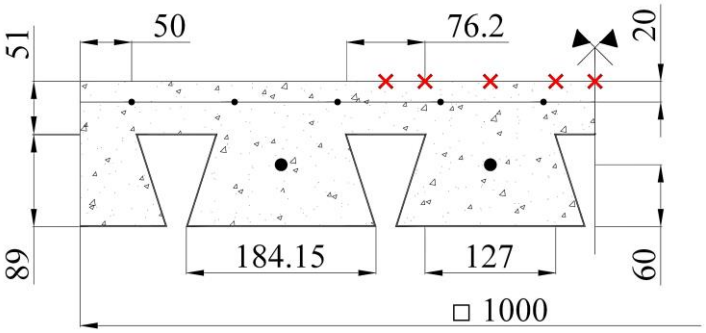

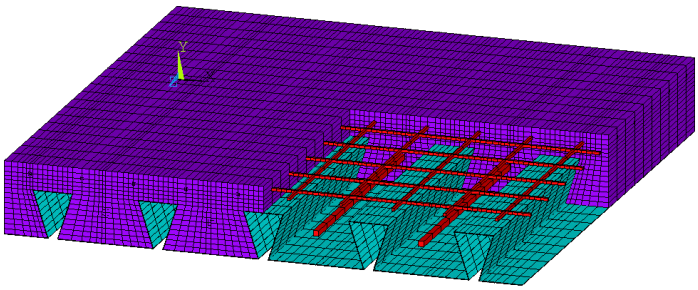

Finite element mesh

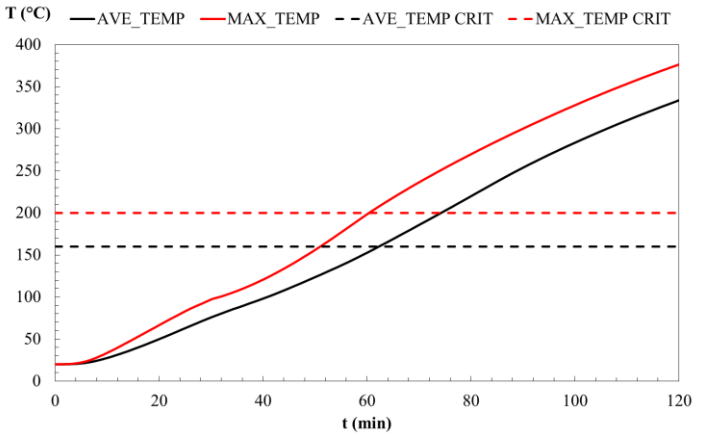

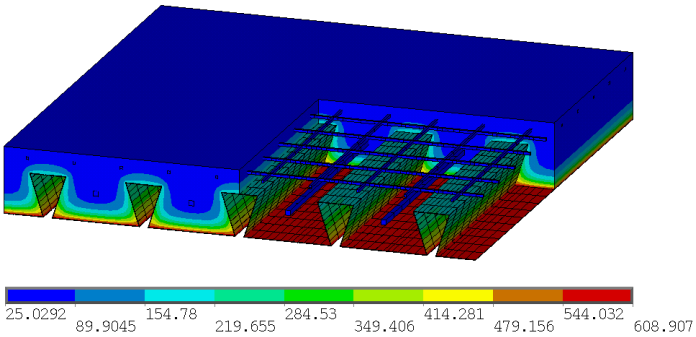

t= 15.1 min

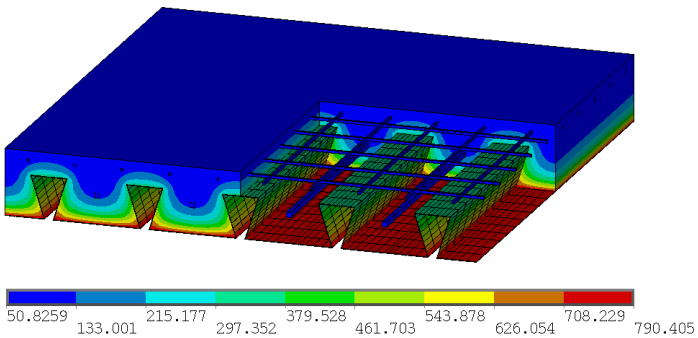

t= 30.2 min

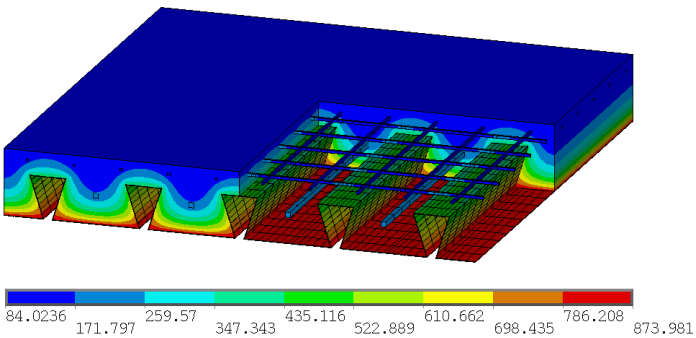

t= 45.3 min

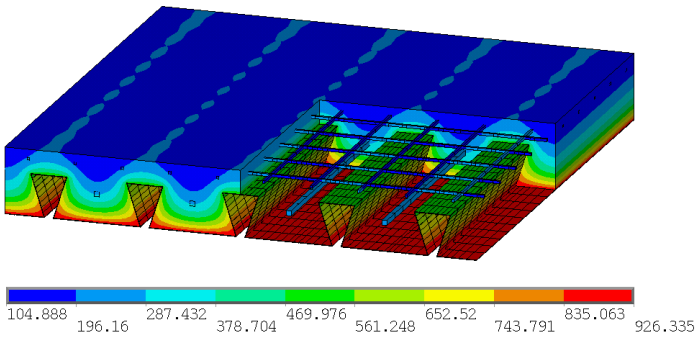

t= 60.4 min

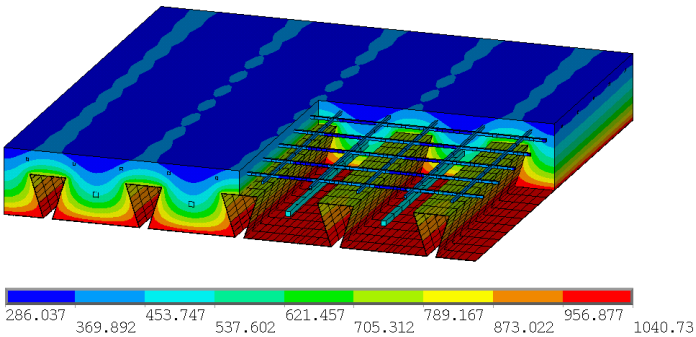

t= 120.0 min

SIM. 134	**Steel deck:** Re-entrant – Vulcraft 3.5D Formlok	**Rebar (mm):** ϕ12	**Fire resistance (min)**	
	Mesh (mm//mm): ϕ6//100 (W4.5)	**h_1 (mm):** 61	Ave: *76.3*	Max: 77.3

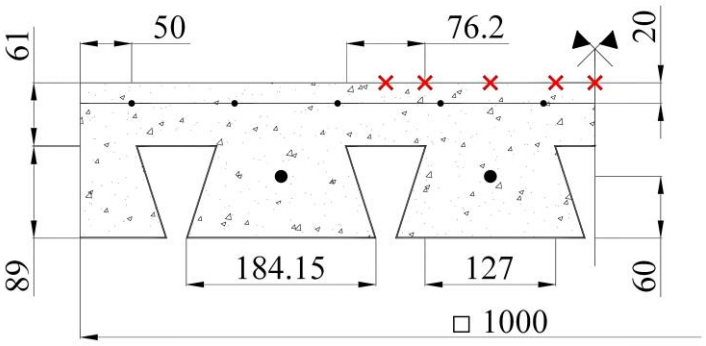

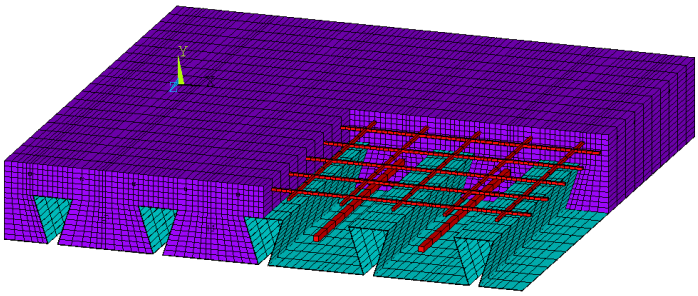

Finite element mesh

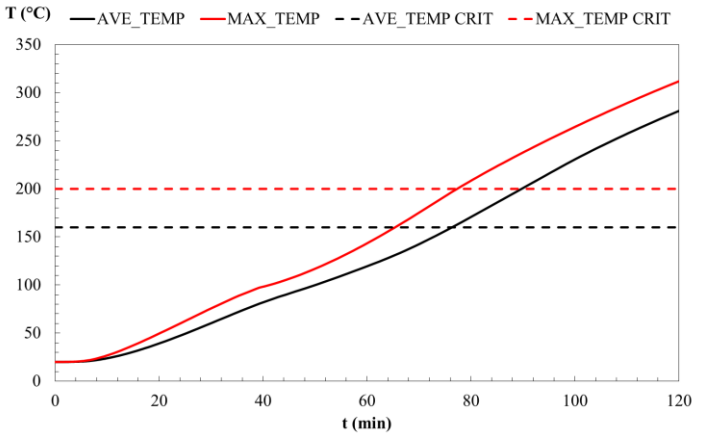

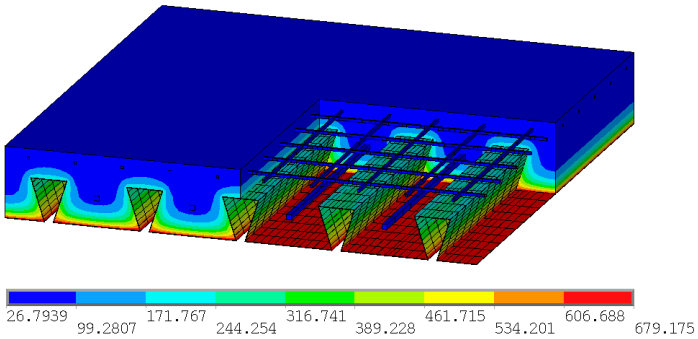

t= 19.1 min

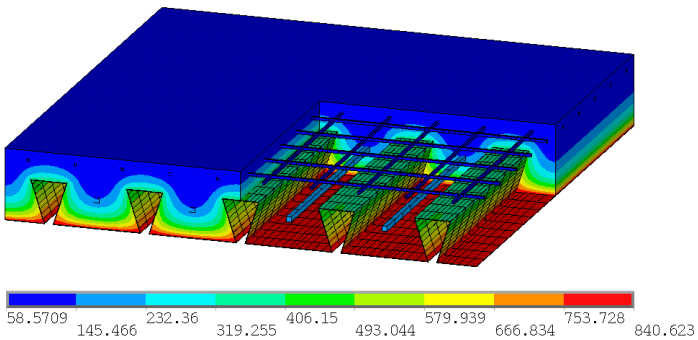

t= 38.2 min

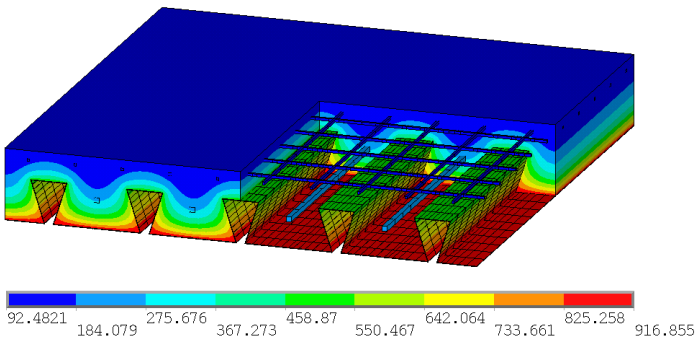

t= 57.2 min

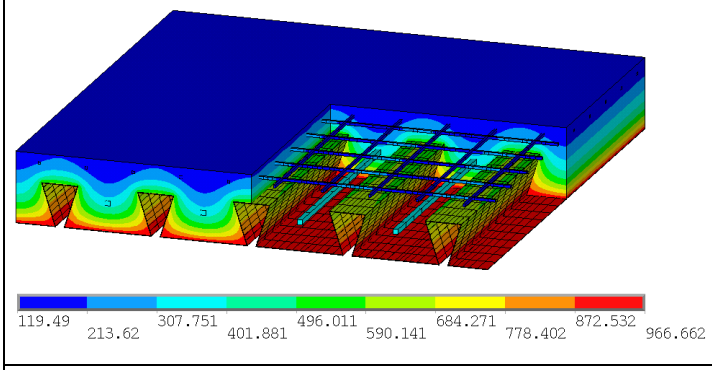

t= 76.3 min

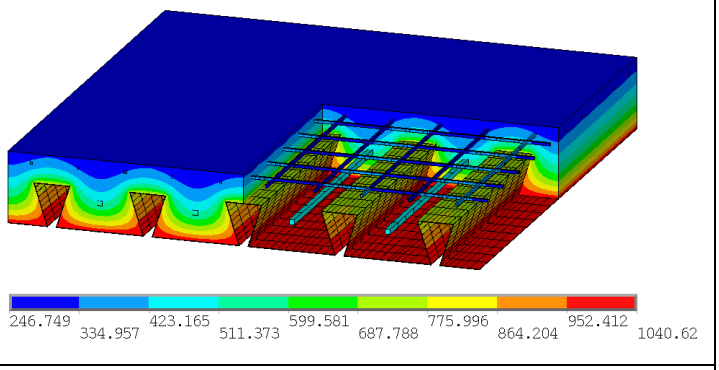

t= 120.0 min

SIM. 135	**Steel deck:** Re-entrant – Vulcraft 3.5D Formlok	**Rebar (mm):** ϕ12	**Fire resistance (min)**	
	Mesh (mm//mm): ϕ6//100 (W4.5)	**h_1 (mm):** 71	Ave: *91.3*	Max: 95.9

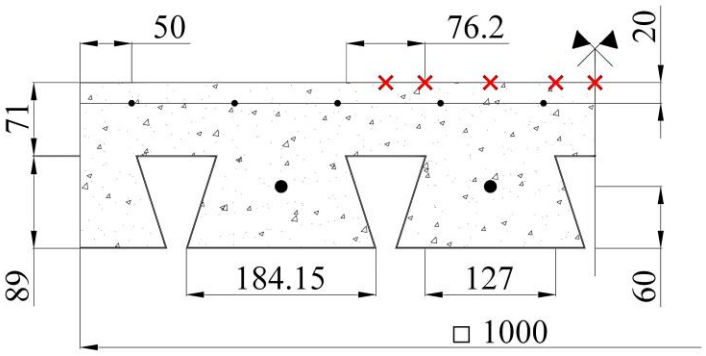

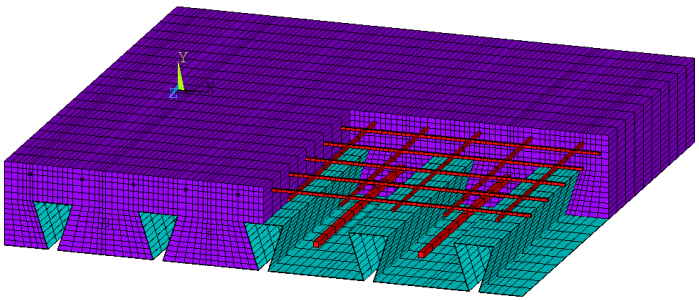

Finite element mesh

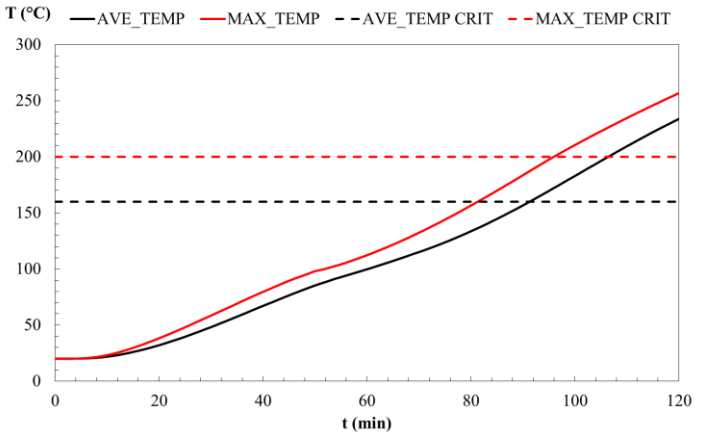

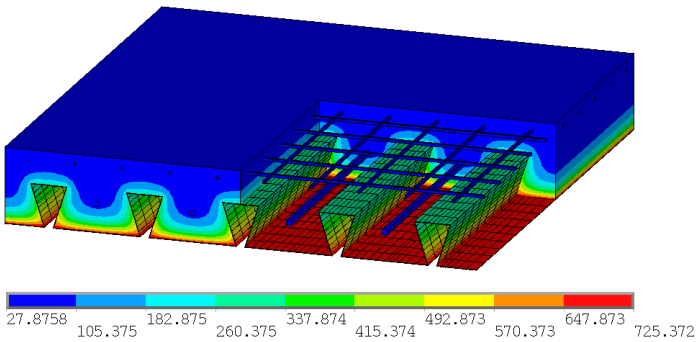

t= 22.8 min

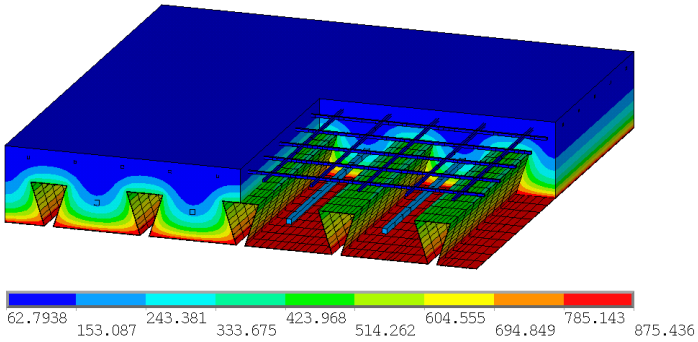

t= 45.7 min

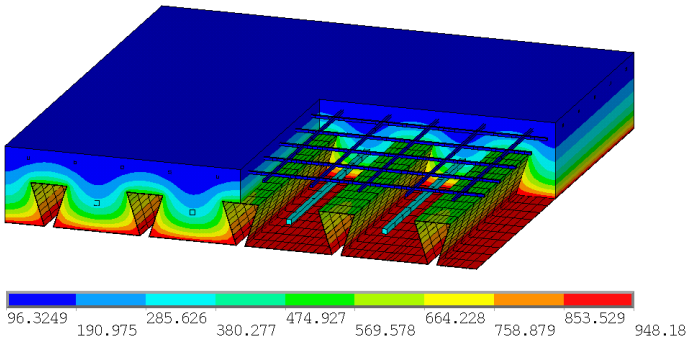

t= 68.5 min

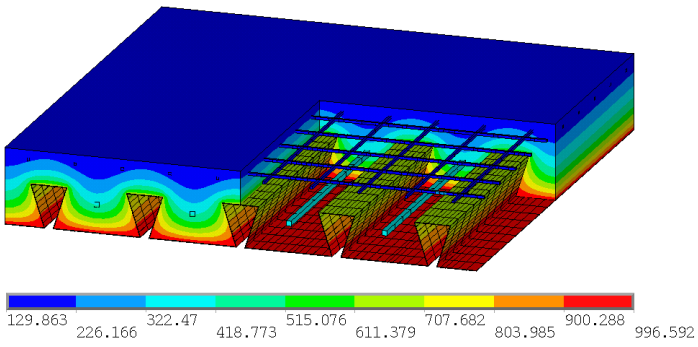

t= 91.3 min

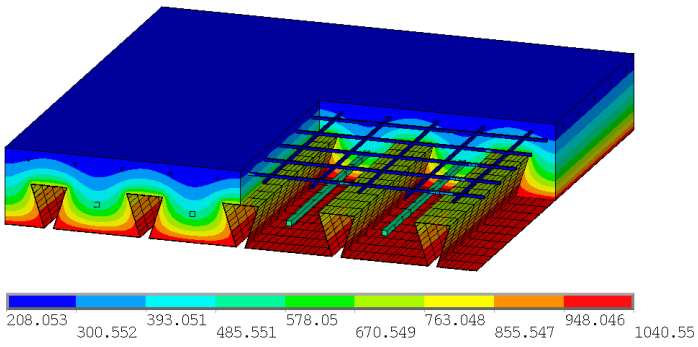

t= 120.0 min

SIM. 136	**Steel deck:** Re-entrant – Vulcraft 3.5D Formlok	**Rebar (mm):** ϕ12	**Fire resistance (min)**	
	Mesh (mm//mm): ϕ6//100 (W4.5)	**h_1 (mm):** 81	Ave: *107.2*	Max: 116.0

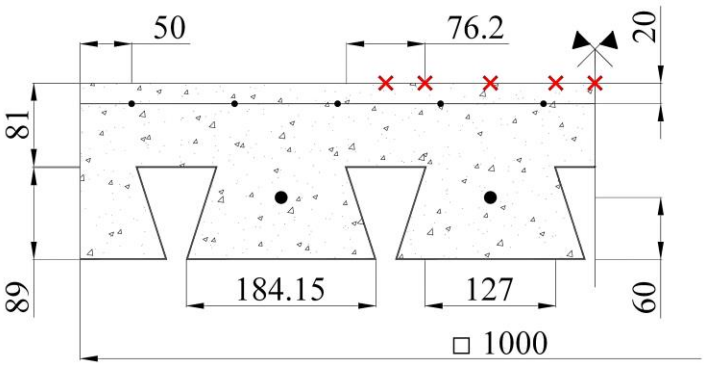

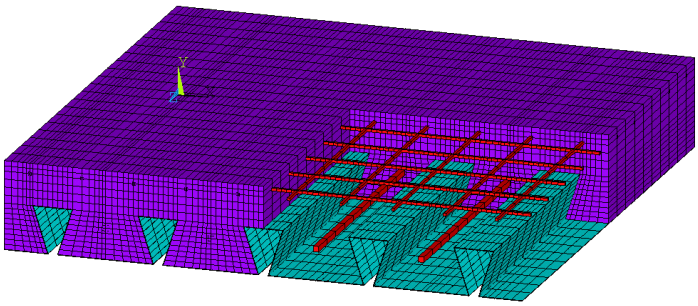

Finite element mesh

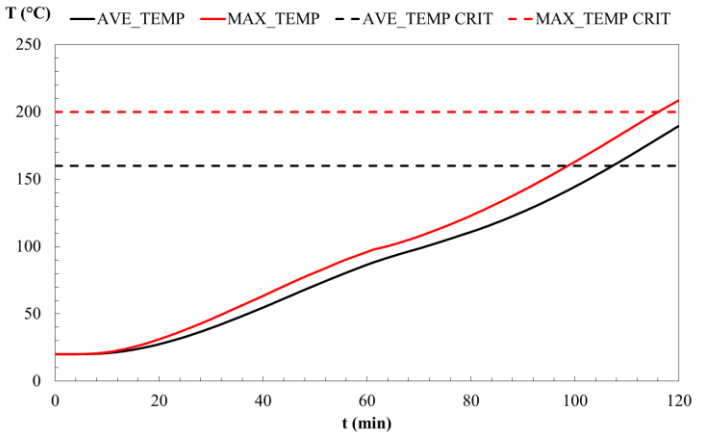

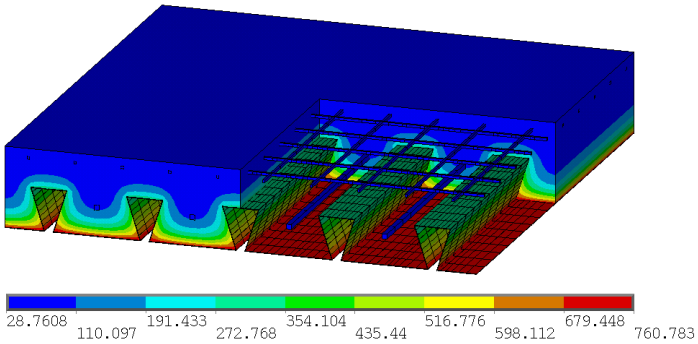

t= 26.8 min

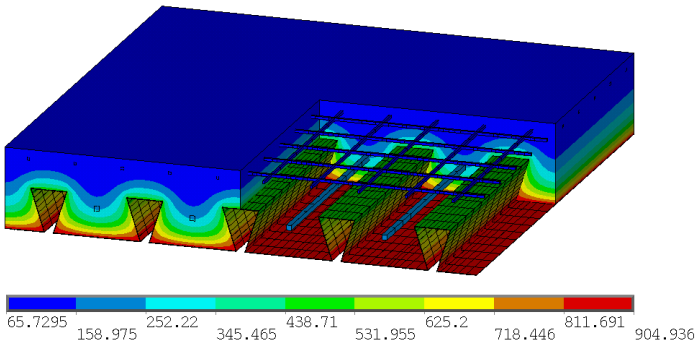

t= 53.6 min

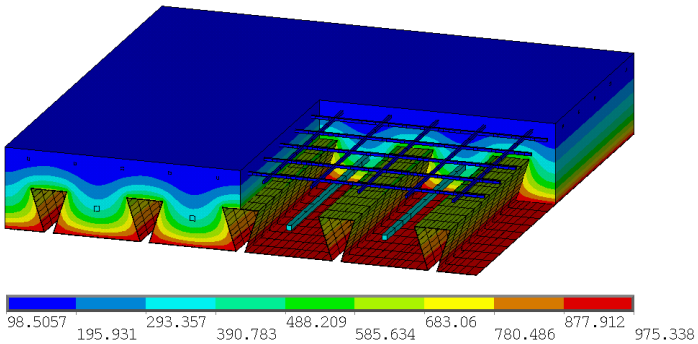

t= 80.4 min

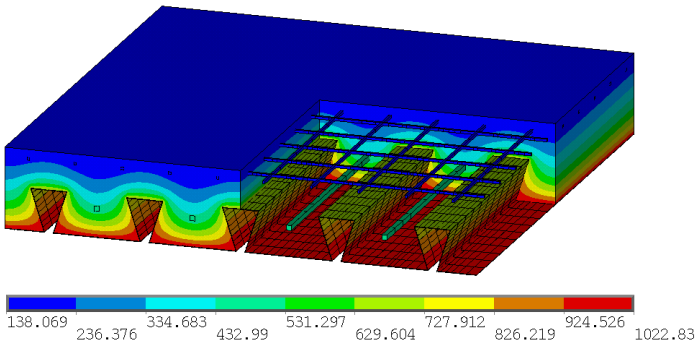

t= 107.2 min

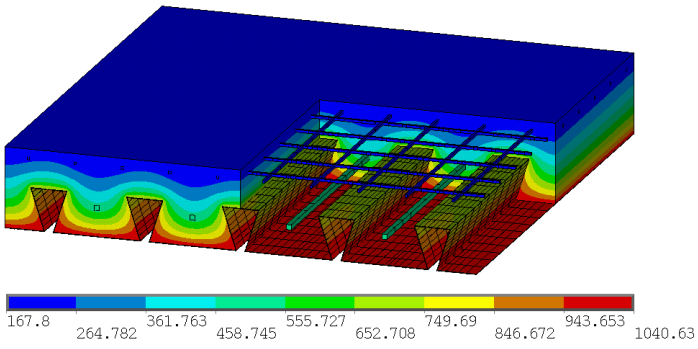

t= 120.0 min

SIM. 137	**Steel deck:** Re-entrant – Vulcraft 3.5D Formlok	**Rebar (mm):** ϕ12	**Fire resistance (min)**	
	Mesh (mm//mm): ϕ6//150 (W4.5)	**h_1 (mm):** 51	Ave: 62.5	Max: *61.6*

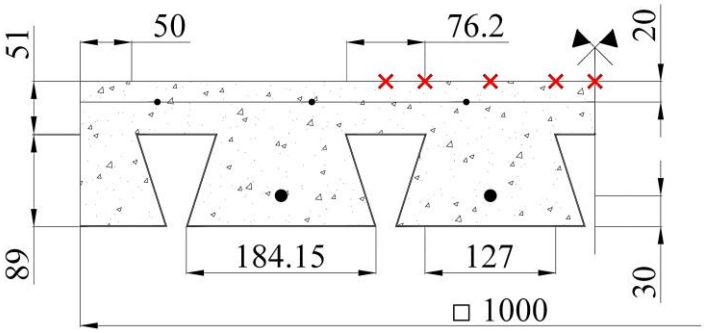

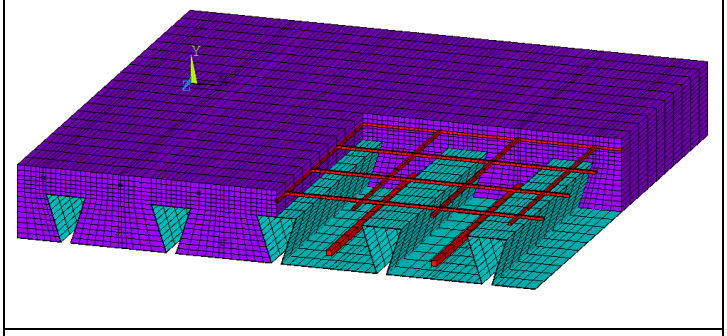

Finite element mesh

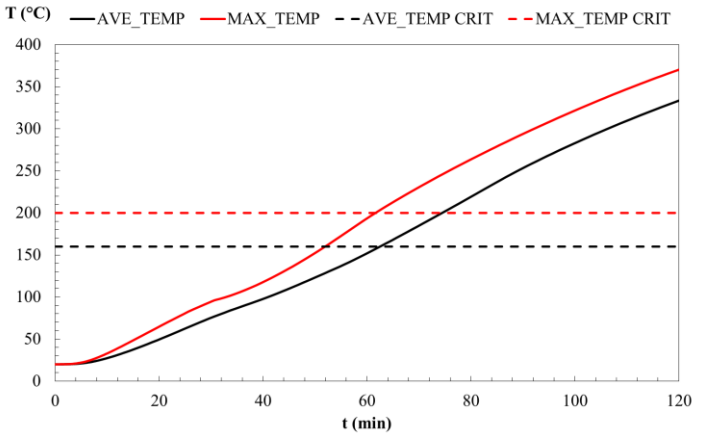

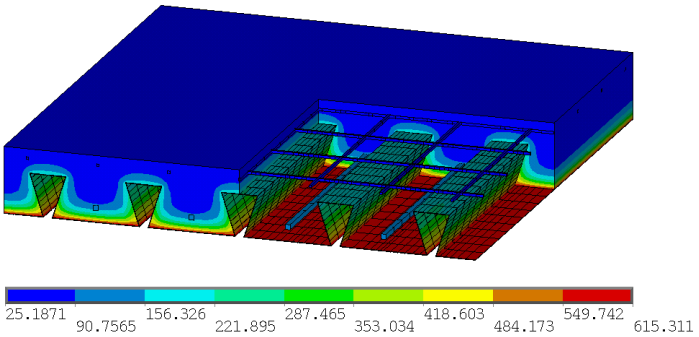

t= 15.4 min

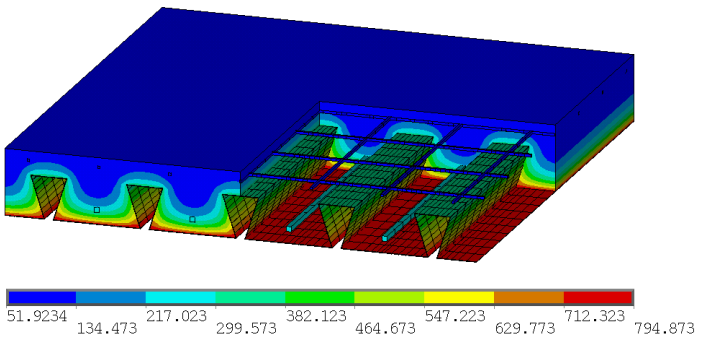

t= 30.8 min

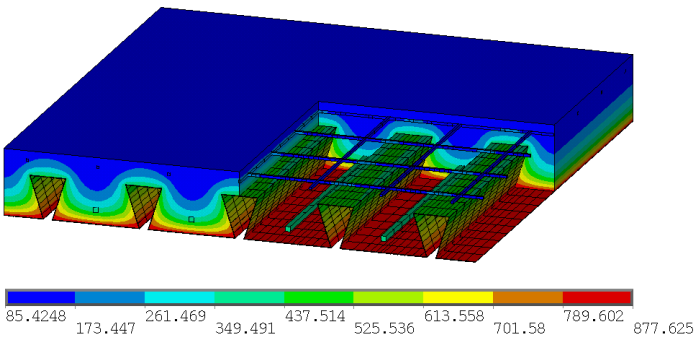

t= 46.2 min

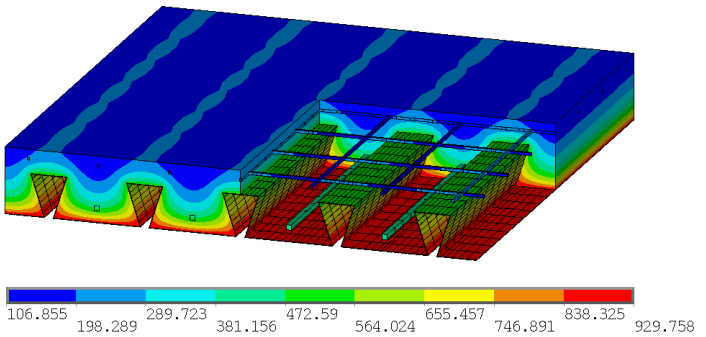

t= 61.6 min

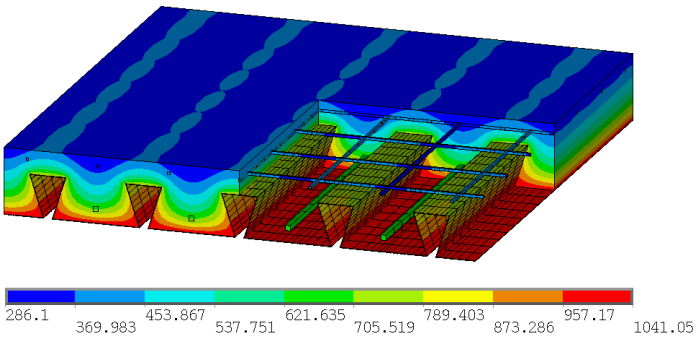

t= 120.0 min

SIM. 138	**Steel deck:** Re-entrant – Vulcraft 3.5D Formlok	**Rebar (mm):** ϕ12	**Fire resistance (min)**	
	Mesh (mm//mm): ϕ6//150 (W4.5)	**h_1 (mm):** 61	Ave: *76.5*	Max: 78.5

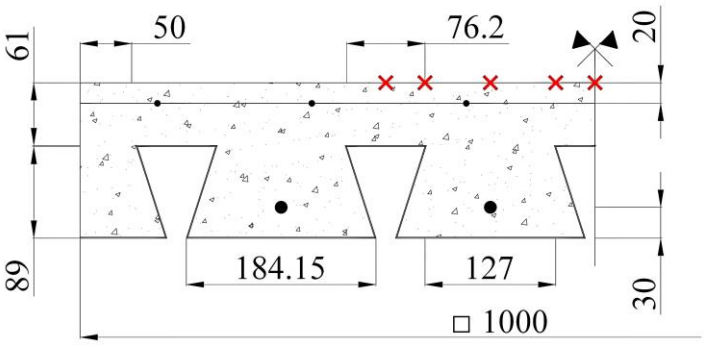

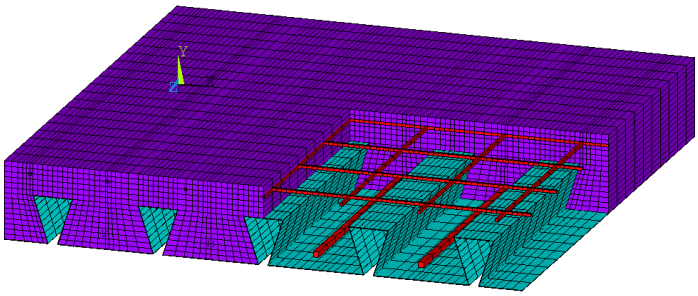

Finite element mesh

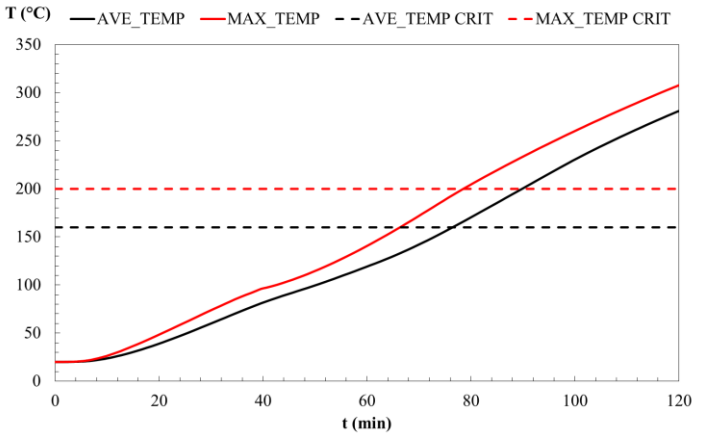

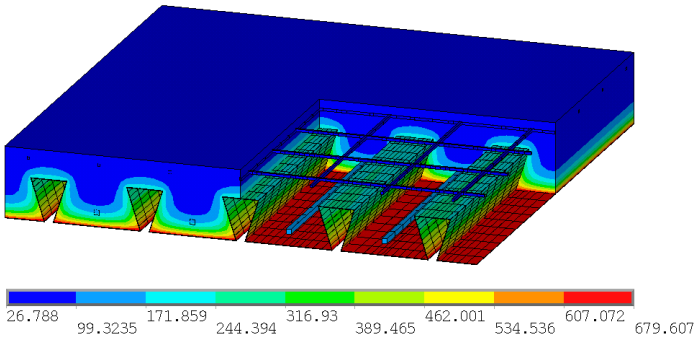

t= 19.1 min

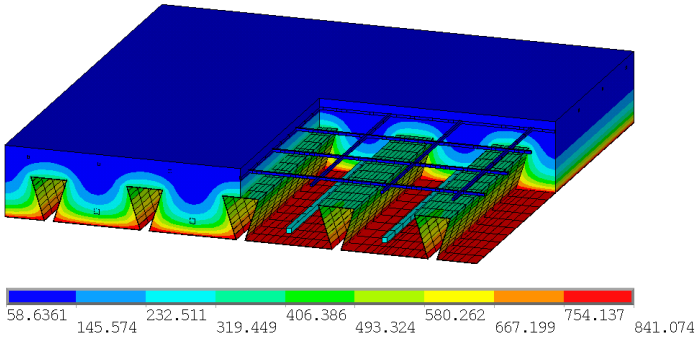

t= 38.3 min

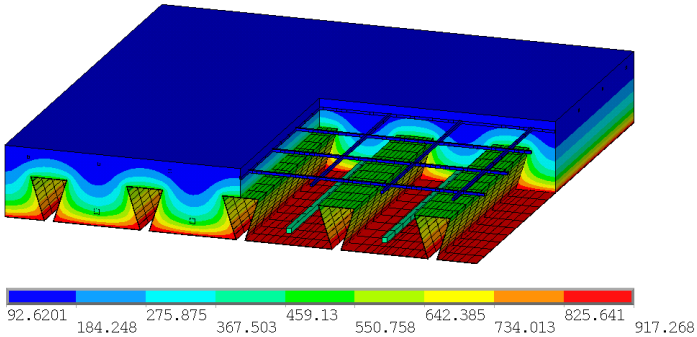

t= 57.4 min

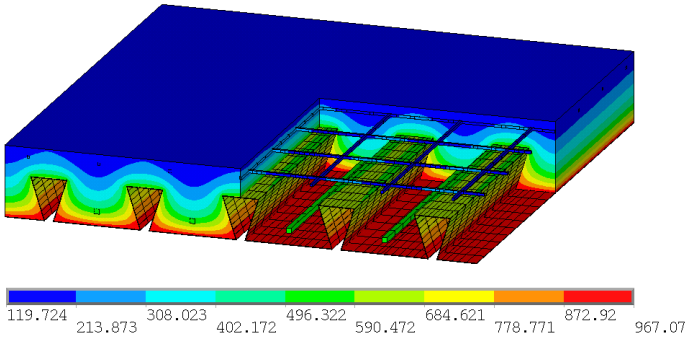

t= 76.5 min

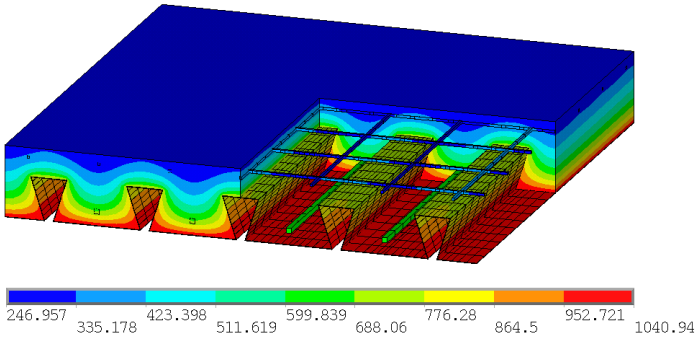

t= 120.0 min

SIM. 139	**Steel deck:** Re-entrant – Vulcraft 3.5D Formlok	**Rebar (mm):** ϕ12	**Fire resistance (min)**	
	Mesh (mm//mm): ϕ6//150 (W4.5)	**h_1 (mm):** 71	Ave: *91.3*	Max: 97.0

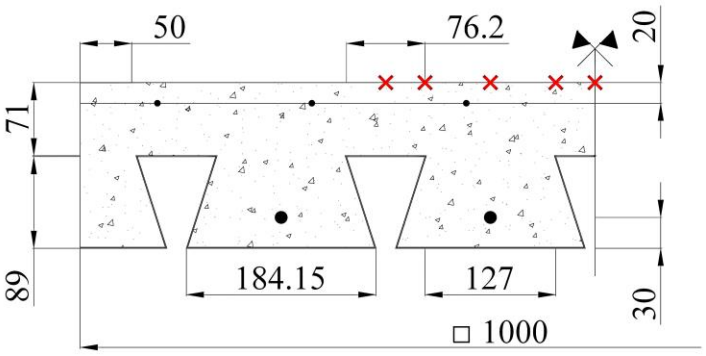

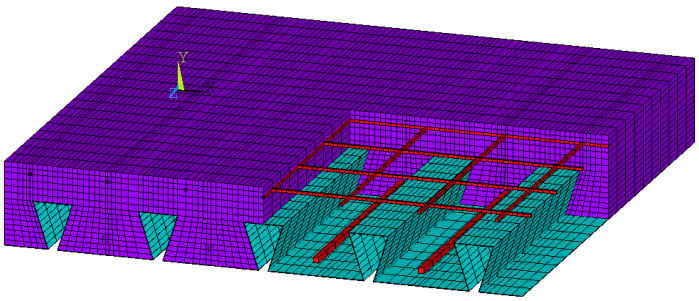

Finite element mesh

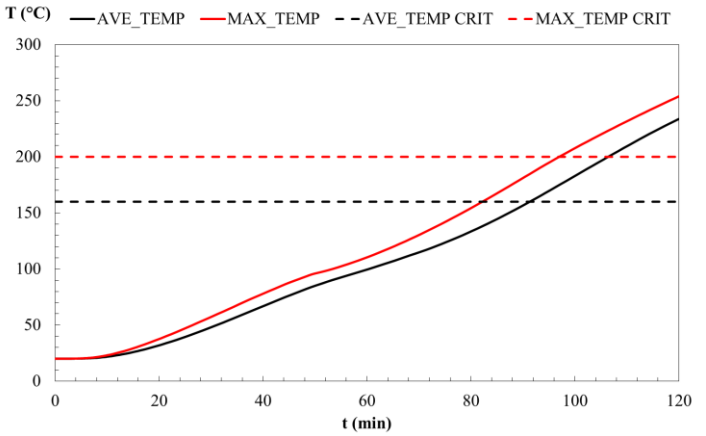

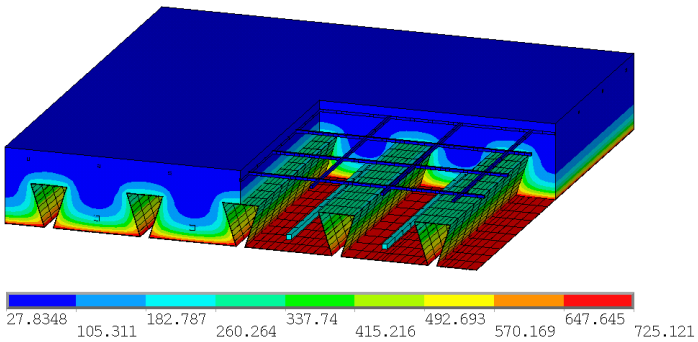

t= 22.8 min

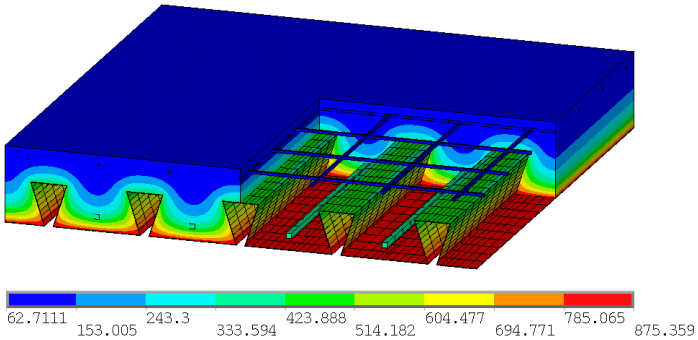

t= 45.7 min

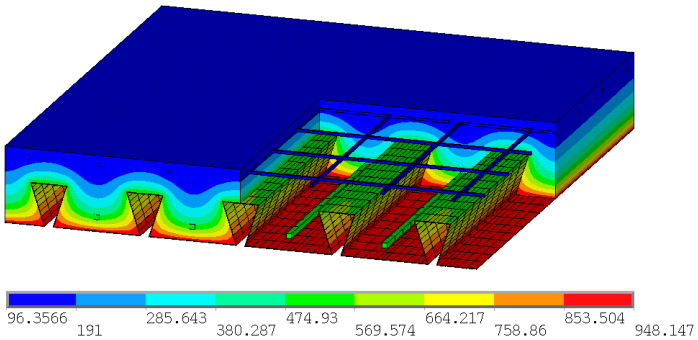

t= 68.5 min

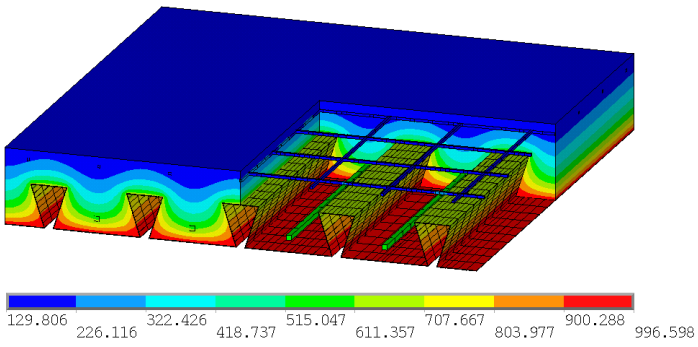

t= 91.3 min

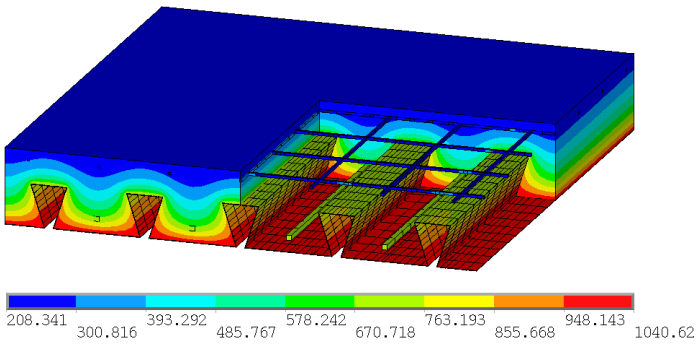

t= 120.0 min

SIM. 140	**Steel deck:** Re-entrant – Vulcraft 3.5D Formlok	**Rebar (mm):** ϕ12	**Fire resistance (min)**	
	Mesh (mm//mm): ϕ6//150 (W4.5)	**h_1 (mm):** 81	Ave: *107.2*	Max: 116.8

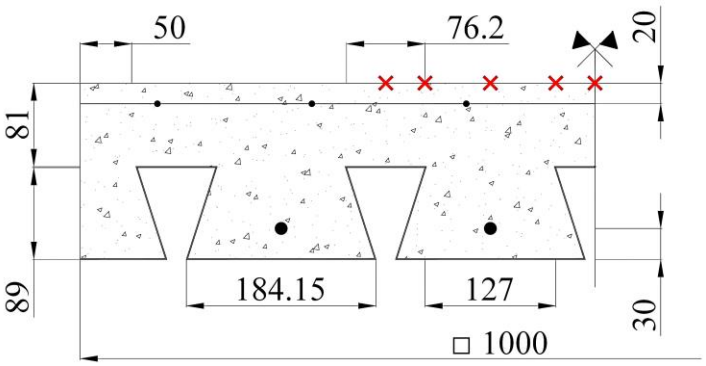

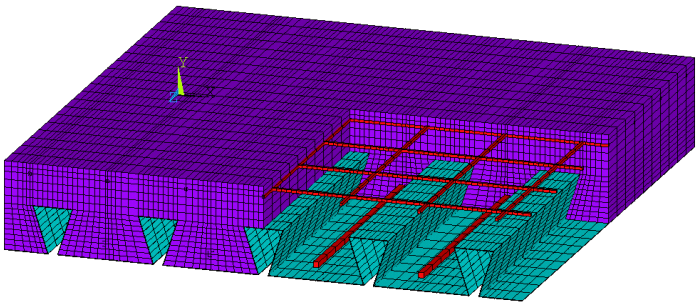

Finite element mesh

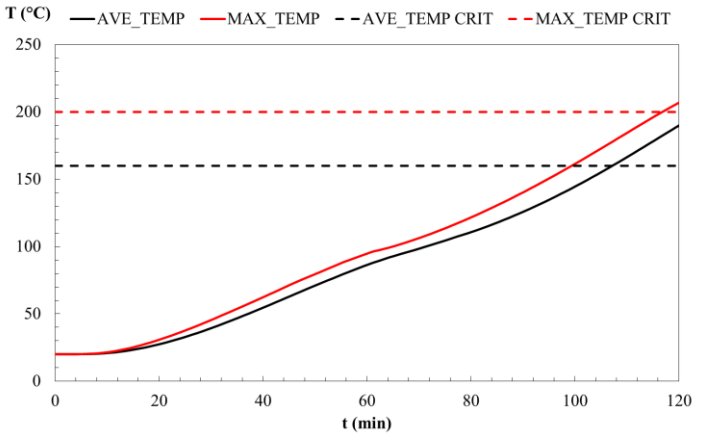

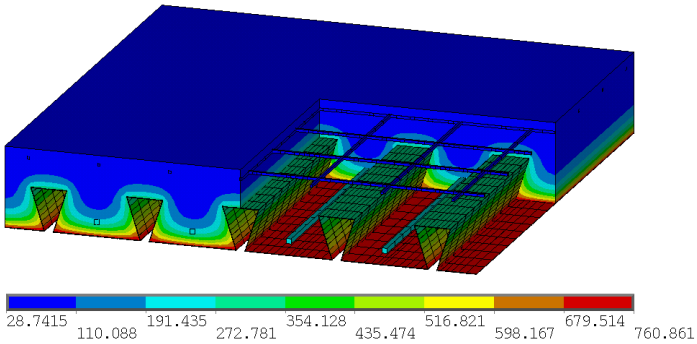

t= 26.8 min

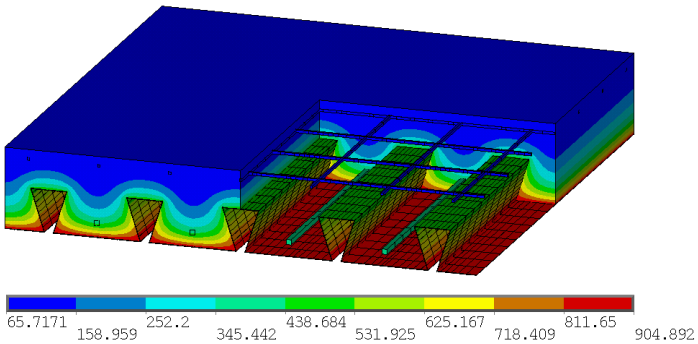

t= 53.6 min

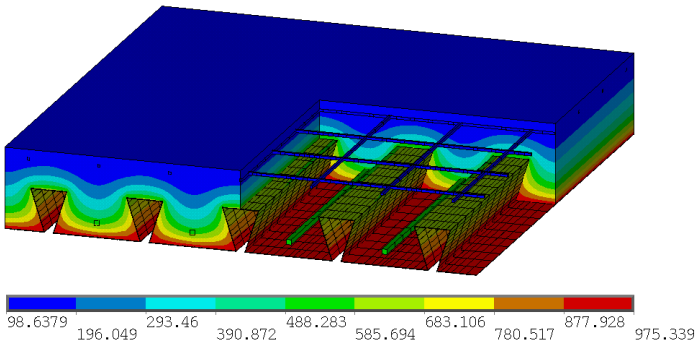

t= 80.4 min

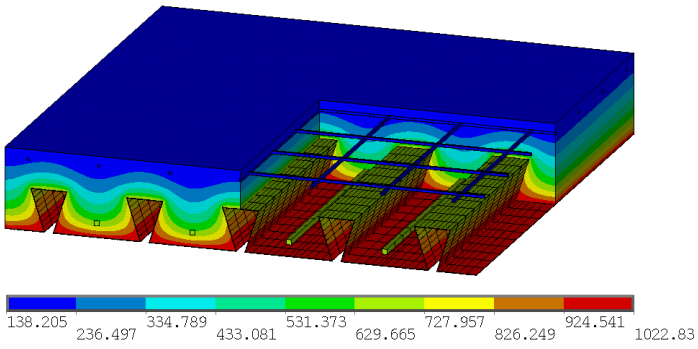

t= 107.2 min

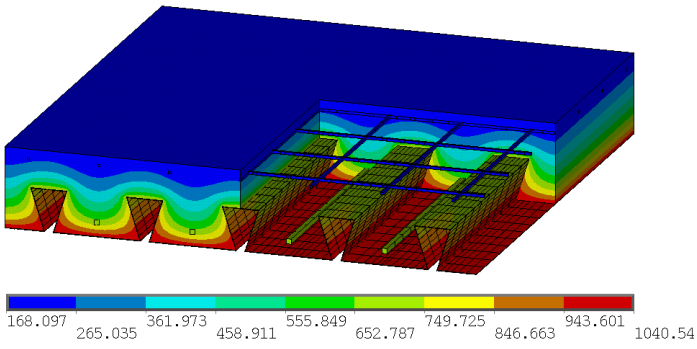

t= 120.0 min

SIM. 141	**Steel deck:** Re-entrant – Vulcraft 3.5D Formlok	**Rebar (mm):** ϕ12	**Fire resistance (min)**	
	Mesh (mm//mm): ϕ6//150 (W4.5)	**h_1 (mm):** 51	Ave: 62.5	Max: *61.6*

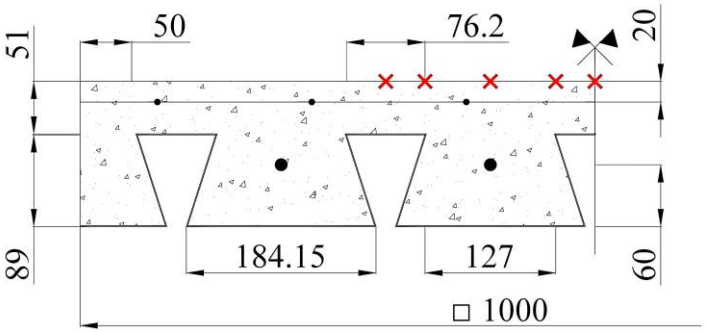

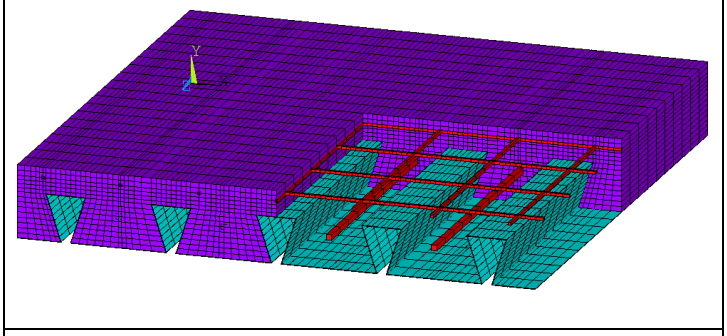

Finite element mesh

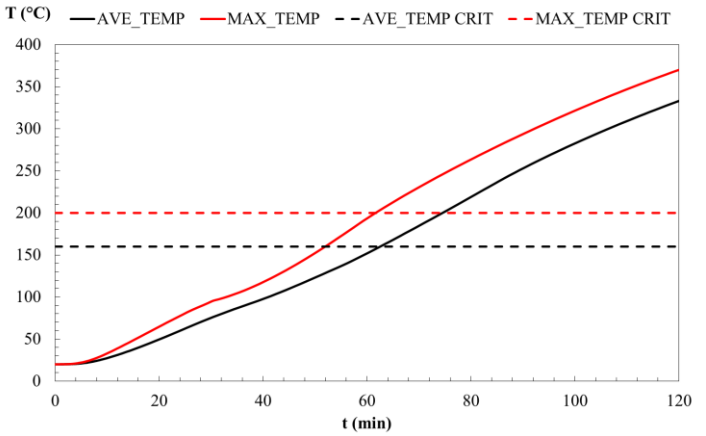

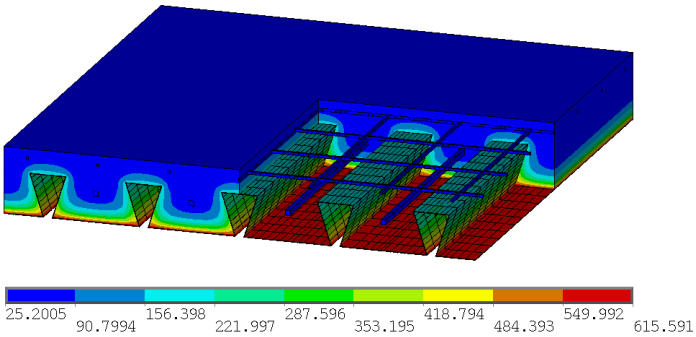

t= 15.4 min

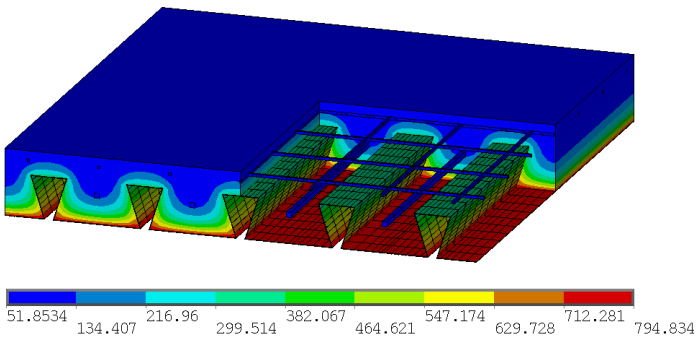

t= 30.8 min

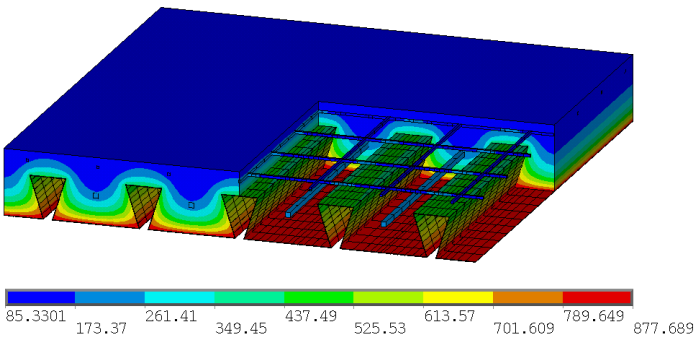

t= 46.2 min

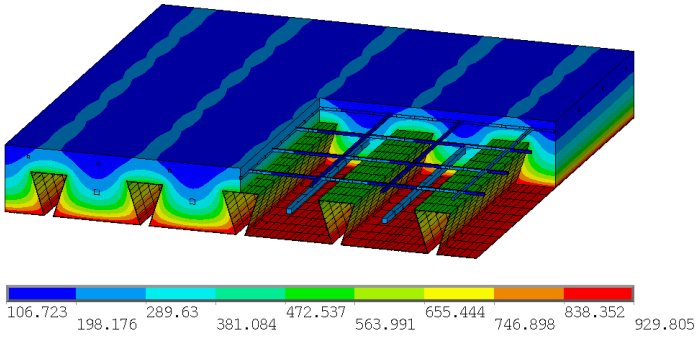

t= 61.6 min

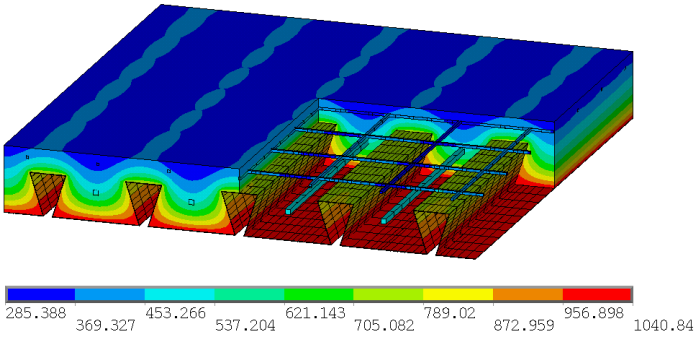

t= 120.0 min

SIM. 142	**Steel deck:** Re-entrant – Vulcraft 3.5D Formlok	**Rebar (mm):** ϕ12	**Fire resistance (min)**	
	Mesh (mm//mm): ϕ6//150 (W4.5)	**h_1 (mm):** 61	Ave: *76.5*	Max: 78.5

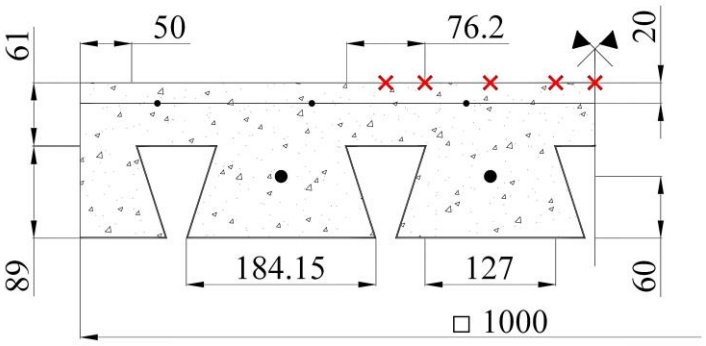

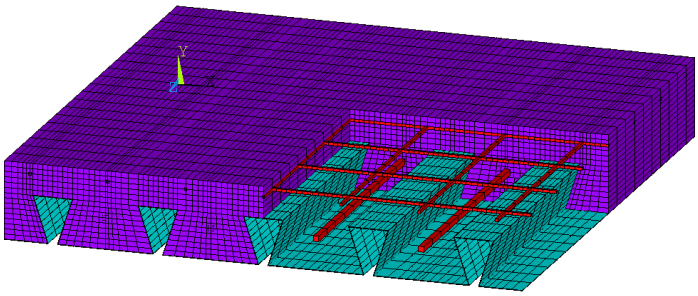

Finite element mesh

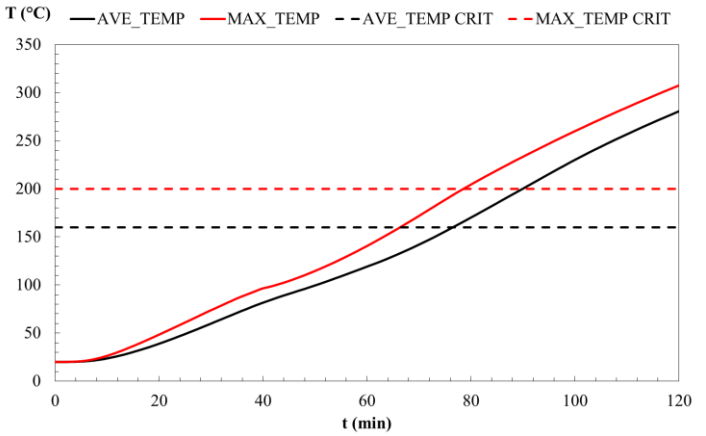

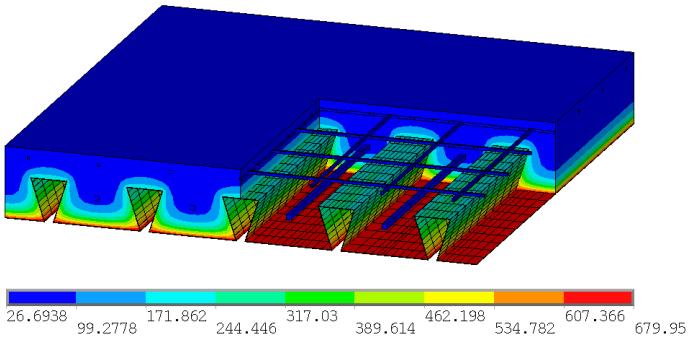

t= 19.1 min

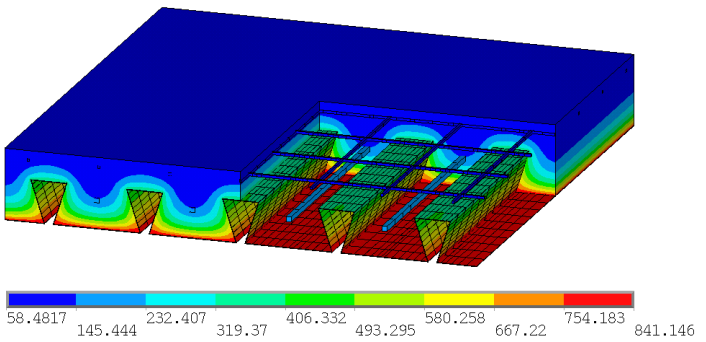

t= 38.3 min

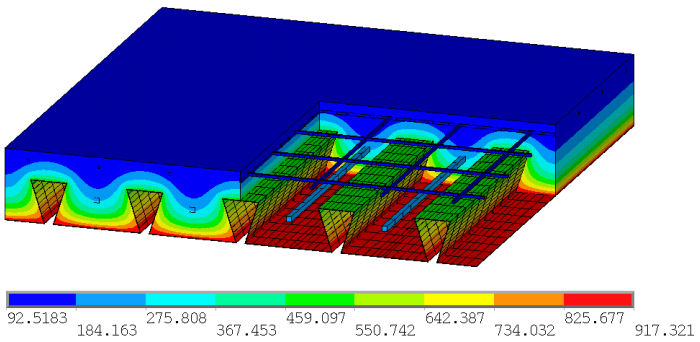

t= 57.4 min

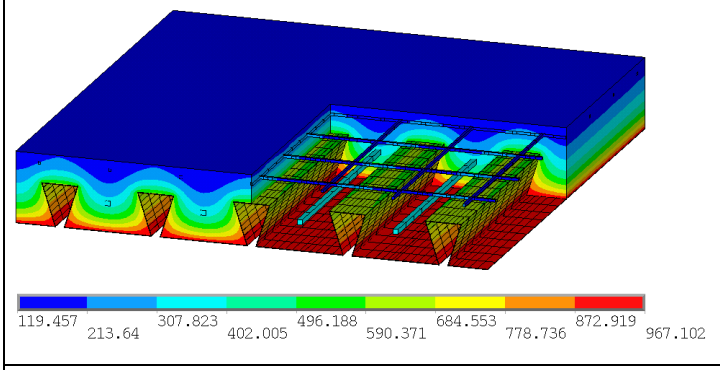

t= 76.5 min

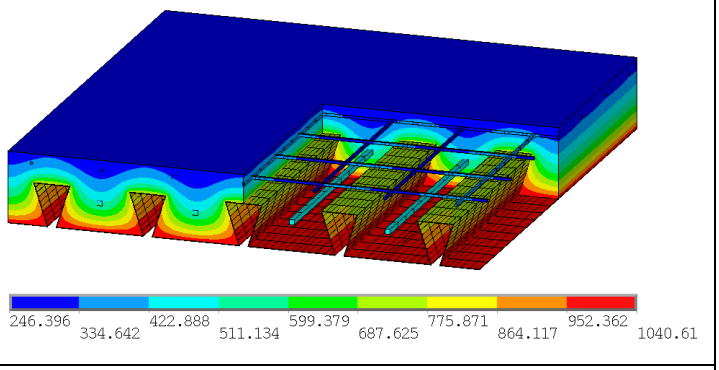

t= 120.0 min

SIM. 143	**Steel deck:** Re-entrant – Vulcraft 3.5D Formlok	**Rebar (mm):** ϕ12	**Fire resistance (min)**	
	Mesh (mm//mm): ϕ6//150 (W4.5)	**h_1 (mm):** 71	Ave: *91.4*	Max: 97.0

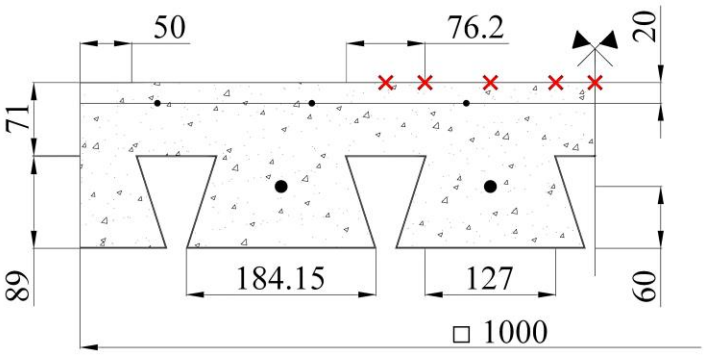

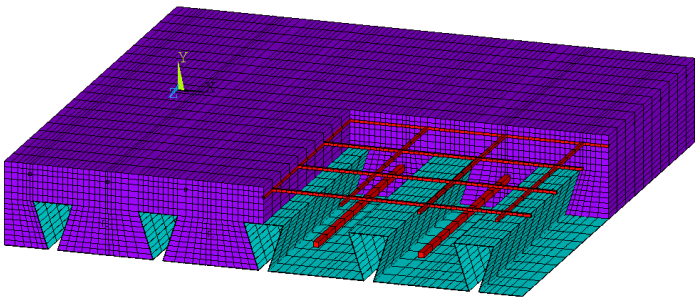

Finite element mesh

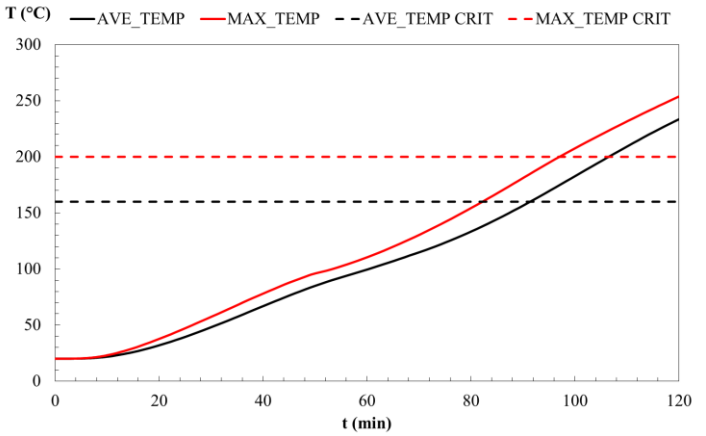

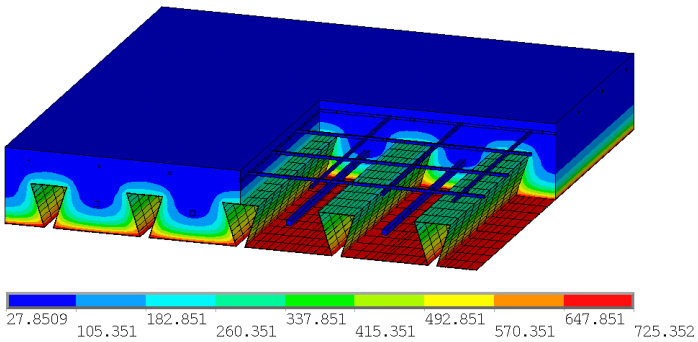

t= 22.9 min

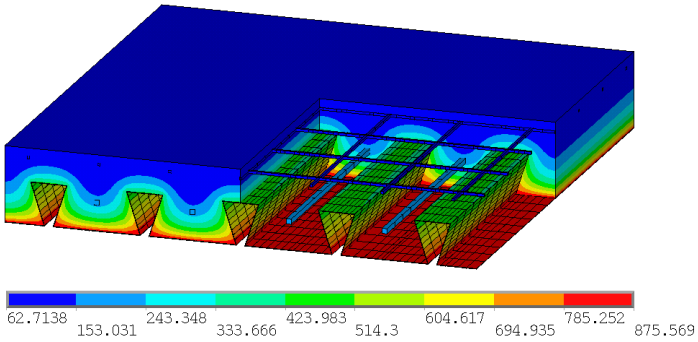

t= 45.7 min

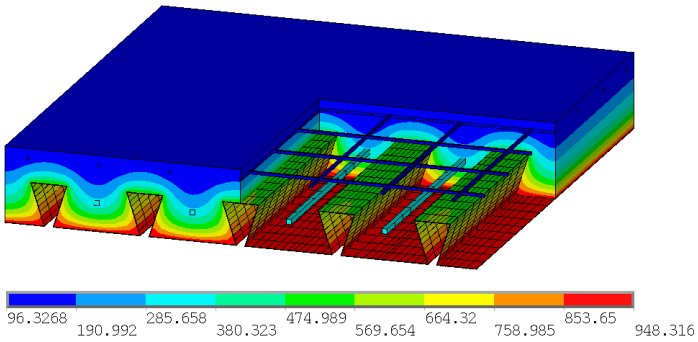

t= 68.6 min

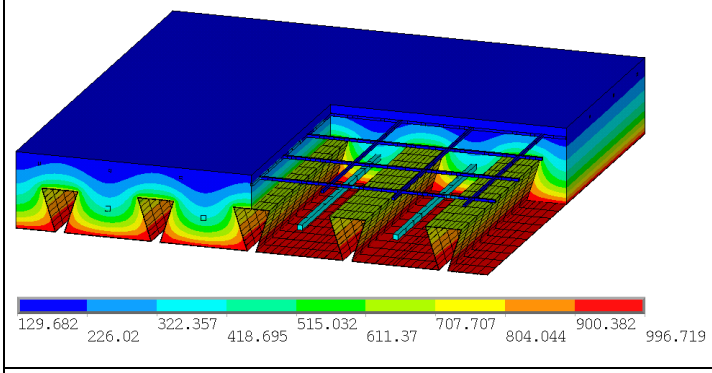

t= 91.4 min

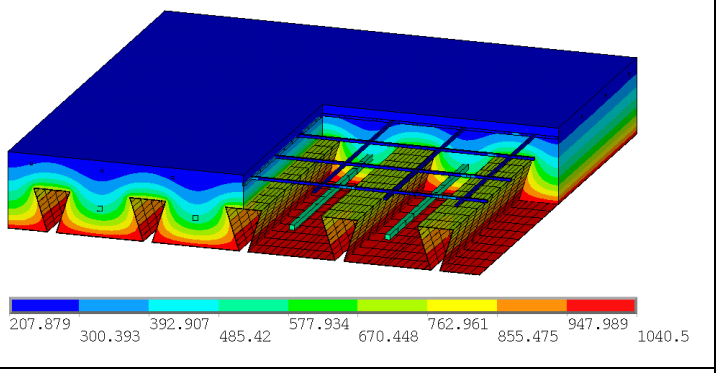

t= 120.0 min

SIM. 144	**Steel deck:** Re-entrant – Vulcraft 3.5D Formlok	**Rebar (mm):** ϕ12	**Fire resistance (min)**	
	Mesh (mm//mm): ϕ6//150 (W4.5)	**h_1 (mm):** 81	Ave: *107.3*	Max: 116.9

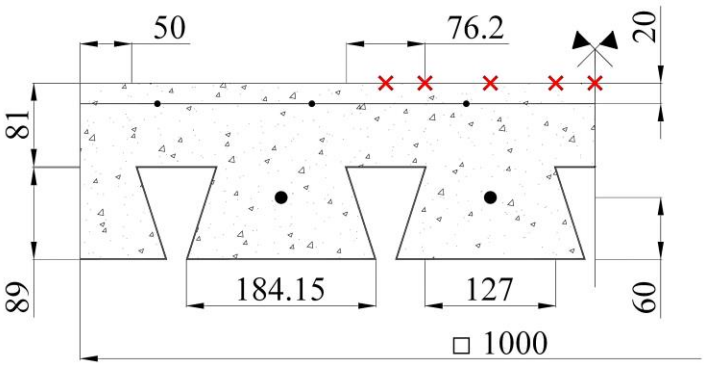

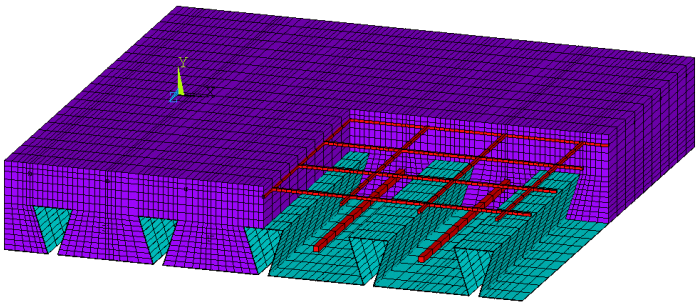

Finite element mesh

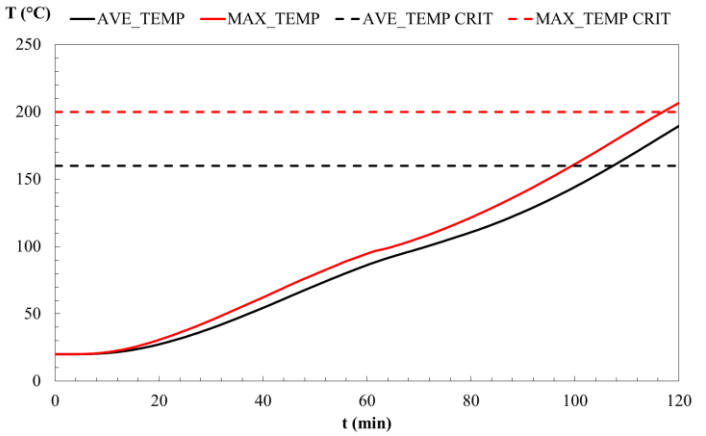

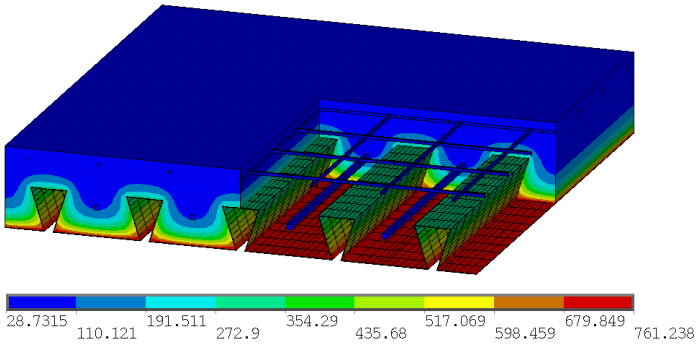

t= 26.8 min

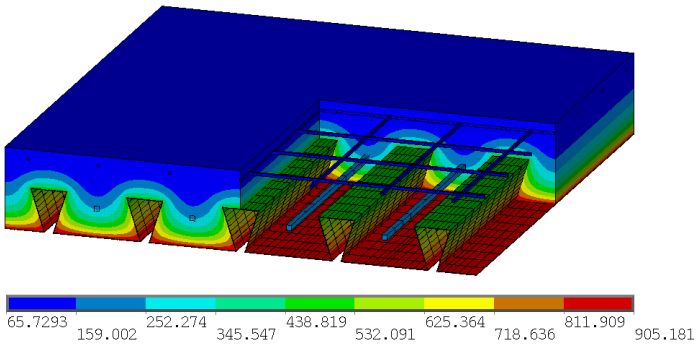

t= 53.7 min

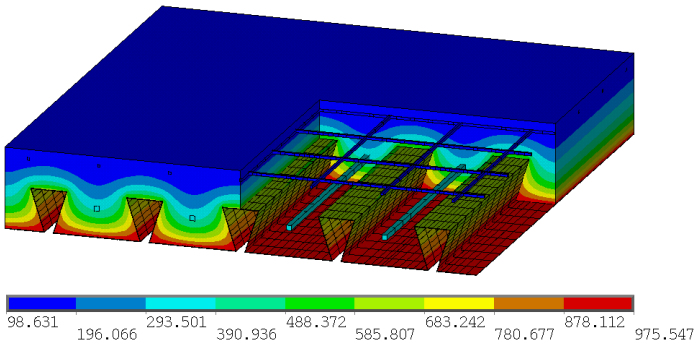

t= 80.5 min

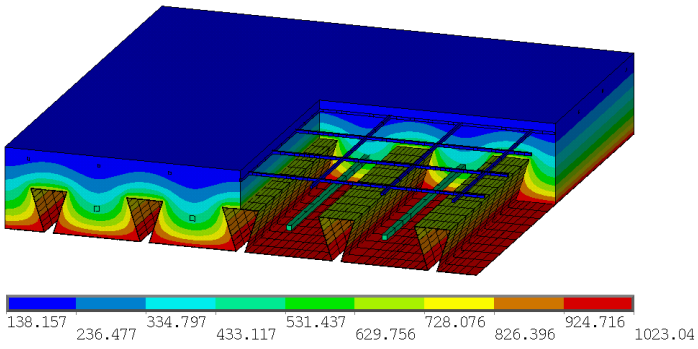

t= 107.3 min

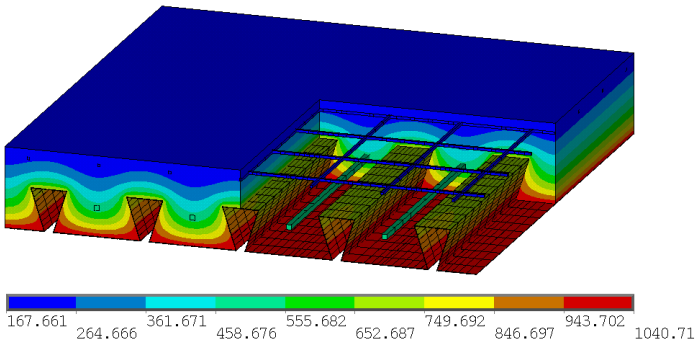

t= 120.0 min

SIM. 145	**Steel deck:** Lysaght Bondek	**Rebar (mm):** ϕ8	**Fire resistance (min)**	
	Mesh (mm//mm): ϕ6.75//200 (RM72)	**h_1 (mm):** 56	Ave: *69.5*	Max: 71.6

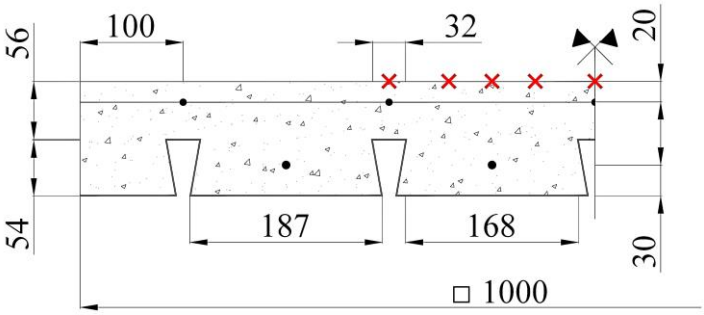

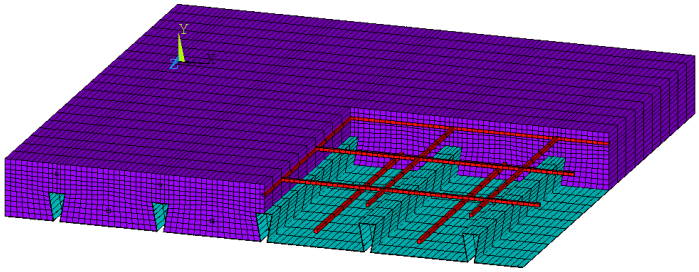

Finite element mesh

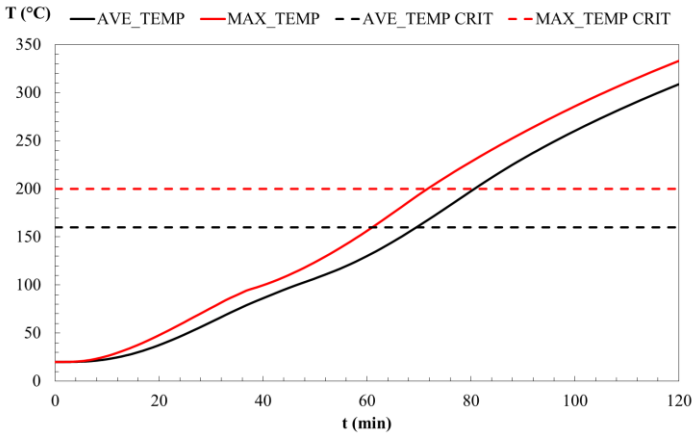

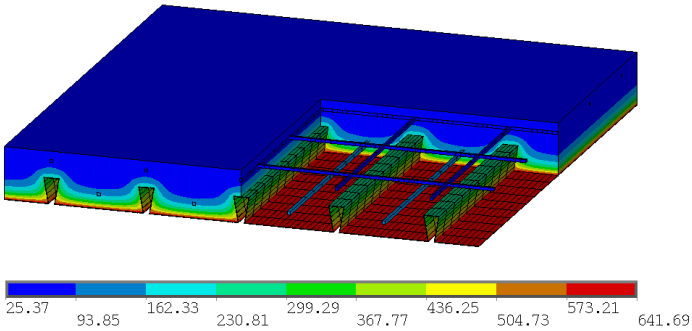

t= 17.4 min

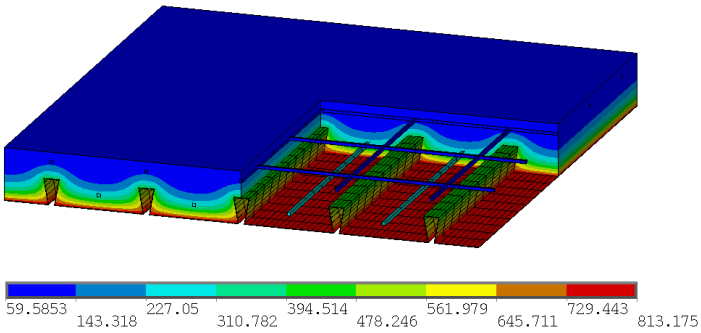

t= 34.8 min

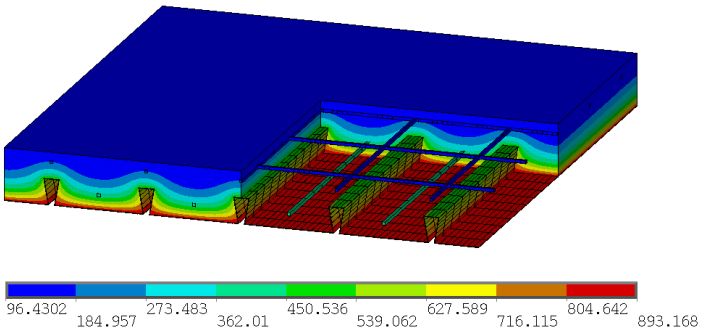

t= 52.1 min

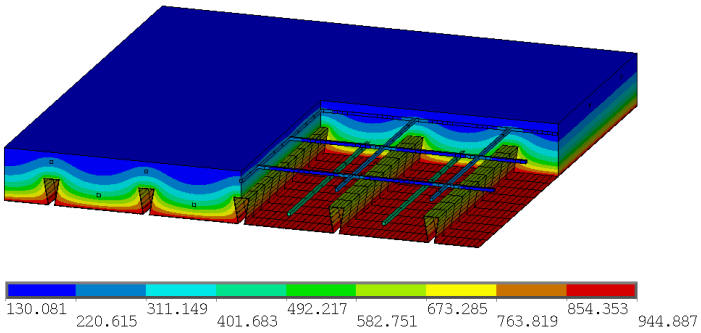

t= 69.5 min

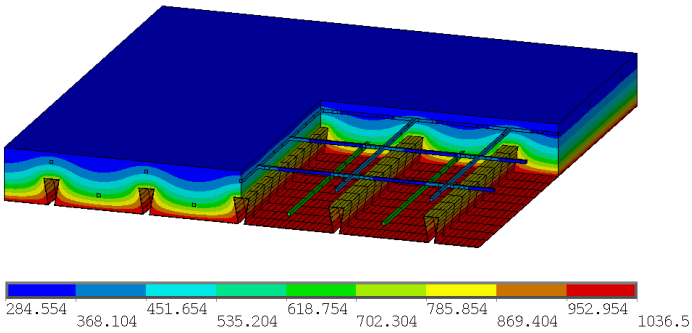

t= 120.0 min

SIM. 146	**Steel deck:** Lysaght Bondek	**Rebar (mm):** ϕ8	**Fire resistance (min)**	
	Mesh (mm//mm): ϕ6.75//200 (RM72)	**h_1 (mm):** 66	Ave: *83.2*	Max: 88.9

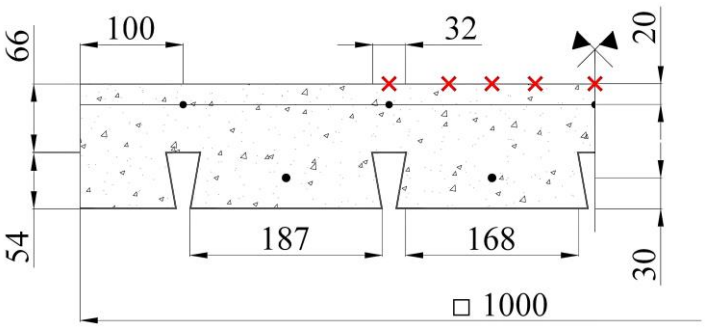

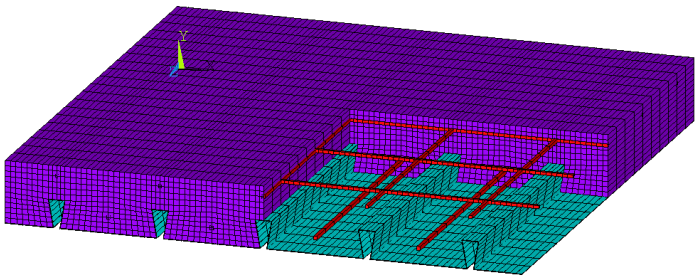

Finite element mesh

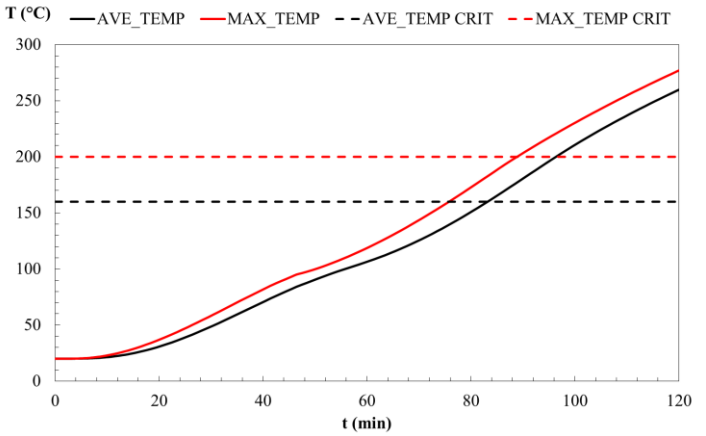

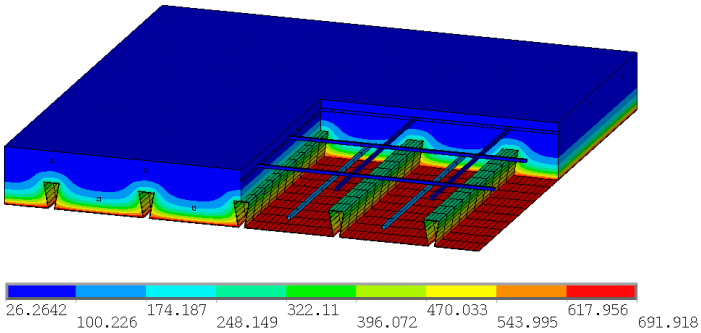

t= 20.8 min

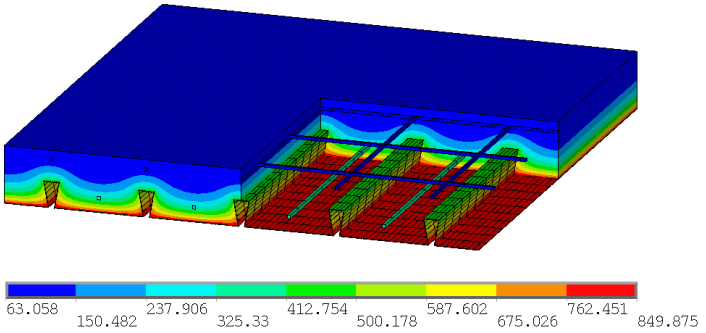

t= 41.6 min

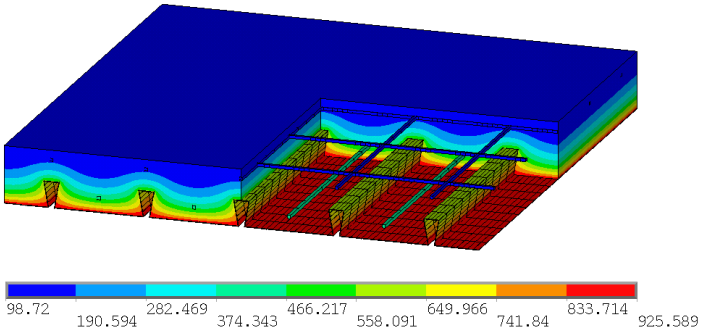

t= 62.4 min

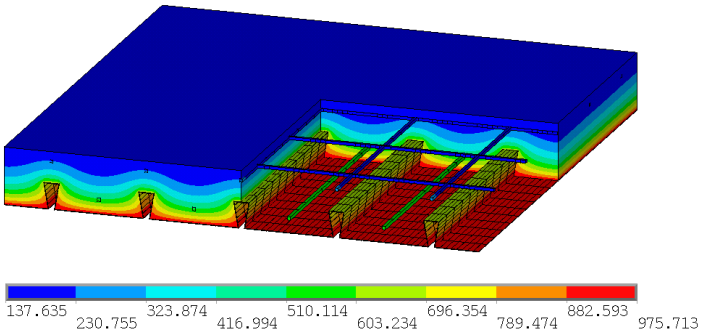

t= 83.2 min

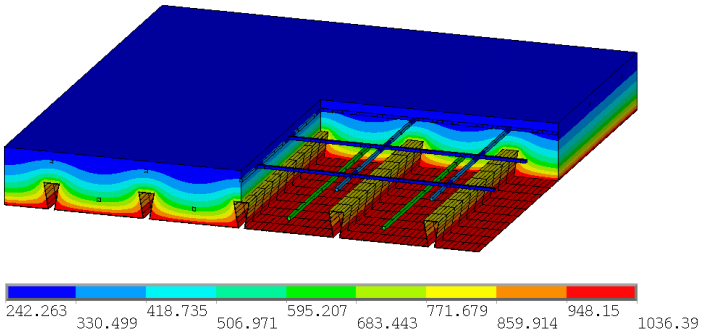

t= 120.0 min

SIM. 147	**Steel deck:** Lysaght Bondek	**Rebar (mm):** ϕ8	**Fire resistance (min)**	
	Mesh (mm//mm): ϕ6.75//200 (RM72)	**h_1 (mm):** 76	Ave: *98.1*	Max: 107.6

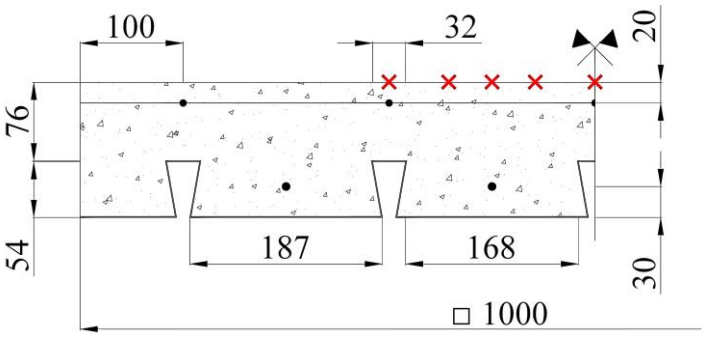

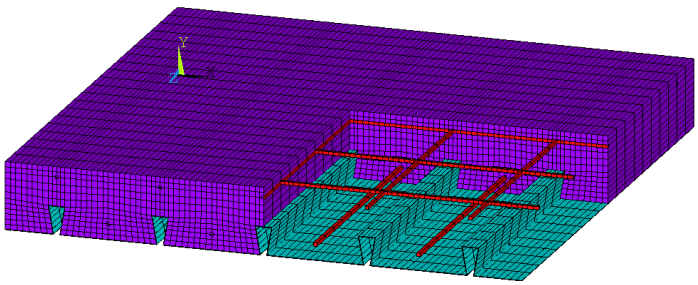

Finite element mesh

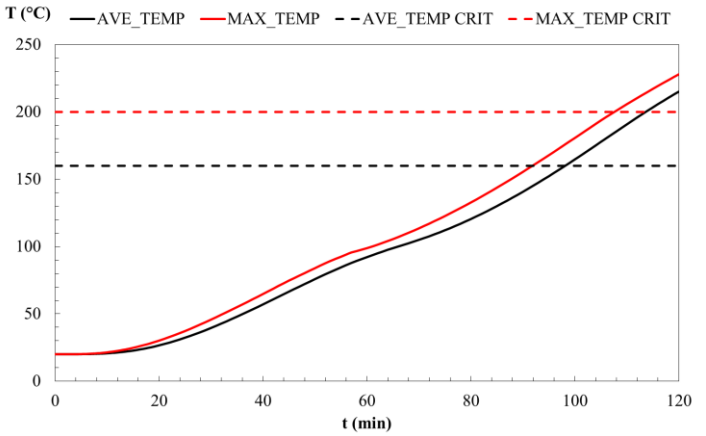

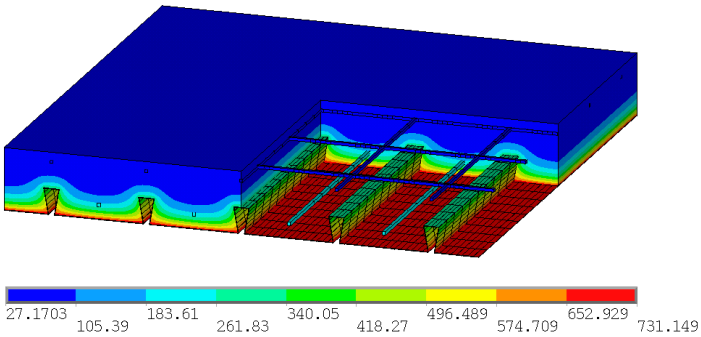

t= 24.5 min

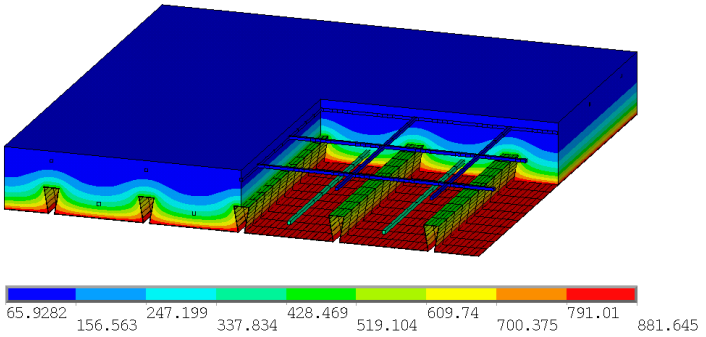

t= 49.1 min

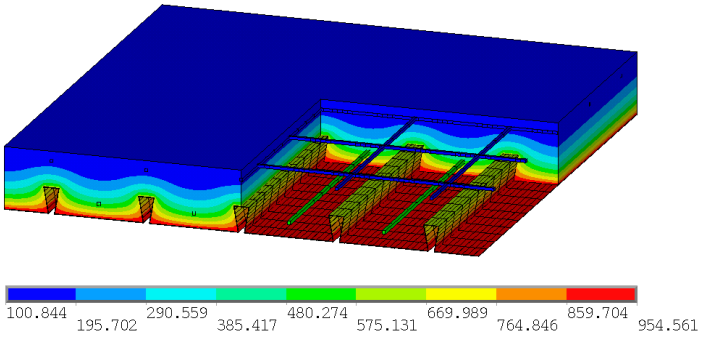

t= 73.6 min

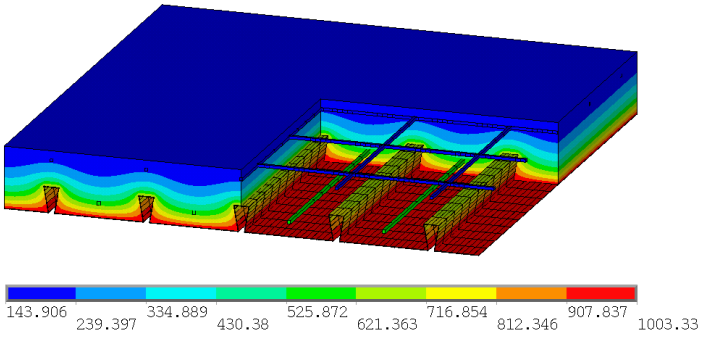

t= 98.1 min

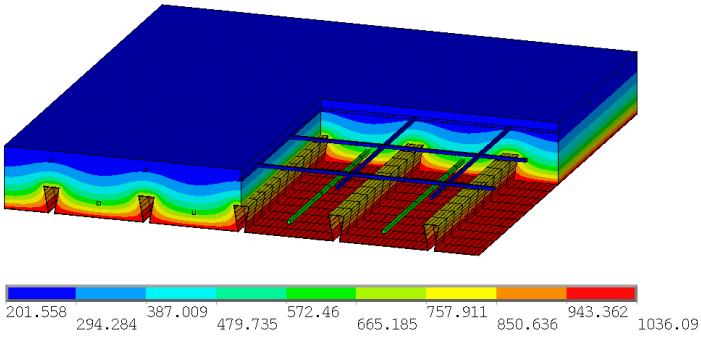

t= 120.0 min

SIM. 148	**Steel deck:** Lysaght Bondek	**Rebar (mm):** ϕ8	**Fire resistance (min)**	
	Mesh (mm//mm): ϕ6.75//200 (RM72)	**h_1 (mm):** 86	Ave: *114.4*	Max: 127.8

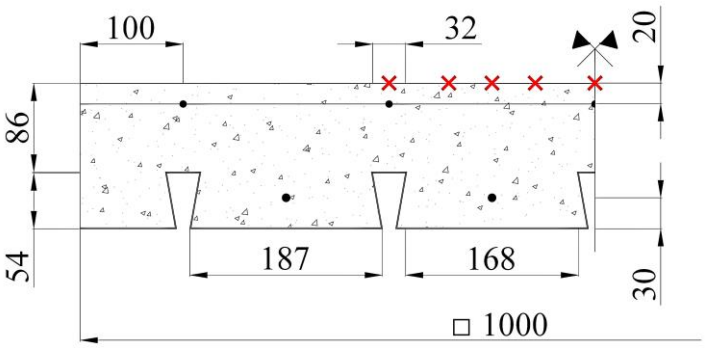

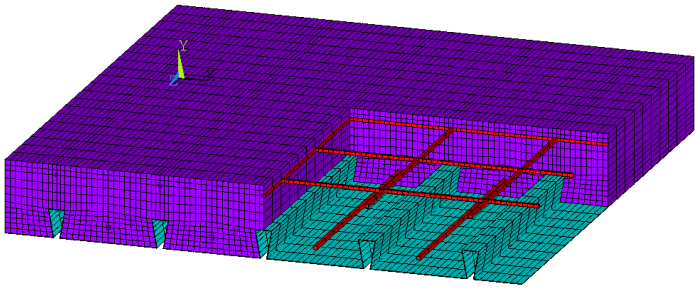

Finite element mesh

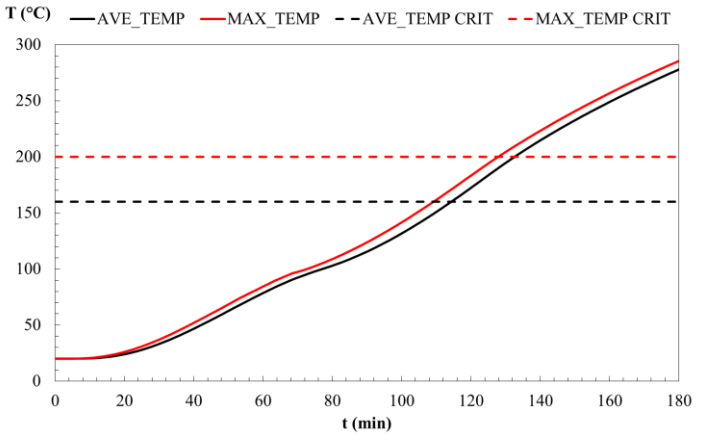

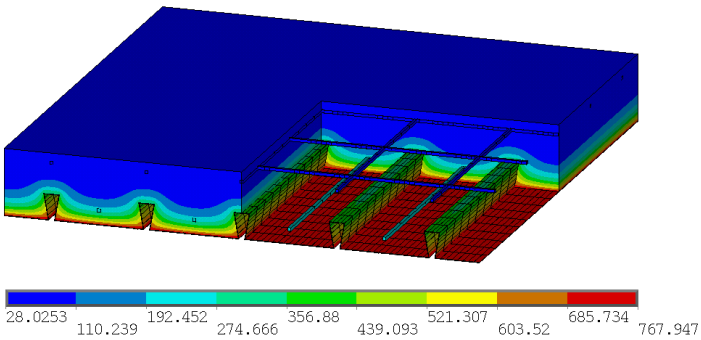

t= 28.6 min

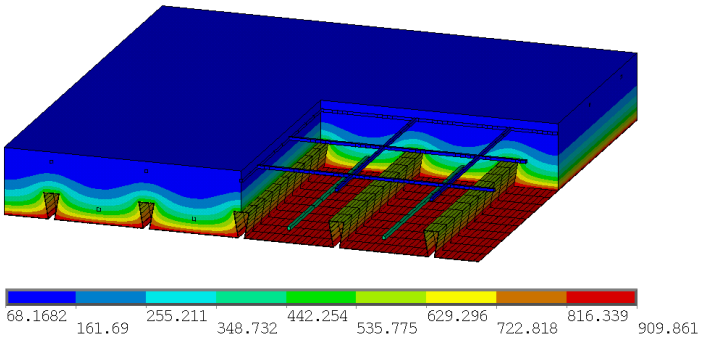

t= 57.2 min

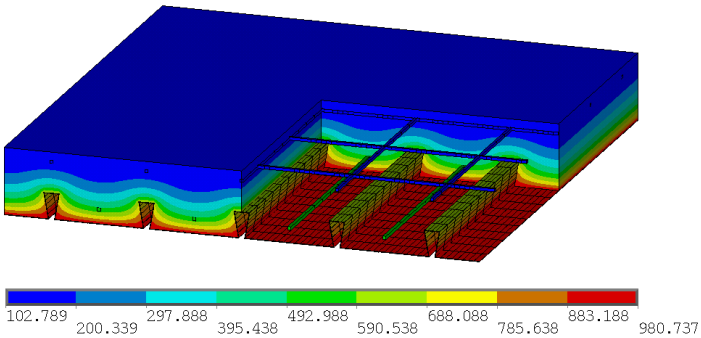

t= 85.8 min

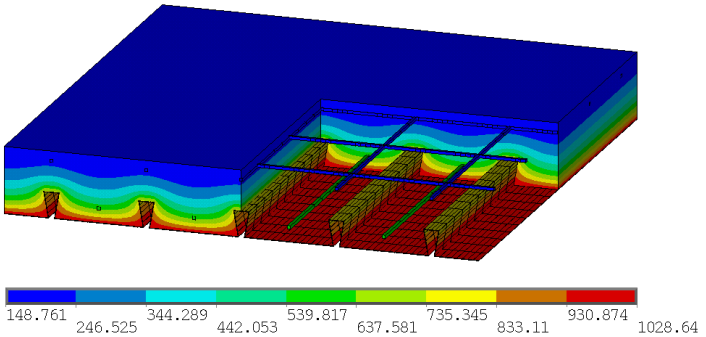

t= 114.4 min

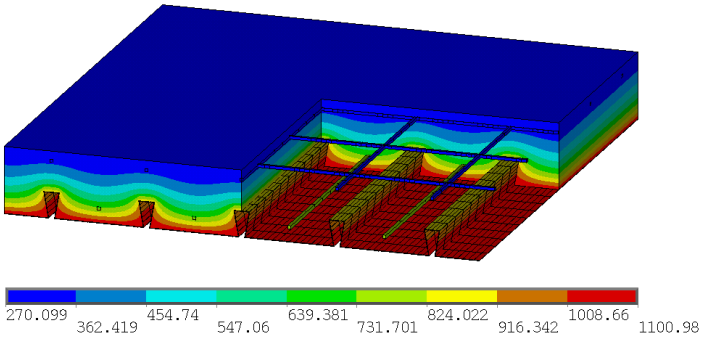

t= 180.0 min

SIM. 149	**Steel deck:** Lysaght Bondek	**Rebar (mm):** ϕ8	**Fire resistance (min)**	
	Mesh (mm//mm): ϕ6.75//200 (RM72)	**h_1 (mm):** 56	Ave: *69.5*	Max: 71.6

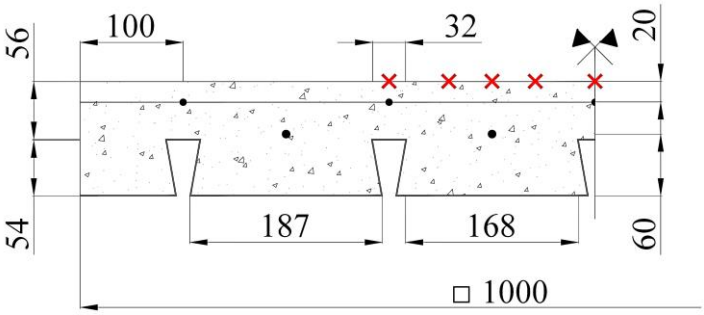

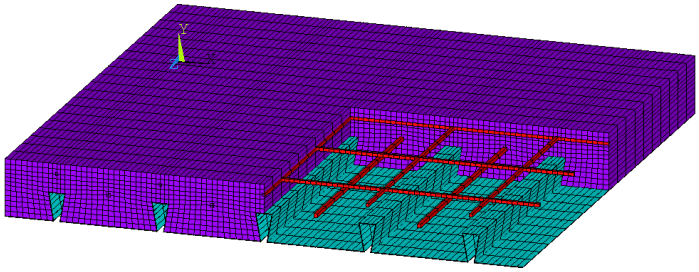

Finite element mesh

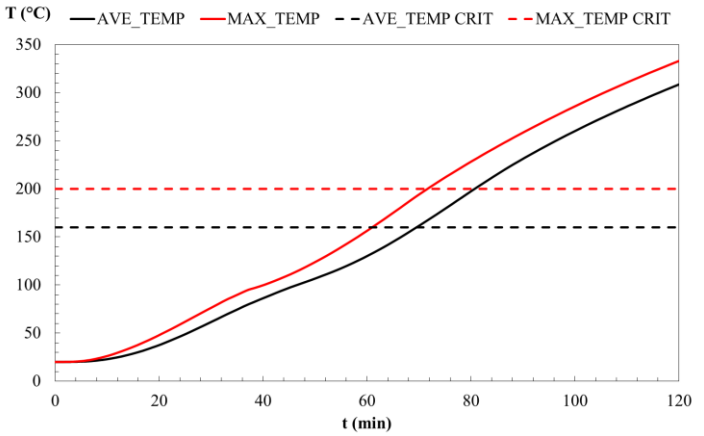

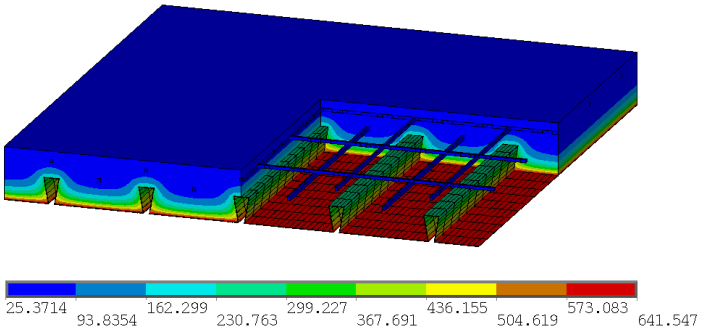

t= 17.4 min

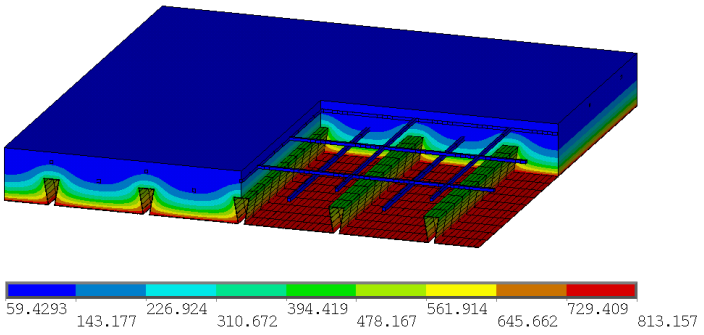

t= 34.8 min

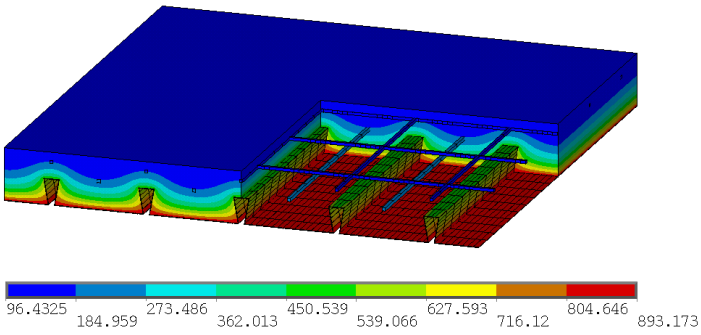

t= 52.1 min

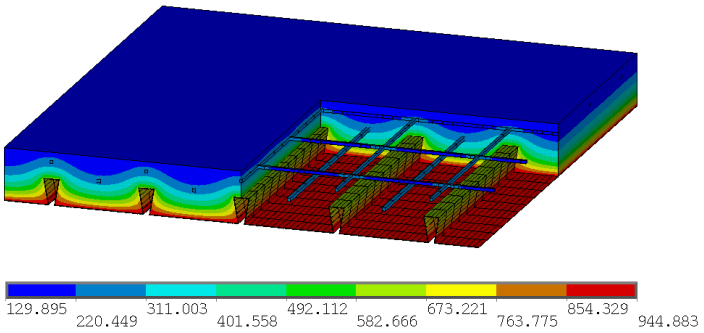

t= 69.5 min

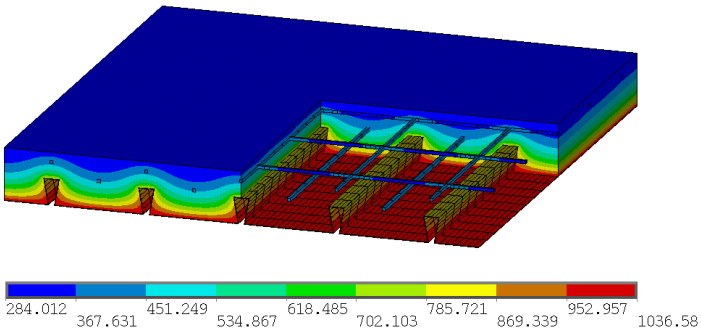

t= 120.0 min

SIM. 150	**Steel deck:** Lysaght Bondek	**Rebar (mm):** ϕ8	**Fire resistance (min)**	
	Mesh (mm//mm): ϕ6.75//200 (RM72)	**h_1 (mm):** 66	Ave: *83.2*	Max: 88.8

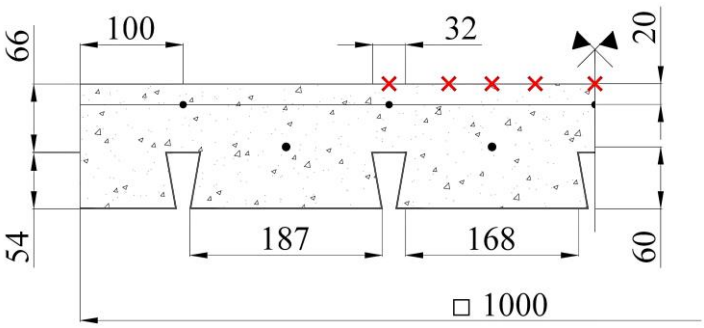

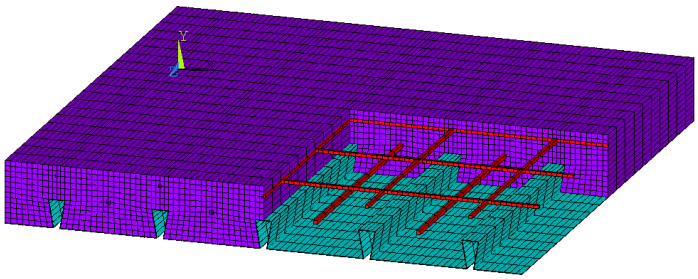

Finite element mesh

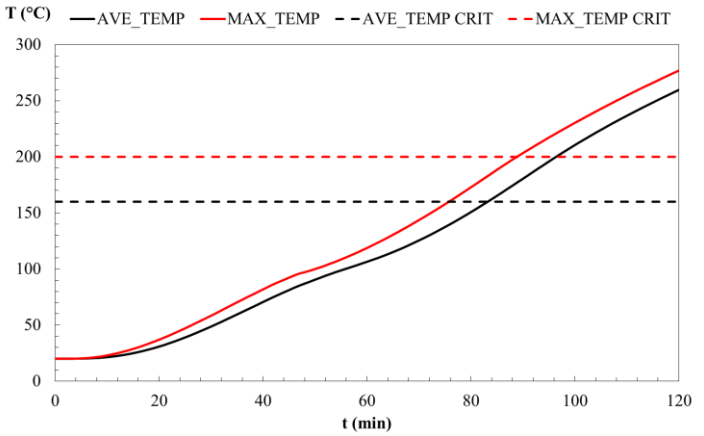

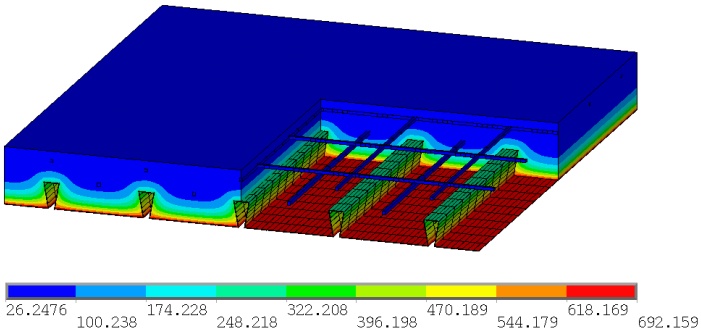

t= 20.8 min

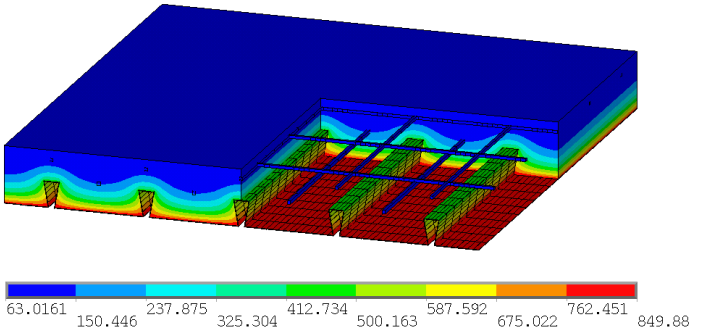

t= 41.6 min

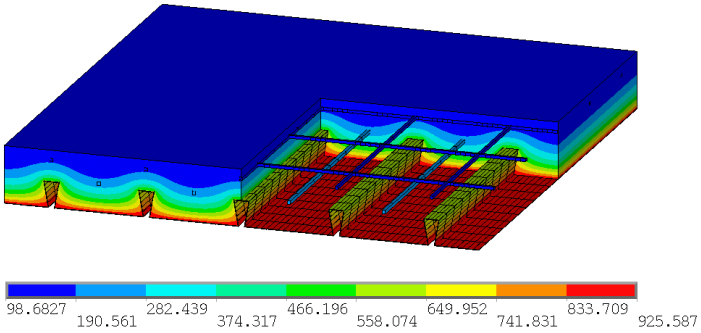

t= 62.4 min

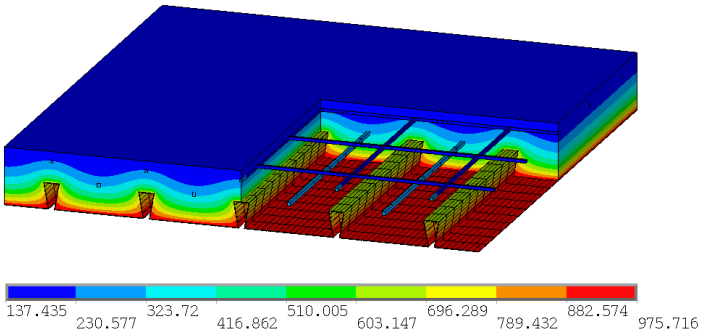

t= 83.2 min

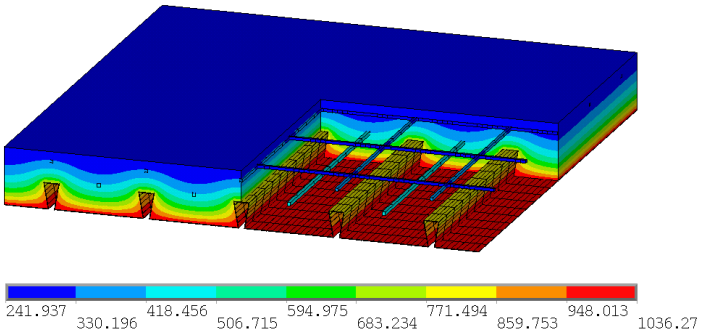

t= 120.0 min

SIM. 151	**Steel deck:** Lysaght Bondek	**Rebar (mm):** ϕ8	**Fire resistance (min)**	
	Mesh (mm//mm): ϕ6.75//200 (RM72)	**h_1 (mm):** 76	Ave: *98.2*	Max: 107.6

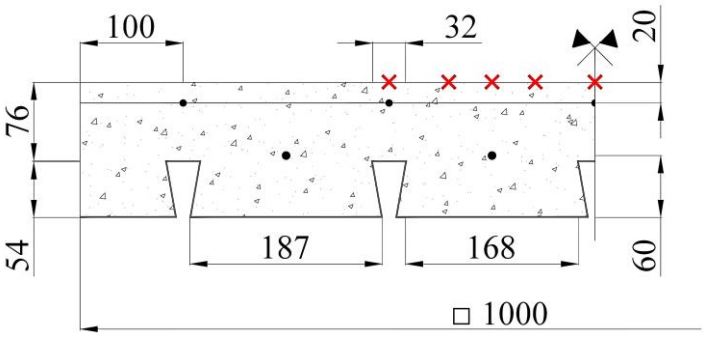

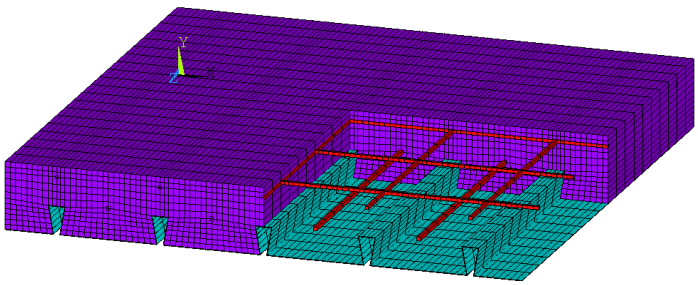

Finite element mesh

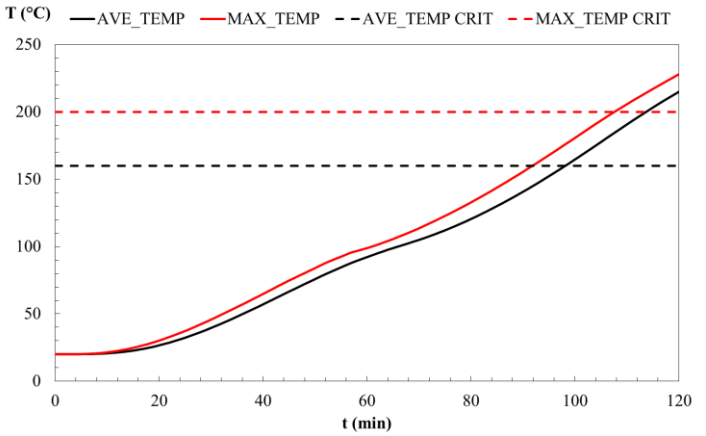

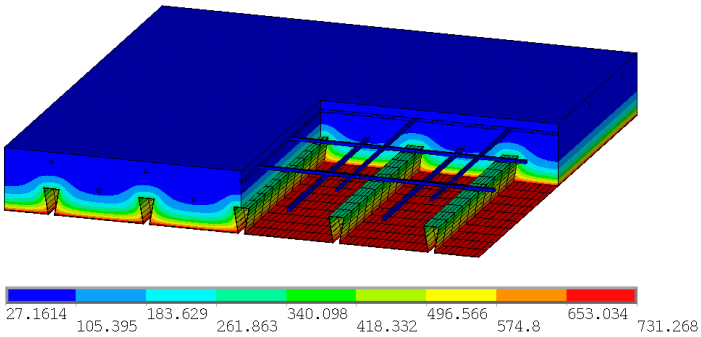

t= 24.6 min

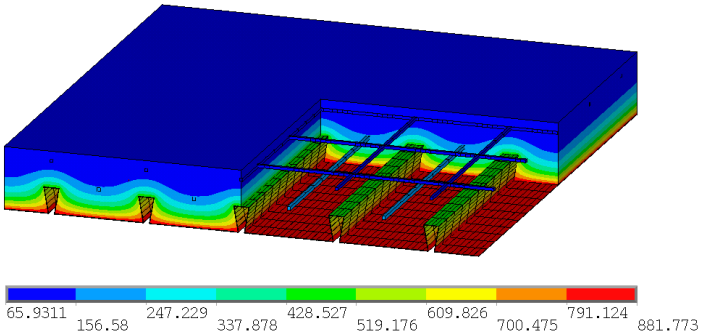

t= 49.1 min

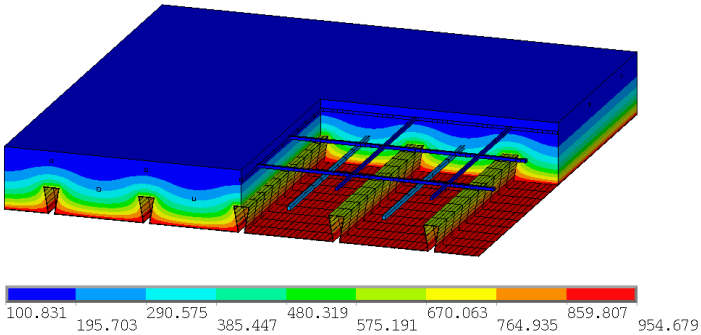

t= 73.7 min

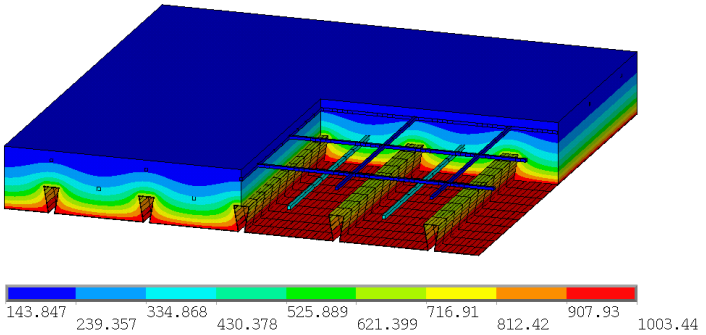

t= 98.2 min

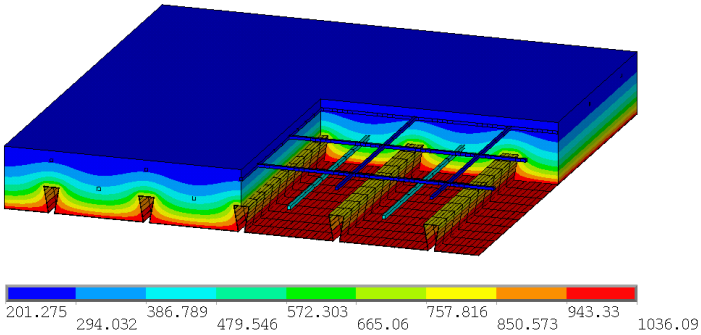

t= 120.0 min

SIM. 152	**Steel deck:** Lysaght Bondek	**Rebar (mm):** ϕ8	**Fire resistance (min)**	
	Mesh (mm//mm): ϕ6.75//200 (RM72)	**h_1 (mm):** 86	Ave: *114.4*	Max: 127.9

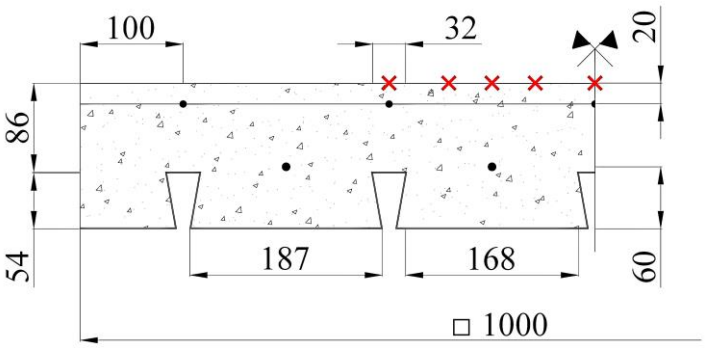

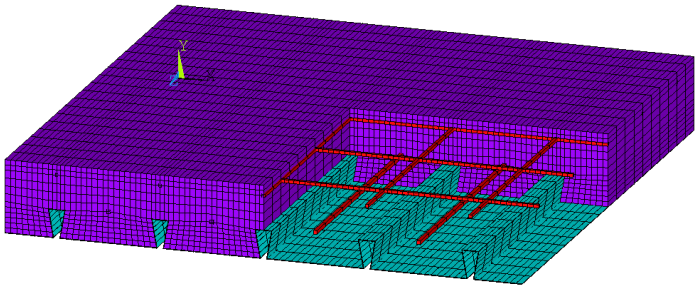

Finite element mesh

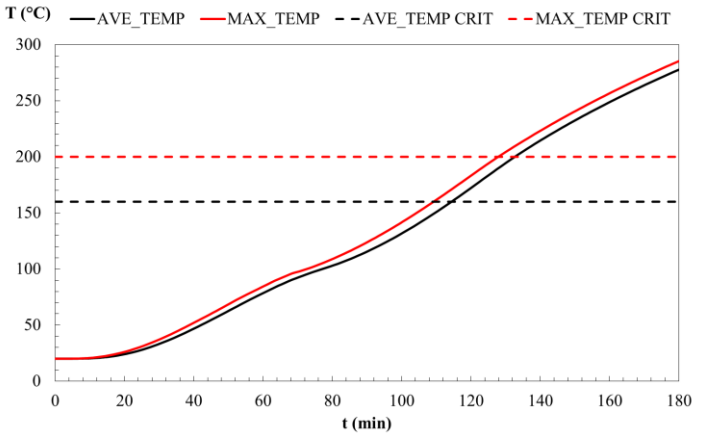

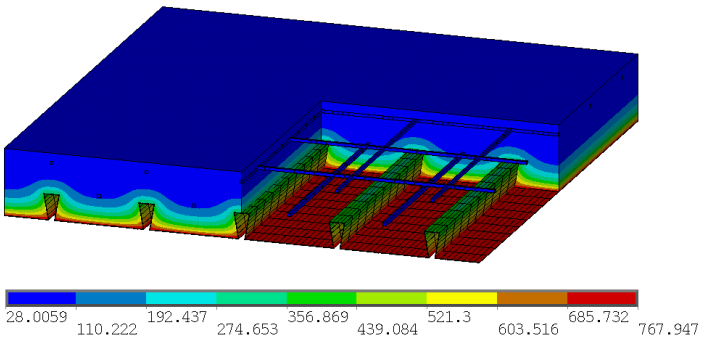

t= 28.6 min

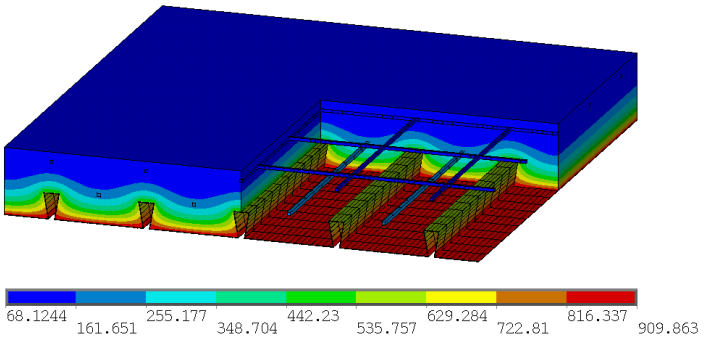

t= 57.2 min

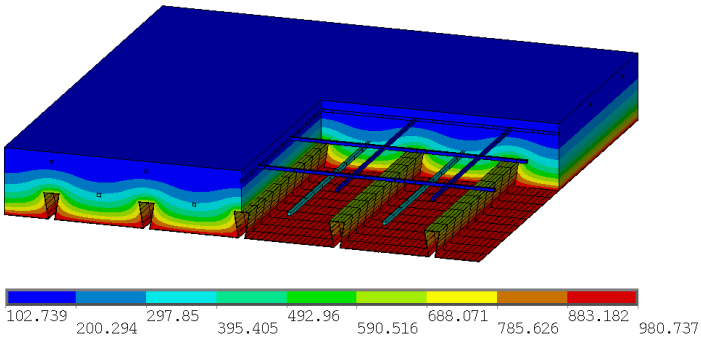

t= 85.8 min

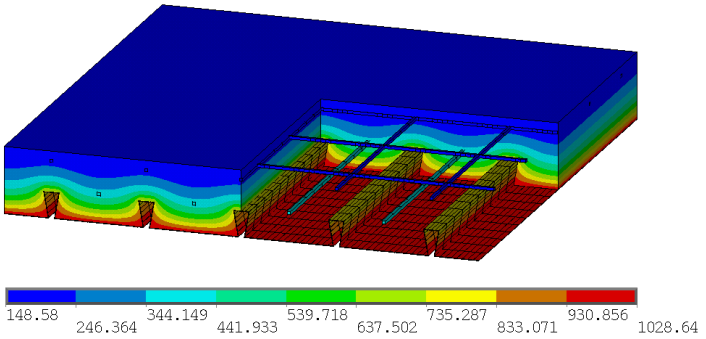

t= 114.4 min

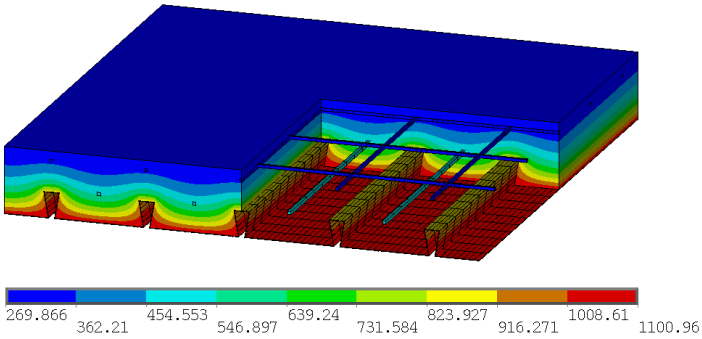

t= 180.0 min

SIM. 153	**Steel deck:** Lysaght Bondek	**Rebar (mm):** ϕ8	**Fire resistance (min)**	
	Mesh (mm//mm): ϕ7.6//200 (RM82)	**h_1 (mm):** 56	Ave: *69.6*	Max: 72.2

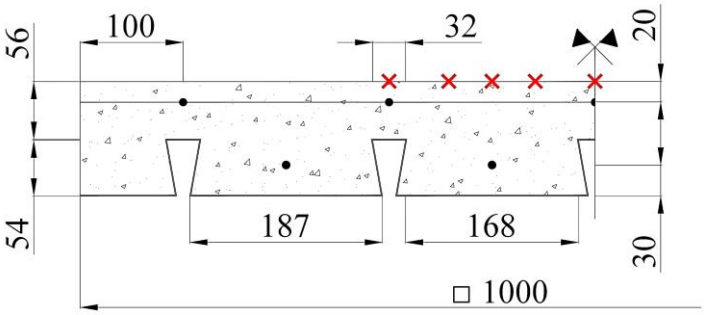

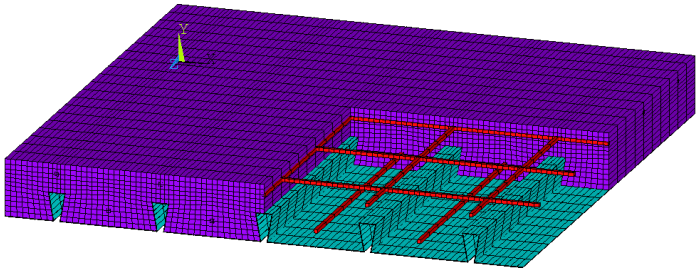

Finite element mesh

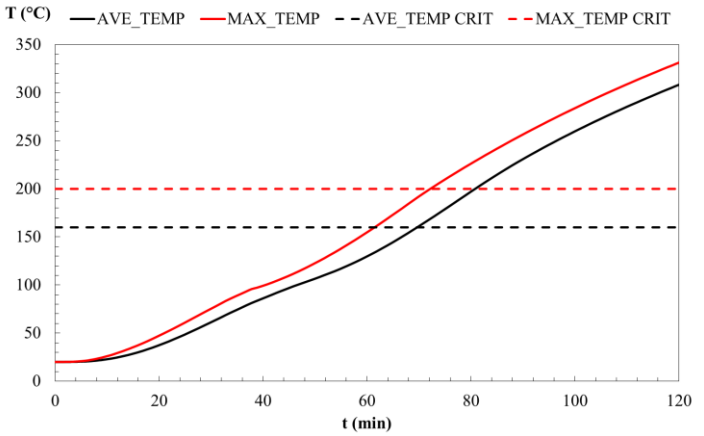

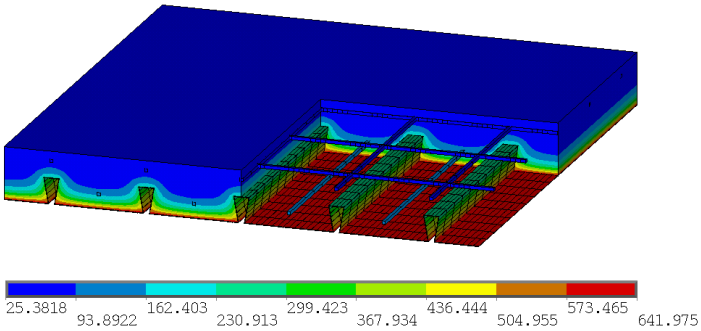

t= 17.4 min

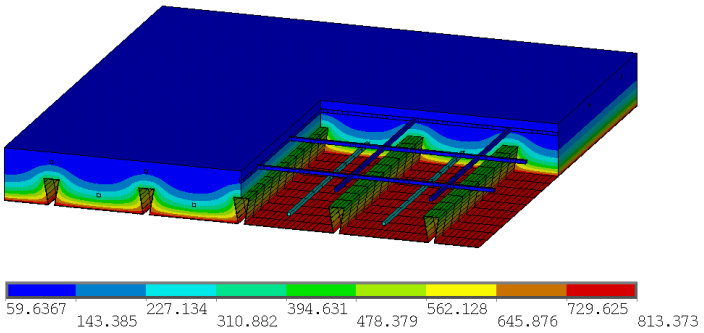

t= 34.8 min

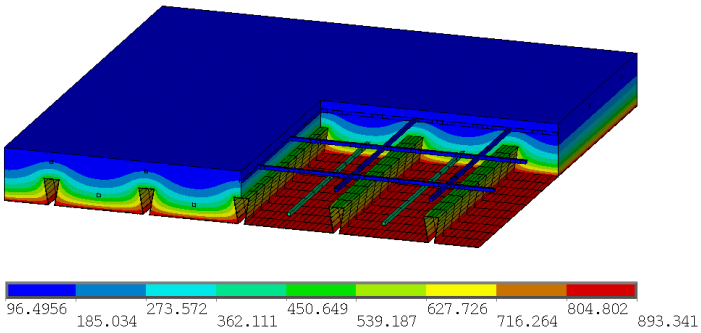

t= 52.2 min

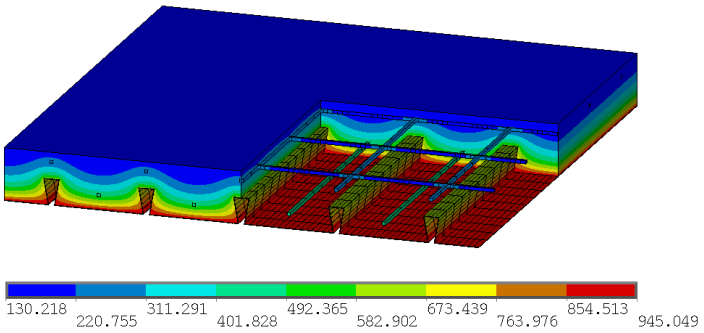

t= 69.6 min

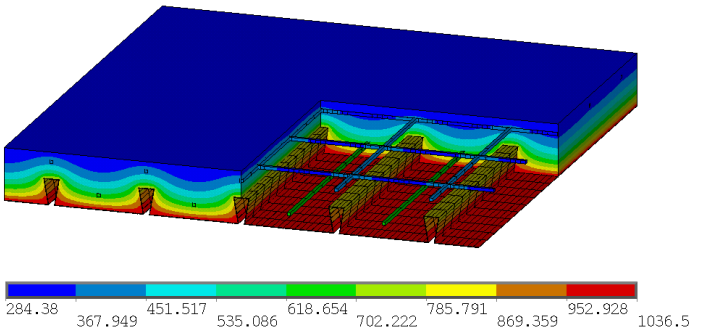

t= 120.0 min

SIM. 154	**Steel deck:** Lysaght Bondek	**Rebar (mm):** ϕ8	**Fire resistance (min)**	
	Mesh (mm//mm): ϕ7.6//200 (RM82)	**h_1 (mm):** 66	Ave: *83.3*	Max: 89.4

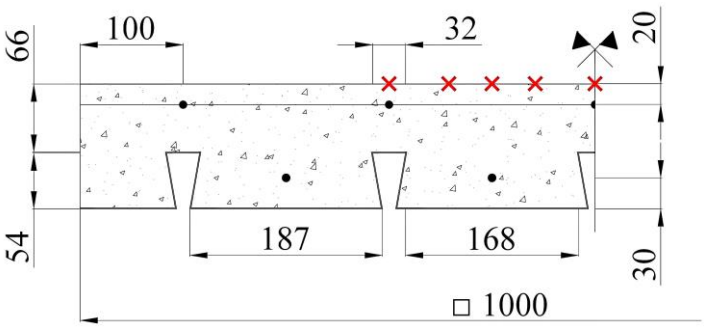

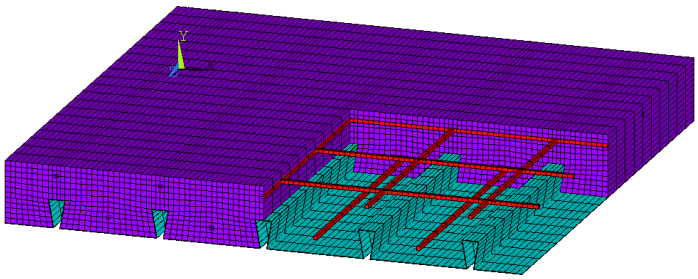

Finite element mesh

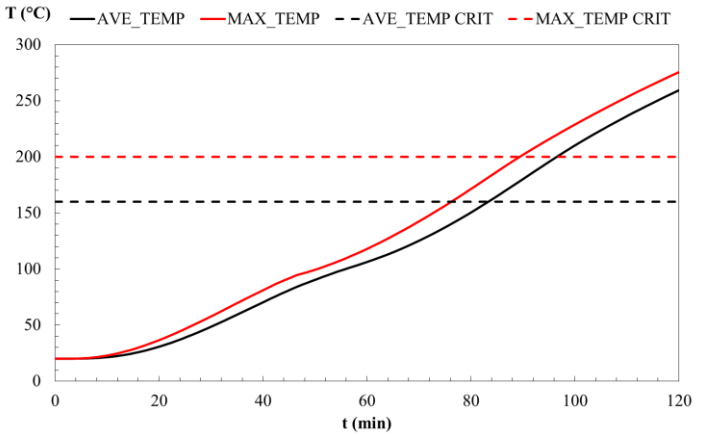

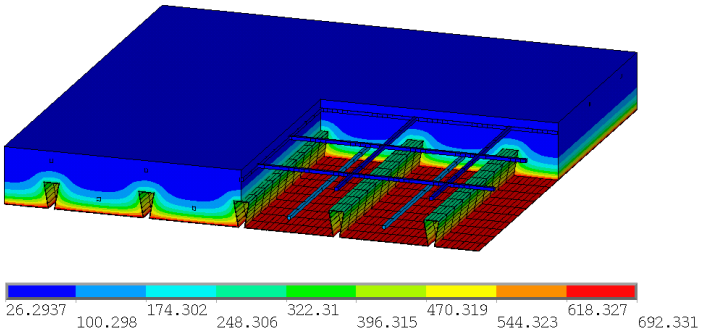

t= 20.8 min

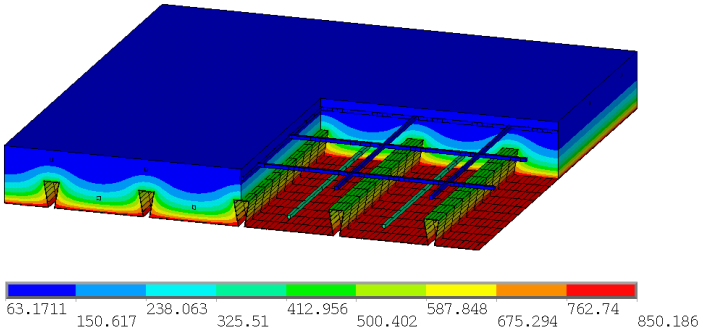

t= 41.7 min

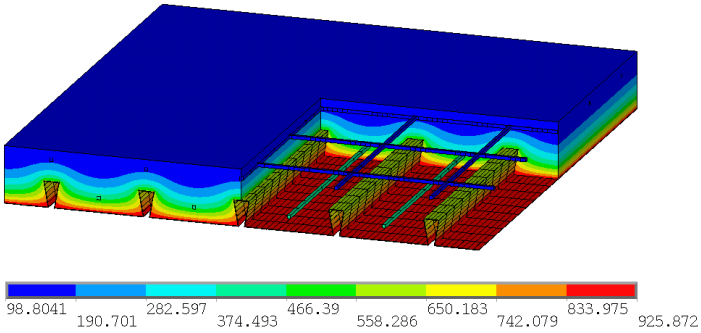

t= 62.5 min

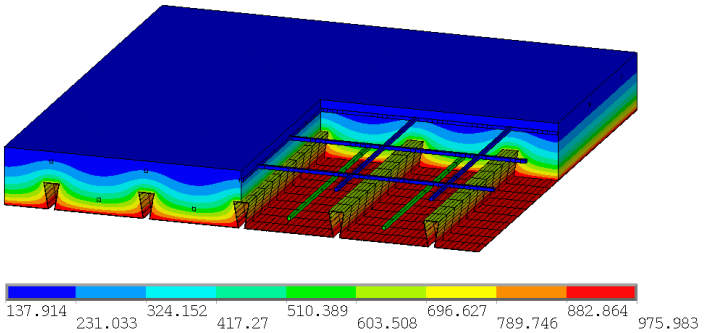

t= 83.3 min

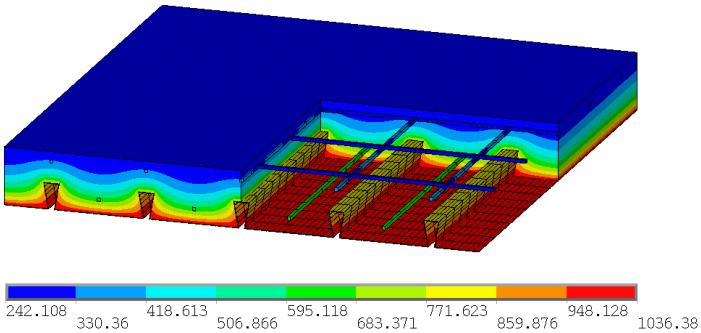

t= 120.0 min

SIM. 155	**Steel deck:** Lysaght Bondek	**Rebar (mm):** ϕ8	**Fire resistance (min)**	
	Mesh (mm//mm): ϕ7.6//200 (RM82)	**h_1 (mm):** 76	Ave: *98.3*	Max: 108.1

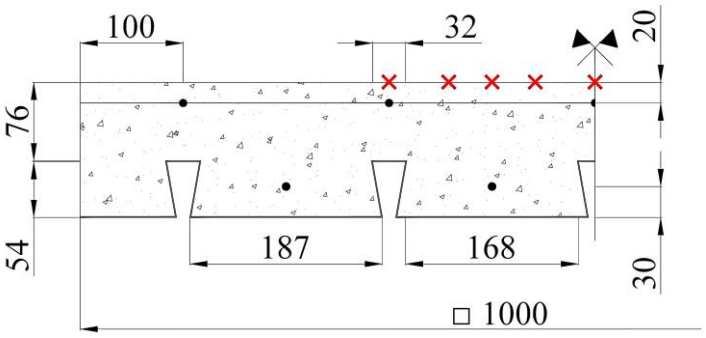

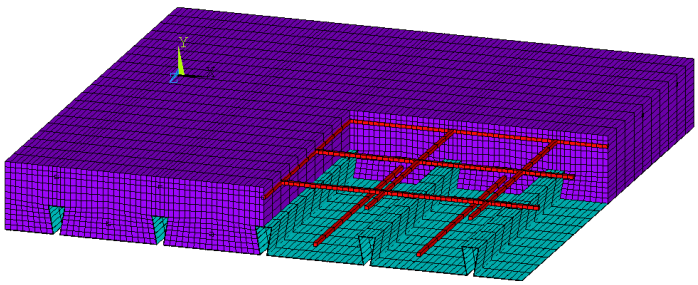

Finite element mesh

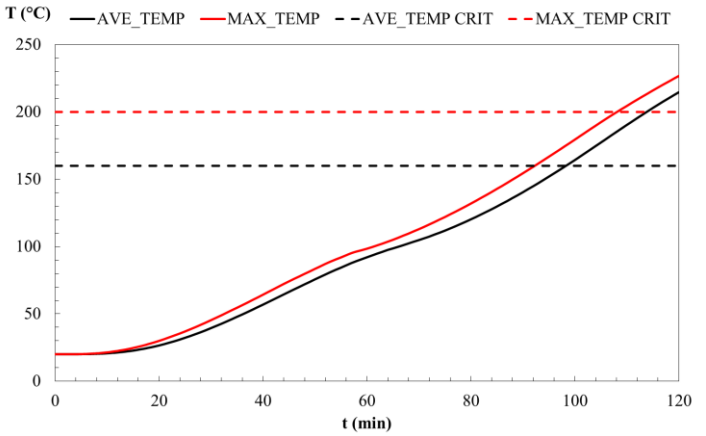

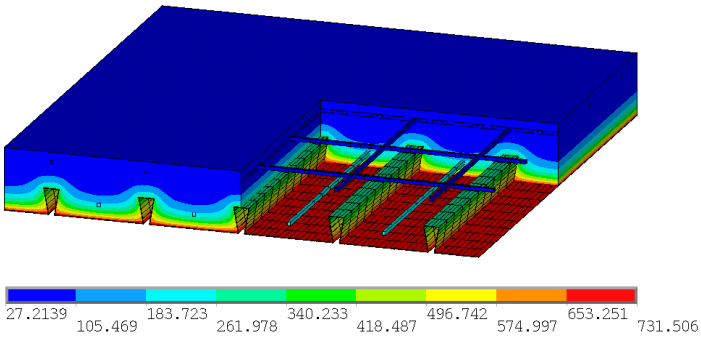

t= 24.6 min

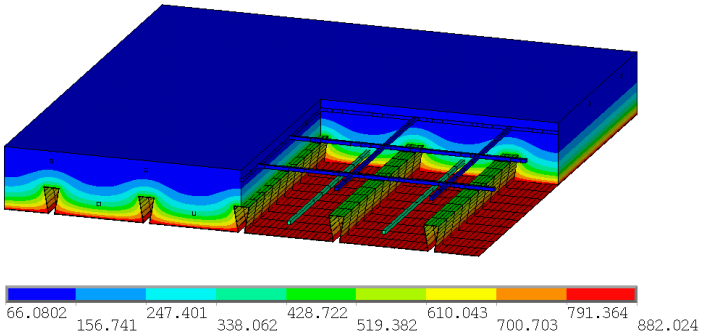

t= 49.2 min

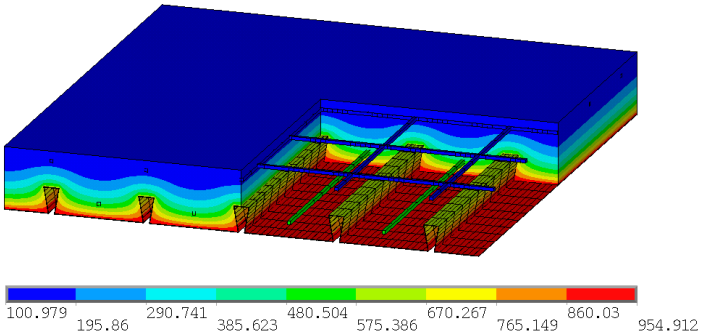

t= 73.7 min

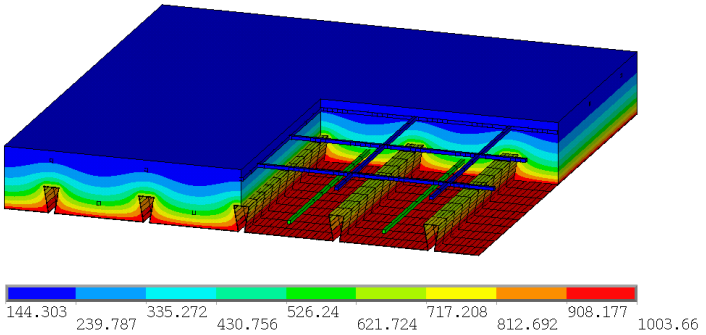

t= 98.3 min

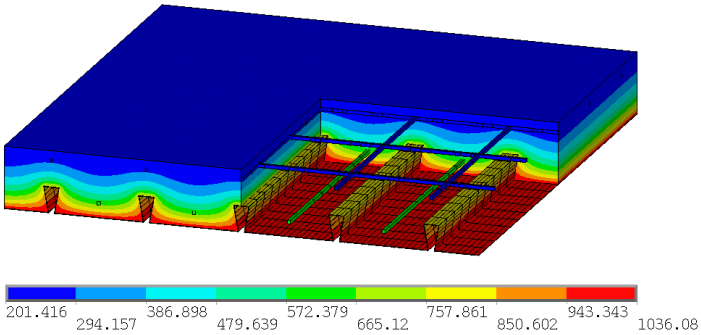

t= 120.0 min

SIM. 156	**Steel deck:** Lysaght Bondek	**Rebar (mm):** ϕ8	**Fire resistance (min)**	
	Mesh (mm//mm): ϕ7.6//200 (RM82)	**h_1 (mm):** 86	Ave: *114.5*	Max: 128.3

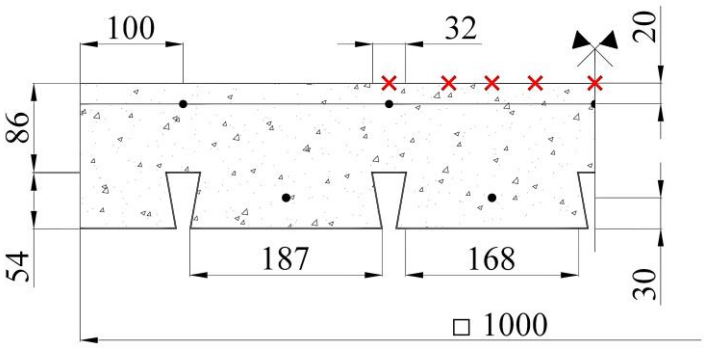

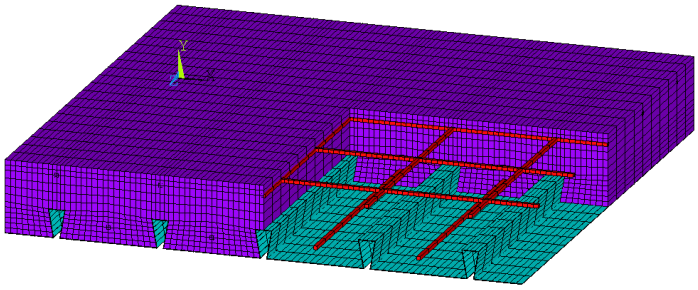

Finite element mesh

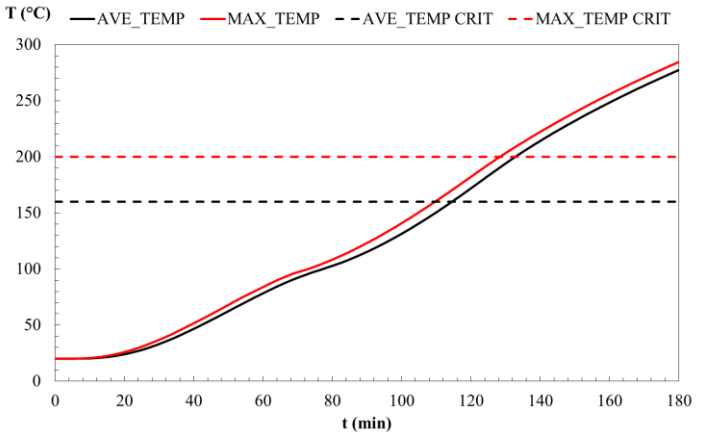

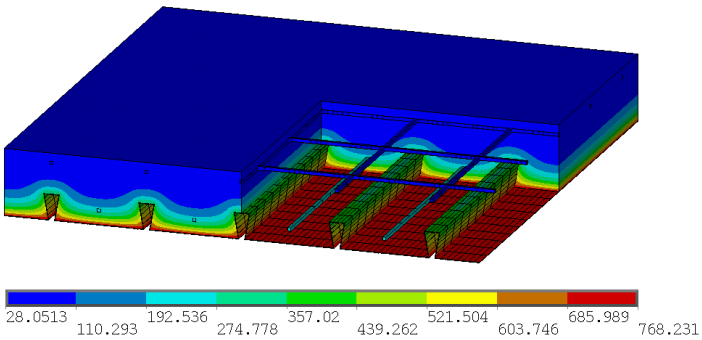

t= 28.6 min

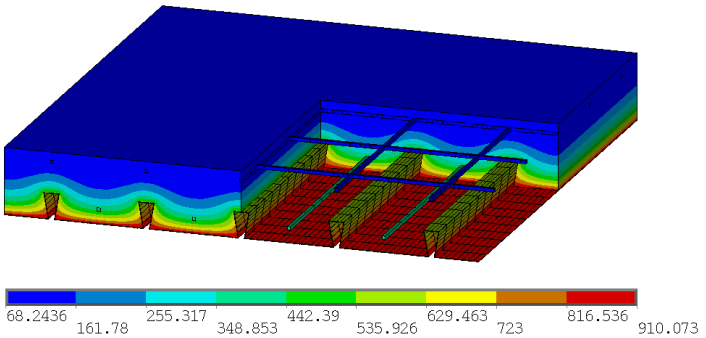

t= 57.3 min

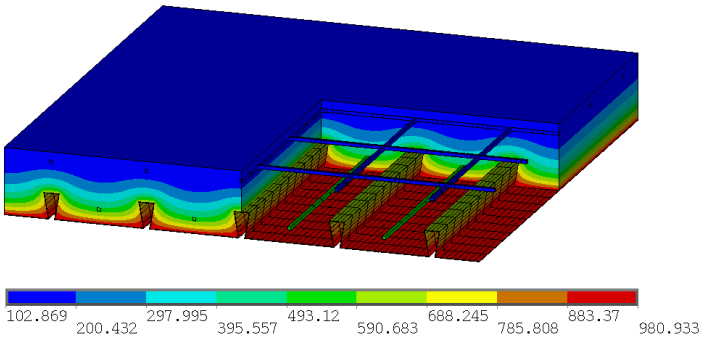

t= 85.9 min

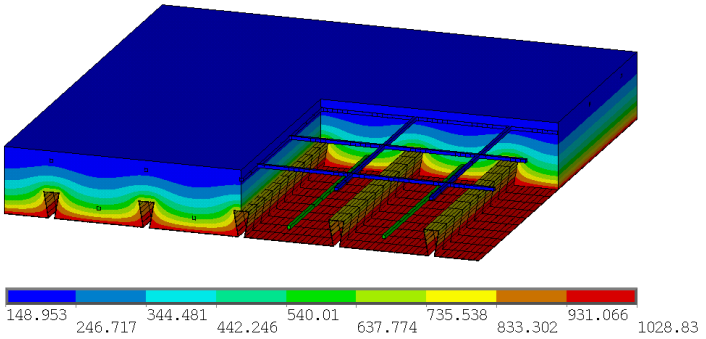

t= 114.5 min

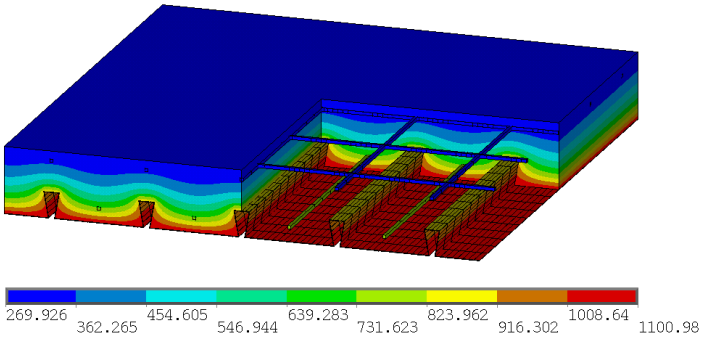

t= 180.0 min

SIM. 157	**Steel deck:** Lysaght Bondek	**Rebar (mm):** ϕ8	**Fire resistance (min)**	
	Mesh (mm//mm): ϕ7.6//200 (RM82)	**h_1 (mm):** 56	Ave: *69.7*	Max: 72.2

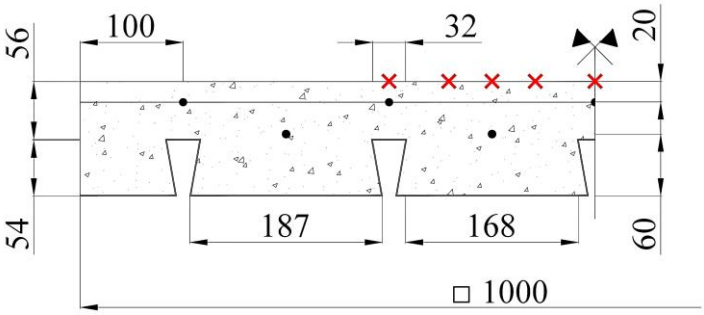

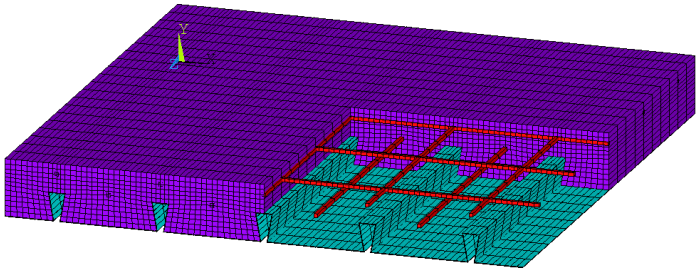

Finite element mesh

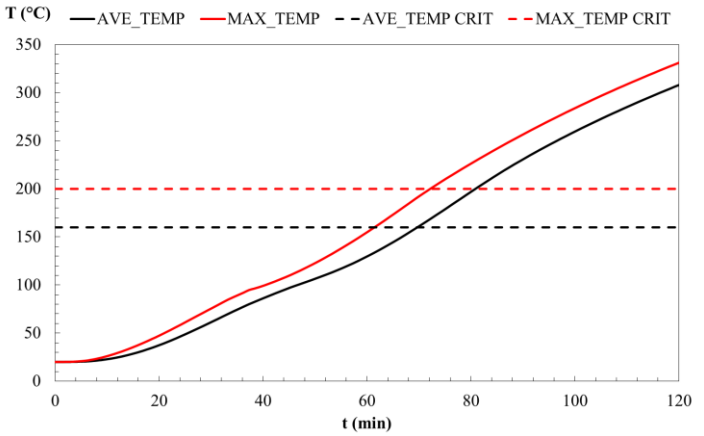

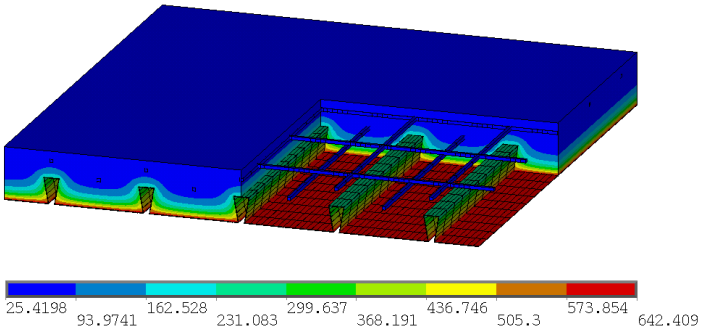

t= 17.4 min

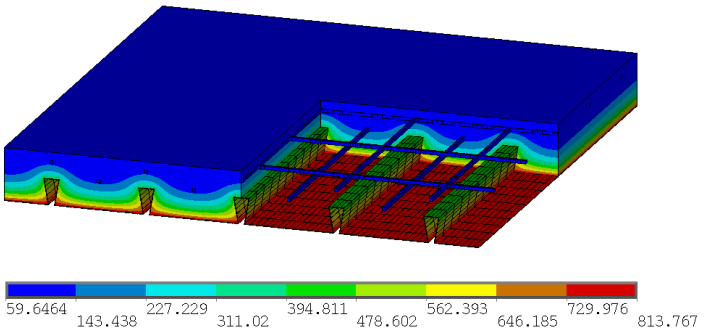

t= 34.9 min

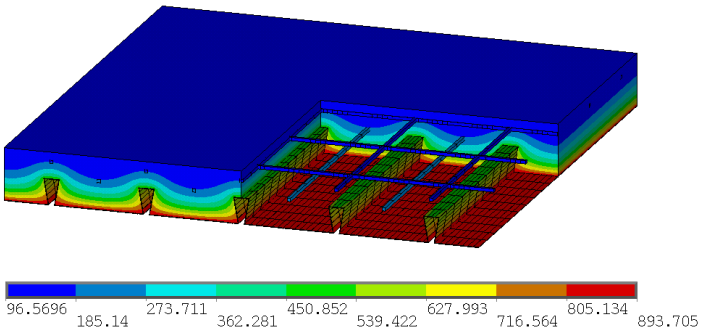

t= 52.3 min

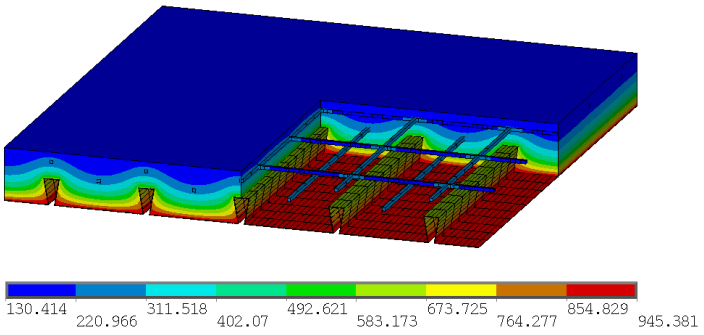

t= 69.7 min

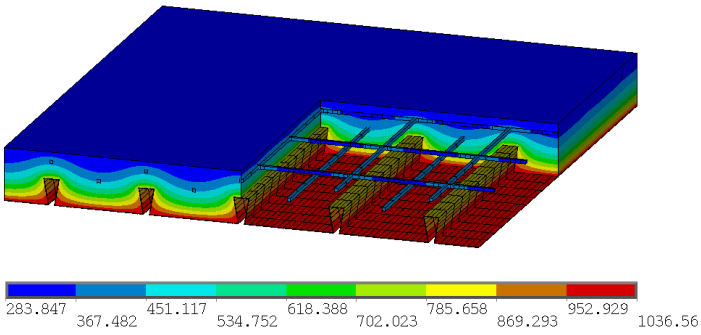

t= 120.0 min

SIM. 158	**Steel deck:** Lysaght Bondek	**Rebar (mm):** ϕ8	**Fire resistance (min)**	
	Mesh (mm//mm): ϕ7.6//200 (RM82)	**h_1 (mm):** 66	Ave: *83.4*	Max: 89.4

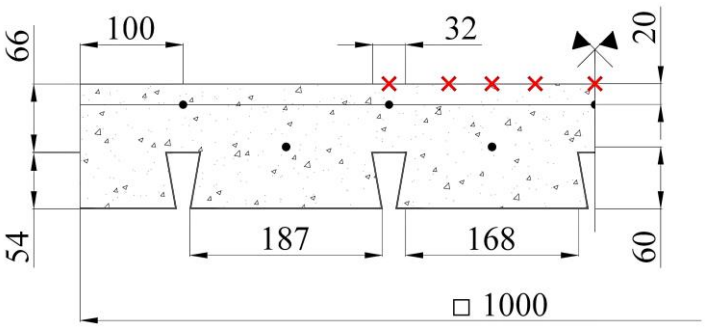

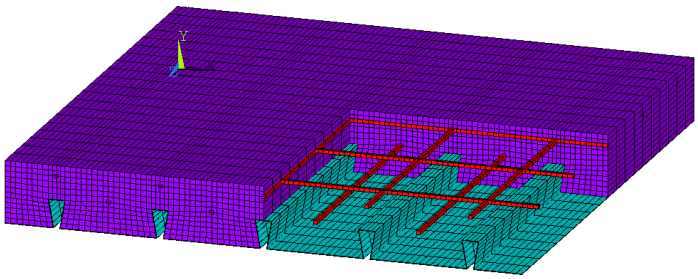

Finite element mesh

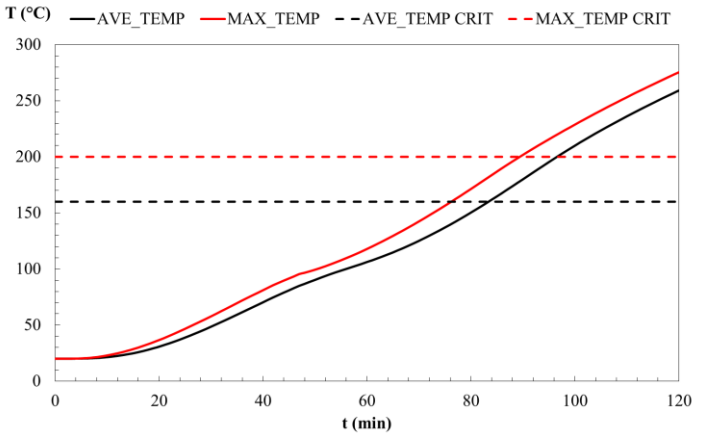

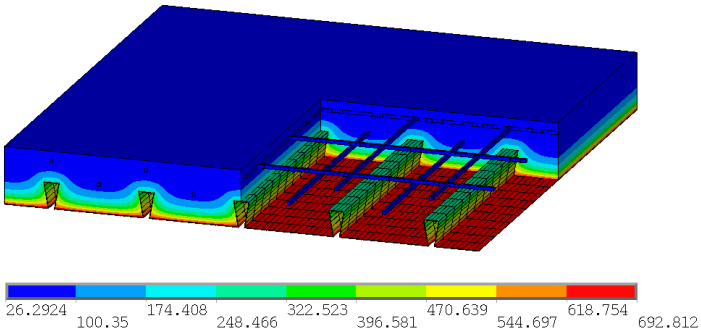

t= 20.9 min

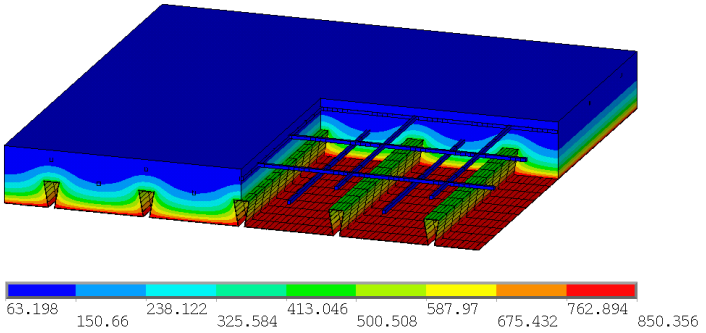

t= 41.7 min

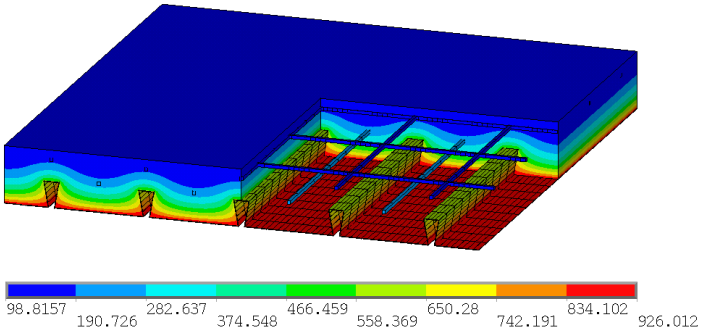

t= 62.6 min

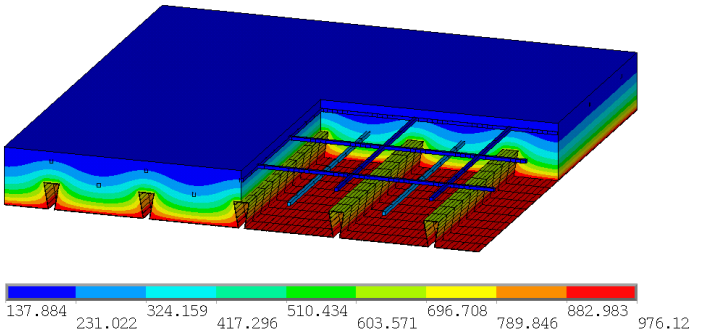

t= 83.4 min

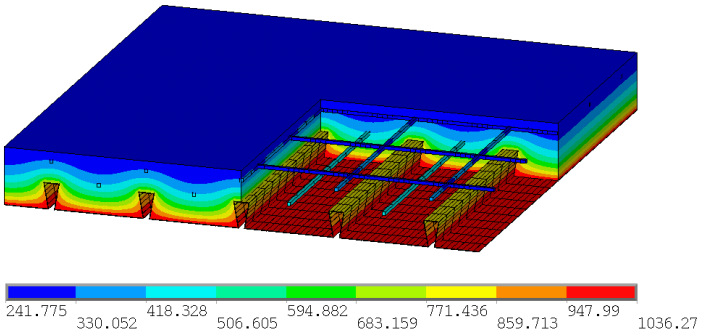

t= 120.0 min

SIM. 159	**Steel deck:** Lysaght Bondek	**Rebar (mm):** ϕ8	**Fire resistance (min)**	
	Mesh (mm//mm): ϕ7.6//200 (RM82)	**h_1 (mm):** 76	Ave: *98.3*	Max: 108.1

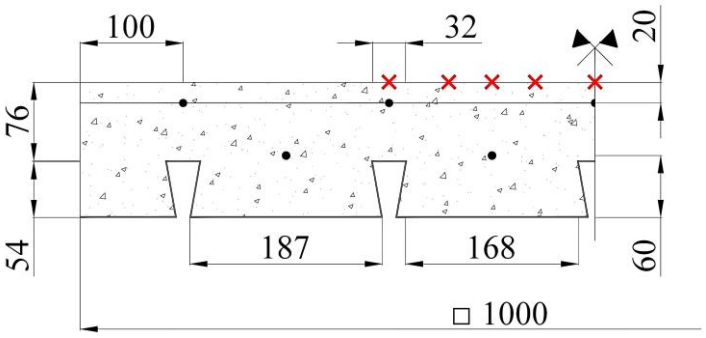

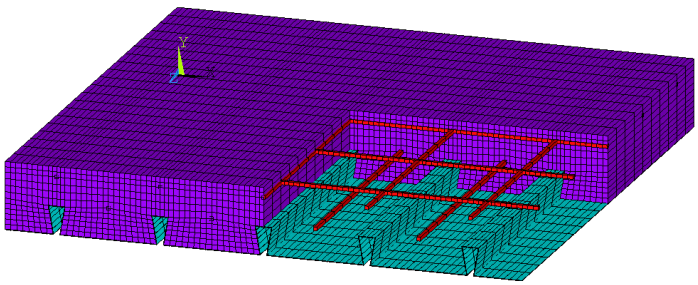

Finite element mesh

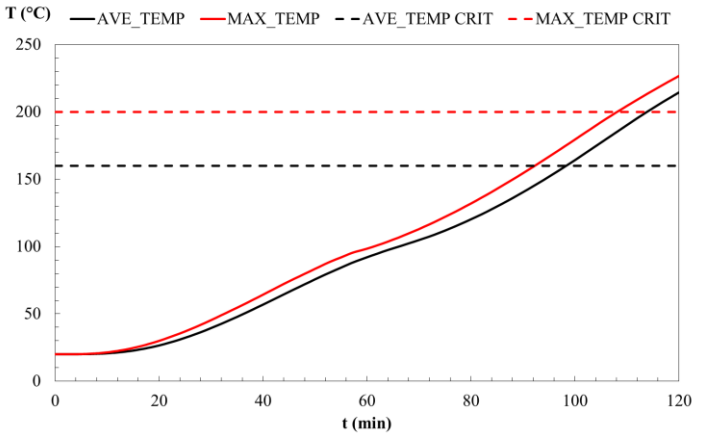

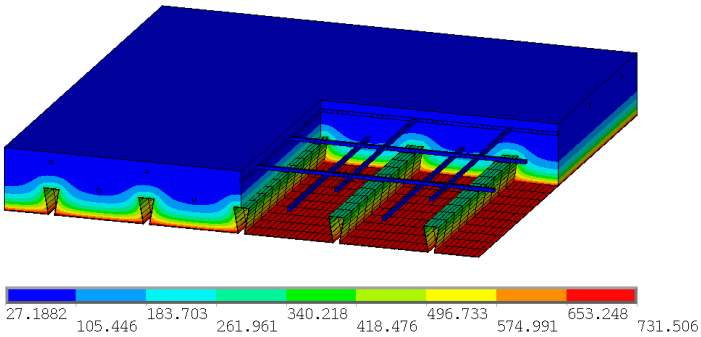

t= 24.6 min

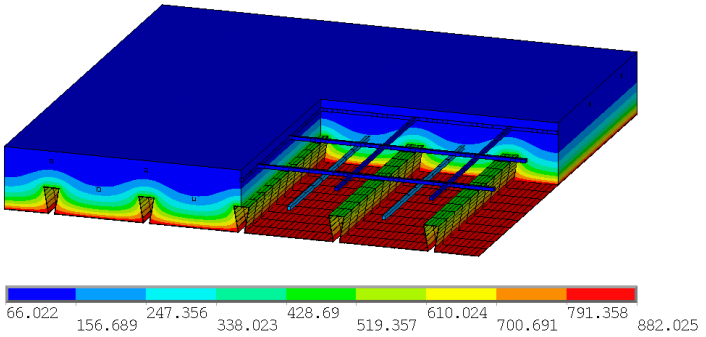

t= 49.2 min

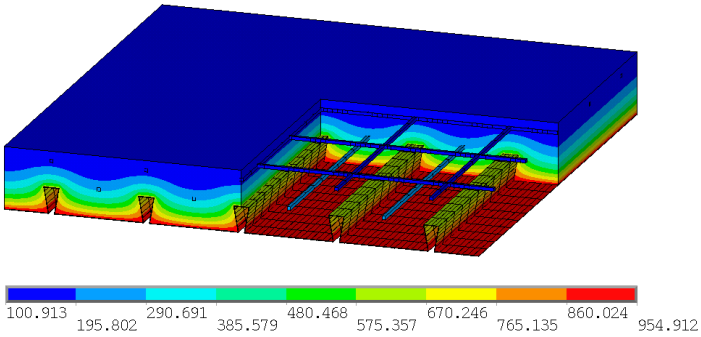

t= 73.7 min

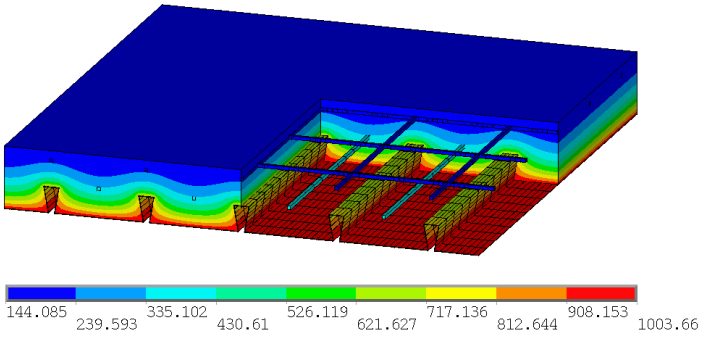

t= 98.3 min

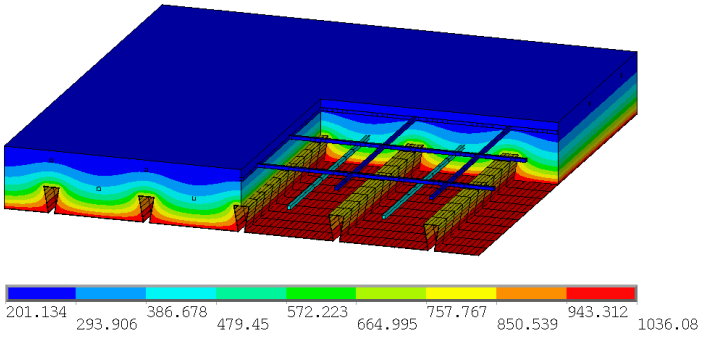

t= 120.0 min

SIM. 160	**Steel deck:** Lysaght Bondek	**Rebar (mm):** ϕ8	**Fire resistance (min)**	
	Mesh (mm//mm): ϕ7.6//200 (RM82)	**h_1 (mm):** 86	Ave: *114.6*	Max: 128.4

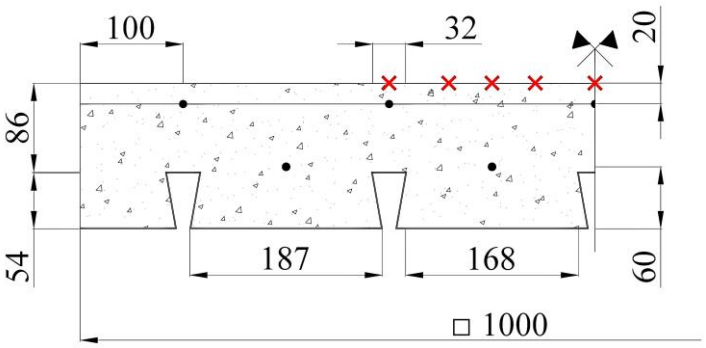

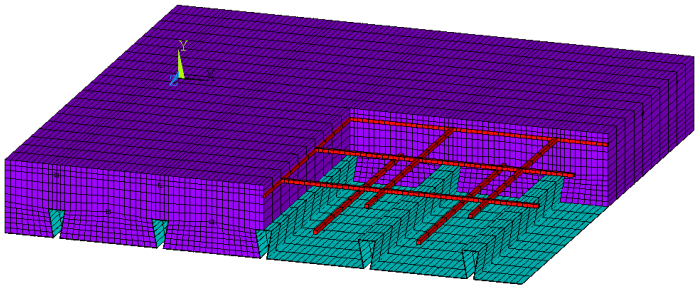

Finite element mesh

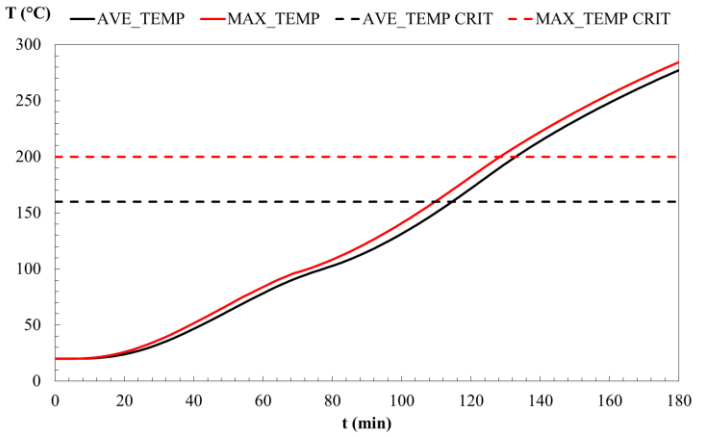

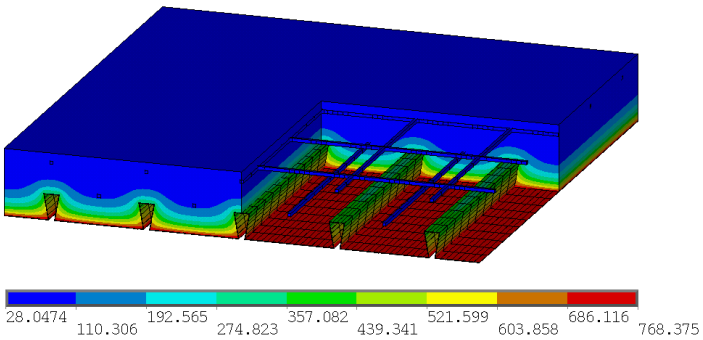

t= 28.7 min

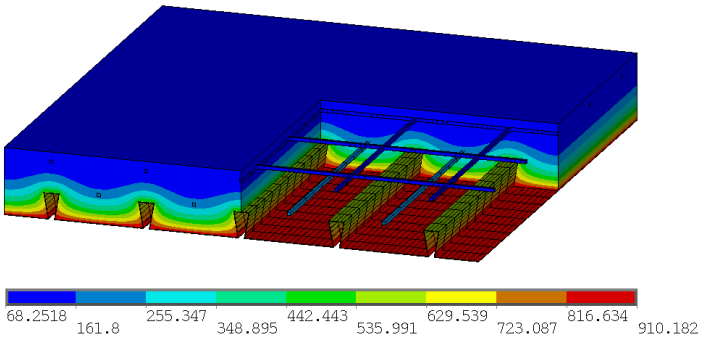

t= 57.3 min

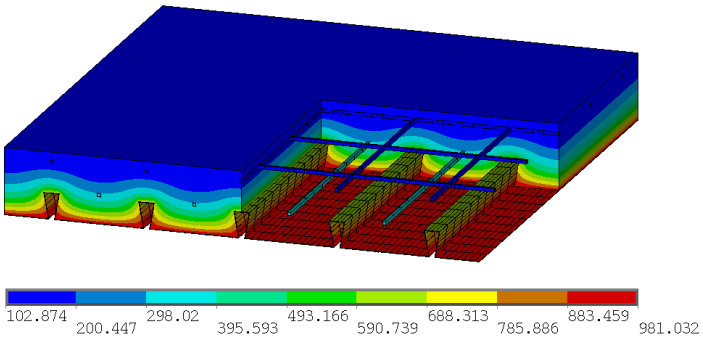

t= 86.0 min

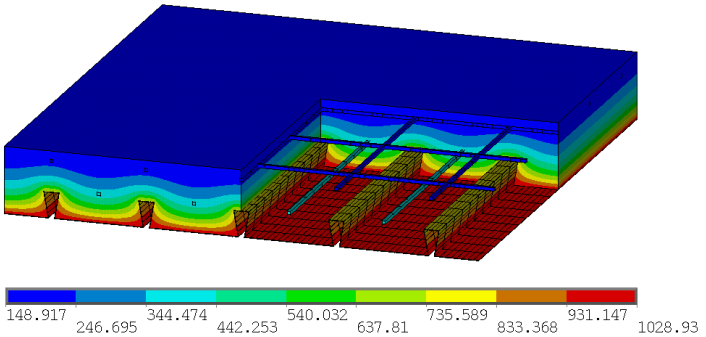

t= 114.6 min

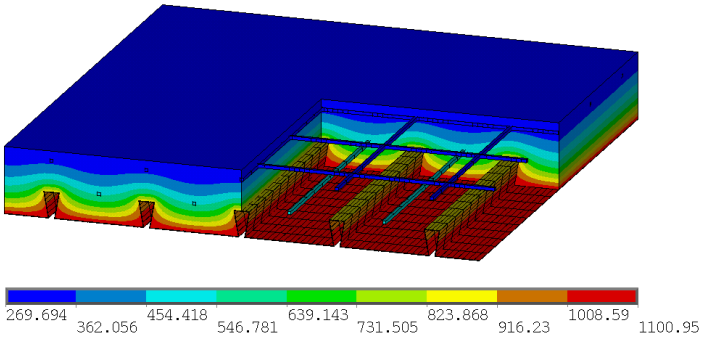

t= 180.0 min

SIM. 161	**Steel deck:** Lysaght Bondek	**Rebar (mm):** ϕ10	**Fire resistance (min)**	
	Mesh (mm//mm): ϕ6.75//200 (RM72)	**h_1 (mm):** 56	Ave: *69.6*	Max: 71.7

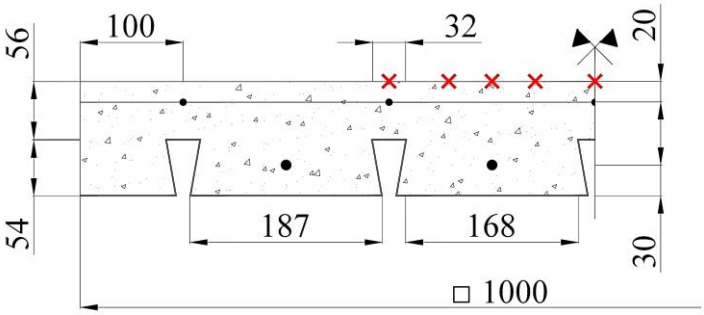

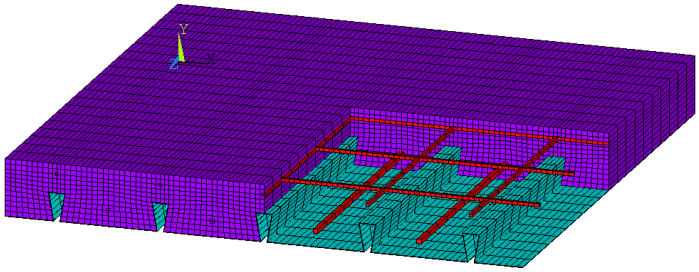

Finite element mesh

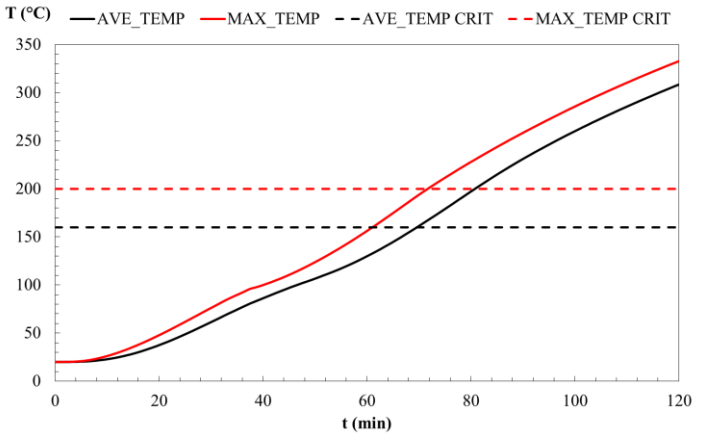

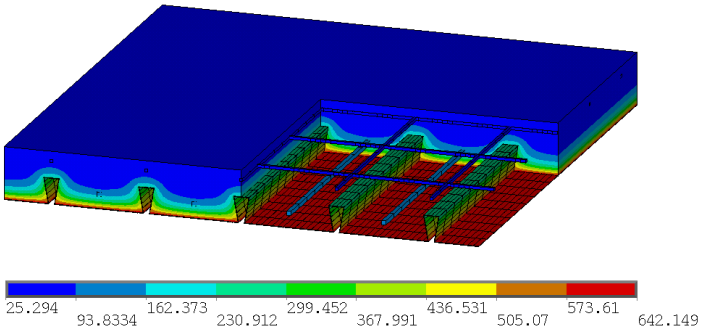

t= 17.4 min

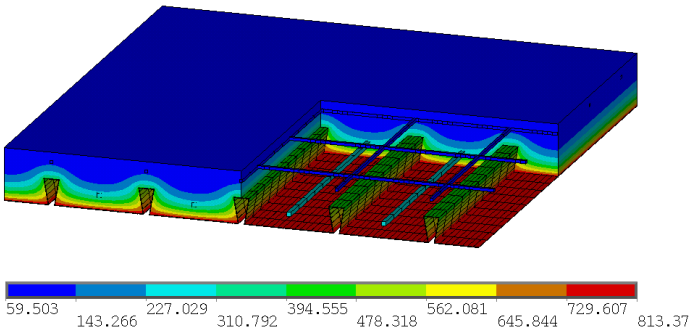

t= 34.8 min

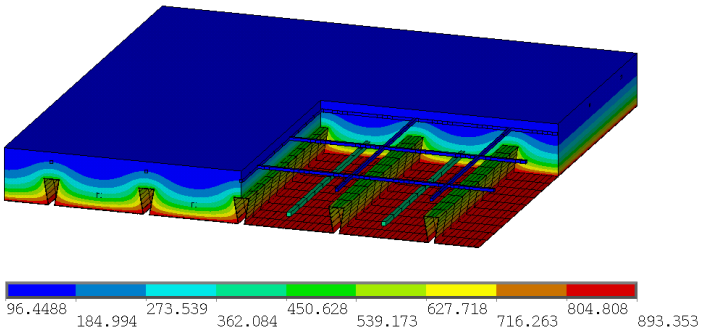

t= 52.2 min

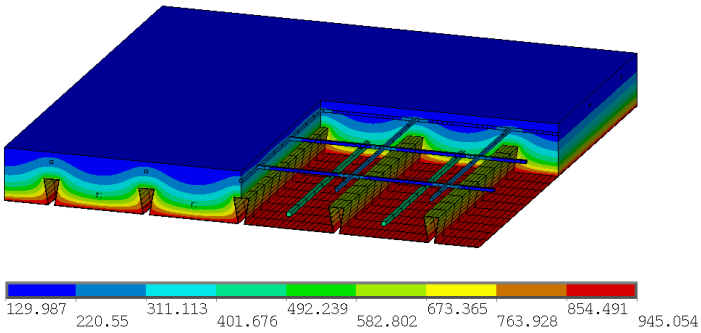

t= 69.6 min

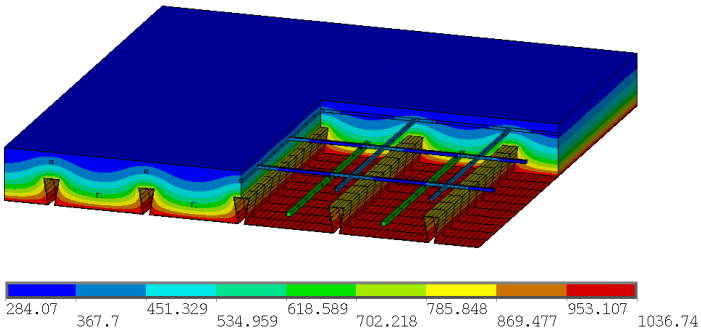

t= 120.0 min

SIM. 162	**Steel deck:** Lysaght Bondek	**Rebar (mm):** ϕ10	**Fire resistance (min)**	
	Mesh (mm//mm): ϕ6.75//200 (RM72)	**h_1 (mm):** 66	Ave: *83.3*	Max: 88.9

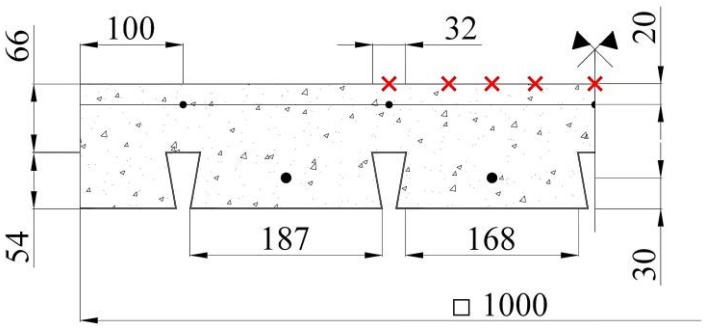

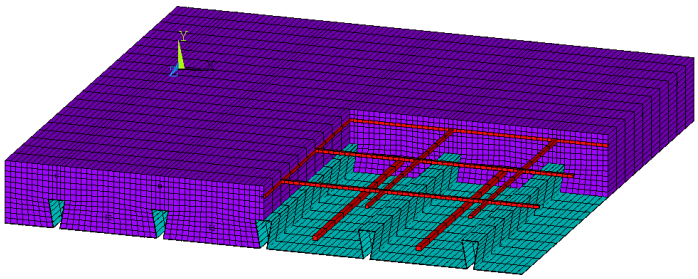

Finite element mesh

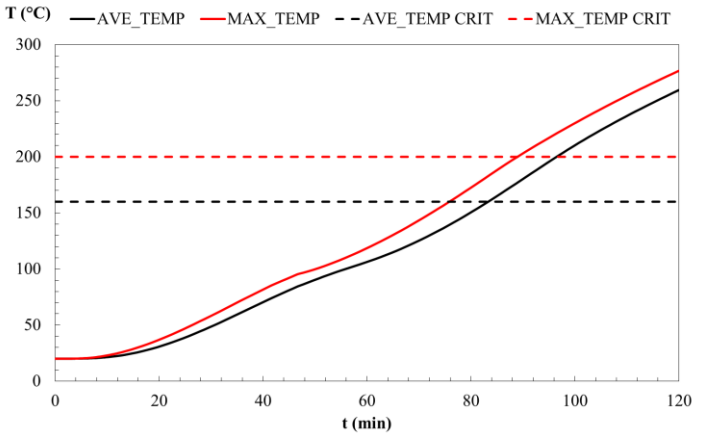

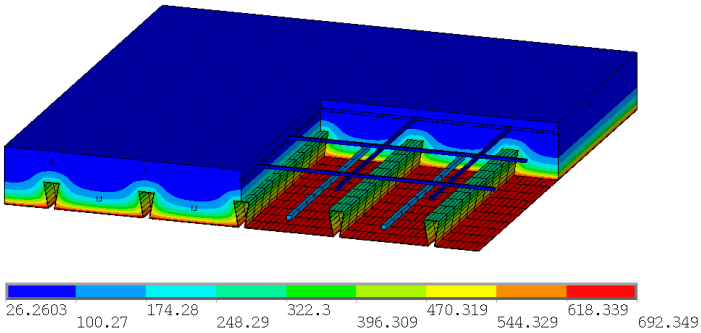

t= 20.8 min

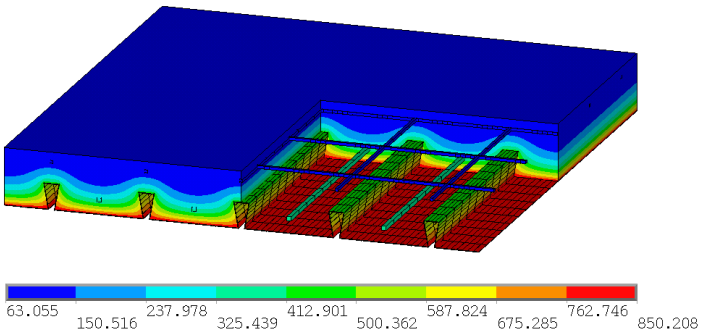

t= 41.7 min

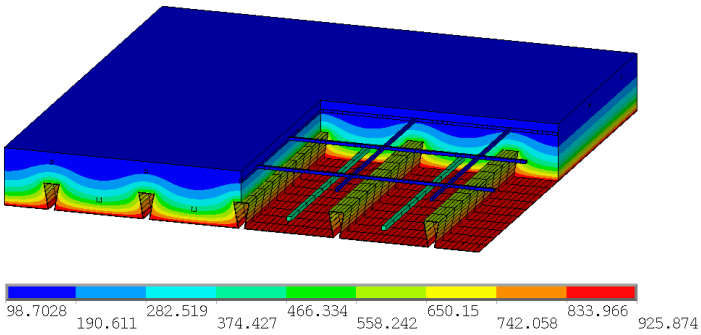

t= 62.5 min

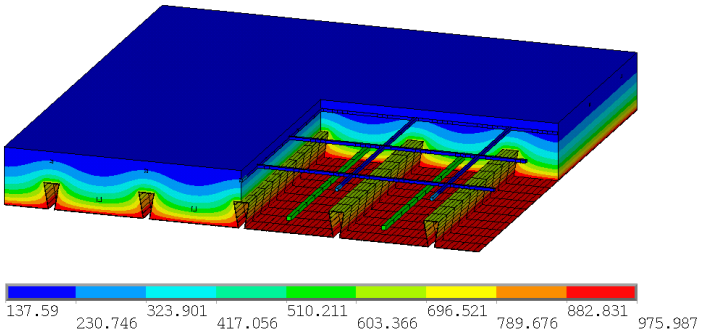

t= 83.3 min

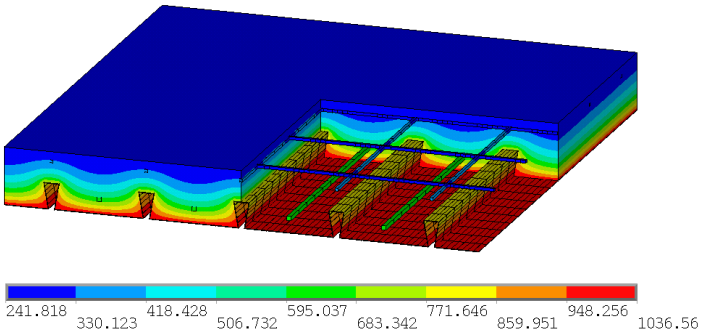

t= 120.0 min

SIM. 163	**Steel deck:** Lysaght Bondek	**Rebar (mm):** ϕ10	**Fire resistance (min)**	
	Mesh (mm//mm): ϕ6.75//200 (RM72)	**h_1 (mm):** 76	Ave: *98.2*	Max: 107.7

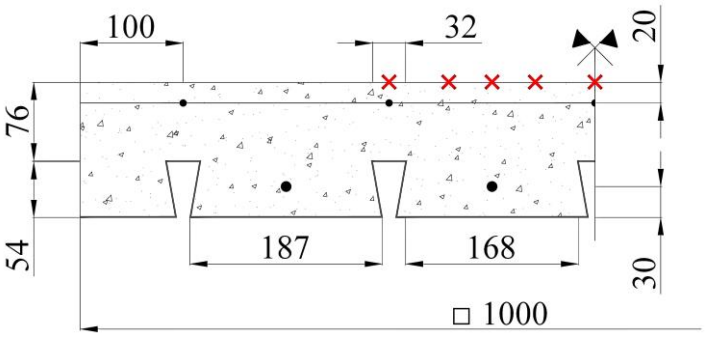

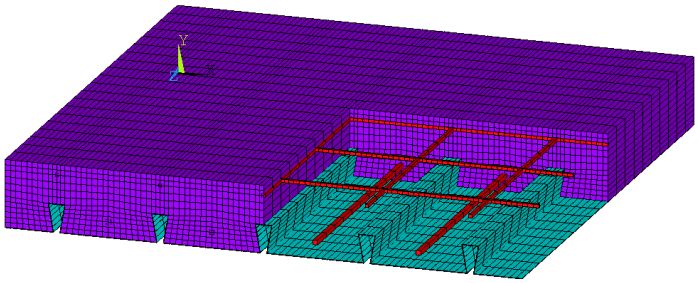

Finite element mesh

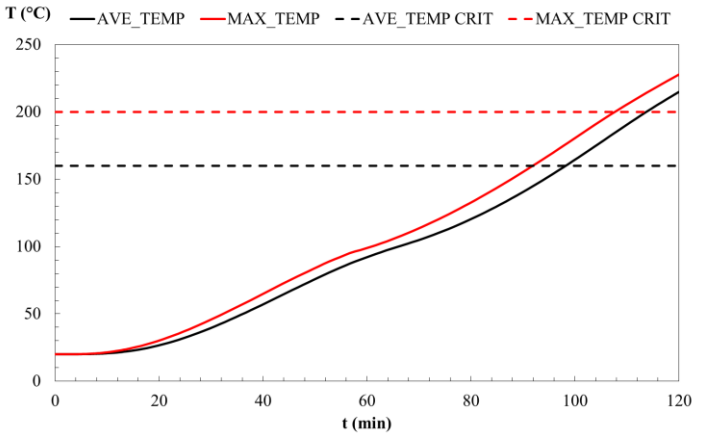

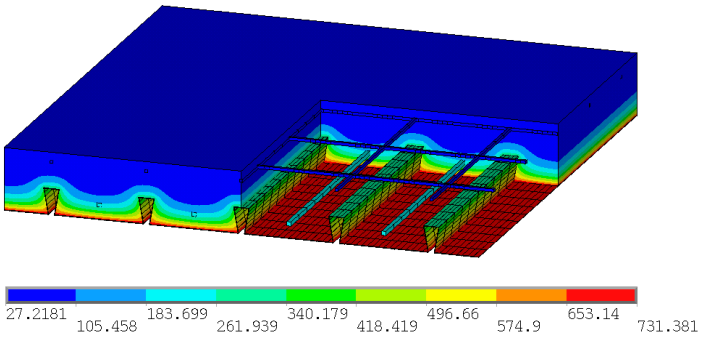

t= 24.6 min

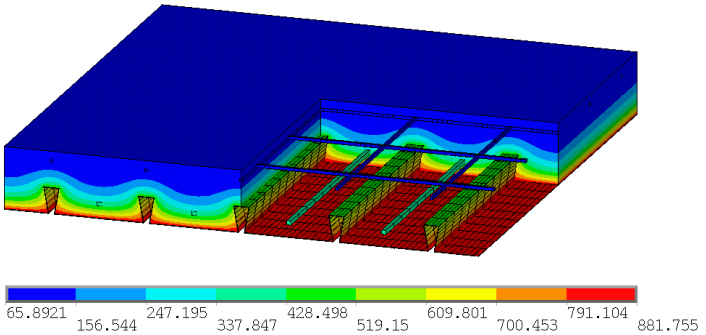

t= 49.1 min

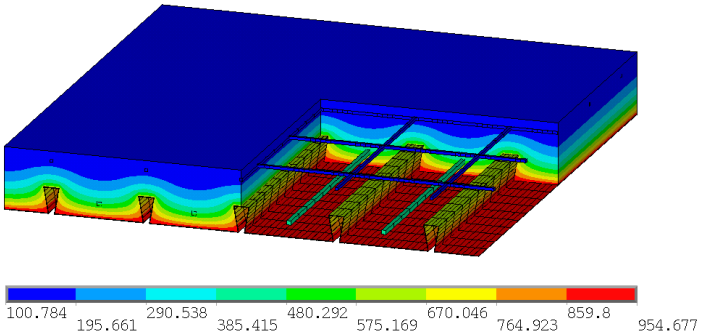

t= 73.7 min

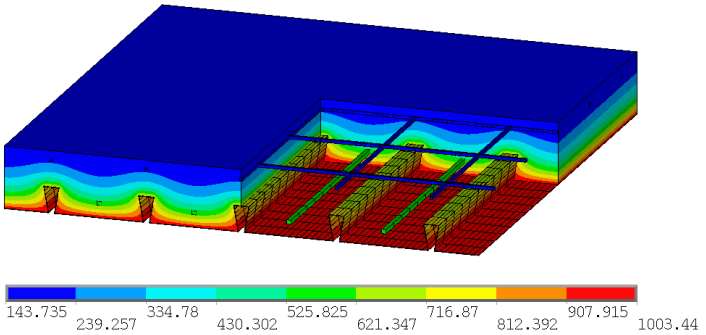

t= 98.2 min

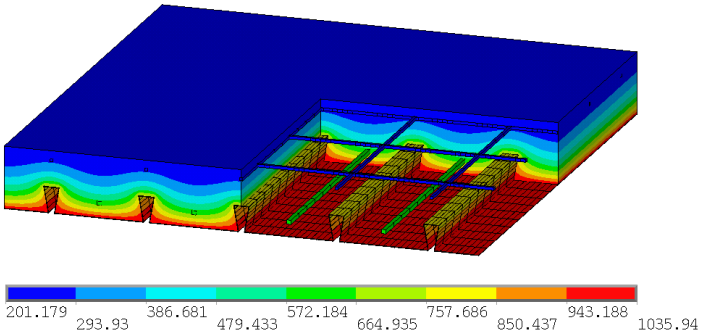

t= 120.0 min

SIM. 164	**Steel deck:** Lysaght Bondek	**Rebar (mm):** ϕ10	**Fire resistance (min)**	
	Mesh (mm//mm): ϕ6.75//200 (RM72)	**h_1 (mm):** 86	Ave: *114.5*	Max: 128.0

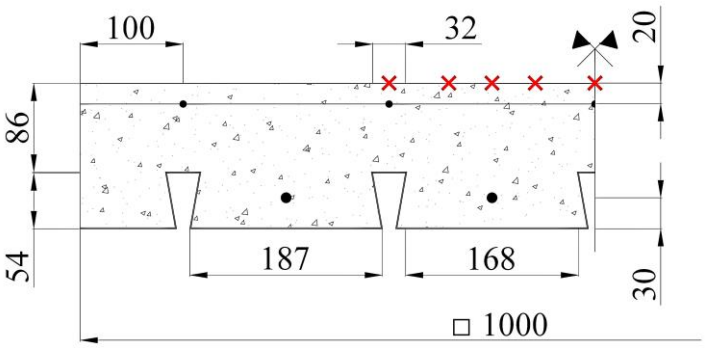

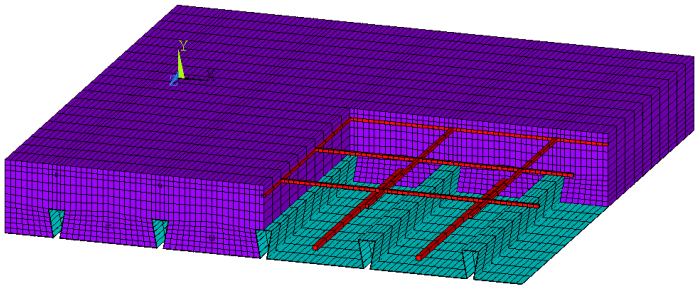

Finite element mesh

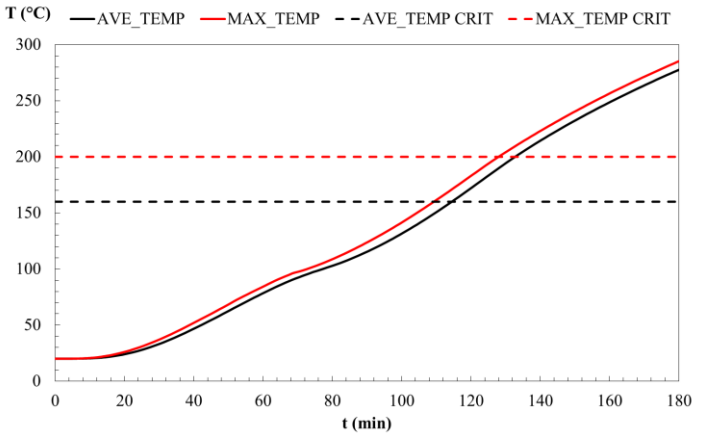

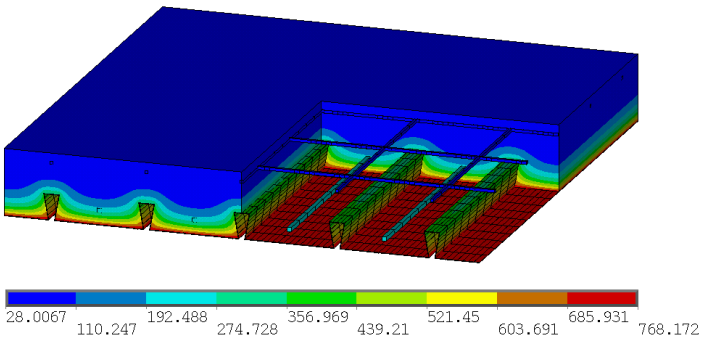

t= 28.6 min

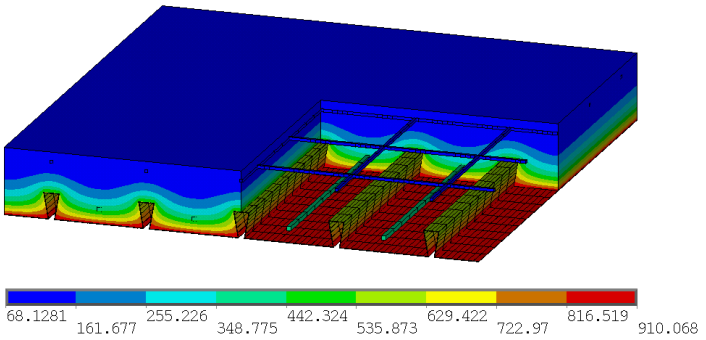

t= 57.3 min

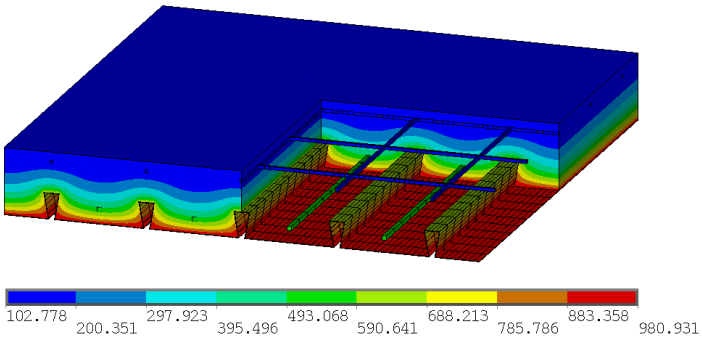

t= 85.9 min

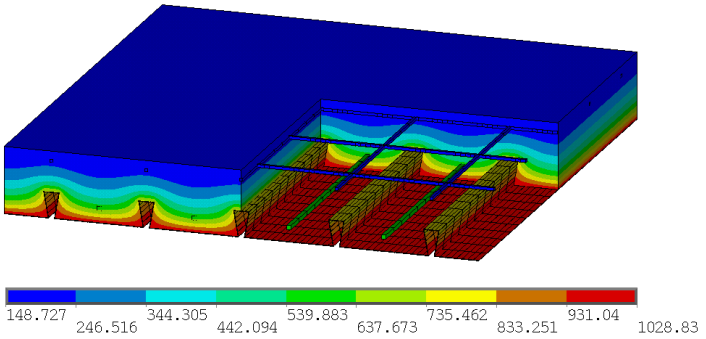

t= 114.5 min

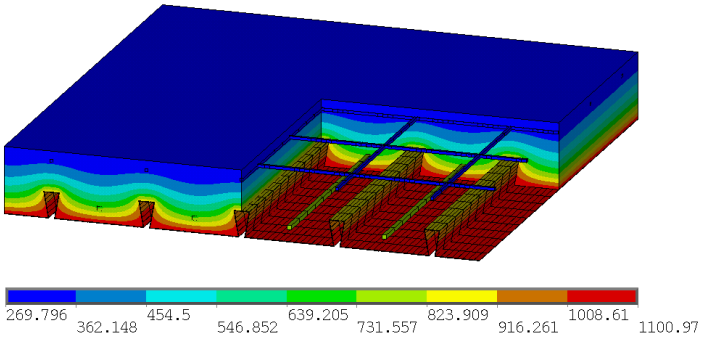

t= 180.0 min

SIM. 165	**Steel deck:** Lysaght Bondek	**Rebar (mm):** ϕ10	**Fire resistance (min)**	
	Mesh (mm//mm): ϕ6.75//200 (RM72)	**h_1 (mm):** 56	Ave: *69.6*	Max: 71.7

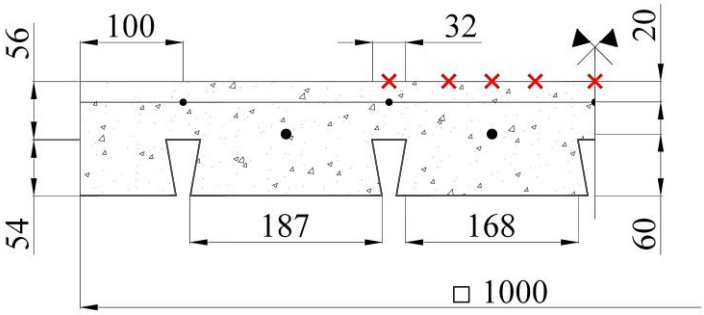

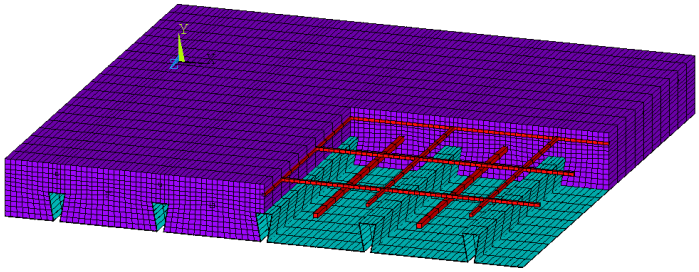

Finite element mesh

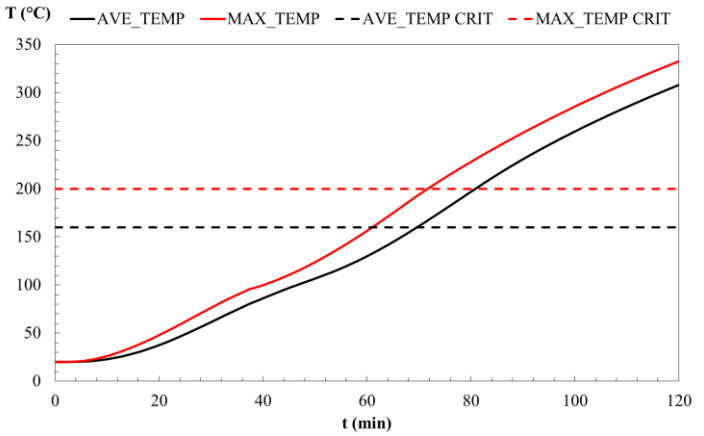

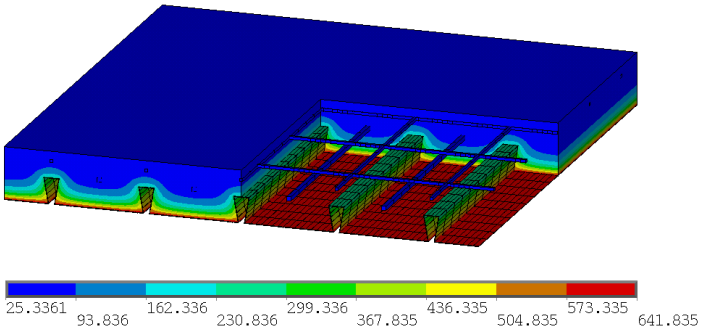

t= 17.4 min

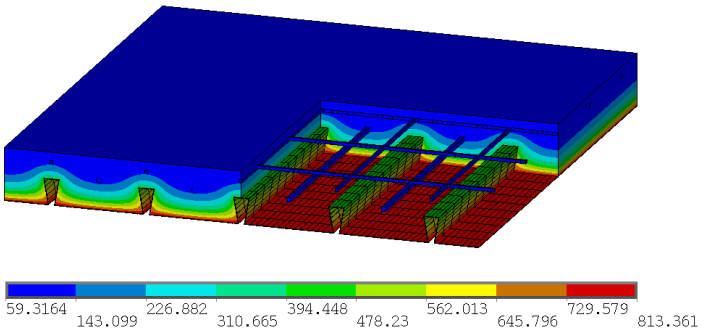

t= 34.8 min

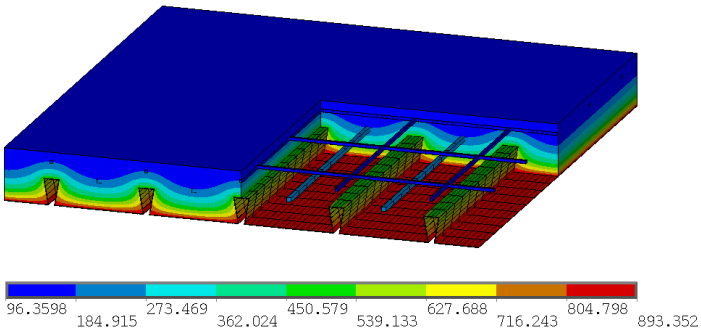

t= 52.2 min

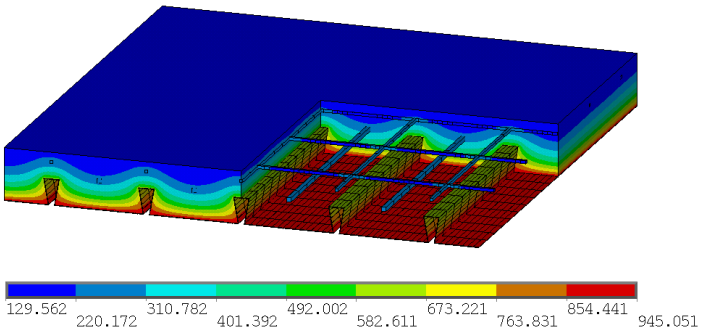

t= 69.6 min

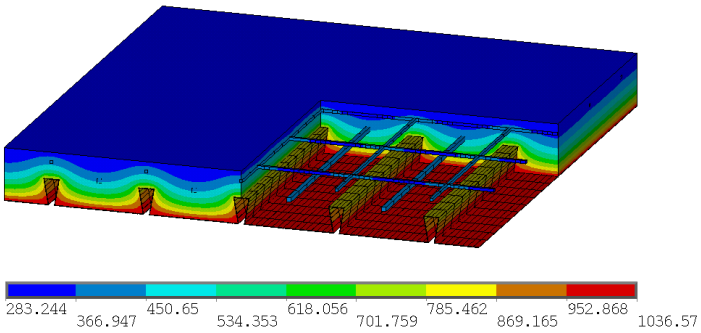

t= 120.0 min

SIM. 166	**Steel deck:** Lysaght Bondek	**Rebar (mm):** ϕ10	**Fire resistance (min)**	
	Mesh (mm//mm): ϕ6.75//200 (RM72)	**h_1 (mm):** 66	Ave: *83.3*	Max: 88.9

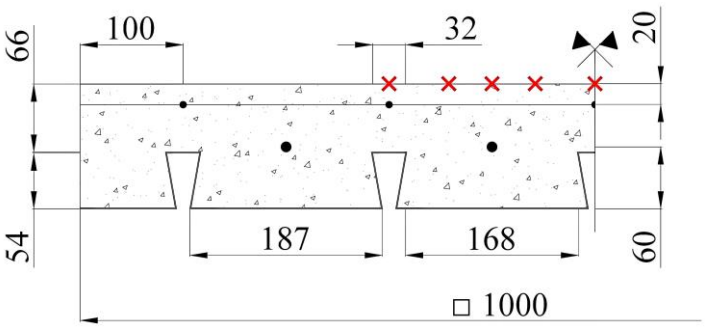

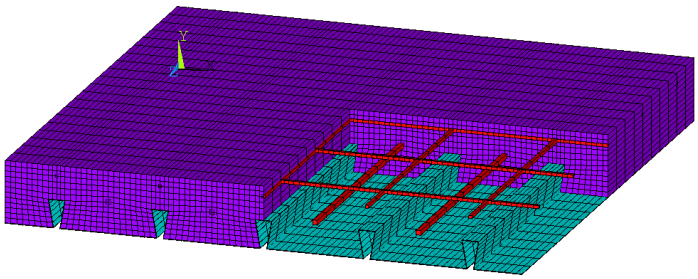

Finite element mesh

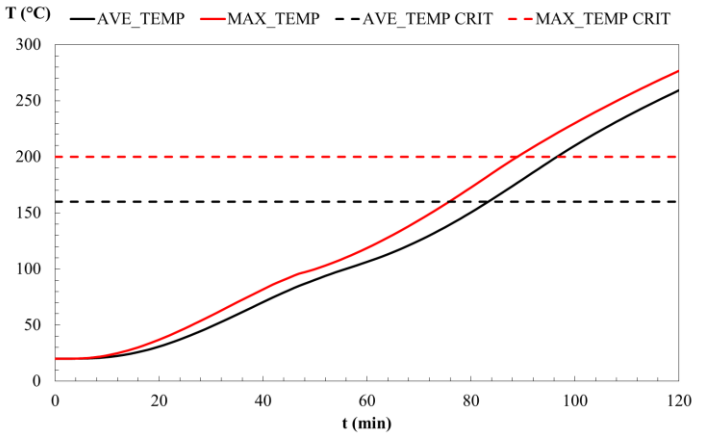

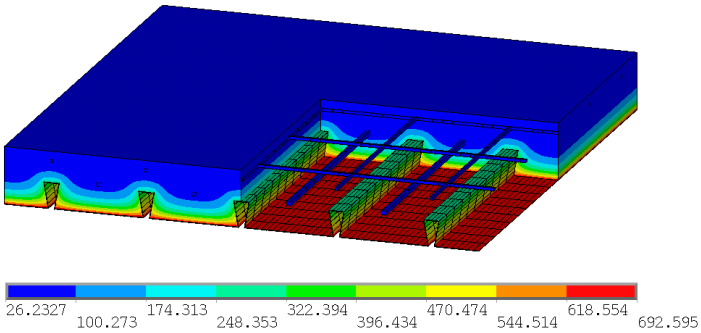

t= 20.8 min

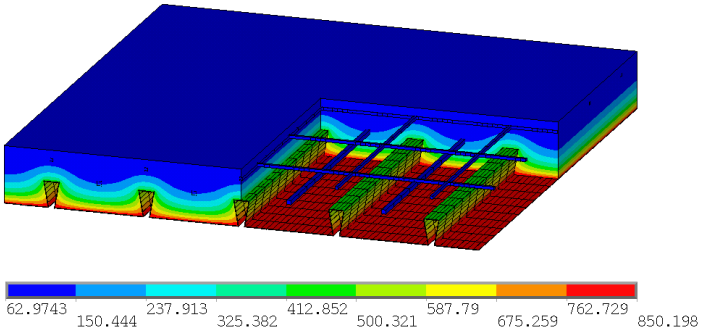

t= 41.7 min

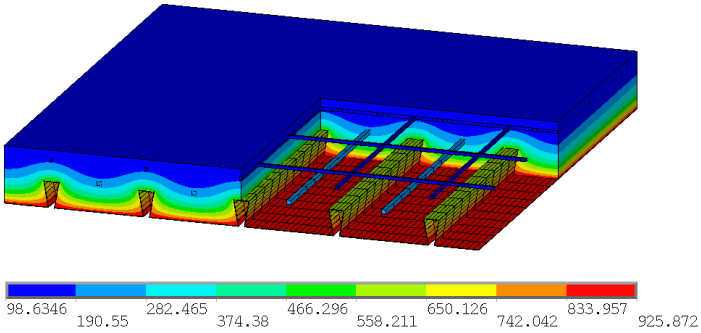

t= 62.5 min

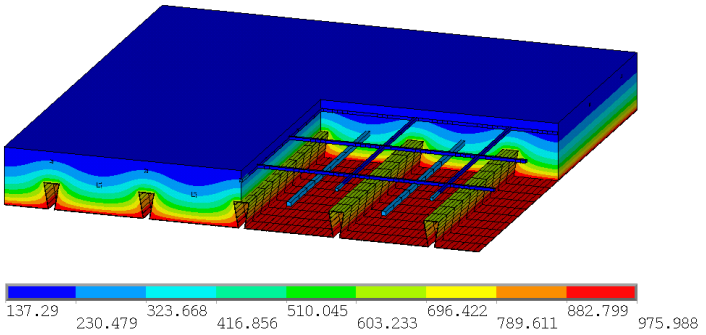

t= 83.3 min

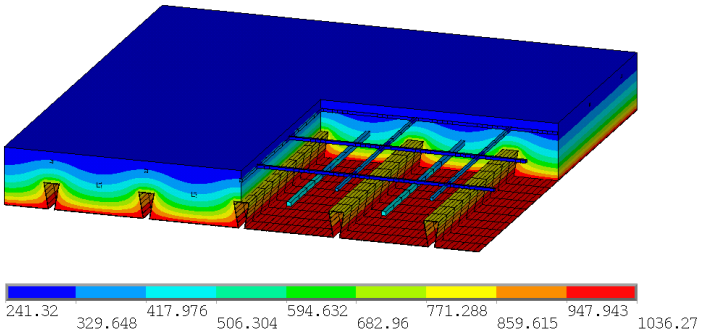

t= 120.0 min

SIM. 167	**Steel deck:** Lysaght Bondek	**Rebar (mm):** ϕ10	**Fire resistance (min)**	
	Mesh (mm//mm): ϕ6.75//200 (RM72)	**h_1 (mm):** 76	Ave: *98.3*	Max: 107.7

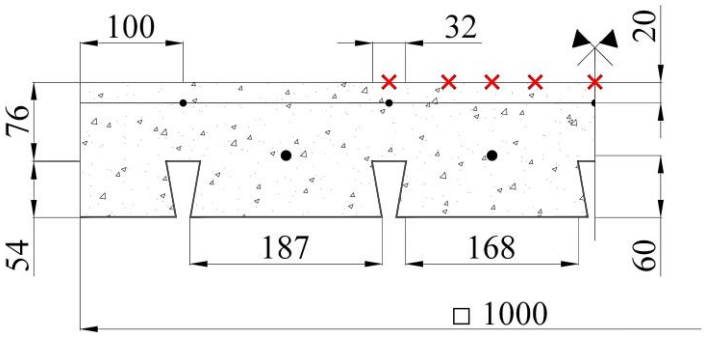

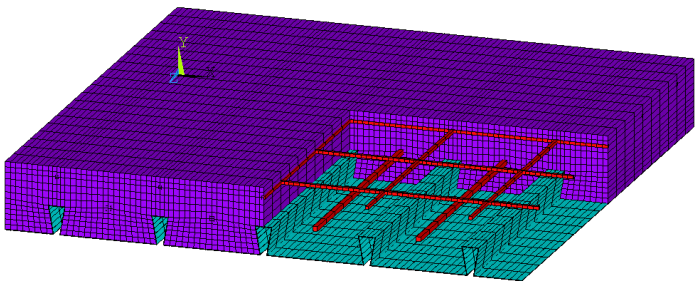

Finite element mesh

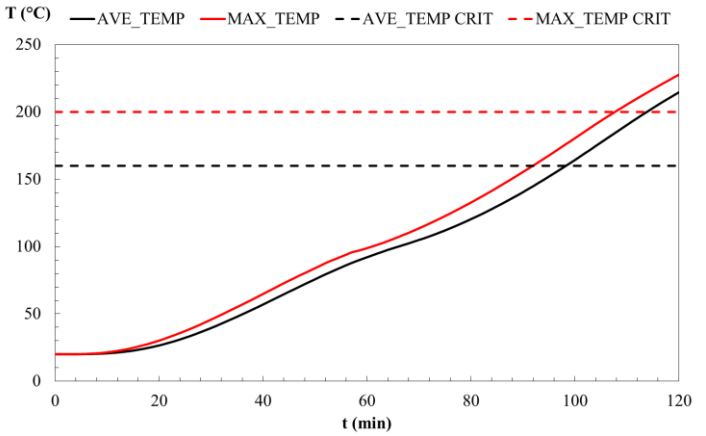

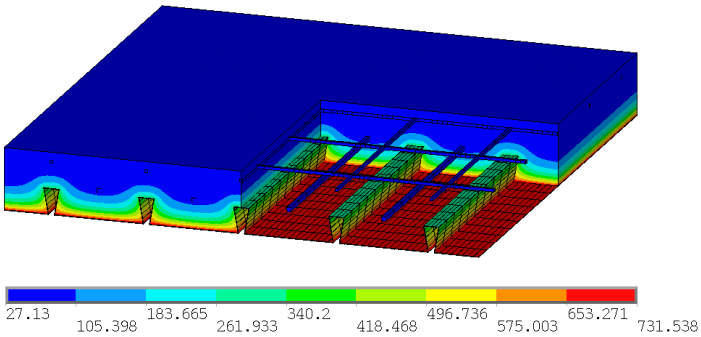

t= 24.6 min

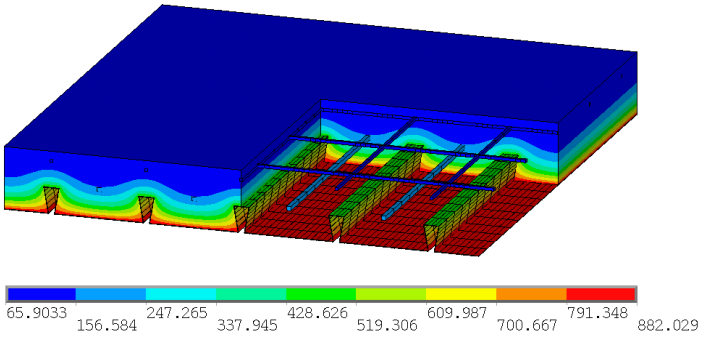

t= 49.2 min

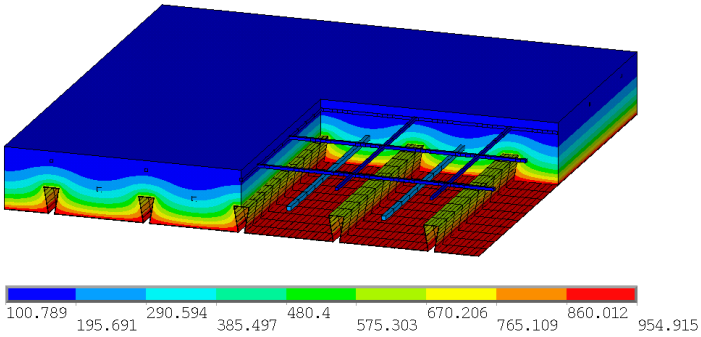

t= 73.7 min

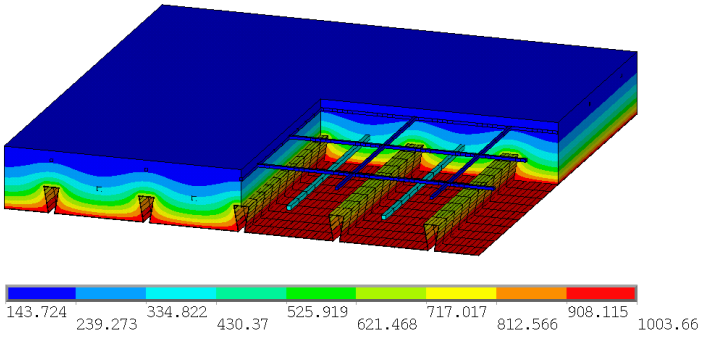

t= 98.3 min

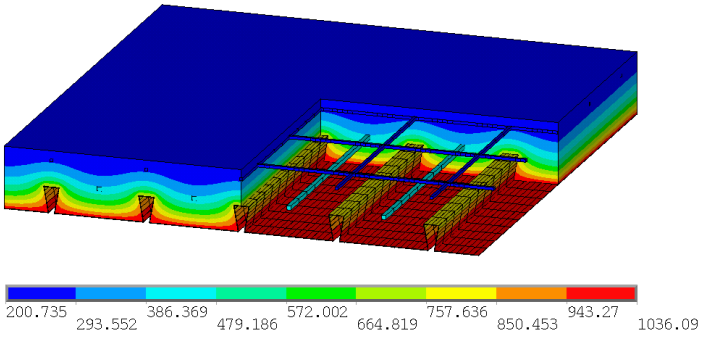

t= 120.0 min

SIM. 168	**Steel deck:** Lysaght Bondek	**Rebar (mm):** ϕ10	**Fire resistance (min)**	
	Mesh (mm//mm): ϕ6.75//200 (RM72)	**h_1 (mm):** 86	Ave: *114.5*	Max: 128.0

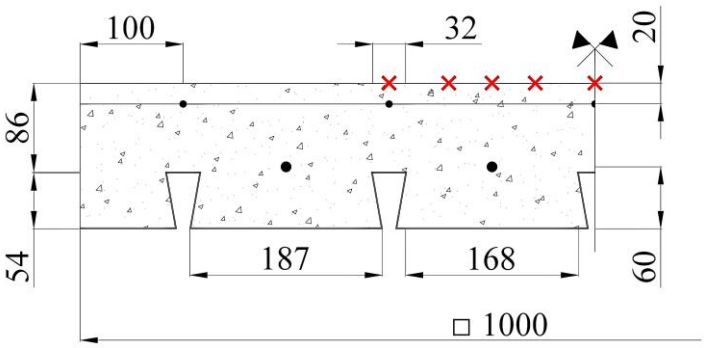

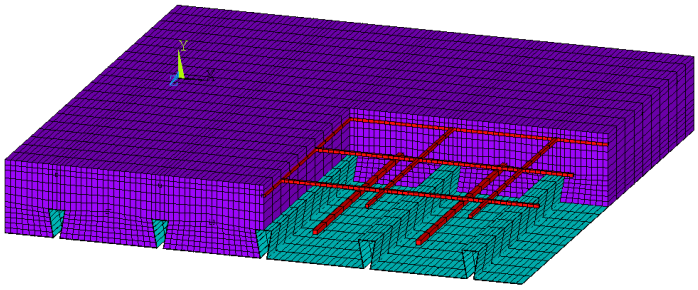

Finite element mesh

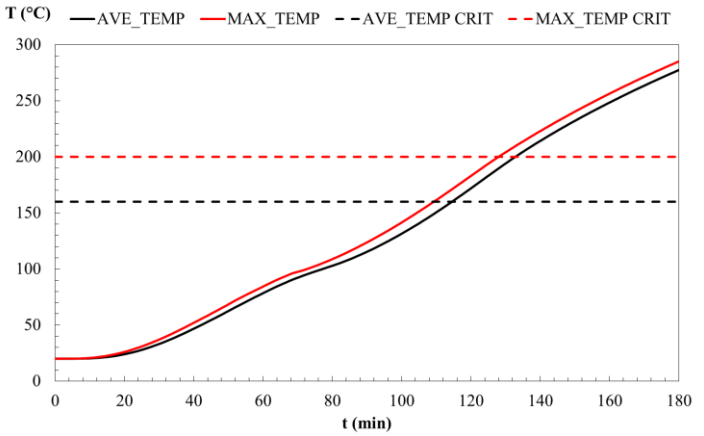

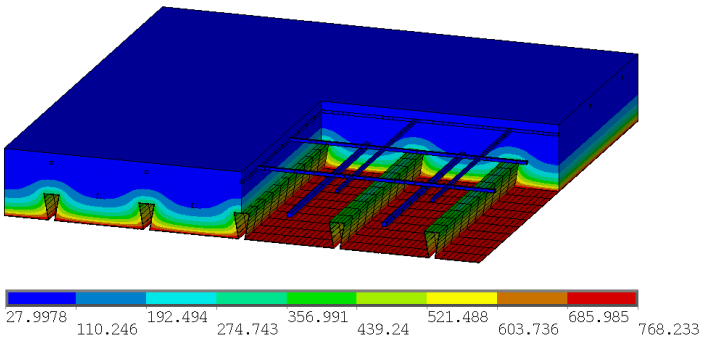

t= 28.6 min

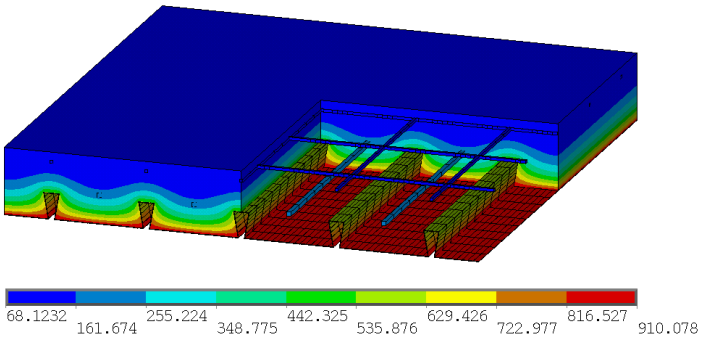

t= 57.3 min

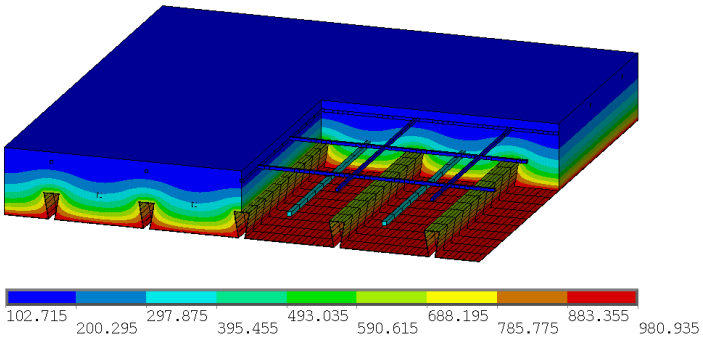

t= 85.9 min

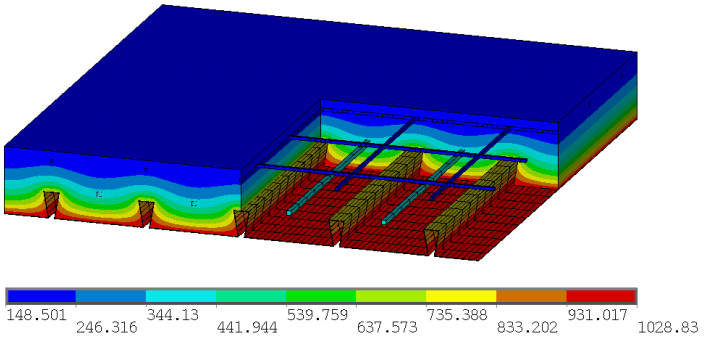

t= 114.5 min

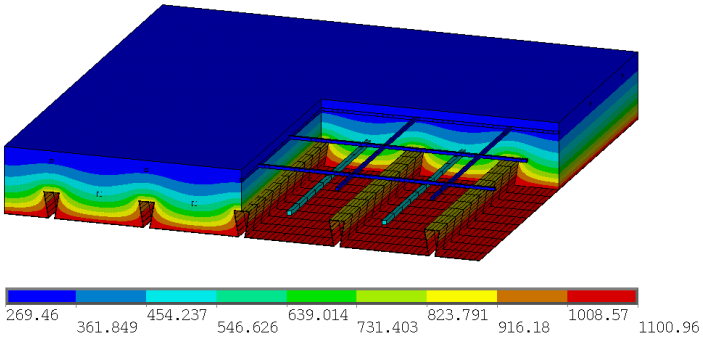

t= 180.0 min

SIM. 169	**Steel deck:** Lysaght Bondek	**Rebar (mm):** ϕ10	**Fire resistance (min)**	
	Mesh (mm//mm): ϕ7.6//200 (RM82)	**h_1 (mm):** 56	Ave: *69.7*	Max: 72.2

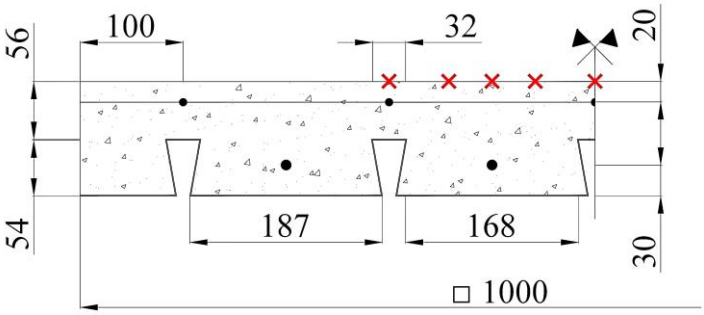

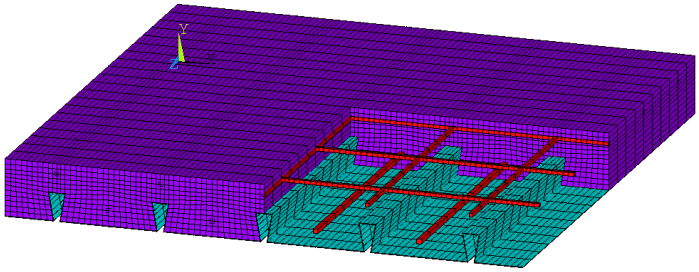

Finite element mesh

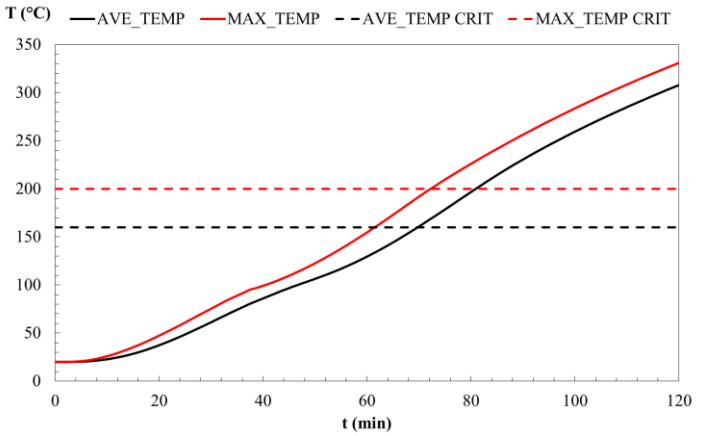

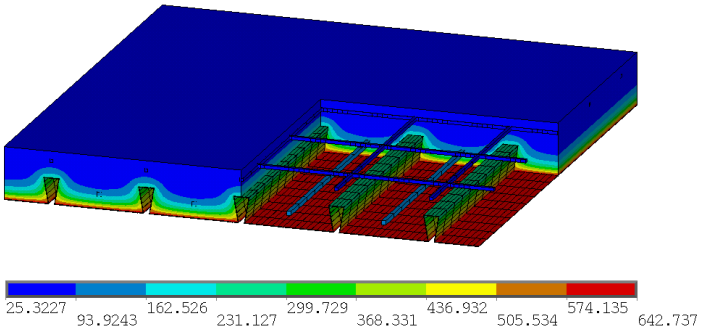

t= 17.4 min

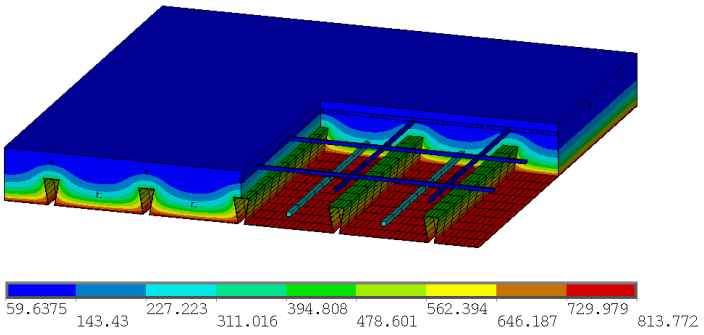

t= 34.9 min

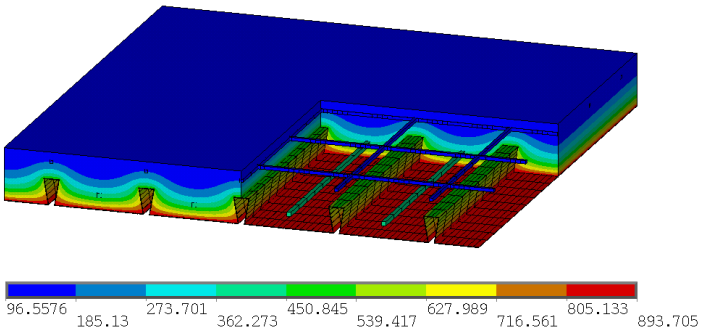

t= 52.3 min

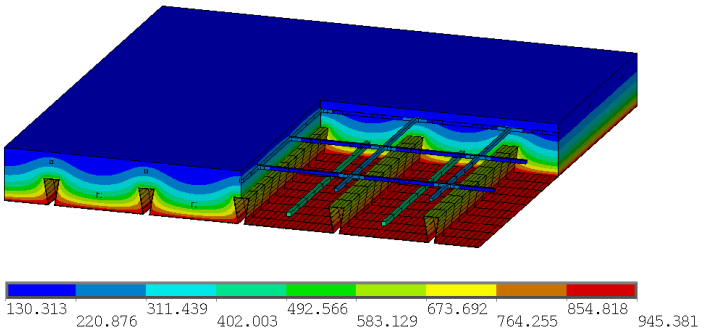

t= 69.7 min

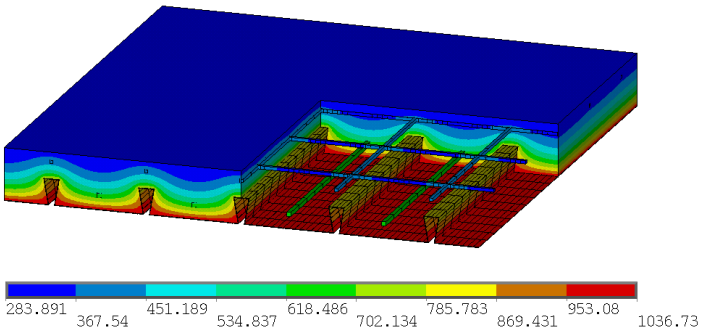

t= 120.0 min

SIM. 170	**Steel deck:** Lysaght Bondek	**Rebar (mm):** ϕ10	**Fire resistance (min)**	
	Mesh (mm//mm): ϕ7.6//200 (RM82)	**h_1 (mm):** 66	Ave: *83.5*	Max: 89.5

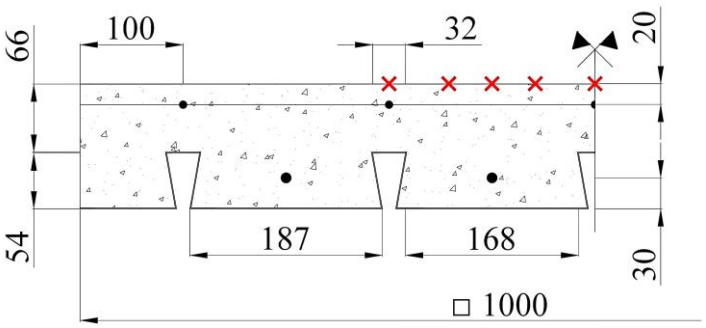

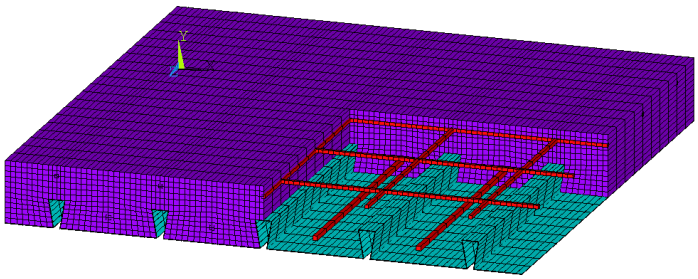

Finite element mesh

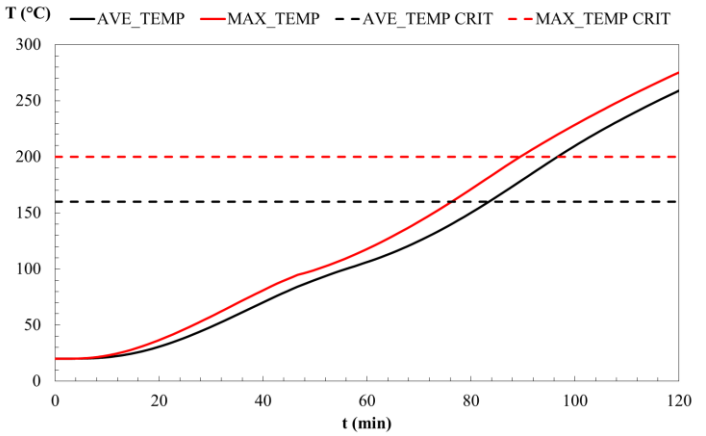

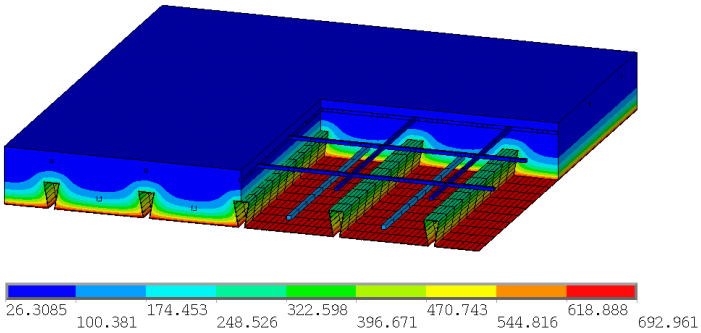

t= 20.9 min

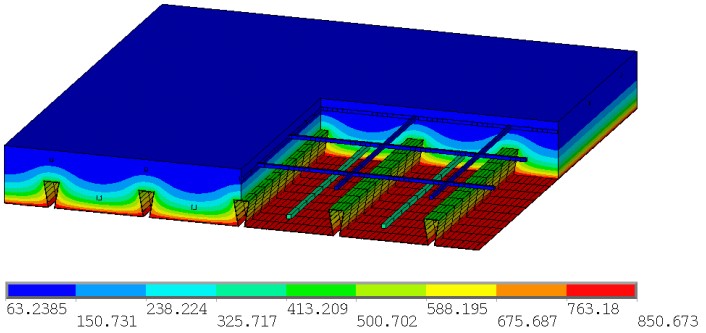

t= 41.8 min

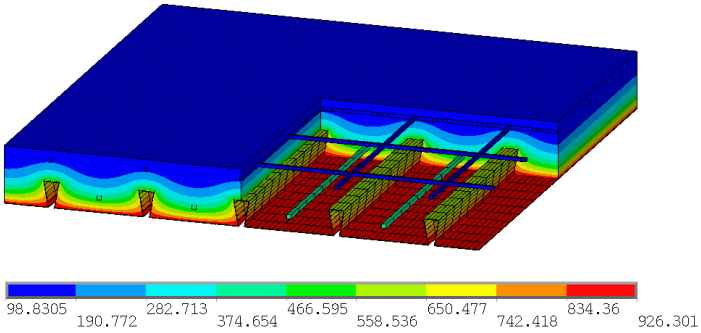

t= 62.6 min

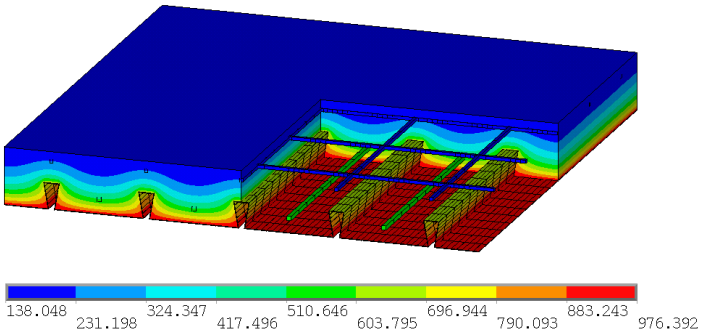

t= 83.5 min

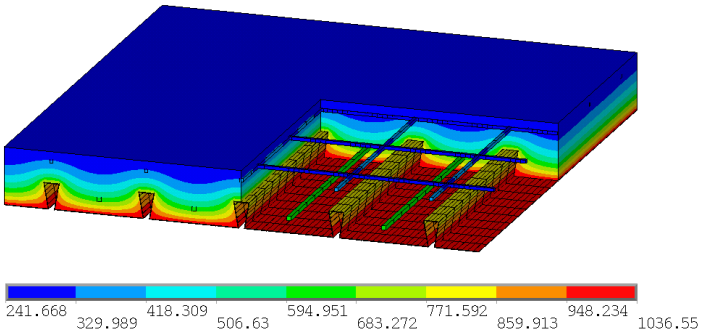

t= 120.0 min

SIM. 171	**Steel deck:** Lysaght Bondek	**Rebar (mm):** ϕ10	**Fire resistance (min)**	
	Mesh (mm//mm): ϕ7.6//200 (RM82)	**h_1 (mm):** 76	Ave: *98.4*	Max: 108.2

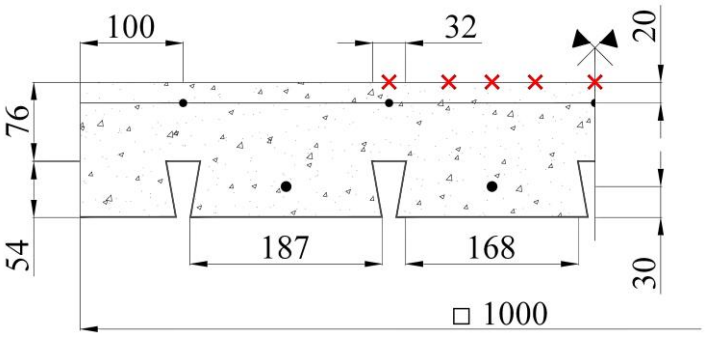

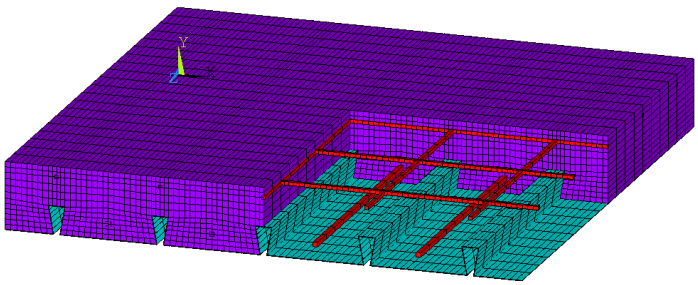

Finite element mesh

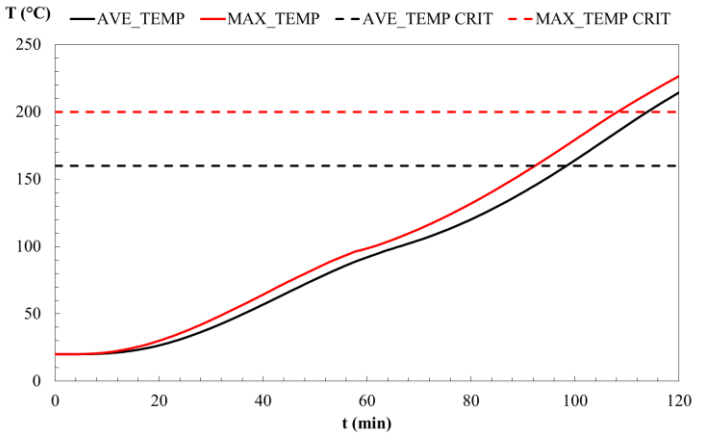

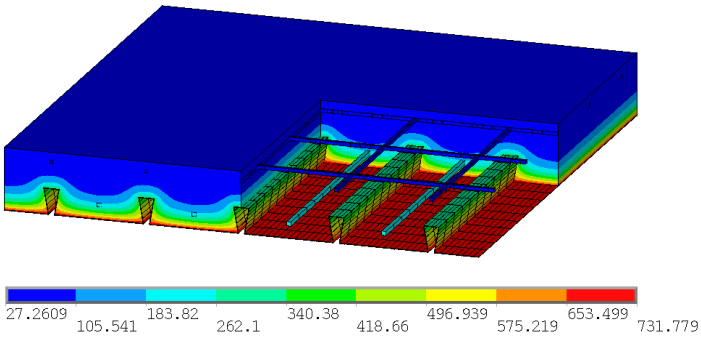

t= 24.6 min

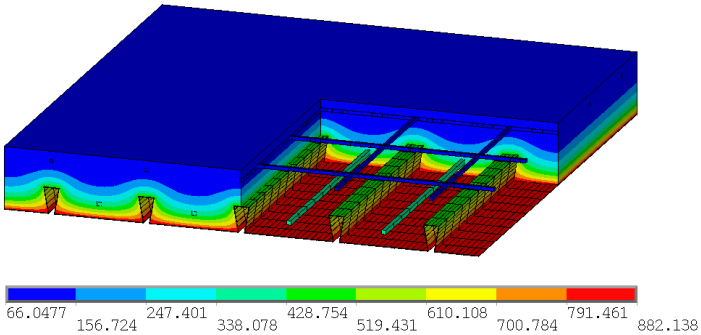

t= 49.2 min

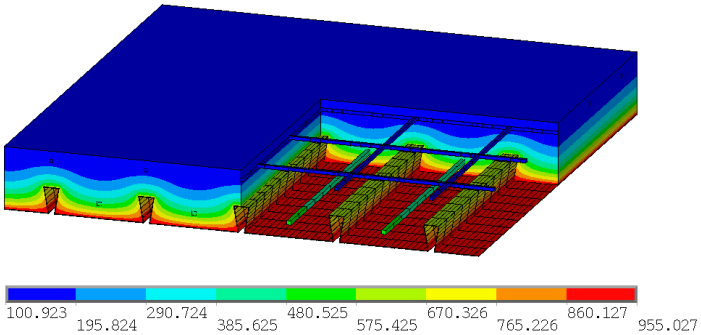

t= 73.8 min

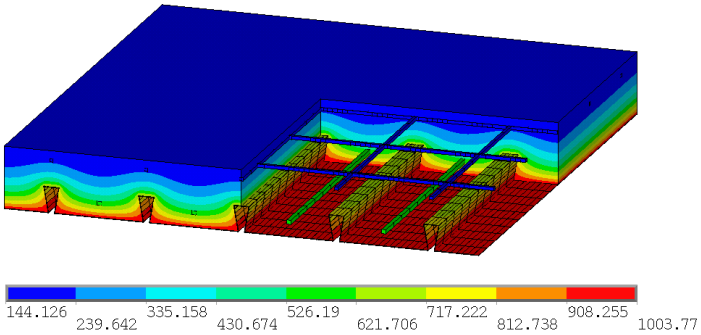

t= 98.4 min

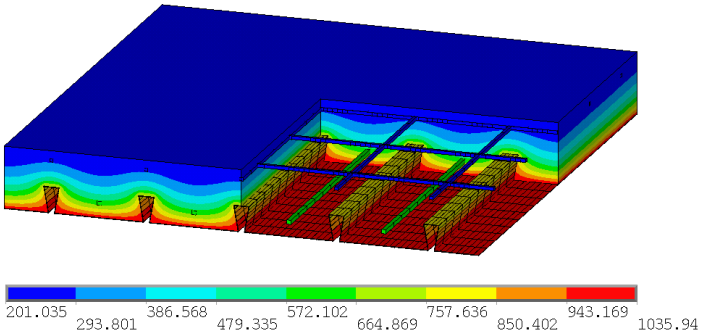

t= 120.0 min

SIM. 172	**Steel deck:** Lysaght Bondek	**Rebar (mm):** ϕ10	**Fire resistance (min)**	
	Mesh (mm//mm): ϕ7.6//200 (RM82)	**h_1 (mm):** 86	Ave: *114.7*	Max: 128.5

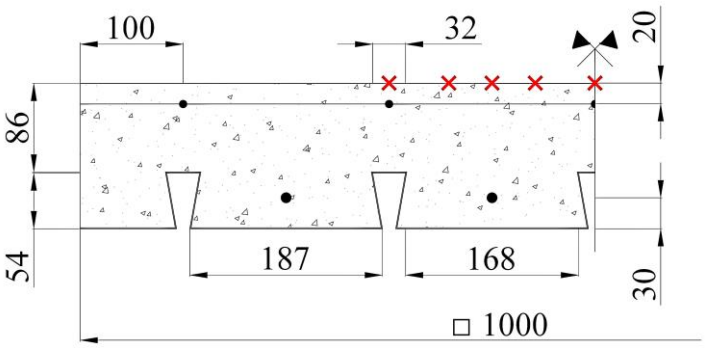

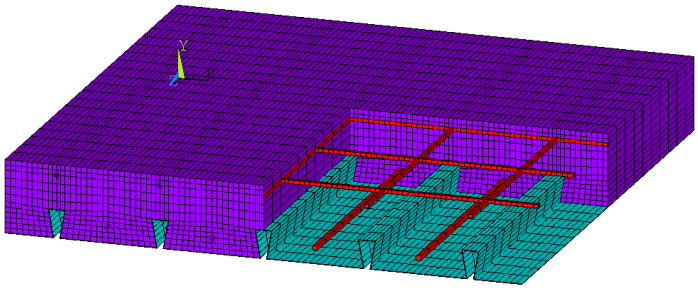

Finite element mesh

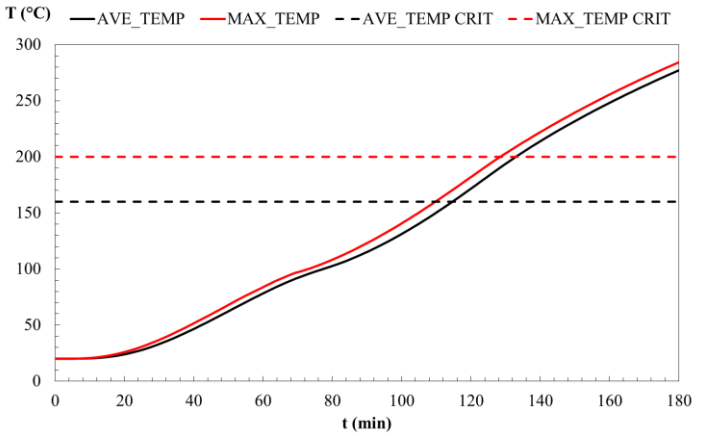

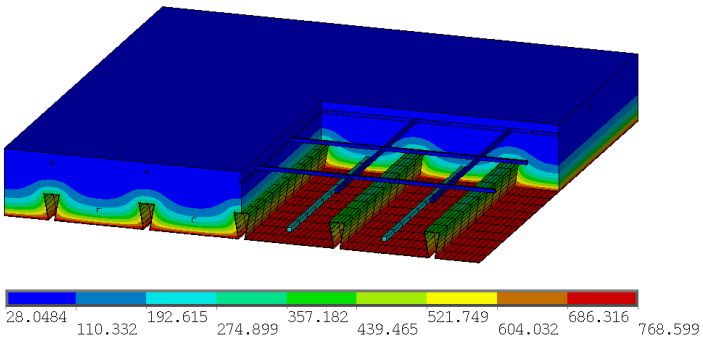

t= 28.7 min

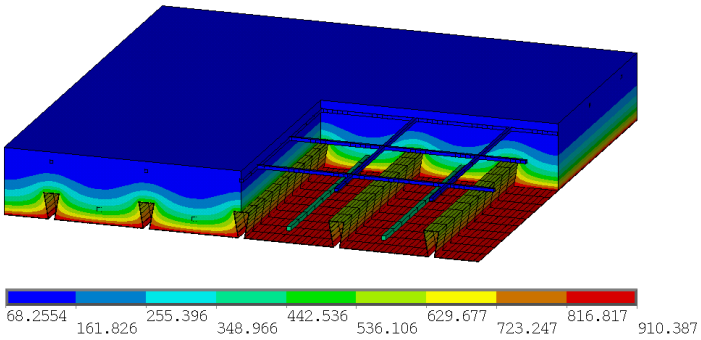

t= 57.4 min

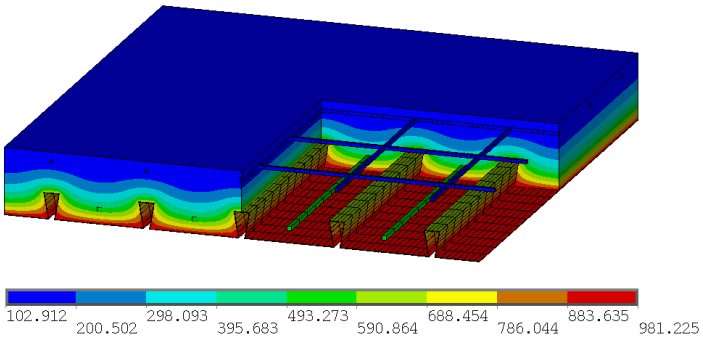

t= 86.0 min

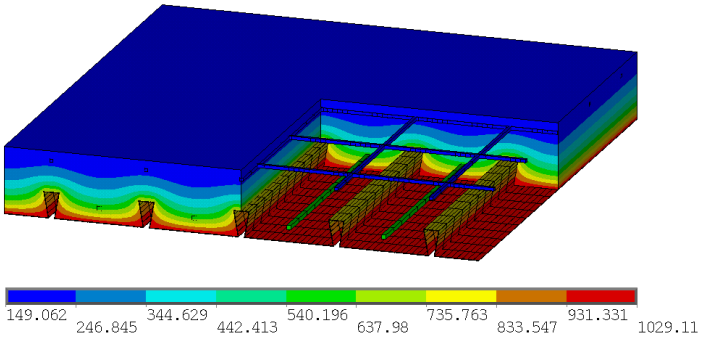

t= 114.7 min

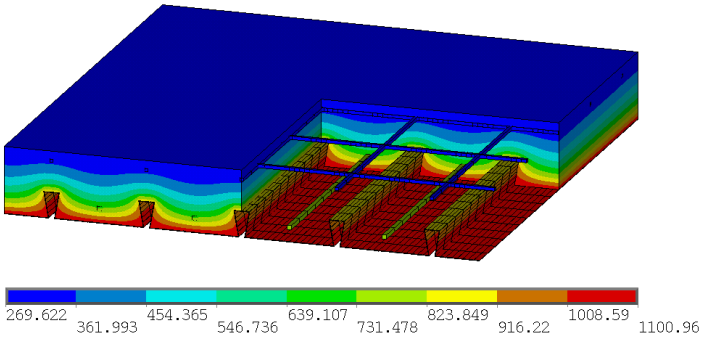

t= 180.0 min

SIM. 173	**Steel deck:** Lysaght Bondek	**Rebar (mm):** ϕ10	**Fire resistance (min)**	
	Mesh (mm//mm): ϕ7.6//200 (RM82)	**h_1 (mm):** 56	Ave: *69.8*	Max: 72.2

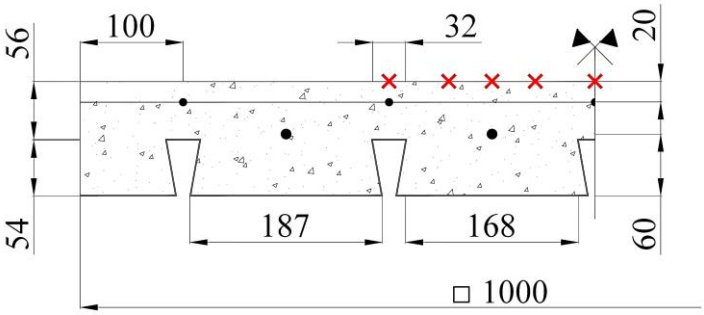

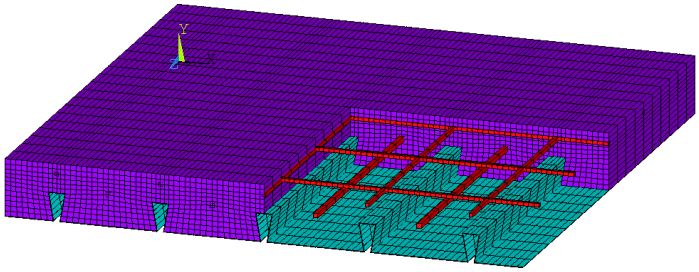

Finite element mesh

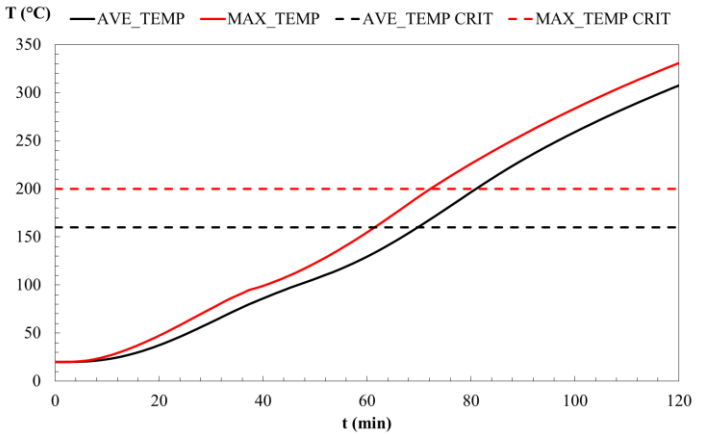

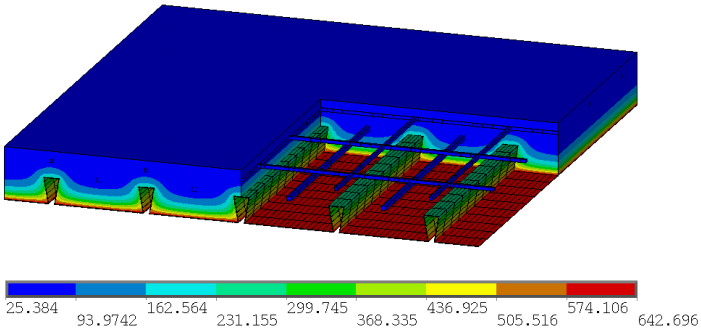

t= 17.5 min

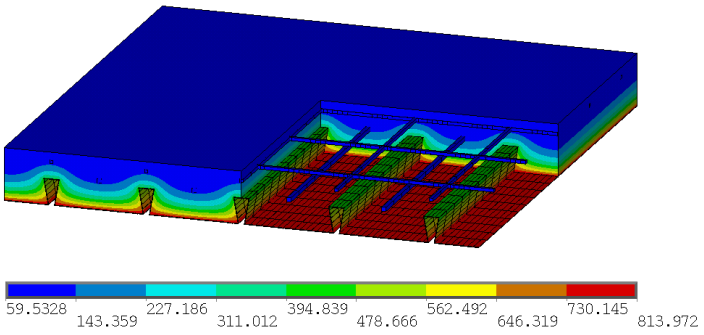

t= 34.9 min

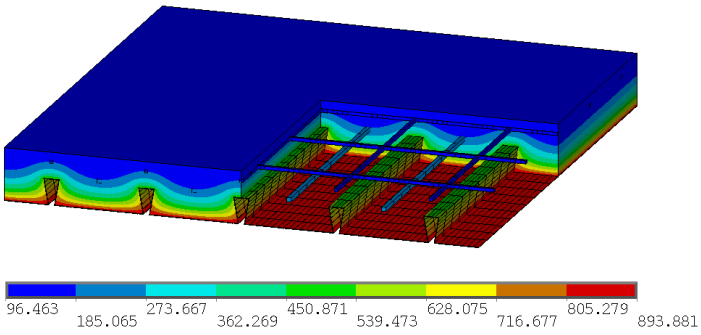

t= 52.4 min

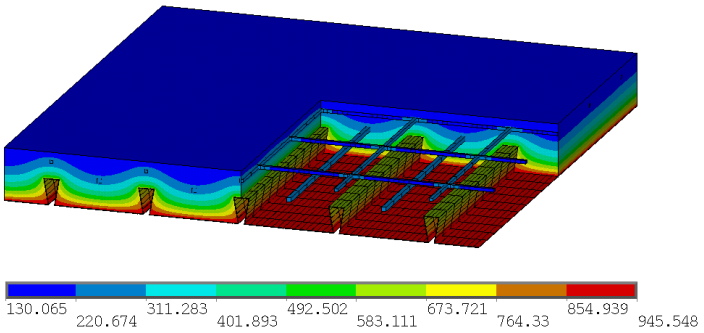

t= 69.8 min

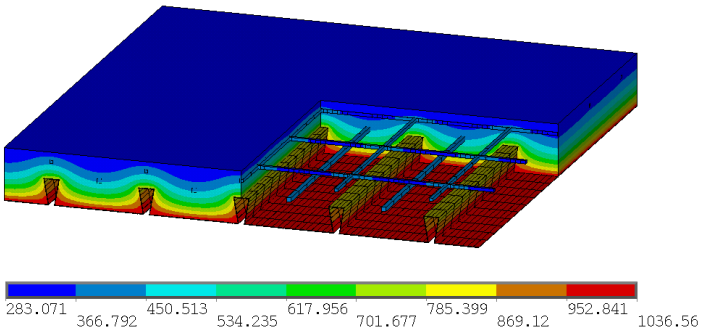

t= 120.0 min

SIM. 174	**Steel deck:** Lysaght Bondek	**Rebar (mm):** ϕ10	**Fire resistance (min)**	
	Mesh (mm//mm): ϕ7.6//200 (RM82)	**h_1 (mm):** 66	Ave: *83.5*	Max: 89.5

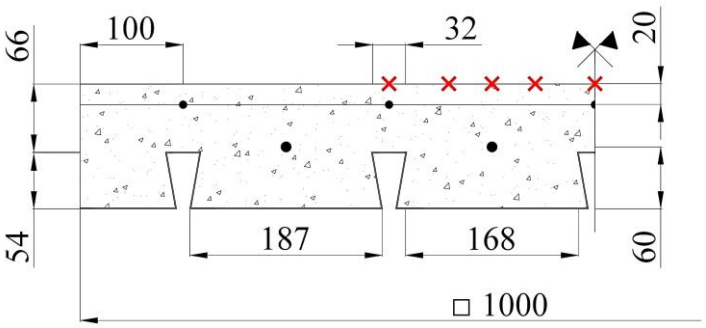

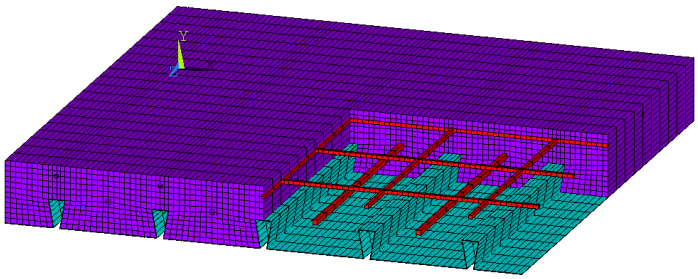

Finite element mesh

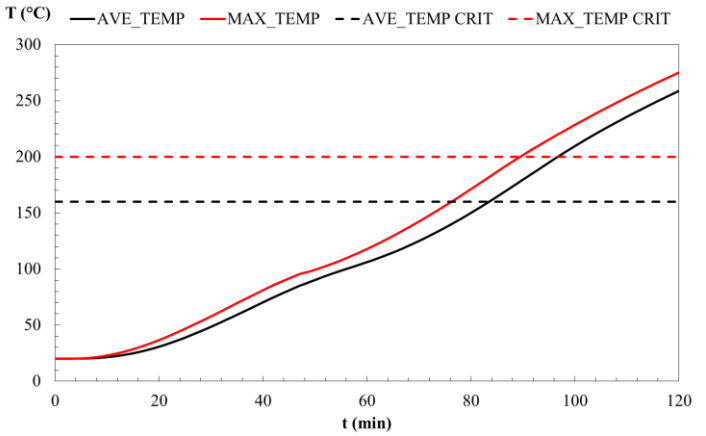

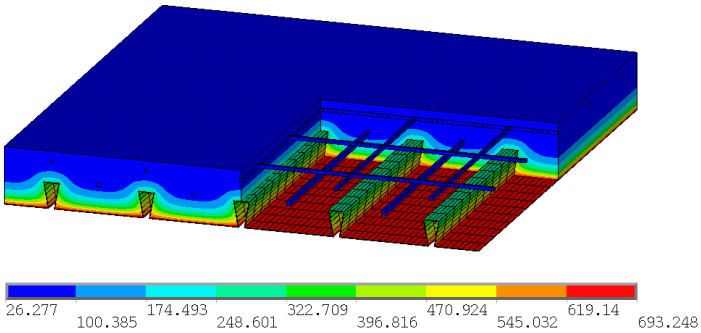

t= 20.9 min

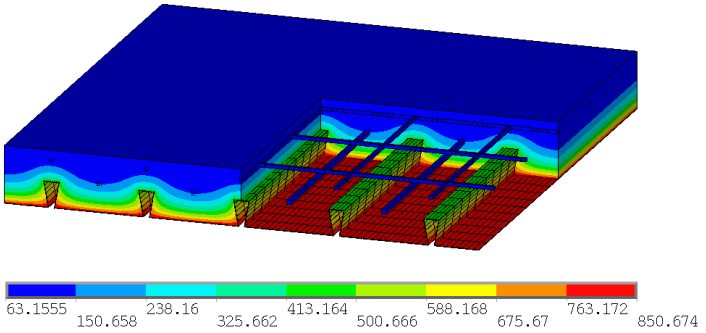

t= 41.8 min

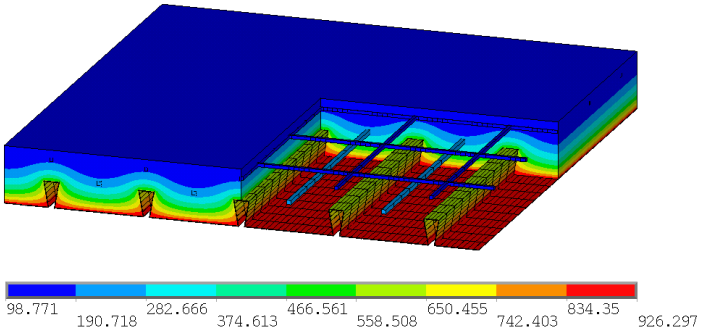

t= 62.6 min

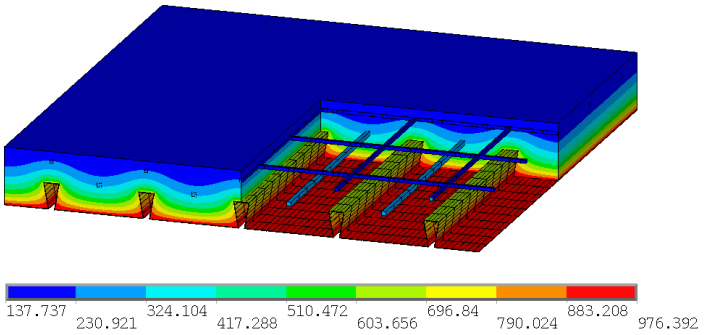

t= 83.5 min

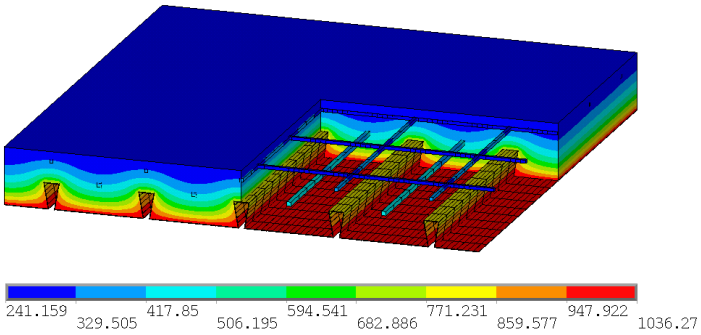

t= 120.0 min

SIM. 175	**Steel deck:** Lysaght Bondek	**Rebar (mm):** ϕ10	**Fire resistance (min)**	
	Mesh (mm//mm): ϕ7.6//200 (RM82)	**h_1 (mm):** 76	Ave: *98.4*	Max: 108.2

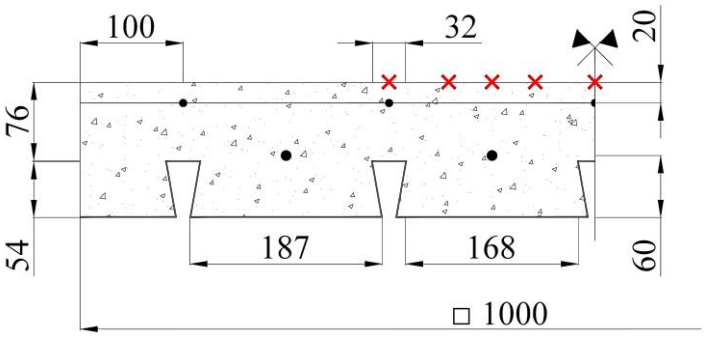

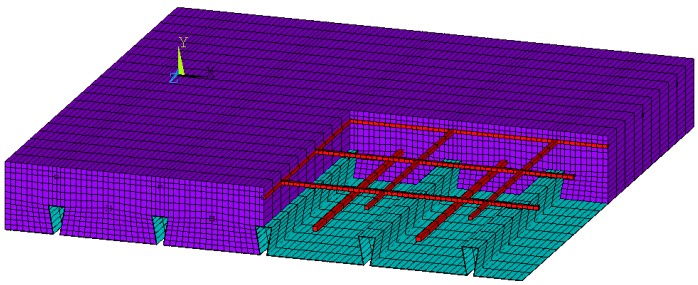

Finite element mesh

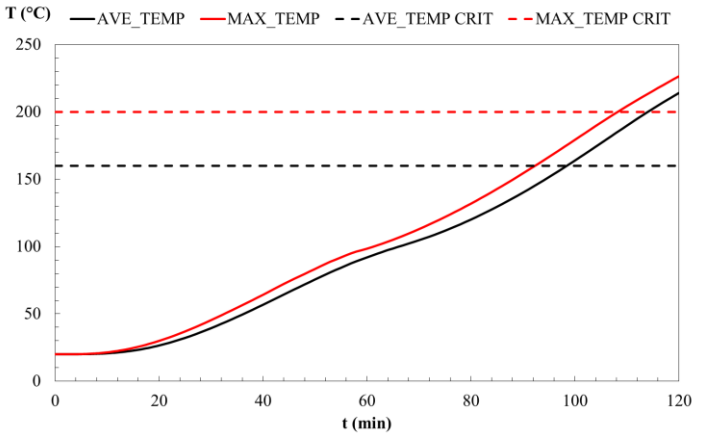

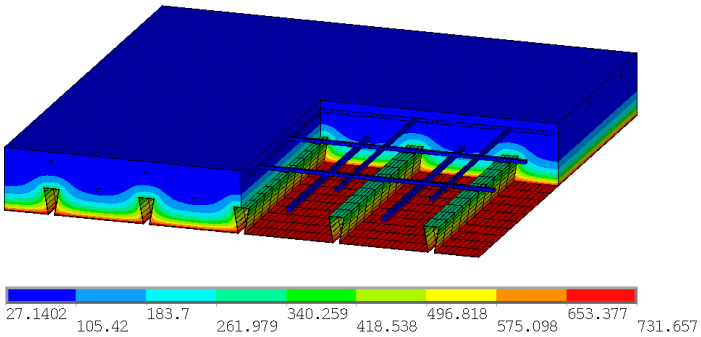

t= 24.6 min

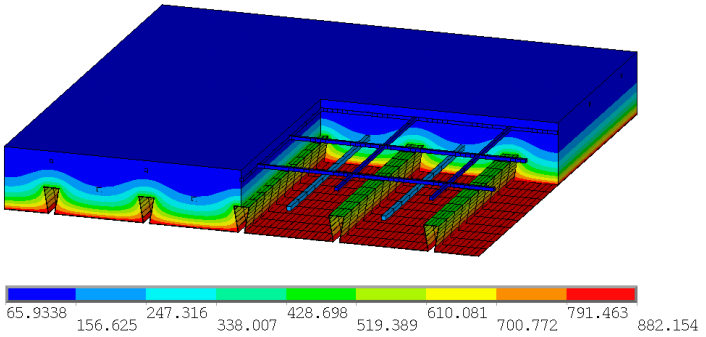

t= 49.2 min

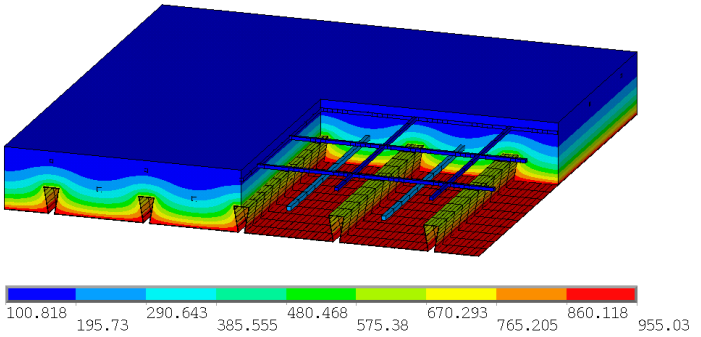

t= 73.8 min

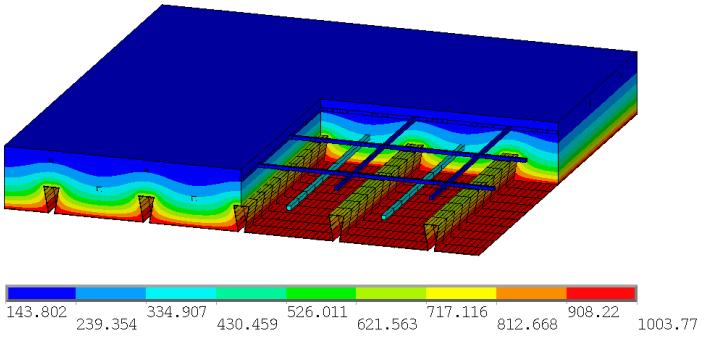

t= 98.4 min

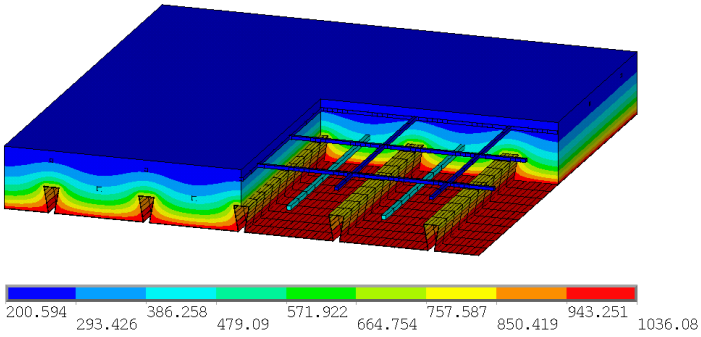

t= 120.0 min

SIM. 176	**Steel deck:** Lysaght Bondek	**Rebar (mm):** ϕ10	**Fire resistance (min)**	
	Mesh (mm//mm): ϕ7.6//200 (RM82)	**h_1 (mm):** 86	Ave: *114.7*	Max: 128.5

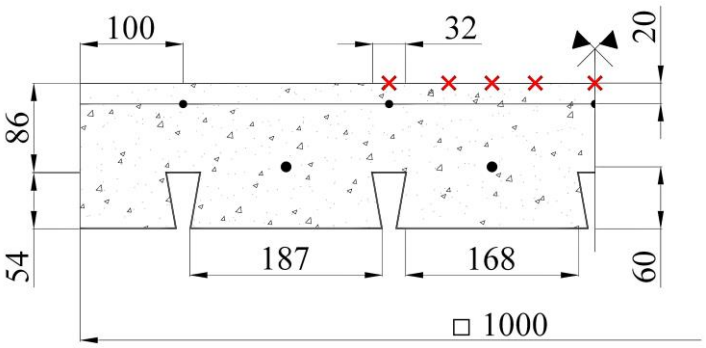

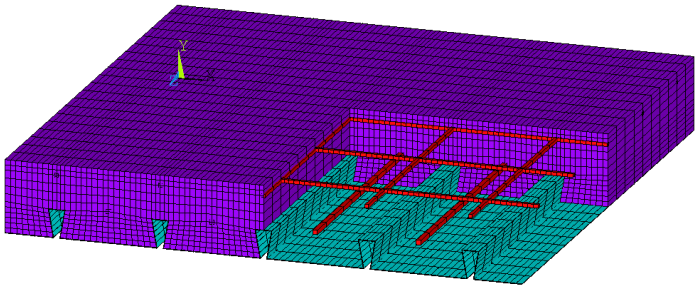

Finite element mesh

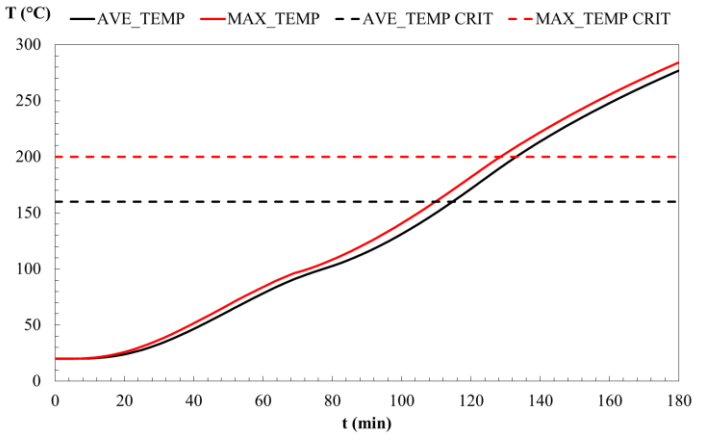

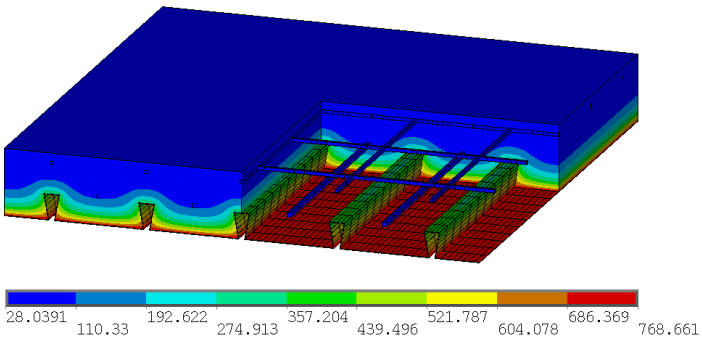

t= 28.7 min

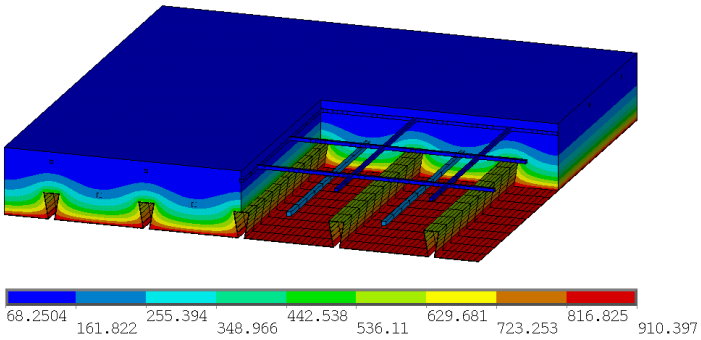

t= 57.4 min

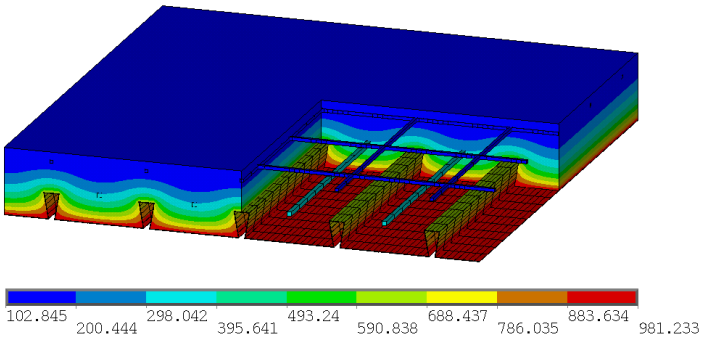

t= 86.0 min

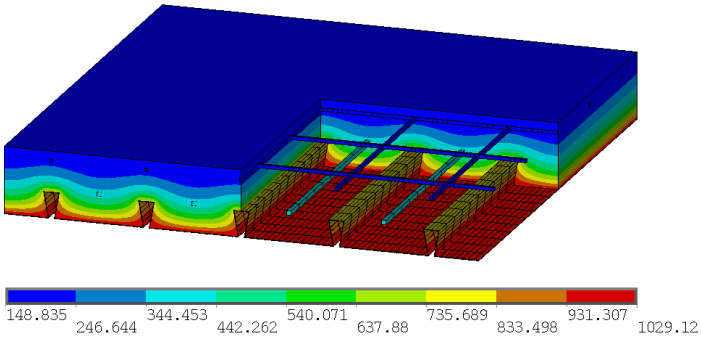

t= 114.7 min

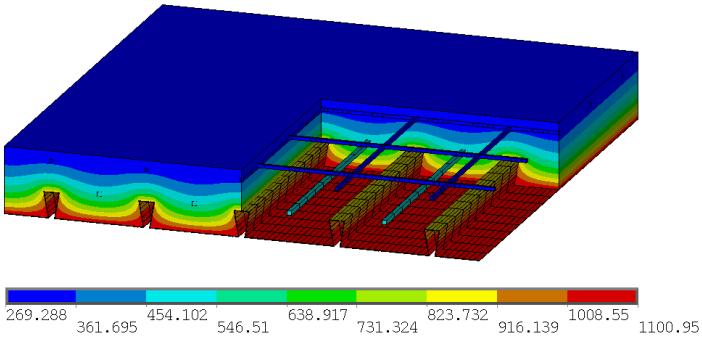

t= 180.0 min

SIM. 177	**Steel deck:** Lysaght Bondek	**Rebar (mm):** ϕ12	**Fire resistance (min)**	
	Mesh (mm//mm): ϕ6.75//200 (RM72)	**h_1 (mm):** 56	Ave: *69.7*	Max: 71.7

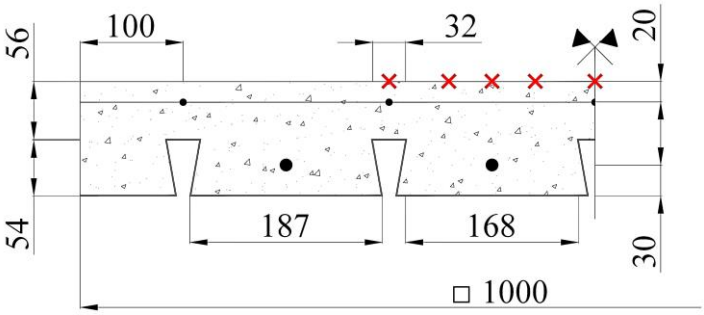

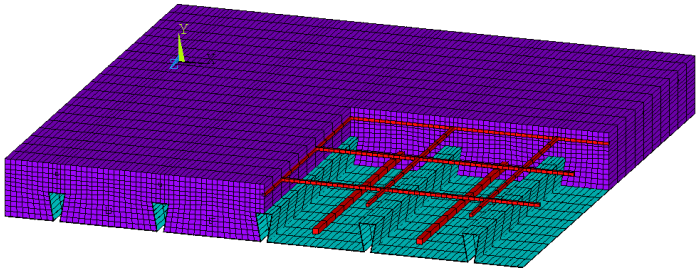

Finite element mesh

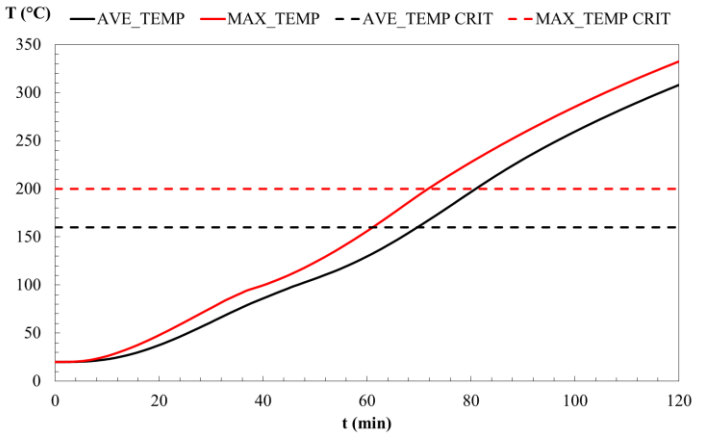

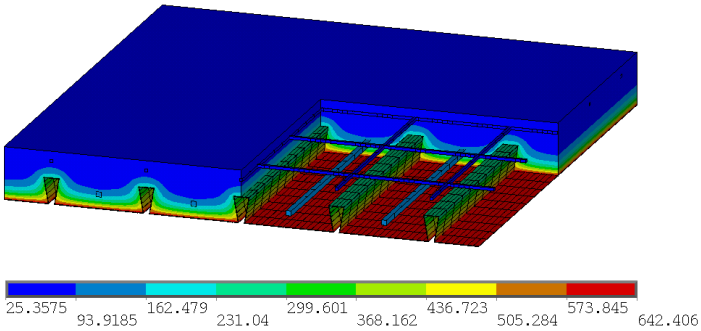

t= 17.4 min

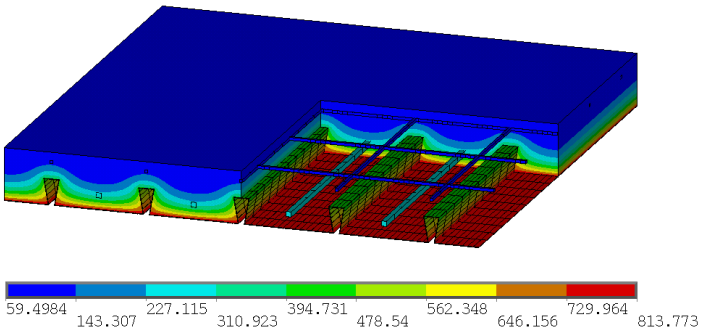

t= 34.9 min

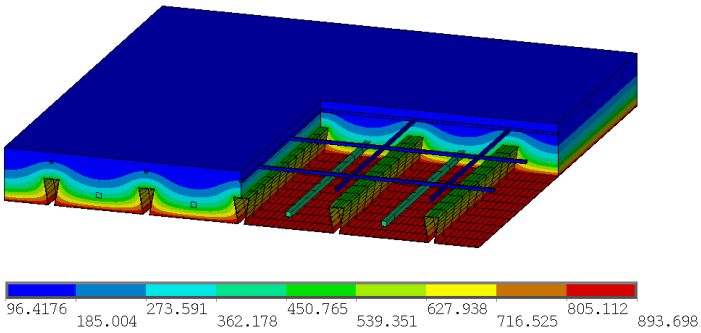

t= 52.3 min

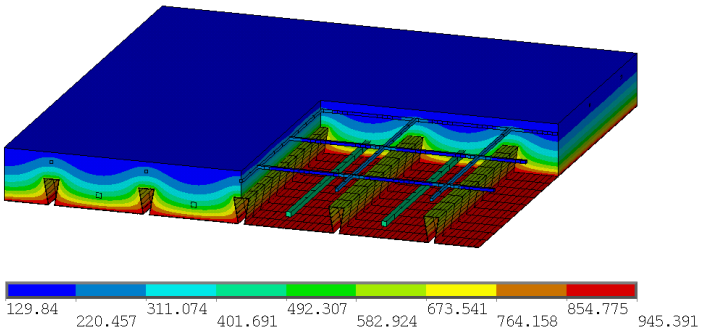

t= 69.7 min

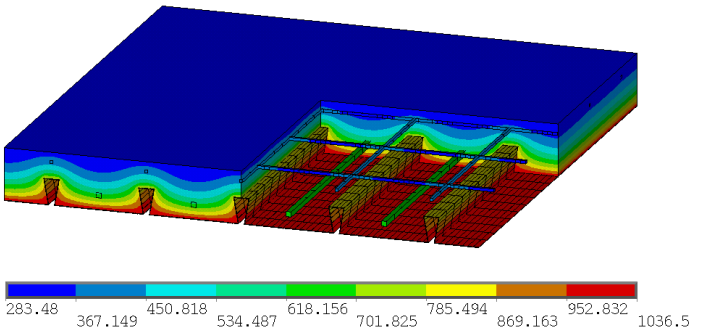

t= 120.0 min

SIM. 178	**Steel deck:** Lysaght Bondek	**Rebar (mm):** ϕ12	**Fire resistance (min)**	
	Mesh (mm//mm): ϕ6.75//200 (RM72)	**h_1 (mm):** 66	Ave: *83.4*	Max: 89.0

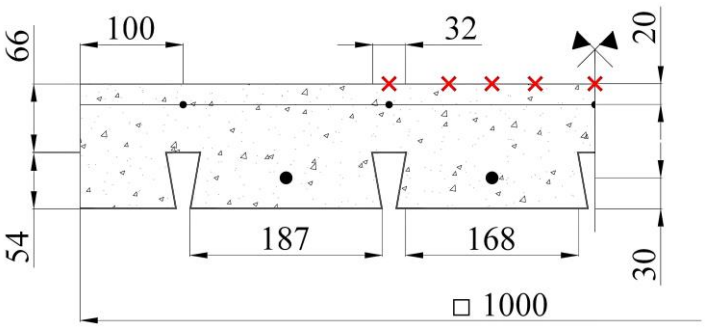

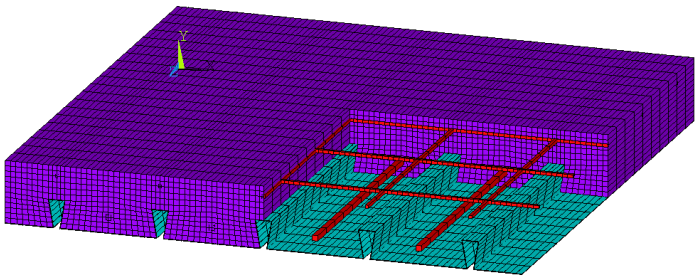

Finite element mesh

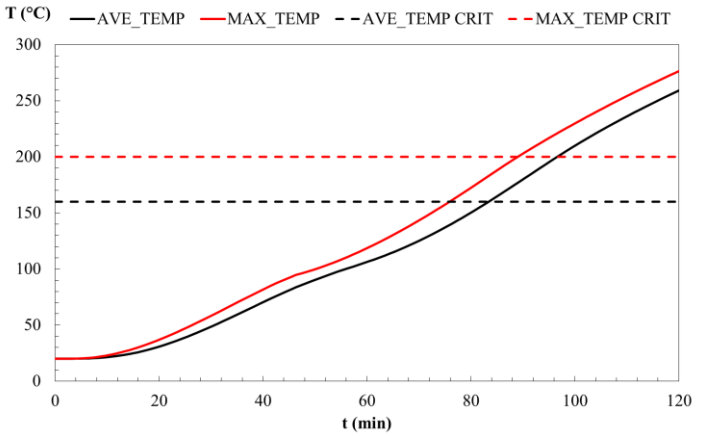

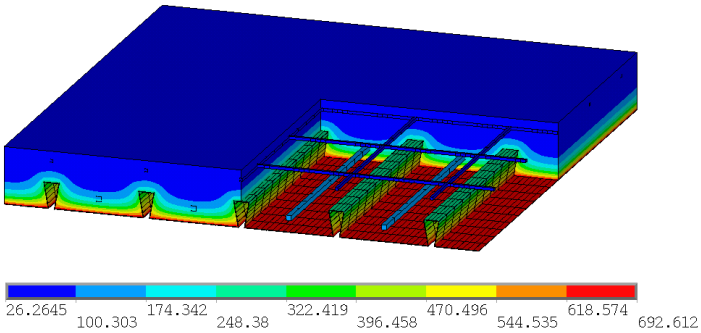

t= 20.9 min

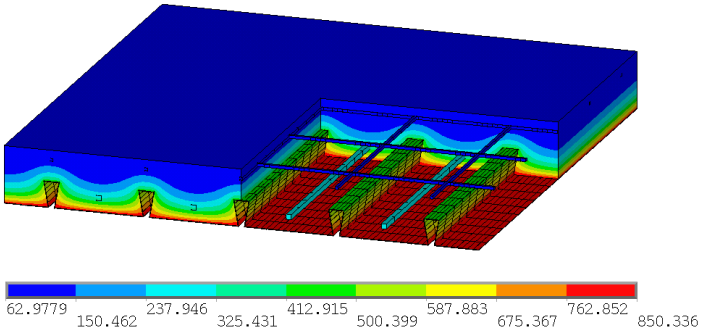

t= 41.7 min

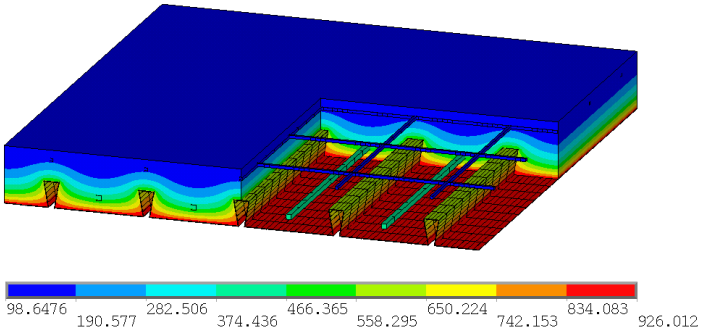

t= 62.6 min

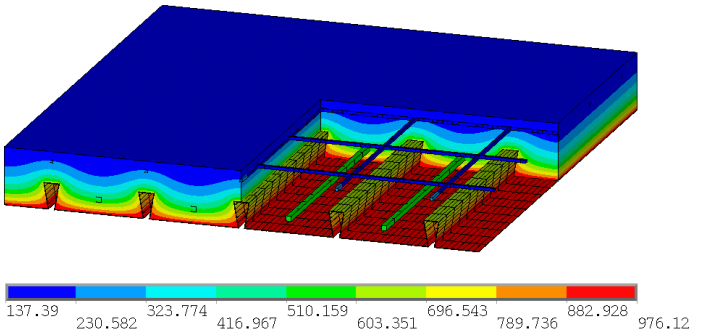

t= 83.4 min

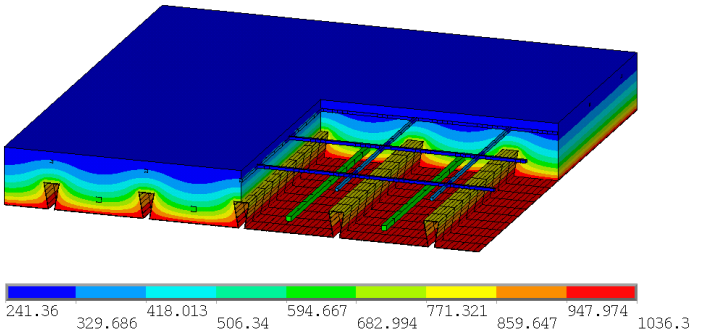

t= 120.0 min

SIM. 179	**Steel deck:** Lysaght Bondek	**Rebar (mm):** ϕ12	**Fire resistance (min)**	
	Mesh (mm//mm): ϕ6.75//200 (RM72)	**h_1 (mm):** 76	Ave: *98.3*	Max: 107.7

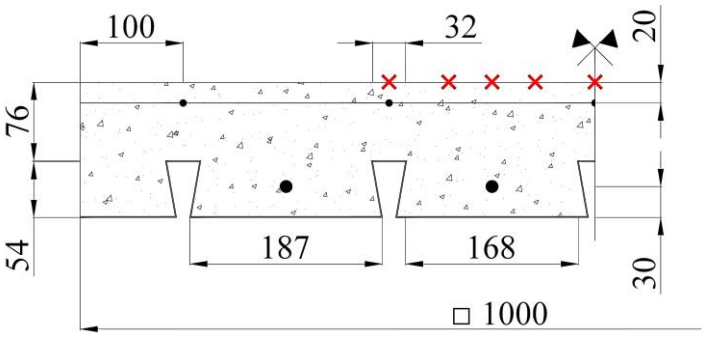

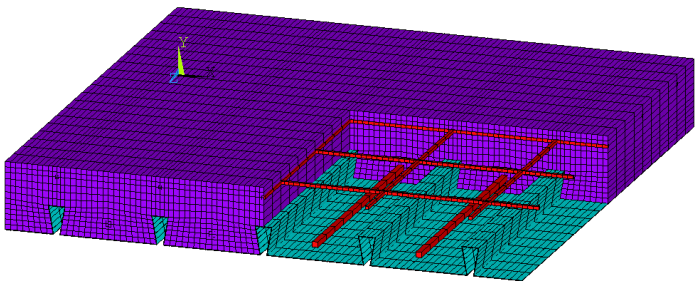

Finite element mesh

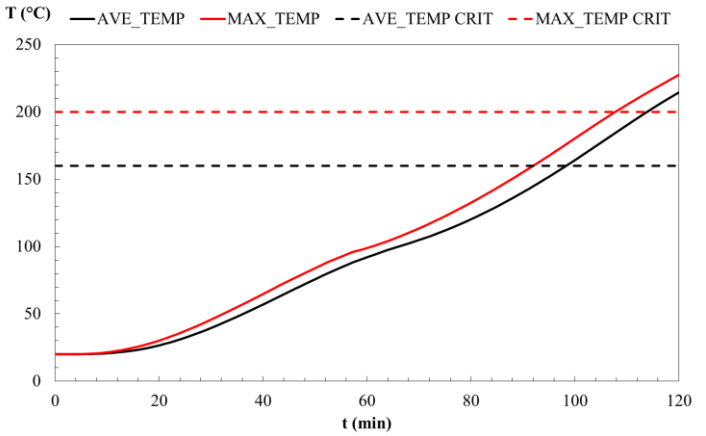

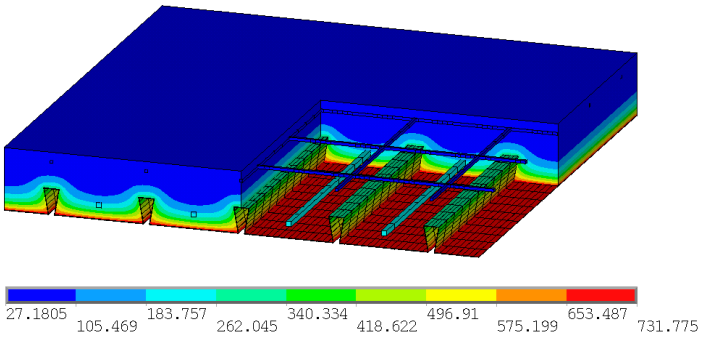

t= 24.6 min

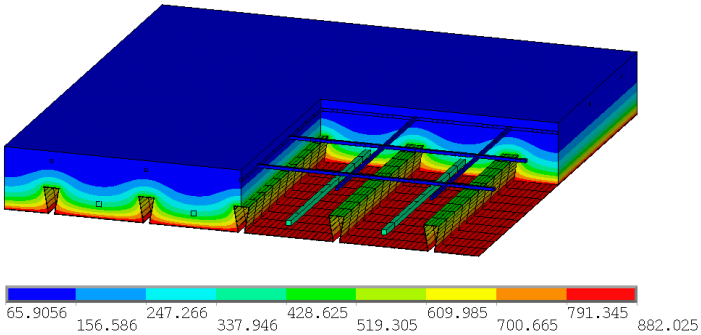

t= 49.2 min

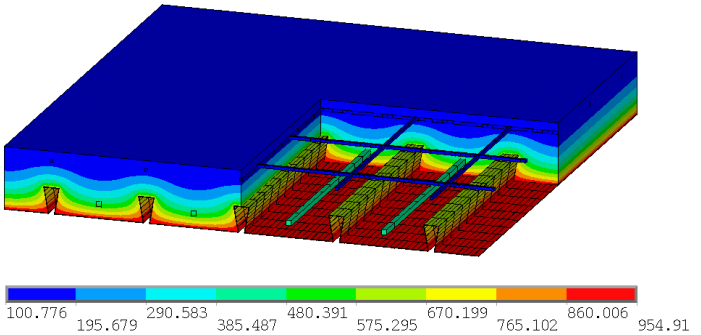

t= 73.7 min

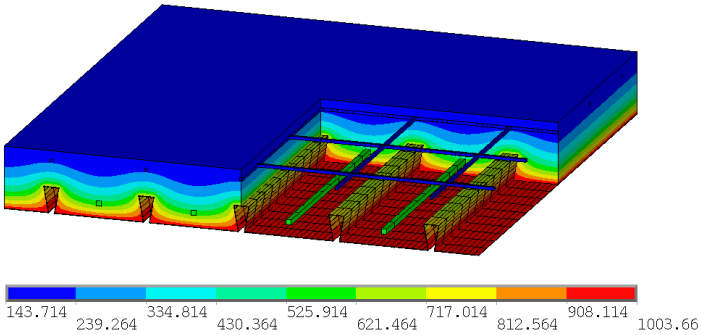

t= 98.3 min

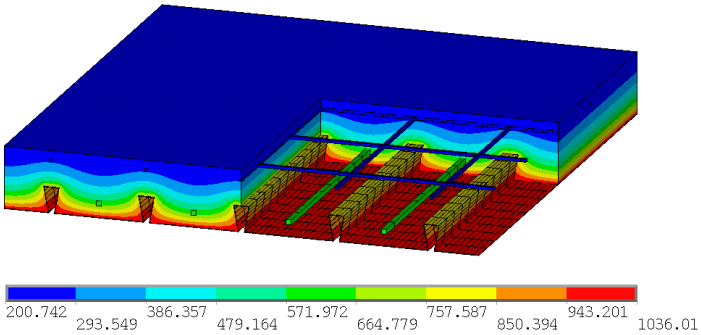

t= 120.0 min

SIM. 180	**Steel deck:** Lysaght Bondek	**Rebar (mm):** ϕ12	**Fire resistance (min)**	
	Mesh (mm//mm): ϕ6.75//200 (RM72)	**h_1 (mm):** 86	Ave: *114.6*	Max: 128.0

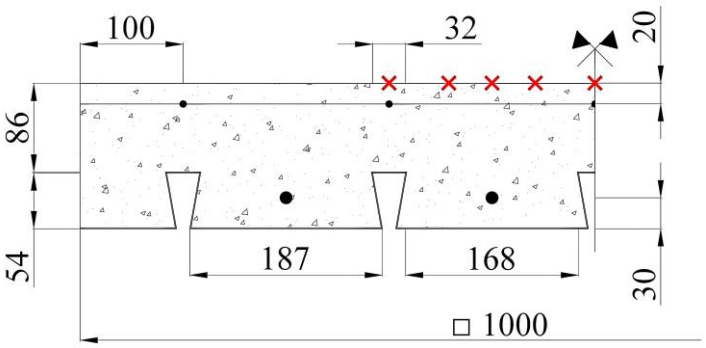

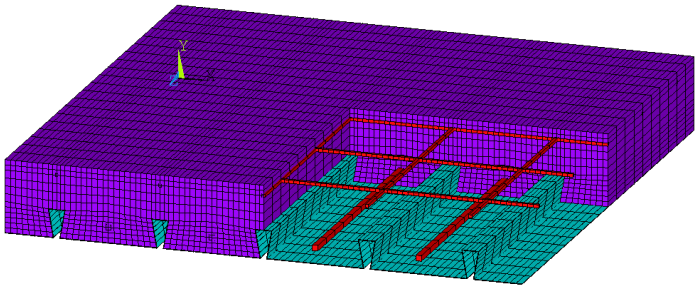

Finite element mesh

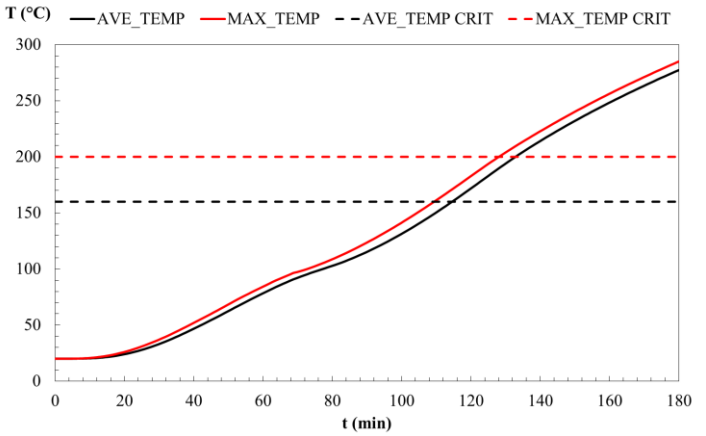

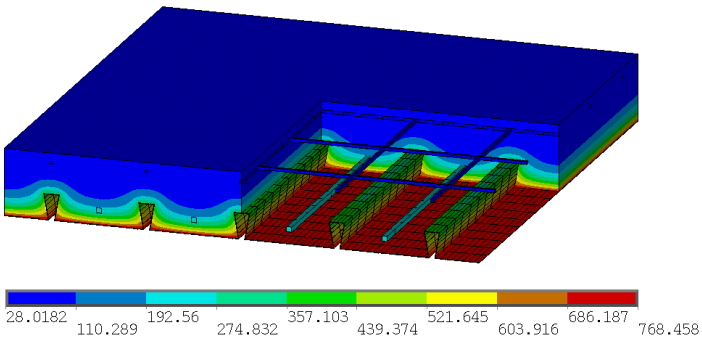

t= 28.7 min

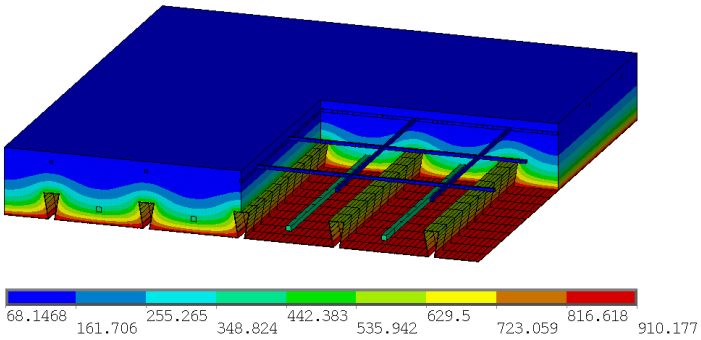

t= 57.3 min

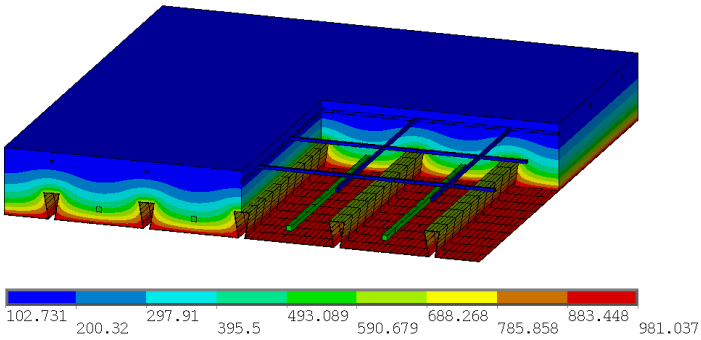

t= 86.0 min

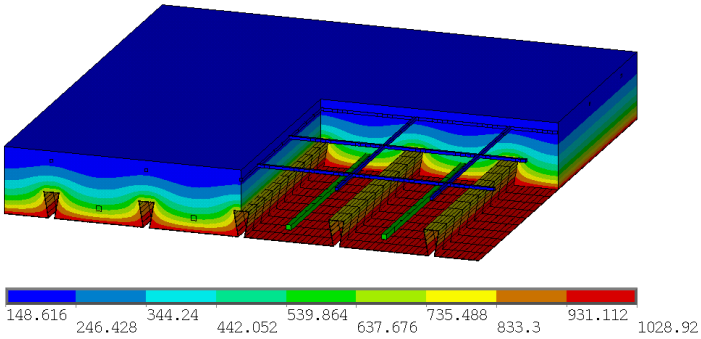

t= 114.6 min

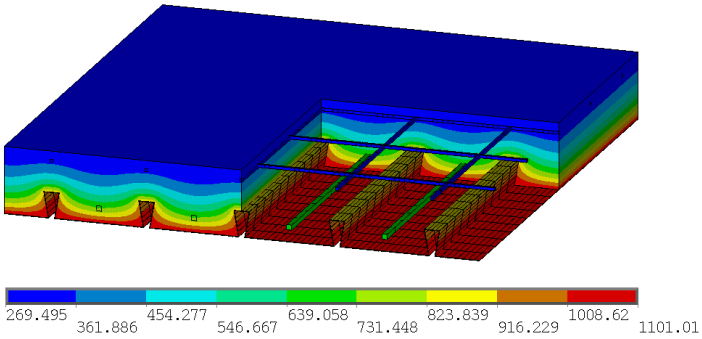

t= 180.0 min

SIM. 181	**Steel deck:** Lysaght Bondek	**Rebar (mm):** ϕ12	**Fire resistance (min)**	
	Mesh (mm//mm): ϕ6.75//200 (RM72)	**h_1 (mm):** 56	Ave: *69.7*	Max: 71.7

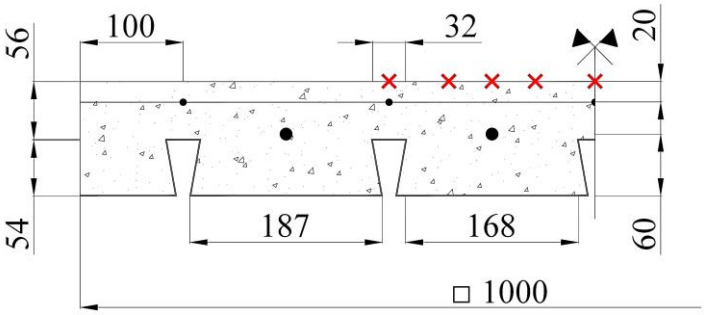

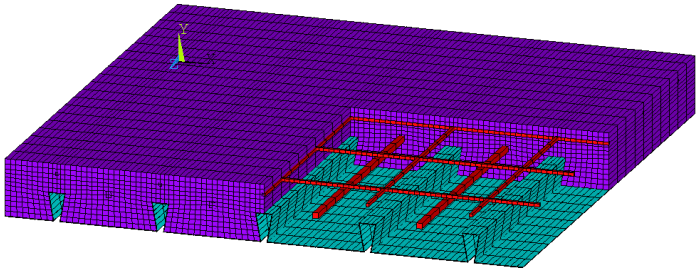

Finite element mesh

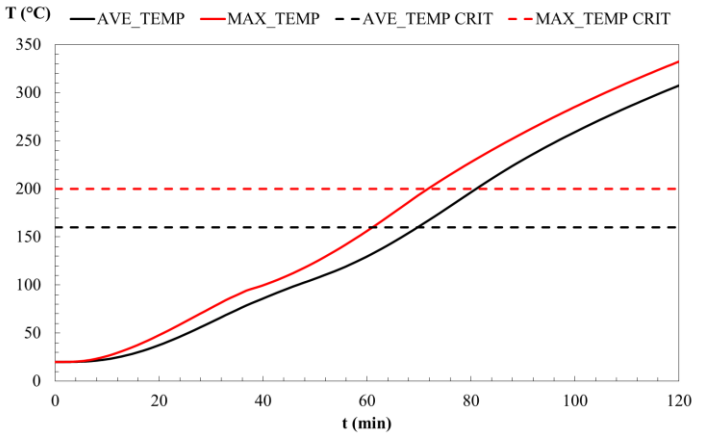

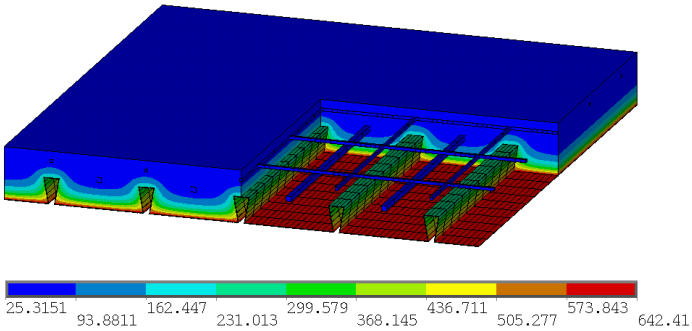

t= 17.4 min

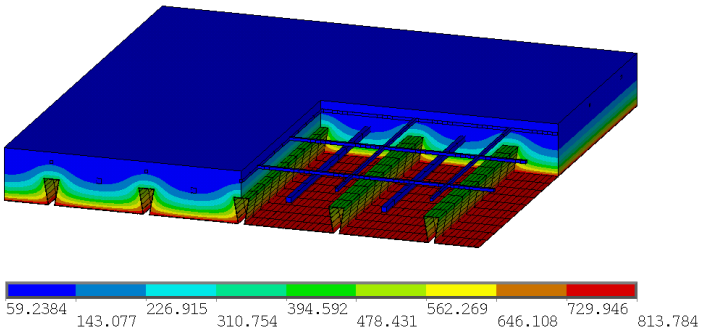

t= 34.9 min

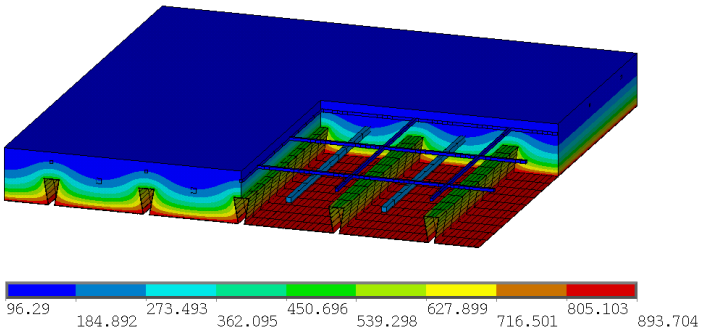

t= 52.3 min

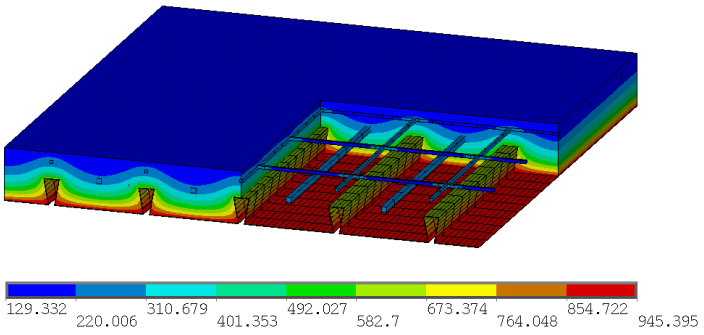

t= 69.7 min

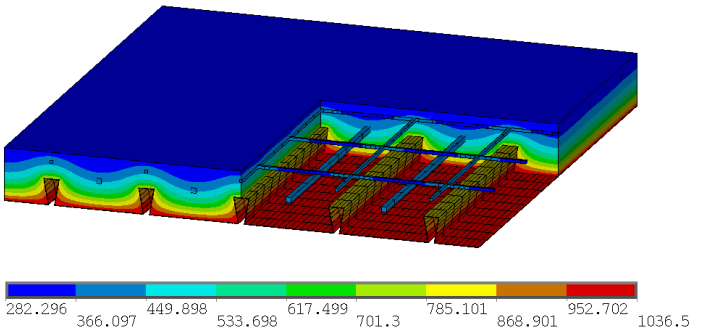

t= 120.0 min

SIM. 182	**Steel deck:** Lysaght Bondek	**Rebar (mm):** ϕ12	**Fire resistance (min)**	
	Mesh (mm//mm): ϕ6.75//200 (RM72)	**h_1 (mm):** 66	Ave: *83.5*	Max: 89.0

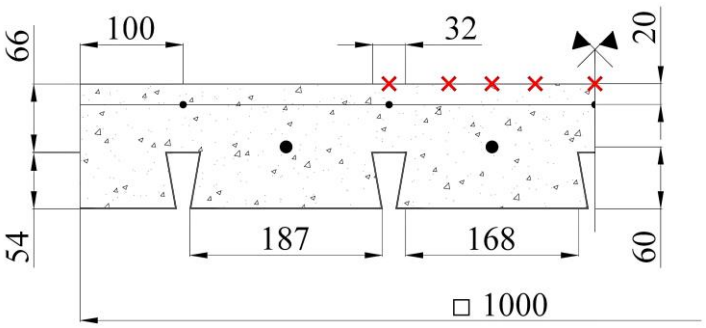

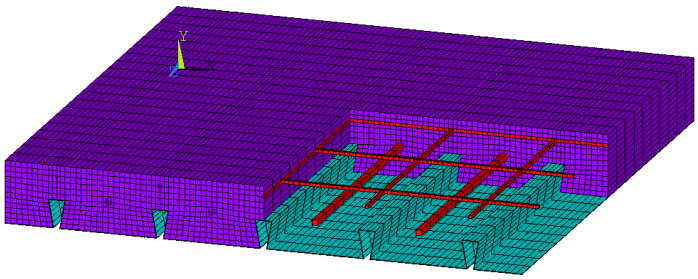

Finite element mesh

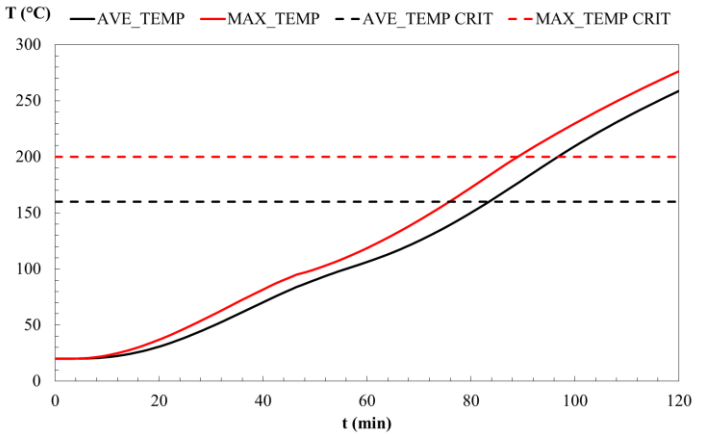

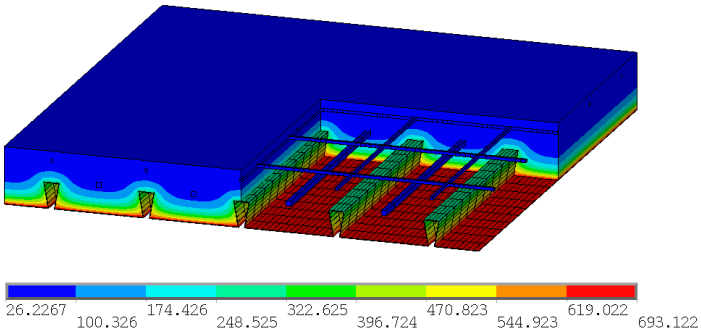

t= 20.9 min

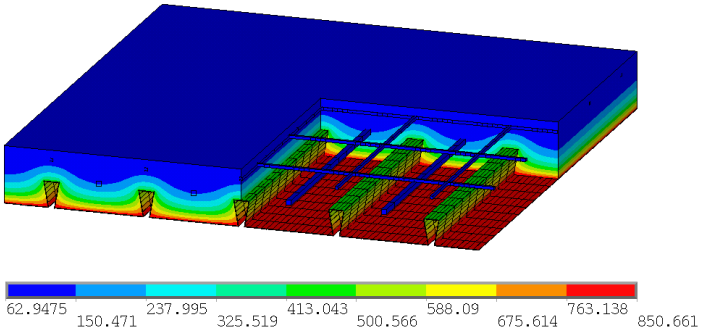

t= 41.8 min

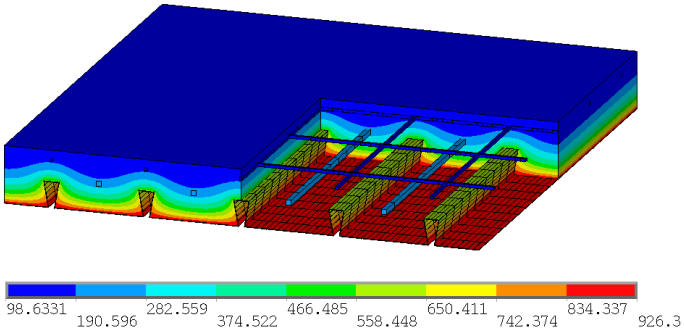

t= 62.6 min

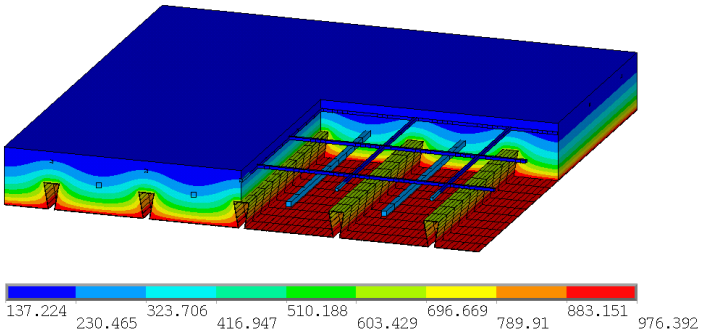

t= 83.5 min

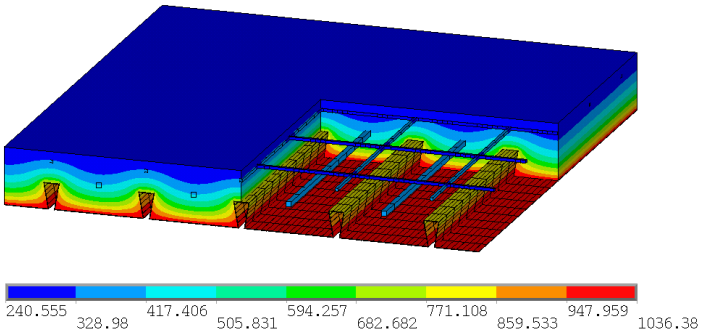

t= 120.0 min

SIM. 183	**Steel deck:** Lysaght Bondek	**Rebar (mm):** ϕ12	**Fire resistance (min)**	
	Mesh (mm//mm): ϕ6.75//200 (RM72)	**h_1 (mm):** 76	Ave: *98.4*	Max: 107.8

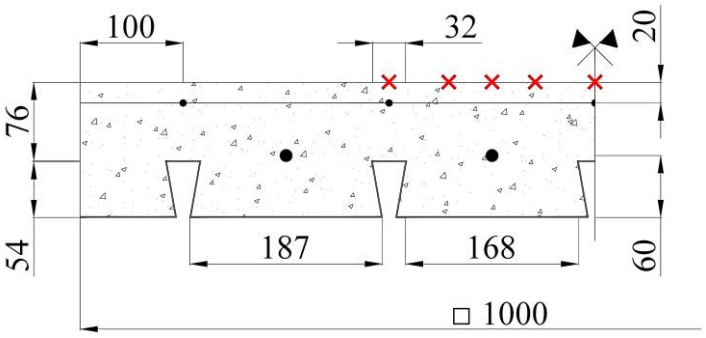

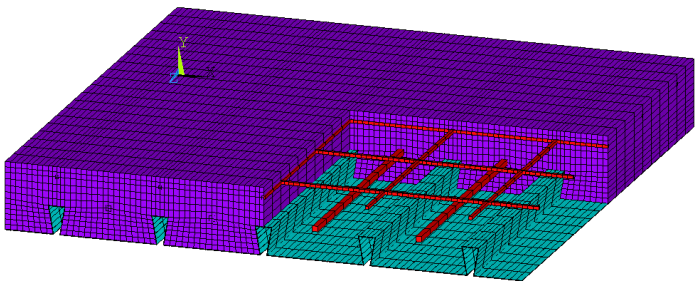

Finite element mesh

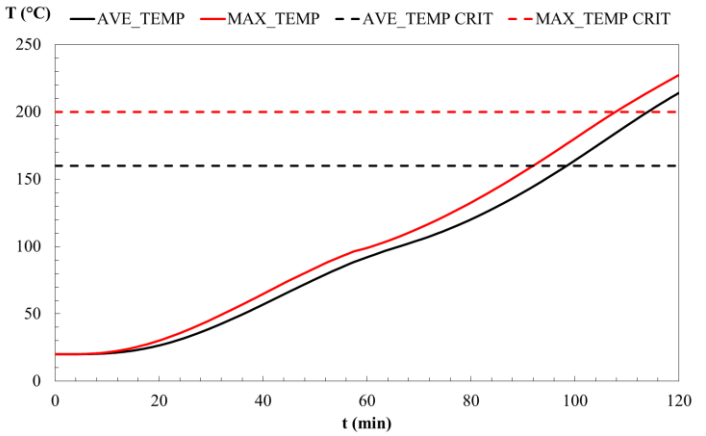

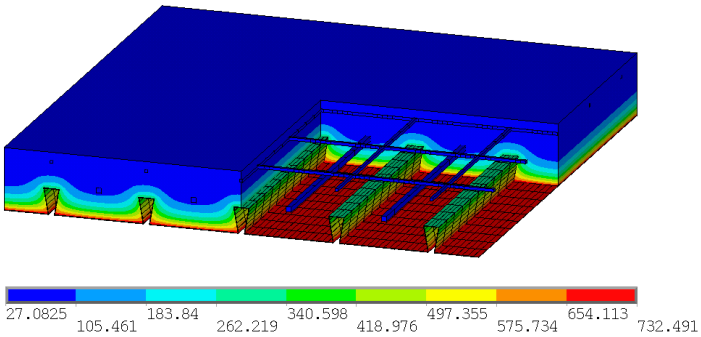

t= 24.6 min

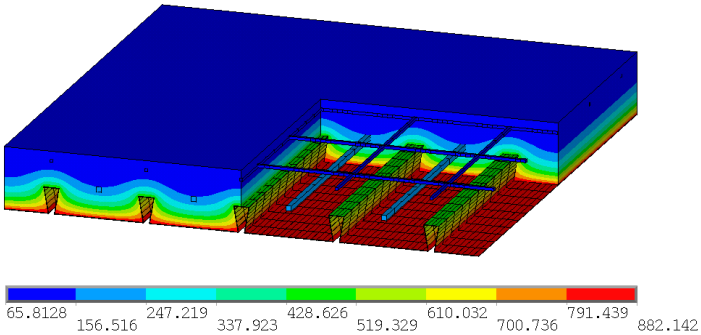

t= 49.2 min

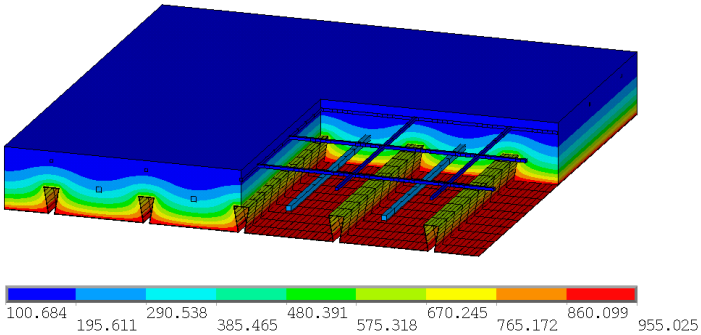

t= 73.8 min

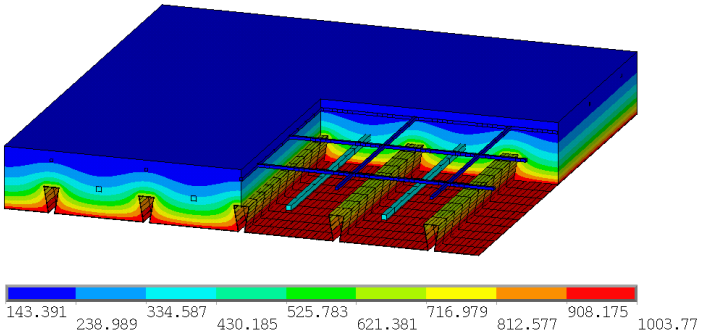

t= 98.4 min

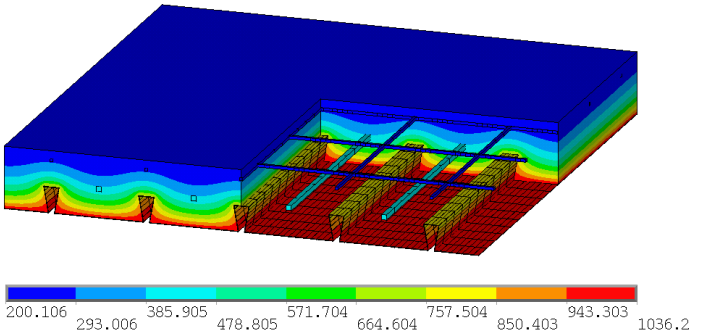

t= 120.0 min

SIM. 184	**Steel deck:** Lysaght Bondek	**Rebar (mm):** ϕ12	**Fire resistance (min)**	
	Mesh (mm//mm): ϕ6.75//200 (RM72)	**h_1 (mm):** 86	Ave: *114.7*	Max: 128.1

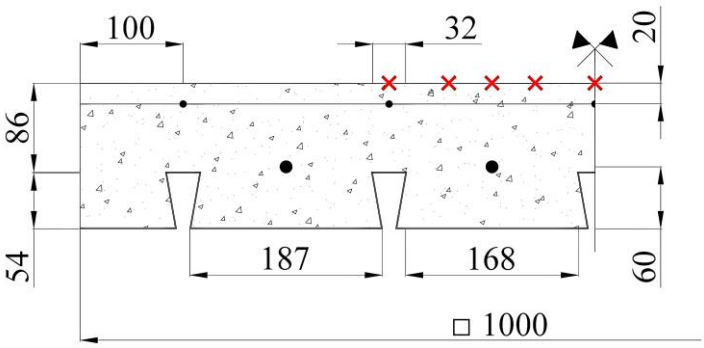

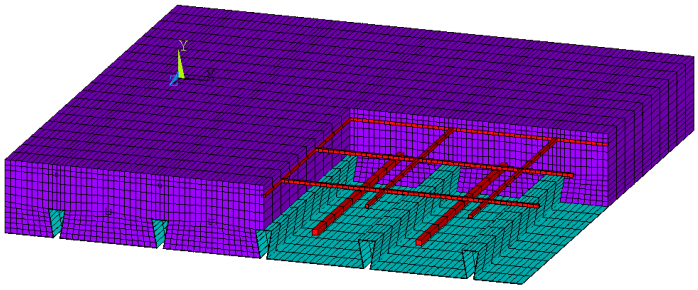

Finite element mesh

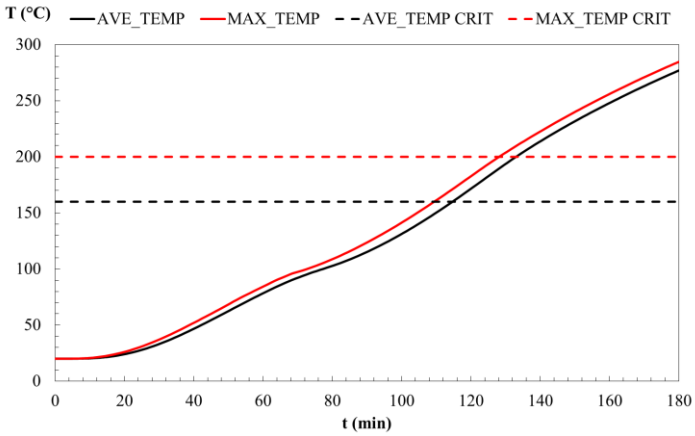

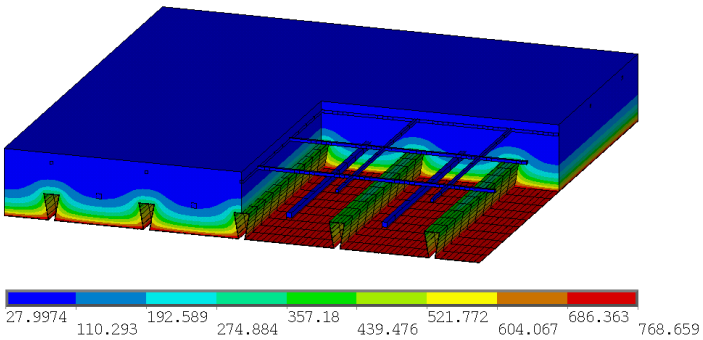

t= 28.7 min

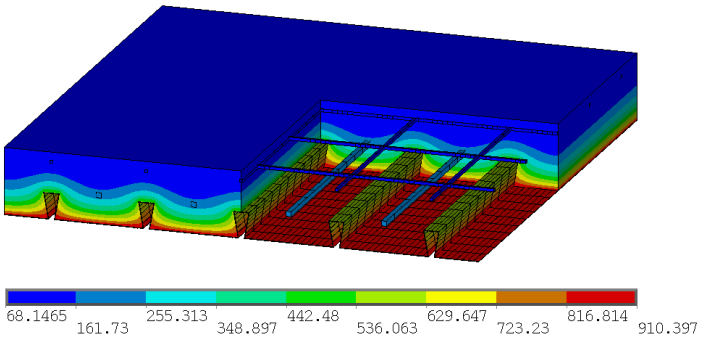

t= 57.4 min

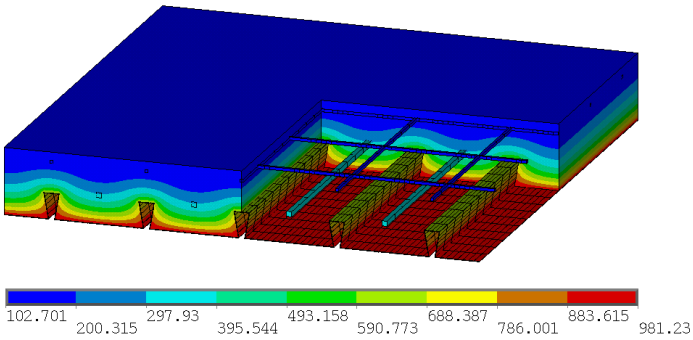

t= 86.0 min

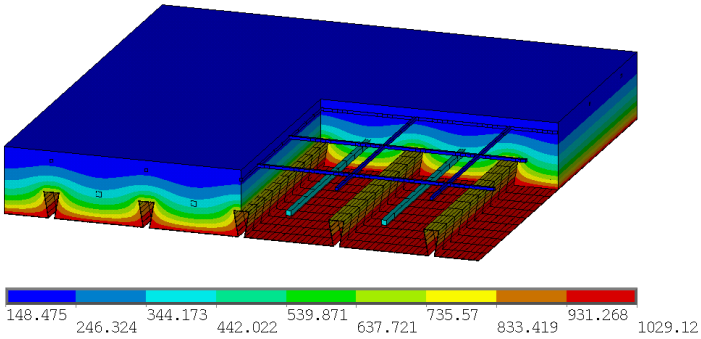

t= 114.7 min

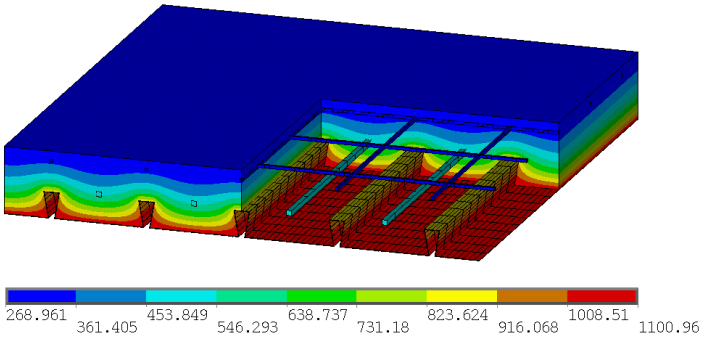

t= 180.0 min

SIM. 185	**Steel deck:** Lysaght Bondek	**Rebar (mm):** ϕ12	**Fire resistance (min)**	
	Mesh (mm//mm): ϕ7.6//200 (RM82)	**h_1 (mm):** 56	Ave: *69.8*	Max: 72.3

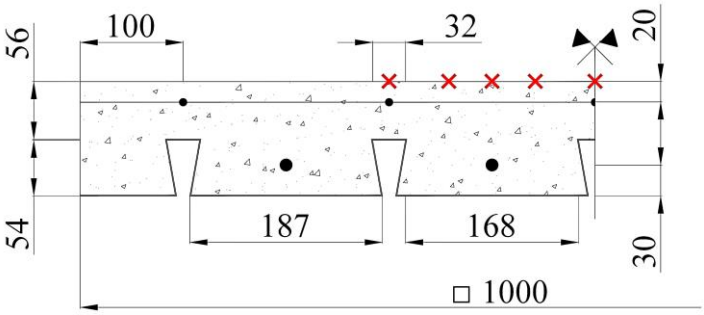

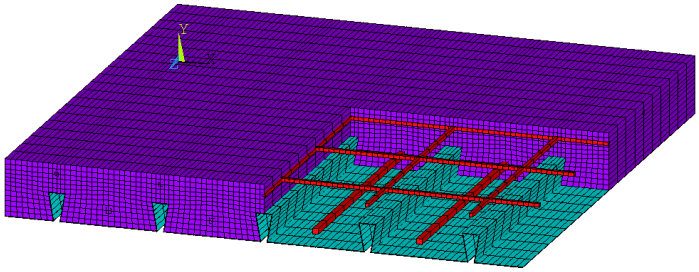

Finite element mesh

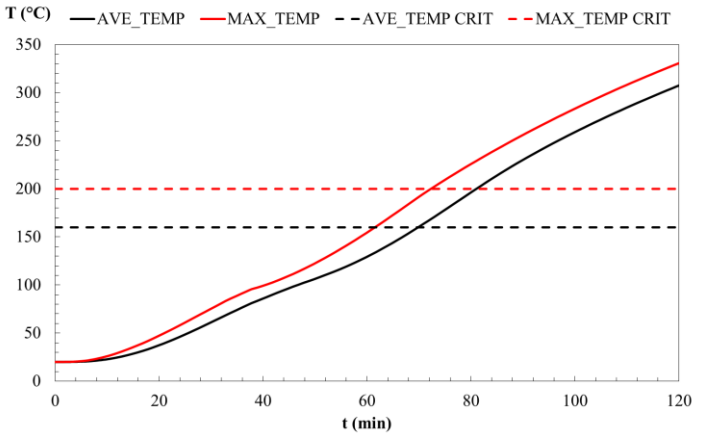

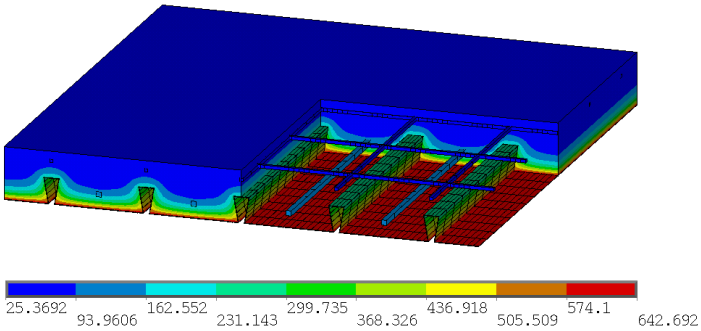

t= 17.5 min

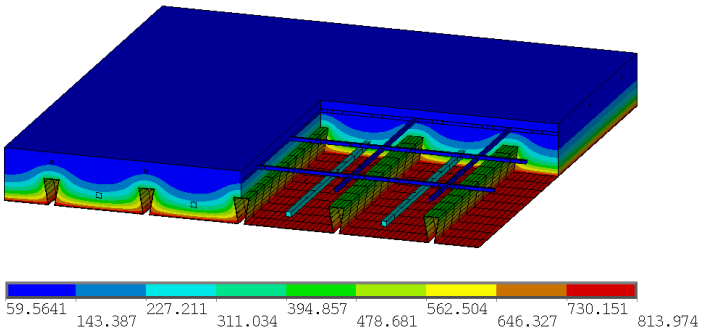

t= 34.9 min

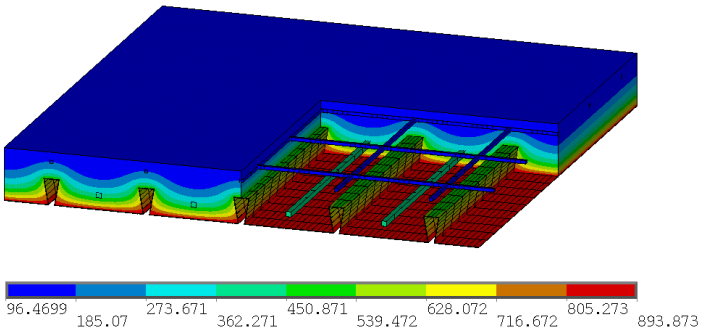

t= 52.4 min

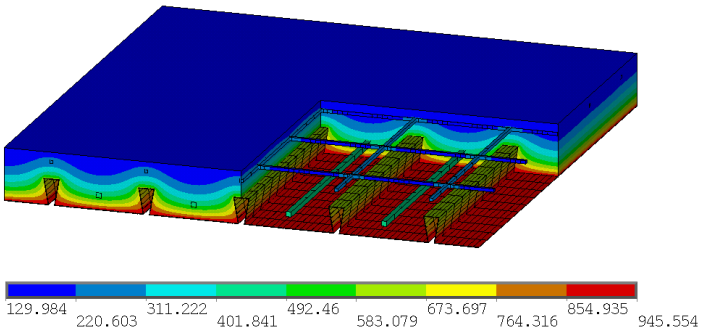

t= 69.8 min

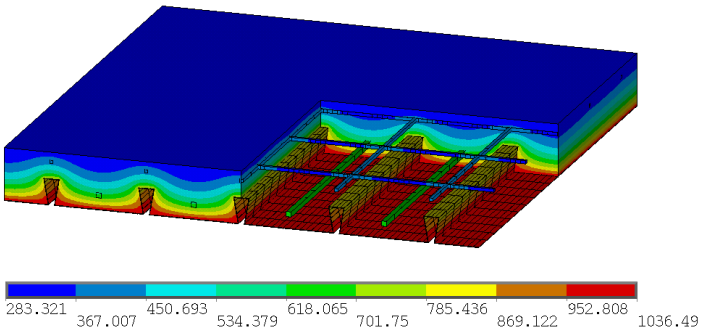

t= 120.0 min

SIM. 186	**Steel deck:** Lysaght Bondek	**Rebar (mm):** ϕ12	**Fire resistance (min)**	
	Mesh (mm//mm): ϕ7.6//200 (RM82)	**h_1 (mm):** 66	Ave: *83.6*	Max: 89.5

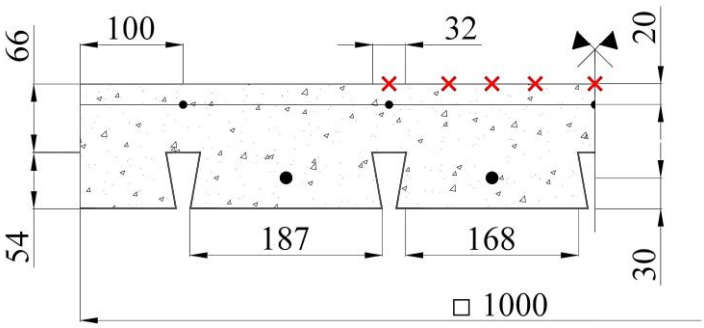

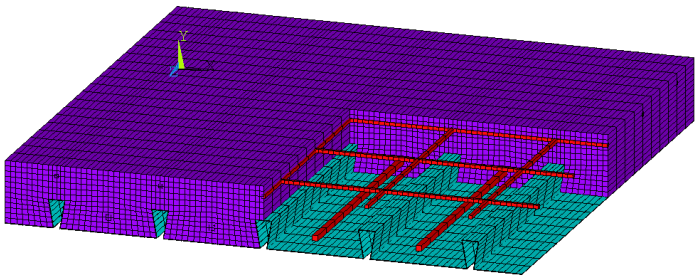

Finite element mesh

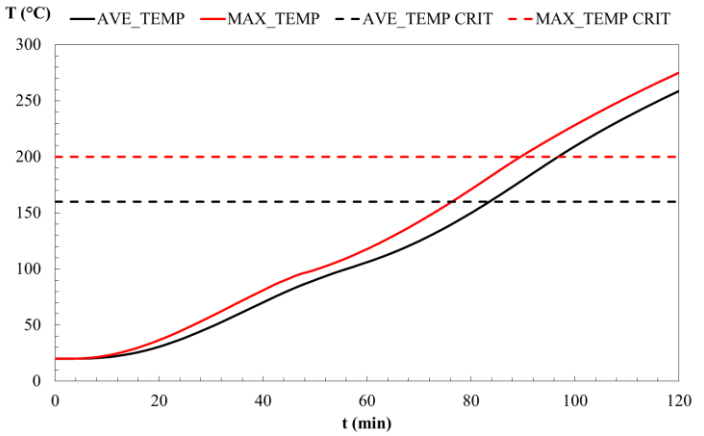

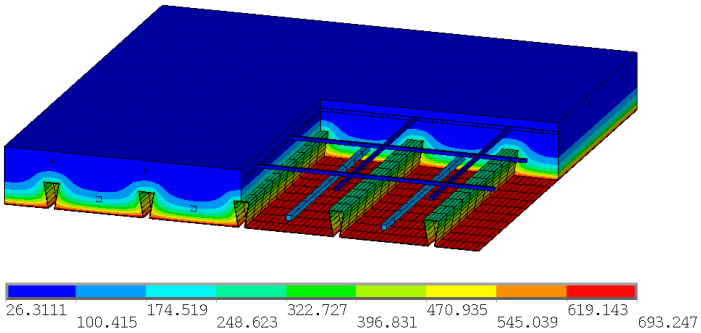

t= 20.9 min

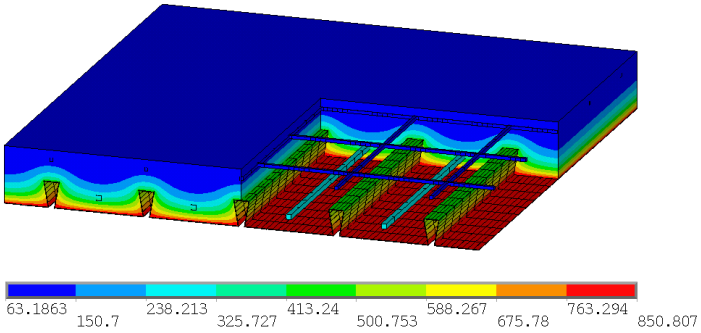

t= 41.8 min

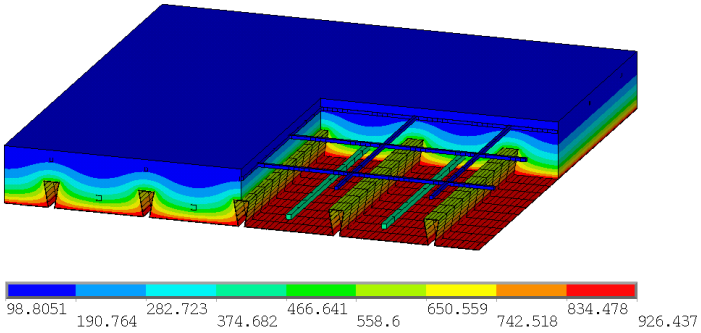

t= 62.7 min

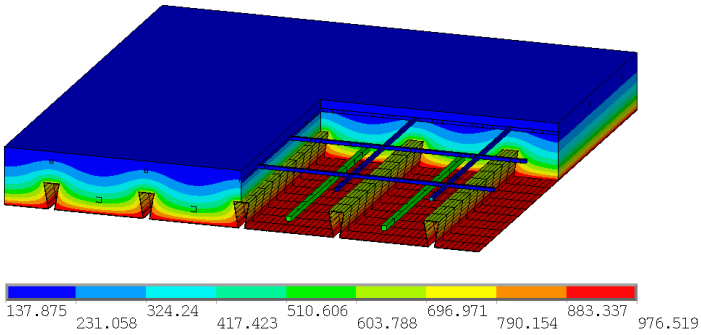

t= 83.6 min

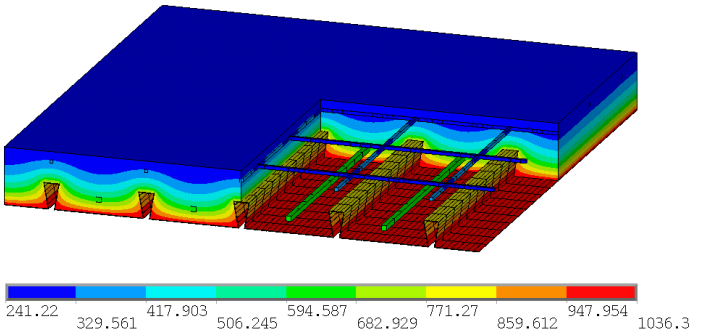

t= 120.0 min

SIM. 187	**Steel deck:** Lysaght Bondek	**Rebar (mm):** ϕ12	**Fire resistance (min)**	
	Mesh (mm//mm): ϕ7.6//200 (RM82)	**h_1 (mm):** 76	Ave: *98.5*	Max: 108.3

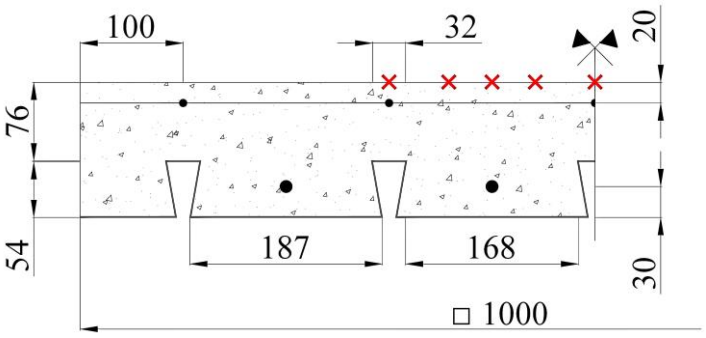

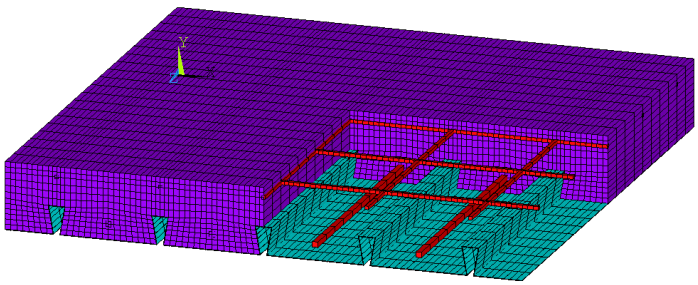

Finite element mesh

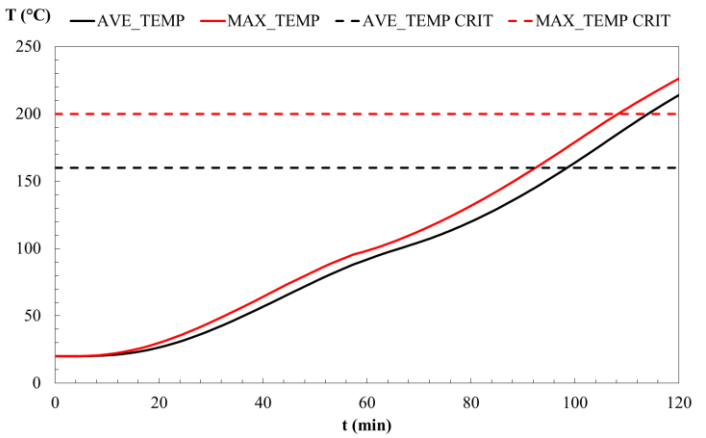

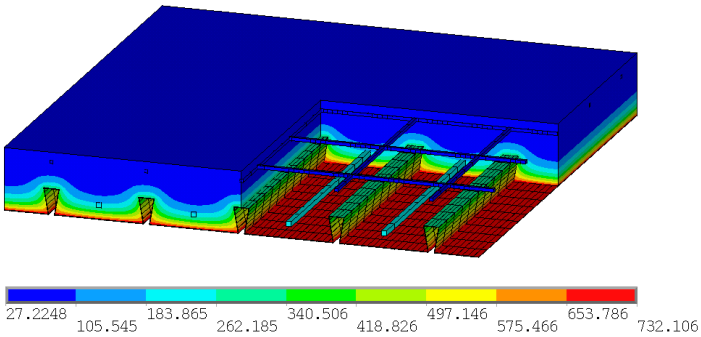

t= 24.6 min

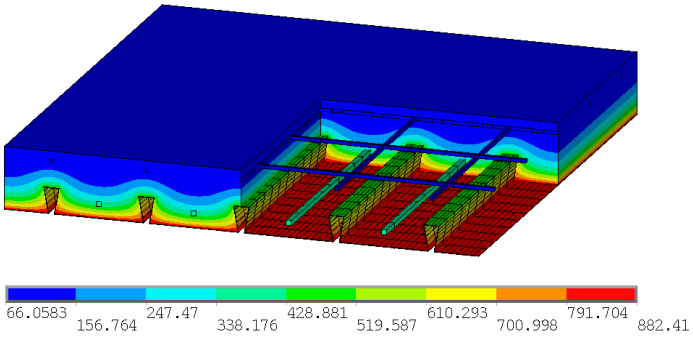

t= 49.3 min

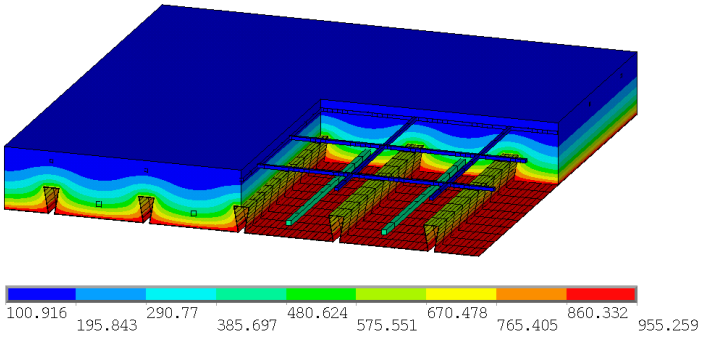

t= 73.9 min

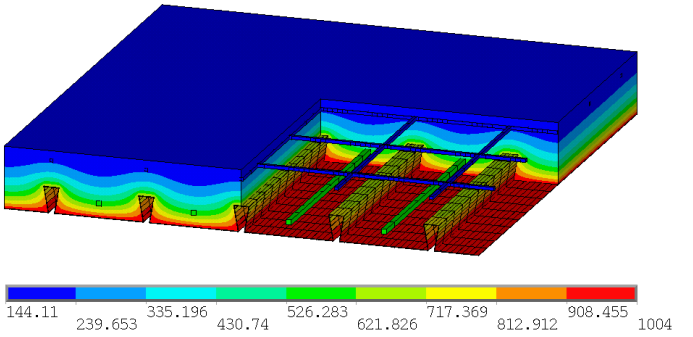

t= 98.5 min

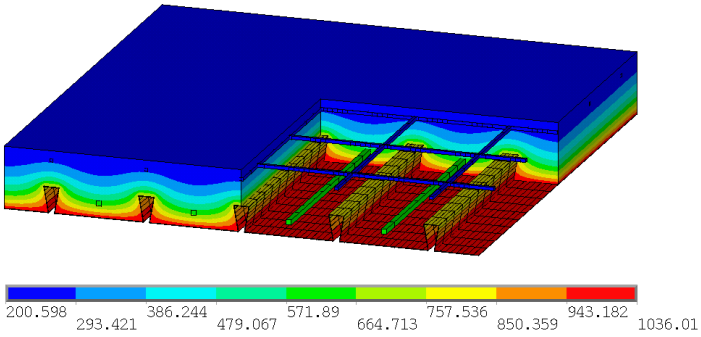

t= 120.0 min

SIM. 188	**Steel deck:** Lysaght Bondek	**Rebar (mm):** ϕ12	**Fire resistance (min)**	
	Mesh (mm//mm): ϕ7.6//200 (RM82)	**h_1 (mm):** 86	Ave: *114.7*	Max: 128.5

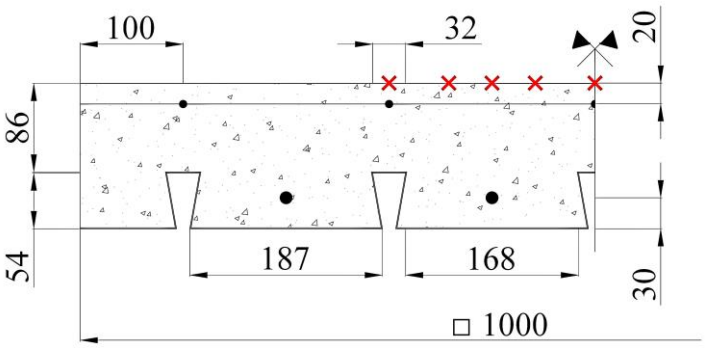

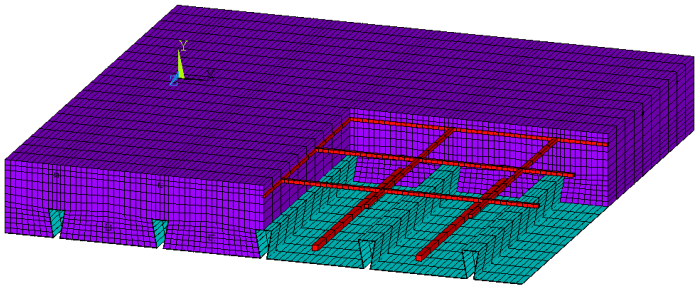

Finite element mesh

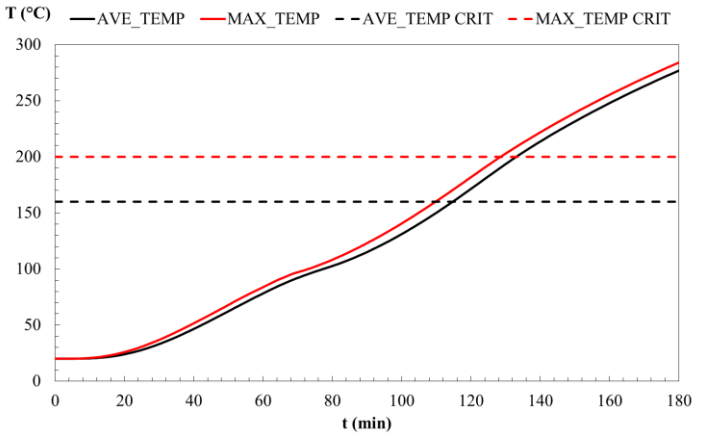

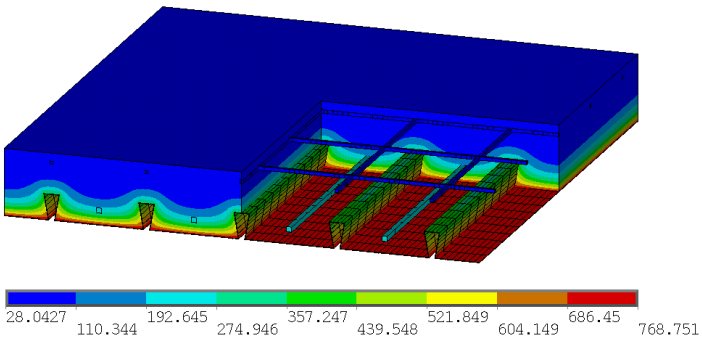

t= 28.7 min

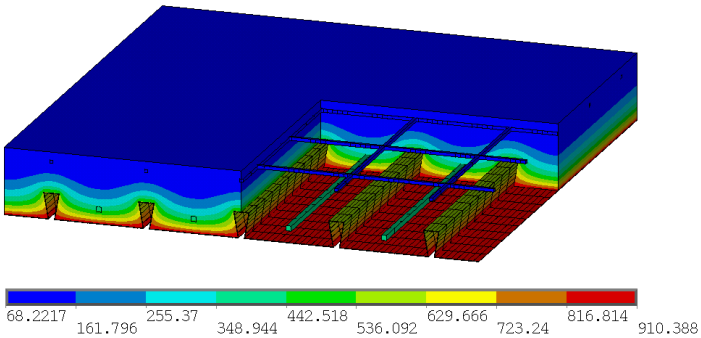

t= 57.4 min

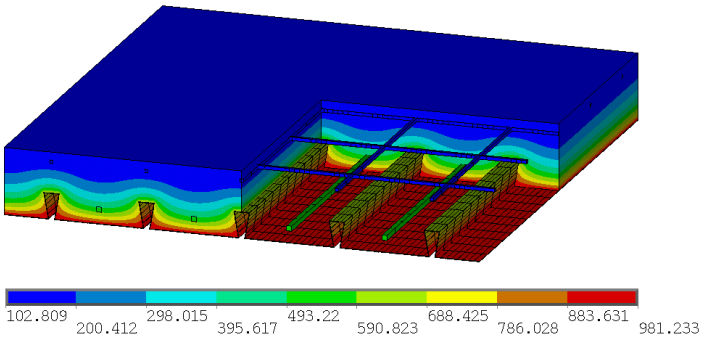

t= 86.0 min

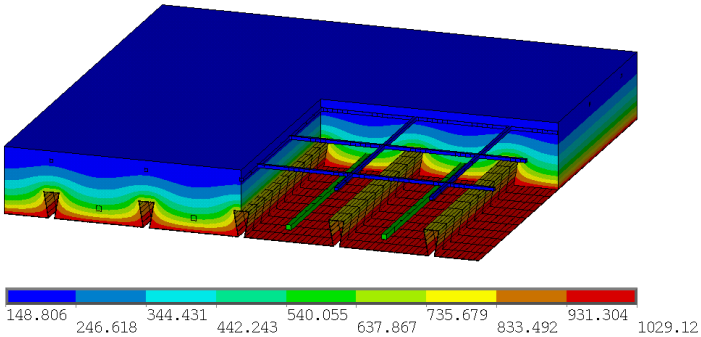

t= 114.7 min

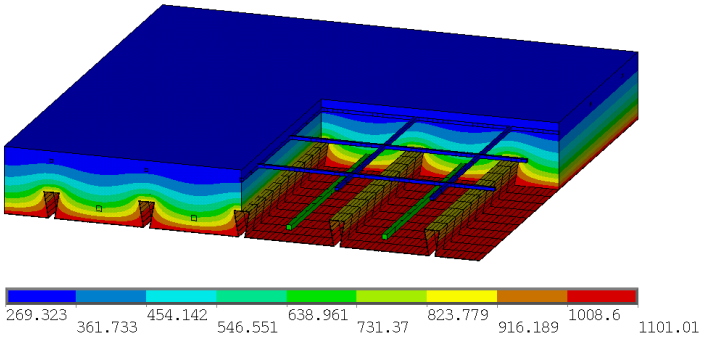

t= 180.0 min

SIM. 189	**Steel deck:** Lysaght Bondek	**Rebar (mm):** ϕ12	**Fire resistance (min)**	
	Mesh (mm//mm): ϕ7.6//200 (RM82)	**h_1 (mm):** 56	Ave: *69.9*	Max: 72.2

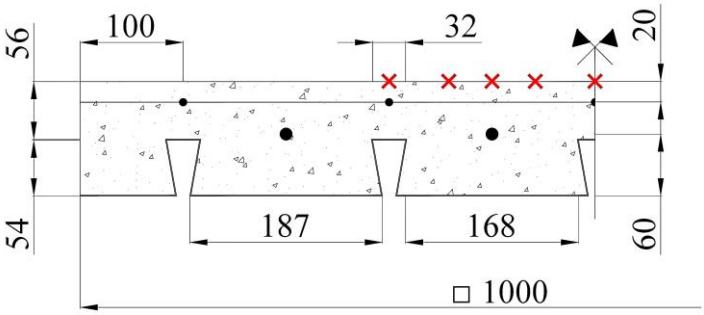

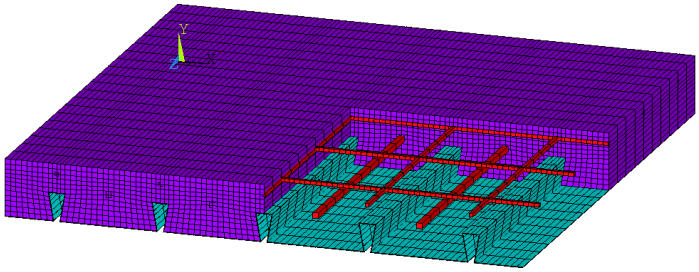

Finite element mesh

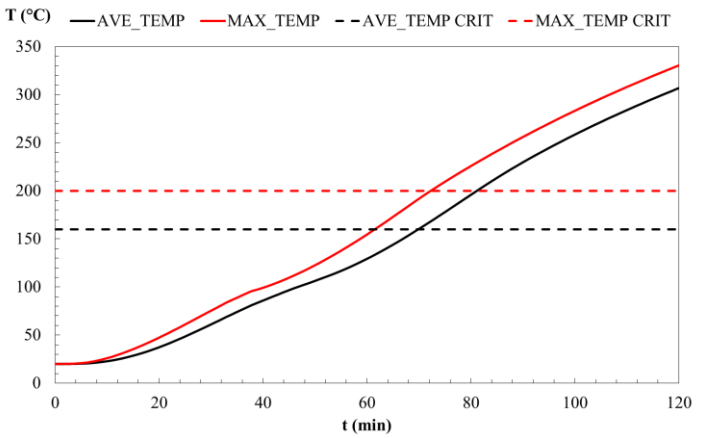

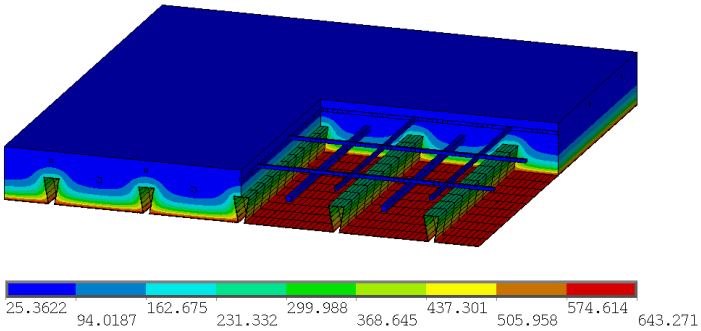

t= 17.5 min

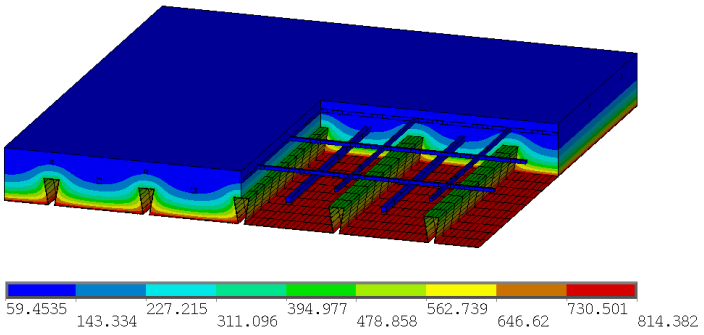

t= 35.0 min

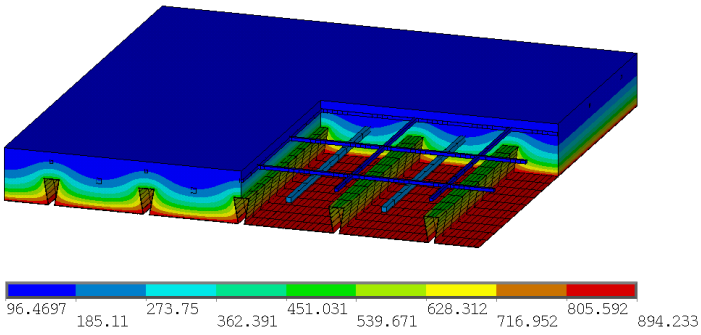

t= 52.4 min

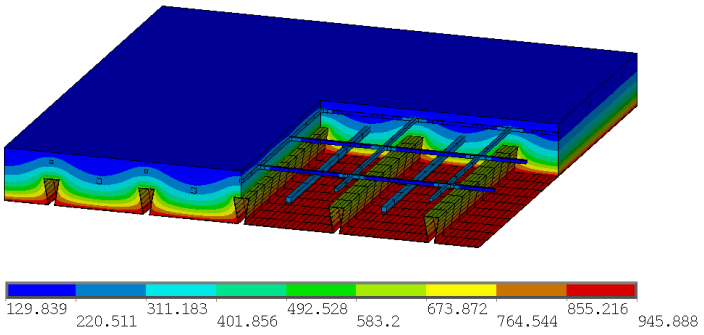

t= 69.9 min

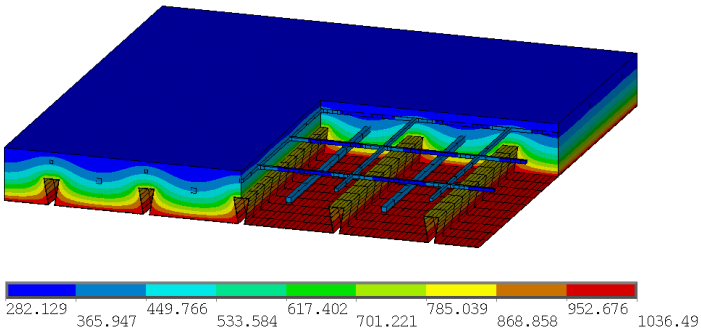

t= 120.0 min

SIM. 190	**Steel deck:** Lysaght Bondek	**Rebar (mm):** ϕ12	**Fire resistance (min)**	
	Mesh (mm//mm): ϕ7.6//200 (RM82)	**h_1 (mm):** 66	Ave: *83.6*	Max: 89.5

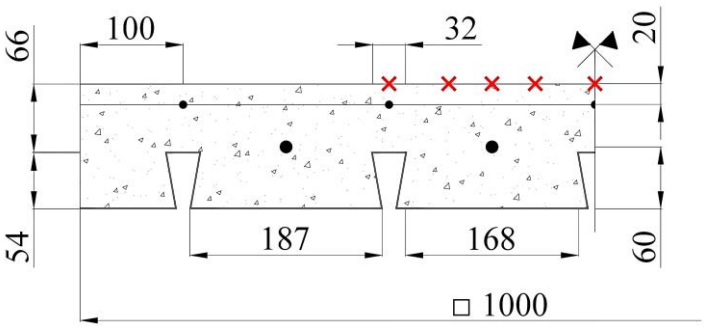

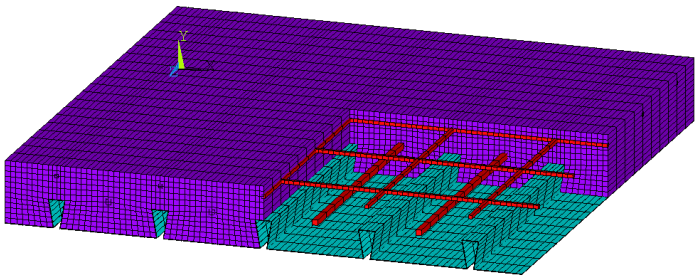

Finite element mesh

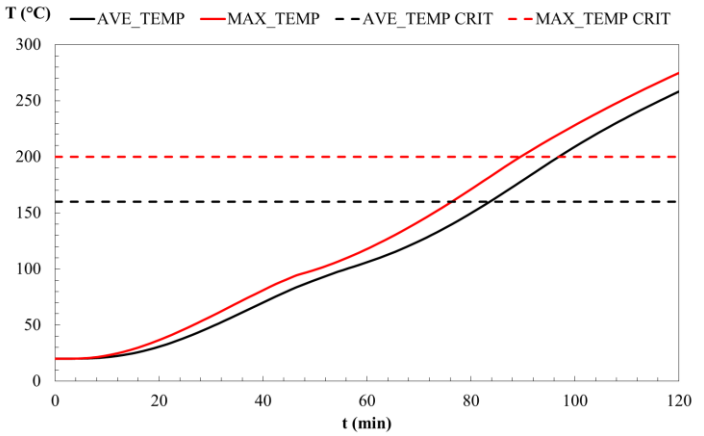

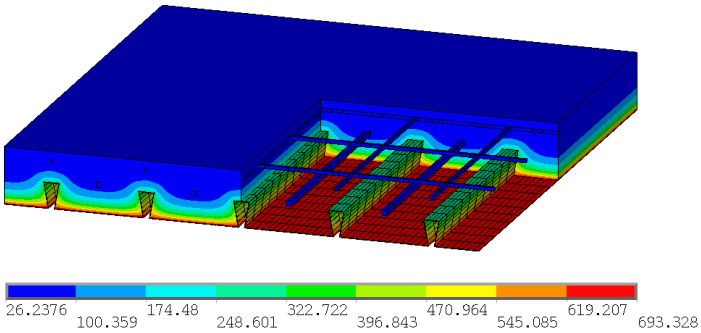

t= 20.9 min

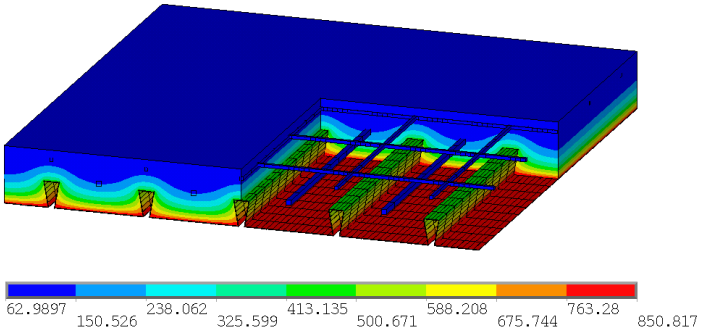

t= 41.8 min

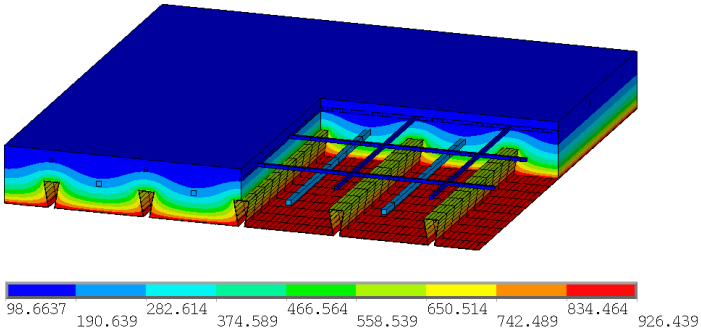

t= 62.7 min

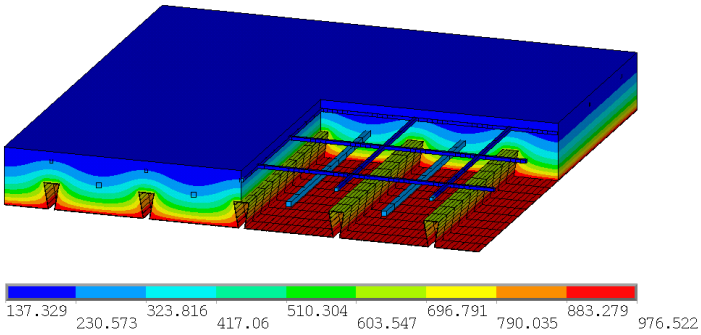

t= 83.6 min

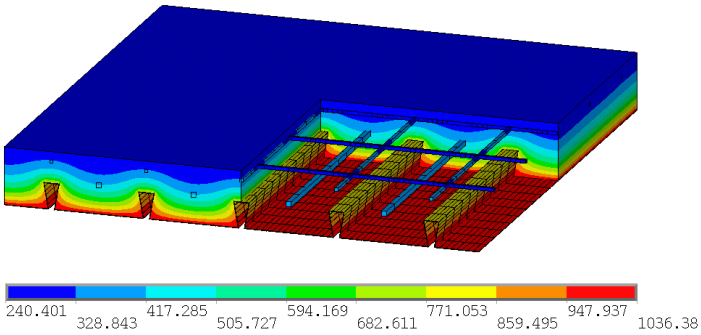

t= 120.0 min

SIM. 191	**Steel deck:** Lysaght Bondek	**Rebar (mm):** ϕ12	**Fire resistance (min)**	
	Mesh (mm//mm): ϕ7.6//200 (RM82)	**h_1 (mm):** 76	Ave: *98.6*	Max: 108.3

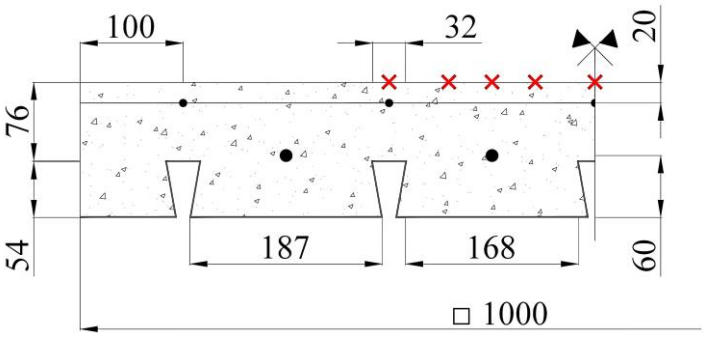

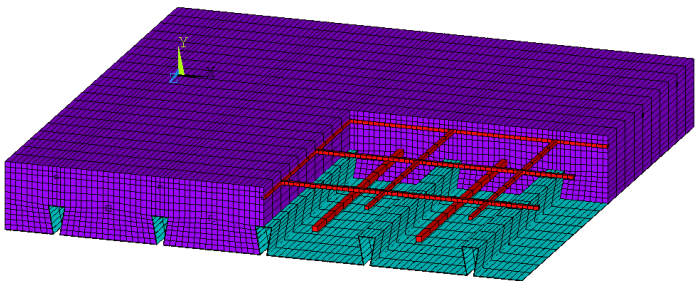

Finite element mesh

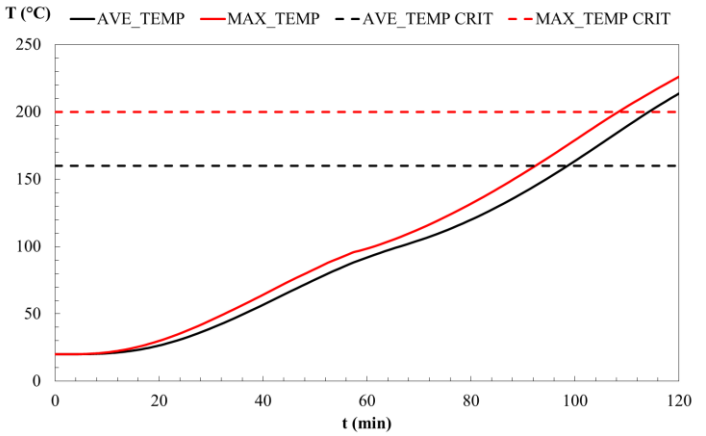

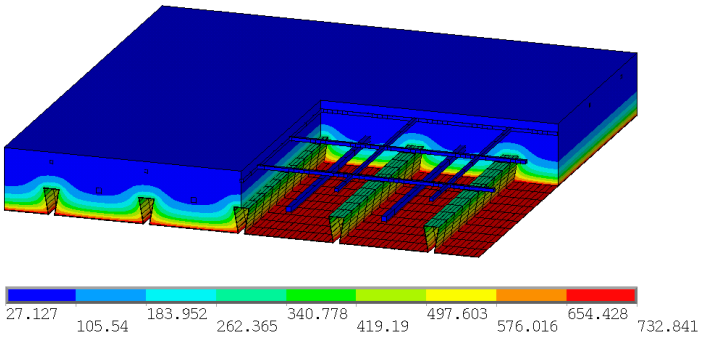

t= 24.7 min

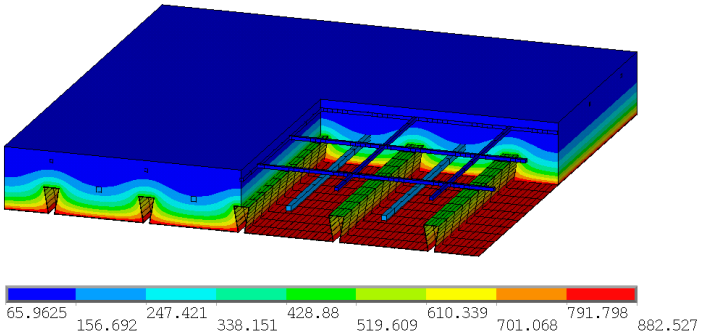

t= 49.3 min

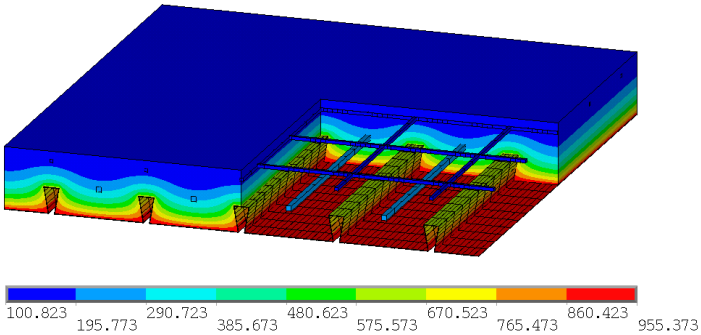

t= 74.0 min

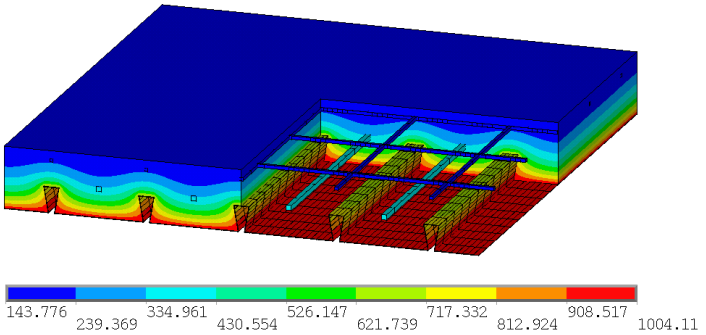

t= 98.6 min

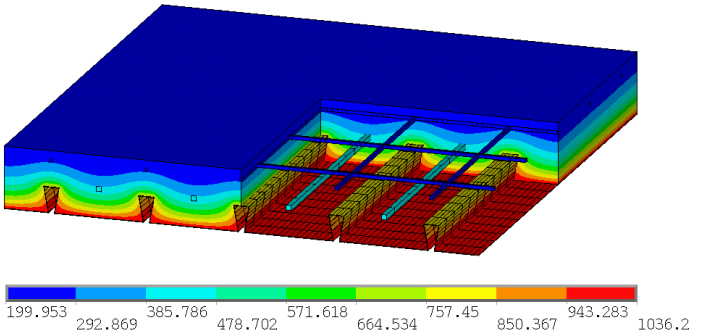

t= 120.0 min

SIM. 192	**Steel deck:** Lysaght Bondek	**Rebar (mm):** ϕ12	**Fire resistance (min)**	
	Mesh (mm//mm): ϕ7.6//200 (RM82)	**h_1 (mm):** 86	Ave: *114.9*	Max: 128.6

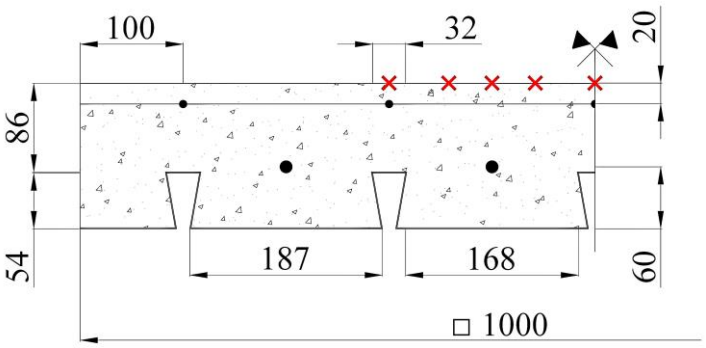

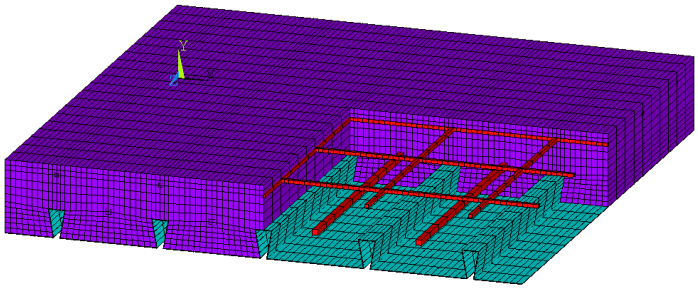

Finite element mesh

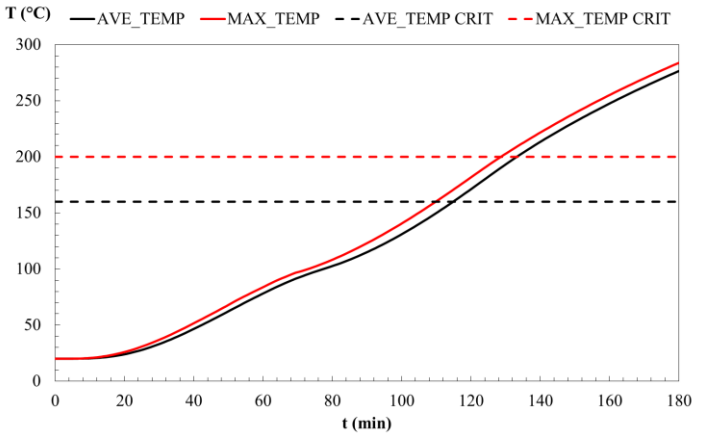

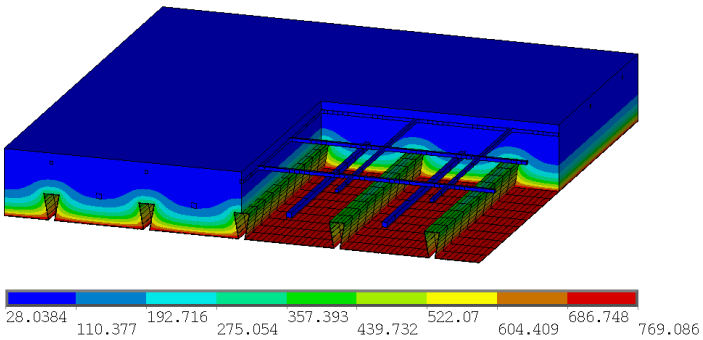

t= 28.7 min

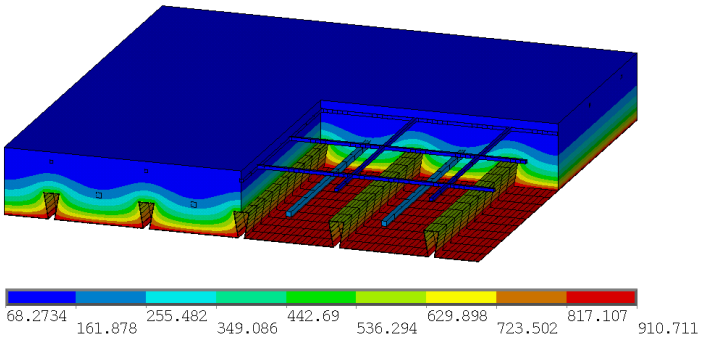

t= 57.5 min

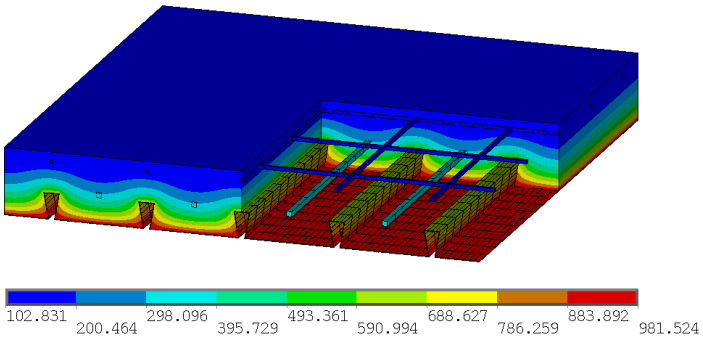

t= 86.2 min

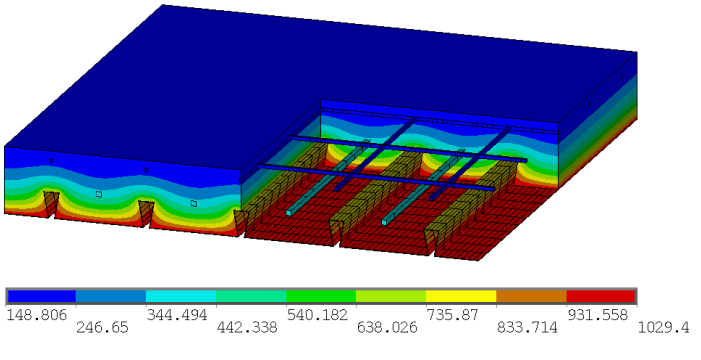

t= 114.9 min

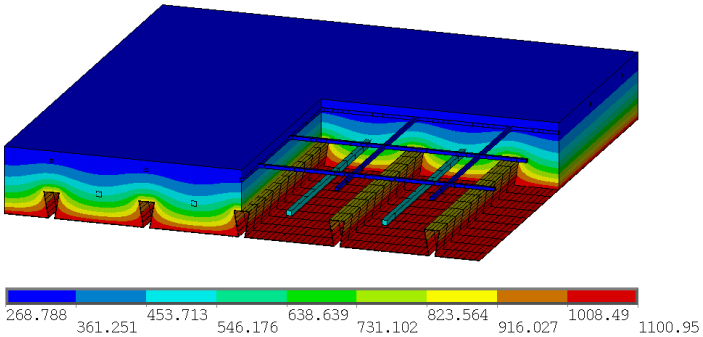

t= 180.0 min

SIM. 193	**Steel deck:** Trapezoidal – O Feliz H60	**Rebar (mm): -**	**Fire resistance (min)**	
	Mesh (mm//mm): ϕ6//100 (FNQ 60)	**h_1 (mm):** 50	Ave: 36.1	Max: *34.5*

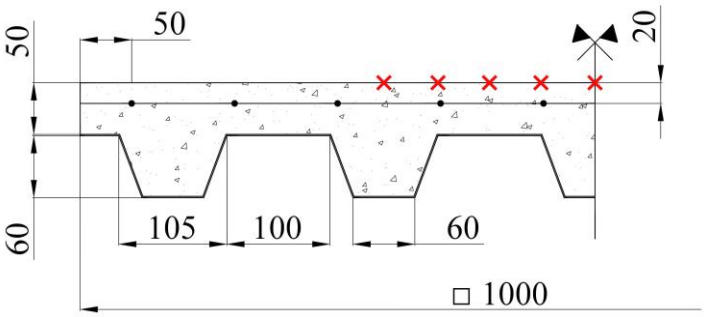

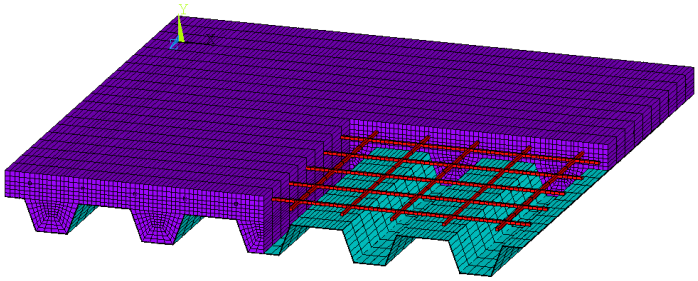

Finite element mesh

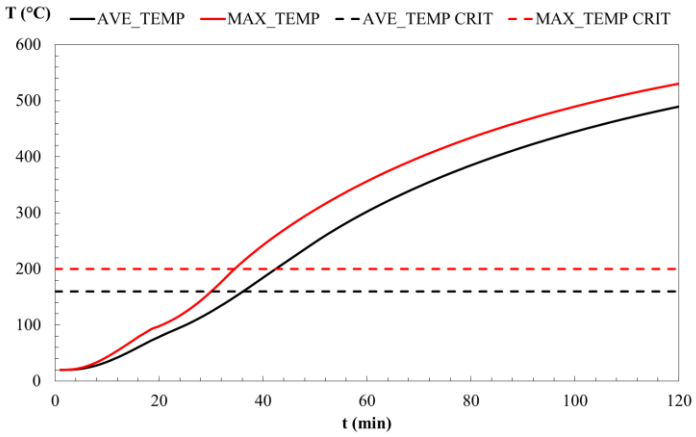

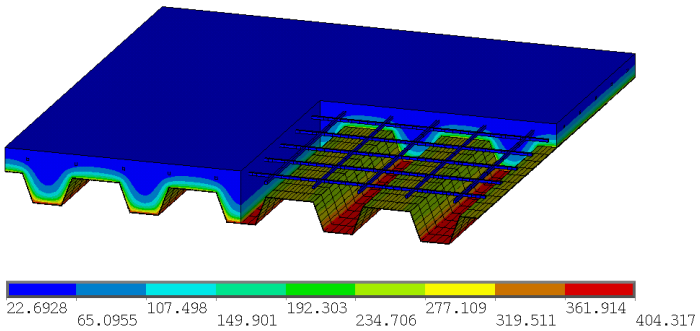

t= 8.6 min

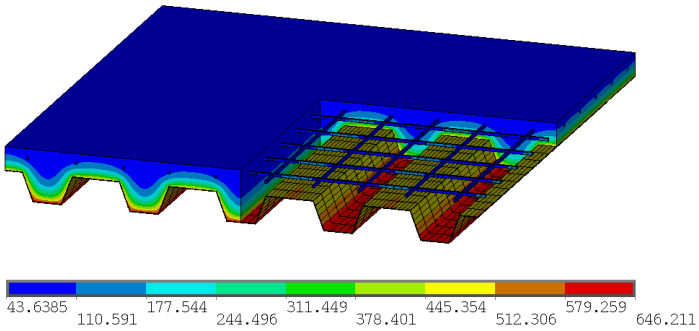

t= 17.3 min

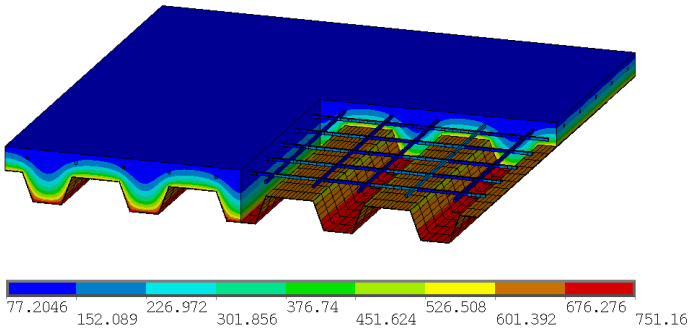

t= 25.9 min

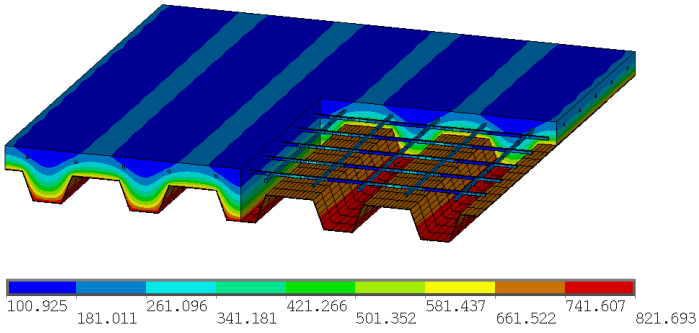

t= 34.5 min

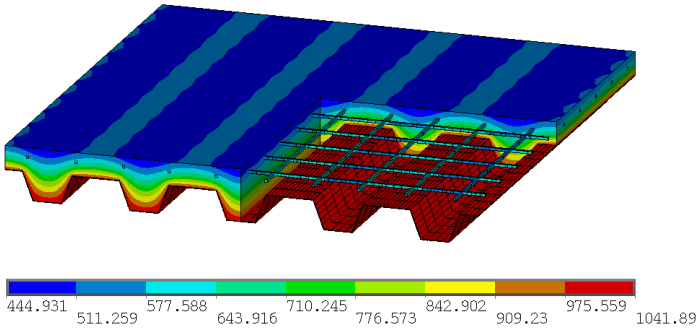

t= 120.0 min

SIM. 194	**Steel deck:** Trapezoidal – O Feliz H60	**Rebar (mm): -**	**Fire resistance (min)**	
	Mesh (mm//mm): ϕ6//100 (FNQ 60)	**h_1 (mm):** 60	Ave: 46.2	Max: *45.8*

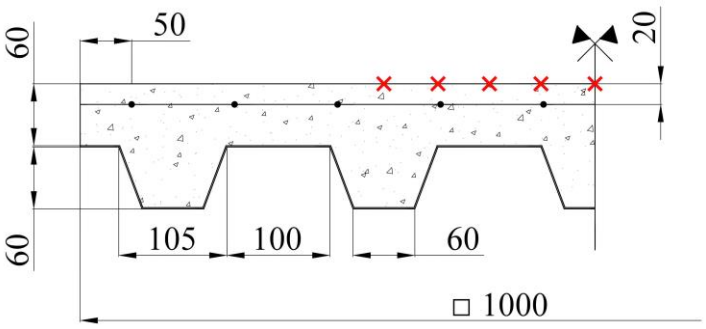

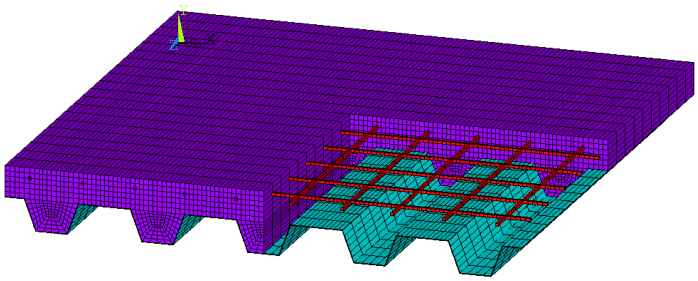

Finite element mesh

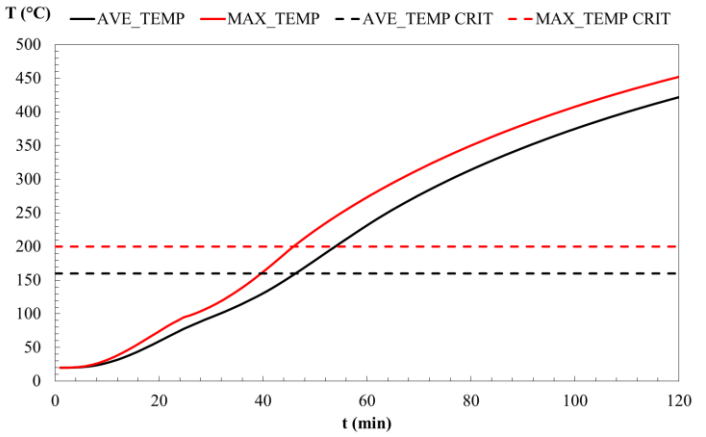

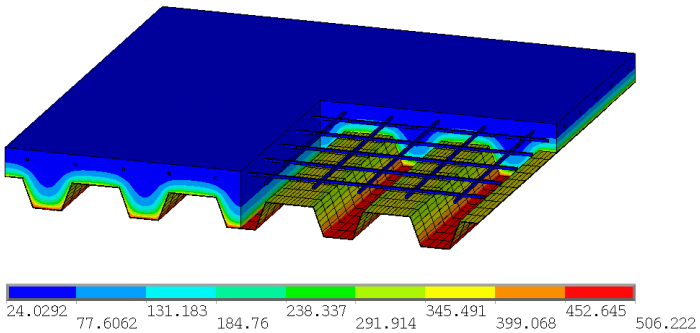

t= 11.5 min

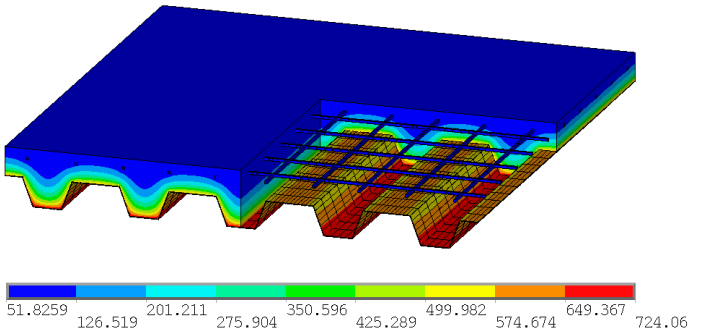

t= 22.9 min

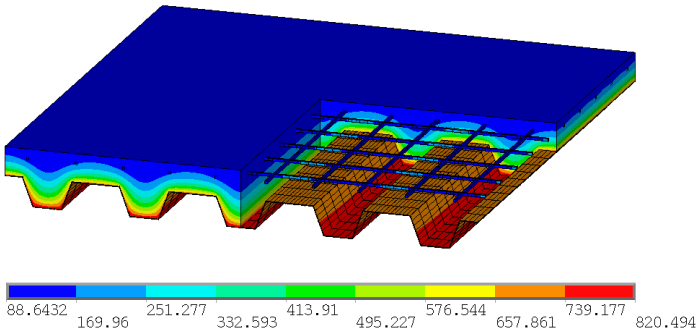

t= 34.4 min

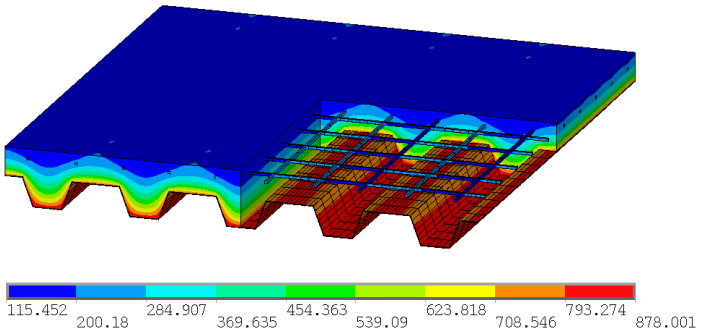

t= 45.8 min

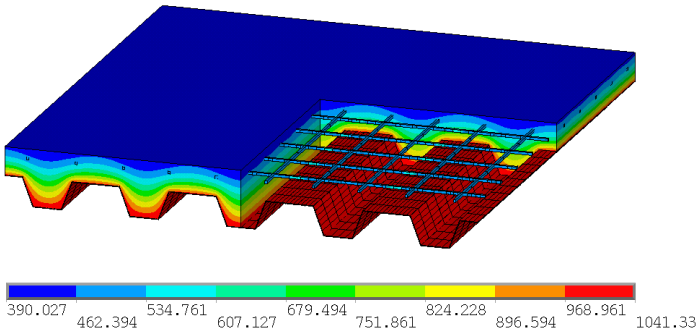

t= 120.0 min

SIM. 195	**Steel deck:** Trapezoidal – O Feliz H60	**Rebar (mm): -**	**Fire resistance (min)**	
	Mesh (mm//mm): ϕ6//100 (FNQ 60)	**h_1 (mm):** 70	Ave: *57.4*	Max: 59.1

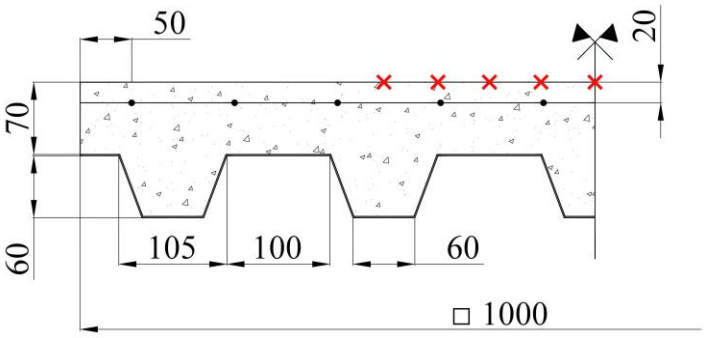

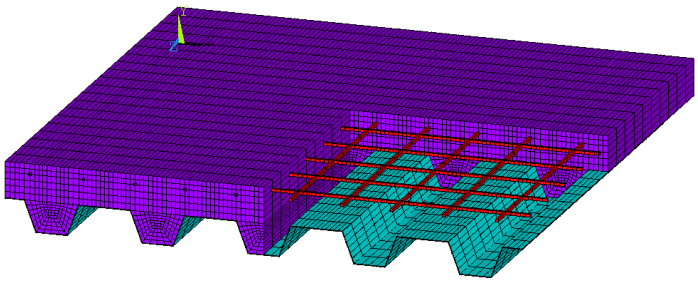

Finite element mesh

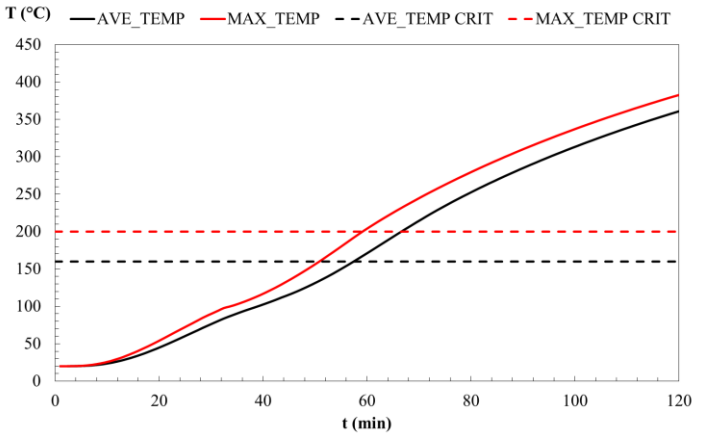

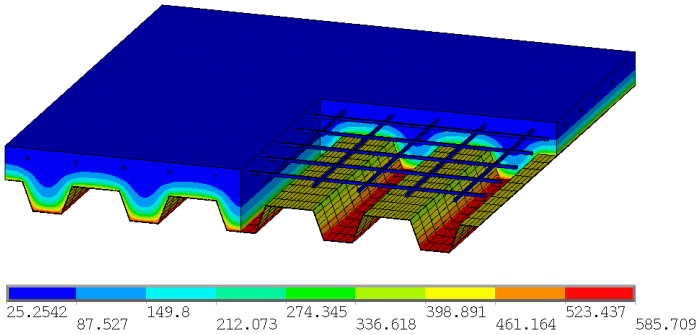

t= 14.4 min

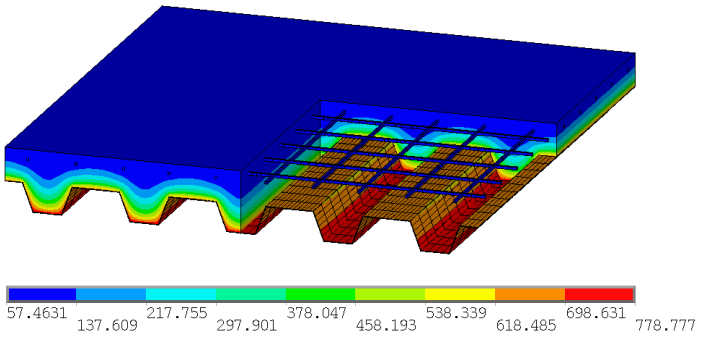

t= 28.7 min

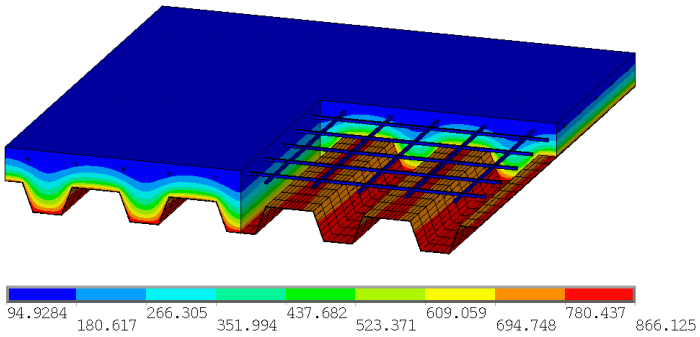

t= 43.1 min

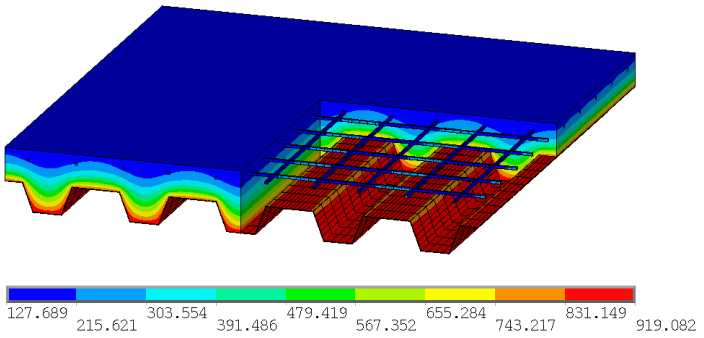

t= 57.4 min

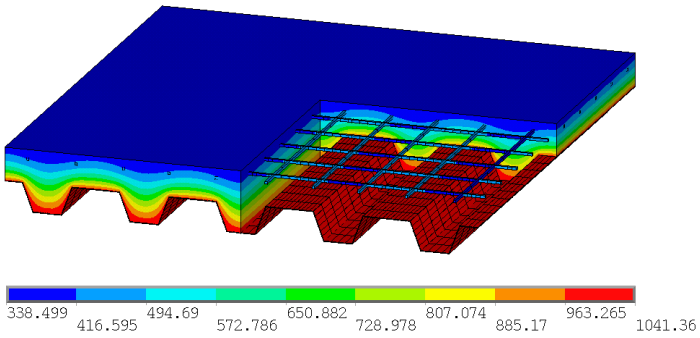

t= 120.0 min

SIM. 196	**Steel deck:** Trapezoidal – O Feliz H6	**Rebar (mm): -**	**Fire resistance (min)**	
	Mesh (mm//mm): ϕ6//100 (FNQ 60)	**h_1 (mm):** 80	Ave: *69.8*	Max: 74.3

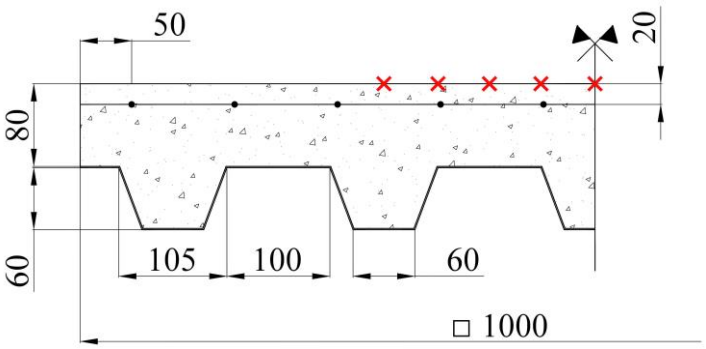

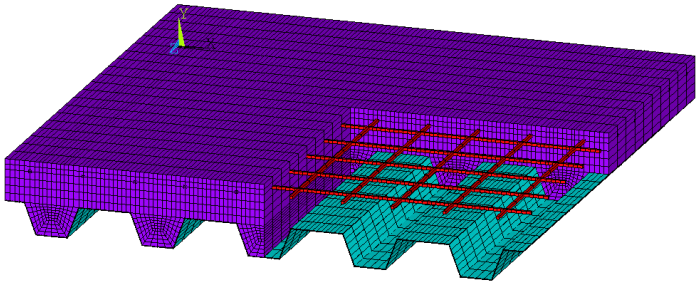

Finite element mesh

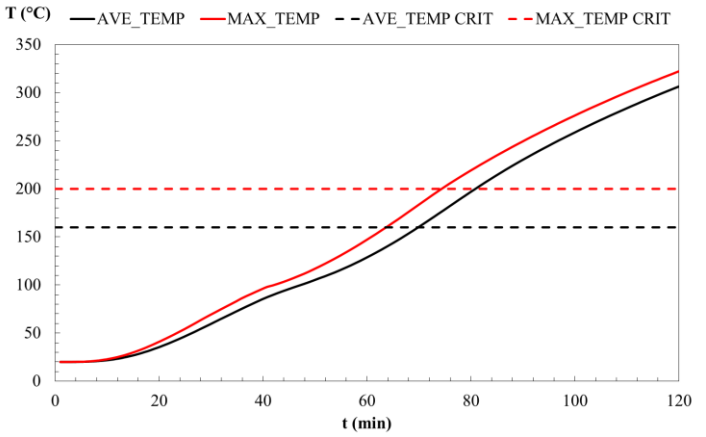

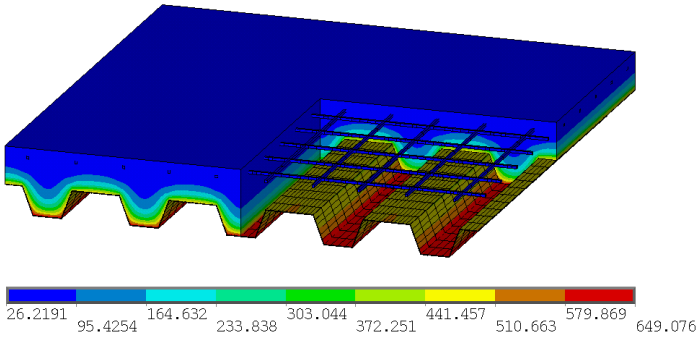

t= 17.5 min

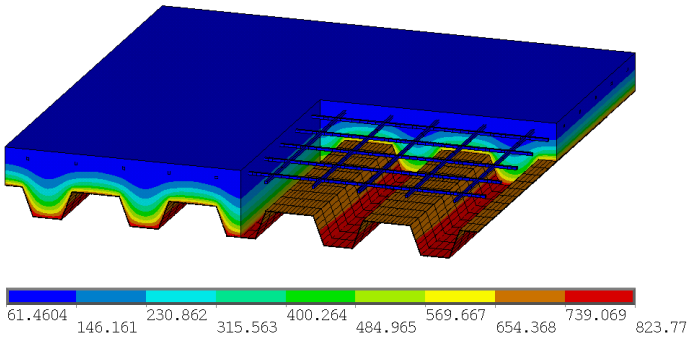

t= 34.9 min

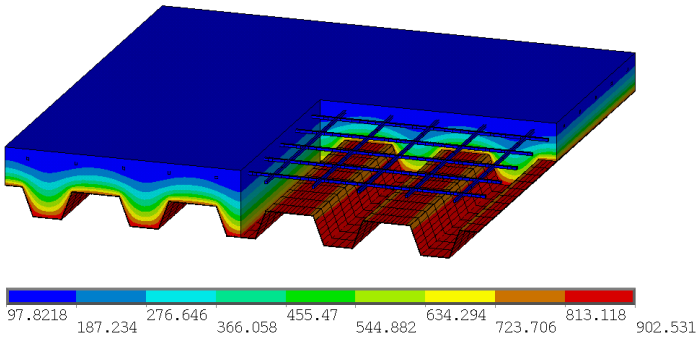

t= 52.4 min

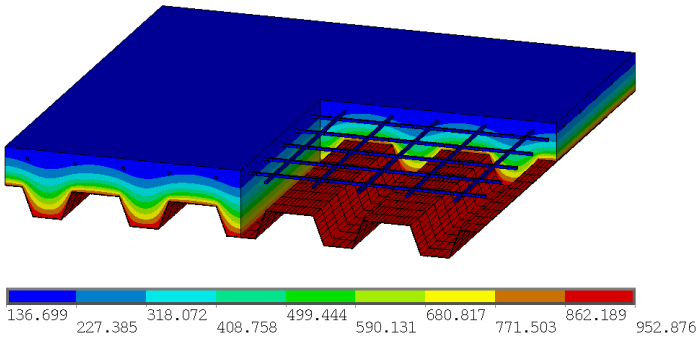

t= 69.8 min

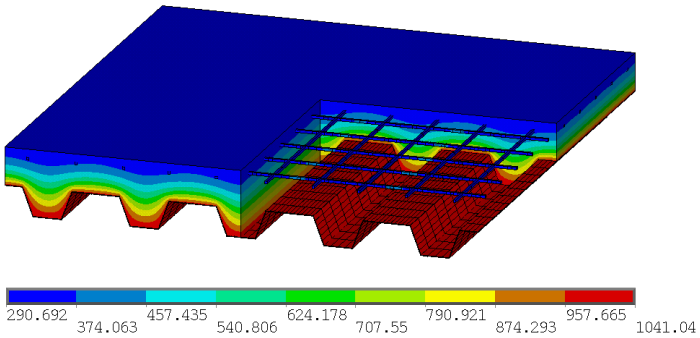

t= 120.0 min

SIM. 197	**St. deck:** Trapezoidal – ArcelorMittal Polydeck 59S	**Rebar (mm): -**	**Fire resistance (min)**	
	Mesh (mm//mm): ϕ6//100 (Q 283)	**h_1 (mm):** 51	Ave: 38.3	Max: *36.2*

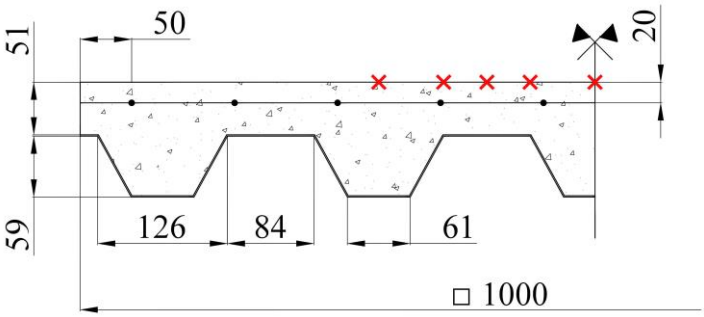

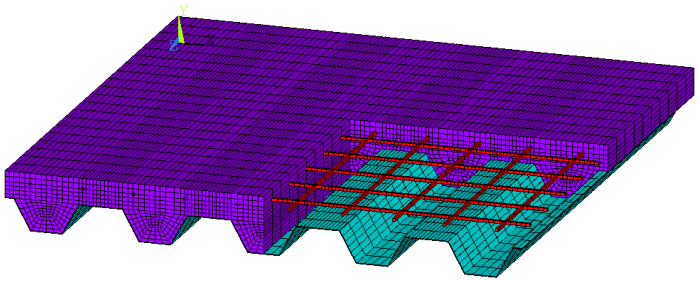

Finite element mesh

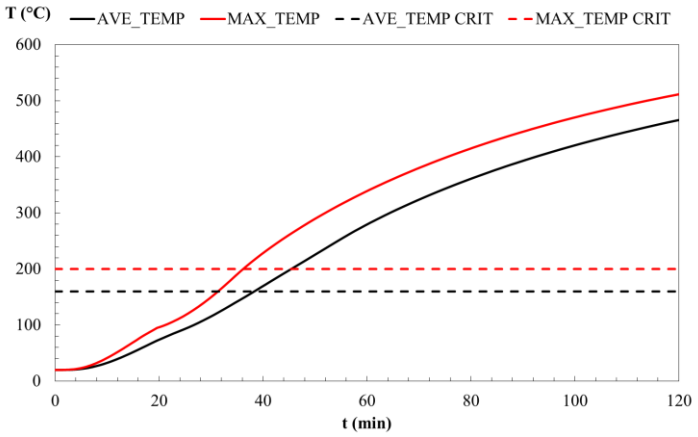

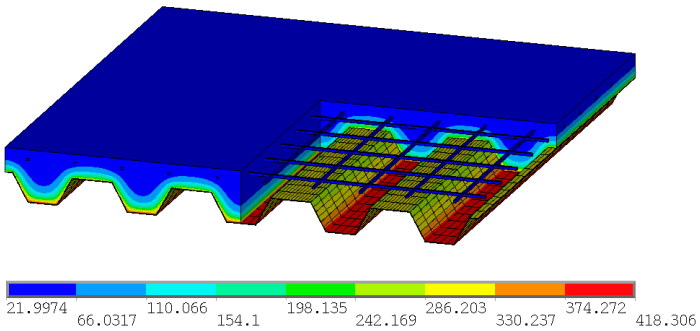

t= 9.1 min

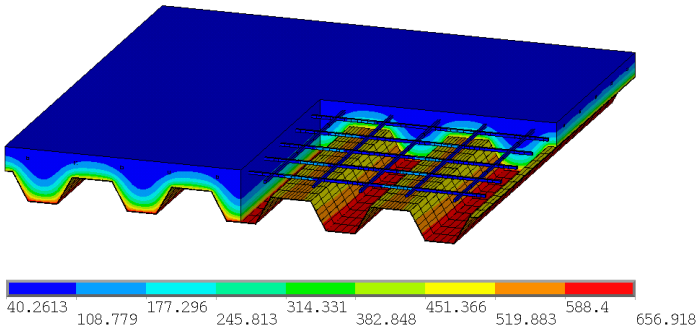

t= 18.1 min

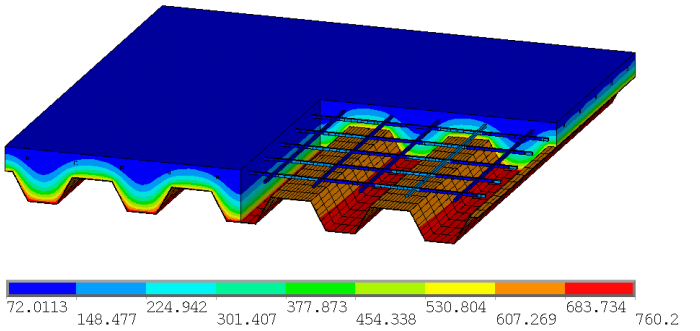

t= 27.2 min

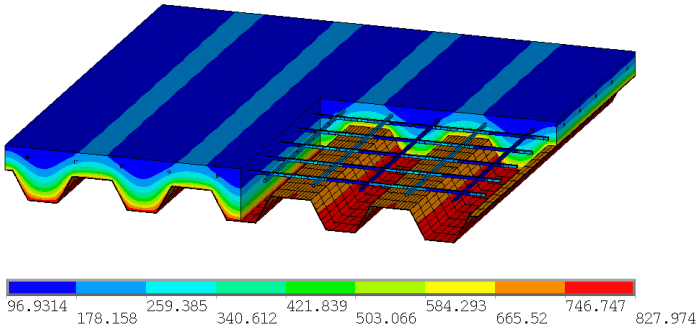

t= 36.2 min

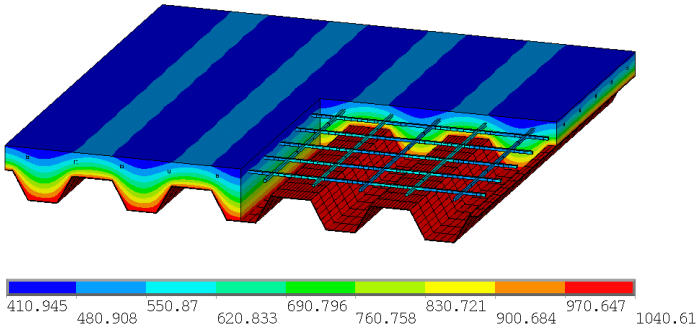

t= 120.0 min

SIM. 198	**St. deck:** Trapezoidal – ArcelorMittal Polydeck 59S	**Rebar (mm): -**	**Fire resistance (min)**	
	Mesh (mm//mm): ϕ6//100 (Q 283)	**h_1 (mm):** 61	Ave: 49.1	Max: *48.2*

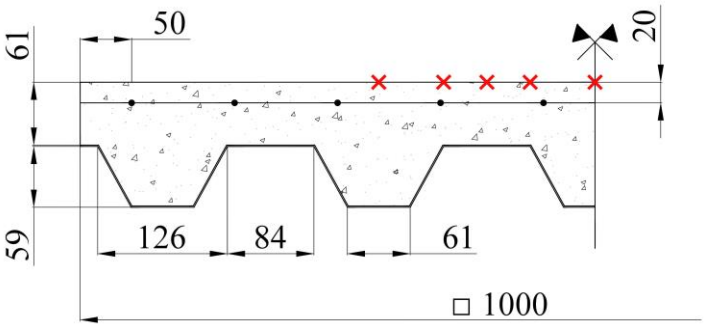

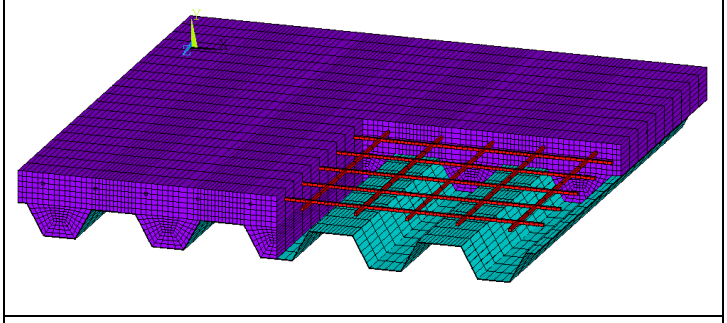

Finite element mesh

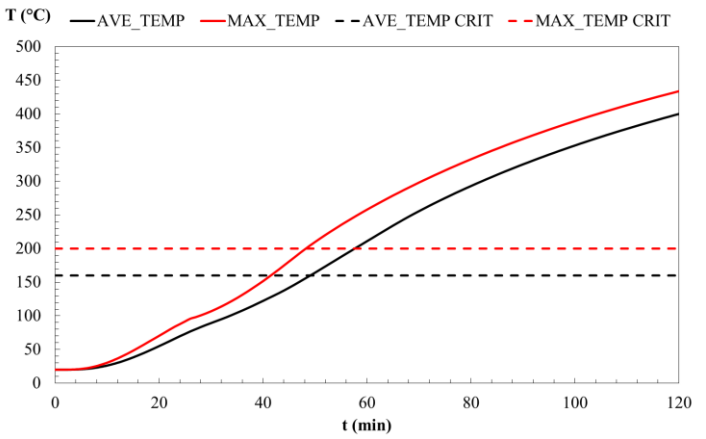

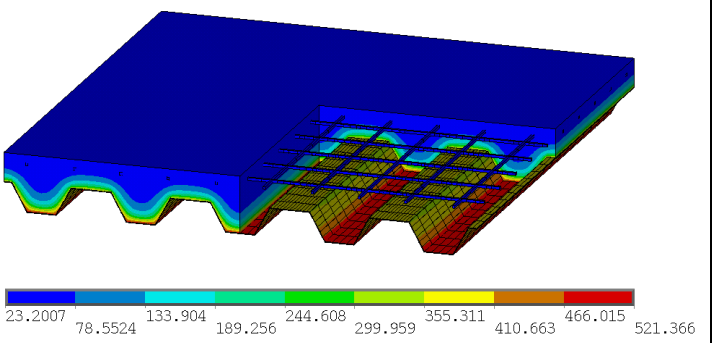

t= 12.1 min

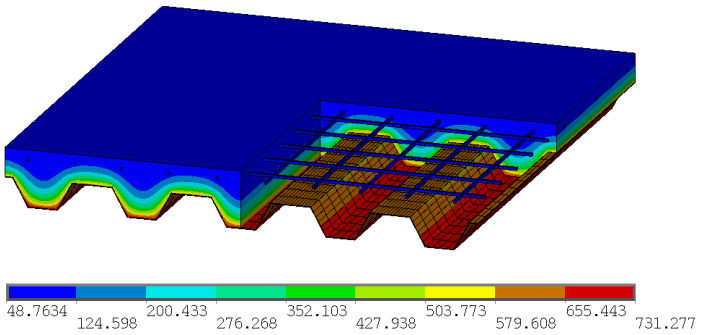

t= 24.1 min

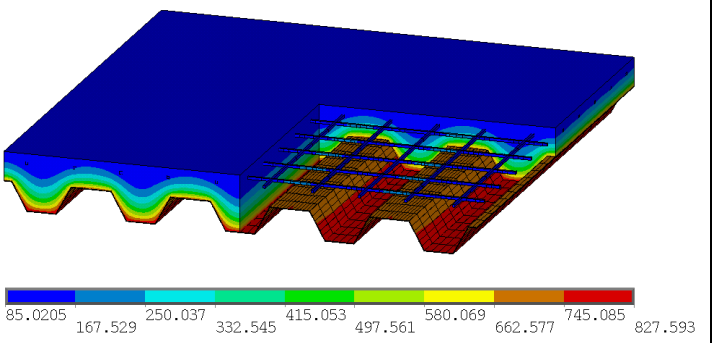

t= 36.2 min

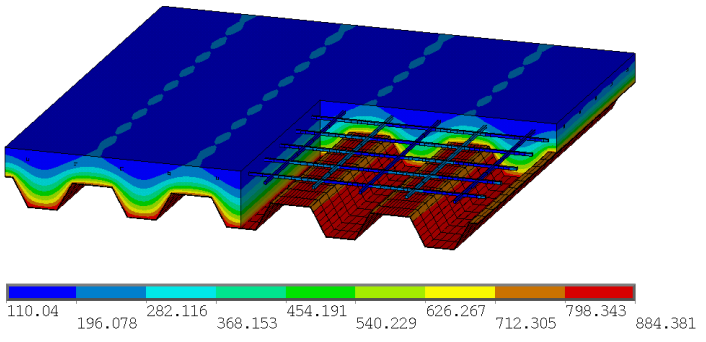

t= 48.2 min

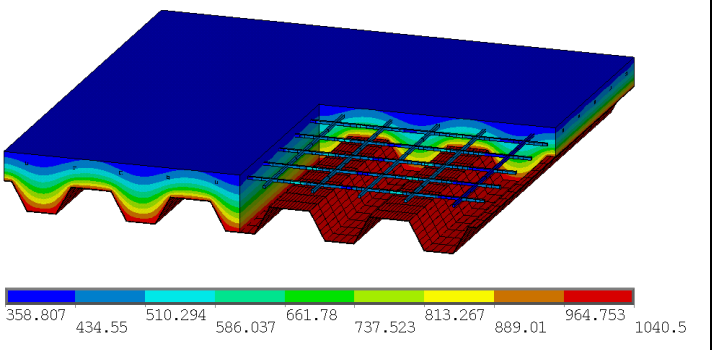

t= 120.0 min

SIM. 199	**St. deck:** Trapezoidal – ArcelorMittal Polydeck 59S	**Rebar (mm): -**	**Fire resistance (min)**	
	Mesh (mm//mm): ϕ6//100 (Q 283)	**h_1 (mm):** 71	Ave: *60.9*	Max: 62.3

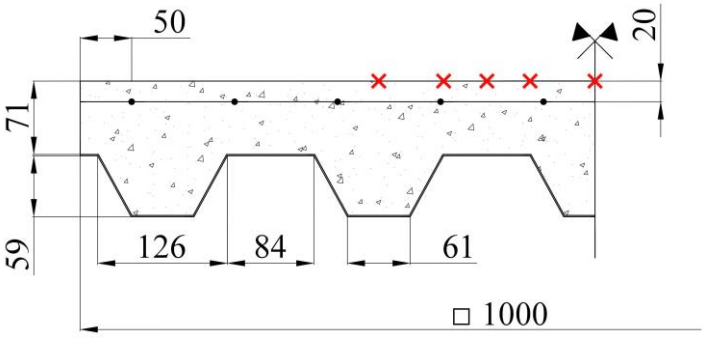

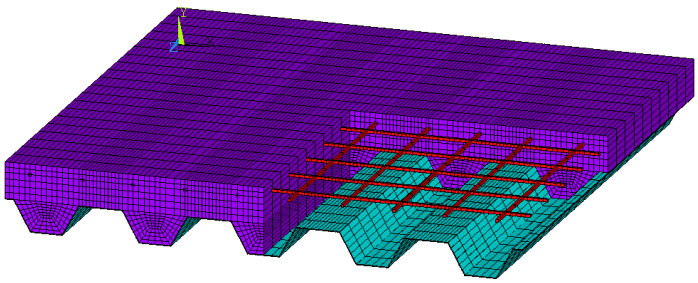

Finite element mesh

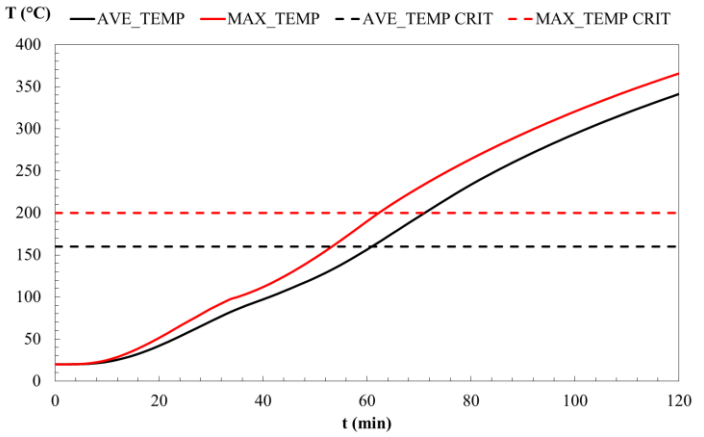

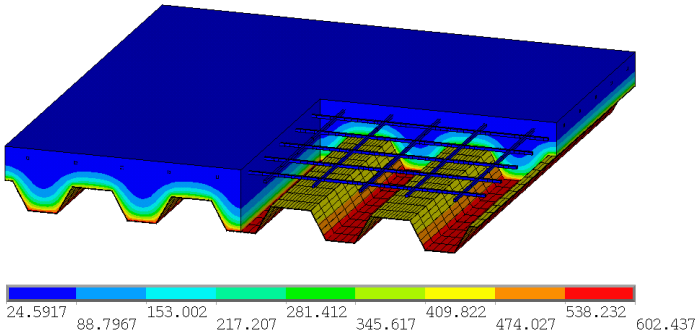

t= 15.2 min

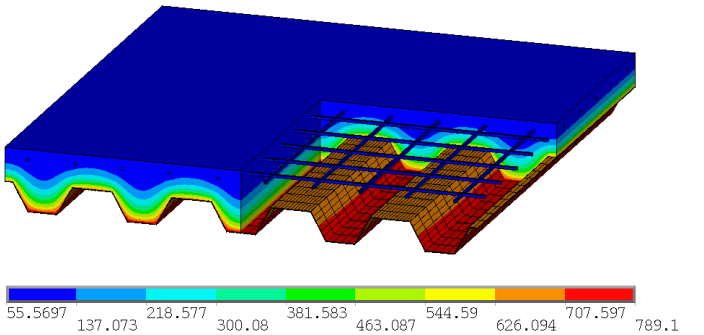

t= 30.5 min

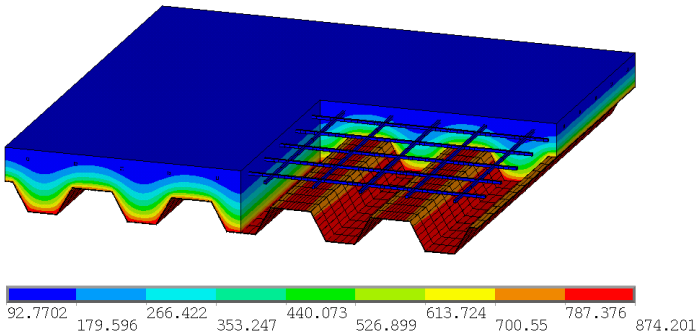

t= 45.7 min

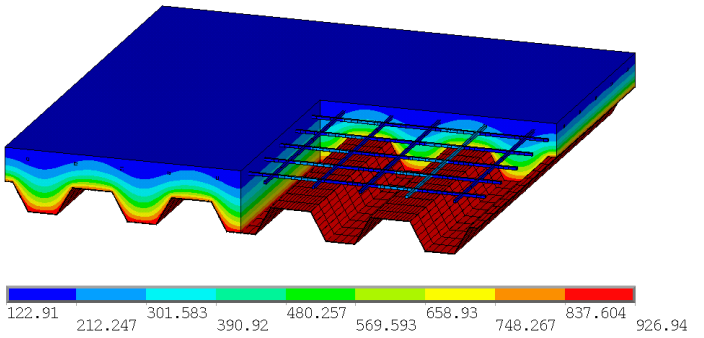

t= 60.9 min

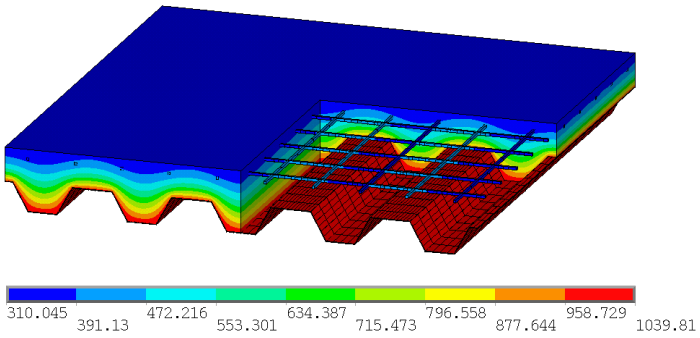

t= 120.0 min

SIM. 200	**St. deck:** Trapezoidal – ArcelorMittal Polydeck 59S	**Rebar (mm): -**	**Fire resistance (min)**	
	Mesh (mm//mm): ϕ6//100 (Q 283)	**h_1 (mm):** 81	Ave: *74.0*	Max: 78.4

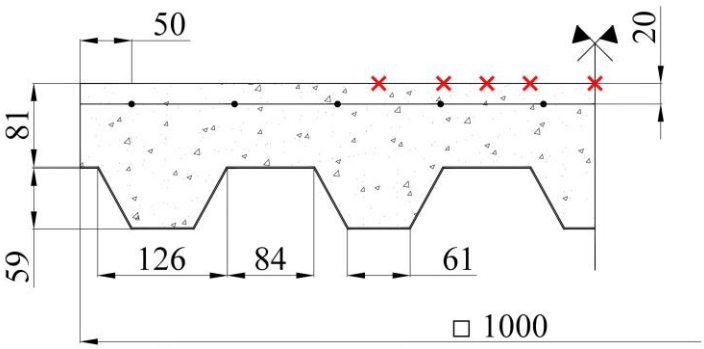

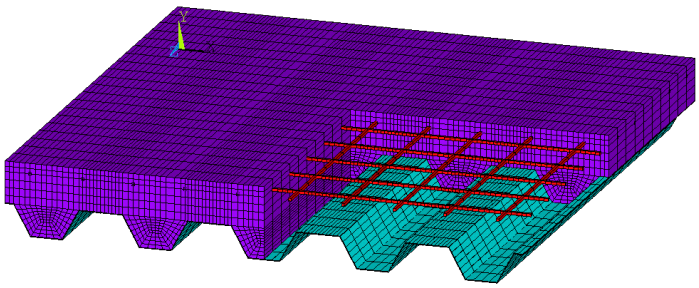

Finite element mesh

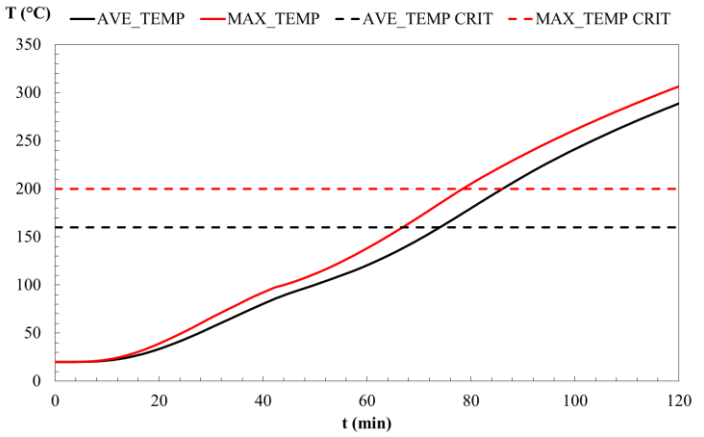

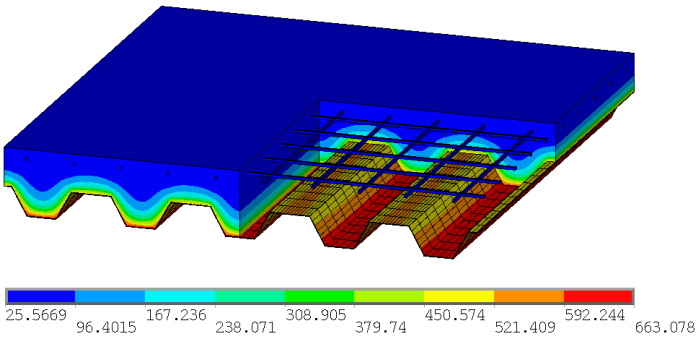

t= 18.5 min

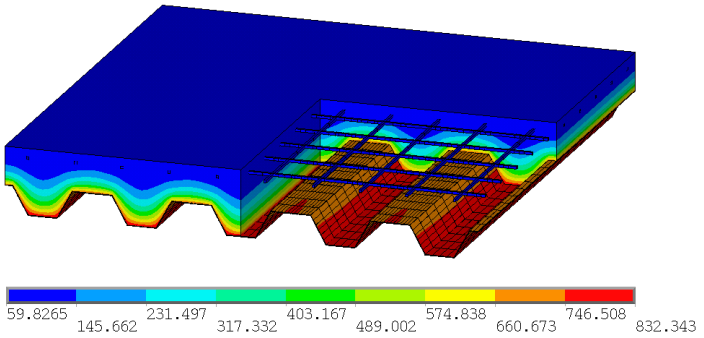

t= 37.0 min

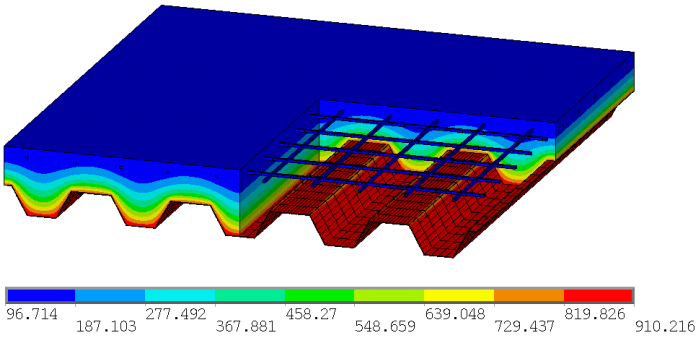

t= 55.5 min

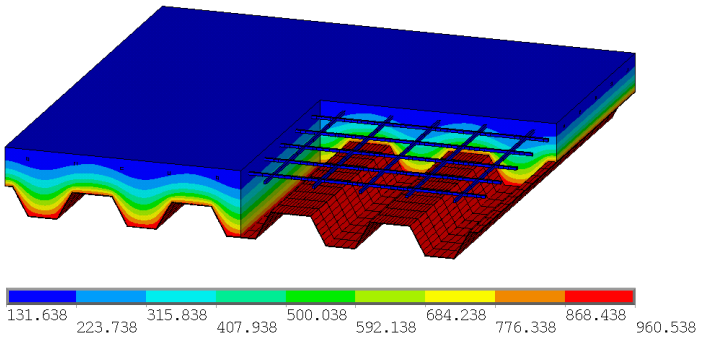

t= 74.0 min

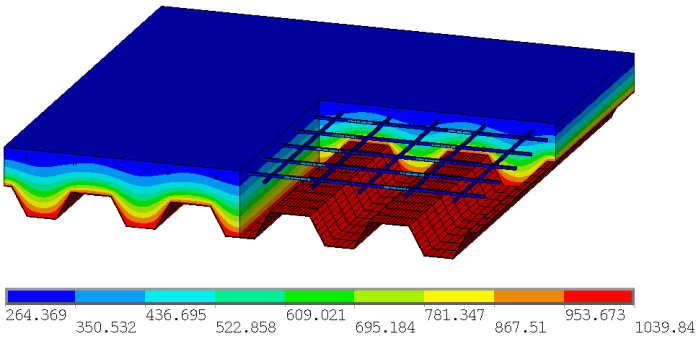

t= 120.0 min

SIM. 201	**Steel deck:** Re-entrant – Vulcraft 3.5D Formlok	**Rebar (mm): -**	**Fire resistance (min)**	
	Mesh (mm//mm): ϕ6//100 (W4.5)	**h_1 (mm):** 51	Ave: 62.1	Max: *60.3*

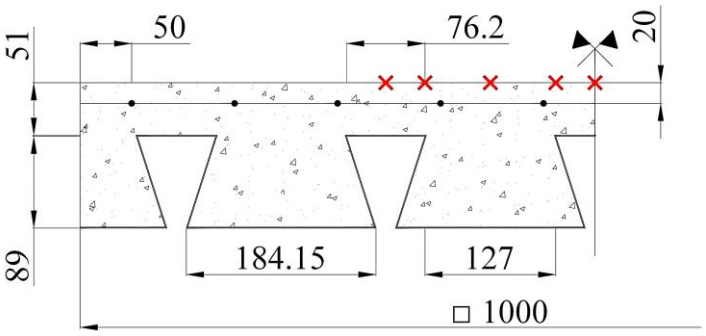

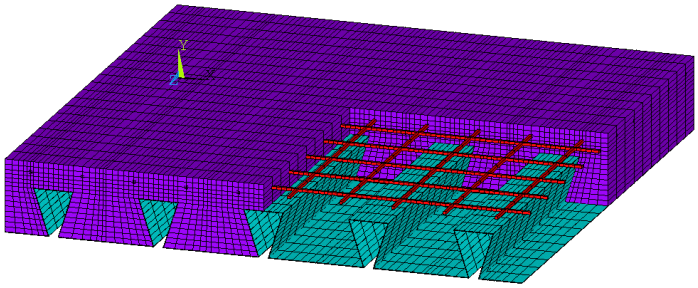

Finite element mesh

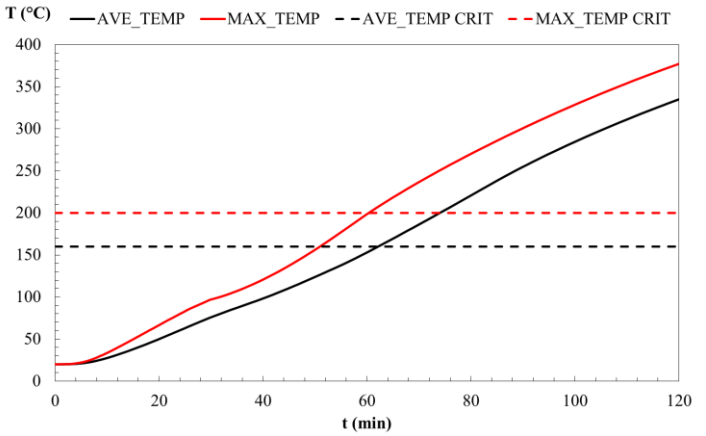

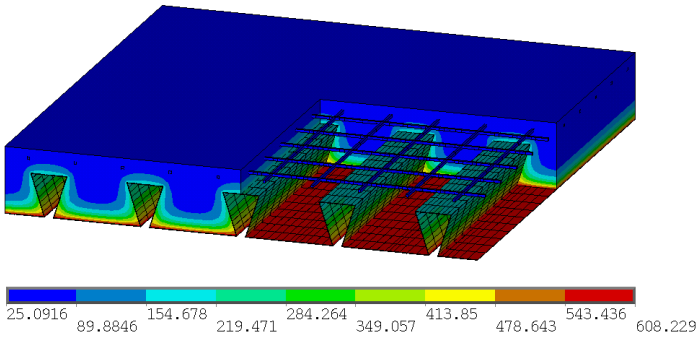

t= 15.1 min

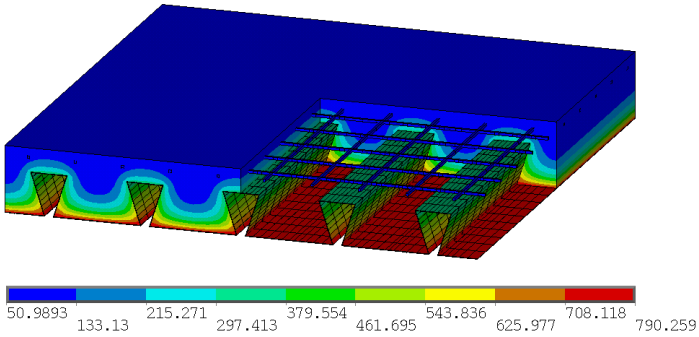

t= 30.2 min

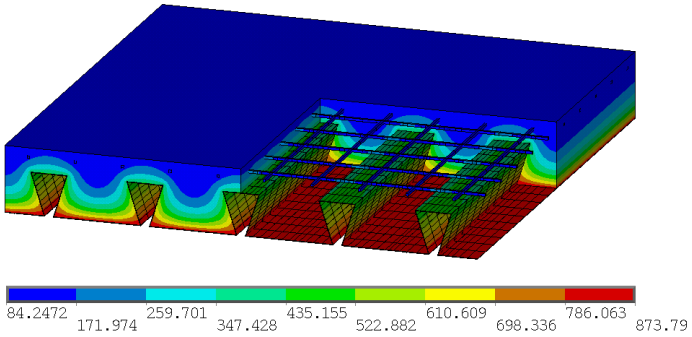

t= 45.2 min

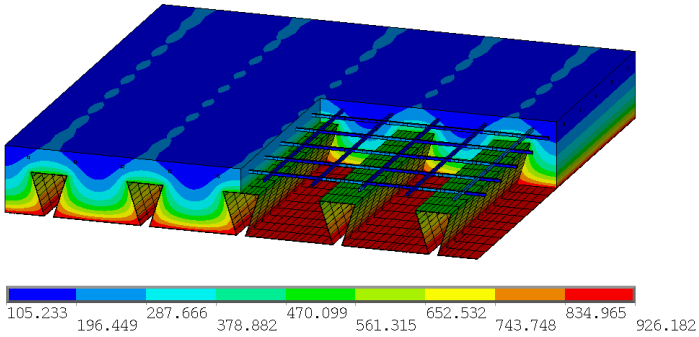

t= 60.3 min

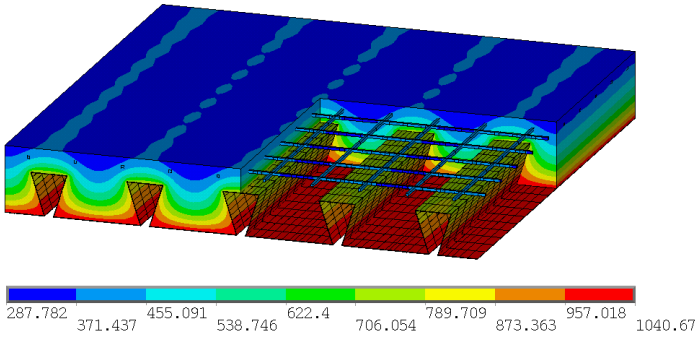

t= 120.0 min

SIM. 202	**Steel deck:** Re-entrant – Vulcraft 3.5D Formlok	**Rebar (mm): -**	**Fire resistance (min)**	
	Mesh (mm//mm): ϕ6//100 (W4.5)	**h_1 (mm):** 61	Ave: *76.2*	Max: 77.2

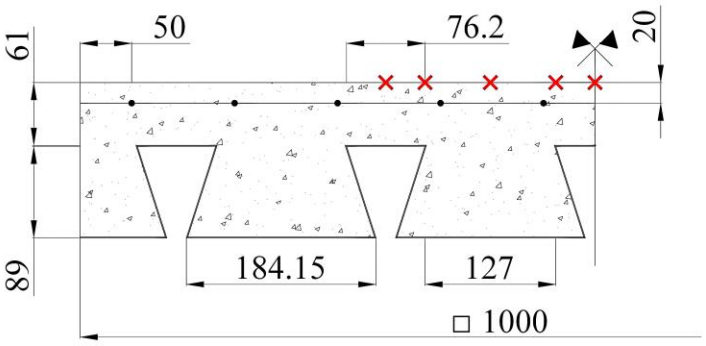

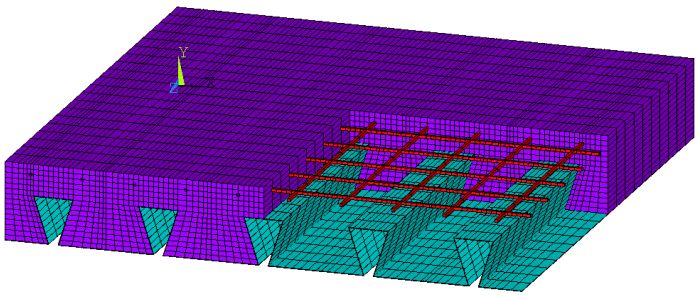

Finite element mesh

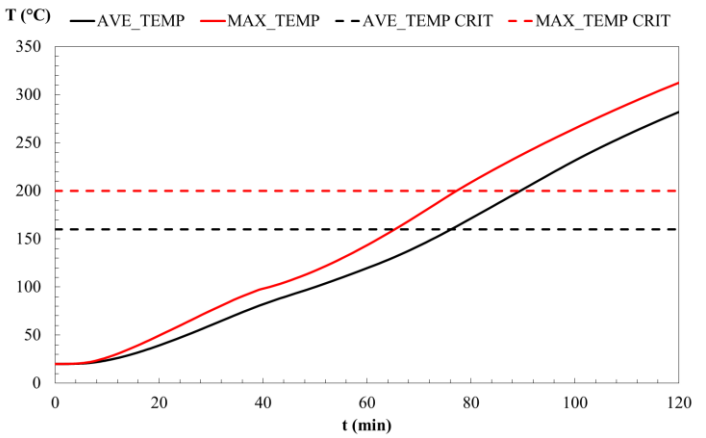

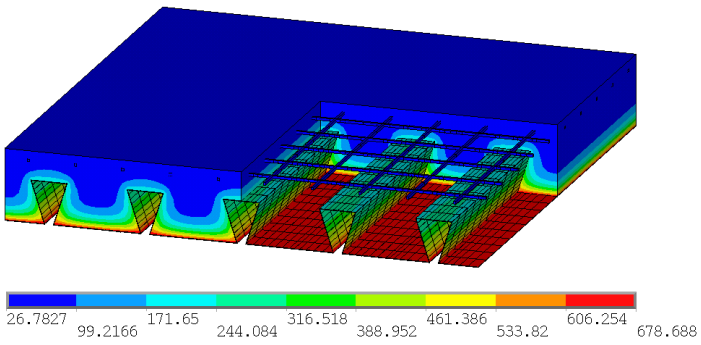

t= 19.1 min

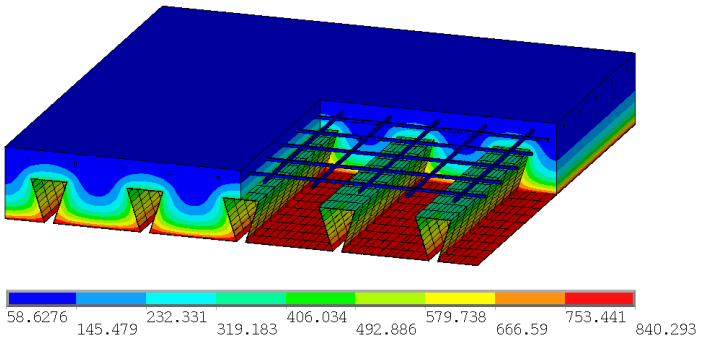

t= 38.1 min

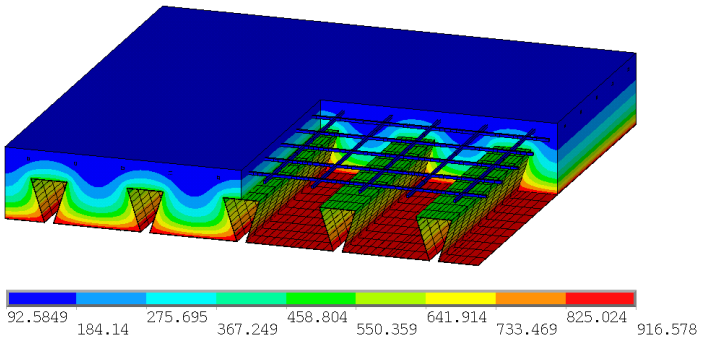

t= 57.2 min

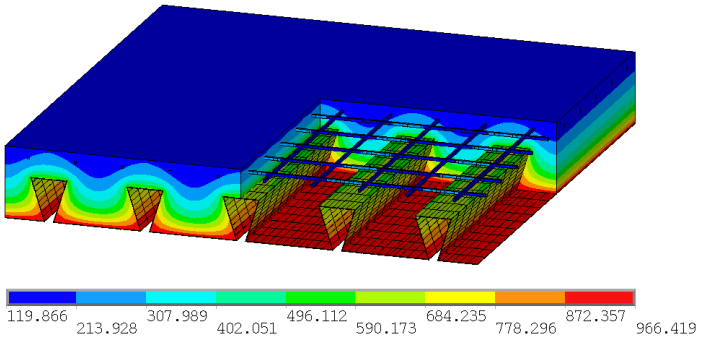

t= 76.2 min

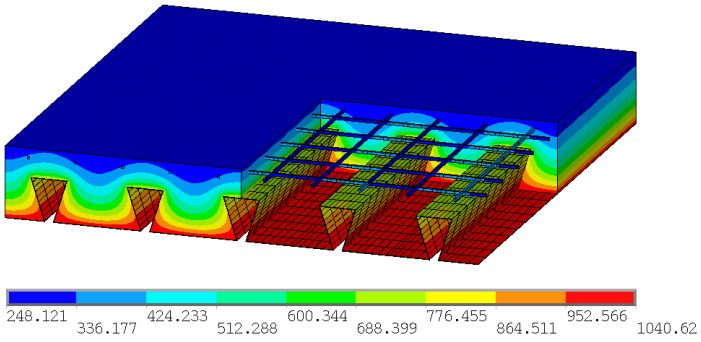

t= 120.0 min

SIM. 203	**Steel deck:** Re-entrant – Vulcraft 3.5D Formlok	**Rebar (mm):** -	**Fire resistance (min)**	
	Mesh (mm//mm): ϕ6//100 (W4.5)	**h_1 (mm):** 71	Ave: *91.1*	Max: 95.8

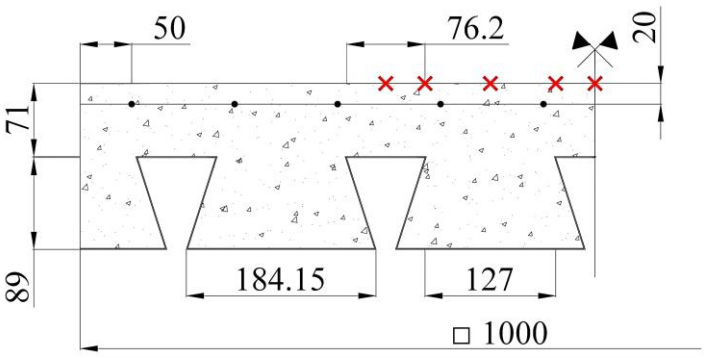

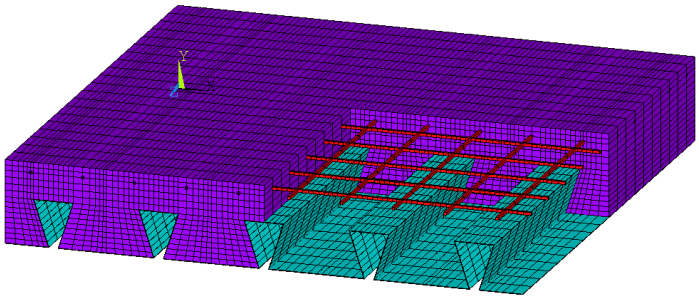

Finite element mesh

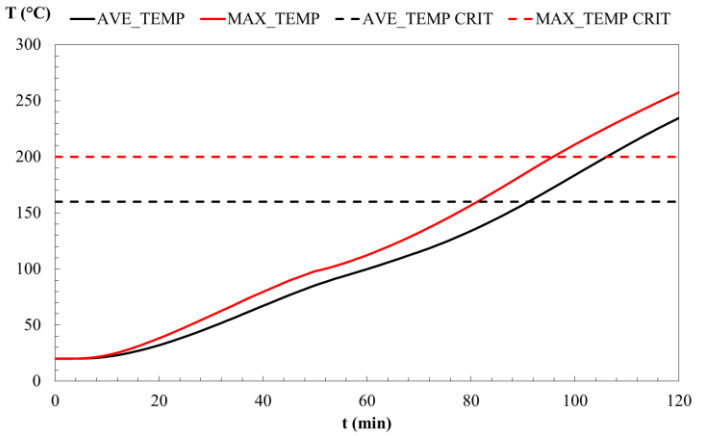

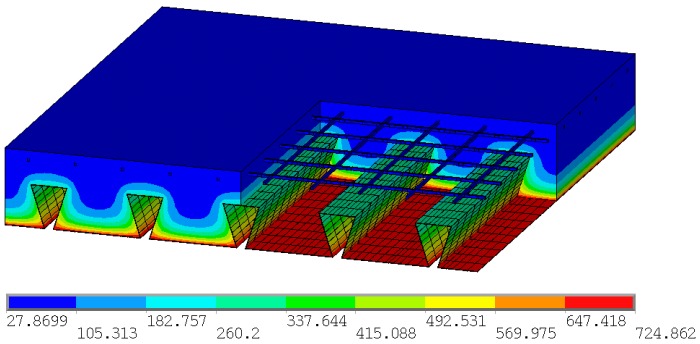

t= 22.8 min

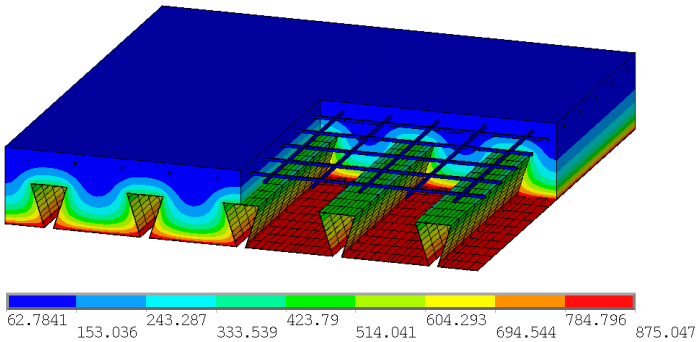

t= 45.6 min

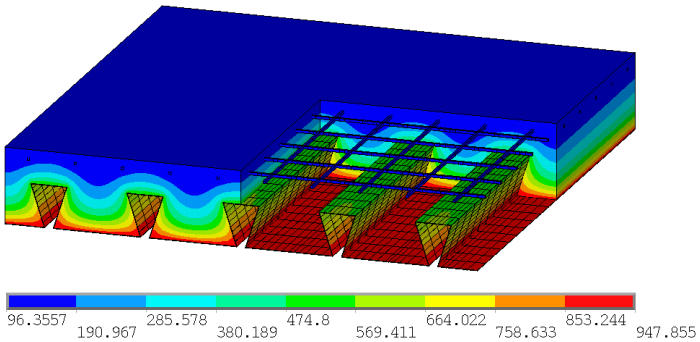

t= 68.3 min

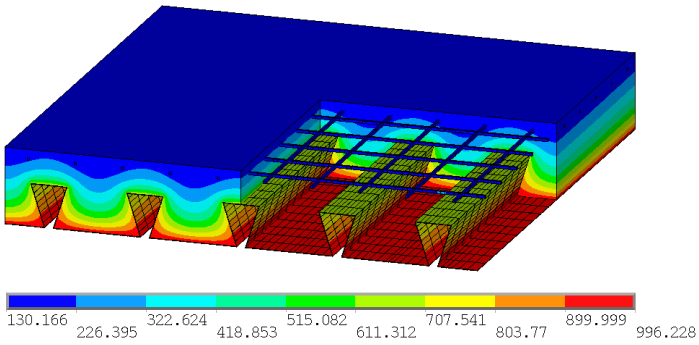

t= 91.1 min

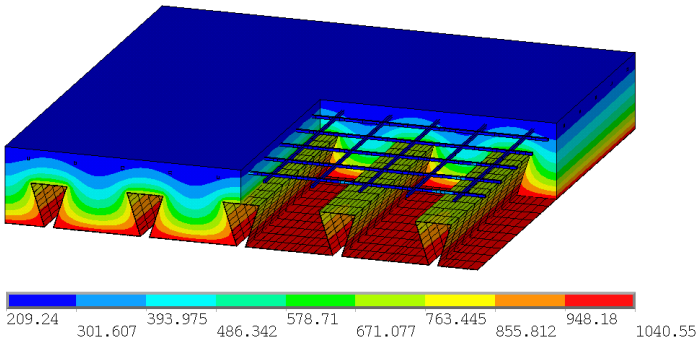

t= 120.0 min

SIM. 204	**Steel deck:** Re-entrant – Vulcraft 3.5D Formlok	**Rebar (mm): -**	**Fire resistance (min)**	
	Mesh (mm//mm): ϕ6//100 (W4.5)	**h_1 (mm):** 81	Ave: *107.0*	Max: 115.8

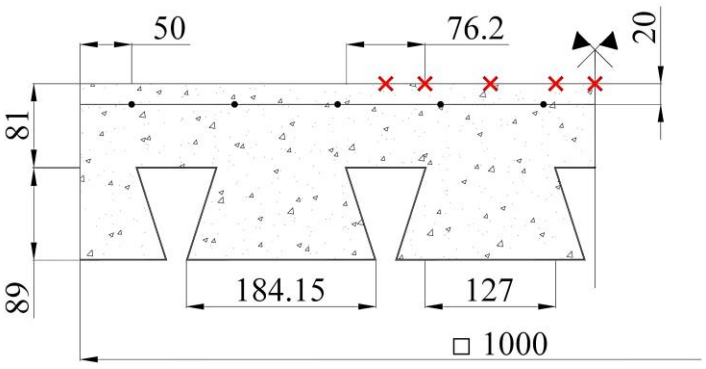

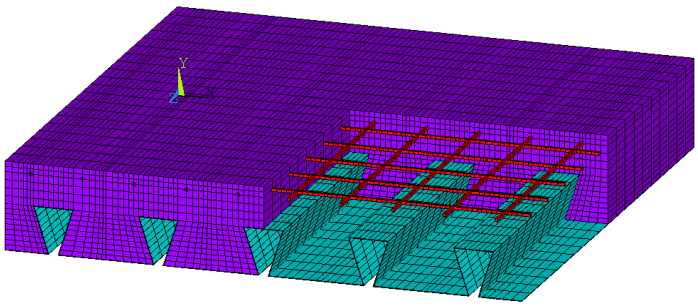

Finite element mesh

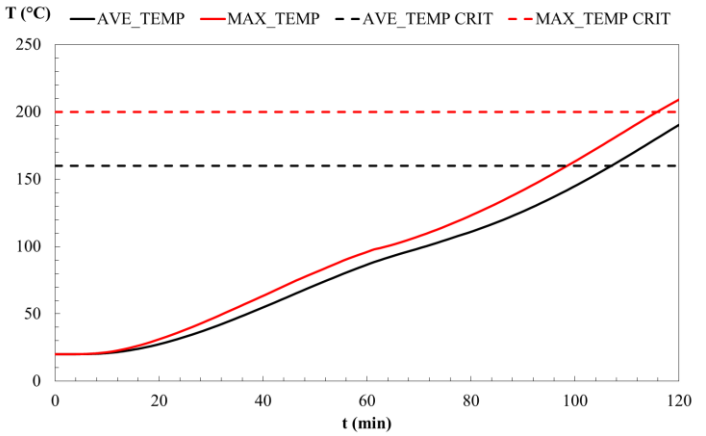

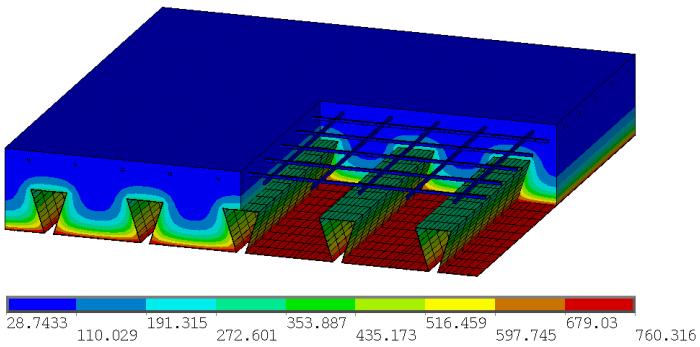

t= 26.8 min

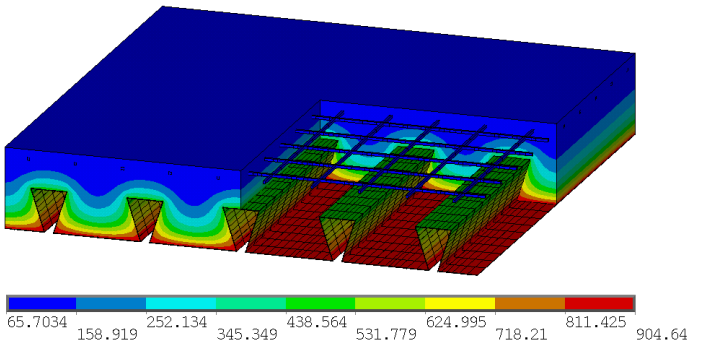

t= 53.5 min

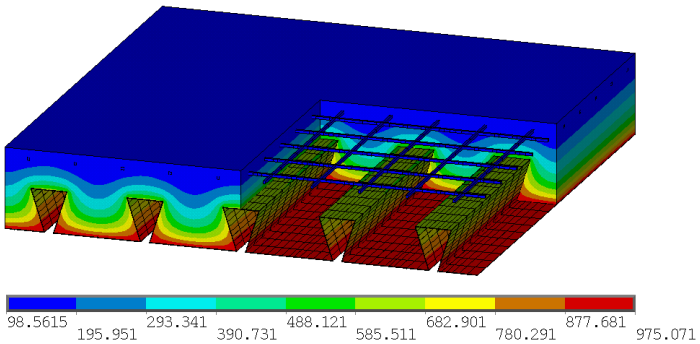

t= 80.3 min

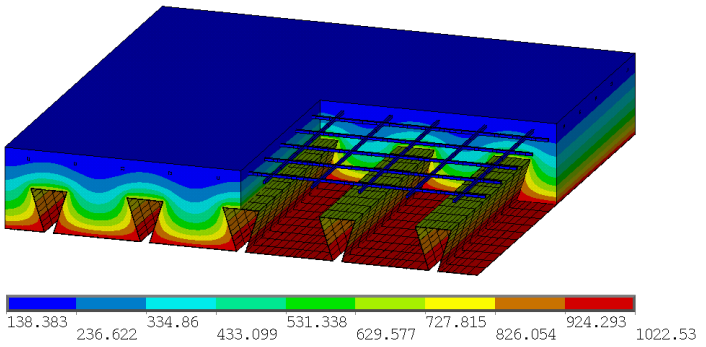

t= 107.0 min

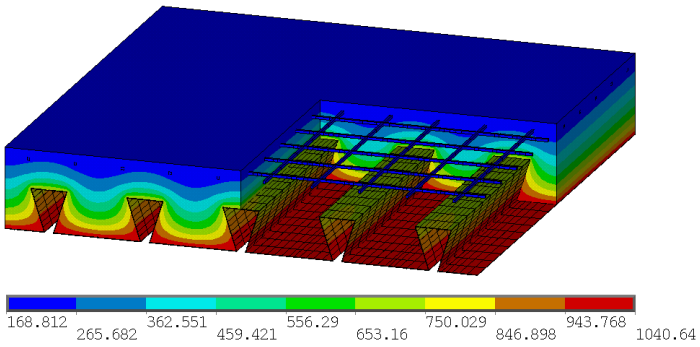

t= 120.0 min

SIM. 205	**Steel deck:** Lysaght Bondek	**Rebar (mm): -**	**Fire resistance (min)**	
	Mesh (mm//mm): ϕ7.6//200 (RM82)	**h_1 (mm):** 56	Ave: *69.5*	Max: 72.1

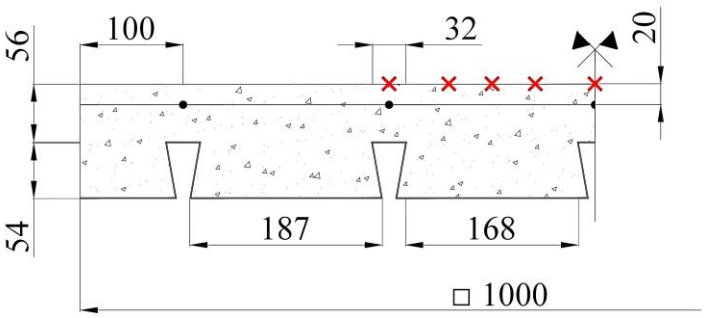

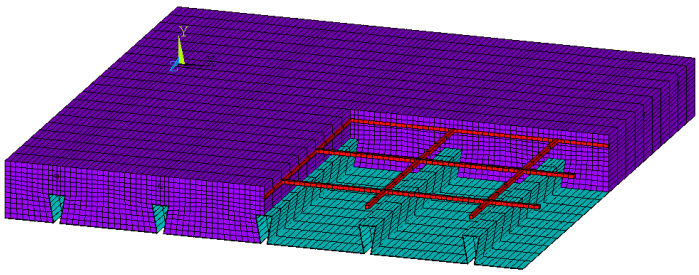

Finite element mesh

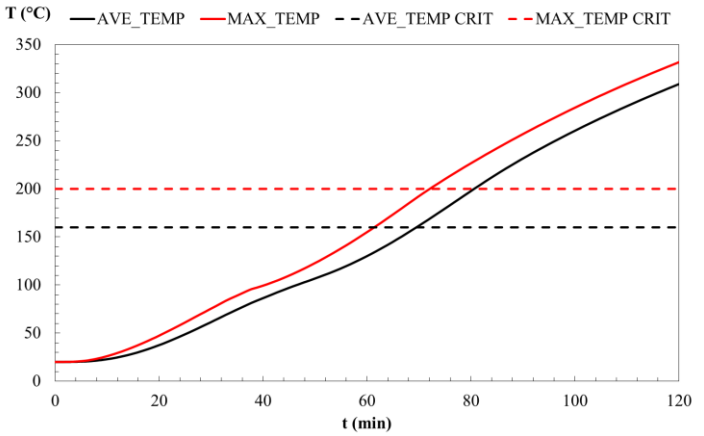

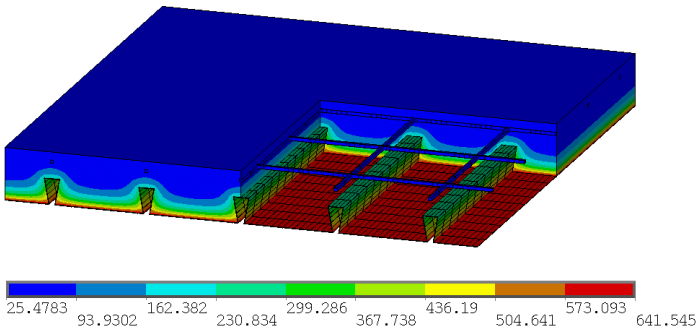

t= 17.4 min

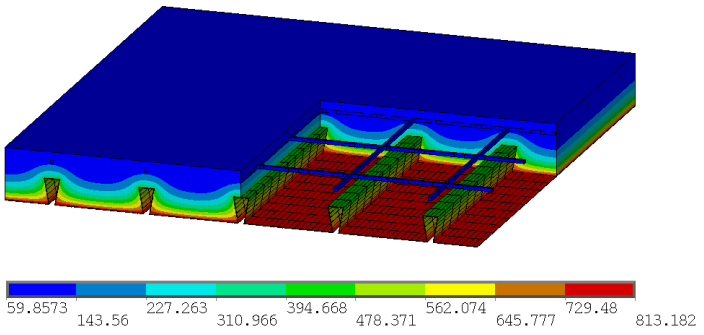

t= 34.8 min

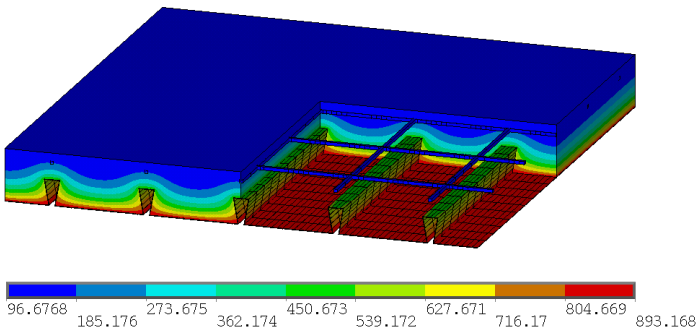

t= 52.1 min

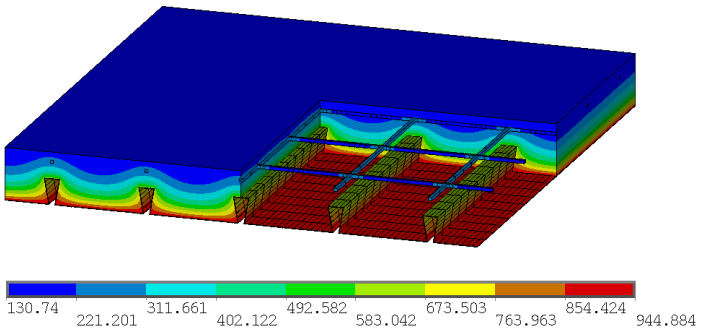

t= 69.5 min

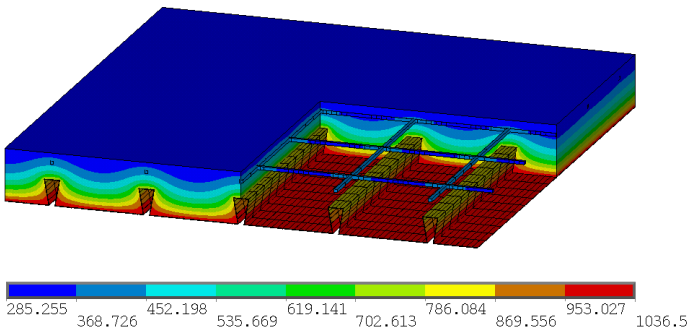

t= 120.0 min

SIM. 206	**Steel deck:** Lysaght Bondek	**Rebar (mm):** -	**Fire resistance (min)**	
	Mesh (mm//mm): ϕ7.6//200 (RM82)	**h_1 (mm):** 66	Ave: *83.2*	Max: 89.3

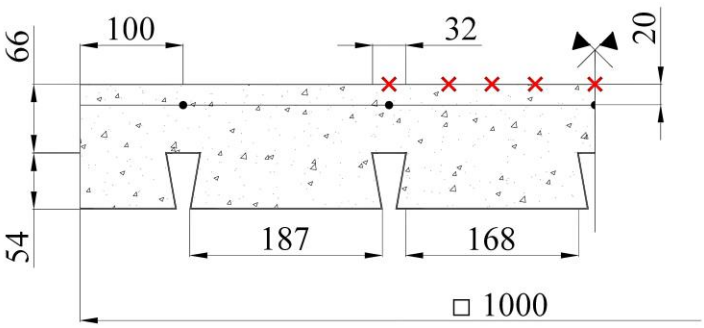

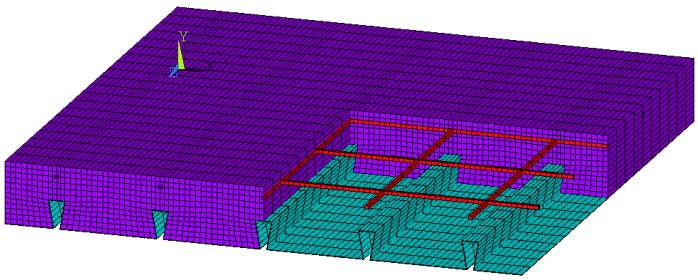

Finite element mesh

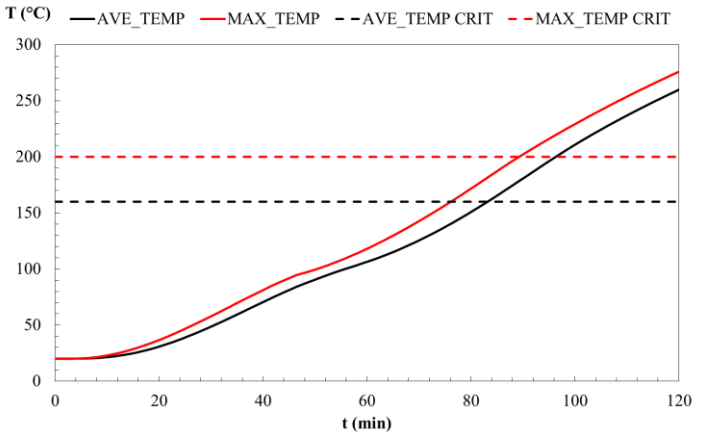

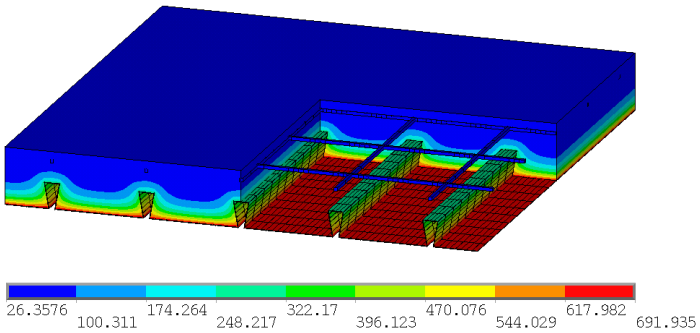

t= 20.8 min

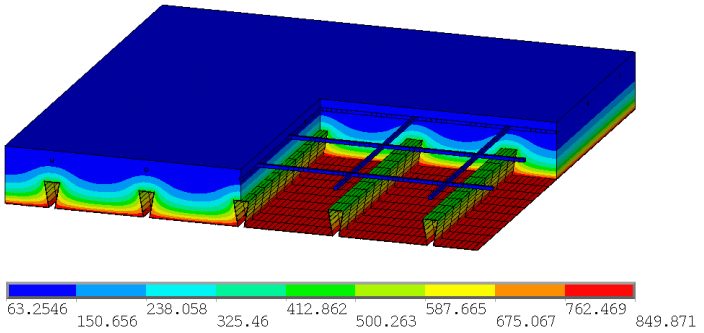

t= 41.6 min

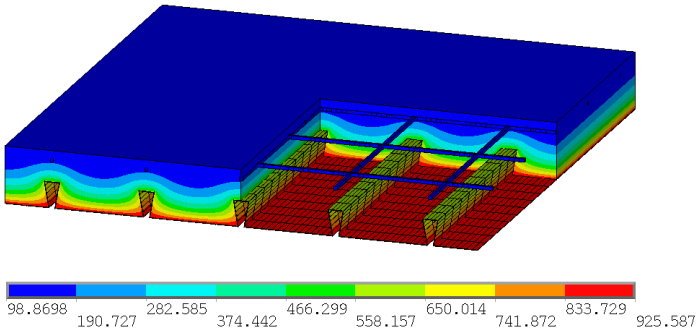

t= 62.4 min

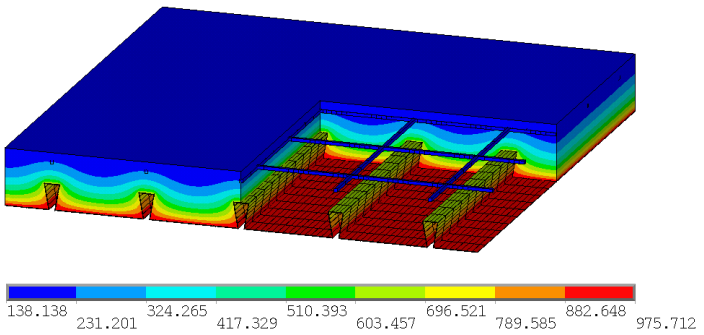

t= 83.2 min

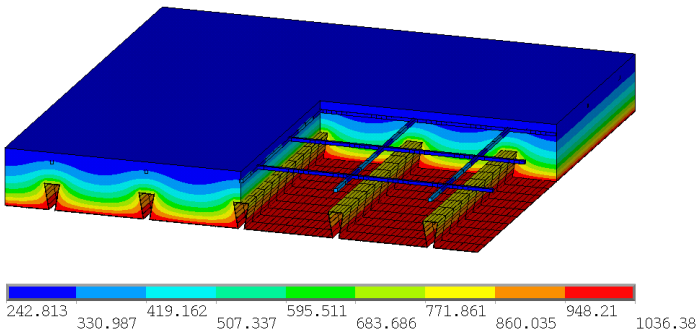

t= 120.0 min

SIM. 207	**Steel deck:** Lysaght Bondek	**Rebar (mm):** -	**Fire resistance (min)**	
	Mesh (mm//mm): ϕ7.6//200 (RM82)	**h_1 (mm):** 76	Ave: *98.1*	Max: 107.9

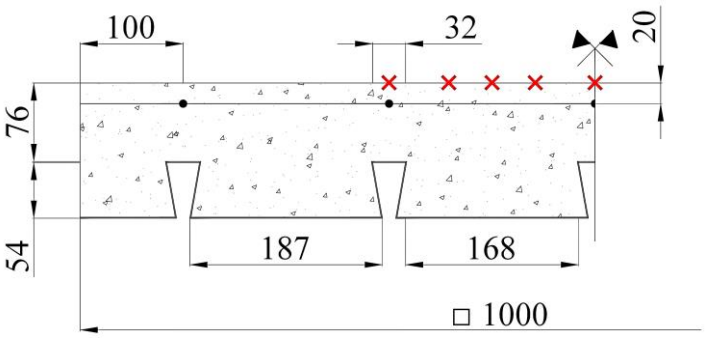

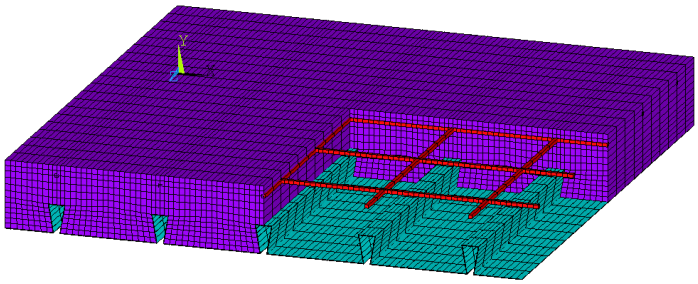

Finite element mesh

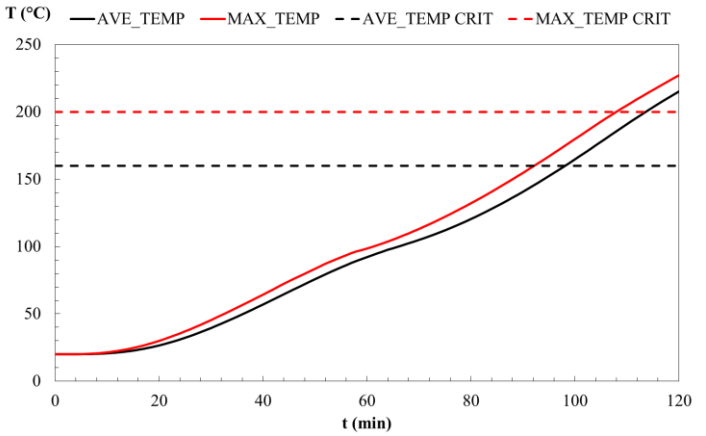

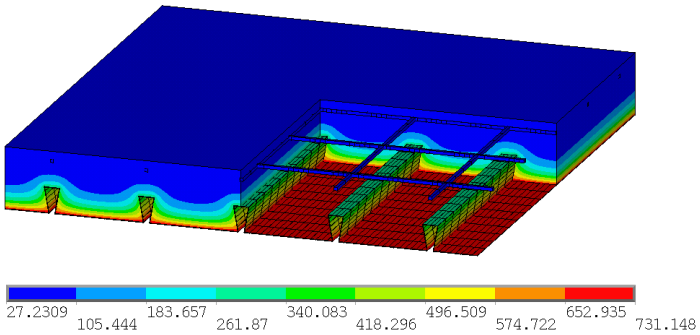

t= 24.5 min

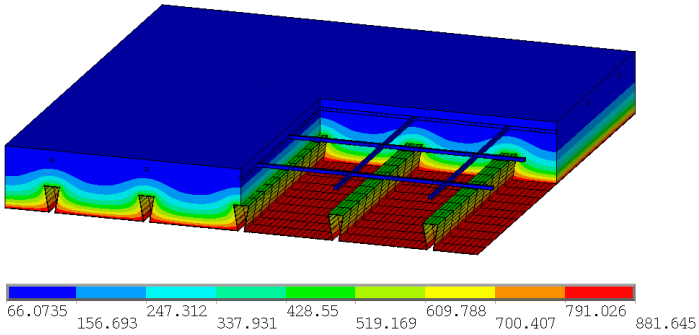

t= 49.1 min

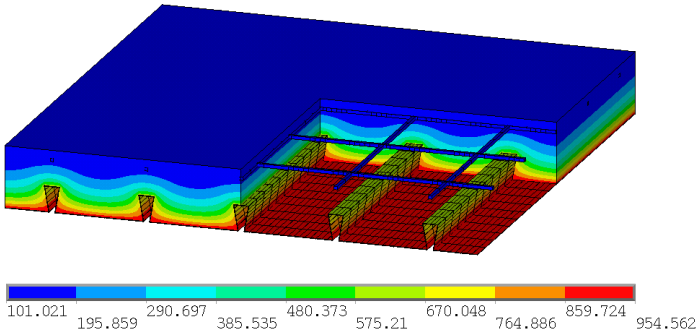

t= 73.6 min

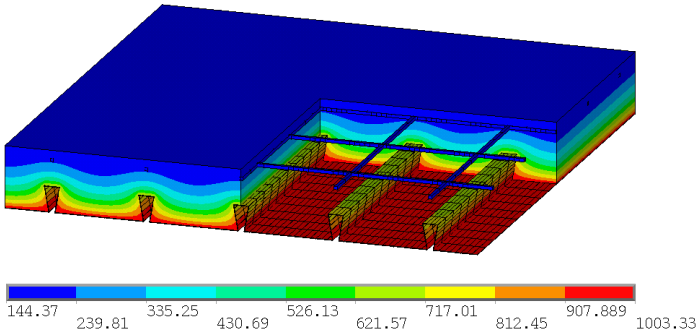

t= 98.1 min

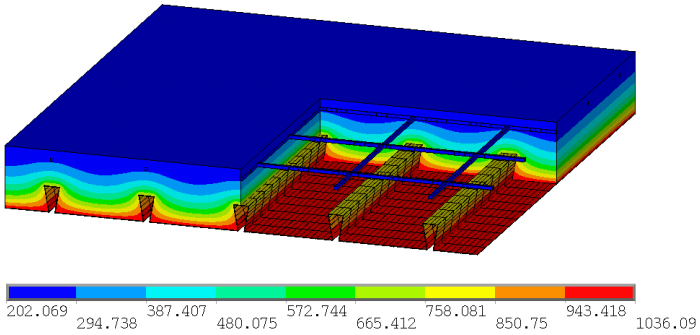

t= 120.0 min

SIM. 208	**Steel deck:** Lysaght Bondek	**Rebar (mm): -**	**Fire resistance (min)**	
	Mesh (mm//mm): ϕ7.6//200 (RM82)	**h_1 (mm):** 86	Ave: *114.3*	Max: 128.1

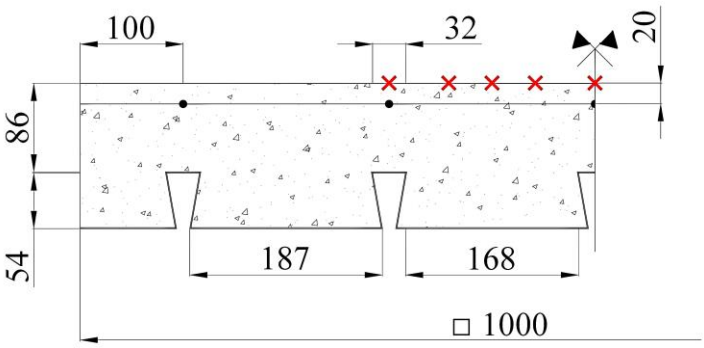

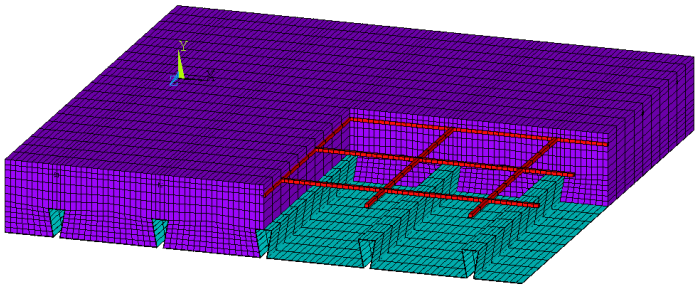

Finite element mesh

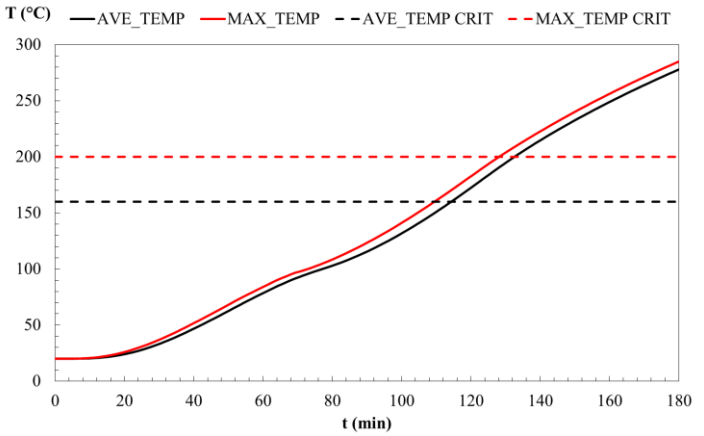

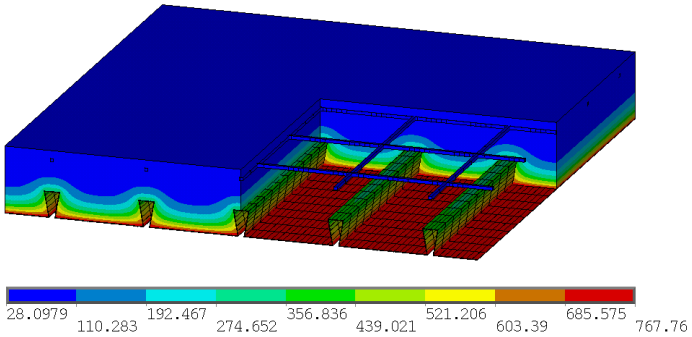

t= 28.6 min

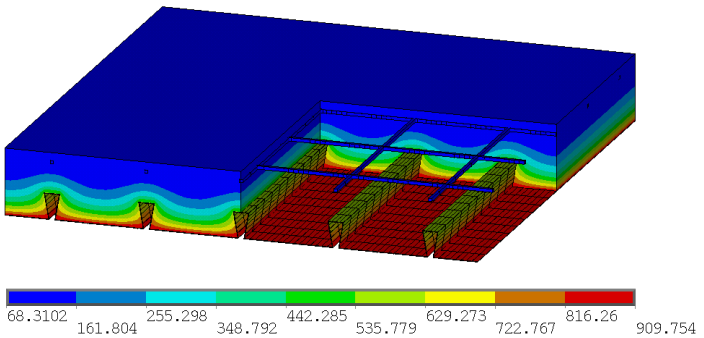

t= 57.2 min

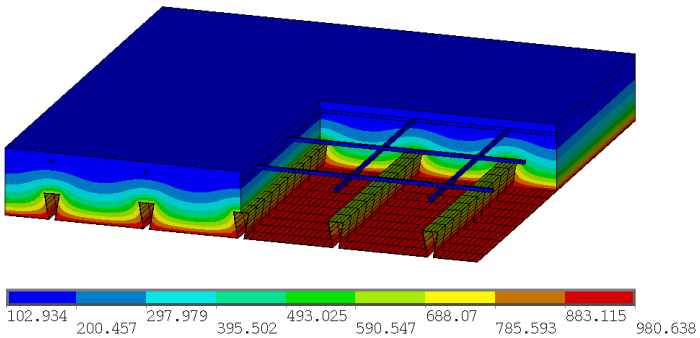

t= 85.7 min

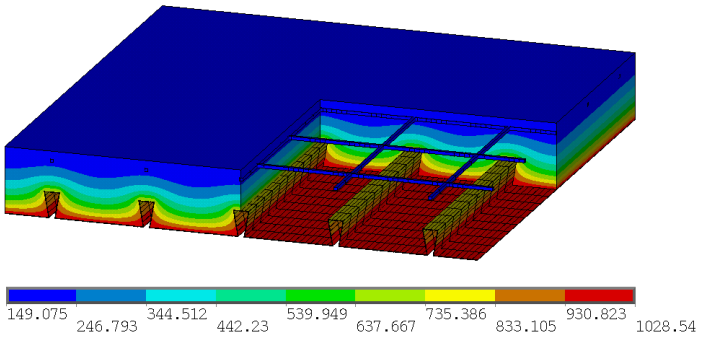

t= 114.3 min

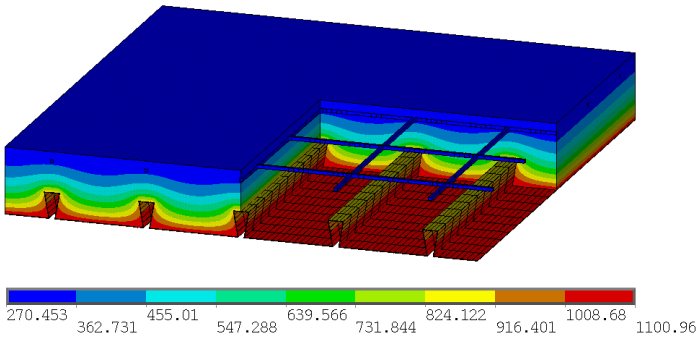

t= 180.0 min

APPENDIX C

CRITICAL TEMPERATURES OF THE STEEL COMPONENTS FOR THE FIRST PARAMETRIC STUDY

O FELIZ H60 (PORTUGAL)																
Numerical simulation												**t_{fi} (min)**		**T_{crit} (°C)**		
No.	l_1 (mm)	l_2 (mm)	l_3 (mm)	h_1 (mm)	h_2 (mm)	h_{tot} (mm)	ϕ_{reb} (mm)	d'_{reb} (mm)	ϕ_{mesh} (mm)	s_{mesh} (mm/mm)	h_{eff} (mm)	AVE_T crit.	MAX_T crit.	Steel deck	Rebar	Mesh
1	105	60	100	50	60	110	8	30	6	100	74.1	36.3	**34.6**	746.9	403.7	199.4
2	105	60	100	60	60	120	8	30	6	100	84.1	46.4	**45.9**	814.9	501.8	202.8
3	105	60	100	70	60	130	8	30	6	100	94.1	**57.7**	59.3	867.6	581.1	201.4
4	105	60	100	80	60	140	8	30	6	100	104.1	**70.1**	74.5	908.2	646.7	197.6
5	105	60	100	50	60	110	8	60	6	100	74.1	36.2	**34.5**	746.3	223.2	199.2
6	105	60	100	60	60	120	8	60	6	100	84.1	46.3	**45.9**	814.6	307.9	203.3
7	105	60	100	70	60	130	8	60	6	100	94.1	**57.5**	59.2	866.6	377.7	201.1
8	105	60	100	80	60	140	8	60	6	100	104.1	**70.0**	74.4	907.7	440.1	197.7
9	105	60	100	50	60	110	8	30	6	150	74.1	36.4	**35.1**	750.7	408.5	198.6
10	105	60	100	60	60	120	8	30	6	150	84.1	**46.5**	**46.5**	818.3	506.4	203.0
11	105	60	100	70	60	130	8	30	6	150	94.1	**57.8**	60.0	868.0	581.7	199.6
12	105	60	100	80	60	140	8	30	6	150	104.1	**70.2**	75.2	908.5	647.1	196.6
13	105	60	100	50	60	110	8	60	6	150	74.1	36.3	**35.0**	750.2	227.4	198.4
14	105	60	100	60	60	120	8	60	6	150	84.1	**46.4**	46.5	817.5	311.3	202.8
15	105	60	100	70	60	130	8	60	6	150	94.1	**57.6**	59.9	867.1	378.3	199.4
16	105	60	100	80	60	140	8	60	6	150	104.1	**70.0**	75.1	907.8	440.2	196.4
17	105	60	100	50	60	110	10	30	6	100	74.1	36.3	**34.6**	746.6	391.1	199.3
18	105	60	100	60	60	120	10	30	6	100	84.1	46.4	**45.9**	814.6	489.6	202.7
19	105	60	100	70	60	130	10	30	6	100	94.1	**57.8**	59.3	867.7	569.8	201.7
20	105	60	100	80	60	140	10	30	6	100	104.1	**70.2**	74.6	908.3	635.8	197.8
21	105	60	100	50	60	110	10	60	6	100	74.1	36.2	**34.5**	746.2	216.5	199.0
22	105	60	100	60	60	120	10	60	6	100	84.1	46.4	**45.9**	814.5	301.1	202.9

Continue on next page

23	105	60	100	70	60	130	10	60	6	100	94.1	**57.6**	59.2	866.9	371.8	201.3
24	105	60	100	80	60	140	10	60	6	100	104.1	**70.0**	74.4	907.6	434.0	197.5
25	105	60	100	50	60	110	10	30	6	150	74.1	36.4	**35.1**	750.4	396.2	198.5
26	105	60	100	60	60	120	10	30	6	150	84.1	**46.6**	**46.6**	818.7	496.2	203.1
27	105	60	100	70	60	130	10	30	6	150	94.1	**57.8**	60.0	867.8	569.8	199.4
28	105	60	100	80	60	140	10	30	6	150	104.1	**70.2**	75.2	908.3	635.8	196.3
29	105	60	100	50	60	110	10	60	6	150	74.1	36.3	**35.0**	750.1	220.7	198.1
30	105	60	100	60	60	120	10	60	6	150	84.1	**46.4**	46.5	817.4	304.6	202.5
31	105	60	100	70	60	130	10	60	6	150	94.1	**57.6**	59.9	866.9	371.8	199.1
32	105	60	100	80	60	140	10	60	6	150	104.1	**70.1**	75.1	907.9	434.5	196.4
33	105	60	100	50	60	110	12	30	6	100	74.1	36.3	**34.6**	746.2	376.7	199.3
34	105	60	100	60	60	120	12	30	6	100	84.1	46.5	**46.0**	814.8	476.1	203.1
35	105	60	100	70	60	130	12	30	6	100	94.1	**57.8**	59.3	867.4	556.0	201.5
36	105	60	100	80	60	140	12	30	6	100	104.1	**70.2**	74.6	908.0	622.4	197.7
37	105	60	100	50	60	110	12	60	6	100	74.1	36.2	**34.5**	746.1	209.0	198.7
38	105	60	100	60	60	120	12	60	6	100	84.1	46.4	**45.9**	814.3	293.2	202.5
39	105	60	100	70	60	130	12	60	6	100	94.1	**57.6**	59.2	866.7	364.2	201.0
40	105	60	100	80	60	140	12	60	6	100	104.1	**70.1**	74.5	907.7	427.1	197.6
41	105	60	100	50	60	110	12	30	6	150	74.1	36.4	**35.1**	750.1	381.8	198.4
42	105	60	100	60	60	120	12	30	6	150	84.1	**46.5**	**46.5**	817.7	480.5	202.7
43	105	60	100	70	60	130	12	30	6	150	94.1	**57.9**	60.1	867.9	556.6	199.7
44	105	60	100	80	60	140	12	30	6	150	104.1	**70.3**	75.3	908.4	622.9	196.6
45	105	60	100	50	60	110	12	60	6	150	74.1	36.3	**35.0**	750.0	213.0	197.8
46	105	60	100	60	60	120	12	60	6	150	84.1	**46.5**	**46.5**	817.8	297.3	202.6
47	105	60	100	70	60	130	12	60	6	150	94.1	**57.7**	59.9	867.1	364.7	199.2
48	105	60	100	80	60	140	12	60	6	150	104.1	**70.1**	75.1	907.8	427.2	196.1

ARCELORMITTAL POLYDECK 59S (BRAZIL)																
Numerical simulation												**t_{fi} (min)**		**T_{crit} (°C)**		
No.	l_1 (mm)	l_2 (mm)	l_3 (mm)	h_1 (mm)	h_2 (mm)	h_{tot} (mm)	ϕ_{reb} (mm)	d'_{reb} (mm)	ϕ_{mesh} (mm)	s_{mesh} (mm/mm)	h_{eff} (mm)	AVE_T crit.	MAX_T crit.	Steel deck	Rebar	Mesh
49	126	61	84	51	59	110	8	30	5	100	77.3	38.2	**36.0**	761.9	388.2	193.1
50	126	61	84	61	59	120	8	30	5	100	87.3	49.0	**48.1**	830.4	483.6	197.1
51	126	61	84	71	59	130	8	30	5	100	97.3	**60.9**	62.1	882.0	561.4	197.7
52	126	61	84	81	59	140	8	30	5	100	107.3	**73.9**	78.1	920.9	624.1	193.9
53	126	61	84	51	59	110	8	60	5	100	77.3	38.2	**36.0**	762.2	202.4	192.9
54	126	61	84	61	59	120	8	60	5	100	87.3	49.0	**48.1**	830.6	283.9	196.9
55	126	61	84	71	59	130	8	60	5	100	97.3	**60.9**	62.1	882.1	353.8	197.5
56	126	61	84	81	59	140	8	60	5	100	107.3	**73.9**	78.2	921.0	412.2	193.7
57	126	61	84	51	59	110	8	30	6	100	77.3	38.3	**36.2**	763.1	390.2	192.8
58	126	61	84	61	59	120	8	30	6	100	87.3	49.2	**48.3**	831.3	485.0	196.7
59	126	61	84	71	59	130	8	30	6	100	97.3	**61.0**	62.4	882.3	562.0	196.8
60	126	61	84	81	59	140	8	30	6	100	107.3	**74.1**	78.4	921.4	624.9	193.4
61	126	61	84	51	59	110	8	60	6	100	77.3	38.3	**36.2**	763.5	204.2	192.6
62	126	61	84	61	59	120	8	60	6	100	87.3	49.2	**48.2**	831.0	284.7	196.1
63	126	61	84	71	59	130	8	60	6	100	97.3	**61.0**	62.3	882.4	354.2	196.7
64	126	61	84	81	59	140	8	60	6	100	107.3	**74.1**	78.4	921.5	413.0	193.2
65	126	61	84	51	59	110	10	30	5	100	77.3	38.2	**36.0**	761.6	377.2	193.0
66	126	61	84	61	59	120	10	30	5	100	87.3	49.0	**48.1**	830.2	472.9	197.0
67	126	61	84	71	59	130	10	30	5	100	97.3	**60.9**	62.1	881.8	551.2	197.6
68	126	61	84	81	59	140	10	30	5	100	107.3	**74.0**	78.1	921.1	614.6	194.1
69	126	61	84	51	59	110	10	60	5	100	77.3	38.2	**36.0**	762.2	196.9	192.7
70	126	61	84	61	59	120	10	60	5	100	87.3	49.0	**48.1**	830.5	278.2	196.6

Continue on next page

71	126	61	84	71	59	130	10	60	5	100	97.3	**60.9**	62.1	882.0	348.3	197.2
72	126	61	84	81	59	140	10	60	5	100	107.3	**74.0**	78.2	921.2	407.4	193.8
73	126	61	84	51	59	110	10	30	6	100	77.3	38.4	**36.2**	762.8	379.0	192.6
74	126	61	84	61	59	120	10	30	6	100	87.3	49.2	**48.3**	831.1	474.2	196.6
75	126	61	84	71	59	130	10	30	6	100	97.3	**61.0**	62.4	882.1	551.7	196.7
76	126	61	84	81	59	140	10	30	6	100	107.3	**74.1**	78.4	921.3	615.0	193.3
77	126	61	84	51	59	110	10	60	6	100	77.3	38.4	**36.2**	763.4	198.7	192.5
78	126	61	84	61	59	120	10	60	6	100	87.3	49.2	**48.3**	831.4	279.6	196.3
79	126	61	84	71	59	130	10	60	6	100	97.3	**61.1**	62.3	882.7	349.3	196.9
80	126	61	84	81	59	140	10	60	6	100	107.3	**74.2**	78.4	921.7	408.2	193.3
81	126	61	84	51	59	110	12	30	5	100	77.3	38.2	**36.0**	761.4	364.3	192.9
82	126	61	84	61	59	120	12	30	5	100	87.3	49.0	**48.1**	830.0	460.2	196.8
83	126	61	84	71	59	130	12	30	5	100	97.3	**60.9**	62.1	881.6	538.9	197.3
84	126	61	84	81	59	140	12	30	5	100	107.3	**74.0**	78.2	920.9	602.7	193.9
85	126	61	84	51	59	110	12	60	5	100	77.3	38.2	**36.0**	762.1	190.7	192.5
86	126	61	84	61	59	120	12	60	5	100	87.3	49.0	**48.0**	829.9	270.8	195.9
87	126	61	84	71	59	130	12	60	5	100	97.3	**61.0**	62.2	882.2	342.2	197.3
88	126	61	84	81	59	140	12	60	5	100	107.3	**74.1**	78.2	921.4	401.6	193.8
89	126	61	84	51	59	110	12	30	6	100	77.3	38.4	**36.2**	762.5	366.1	192.4
90	126	61	84	61	59	120	12	30	6	100	87.3	49.2	**48.2**	830.4	460.9	195.9
91	126	61	84	71	59	130	12	30	6	100	97.3	**61.0**	62.3	881.9	539.5	196.6
92	126	61	84	81	59	140	12	30	6	100	107.3	**74.2**	78.5	921.4	603.6	193.4
93	126	61	84	51	59	110	12	60	6	100	77.3	38.4	**36.2**	763.4	192.3	192.2
94	126	61	84	61	59	120	12	60	6	100	87.3	49.2	**48.3**	831.3	272.7	195.9
95	126	61	84	71	59	130	12	60	6	100	97.3	**61.2**	62.4	882.9	343.2	196.9
96	126	61	84	81	59	140	12	60	6	100	107.3	**74.3**	78.5	921.9	402.4	193.3

VULCRAFT 3.5D DOVETAIL FORMLOK (USA)																
Numerical simulation												**t_{fi} (min)**		**T_{crit} (°C)**		
No.	l_1 (mm)	l_2 (mm)	l_3 (mm)	h_1 (mm)	h_2 (mm)	h_{tot} (mm)	ϕ_{reb} (mm)	d'_{reb} (mm)	ϕ_{mesh} (mm)	s_{mesh} (mm/mm)	h_{eff} (mm)	AVE_T crit.	MAX_T crit.	Steel deck	Rebar	Mesh
97	127	184.15	76.2	51	89	140	8	30	6	100	109.6	62.2	**60.4**	712.9	469.8	189.5
98	127	184.15	76.2	61	89	150	8	30	6	100	129.1	**76.2**	77.3	767.2	545.3	194.7
99	127	184.15	76.2	71	89	160	8	30	6	100	139.1	**91.2**	95.8	809.4	604.8	193.7
100	127	184.15	76.2	81	89	170	8	30	6	100	149.1	**107.1**	115.8	847.2	658.2	192.4
101	127	184.15	76.2	51	89	140	8	60	6	100	109.6	62.2	**60.4**	712.9	284.3	189.4
102	127	184.15	76.2	61	89	150	8	60	6	100	129.1	**76.2**	77.3	767.2	356.6	194.6
103	127	184.15	76.2	71	89	160	8	60	6	100	139.1	**91.2**	95.9	809.3	414.9	193.6
104	127	184.15	76.2	81	89	170	8	60	6	100	149.1	**107.1**	115.9	847.1	468.6	192.2
105	127	184.15	76.2	51	89	140	8	30	6	150	109.6	62.5	**61.6**	717.5	476.1	193.7
106	127	184.15	76.2	61	89	150	8	30	6	150	129.1	**76.4**	78.5	767.4	546.1	194.4
107	127	184.15	76.2	71	89	160	8	30	6	150	139.1	**91.3**	96.9	809.0	605.1	192.8
108	127	184.15	76.2	81	89	170	8	30	6	150	149.1	**107.1**	116.7	846.5	658.2	190.8
109	127	184.15	76.2	51	89	140	8	60	6	150	109.6	62.5	**61.6**	717.5	290.4	193.6
110	127	184.15	76.2	61	89	150	8	60	6	150	129.1	**76.4**	78.5	767.4	357.5	194.3
111	127	184.15	76.2	71	89	160	8	60	6	150	139.1	**91.3**	96.9	809.0	415.3	192.6
112	127	184.15	76.2	81	89	170	8	60	6	150	149.1	**107.2**	116.8	846.6	469.0	190.9
113	127	184.15	76.2	51	89	140	10	30	6	100	109.6	62.2	**60.4**	712.8	462.7	189.4
114	127	184.15	76.2	61	89	150	10	30	6	100	129.1	**76.2**	77.3	767.1	538.4	194.6
115	127	184.15	76.2	71	89	160	10	30	6	100	139.1	**91.2**	95.9	809.3	597.8	193.6
116	127	184.15	76.2	81	89	170	10	30	6	100	149.1	**107.1**	115.9	847.0	651.4	192.2
117	127	184.15	76.2	51	89	140	10	60	6	100	109.6	62.2	**60.4**	712.8	279.5	189.3
118	127	184.15	76.2	61	89	150	10	60	6	100	129.1	**76.3**	77.3	767.4	352.3	194.7

Continue on next page

119	127	184.15	76.2	71	89	160	10	60	6	100	139.1	**91.2**	95.9	809.2	410.1	193.5
120	127	184.15	76.2	81	89	170	10	60	6	100	149.1	**107.2**	116.0	847.2	464.1	192.3
121	127	184.15	76.2	51	89	140	10	30	6	150	109.6	62.5	**61.6**	717.4	469.1	193.6
122	127	184.15	76.2	61	89	150	10	30	6	150	129.1	**76.5**	78.5	767.6	539.6	194.7
123	127	184.15	76.2	71	89	160	10	30	6	150	139.1	**91.3**	97.0	808.9	598.2	192.6
124	127	184.15	76.2	81	89	170	10	30	6	150	149.1	**107.2**	116.7	846.6	651.7	190.9
125	127	184.15	76.2	51	89	140	10	60	6	150	109.6	62.5	**61.6**	717.4	285.6	193.5
126	127	184.15	76.2	61	89	150	10	60	6	150	129.1	**76.5**	78.5	767.6	353.1	194.5
127	127	184.15	76.2	71	89	160	10	60	6	150	139.1	**91.3**	97.0	808.9	410.5	192.4
128	127	184.15	76.2	81	89	170	10	60	6	150	149.1	**107.2**	116.8	846.5	464.2	190.8
129	127	184.15	76.2	51	89	140	12	30	6	100	109.6	62.2	**60.4**	712.7	454.4	189.3
130	127	184.15	76.2	61	89	150	12	30	6	100	129.1	**76.3**	77.3	767.3	530.6	194.8
131	127	184.15	76.2	71	89	160	12	30	6	100	139.1	**91.2**	95.9	809.2	589.7	193.5
132	127	184.15	76.2	81	89	170	12	30	6	100	149.1	**107.2**	115.9	847.1	643.6	192.4
133	127	184.15	76.2	51	89	140	12	60	6	100	109.6	62.3	**60.4**	712.7	273.9	189.1
134	127	184.15	76.2	61	89	150	12	60	6	100	129.1	**76.3**	77.3	767.3	346.6	194.6
135	127	184.15	76.2	71	89	160	12	60	6	100	139.1	**91.3**	95.9	809.3	404.8	193.6
136	127	184.15	76.2	81	89	170	12	60	6	100	149.1	**107.2**	116.0	847.0	458.4	192.2
137	127	184.15	76.2	51	89	140	12	30	6	150	109.6	62.5	**61.6**	717.3	460.7	193.5
138	127	184.15	76.2	61	89	150	12	30	6	150	129.1	**76.5**	78.5	767.5	531.4	194.6
139	127	184.15	76.2	71	89	160	12	30	6	150	139.1	**91.3**	97.0	808.8	589.9	192.4
140	127	184.15	76.2	81	89	170	12	30	6	150	149.1	**107.2**	116.8	846.4	643.5	190.8
141	127	184.15	76.2	51	89	140	12	60	6	150	109.6	62.5	**61.6**	717.3	279.9	193.4
142	127	184.15	76.2	61	89	150	12	60	6	150	129.1	**76.5**	78.5	767.4	347.3	194.3
143	127	184.15	76.2	71	89	160	12	60	6	150	139.1	**91.4**	97.0	809.0	405.1	192.5
144	127	184.15	76.2	81	89	170	12	60	6	150	149.1	**107.3**	116.9	846.5	458.7	190.8

LYSAGHT BONDEK (AUSTRALIA)																
Numerical simulation												**t_{fi} (min)**		**T_{crit} (°C)**		
No.	l_1 (mm)	l_2 (mm)	l_3 (mm)	h_1 (mm)	h_2 (mm)	h_{tot} (mm)	ϕ_{reb} (mm)	d'_{reb} (mm)	ϕ_{mesh} (mm)	s_{mesh} (mm/mm)	h_{eff} (mm)	AVE_T crit.	MAX_T crit.	Steel deck	Rebar	Mesh
145	168	187	32	56	54	110	8	30	6.75	200	103.9	**69.5**	71.6	777.5	472.8	208.9
146	168	187	32	66	54	120	8	30	6.75	200	113.9	**83.2**	88.9	817.9	522.1	201.9
147	168	187	32	76	54	130	8	30	6.75	200	123.9	**98.1**	107.6	854.7	567.7	196.8
148	168	187	32	86	54	140	8	30	6.75	200	133.9	**114.4**	127.8	888.3	610.7	193.2
149	168	187	32	56	54	110	8	60	6.75	200	103.9	**69.5**	71.6	777.6	266.1	208.7
150	168	187	32	66	54	120	8	60	6.75	200	113.9	**83.2**	88.8	818.0	309.6	201.8
151	168	187	32	76	54	130	8	60	6.75	200	123.9	**98.2**	107.6	855.0	351.3	197.0
152	168	187	32	86	54	140	8	60	6.75	200	133.9	**114.4**	127.9	888.3	391.0	193.1
153	168	187	32	56	54	110	8	30	7.6	200	103.9	**69.6**	72.2	777.6	473.2	209.0
154	168	187	32	66	54	120	8	30	7.6	200	113.9	**83.3**	89.4	818.1	522.5	201.9
155	168	187	32	76	54	130	8	30	7.6	200	123.9	**98.3**	108.1	855.1	568.3	197.0
156	168	187	32	86	54	140	8	30	7.6	200	133.9	**114.5**	128.3	888.4	610.9	193.1
157	168	187	32	56	54	110	8	60	7.6	200	103.9	**69.7**	72.2	778.0	267.0	209.1
158	168	187	32	66	54	120	8	60	7.6	200	113.9	**83.4**	89.4	818.4	310.2	202.1
159	168	187	32	76	54	130	8	60	7.6	200	123.9	**98.3**	108.1	855.1	351.6	196.9
160	168	187	32	86	54	140	8	60	7.6	200	133.9	**114.6**	128.4	888.7	391.4	193.2
161	168	187	32	56	54	110	10	30	6.75	200	103.9	**69.6**	71.7	777.8	467.6	209.0
162	168	187	32	66	54	120	10	30	6.75	200	113.9	**83.3**	88.9	818.1	517.0	201.9
163	168	187	32	76	54	130	10	30	6.75	200	123.9	**98.2**	107.7	854.9	562.8	196.9
164	168	187	32	86	54	140	10	30	6.75	200	133.9	**114.5**	128.0	888.3	605.8	193.2
165	168	187	32	56	54	110	10	60	6.75	200	103.9	**69.6**	71.7	777.9	262.9	208.7
166	168	187	32	66	54	120	10	60	6.75	200	113.9	**83.3**	88.9	818.2	306.5	201.8

Continue on next page

167	168	187	32	76	54	130	10	60	6.75	200	123.9	**98.3**	107.7	855.2	348.4	196.9
168	168	187	32	86	54	140	10	60	6.75	200	133.9	**114.5**	128.0	888.4	388.1	193.1
169	168	187	32	56	54	110	10	30	7.6	200	103.9	**69.7**	72.2	777.8	468.0	209.0
170	168	187	32	66	54	120	10	30	7.6	200	113.9	**83.5**	89.5	818.6	517.7	202.3
171	168	187	32	76	54	130	10	30	7.6	200	123.9	**98.4**	108.2	855.2	563.4	197.1
172	168	187	32	86	54	140	10	30	7.6	200	133.9	**114.7**	128.5	888.7	606.3	193.3
173	168	187	32	56	54	110	10	60	7.6	200	103.9	**69.8**	72.2	778.3	263.8	209.2
174	168	187	32	66	54	120	10	60	7.6	200	113.9	**83.5**	89.5	818.6	307.1	202.1
175	168	187	32	76	54	130	10	60	7.6	200	123.9	**98.4**	108.2	855.3	348.6	196.9
176	168	187	32	86	54	140	10	60	7.6	200	133.9	**114.7**	128.5	888.8	388.6	193.2
177	168	187	32	56	54	110	12	30	6.75	200	103.9	**69.7**	71.7	778.0	461.1	209.0
178	168	187	32	66	54	120	12	30	6.75	200	113.9	**83.4**	89.0	818.3	510.8	201.9
179	168	187	32	76	54	130	12	30	6.75	200	123.9	**98.3**	107.7	855.0	556.8	196.9
180	168	187	32	86	54	140	12	30	6.75	200	133.9	**114.6**	128.0	888.5	600.1	193.3
181	168	187	32	56	54	110	12	60	6.75	200	103.9	**69.7**	71.7	778.1	259.0	208.7
182	168	187	32	66	54	120	12	60	6.75	200	113.9	**83.5**	89.0	818.7	303.0	202.0
183	168	187	32	76	54	130	12	60	6.75	200	123.9	**98.4**	107.8	855.3	344.8	196.9
184	168	187	32	86	54	140	12	60	6.75	200	133.9	**114.7**	128.1	888.7	384.9	193.2
185	168	187	32	56	54	110	12	30	7.6	200	103.9	**69.8**	72.3	778.1	461.5	209.1
186	168	187	32	66	54	120	12	30	7.6	200	113.9	**83.6**	89.5	818.7	511.5	202.3
187	168	187	32	76	54	130	12	30	7.6	200	123.9	**98.5**	108.3	855.4	557.4	197.1
188	168	187	32	86	54	140	12	30	7.6	200	133.9	**114.7**	128.5	888.6	600.3	193.1
189	168	187	32	56	54	110	12	60	7.6	200	103.9	**69.9**	72.2	778.6	259.9	209.1
190	168	187	32	66	54	120	12	60	7.6	200	113.9	**83.6**	89.5	818.8	303.3	202.0
191	168	187	32	76	54	130	12	60	7.6	200	123.9	**98.6**	108.3	855.7	345.3	197.1
192	168	187	32	86	54	140	12	60	7.6	200	133.9	**114.9**	128.6	889.1	385.3	193.4

O FELIZ H60 (PORTUGAL)																
Numerical simulation												**t_{fi} (min)**		**T_{crit} (°C)**		
No.	l_1 (mm)	l_2 (mm)	l_3 (mm)	h_1 (mm)	h_2 (mm)	h_{tot} (mm)	ϕ_{reb} (mm)	d'_{reb} (mm)	ϕ_{mesh} (mm)	s_{mesh} (mm/mm)	h_{eff} (mm)	AVE_T crit.	MAX_T crit.	Steel deck	Rebar	Mesh
193	105	60	100	50	60	110	-	-	6	100	74.1	36.1	**34.5**	746.5	-	199.7
194	105	60	100	60	60	120	-	-	6	100	84.1	46.2	**45.8**	814.3	-	203.4
195	105	60	100	70	60	130	-	-	6	100	94.1	**57.4**	59.1	866.5	-	201.2
196	105	60	100	80	60	140	-	-	6	100	104.1	**69.8**	74.3	907.4	-	197.5

ARCELORMITTAL POLYDECK 59S (BRAZIL)																
Numerical simulation												**t_{fi} (min)**		**T_{crit} (°C)**		
No.	l_1 (mm)	l_2 (mm)	l_3 (mm)	h_1 (mm)	h_2 (mm)	h_{tot} (mm)	ϕ_{reb} (mm)	d'_{reb} (mm)	ϕ_{mesh} (mm)	s_{mesh} (mm/mm)	h_{eff} (mm)	AVE_T crit.	MAX_T crit.	Steel deck	Rebar	Mesh
197	126	61	84	51	59	110	-	-	6	100	77.3	38.3	**36.2**	763.6	-	193.0
198	126	61	84	61	59	120	-	-	6	100	87.3	49.1	**48.2**	831.2	-	196.6
199	126	61	84	71	59	130	-	-	6	100	97.3	**60.9**	62.3	882.2	-	196.9
200	126	61	84	81	59	140	-	-	6	100	107.3	**74.0**	78.4	921.4	-	193.4

VULCRAFT 3.5D DOVETAIL FORMLOK (USA)																
Numerical simulation												**t_{fi} (min)**		**T_{crit} (°C)**		
No.	l_1 (mm)	l_2 (mm)	l_3 (mm)	h_1 (mm)	h_2 (mm)	h_{tot} (mm)	ϕ_{reb} (mm)	d'_{reb} (mm)	ϕ_{mesh} (mm)	s_{mesh} (mm/mm)	h_{eff} (mm)	AVE_T crit.	MAX_T crit.	Steel deck	Rebar	Mesh
201	127	184.15	76.2	51	89	140	-	-	6	100	109.6	62.1	**60.3**	712.7	-	189.3
202	127	184.15	76.2	61	89	150	-	-	6	100	129.1	**76.2**	77.2	767.4	-	194.8
203	127	184.15	76.2	71	89	160	-	-	6	100	139.1	**91.1**	95.8	809.3	-	193.6
204	127	184.15	76.2	81	89	170	-	-	6	100	149.1	**107.0**	115.8	847.1	-	192.3

LYSAGHT BONDEK (AUSTRALIA)																
Numerical simulation												**t_{fi} (min)**		**T_{crit} (°C)**		
No.	l_1 (mm)	l_2 (mm)	l_3 (mm)	h_1 (mm)	h_2 (mm)	h_{tot} (mm)	ϕ_{reb} (mm)	d'_{reb} (mm)	ϕ_{mesh} (mm)	s_{mesh} (mm/mm)	h_{eff} (mm)	AVE_T crit.	MAX_T crit.	Steel deck	Rebar	Mesh
205	168	187	32	56	54	110	-	-	7.6	200	103.9	**69.5**	72.1	777.4	-	209.1
206	168	187	32	66	54	120	-	-	7.6	200	113.9	**83.2**	89.3	818.0	-	202.0
207	168	187	32	76	54	130	-	-	7.6	200	123.9	**98.1**	107.9	854.8	-	196.9
208	168	187	32	86	54	140	-	-	7.6	200	133.9	**114.3**	128.1	888.2	-	193.0

APPENDIX D

NUMERICAL AND EUROCODE 4 RESULTS FOR THE TEMPERATURES OF THE PARTS OF THE STEEL DECK AND THE REBARS FOR THE FIRST PARAMETRIC STUDY

	Temp. of the parts of the steel deck (°C) - R60						Temp. of the parts of the steel deck (°C) - R90						Temp. of the parts of the steel deck (°C) - R120					
No.	Lower flange		Web		Upper flange		Lower flange		Web		Upper flange		Lower flange		Web		Upper flange	
	ANS	EC4	ANS	EC4	ANS	EC4	ANS	EC4	ANS	EC4	ANS	EC4	ANS	EC4	ANS	EC4	ANS	EC4
1	923.2	861.7	881.0	779.6	859.2	713.4	993.3	959.4	965.3	906.6	950.7	851.5	1040.4	1016.9	1019.0	976.7	1007.6	931.8
2	922.9	861.7	877.8	779.6	853.7	713.4	993.0	959.4	962.5	906.6	946.3	851.5	1040.0	1016.9	1017.0	976.7	1004.5	931.8
3	922.8	861.7	875.9	779.6	850.7	713.4	992.7	959.4	960.2	906.6	942.7	851.5	1039.8	1016.9	1015.0	976.7	1001.7	931.8
4	922.7	861.7	874.7	779.6	849.1	713.4	992.5	959.4	958.4	906.6	940.1	851.5	1039.6	1016.9	1013.3	976.7	999.2	931.8
17	923.0	861.7	880.8	779.6	859.1	713.4	993.2	959.4	965.2	906.6	950.6	851.5	1040.2	1016.9	1018.9	976.7	1007.5	931.8
18	922.7	861.7	877.6	779.6	853.6	713.4	992.8	959.4	962.3	906.6	946.1	851.5	1039.9	1016.9	1016.8	976.7	1004.4	931.8
19	922.5	861.7	875.7	779.6	850.6	713.4	992.5	959.4	960.0	906.6	942.6	851.5	1039.6	1016.9	1014.9	976.7	1001.6	931.8
20	922.4	861.7	874.5	779.6	849.0	713.4	992.4	959.4	958.3	906.6	940.0	851.5	1039.4	1016.9	1013.2	976.7	999.1	931.8
33	922.7	861.7	880.5	779.6	858.9	713.4	993.0	959.4	965.0	906.6	950.5	851.5	1040.0	1016.9	1018.7	976.7	1007.4	931.8
34	922.4	861.7	877.3	779.6	853.4	713.4	992.6	959.4	962.2	906.6	946.0	851.5	1039.7	1016.9	1016.6	976.7	1004.3	931.8
35	922.3	861.7	875.4	779.6	850.4	713.4	992.4	959.4	959.8	906.6	942.4	851.5	1039.4	1016.9	1014.7	976.7	1001.5	931.8
36	922.2	861.7	874.2	779.6	848.8	713.4	992.2	959.4	958.1	906.6	939.9	851.5	1039.2	1016.9	1013.0	976.7	999.0	931.8
49	921.1	851.0	883.2	773.0	861.9	706.5	991.8	952.1	966.1	899.5	951.7	845.0	1038.8	1011.3	1019.1	970.0	1007.9	925.0
50	920.8	851.0	880.4	773.0	857.0	706.5	991.4	952.1	963.4	899.5	947.5	845.0	1038.4	1011.3	1017.1	970.0	1004.9	925.0
51	920.7	851.0	878.8	773.0	854.4	706.5	991.1	952.1	961.4	899.5	944.3	845.0	1038.2	1011.3	1015.4	970.0	1002.3	925.0
52	920.6	851.0	877.7	773.0	852.9	706.5	991.0	952.1	959.8	899.5	941.9	845.0	1038.1	1011.3	1013.9	970.0	1000.0	925.0
65	920.9	851.0	883.0	773.0	861.8	706.5	991.6	952.1	965.9	899.5	951.6	845.0	1038.7	1011.3	1019.0	970.0	1007.9	925.0
66	920.6	851.0	880.2	773.0	856.9	706.5	991.2	952.1	963.3	899.5	947.5	845.0	1038.3	1011.3	1017.0	970.0	1004.8	925.0
67	920.5	851.0	878.6	773.0	854.3	706.5	991.0	952.1	961.3	899.5	944.2	845.0	1038.1	1011.3	1015.3	970.0	1002.3	925.0
68	920.4	851.0	877.5	773.0	852.9	706.5	990.9	952.1	959.7	899.5	941.9	845.0	1038.3	1011.3	1014.0	970.0	1000.1	925.0
81	920.7	851.0	882.8	773.0	861.7	706.5	991.5	952.1	965.8	899.5	951.5	845.0	1038.7	1011.3	1019.0	970.0	1007.9	925.0
82	920.4	851.0	880.0	773.0	856.8	706.5	991.1	952.1	963.2	899.5	947.4	845.0	1038.1	1011.3	1016.8	970.0	1004.7	925.0
83	920.2	851.0	878.4	773.0	854.2	706.5	990.8	952.1	961.2	899.5	944.1	845.0	1038.3	1011.3	1015.5	970.0	1002.4	925.0

Continue on next page

84	920.2	851.0	877.3	773.0	852.7	706.5	990.7	952.1	959.6	899.5	941.8	845.0	1037.8	1011.3	1013.6	970.0	999.8	925.0
97	914.9	855.7	706.9	588.9	524.7	305.3	986.7	954.5	812.7	763.2	667.9	585.4	1035.0	1015.7	888.5	875.8	772.2	729.8
98	914.8	855.7	704.1	588.9	517.9	305.3	986.5	954.5	806.8	763.2	654.9	585.4	1034.7	1015.7	881.5	875.8	757.7	729.8
99	914.7	855.7	702.2	588.9	514.0	305.3	986.4	954.5	803.1	763.2	646.8	585.4	1034.2	1015.7	876.2	875.8	746.4	729.8
100	914.7	855.7	700.6	588.9	511.1	305.3	986.4	954.5	800.9	763.2	642.3	585.4	1034.2	1015.7	873.2	875.8	739.2	729.8
113	914.8	855.7	706.8	588.9	524.6	305.3	986.7	954.5	812.6	763.2	667.7	585.4	1034.8	1015.7	888.2	875.8	771.9	729.8
114	914.8	855.7	703.9	588.9	517.8	305.3	986.5	954.5	806.6	763.2	654.7	585.4	1034.5	1015.7	881.3	875.8	757.4	729.8
115	914.7	855.7	702.1	588.9	513.9	305.3	986.4	954.5	803.0	763.2	646.7	585.4	1034.4	1015.7	876.2	875.8	746.4	729.8
116	914.6	855.7	700.5	588.9	510.9	305.3	986.3	954.5	800.7	763.2	642.2	585.4	1034.3	1015.7	873.0	875.8	739.0	729.8
129	914.8	855.7	706.7	588.9	524.5	305.3	986.7	954.5	812.5	763.2	667.6	585.4	1034.8	1015.7	888.0	875.8	771.7	729.8
130	914.7	855.7	703.8	588.9	517.7	305.3	986.5	954.5	806.5	763.2	654.5	585.4	1034.5	1015.7	881.1	875.8	757.3	729.8
131	914.7	855.7	702.0	588.9	513.8	305.3	986.4	954.5	802.8	763.2	646.5	585.4	1034.4	1015.7	876.1	875.8	746.2	729.8
132	914.6	855.7	700.4	588.9	510.8	305.3	986.3	954.5	800.6	763.2	642.0	585.4	1034.4	1015.7	873.0	875.8	738.9	729.8
145	906.9	846.6	736.1	596.4	576.5	276.0	980.5	947.7	837.7	763.5	705.1	555.0	1029.7	1009.5	910.6	872.5	801.7	702.2
146	906.6	846.6	733.8	596.4	572.1	276.0	979.9	947.7	832.6	763.5	695.7	555.0	1029.3	1009.5	904.3	872.5	789.6	702.2
147	906.5	846.6	731.9	596.4	568.8	276.0	977.4	947.7	829.7	763.5	690.2	555.0	1028.8	1009.5	899.3	872.5	780.2	702.2
148	906.3	846.6	730.3	596.4	566.2	276.0	979.5	947.7	827.6	763.5	686.7	555.0	1028.7	1009.5	896.4	872.5	774.3	702.2
161	906.8	846.6	736.0	596.4	576.4	276.0	980.4	947.7	837.6	763.5	705.0	555.0	1029.9	1009.5	910.6	872.5	801.7	702.2
162	906.6	846.6	733.7	596.4	572.0	276.0	979.9	947.7	832.5	763.5	695.5	555.0	1029.4	1009.5	904.2	872.5	789.5	702.2
163	906.5	846.6	731.9	596.4	568.7	276.0	979.8	947.7	829.6	763.5	690.0	555.0	1028.6	1009.5	899.1	872.5	780.0	702.2
164	906.3	846.6	730.2	596.4	566.0	276.0	979.5	947.7	827.5	763.5	686.5	555.0	1028.9	1009.5	896.1	872.5	774.1	702.2
177	906.8	846.6	735.9	596.4	576.3	276.0	980.2	947.7	837.4	763.5	704.8	555.0	1029.6	1009.5	910.3	872.5	801.4	702.2
178	906.6	846.6	733.6	596.4	571.8	276.0	979.5	947.7	832.4	763.5	695.4	555.0	1029.2	1009.5	903.9	872.5	789.2	702.2
179	906.4	846.6	731.8	596.4	568.6	276.0	979.8	947.7	829.5	763.5	689.9	555.0	1028.7	1009.5	899.1	872.5	779.9	702.2
180	906.3	846.6	730.2	596.4	566.0	276.0	977.1	947.7	827.5	763.5	686.4	555.0	1028.9	1009.5	896.0	872.5	774.0	702.2

No.	Temperature of the rebars (°C)					
	R60		R90		R120	
	ANS	EC4	ANS	EC4	ANS	EC4
1	598.9	524.2	731.3	695.1	837.0	797.7
2	595.8	524.2	-	-	-	-
3	594.6	524.2	-	-	-	-
4	593.8	524.2	-	-	-	-
17	586.8	524.2	723.1	695.1	822.4	797.7
18	584.0	524.2	-	-	-	-
19	582.8	524.2	-	-	-	-
20	582.1	524.2	-	-	-	-
33	572.7	524.2	712.0	695.1	799.2	797.7
34	570.1	524.2	-	-	-	-
35	569.0	524.2	-	-	-	-
36	568.3	524.2	-	-	-	-
49	560.6	491.9	698.6	659.0	789.1	760.6
50	557.8	491.9	-	-	-	-
51	556.5	491.9	-	-	-	-
52	555.8	491.9	-	-	-	-
65	549.9	491.9	688.4	659.0	769.6	760.6
66	547.3	491.9	-	-	-	-
67	546.2	491.9	-	-	-	-
68	545.4	491.9	-	-	-	-
81	537.4	491.9	676.6	659.0	749.4	760.6
82	535.0	491.9	-	-	-	-
83	534.0	491.9	-	-	-	-
84	533.2	491.9	-	-	-	-
145	431.4	363.0	549.0	538.2	640.6	656.9
146	429.8	363.0	-	-	-	-
147	428.9	363.0	-	-	-	-
148	427.9	363.0	-	-	-	-
161	425.6	363.0	543.4	538.2	634.9	656.9
162	424.0	363.0	-	-	-	-
163	423.1	363.0	-	-	-	-
164	422.2	363.0	-	-	-	-
177	418.6	363.0	536.7	538.2	628.1	656.9
178	417.1	363.0	-	-	-	-
179	416.3	363.0	-	-	-	-
180	415.5	363.0	-	-	-	-

APPENDIX E

TECHNICAL FILES FOR THE SECOND PARAMETRIC STUDY

SIM. 1	**Steel deck:** Trapezoidal – O Feliz H60	**Rebar (mm):** ϕ8	**t_a (mm):** 0	**Fire resistance (min)**	
	Mesh (mm//mm): ϕ6//100 (FNQ 60)	**h_1 (mm):** 50		Ave: 36.3	Max: *34.6*

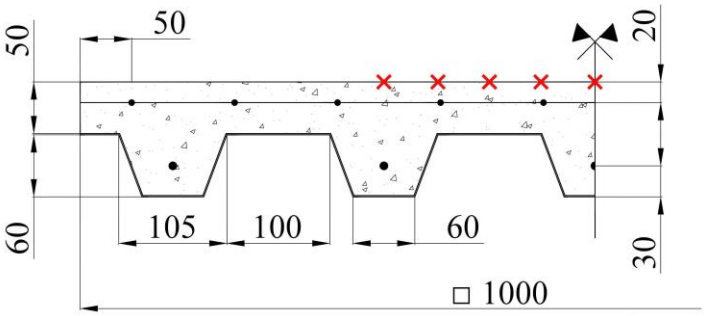

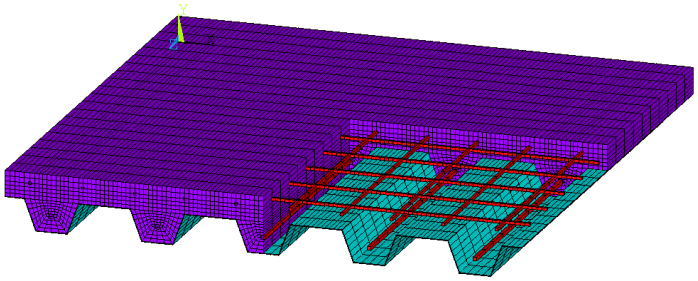

Finite element mesh

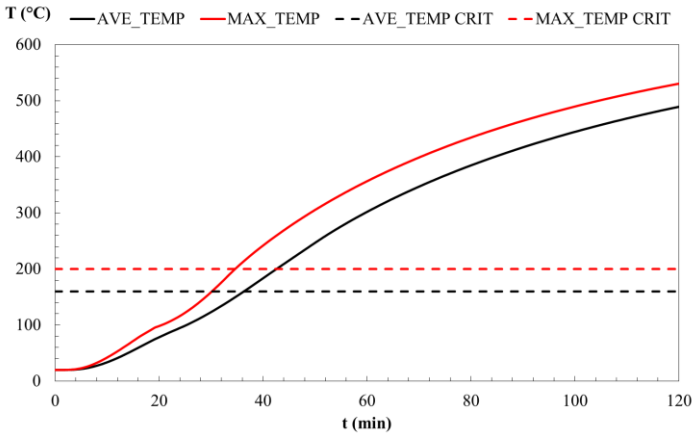

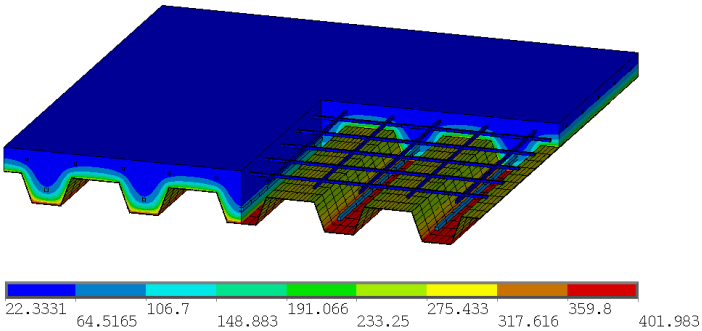

t= 8.7 min

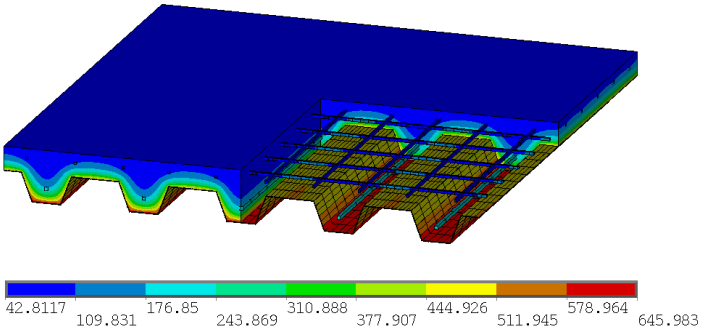

t= 17.3 min

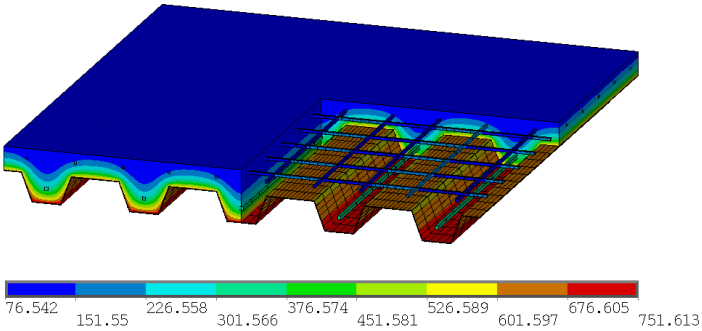

t= 26.0 min

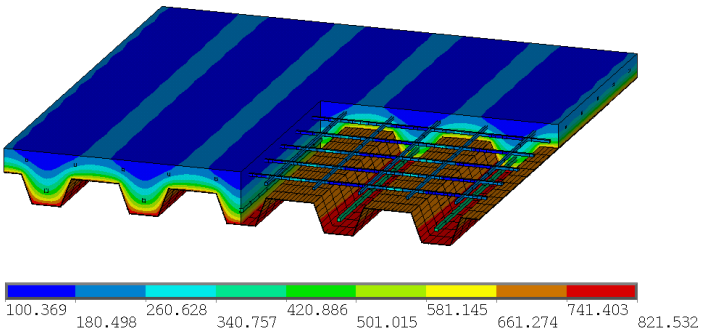

t= 34.6 min

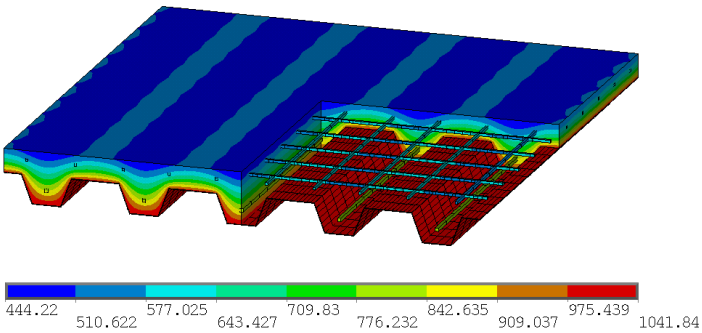

t= 120.0 min

SIM. 2	**Steel deck:** Trapezoidal – O Feliz H60	**Rebar (mm):** ϕ8	**t_a (mm):** 0	**Fire resistance (min)**	
	Mesh (mm//mm): ϕ6//100 (FNQ 60)	**h_1 (mm): 60**		Ave: 46.4	Max: *45.9*

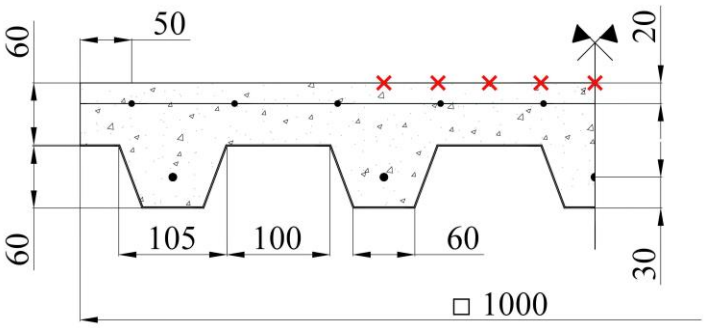

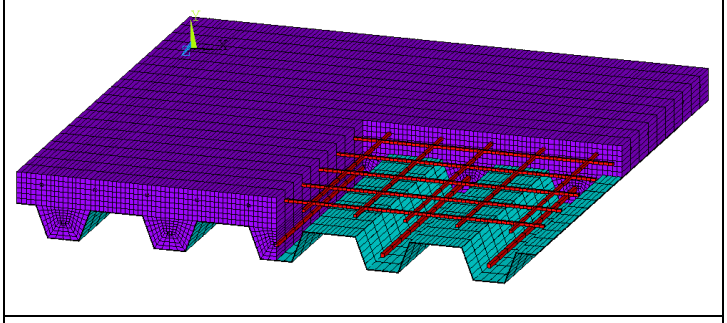

Finite element mesh

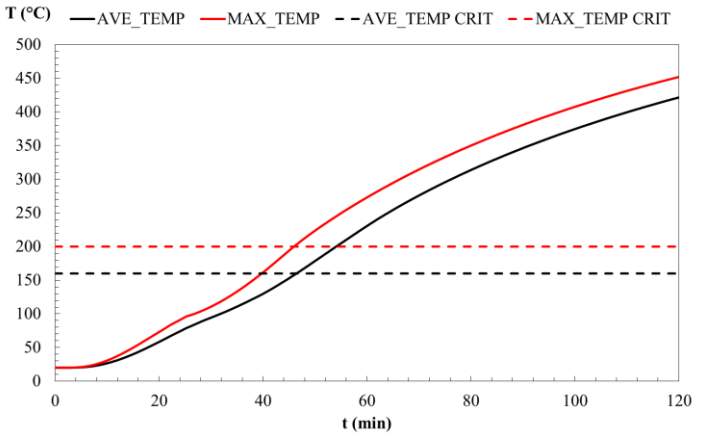

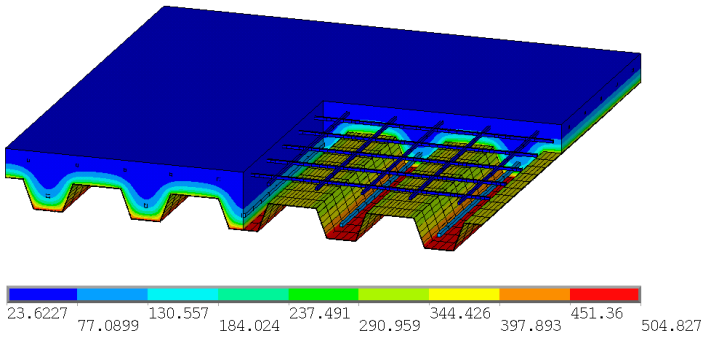

t= 11.5 min

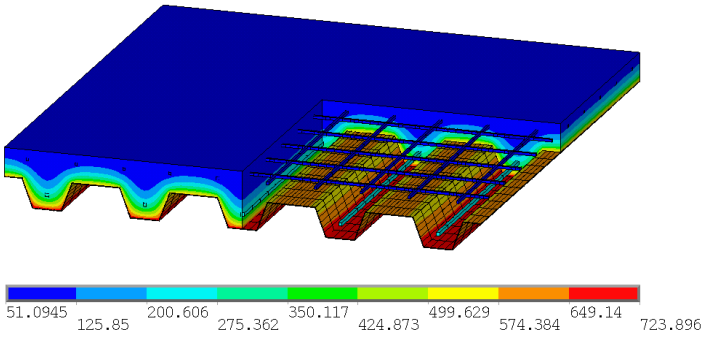

t= 23.0 min

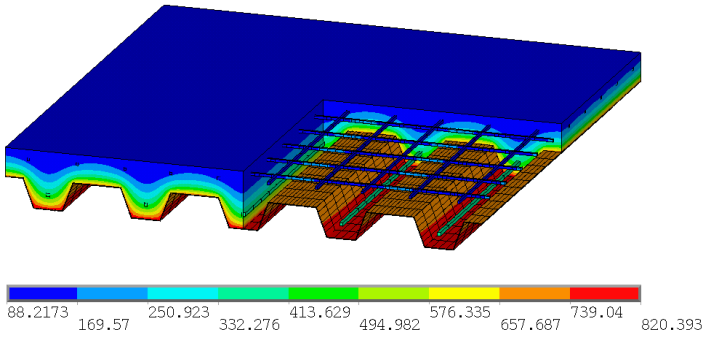

t= 34.4 min

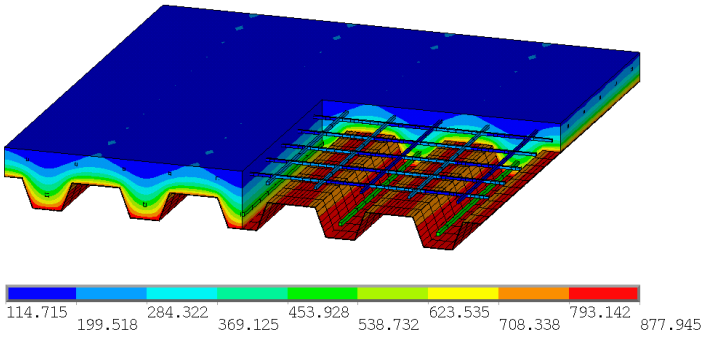

t= 45.9 min

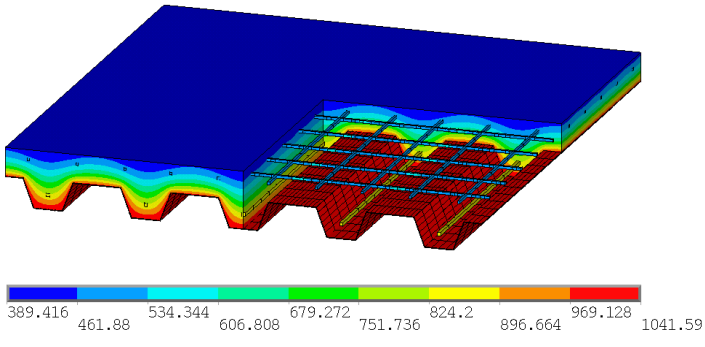

t= 120.0 min

SIM. 3	**Steel deck:** Trapezoidal – O Feliz H60	**Rebar (mm):** ϕ8	**t_a (mm):** 0	**Fire resistance (min)**	
	Mesh (mm//mm): ϕ6//100 (FNQ 60)	**h_1 (mm):** 70		Ave: *57.7*	Max: 59.3

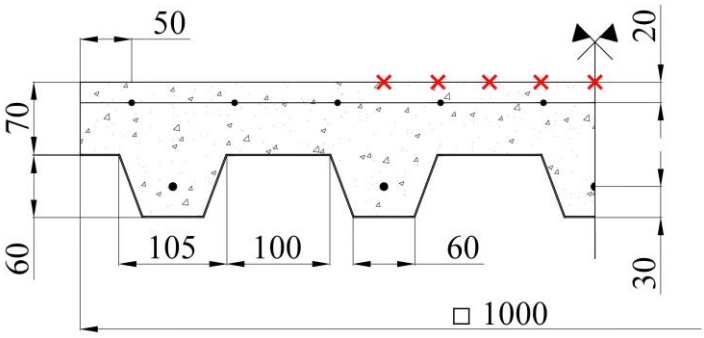

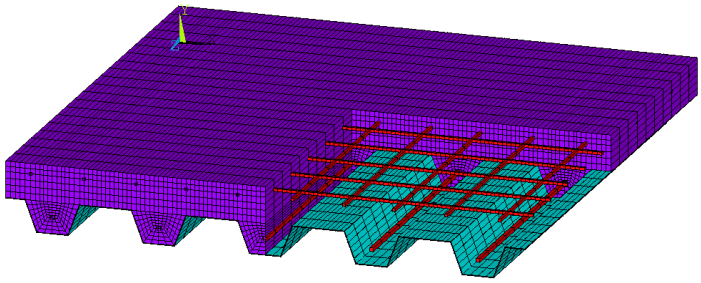

Finite element mesh

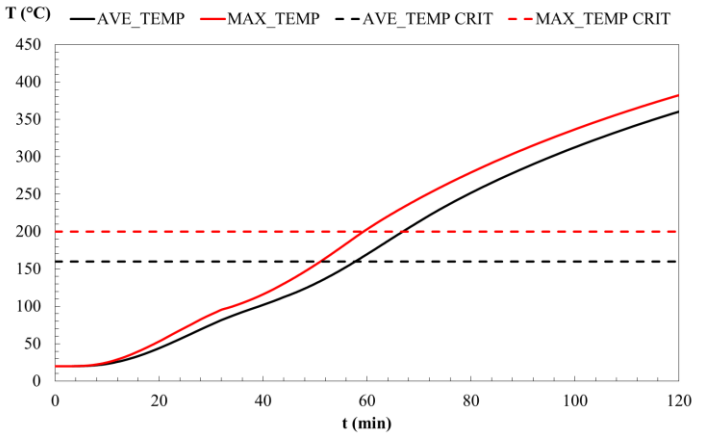

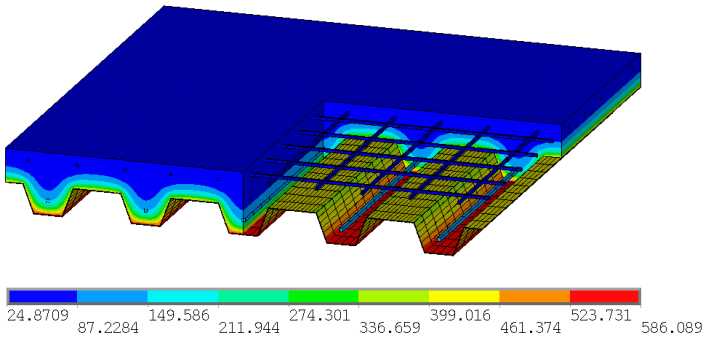

t= 14.4 min

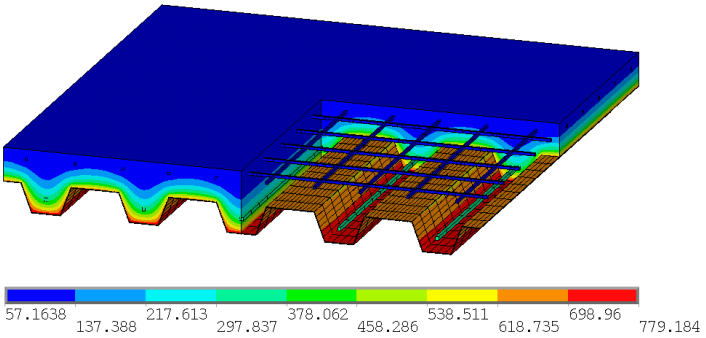

t= 28.9 min

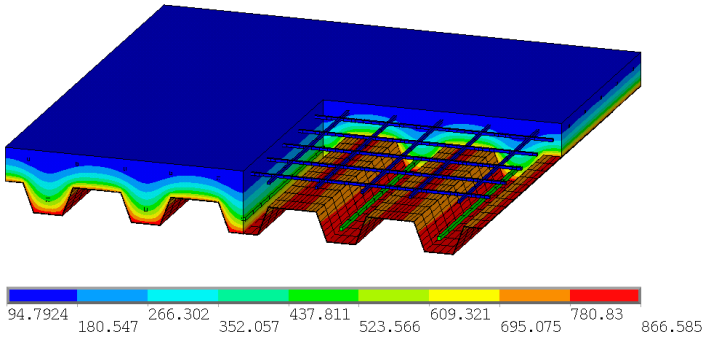

t= 43.3 min

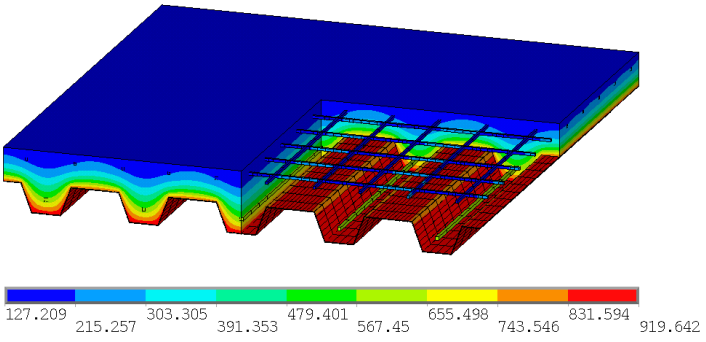

t= 57.7 min

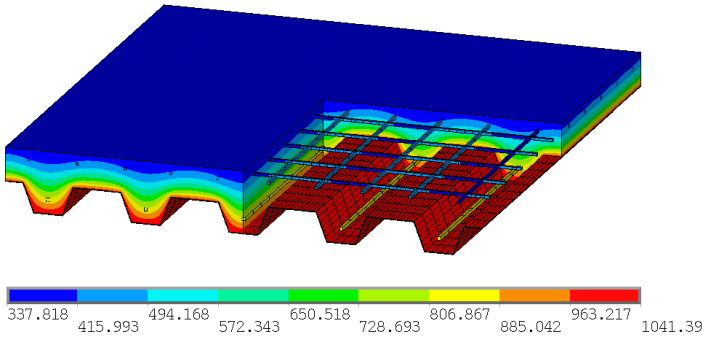

t= 120.0 min

SIM. 4	**Steel deck:** Trapezoidal – O Feliz H60	**Rebar (mm):** ϕ8	**t_a (mm):** 0	**Fire resistance (min)**	
	Mesh (mm//mm): ϕ6//100 (FNQ 60)	**h_1 (mm):** 80		Ave: *70.1*	Max: 74.5

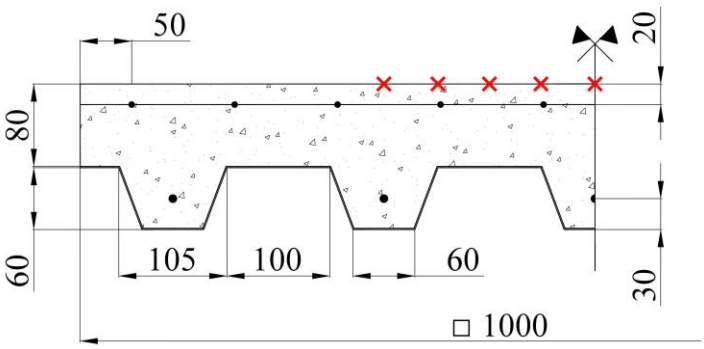

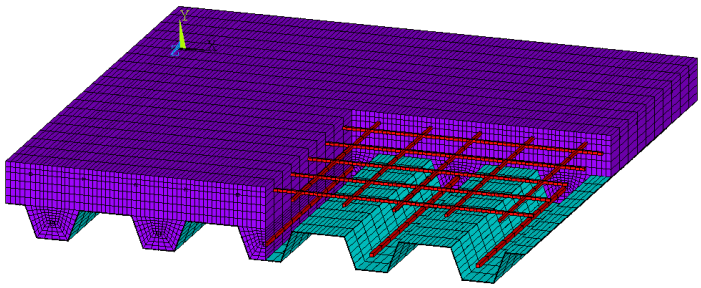

Finite element mesh

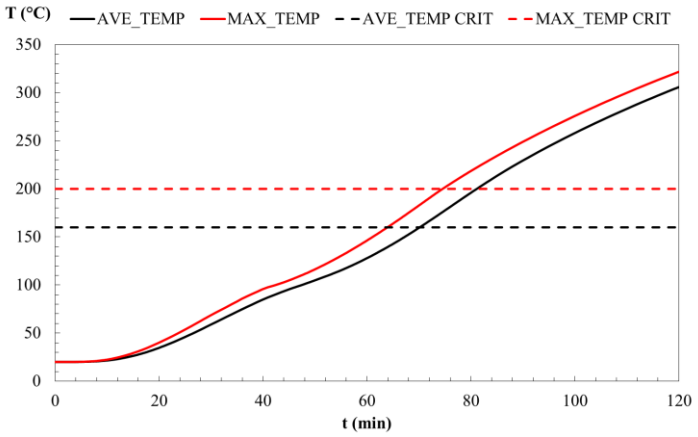

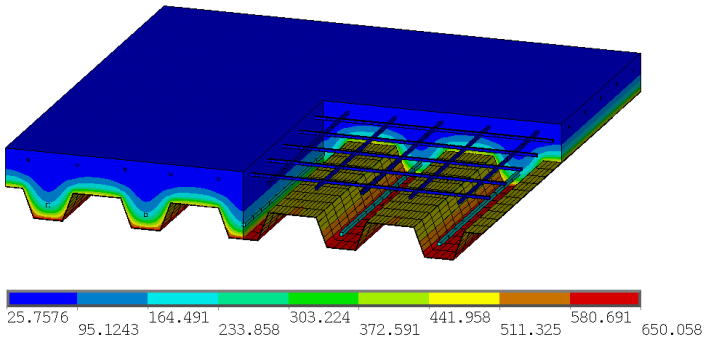

t= 17.5 min

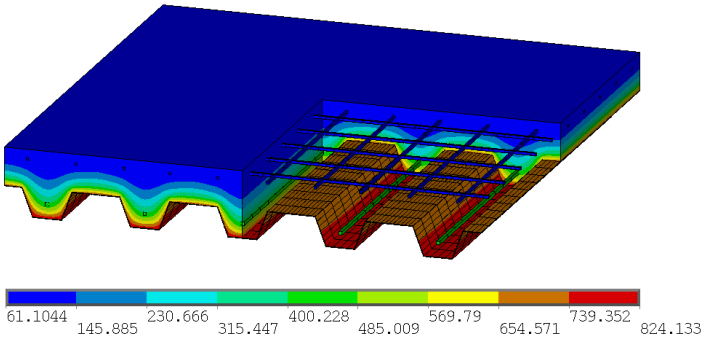

t= 35.1 min

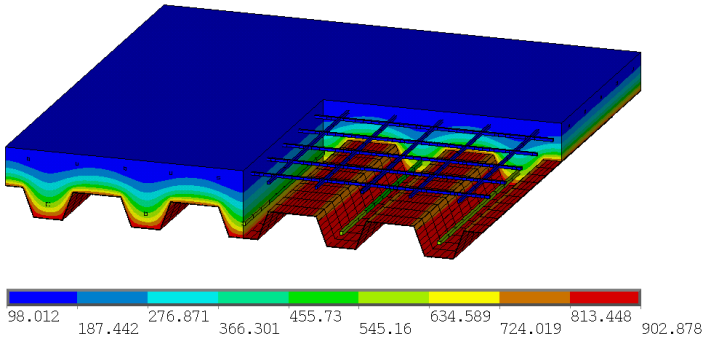

t= 52.6 min

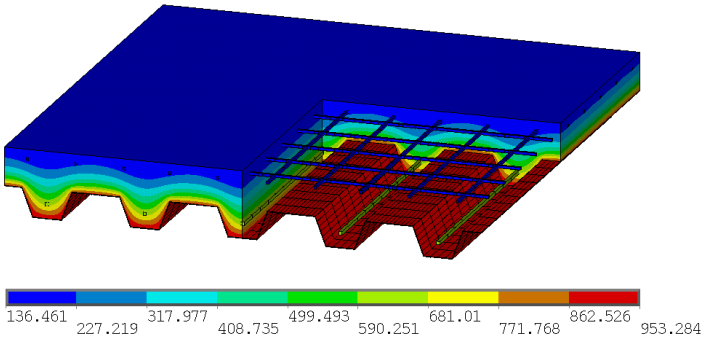

t= 70.1 min

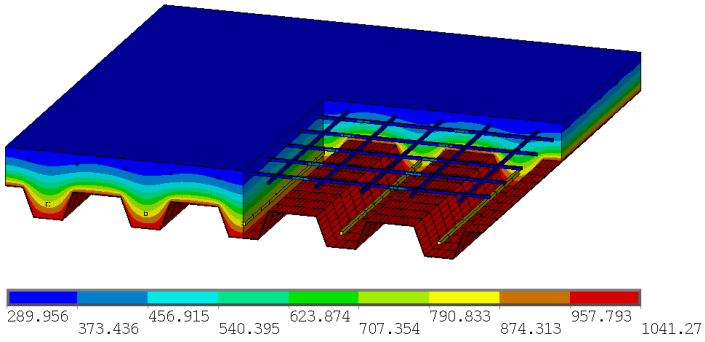

t= 120.0 min

SIM. 5	**Steel deck:** Trapezoidal – O Feliz H60	**Rebar (mm):** ϕ8	**t_a (mm):** 0	**Fire resistance (min)**	
	Mesh (mm//mm): ϕ6//100 (FNQ 60)	**h_1 (mm):** 90		Ave: *83.6*	Max: 91.4

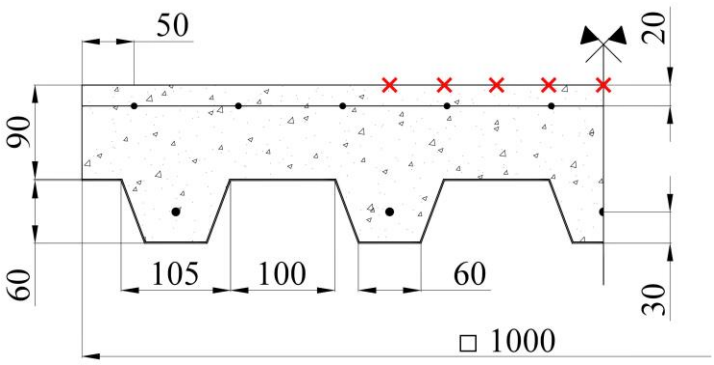

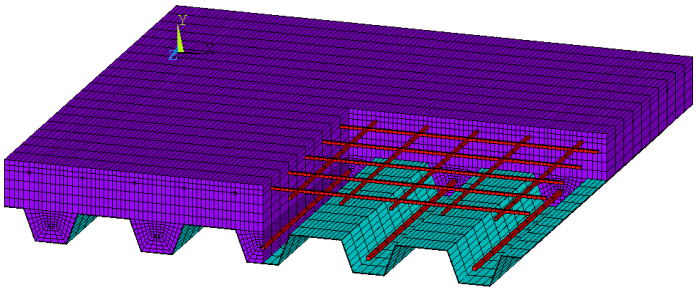

Finite element mesh

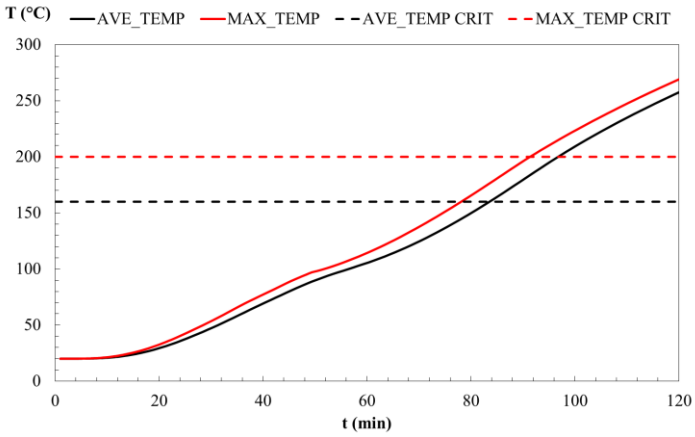

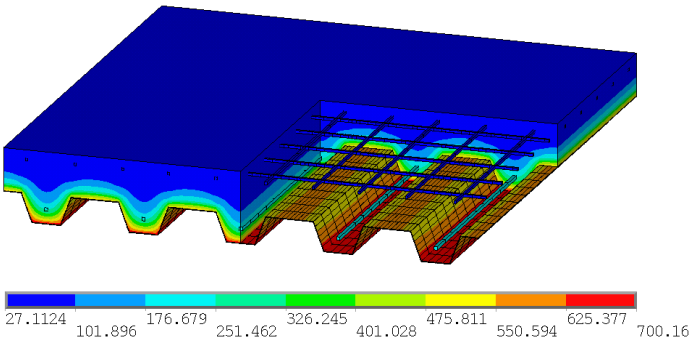

t= 20.9 min

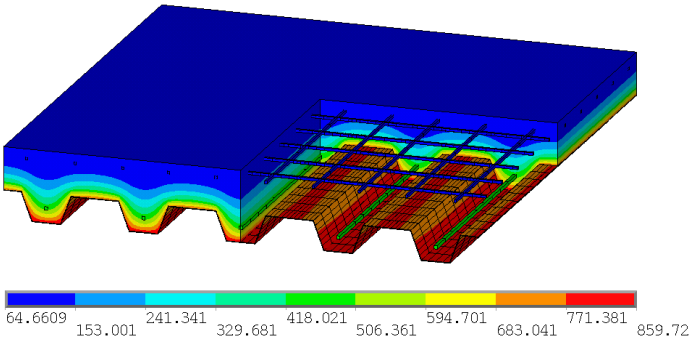

t= 41.8 min

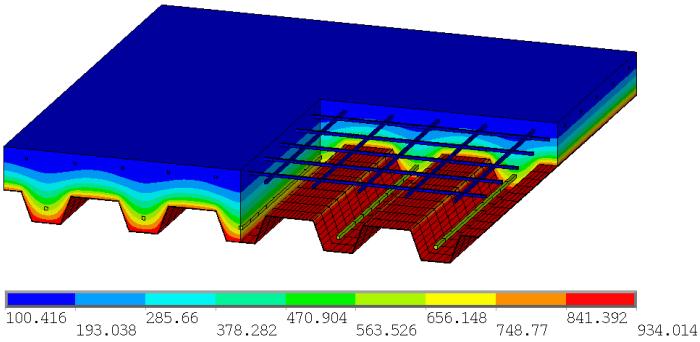

t= 62.7 min

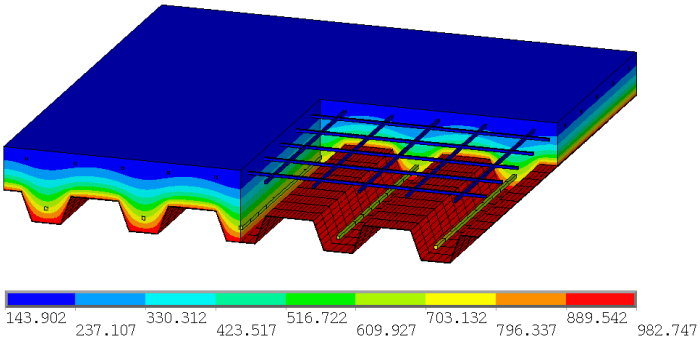

t= 83.6 min

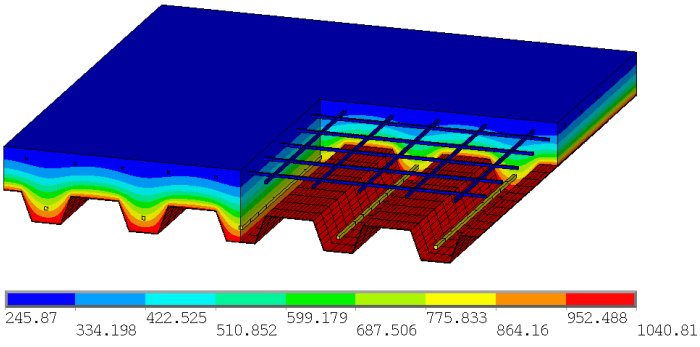

t= 120.0 min

SIM. 6	**Steel deck:** Trapezoidal – O Feliz H60	**Rebar (mm):** ϕ8	**t_a (mm):** 0	**Fire resistance (min)**	
	Mesh (mm//mm): ϕ6//100 (FNQ 60)	**h_1 (mm):** 100		Ave: *99.1*	Max: 110.3

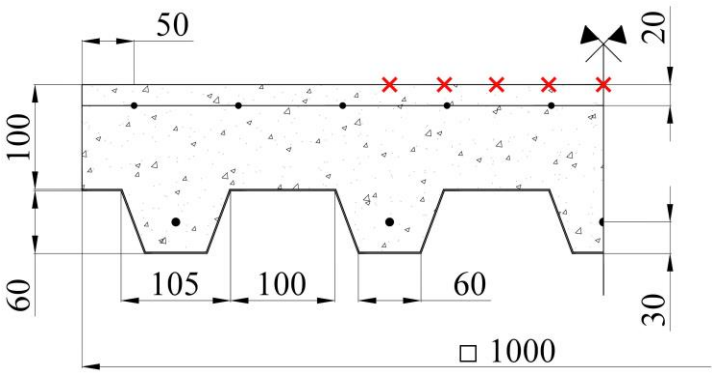

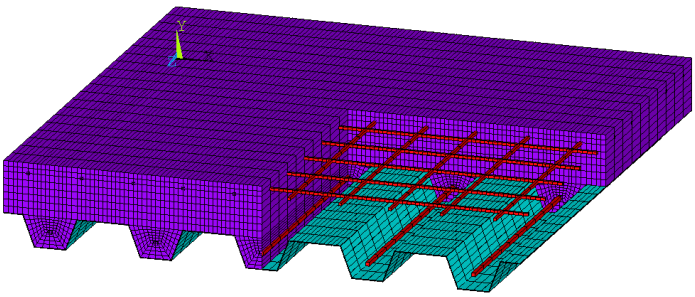

Finite element mesh

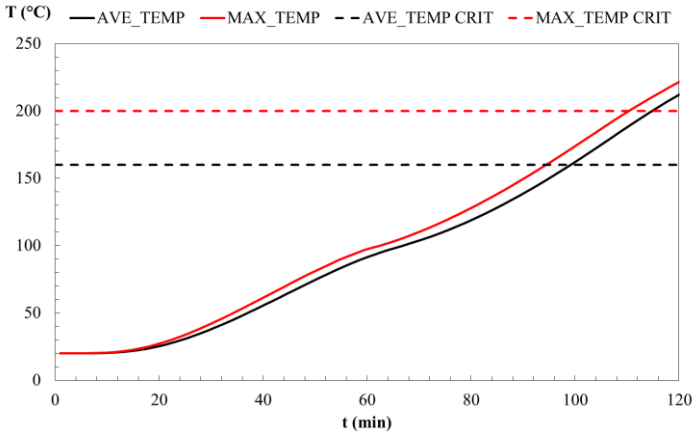

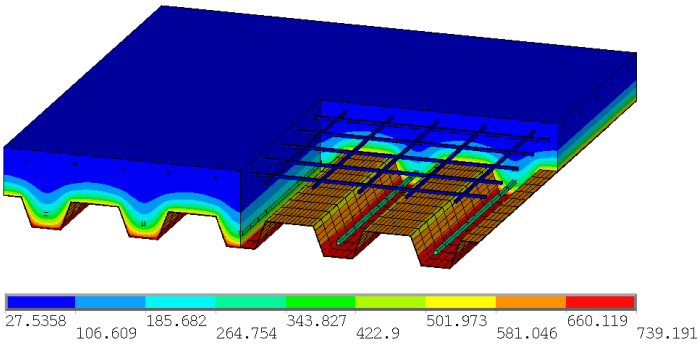

t= 24.8 min

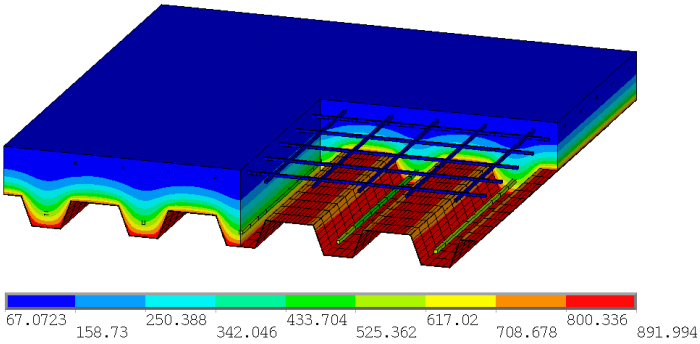

t= 49.6 min

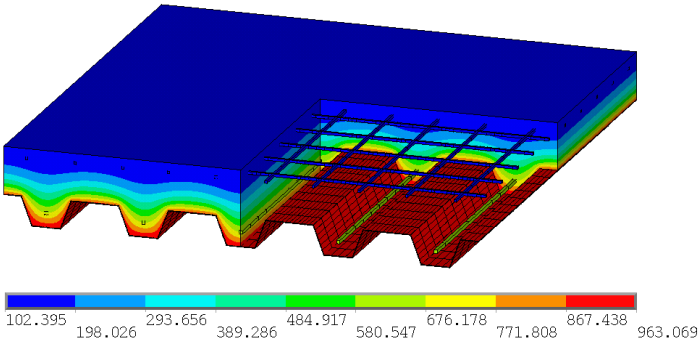

t= 74.3 min

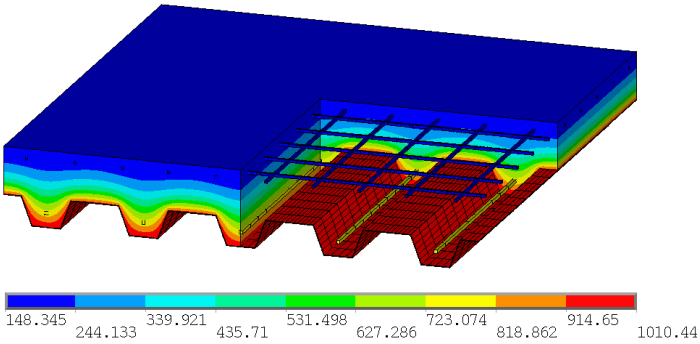

t= 99.1 min

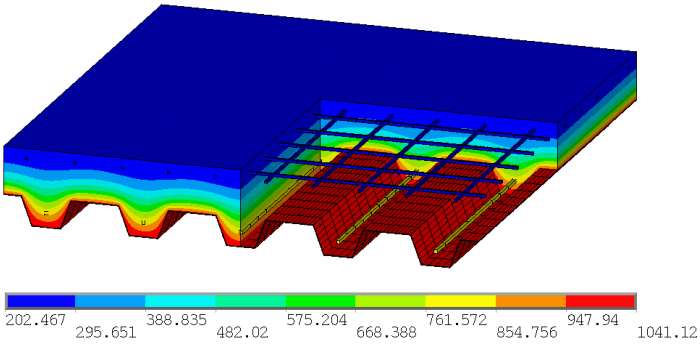

t= 120.0 min

SIM. 7	**Steel deck:** Trapezoidal – O Feliz H60	**Rebar (mm):** ϕ8	**t_a (mm):** 0	**Fire resistance (min)**	
	Mesh (mm//mm): ϕ6//100 (FNQ 60)	**h_1 (mm):** 110		Ave: *115.6*	Max: 130.6

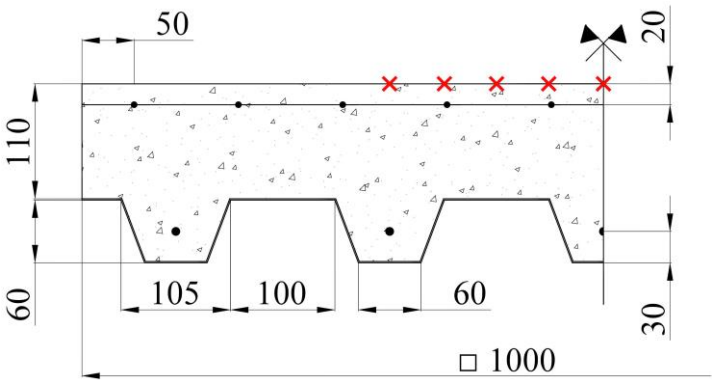

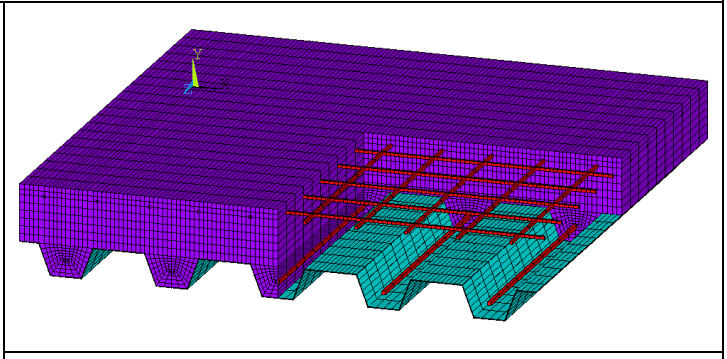

Finite element mesh

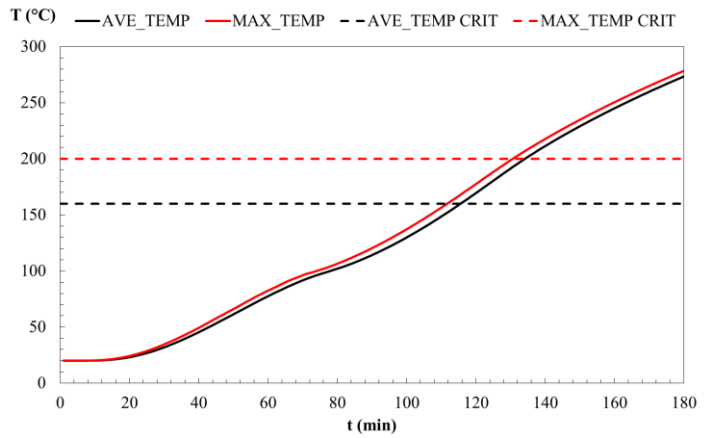

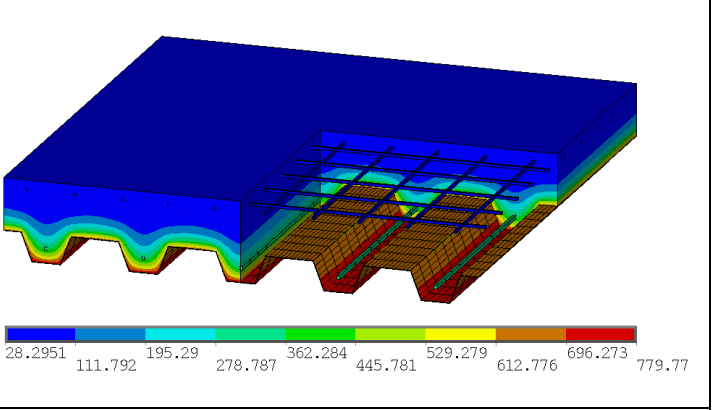

t= 28.9 min

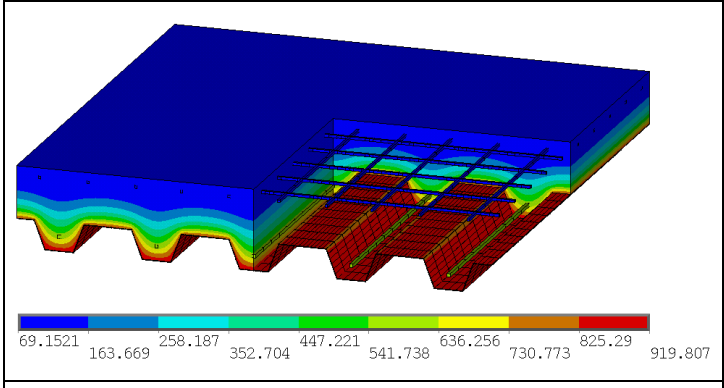

t= 57.8 min

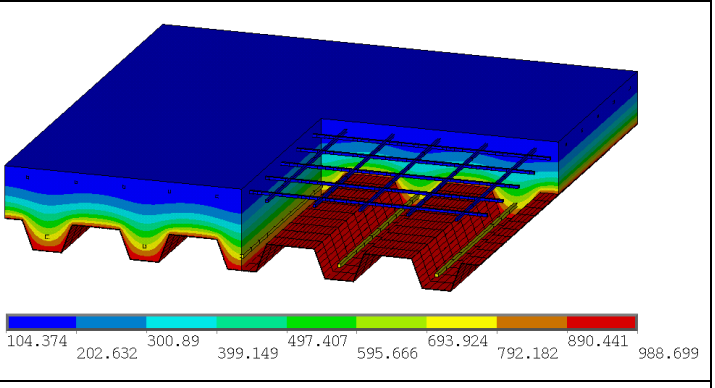

t= 86.7 min

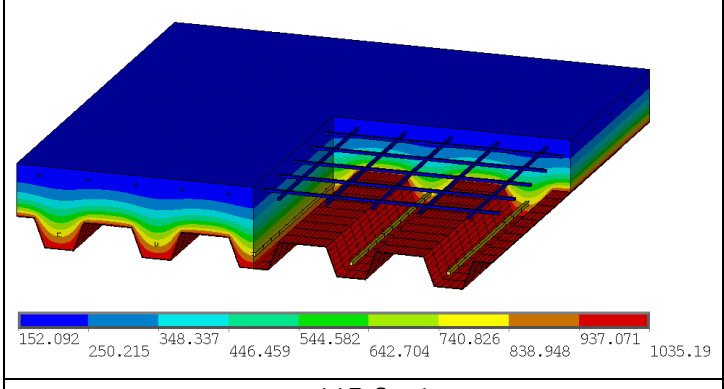

t= 115.6 min

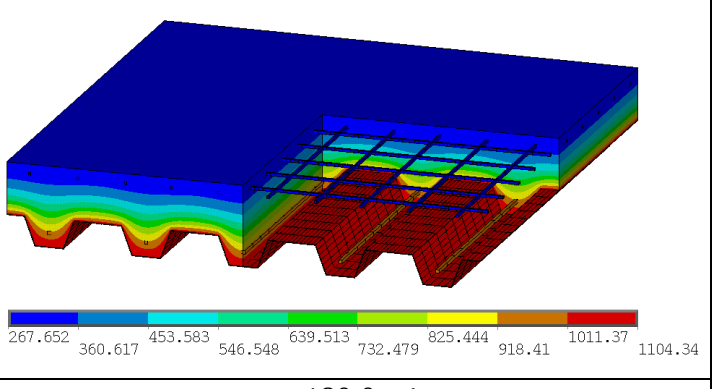

t= 180.0 min

SIM. 8	**Steel deck:** Trapezoidal – O Feliz H60	**Rebar (mm):** ϕ8	**t_a (mm):** 0	**Fire resistance (min)**	
	Mesh (mm//mm): ϕ6//100 (FNQ 60)	**h_1 (mm):** 120		Ave: *133.5*	Max: 152.7

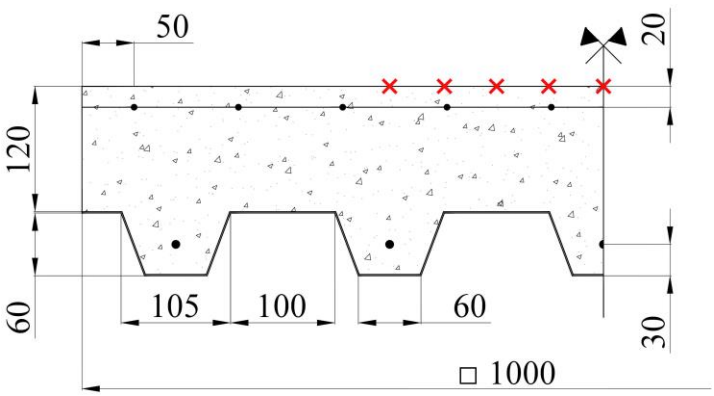

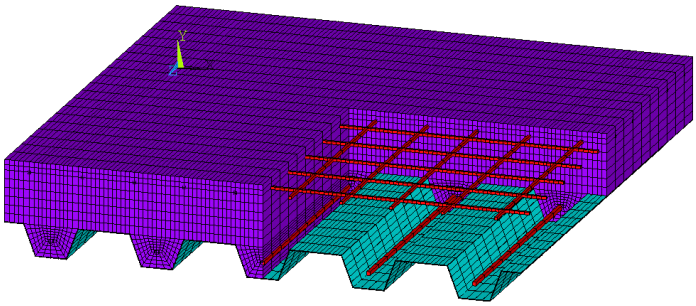

Finite element mesh

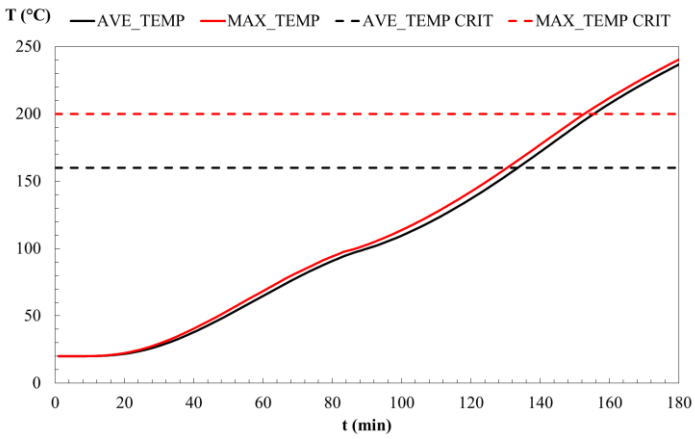

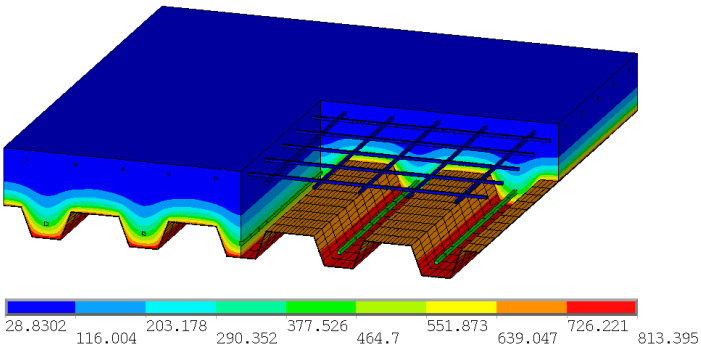

t= 33.4 min

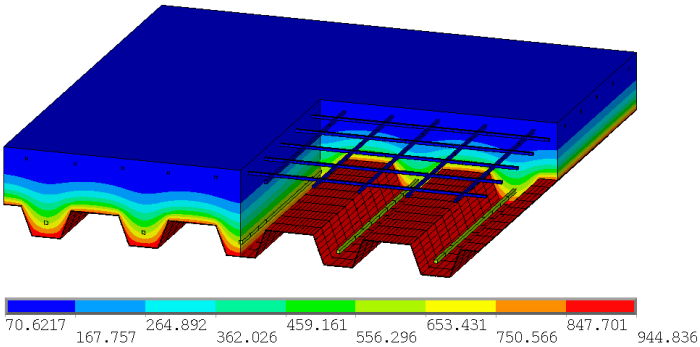

t= 66.8 min

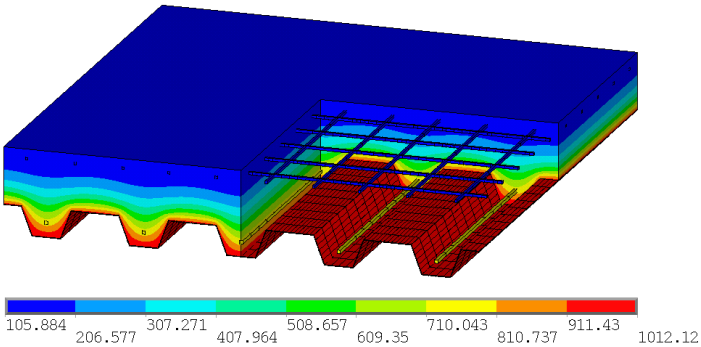

t= 100.1 min

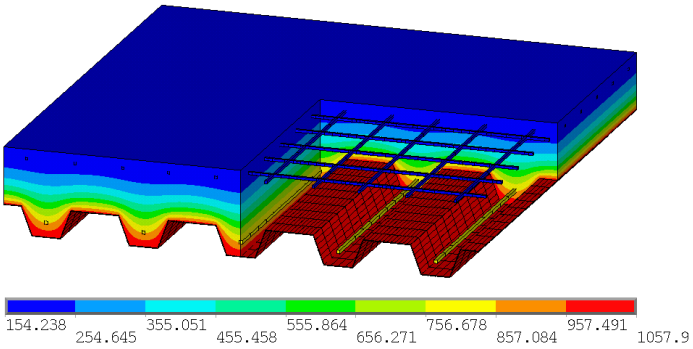

t= 133.5 min

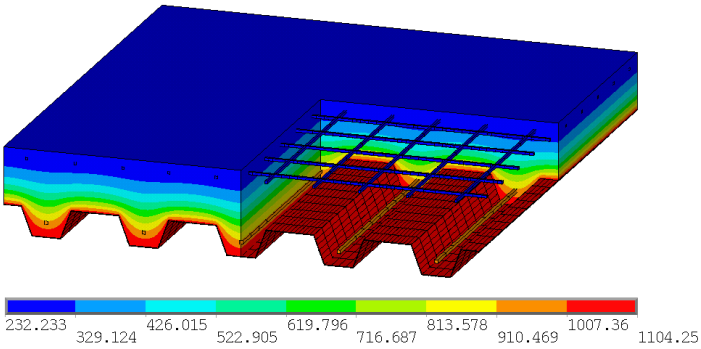

t= 180.0 min

SIM. 9	**Steel deck:** Trapezoidal – O Feliz H60	**Rebar (mm):** ϕ8	**t_a (mm):** 1	**Fire resistance (min)**	
	Mesh (mm//mm): ϕ6//100 (FNQ 60)	**h_1 (mm):** 50		Ave: 49.6	Max: *48.7*

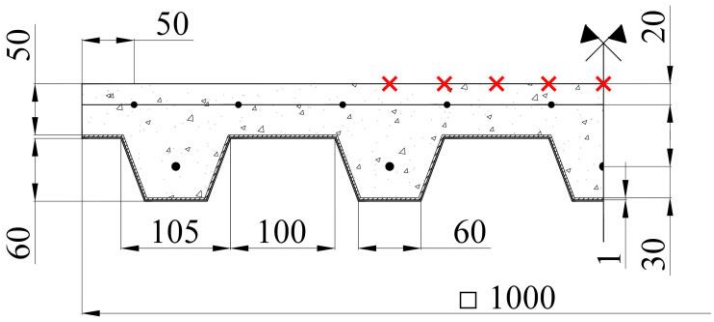

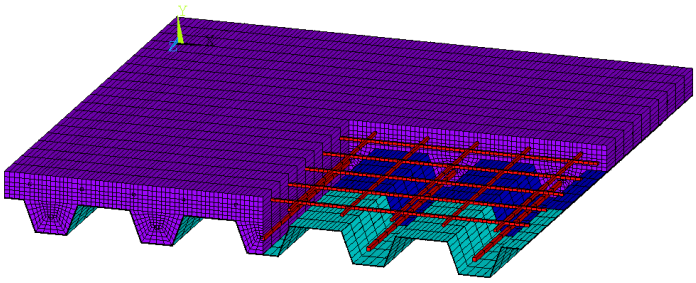

Finite element mesh

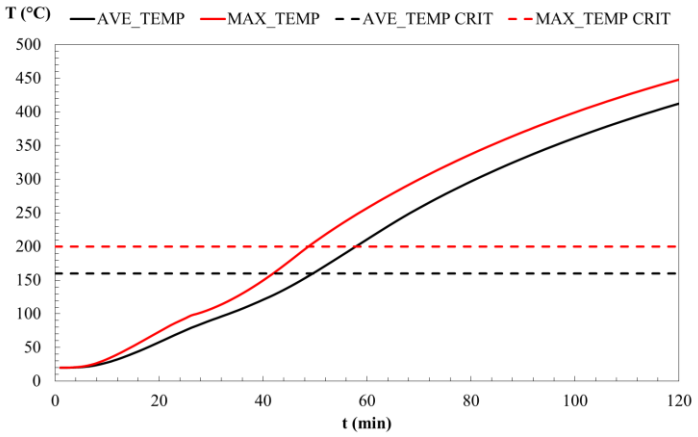

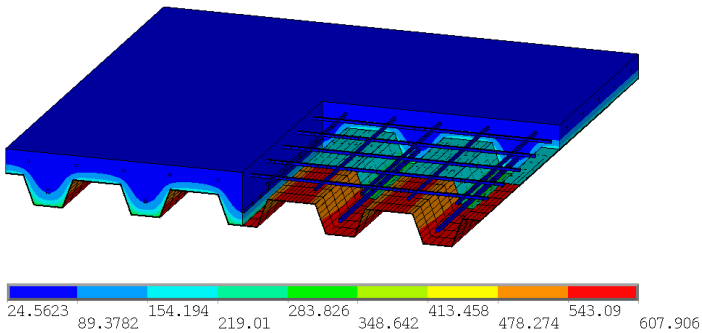

t= 12.2 min

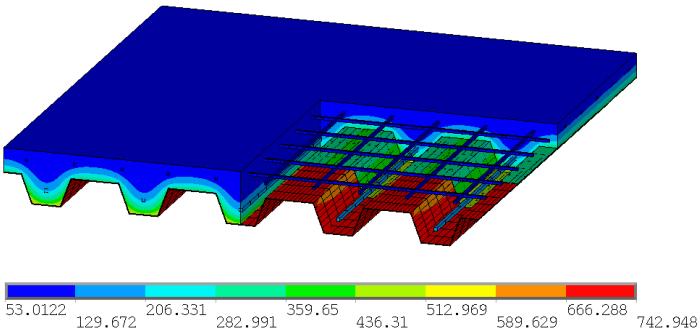

t= 24.4 min

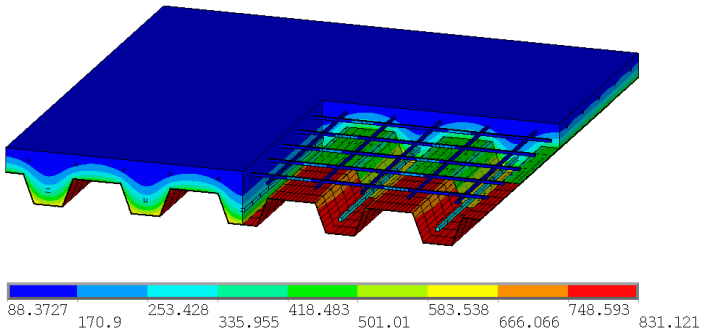

t= 36.5 min

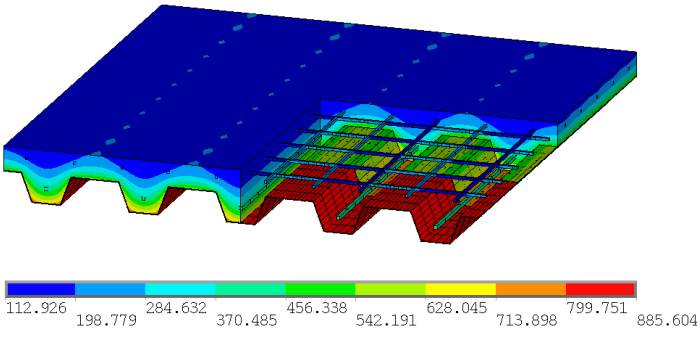

t= 48.7 min

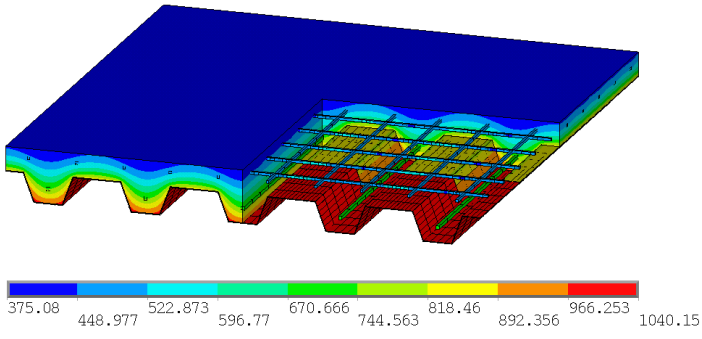

t= 120.0 min

SIM. 10	**Steel deck:** Trapezoidal – O Feliz H60	**Rebar (mm):** ϕ8	**t_a (mm):** 1	**Fire resistance (min)**	
	Mesh (mm//mm): ϕ6//100 (FNQ 60)	**h_1 (mm):** 60		Ave: *61.3*	Max: 62.6

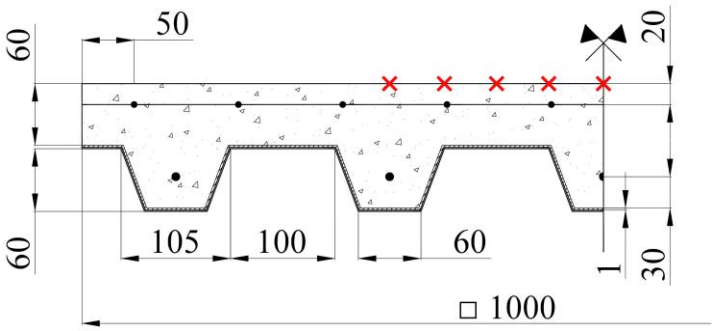

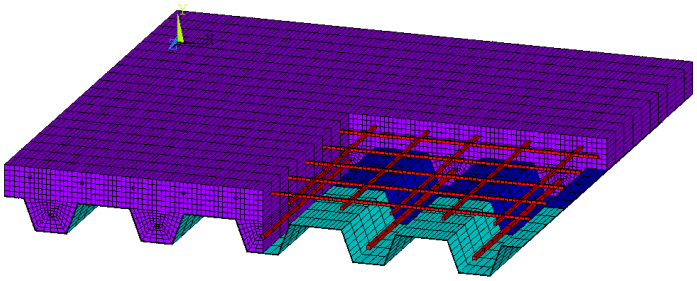

Finite element mesh

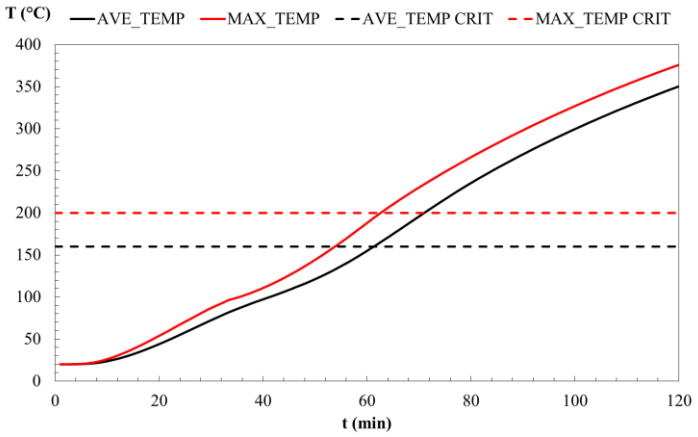

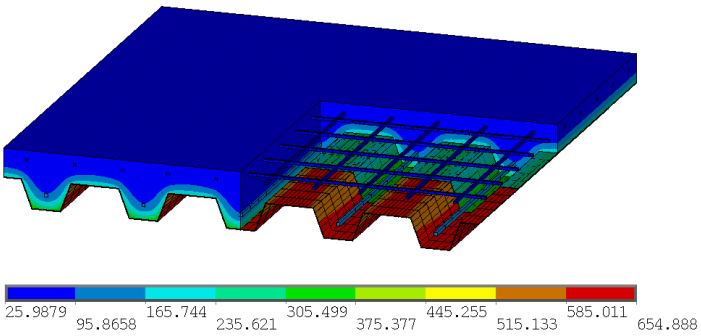

t= 15.3 min

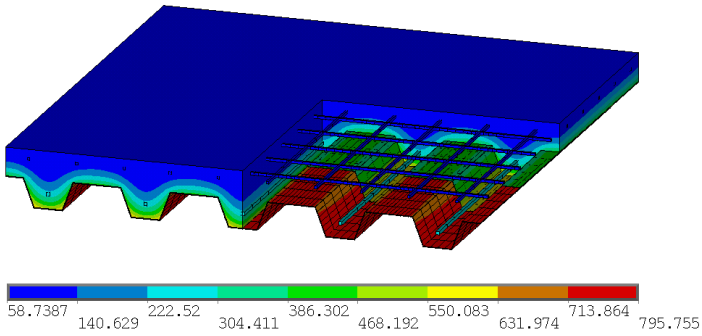

t= 30.7 min

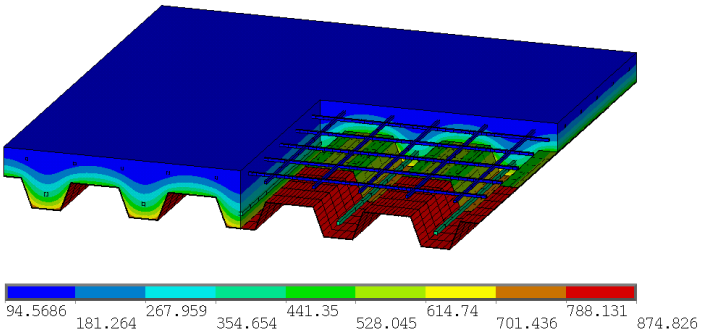

t= 46.0 min

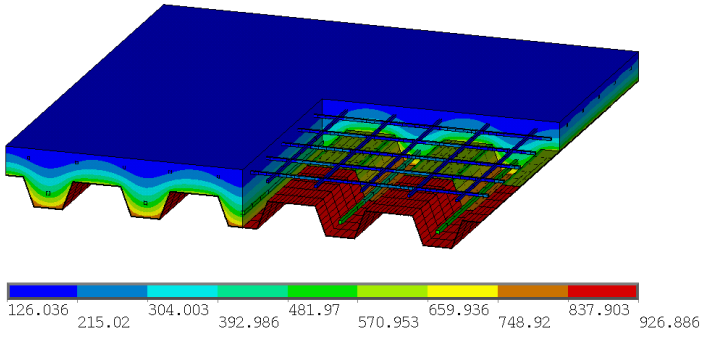

t= 61.3 min

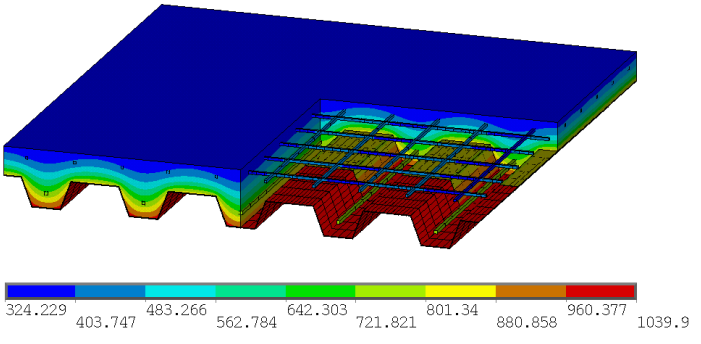

t= 120.0 min

SIM. 11	**Steel deck:** Trapezoidal – O Feliz H60	**Rebar (mm):** ϕ8	**t_a (mm):** 1	**Fire resistance (min)**	
	Mesh (mm//mm): ϕ6//100 (FNQ 60)	**h_1 (mm):** 70		Ave: *74.1*	Max: 78.2

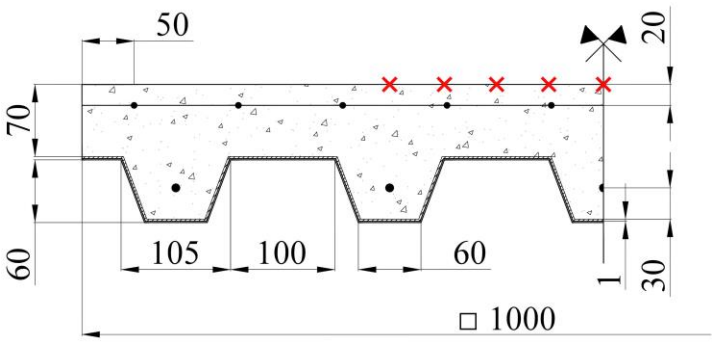

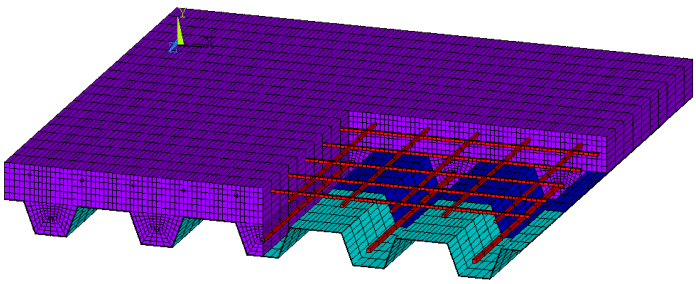

Finite element mesh

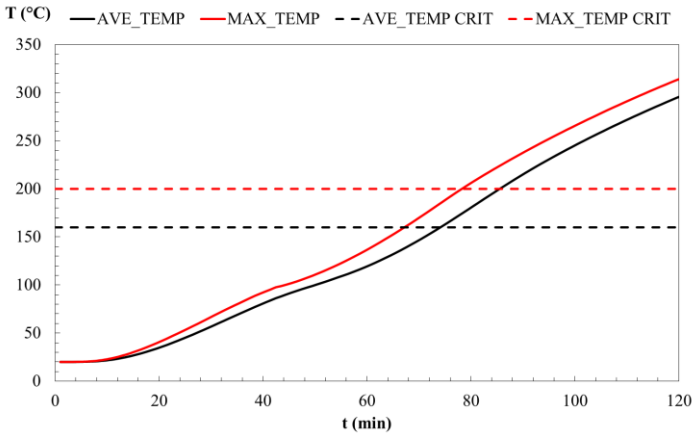

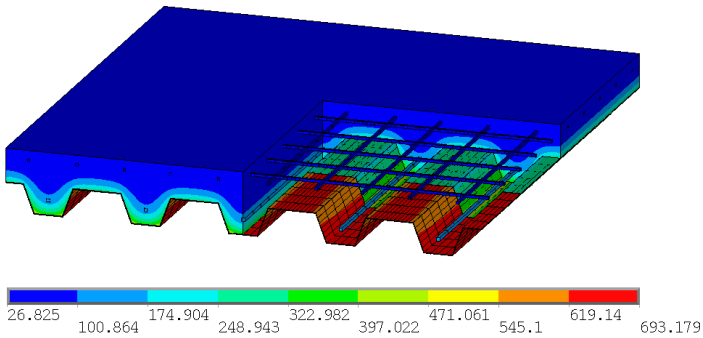

t= 18.5 min

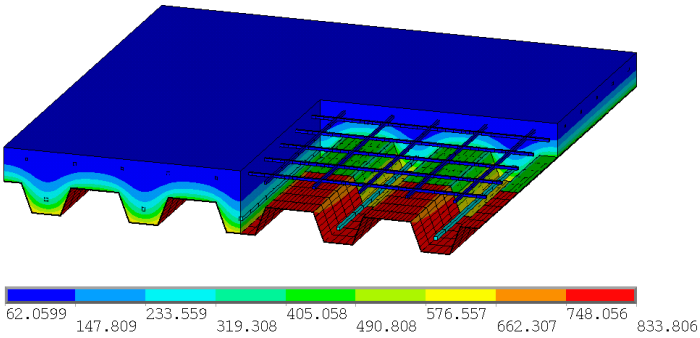

t= 37.1 min

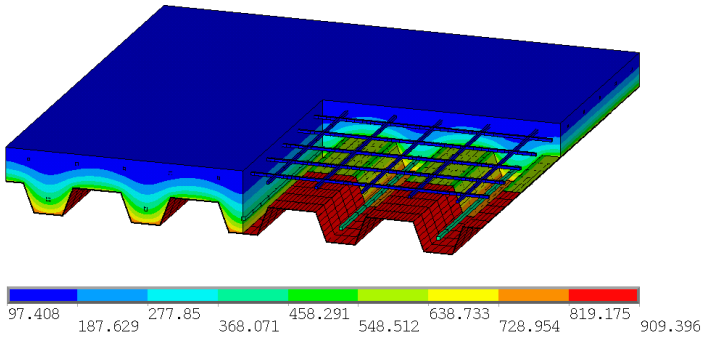

t= 55.6 min

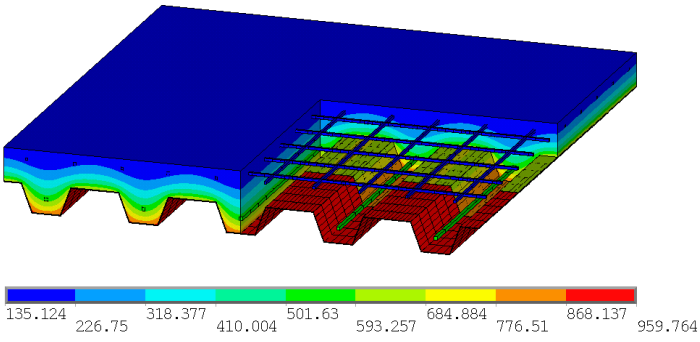

t= 74.1 min

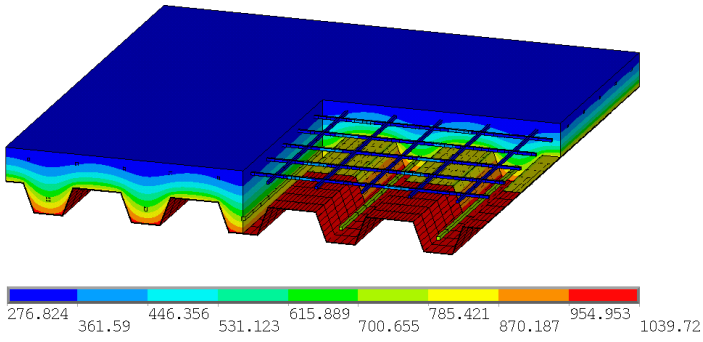

t= 120.0 min

SIM. 12	**Steel deck:** Trapezoidal – O Feliz H60	**Rebar (mm):** ϕ8	**t_a (mm):** 1	**Fire resistance (min)**	
	Mesh (mm//mm): ϕ6//100 (FNQ 60)	**h_1 (mm):** 80		Ave: *88.1*	Max: 95.5

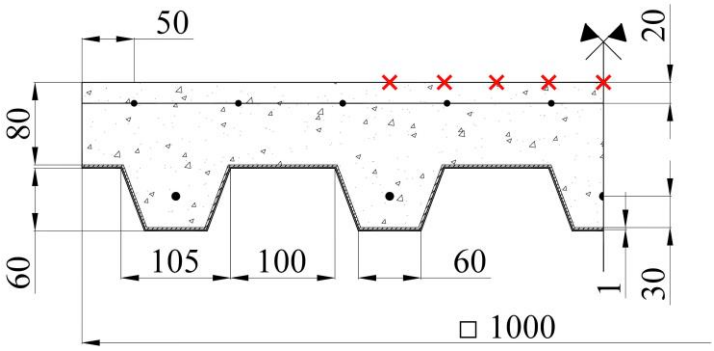

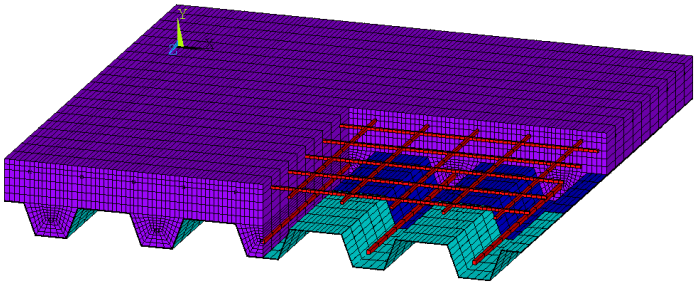

Finite element mesh

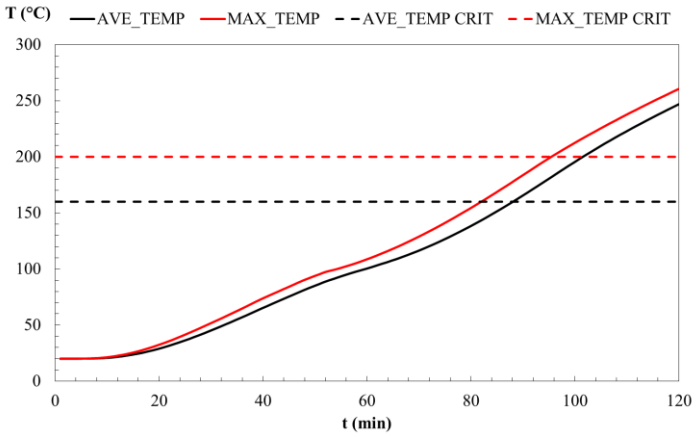

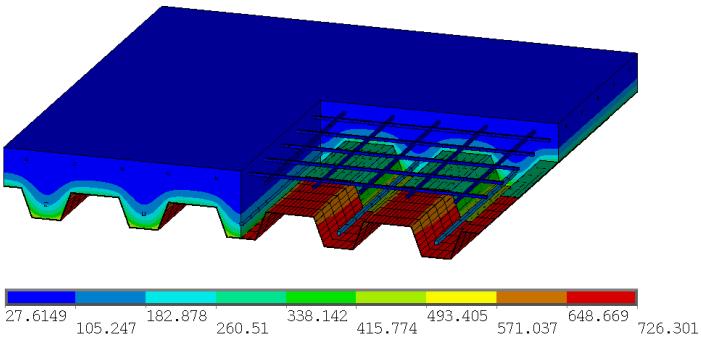

t= 22.0 min

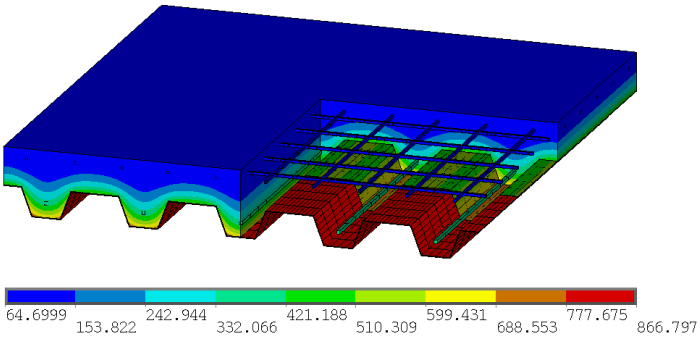

t= 44.1 min

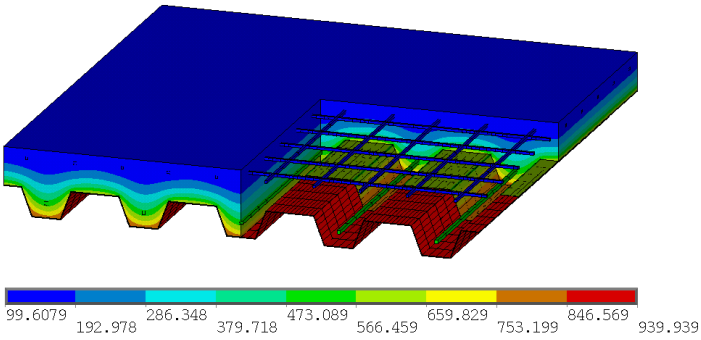

t= 66.1 min

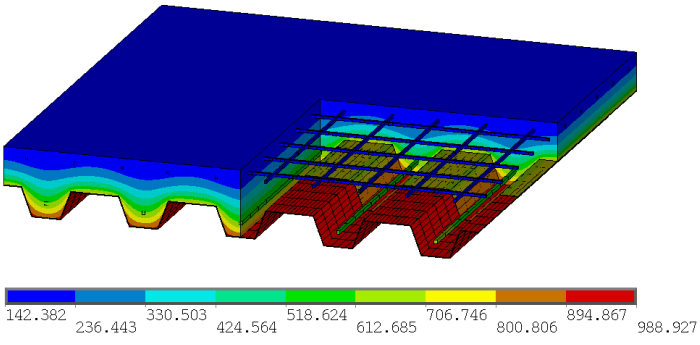

t= 88.1 min

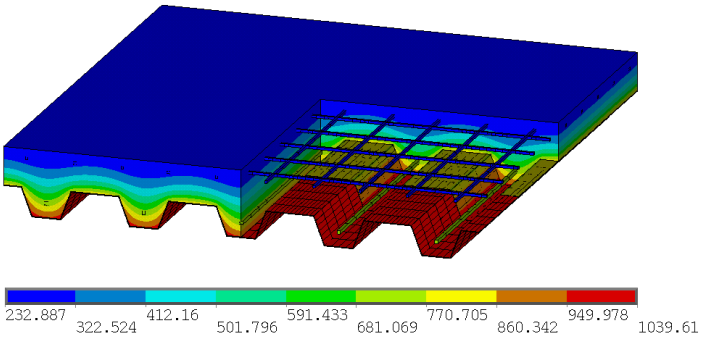

t= 120.0 min

SIM. 13	**Steel deck:** Trapezoidal – O Feliz H60	**Rebar (mm):** ϕ8	**t_a (mm):** 1	**Fire resistance (min)**	
	Mesh (mm//mm): ϕ6//100 (FNQ 60)	**h_1 (mm):** 90		Ave: *103.2*	Max: 114.2

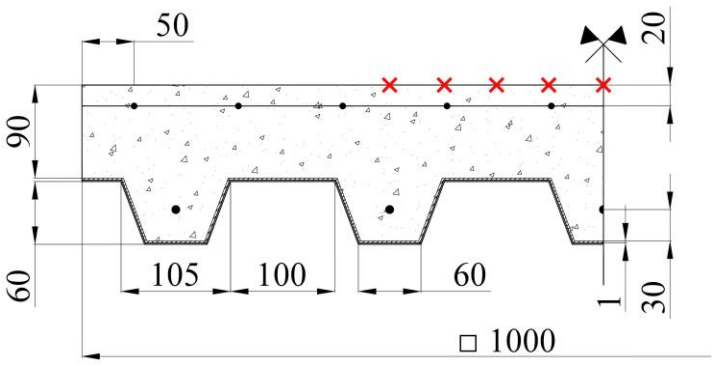

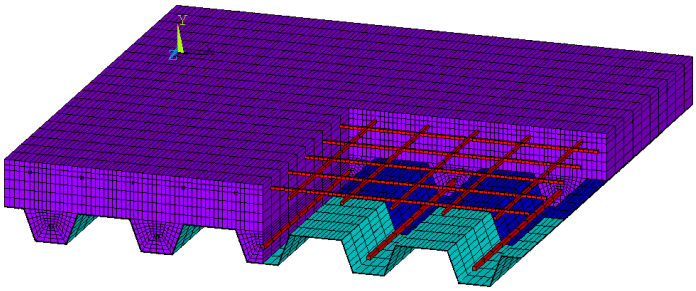

Finite element mesh

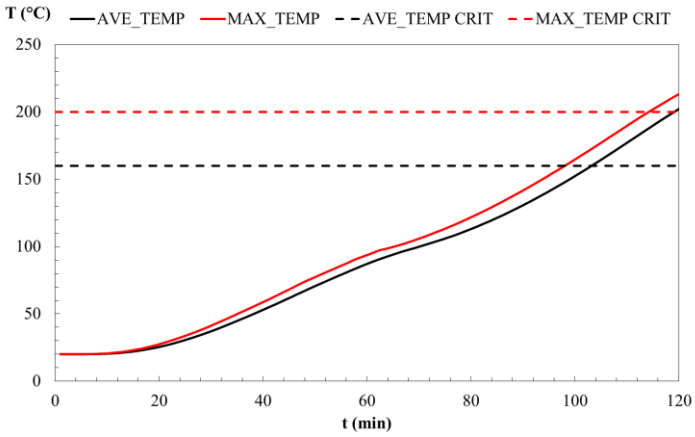

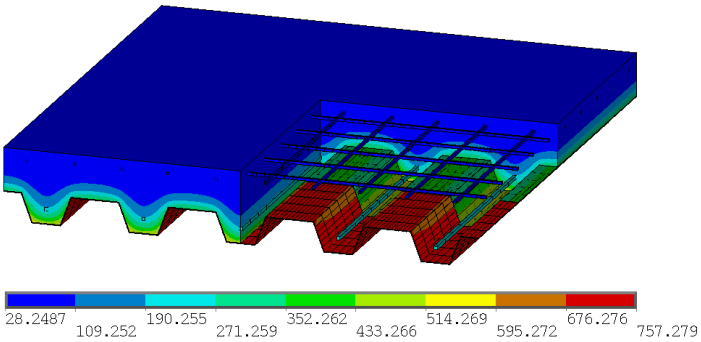

t= 25.8 min

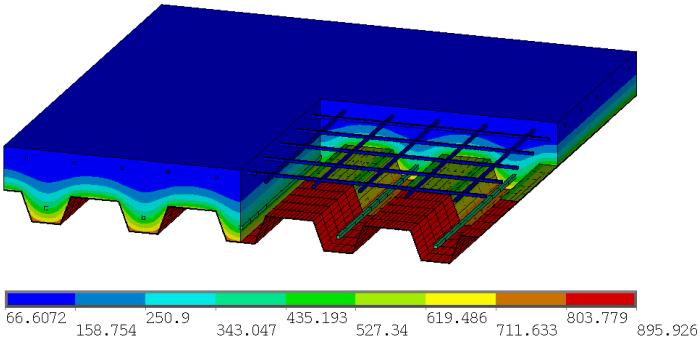

t= 51.6 min

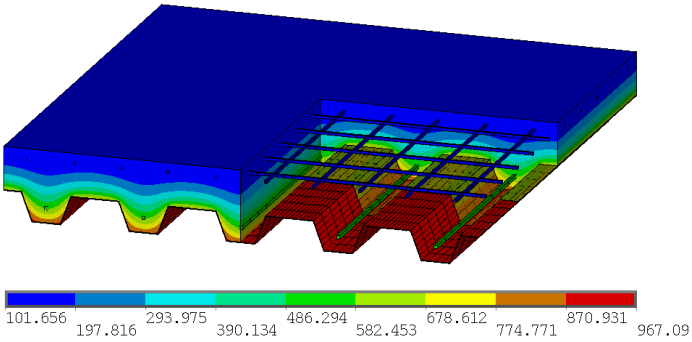

t= 77.4 min

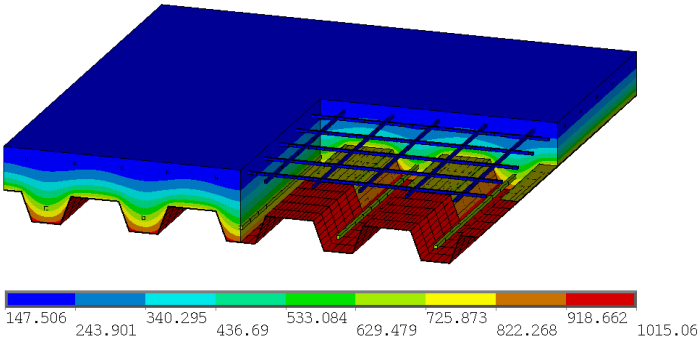

t= 103.2 min

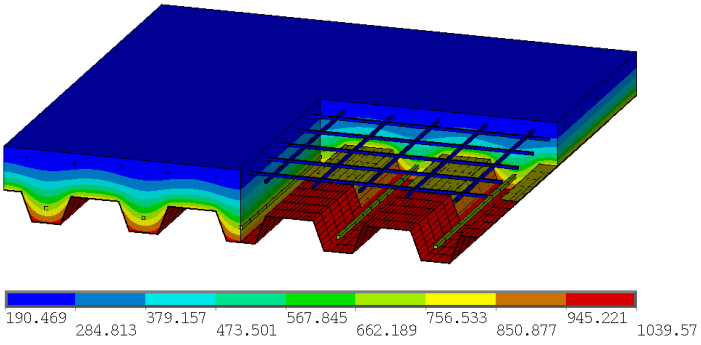

t= 120.0 min

SIM. 14	**Steel deck:** Trapezoidal – O Feliz H60	**Rebar (mm):** ϕ8	**t_a (mm):** 1	**Fire resistance (min)**	
	Mesh (mm//mm): ϕ6//100 (FNQ 60)	**h_1 (mm):** 100		Ave: *120.1*	Max: 134.7

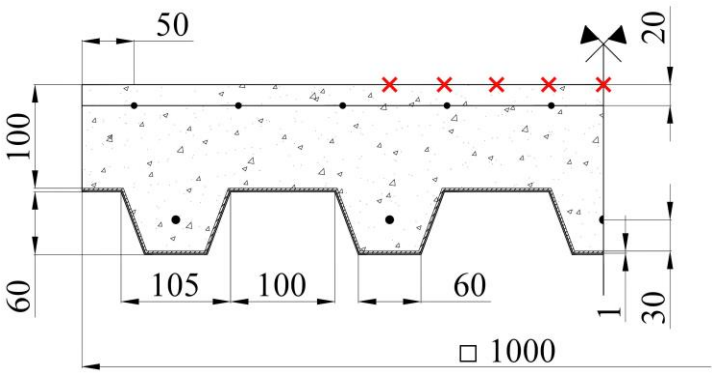

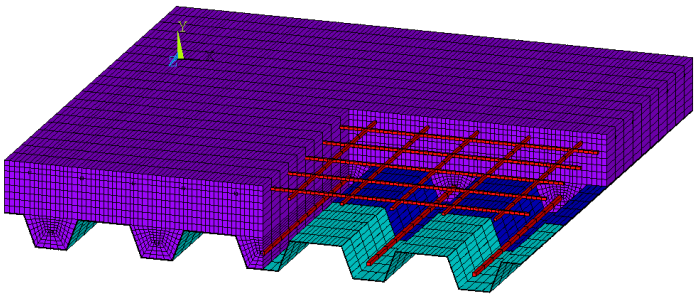

Finite element mesh

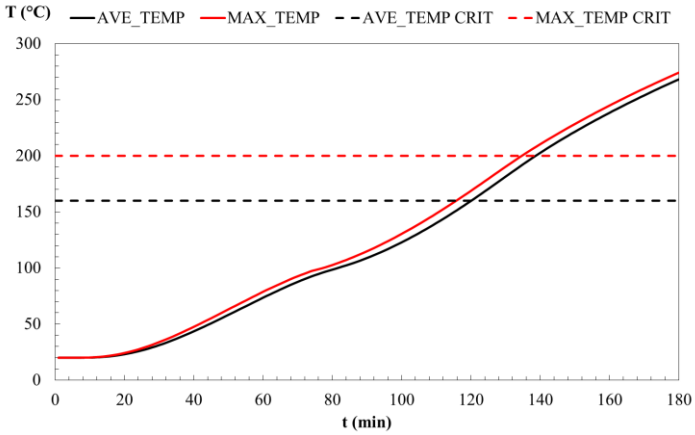

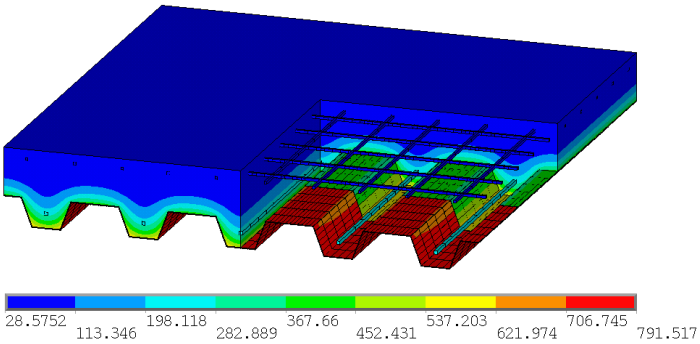

t= 30.0 min

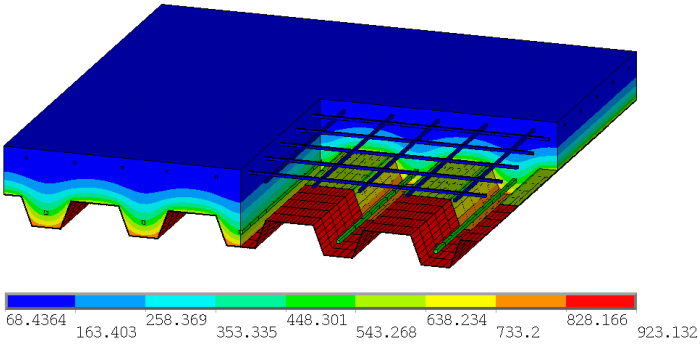

t= 60.1 min

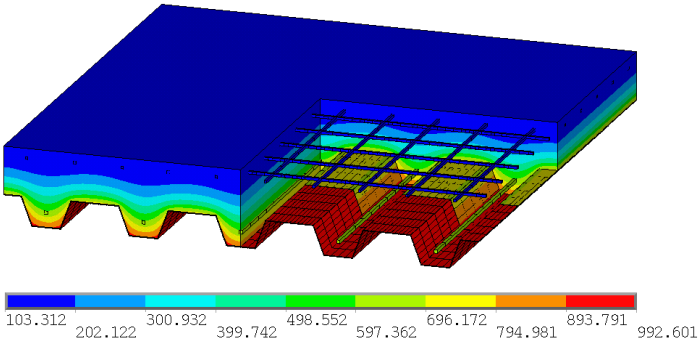

t= 90.1 min

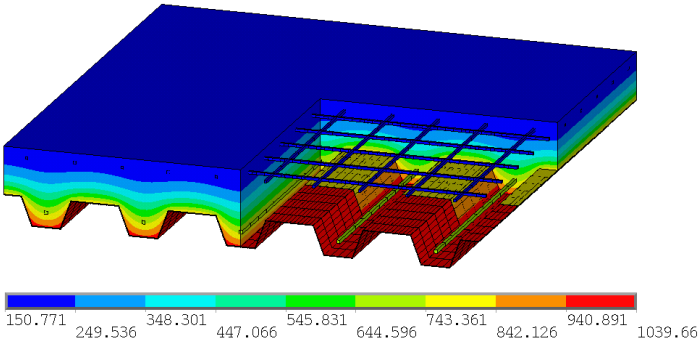

t= 120.1 min

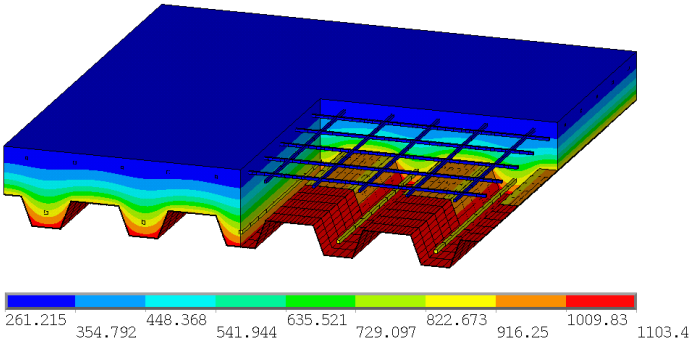

t= 180.0 min

SIM. 15	**Steel deck:** Trapezoidal – O Feliz H60	**Rebar (mm):** ϕ8	**t_a (mm):** 1	**Fire resistance (min)**	
	Mesh (mm//mm): ϕ6//100 (FNQ 60)	**h_1 (mm):** 110		Ave: *138.0*	Max: 156.7

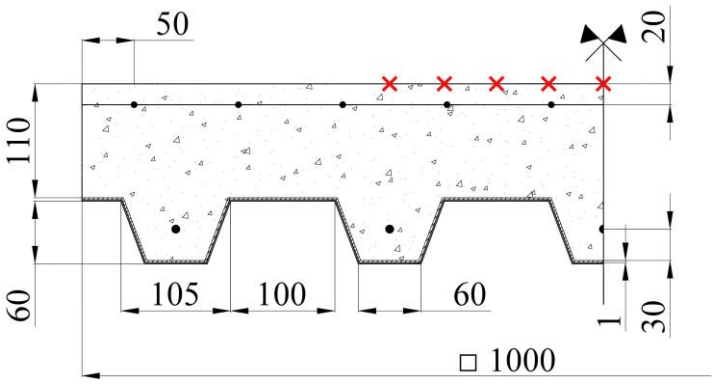

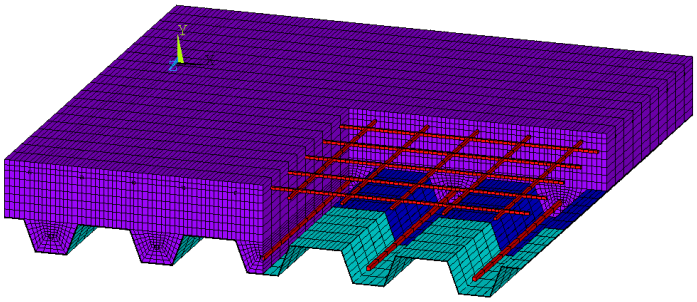

Finite element mesh

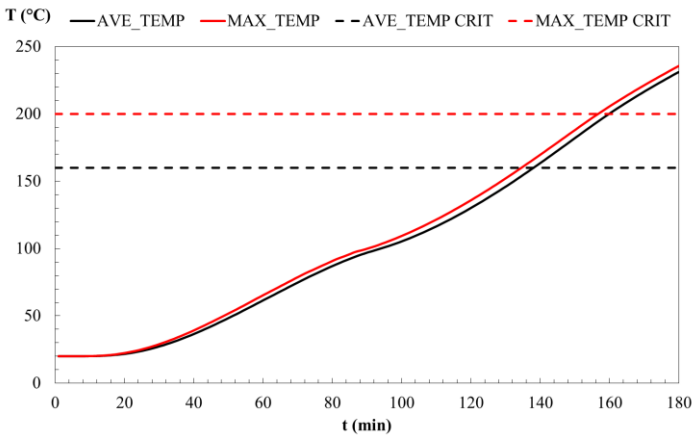

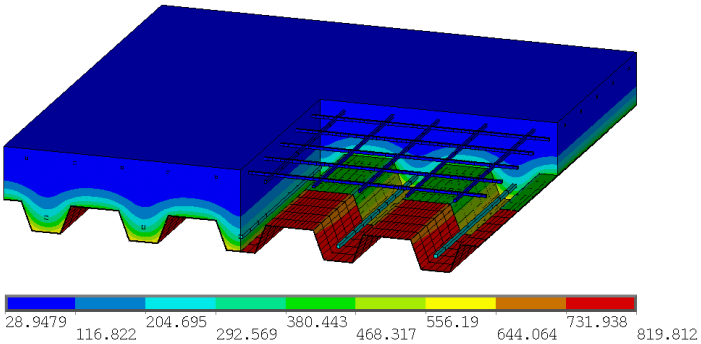

t= 34.5 min

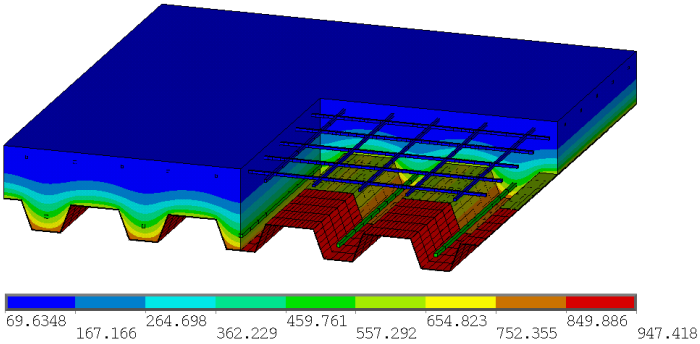

t= 69.0 min

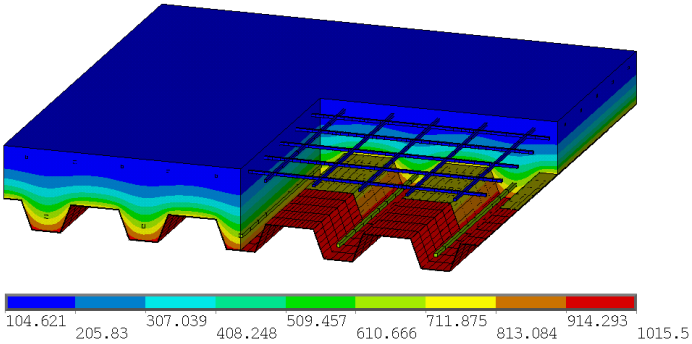

t= 103.5 min

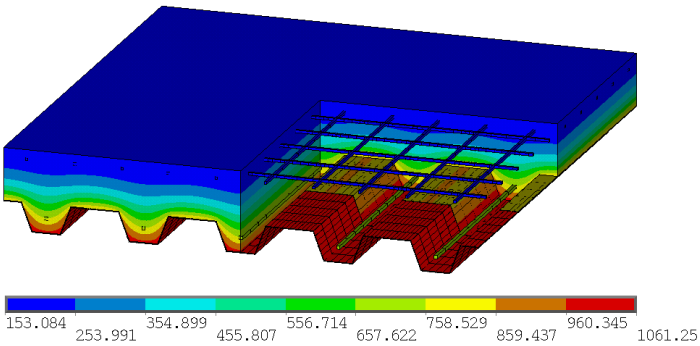

t= 138.0 min

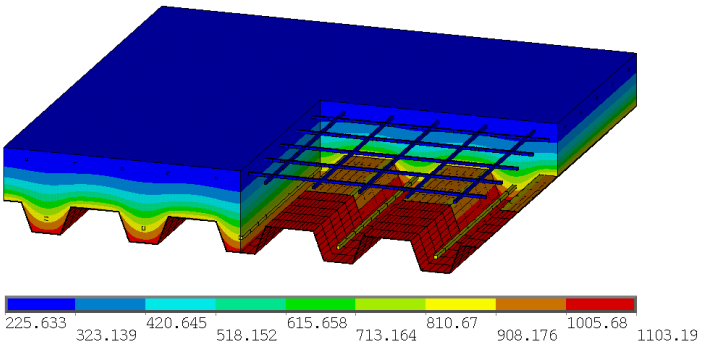

t= 180.0 min

SIM. 16	**Steel deck:** Trapezoidal – O Feliz H60	**Rebar (mm):** ϕ8	**t_a (mm):** 1	**Fire resistance (min)**	
	Mesh (mm//mm): ϕ6//100 (FNQ 60)	**h_1 (mm):** 120		Ave: *157.5*	Max: 180.3

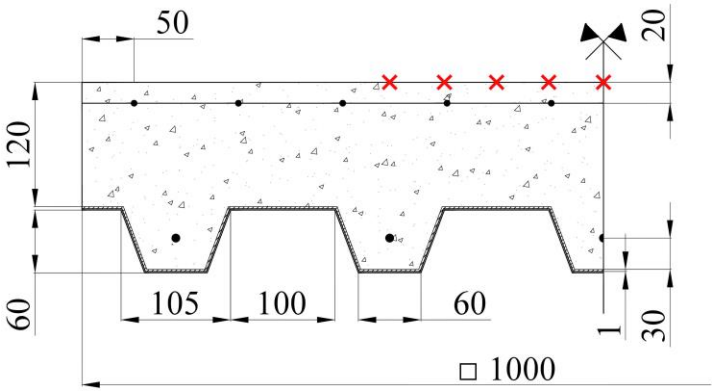

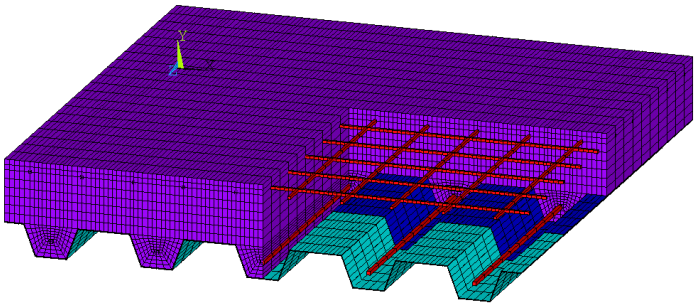

Finite element mesh

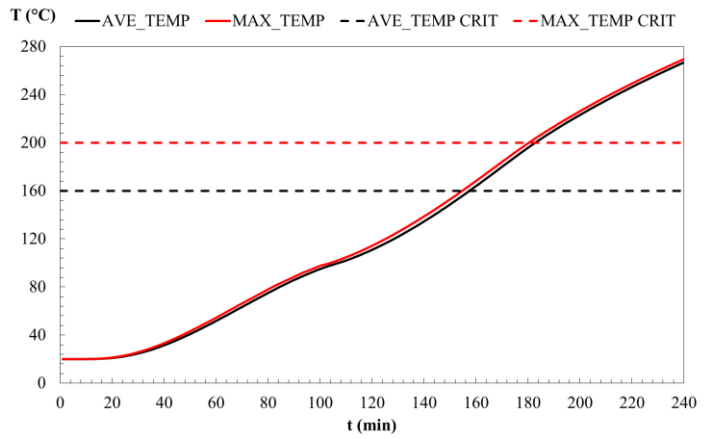

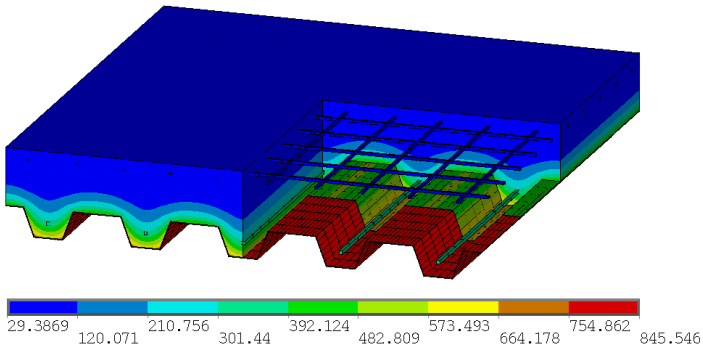

t= 39.4 min

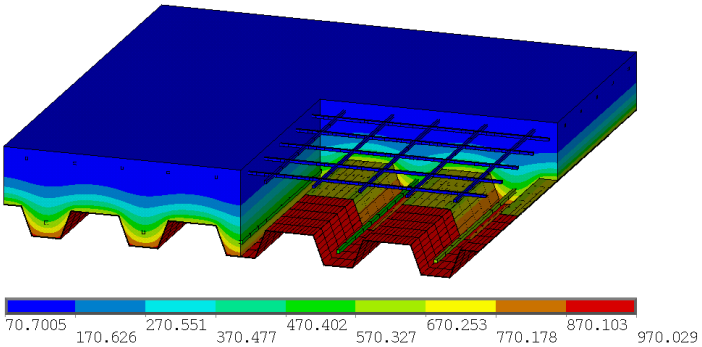

t= 78.8 min

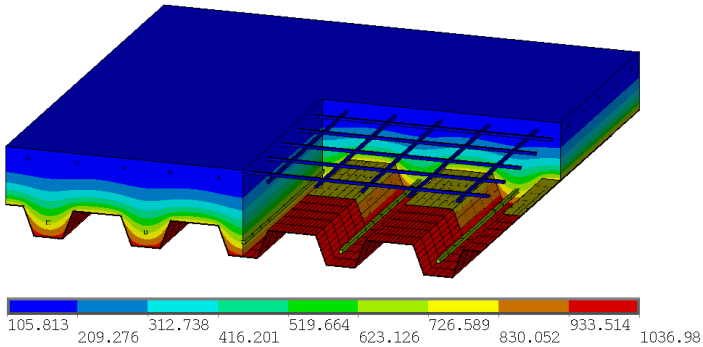

t= 118.1 min

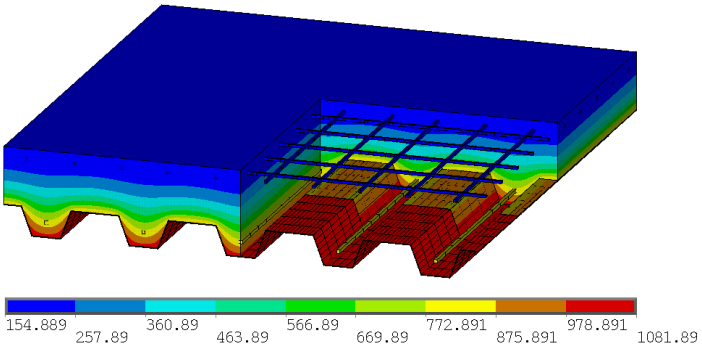

t= 157.5 min

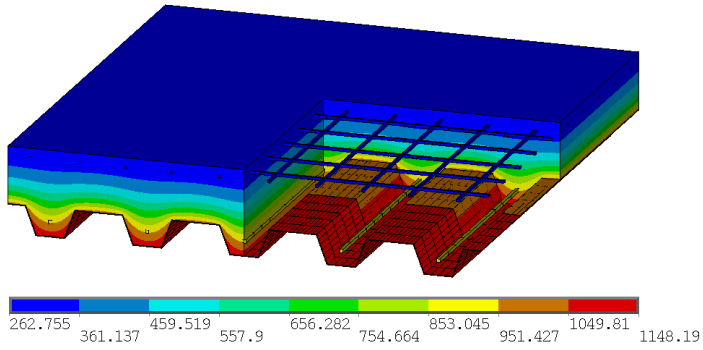

t= 240.0 min

SIM. 17	**Steel deck:** Trapezoidal – O Feliz H60	**Rebar (mm):** ϕ8	**t_a (mm):** 2	**Fire resistance (min)**	
	Mesh (mm//mm): ϕ6//100 (FNQ 60)	**h_1 (mm):** 50		Ave: *62.3*	Max: 63.4

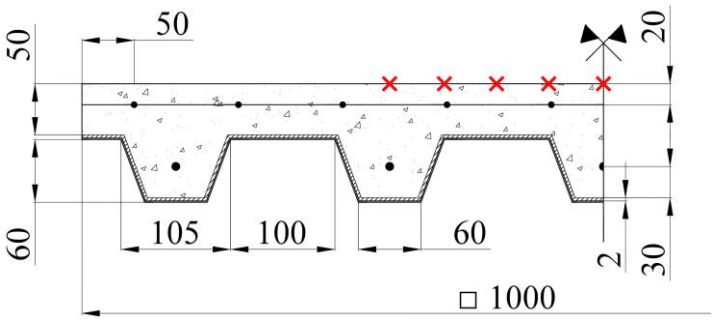

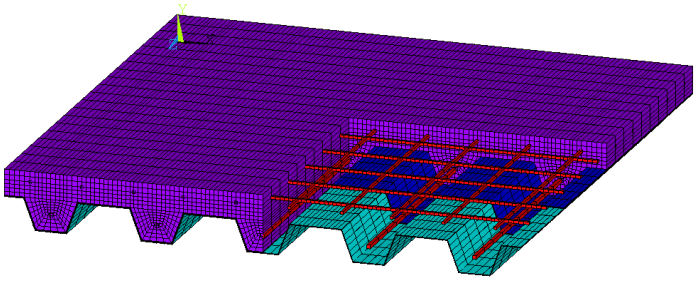

Finite element mesh

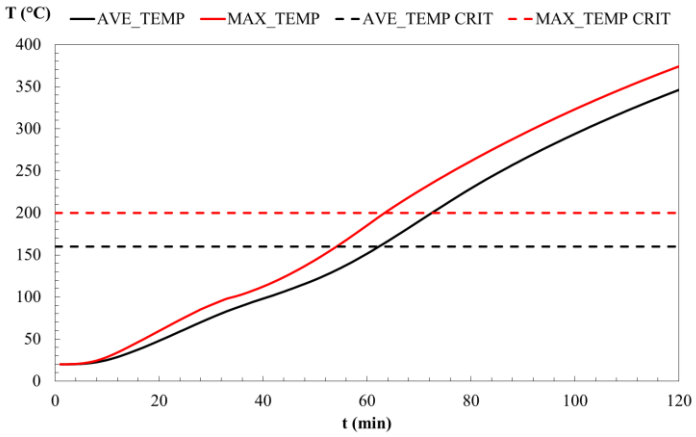

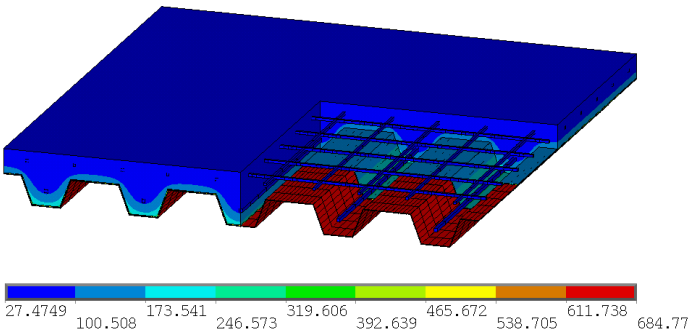

t= 15.6 min

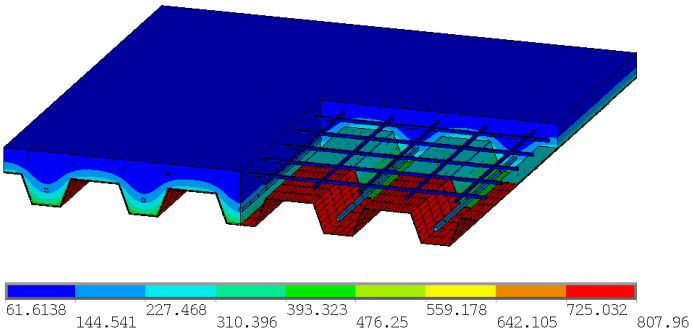

t= 31.2 min

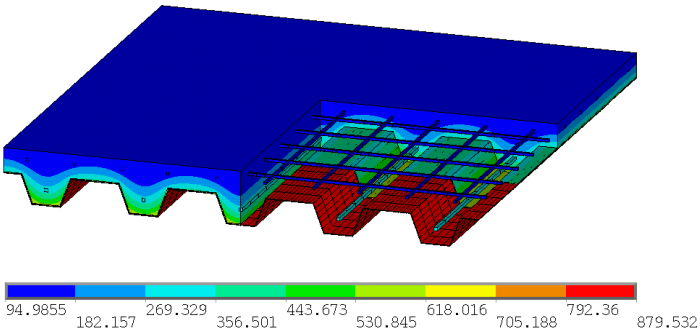

t= 46.7 min

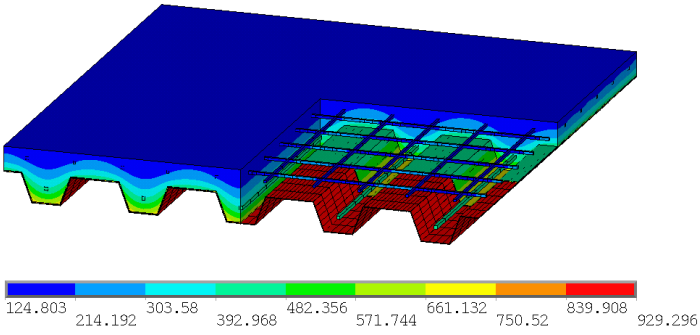

t= 62.3 min

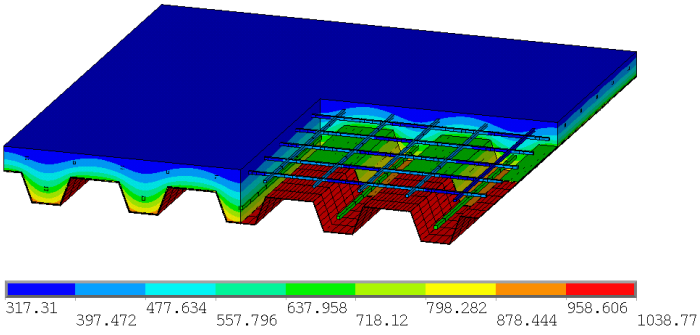

t= 120.0 min

SIM. 18	**Steel deck:** Trapezoidal – O Feliz H60	**Rebar (mm):** ϕ8	**t_a (mm):** 2	**Fire resistance (min)**	
	Mesh (mm//mm): ϕ6//100 (FNQ 60)	**h_1 (mm):** 60		Ave: *75.6*	Max: 79.6

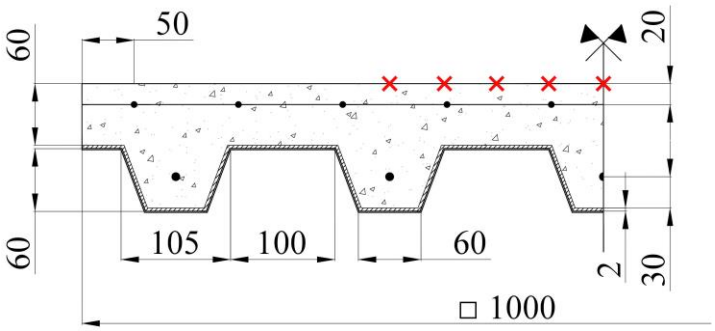

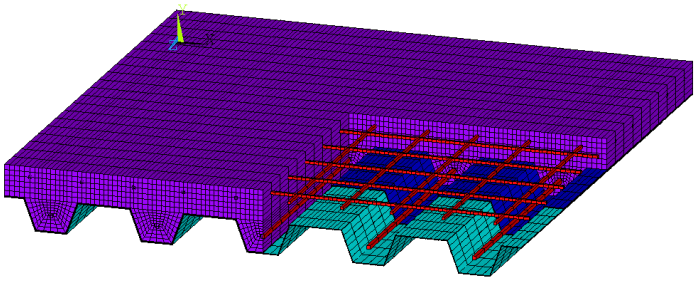

Finite element mesh

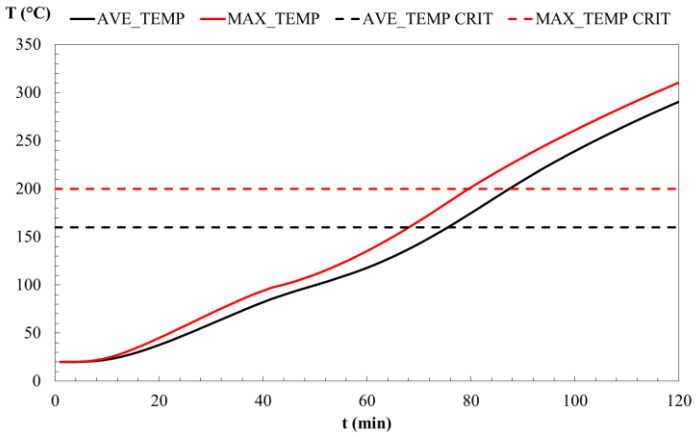

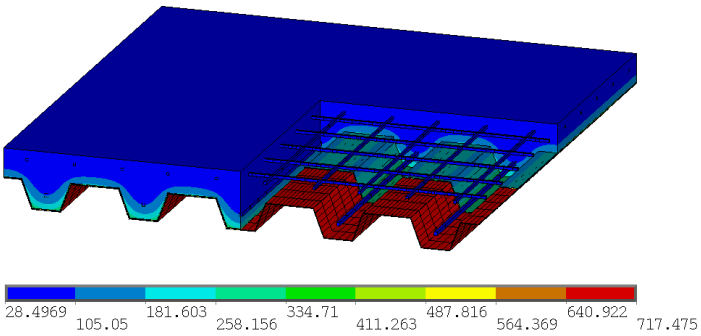

t= 18.9 min

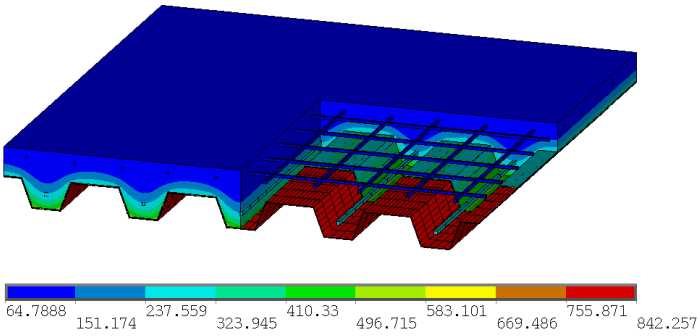

t= 37.8 min

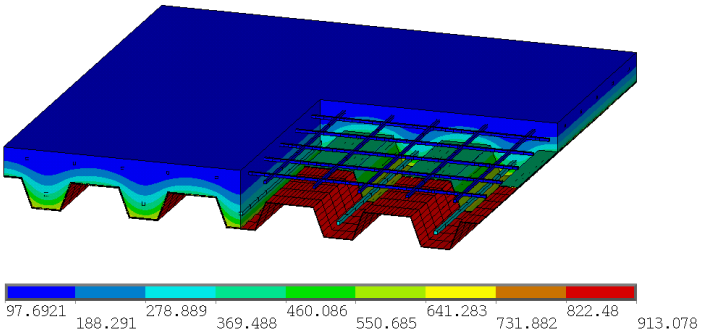

t= 56.7 min

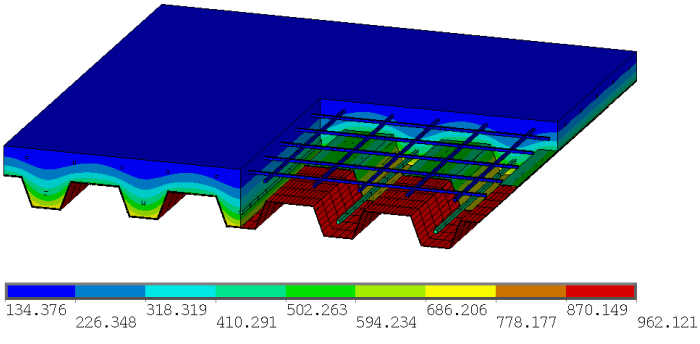

t= 75.6 min

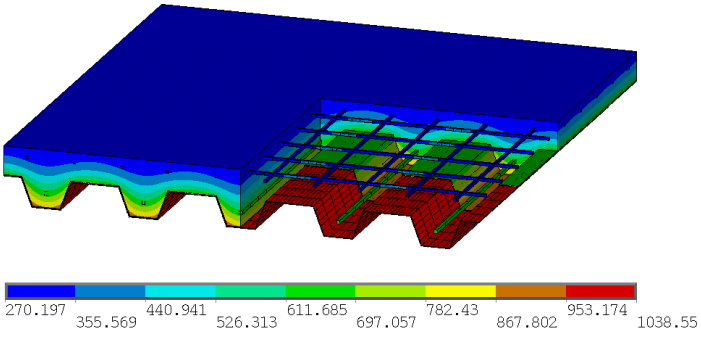

t= 120.0 min

SIM. 19	**Steel deck:** Trapezoidal – O Feliz H60	**Rebar (mm):** ϕ8	**t_a (mm):** 2	**Fire resistance (min)**	
	Mesh (mm//mm): ϕ6//100 (FNQ 60)	**h_1 (mm):** 70		Ave: *89.9*	Max: 97.2

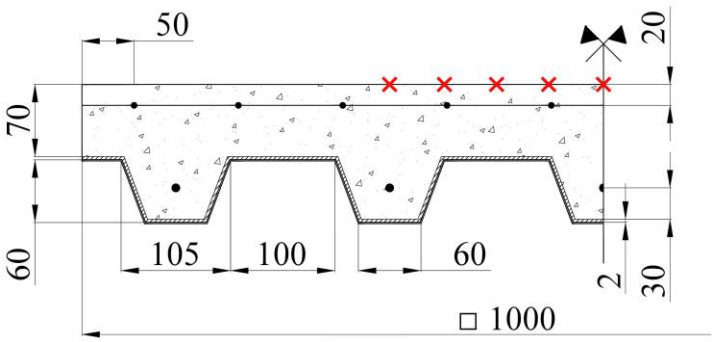

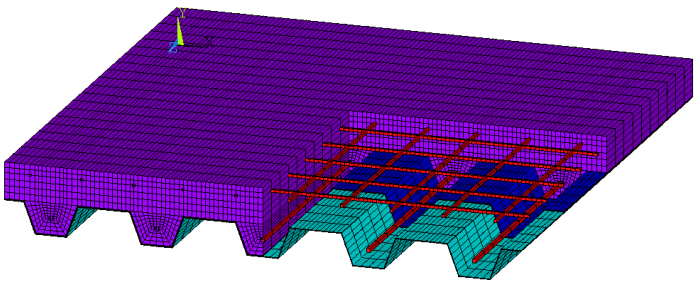

Finite element mesh

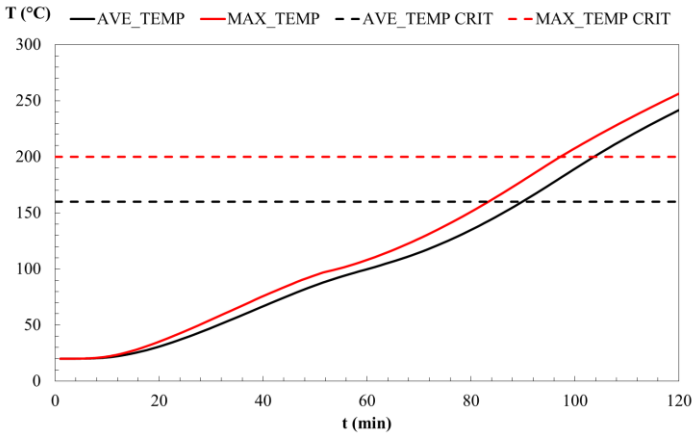

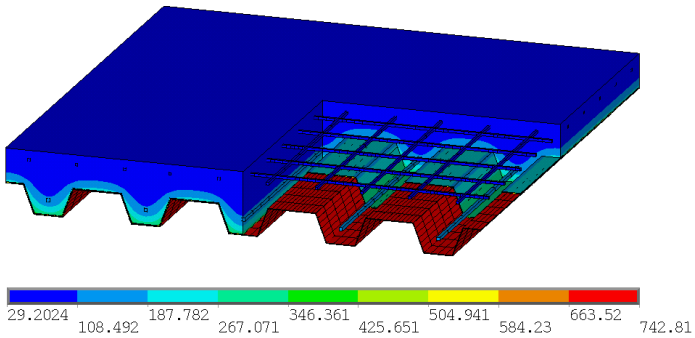

t= 22.5 min

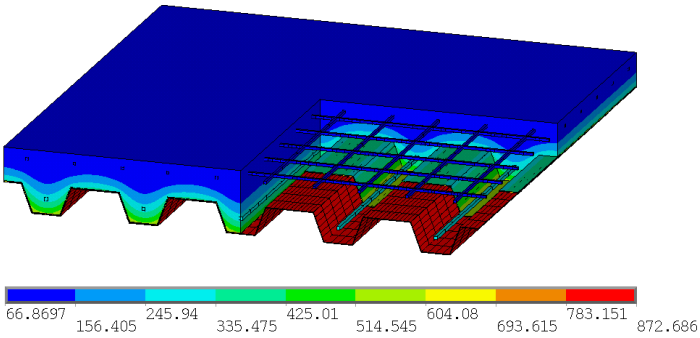

t= 45.0 min

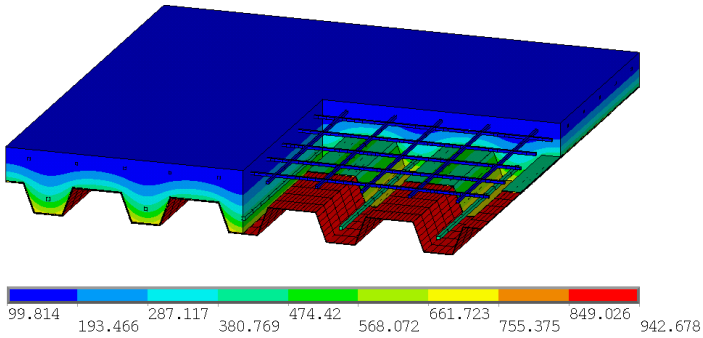

t= 67.4 min

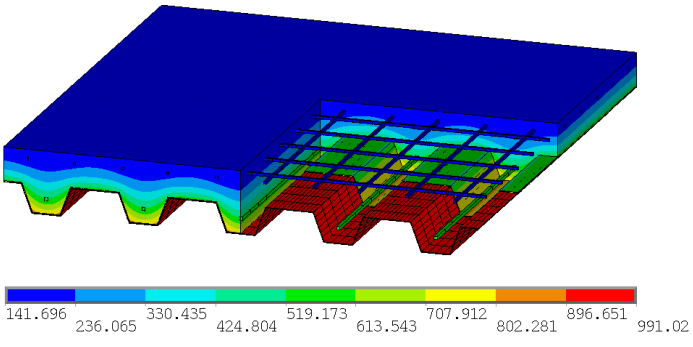

t= 89.9 min

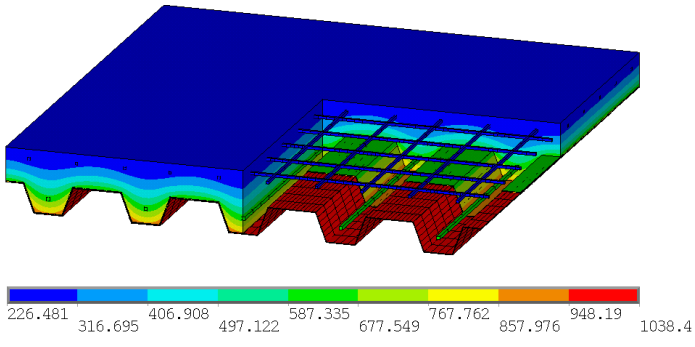

t= 120.0 min

SIM. 20	**Steel deck:** Trapezoidal – O Feliz H60	**Rebar (mm):** ϕ8	**t_a (mm):** 2	**Fire resistance (min)**	
	Mesh (mm//mm): ϕ6//100 (FNQ 60)	**h_1 (mm):** 80		Ave: *105.3*	Max: 116.2

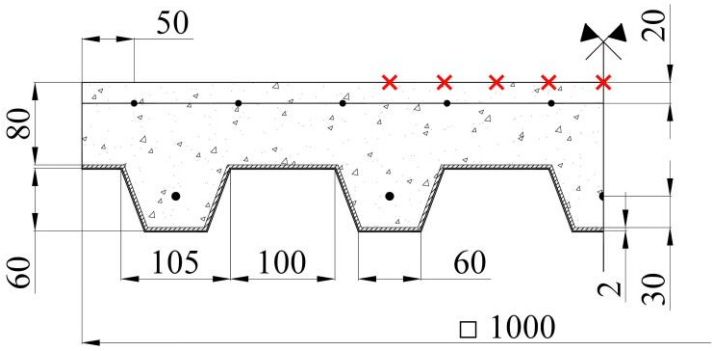

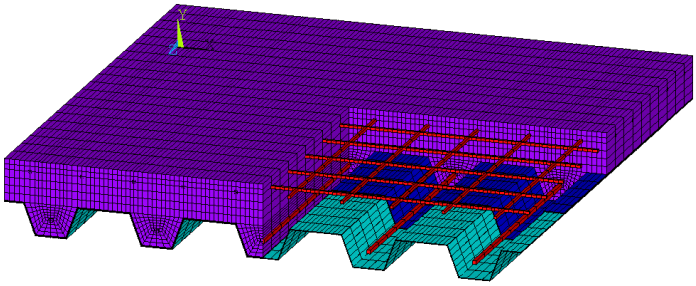

Finite element mesh

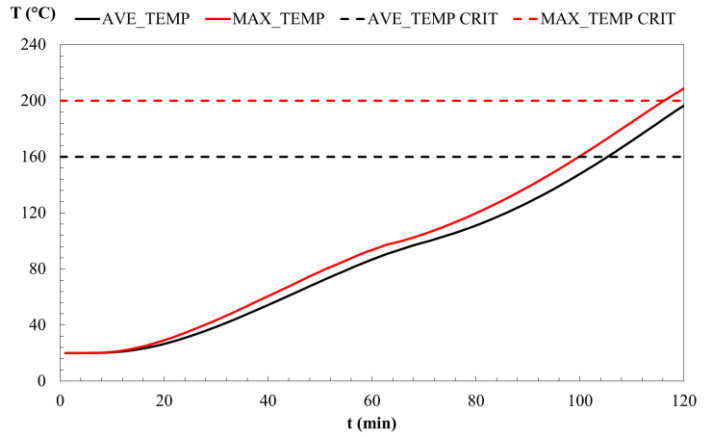

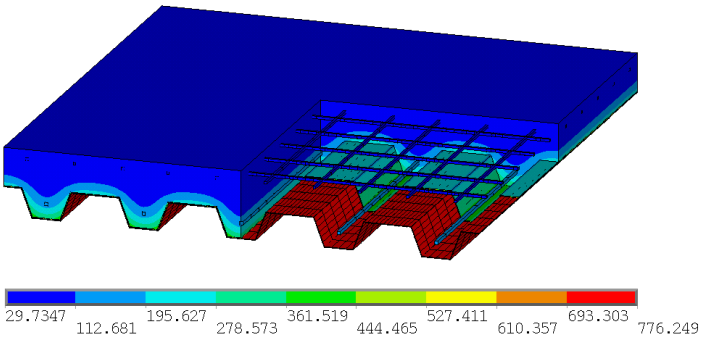

t= 26.3 min

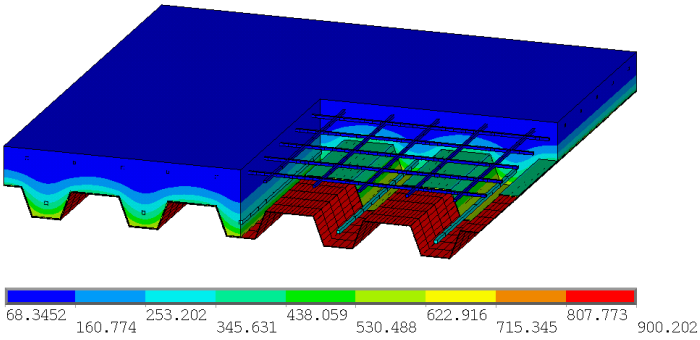

t= 52.7 min

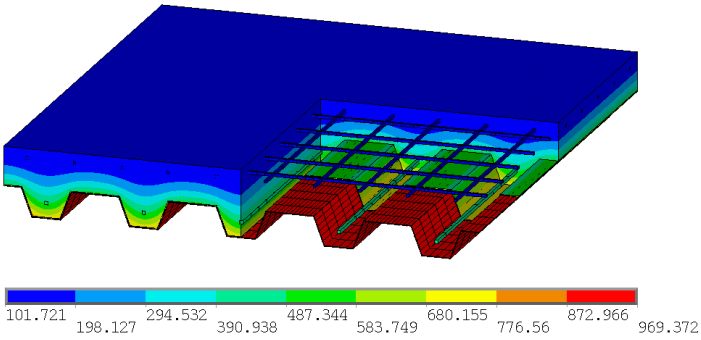

t= 79.0 min

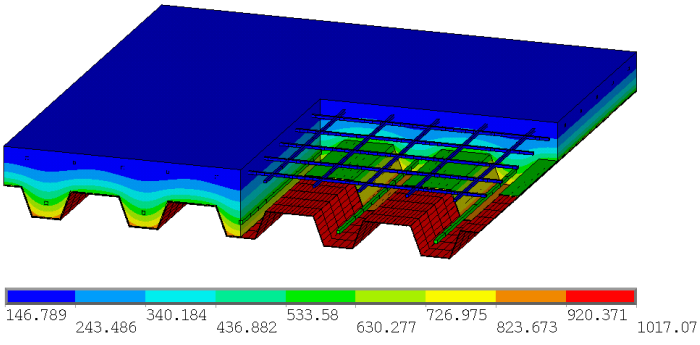

t= 105.3 min

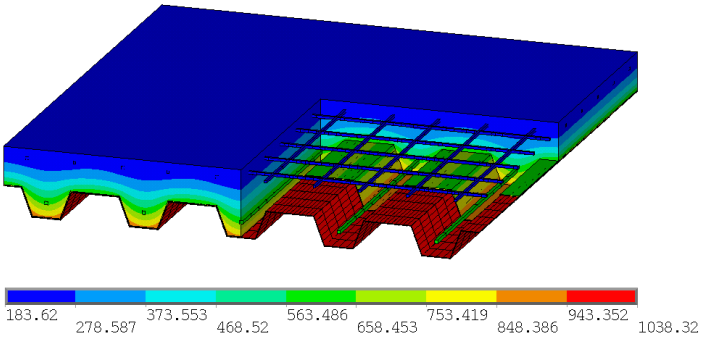

t= 120.0 min

SIM. 21	**Steel deck:** Trapezoidal – O Feliz H60	**Rebar (mm):** ϕ8	**t_a (mm):** 2	**Fire resistance (min)**	
	Mesh (mm//mm): ϕ6//100 (FNQ 60)	**h_1 (mm):** 90		Ave: *121.9*	Max: 136.6

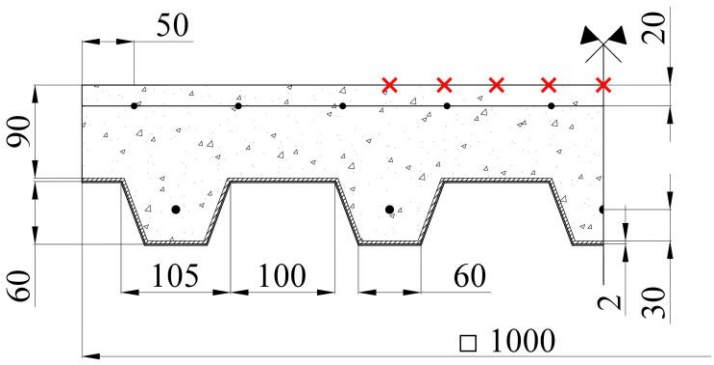

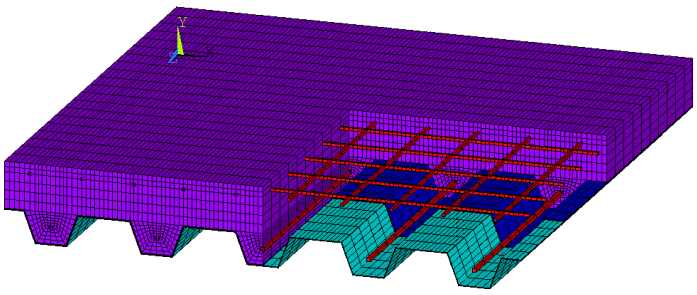

Finite element mesh

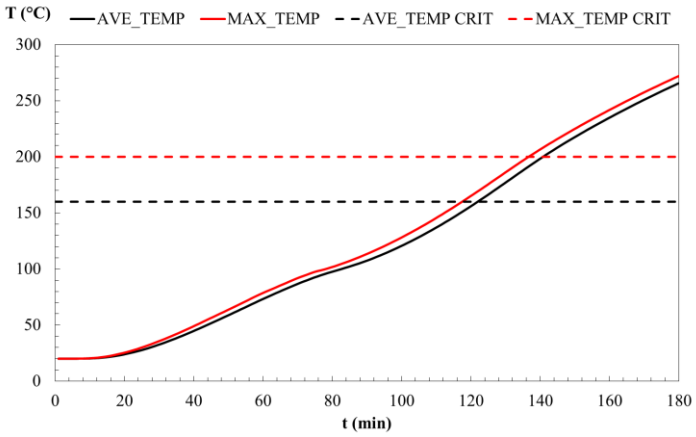

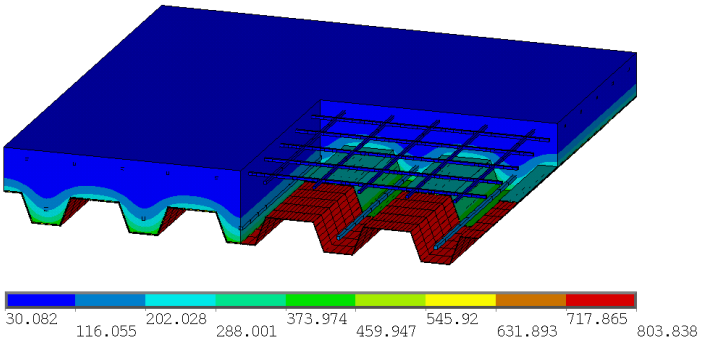

t= 30.5 min

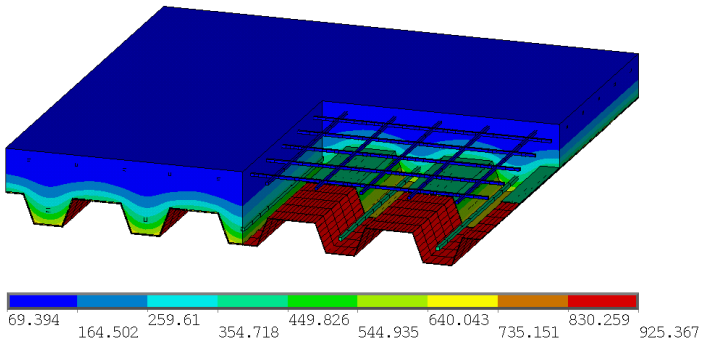

t= 61.0 min

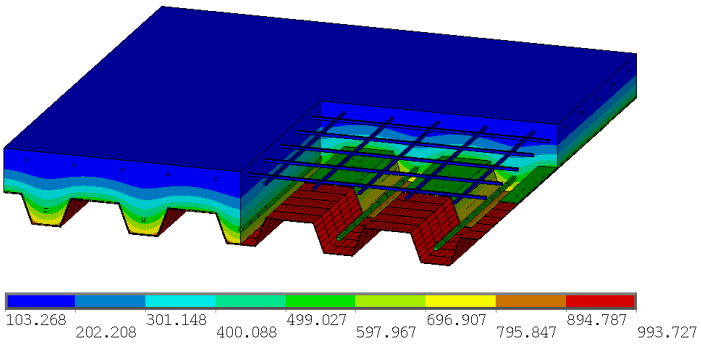

t= 91.4 min

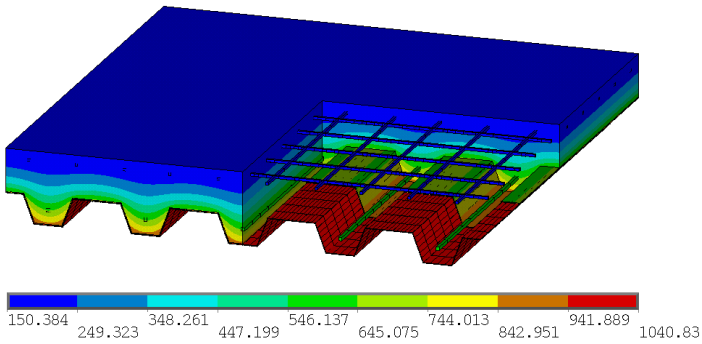

t= 121.9 min

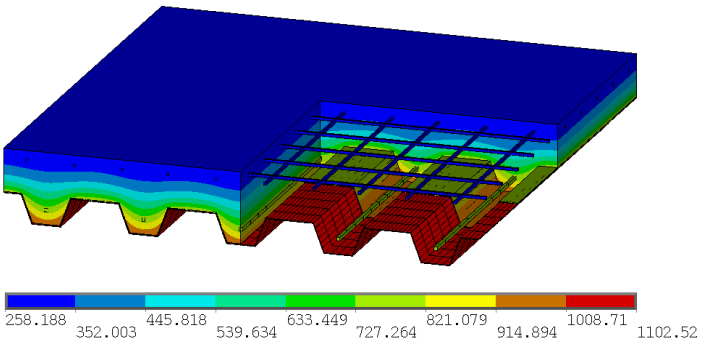

t= 180.0 min

SIM. 22	**Steel deck:** Trapezoidal – O Feliz H60	**Rebar (mm):** ϕ8	**t_a (mm):** 2	**Fire resistance (min)**	
	Mesh (mm//mm): ϕ6//100 (FNQ 60)	**h_1 (mm):** 100		Ave: *140.3*	Max: 158.7

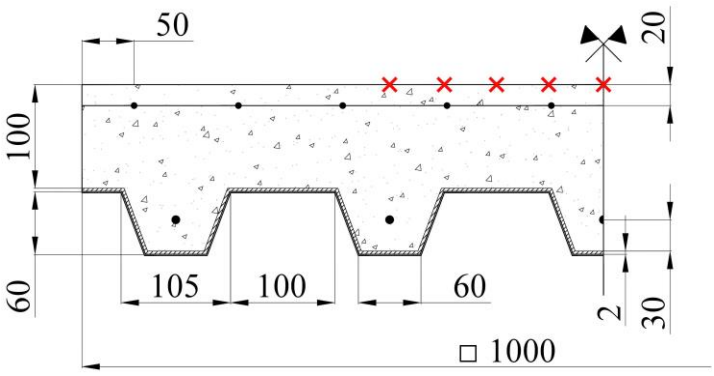

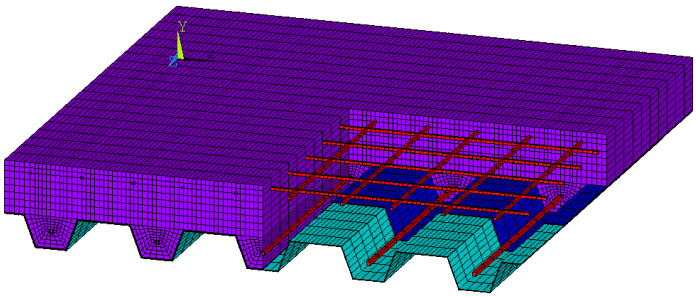

Finite element mesh

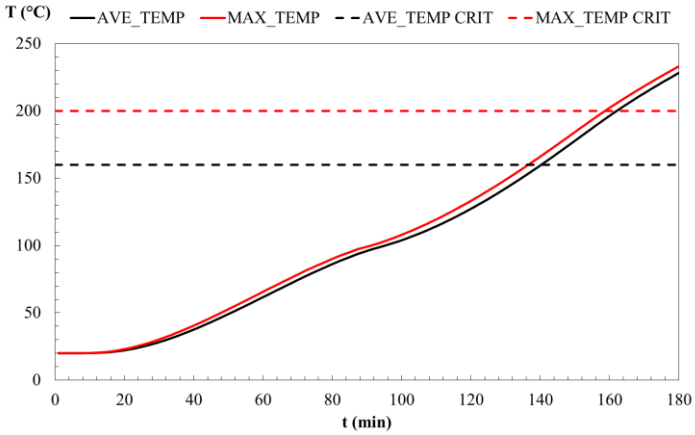

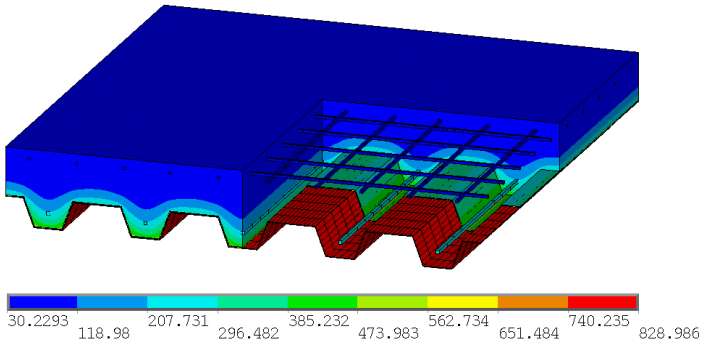

t= 35.1 min

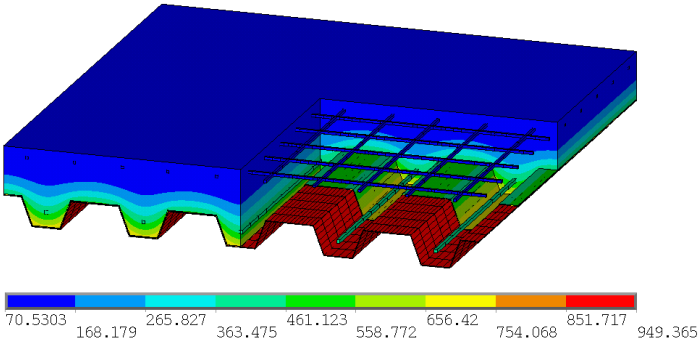

t= 70.2 min

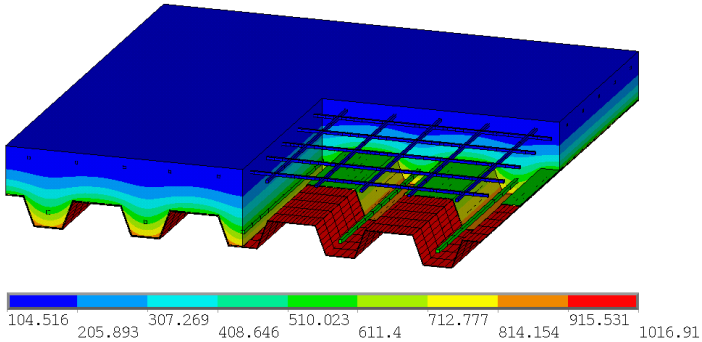

t= 105.2 min

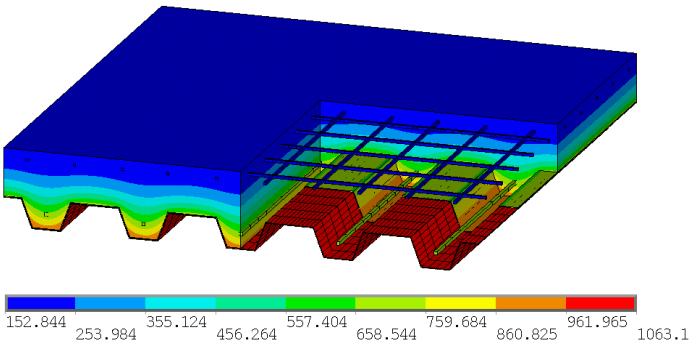

t= 140.3 min

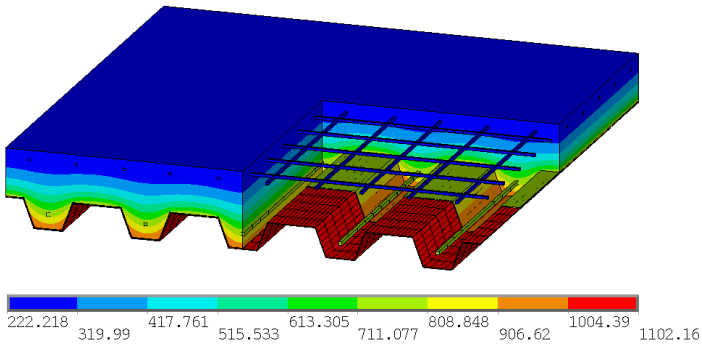

t= 180.0 min

SIM. 23	**Steel deck:** Trapezoidal – O Feliz H60	**Rebar (mm):** ϕ8	**t_a (mm):** 2	**Fire resistance (min)**	
	Mesh (mm//mm): ϕ6//100 (FNQ 60)	**h_1 (mm):** 110		Ave: *159.7*	Max: 182.2

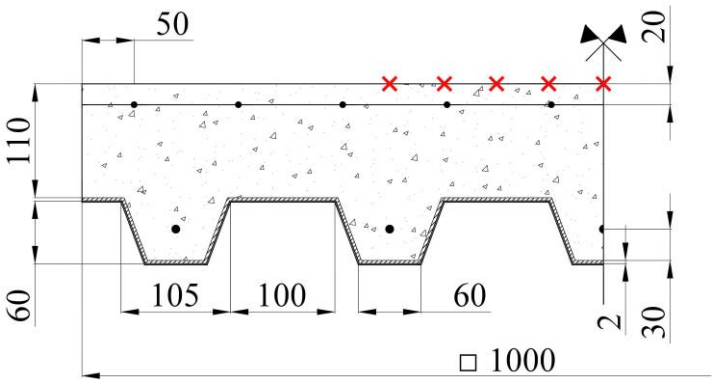

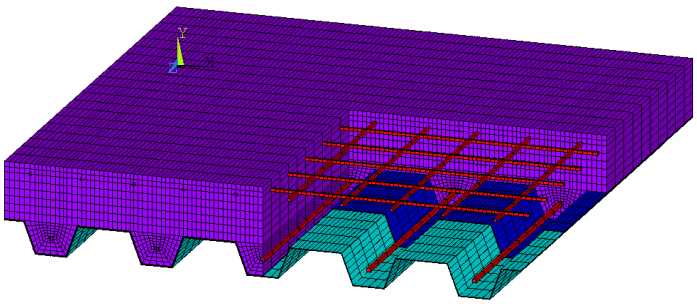

Finite element mesh

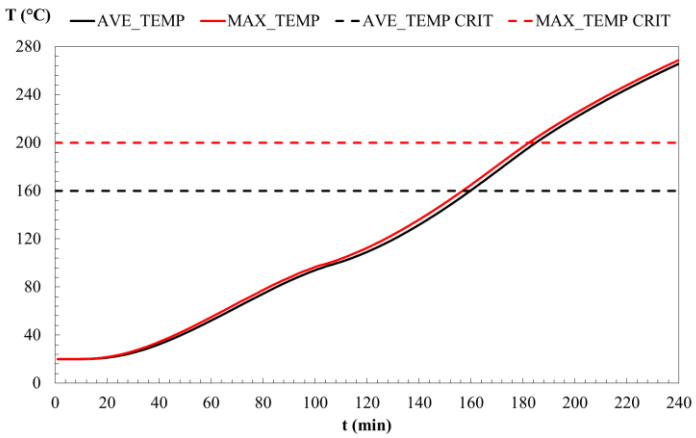

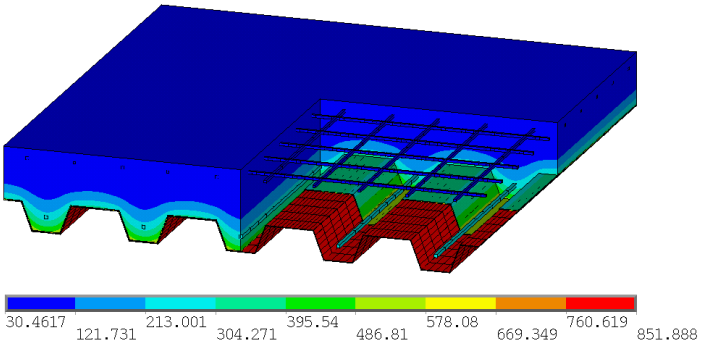

t= 39.9 min

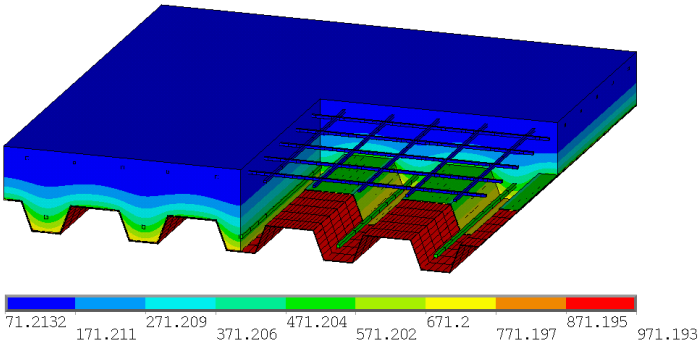

t= 79.9 min

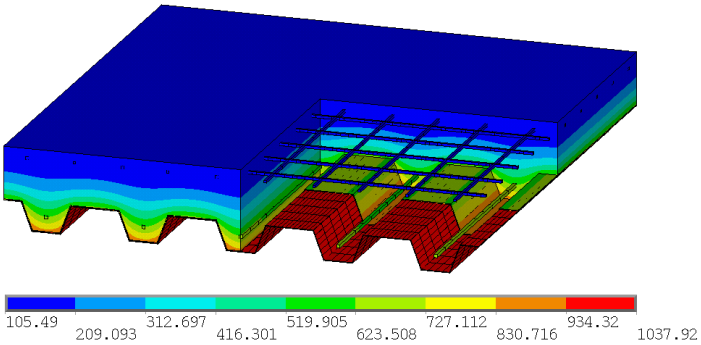

t= 119.8 min

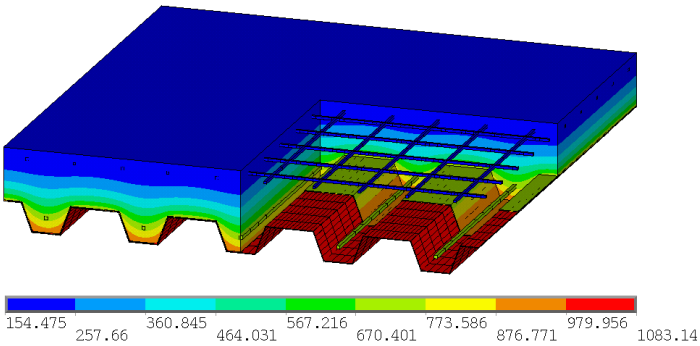

t= 159.7 min

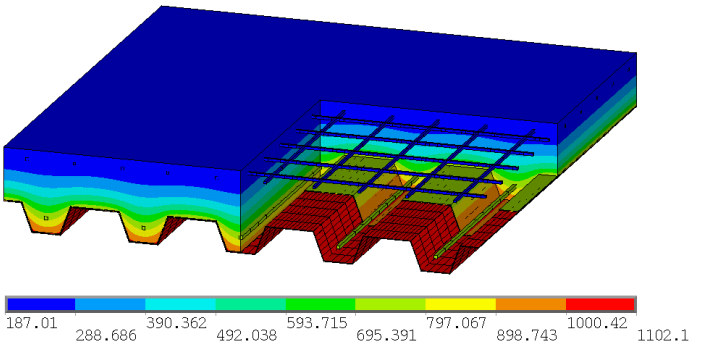

t= 180.0 min

SIM. 24	**Steel deck:** Trapezoidal – O Feliz H60	**Rebar (mm):** ϕ8	**t_a (mm):** 2	**Fire resistance (min)**	
	Mesh (mm//mm): ϕ6//100 (FNQ 60)	**h_1 (mm):** 120		Ave: *180.6*	Max: 207.5

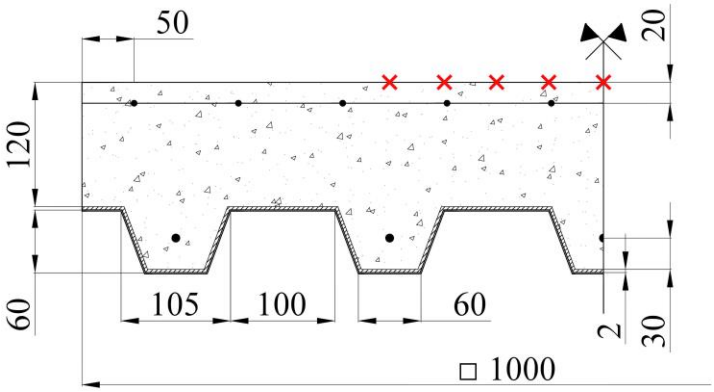

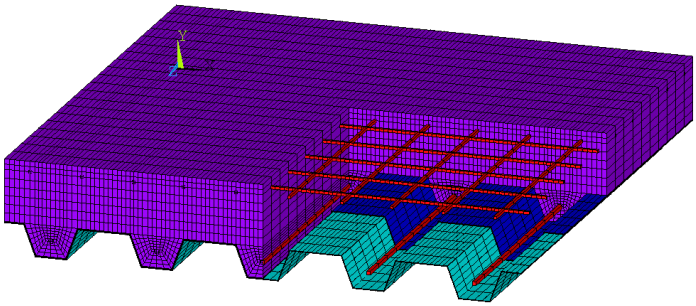

Finite element mesh

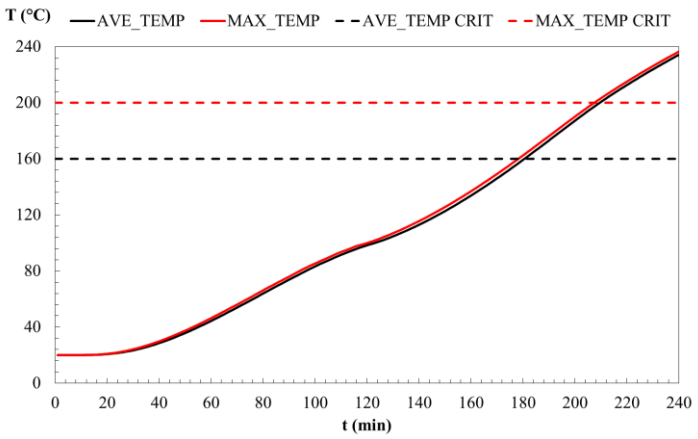

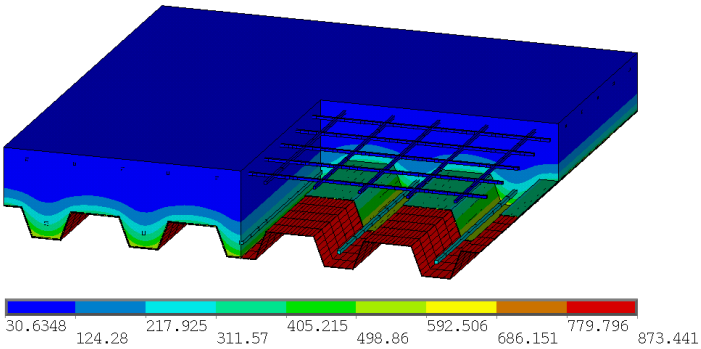

t= 45.2 min

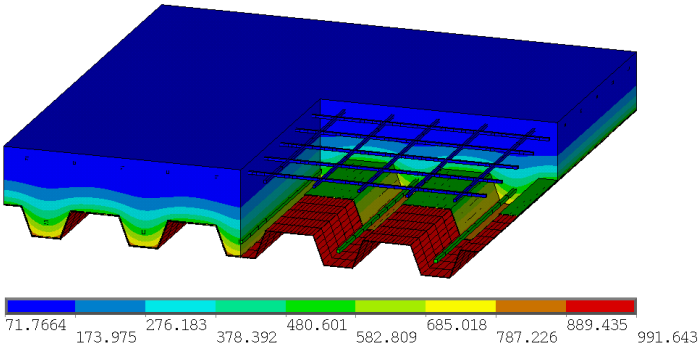

t= 90.3 min

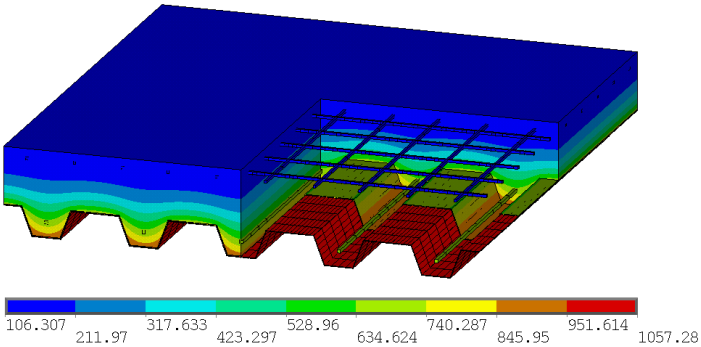

t= 135.5 min

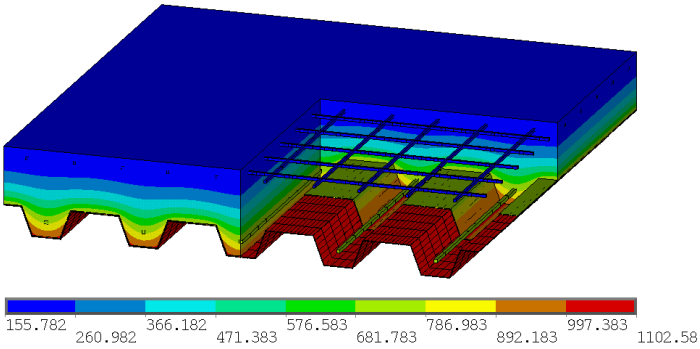

t= 180.6 min

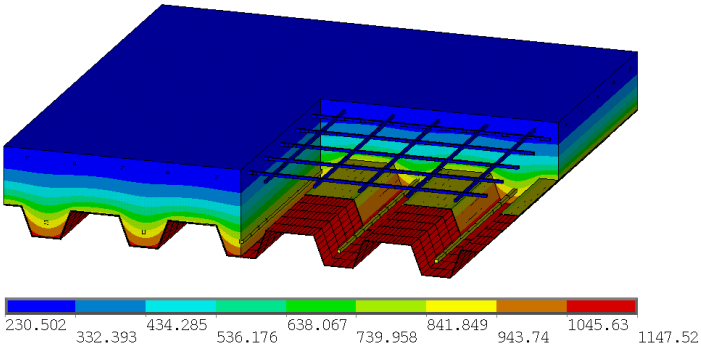

t= 240.0 min

SIM. 25	**Steel deck:** Trapezoidal – O Feliz H60	**Rebar (mm):** ϕ8	**t_a (mm):** 3	**Fire resistance (min)**	
	Mesh (mm//mm): ϕ6//100 (FNQ 60)	**h_1 (mm):** 50		Ave: *74.3*	Max: 77.9

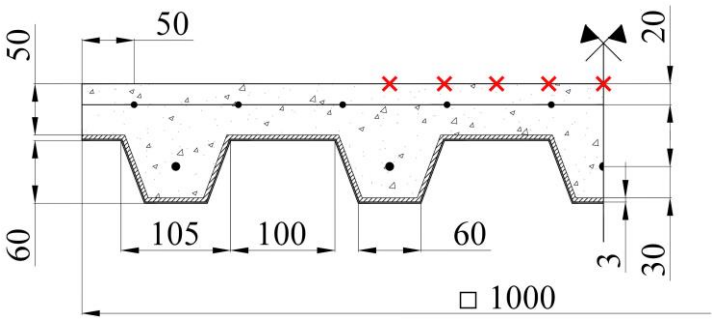

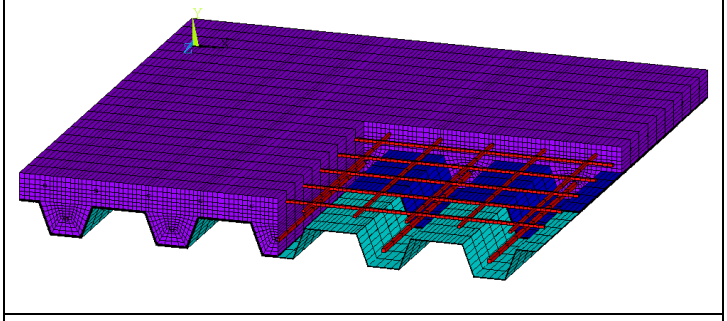

Finite element mesh

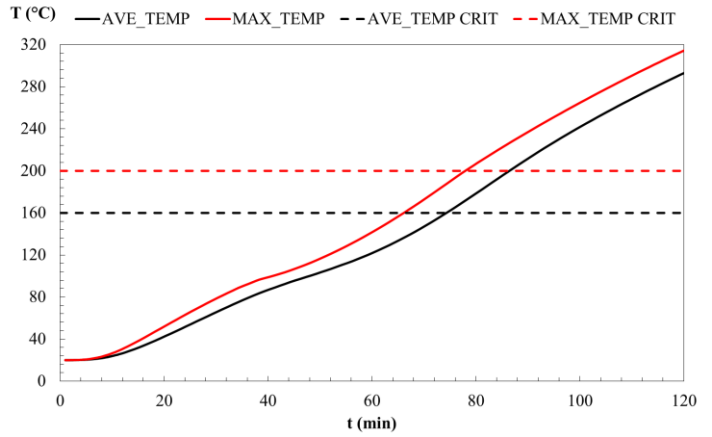

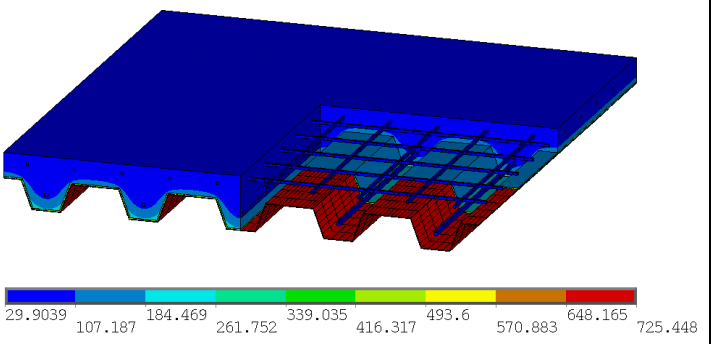

t= 18.6 min

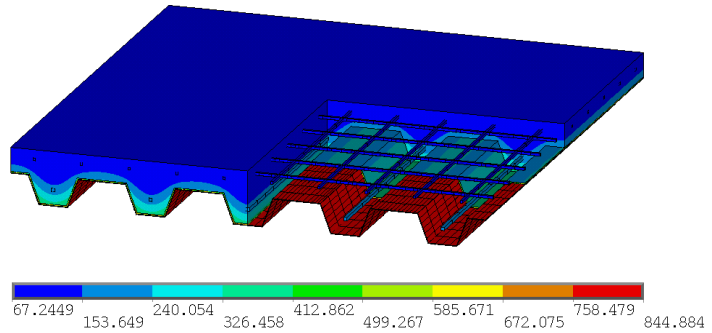

t= 37.2 min

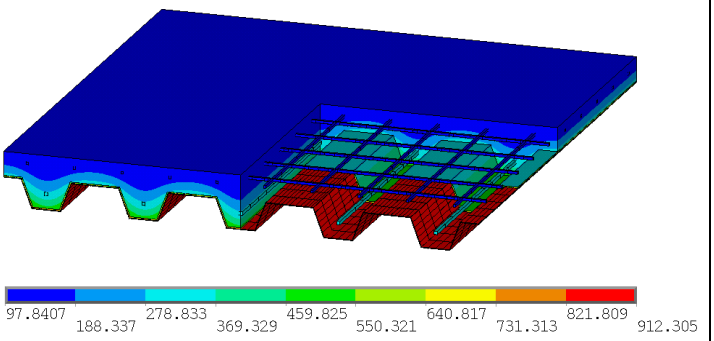

t= 55.7 min

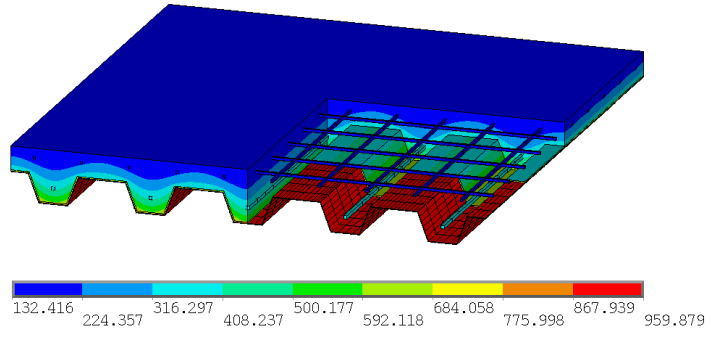

t= 74.3 min

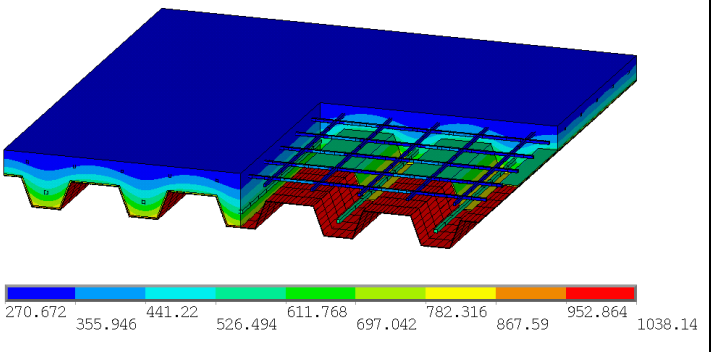

t= 120.0 min

SIM. 26	**Steel deck:** Trapezoidal – O Feliz H60	**Rebar (mm):** ϕ8	**t_a (mm):** 3	**Fire resistance (min)**	
	Mesh (mm//mm): ϕ6//100 (FNQ 60)	**h_1 (mm):** 60		Ave: *89.1*	Max: 96.2

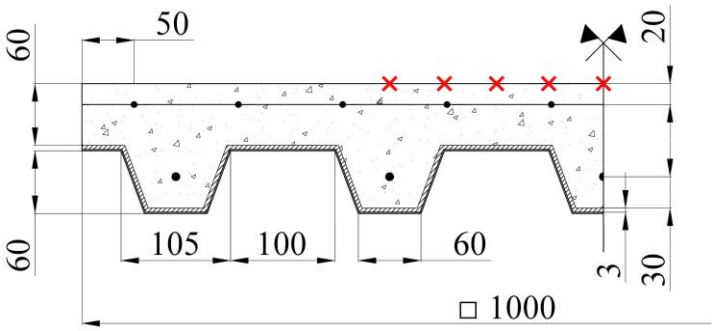

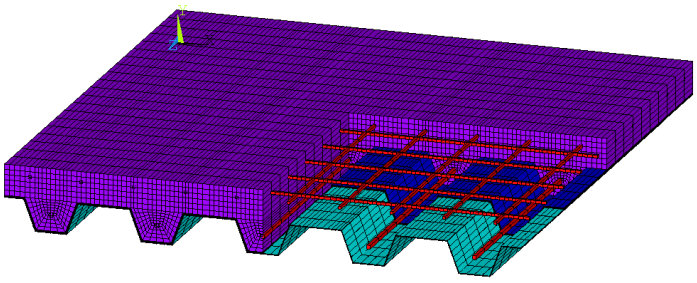

Finite element mesh

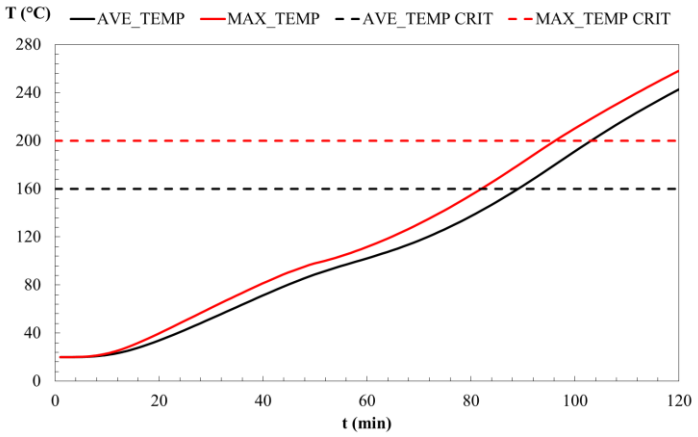

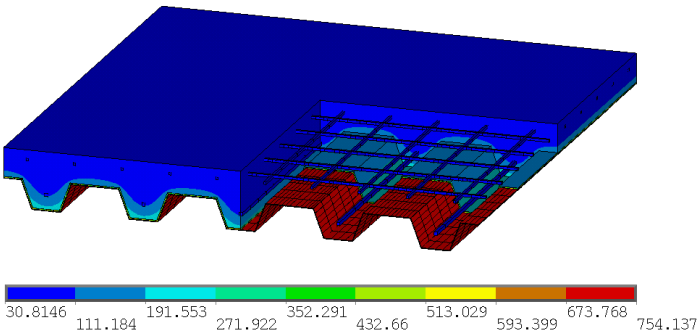

t= 22.3 min

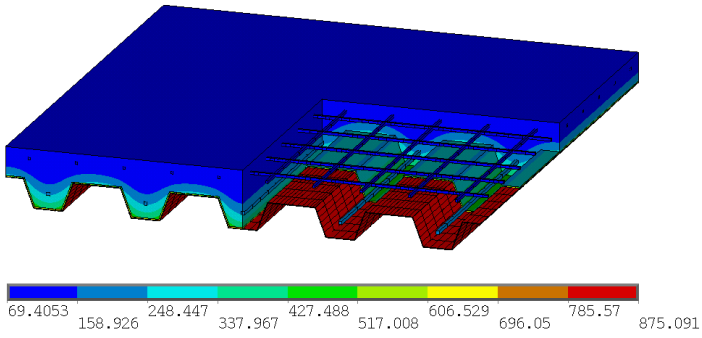

t= 44.6 min

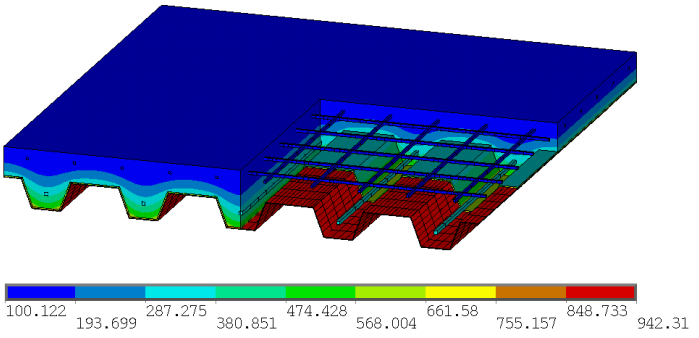

t= 66.8 min

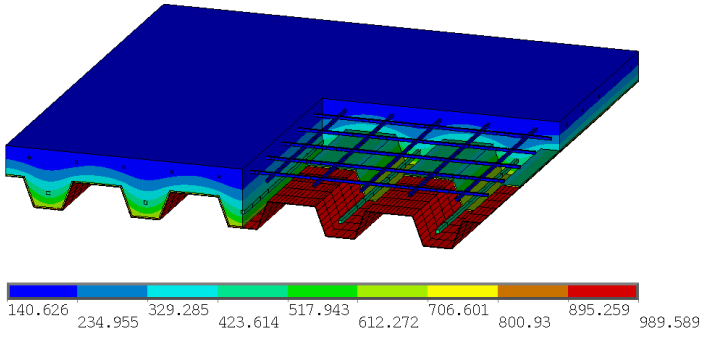

t= 89.1 min

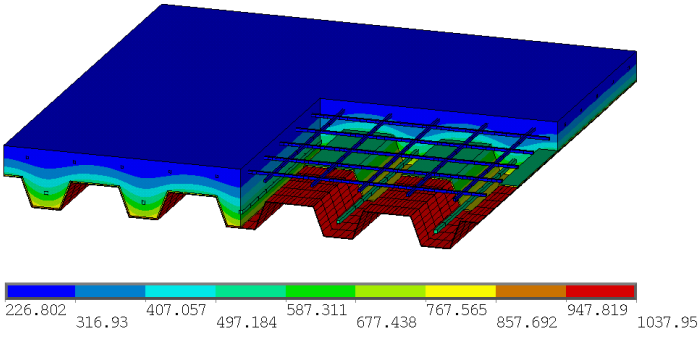

t= 120.0 min

SIM. 27	**Steel deck:** Trapezoidal – O Feliz H60	**Rebar (mm):** ϕ8	**t_a (mm):** 3	**Fire resistance (min)**	
	Mesh (mm//mm): ϕ6//100 (FNQ 60)	**h_1 (mm):** 70		Ave: *104.8*	Max: 115.5

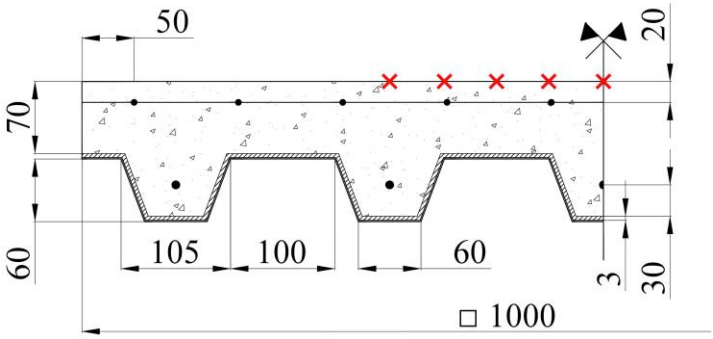

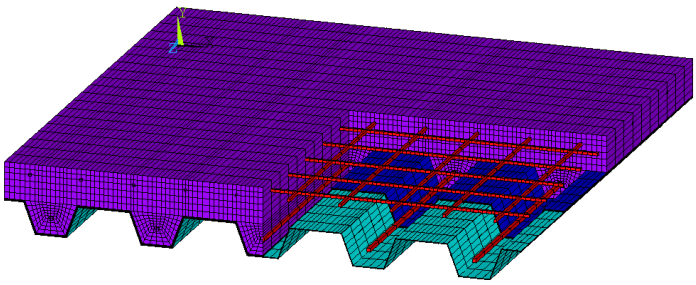

Finite element mesh

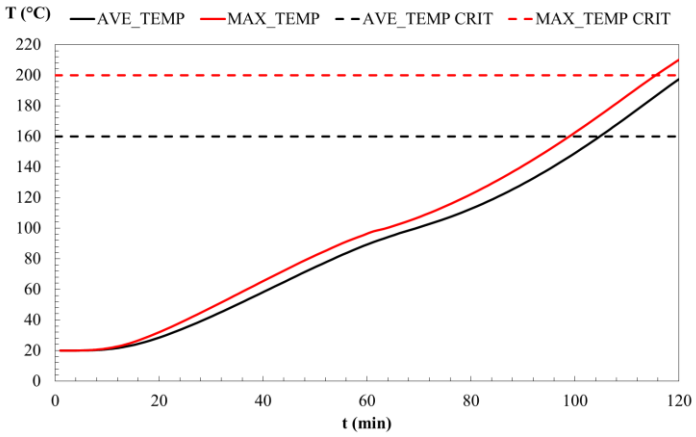

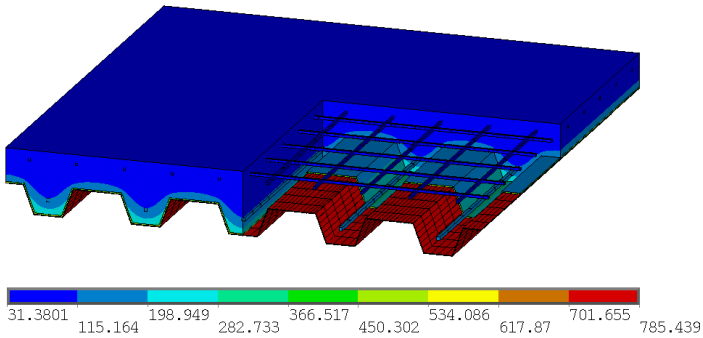

t= 26.2 min

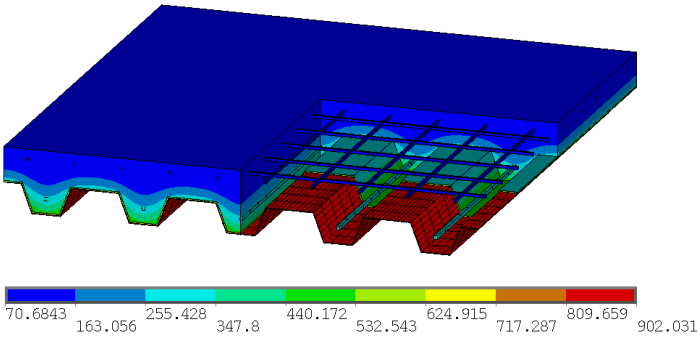

t= 52.4 min

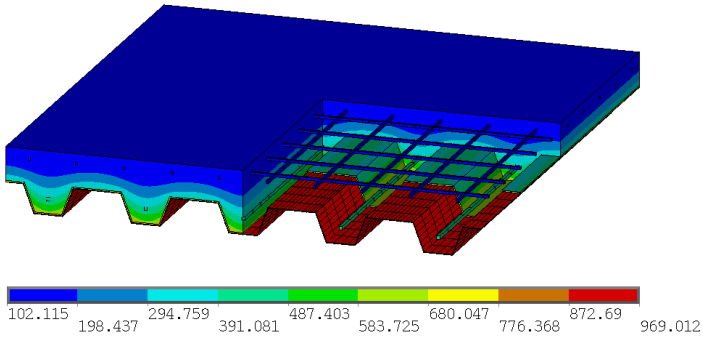

t= 78.6 min

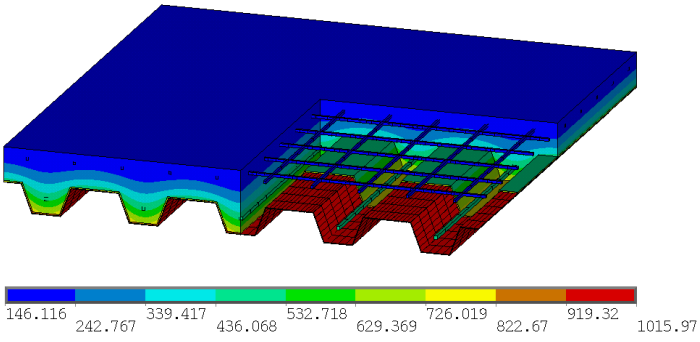

t= 104.8 min

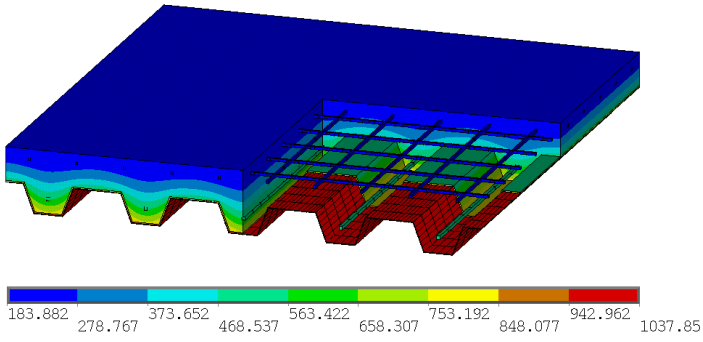

t= 120.0 min

SIM. 28	**Steel deck:** Trapezoidal – O Feliz H60	**Rebar (mm):** ϕ8	**t_a (mm):** 3	**Fire resistance (min)**	
	Mesh (mm//mm): ϕ6//100 (FNQ 60)	**h_1 (mm):** 80		Ave: *121.6*	Max: 136.2

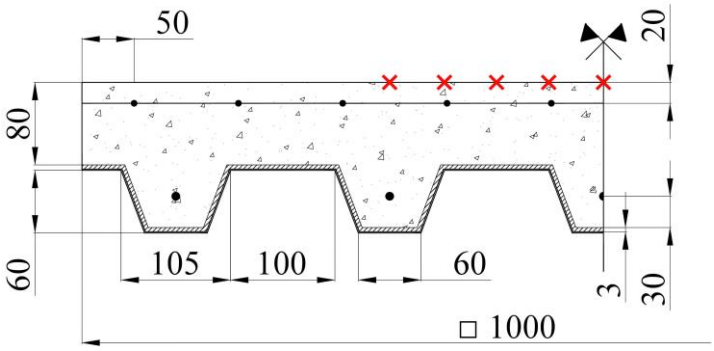

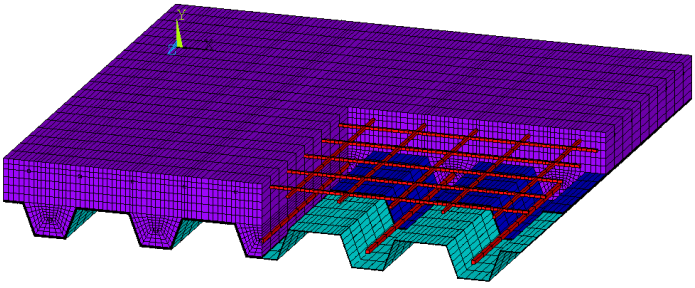

Finite element mesh

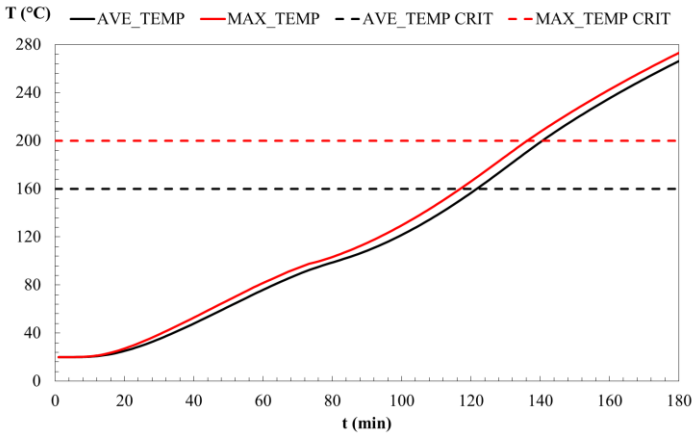

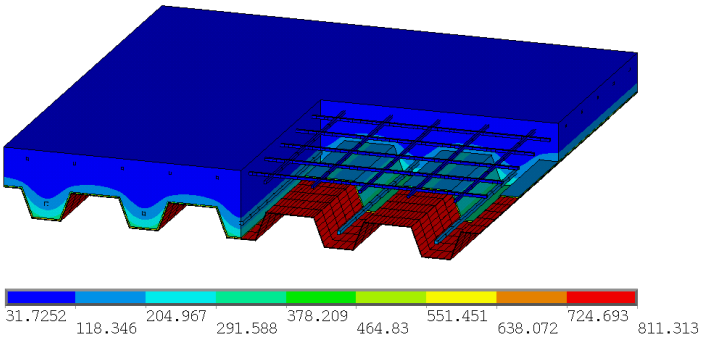

t= 30.4 min

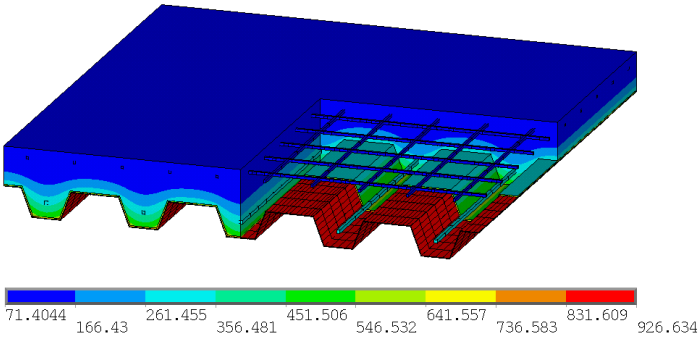

t= 60.8 min

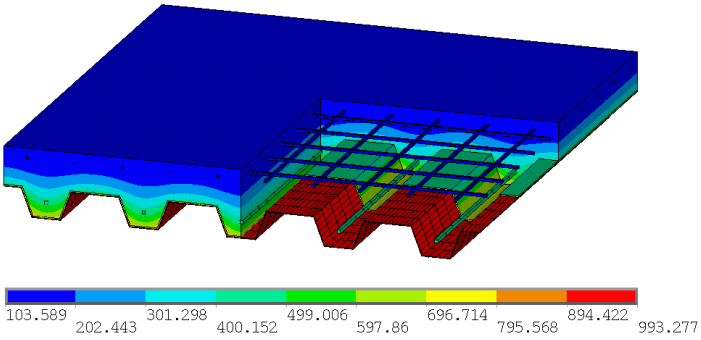

t= 91.2 min

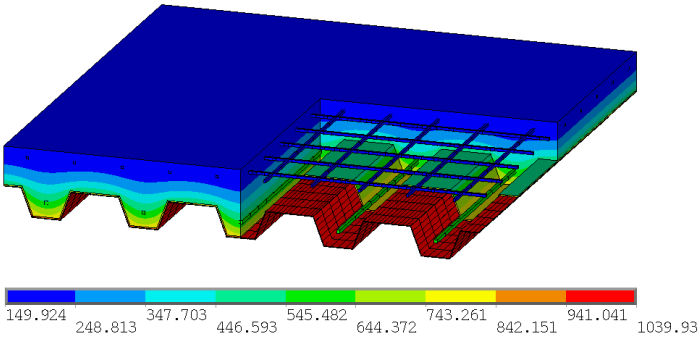

t= 121.6 min

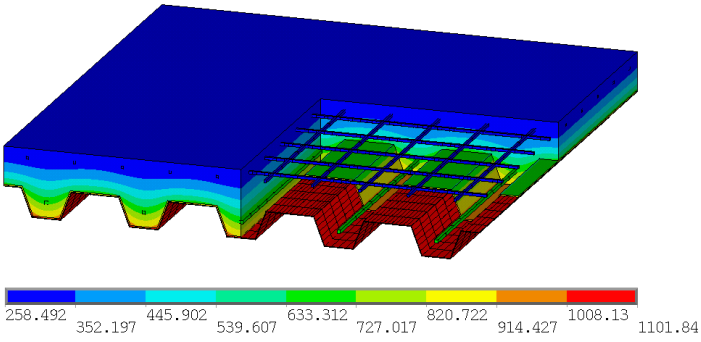

t= 180.0 min

SIM. 29	**Steel deck:** Trapezoidal – O Feliz H60	**Rebar (mm):** ϕ8	**t_a (mm):** 3	**Fire resistance (min)**	
	Mesh (mm//mm): ϕ6//100 (FNQ 60)	**h_1 (mm):** 90		Ave: *139.8*	Max: 158.2

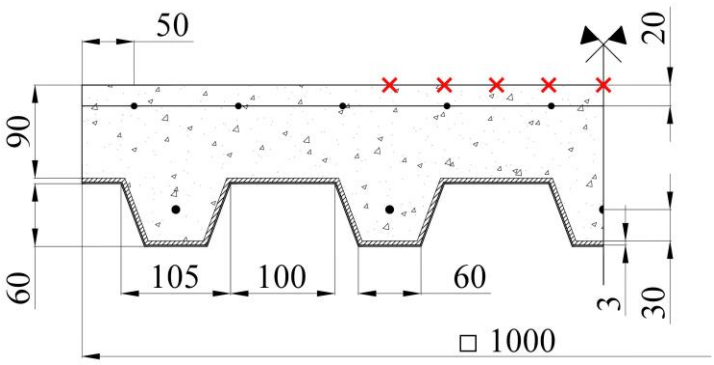

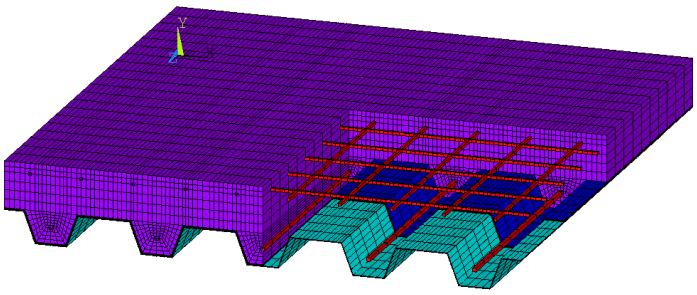

Finite element mesh

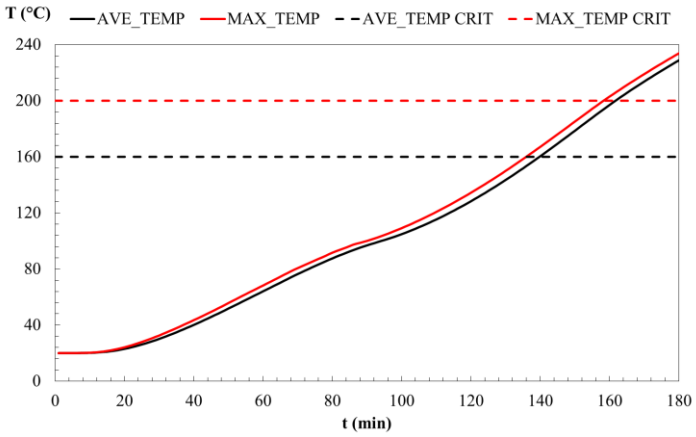

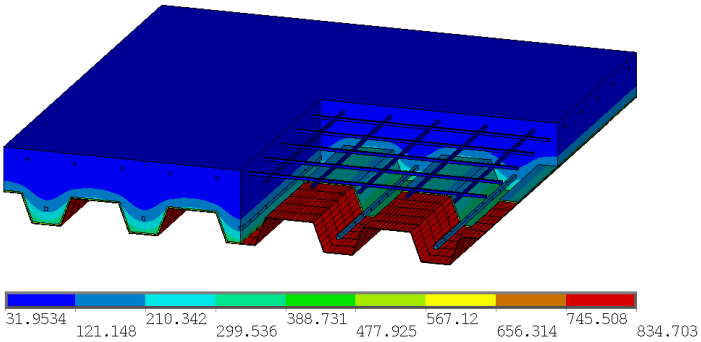

t= 35.0 min

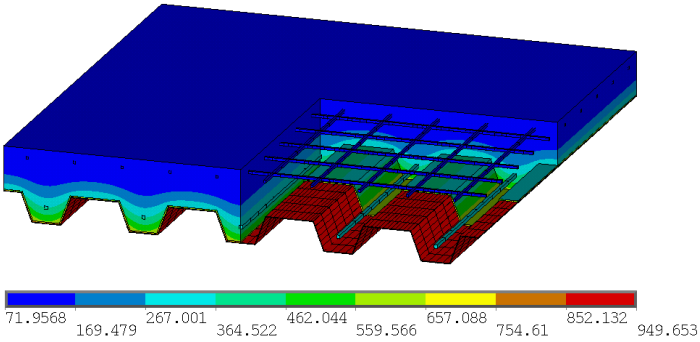

t= 69.9 min

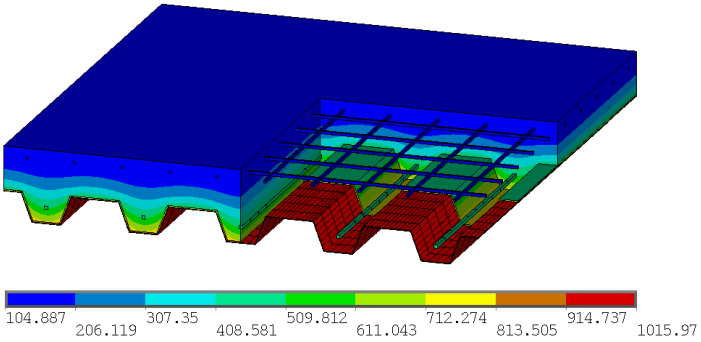

t= 104.9 min

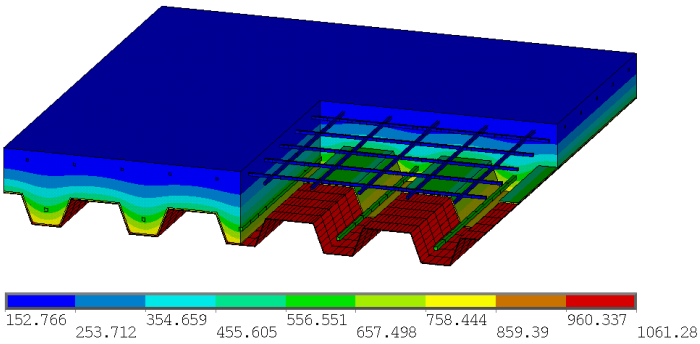

t= 139.8 min

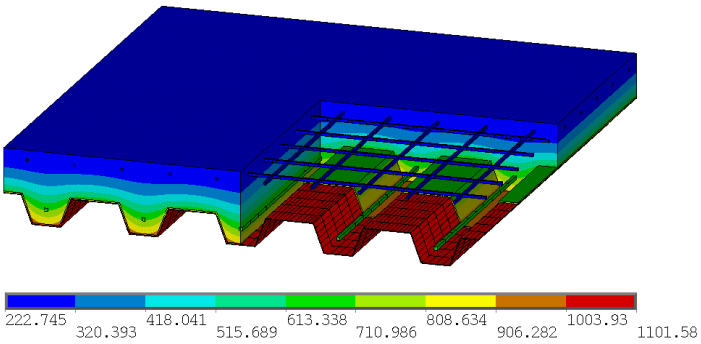

t= 180.0 min

SIM. 30	**Steel deck:** Trapezoidal – O Feliz H60	**Rebar (mm):** ϕ8	**t_a (mm):** 3	**Fire resistance (min)**	
	Mesh (mm//mm): ϕ6//100 (FNQ 60)	**h_1 (mm):** 100		Ave: *159.6*	Max: 181.9

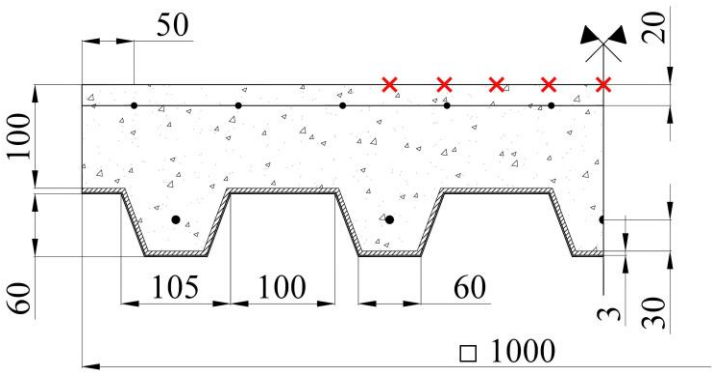

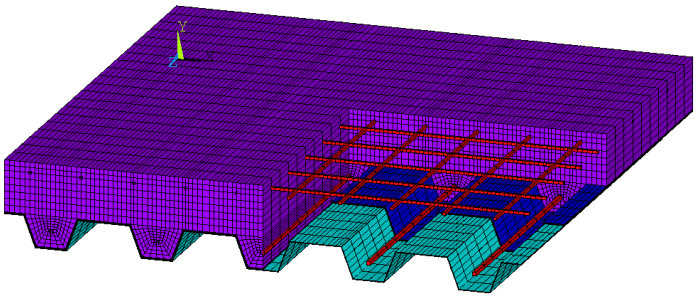

Finite element mesh

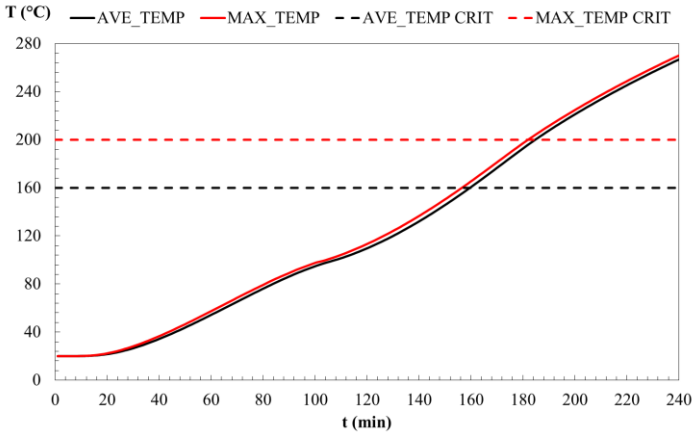

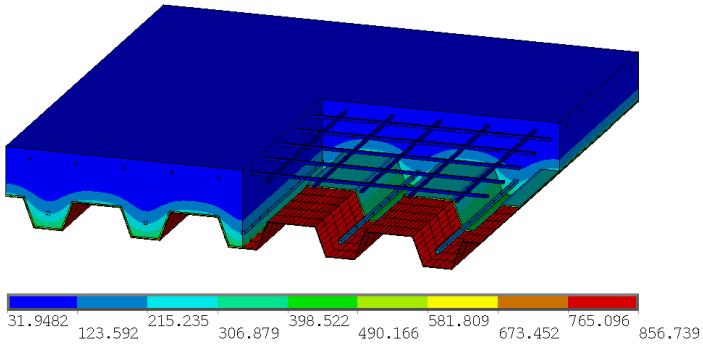

t= 39.9 min

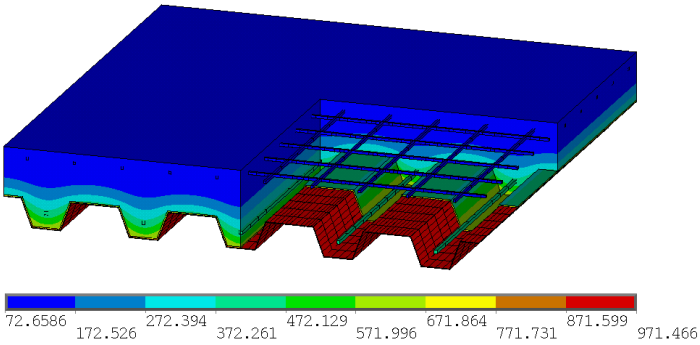

t= 79.8 min

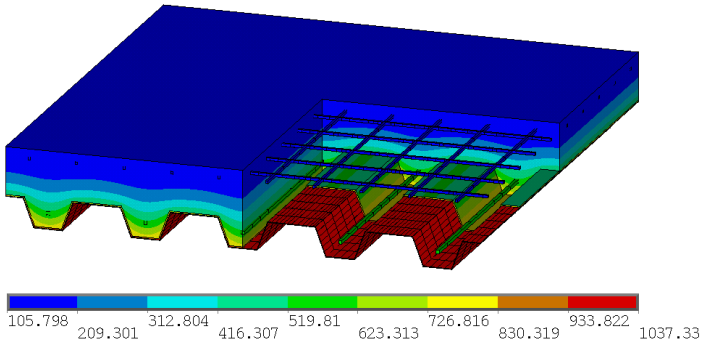

t= 119.7 min

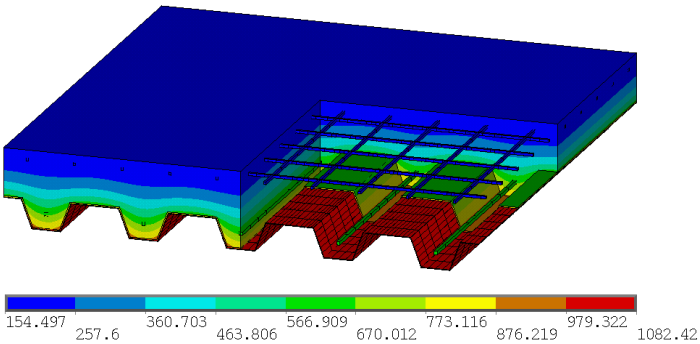

t= 159.6 min

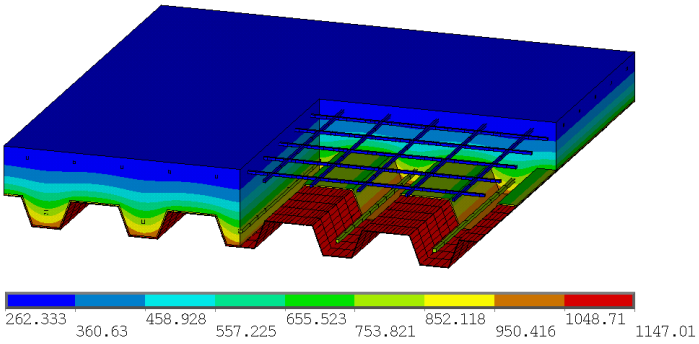

t= 240.0 min

SIM. 31	**Steel deck:** Trapezoidal – O Feliz H60	**Rebar (mm):** ϕ8	**t_a (mm):** 3	**Fire resistance (min)**	
	Mesh (mm//mm): ϕ6//100 (FNQ 60)	**h_1 (mm):** 110		Ave: *180.4*	Max: 207.1

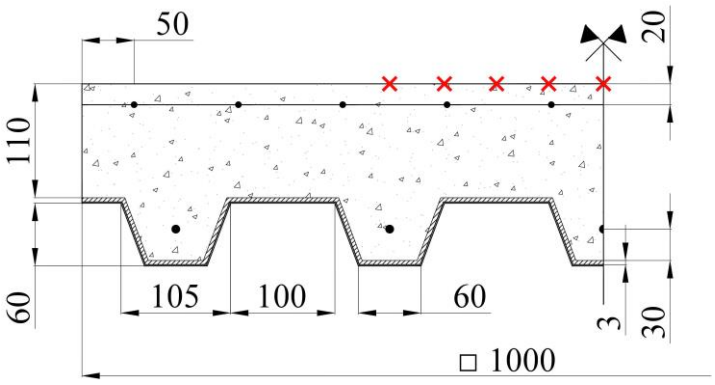

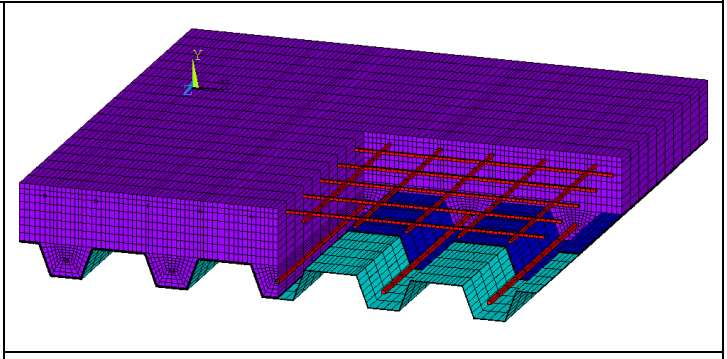

Finite element mesh

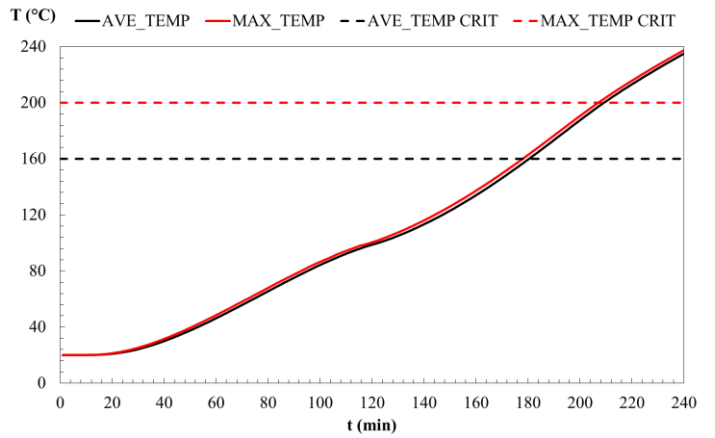

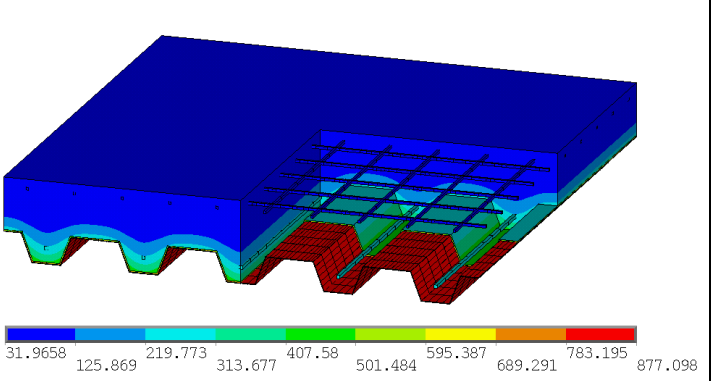

t= 45.1 min

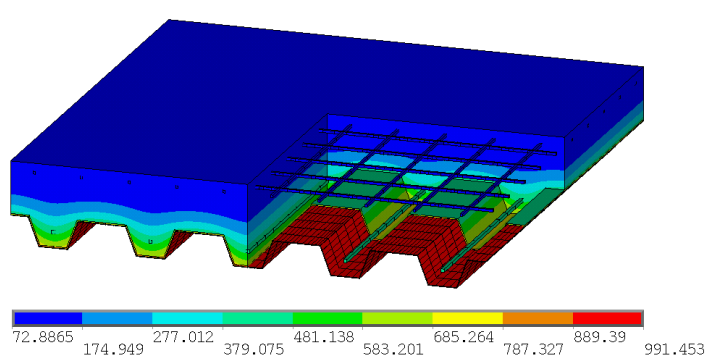

t= 90.2 min

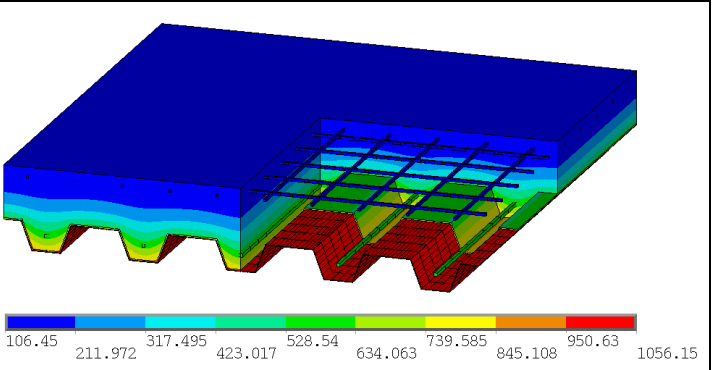

t= 135.3 min

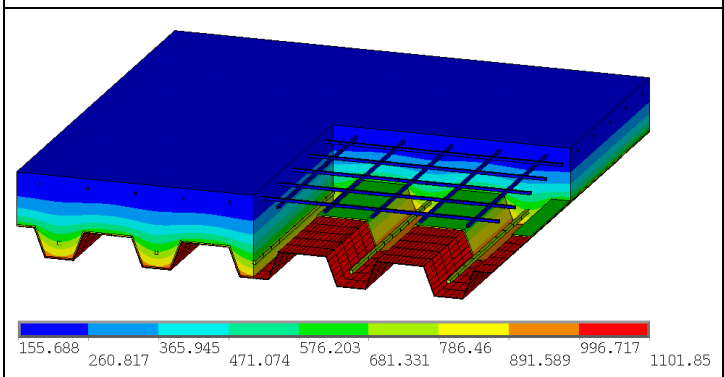

t= 180.4 min

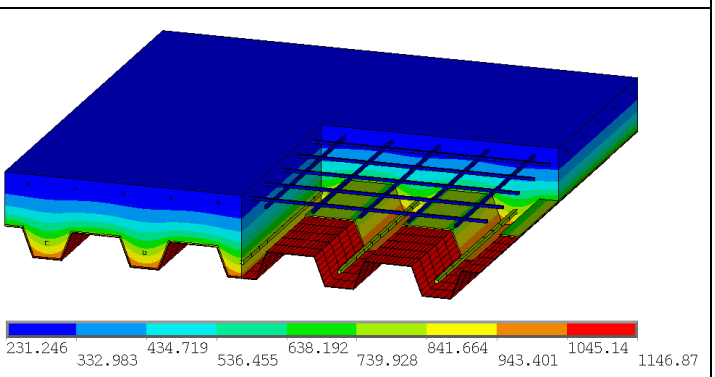

t= 240.0 min

SIM. 32	**Steel deck:** Trapezoidal – O Feliz H60	**Rebar (mm):** ϕ8	**t_a (mm):** 3	**Fire resistance (min)**	
	Mesh (mm//mm): ϕ6//100 (FNQ 60)	**h_1 (mm):** 120		Ave: *202.6*	Max: 233.8

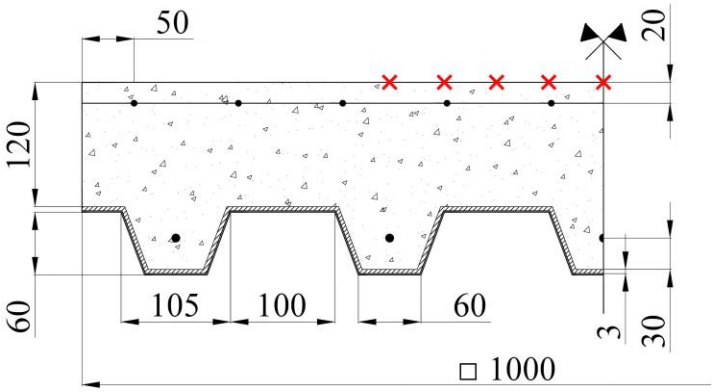

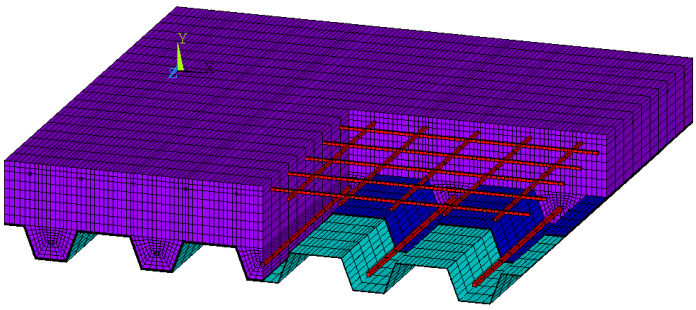

Finite element mesh

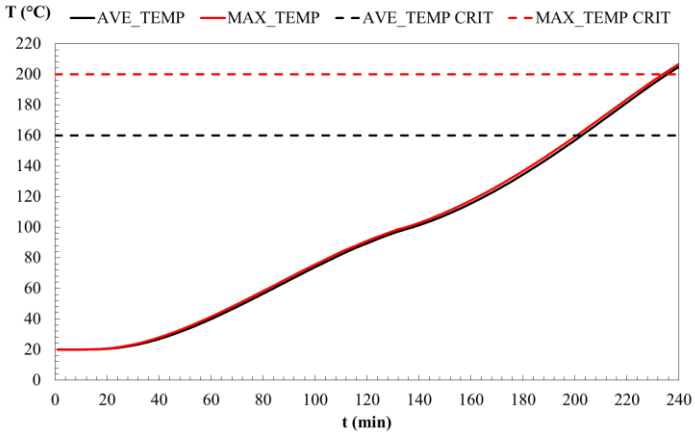

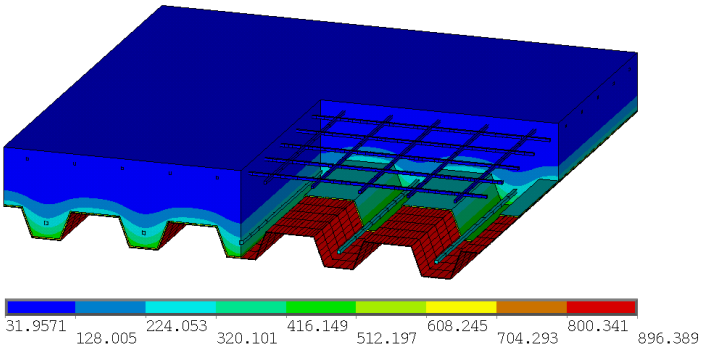

t= 50.7 min

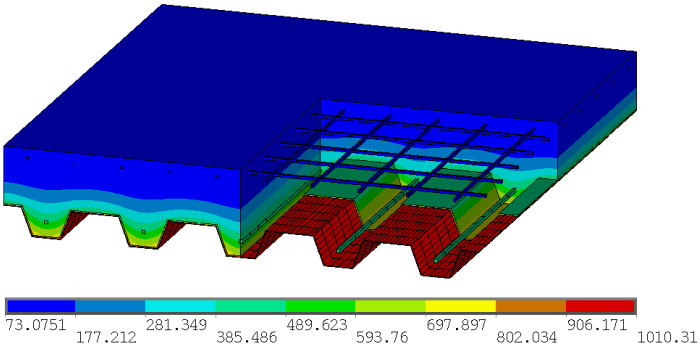

t= 101.3 min

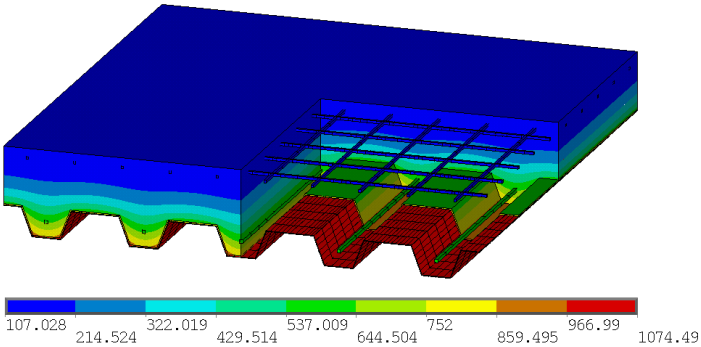

t= 152.0 min

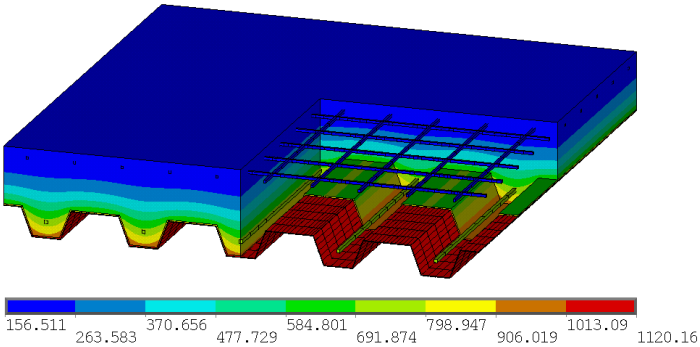

t= 202.6 min

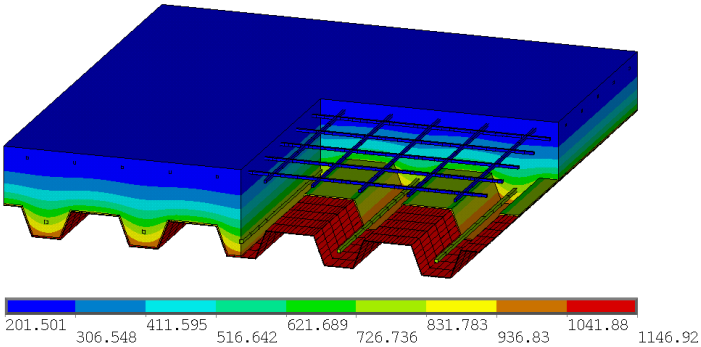

t= 240.0 min

SIM. 33	**Steel deck:** Trapezoidal – O Feliz H60	**Rebar (mm): -**	**t_a (mm):** 3	**Fire resistance (min)**	
	Mesh (mm//mm): -	**h_1 (mm):** 50		Ave: *74.6*	Max: 77.2

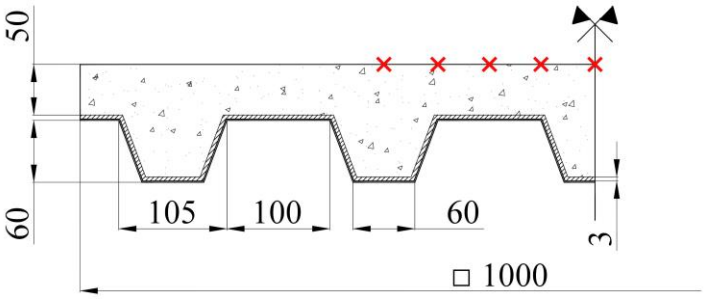

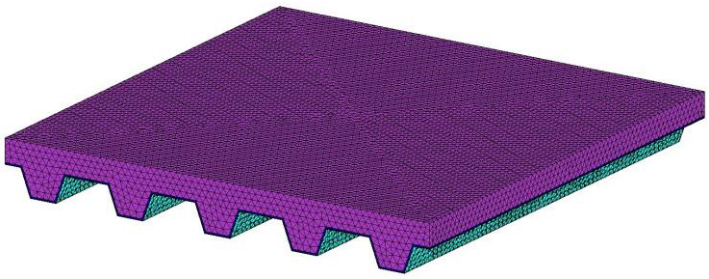

Finite element mesh

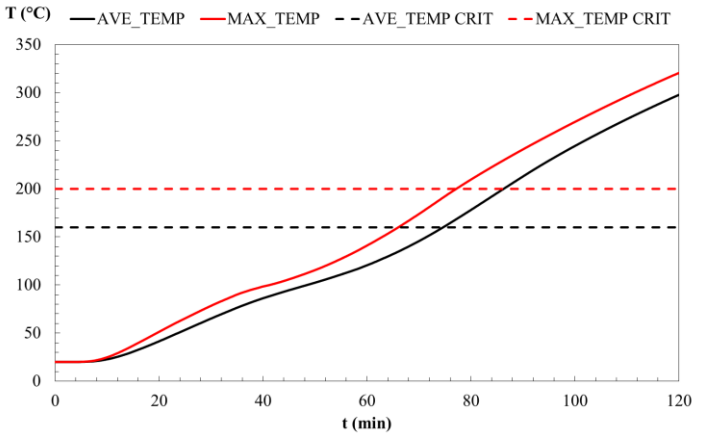

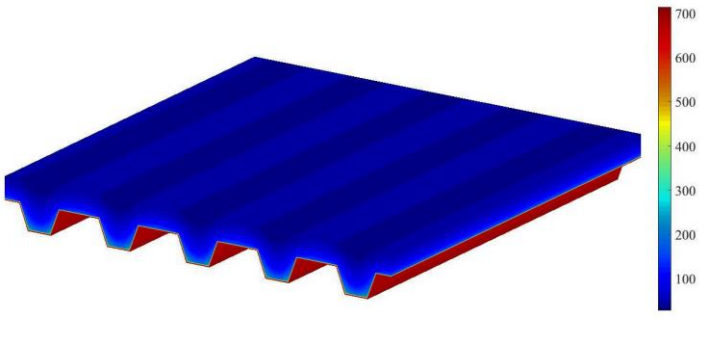

t= 18.7 min

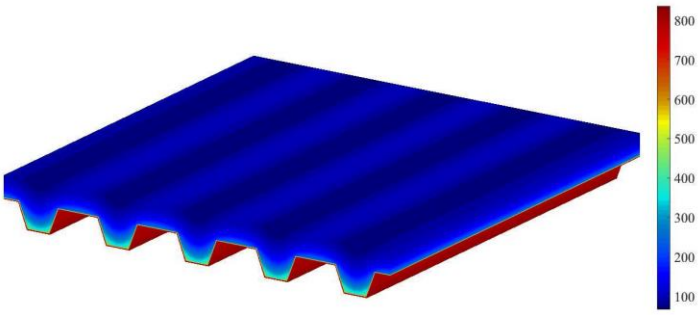

t= 37.3 min

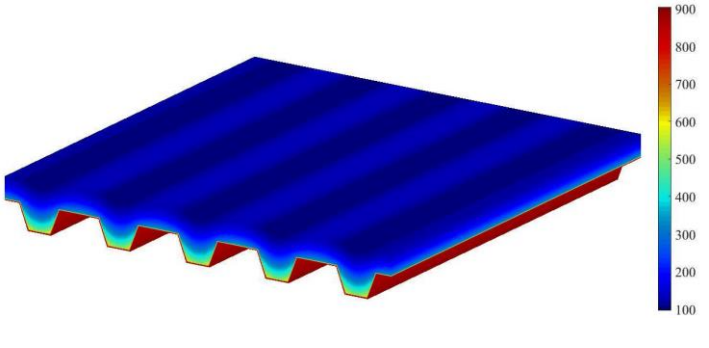

t= 56.0 min

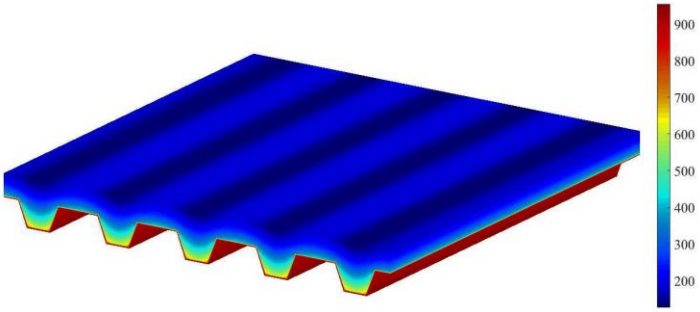

t= 74.6 min

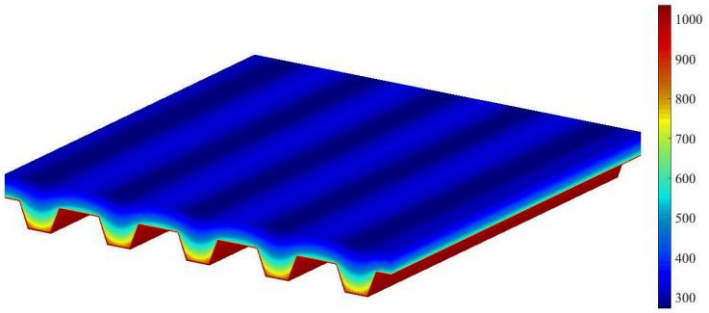

t= 120.0 min

SIM. 34	**Steel deck:** Trapezoidal – O Feliz H60	**Rebar (mm): -**	**t_a (mm):** 3	**Fire resistance (min)**	
	Mesh (mm//mm): -	**h_1 (mm):** 60		Ave: *89.7*	Max: 95.5

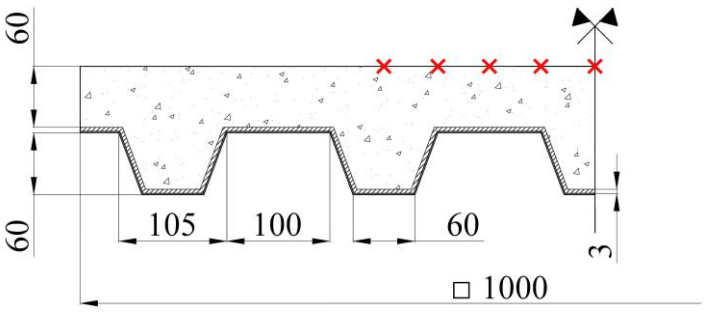

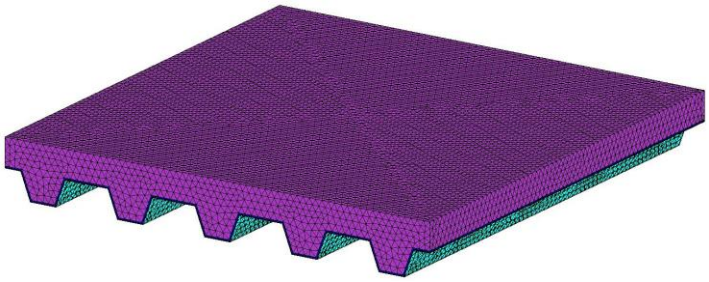

Finite element mesh

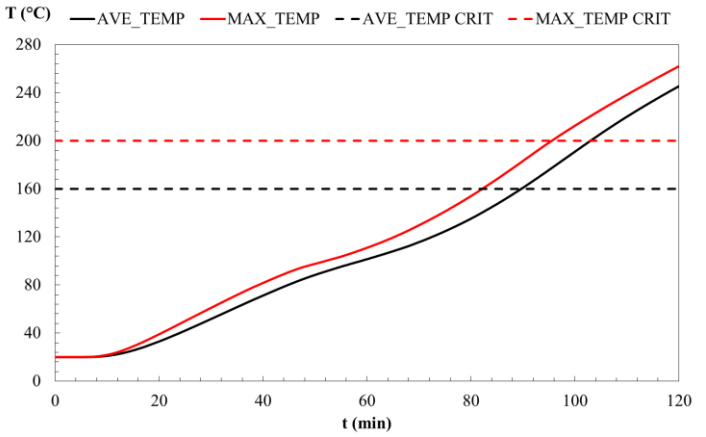

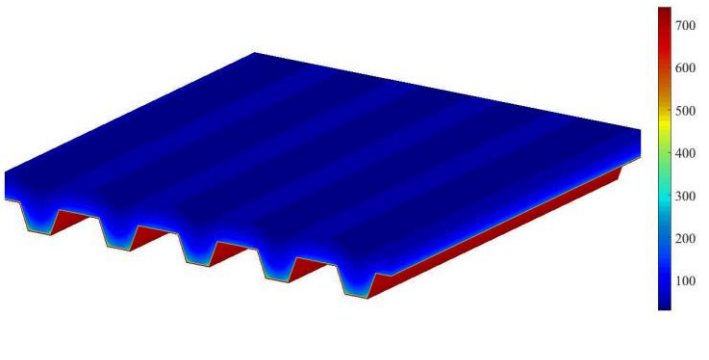

t= 22.4 min

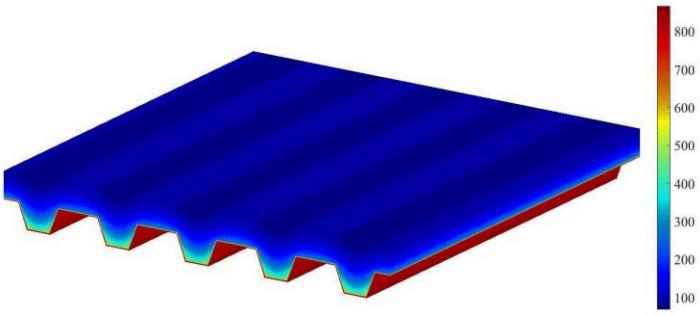

t= 44.9 min

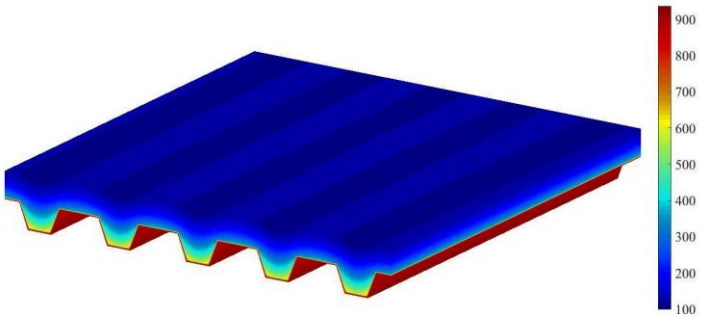

t= 67.3 min

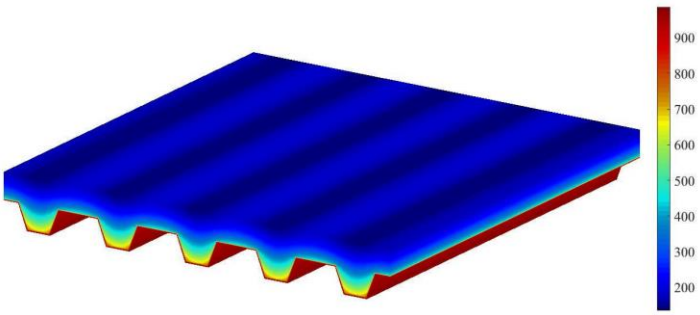

t= 89.7 min

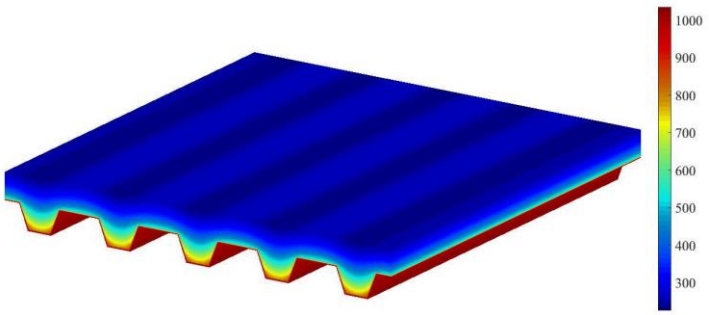

t= 120.0 min

SIM. 35	**Steel deck:** Trapezoidal – O Feliz H60	**Rebar (mm): -**	**t_a (mm):** 3	**Fire resistance (min)**	
	Mesh (mm//mm): -	**h_1 (mm):** 70		Ave: *105.8*	Max: 115.2

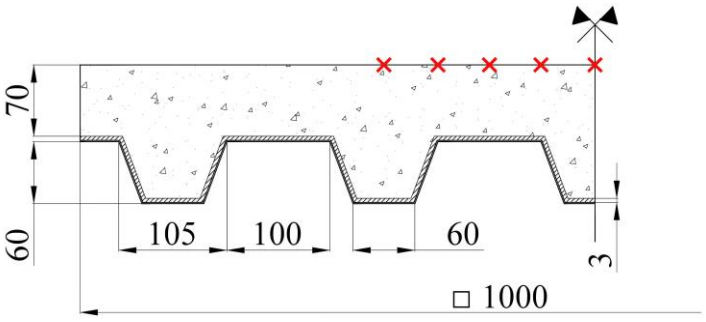

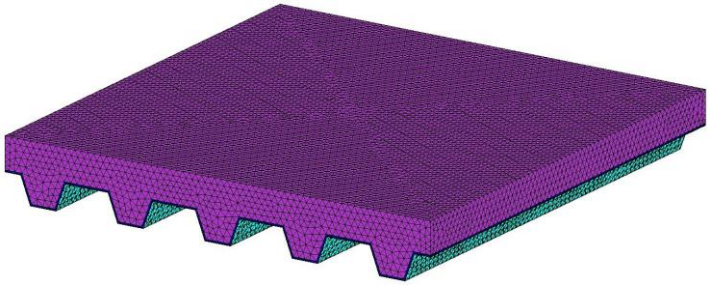

Finite element mesh

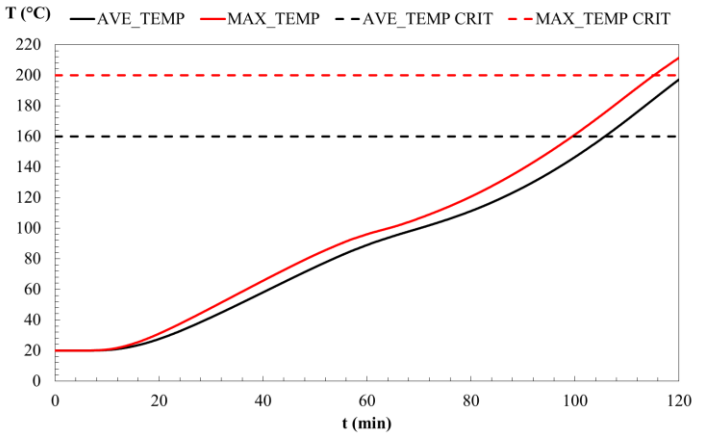

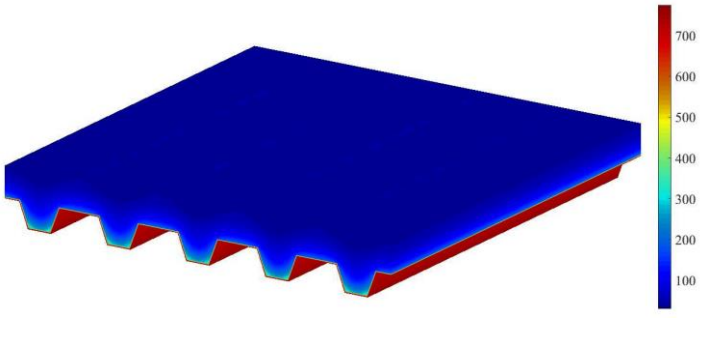

t= 26.5 min

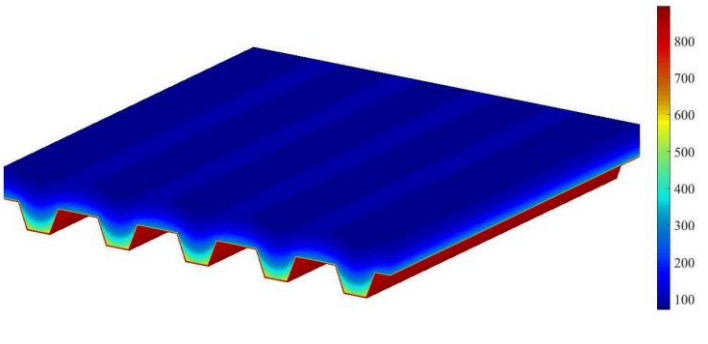

t= 52.9 min

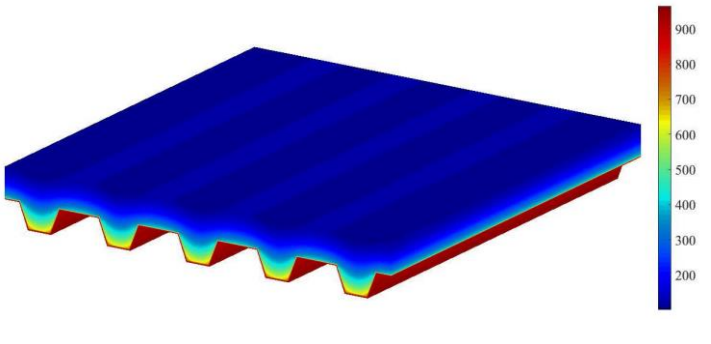

t= 79.4 min

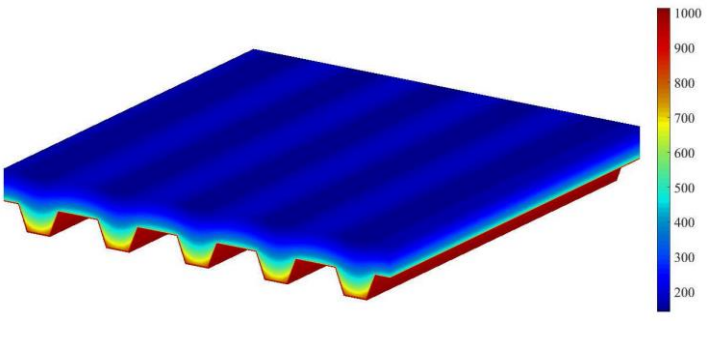

t= 105.8 min

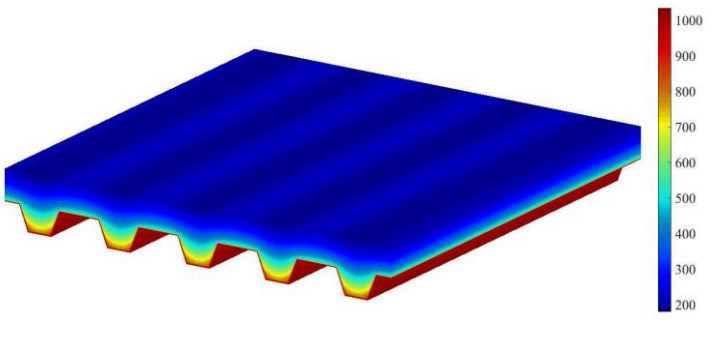

t= 120.0 min

SIM. 36	**Steel deck:** Trapezoidal – O Feliz H60	**Rebar (mm): -**	**t_a (mm):** 3	**Fire resistance (min)**	
	Mesh (mm//mm): -	**h_1 (mm):** 80		Ave: *122.9*	Max: 135.8

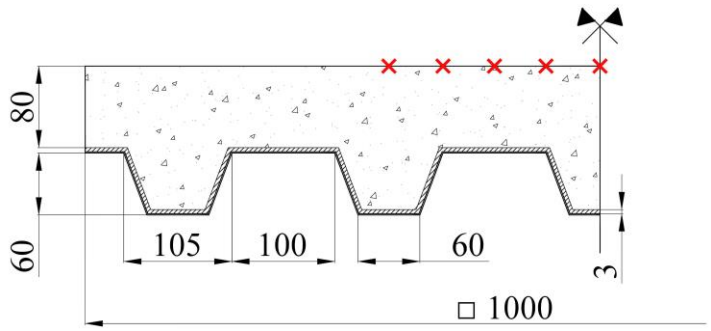

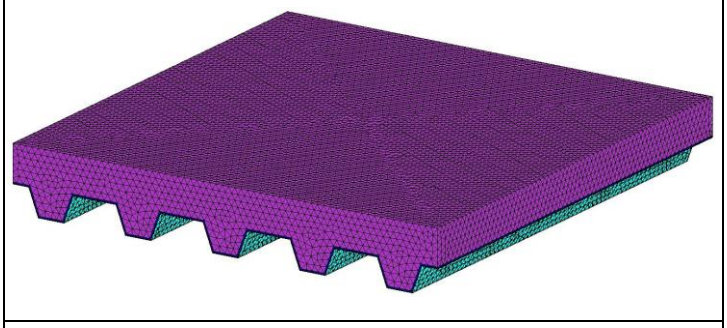

Finite element mesh

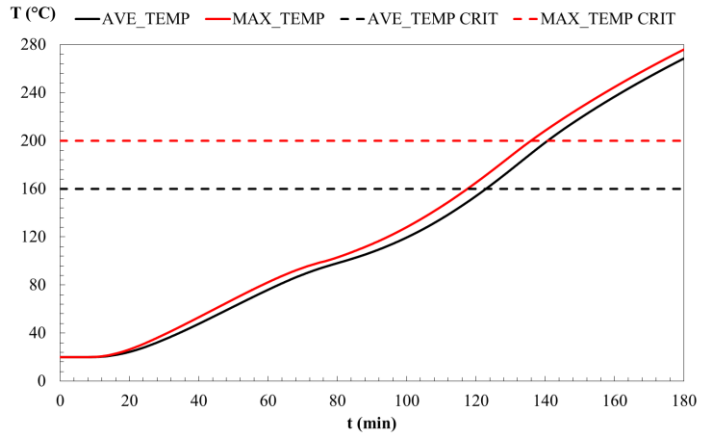

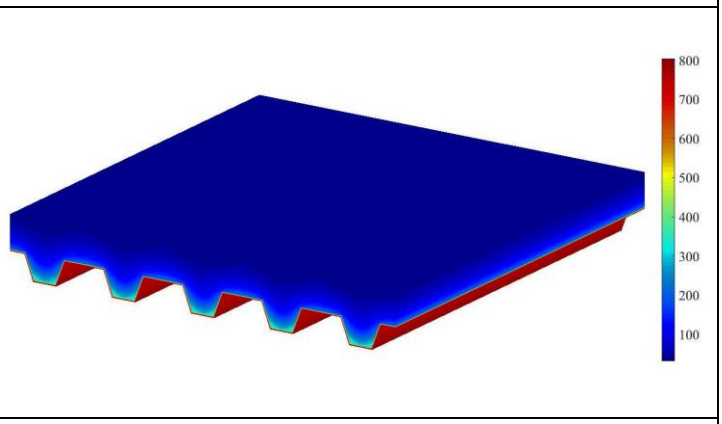

t= 30.7 min

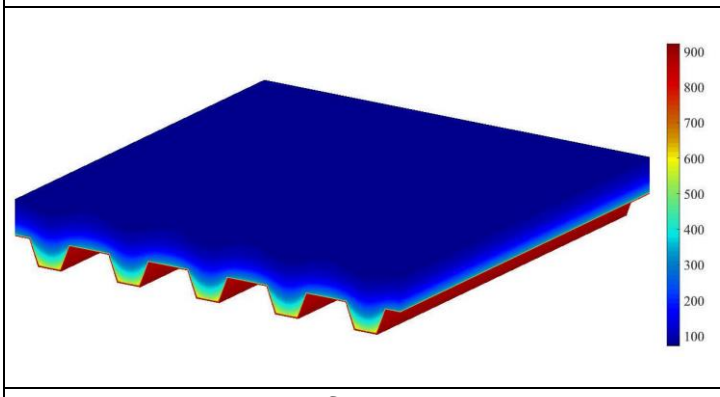

t= 61.5 min

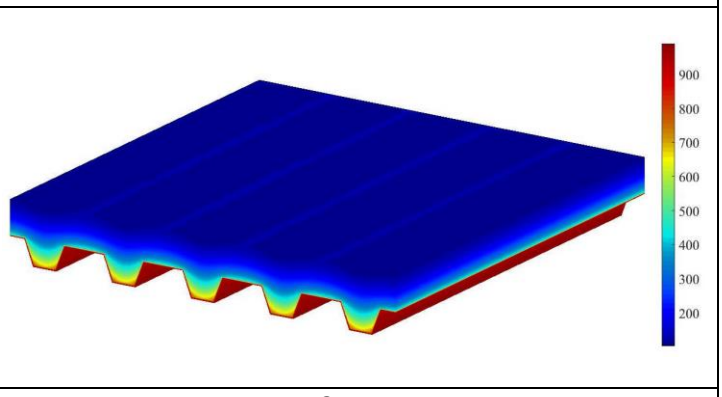

t= 92.2 min

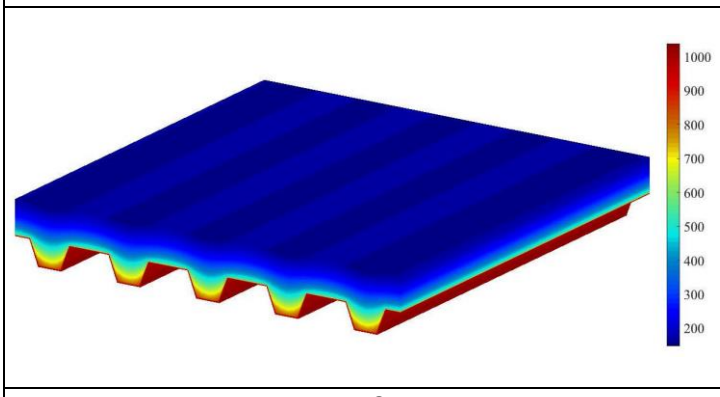

t= 122.9 min

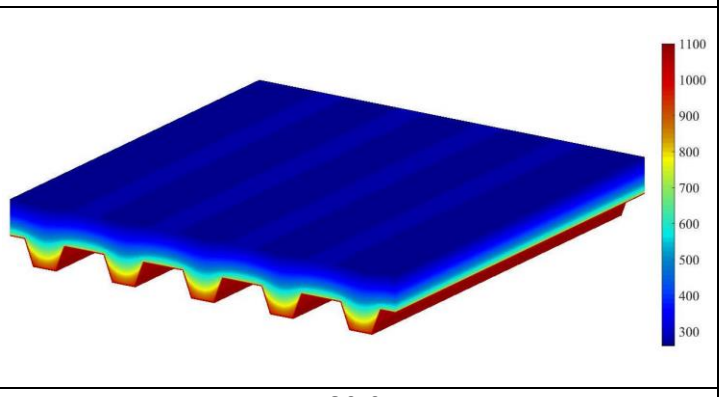

t= 180.0 min

SIM. 37	**Steel deck:** Trapezoidal – O Feliz H60	**Rebar (mm): -**	**t_a (mm):** 3	**Fire resistance (min)**	
	Mesh (mm//mm): -	**h_1 (mm):** 90		Ave: *141.4*	Max: 158.3

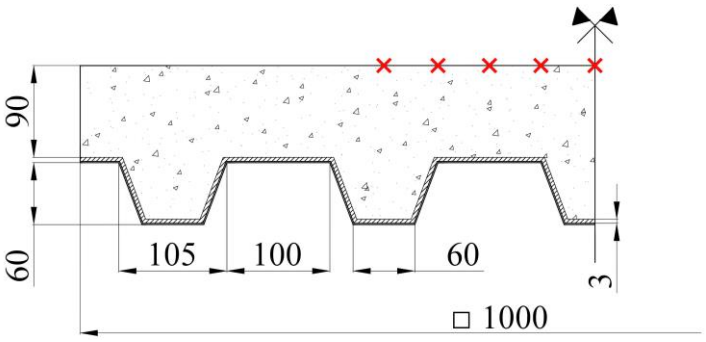

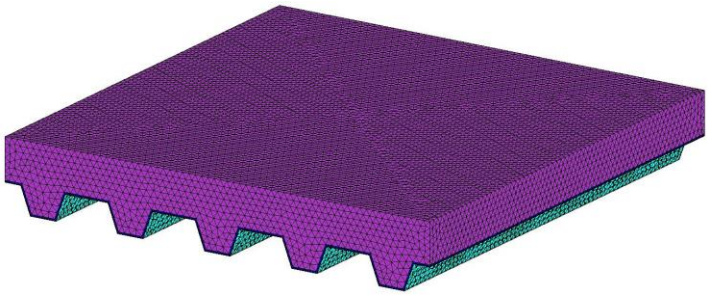

Finite element mesh

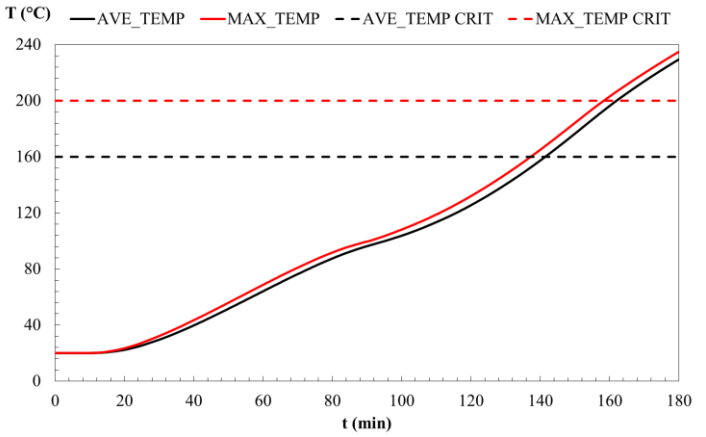

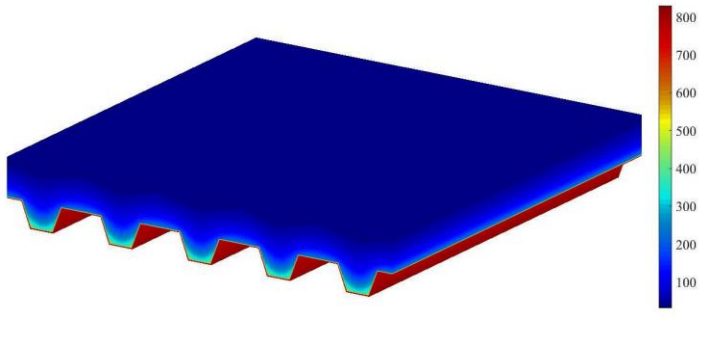

t= 35.4 min

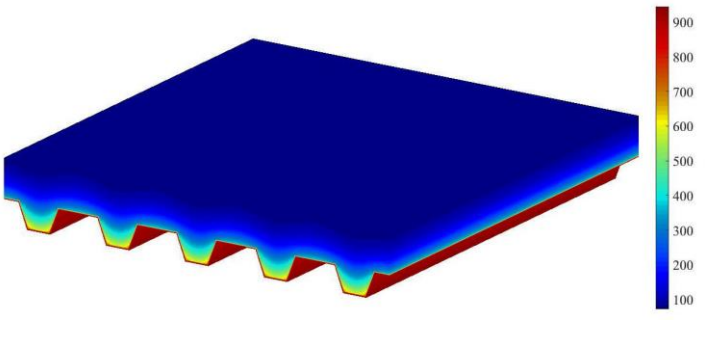

t= 70.7 min

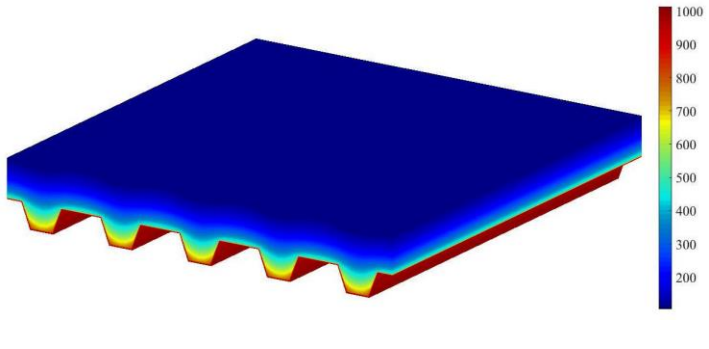

t= 106.1 min

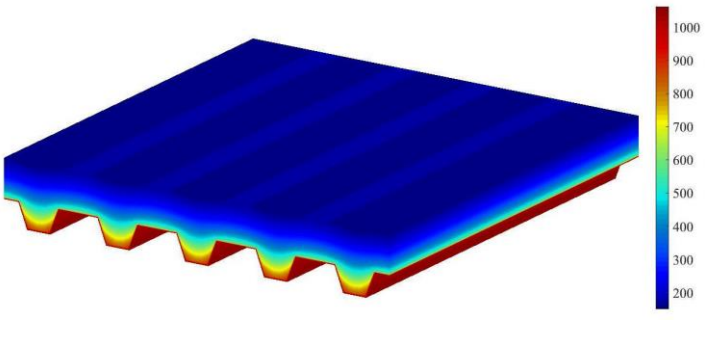

t= 141.4 min

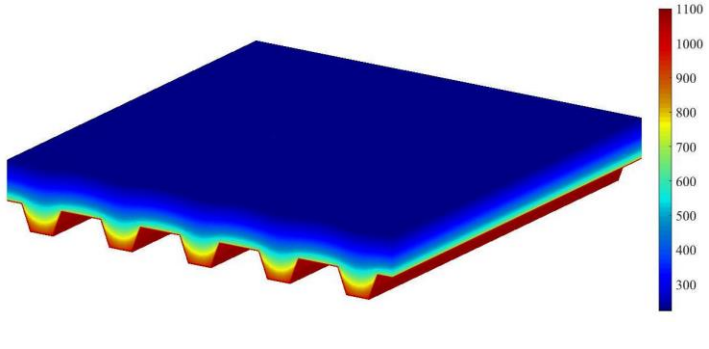

t= 180.0 min

SIM. 38	**Steel deck:** Trapezoidal – O Feliz H60	**Rebar (mm): -**	**t_a (mm):** 3	**Fire resistance (min)**	
	Mesh (mm//mm): -	**h_1 (mm):** 100		Ave: *161.4*	Max: 182.2

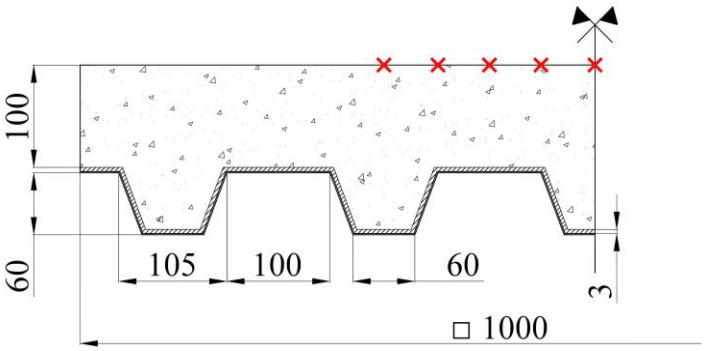

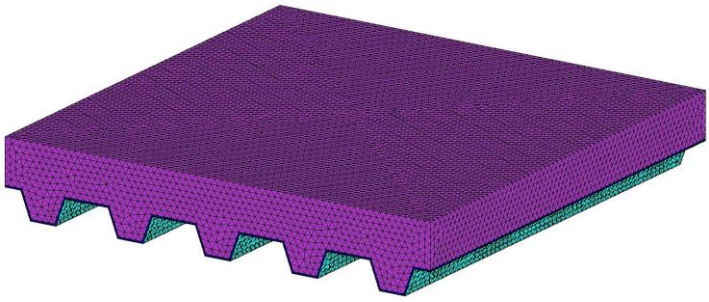

Finite element mesh

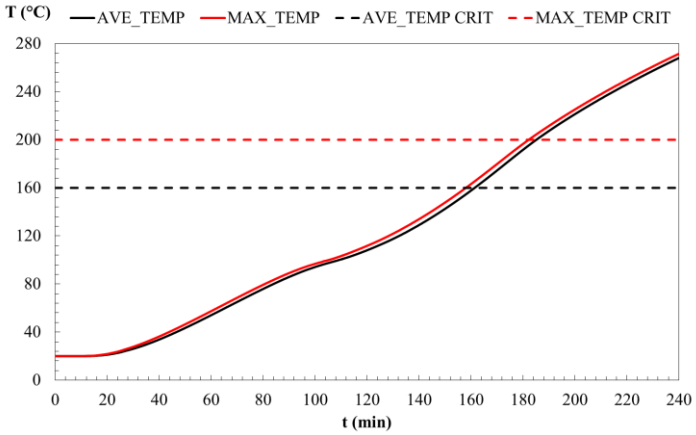

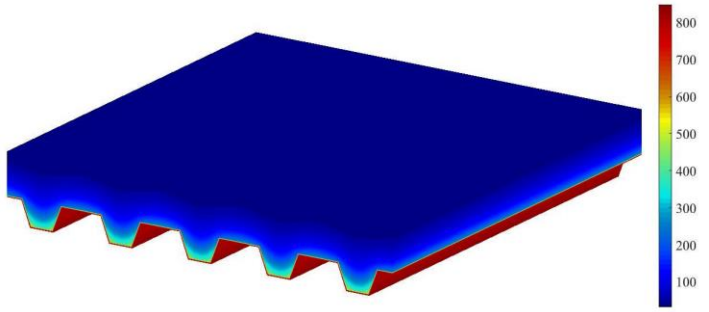

t= 40.4 min

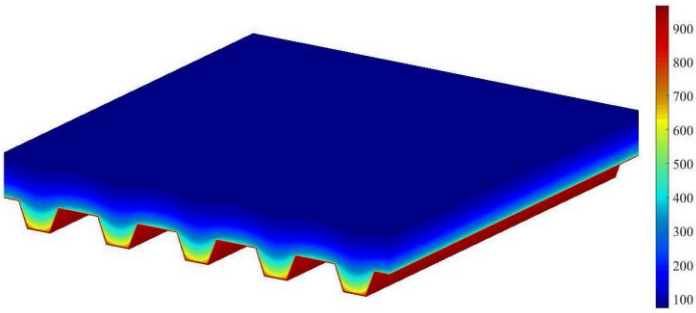

t= 80.7 min

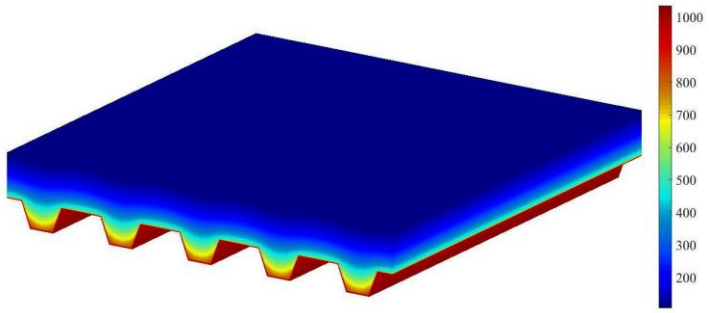

t= 121.1 min

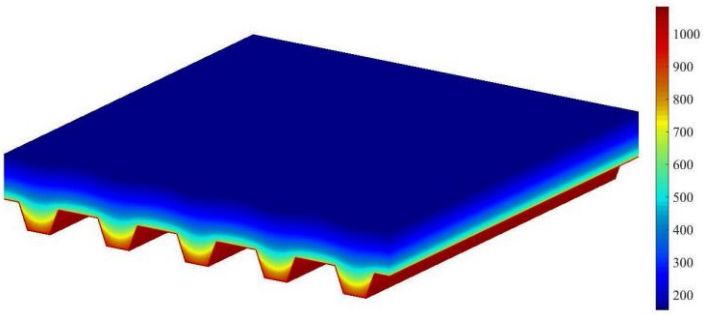

t= 161.4 min

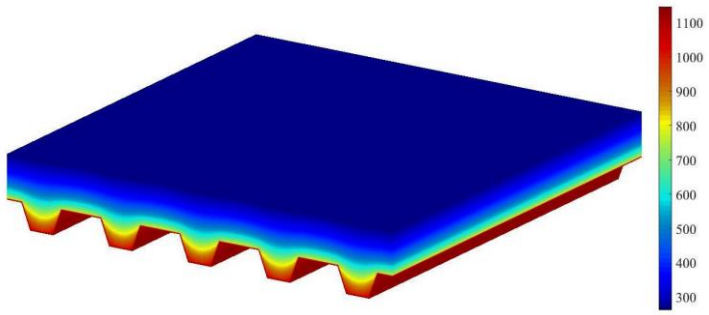

t= 240.0 min

SIM. 39	**Steel deck:** Trapezoidal – O Feliz H60	**Rebar (mm): -**	**t_a (mm):** 3	**Fire resistance (min)**	
	Mesh (mm//mm): -	**h_1 (mm):** 110		Ave: *182.6*	Max: 207.5

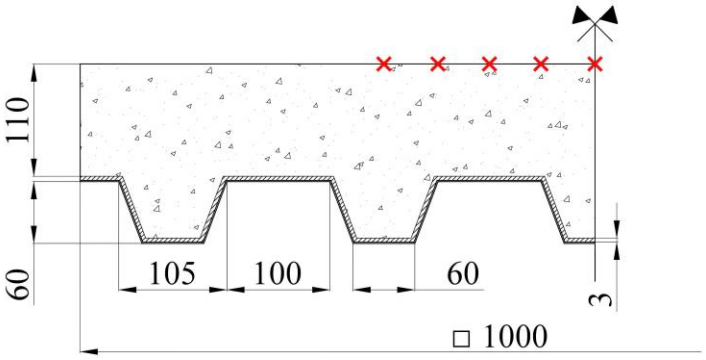

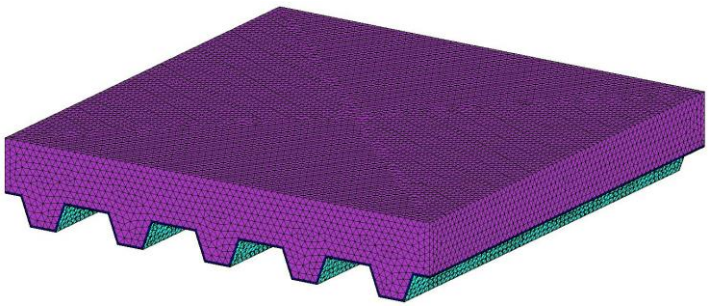

Finite element mesh

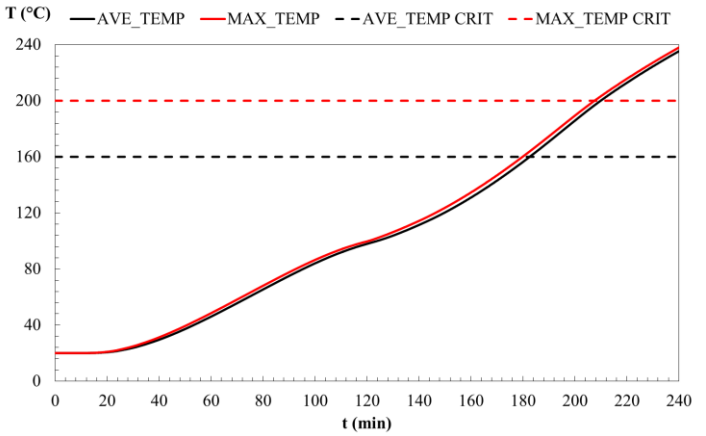

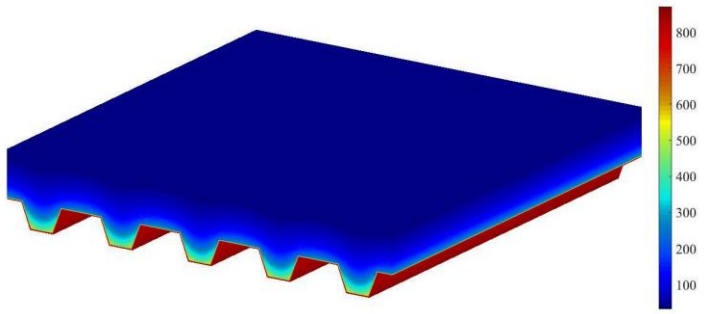

t= 45.7 min

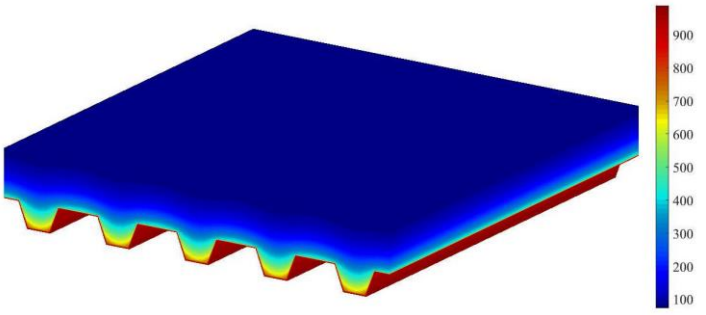

t= 91.3 min

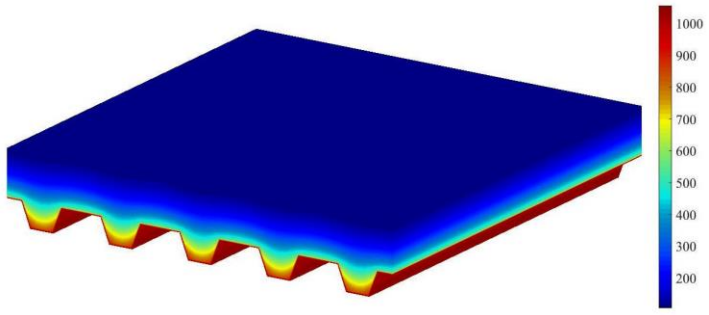

t= 137.0 min

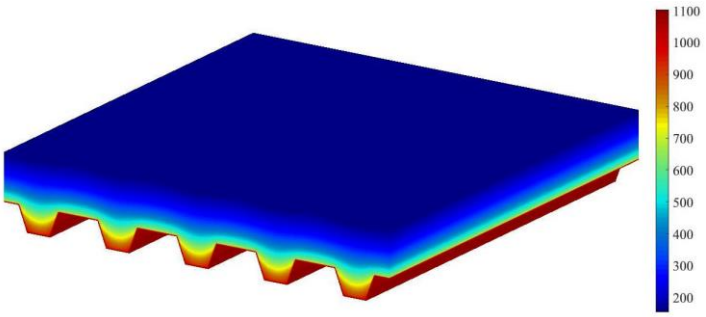

t= 182.6 min

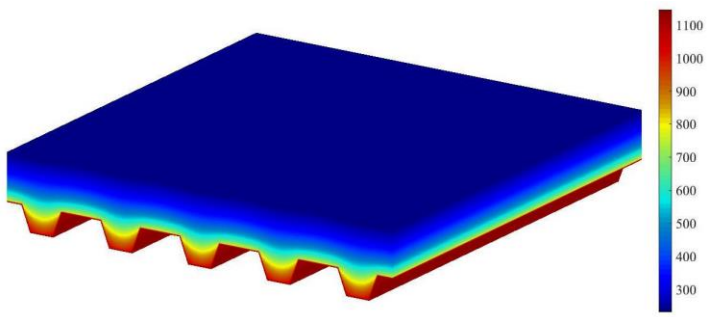

t= 240.0 min

SIM. 40	**Steel deck:** Trapezoidal – O Feliz H60	**Rebar (mm): -**	**t_a (mm):** 3	**Fire resistance (min)**	
	Mesh (mm//mm): -	**h_1 (mm):** 120		Ave: *205.3*	Max: 234.8

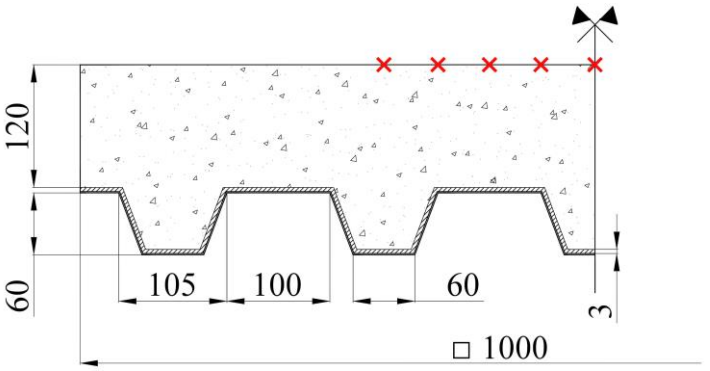

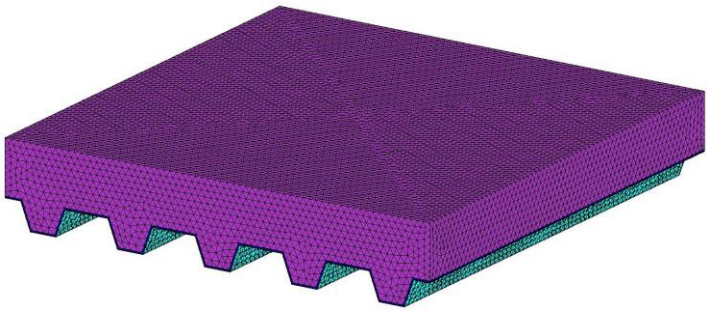

Finite element mesh

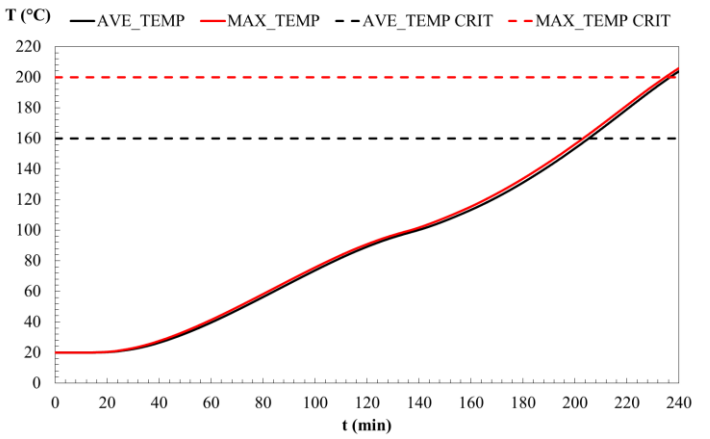

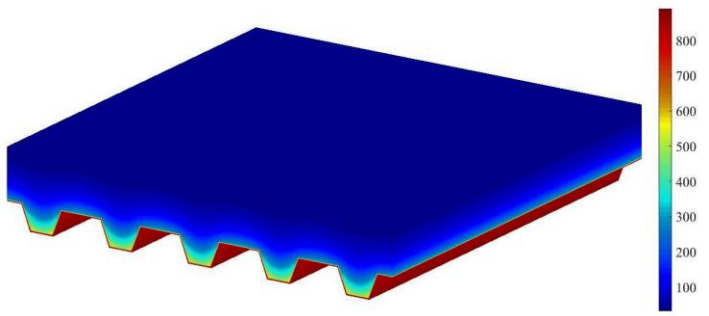

t= 51.3 min

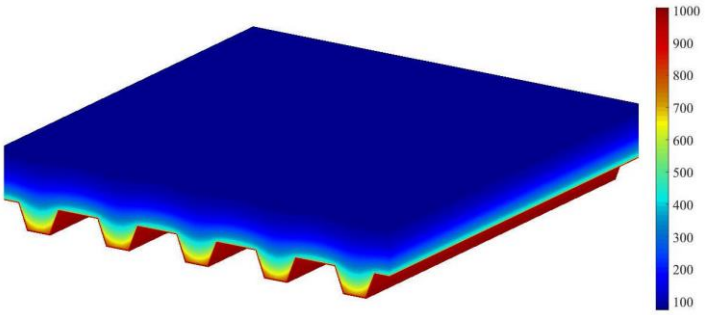

t= 102.7 min

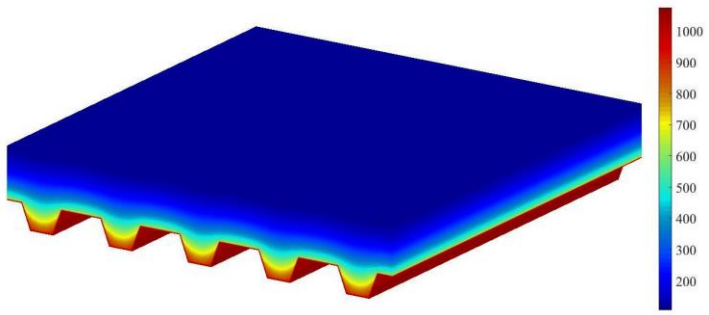

t= 154.0 min

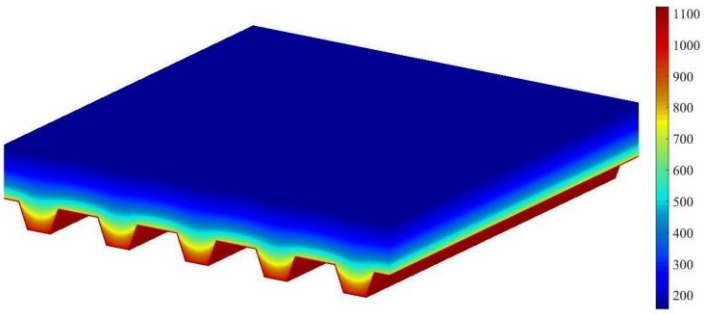

t= 205.3 min

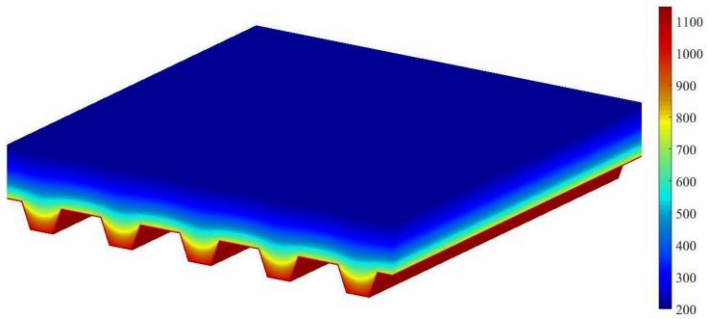

t= 240.0 min

APPENDIX F

DESCRIPTION OF THE PARAMETERS OF THE SIMULATIONS AND FIRE RESISTANCE OF THE COMPOSITE SLABS (I) FOR THE SECOND PARAMETRIC STUDY

O FELIZ H60 (PORTUGAL)														
Numerical simulation													**t_{fi} (min)**	
No.	l_1 (mm)	l_2 (mm)	l_3 (mm)	h_1 (mm)	h_2 (mm)	h_{tot} (mm)	ϕ_{reb} (mm)	d'_{reb} (mm)	ϕ_{mesh} (mm)	s_{mesh} (mm/mm)	h_{eff} (mm)	t_a (mm)	AVE_T crit.	MAX_T crit.
1	105	60	100	50	60	110	8	30	6	100	74.1	0	36.3	**34.6**
2	105	60	100	60	60	120	8	30	6	100	84.1	0	46.4	**45.9**
3	105	60	100	70	60	130	8	30	6	100	94.1	0	**57.7**	59.3
4	105	60	100	80	60	140	8	30	6	100	104.1	0	**70.1**	74.5
5	105	60	100	90	60	150	8	30	6	100	114.1	0	**83.6**	91.4
6	105	60	100	100	60	160	8	30	6	100	124.1	0	**99.1**	110.3
7	105	60	100	110	60	170	8	30	6	100	134.1	0	**115.6**	130.6
8	105	60	100	120	60	180	8	30	6	100	144.1	0	**133.5**	152.7
9	105	60	100	50	60	110	8	30	6	100	74.1	1	49.6	**48.7**
10	105	60	100	60	60	120	8	30	6	100	84.1	1	**61.3**	62.6
11	105	60	100	70	60	130	8	30	6	100	94.1	1	**74.1**	78.2
12	105	60	100	80	60	140	8	30	6	100	104.1	1	**88.1**	95.5
13	105	60	100	90	60	150	8	30	6	100	114.1	1	**103.2**	114.2
14	105	60	100	100	60	160	8	30	6	100	124.1	1	**120.1**	134.7
15	105	60	100	110	60	170	8	30	6	100	134.1	1	**138.0**	156.7
16	105	60	100	120	60	180	8	30	6	100	144.1	1	**157.5**	180.3
17	105	60	100	50	60	110	8	30	6	100	74.1	2	**62.3**	63.4
18	105	60	100	60	60	120	8	30	6	100	84.1	2	**75.6**	79.6
19	105	60	100	70	60	130	8	30	6	100	94.1	2	**89.9**	97.2
20	105	60	100	80	60	140	8	30	6	100	104.1	2	**105.3**	116.2
21	105	60	100	90	60	150	8	30	6	100	114.1	2	**121.9**	136.6
22	105	60	100	100	60	160	8	30	6	100	124.1	2	**140.3**	158.7

Continue on next page

23	105	60	100	110	60	170	8	30	6	100	134.1	2	**159.7**	182.2
24	105	60	100	120	60	180	8	30	6	100	144.1	2	**180.6**	207.5
25	105	60	100	50	60	110	8	30	6	100	74.1	3	**74.3**	77.9
26	105	60	100	60	60	120	8	30	6	100	84.1	3	**89.1**	96.2
27	105	60	100	70	60	130	8	30	6	100	94.1	3	**104.8**	115.5
28	105	60	100	80	60	140	8	30	6	100	104.1	3	**121.6**	136.2
29	105	60	100	90	60	150	8	30	6	100	114.1	3	**139.8**	158.2
30	105	60	100	100	60	160	8	30	6	100	124.1	3	**159.6**	181.9
31	105	60	100	110	60	170	8	30	6	100	134.1	3	**180.4**	207.1
32	105	60	100	120	60	180	8	30	6	100	144.1	3	**202.6**	233.8
33	105	60	100	50	60	110	-	-	-	-	74.1	3	**74.6**	77.2
34	105	60	100	60	60	120	-	-	-	-	84.1	3	**89.7**	95.5
35	105	60	100	70	60	130	-	-	-	-	94.1	3	**105.8**	115.2
36	105	60	100	80	60	140	-	-	-	-	104.1	3	**122.9**	135.8
37	105	60	100	90	60	150	-	-	-	-	114.1	3	**141.4**	158.3
38	105	60	100	100	60	160	-	-	-	-	124.1	3	**161.4**	182.2
39	105	60	100	110	60	170	-	-	-	-	134.1	3	**182.6**	207.5
40	105	60	100	120	60	180	-	-	-	-	144.1	3	**205.3**	234.8

APPENDIX G

COMPARISON BETWEEN THE RESULTS OF THE PROPOSED NEW EQUATIONS, ANSYS AND EUROCODE 4 FOR THE TEMPERATURE OF THE PARTS OF THE STEEL DECK, AND THE TEMPERATURE OF THE REBARS IN THE RIB

Temperature of the parts of the steel deck (°C)									
R60	**Lower flange**			**Web**			**Upper flange**		
SIM.	ANSYS	EC4	New Eq.	ANSYS	EC4	New Eq.	ANSYS	EC4	New Eq.
1	923.2	861.7	927.3	881.0	779.6	881.1	859.2	713.4	859.8
2	922.9	861.7	927.3	877.8	779.6	881.1	853.7	713.4	859.8
3	922.8	861.7	927.3	875.9	779.6	881.1	850.7	713.4	859.8
4	922.7	861.7	927.3	874.7	779.6	881.1	849.1	713.4	859.8
17	923.0	861.7	927.3	880.8	779.6	881.1	859.1	713.4	859.8
18	922.7	861.7	927.3	877.6	779.6	881.1	853.6	713.4	859.8
19	922.5	861.7	927.3	875.7	779.6	881.1	850.6	713.4	859.8
20	922.4	861.7	927.3	874.5	779.6	881.1	849.0	713.4	859.8
33	922.7	861.7	927.3	880.5	779.6	881.1	858.9	713.4	859.8
34	922.4	861.7	927.3	877.3	779.6	881.1	853.4	713.4	859.8
35	922.3	861.7	927.3	875.4	779.6	881.1	850.4	713.4	859.8
36	922.2	861.7	927.3	874.2	779.6	881.1	848.8	713.4	859.8
49	921.1	851.0	916.8	883.2	773.0	878.8	861.9	706.5	858.7
50	920.8	851.0	916.8	880.4	773.0	878.8	857.0	706.5	858.7
51	920.7	851.0	916.8	878.8	773.0	878.8	854.4	706.5	858.7
52	920.6	851.0	916.8	877.7	773.0	878.8	852.9	706.5	858.7
65	920.9	851.0	916.8	883.0	773.0	878.8	861.8	706.5	858.7
66	920.6	851.0	916.8	880.2	773.0	878.8	856.9	706.5	858.7
67	920.5	851.0	916.8	878.6	773.0	878.8	854.3	706.5	858.7
68	920.4	851.0	916.8	877.5	773.0	878.8	852.9	706.5	858.7
81	920.7	851.0	916.8	882.8	773.0	878.8	861.7	706.5	858.7
82	920.4	851.0	916.8	880.0	773.0	878.8	856.8	706.5	858.7
83	920.2	851.0	916.8	878.4	773.0	878.8	854.2	706.5	858.7
84	920.2	851.0	916.8	877.3	773.0	878.8	852.7	706.5	858.7
97	914.9	855.7	919.8	706.9	588.9	707.5	524.7	305.3	523.4
98	914.8	855.7	919.8	704.1	588.9	707.5	517.9	305.3	523.4
99	914.7	855.7	919.8	702.2	588.9	707.5	514.0	305.3	523.4
100	914.7	855.7	919.8	700.6	588.9	707.5	511.1	305.3	523.4
113	914.8	855.7	919.8	706.8	588.9	707.5	524.6	305.3	523.4
114	914.8	855.7	919.8	703.9	588.9	707.5	517.8	305.3	523.4
115	914.7	855.7	919.8	702.1	588.9	707.5	513.9	305.3	523.4
116	914.6	855.7	919.8	700.5	588.9	707.5	510.9	305.3	523.4
129	914.8	855.7	919.8	706.7	588.9	707.5	524.5	305.3	523.4
130	914.7	855.7	919.8	703.8	588.9	707.5	517.7	305.3	523.4
131	914.7	855.7	919.8	702.0	588.9	707.5	513.8	305.3	523.4
132	914.6	855.7	919.8	700.4	588.9	707.5	510.8	305.3	523.4
145	906.9	846.6	910.6	736.1	596.4	736.1	576.5	276.0	573.1

Continue on next page

146	906.6	846.6	910.6	733.8	596.4	736.1	572.1	276.0	573.1
147	906.5	846.6	910.6	731.9	596.4	736.1	568.8	276.0	573.1
148	906.3	846.6	910.6	730.3	596.4	736.1	566.2	276.0	573.1
161	906.8	846.6	910.6	736.0	596.4	736.1	576.4	276.0	573.1
162	906.6	846.6	910.6	733.7	596.4	736.1	572.0	276.0	573.1
163	906.5	846.6	910.6	731.9	596.4	736.1	568.7	276.0	573.1
164	906.3	846.6	910.6	730.2	596.4	736.1	566.0	276.0	573.1
177	906.8	846.6	910.6	735.9	596.4	736.1	576.3	276.0	573.1
178	906.6	846.6	910.6	733.6	596.4	736.1	571.8	276.0	573.1
179	906.4	846.6	910.6	731.8	596.4	736.1	568.6	276.0	573.1
180	906.3	846.6	910.6	730.2	596.4	736.1	566.0	276.0	573.1

Temperature of the parts of the steel deck (°C)									
R90	**Lower flange**			**Web**			**Upper flange**		
SIM.	ANSYS	EC4	New Eq.	ANSYS	EC4	New Eq.	ANSYS	EC4	New Eq.
1	993.3	959.4	993.1	965.3	906.6	968.1	950.7	851.5	950.8
2	993.0	959.4	993.1	962.5	906.6	968.1	946.3	851.5	950.8
3	992.7	959.4	993.1	960.2	906.6	968.1	942.7	851.5	950.8
4	992.5	959.4	993.1	958.4	906.6	968.1	940.1	851.5	950.8
17	993.2	959.4	993.1	965.2	906.6	968.1	950.6	851.5	950.8
18	992.8	959.4	993.1	962.3	906.6	968.1	946.1	851.5	950.8
19	992.5	959.4	993.1	960.0	906.6	968.1	942.6	851.5	950.8
20	992.4	959.4	993.1	958.3	906.6	968.1	940.0	851.5	950.8
33	993.0	959.4	993.1	965.0	906.6	968.1	950.5	851.5	950.8
34	992.6	959.4	993.1	962.2	906.6	968.1	946.0	851.5	950.8
35	992.4	959.4	993.1	959.8	906.6	968.1	942.4	851.5	950.8
36	992.2	959.4	993.1	958.1	906.6	968.1	939.9	851.5	950.8
49	991.8	952.1	994.5	966.1	899.5	964.9	951.7	845.0	956.4
50	991.4	952.1	994.5	963.4	899.5	964.9	947.5	845.0	956.4
51	991.1	952.1	994.5	961.4	899.5	964.9	944.3	845.0	956.4
52	991.0	952.1	994.5	959.8	899.5	964.9	941.9	845.0	956.4
65	991.6	952.1	994.5	965.9	899.5	964.9	951.6	845.0	956.4
66	991.2	952.1	994.5	963.3	899.5	964.9	947.5	845.0	956.4
67	991.0	952.1	994.5	961.3	899.5	964.9	944.2	845.0	956.4
68	990.9	952.1	994.5	959.7	899.5	964.9	941.9	845.0	956.4
81	991.5	952.1	994.5	965.8	899.5	964.9	951.5	845.0	956.4
82	991.1	952.1	994.5	963.2	899.5	964.9	947.4	845.0	956.4
83	990.8	952.1	994.5	961.2	899.5	964.9	944.1	845.0	956.4
84	990.7	952.1	994.5	959.6	899.5	964.9	941.8	845.0	956.4
97	986.7	954.5	986.4	812.7	763.2	812.7	667.9	585.4	660.4
98	986.5	954.5	986.4	806.8	763.2	812.7	654.9	585.4	660.4
99	986.4	954.5	986.4	803.1	763.2	812.7	646.8	585.4	660.4
100	986.4	954.5	986.4	800.9	763.2	812.7	642.3	585.4	660.4
113	986.7	954.5	986.4	812.6	763.2	812.7	667.7	585.4	660.4
114	986.5	954.5	986.4	806.6	763.2	812.7	654.7	585.4	660.4
115	986.4	954.5	986.4	803.0	763.2	812.7	646.7	585.4	660.4
116	986.3	954.5	986.4	800.7	763.2	812.7	642.2	585.4	660.4
129	986.7	954.5	986.4	812.5	763.2	812.7	667.6	585.4	660.4
130	986.5	954.5	986.4	806.5	763.2	812.7	654.5	585.4	660.4
131	986.4	954.5	986.4	802.8	763.2	812.7	646.5	585.4	660.4
132	986.3	954.5	986.4	800.6	763.2	812.7	642.0	585.4	660.4
145	980.5	947.7	984.4	837.7	763.5	836.6	705.1	555.0	694.3

Continue on next page

146	979.9	947.7	984.4	832.6	763.5	836.6	695.7	555.0	694.3
147	977.4	947.7	984.4	829.7	763.5	836.6	690.2	555.0	694.3
148	979.5	947.7	984.4	827.6	763.5	836.6	686.7	555.0	694.3
161	980.4	947.7	984.4	837.6	763.5	836.6	705.0	555.0	694.3
162	979.9	947.7	984.4	832.5	763.5	836.6	695.5	555.0	694.3
163	979.8	947.7	984.4	829.6	763.5	836.6	690.0	555.0	694.3
164	979.5	947.7	984.4	827.5	763.5	836.6	686.5	555.0	694.3
177	980.2	947.7	984.4	837.4	763.5	836.6	704.8	555.0	694.3
178	979.5	947.7	984.4	832.4	763.5	836.6	695.4	555.0	694.3
179	979.8	947.7	984.4	829.5	763.5	836.6	689.9	555.0	694.3
180	977.1	947.7	984.4	827.5	763.5	836.6	686.4	555.0	694.3

Temperature of the parts of the steel deck (°C)									
R120	**Lower flange**			**Web**			**Upper flange**		
SIM.	ANSYS	EC4	New Eq.	ANSYS	EC4	New Eq.	ANSYS	EC4	New Eq.
1	1040.4	1016.9	1045.7	1019.0	976.7	1020.0	1007.6	931.8	1013.5
2	1040.0	1016.9	1045.7	1017.0	976.7	1020.0	1004.5	931.8	1013.5
3	1039.8	1016.9	1045.7	1015.0	976.7	1020.0	1001.7	931.8	1013.5
4	1039.6	1016.9	1045.7	1013.3	976.7	1020.0	999.2	931.8	1013.5
17	1040.2	1016.9	1045.7	1018.9	976.7	1020.0	1007.5	931.8	1013.5
18	1039.9	1016.9	1045.7	1016.8	976.7	1020.0	1004.4	931.8	1013.5
19	1039.6	1016.9	1045.7	1014.9	976.7	1020.0	1001.6	931.8	1013.5
20	1039.4	1016.9	1045.7	1013.2	976.7	1020.0	999.1	931.8	1013.5
33	1040.0	1016.9	1045.7	1018.7	976.7	1020.0	1007.4	931.8	1013.5
34	1039.7	1016.9	1045.7	1016.6	976.7	1020.0	1004.3	931.8	1013.5
35	1039.4	1016.9	1045.7	1014.7	976.7	1020.0	1001.5	931.8	1013.5
36	1039.2	1016.9	1045.7	1013.0	976.7	1020.0	999.0	931.8	1013.5
49	1038.8	1011.3	1038.7	1019.1	970.0	1018.6	1007.9	925.0	1017.3
50	1038.4	1011.3	1038.7	1017.1	970.0	1018.6	1004.9	925.0	1017.3
51	1038.2	1011.3	1038.7	1015.4	970.0	1018.6	1002.3	925.0	1017.3
52	1038.1	1011.3	1038.7	1013.9	970.0	1018.6	1000.0	925.0	1017.3
65	1038.7	1011.3	1038.7	1019.0	970.0	1018.6	1007.9	925.0	1017.3
66	1038.3	1011.3	1038.7	1017.0	970.0	1018.6	1004.8	925.0	1017.3
67	1038.1	1011.3	1038.7	1015.3	970.0	1018.6	1002.3	925.0	1017.3
68	1038.3	1011.3	1038.7	1014.0	970.0	1018.6	1000.1	925.0	1017.3
81	1038.7	1011.3	1038.7	1019.0	970.0	1018.6	1007.9	925.0	1017.3
82	1038.1	1011.3	1038.7	1016.8	970.0	1018.6	1004.7	925.0	1017.3
83	1038.3	1011.3	1038.7	1015.5	970.0	1018.6	1002.4	925.0	1017.3
84	1037.8	1011.3	1038.7	1013.6	970.0	1018.6	999.8	925.0	1017.3
97	1035.0	1015.7	1038.9	888.5	875.8	887.8	772.2	729.8	765.8
98	1034.7	1015.7	1038.9	881.5	875.8	887.8	757.7	729.8	765.8
99	1034.2	1015.7	1038.9	876.2	875.8	887.8	746.4	729.8	765.8
100	1034.2	1015.7	1038.9	873.2	875.8	887.8	739.2	729.8	765.8
113	1034.8	1015.7	1038.9	888.2	875.8	887.8	771.9	729.8	765.8
114	1034.5	1015.7	1038.9	881.3	875.8	887.8	757.4	729.8	765.8
115	1034.4	1015.7	1038.9	876.2	875.8	887.8	746.4	729.8	765.8
116	1034.3	1015.7	1038.9	873.0	875.8	887.8	739.0	729.8	765.8
129	1034.8	1015.7	1038.9	888.0	875.8	887.8	771.7	729.8	765.8
130	1034.5	1015.7	1038.9	881.1	875.8	887.8	757.3	729.8	765.8
131	1034.4	1015.7	1038.9	876.1	875.8	887.8	746.2	729.8	765.8
132	1034.4	1015.7	1038.9	873.0	875.8	887.8	738.9	729.8	765.8
145	1029.7	1009.5	1029.1	910.6	872.5	907.4	801.7	702.2	795.1

Continue on next page

146	1029.3	1009.5	1029.1	904.3	872.5	907.4	789.6	702.2	795.1
147	1028.8	1009.5	1029.1	899.3	872.5	907.4	780.2	702.2	795.1
148	1028.7	1009.5	1029.1	896.4	872.5	907.4	774.3	702.2	795.1
161	1029.9	1009.5	1029.1	910.6	872.5	907.4	801.7	702.2	795.1
162	1029.4	1009.5	1029.1	904.2	872.5	907.4	789.5	702.2	795.1
163	1028.6	1009.5	1029.1	899.1	872.5	907.4	780.0	702.2	795.1
164	1028.9	1009.5	1029.1	896.1	872.5	907.4	774.1	702.2	795.1
177	1029.6	1009.5	1029.1	910.3	872.5	907.4	801.4	702.2	795.1
178	1029.2	1009.5	1029.1	903.9	872.5	907.4	789.2	702.2	795.1
179	1028.7	1009.5	1029.1	899.1	872.5	907.4	779.9	702.2	795.1
180	1028.9	1009.5	1029.1	896.0	872.5	907.4	774.0	702.2	795.1

Temperature of the rebars in the rib (°C)					
Standard fire resistance	SIM.	ϕ_{reb} (mm)	ANSYS	EC4	New Eq.
R60	1	8	598.9	524.2	599.0
	17	10	586.8	524.2	586.8
	33	12	572.7	524.2	572.8
	49	8	560.6	491.8	566.6
	65	10	549.9	491.8	554.5
	81	12	537.4	491.8	540.4
	145	8	431.4	363.0	431.4
	161	10	425.6	363.0	425.7
	177	12	418.6	363.0	418.6
R90	1	8	731.3	695.1	734.7
	17	10	723.1	695.1	724.5
	33	12	712.0	695.1	712.8
	49	8	698.6	658.9	698.5
	65	10	688.4	658.9	688.3
	81	12	676.6	658.9	676.5
	145	8	549.0	538.2	549.0
	161	10	543.4	538.2	543.4
	177	12	536.7	538.2	536.7
R120	1	8	837.0	797.7	839.3
	17	10	822.4	797.7	822.5
	33	12	799.2	797.7	799.6
	49	8	789.1	760.6	789.0
	65	10	769.6	760.6	772.1
	81	12	749.4	760.6	749.3
	145	8	640.6	656.9	640.6
	161	10	634.9	656.9	634.9
	177	12	628.1	656.9	628.1